

# Proceedings

Science, Engineering & Environment

Edited by  
Zakaria Hossain  
Jim Shiau



UNIVERSITY  
OF SOUTHERN  
QUEENSLAND

SPRINGFIELD CAMPUS

**13-16 November 2017**

University of Southern Queensland

Springfield, Brisbane, Australia

<https://www.usq.edu.au/springfield>

SEE 2017 USQ SPRINGFIELD BRISBANE, AUSTRALIA  
SCIENCE, ENGINEERING AND ENVIRONMENT



PROCEEDINGS OF THIRD INTERNATIONAL CONFERENCE – SEE 2017  
SCIENCE, ENGINEERING & ENVIRONMENT USQ SPRINGFIELD BRISBANE, AUSTRALIA  
13-15 November, 2017

# Science, Engineering and Environment

*Edited by*

**Prof. Dr. Zakaria Hossain**  
*Graduate School of Bioresources  
Mie University, Japan*

**Dr. Jim Shiau**  
*School of Civil Engineering and Surveying  
University of Southern Queensland, Australia*



THE GEOMATE INTERNATIONAL SOCIETY

Copyright © 2017 by The GEOMATE International Society

All rights reserved. In principle, no part of this publication or the information contained herein may be reproduced in any form or by any means, translated in any language, stored in any data base or retrieval system, or transmitted in any form or by any means without prior permission in writing from the publisher.

Disclaimer: The editors and the publisher have tried their best effort to ensure the integrity and the quality of this publication and information herein. However, they give no warranty of any kind, expressed or implied with regard to the material contained in this book, and will not be liable in any event for the consequences of its use.

Published by:  
The GEOMATE International Society  
Tsu city, Mie, Japan  
E-mail: [society@geomate.org](mailto:society@geomate.org)  
<http://www.geomate.org/>

ISBN Number: 978-4-9905958-9-0 C3051

## Table of Contents

	Preface	xi
	Organization	xii
<b>ID</b>	<b><i>Keynote Papers</i></b>	<b>1</b>
1k	MECHANICS OF GEOSYNTHETICS SUBJECTED TO CHEMICAL EXPOSURE: EXPERIMENTS, CONSTITUTIVE MODELS AND COMPUTATIONS A.P.S. Selvadurai	<b>2</b>
2k	MEETING THE CHALLENGES OF ENGINEERING A SUSTAINABLE FUTURE David Thorpe	<b>12</b>
3k	STATISTICS FOR EVIDENCE-BASED DECISIONS – USE, MISUSE AND ABUSE Shahjahan Khan and M Ashraf Memon	<b>22</b>
	<b><i>Technical Papers</i></b>	<b>31</b>
<b>ID</b>	<b><i>Science</i></b>	<b>32</b>
3522	SEA LEVEL IN A CHANGING CLIMATE Maria McCrann, Dr John Russell, Dr Daniela Ionescu and Dr Bandita Mainali	<b>33</b>
3534	EBOLA VIRAL PROTEIN 24 (VP24) INHIBITOR DISCOVERY BY IN SILICO FRAGMENT-BASED DESIGN Syafrika Siregar, Erwin Prasetya Toepak, Usman Sumo Friend Tambunan	<b>39</b>
3535	FRAGMENT-BASED LEAD COMPOUND DESIGN TO INHIBIT EBOLA VP35 THROUGH COMPUTATIONAL STUDIES Atika Marnolia, Erwin Prasetya Toepak, Usman Sumo Friend Tambunan	<b>45</b>
3547	DEVELOPMENT OF SPECIFIC ELECTROCHEMICAL BIOSENSOR BASED ON CHITOSAN MODIFIED SCREEN PRINTED CARBON ELECTRODE FOR THE MONITORING OF CAPTAN FUNGICIDE Porntip Wongkaew, Buddhapala Wongkaew, Suwita Saepaisan, and Panupong Thanutong	<b>51</b>
3548	A BASIC STUDY ON FLUID PREDICTION OF MORTAR WITH VARIOUS POWDERS Yuki takagi, Koji Takasu, Hidehiro Koyamada and Hiroki Suyama	<b>57</b>
3549	PHYTOCHEMICALS AND ANTIOXIDANT ACTIVITIES OF THAI RED RICE SEEDS FROM DIFFERENT CULTIVATED AREAS Muntana Nakornriab, Jiraporn Krasaetep, Maratree Plainsirichai and Sisikka Wannajun	<b>62</b>
3550	A STUDY ON PROPERTIES OF MORTAR WITH FLY ASH REMOVED UNBURNED CARBON BY FLOTATION METHOD Rika Oie, Koji Takasu, Hidehiro Koyamada and Hiroki Suyama	<b>67</b>



3551	A STUDY ON PROPERTIES OF WITH FLY ASH REMOVED UNBURNED CARBON BY FLOTATION METHOD Yuto Murakami, Koji Takasu, Hidehiro Koyamada and Hiroki Suyama	72
3559	CHARACTERIZATION OF CERIUM OXIDE-CHITOSAN NANOCOMPOSITE–MODIFIED SCREEN PRINTED CARBON ELECTRODE AND APPLICATION IN MELATONIN DETERMINATION Pachanuporn Sunon, Porntip Wongkaew, Jeffrey Johns, Nutjaree Johns	77
3564	COMPARISON OF HEART RATE VARIABILITY BETWEEN PATIENTS WITH MAJOR DEPRESSIVE DISORDER AND NORMAL SUBJECTS Warangkana Chompoopan, Sipanut Silaket, Wichai Eungpinichpong, Suwanna Arunpongpaisal and Niramol Patjanasootorn	83
3566	EFFECT OF ARM SWING EXERCISES ON CARDIOVASCULAR RESPONSE AND BALANCE OF OLDER WOMEN Worawut Chompoopan, Piyathida Kuhirunyaratn	87
3578	PLASTIC FLOW HETEROGENEITY AND FAILURE OF BIMETAL MATERIAL Svetlana Barannikova, Lev Zuev and Yulia Li	91
3606	SEARCHING OF NEW ANTIVIRAL COMPOUNDS OF SUDAN EBOLAVIRUS GLYCOPROTEIN BASED ON FLAVONOID COMPOUNDS USING IN SILICO METHODS Rendy Pramuda Putra, Ahmad Husein Alkaff, Mochammad Arfin Fardiansyah Nasution and Agustinus C. B. Kantale, and Usman Sumo Friend Tambunan	97
3622	NEW ESTIMATION IN AR MODELS WITH EXPONENTIAL WHITE NOISE BY USING REVERSIBLE JUMP MCMC ALGORITHM Suparman	103
3623	ECOLOGY AND CONSERVATION OF INDIAN HORNBILLS WITH PARTICULAR REFERENCE TO NARCONDAM HORNBILL (ACEROS NARCONDAMI) OCCURRING ON NARCONDAM ISLAND OF ANDAMAN& NICOBAR ISLAND ARCHIPELAGO Hafiz S.A. Yahya	107
3630	THE IMMEDIATE EFFECTS OF FOOT MASSAGE WITH COCONUT SHELL ON PRESSURE PAIN THRESHOLD AND FOOT GRIP STRENGTH IN HEALTHY SUBJECTS: A PILOT STUDY Laojeenwong P, Eungpinichpong W	113
3633	MOCAP TEMPEH DATES BISCUIT FOR THE IMPROVEMENT NUTRITIONAL STATUS OF UNDERWEIGHT CHILDREN Fatmah	117
3637	SPATIAL VARIATION OF WATERBIRDS IN PALLAI AND THADDUVANKODDY IN THE NORTHERN PROVINCE, SRI LANKA G. Kandasamy, D. K. Weerakoon, and A. Sivaruban	124
3645	FACTORS RELATED TO SELF-CARE ABILITY AMONG ELDERLY WOMEN IN SEMI-URBAN COMMUNITIES, KHON KAEN, THAILAND. Kanchana Nimsuntorn, Piyathida Kuhirunyaratn and Kanaporn Tansriprapasiri	130
3646	IMMEDIATE EFFECTS OF THAI MASSAGE ON GAIT PARAMETERS IN NORMAL ADULTS: A PILOT STUDY Nutthanun Tatchananusorn, Wichai Eungpinichpong, Uraiwan Chatchawan and Donlaya Promkaew	136
3648	THAI MASSAGE COMBINED WITH MUSCLE ENERGY AND PASSIVE STATIC STRENGTHENING TECHNIQUE COULD IMPROVE HEIGHT OF SEPAKTAKRAW SERVES Apichat Deeminoi, Dr.Wichai Eungpinichpong, Dr.Maitree Pakarasang, Dr.Thanarat Sripongngam	140
3652	A STUDY OF THE CORRELATION BETWEEN FOUR CLINICAL TRIALS FOR THE MEASUREMENT OF HAMSTRING MUSCLE FLEXIBILITY Apichat Deeminoi, Dr.Thanarat Sripongngam	146
3665	EFFECTS OF KAEMPFERIA PARVIFLORA ON PHYSICAL AND PSYCHOLOGICAL STRESSES IN ADULTS Wichai Eungpinichpong, Uraiwan Chatchawan, Bung-orn Sripanidkulchai Suwanna Arunpongpaisal	150

3673	DEVELOPMENT OF POLY (D, L-LACTIC ACID) WITH POLYBENZOXAZINE VIA SOLUTION BLENDING Kansiri Pakkethati and Yodthong Baimark	154
3677	BIOCHEMICAL CHANGES IN CHEMICAL INGRADIENTS OF SILK COCOONS UNDER ENVIRONMENTAL FACTORS H.N.P. Singh, Sunita Kumari and M.M. Prasad	159
3711	ACUTE EFFECTS OF TRADITONAL THAI MASSAGE ON HEART RATE VARIABILITY, HEART RATE AND SALIVARY ALPHA AMYLASE Jaruk Keawsod Wichai Eungpinichpong	163
<b>ID</b>	<b><i>Engineering</i></b>	<b>166</b>
3503	SHEAR STRENGTH OF SOIL BY USING SHELL HUSKS WASTE AS RECYCLE AGGREGATE Siti Hanggita Rachmawati, Zakaria Hossain	167
3504	ANALYTICAL STUDY ON SINGLE PILE DESIGN FOR SOLAR FOUNDATIONS FOR SLOPING LAND. Alex Otieno Owino, Hossain, M.Z., Ojiro C., Ozumi, S., Harada, H. and Okuyama, S.	172
3510	EXPERIMENTAL BEHAVIORAL INSPECTION OF COMPOSITE CONCRETE-OPEN WEB EXPANDED STEEL BEAMS EXPOSED TO STATIC LOADING Nazar K. Oukaili and Seezar Sh. Abdullah	178
3512	RESIDENTIAL CUSTOMER DEMAND RESPONSE PROGRAM IN MICROGRID SYSTEM: A SURVEY LITERATURE Ignatius Rendroyoko, and Ngapuli I Sinisuka	184
3514	CRACKING AND DEFORMABILITY OF BONDED AND UNBONDED PRESTRESSED CONCRETE BEAMS UNDER MONOTONIC STATIC LOADING Nazar K. Oukaili and Mohammed M. Khattab	190
3515	DISTRIBUTED MODEL OF HYDROLOGICAL AND SEDIMENT TRANSPORT PROCESS IN MEKONG RIVER BASIN Zuliziana Suif, Chihiro Yoshimura, Nordila Ahmad and Sengheng Hul	196
3516	EVALUATION OF PIER-SCOUR PREDICTIONS FOR WIDE PIERS USING FIELD DATA Nordila Ahmad, Bruce W. Melville, Thamer Mohammad, Zuliziana Suif	202
3521	MECHANICAL CHARACTERISTICS OF ARTIFICIAL STONE MADE FROM WASTE OF SILICEOUS TUFF Hiroaki Shigematsu and Shogo Hashimoto	208
3528	3 DIMENSION REAL TIME IMAGES OF RAINFALL INFILTRATION INTO UNSATURATED SOIL SLOPE Aniza Ibrahim, Irfana Kabir Ahmad, Hapsa Husen, Jestin Jelani1and Mohd. Raihan Taha	214
3529	STEREO ECHO CANCELLATION USING ADAPTIVE NON-LINEAR NETWORK FILTER FOR HOME THEATRE ROOM Sunisa Kunarak	219
3530	FINITE ELEMENT ANALYSIS OF EWECs COLUMNS WITH VARYING SHEAR SPAN RATIO Fauzan, Ruddy Kurniawan and Zev Al Jauhari	224
3538	EXPERIMENTAL INVESTIGATION ON BOX-UP COLD-FORMED STEEL COLUMNS IN FIRE Fadhluhartini Muftah, Mohd Syahrul Hisyam Mohd Sani, Ahmad Rasidi Osman, Shahrin Mohammad, Shek Poi Ngian	231

3539	EXPERIMENTAL INVESTIGATION OF COLD-FORMED STEEL CHANNEL SECTION WITH NOTCH Mohd Syahrul Hisyam Mohd Sani, Fadhluhartini Muftah, Muhammad Isha Ismail	237
3542	A REVIEW OF UNEXPECTED LARGE SLOPE FAILURES Marthinus Sonnekus and John Victor Smith	243
3563	THE EFFECT OF STEEL FIBERS EXTRACTED FROM WASTE TYRE ON CONCRETE CONTAINING PALM OIL FUEL ASH Fauzan, Febrin Anas Ismail and Rio Sandi	249
3574	ACCURACY OF CENTRALIZED AND DECENTRALIZED MANUFACTURING SYSTEMS TOWARDS AN INDUSTRY 4.0'S PERSPECTIVE Poonpakdee, P. , Koiwanit, J., Yuangyai, C.	254
3576	NUMERICAL ANALYSIS OF NONLINEAR MODEL OF SFRC SLAB AND NONLINEAR SUBSOIL MODEL IN INTERACTION Jana VASKOVA, Radim CAJKA	260
3583	AN OVERVIEW OF THE IMPACTS OF SUSTAINABLE HOUSING DESIGN ON ENERGY EFFICIENCY OF THE AUSTRALIAN HOUSING Javad Asad Poor , David Thorpe, Yong Goh	266
3590	VULNERABILITY ASSESSMENT OF SURIGAO METRO WATER DISTRICT UNDER SEISMIC HAZARD Sheena I. Better and Lessandro Estelito O. Garciano	276
3591	A COMPARISON OF ESTIMATED SHEAR STRENGTH OF SOUTH-EAST QUEENSLAND RESIDUAL SOIL USING FIELD AND LABORATORY TESTING Darren Newell and Choo Yong	283
3593	STUDY ON LANDSLIDE CATEGORY BASE ON TEMPORAL– SPATIAL CHARACTERISTIC DISTRIBUTION IN NORTHERN VIETNAM USING SATELLITE IMAGES Thuy Thi Thanh LE and Seiki KAWAGOE	287
3597	THE QUALITY ANALYSIS OF BICYCLE ROUTES FOR SUSTAINABLE URBAN MOBILITY IN THE WESTERN ZONE OF RIO DE JANEIRO Guilherme Marins Pessanha, Jaime Massaguer Hidalgo Jr	293
3599	COMPARATIVE ANALYSIS OF PAVEMENT FRICTION PREDICTION MODELS Luciana Omar, Karim Ismail and Abd El Halim O. Abd El Halim	299
3608	APPLICATION OF MEMETIC ALGORITHM FOR SOLVING THE VEHICLE ROUTING PROBLEM WITH TIME WINDOWS Chaowalit Hamontree , Jiraporn Chuenjai and Nawaporn Chamnanketgorn	305
3614	THE EFFECT OF MODEL DOMAIN SIZE FOR UNSUPPORTED PLAIN STRAIN TUNNEL HEADINGS IN UNDRAINED CLAY Jim Shiau, Fadhil Al-Asadi	309
3656	APPLICATION OF HEC-RAS AND ARC GIS FOR FLOODPLAIN MAPPING IN SEGAMAT TOWN, MALAYSIA Noor Suraya Romali, Zulkifli Yusop and Ahmad Zuhdi Ismail	315
3658	EFFECT OF SATURATION ON STRENGTH BEHAVIOR OF SOAPSTONE Ravikant R Singh, Darga Kumar Nandyala and Faijal Ali	321
3659	MEASUREMENT ACCURACY OF ORIENTATION CODE MATCHING FOR SLOPE DEFORMATION MONITORING Takeshi YAMAMOTO, Keigo KOIZUMI, Kazuhiro ODA, and Yoshio FUKUDA	327



3670	NANOSTRUCTURAL CHARACTERIZATION OF GLUTATHIONE-S-TRANSFERASE IMMOBILIZING CHITOSAN MODIFIED SCREEN PRINTED CARBON ELECTRODE BY ATOMIC FORCE MICROSCOPY Buddhapala Wongkaew, Porntip Wongkaew, Panupong Thanutong and Chitsanuphong Thanutong	332
3672	COLUMN BASED INFILTRATION EXPERIMENT FOR CONSIDERING INITIAL QUASI-SATURATED VOLUMETRIC WATER CONTENT DUE TO DIFFERENCES OF WATER SPRAY INTENSITY AND GRAIN SIZE DISTRIBUTION Hiroshi Kita, Keigo Koizumi and Kazuhiro Oda and Mitsuru Komatsu	338
3683	ENVIRONMENTAL RISK ASSESSMENT AND MANAGEMENT OF BIOMASS POWER PLANTS FOR SUSTAINABILITY IN THAILAND Manutchanok Jongprasithporn, Adisak Martsri, Supapat Phuangkaew, Wannapong Yeamma, and Nantakrit Yodpijit	342
3686	THE DESIGN OF AN ALTERNATIVE ENERGY DATABASE IN THAILAND Manutchanok Jongprasithporn, Supapat Phuangkaew, Siravitch Atipatha, and Nantakrit Yodpijit	348
3691	NUMERICAL INVESTIGATION OF 2D TRAPDOOR STABILITY Jim Shiau, Mohammad Mirza Hassan	354
3695	INSTALLATION CONSTRAINTS OF SUCTION ASSISTED FOUNDATIONS AND ANCHORS FOR OFFSHORE ENERGY DEVELOPMENT Kingsley Osezua Akeme, Alireza Rezagholilou and Meysam Banimahd	360
3706	DIFFERENTIAL THERMAL ANALYSIS OF PMMA (POLY METHYL METHACRYLATE) - EXPERIMENTAL CONCERNS Sam M Dakka	368
3717	INVESTIGATION OF CURING PERIOD OF CEMENTITIOUS ADHESIVE AND PERFORMANCE OF RUST PREVENTION Yoichi Mimura, Vanissorn Vimonsatit and Isamu Yoshitake	373
3721	REGIONAL DEPOSITION CHARACTERISTICS OF NANOPARTICLES IN A RAT NASAL CAVITY Yidan Shang, Jingliang Dong, Kiao Inthavong and Jiyuan Tu	379
3733	SEGMENTATION OF PAP SMEAR IMAGES TO IDENTIFY AND DETECT CERVICAL CANCER Vasundhara Acharya, Preetham Kumar	383
<b>ID</b>	<b><i>Environment</i></b>	<b>390</b>
3506	NUTRIENT LOADS AND SELF-REMEDIATION ASSESSMENT IN KHLONG RUNGSIT TAI, PATHUM THANI PROVINCE, THAILAND Boontarika Thongdonphum, Kittima Vanichkul, Saming Champasri and Jirapon Kulkham	391
3517	INFLUENCE OF ABIOTIC STRESS FACTORS ON BLACKCURRANT RESISTANCE TO PESTS I.V. Mashkova, T.G. Krupnova, A.M. Kostryukova	395
3518	USING BIRCH LEAVES TO INDICATE AIR POLLUTION T.G. Krupnova, I.V. Mashkova and A.M. Kostryukova	399
3519	STUDY OF SYNANTHROPIC PLANTS OF THE SOUTH URAL A.M. Kostryukova, I.V. Mashkova, T.G. Krupnova and E.E. Shchelkanova	405
3531	A STUDY ON THE EFFECTIVENESS OF LIQUID SMOKE PRODUCED FROM PALM KERNEL SHELLS IN INHIBITING BLACK POD DISEASE IN CACAO FRUIT IN VITRO M. Faisal, Tjut Chamzurni, Hiroyuki Daimon	411

3543	HEAVY METALS IN MICROALGAE BIOMASS ADDED WITH DIFFERENT CONCENTRATION OF WET MARKET WASTEWATER Radin Maya Saphira Radin Mohamed, Najeeha Apendi, Siti Nor Hidayah Arifin, A.A.S. Al-Gheethi and Amir Hashim Mohd Kassim	417
3546	INFLUENCING PARAMETER OF SELF PURIFICATION PROCESS IN THE URBAN AREA OF CIKAPUNDUNG RIVER, INDONESIA Yonik Meilawati Yustiani, Mia Nurkanti, Neneng Suliasih and Annisa Novantri	422
3562	THE PHYSICAL MICROHABITAT REQUIREMENTS OF FRESHWATER MUSSEL, WESTRALUNIO CARTERI, (BIVALVIA: HYRIIDAE) IN SOUTH-WESTERN AUSTRALIA Le Ma1, Alan Lymberry, Stephen Beatty and David Morgan	426
3567	EVALUATING THE EFFECTIVENESS OF VIRGINIA BUTTONWEED FOR EROSION CONTROL OF DAM RESERVOIR SLOPES IN JAPAN. Taizo Uchida, Yuya Imamura, Yoshifumi Kochi, Mamoru Yamada, Kunihiro Fukaura, Aki Matsumoto, William T. Haller and Lyn A. Gettys	432
3577	NANOCOMPOSITE WITH DUAL FUNCTIONALITY IN SIMULTANEOUS REMOVAL OF HEAVY METALS, DYE AND ANIONIC SURFACTANT FROM MULTICOMPONENT WASTEWATER Maria Visa, Nicoleta Popa, Andreea Maria Chelaru	437
3600	EFFECT OF WATER ACTIVITY ON ENZYMES ADSORBED ON BIOMASS CHARCOAL IN ORGANIC MEDIA Hidetaka Noritomi, Jumpei Nishigami, Nobuyuki Endo, Satoru Kato and Katsumi Uchiyama	443
3602	EVALUATION OF ENERGY EFFICIENCY AND ENVIRONMENTAL PERFORMANCE IN LOBLAW COMPANIES LIMITED IN CANADA Koiwanit, J., Chan, V. K., Piewkhow, L., Katipelly, N. D.	449
3611	AN EVALUATION FOR EFFECTIVE PUBLIC PARTICIPATION IN EIA IN THAILAND Chutarat Chompunth	455
3649	ACHIEVING WATER SENSITIVE CITY CONCEPT THROUGH MUSRENBANG MECHANISM IN SURABAYA CITY, INDONESIA Eddy Setiadi Soedjono, Nurina Fitriani, Rifda Rahman, I Made Wahyu Wijaya	462
3651	THE STUDY ON MITIGATION METHOD OF BEACH EROSION USING THE CORAL CELLS Sang Kil Park, Hong Bum Park, Kyeong Mo Lim	467
3662	THE DESCRIPTION OF LIGHTING ENVIRONMENTAL ON THE URBAN STREET Shuto Takeuchi, Kazunari Tanaka and Shin Yoshikawa	473
3684	SOCIAL AND ENVIRONMENTAL RESPONSIBILITY IN DEVELOPING COUNTRIES: A THEORETICAL APPROACH OF REGULATION Lindrianasari, Mahatma Kufepaksi, Yuztitya Asmaranti, and Agrianti Komalasari	477
3688	ASSESSMENT OF URBAN CLIMATE CHANGE IN IPOH CITY, PERAK, MALAYSIA Mohd Hairry Ibrahim, Mazlini Adnan, Nor Kalsum Mohd Isa & Kamarul Ismail,	482
3707	TREND OF DAILY RAINFALL AND TEMPERATURE IN PENINSULAR MALAYSIA BASED ON GRIDDED DATA SET Chee-Loong Wong, Zulkifli Yusop, Tarmizi Ismail	488
3708	SPATIO-TEMPORAL ANALYSIS OF LAND USE AND LAND COVER CHANGES IN ARID REGION OF SAUDI ARABIA Eman Albalawi, Ashraf Dewan and Robert Corner	496

3718	COMPARISON OF LUNG DAMAGES DUE TO PETROL AND DIESEL CAR SMOKE EXPOSURES: HISTOLOGICAL STUDY Wardoyo, Arinto Y.P.a, Juswono, Unggul P., Noor, Johan A. E.	502
3723	SPATIAL VARIATIONS OF SURFACE WATER QUALITY AND POLLUTION SOURCES IN KHLONG U-TAPAO RIVER BASIN Saudee Maprasit, Chaisri Suksaroj, Vichit Rangpan, and Rotchanatch Darnsawasdi	508
3724	DIVESIRY AND POLLEN MORPHOLGY OF IMPORTANT TREE SPECIES OF RANIKOT FORT, SINDH, PAKISTAN. Nabila Shah Jilani, S.S Hassney, Muhammad Tahir Rajput and Feroza shar Baloch	514
3727	RELATIONSHIP BETWEEN PAVEMENT TEXTURE AND MOVEMENT Yuki OGIMOTO,Kazunari TANAKA and shin YOSHIKAWA	517
3728	REMOVAL AMMONIA FROM LANDFILL LEACHATE USING ULTRASONIC IRRADIATION PROCESS Sartaj M., Tobalt A., and Kennedy K.	521
3729	THE IMPLEMENTATION OF WATER SENSITIVE CITY AT DEPOK -MIDDLE CITY IN INDONESIA Firdaus Ali, Irene Sondang, Esty Suyanti and Ahmad Zubair	524
3730	RISK MAPPING STUDIES OF HYDRO-METEOROLOGICAL HAZARD IN DEPOK MIDDLE CITY R. Jachrizal Soemabrata, Ahmad Zubair, Irene Sondang and Esty Suyanti	528
3698	ROLE OF GOVERNMENT AND PRIVATE SECTOR IN MARINE ECOTOURISM RELATED TO CONSERVATION OF BIODIVERSITY IN SERIBU ISLANDS Lily Surayya Eka Putri and Kristiyanto	534
3689	SEISMIC MICROZONATION FOR URBAN PLANNING AND VULNERABILITY ASSESSMENT OF NON-ENGINEERED STRUTURE IN EARTHQUAKE PRONE AREA, PADANG, INDONESIA Rusnardi Rahmat Putra, Junji Kiyono, Ganefri Fahmi Rijal and Syahril	540
3545	RAINWATER HARVESTING STUDY AT MASJID JAMEK RIYAHDUS SOLIHIN, PINTAS PUDING, BATU PAHAT JOHOR MALAYSIA Amir Hashim Mohd Kassim, Siti Mariam Sulaiman, Radin Maya Saphira Radin Mohamed and Adel Ali Saeed Al Gheethi	549

Authors Index



## Preface

On behalf of the SEE 2017 Organizing Committee, it is our great pleasure to welcome you to the Third International Conference on Science, Engineering & Environment, held at the USQ Springfield Brisbane Australia organized in conjunction with University of Southern Queensland, Mie University Research Center for Environmental Load Reduction, The GEOMATE International Society, Useful Plant Spread Society, Glorious International, AOI Engineering, HOJUN, JCK, CosmoWinds and Beppu Construction, Japan.

The conference covers three major themes with many specific themes including:

Engineering	Science	Environment
<ul style="list-style-type: none"> <li>· Environmental Engineering</li> <li>· Chemical Engineering</li> <li>· Civil and Structural Engineering</li> <li>· Computer Software Web Engineering</li> <li>· Electrical and Electronic Engineering</li> <li>· Energy and Thermal Engineering</li> <li>· Aerospace Engineering</li> <li>· Agricultural Engineering</li> <li>· Biological Engineering and Sciences</li> <li>· Biological Systems Engineering</li> <li>· Biomedical and Genetic Engineering</li> <li>· Bioprocess and Food Engineering</li> <li>· Geotechnical Engineering</li> <li>· Industrial and Process Engineering</li> <li>· Manufacturing Engineering</li> <li>· Mechanical and Vehicle Engineering</li> <li>· Materials and Nano Engineering</li> <li>· Nuclear Engineering</li> <li>· Petroleum and Power Engineering</li> <li>· Forest Industry Engineering</li> </ul>	<ul style="list-style-type: none"> <li>· Environmental Sciences</li> <li>· Chemistry and Chemical Sciences</li> <li>· Fisheries and Aquaculture Sciences</li> <li>· Astronomy and Space Sciences</li> <li>· Atmospheric Sciences</li> <li>· Botany and Biological Sciences</li> <li>· Genetics and Bacteriology</li> <li>· Forestry Sciences</li> <li>· Geological Sciences</li> <li>· Materials Science and Mineralogy</li> <li>· Statistics and Mathematics</li> <li>· Microbiology and Medical Sciences</li> <li>· Meteorology and Palaeo Ecology</li> <li>· Pharmacology</li> <li>· Physics and Physical Sciences</li> <li>· Plant Sciences and Systems Biology</li> <li>· Psychology and Systems Biology</li> <li>· Zoology and Veterinary Sciences</li> </ul>	<ul style="list-style-type: none"> <li>· Environmental Technology</li> <li>· Recycle Solid Wastes</li> <li>· Environmental dynamics</li> <li>· Meteorology and Hydrology</li> <li>· Atmospheric and Geophysics</li> <li>· Physical oceanography</li> <li>· Bio-engineering</li> <li>· Environmental sustainability</li> <li>· Resource management</li> <li>· Modelling and decision support tools</li> <li>· Institutional development</li> <li>· Suspended and biological processes</li> <li>· Anaerobic and Process modelling</li> <li>· Modelling and numerical prediction</li> <li>· Interaction between pollutants</li> <li>· Water treatment residuals</li> <li>· Quality of drinking water</li> <li>· Distribution systems on potable water</li> <li>· Reuse of reclaimed waters</li> </ul>

This year we have received many submissions over 50 universities of different countries all over the world including Australia, Brazil, Canada, Czech Republic, Fiji, India, Indonesia, Iraq, Japan, Malaysia, Philippines Romania, Russia, South Korea, Sri Lanka and Thailand. The technical papers were selected from the vast number of contributions submitted after a review of the abstracts. The final papers in the proceedings have been peer reviewed rigorously and revised as necessary by the authors. It relies on the solid cooperation of numerous people to organize a conference of this size. Hence, we appreciate everyone who support as well as participate in the joint conferences.

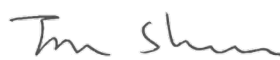
Last but not least, we would like to express our gratitude to all the authors, session chairs, reviewers, participants, institutions and companies for their contribution to SEE 2017. We hope you enjoy the conference and find this experience inspiring and helpful in your professional field. We look forward to seeing you at our upcoming conference next year.

Best regards,

Prof. Dr. Zakaria Hossain, Conference Chairman (General)



Dr. Jim Shiau, Conference Chairman (Program)



## Organization

*Third International Conference on Science, Engineering & Environment,  
USQ Springfield Brisbane, Australia, Nov.13-15, 2017, ISBN: 978-4-9905958-9-0*

### *Scientific Committees:*

#### Conference Honorary Chairmen:

Dr. John Yeaman, Professor, Univ. of the S/Coast, Australia

Dr. Sohji Inoue, Emeritus Professor, Mie University, Japan

#### Conference Chairmen:

Dr. Jim Shiau, Senior Lecturer, USQ, Australia (Program Chair)

Dr. Zakaria Hossain, Prof. Mie Univ., Japan (General Chair)

#### Conference Organizing Committee:

Dr. Jim Shiau, S./Lec. Univ. of Southern Queensland, Australia

Dr. Stephen Buttlings, Principal, National Geo. Cons., Australia

Dr. Karu Karunasena, Prof. USQ, Australia

Dr. David Thorpe, A/Prof., USQ, Australia

Dr. Toshinori Sakai, Prof. Mie University, Japan

Dr. Zakaria Hossain, Prof. Mie University, Japan

#### National & International Advisory Committee:

Dr. Allan Manalo, Senior Lecturer, USQ, Australia

Dr. Soma Somasundaraswaran, Lecturer, USQ, Australia

Dr. John Smith, A/Prof. RMIT University, Australia

Dr. Arul Arulrajah, Prof. Swinburne Univ. of Tech., Australia

Dr. Robert Evans, A/Prof., Swinburne Univ. of Tech., Australia

Dr. Chaminda Gallage, A/Prof, Queensland Uni. of Tec, Australia

Dr. Iyad Alkroosh, A/Prof., Curtin University, Australia

Dr. Sammy Kwok, Geo. Eng. Cardno Bowler, Australia

Dr. Jun Sugawara, S/Eng. Golder Associates Pty Ltd, Australia

Dr. N. Sivakugan, A/Prof. James Cook Univ., Australia

Dr. Erwin Oh, Senior Lecturer, Griffith University, Australia

Dr. Fumio Tatsuoka, Prof. Tokyo University of Science, Japan

Dr. Jing-Cai Jiang, Prof. University of Tokushima, Japan

Dr. Toshihiro Morii, Prof. Niigata University, Japan

Dr. Kimitoshi Hayano, Prof. Yokohama National Univ., Japan

Dr. Sai Vanapalli, Prof. University of Ottawa, Canada

Dr. Musharraf Zaman, Prof. Univ. of Oklahoma, USA

Dr. Rafiqul Tarefder, Prof. University of New Mexico, USA

Dr. M. Bouassida, Prof. National Sch. of Engg. of Tunis

Dr. L.R. Austriaco, Prof. Angeles Univ. Found., Philippines

Dr. A.S.M. Abdul Awal, Prof., UTHM, Malaysia

Dr. Bujang B.K. Huat, Prof. Univ. Putra Malaysia

Dr. Nemy Banthia, Prof. UBC, Canada

Dr. Ian Jefferson, Prof. Univ. of Birmingham, UK

Dr. John Bolander, Prof. Univ. of California, USA

Dr. Shamsul Chowdhury, Prof. Roosevelt Univ., USA

Dr. Isabel Pinto, Prof. University of Coimbra, Portugal

Dr. Hj. Ramli Bin Hj. Nazir, A/Prof.. UTM, Malaysia

Dr. Aly Ahmed, A/Prof.. Beni-Suef University, Egypt

Dr. Chang-Yu Ou, Prof. National Taiwan Univ. of Sci. &Tech.

### *International Technical Program Committee:*

Prof. Adolf Heinrich Horn, Geological Institute - Federa University of Minas Gerais, Brazil

Prof. Bang-Fuh Chen, National Sun Yat-sen University, Taiwan

Prof. Bindeshwar Singh, Kamla Nehru Institute of Technology, India

Prof. Catherine Mulligan, Concordia Institute of Water, Energy and Sustainable Systems, Canada  
 Prof. Chi-Min Liu Chienkuo Technology University, Taiwan  
 Prof. Daffalla Rabih, Kenana Sugar Company, Sudan  
 Prof. Essaid Bilal, Ecole Nationale Supérieure Des Mines De Saint Etienne, France  
 Prof. Hakan Caliskan, Usak University, Faculty of Engineering, Turkey  
 Prof. Ibrahim Maiyza, National Institute of Oceanography & Fisheries, Egypt  
 Prof. Loc Nguyen, Sunflower Soft Company, Vietnam  
 Prof. Marilia Hagen, Indiana University, United States  
 Prof. Md Najib bin Ibrahim, Universiti Teknologi MARA, Malaysia  
 Prof. Md. Abdul Baset Mia, BSMR Agri. Univ., Bangladesh  
 Prof. Mihaela Popescu, University of Craiova, Romania  
 Prof. Mohamed Abdou, Faculty of Education Department of Mathematics, Egypt  
 Prof. Mohamed Tahiri, Présidnce de l'Université Hassan II de Casablanca, Morocco  
 Prof. Nazar Oukaili, University of Baghdad, Iraq  
 Prof. Radim Cajka, Technical University Ostrava, Faculty of Civil Engineering, Czech Republic  
 Prof. Rajaraman Jambunathan, AMET University, India  
 Prof. Saad Farhan Ibrahim Alabdullah, University of Almustansiriyah, Iraq  
 Prof. Salem Alsanusi, Benghazi, Libya  
 Prof. Sudhir Kumar Das, Retired Senior Project Manager of Indian Railways, India  
 Prof. Zachary Senwo, Alabama A&M University, United States  
 Prof. Imed Jabri, University of Tunis, Tunisia  
 A/Prof. Bindeshwar Singh Kamla Nehru Institute of Technology, India  
 A/Prof. Hasi Rani Barai, Yeungnam University, South Korea  
 A/Prof. Jamaluddin Mahmud, Universiti Teknologi MARA, Malaysia  
 A/Prof. Mohamed Ramadan, University of Hail, Saudi Arabia  
 A/Prof. Najam Hasan, Dhofar University, Oman  
 A/Prof. Nosina Krishna Chaitanya, Jawaharlal Nehru Technological University, India  
 A/Prof. Nurbek Saparkhojayev, Almaty Management University, Kazakhstan  
 A/Prof. Pandian Vasant, Universiti Teknologi Petronas, Malaysia  
 A/Prof. Teodor Lucian Grigorie, University of Craiova, Romania  
 A/Prof. Zawawi Daud, Universiti Tun Hussein Onn Malaysia  
 A/Prof. Abdull Halim Abdul, Oil and Gas department, Malaysia  
 A/Prof. Baoping Cai, China University of Petroleum, China  
 A/Prof. Dariusz Jakóbczak, Koszalin University of Technology, Poland  
 A/Prof. Edgar Allan Mendoza, University of the Philippines  
 A/Prof. Lakhveer Singh, Universiti Malaysia Pahang (UMP) Malaysia, Malaysia  
 A/Prof. Lidia Sas Paszt, Research Institute of Pomology, Poland  
 A/Prof. Mahmood Barbooti, University of Yechology, Iraq  
 A/Prof. Majid Mirzaei, Universiti Tunku Abdul Rahman, Malaysia  
 A/Prof. Najeh Lakhoua, University of Carthage, Tunisia  
 A/Prof. Ryan Joseph Calinao, Lyceum of the Philippines University-Laguna  
 A/Prof. Sarawut Thepanondh, Mahidol University, Thailand  
 A/Prof. Yasir Al Hussein, Jerash University, Faculty of Engineering, Jordan  
 A/Prof. Grigorie Teodor Lucian, University of Craiova, Romania  
 A/Prof. Hêriş Golpîra, Islamic Azad University, Sanandaj, Iran  
 A/Prof. Muhammad Aslam, King Abdulaziz University, Saudi Arabia  
 A/Prof. Tomasz Plech, Medical University of Lublin, Poland  
 A/Prof. Fellah Mamoun, Abbes laghrour University, Algeria  
 A/Prof. R. S. Ajin, GeoVin Solutions Pvt. Ltd., India  
 A/Prof. Roman Szewczyk, Industrial Research Institute for Automation and Measurements, Poland  
 Dr. Abolghasem Akbari, University Malaysia Pahang, Malaysia  
 Dr. Ahmad Safuan A Rashid, Universiti Teknologi Malaysia, Malaysia  
 Dr. Akinola Johnson Olarewaju, Federal Polytechnic Ilaro, Ogun State, Nigeria  
 Dr. Alexandre Costa, Federal University of the valleys of Jequitinhonha and Mucuri, Brazil  
 Dr. Angelo Gallone, Scotland's Rural College (SRUC), United Kingdom  
 Dr. Azizul Azhar Ramli, Universiti Tun Hussein Onn Malaysia  
 Dr. Bashir Dar, University of kashmir Delina Baramulla J&K India, India  
 Dr. Bassam Abdellatif, National Authority for Remote Sensing and Space Sciences, Egypt



Dr. Binh Phu Nguyen, National University of Singapore, Singapore  
 Dr. Cazacu Gabriela, S.C. Geotech Dobrogea, Romania  
 Dr. Chengen Yang, Intel Corporation, United States  
 Dr. Dayang Norulfairuz Abang Zaidel, Universiti Teknologi Malaysia  
 Dr. Evgeni Starikov, KIT, Karlsruhe, Germany; Chalmers, Gothenburg Sweden, Germany  
 Dr. Fatma Khanchel, University of Tunis El Manar, Tunisia  
 Dr. Hamidreza Khataee, Griffith University, Australia  
 Dr. Hêriş Golpîra, Islamic Azad University, Iran  
 Dr. Iskhaq Iskandar, Dept. Physics, University of Sriwijaya, Indonesia  
 Dr. Jingwei Zhao, University of Wollongong, Australia  
 Dr. Jitendra Agrawal, Rajiv Gandhi Proudhyogiki Vishwavidyalaya, India  
 Dr. Liza Patacsil, Malayan Colleges Laguna, Philippines  
 Dr. Mohamed Amine, Ferrag Guelma University, Algeria  
 Dr. Mohd Afendi Rojan, Universiti Malaysia Perlis, Malaysia  
 Dr. Mohd Altaf, University of Kashmir Delina Baramulla J&K India, India  
 Dr. Mohd Hairy Ibrahim, Sultan Idris Education University, Malaysia  
 Dr. Mostafa Khater, Egypt - El shargia - Zagazig, Egypt  
 Dr. Najam Hasan, Dhofar University, Oman  
 Dr. Namir Alkawaaz, University of Almustansiriyah, Iraq  
 Dr. Nashrul Fazli Mohd Nasir, Universiti Malaysia Perlis, Malaysia  
 Dr. Naufal Mansor Kampus Uniciti Alam, Universiti Malaysia Perlis (UniMAP), Malaysia  
 Dr. Obed Majeed Ali, Northern Technical University, Iraq  
 Dr. Piyapong Janmaimool, King Mongkut' University of Technology, Thailand  
 Dr. Po-Sheng Chiu, National Cheng Kung University, Taiwan  
 Dr. Prabu Mohandas, Adhiyamaan College of Engineering, India  
 Dr. Raman Kumar, D A V Institute of Engineering and Technology, India  
 Dr. Riccardo Colella, University of Salento, Italy  
 Dr. Rolando Javellonar, Romblon State University, Philippines  
 Dr. Shikha Agrawal, Rajeev Gandhi Technical University, India  
 Dr. Stefania Tomasiello CORISA, University of Salerno, Italy  
 Dr. Sumiyyah Sabar, Universiti Sains Malaysia, Malaysia  
 Dr. Suphaphat Kwonpongsagoon, Mahidol University, Thailand  
 Dr. Wei Hong Tan, Universiti Malaysia Perlis, Malaysia  
 Dr. Yoshiro Fujii, Shin Kobe Dental Clinic, Japan  
 Dr. Yuk Feng Huang, Universiti Tunku Abdul Rahman (UTAR), Malaysia  
 Dr. Zongyan Zhou, Monash University, Australia  
 Dr. Purnanand Savoikar, Goa Engineering College, India  
 Dr. Ahmed Toaha Mobashsher, University of Queensland, Australia  
 Dr. Chupong Pakpum, Maejo University  
 Dr. Emanuele Quaranta, Politecnico di Torino, Italy  
 Dr. Jiangling Yin, Apple Inc., Cupertino, CA, United States  
 Dr. Khor Shing Fhan, Universiti Malaysia Perlis, Malaysia  
 Dr. Mario Chauca, Ricardo Palma University, Peru  
 Dr. Santosh Gaikwad, Model College, Ghansawangi, India  
 Dr. Tse Guan Tan, Universiti Malaysia Kelantan  
 Dr. Vikas Panthi, National Institute of Technology, India  
 Dr. Watoo Phrompittayarat, Naresuan University, Thailand  
 Dr. Hamidreza Namazi, Nanyang Technological University, Singapore  
 Dr. Parichat Phumkhachorn, Ubon Ratchathani University, Thailand  
 Dr. Subhasis Roy, University of Calcutta, India

*Conference Correspondence:*

Dr. Jim Shiau, Senior Lecturer, USQ, Australia, Program Chair  
 Dr. Zakaria Hossain, General Chair,  
 Prof. Graduate School of Bioresources,  
 Mie University 1577 Kurima Machiya-cho, Tsu-city,

Mie 514-8507 Japan, E-mail: editor@geomate.org  
Tel & Fax: +81-59-231-9578

*Conference History:*

SEE-Mie, Japan, Nov. 19-21, 2015  
Chairman: Prof. Dr. Satoshi Kaneco, Mie University, Japan  
SEE-Osaka, Japan, Nov. 21-23, 2016  
Chairman: Prof. Dr. Zakaria Hossain, Mie University, Japan

*Editorial and Executive Committee:*

Prof. Dr. Zakaria Hossain  
Dr. Jim Shiau  
Ms. Siti Hanggita Rachmawati  
Mr. Md. Aminul Islam  
Mr. Alex Otieno Owino

Note- A: Associate, E-Emeritus

***Keynote Papers***

# **MECHANICS OF GEOSYNTHETICS SUBJECTED TO CHEMICAL EXPOSURE: EXPERIMENTS, CONSTITUTIVE MODELS AND COMPUTATIONS**

A.P.S. Selvadurai

Department of Civil Engineering and Applied Mechanics  
McGill University, Canada.

## **ABSTRACT**

This article is a review of recent research related to the development of advanced mathematical models for describing the behaviour of strain rate sensitive materials such as geosynthetics that are used extensively as barriers to the migration of contaminants and other hazardous materials. The important finding of the research is that the leaching of the plasticizer from the geosynthetic can lead to a loss of hyperelasticity of the material, which is a key functional requirement for a geosynthetic. It is also shown that constitutive models can be developed to describe the mechanical behaviour of the geosynthetic in its virgin state and upon direct exposure to pure ethanol for thirteen months. The mathematical models developed using results of uniaxial tests can be incorporated in a general purpose finite element code. This computational approach is used to evaluate the results of separate laboratory experiments involving transverse indentation of geosynthetic membranes that are fixed along a circular boundary and tested in either its untreated state or after prolonged exposure to ethanol. The computational predictions compare very accurately with experimental results in the loading mode of both treated and untreated geosynthetics. The irreversible deformations of the geosynthetic subjected to transverse loading is satisfactory and can be further improved by re-examining the rate-sensitive plasticity model used in the modelling.

*Keywords: Geosynthetics, Chemical exposure, Loss of elasticity properties; Embrittlement, Computational modelling, Rate-sensitive materials, Indentation tests for membranes*

## **INTRODUCTION**

Polyvinyl chloride (PVC) membranes, also referred to as geosynthetics or geomembranes, are used quite extensively in geoenvironmental endeavours in order to prevent groundwater contamination due to leakage of leachates from landfill and from hazardous waste sites such as mine tailings ponds. PVC membranes constitute an important component of multi-barrier containment systems that also consist of alternate layers of impermeable clay and collection systems. Geosynthetic membranes used as landfill liners can be exposed to adverse environments, including heat, ultra-violet light (prior to commissioning of a landfill site), bacteria and chemicals [1]. Although geosynthetics are widely used in geoenvironmental engineering practice, the assessment of the long term effectiveness of these materials under exposure to chemicals, ultra-violet light, radiation, etc., still needs concerted attention. The chemical properties and other details of the untreated PVC material are given in [1].

A primary requirement of a geosynthetic relates to its ability to undergo large deformations and to maintain its integrity, thereby impeding the migration of hazardous chemicals and contaminants to the environment. Experiments conducted in connection with this research indicate that the

interaction of the geosynthetic with chemicals such as acetone and ethanol leads to the loss of plasticizers that contribute to the *hyperelasticity* of the material. The flexibility of a geosynthetic is derived largely from plasticizers incorporated into its chemical composition. Recent research has shown that the exposure of the geosynthetic membranes to chemicals such as *acetone* and *ethanol* can lead to *embrittlement* of the membrane through the leaching of the plasticizer. The longevity of the containment provided by PVC geosynthetics can be influenced by these factors, specifically in situations involving the thermal desiccation of clay. Desiccation cracking can be caused by moisture depletion in the clay barrier following exothermic processes associated with the decay of organic matter in the landfill. A cracked clay barrier provides a pathway for contaminants to come into direct contact with a geosynthetic barrier. The direct exposure of the plasticized PVC membrane to chemical action is a problem of major concern. The exposure of the PVC to chemicals can result in mechanical alterations in the material, largely as a result of leaching of the plasticizer, which contributes to the flexibility of the PVC [2]. Exposure to commonly occurring chemicals such as acetone and ethanol can lead to a loss of hyperelasticity in the geosynthetics [3,4].

Uniaxial experiments (Figure 1) conducted in connection with this research also show an alteration

in the mechanical properties of a PVC membranes during exposure to pure ethanol. These alterations include a progressive loss of large strain flexibility, embrittlement, the development of a distinct initial linear elastic modulus and the development of a yield point (Figure 2). The initial linear elastic modulus and the yield stress of the material continuously increase over an exposure period of 2 months after which there is a slight decrease in the peak yield value, which remains unaltered during further exposure.

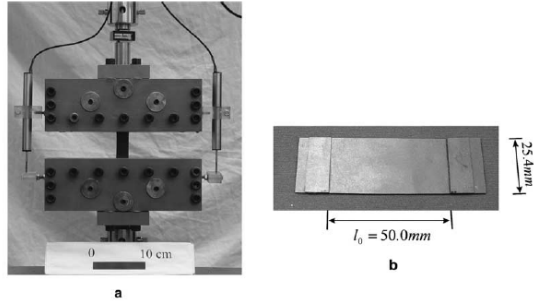


Fig. 1 Uniaxial testing of specimens of PVC membranes

The rapid alteration in the mechanical properties of the geosynthetic membrane in the first two months correlates well with the X-Ray fluorescence evidence, which also indicates a loss of plasticizer during this period. The plasticizer content is identified through the weight ratio  $R_{O/Cl}$  of the oxygen element and chloride element in the geosynthetic specimen that has been originally plasticized with 25-35% weight content of a phthalate plasticizer. The loss of plasticizer after a two-month exposure to pure ethanol leads to (i) a reduction in the flexibility of the geosynthetic, (ii) an increase in the failure stress and (iii) the development of a strain-hardening regime in the stress-strain response (Figure 2).

For PVC geosynthetics that have been exposed to ethanol for a period of 13 months, the stress-strain behaviour of the specimen exhibits a mechanical response similar to a PVC material containing a very low content of DOP (Diethyl phthalate) plasticizer (less than 15%) [2]. With significant loss of plasticizer from the specimen, the PVC geosynthetic subjected to a 13-month chemical exposure shows only moderate deformability with a failure strain of about 20%. For a specimen that is loaded at a lower strain-rate (e.g.  $0.05 \text{ min}^{-1}$ ), however, the large strain deformability of a PVC material with a low content of plasticizer can be recovered [5]. The results of the computational simulations are compared with the experimental results. We observe that the constitutive models that use a basic hyperelastic constitutive relationship of the Mooney-Rivlin form, where the parameters are strain rate- and chemical exposure-dependent, provides a

convenient model for the examination of the constitutive behaviour of a geosynthetic both in its untreated state and after prolonged exposure to ethanol.

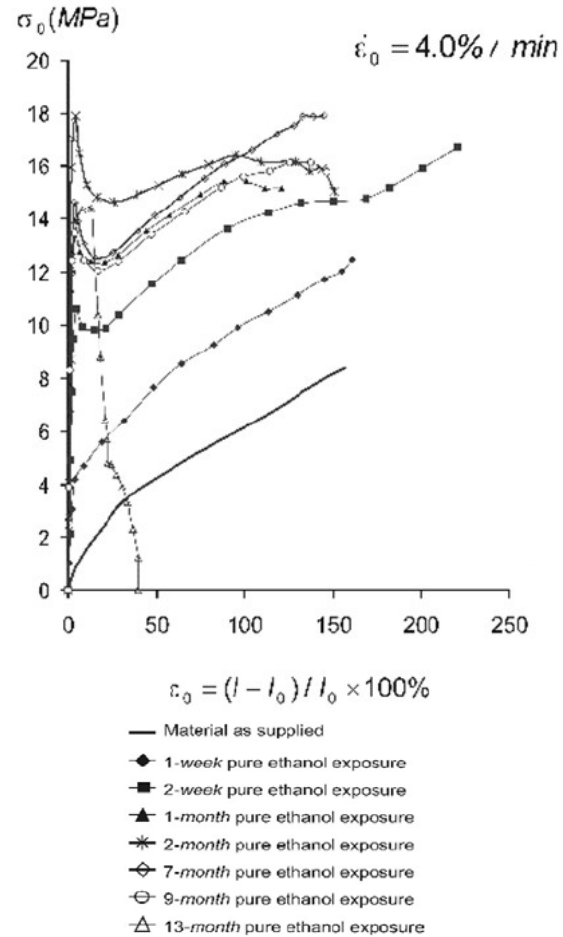


Fig. 2 Behaviour of PVC specimens during exposure to pure ethanol.

## CONSTITUTIVE MODELLING

Purely hyperelastic rubber-like materials exhibit virtually no irreversible phenomena in terms of permanent deformations and energy dissipation during quasi-static load cycling [6-11]. In contrast, glassy polymeric materials exhibit appreciable irreversible effects including development of permanent strains during loading-unloading cycles and strain-rate effects [12]. The constitutive modelling of such materials can be approached at a variety of levels ranging from elementary power law creep models to generalized continuum models applicable to non-linear viscoelastic materials. This paper presents constitutive models that first describe the hyperelastic behaviour of a geosynthetic material in its as supplied condition. The modelling accounts for both reversible and irreversible components of hyperelastic behaviour and incorporates strain rate dependency in the

constitutive response. The constitutive modelling is then extended to include the loss of hyperelasticity as a result of exposure to pure ethanol. The constitutive parameters were determined from uniaxial tests and constrained tests conducted at different strain rates. The constitutive models were implemented in a general purpose finite element code to examine the mechanics of a membrane fixed along a circular boundary and loaded by a hemispherical indenter. chemical action on these materials is to leach out the plasticizer that provides large strain capability without initiation of fracture and/or damage. This paper presents the results of experiments conducted on PVC in its as supplied state and subjected to chemical treatment, in order to determine the constitutive relationships that govern hyperelastic behaviour as well as loss of hyperelasticity during chemical action (Selvadurai and Yu [13-15]; Yu and Selvadurai [1,16]). The constitutive models developed, take into consideration strain-rate sensitivity and large strain effects in the *untreated material* and distinct yield and strain-rate sensitivity in the *chemically treated material*. The modelling uses forms of constitutive potentials that are derived from hyperelastic rubberlike materials undergoing moderately large strains. We consider the deformation such that the position of a generic particle in the deformed configuration is denoted by  $x_i$  ( $i=1,2,3$ ) and the coordinates of the same particle in the reference configuration are denoted by  $X_A$  ( $A=1,2,3$ ). Restricting attention to an incompressible materials (for which  $\det \mathbf{F}=1$ ), the deformation gradient tensor is given by

$$\mathbf{F} = \left\| \partial x_i / \partial X_A \right\| \quad (1)$$

As suggested by Lee [17] and others, the total deformation gradient tensor  $\mathbf{F}$  can be decomposed into its elastic ( $e$ ) and irreversible ( $u$ ) components, i.e.

$$\mathbf{F} = \mathbf{F}^e \mathbf{F}^u \quad (2)$$

Strain tensors in terms of  $\mathbf{B}^e$  and  $\mathbf{B}^u$  are defined by

$$\mathbf{B}^e = \mathbf{F}^e (\mathbf{F}^e)^T ; \quad \mathbf{B}^u = \mathbf{F}^u (\mathbf{F}^u)^T \quad (3)$$

and the strain-rate is defined (Spencer, [18]) by

$$\begin{aligned} \mathbf{L} &= \dot{\mathbf{F}} \mathbf{F}^{-1} = \mathbf{D} + \mathbf{W} = \dot{\mathbf{F}}^e (\mathbf{F}^e)^{-1} + \mathbf{F}^e [\dot{\mathbf{F}}^u (\mathbf{F}^u)^{-1}] (\mathbf{F}^e)^{-1} \\ \mathbf{L}^u &= \dot{\mathbf{F}}^u (\mathbf{F}^u)^{-1} ; \quad \mathbf{D}^u = \frac{1}{2} [\mathbf{L}^u + (\mathbf{L}^u)^T] \end{aligned} \quad (4)$$

The invariants of  $\mathbf{B}^e$ ,  $\mathbf{B}^u$  are

$$\begin{aligned} I_1^h &= (\lambda_1^h)^2 + (\lambda_2^h)^2 + (\lambda_3^h)^2 \\ I_2^h &= \frac{1}{(\lambda_1^h)^2} + \frac{1}{(\lambda_2^h)^2} + \frac{1}{(\lambda_3^h)^2} \\ I_3^h &= \lambda_1^h \lambda_2^h \lambda_3^h = 1 ; (h=e,u) \end{aligned} \quad (5)$$

and  $\lambda_i^e$  and  $\lambda_i^u$  ( $i=1,2,3$ ) are, respectively, the principal stretches of the elastic and irreversible components. In this research, the general constitutive model for both the *untreated* and *chemically treated* PVC has been selected to conform to a single generic form (Figure 3). The large elastic deformation can be modelled through the introduction of a strain energy function  $W^e$  (component  $C$ ) of a modified Mooney-Rivlin form, which is considered to be a satisfactory form of a strain energy function for hyperelastic materials that experience moderately large strains [17-26]. The irreversible deformation can be characterized by a visco-plastic model, which can be visualized as consisting of an elastic component  $A$  of the finite strain contributing to the elastic recovery, in parallel with a visco-plastic component  $B$  that accounts for the rate-dependent effects during unloading. The finite strain component  $A$ , which is similar to component  $C$ , can be characterized by a strain energy function  $W^u$  of the Mooney-Rivlin form.

The component  $C$  is sufficient to characterize the constitutive behaviour of an *untreated* material during *monotonic loading without unloading* or a *chemically treated* material experiencing strains prior to the yield point. In this case, there are no irreversible effects and the total deformation gradient  $\mathbf{F}$  is the same as the elastic deformation gradient  $\mathbf{F}^e$ .

The stress  $\mathbf{T}_C$  associated with the component  $C$ , which is the total Cauchy stress  $\mathbf{T}$  of the *untreated* or *chemically treated* material, is an isotropic function of elastic strain tensor  $\mathbf{B}^e$  and takes the form

$$\begin{aligned} \mathbf{T} = \mathbf{T}_C &= -\tilde{p}^e \mathbf{I} + \psi_1^e \mathbf{B}^e + \psi_2^e (\mathbf{B}^e)^2 \\ \psi_1^e &= 2 \left( \frac{\partial W^e}{\partial I_1^e} + I_1^e \frac{\partial W^e}{\partial I_2^e} \right) ; \quad \psi_2^e = -2 \frac{\partial W^e}{\partial I_2^e} \end{aligned} \quad (6)$$

where  $\tilde{p}^e$  is a scalar pressure. Following the approach proposed by Sweeny and Ward [12] to account for the influence of the strain rate on the strain energy function, we adopt the following type of strain energy function for the *untreated* material:

$$W^e(I_1^e, I_2^e) = C_1'(I_1^e - 3) + C_2'(I_2^e - 3)$$

(7)

where

$$C_1' = C_1 + \begin{cases} \kappa_1 \ln(|\dot{\gamma}_0|/\dot{\gamma}_c); & (|\dot{\gamma}_0| \geq \dot{\gamma}_c) \\ 0 & ; \quad (|\dot{\gamma}_0| < \dot{\gamma}_c) \end{cases}$$

$$C_2' = C_2 + \begin{cases} \kappa_2 \ln(|\dot{\gamma}_0|/\dot{\gamma}_c); & (|\dot{\gamma}_0| \geq \dot{\gamma}_c) \\ 0 & ; \quad (|\dot{\gamma}_0| < \dot{\gamma}_c) \end{cases} \quad (8)$$

Rate-dependent elastic constitutive component C

$$W^e = C_1'(\dot{\gamma}_0)(I_1^e - 3) + C_2'(\dot{\gamma}_0)(I_2^e - 3)$$

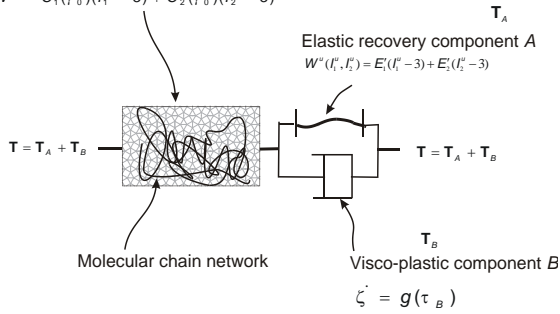


Fig. 3 Schematic representation of the constitutive components

In (8),  $\dot{\gamma}_0$  is a generalized form of a combined stretch-rate that depends only on the in-plane principal stretches  $\lambda_i$  ( $i = 1, 2$ ), such that

$$\dot{\gamma}_0 = \frac{d\gamma_0}{dt} \quad ; \quad \gamma_0 = [(\bar{\lambda}_1 - 1)^\alpha + (\bar{\lambda}_2 - 1)^\alpha]^{1/\alpha} \quad (9)$$

where,  $\bar{\lambda}_i$  have a conditional dependence on the total principal stretches  $\lambda_i$  to take into consideration either the stretching or the unloading response: i.e.

$$\bar{\lambda}_i = \begin{cases} \lambda_i & ; \quad (\lambda_i \geq 1) & ; \quad i = (1, 2) \\ 1 & ; \quad (\lambda_i < 1) & ; \quad i = (1, 2) \end{cases} \quad (10)$$

and  $\alpha$  is a *material (combination) parameter*. When the geosynthetic specimen is subjected to a uniaxial stretch, the principal stretches in the other direction are less than unity and therefore the definition of  $\gamma_0$  reduces to that of the uniaxial strain  $\varepsilon_0$ . In (8),  $C_1'$  and  $C_2'$  are the modified Mooney-Rivlin parameters,  $\kappa_1$  and  $\kappa_2$  are parameters that define the strain-rate sensitivity and  $\dot{\gamma}_c$  is defined as the *rate-independent threshold strain-rate*. At loading rates  $|\dot{\gamma}_0| \leq \dot{\gamma}_c$ , the strain-

rate effects are disregarded. For a chemically treated material, a classical Hookean isotropic incompressible elastic model, without the consideration of large strain effects, can adequately describe its initial elastic behaviour prior to the yield point. To conform to the description of the model for the *untreated* material, we adopt a neo-Hookean form of the strain energy function, which can be derived from a Mooney-Rivlin form of strain energy function (7) with  $C_2'$  independent of the strain-rate and always equal to zero, i.e.,  $C_2' = 0$ . When examining the *untreated* material during unloading or the *chemically treated* material experiencing strains beyond the yield point, permanent strains ensue. Therefore, the additional visco-plastic model characterized by an elastic recovery component A in parallel to a visco-plastic component B should be added in series to the component C. The component A is described by a further conventional finite strain approach with a strain energy function  $W^u$  of a Mooney-Rivlin form:

$$\mathbf{T}_A = -\tilde{p}^u \mathbf{I} + \psi_1^u \mathbf{B}^u + \psi_2^u (\mathbf{B}^u)^2$$

$$\psi_1^u = 2 \left( \frac{\partial W^u}{\partial I_1^u} + I_1^u \frac{\partial W^u}{\partial I_2^u} \right); \quad \psi_2^u = -2 \frac{\partial W^u}{\partial I_2^u} \quad (11)$$

where  $\tilde{p}^u$  is a scalar pressure and

$$W^u(I_1^u, I_2^u) = E_1'(I_1^u - 3) + E_2'(I_2^u - 3) \quad (12)$$

In (12),  $E_1'$  has the conditional constraint for an *untreated* material: i.e.

$$E_1' = \begin{cases} \rightarrow \infty & ; \quad (\dot{\gamma}_0 \geq -\dot{\gamma}_c^v) \\ 0 & ; \quad (\dot{\gamma}_0 < -\dot{\gamma}_c^v) \end{cases} \quad (13)$$

and  $E_2'$  is a constant. The choice of  $E_1'$  in (13) is intended to take into account the non-symmetric behaviour of the elastic recovery component A during the loading-unloading response, where, at the loading stage,  $\dot{\gamma}_0 \geq 0$ , and at the extremely low loading rate  $|\dot{\gamma}_0| \leq \dot{\gamma}_c^v$  (where  $\dot{\gamma}_c^v$  is *viscous threshold strain-rate*). The visco-plastic deformation that applies to components A and B is restricted due to the choice of an infinite value for  $E_1'$ . As a result, only the elastic deformation of component C is applicable for the *untreated* material. Upon unloading, however, the visco-plastic deformation is fully released due to the zero value of  $E_1'$  chosen in (13). All three components A, B and C take effect during the unloading of the *untreated* material. For a *chemically treated* specimen,  $E_1'$  must also take



into consideration the yield of the material and has the form

$$\begin{aligned} E'_1 &\rightarrow \infty \quad ; \quad \dot{\gamma}_0 \geq -\dot{\gamma}_c^v \quad \text{and} \quad \gamma_0 \leq \zeta_y \\ E'_1 &= E'_y \quad ; \quad \dot{\gamma}_0 \geq -\dot{\gamma}_c^v \quad \text{and} \quad \gamma_0 > \zeta_y \quad (14) \\ E'_1 &= 0 \quad ; \quad \dot{\gamma}_0 < -\dot{\gamma}_c^v \end{aligned}$$

where  $\zeta_y$  is the yield strain and  $E'_y$  is the post-yield *hardening modulus*. Prior to the yield point, the visco-plastic deformation is restricted; beyond the yield point, however, the visco-plastic deformation is released due to the finite value of  $E'_y$ . This leads to the deviation of the material behaviour from an initial linear elastic behaviour to a softening behaviour followed by hardening behaviour at larger strains. The possibility of rate-dependency of the *hardening modulus*  $E'_y$  is also considered; i.e.

$$E'_y = E_y + \begin{cases} \kappa_y \ln(|\dot{\gamma}_0|/\dot{\gamma}_c^v) & ; \quad (|\dot{\gamma}_0| \geq \dot{\gamma}_c^v) \\ 0 & ; \quad (|\dot{\gamma}_0| < \dot{\gamma}_c^v) \end{cases} \quad (15)$$

where  $\kappa_y$  is the rate sensitivity,  $E_y$  is the *rate-independent hardening modulus*, and, at  $|\dot{\gamma}_0| \leq \dot{\gamma}_c^v$ , the viscous effect is omitted.

The stress  $\mathbf{T}_B$  in component  $B$  is defined in terms of the finite plastic strain-rate  $\mathbf{D}^u$ , which is assumed to be related to the deviatoric component of the normalized effective stress tensor  $\mathbf{N}_B$ . In the component  $B$ , the visco-plastic effects are modelled through a relationship of the form

$$\mathbf{D}^u = \dot{\zeta} \mathbf{N}_B; \quad \mathbf{N}_B = \frac{1}{\sqrt{2}\tau_B} \mathbf{T}'_B; \quad \tau_B = \left\{ \frac{1}{2} \text{tr} \left[ (\mathbf{T}'_e)^2 \right] \right\}^{1/2} \quad (16)$$

and  $\mathbf{T}'_B$  is the deviatoric component of the Cauchy stress tensor  $\mathbf{T}_B$  applicable to visco-plastic phenomena, as depicted in Figure 2. Also, in (16) the visco-plastic strain-rate  $\dot{\zeta}$  is generally assumed to be a function of the effective stress  $\tau_B$  and the strain-rate  $\dot{\gamma}_0$ , i.e.

$$\dot{\zeta} = \left( \frac{\tau_B}{q} \right)^{1-s} |\dot{\gamma}_0| \begin{cases} \frac{1}{(|\dot{\gamma}_0|/\dot{\gamma}_c^v)^s} & ; \quad (|\dot{\gamma}_0| \geq \dot{\gamma}_c^v) \\ 1 & ; \quad (|\dot{\gamma}_0| < \dot{\gamma}_c^v) \end{cases} \quad (17)$$

In (17),  $s$  is the *viscous sensitivity* to the rate effect. Also at extremely low loading rates  $|\dot{\gamma}_0| \leq \dot{\gamma}_c^v$ , the

dependency of  $\dot{\zeta}$  on the strain-rate  $\dot{\gamma}_0$  is neglected; therefore, the parameter  $q$  can be interpreted as the *static yielding stress* of the material. It should also be noted that when  $s \approx 0$ , the value of  $\dot{\gamma}_c^v$  is inapplicable and the response of the material reduces to a pure plastic response.

The stress states in the elastic recovery responses, denoted by  $\mathbf{T}_A$  and the visco-plastic responses, denoted by  $\mathbf{T}_B$ , are added to generate the Cauchy stress: i.e.

$$\mathbf{T} = \mathbf{T}_C = \mathbf{T}_A + \mathbf{T}_B \quad (18)$$

In summary, a single generalized form of a constitutive model intended for describing large strain hyperelastic behaviour, strain-rate effects and moderately large irreversible plastic strains has been adopted for modelling both the *untreated* and *chemically treated* materials. The mechanical response of the *untreated* material, however, has to distinguish between loading and unloading through a selective treatment of the elastic parameter of the elastic recovery component. During loading, the visco-plastic deformation of the *untreated* material is restricted and the only deformation is attributed to elastic effects; upon unloading, however, the visco-plastic component is fully released and the unloading behaviour is accompanied by irreversible deformations. For the *chemically treated* material, the material responses also have to take into account the yield point. Prior to yield, the visco-plastic deformation is restricted; beyond the yield point, however, the visco-plastic component is released, which accounts for further softening and hardening behaviour. The equations used to describe the general form of the constitutive model for both the *untreated* and *chemically treated* material, can be summarized as follows:

#### **Constitutive Equations used for modelling the Untreated Material**

##### **Loading:**

Deformation Gradient:  $\mathbf{F} = \mathbf{F}^e$

Component A ( $\mathbf{T}_A$ ): Deformation restricted

Component B ( $\mathbf{T}_B$ ): Deformation restricted

Component C ( $\mathbf{T}_C$ ): Eq. (6), (7), (8), (9), (10)

##### **Unloading:**

Deformation Gradient:  $\mathbf{F} = \mathbf{F}^e \mathbf{F}^u$

Component A ( $\mathbf{T}_A$ ): Eq. (11), (12) with  $E'_1 = 0$

Component B ( $\mathbf{T}_B$ ): Eq. (16), (17)

Component C ( $\mathbf{T}_C$ ): Eq. (6), (7), (8), (9), (10)

### Constitutive Equations used for modelling the Chemically Treated Material

#### Loading prior to Yield Point:

Deformation Gradient:  $\mathbf{F} = \mathbf{F}^e$

Component A ( $\mathbf{T}_A$ ): Deformation restricted

Component B ( $\mathbf{T}_B$ ): Deformation restricted

Component C ( $\mathbf{T}_C$ ): Eq. (6) with  $C'_2 = 0$ , (7), (8), (9), (10)

#### Loading beyond Yield Point:

Deformation Gradient:  $\mathbf{F} = \mathbf{F}^e \mathbf{F}^u$

Component A ( $\mathbf{T}_A$ ): Eq. (11), (12) with  $E'_1 = E'_y$ , and (15)

Component B ( $\mathbf{T}_B$ ): Eq. (16), (17)

Component C ( $\mathbf{T}_C$ ): Eq. (6) with  $C'_2 = 0$ , (7), (8), (9), (10)

#### Unloading:

Deformation Gradient:  $\mathbf{F} = \mathbf{F}^e \mathbf{F}^u$

Component A ( $\mathbf{T}_A$ ): Eq. (11), (12) with  $E'_1 = 0$

Component B ( $\mathbf{T}_B$ ): Eq. (16), (17)

Component C ( $\mathbf{T}_C$ ): Eq. (6) with  $C'_2 = 0$ , (7), (8), (9), (10)

The material properties required to model the *untreated* and *chemically treated* PVC geosynthetics are determined from uniaxial tests. The experiments were conducted at strain-rates of  $\dot{\epsilon}_0 = 4\%/min$  and  $\dot{\epsilon}_0 = 40\%/min$  with a peak strain of 140%, followed by unloading. The specific material parameters applicable for *untreated* PVC material are as follows:

$$\begin{aligned} C_1 &\approx 0.23 \text{ MPa}; & C_2 &\approx 0.53 \text{ MPa}; \\ \kappa_1 &= \kappa_2 = \kappa \approx 0.13; & \dot{\gamma}_c &\approx 5.67 \times 10^{-7} \text{ sec}^{-1}; \\ q &\approx 2.0 \text{ MPa}; & s &\approx 0; & E'_2 &\approx 0.5 \text{ MPa} \end{aligned} \quad (19)$$

Similarly, the constitutive parameters applicable to the *chemically treated* material are summarized below:

$$\begin{aligned} C_1 &\approx 9.0 \text{ MPa}; & \kappa_1 &\approx 12.6; & \dot{\gamma}_c &\approx 5.6 \times 10^{-7} \text{ sec}^{-1} \\ q &\approx 2.64 \text{ MPa}; & s &\approx 0.1; & \dot{\gamma}_c^v &\approx 3.2 \times 10^{-10} \text{ sec}^{-1}; \quad (20) \\ \kappa_y &= \kappa \approx 0.13; & E_y &\approx 1.13 \text{ MPa}; & E_2 &\approx 1.2 \text{ MPa} \end{aligned}$$

### MEMBRANE INDENTATION EXPERIMENTS

The membrane indentation test facility shown in Figure 4 is designed to apply a controlled movement

( $\Delta$ ) to a rigid spherical indenter (with a diameter 50.8mm) that interacts with a membrane fixed along a circular boundary. All tests were conducted on PVC specimens that had been exposed to ethanol for a period of 9 months. The rate of indentation  $\dot{\Delta}$  is set constant during a test. The test facility has provisions for securing a plane membrane specimen in a fixed condition along a circular boundary of diameter 250mm (see Figure 4b). The fixed boundary condition is achieved by clamping of the PVC specimen between two aluminum plates (5mm in thickness) using eight 4mm screws. To reduce the possibility of slippage at the clamped boundary, a rubber sheet of thickness 3mm with an opening of diameter 250mm was bonded to the PVC specimen, using a non-reactive instant adhesive. During axisymmetric indentation, the contacts were initiated at the center of the circular membrane (Figure 5a). The indentation response was prescribed through the application of the indentation displacement in an incremental manner up to a maximum displacement of  $\Delta_{\max} = 50.8\text{mm}$ . During axisymmetric loading of the chemically-treated PVC, the ratio of the maximum axial displacement to the membrane diameter reached approximately 0.20. This corresponds to a maximum strain of 8% in the radial direction. The load ( $P$ )-indenter displacement ( $\Delta$ ) response during axisymmetric indentation and the displaced profiles of the membrane are shown in Figure 5a.

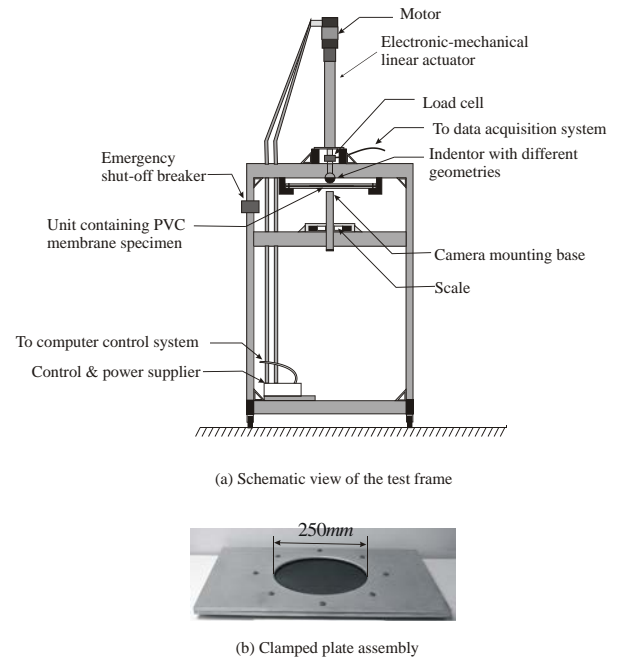


Fig. 4 Apparatus used for membrane indentation tests

The results show a good repeatability between the sets of experiments. The visual images of the

deflected shapes were recorded using a high precision (5 Mega pixels) digital camera, which was positioned 1.5m from the test specimen. The digital camera was mounted on the test frame in such a way that the image plane was parallel to the plane of the symmetry of the indentation of the membrane. The chemically-treated PVC material exhibited pronounced irreversible deformations after a loading-unloading cycle. During asymmetric indentation, the contacts were initiated at a distance of 42mm from the central axis of the circular membrane (Figure 5b). The indentation responses were examined up to a maximum displacement of  $\Delta_{\max} = 38.1\text{mm}$ , which gave rise to a maximum strain of approximately 10%. In comparison to the case of the axisymmetric indentation, larger forces are needed to induce the same indentational displacement (Figure 8b).

### COMPUTATIONAL MODELLING

The constitutive models for both *untreated* and *chemically treated* polymeric materials can be implemented in computational approaches to examine the mechanical behaviour. In this research program attention focused on membranes that were fixed along a circular boundary and subjected to axisymmetric and asymmetric indentation using a spherical rigid indenter. The computational code used for this purpose was the general purpose finite element code ABAQUS/ Standard™ and the material sub-routine U-MAT was used to implement the constitutive relationships within the computational algorithm. The computational modelling takes into account the rate-sensitive constitutive models and frictional contact between the spherical indenter and the PVC membrane (See also [1], [13-15], [27]). In the nonlinear analysis of frictional contact performed using the ABAQUS™ code, each step is divided into iteration increments. The size of the displacement increment is first chosen and the ABAQUS/Standard™ code automatically assigns the size of subsequent increments. During each increment, the code employs a Newton-Raphson algorithm to perform the iterations and the equilibrium is determined through consideration of the principle of virtual work. The ABAQUS/Standard™ further utilizes a Backward-Euler scheme as a default finite difference scheme to update variables. Those variables determined from previous iterations that do not change during the iteration between  $[t, t + dt]$  can be defined as state variables. The state variables adopted in the analysis include the components of the irreversible deformation gradient  $\mathbf{F}^u$  at time  $t$  and the stress tensors at time  $t$  in the visco-plastic component included in models A and B. When a fully backward-Euler finite difference scheme in time is

implemented, the updating of  $\gamma_0$  requires information on the material configuration at  $t + dt$ . The updated value of  $\gamma_0$  will have a direct influence on the elasticity parameters for the component C in the chosen constitutive model, with the result that the computations will exhibit non-convergence.

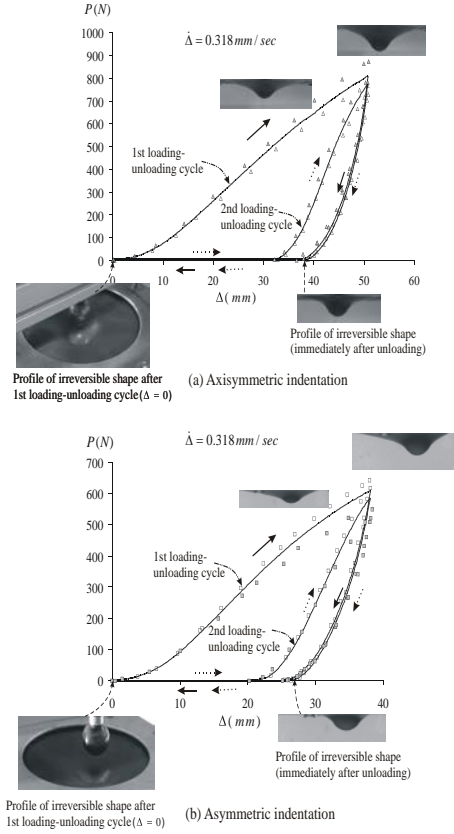


Fig. 5 Load-displacement responses of the treated PVC membrane (exposed to pure ethanol for 9 months): (a) subjected to axisymmetric indentation and (b) asymmetric indentation (symbols represent experimental scatter)

The value of  $\gamma_0$  is thus assumed to remain unchanged during iterations and is taken as a further state variable. For the problems examined here, the PVC membrane only experiences incremental loading during the initial stage where irreversible deformations are absent; the initial values of the state variables can, therefore, be obtained by treating the material as fully elastic. The state variables are updated only when the iteration converges. Both a quadratic triangular membrane element (3M6) and a linear solid triangular prism element (C3D6) were used in the computational modelling. The results indicated no noticeable differences between the two types of elements. The computations presented in the paper were developed using the solid triangular prism element. Figure 6 shows the mesh discretization used in the computational simulation of

the axisymmetric indentation problem for the circular membrane. Figure 7 illustrates the comparison of deflection profiles during loading and unloading of an as supplied membrane obtained from the experiments and the computational simulations. Corresponding results for the asymmetric indentation of the edge supported, as supplied circular membrane

are shown in Figures 8 and 9. Further details of the

computational procedures and results of comparisons between computational estimates and experimental results can be found in [13-16].

## CONCLUDING COMMENTS

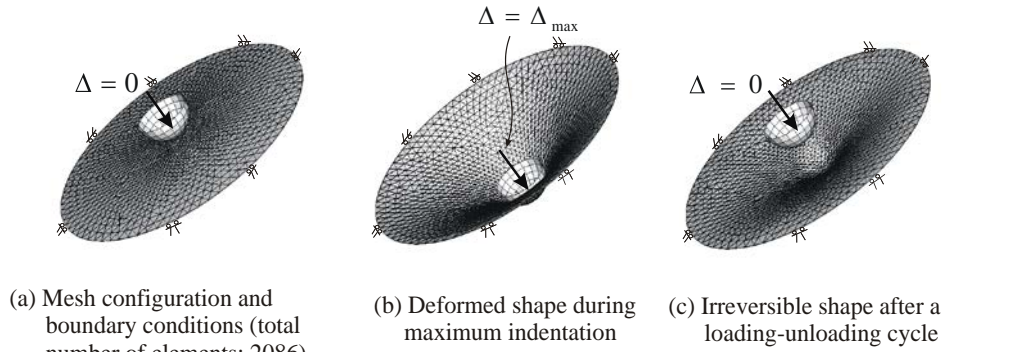


Fig. 6 Computational simulations of the untreated PVC membrane-symmetric indentation

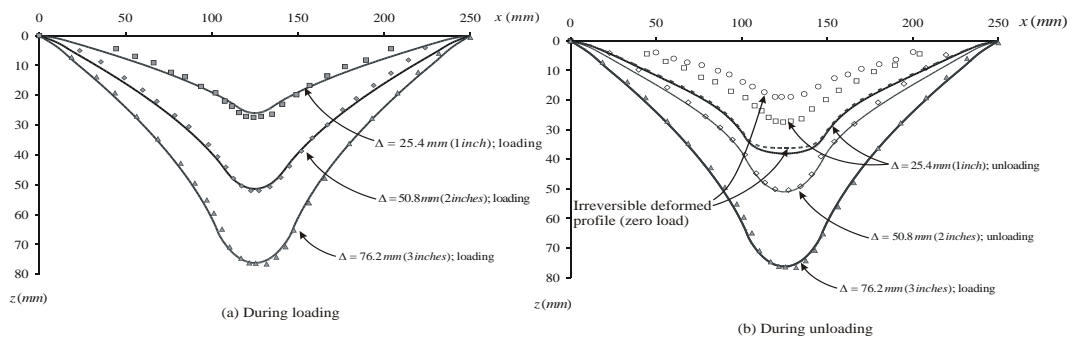


Fig. 7 Deflected shapes of untreated membrane during symmetric loading and unloading

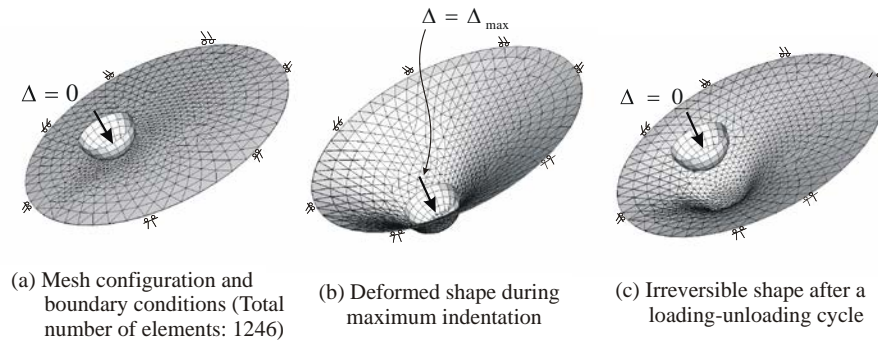


Fig. 8 Computational simulations of the untreated PVC membrane-non-symmetric indentation

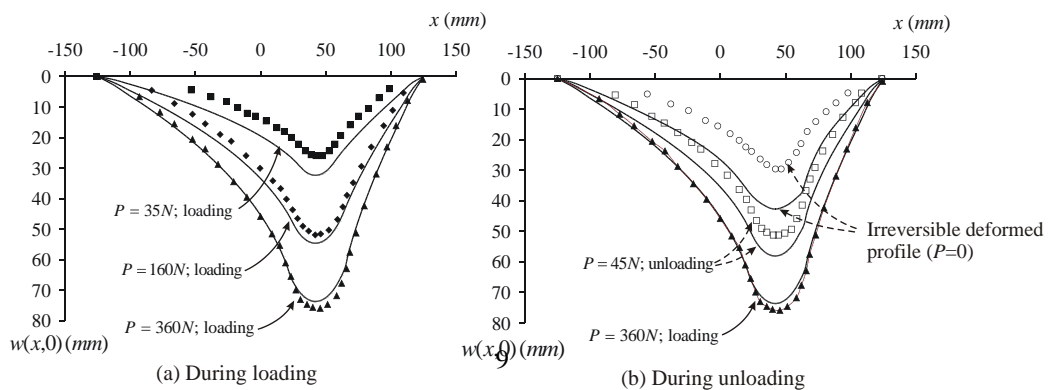


Fig. 9 Deflected shapes of untreated membrane during asymmetric loading and unloading

The loss of hyperelasticity during exposure to chemicals that can leach out the plasticizer in PVC membranes is a further factor that needs to be accounted for in the development of the constitutive models. In this study we have considered a unified model that can accommodate the large strain and strain-rate sensitive responses of a PVC membrane in an untreated and chemically treated state. The validity of the modelling can be assessed either through predictions of uniaxial test results conducted at different strain rates or through predictions of experiments involving three-dimensional deformations of membranes subjected to transverse loading. The latter approach is the more general and requires the implementation of the constitutive models developed in a suitable computational approach. The paper summarizes the results of previous research that involved the implementation of the constitutive models in a general purpose computational code. The computational results accurately predict the response of the transverse deflections of the symmetrically and asymmetrically loaded PVC membranes composed of either untreated or ethanol treated PVC particularly in the loading mode. The irreversible deformations during unloading of both the untreated and ethanol- treated unloading of both the untreated and ethanol-treated circular membranes show that while the trends are accurate, the computational modeling generally underestimates the experimental data. Both the constitutive modelling and the computational approach can be considered as useful for examining the mechanics of hyperelastic rate-sensitive polymeric materials used in geoenvironmental applications.

## ACKNOWLEDGEMENTS

The work described in this paper was supported by an *NSERC Discovery Grant*, the 2003 *Max Planck Research Prize in the Engineering Sciences* awarded by the Max Planck Gesellschaft, Berlin, Germany and the James McGill Research Chairs program. The author is grateful to Dr. Qifeng Yu for his important contributions to the research work.

## REFERENCES

- [1] Yu Q, Selvadurai APS, 2005, Mechanical behaviour of a plasticized PVC membrane subjected to ethanol exposure, *Polymer Degradation and Stability*, 89, 109-124.
- [2] Pita VJRR., Sampaio EEM, Monteiro EEC, 2002, Mechanical properties evaluation of PVC/plasticizers and PVC/thermoplastic polyurethane blends from extrusion processing, *Polymer Testing*, 21, 545-550.
- [3] Haedrich T, 1995, *The Effect of Chemical Exposure on the Burst Strength of a Geomembrane*, Master's Thesis, Carleton University, Ottawa (Canada).
- [4] Contamin B, Debeauvais V, 1998, *The Effect of Ethanol Exposure on Burst Strength of a Geomembrane*, Research Report, McGill University, Montreal (Canada).
- [5] Pezzin G, Ajroldi T, Casiraghi T, Garbuglio C, Vittadini G, 1972, Dynamic-mechanical and tensile properties of poly (vinyl chloride). Influence of thermal history and crystallinity, *Journal of Applied Polymer Science*, 16, 1839-1849.
- [6] Treloar LRG, 1943, Stress-strain data for vulcanized rubber under various types of deformation, *Transactions of the Faraday Society*, 39, 59-70.
- [7] Rivlin RS, 1948, Large elastic deformations of isotropic materials. IV. Further developments of the general theory. *Philosophical Transactions of the Royal Society, A* 241, 379-397.
- [8] Green AE, Adkins JE, 1970, *Large Elastic Deformations*, Oxford University Press, London.
- [9] Spencer AJM, 1970, The static theory of finite elasticity, *Journal of the Institute of Mathematics and its Applications*, 6, 164-200.
- [10] Selvadurai APS, 2002, Second-order elasticity for axisymmetric torsion: a spheroidal coordinates formulation. In Croitoro., E. (Ed.), *Proceedings of the 2<sup>nd</sup> Canadian Conf. on Nonlinear Solid Mechanics*, Vancouver, 1, 27-49.
- [11] Selvadurai APS, Suvorov AP, 2016, Coupled hydro-mechanical effects in a poro-hyperelastic material, *Journal of the Mechanics and Physics of Solids*, 91, 311-333.
- [12] Sweeney J, Ward IM, 1995, Rate dependent and network phenomena in the multi-axial drawing of poly (vinyl chloride), *Polymer*, 36, 299-308.
- [13] Selvadurai APS, Yu Q, 2006, On the indentation of a polymeric membrane, *Proceedings of the Royal Society, Mathematics and Physics Series A*, 462, 189-209.
- [14] Selvadurai APS, Yu Q, 2006, Constitutive modelling of a polymeric material subjected to chemical exposure, *International Journal of Plasticity*, 22, 1089-1122.
- [15] Selvadurai APS, Yu Q, 2008, Mechanics of polymeric membranes subjected to chemical exposure, *International Journal of Non-Linear Mechanics*, 43, 264-276.
- [16] Yu Q, Selvadurai APS, 2007, Mechanics of a rate-dependent polymer network, *Philosophical Magazine*, 87, 3519-3530.
- [17] Lee EH, 1969. Elastic-plastic deformation at finite strains, *Journal of Applied Mechanics, Transactions of the ASME*, 36, 1-6.

- [18] Spencer AJM, 2004, *Continuum Mechanics*, 3<sup>rd</sup> Ed., Dover Publications, Longman Group, London.
- [19] Mooney M, 1940, A theory of large elastic deformation, *Journal of Applied Physics*, 11, 583-593.
- [20] Rivlin RS, 1960, Some topics in finite elasticity, *Structural Mechanics: Proceedings of the 1<sup>st</sup> Symposium on Naval Structural Mechanics*, (J.N. Goodier & N.J. Hoff, Eds.), 169-198, Pergamon Press, New York.
- [21] Selvadurai APS, Spencer AJM, 1972, Second order elasticity with axial symmetry. I. General theory, *International Journal of Engineering Science*, 10, 97-114.
- [22] Selvadurai APS, 1974, Second-order effects in the torsion of a spherical annular region, *International Journal of Engineering Science*, 12, 295-310.
- [23] Selvadurai APS, 1975, Distribution of stress in a rubber-like elastic material bounded internally by a rigid spherical inclusion subjected to a central force, *Mechanics Research Communications*, 2, 99-106.
- [24] Selvadurai APS, 2006, Deflections of a rubber membrane, *Journal of the Mechanics and Physics of Solids*, 54, 1093-1119.
- [25] Selvadurai APS, Spencer AJM, Rudgyard MA, 1988, Second order elasticity with axial symmetry. II. Spherical cavity and spherical rigid inclusion problems, *International Journal of Engineering Science*, 26, 343-360.
- [26] Selvadurai APS, Shi M, 2012, Fluid pressure loading of a hyperelastic membrane, *International Journal of Non-Linear Mechanics*, 47, 228-239.
- [27] Selvadurai APS, Yu Q, 2005, Mechanics of a discontinuity in a geomaterial, *Computers and Geotechnics*, 32, 92-106.

# MEETING THE CHALLENGES OF ENGINEERING A SUSTAINABLE FUTURE

David Thorpe

School of Civil Engineering and Surveying, University of Southern Queensland, Australia

## ABSTRACT

Engineers have a significant role in the sustainable development and management of resources. This responsibility encompasses the three generally accepted dimensions of sustainability – environment, economic and social - and applies to engineering projects throughout their life cycle. Sustainable engineering practice is supported by professional engineering associations, such as Engineers Australia, which includes the promotion of sustainability as one of the four principles of its Code of Ethics, and which has recently published position statements on infrastructure and energy that support sustainable engineering management positions. It has also been given impetus by the recent Paris Agreement on climate change. However, while there has been considerable progress and many advances in this field, such as recycling, use of innovative materials and the use of renewable resources in energy production, there is much work required to achieve a truly sustainable future. While industry has a major role in promoting and encouraging sustainable practices in engineering projects, educators also have a significant role in this process through developing and fostering the knowledge and skills of sustainability in engineers. At the undergraduate level, this task is normally undertaken through the offer of courses that teach the principles of sustainable engineering practice. A major challenge for educators, however, is the ongoing development of the knowledge and skills of sustainable engineering taught in such courses. While postgraduate study in engineering management topics that incorporate sustainable practices can achieve this objective, the majority of practising engineers are unlikely to study them at a formal level. Meeting this gap between sustainable engineering knowledge and its implementation in order to better achieve a sustainable future therefore presents challenges to educators. Possible options proposed to achieve this goal include an ongoing commitment by government and society to sustainability in engineering projects, ongoing implementation of innovative sustainable engineering practices, and lifelong learning in sustainable engineering practices by professional engineers through educational providers, professional associations and personal study.

**Keywords:** *sustainability, life cycle management, resilience, education, professional development*

## INTRODUCTION

Professional engineers are responsible for planning, designing, delivering and maintaining significant public and private works. Increasingly, in undertaking this role, they are expected to undertake sustainable engineering practices and adhere to sustainable management principles. Such practices are supported by professional engineering organizations, such as Engineers Australia [1] [2].

Sustainable management practices have increasingly gained acceptance by both the community and the corporate sector, resulting in a number of global initiatives with respect to sustainability, including the United Nations Paris Agreement of 2015, which recognizes the urgency of managing climate change, a task that requires wide cooperation and participation by all countries in a global response aimed at accelerating the reduction of global greenhouse gas emissions, with a goal of containing the increase in global average

temperatures to below 2 °C, and preferably to no more than 1.5 °C [3].

While there is increasing commitment to sustainable engineering practices, both locally and globally, there are significant challenges in developing engineering and other professionals who have the requisite knowledge, skills and commitment to implement such practices. While some of this work can be accomplished by the University sector, much of its success relies on continued acceptance of the need for sustainability, implementation of sustainable practices by industry, and a commitment to practicing sustainability by individual professionals such as engineers and scientists.

One approach to addressing these challenges is to engineer the future in a sustainable manner. This task will require commitment by all parties in major engineering and other projects to exercising and implementing sustainable practices, and understanding the issues involved. This paper



discusses the issues and challenges in this process through a review of the principles of sustainability, discussing approaches to managing the future sustainably, providing examples of current sustainability initiatives, discussing the development of a sustainable future, outlining the role of professional engineers in sustainable practices, discussing the development of sustainability skills in professional engineers, providing examples of teaching sustainable engineering skills and discussing the opportunities for meeting the challenges of engineering a sustainable future.

## THE PRINCIPLES OF SUSTAINABILITY

### Sustainable Development and Practices

Sustainable development, on which the principles of sustainable practices are based, is normally defined as “development that meets the needs of the present, yet does not compromise future generations from having the ability to meet their own needs” [4]. It is commonly described as balancing economic development, social equity and environmental protection. Some views of sustainable development add the political dimension. For example, the United Nations Educational, Scientific and Cultural Organization (UNESCO) views sustainable development as having natural, economic, social and political dimensions [5].

The United Nations has developed a list of 17 sustainable goals to be achieved by 2030. These goals relate to social areas (for example, poverty, hunger, health, education, gender equality, reducing inequality, safe cities); resources (such as water, energy, sustainable consumption and production, the marine environment); resilience, climate change, sustainable ecosystems and building global partnerships for sustainable development [6].

Sustainability affects all engineering projects and processes. For example, energy efficiency is important in any engineering undertaking that uses power, such as in transportation activities and the lighting and air-conditioning in buildings. Similarly, it is increasingly necessary to consider recycling, and the use of recycled products, in the design and implementation of infrastructure and building projects. Project development using lean principles that save waste will be less wasteful of natural resources. Using extensive community consultation with respect to the planning of engineering projects and considering the views of the community in the final implementation decision is likely to positively impact on the social aspects of projects. Sustainable practices are important in both smaller engineering projects and processes, and larger systems (such as energy delivery) that affect significant populations.

### Resilience

A related concept to sustainability is resilience, which can be described in terms of systems thinking. The resilience of the socio-ecological-economic system, which is the focus of this discussion, is largely underpinned by the following concepts

- We live within socio-ecological systems in which changes in one domain of the system impact other domains.
- Socio-economic systems are complex adaptive systems that do not change in a predictable way and can be driven across a threshold into a different regime
- Resilience can be defined as “the capacity of a system to absorb disturbance, to undergo change and still retain essentially the same function, structure, and feedbacks” or “the capacity to undergo some change without crossing a threshold to a different system regime—a system with a different identity” [7].

A resilient system therefore can be subject to significant change, such as in natural disasters, and return to its previous function, provided that it does not cross a threshold. From this point of view, resilience can be considered as being defined by the characteristics of the amount of disturbance that a system can absorb and still remain within the same state, the degree to which the system can self-organize and the ability to build and increase its capacity for learning and adaptation. This characteristic of persistence connects resilience with sustainability, as sustainable development can also be considered as having the goal of not only creating but also maintaining well-performing social, economic and ecological systems. This persistence is common to both concepts. Resilience thinking can provide a framework for viewing the three components of sustainability as one system operating over linked scales of time and space; and a focus on the change of a system with time and disturbance [8].

Thus, a resilient social-ecological system has a greater capacity to avoid problems as a result of disturbances external to the system, and so has a greater capacity to continue providing us with those goods and services that support our quality of life [9]. A further consideration of this point of view is that if it is accepted that there will be a certain amount of climate change over time as a result of the emissions to date and in the future of greenhouse gases, a resilient engineering installation will be one that is designed and installed in such a way that it will maintain or fairly quickly return to its function should the intensity of a climatic event increase as a result of further climate change. A related argument for a link between sustainability and resilience is that persisting in the achievement of a sustainable world will result in the development of resilient systems of engineering works.



Resilience may also be understood through the concepts of threshold (the magnitude or intensity that must be exceeded for a particular result not to occur), the adaptive cycle (how an ecosystem organizes itself and responds to a changing world) and panarchy (a conceptual framework of systems and their linkages) [10].

A resilient system will therefore have an upper bound to the intensity of a particular event, will be adaptable and be composed of a number of linked sub-systems, or alternatively form part of a larger integrated resilient system. For example, a transportation system of roads could be considered resilient if, during or immediately after a disaster there is a system of key transportation routes (such as roads) available that will enable assistance to be given to a community to evacuate as required, be sustained during the disaster, and return to normal life as quickly as possible after the disaster. These key transportation routes would be supported by sub-systems of other routes that would return to normal service as soon as possible after the disaster, and by other transportation facilities such as sea and air transport.

A further perspective on the concept of resilience from an engineering point of view is that of robustness, or “designed resilience,” of an engineering system. This approach assumes bounded uncertainty, in which the types and ranges of uncertainty are known, and the system is designed to be resilient to the shocks from them. This engineering approach to resilience is different from that of other professions, such as psychologists, who deal with the resilience of individuals and societies; ecologists, who consider both the speed at which a system can recover or if it can recover; and military or disaster focused personnel, who also consider speed and ability to recover [11].

### Uncertainty and Risk

The uncertainty in the sustainability and resilience of a system arises because many events affecting the system have limited predictability, and in some cases cannot be anticipated with certainty. Such uncertainty arises from the limited predictability of the events on a global scale, such as weather conditions, the economy, wars, seismic activity and the extent of rise in sea level as a result of global warming. It is incumbent on the engineering profession to limit the extent of such uncertainty. One approach for working with uncertainty and managing it is managing risk [12]. This process is discussed in the Risk Management Standard AS/NZS ISO 31000:2009, “Risk management- Principles and guidelines.” According to this Standard, risk may be defined as the “effect of uncertainty on objectives”, where:

- An effect is a deviation from the expected,

which may be either positive and/or negative.

- Objectives can have different aspects (such as financial, health and safety, and environmental goals), and can apply at different levels (such as strategic, organization-wide, project, product and process).
- Risk is often characterized by reference to potential events and consequences, or their combination. It can be positive or negative.
- Uncertainty is the state, even partial, of deficiency of information related to, understanding or knowledge of an event, its consequence, or likelihood.

Risk is often expressed in terms of a combination of the consequences of an event and the associated likelihood of occurrence. It is managed through a system that is based on a number of principles; uses a framework based on mandate and commitment and that uses a continual improvement approach; and uses a process of seven steps consisting of communication and consultation, establishing the context, risk assessment (risk identification, analysis and evaluation), risk treatment, and monitoring and review [13].

An alternative view of risk is to distinguish unfavourable or favourable outcomes by using the word “risk” for possible unfavourable outcomes and “opportunity” for possible favourable outcomes [14].

This approach to risk management is both rigorous and collaborative. Properly applied, a good risk management approach like that described will assess and make provision to take advantage of the benefits and minimize the adverse effects arising from the sustainability risks in a system. It will therefore provide a basis for managing the benefits and issues from the risks in the sustainability and resilience of a given engineering system, and aid in the developing solutions to understanding, designing and implementing measures to manage and improve the sustainability and resilience of the system.

In summary, the concepts of sustainability, resilience and managing uncertainty through a risk management process are closely linked, and require consideration at all levels of engineering systems if an ongoing sustainable future is to be achieved.

The relationship between sustainability, uncertainty/risk and resilience is shown in Figure 1, which is based on a similar figure in a paper on food system resilience [15]. In this figure, factors in sustainability, like global warming, lead to uncertainty in the global environment which results in the uncertainty and risk of increased instability in the weather and climate, which in turn may lead to disruption of and damage to the infrastructure and services system. This simplified picture can be extended to a considerable number of events and risks, all of which may jointly interact with the resilience of the world system. Therefore, the management of sustainability is highly desirable if

the risk of negative impacts on the global environmental, societal and economic systems is to successfully managed.

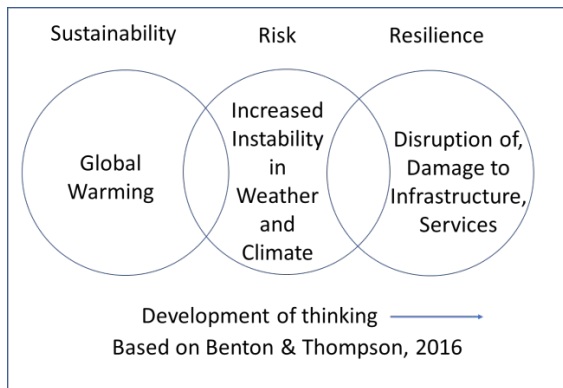


Fig 1 Sustainability, Resilience, Uncertainty

## MANAGING A SUSTAINABLE FUTURE

The 2015 Paris Agreement recognizes that climate change represents an urgent and potentially irreversible threat to human society and the Earth, which requires cooperation by all countries in an international response aimed at accelerating the reduction of global greenhouse gas emissions, and that significant reductions are required in global emissions to achieve the emissions reduction of the Agreement. It also recognizes that climate change is a common concern of the human race, and that parties should, when implementing climate change, respect human rights, health and related matters, including indigenous rights. The need to promote access to sustainable energy in developing countries through the enhanced deployment of renewable energy is acknowledged [3]. As an example of the commitment to climate change by many world governments, the Australian Government has a goal to reduce carbon emissions by 26 per cent to 28 per cent over 2005 levels by 2030 [16].

The importance of managing climate change is underscored by the significant increase in greenhouse gas emissions and other climate indicators. Data from the World Bank indicates that world greenhouse gas emissions rose by 40 per cent from 1990 to 2012 [17], with the main industry sectors responsible for carbon dioxide emissions in 2013 being electricity and heat production (49.4 per cent), manufacturing industries and construction (19.7 per cent) and transport (20.2 per cent [18]. Overall, the World Bank estimated that total world carbon dioxide emissions in 2013 were 34,848.6 million metric tonnes [19]. This position is complemented by the United Nations Environment Programme (UNEP) Sustainable Buildings & Climate Initiative (SBCI), which have stated that the building sector, which would span a number of

industry sectors, contributes up to 30 per cent of global greenhouse gas emissions per year and consumes up to 40 per cent of all energy, a figure which between 1971 and 2004 had been growing at 2.5 per cent per year for commercial buildings and 1.7 per cent per year for residential buildings [20].

The Paris Agreement is complemented by the United Nations' 17 sustainable development goals to be achieved by 2030 [6].

The Paris Agreement of 2015 also has a number of technological goals, and notes the role of technology research, development and demonstration; and the development and enhancement of endogenous capacities and technologies. It also establishes a process for technology development and transfer to support its long-term vision. Some of the technology initiatives include technology needs assessments and their implementation, technology action plans and project ideas; provision of financial and technical support for the implementation of the results of the technology needs assessments; the assessment of technologies that are ready for transfer; and enabling environments for addressing barriers to the development and transfer of technologies that meet social and environmental requirements [21].

The above requirements recognize the role of engineering in the sustainable development process. Examples of such initiatives could include, as well as the initiatives of energy efficiency, recycling and waste management, other initiatives like the use of advanced materials, nanotechnology, management of the natural environment including less dependence on non-renewable resources and a range of other initiatives. Sustainable processes might include smart design for sustainability and resilience, sustainable asset management, recycling, lean manufacturing and construction that reduces waste, rehabilitation rather than replacement, design of materials to match the expected product life cycle, and reuse of waste materials in other applications and products. Further insight into some of these processes are provided by Allwood and Cullen, who have discussed, in addition to energy efficiency, ways to achieve efficiency in the use of material, including re-using metal components, longer life products and achieving a sustainable material future through business activity evaluation, the influence of policy and the actions of individuals [22].

In summary, there is global recognition of the existing and potential future consequences of climate change and other components of a sustainable future, and a commitment by many governments to address these issues, and in particular global warming. The challenge that now faces the world, and the engineering profession in particular, is how to address the positively and sustainably manage climate change and other sustainability initiatives through positive

management of emissions, waste, resources and global infrastructure. Achieving this goal will achieve a more livable future world, conserve our resources for the future, improve global resilience to the effects of climate change by infrastructure and buildings and, through positive risk management, reduce the uncertainty of the future. This process should also deliver global social and economic benefits. Engineers have a significant role in planning, designing, developing and managing this sustainable future.

## **EXAMPLES OF CURRENT SUSTAINABILITY INITIATIVES**

Engineering a sustainable future presents many challenges to the engineering profession. It also provides many opportunities. Areas in which engineers can play an active role in developing a sustainable future include planning and designing infrastructure and other installations that not only meet the needs of society, but also use sustainable materials and methods, waste minimization, developing and implementing systems and processes to minimize greenhouse gas emissions, undertaking renewable energy projects, improving the manufacture and use of engineering material including developing and implementing advanced and green materials, minimizing waste, recycling and designing installations to maximize resilience and minimize the adverse impacts of climate change.

These challenges and opportunities can be illustrated through considering three areas of engineering practice – the use of advanced design and development including material reuse, the development and use of advanced engineering and construction materials, and the challenges in the energy sector.

### **Advanced engineering design and development**

Advanced engineering design and development processes, including the application of advanced software, can be a significant contributor to sustainable and resilient engineering practices.

One example of using advanced engineering to improve efficiency in material usage, by Allwood and Cullen, has previously been discussed [22]. A further example is research into the use of bioclimatic design principles, which tend to mimic natural approaches and aim to both enable buildings to function satisfactorily in existing and future climatic conditions and reduce building energy use and greenhouse gas emissions. Such principles aim at minimizing energy consumption in mining and manufacturing, minimizing transportation; optimizing resource use through material reuse and recycling, and maximizing the use of renewable energy [23].

The use of lean design and construction principles, which aim at reducing waste throughout the production or construction process [24], similarly aim to optimize the use of both materials and energy in these processes.

Recycling is also used in a range of engineering processes. For example, achieving sustainability in road design, construction and management requires the use of not only sound environmental management, but also practices like water sensitive urban design, use of advanced and recycled materials, and environmentally responsible project management and construction, subject to precautions being taken to ensure that recycled materials are free from contaminants. An alternative approach in roadworks is to stabilize existing materials rather than obtain new materials, using materials like cement, lime, or powdered polymers [25].

### **Developments in engineering and construction materials**

Modern Engineering uses a range of traditional and new materials. Such materials are used across the engineering spectrum, and in buildings, infrastructure, machinery and electrical applications. In the construction area, for example, there has been considerable research in low carbon concrete applications in buildings and other engineering projects.

There have been enhancements to the physical and mechanical properties of concrete, a stronger focus on more efficient use of resources and the use of smart concretes in building energy efficiency [26]. For example, geopolymers, which result from the reaction of amorphous aluminosilicates with alkali hydroxide and silicate solutions, have been claimed to be used in concrete of up to 70 MPa compressive strength and have been used in applications like retaining walls, water tanks, precast bridge decks and precast beams [27].

Alternative materials may have both advantages and disadvantages over traditional materials. Thus, while cement made with fly ash cementitious additives uses waste from coal-fired power stations and can have useful properties fitting it for a range of uses like mass structures its relatively slow rate of strength development can make it not suitable for high early strength applications. Similarly, concrete made from recycled aggregate may have lower densities than concrete made from naturally occurring aggregate because some mortar remains attached to it and resulting larger water absorption than naturally occurring material [28]. There is also the risk that fly ash may become less readily available as the world moves away from coal fired power stations.

Finally, research into the use of advanced and green materials by the small and medium sector of

industry has indicated that there may be challenges in using some building materials, such as advanced concrete materials, materials using native earth such as adobe and rammed earth, advanced timber products, green roof and pervious concrete. These challenges included whether the firm had previously had experience with using the material, cost of the material and the availability of standards and codes of practice [29].

In summary, while there will continue to be considerable research into the development and application of both advanced and sustainable engineering materials, there are likely to be some challenges with their acceptance by the broader engineering and construction community. It is probable that a number of these challenges arise from the novelty of some of the material, and the reluctance of industry to use new materials until they are proven to be reliable, durable, safe and cost-effective. This may take time, given the innovation decision process of knowledge of the innovation, persuasion of its use through its perceived characteristics, a decision to use it, implementation of the innovation and confirmation of its value or otherwise [30].

### **Energy production and management**

The figures estimated by the World Bank in its 2017 World Development Indicators publication included a global electricity production figure in 2014 of 23,869.3 billion kilowatt hours, and an energy use per capita of 1,929 watts [19]. Given this ongoing demand for energy, and an increasing demand for energy, one area in which to improve the total carbon emissions is through improved management of energy, such as electricity, both through managing demand and moving away from fossil fuel production.

In Australia, a review of the future security of the national electricity market was undertaken by Chief Scientist Alan Finkel. In summary, the report on the review recommended increased security, future reliability, rewarding consumers and lower emissions. [31].

The Engineers Australia organization, which represents professional engineers in Australia, has recently released an energy position paper, which discusses energy productivity, transport energy and electricity generation. Among its recommendations are that the Australian government adopts an energy efficiency target of 30 per cent by 2030 as the means to drive progress under the Australian Government National Energy Productivity Plan, that the Australian government introduces policies and programs that lead to energy efficiency in the transport sector, including active integration of more efficient transport modal mixes, and that all levels of government proactively develop plans to restructure

electricity generation in Australia [2].

### **DEVELOPING A SUSTAINABLE FUTURE**

Developing a sustainable, resilient future is a challenging task. It is a process subject to considerable uncertainty, which requires the management of the negative risks involved and presents many opportunities. The goal of this task is to develop a rewarding and livable future for both ourselves and our descendants, in which global warming is contained and cities and other infrastructure quickly recovers from disasters. Achieving this target requires assessment of the current position and balance of the environmental, economic and social state of the world; evaluation of the options in managing climate change and the ongoing use of resources; and development of solutions that not only achieve a sustainable future but also ensures resilience of key infrastructure and productive facilities in times of challenges and disasters.

Fundamental to this process is an understanding of the options and initiatives that can result in much more sustainable world. Examples have been given of such initiatives in engineering design and development, improved and new engineering and construction materials and significant advances in energy production and management. These developments can be considered as part of a much wider focus on building a sustainable future, and linking us, through the lens of resilience, with a wider systems approach in understanding not only the immediate impact of sustainability, but also its longer-term evaluation.

Because of the increasing role of sustainable practices in the engineering profession, the effectiveness of teaching these practices to engineering students, and of the use of these practices in professional engineering, is developing with the passage of time. Such teaching should not only encourage students to understand the principles of sustainable development, but also should provide them with the understanding, knowledge and skills in this area to motivate them to make sustainable engineering practices a significant component of their professional career. The first step in discussing this process is to review the role of the professional engineer in these practices.

### **THE ROLE OF PROFESSIONAL ENGINEERS IN SUSTAINABLE PRACTICES**

Professional engineers have a significant role in providing a sustainable, resilient future. As an example of the recognition of this role by professional engineering member organizations, Engineers Australia, of which many Australian professional engineers are members, states that

professional Engineers are “responsible for bringing knowledge to bear from multiple sources to develop solutions to complex problems and issues, for ensuring that technical and non-technical considerations are properly integrated, and for managing risk as well as sustainability issues.” Engineers Australia prescribes two levels of engineering practice competency. Stage 1 competencies qualify students as graduate engineers, at which they are expected to understand sustainable engineering practice in their discipline, and demonstrate commitment to sustainable engineering practices and the achievement of sustainable outcomes [32]. The second stage of competencies, Stage 2 competencies, is the Chartered Professional Engineer level, for which graduates must have minimum of at least three years of professional experience and are required to show competencies in personal commitment, obligation to community, value in the workplace and technical proficiency. These competencies include the sustainability related skills of developing safe and sustainable solutions; engaging with community and stakeholders; communication and risk assessment [33].

These competencies are supported by the Code of Ethics of Engineers Australia, which contains guidelines to professional conduct that is based on ethical engineering practice that requires judgment, interpretation and balanced decision-making in context. Engineers in their course of professional practice are required to demonstrate integrity, practice competently, exercise leadership and promote sustainability. As part of promoting sustainability, professional engineers are required to engage responsibly with the community and other stakeholders; practise engineering to foster the health, safety and wellbeing of the community and the environment; and balance the needs of the present with the needs of future generations [1].

These ethics, combined with required engineering competencies, provide a strong focus on sustainable practice within the engineering profession. At the same time, there are some engineering related disciplines, such as construction, which do not rate sustainable management skills as highly as some other skills. For example, a survey of recruiters for over 100 construction companies located in the eastern United States of America found that they rated environmental awareness, along with communication skills, lowest among 14 key competencies, while other skills like ethical issues, problem-solving skills, and interpersonal skills were rated highly [34]. On the other hand, an Australian survey noted both the connections and differences between educational and professional employment requirements with respect to education for sustainability [35].

In summary, sustainable management skills are

increasingly recognized by professional engineering and other organizations, and are increasingly required by industry. There is however a challenge to develop the skills in engineering students by both educational institutions and industry so that they become not only part of their undergraduate education, but are also embedded in their professional practice.

## **DEVELOPMENT OF SUSTAINABILITY SKILLS IN PROFESSIONAL ENGINEERS**

The support of sustainable engineering practices by professional engineering organizations, government and industry has resulted in sustainable engineering practice is increasingly being taught to engineering students. Such teaching would be likely to consider the principles of the United Nations Scientific and Cultural Organization (UNESCO) in the education of sustainable development (ESD) These competencies include that such education:

- is based on the principles and values that underlie sustainable development
- promotes life-long learning
- is locally relevant and culturally appropriate
- is based on local needs but acknowledges their international consequences
- engages formal, non-formal and informal education
- accommodates the evolving nature of sustainability addresses content
- builds civil capacity
- is interdisciplinary and promotes participatory learning and higher-order thinking skills [36].

In engineering, sustainability teaching tends to follow one of three models – integration of sustainability into traditional courses, stand-alone sustainable engineering, and embedding sustainable engineering modules within the framework of existing courses. Challenges in sustainable engineering education include a full curriculum, the engineering educational structure and a focus on the environmental aspects of sustainability, with less emphasis on its social and cultural aspects [37]. Thus, there is an opportunity to improve the learning of engineering students in the social dimension of sustainability [38]. This need for a seamless interface between engineering and society has been reinforced by other studies, once of which considered the link between science, technology and society courses and engineering, and which highlighted the three categories of participation, politics and policy, and citizenship, which were reflected themes that were not discussed often in engineering curricula, but were significant in science, technology and society [39].

In conclusion, while teaching in sustainable engineering practices is undertaken in universities, there is a still a gap in teaching the social and

cultural aspects of sustainability as outlined in the UNESCO competencies for sustainable education.

## EXAMPLES OF TEACHING SUSTAINABLE ENGINEERING SKILLS

One of the main expected outcomes of teaching sustainable engineering skills is the development of engineers who can practice, on an ongoing basis, the sustainable design and management of engineering projects and processes as expected by society and professional engineering organizations. As an example of such teaching, the University of Cambridge, in recognition of the increasing recognition by the United Kingdom construction and civil engineering industries, and their professional bodies, of sustainable engineering practice, engaged with sustainable development issues.

This approach recognized that many sustainability problems requires a systems view of the world that accounted for complexity, interdisciplinary understanding and a broader view of system performance. This process requires not only the use of mathematics, but also making judgments and understanding of differences.

As a result, a number of initiatives were undertaken in the Cambridge University Engineering Department. Such initiatives focused on embedding sustainable development within the Department. Initiatives have included:

- introduction of sustainable development thinking into undergraduate teaching
- the development of a Master of Philosophy in Engineering for Sustainable Development
- formalizing sharing of sustainable development
- developing sustainable development as a key theme of departmental strategy.

This approach required achieving a quantitative and qualitative balance, dealing with pedagogical issues, and initiating change. It has been successful. Lessons were also learnt in managing change [40].

It is also noted that the Engineering Department of Cambridge University is undertaking research in modelling, simulation and analysis of complex systems. This research is aimed at better managing their uncertainties through absorbing variations naturally. Part of this research is in developing a new understanding of uncertainty and risk [41].

The University of Southern Queensland offers the *Technology, Sustainability and Society* course, an example of a stand-alone sustainable engineering course, to all Engineering and Built Environment students studying a three or four year undergraduate degree program. This course, which discusses topics like the history of technology, sustainability including environmental impact management, politics and power, the economy, models of society, cultural impacts, law and regulation and management concepts, has been successful [42].

The University also incorporates sustainable engineering management principles included as part of other courses, including postgraduate study up to Doctor of Professional Engineering level. For example, *Technological Impact and its Management* is a stand-alone sustainable management focused course that reviews current technological development and evaluates its impact on the world on we live. There are also courses offered at the University postgraduate level that integrate sustainability with the course material. Such courses include:

- *Asset Management in an Engineering Environment*, which discusses the strategic life cycle management of engineering asset systems
- *Advanced Engineering Project Management*, which is designed to teach higher level project and program management knowledge and skills
- *Whole of Life Facilities Management*, which teaches the life cycle operations, maintenance and renewal of engineering facilities [43].

In addition, the University offers a postgraduate courses *Management of Technological Risk* course [43]. This course teaches risk management principles based on the Australian Standard for Risk Management [13], and the applications of risk management principles in engineering projects and processes. A text on managing project opportunity and risk [14] supports the course.

These courses place a strong emphasis on assignments that are designed to challenge students to demonstrate their competencies in problems similar to those of professional practice, and which are assessed using the principles of authentic assessment [44]. Similarly, students are also encouraged to apply experiential learning principles [45] through applying practical examples in examinations in those courses with examinations and applying marking feedback from a first assignment to a second, more complex assignment in those courses, like *Advanced Engineering Project Management*, that are assessed solely by assignments. There is also an increasing use of guest lecturers from industry.

## OPPORTUNITIES FOR MEETING THE CHALLENGES

As shown above, there is a developing emphasis on teaching sustainable engineering practices in both undergraduate and postgraduate engineering programs. Such teaching tends, however, not to be a large component of the engineering curriculum. It is therefore desirable that graduate engineers further develop the knowledge and skill of sustainability during their professional practice. One way in which such ongoing development could be addressed would be for industry to lead this development through initiatives like providing environments in

which these skills can be enhanced. Further formal education in sustainable engineering practice is also desirable. Because most professionals are very busy, this approach may only be suitable for those engineers who have the time to undertake additional study.

Another possible opportunity for both the tertiary education sector and industry to have a role in developing sustainable engineering knowledge and skills this area is for industry to develop links with universities with respect to teaching sustainable engineering practice. This approach would benefit those industries that are becoming more sustainable in their outlook and practices, and would therefore benefit by having a positive role to play in sustainable engineering education. This process has the potential to elevate the profile of sustainability to engineering students. A further option could be for universities to develop links with industry partners and professional associations in encouraging sustainable practices and offering short courses in them, along with the related areas of risk and resilience, to both students and practicing professionals.

The amount of teaching in sustainable engineering at an undergraduate level could be reviewed to see if it can be better incorporated into the engineering curriculum, perhaps by incorporating an increased number of components of it in selected courses in each year of the engineering curriculum. Engineering teaching could also benefit from more emphasis on the social aspects of sustainability.

There is also an opportunity for further understanding between sustainability, the risks of not using sustainable practices, and the impact at a systems wide level on resilience, or the ability to better withstand and more quickly recover from the impacts of more extreme and frequent events in areas like the weather, or economic or social conditions resulting from increased risk.

## CONCLUSION

While there has been considerable progress in the teaching and practice of sustainability in engineering, there is still much work to be undertaken to make it a part of day to day professional practice and thereby minimize the impacts of climate change, as well as to optimize the social and economic aspects of a sustainable future. In particular, there should be a better understanding of the effect, on the resilience of the built environment, of not managing this future well.

Engineers have a significant role in sustainable management and in designing, developing, operating and maintaining infrastructure sustainably and with the resilience to minimize the effect of negative climatic and other impacts on the functioning of

infrastructure and services, and which can quickly be restored to functionality following such events. While current engineering education would be expected to should provide them with a basic understanding of these principles, it is considered that such education be further reinforced through government and industry support of sustainable practices, postgraduate education and training.

## REFERENCES

- [1] Engineers Australia, Our Code of Ethics, Canberra, Australia, 2013.
- [2] Engineers Australia, Energy Position Statement, Canberra, Australia, 2016.
- [3] United Nations, Adoption of the Paris Agreement. United Nations Framework Convention in Climate Change, Paris, 2015, pp.1, 2.
- [4] Brundtland, GH, Report of the World Commission on Environment and Development – Our Common Future, United Nations General Assembly, New York, 1987.
- [5] United Nations Educational, Scientific and Cultural Organization, “Four Dimensions of Sustainable Development”, viewed May 9, 2014, [http://www.unesco.org/education/tlsf/mods/theme\\_a/popups/mod04t01s03.html](http://www.unesco.org/education/tlsf/mods/theme_a/popups/mod04t01s03.html), 2010.
- [6] United Nations, Transforming our World: The 2030 Agenda for Sustainable Development, New York, 2015, p.14.
- [7] Walker, B & Salt, D, Resilience thinking: sustaining ecosystems and people in a changing world. Island Press, Washington, 2006, pp. 31, 32.
- [8] Pisano, U, Resilience and Sustainable Development: Theory of resilience, systems thinking and adaptive governance - ESDN Quarterly Report Number 26, European Sustainable Development Network, Vienna, 2012, p.6.
- [9] Walker, B & Salt, D, Resilience thinking: sustaining ecosystems and people in a changing world. Island Press, Washington, 2006, p. 37.
- [10] Pisano, U, Resilience and Sustainable Development: Theory of resilience, systems thinking and adaptive governance - ESDN Quarterly Report Number 26, European Sustainable Development Network, Vienna, 2012, p.19.
- [11] Walker, B & Salt, D, Resilience practice – building capacity to absorb disturbance and maintain function. Island Press, Washington, 2012, p.2, 3.
- [12] Trevelyan, J, The Making of an Expert Engineer. CRC Press, 2014, p. 321.
- [13] Standards Australia, Risk management – Principles and guidelines: AS/NZS ISO 31000:2009, Standards Australia, Sydney, 2009.
- [14] Chapman, C & Ward, S, How to Manage Project Opportunity and Risk, 3rd edn, Wiley, Chichester, United Kingdom, 2011, p.3.



- [15] Benton, TG & Thompson, C, "Food system resilience", Food Science and Technology, 2016, September.
- [16] Australia's 2030 climate change target, Australian Government, Canberra, 2015.
- [17] The World Bank, World Development Indicators, Table 3.9, Trends in greenhouse gas emissions, accessed May 25, 2017, <http://wdi.worldbank.org/table/3.9>.
- [18] The World Bank, World Development Indicators, Table 3.10, Carbon dioxide emissions by sector, accessed May 25, 2017, <http://wdi.worldbank.org/table/3.10>.
- [19] The World Bank, World Development Indicators 2017. Washington, DC, p. 58.
- [20] United Nations Environment Programme Sustainable Building and Construction Initiative, United Nations Environment Programme, Paris, 2009, pp. 3, 9.
- [21] United Nations, Adoption of the Paris Agreement. United Nations Framework Convention in Climate Change, Paris, 2015, pp.2-28.
- [22] Allwood, JM & Cullen, JM With Both Eyes Open, UIT Cambridge Limited, Cambridge, 2012.
- [23] Sattary, S and Thorpe, D, "Potential carbon emission reductions in Australian construction systems through bioclimatic principles" Sustainable Cities and Society, 2016, vol. 23, pp. 105-113.
- [24] Howell, G.A., What is Lean Construction - 1999, Proceedings IGLC-7, 1999.
- [25] Wilmot, T.D. and Wilmot, S.D., "Strategies for Sustainable Roads", 21st ARRB Conference, Cairns, Queensland, 2003.
- [26] D'Alessandro, A, Fabiani, C, Pisello, AL, Ubertini F, Materazzi, AL & Cotana, F, "Innovative concretes for low carbon constructions: a review", International Journal of Low-Carbon Technologies, May 2016.
- [27] Aldred, J and Day, J, "Is Geopolymer Concrete a Suitable Alternative to Traditional Concrete?" in 37th Conference on our World in Concrete & Structures", Singapore, Aug. 2012.
- [28] Meyer C, "The greening of the concrete industry", Cement and Concrete Composites, Vol. 33, 2009, pp. 601-605.
- [29] Wright, C. and Thorpe, D, Use of advanced and green construction materials by small and medium-sized enterprises. In Proc. Of 31st Annual ARCOM Conference, 7-9 September 2015, pp. 227-236.
- [30] Rogers, E.M. The diffusion of innovations, Free Press, New York, 5<sup>th</sup> edn., 2003, pp. 168-215.
- [31] Finkel A, Independent Review into the Future Security of the National Electricity Market – Blueprint for the Future, Australian Government, Department of the Environment and Energy, Canberra, Australia, 2017.
- [32] Engineers Australia, Guide to Assessment of Eligibility for Membership (Stage 1 Competency), Canberra, ACT, Australia, 2013.
- [33] Engineers Australia, Australian Engineering Competency Standards Stage 2 – Experienced Professional Engineer, Canberra, ACT, Australia, 2012.
- [34] Ahn YH, Pearce A & Kwon H, "Key Competencies for U.S. Construction Graduates: Industry Perspective", Journal of Professional Issues in Engineering Education and Practice, 2013, vol. 138, pp. 123-130.
- [35] Thomas I, Barth M & Day T, "Education for Sustainability, Graduate Capabilities, Professional Employment: How They All Connect", Australian Journal of Environmental Education, 2013, vol. 29, no. 1, pp. 33-51.
- [36] Mochizuki Y & Fadeeva Z, "Competences for sustainable development and sustainability: significance and challenges for ESD", International Journal of Sustainability in Higher Education, 2010, vol. 11, no. 4, pp. 391-403.
- [37] Allenby B, Murphy CF, Allen, D & Davidson, C, "Sustainable engineering education in the United States", Sustainability Science, 2009, vol.4, no.7.
- [38] Valdes-Vasquez R & Klotz L, "Incorporating the Social Dimension of Sustainability into Civil Engineering Education", 2011, Journal of Professional Issues in Engineering Education and Practice, vol. 137, pp. 189-197.
- [39] Pritchard J. & Baillie C, "How can engineering education contribute to a sustainable future?", European Journal of Engineering Education, 2006, Vol. 31, No. 5, pp. 555-565.
- [40] Fenner RA, Ainger CA, Cruickshank HJ & Guthrie PM, "Embedding sustainable development at Cambridge Engineering Department", International Journal of Sustainability in Higher Education, 2005, vol. 6, no. 5, pp. 229-241.
- [41] Cambridge University, Complex, Resilient and Intelligent Systems, viewed 1 September 2017, <http://www.eng.cam.ac.uk/research/strategic-themes/complex-resilient-and-intelligent-systems>, 2017.
- [42] University of Southern Queensland, Course Specification: ENG2002 Technology, Sustainability and Society, 2017, Toowoomba, Australia.
- [43] University of Southern Queensland, Doctor of Professional Engineering, 2017, Toowoomba, Australia.
- [44] Gulikers JTM, Bastiaens ThJ, & Kirschner PA, "Perceptions of authentic assessment: Five dimensions of authenticity", Second biannual Northumbria/EARLI SIG assessment conference, 2004, Bergen.
- [45] Kolb DA Experiential Learning: Experience as the Source of Learning and Development, 1984 Englewood Cliffs, N.J.: Prentice-Hall.



## **STATISTICS FOR EVIDENCE-BASED DECISIONS – USE, MISUSE AND ABUSE**

Shahjahan Khan<sup>1</sup> and M Ashraf Memon<sup>1,2,3,4</sup>

<sup>1</sup>Faculty of Health, Engineering and Sciences, University of Southern Queensland, Australia

<sup>2</sup>Faculty of Medicine, University of Queensland, Australia

<sup>3</sup>Faculty of Health Sciences and Medicine, Bond University, Australia

<sup>4</sup>Faculty of Health and Social Science, Bolton University, UK

### **ABSTRACT**

Increasingly decision-makers are relying on an evidenced-based approach, using results extracted by analysing exponentially growing data. Statistical methods have become an integral part of analysing and interpreting simple or complex data to make valid and accurate decisions for society and science in the face of uncertainty. Because of its power to uncover, otherwise unavailable, valuable information from data, statistics is increasingly being applied for both private and public benefit including business and trade, not to mention its crucial role in research and innovative technologies. The key role of statistics is engraved in the planning and development of every successful nation and international agency. In fact, the scope of statistics is not confined by borders as it disseminates through regional and international organisations and agencies driving social, economic, environmental, health, poverty elimination, education and other agendas for planned development. Obviously statistical methods are capable of analysing data to determine various indices, indicators, predictions, estimates, and perform tests to help identify any problems and take appropriate measures to remedy them. Because of the obvious power of statistics it has been used, misused and abused by those who are in authority and power.

*Keywords: Evidence-based decision, Analysis of data, Estimation and test, P-value, Society and Science*

### **INTRODUCTION**

In recent years, statistics is receiving growing attention, acknowledgement, recognition and appreciation from the key decision makers in every corner of the globe due its incredible power to reveal, otherwise unavailable, precious information from various databases for the benefit of mankind. Even the Secretary General of the United Nations (UN) and its General Assembly have highlighted the crucial role of statistics in the modern world by adopting a resolution in the UN General Assembly to celebrate World Statistics Day in 2015. As in [1], the theme of the celebration 'Better data. Better lives' impresses upon the importance of quality data to better lives in a very wide sense encompassing every aspect of life and society. A UN Economic and Social Affairs video on better data is found at [2].

The increasing popularity of statistics is underpinned by its widespread use and the growing awareness of its public benefit whether that be in everyday work, business strategy and decision making process. Recent global interest in evidence based decision-making practice has also brought statistics to the spotlight. The emergence of 'Big Data' and Data Science have further expanded the applications and benefits of statistics. The appointment of the Chief Data Scientist by the President of the USA is clear evidence of the

recognition of statistics at the highest level of administration.

Not surprisingly statistical literacy is gradually becoming an essential component of this basic skill set in today's modern world. Every society is increasingly embracing statistical information as an effective means of communication, reasoning, and evidence representation. With the exponential growth of data due to its never ending mass production on the internet and elsewhere, more in-depth understanding of statistics, and its power is becoming inevitable. Statistical literacy, if not expertise, is an essential skill for policy makers, government officials, business executives, scientific researchers and ordinary citizens.

In the past, there was lack of data, but now, there is an influx and oversupply of data in many ways. However, there is no value or real use of this raw data until and unless it is properly scrutinized and analysed, only then highly precious information can be retrieved and presented in lay terms to inform mass population of its value. Statistics has the means to unlock the secret of data and reveal important information to make it beneficial for real life applications. Thus, the tremendous power of statistics has started to get due recognition from many fair-minded professionals and decision-makers in research, business, management, and government and non-government agencies.

Although, the power of statistics is often not highlighted, statistical information is an excellent way to create awareness, and change the perception, in the community and society on crucial national and global issues. It can send the strongest possible message to shake up views and opinions of the people, and inspire/convince them to do things differently. Two recent examples of how statistics have impacted on the ordinary people and decision makers are presented below. The first example pertains to statistics on the unemployment rate and its power to impact on the choice of voters in the USA. The second example is relates to vital statistics in the area of public health sector in Australia.

In the recent past, the power of statistics has been reflected in the presidential election campaign of the USA. In the 2012 re-election campaign of President Barack Hussein Obama the number one issue was the unemployment rate. Just one month before the November election, on 5 October the Bureau of Labor Statistics released that the official unemployment rate [3] had dropped from 8.1 percent to 7.8 percent in September (see Table 1). Although the drop was only 0.3 percent, undoubtedly, this was not a simple 'rate' or 'number' for President Obama and his opponent (Mitt Romney). It was make or break information, and most likely the most powerful statistic in dictating the 2012 presidential election result.

Table 1 Unemployment rate by Labor Force Statistics from the Current Population Survey

Year	Jan	Feb	Mar	Apr	May	Jun	Jul	Aug	Sep	Oct	Nov	Dec
2008	5.0	4.9	5.1	5.0	5.4	5.6	5.8	6.1	6.1	6.5	6.8	7.3
2009	7.8	8.3	8.7	9.0	9.4	9.5	9.5	9.6	9.8	10.0	9.9	9.9
2010	9.8	9.8	9.9	9.9	9.6	9.4	9.4	9.5	9.5	9.4	9.8	9.3
2011	9.1	9.0	9.0	9.1	9.0	9.1	9.0	9.0	9.0	8.8	8.6	8.5
2012	8.3	8.3	8.2	8.2	8.2	8.2	8.2	8.1	7.8	7.8	7.7	7.9
2013	8.0	7.7	7.5	7.6	7.5	7.5	7.3	7.3	7.3	7.2	6.9	6.7
2014	6.6	6.7	6.7	6.2	6.2	6.1	6.2	6.2	6.0	5.7	5.8	5.6
2015	5.7	5.5	5.5	5.4	5.5	5.3	5.3	5.1	5.1	5.0	5.0	5.0
2016	4.9	4.9	5.0	5.0	4.7							

Obviously, the Republican camp claimed that the drop of the unemployment rate was 'cooked' by the influence of the administration. Steve Haugen, an economist at the Bureau of Labor Statistics, "flatly dismissed the idea that there was any way the White House or Obama campaign could have had a hand in how the numbers turned out." "The data is not manipulated for political reasons. I've been involved in the process myself for almost three decades. There's never been any political manipulation of the data, period," Haugen told CBSNews [4]. Table 1 shows the statistics on the

unemployment rate in the USA before and after the re-election of President Obama.

For the second example, we consider a statistic on cancer from the 'authoritative information and statistics to promote better health and wellbeing' (AIHW), Australia report [5], "In Australia 1 in 3 men and 1 in 4 Australian women will be diagnosed by cancer before the age of 75." This is a chilling statement, not just some figures, but a stern warning about the very high risk of cancer for real people. This simple statistic sends a very powerful message to society on how extensive the risk is of getting cancer. This statistic also demands policy from the decision makers, to be proactive in saving lives.

The chart in Figure 1 shows that the incidence of cancer in Australia is still increasing over the years with some fluctuations for both male and female population.

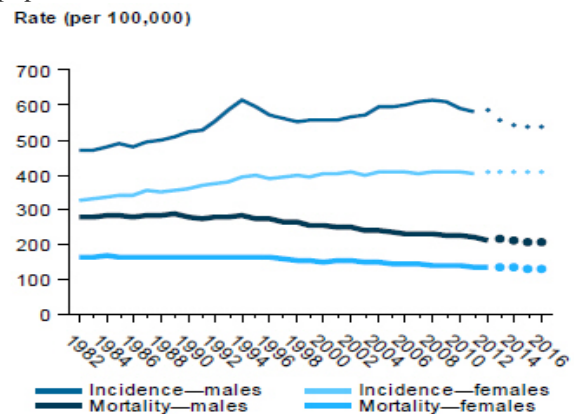


Fig. 1 Incidence and mortality of all cancers combined, 1982-2016

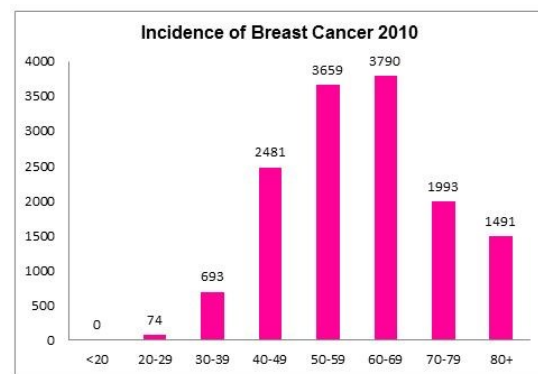


Fig. 2 Incidence of breast cancer by age for Australian women in 2010

Another statistical fact presented in a simple bar chart in Figure 2 reveals the incidences of breast cancer in Australian women [6]. Clearly, a large number of women above the age of 40 years are reported to have breast cancer. This statistic sends alarm bells to the health authorities and other relevant policy makers to tackle this serious health

problem with appropriate policy and measures, particularly for middle and older age women.

## WHY STATISTICS IS ESSENTIAL?

What makes statistics so important in life? Why is it so relevant in so many aspects of society? The answer to these questions requires understanding and appreciation of three crucial realities of life i.e. uncertainty, variability and error.

### Uncertainty

Life is full of uncertainties. The weather is uncertain, the gender of the conceived baby is uncertain, the amount of sale/income is uncertain, the profit/loss is uncertain, the list goes on and on. There is no certainty in almost every natural phenomena and human behaviour. *In this world uncertainty is the only certainty.* Like it or not, uncertainty is here to stay for ever. Is there any way to measure the degree of uncertainty? Fortunately, statistical methods are capable of dealing with uncertainty and it relies on the laws of probability and statistical distributions. Actually, statistical methods make use of the magnitude of uncertainty to create models and enables us to find and study different attributes of uncertain phenomenon. Measuring uncertainty has important economic consequences for calibration and measurement activities. In calibration reports, the magnitude of uncertainty is often taken as an indication of the quality of the laboratory, and smaller uncertainty values generally are of higher value and of higher cost.

### Variability

We live in a world of variables. People vary in gender, age, height, weight, income, education, ethnicity, hair colour, nationality, size of shirt/shoe, type of car, and so on. Society varies in household, dwelling, population, culture, language, religion, standard of life, quality of life, health care, welfare system etc. Business vary in size, sale, profit, type, customer base, product, staff, marketing, wage, commission/bonus, location, and so on. Almost everything around us varies and that is the reality of life and society. Statistical methods utilise the measure of variability in describing and analysing the nature and characteristics of the variable. In fact, variables are the key raw materials of statistical methods.

### Error

The world is full of errors. Error is everything and everywhere. We always refer to measurement error, assessment error, human error, machine error,

model error, judgement error and so on. Unfortunately, we can't avoid or ignore error, because this is a reality of life. Therefore, we need to learn how to deal with error, and how to prevent or reduce it. Statistical methods such as regression model and analysis of variance model include error in the model as a way of representing the reality of life. The most commonly used normal distribution introduced by Gauss [7] is related to measurement of errors. In fact normal distribution is also known as the law of error, the law of facility of errors, Laplace's second law, Gaussian law etc. By the end of the 19th century some authors had started using the name *normal distribution*, where the word "normal" was used as an adjective – the term now being seen as a reflection of the fact that this distribution was seen as typical, common – and thus "normal".

Certainly, we live in a world that is full of uncertainty, variability, and errors of various kinds. Needless to say that these three realities of life – variation, error and uncertainty - are everywhere and in everything, and hence the use of statistics is unavoidable, rather inevitable. Life becomes more complicated and challenging if the three factors act simultaneously or in combination leading to further complexities, demanding further sophistication of statistical methods. This obvious and ongoing challenge has helped develop statistics faster than any other scientific discipline in the last several decades. Often statistical methods evolved on the way of solving problems in other disciplines, and later it has found applications in many new areas of modern life.

According to the LinkedIn [8] statistics graduates were the most in-demand skill in 2014 and it is the second most-in-demand in 2017. Among the hottest skill for jobs in 2016 were statistical analysis with data mining listing second. LinkedIn blog reports, "Our top skill category last year, statistical analysis and data mining, is still sitting comfortably at #2. It is the only skill category that is consistently ranked in the top 4 across *all* of the countries we analyzed. We still live in an increasingly data-driven world, and businesses are *still* aggressively hiring experts in data storage, retrieval and analysis."

Statistics is among the fastest-growing disciplines of for jobs in the USA. The McKinsey Global Institute predicts a shortage of up to 190,000 people with the data analysis skills to work with Big Data. Statistics is ranked by *Fortune* as the top graduate degree based on salary, growth and job satisfaction. The starting salaries for statistics graduates are among the highest in the USA. No wonder demand for statisticians is very high.

## DEVELOPMENT OF STATISTICS

The development of statistics to its current state as a scientific discipline is relatively recent. But the ancient rulers - kings and emperors - used statistics to take an account of the state of affairs of their territory; population, soldiers, horses, food stock, etc. As far back as the Bible, God ordered Prophet Moses to conduct a census of all males over the age of 20, and he did it. So the history of census, an integral part of modern statistics, is at least as old as the Bible.

In the pre-twentieth century statistics was viewed as a branch of mathematics dealing with data. As a discipline lacking rigorous scientific validity, at that time, its main emphasis was on collection, analysis, and exploration of observational data. After Kolmogorov [9] proposed his famous Axioms of Probability, and its English translation published by Morrison [10], statistics received a boost as a scientific discipline. This laid the much needed scientific foundation of statistical theory and methods enabling the use of various probability distributions and sampling distributions of sample statistics for making valid inferences.

The introduction of high power computers has done a tremendous service making statistical computing easy and quick, and thus helped popularise statistics and widen its applications. In fact, this is what the statistics community was waiting for; the full manifestation of what statistics could offer to humanity (see Nolan and Lang, [11]). In addition to performing different analyses of a wide range of observational and experimental data in a very short time, computer technology has provided a way to easily prove and illustrate many complicated statistical results (cf. Klemens [12]). Furthermore, it enables statisticians to conduct Monte Carlo simulations and numerical computations in a variety of statistical setups when analytical methods are unavailable.

Statistics is a science that enables making reliable decisions in the face of uncertainty. It provides methods to minimise the risk, and predicts the value of a response variable for given values of related explanatory variables. Statistics is like a mirror of society that reflects the true state of different aspects of the society and their characteristics. To know the attributes of a society, one needs to know the relevant statistics.

Florence Nightingale said, "To understand God's thoughts we must study statistics, for these are the measure of His purpose."

## MAJOR CONTRIBUTIONS OF STATISTICS

Statistics has been widely used for different reasons by people from all walks of life. Among the frequent users of statistics are the policy/decision

makers and researchers both in the private and public sectors. Often, the contribution of statistics is not fully understood, realised or recognised due to lack of understanding the depth and extent of its impact on the society and appreciation of its value and importance in real life. Some of the major contributions of statistics are highlighted below.

*Big Data:* The recent emergence of big data has changed the way people look at statistics, and how it could extract the hidden information in the mess of huge data for their business and other needs. The analysis of big data involves a number of computing tools in addition to statistical techniques such as factor analysis, principal component analysis, support vector machine, artificial neural networks, multiple regression, analysis of variance, k-means, prediction analysis etc.

## Census

Population census is an ancient statistical method to collect data on every household and individual residing in a country. Normally census is conducted every 5 or 10 years to gather information on vital demographic, social and economic variables. The census data is used by governments and other development/welfare agencies to determine the vital needs of the communities including infrastructure, education, welfare, healthcare, recreation etc. In many countries, regular census is also conducted on agriculture and industry sectors.

## Sample Survey

Introduction of random sample is a remarkable contribution of statistics for the mankind. The random sampling techniques not only reduces the cost, time and resources of data collection, but also ensures scientific validity of results derived from the sample data by avoiding selection bias. This allows studies to collect data from a very small representative part of a population to make valid conclusion or inference on the characteristics of the whole population. The frequently used sample survey is the most convenient, timely, cost effective and popular way of collecting data.

## Design of Experiment

Properly conducted experiments following the principle of random allocation of treatments to experimental units, introduction of control, block and replications enable the experimenters to isolate out the effect of the treatment of interest from many potential latent and confounding factors. Controlled experiment is the only way to establish 'cause and effect' relationship between variables.

This is extensively used in the agricultural, industrial and engineering problems.

### **Randomised Controlled Trial**

In a study in which subjects are allocated at random (by chance alone) to receive one of several clinical interventions including one control in the form of a standard practice, a placebo, or no intervention at all. The aim is to compare the effect of the intervention (treatment) with that of the control to find out if the intervention effect is significant. No new drug is allowed to be in the market for the use of the patients without undergoing clinical trials and proving its effectiveness through statistical test. This is regularly used in the health and medical studies.

### **Estimation and Hypothesis Test**

Point and interval estimations allow people to compute the value of the sample counterpart of any relevant unknown parameter/characteristic of the population at large without knowing the population data. The confidence interval is a very popular way to estimate unknown parameter with a preselected level of confidence. Test of hypothesis is the only way to check manufacturer's claim on the quality of a product or any statement about specific value of parameters of a population. This is frequently used by the researchers in many different fields to find out if the observational or experimental results are statistically significant. Introduction of any new drug in the market requires compulsory clinical trials and results must be supported by statistical test. The sampling distribution of the underlying statistic is in the centre of both interval estimation and test of hypothesis. These methods are widely used in business, education, and all branches of sciences.

### **Analysis of Variance**

This is a very frequently used statistical technique by many people who wish to compare the means of several treatments or populations. The underlying mechanism is to use the between treatment variance in determining if there is significant difference among the treatment means. It is popularly known as ANOVA. Its multivariate version, MANOVA is used for multivariate data analysis.

### **Regression Model**

The linear (and nonlinear) regression analysis is a method to establish relationship between a response/dependent variable and one or more explanatory/predictor variables. In most of the

modelling exercises, regression analysis plays a crucial role for prediction or estimation or test. The regression model is used in varieties of forecasting and analytical problems.

### **Total Quality Management**

The quality control is a routine statistical practice in manufacturing industries to ensure the effectiveness of the production system. Various types of control charts are used to detect any problems in the quality of the final products, so that the underlying defects are rectified to resume normal production before it is too late. The ground breaking work of Taguchi and Deming has changed the way manufacturing industry used to work in the past.

### **Opinion Poll**

This statistical tool allows collection of data on different issues and problems faced by the society or nation. It is more popular in checking the level of popular support for political parties and government plans and programs. It is equally useful to find the views of the people on different crucial and controversial issues of the day. Often politicians assesse, review and revise their party policies and programs based on the outcome of opinion polls.

### **Research Methodology**

After determining the research questions the main concern of every researcher is to gather relevant data following an appropriate survey design along with a properly constructed questionnaire or controlled experiment, analyse the data at hand, and then interpret the results to answer the questions. Statistics is an integral part of many successful research projects starting from the initial planning stage to finally publishing the outcomes in professional journals.

There are many disciplines taught at various tertiary levels all over the world that are either statistics in disguise or highly dominated by statistical contents including, but not limited to, (1) Actuarial Science, (2) Bioinformatics, (3) Biometry, (4) Biostatistics, (5) Climatology, (6) Data Mining, (7) Data Science, (8) Demography, (9) Econometrics, (10) Epidemiology, (11) Environmetrics, (12) Forecasting, (13) Image Processing, (14) (Bio)Informatics, (15) Management Science, (16) Meta-analysis, (17) Quality/Process Control, (18) Quantitative Methods, (19) Queuing Methods, (20) Reliability Analysis, (21) Risk Analysis, (22) Research Methods, (23) Survival Analysis, (24) Stochastic Process, (25) Time Series Analysis etc. Further details on

importance and use of statistics is found in Khan [13].

## IMPACT OF STATISTICS ON RESEARCH AND SCIENCE

Would it be too much to say, 'No research without statistics'? Not really, as it is almost correct for any research involving collection, analysis and interpretation of data with the very small exception of some qualitative researches in some disciplines. Many research projects are highly dependent on statistics in many different ways. There is hardly any research that does not involve data and hence require some form of statistical support. In fact, statistics has changed the way people used to look at and conduct research.

Every credible quantitative research requires some kind of data handling. This varies from planning and implementation of collection or production of data to screening and analysis of data, and the interpretation of results. In the heart of any social and scientific research there is data of one kind or another. The question is how is this data collected? What sampling or experimental design is used to collect the data? How is the questionnaire prepared or how are the experimental treatments allocated? Answers to these fundamental questions are crucial in determining if the data at hand meets the requirements to be scientifically valid, and hence the results derived from them are accurate. The quality of data is the key into producing any credible statistics. Inappropriate or invalid or defective data can't produce any valid or useful statistics, regardless of what or how sophisticated methods are used. Statisticians must be involved in the planning stage of any project involving data to make sure that the data is collected scientifically and it captures all information on relevant variables of interest and whether to conduct planned or post hoc analyses.

In many research studies the main objective is to find confidence intervals for unknown parameters or perform test of hypotheses, or both. The validity of the sampling distribution of the underlying statistic in both cases is crucial, and hence checking the assumptions of normality, random samples, equality of variances etc are essential. The commonly used  $z$ ,  $t$ , chi-squared, and  $F$  statistics are based on the assumption of normal population. Blind use of these procedures, without properly checking the data on the validity of the underlying assumptions, is likely to produce inappropriate and misleading results and therefore lead to the wrong conclusions.

Inclusion of statistical analyses in research/scientific papers prepared for possible publication in international journals has become a universal practice in almost every field. Often there

are serious issues in the reported statistical results due to oversight or lack of statistical knowledge on the part of the authors. No wonder, many reputed journals mandate checking of statistical contents of manuscripts by statistics reviewer/editor. Even then, there are many published articles with questionable statistical content. This is because some authors opt to use dishonest statistics as a way to get their papers published without having proper statistical understanding and clearly any insight into its adverse consequences.

One highly controversial issue relating to statistical contents in research papers intended to publish in high impact journals, is the inappropriate use of the  $p$ -value in the context of test of hypotheses. One of the well reputed psychology journals decided not to publish any articles with  $p$ -value. Although, the  $p$ -value can be misused and its use as a means to make an acceptance or rejection decision on the null hypothesis can be problematic, it can still be used as a statistical tool under the correct conditions and with appropriate caution, if the context is clarified. A better option is to provide the confidence interval, rather than suggesting acceptance or rejection of the null hypothesis, so that the readers can see a wider picture on the tenability of the parameter of interest. Instead of depending on the  $p$ -value of a single study, combining results from many studies on the same topic by conducting meta-analysis may be a way to increase statistical power through increased sample size and avoid the danger of misusing  $p$ -value.

## STATISTICS IN SHAPING SOCIETY

Planning is the core mechanism of the government to direct and manage programs and activities through allocation of funds to ensure balanced and targeted development. The intention is to come up with a budget that helps achieve desired progress and development in priority sectors of economy and society. Statistical data is the back bone and plays a key role in directing resources to priority areas of every contemporary planning and allocation of budget. Limited resources and competing demands in various sectors, the challenge is to determine the areas of priority for investment, and statistical evidence provides the necessary guidance to rationalise the allocation. Further explanations on the role of statistics in planning and development is found in Khan [14].

The strategic use of statistics in decision-making by governments, welfare agencies, research scientists, international organisations and businesses are making a huge impact on reshaping societies in several ways. Allocation of resources for various directed development programs, focussed interventions, priority engagements,

targeted human development and management, universal health and education strategies etc are based on population statistics.

We are living in a global information society where the flow of information is ever increasing. Statistics plays a major role in shaping and providing scientific information that are useful in almost every aspect of human life, and beyond. It has successfully made its mark on as diverse areas as from astronomy to administration, from business to biology, from housing to health, from engineering to environment, from commerce to community, from manufacturing to ministry, from marketing to management, from industry to infrastructure, from politics to policy, from tourism to trade-union, from sports to strategy. Modern decision-making, be it for an individual or a business or any national government or an international agency, is increasingly using statistical methods to improve the quality of information and/or decision.

Some of the important features of modern statistics are highlighted in the following quotation: "Statistics have a key role to play in opening up government because of the role they play to holding the Government to account. They used to be called the 'Government's statistics' – now they will be the public's." Jack Straw.

Statistics is used to solve many complex real life problems which directly contribute to planning and development. Among popular applications, it is used to (1) prove the effectiveness of a new drug, (2) assess the effect or impact of air or water pollution on living creatures, (3) measure the demographic or economic growth, (4) forecast economic outlook or growth of different types of crops and produce, (5) create awareness on national or global issues, (6) judge popularity of a government, party or leader, (7) determine the needs for doctors, engineers and other professionals, (8) plan for traffic flow on roads and highways, (9) analyse contributions of different sectors of the economy on the gross national product, (10) formulate/adopt appropriate population and human development programs, (11) highlight the state of unemployment, (12) estimate agricultural and natural resources, (13) evaluate performance and efficiency gains of the labour force, (14) find the consumers' price index, (15) study the performance of the stock market, (16) enhance the use of the information highway, (17) compare among nations and regions, (18) decide on bank/interest rates, (19) make insurance profitable, (20) evaluate the crime rate, (21) improve the quality of industrial products, (22) settle claims of insurance and pay rises for employees etc.

The Millennium Development Goal (MDG) 2015 of the UN was planned, monitored, assessed/evaluated and compared by using relevant

statistics and indices on the specific eight different areas of health, education, and social status of people globally. See [15] the MDG Report for details.

The power of statistics is highly dependent on its quality and absolute public trust in the offices that produce statistics. As such, one of the main tasks of any Statistics Office is to earn and maintain the absolute confidence of the users of statistics and the general public. Public perception of statistics is key to the success of official statistics. Keeping the clients satisfied is absolutely essential for the producers of statistics. This is achieved by observing some fundamental principles of official statistics and promoting them. Any government statistics office must (1) retain users' trust using strictly professional considerations for decisions on methodology, terminology and data presentation; (2) establish accountability and transparency by making sources and methods used to compile statistics readily available to users so that they can judge the fitness of use of the data; (3) address erroneous interpretation and preventing misuse of statistics by explaining perceived erroneous interpretation and misuse of statistics; (4) safeguard the confidentiality of individual's data; and (5) strictly adhere to the legislation by following laws, regulations and measures under which the statistical systems operate for public benefit.

The importance of statistics in economic development has been recognised by the Government of Japan [16] via observing 18 October as 'the Statistics Day' every year. This day was fixed on 3 July 1973 by the Japanese Cabinet for the purpose of strengthening the national concern and understanding of the importance of statistics and promoting their cooperation in surveys held by the central and local governments. Interestingly, 18 October is the day when the Japanese Government proclaimed the order to compile its first modernistic statistics, 'Fuken Bussan-hyo' in 1870. The day was converted from the lunar calendar day, 24 September, to the solar calendar day, 18 October (see Statistics Day in Japan). The United Nations Statistical Commission in collaboration with the International Statistical Institute (ISI) celebrated the second World Statistics Day [17] on 20 October 2015 to raise awareness of the many achievements of official statistics premised on the core values of service, professionalism, and integrity. The event was celebrated in various ways in over 130 countries. Details on this are found on the World of Statistics website.

## MISUSE AND ABUSE OF STATISTICS

In spite of world-wide recognition of statistics and its benefits, the vast majority of ordinary

citizens are not well versed with the statistics and what it has done for them. Worse even is the deliberate abuse of statistics for unfair benefit and ignorantly spreading misgivings on statistics. This is a challenge for all statisticians as well as the producers and users of statistics to reach out to people in the community and to remove misconceptions and present statistics to them in a way that is easily understood and appreciated and thereby removing any misconception.

To undermine statistics and its phenomenal contribution to humanity, some ignorant people and learned sceptics call upon a quote falsely attributed to the American author and humourist Mark Twain (actual name Samuel Langhorne Clemens), "There are three kinds of lies: lies, damned lies and statistics". Stephen Goranson wrote on the Mark Twain Forum on 31 July 2002: Twain's Autobiography attribution of a remark about lies and statistics to a former Prime Minister of the UK, Benjamin Disraeli is generally not accepted. However, the phrase appeared in 1895 in an article by Leonard H. Courtney [18] suggests that the origin of the phrase is still uncertain, but suspected to be from another British politician Sir Charles Dilke (The Bristol Mercury, 19 October 1891) who said, false statements might be arranged according to their degree under three heads, fibs, lies, and statistics. It may not be at all wrong to replace the word 'statistics' in the above quote with 'politics'.

Regardless of the source, the inclusion of the term 'statistics' in the phrase is misleading, at least in the modern sense of the word, and as a key scientific discipline. Should we then be blaming the person behind the abuse or the discipline being abused? Isn't it, then, synonymous with rewarding the criminal and punishing the victim? Unfortunately, the so called quote is not going away anytime soon. So we have to live with it not only preserving the innocence of statistics but also promoting its enormous goodness to society. It is worth remembering the fact, 'figures don't lie, but liars can figure' or 'figures fool, when fools figure'.

The abuse of statistics is not new, and has been occurring as a result of ignorance or deliberate acts of dishonest people, as noted by Josefina Mota, "There are two ways of lying. One, not telling the truth and the other, making up statistics." And "There are two kinds of statistics, the kind you look up and the kind you make up" Rex Stout. The problem is with the 'make up' and the one who is 'making up', but not with statistics as a discipline. Stephen Leacock stated, "In ancient times they had no statistics so they had to fall back on lies." In the contemporary world statistics is being used even in the courts to identify and punish the criminals.

Controversial Canadian psychology professor John Philippe Rushton [19] at the University of

Western Ontario claimed in the early nineties that the Whites tend on average to score higher than test takers of African ancestry on IQ tests, and subsequent findings that test takers of East Asian background tend to score higher than whites. Rushton's controversial work was heavily criticized by the scientific community for the questionable quality of its research based on highly biased convenience sampling with many alleging that it was conducted under a racist agenda. Since 2002, he was head of the Pioneer Fund, a research foundation that has been widely accused of being racist.

Flaherty [20] wrote, "In 1998, Dr Andrew Wakefield, a British gastroenterologist, described a new autism phenotype called the regressive autism-enterocolitis syndrome triggered by environmental factors such as measles, mumps, and rubella (MMR) vaccination. The speculative vaccination-autism connection decreased parental confidence in public health vaccination programs and created a public health crisis in England and questions about vaccine safety in North America. After 10 years of controversy and investigation, Dr Wakefield was found guilty of ethical, medical, and scientific misconduct in the publication of the autism paper. Additional studies showed that the data presented were fraudulent. The alleged autism-vaccine connection is, perhaps, the most damaging medical hoax of the last 100 years." (c.f. DOI: 10.1345/aph.1Q318).

In November 2015, the republican Presidential Candidate in the USA, Donald Trump tweeted "Whites killed by blacks – 81%", citing "Crime Statistics Bureau – San Francisco". The US fact-checking site *PolitiFact* says – "Bureau" did not exist, and the true figure is around 15%. When confronted, Trump shrugged and said, "Am I going to check every statistic?" During the recent Brexit movement in the UK, Boris Johnson's campaign bus slogan was "We send the EU £350m a week." This is another political abuse of statistics as the UK's net contribution is more like £250m a week when rebates are taken into account – and after subsidies and grants the figure reduces to £136m. Once again the people of power know the power of statistics and hence they conveniently abuse statistics to their benefit, even if it compromises their honesty and knowledge, and at the end blame the victim.

## CONCLUDING REMARKS

The best sellers of statistics are the main users of statistics. Among them are the policy makers in the government departments, business executives in the private sector, research communities, and international agencies. Everyone who is part of these agencies should take responsibility to produce



high quality statistics to ensure its appropriateness, accuracy, and expected benefits. All good journalists use statistics to prepare reliable reports on various socio-economic and administrative issues. The value and power of good statistics are well known to them. They play a key role in promoting and popularising statistics to the public. Media related people should have sound knowledge and understanding of statistics to ensure correct interpretation and avoid its unintentional misuse or abuse. There are many users of statistics engaged in the consultancy business as administrators or experts. These people could directly promote the use and benefits of statistics in industry and business.

As a continually growing subject, statistics is always in search of better methods to improve on the existing ones, and introducing new methods for emerging problems. The researchers and producers of statistics must be abreast all the time so that the users get the best results possible. This is equally applicable to everyone engaged in providing crucial information for planning and development for public or private institutions. In this context the goals of World Statistics Day, "Official statistics help decision makers develop informed policies that impact millions of people. Improved data sources, sound statistical methods, new technologies and strengthened statistical systems enable better decisions that eventually result in better lives for all of us" is absolutely important to the statistics community everywhere. The old rule 'use it or lose it' applies.

## REFERENCES

- [1] UN Better Data, <http://www.un.org/en/development/desa/news/statistics/better-data-better-lives.html>
- [2] UN Economic and Social Affairs video, <https://www.youtube.com/watch?v=TIpF3iyiT2g>
- [3] S Unemployment Rate, <https://data.bls.gov/timeseries/LNS14000000>
- [4] CBS News <http://www.cbsnews.com/news/jobs-report-unemployment-rate-drops-to-78-percent/>
- [5] Australian Institute of Health and Welfare (AIHW). <http://www.aihw.gov.au/cancer/cancer-in-australia-overview-2014/appendixb/#t1>
- [6] Breast Cancer Network Australian (BCNA). <https://www.bcna.org.au/understanding-breast-cancer/#sthash.iJyB2HVg.dpuf>
- [7] Gauss CF, Theoria motus corporum coelestium in sectionibus conicis solem ambientium, 1809.
- [8] LinkedIn Blog, <https://blog.linkedin.com/2016/01/12/the-25-skills-that-can-get-you-hired-in-2016>
- [9] Kolmogorov AN, Grundbegriffe der Wahrscheinlichkeitsrechnung. Berlin, Springer, 1933.
- [10] Morrison N. Foundations of the Theory of Probability. New York, Chelsea, 1950.
- [11] Nolan, D and Lang, TD, "Computing in the Statistics Curricula", The American Statistician, 64 (2), 2010, pp.97-107.
- [12] Klemens B. Modeling with Data: Tools and Techniques for Statistical Computing, Princeton University Press, 2008.
- [13] Khan S, "Statistics on Spotlight: World Statistics Day 2015", 2015. World of Statistics Website, <http://www.worldofstatistics.org/files/2015/10/Article-WSD-2015-2.pdf>
- [14] Khan S, "Statistics in planning and development", Pakistan Journal of Statistics, 29 (4), 2013, pp. 513-524.
- [15] MDG Report 2015, [http://www.un.org/millenniumgoals/2015\\_MDG\\_Report/pdf/MDG%202015%20rev%20\(July%201\).pdf](http://www.un.org/millenniumgoals/2015_MDG_Report/pdf/MDG%202015%20rev%20(July%201).pdf)
- [16] MDG Report 2015, [http://www.un.org/millenniumgoals/2015\\_MDG\\_Report/pdf/MDG%202015%20rev%20\(July%201\).pdf](http://www.un.org/millenniumgoals/2015_MDG_Report/pdf/MDG%202015%20rev%20(July%201).pdf)
- [17] Hoss Statistics Day in Japan, <http://www.stat.go.jp/english/index/seido/8-i166.htm>
- [18] World Statistics Day, <http://unstats.un.org/unsd/wsd/>
- [19] Courtney LH, 1895, <http://www.york.ac.uk/depts/maths/histstat/lies.htm>
- [20] Rushton, J P. [https://en.wikipedia.org/wiki/J.\\_Philippe\\_Rushton](https://en.wikipedia.org/wiki/J._Philippe_Rushton)
- [21] Flaherty DK, "The Vaccine-Autism Connection: A Public Health Crisis Caused by Unethical Medical Practices and Fraudulent Science", Annals of Pharmacotherapy, 45(10), 2011, pp.1302-4.

***Technical Papers***

## ***Science***

## SEA LEVEL IN A CHANGING CLIMATE

Maria McCrann<sup>1</sup>, Dr John Russell<sup>2</sup>, Dr Daniela Ionescu<sup>3</sup> and Dr Bandita Mainali<sup>4</sup>  
1,2,3,4 School of Engineering and Mathematical Sciences, La Trobe University, Australia

### ABSTRACT

The rise of the oceans level could have devastating consequences for coastal settlements and it can easily be one of the most critical effects of Climate Change. Thus, all factors affecting sea level need to be considered. One of these factors discussed in this paper is the natural variability originated in the oscillation of the planets and solar activity. The effect of Sun's activity on Earth's climate has been identified since the eighteen hundreds. However, there are still many unknowns regarding the mechanisms connecting the Earth's climate to the variation in solar irradiance. Climate modelling implementing the solar sciences is a novel approach that accounts for the considerable effect that natural factors has on the climate especially at regional level. This paper discusses the noticeable effect that the planets oscillations have on the Sun's activity, which is in very good correlation with the observed patterns in global surface temperatures, rainfall records, and sea levels. In agreement with many studies that identified a 60-years cycle in the variation of Earth's temperature, it is expected that the surface temperatures will reach a trough of the cycle around 2030-2040. Furthermore, considering the influence of the Solar Inertial Motion, a solar slowdown is predicted for Solar Cycles 24 and 25, which will create a weak grand minimum. It is anticipated that this weak grand minimum to be reflected in a dampening effect of global temperatures and a subsequent moderation in the rate of sea level rise.

*Keywords: Solar Activity, Sea Level Rise, Planetary Oscillations, 60-years Cycle*

### INTRODUCTION

There is abundant evidence of large changes in sea level during the Earth's past history. For example, about 120,000 years ago during the warm period, the average global temperature was about 2 degrees Celsius higher than today and the sea level exceeded 5 meters above present levels. Then, 22,000 years ago during the Ice Age, sea level was 120 meters lower than today [1].

Paleoclimate reconstructions based on climate proxies such as ice cores, tree rings, and lake sediments, enable links between the Earth's warm and cool periods with the Sun's activity. Most reconstructions of the solar activity are based on the sunspot number, and the solar cycles' length or frequency. Eddy [2] noted a correlation between periods of significant change in the number of sunspots in the past millennium and large changes in the climate of the Earth. Hence, many studies reported that during periods of low solar activity, lower than average European temperatures were recorded [3]–[7]. Such periods of low solar activity are, the Maunder minimum (1645-1715), Dalton minimum (1800-1820), 1900 minimum (1880-1900), and a slight decrease between 1940 and 1970. Also, a sharp maximum in the global temperatures around 1830 is connected to high solar activity. Superimposed on these long-term trends of minima and maxima are short-term fluctuations caused by the Schwabe cycle [8], [9]. Furthermore, other studies suggest that the climate and atmospheric oscillations such as the Pacific Decadal Oscillation (PDO), the Atlantic Multi-decadal Oscillation (AMO) and El Nino Southern Oscillation (ENSO) are synchronized to the natural oscillations of the Solar System, which are driven by the movements of the planets around the Sun and lunar gravitational tides [7], [10]–[12]. In addition, Chambers et al. [13] identified multi-decadal oscillations of about 60-years in most of the ocean tide

gauges examined, believed to be related to wind forcing and currents variation [14]. As such, they are not spatially uniform and are directly associated with atmospheric oscillations such as the PDO, AMO and ENSO, and they influence sea surface temperatures, pressure levels and surface winds [15]. Moreover, Reid [16] compared the long term trend of Sea Surface Temperature (SST) with the corresponding trend of solar activity and found a significant correlation especially during the minima periods.

Numerous studies reported that the Sun's activity is moderated by the planets oscillation on the Solar system, modifying so the relative location of the Barycenter to the Sun's centre of mass [10], [17], [18]. These studies also noted that the oscillations of the planets have a close link with the variations of Earth's global average temperatures, sea temperatures, and sea levels.

Church and Zhang [19] suggested that coastal regions are mainly impacted by the combined effect of long term sea-level rise and natural variability. The fact that sea-level rise is not uniform across the worldwide oceans, makes it difficult to separate natural variability from the signal of climate change at a regional scale. In agreement with the Intergovernmental Panel for Climate Change (IPCC) physics-based projections models, Church and Zhang [20] indicated that sea-level changes are likely to show over 80% of the world's oceans by 2030. However, Lyu et al. [21] suggested that, in the next 20 years, at a regional scale, the signature of natural variability is likely to exceed the effect of the anthropogenic climate change on the rise of sea level for many areas of the globe.

In spite of the general agreement that Solar activity affects the Earth's climate, opinion that is supported by the broad data and re-emerging theories, the solar effects on climate are not yet well defined. Jones et al. [22] used a simple climate model to assess the potential

implications for future climate projections for a range of solar radiance scenarios. However, this study was based on Total Solar Irradiance (TSI) variations and concluded that the use of TSI may not capture the net effect of solar variability as it fails to incorporate UV variability and 'top-down' influences through stratospheric changes. Even though the solar influence shows small effects on global temperatures when compared with the modelled anthropogenic effects, the regional and seasonal variations around the globe have a closer link to the solar activity. Hence, modelling regional climate needs to consider a larger forcing due to solar and natural variability [4], [23]. Subsequently, it is expected that the regional sea level changes will be closely related to the natural variability and solar forcing.

Van Loon and Meehl [7] found that when the sunspots peak and the North Atlantic Oscillation (NAO) are in phase, there is an intensified positive NAO with negative Sea Level Pressures (SLP) anomalies in the North Atlantic greater than 6 hPa and positive anomalies of about 3 hPa in the subtropical North Atlantic. This is likely to have a considerable effect in ocean's basins given that under a positive NAO index (NAO+), the 'inverse barometer effect' is observed on regional basis, where the reduction in atmospheric pressure creates a regional rise in sea level. This effect is important to both the interpretation of historic sea level records and the predictions of future sea level trends, as mean pressure fluctuations of the order of few hectopascals can lead to sea level fluctuations of the order of centimetres [24].

There are various factors contributing to sea level rise, though the thermal expansion of water in the oceans is the most influential and accounts for about 35% of the predicted sea level rise [25]. Thermal expansion of the oceans is complex and depends on the water temperature, the global surface temperature, and the oceans thermal inertia. Therefore, observing the trends and oscillations of global temperature can serve as a guide on how oceans will behave.

Some studies [26], [27], reported that the average global temperature records are characterised by decadal and bi-decadal oscillations. In general, these oscillations are in good correlation with the 11-years Schwabe and the 22-years Hale Solar cycles, with higher global temperatures related to higher solar activity. Current predictions on the Solar activity show that we are in a low sunspot cycle similar to that of the 1900 Minimum and the subsequent cycles are predicted to present even lower Solar activity, therefore a drop in global temperatures is expected [28]–[30]. Considering the significant influence of the thermal expansion of the oceans, it is predicted that the sea level will follow the global temperature oscillations (with a lag due to thermal inertia), resulting in a subsequent moderation in the rate of sea level rise, as it happened in 2010-2011 due to an exceptionally strong La Nina event [31].

## SEA LEVEL

There are two main data sources for global sea level namely satellite altimeters and tide gauges. Figure 1 presents the Global Mean Sea Level (GMSL) monitored

between 1993 and 2015 by the satellite TOPEX/Poseidon, Jason-1, and Jason-2, which shows a linear trend and a rate of increase of  $3.4 \pm 0.4$  mm/yr [32].

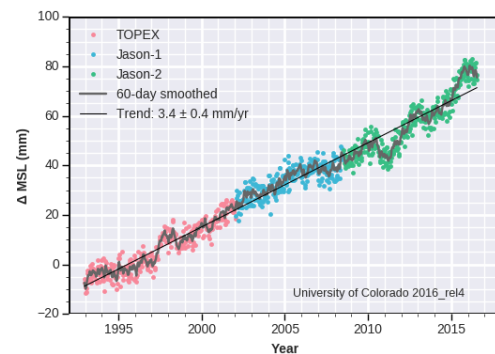


Fig. 1 Satellite altimetry time series 1993-2016 [32]

It is important to note that there are many methods used to review the sea level rise, employing different trend approaches and assumptions, which at times lead to contradictory acceleration – deceleration inferences. This aspect has been reviewed in detail by Visser et al. [33]. They explored the sea level trends using more than one method in addition to cyclic or additional information such as the SOI or PDO to provide a better trend description. Furthermore, Watson [34] developed a methodology to provide a consistent transparent appraisal of acceleration in mean sea level records using the Singular Spectrum Analysis (SSA). This technique readily separates the trend of sea level from the 60 years dynamic ocean oscillations and noise.

The limitation of Satellite data (Fig. 1) is that spans only over 20 years, hence cannot encapsulate and describe larger multi-decadal scale natural oscillations. In contrast, tide gauges offer a long term view of the changes in mean sea level. Though, the tide gauges are located in the Northern Hemisphere (Europe, Japan, the United States), providing poor sampling. Additionally, tide gauge records do not cover the same time period [35]. Therefore, it is useful to define sea level variation on a regional base considering a wide range of local processes to eliminate misleading estimates that global ocean level average could introduce. Furthermore, the effects of natural variability are likely to influence ocean levels without adding to the volume.

## FUNDAMENTAL DRIVERS FOR NATURAL CLIMATE CHANGE VARIABILITY

Fluctuations in the oceans levels are common and this paper investigates their relationship with natural variability and oscillations. These natural oscillations have drivers such as the solar variations, the planetary forces, and Earth's orbital changes. It is suggested that these three natural drivers for climate variability have noticeable influence in surface temperature patterns and consequently sea level rise. Other natural drivers such as volcanic eruptions and regular, repeatable lunar motions are excluded from this paper [36].

## Solar Variation

In 1843, astronomer Henrich Schwabe was the first to demonstrate the 11-years cycle of the sunspots. English astronomer Walter Maunder reported that from 1645 to 1715 sunspots had been generally absent. Such period with a minimum number of sunspots is now known as the Maunder Minimum and was accompanied, in Europe and other regions, by the most severe temperature dip for several millennia [37].

Eddy [2] noted a correlation between periods of significant change in the number of Sunspots in the past millennium and large changes in the climate of the Earth. Figure 2 illustrates the correlation between the Sunspots activity and the drops of temperature registered in history. It is clear the periods of minimum temperature occurred when the number of sunspots registered was considerably lower than for other periods.

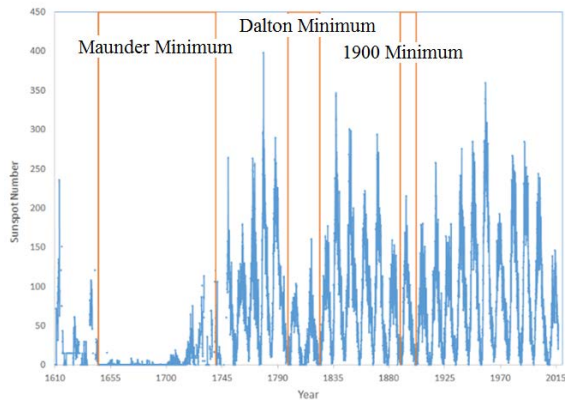


Fig. 2 Sunspots numbers and the periods of reduced Solar activity (after [8], [45]).

The solar activity alternates between active and quiet phases with a frequency of 11 years known as the Schwabe cycle. Figure 3 presents the 11-years cycles of solar activity. It shows a maximum of 150 sunspots for Cycle 24, contrasting with 81.9 sunspots reported NOAA in April 2014. This is the cycle with the lowest maximum of sunspots since Cycle 14, which had a maximum of 64.2 sunspots in February of 1906. Cycle 14 coincides with the 1900 Minimum [30].

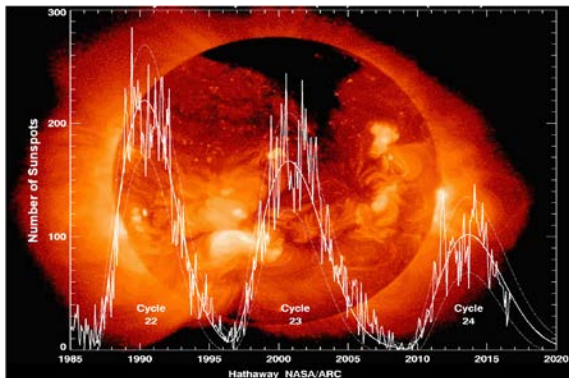


Fig. 3 Projected and observed sunspots [38].

The variations in the sunspot number reflects the solar activity and therefore is related to the changes in TSI. The monitored values of TSI since the beginning of the 1990s shows a decline and the last value measured for Cycle 24 was  $1361.53 \text{ W/m}^2$ .

According to research undertaken by Hathaway [38], it is expected that Solar Cycle 25, peaking around 2022, be the weakest one [30]. It is anticipated that the reduction in Sun's activity to result in temperature drops due to reduced energy received. These changes in TSI would be level out by the thermal inertia of the ocean. However, low TSI for two or more consecutive cycles will cause temperatures drop and delayed sea level rise decline due to the thermal inertia of the ocean. It is worth noting that the variation of the TSI might be increased by feedback mechanisms that amplify the solar variations generating large weather effects. It is believed that some of these mechanisms are radiative forcing, cosmic rays, the stratospheric solar vortex, cloud cover and albedo, cosmic rays related to changes of the ozone layer, etc. [39], [40]. However, these mechanisms are outside the scope of this paper.

## Planet forces

In addition to the findings reported earlier, many studies indicated that the Sun's activity is moderated by the Solar System planets oscillations which shift the location of the Solar System Center of Mass (SSCM) or the Solar System Barycenter (SSB) [29], [41]–[43]. Furthermore, it has been noted a close link between planetary oscillations and Earth's global average temperatures variation, thus with the sea temperatures and the sea levels.

Charvátová [44] reviewed work by Paul Jose who was one of the first researcher to link solar modulation with planetary movements. Jose observed that the Sun oscillates around the center of mass of the Solar System (Barycenter), in order to balance the variation in planets position, hence the center of gravity remains at rest. The Solar Inertial Motion (SIM) and Solar variability studies found that the planets returned to roughly the same position every 178.8 years or 172 years as suggested by others, a frequency that is similar to that of sunspots activity [53].

The extent of Sun oscillation around the Solar System Barycenter is affected by the relative mass of the planets as displayed in Fig. 4. Figure 4(a) shows the position of the center of gravity of the Solar System. Figure 4(b) simulates the significant shift in the position of Barycenter when Jupiter is removed from the Solar System. Figure 4(c) presents the change in the location of the center of gravity if both Jupiter and Saturn are removed. Once Neptune is removed, the effect of the remaining planets is barely noticeable. Hence, Jupiter has the highest effect on SIM due to its largest mass [10], [29].

The gravitational forces between planet and Sun affect the Solar System dynamics causing harmonic resonances that also modify magnetic and electrical forces. According to Sharp [29], these harmonic drivers can be separated into three levels.



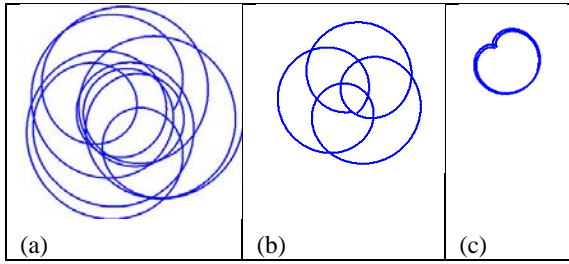


Fig. 4 Sun's path around the Barycenter (not to scale) when: (a) including all planets; (b) removing Jupiter; (c) removing Jupiter and Saturn [45].

Level 1 includes the Ice Age Cycles due to orbital changes as stated by Sharp, reporting on work by Milankovitch [36]. These cycles are very long and affect long term climate variations such as glacial and interglacial periods.

Level 2 comprises of Solar Grand Minimum and Solar Modulation Cycles. This level is governed by the SIM theory, which states that the Sun follows a kaleidoscope like pattern orbit around the SSB [46] as shown in Fig. 4. The wobble of the Sun generates changes in its Angular Momentum (AM), velocity, acceleration, and torque. Several studies have found a correspondence between the Grand Minima and the variations of the position of the Sun relative to the Barycenter [29], [43], [47], [48]. Sharp [29] stated that this level is modulated by the 172 years conjunction of Neptune and Uranus and suggested a spacing of 172-179 years between Grand Minima. Based on the influence of the Solar Inertial Motion a solar slowdown is expected for Solar Cycles 24 and 25 that will create a weak grand minimum expected to trough around 2030. The implications of this predicted weak grand minimum can be expected to be observed in a decline in global temperatures and a subsequent moderation in the rate of sea level rise.

Level 3 refers to the well-known 60-years cycle in the Earth's temperature record that seems to align with the PDO/ENSO records. There is significant evidence [11], [26] showing a coincidence between the global temperature record and two Solar System harmonic patterns, the Solar velocity 60-years cycle and the Jupiter/Saturn synodic harmonic cycle along with Lunar harmonics.

### THE 60-YEARS OSCILLATION AND SEA LEVEL

Chambers et al. [13] identified a significant oscillation of about 60-years in the majority of the tide gauges examined. Using the average of tide gauges in five ocean regions, Chambers team found similar phase and amplitude for North Atlantic, Western North Pacific and Indian Oceans, while for the Western South Pacific there was a 10 years lag in the monitored tide gauges. Though, the mean sea level measured in the Central/Eastern North Pacific region did not show a 60 years fluctuation. As mentioned earlier, Chambers [14] suggested that these fluctuations are related to wind forcing and currents variation, which are not spatially

uniform. Although, Baldwin and Dunkerton [15] found a direct correlation between these atmospheric factors and the atmospheric oscillations (PDO, AMO, ENSO), which have a significant effect on the sea surface temperatures, pressure levels pressure, and the surface winds.

Merrifield et al. [49] reviewing several studies found that on decadal to multi-decadal time scales, variations of up to 1 cm in the level of the Pacific Ocean, believed to be caused by a combination of Pacific trade winds. There is a consensus regarding the sea level fluctuations in the Western Pacific Ocean with the PDO index, finding based on tide gauge observations that provide a 60-years long record. Also, Van Loon and Meehl [7] stated that the decadal time scale climate variability in the Pacific region was due to external forcing from variations in the solar irradiance and the internal climate variability associated with the PDO. Therefore, Chambers [14] concluded that the regional variability and strong effects of wind stresses in the Pacific Ocean could be the reason why there was no 60-years oscillation found in his analysis for the Central/Eastern North Pacific. Furthermore, Chambers et al. [13] pointed out that incorporating the 60-years oscillation in the mean sea level variation, did not change the overall conclusion that sea levels have been rising on average by 1.7mm/yr over the last 110 years. It simply shows a natural oscillation that permeates into the sea level measurements [13]. Therefore, this natural oscillation should be considered when estimating future sea level rise as proved to be directly related to the planetary orbits and solar activity, which in time modulates atmospheric variables such as PDO, AMO, ENSO, etc.

Figure 5 presents Chambers et al. [13] findings,

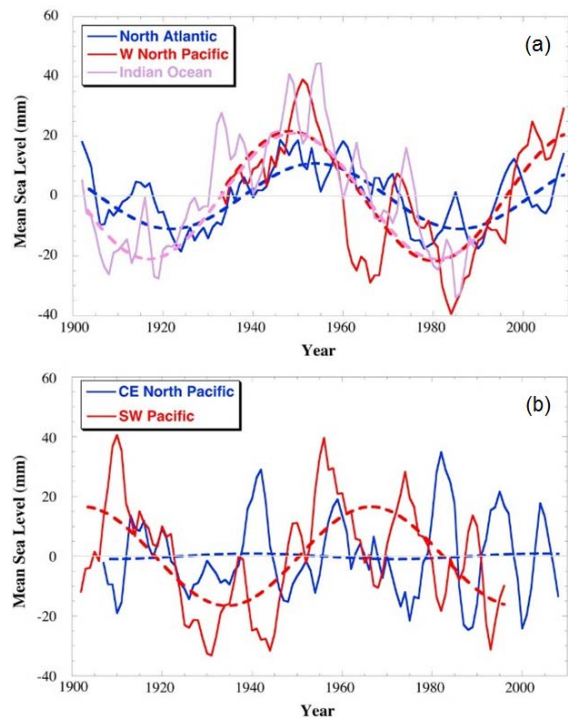


Fig. 5 Sixty-year cycle in Mean Sea Level for world's oceans [13].

which shows a 60-year cycle in the sea level data, smoothed with a 5-years running mean. The North Atlantic variation has an optimal period of 64-years. However, this 64-years oscillation is not evident in the Central Eastern Pacific gauges (Fig. 5). The Western North Pacific and Indian Ocean levels seem to be in phase, whilst the North Atlantic gauges are slightly delayed. The minimum level is around 1915–25, with a peak around 1950–60, and another minimum around 1980–90. The phase of the South Pacific gauges around Australia/New Zealand lags by about 10 years (Fig. 5.b).

Concerns were raised by Chambers et al. [13] in using sea level records shorter than two cycles of 60-years, as at this point it is not fully understood if there is a 60 year oscillation present in the GMSL. High hesitation was articulated by some researchers in lieu with the interpretation of acceleration in GMSL based on only 20-years record from satellite altimetry [13].

Chambers and his team's research (particularly findings presented in Fig. 5), supports the theory of a natural variability underlining the changes in sea level. On the other hand, assuming that thermal expansion may be a key factor contributing to the sea level rise and based on the premise of the effects of solar activity, it is logical to predict that a reduction in the global average temperatures might manifest in a consequent slowing of the rate of sea level rise.

## CONCLUSION

The oscillations of the planets have a noticeable effect on the Sun's activity and shows a good correlation with the observed patterns in global surface temperatures and sea levels.

Based on the influence of the Solar Inertial Motion a solar slowdown is expected for Solar Cycles 24 and 25 that will create a weak grand minimum which combined with the 60-years cycle is likely to dip around 2030-2040. The implications of this weak grand minimum can be expected to be reflected in a dampening effect of global temperatures and a subsequent slowing in the rate of sea level rise. This dampening effect is expected to be more noticeable when assessing climate variability on a regional scale for decadal and multi-decadal projections.

The combination of natural forces and anthropogenic effects is paramount when analyzing our climate, as the natural variability has a larger effect at a regional scale. Therefore, the inclusion of solar and planetary influences in regional models is recommended.

## ACKNOWLEDGEMENTS

The authors would like to thank Phil Watson from the University of New South Wales, Nicola Scafetta, Don Chambers and Geoff Sharp, for clarification and comments. This work is sponsored by the Australian Postgraduate Award (APA).

## REFERENCES

[1] Masson-Delmotte V, Schulz M, Abe-Ouchi A, Beer J,

Ganopolski A, González Rouco J, Jansen E, Lambeck K, Luterbacher J, Naish T, Osborn T, Otto-Bliesner B, Quinn T, Ramesh R, Rojas M, Shao X, and Timmermann A, "Information from paleoclimate archives climate", *Clim. Chang.* 2013: Phys. Sci. Basis. Contrib. Work. Gr. I to Fifth Assess. Rep. Intergov. Panel Clim. Chang., Cambridge University Press, 2013.

[2] Eddy JA, "The Maunder Minimum", *Science*, Vol. 192, No. 4245, 1976, pp. 1189–81202.

[3] Ineson A, Scaife AA, Knight JR, Manners JC, Dunstone NJ, Gray LJ, and Haigh JD, "Solar forcing of winter climate variability in the northern hemisphere", *Nat. Geosci.*, Vol. 4, No. 11, pp. 753–757, 2011.

[4] Lockwood M, "Solar influence on global and regional climates", *Surv. Geophys.*, Vol. 33, No. 3–4, 2012, pp. 503–534.

[5] Scafetta N, "Discussion on climate oscillations: CMIP5 general circulation models versus a semi-empirical harmonic model based on astronomical cycles", *Earth-Science Rev.*, Vol. 126, 2013, pp. 321–357.

[6] Scafetta N, "Multi-scale dynamical analysis (MSDA) of sea level records versus PDO, AMO, and NAO indexes", *Clim. Dyn.*, Vol. 43, No. 1–2, 2014, pp. 175–192.

[7] Van Loon H and Meehl GA, "Interactions between externally forced climate signals from sunspot peaks and the internally generated Pacific Decadal and North Atlantic Oscillations", *Geophys. Res. Lett.*, Vol. 41, pp. 161–166, 2014.

[8] Beer J, Mende W, and Stellmacher R, "The role of the sun in climate forcing", *Quat. Sci. Rev.*, Vol. 19, No. 1–5, 2000, pp. 403–415.

[9] Gray LJ, Beer J, Geller M, Haigh JD, Lockwood M, Matthes K, Cubasch U, Fleitmann D, Harrison G, Hood L, Luterbacher J, Meehl GA, Shindell D, Van Geel B, and White W, "Solar influence on climate", *Rev. Geophys.*, Vol. 48, No. 2009, 2010, p. RG4001.

[10] Scafetta N, "Empirical evidence for a celestial origin of the climate oscillations and its implications", *J. Atmos. Solar-Terrestrial Phys.*, Vol. 72, No. 13, 2010, pp. 951–970.

[11] Mazzearella A and Scafetta N, "Evidences for a quasi 60-year North Atlantic Oscillation since 1700 and its meaning for global climate change", *Theor. Appl. Climatol.*, Vol. 107, No. 3–4, 2012, pp. 599–609.

[12] Wang Z, Wu D, Song X, Chen X, and Nicholls S, "Sun-Moon gravitation-induced wave characteristics and climate variation", *J. Geophys. Res. Atmos.*, Vol. 117, No. 7, 2012, pp. 1–20.

[13] Chambers DP, Merrifield MA, and Nerem RS, "Is there a 60-year oscillation in global mean sea level?", *Geophys. Res. Lett.*, Vol. 39, No. 17, 2012, pp. 1–6.

[14] Chambers DP, "Personal communication", 2015.

[15] Baldwin MP and Dunkerton TJ, "The solar cycle and stratosphere – troposphere dynamical coupling", *Geophys. Res. Lett.*, Vol. 34, No. 16, 2007, pp. 71–82.

[16] Reid GC, "Solar total irradiance variations and the global sea surface temperature record", *J. Geophys. Res.*, Vol. 96, No. 2, 1991, pp. 2835–2844.

[17] Lockwood M Bell C, Woolings TH Harrison RG Gray LJ and Haigh D, "Top-down solar modulation of climate: evidence for centennial-scale change," *Environ. Res. Lett.*, Vol. 5, No. 3, 2010, p. 34008.



- [18] Scafetta N, "Does the Sun work as a nuclear fusion amplifier of planetary tidal forcing? A proposal for a physical mechanism based on the mass-luminosity relation", *J. Atmos. Solar-Terrestrial Phys.*, Vol. 81–82, 2012, pp. 27–40.
- [19] Zhang X and Church JA, "Sea level trends, interannual and decadal variability in the Pacific Ocean", *Geophys. Res. Lett.*, Vol. 39, No. 21, 2012, pp. 1–8.
- [20] Church JA and Zhang X, "15 years from now, our impact on regional sea level will be clear", *The conversation*, 2014.
- [21] Lyu K, Zhang X, Church JA, Slangen ABA, and Hu J, "Time of emergence for regional sea-level change", *Nat. Clim. Chang.*, Vol. 4, No. 11, 2014, pp. 1006–1010.
- [22] Jones GS, Lockwood M, and Stott PA, "What influence will future solar activity changes over the 21st century have on projected global near-surface temperature changes?", *J. Geophys. Res. Atmos.*, Vol. 117, No. 5, 2012, pp. 1–13.
- [23] Kirtman B, Power SB, Adedoyin JA, Boer GJ, Bojariu R, Camilloni I, Doblas-Reyes FJ, Fiore AM, Kimoto M, Meehl GA, Prather M, Sarr A, Schär C, Sutton R, Van Oldenborgh GJ, Vecchi G, and Wang H-J, "Near-term climate change: projections and predictability", *Clim. Chang. 2013: Phys. Sci. Basis. Contrib. Work. Gr. I to Fifth Assess. Rep. Intergov. Panel Clim. Chang.*, Cambridge University Press, 2013, pp. 953–1028.
- [24] Woolf DK, Shaw AGP, and Tsimplis MN, "The influence of the North Atlantic Oscillation on sea-level variability in the North Atlantic region", *J. Atmos. Ocean Sci.*, Vol. 9, No. 4, 2003, pp. 145–167.
- [25] Church JA, Clark PU, Cazenave A, Gregory JM, Jevrejeva S, Levermann SA, Merrifield MA, Milne GA, Nerem R, Nunn PD, Payne AJ, Pfeffer WT, Stammer D, and Unnikrishnan AS, "Sea level change: the physical science basis", *Clim. Chang. 2013: Phys. Sci. Basis. Contrib. Work. Gr. I to Fifth Assess. Rep. Intergov. Panel Clim. Chang.*, Cambridge University Press, 2013, pp. 1137–1216.
- [26] Ghil M and Vautard R, "Interdecadal oscillations and the warming trend in global temperature time series", *Nature*, Vol. 350, 1991, pp. 324–327.
- [27] Lockwood M, Owens MJ, Barnard L, Davis CJ, and Steinhilber F, "The persistence of solar activity indicators and the descent of the Sun into Maunder Minimum conditions", *Geophys. Res. Lett.*, Vol. 38, No. 22, 2011, pp. 1–5.
- [28] Sharp G, "Are Uranus and Neptune responsible for Solar Grand Minima and Solar Cycle Modulation?", *Int. J. Astron. Astrophys.*, Vol. 3, 2013, pp. 260–273.
- [29] Hathaway DD, "Solar cycle prediction", *NASA Solar Physics*, 2016. [Online]. Available: <https://solarscience.msfc.nasa.gov/>.
- [30] Fasullo JT, Boening C, Landerer LW, and Nerem RS, "Australia's unique influence on global sea level in 2010-2011", *Geophys. Res. Lett.*, Vol. 40, No. 16, 2013, pp. 4368–4373.
- [31] Nerem R, Chambers D, Choe C, and Mitchum GT, "Estimating mean sea level change from the TOPEX and Jason Altimeter Missions", *Mar. Geod.*, Vol. 33, No. 1, Supp 1, 2010, p. 435.
- [32] Visser H, Dangendorf S, and Petersen AC, "A review of trend models applied to sea level data with reference to the 'acceleration-deceleration debate'", *J. Geophys. Res. Ocean.*, Vol. 120, No. 6, 2015, pp. 3873–3895.
- [33] Watson PJ, "Acceleration in U.S. mean sea level? A new insight using improved tools", *J. Coast. Res.*, 2016.
- [34] Jevrejeva S, Grinsted A, Moore J, and Holgate S, "Nonlinear trends and multiyear cycles in sea level records", *J. Geophys. Res. Ocean.*, Vol. 111, No. 9, 2006, pp. 1–11.
- [35] Fasullo JT, Nerem RS, and Hamlington B, "Is the detection of accelerated sea level rise imminent?", *Sci. Rep.*, No. 6:31245, Aug. 2016, pp. 1–6.
- [36] Hoyt DV and Schatten KH, *The role of the sun in climate change*. 1997.
- [37] NASA, "NASA long range solar forecast", 2016. Available: [http://science.nasa.gov/science-news/science-at-nasa/2006/10may\\_longrange/](http://science.nasa.gov/science-news/science-at-nasa/2006/10may_longrange/). [Accessed: 01-Nov-2016].
- [38] Mufti S and Shah GN, "Solar-geomagnetic activity influence on Earth's climate", *J. Atmos. Solar-Terrestrial Phys.*, vol. 73, no. 13, pp. 1607–1615, 2011.
- [39] Lean J, "Cycles and trend in solar irradiance and Climate", vol. 1, no. February, pp. 111–122, 2010.
- [40] Charvátová I, "Can origin of the 2400-year cycle of solar activity be caused by solar inertial motion?", *Ann. Geophys.*, Vol. 18, No. 4, 2000, pp. 399–405.
- [41] Wolff CL and Patrone PN, "A new way that planets can affect the Sun", *Sol. Phys.*, Vol. 266, No. 2, 2010, pp. 227–246.
- [42] Abreu JA, Beer J, McCracken KG, and Steinhilber F, "Is there a planetary influence on solar activity?", *Astron. Astrophys.*, Vol. 548, 2012, pp. A88, 1–9.
- [43] Charvátová I, "Long-term predictive assessments of solar and geomagnetic activities made on the basis of the close similarity between the solar inertial motions in the intervals 1840-1905 and 1980-2045", *New Astron.*, Vol. 14, No. 1, 2009, pp. 25–30.
- [44] Dunn T, "The Solar System Barycenter" 2000 <http://www.orbitsimulator.com/gravity/articles/ssbarycenter.html> [Accessed: 01-Nov-2016]
- [45] Charvátová I, "Solar-terrestrial and climatic phenomena in relation to solar inertial motion", *Surv. Geophys.*, Vol. 18, No. 2–3, 1997, pp. 131–146.
- [46] Paluš M, Kurths J, Schwarz U, Seehafer N, Novotná D, and Charvátová I, "The solar activity cycle is weakly synchronized with the solar inertial motion", *Phys. Lett. Sect. A Gen. At. Solid State Phys.*, Vol. 365, No. 5–6, 2007, pp. 421–428.
- [47] McCracken KG, Beer J, and Steinhilber F, "Evidence for planetary forcing of the cosmic ray intensity and Solar activity throughout the past 9400 years", *Sol. Phys.*, Vol. 289, No. 8, 2014, pp. 3207–3229.
- [48] Merrifield MA, Thompson PR, and Lander M, "Multidecadal sea level anomalies and trends in the western tropical Pacific", *Geophys. Res. Lett.*, Vol. 39, No. 13, 2012, pp. 2–6.

## EBOLA VIRAL PROTEIN 24 (VP24) INHIBITOR DISCOVERY BY IN SILICO FRAGMENT-BASED DESIGN

Syafrida Siregar<sup>1</sup>, Erwin Prasetya Toepak<sup>1</sup>, Usman Sumo Friend Tambunan<sup>1\*</sup>

<sup>1</sup>Bioinformatics Research Group, Department of Chemistry, Faculty of Mathematics and Natural Science,  
Universitas Indonesia, Kampus UI Depok, West Java 16424, Indonesia

### ABSTRACT

Ebola hemorrhagic fever (EHF) is a fatal disease caused by *Ebolavirus* that can potentially lead to death. The number of fatalities reached 11.000 of the 28.000 reported cases. A serious concern should be taken because neither drug nor treatment to cure this disease has been found until now. Recent studies show that viral protein 24 (VP24) is one of the structural protein that plays a key role in EBOV proliferation and viral life cycle. In this study, we tried to find the potential inhibitor for EBOV VP24 through in silico experiment. About 242.520 compounds from ZINC15 In Vitro Database were obtained and screened according to the Rules of Three and pharmacological properties to get a proper lead-like fragment compounds. These compounds were docked into the active site of VP24 using MOE 2014.09 software. The potential fragment compounds were linked to generate potential inhibitor ligands. These ligands were screened earlier based on Lipinski's Rule of Five and toxicity prediction, then they were docked once again to obtain the favourable ligand. Furthermore, the dynamics simulation of best ligand, namely L833, L217 and L595, were performed to predict the ligand-enzyme complex stability. In the end, we conclude that L595 is the best ligand. Moreover, the pharmacological and toxicity prediction also confirm that L595 can be developed as the potential inhibitor for EBOV VP24.

**Keywords:** *Ebolavirus*, *Viral Protein 24*, *Molecular Docking*, *Pharmacological*, *Toxicity Prediction*

### INTRODUCTION

*Ebolavirus* is a part of *Filoviridae* family that can cause a fatal disease like Ebola hemorrhagic fever [1]. The virus is endemic and deadly in humans and nonprimate [2]. Fever, sore throat, muscle aches, and headache are symptoms of Ebola hemorrhagic fever [3]. The spread of this virus has occurred from one country to another such as in West Africa. Liberia, Guinea, Sierra Leone was attacked by *Ebolavirus* in 2014-2015. This disease causes up to 11.297 deaths as reported by WHO [4].

RNA of the *Ebolavirus* genome encodes seven structural protein and one non-structural protein [5]. The encoded structural proteins are transmembrane glycoprotein (GP), nucleoprotein (NP), four viral protein (VP24, VP30, VP35, and VP40) and RNA polymerase (L) [4,5]. VP40 is known to be the principal protein matrix and the most abundant viral protein. It contributes to the proliferation process of EBOV. The viral maturation involves VP40 that joins the cell membrane. The process of viral maturation of infected cells by inducing virion assembly in the plasma membrane [7]. VP24 is the second protein matrix and a minor portion of the viral protein [8]. The VP24 function as viral protein is not known certainly [6,7]. However, as a structural protein, VP24 may play a role in the virion assembly process [8]. Other supporting statements are put forward by Shinji Watanabe et al., 2007. They reported that VP24 can reduce transcription and

replication process of the *Ebolavirus* genome. The direct association of the ribonucleoprotein complex in the infected cells occurs in both processes [9].

In silico study has been used for several years by researchers. This study provides efficient and effective results, as it provides accelerated identification and optimization of drug discovery. Not only researchers, but the pharmaceutical industry has also utilized In silico analysis in their drug design pipeline because it can recommend affinity selectivity to a small number of compounds. Study In silico utilizes the 3D structure of the protein as the starting point of the pharmacological test, and this structure provides a visualization of the interaction occurring in proteins. Vincent Zoete et al. 2009 reported that there are more than 50 compounds of In silico study results that have entered the clinical trial stage and some of them have been approved by The Food and Drug Administration (FDA) [10].

The fragment-based design is one of the drug discovery approaches in Silico study. In a fragment-based approach, the small-molecule formed from low molecular fragments from the molecule period is different from the high throughput screening (HTS) approach. HTS is not yet clear which part of the molecule is heavily involved in the binding energy even though HTS hit binding is obtained by this approach [11].

## METHOD

### Preparation Of Protein VP24

The 3D structure of the target protein become a new approach to structure-based drug design [12]. In this study, the 3D structure of VP24 was obtained from the Protein Data Bank (<http://www.rcsb.org/pdb>), water molecules, and heteromolecules that attached to the protein structures were removed [13]. Lig X function in MOE 2014.09 was applied to viral protein for designing optimized process of VP24.

### Preparation Of Fragment

Fragment database was obtained by downloading the molecules from ZINC15. ZINC15 is a database developed by combining biology and chemoinformatics together. With this database, researchers can access ready-made compounds for virtual screening, ligand discovery [14]. Compounds from the database then screened using RO3 (rule of-three). The main purpose of the screening process is to get molecules that have the desired properties so that it becomes a more efficient sample [15]. The rule of three was applied by using Osiris DataWarrior software, ([www.openmolecules.org/datawarrior/](http://www.openmolecules.org/datawarrior/)). MOE 2014.09 software was applied to get energy minimize and also the partial charge with the same software in an MMFF94x force field software.

### Molecular Docking Simulation Of Oleuropein, Ouabain, And Fragment Database

In this step, we did molecular docking simulation by applying MOE 2014.09 [16] in oleuropein, ouabain and fragment database. Oleuropein is one of phenolic compound in olive leaves. It has been proved by Sebastian Pleško et al. 2015 that oleuropein can act as an inhibitor of VP24 [6]. Edwige Picazo, 2015 reported that ouabain has the possibility to inhibit the activity of VP24 [17]. Molecular docking is to prophesy the natural position, orientation, and conformation of the small-molecule ligand within the binding site of a targeted molecule [10]. The first molecular docking use retains 30. It means 30 times of placement pose as parameters.

### Molecular Redocking Of Oleuropein, Ouabain, And Fragment Database

In addition, redocking also to validate the results from the previous docking simulation. To validate the docking retain 30, we continued redocking retain 100. Redocking was done by using MOE 2014.09 software. The ligands with root mean square deviation (RMSD) values lower than 2.0 and Gibbs binding energy ( $\Delta G_{\text{binding}}$ ) lower than standards will be selected as the best ligand [10].

### Hits Determination, Fragment Linking, And Screening

In the initial stage, we determined the fragment that bound to an amino acid. Then, we searched for a fragment that did not overlap to the first fragment. Both of these fragments were linked by using linker database in MOE 2014.09 to generate potential inhibitor ligands. The results are screened using Lipinski's Rule of Five (RO5). RO5 was applied because it can predict drug-like feature closely related to the efficacy of the drug in clinical trials [18]. Then we performed molecular docking and redocking with the same retain as the previous molecular docking parameter. The results obtained from the simulation were saved in mdb format.

### Analysis Of Protein-Ligand Interaction, Pharmacological And Toxicity Prediction

We determined the protein-ligand interaction by finding the active site of VP24 that bound with low binding energies ligand. At this step, we also applied Toxtree, Osiris DataWarrior VEGA, and experiment to predict pharmacological and toxicity characteristic.

### Molecular Dynamics

In this study, we performed dynamic simulation using MOE 2014.09 as the final step. The first stage in the simulation is ligand preparation. Energy minimization and geometry optimization are applied in dynamics simulation. The process of minimizing energy and optimization is almost similar to the docking simulation stage as well as the parameter except for Generalized Born solvation is applied to dynamics simulation consisting of initialization, equilibration, production. At the initialization, the heating process was performed for 10 ps from 300 K to 312 K. At the equilibration stage was done for 100 ps at 312 K, while in the production phase was set to 20,000 ps at 312 K.

## RESULTS AND DISCUSSION

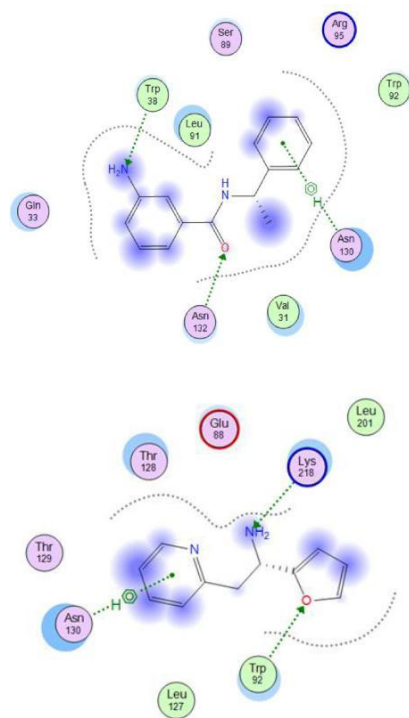
### Set Up Protein VP24

The protein used in this study was obtained from Protein Data Bank (PDB ID 4U2X) as reported by Sebastian Pleško (2015) [6] and Wei Xu (2014) [19] with some modification. The interaction between ligand and one of amino acid residues was considered as a potential inhibitor candidate for EBOV VP24. We minimized the structure of VP24 when RMS Gradient structure of this protein is 0.05 kcal/mol/ Å<sup>2</sup> by using ligX in MOE 2014.09 in Amber10:EHT force field.

## Set Up Fragment Libraries

From ZINC15, we obtained 242,520 compounds. Osiris DataWarrior was used to screen and create the fragment libraries. The rule of three (RO3) was applied for ensuring that fragment libraries contained fragment-like properties and only consisted of simple molecules that can be easy to elaborate [9,12]. The molecule properties in the Rule of Three were applied to screen compounds, and it resulted in 6662 fragments. The criteria of Rule of Three (RO3) follow rules such as [20]: the value of molecular weight are less than 300g/mol; the amount of hydrogen bond acceptor and donor are less than or equal three; the value of cLogP is 3, and have less than or equal with three hydrogen bond donor.

Besides that, some rules are added in RO3, which is the number of rotatable bonds is less than or equal to three and the value of the polar surface area is  $60 \text{ \AA}^2$ . The construction of fragment libraries used Osiris DataWarrior. Toxicity parameters, such as mutagenic, tumorigenic, irritant and developmental toxicity were applied. We obtained 1285 ligands after toxicity screening assay.



**Fig. 1.** Molecular interaction of the protein EBOV VP24 with fragment 30 (top) and fragment 300 (bottom)

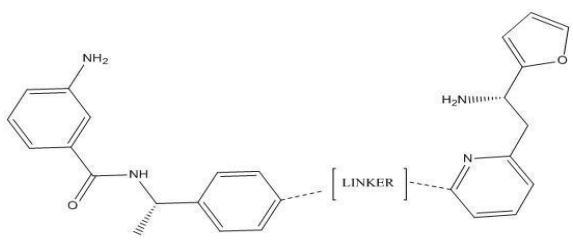
## Molecular Docking Simulation Of Oleuropein, Ouabain, And Fragment Database


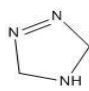

Molecular docking simulation to oleuropein, ouabain, as ligand standards and the fragment database as a sample by using MOE 2014.09 software produced 1285 ligands and delivered a score of binding energy ( $\Delta G_{\text{binding}}$ ) from each ligand. Gibbs free energy binding energy ( $\Delta G_{\text{binding}}$ ) is used to predict which ligand-protein conformation that binds stronger. We also obtained the active site of VP24 at asparagine and tryptophan (Asn130, Asn132, and Trp38). Moreover, we acquired interactions among VP24 with ligands. The first, among asparagine (N130) with fragment number 30 as shown in **Figure 1**. This residue in line with what has been reported by Sebastian Pleško, 2015 [21]. The other with fragment number 300 as shown in **Figure 1**. These fragments are the candidate that would be linked to the next phase and each fragment has RMSD value of 0,8359 and 1,4322, respectively.

## Prediction Of Linking Fragment And Molecular Docking Of Ligands And Potential Fragment

In this step, we linked fragments that resulted from the previous step. Both of fragments were linked with residue amino acids to form a linking fragment. It was expected that all of the linked fragments will produce higher affinity [20]. The linking process was done by using Link Multiple Fragments features in MOE 2014.09 software. The result of linked fragments was screening according to energy minimized and partial charge.

Molecular docking was applied twice with different retain. The docked ligands were given code L and followed by mseq number. In this study, we chose three ligands for selecting. The redocking process was applied to get root mean square deviation (RMSD) score lower than  $2.0 \text{ \AA}$  [10]. The best ligand is L595, 3-amino-*N*-((*S*)-1-(4-((*E*)-1-(6-((*S*)-2-amino-2-(furan-2-yl)ethyl)pyridin-2-yl)-4-hydroxybut-2-en-2-yl)phenyl)ethyl)benzamide which has  $\Delta G_{\text{binding}}$  -54,2638, pKi (inhibition constants) 39,5304 and RMSD 1.5134. Scores  $\Delta G_{\text{binding}}$ , RMSD, pKi and Osiris DataWarrior for three ligands and standard ligands were shown in **Table 1** below.

**Table 1.**  $\Delta G_{\text{binding}}$  energy, pKi, RMSD scores from the selected linked compounds and standard ligands


Ligand	Linker	$\Delta G_{\text{binding}}$ (RMSD)	pKi	Molecular weight	H- Donor	H- Acceptor	C log- P	Polar Surface Area
L833		-54,8520 kcal/mol 1.7644	39,9986	496,633	4	7	2,9530	123,78
L217		-54,8511 kcal/mol 1.9861	39,9582	495,585	3	9	1,8767	135,13
L595		-54,2638 kcal/mol 1.5134	39,5304	496,609	4	7	2,9814	127,40
Oleuropein*		-44,1153 kcal/mol 2,8153	32,1373	540,516	6	13	0,3124	201,67
Ouabain*		-41,2201 kcal/mol 1,1113	30,0282	584,656	8	12	1,4423	206,60

Note: \* standard ligand

**Prediction Drug Scan**

We predicted toxicity and drug likeness for all of ligands and standards ligands by using Osiris DataWarrior, VEGA and Toxtree analysis [22]. Parameters mutagenicity, tumorigenic, irritant effect, and developmental toxicity are showed in Osiris DataWarrior analysis. The result from Osiris

DataWarrior analysis is shown in **Table 2** below. Parameters developmental/reproductive toxicity, potential S Typhimurium TA100 mutagen based on QSAR, potential carcinogen based on QSAR in VEGA analysis are showed in Toxtree. The result from VEGA analysis is shown in **Table 2** below.

**Table 2.** Toxicity prediction by Toxtree and VEGA

No	Ligand	Mutagenic	Tumorigenic	Irritant	Develop- mental Toxicity	Repro- ductive Toxicity	Mutagenicity (S.Thypium)	QSAR Carci- nogenicity
1	L833	None	None	None	None	No	No	No
2	L217	Low	High	None	High	No	No	No
3	L595	None	None	None	None	No	No	No
4	oleuropein*	None	None	None	None	No	No	No
5	ouabain*	None	None	None	None	No	No	No

Note: \* standard ligand

The results toxicity prediction by OSIRIS DataWarrior, Toxtree and Vega analysis showed, L595 has same characteristics with ligands standard oleuropein, ouabain. The drug-likeness characteristics according to Lipinski's RO5 and Veber rules. Lipinski's RO5 has several parameters[23]. Ligands have these parameters are

considered as potential inhibitor candidates. The molecular weight (MW) of the ligands is less than 500 g/mol, clogP is less than 5.0, have less than 5 hydrogen bond donor and no more 10 hydrogen bond acceptor. The parameters of Veber rules are different with Lipinski's RO5. Veber rules only have 2 characteristics for candidate inhibitor. The first



parameter is no more 10 rotatable bonds. The last, polar surface area is equal to or less than 140 Å.

### Dynamics Simulation

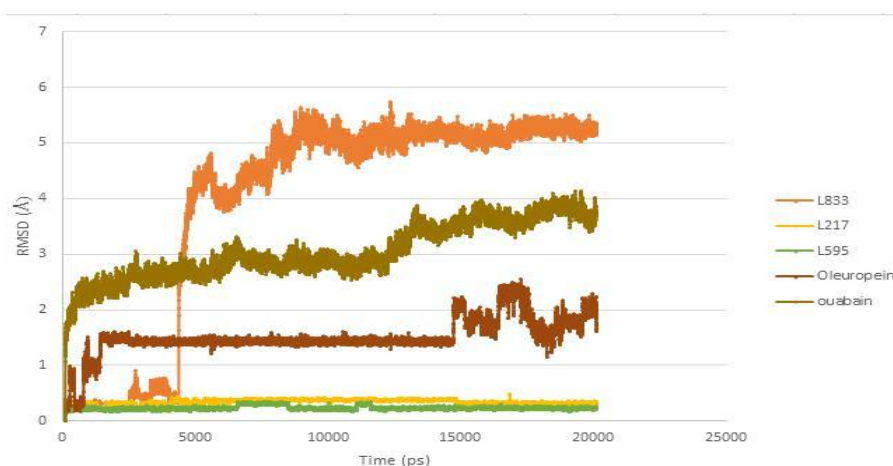
From dynamic simulation of the production stage, we obtained interactions with amino acid residues from three ligands with lowest

$\Delta G_{\text{binding}}$  and RMSD smaller than 2 (table is shown below). Another consideration in choosing the best ligand is the change in RMSD value of not more than 3Å every 1 nanosecond (ns). The meaning of this change value indicates the stability of the ligand [24]. The change of RMSD value of dynamic simulation result is shown in **Figure 2**.

**Table 3.** Interaction L833, L217, L595 with amino acid residues

	L833	L217	L595
Molecular docking	Q33, <b>W38</b> , N132, V31, L91, <b>W92</b> , L127, <b>K218</b> , L201, <b>E88</b> , T128, S89, I87, T129, <b>N130</b>	L201, <b>K218</b> , L127, S89, L91, <b>W92</b> , T128, T129, <b>N130</b> , E88, V31, <b>N132</b> , <b>Q33</b> , <b>W38</b>	L201, <b>K218</b> , L127, S89, L91, <b>W92</b> , T128, T129, <b>N130</b> , E88, V31, <b>N132</b> , <b>Q33</b> , <b>W38</b>
MD simulation	N30, <b>E88</b> , <b>K218</b> , T86, T129, <b>T128</b> , I87, S85, P216, K61, <b>P83</b> , N82, N84	<b>E88</b> , K218, L201, T28, <b>S89</b> , W92, N130, T129, L127, L91, <b>W38</b> , <b>Q33</b> , V31, N132	E88, W92, L201, L127, K218, T128, L91, N130, V31, <b>N132</b> , S89, I87, <b>W38</b> , <b>Q33</b>

Note: red color is amino acid residues that found in the binding site of the protein. Bold font is residues that found in the protein.



**Fig. 2.** Graph of RMSD (Å) against time (ps)

### CONCLUSION

We concluded that L595 is the best ligand from L833 and L217. The L595 have  $\Delta G_{\text{binding}}$  -54.2638 kcal/mol, and RMSD 1.5134. Toxicity prediction by Osiris Data Warrior, Toxtree, and VEGA showed that L595 can be developed to be a promising lead candidate for inhibiting *Ebolavirus* and more stable than L833 and L217 which have smaller  $\Delta G_{\text{binding}}$ . It is expected that this research will be continued in vitro and in vivo experiments.

### CONFLICT OF INTEREST

We declare that there is no conflict of interest in this research for publication

### ACKNOWLEDGEMENTS

We would like to thank Directorate of Research and Community Engagement of Universitas Indonesia (DRPM UI) for funding the research and publication of this article through Hibah Publikasi

International Terindeks untuk Tugas Akhir Mahasiswa No: 693/UN2.R3.1/HKP.05.00/2017. USFT designed the study and supervised this research, while EPT and SS were performed the experimental details. We also would like to thank Mr. Mochammad Arfin Fardiansyah Nasution for helping us to proofread this paper.

### REFERENCES

- [1] D. W. Leung, K. C. Prins, C. F. Basler, and G. K. Amarasinghe, "Ebola virus VP30 is a multifunctional virulence factor," *Virulence*, vol. 1, no. 6, pp. 526–31, 2010.
- [2] A. Sanchez, T. G. Ksiazek, P. E. Rollin, M. E. G. Miranda, S. G. Trappier, A. S. Khan, C. J. Peters, and S. T. Nichol, "Detection and molecular characterization of Ebola viruses causing disease in human and nonhuman primates," *J. Infect. Dis.*, vol. 179, no. Suppl 1, pp. S164–S169, 1999.
- [3] G. L. Shapiro, "Ebola Virus Disease."

- [4] R. R. Assessment, "Outbreak of Ebola virus disease in West Africa Epidemiological update," *Eur. Cent. Dis. Prev. Control*, no. February, 2015.
- [5] J. A. Wilson, M. Bray, R. Bakken, and M. K. Hart, "Vaccine Potential of Ebola Virus VP24 , VP30 , VP35 , and VP40 Proteins," vol. 390, pp. 384–390, 2001.
- [6] S. Ple, H. Volk, and M. Luk, "In Silico Study of Plant Polyphenols ' Interactions with VP24 – Ebola Virus Membrane-associated Protein," pp. 555–564, 2015.
- [7] J. a Wilson, M. Bray, R. Bakken, and M. K. Hart, "Vaccine potential of Ebola virus VP24, VP30, VP35, and VP40 proteins.," *Virology*, vol. 286, no. 2, pp. 384–390, 2001.
- [8] Z. Han, H. Boshra, J. O. Sunyer, S. H. Zwiers, J. Paragas, and R. N. Harty, "Biochemical and Functional Characterization of the Ebola Virus VP24 Protein : Implications for a Role in Virus Assembly and Budding," vol. 77, no. 3, pp. 1793–1800, 2003.
- [9] S. Watanabe, T. Noda, P. Halfmann, L. Jasenosky, and Y. Kawaoka, "Ebola Virus ( EBOV ) VP24 Inhibits Transcription and Replication of the EBOV Genome," vol. 196, no. Suppl 2, 2007.
- [10] V. Zoete, A. Grosdidier, and O. Michielin, "Docking , virtual high throughput screening and in silico fragment-based drug design," vol. 13, no. 2, pp. 238–248, 2009.
- [11] D. E. Scott, A. G. Coyne, S. A. Hudson, and C. Abell, "Fragment based approaches in drug discovery and chemical biology," *Biochemistry*, vol. 51, pp. 4990–5003, 2012.
- [12] A. E. Muryshev, D. N. Tarasov, A. V. Butygin, O. Y. Butygina, and A. B. Aleksandrov, "A novel scoring function for molecular docking," pp. 597–605, 2003.
- [13] U. Raj and P. Kumar, "Flavonoids as Multi-target Inhibitors for Proteins Associated with Ebola Virus : In Silico Discovery Using Virtual Screening and Molecular Docking Studies," *Interdiscip. Sci. Comput. Life Sci.*, 2015.
- [14] T. Sterling and J. J. Irwin, "ZINC 15 - Ligand Discovery for Everyone," *J. Chem. Inf. Model.*, vol. 55, no. 11, pp. 2324–2337, 2015.
- [15] H. Jhoti, G. Williams, D. C. Rees, and C. W. Murray, "The 'rule of three' for fragment-based drug discovery: where are we now?," *Nat. Rev. Drug Discov.*, vol. 12, no. 8, pp. 644–644, 2013.
- [16] U. S. F. Tambunan, A. A. Parikesit, A. S. Ghifari, C. P. Satriyanto, C. P. S. Usman S.F. Tambunan, , Arli A. Parikesit , Abi S. Ghifari, U. S. F. Tambunan, A. A. Parikesit, A. S. Ghifari, and C. P. Satriyanto, "In silico identification of 2-oxo-1,3-thiazolidine derivatives as novel inhibitors candidate of class II histone deacetylase (HDAC) in cervical cancer treatment," *Arab. J. Chem.*, 2015.
- [17] E. Picazo and F. Giordanetto, "Small molecule inhibitors of ebola virus infection," *Drug Discov. Today*, vol. 20, no. 2, pp. 277–286, 2015.
- [18] C. A. Lipinski, "Lead- and drug-like compounds: The rule-of-five revolution," *Drug Discov. Today Technol.*, vol. 1, no. 4, pp. 337–341, 2004.
- [19] W. Xu, M. R. Edwards, D. M. Borek, A. R. Feagins, A. Mittal, J. B. Alinger, K. N. Berry, B. Yen, J. Hamilton, T. J. Brett, R. V Pappu, D. W. Leung, C. F. Basler, and G. K. Amarasinghe, "Article Ebola Virus VP24 Targets a Unique NLS Binding Site on Karyopherin Alpha 5 to Selectively Compete with Nuclear Import of Phosphorylated STAT1," *Cell Host Microbe*, vol. 16, no. 2, pp. 187–200, 2014.
- [20] D. C. Rees, M. Congreve, C. W. Murray, and R. Carr, "Fragment-based lead discovery," *Nat. Rev. Drug Discov.*, vol. 3, no. 8, pp. 660–672, 2004.
- [21] S. Pleško, H. Volk, M. Lukšič, and Č. Podlipnik, "In silico study of plant polyphenols' interactions with VP24-ebola virus membrane-associated protein," *Acta Chim. Slov.*, vol. 62, no. 3, pp. 555–564, 2015.
- [22] M. W. El-saadi, T. Williams-hart, B. A. Salvatore, and E. Mahdavian, "Use of in-silico assays to characterize the ADMET profile and identify potential therapeutic targets of fusarochromanone , a novel anti-cancer agent," *Silico Pharmacol.*, pp. 1–20, 2015.
- [23] C. A. L. Ā, "Lead profiling Lead- and drug-like compounds : the rule-of-five revolution," pp. 337–341, 2004.
- [24] U. S. F. Tambunan, A. H. Alkaff, M. A. F. Nasution, A. A. Parikesit, and D. Kerami, "Screening of Commercial Cyclic Peptide Conjugated to HIV-1 Tat Peptide as Inhibitor of N-Terminal Heptad Repeat Glycoprotein-2 Ectodomain Ebola Virus Through In Silico Analysis," *J. Mol. Graph. Model.*, vol. 74, pp. 366–378, 2017.

## FRAGMENT-BASED LEAD COMPOUND DESIGN TO INHIBIT EBOLA VP35 THROUGH COMPUTATIONAL STUDIES

Atika Marnolia<sup>1</sup>, Erwin Prasetya Toepak<sup>2</sup>, Usman Sumo Friend Tambunan<sup>3</sup>

<sup>1</sup>Bioinformatics Research Group, Departement of Chemistry, Faculty of Mathematics and Natural Science, Universitas Indonesia, Kampus UI Depok, West Java 16424, Indonesia

### ABSTRACT

Ebola virus (EBOV) is a virus that is classified under *Filoviridae* family as a pathogenic organism. On March 2016, World Health Organization (WHO) reported that 28,646 cases caused by EBOV. Thus, it is important to find the antiviral drug for this disease because it can create the epidemic around the world. EBOV VP35 is a potential drug target because it has the component of the viral RNA polymerase complex that will hamper the host interferon (IFN) production. In this research, about 6,662 fragments were obtained from ZINC15 Biogenic Database after the Rules of Three, and pharmacological properties parameters were applied. After that, these fragments were docked into the active side of EBOV VP35 using MOE 2014.09 software. The potential fragments from previous docking simulations were linked each other, resulting 91 ligands in the process. Furthermore, the docking simulation was conducted again, and we discovered the best three ligands that have lower Gibbs free binding energy than the standards. Moreover, the pharmacological prediction tests were also done to find the ligand with excellent molecular properties. The best three ligands from these tests were continued into molecular dynamics simulation. In the end, we conclude that the LEB 31 ligand can be the new drug candidate as EBOV VP35 inhibitor based on molecular docking, pharmacological prediction test, and molecular dynamic.

**Keywords:** *Fragment-Based Drug Design, Ebola Virus, VP35, Molecular Docking, Pharmacological Prediction*

### INTRODUCTION

The Ebola virus (EBOV) is pathogenic, single-stranded RNA virus of *Filoviridae* family causing fatal hemorrhagic fever in human and non-human primates [1],[2]. Ebola virus was found in Africa for the first time in 1976. On July 2015, there are 11,268 people deaths from 27,621 cases reported. In Africa, this case is an epidemic, but Ebola virus may develop and infected populations in other parts of the world [3].

There are seven codes of protein for EBOV such as RNA-polymerase (L), nucleoprotein (NP), glycoprotein (GP), VP24, VP30, VP35 and VP40 [2]. In this study, we focused on VP35. Viral protein (VP) 35 is the important host for EBOV infection that has functions in the filoviral replication cycle and an essential cofactor of the viral RNA polymerase complex [4]-[6]. The EBOV VP35 is a potential drug target because it has the component of the viral RNA polymerase complex that will hamper the transcription of type I interferon (IFN) and the production of IFN will decrease [2],[7]. Initial studies said that the virus target the RIG-I signal pathway inhibit the activation of IRF-3 and production of interferon from infected cells [6].

Raj et al. (2015) used the flavonoid as an inhibitor for EBOV [2]. In this study, we designed EBOV VP35 inhibitor based on in

silico biogenic fragment database. Fragment-based has been widely used in the pharmaceuticals and biotechnology industry as it is easy to synthesize and show good results in chemical properties analysis [8]. We used the molecular docking to know the VP35-ligand interaction [9]. To docking fragment database, we used MOE 2014.09 software [10]. In this research, we tried to design a potential VP35 inhibitor using fragment-based drug methods. We expected the outcome from this study could provide a promising drugs for Ebola virus infection.

### METHODS

#### Protein Structure

In this study, we used the three-dimensional structure of EBOV VP35 with PDB ID: 3FKE [2] that available in Protein Data Bank (<http://www.rcsb.org/pdb>). Before protein preparation process, the water molecules were removed [11]. We used MOE 2014.09 to minimized and optimized the 3D structure of protein [10].



### Construction of Fragment Database

Biogenic compounds database were downloaded from ZINC15 database [8]. All of the fragment was created based on Rule of Three and toxicity prediction using Osiris Data Warrior [5]. The energy minimized and partial charge of both fragments used the MOE 2014.09 with MMFF94x as a forcefield [11].

### Molecular Docking of Fragment Database and Standard Compound

Three-dimensional structure of standard ligands were obtained from ChemSpider.. Molecular docking simulation for the standard and fragment database was performed using MOE 2014.09 software. We used Triangle Matcher as placements methods, London dG as scoring function and 30 to 100 times of placement retain as parameters. The other parameters were set according to MOE 2014.09 default parameters with AMBER10: EHT as a forcefield [11].

### Fragment Linking

Potential fragments were linked in MOE 2014.09 to generated new ligands. These new ligands were docked with the EBOV VP35. Three of new ligands that have low binding energy were used to the pharmacological prediction test.

### Analysis of Ligand Interactions and Pharmacological Properties

Three new ligand and standard ligand were analyzed their interaction with the active side of EBOV VP35. In this study, we used Osiris Data Warrior, VEGA and Toxtree to predict the drug-likeness and the toxicity.

### Molecular Dynamics Simulation

In this study, we chose the best three ligands from molecular docking and pharmacological properties prediction. The heating process was conducted for ten picoseconds (ps) at 300 K and 312 K in the first step. After that, equilibrium step simulation was conducted for 100 ps at 312 K and production in 20000 ps at 312 K. For the last step, cooling simulation is conducted in 10 ps at 300 K [12]. The result for this simulation was analyzed.

## RESULT AND DISCUSSION

### Protein Structure

In this study, we used EBOV VP35 chain A (Fig. 1) as potential protein target because this protein has a function to protective immune responses to EBOV [13]. This protein has the interaction with Gln244, one of the key amino acid residues in the protein [2]. We used LigX in MOE 2014.09 to prepare the protein with AMBER 10: EHT as a forcefield.

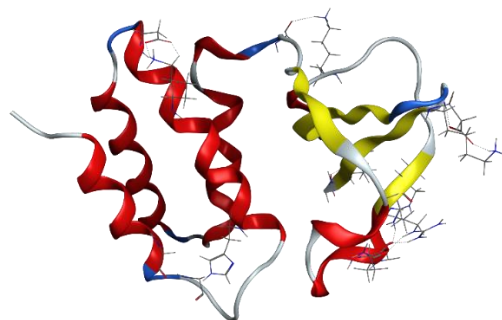


Fig.1 Structure of EBOV VP35

### Construction of Fragment Database

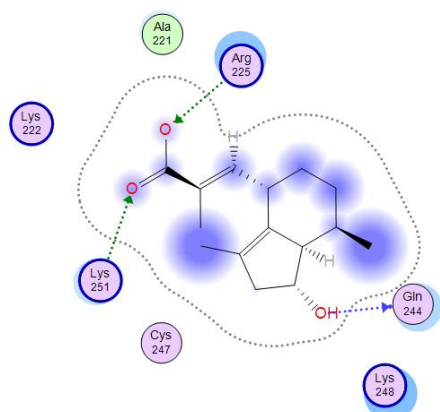
We got 246.244 compounds from biogenic database. We used the Rule of Three to reduce the amount of the compounds to find the potential fragment in Osiris Data Warrior. Three things must be followed in Rule of Three: (1) molecules have a mass less than 300Da, (2) molecules has the hydrogen donor, and acceptor up to three, and (3) the value of clogP is 3 [14]. Toxicity screening could also be used to reduce the risk of toxicity or metabolic instability [11]. We used mutagenic, tumorigenic, irritant and reproductive prediction as a parameter in Osiris Data Warrior. We got 6.662 fragments after toxicity and Rule of Three screening. In this study, we used the chloroquine as a ligand standard [9], [13]. The energy minimizes, and partial charges of both fragments were applied using the MOE 2014.09 with MMFF94x as a force field.

### Molecular Docking and Linking Process

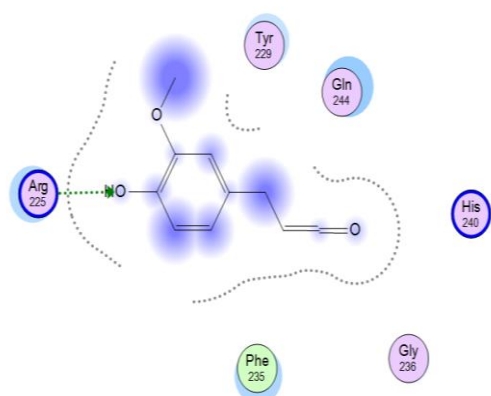
Molecular docking is the way to predict the position, orientation, and conformation of the protein target binding the ligand [15]. We used the MOE 2014.09 to performed molecular docking of 6.662 fragments into the active site of VP35. We docked 6.662 fragments towards VP35.

After docking, we search two potential candidates of the fragment for the linker. Fragment 1 is the fragment that has interaction

with Gln244 residue [2]. Fragment 1 has the root mean square deviation (RMSD) 1.4186 Å (**Fig. 2**). Fragment 2 is another ligand that not overlap with fragment 1. Fragment 2 has the value of RMSD 1.5146 Å (**Fig. 3**). Interaction of key amino acid residues and ligands is important to inhibiting the protein activity.



**Fig. 2** The interaction between Fragment 1 with the binding site of EBOV VP35



**Fig. 3** The interaction between Fragment 2 with EBOV VP35 at its active site

We linked two fragments using Link Multiple Fragments feature in MOE 2014.09 to generated higher affinity binding compounds that have interaction with the active site of VP35. We got 91 ligands as result of linked, and then we docked these ligands. After docking simulation with rescoring 30, we found ligands with the low

value of  $\Delta G_{\text{binding}}$ , but the RMSD score is higher than 2.0 Å in LEB 31 (3.26920 Å). In general, a docking pose would be acceptable if the value of RMSD that generated during the docking simulation is lower than 2.0 Å [16]. Because of this reason, we re-docked the fragment into rescoring 100, and the result showed that the RMSD of LEB 31 decrease to 1.0642 Å.

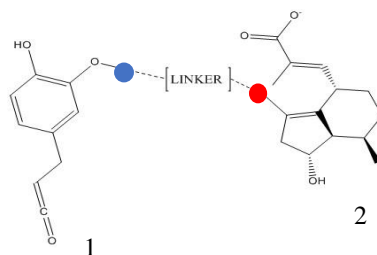
In this step, we found three best ligands that have potential as a drug for EBOV VP35 based on the value of  $\Delta G_{\text{binding}}$ , inhibition constant (pKi) and RMSD. The ligand with the code LEB 31 is the best ligand that showed the  $\Delta G_{\text{binding}}$  - 50.5453 kcal/mol with an inhibition constant (pKi) of 36.8215 and RMSD is 1.0642 Å. The value of  $\Delta G_{\text{binding}}$ , inhibition constant (pKi) and RMSD of the three best ligands and standard ligands that used in our work showed in **Table 1**.

### Pharmacological Analysis

The toxicity and drug-likeness analysis of the best ligands were performed using Osiris Data Warrior, VEGA and Toxtree [17], [18]. The parameter of toxicity like as mutagenic, tumorigenic, toxicity and irritant was predicted using Osiris Data Warrior, while development or reproductive toxicity using VEGA and potential *S. typhimurium* TA100 mutagen and potential carcinogen using Toxtree (**Table 2**). In **Table 2**, chloroquine as standard ligand shows that it has a high mutagenic and irritant than another ligand when using Osiris Data Warrior in toxicity test. Toxicity prediction test using VEGA and Toxtree show that all of the ligands have not toxicity properties in three parameters.

The bioavailability properties prediction based on Lipinski and Veber rules such as rotatable bonds, clogP, hydrogen bond donor and acceptor and also the polar surface area. These parameter was determined using Osiris Data Warrior (**Table 3**).

**Table 3**. show that all of ligands give the good result based on Lipinski rules: the value of clogP less than 5, have five hydrogen donors and ten hydrogen acceptors and also Veber rules: (1) ligand have a number of rotatable bonds no more than 10 and (2) polar surface area equal or less than 140 Å [19].

**Table 1.**  $\Delta G$  energy, pKi, and RMSD value from the selected linked compounds and standard ligands

Ligands	Linker	$\Delta G$ (kcal/mol)	pKi	RMSD (Å)
LEB 31		-50.5453	36.8215	1.0642
LEB 39		-47.8037	34.8243	1.3152
LEB 89		-47.4118	34.5388	1.5913
*Chloroquine	-	-29.0212	21.1415	1.9169

Note: \* Standard Ligand; the blue circle in linker is linking with the blue circle in fragment 1 while the red circle is linking with the red circle in another fragment.

**Table 2.** Toxicity test using Osiris Data Warrior, VEGA and Toxtree

Ligands	Parameters						
	Mutagenic	Tumorigenic	Irritant	Toxicity	Developmental /Reproductive Toxicity	Potential <i>S. typhimurium</i> TA100 mutagen	Potential carcinogen
LEB 31	None	None	None	None	NO	NO	NO
LEB 39	None	None	None	None	NO	NO	NO
LEB 89	None	None	None	None	NO	NO	NO
*Chloroquine	High	None	High	None	NO	NO	NO

Note: \* Standard Ligand

**Table 3.** The molecular properties using Osiris DataWarrior

Ligands	Parameters					
	Molecular Weight	Number of H-Donor	Number of H-Acceptor	cLog P	Polar Surface Area	Number of Rotatable bonds
LEB 31	495.594	3	8	0.6552	111.33	9
LEB 39	497.586	3	2	1.0868	120.56	9
LEB 89	495.641	3	7	2.4432	134.53	10
*Chloroquine	321.894	1	3	4.2018	28.16	8

Note: \*Standard Ligand

### Molecular Dynamics Simulation

The best three ligands was analyzed with molecular dynamics simulation to observe protein-ligand complex stability. **Table 4.** showed the amino acid residues that interact with

protein target. The result shows that some of the amino acid residues in molecular docking are also found in molecular dynamics. This result indicated the complex ligan-protein is quit stable. RMSD score is also the parameter that show the stability of protein-ligand interaction because the

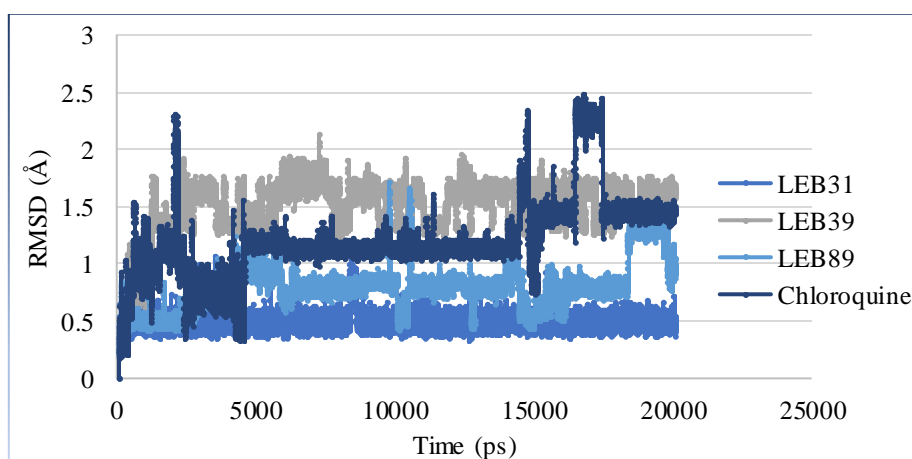
distance of the particular atom in the complex can indicate from this value. Protein-ligand complex is stable when the changes in the value of RMSD does not exceed 3 Å in a reach of 1

nanosecond (ns) [12]. In Fig.4, all of the ligands have RMSD low than 3 Å. LEB 31 is the most stable than another ligand and standard.

**Table 4.** Amino acid residues based on molecular docking and dynamics simulation

Ligand	LEB 31	LEB 39	LEB 89	Chloroquine
<b>Molecular docking</b>	<b>Q241, Q244</b> , K248, <b>K251, R225</b> , A221, W229, K222, F235, P304	H240, K248, <b>Q244</b> , G236, F235, <b>K251</b> , C247, K222, A221, N226, <b>R225</b> , Y229	K248, <b>Q244</b> , F235, <b>R225</b> , N226, Y229, A221, K222, <b>K251</b> , C247	R225, Q241, Q244, V245, I295, K248, P293, L249, V1294
<b>Molecular dynamics</b>	<b>K222, R225</b> , Q244, A221, K251, K248, Cs247	P239, Q244, <b>K251</b> , <b>R225</b> , A221, L249, Q241, K248, I295, V249	K248, <b>Q244, Q241</b> , F328, I295, D302, P304, <b>R225, A221</b> , K222, <b>K251</b>	K248, PP293, H296, I295, L249, V249

Note: amino acid residues in red color are the residues found in the binding site of protein. Residues in bold font are the residues that can be found in molecular docking and dynamics simulation.



**Fig. 4** Graph of RMSD (Å) Vs time (ps)

## Conclusion

In this research, we constructed fragment database and docked it into the active site of VP35. After docked, we linked the two potential fragment and then docked again with VP35. We obtained 91 ligands from this fragment linking process. In the next step of the study, we used three best ligands from molecular docking simulation to analyzed in molecular dynamics simulation. In generally, all of the ligands showed the good pharmacological properties and gave the value of RMSD lower than 3 Å in molecular dynamics. Among all ligands, LEB 31 is the best inhibitor based on result of molecular docking, pharmacological properties prediction, and molecular dynamics simulation.

## Acknowledgements

This research has been supported and funded by Directorate of Research and Community Engagement (DRPM) Universitas Indonesia

through Hibah Publikasi Internasional Terindeks Untuk Tugas Akhir Mahasiswa (PITTA) No: 693/UN2.R3.1/HKP.05.00/2017. Usman Sumo Friend Tambunan supervised this study, while Atika Marnolia and Erwin Prasetya Toepak did the experimental and wrote the manuscript. We also would like to thank Mr. Mochammad Arfin Fardiansyah Nasution for helping proofread this paper.

## References

- [1] Ž. Selaković, V. Soloveva, D. N. Gharaibeh, J. Wells, S. Šegan, R. G. Panchal, and B. A. Šolaja, "Anti-Ebola Activity of Diazachrysene Small Molecules," *ACS Infect. Dis.*, vol. 1, no. 6, pp. 264–271, 2016.
- [2] U. Raj and P. K. Varadwaj, "Flavonoids as Multi-target Inhibitors for Proteins Associated with Ebola Virus: In Silico Discovery Using Virtual Screening and

- Molecular Docking Studies,” *Interdiscip. Sci. Comput. Life Sci.*, vol. 8, no. 2, pp. 132–141, 2016.
- [3] A. Haque, D. Hober, and J. Blondiaux, “Addressing therapeutic options for Ebola virus infection in current and future outbreaks,” *Antimicrob. Agents Chemother.*, vol. 59, no. 10, pp. 5892–5902, 2015.
- [4] L. W. Leung, M.-S. Park, O. Martinez, C. Valmas, C. B. López, and C. F. Basler, “Ebola virus VP35 suppresses IFN production from conventional but not plasmacytoid dendritic cells,” *Immunol. Cell Biol.*, vol. 89, no. 7, pp. 792–802, 2011.
- [5] J. M. Binning, T. Wang, P. Luthra, R. S. Shabman, D. M. Borek, G. Liu, W. Xu, D. W. Leung, C. F. Basler, and G. K. Amarasinghe, “Development of RNA aptamers targeting Ebola virus VP35,” *Biochemistry*, vol. 52, no. 47, pp. 8406–8419, 2013.
- [6] D. W. Leung, K. C. Prins, C. F. Basler, and G. K. Amarasinghe, “Ebola virus VP35 is a multifunctional virulence factor,” *Virulence*, vol. 1, no. 6, pp. 526–31, 2010.
- [7] A. Rivera and I. Messaoudi, “Pathophysiology of Ebola Virus Infection: Current Challenges and Future Hopes,” *ACS Infect. Dis.*, vol. 1, no. 5, pp. 186–197, 2015.
- [8] T. Sterling and J. J. Irwin, “ZINC 15 - Ligand Discovery for Everyone,” *Journal of Chemical Information and Modeling*, vol. 55, no. 11, pp. 2324–2337, 2015.
- [9] D. E. Scott, A. G. Coyne, S. A. Hudson, and C. Abell, “Fragment-Based Approaches in Drug Discovery and Chemical Biology,” 2012.
- [10] A. A. Parikesit, B. Ardiansah, D. M. Handayani, S. F. Tambunan, D. Kerami, U. S. F. Tambunan, and D. Kerami, “Virtual screening of Indonesian flavonoid as neuraminidase inhibitor of influenza a subtype H5N1,” *Mater. Sci. Eng*, vol. 107, no. 1, p. 12053, 2016.
- [11] D. C. Rees, M. Congreve, C. W. Murray, and R. Carr, “Fragment-based lead discovery,” *Nat. Rev. Drug Discov.*, vol. 3, no. 8, pp. 660–672, 2004.
- [12] U. S. F. Tambunan, A. H. Alkaff, M. A. F. Nasution, A. A. Parikesit, and D. Kerami, “Screening of Commercial Cyclic Peptide Conjugated to HIV-1 Tat Peptide as Inhibitor of N-Terminal Heptad Repeat Glycoprotein-2 Ectodomain Ebola Virus Through In Silico Analysis,” *J. Mol. Graph. Model.*, vol. 74, pp. 366–378, 2017.
- [13] J. G. Glanzer, B. M. Byrne, A. M. McCoy, B. J. James, J. D. Frank, and G. G. Oakley, “In silico and in vitro methods to identify ebola virus VP35-dsRNA inhibitors,” *Bioorganic Med. Chem.*, vol. 24, no. 21, pp. 5388–5392, 2016.
- [14] D. E. Scott, A. G. Coyne, S. A. Hudson, and C. Abell, “Fragment based approaches in drug discovery and chemical biology,” *Biochemistry*, vol. 51, pp. 4990–5003, 2012.
- [15] V. Zoete, A. Grosdidier, and O. Michielin, “Docking, virtual high throughput screening and *in silico* fragment-based drug design,” *J. Cell. Mol. Med.*, vol. 13, no. 2, pp. 238–248, 2009.
- [16] U. Gowthaman, M. Jayakanthan, and D. Sundar, “Molecular docking studies of dithionitrobenzoic acid and its related compounds to protein disulfide isomerase: computational screening of inhibitors to HIV-1 entry,” *BMC Bioinformatics*, vol. 9 Suppl 12, p. S14, 2008.
- [17] M. W. El-Saadi, T. Williams-Hart, B. A. Salvatore, and E. Mahdavian, “Use of in-silico assays to characterize the ADMET profile and identify potential therapeutic targets of fusarochromanone, a novel anti-cancer agent,” *silico Pharmacol.*, vol. 3, no. 1, p. 6, 2015.
- [18] S. J. Enoch, M. Hewitt, M. T. D. Cronin, S. Azam, and J. C. Madden, “Classification of chemicals according to mechanism of aquatic toxicity: An evaluation of the implementation of the Verhaar scheme in Toxtree,” *Chemosphere*, vol. 73, no. 3, pp. 243–248, 2008.
- [19] D. F. Veber, S. R. Johnson, H. Cheng, B. R. Smith, K. W. Ward, and K. D. Kopple, “Molecular Properties That Influence the Oral Bioavailability of Drug Candidates,” pp. 2615–2623, 2002.

## DEVELOPMENT OF SPECIFIC ELECTROCHEMICAL BIOSENSOR BASED ON CHITOSAN MODIFIED SCREEN PRINTED CARBON ELECTRODE FOR THE MONITORING OF CAPTAN FUNGICIDE

Pornpip Wongkaew<sup>1\*</sup>, Buddhapala Wongkaew<sup>2</sup>, Suwita Saepaisan<sup>3</sup>, and Panupong Thanutong<sup>4</sup>

<sup>1</sup>Division of Plant Pathology, Faculty of Agriculture, Khon Kaen University, Khon Kaen 40002, Thailand;

<sup>2</sup>Metropolitan Waterworks Authority, Bangkok 10210, Thailand.

### ABSTRACT

Harmful chemicals predominantly used in modern agriculture for pest control have raised a long term accumulation in environment and serious problems concerning food safety and health. Excellent detection tools for environmental monitoring are thus urgently needed. The recent biosensor technology is proposed to fulfill this purpose. In this study, an expedient biosensor for captan fungicide determination has been fabricated using its specific reacting enzyme glutathione-s-transferase (GST) covalently immobilized on natural biopolymer chitosan (Chi). The screen printed carbon electrode (SPCE) has been selected as a basal platform for the biosensor development. Modification of SPCE was made by self-assembled deposition of 1% chitosan in 1% acetic acid solution onto the basal SPCE. Progressive characteristics of the assembled SPCE-Chi-GST have been clearly approved by atomic force microscopy, impedance spectroscopy and cyclic voltammetry (CV). Two sequential oxidation peak currents were arisen in the electrochemical behavior analysis of captan in the presence of GST substrate electrolyte solution by CV and linear sweep voltammetry (LSV). Dose response to various captan concentrations was investigated in the range 0 – 20 µg/ml by LSV and a similar good linear relationship between peak current and concentration of captan could be obtained by both oxidation steps with the limit of detection (LOD) at 0.2 µg/ml. Thus the sensitive, rapid, inexpensive and miniature quantitative system for captan monitoring could now be successfully achieved by this proposed biosensor.

*Keywords: Electrochemical biosensor · Screen printed electrode · Captan · Chitosan · Glutathione-s-transferase · Voltammetry*

### INTRODUCTION

The fungicide captan is one of the most frequently applied pesticides due to its broad actions. It has been widely used in a variety of crop production at every growing stage of plant and in various industries including household applications. It is highly toxic to very highly toxic to livestock, poultry, and fish. The evidence of human cardiotoxic effects has also been reported in a rare case of captan ingestion by skinny person [1]. Overuse of captan has several drawbacks including pollution in environment and water ecosystem electrochemical technique. The toxicity of captan is primarily due to an inhibitory effect on enzymes and essential amino compounds production according to several toxicokinetic studies [2]. In captan metabolism, a major functional group, trichloromethylthio (SCCl<sub>3</sub>) is generally metabolized to the reactive thiophosgene (S=CCl<sub>2</sub>) along with a relatively stable 1,2,3,6-tetrahydrophthalimide (THPI) in the presence of exposed thiol group. While a cellular detoxification response against this xenobiotic is activated through an enzyme glutathione-s-transferase (GST) that metabolizes a broad range of

electrophilic substrates via glutathione (GSH) conjugation. This principal role of GST in xenobiotic-GSH conjugation especially in the reaction with transient thiophosgene to form a product thiazolidine-2-thione-4-carboxylic acid (TTCA) thus has been considered as a basis for captan determination using high performance liquid chromatography (HPLC), in coupled with mass spectrometry (MS) but these systems are very sophisticated, highly expensive, laborious and time-consuming. Electrochemical sensor using enzyme reaction is one among advanced effective tools alternative to such conventional methods. A field-based and in situ environmental monitoring is expected to handle easily on site with several order lower cost by this novel approach.

Our previous studies presented an approved effective and afford able electrochemical implement by a combination of a screen printed carbon electrode (SPCE) and biopolymer chitosan [3]. In this present study, the chitosan modified screen printed carbon electrode (SPCE-Chi) was employed for a novel fabrication of GST based biosensor. Characterization of the prepared electrodes was carried out using atomic force microscopy (AFM),

electrochemical impedance spectroscopy (EIS), and cyclic voltammetry (CV). Statistics calibration was subsequently explored by linear sweep voltammetry (LSV) with varying captan concentration. The present issue also firstly demonstrates catalytic ability of this SPCE-Chi-GST in the oxidation of captan that liberated significant two sensing mechanisms owing to the simultaneous formation of two different electrophillic complexes from a distinct function of xenobiotic-GSH conjugation.

## MATERIALS AND METHODS

### Materials and apparatus

Chitosan (85% degree of deacetylation) with a molecular weight of 0.28 kDa was obtained from Bioline Lab, Co., Thailand. Glutathione-S-transferase from equine liver, glutathione (GSH) and captan were purchased from Sigma-Aldrich Co. LLC, USA. Other chemicals for reagent preparation were purchased from Ajax Finechem Pty, Ltd., Australia. All solutions and reagents were prepared using high purity deionized water of 18.2 MΩ from Milli-Q RG system (Millipore Corporation, MA, USA.). Screen printed carbon electrode DRP-150 was provided by DropSens, ParqueTecnológico de Asturias, S.L. Llanera (Asturias) Spain. An XE-120 Atomic force microscope (Park Systems Corp., Suwon, Korea) was acquired for electrode surface observation and a PGSTAT 302N ECoChemie Autolab (Metrohm Autolab B.V., Utrecht, The Netherlands) was used for electrochemical analyses.

### Modification of working electrode and fabrication of GST enzyme based biosensor

Modification of working electrode was performed by self assembled deposition of chitosan onto a SPCE as previously developed [3]. Fabrication of the enzyme biosensor was executed following an immobilization of GST enzyme (3 U) on SPCE-Chi via the incorporation of glutaraldehyde covalent attachment to ensure the stability of GST as previously described [4].

### Atomic force microscopic observation

Morphological characteristics at nanoscale of original SPCE, SPCE-Chi and SPCE-Chi-GST working surfaces were allocated by a true non contact mode AFM with a PPP-NCHR silicon cantilever of < 10 nm tip radius bearing a spring constant of 42 N/m force constant and 320 kHz resonant frequency (Nanosensors TM, Neuchâtel, Switzerland). Inspection of the surface profile was carried out on an x-y accessible 1×1 μm area at 0.5 Hz scan rate with XEP and XEI software for data acquisition and image processing.

## Electrochemical characterization studies

Electrochemical inspections were done at room temperature on a 50 μl droplet of an electrolyte solution at the working electrode surface area. A solution of 0.05 M PBE containing 1.0 mM K<sub>3</sub>Fe(CN)<sub>6</sub> at pH 6.5 was used as the basal electrolyte reagent throughout all experiments. Electrochemical impedance spectroscopy (EIS) measurements were performed in potentiostatic state as a single sine wave at a frequency range of 0.01–10<sup>5</sup> Hz and a frequency number of 50 with the amplitude of 10 mV and estimated duration of 6 minutes. Cyclic voltammetric (CV) profiles were obtained over the potential scan range from – 0.6 to + 0.6 V at a scan rate of 25, 50, 100, 150 and 200 mVs<sup>-1</sup>. Linear sweep voltammetry (LSV) was carried out at similar potential scan range at a scan rate of 50 mVs<sup>-1</sup>.

### Enzyme activity determination

The GST enzyme activity was determined in accordance of an approved procedure [4] using a substrate solution containing 1 mM reduced GSH and 1 mM CDNB in 0.05 M PBE at pH 6.5 as an electrolyte for electrochemical sensing of the prepared SPCE-Chi-GST biosensor. Standard calibration of captan was acquired by fortifying authentic captan at various concentrations ranged from 0 - 20 μg/ml and reacting with the substrate solution by 1:1 ratio. The enzyme sensing activity was assessed before and after captan accretion with an incubation period of 15 minutes. Inhibition of enzyme activity was calculated from the rest of current peak obtained by the equation, Inhibition (%) = ((*I*<sub>pe</sub> – *I*<sub>pf</sub>) / *I*<sub>pe</sub>) × 100, where *I*<sub>pe</sub> and *I*<sub>pf</sub> represent the peak height current of GSH-CDNB reaction product on the SPCE-Chi-GST before and after the addition of captan fungicide, respectively.

## RESULTS AND DISCUSSION

### Morphological characteristics of the prepared electrode working surfaces

The surface morphology of each working electrode type could be manifested directly by their topographic inspection under atomic force microscope. Typical AFM images in three dimensions from the nanoscale surface scanning are as shown in Fig. 1 which representing the original SPCE in image A, the chitosan modified electrode (SPCE-Chi) in image B and the SPCE-Chi that was immobilized with GST enzyme (SPCE-Chi-GST) in image C. It appears that the chitosan nanoparticle layer is thoroughly covered onto SPCE basement upon this surface modification (Fig. 1B). On the



other hand, a prominent distinction can be realized following the electrode working surface transformation and a conspicuous layer of the GST enzyme bound to the surface after immobilization was apparently formed as shown in image C in Fig. 1. Therefore a successful immobilization of GST enzyme can be stated according to these circumstantiated images.

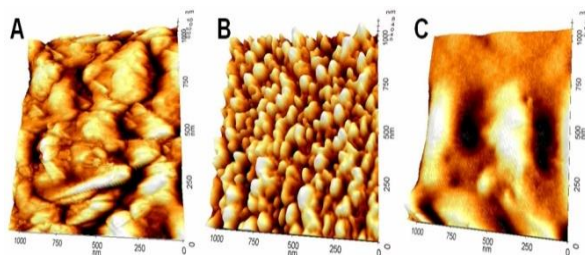


Fig. 1 Three-dimensional AFM surface micrographs at nanoscale of (A) original bare SPCE, (B) SPCE-Chi, and (C) SPCE-Chi-GST

### Electrochemical impedance spectroscopy (EIS)

An EIS assay is exploited to estimate the electrocatalytic properties of original bare SPCE, SPCE-Chi and SPCE-Chi-GST as shown in Fig. 2A with an enlarge view of them at high frequency region in Fig. 2B. The spectral character of each could be obviously distinguished and thus signifies the alteration upon stepwise manipulation according to the assumption of Warburg impedance for a semi-infinite diffusion on smooth surface [5]. In this figure, a broad semicircle at high frequency range has been arisen in the spectra of SPCE as typical characteristic for a high electron transfer resistance. Notable plot from SPCE-Chi is evident by its almost straight line which indicates an extremely fast electron transfer phenomenon due to numerous positive charges holding quality of the chitosan. While a distinct small semicircle has derived in the spectrum of SPCE-Chi-GST which implied for a deceleration of electron transfer after GST immobilization. The reference impedance model using a modified Randles equivalent circuit in this relationship can be written as  $Rs(Cdl(Rct(W)))$  where  $Rs$  is the cell resistance,  $Rct$  is the charge transfer resistance,  $Cdl$  is double-layer capacitance and  $W$  is the Warburg element. The charge transfer resistance ( $Rct$ ) values could be approximated 4,697, 395 and 483  $\Omega\text{cm}^{-2}$  for bare SPCE, SPCE-Chi and SPCE-Chi-GST, respectively. It seems that the  $Rct$  of SPCE-Chi appears to decrease down to almost 12 folds in corresponding to an expedite activity of the  $\text{Fe}^{3+}/\text{Fe}^{2+}$  redox couple by the influence of chitosan assembly onto the original SPCE surface. A bit raised up in  $Rct$  value than the basal SPCE-Chi has been observed after an immobilization of GST enzyme to make the SPCE-Chi-GST. This incidence

probably informs the presence of a barrier that resulted from negative charges repulsion of the enzyme which retarded the electrolyte  $[\text{K}_3\text{Fe}(\text{CN})_6]^{3-/4-}$  redox action and detained the ion charges associated to a successful GST immobilization on SPCE-Chi surface.

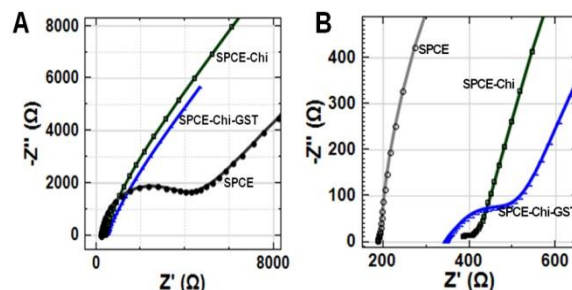


Fig. 2 Impedance spectra of SPCE, SPCE-Chi and SPCE-Chi-GST revealed by nyquist plots (A) and the enlarge view (B).

### Cyclic voltammetric characterization

Typical peak curve of the reductive and reverse oxidative current vs. electrode potential indicating ideal reversible reaction governed by freely diffusion of  $\text{Fe}^{3+}/\text{Fe}^{2+}$  to the planar surface was gained in each electrode at about 0.09 to 0.21 V with the peak separation around 0.1 V at 100  $\text{mV s}^{-1}$  scan rate and a potential window of -0.6 to 0.6 V as shown in Fig. 3. The oxidation/reduction peak currents of SPCE-Chi and SPCE-Chi-GST were almost 2-3 times bigger than that of original bare SPCE (curve a) as a successive superb improvement in electroactive response due to the surface furnishing by an enriched cationic chitosan biopolymer [6, 7]. A high rate of electron transfer process was thus accelerated via this highly conductive chitosan composing as demonstrated by the curve b for SPCE-Chi and curve c for SPCE-Chi-GST. Even though a bit smaller peak current curves were appeared due to a small electron transfer deducted by subsequent GST enzyme immobilization stepwise. Graphical plots in Fig. 4 illustrate the representative cyclic voltammogram of an electrochemical responding to scan rate effect including their linear regression relationship from SPCE-Chi-GST that implies for good diffusion effect.

The results from cyclic voltammetry on the confirmation of self assembled layers were in agreement with those from EIS that inferred an efficient electrochemical catalytic activity after the stepwise preparation. Therefore this prepared SPCE-Chi-GST is capable to use for the further study on captan detection.



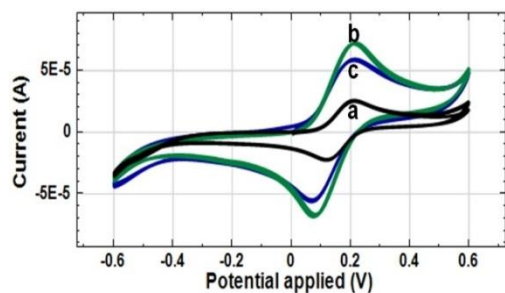


Fig. 3 Cyclic voltammograms of (a) bare SPCE, (b) SPCE-Chi and (c) SPCE-Chi-GST in  $\text{Fe}^{3+}/\text{Fe}^{2+}$  redox probe at  $100 \text{ mV s}^{-1}$  scan rate.

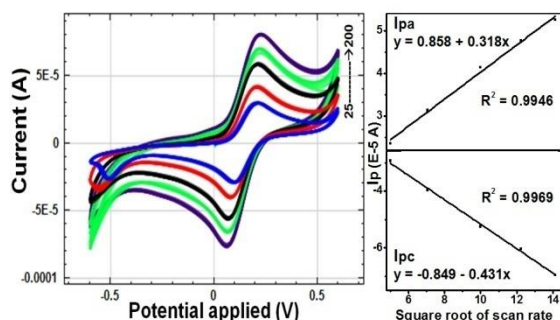


Fig. 4 Cyclic voltammograms of SPCE-Chi-GST in  $\text{Fe}^{3+}/\text{Fe}^{2+}$  probe accounted by curves from inner to outer corresponding to 25, 50, 100, 150 and  $200 \text{ mV s}^{-1}$  scan rates, respectively, with their coordinate linear relationship of anodic and cathodic peak current vs. square root of scan rate on the right plots.

### Electrochemical sensing mechanisms of SPCE-Chi-GST

The CV profiles of the GST immobilized working electrode, SPCE-Chi-GST, as well as their corresponding bare SPCE and SPCE-Chi were gained in the absence and presence of  $2.5 \text{ } \mu\text{g/ml}$  captan in  $0.1 \text{ M}$  PBE ( $\text{pH } 6.5$ ) containing  $1.0 \text{ mM}$   $[\text{K}_3\text{Fe}(\text{CN})_6]^{3-/4-}$  with  $1 \text{ mM}$  reduced GSH and  $1 \text{ mM}$  CDNB as analytic substrate buffer with scan rate of  $100 \text{ mV s}^{-1}$  as shown in Fig. 5. In the sole substrate buffer, almost obvious one oxidation and one reduction charging current peaks were appeared at  $E_{\text{pa}}$  of  $0.27 \text{ V}$  and  $E_{\text{pc}}$  of  $0.16 \text{ V}$  owing to the traditional GSH-CDNB conjugation reaction by GST catalysis [8] that can be summarized as  $\text{CDNB} + \text{GSH} \xrightarrow{\text{GST}} \text{GS-DNB} + \text{HCl}$ . The peak separation between them was about  $0.1 \text{ V}$  indicating profuse diffusion behaviour of the analytic substrate toward the electrode surfaces (Fig. 5 curve a-c). An explicit CV current response was generated in the presence of captan containing analysis buffer in SPCE-Chi-GST with two oxidation and two

reduction peaks as seen in Fig. 5 curve d, suggesting a differentiation due to captan catalytic reaction in the system. The first oxidation peak at  $E_{\text{pa}}$  of  $0.12 \text{ V}$  and the second oxidation peak at  $E_{\text{pa}}$  of  $0.27 \text{ V}$  altogether with the other two prominent reduction peaks at  $E_{\text{pc}}$  of  $-0.078 \text{ V}$  and  $0.145 \text{ V}$  were emerged.

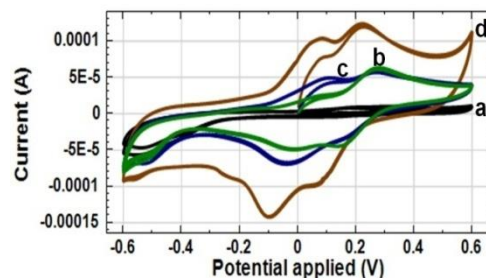


Fig. 5 Cyclic voltammograms at  $100 \text{ mV s}^{-1}$  scan rate of (a) bare SPCE, (b) SPCE-Chi-GST, (c) SPCE-Chi-GST in  $0.1 \text{ M}$  PBE ( $\text{pH } 6.5$ ) containing  $1.0 \text{ mM}$   $[\text{K}_3\text{Fe}(\text{CN})_6]^{3-/4-}$  with  $1 \text{ mM}$  reduced GSH and  $1 \text{ mM}$  CDNB analysis buffer as a blank GST enzyme substrate; and of (d) SPCE-Chi-GST in  $2.5 \text{ } \mu\text{g/ml}$  captan included analysis buffer.

The effect of scan rate on the peak currents and the peak potentials in the presence of captan by the GST immobilized electrodes is illustrated in Fig. 6. A linear relationship between the peak currents and square root of the scan rates with the correlation coefficient  $R^2$  around  $0.99$  of each could be assumed as an evidence for diffusion controlled process.

According to the postulation of captan reaction mechanism [2, 9], this fungicide reacts extremely rapidly with thiol-containing compounds such as glutathione to produce THPI (1,2,3,6-tetrahydro-phthalimide) and reactive thiophosgene by the equation:

$\text{Captan} + \text{GSH} \rightarrow \text{Thiophosgene} + \text{THPI} + \text{HCl}$ . The thiophosgene immediately undergoes further reaction by GST catalysis to form thiazolidine-GSH complex that is spontaneously transformed to an electroactive thiazolidine ring compound, thiazolidine-2-thione-4-carboxylic acid (TTCA). The last oxidation step is proposed by the equation:

$\text{Thiophosgene} + \text{GSH} \xrightarrow{\text{GST}} \text{TTCA} + 2\text{HCl}$ . Considering the GSH oxidation catalysed by GST, the two separated oxidation peaks emergence following the CV measurement in the presence of captan altogether with universal substrate CDNB thus could be presumed as the occurrence of two different xenobiotic-GSH conjugation complexes from the reaction of GSH with thiophosgene intermediate of captan at the  $E_{\text{pa}}$  of  $0.12 \text{ V}$  and from the reaction of GSH with CDNB at the  $E_{\text{pa}}$  of  $0.27 \text{ V}$ .

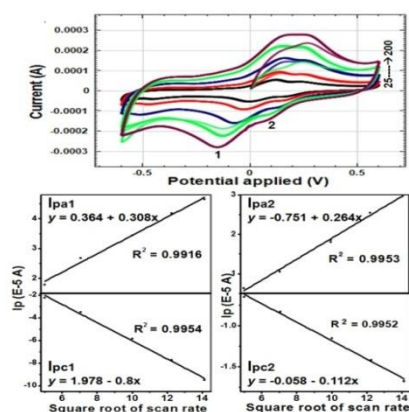


Fig. 6 Cyclic voltammograms of SPCE-Chi-GST in analysis buffer containing 2.5  $\mu\text{g/ml}$  captan accounted by curves from inner to outer corresponding to 25, 50, 100, 150 and 200  $\text{mV s}^{-1}$  scan rates, respectively, with the coordinate linear relationship of their two anodic (Ipa1 and Ipa2) and two cathodic peak (Ipc1 and Ipc2) currents vs. square root of scan rate.

#### Linear detection range of captan

Linear sweep voltammetry (LSV) method was employed to determine the sensing performance of SPCE-Chi-GST and the resulting voltammograms were recorded at 0 up to 20  $\mu\text{g/ml}$  captan concentration in 0.1 M PBE (pH 6.5) containing 1.0 mM  $[\text{K}_3\text{Fe}(\text{CN})_6]^{3-/4-}$  with 1 mM reduced GSH and 1 mM CDNB. Similar electrochemical behaviour to the CV profile was arisen by the appearance of two step oxidation peaks around the potential position 0.04 to 0.12 V for the first peak that continued growing and around 0.2 to 0.27 V for the second peak that continued decreasing in the presence of varying up captan concentrations as shown in Fig. 7. As the first peak currents or peak 1 (p1) gradually increased with an increase of captan concentration, this behaviour could be assumed as a result from the reaction of GSH with thiophosgene intermediate of captan. While the response in the second peak currents or peak 2 (p2) were gradually decreased by typical reaction of GST inhibition.

Calibration plot and detection limit were thus comparatively calculated from either p1 or p2 current against captan concentration. Fig. 8 demonstrates a linear relationship between the current response of SPCE-Chi-GST and captan concentration in two dynamic ranges of 0-1.25  $\mu\text{g/ml}$  and 2.5-15  $\mu\text{g/ml}$  in both cases. The growing p1 currents gradually increased with an increase in captan concentration and the linear regression equations can be expressed as  $y = 1.613 + 0.99x$  with  $R^2 = 0.974$  for the first range, and  $y = 2.93 +$

$0.071x$  with  $R^2 = 0.984$  for the second range, where  $y$  represents the peak current in e-5 ampere (A) and  $x$  represents the captan concentration in  $\mu\text{g/ml}$  as seen in Fig 8A segment p1a and p1b. The detection limit (LOD) for captan in this case is estimated to be 0.225  $\mu\text{g/ml}$  based on the formula:  $\text{LOD} = 3S/b$  where  $S$  is the blank standard deviation ( $n=15$ ) and  $b$  is the slope of the regression. In case of the p2 currents, their two linear regression equations are  $y = 5.066 - 1.205x$  with  $R^2 = 0.995$  in the ranges 0-1.25  $\mu\text{g/ml}$  and  $y = 2.492 - 0.102x$  with  $R^2 = 0.977$  in the ranges 2.5-15  $\mu\text{g/ml}$ . The LOD of 0.198  $\mu\text{g/ml}$  can be acquired in this p2 current case. Notable differences between the slopes of the calibration plots from the first range and the second range of captan concentrations in both p1 and p2 currents are probably due to kinetic limitation at the confine electrode surfaces. The slope obtained from the first concentration range is apparently higher because the active sites number containing on the working surface still be excess in relation to the total number of lower analyte molecules. Statistical analysis between the p1 and p2 current measurements has yielded the value of  $t_{\text{exp}}$  at 0.69 and  $F_{\text{exp}}$  at 1.03 in comparison to the null hypothesis student  $t$ -test of 1.96 critical value and  $F$ -test of 1.00 critical value ( $n = 16$ ) at 95% confidence level. As the  $t_{\text{exp}}$  value was lower than the student  $t$ -test critical value hence their population means are not significantly different. This result also showed an accuracy of the system. While the  $F_{\text{exp}}$  gained was around the  $F_{\text{critical}}$  that should be considered acceptable for the null hypothesis in the population variance. Therefore both the p1 and p2 current delivery cases could be similarly accepted.

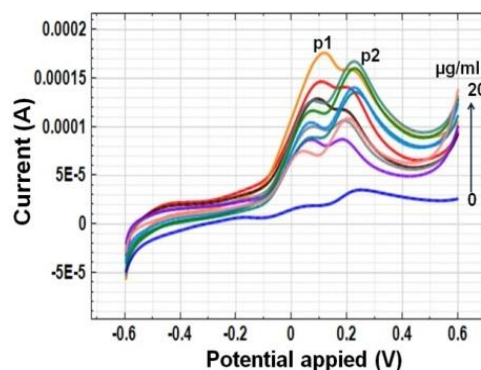
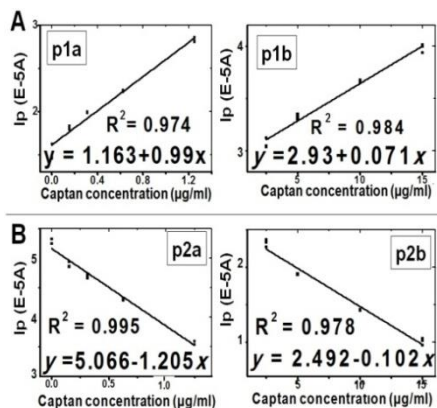


Fig. 7 LSV performance of SPCE-Chi-GST with simultaneous peak 1 (p1) and peak 2 (p2) currents corresponding to different captan concentrations.

The detection range in every regression performance is comparably more competent than the previous reports based on GST activity that were carried through 0.25 to 16 ppm using aminopropyltriethoxysilane-modified gold electrode [4] and 0 to 2 ppm using optical biosensor system

[10]. These repetitive measurement series with different concentrations of captan in all cases gave a correlation coefficient over 0.9 and a relative standard deviation within 3% ( $n = 30$ ), thus demonstrating a high reliability and good repeatability of the measurements including a



reproducibility of the SPCE-Chi-GST fabrication.

Fig. 8 Linear regression relationships from LSV performance of SPCE-Chi-GST between peak 1 current (A) vs. captan concentration ranged from 0-1.25  $\mu\text{g/ml}$  (p1a), and from 2.5-15  $\mu\text{g/ml}$  (p1b); and between peak 2 current (B) vs. the range from 0-1.25  $\mu\text{g/ml}$  (p2a), and from 2.5-15  $\mu\text{g/ml}$  (p2b).

## CONCLUSION

In this present study, a facile electrochemical biosensor has been developed based on the modification of SPCE with chitosan and immobilization of GST enzyme for specific and practical monitoring of captan fungicide. Two sensing mechanisms from this system has been proposed with reference to an occurrence of two simultaneous oxidation peak occurrences in CV and LSV analyses by the formation of two different xenobiotic-GSH conjugation complexes in the reaction system. Quantitative measurements were carried out by their converse concomitance, the peak 1 growing current and the peak 2 decreasing current. A good progressive linear relationship between peak current and captan concentration could be seen in both cases with the LOD around 0.2  $\mu\text{g/ml}$ . All calibrations were attested to be high reliability and reproducibility with the RSD lower than 3% and the correlation coefficient above 0.9. Therefore the detection and quantification of captan are enabled by newly proposed peak 1 current as well as the traditional peak 2 current providing suitable confirmation of the gaining results in parallel.

## ACKNOWLEDGEMENTS

The authors gratefully acknowledge Khon Kaen

University's Division of Research and Technology Transfer Affair for partial funding to both individual and research group (KKU-56-57) and the KKU Research Instrument Center for instrument facilities.

## REFERENCES

- [1] Gottzein AK, Musshoff F, Madea B, "Systematic toxicological analysis revealing a rare case of captan ingestion", *J. of Forensic Sciences*, Vol. 58, Jul. 2013, pp. 1099-1103.
- [2] Gordon EB, "Captan and folpet", *Handbook of Pesticide Toxicology*, Krieger RI, Ed. New York: Elsevier, 2010, pp. 1915-1949.
- [3] Wongkaew P, Poosittisak S, "Atomic force microscopic and electrochemical characterization of the modified screen printed carbon electrode by self assembled deposition of chitosan and activated carbon", *Int. J. of GEOMATE*, Vol. 11, Aug. 2016, pp. 2356-2362.
- [4] Singh RP, Kim YJ, Oh BK, Choi JW, "Glutathione-s-transferase based electrochemical biosensor for the detection of captan", *Electrochemistry Communications*, Vol. 11, Jan. 2009, pp.181-185.
- [5] Orazem ME, Tribollet B, *Electrochemical Impedance Spectroscopy*. New York:Wiley, 2008, pp. 1-459.
- [6] Wongkaew P, Poosittisak S, "Electro-affinity of SCWL-dsDNA on different high deacetylation degree chitosans deposited glassy carbon electrode", *Advances in Developing Affordable In-Vitro Molecular Diagnostics*, Puri CP, Abidi N, Bhanushali, P, Pere A, Gupta SK, Eds. Mumbai: Yashraj Research Foundation, 2012, pp. 249-258.
- [7] Wongkaew P, Poosittisak S, "Diagnosis of sugarcane white leaf disease using the highly sensitive DNA based voltammetric electrochemical determination" *Amer. J. of Plant Sciences*, Vol.5, Jul. 2014, pp. 2256-2268.
- [8] Van der Aar EM, de Groot MJ, Bouwman T, Bijloo GJ, Commandeur JN, Vermeulen NP. "4-Substituted 1-chloro-2-nitrobenzenes: structure-activity relationships and extension of the substrate model of rat glutathione S-transferase 4-4", *Chem. Res. of Toxicology*, Vol. 10, Apr. 1997, pp. 439-449.
- [9] Wolfe NL, Zepp RG, Doster JC, Hollis RC, "Captan hydrolysis", *J. of Agricultural and Food Chemistry*, Vol. 24, May 1976, pp. 1041-1045.
- [10] Choi JW, Kim YK, Oh BK, Song SY, Lee WH, "Optical biosensor for simultaneous detection of captan and organophosphorus compounds", *Biosensors and Bioelectronics*, Vol. 18, May, 2003, pp. 591-597.

## A BASIC STUDY ON FLUID PREDICTION OF MORTAR WITH VARIOUS POWDERS

Yuki takagi<sup>1</sup>, Koji Takasu<sup>2</sup>, Hidehiro Koyamada<sup>3</sup> and Hiroki Suyama<sup>4</sup>

<sup>1</sup> The University of Kitakyushu Graduate School of Environmental Engineering, Japan

<sup>2</sup> The University of Kitakyushu Faculty of Environmental Engineering, Japan

### ABSTRACT

In the field of concrete, Fly ash and crushed stone powder which are by-product powders and limes stone powder are used as admixture materials for concrete from the viewpoint of environmental load. Then we should use by-product powders as materials of the concrete as a substitute of fine aggregate. Therefore it is necessary to predict fluidity of the concrete with powders in large quantities. In this study, we tried a fluid evaluation of mortar with various by-products powders and a fluid prediction by grasping a fluid tendency of mortar with various powders as a part of fine aggregate, and adopted the thickness of a surplus water film theory and the relative flow area ratio as an evaluation index. We clarified when used by-product powders as a part of fine aggregate, we can use excess water film for an index. But the value of the relative flow area ratio was different because of the same thickness of a surplus water film depending on the kind of the powder. It was thought that the fluidity of mortar was able to predict by applying the correction value proposed by this study in various mixtures that used the by-product powder.

*Keywords: Excess Water Film Thickness, Fresh Properties, Fly Ash, Crashed Stone Sand*

### INTRODUCTION

In late years, measures to depletion of natural resources and realization of the low-carbon society are problems in the field of Japanese concrete. So the technique that using by-products powders such as fly ash and crush stone powder or the limestone fine powder as a concrete material is considered as solution to these problems. Therefore a fluid evaluation and prediction of the concrete using by-product powders are required. In this study, We confirm a fluid tendency of mortar which mixed several kinds of powders as a substitute for fine aggregate and evaluated fluidity using excess water film thickness ( $\delta$ ) and the relative flow area ratio ( $\Gamma$ ).

### EXCESS WATER FILM THICKNESS

In this study, excess water thickness was used as an index to show how the composition of mortar and byproduct-based powders influences fluidity. The excess water theory of Miyake et al.<sup>1)</sup> used in this study considers the liquid phase as water and the solid phase as powder and fine aggregate; the correlation with liquidity was reported, assuming that the excess water forms a uniform water film on each particle. The following formula proposed by Miyake et al.<sup>2)</sup> was used to calculate the thickness of the excess water film.

$$W_{exc} = 10^{-2} \cdot (G - G_s) \quad (1)$$

$$\delta = 10^4 \cdot \frac{W_{exc}}{S_p + S_s} = 10^8 \cdot \frac{G - G_s}{S_p + S_s} \quad (2)$$

Refer to “ $W_{exc}$ ” is excess quantity of water

( $m^3/mortar\ m^3$ ), “ $G$ ” is solid content in aggregate of the thing which mixed fine aggregate with powders (%), “ $G_s$ ” is the volume of powders and fine aggregate ratio in the mortar volume (%), “ $S_p$ ” is surface area of powders in mortar  $1m^3$  ( $cm^2/m^3$ ), “ $S_s$ ” is surface area of fine aggregates in mortar  $1m^3$  ( $m^2/m^3$ ), “ $\delta$ ” is excess water film thickness ( $\mu m$ ).

Further, in order to eliminate the influence of particle size distribution, Miyake et al. performed analyses with a dimensionless value  $\delta/d$ , where  $\delta$  is found from the excess water film and  $d$  is the volume-surface average particle size of the solid. The calculation of  $\delta/d$  is described below.

$$A_{cs} = \frac{S_p + S_s}{10^{-2} \cdot G_s} = \frac{6 \cdot \pi (10^{-6} \cdot d)^2}{\pi (10^{-6} \cdot d)^3}$$

$$\therefore d = 6 \times 10^4 \cdot \frac{G_s}{S_p + S_s} \quad (3)$$

Refer to “ $A_{cs}$ ” is mean ratio surface area of cement and fine aggregate per volume ( $cm^2/m^3$ ), “ $d$ ” is average particle size of cement and fine aggregate ( $\mu m$ ).

It is expressed by equation (4) by dividing equation (2) in equation (3)

$$\frac{\delta}{d} = \frac{G - G_s}{6 \cdot G_s} \quad (4)$$

I found the ratio surface area of fine aggregate in the following equations.

$$S_{su} = 6 \cdot \sum \frac{X_i}{100 \cdot a_i} \quad (5)$$

Refer to “ $S_{su}$ ” is the ratio surface area of fine

aggregate ( $\text{mm}^2/\text{mm}^3$ ), “ $X_i$ ” is Capacity percentage between sieve opening  $l_i$  and  $l_{i+1}$  (%), “ $a_i$ ” is average particle size by the geometric mean between sieve opening  $l_i$  and  $l_{i+1}$  ( $\text{mm}$ )  $= (l_i \cdot l_{i+1})^{0.5}$ .

## THE RELATIVE FLOW AREA RATIO

The relative flow area ratio ( $\Gamma$ ) is a thing used for a self-filling-related index, and fluidity is high so that a value is big.

$$\Gamma = \frac{(d_1 \cdot d_2 - d_0^2)}{d_0^2} \quad (6)$$

Refer to “ $d_0$ ” is the inside diameter of the lower flow corn, “ $d_1$  and  $d_2$ ” is I do it with the value that measured the direction that is a right angle in greatest dimension and that of mortar after the transformation.

## SUMMARY OF THE EXPERIMENT

Used materials showed in table 1. I used fly ash of the prescribed II class equivalency for JIS A 6201, crush stone powder of the prescribed for JIS A 5041, crash sand of the prescribed for JIS A 5005. In addition, I kept it more than 24 hours and used these materials for a constant temperature room of 20 degrees Celsius.

Compounding showed in table 2. The admixture-free mixes NS and N-CS were the standard formulations, and the three byproduct components—fly ash powder, limestone fine powder, and crushed stone powder—mixed to a concentration of 5, 7.5, 10 or 15% by volume were used as partial replacement of fine aggregate. In the experiment, mixing was carried out with the formulation in Table 2. The CSPs 10 and 15 are excluded from the formulation table because they could not be mixed with either sea sand or crushed sand. In contrast, FA/LP15-CS, which was also impossible to mix, is listed in the formulation table because it could be mixed with sea sand. As for

the notation method of the compounding sign, “FA” “LP” “CSP” shows a use powders name followed by the written number shows a substitution rate.

In addition, the “S” “CS” of the end expresses sand name which I used, and the number of the end of the standard compounding expresses a water cement ratio. “P” in the compounding list means powders, and “W/P” expresses water powders mass ratio. I worked it out using a mortar mixer and mixed mortar. I measured a mortar flow and mini-slump, the solid content in aggregate of the thing which mixed fine aggregate with powders. For deriving the solid content concentration in the mixture, a steel mortar form ( $\phi 50$  mm, height 100 mm) was filled with the

Table1: Used materials

Item	Type	Properties	Mark
Cement	Ordinary portland cement	Density 3.16g/cm <sup>3</sup>	C
Water	Tap water	-	W
Admixture	Fly ash (JIS II class)	Density 2.43g/cm <sup>3</sup>	FA
		Ignition loss 1.67%	
		Blain's specific surface area 4270cm <sup>2</sup> /g	
	Limestone powder	Density 2.74g/cm <sup>3</sup>	LP
		Blain's specific surface area 2975cm <sup>2</sup> /g	
	Crush stone powder	Density 2.70g/cm <sup>3</sup>	CSP
		Blain's specific surface area 4624cm <sup>2</sup> /g	
Fine aggregate	Sea sand	Surface dry density 2.59g/cm <sup>3</sup>	S
		Water absorption 0.76%	
		Blain's specific surface area 55.9cm <sup>2</sup> /g	
		Fineness modulus 2.4	
	Crush Sand	Solid content 61.5%	CS
		Surface dry density 2.66g/cm <sup>3</sup>	
		Water absorption 1.96%	
		Blain's specific surface area 33.6cm <sup>2</sup> /g	
		Fineness modulus 3.1	
		Solid content 57.1%	

Table2: Mix proportions and Experimental

Symbol	W/C	W/P	Unit content(kg/m <sup>3</sup> )						G(%)	G <sub>s</sub> (%)	δ(μm)	Flow(mm)	mini-s lump Ms(cm)
	(%)	(%)	W	C	FA	LP	CSP	S (CS)					
N-S30	30	30	280	934	0	0	0	917	70.7	65.0	0.18	142	1.9
N-S40	40	40	280	701	0	0	0	1109	75.8	65.0	0.45	185	6.2
N-S50	50	50	280	560	0	0	0	1223	76.7	65.0	0.60	189	7.6
N-S(CS)60	60	60	280	467	0	0	0	1300(1360)	77.9(78.2)	65(65)	0.79(0.82)	190(189)	7.3(7.7)
N-S70	70	70	280	400	0	0	0	1355	75.9	65.0	0.77	192	6
FA5-S(CS)	60	43	269	449	182	0	0	1157(1211)	75.2(74.1)	66.4(66.4)	0.38(0.33)	204(183)	10(6.2)
FA7.5-S(CS)	60	37	264	440	267	0	0	1090(1140)	74.2(73.8)	67(67)	0.27(0.26)	176(154)	6(3.2)
FA10-S(CS)	60	33	259	432	350	0	0	1025(1072)	72(73.4)	67.6(67.6)	0.15(0.19)	180(152)	5.7(3.2)
FA15-S(CS)	60	27	250	416	505	0	0	902(944)	71.3	68.8	0.07	175	6.6
LP5-S(CS)	60	41	269	449	0	207	0	1157(1211)	73.4(73.4)	66.4(66.4)	0.32(0.32)	184(167)	4.8(3.6)
LP7.5-S(CS)	60	35	264	440	0	305	0	1090(1140)	72.6(71.0)	67(67)	0.23(0.17)	166(163)	3.4(3.1)
LP10-S(CS)	60	31	259	432	0	399	0	1025(1072)	70.7(69.1)	67.6(67.6)	0.12(0.06)	150(142)	1.7(2.0)
LP15-S(CS)	60	25	250	416	0	576	0	902(944)	70.6	68.8	0.06	121	0.4
CSP5-S(CS)	60	41	269	449	0	0	206	1157(1211)	74.4(75.3)	66.4(66.4)	0.32	153	2.7(2.0)
CSP7.5-S(CS)	60	36	264	440	0	0	303	1090(1140)	74.3(73.8)	67(67)	0.25	119	0.6(0.6)



mix in a mixer and tapped using a flow table of once per second, and then the volume was derived from the sinking depth of the material in the container; this volume is divided by the container volume to derive the solid content in aggregate. The number for tapping was set at 500 times on the basis of a preliminary test.

## RESULT AND CONSIDERATION

### Excess water film thickness and fluidity

Figs.1,2 showed a water film thickness and relations of the relative flow area ratio, mini-slump. In both Figs. 1 and 2, there was a tendency in all formulations for the relative flow area and the mini-slump to increase as the excessive water film became thicker. This is taken to indicate that the change in the excess water film thickness influences the fresh state, such as the relative flow area and the mini-slump of mortar. However, when comparing the powders in Figs. 1 and 2, it can be seen that there is a large difference in relative flow area and mini-slump between them, even when the water film thicknesses are the same. This seems to indicate the influence of the properties of the powders. A possible influencing factor is the difference in particle shape. Whereas fly ash has a smooth spherical shape, it is reported that for crushed powder with fine surface irregularities, the BET-specific surface area is larger than for other types of powders<sup>2)</sup>. That is, we assume that the difference in particle shape influenced fluidity. Also, in the process using fly ash, the relative flow area and mini-slump were differed sharply between sea sand and crushed sand, while in the standard formulation, little fine aggregate choice had little influence.

## FLUID PREDICTION

### Examination by Excess water film thickness

From the results of preceding section, it can be inferred that it is difficult to predict fluidity from only water film thickness when comparing between processes that use different powders. We consider whether it is possible to predict the fluidity using water film thickness by applying a correction value for each powder, assuming that the way the unique properties of each powder influences fluidity can be evaluated from its water film thickness. To do so, we need an intermediary indicator that correlates with both water film thickness and relative flow area. It has been confirmed in a previous study<sup>1)</sup> that the unit amount of water relative to the total surface area of the powder is correlated with fluidity. In this, Water volume per total surface area was used as an index to evaluate both water film thickness and relative flow area. Even within this experiment, in each powder, the water volume per total surface area was correlated with the ratio between water film thickness and relative flow area, as shown in Fig. 3.

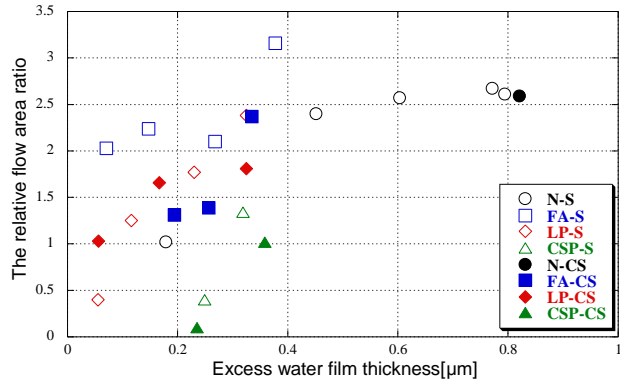


Fig.1 Water film thickness and Relative flow area ratio

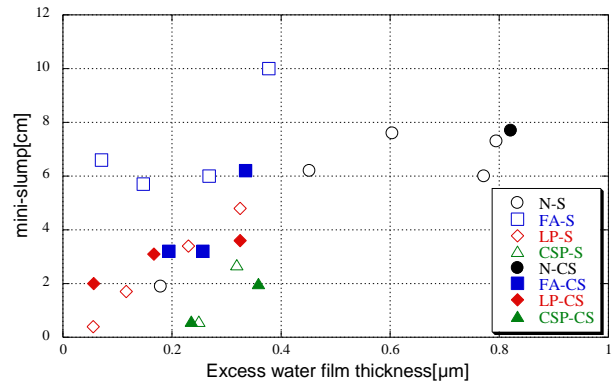


Fig.2 Water film thickness and Mini-slump

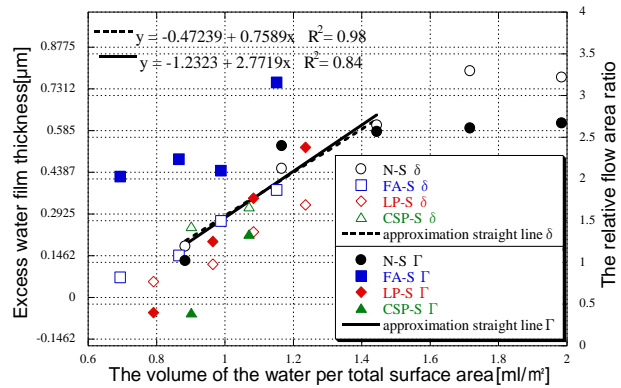
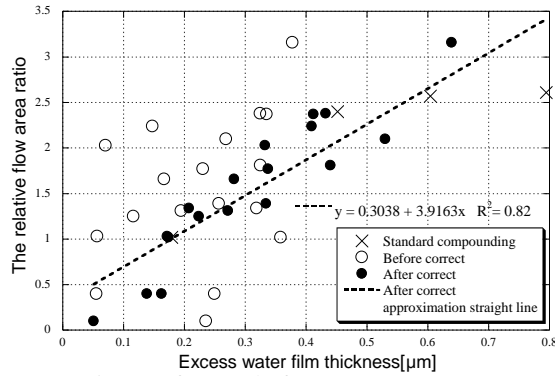


Fig.3 volume of the water per total surface area and  $\delta$ ,  $\Gamma$

In order to evaluate the characteristics peculiar to the powder, the y-axis was adjusted on the graph so that the reference formulation is approximately a straight line. Figure 3 shows the fitted curves. Here, a linear approximation was found for the cases N-S 30, 40, and 50; in these, a linear relationship was clearly observed. It is assumed from this that the differences between the curves of water film thickness and relative flow area for each powder (Fig. 3) are due to the characteristics peculiar to the powder. Therefore, approximately straight lines were drawn for the curves of water film thickness and relative flow area for the powders, and the correction value was obtained by averaging the difference between the straight lines and converting it into water film

Fig.4 Before and after correct-  $\delta$ ,  $\Gamma$ 

thickness; the water film thickness calculated using the correction value was taken as the corrected water film thickness.

A similar technique was also used for the mini-slump. By correcting the water film thickness for each powder using the correction value, it was possible to express the relation between water film thickness and relative flow area and mini-slump as a straight line. In other words, it is assumed that fluidity can be approximately evaluated and predicted using both correction values and straight-line approximations, as seen in Figs. 4 and 5. Looking at the correction values in Table 3, significant differences were observed according to powder. The correction value of fly ash is larger than that of other types of powders. This seems to be due to the ball-bearing effect caused by the smooth and round shape of the fly ash, which improves the fluidity such that the fluidity becomes theoretically large against the water film thickness. In contrast, with the crushed powder, the correction value for the relative flow area and mini slump is negative. This is interpreted as being because fine irregularities on the particle surface of the crushed stone powder decrease the fluidity, and so the fluidity becomes theoretically small against the water film thickness.

#### Examination by $\delta/d$

In comparison with the excess water film thickness, which is derived by dividing excess water volume by total surface area, and so depends on the surface area, the index  $\delta/d$  proposed by Miyake et al.<sup>1)</sup> excludes the influence of the particle size distribution and is more concise than the water film thickness, which does not include the surface area in the derivation. Therefore, a consideration similar to that made for water film thickness was also made for the index  $\delta/d$ . Before the correction, the relative flow area ratio and mini-slump increased with  $\delta/d$ , as in the case of the water film thickness, but when comparing different powders for the same value of  $\delta/d$ , variations were observed from powder to powder. However, we could derive a linear relationship between  $\delta/d$  and relative flow area and mini-slump through corrections. Also, looking at the

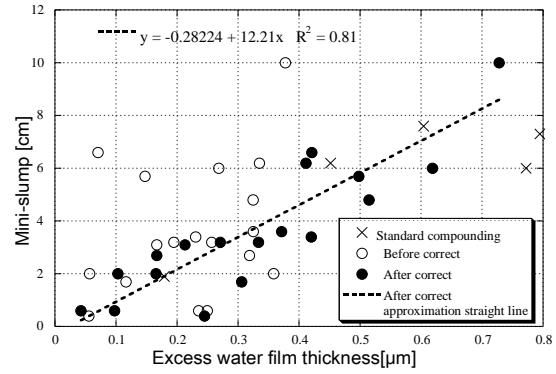
Fig.5 Before and after correct-  $\delta$ , Ms

Table3: Water film correction value

Powder	Fine aggregate	Water film correction value $\Gamma$ ( $\mu\text{m}$ )	Water film correction value Ms ( $\mu\text{m}$ )
FA	S	$2.62 \times 10^{-2}$	$3.50 \times 10^{-2}$
	CS	$7.72 \times 10^{-3}$	$7.65 \times 10^{-3}$
LP	S	$1.07 \times 10^{-2}$	$1.90 \times 10^{-2}$
	CS	$1.12 \times 10^{-2}$	$4.62 \times 10^{-3}$
CSP	S	$-1.12 \times 10^{-2}$	$-1.52 \times 10^{-2}$
	CS	$-1.85 \times 10^{-2}$	$-1.93 \times 10^{-2}$

Table4:  $\delta/d$  correction value

Powder	Fine aggregate	$\delta/d$ correction value $\Gamma$ ( $\mu\text{m}$ )	$\delta/d$ correction value Ms ( $\mu\text{m}$ )
FA	S	$1.62 \times 10^{-2}$	$1.83 \times 10^{-2}$
	CS	$3.59 \times 10^{-3}$	$2.80 \times 10^{-3}$
LP	S	$6.37 \times 10^{-3}$	$8.50 \times 10^{-4}$
	CS	$7.46 \times 10^{-3}$	$2.76 \times 10^{-3}$
CSP	S	$-8.71 \times 10^{-3}$	$-7.59 \times 10^{-3}$
	CS	$-1.30 \times 10^{-2}$	$-1.37 \times 10^{-2}$

correction values in Table 4, the correction value of fly ash was large, and the correction value of the crushed powder was negative, a result similar to the result for water film thickness; therefore,  $\delta/d$  seems adequate to use as an index of fluidity.

#### CONCLUSION

1 – 1) Even when a byproduct-based powder is mixed as a water film thickness as an index of fluidity, though the properties of the powders must be taken into account when doing so.

2 – 1) The correction value was given as a converted water film thickness to indicate the influence of the characteristics of the powder on the fluidity, and the corrected water film was obtained by adding the correction value to the theoretical water film thickness. By using the corrected value for the water film, the relation between corrected water film and relative flow area and mini-slump, which serves as an index of fluidity, can be given by a straight line. From this, it seems that the liquidity can be approximately evaluated and predicted simply by using water film thickness, even for a process using byproduct-based powders.

## **ACKNOWLEDGMENTS**

The experiment was supported by Eiji Mikura, Saori Itanami, Irie Akira. We show gratitude to them.

## **REFERENCES**

- [1]Miyake Jyunichi, Matsushita Hirotsugu , Torii Tsuyoshi “Consideration about the fresh time property of different mortar of paste levels and the powders classification”, Concrete engineering annual memoirs,Vol.2, No.1,2005,pp997~1002
- [2]Fukuyama Tomohiro, “Study on use as mixture materials for high flow concrete of the crush stone powder”, Concrete engineering annual memoirs, Vol.25, No.1, pp977~982, 2003.7



## PHYTOCHEMICALS AND ANTIOXIDANT ACTIVITIES OF THAI RED RICE SEEDS FROM DIFFERENT CULTIVATED AREAS

\*Muntana Nakornriab<sup>1</sup>, Jiraporn Krasaetep<sup>2</sup>, Maratree Plainsirichai<sup>3</sup> and Sisikka Wannajun<sup>4</sup>

<sup>1</sup> Faculty of Science, Mahasarakham University, Mahasarakham 44150, Thailand

<sup>2</sup> Faculty of Technology, Mahasarakham University, Mahasarakham 44150, Thailand

<sup>3</sup> Faculty of Cultural Science, Mahasarakham University, Mahasarakham 44150, Thailand

### ABSTRACT

The objectives of this work were to study total phenolic, flavonoid, anthocyanin contents and antioxidant activities of Thai red rice seed from different 14 areas. Total phenolic, flavonoid and anthocyanin contents were measured using Folin-Ciocalteu, colorimetric aluminum chloride and pH differential methods respectively. The antioxidant activities were measured by DPPH and FRAP assay. The results showed that seed extract from Thai red rice from different areas had total phenolic and flavonoid contents in range of 112.46-278.88 mg GAE/100g sample, 238.55-980.13 mg quercetin/100 g sample, respectively. While the antioxidant activities were found in range of 3.26-8.63 mg/mL and 510.50-2350.41 mM Fe(II)/100 g sample, respectively. The seed extracts from NET area had significantly higher phytochemicals and antioxidant activities than other extracts from different areas. In conclusion, the Thai red rice should be proposed as potential sources of safe natural antioxidants and preservatives for rice industry.

*Keywords: Thai red rice, phytochemical, antioxidant activity, different cultivated area*

### INTRODUCTION

Rice is an important food of Thai people and foreigners for a long time. Currently, rice products produce income to Thailand more than other agricultural products. Rice is cereal which its scientific name is *Oryza sativa* L. It is in a family of Poaceae. Rice grown in Thailand is an indica type. Rice is divided into rice and glutinous rice. The difference between rice and glutinous rice is type of starch that is combined into the endosperm. Rice kernels contain amylase flour about 15-30%, while glutinous rice kernels contain most of amylopectin but very small amylose content. Thailand has many kinds of rice which have many seed colors, indicating the special properties of rice as the source of nutrients and special substances. Eighty of seed rice is flour and 20% of seed rice is bran and rice germ nutrients [1]. Grain consists of two parts: hull or husk, which is outer most part of seed and fruit or pure rice (true fruit or caryopsis or brown rice) which is inside the cracked kernel.

Brown rice consists of 3 main parts, germ, or embryo (germ) rice seed coat (bran) and rice kernel (endosperm). Germ or embryo is at the base of large seed shell which. Germ is the source of food for growth of seed and it contains high the amount of nutrients such as protein, fat, and vitamin E. In addition, the germ also contains substances that have different antioxidants including phenolics tocopherol tocotrienol, oryzanol [2-5]. Seed pericarp is the outer layer of tissue containing pigment mixed with brown rice is made with various colors like brown, russet or

purple or other colors depending on type and rice components. Furthermore, there are important parts like proteins, cellulose and hemicellulose. Next to fruit pericarp, it is seed pericarp or rice bran. It is 10 % of all seed that contains fat and pigment like fruit pericarp. This causes brown rice has high nutrient substances and fiber [6]. There is the report that brown rice or rice with different colors like red, dark purple, and black in inner seed contain higher important nutrients than rice with has no color for example polyphenol, betacarotene, anthocyanin, vitamin E, and gamma oryzanol. These antioxidant activity substances are very useful and prevent aging, obesity, diabetes, cancer, and cardiovascular disease [7-8].

### METHODOLOGY

Thai red rice samples (Taptim-Chumphae rice) collected from 18 different areas of Thailand: 3 provinces from North Thailand (NT), 3 province from Southern Thailand (ST), 3 province from East Thailand (ET), 3 province from West Thailand (WT), 3 provinces from North East Thailand (NET) and 3 provinces from Central Region Thailand (CRT). They were from the 2015 of the Chumphae Rice Research Center in Khon Kaen province and Faculty of Technology, Mahasarakham University, Thailand. All chemical reagents used were analytical grade.

### Extraction of Crude Antioxidants

The seeds from Thai red rice at different area were dried in oven at 25 °C, then ground to a fine powder in a mechanical blender. Dried seed powder (10.0g) were extracted by 95% ethanol containing 1.0% HCl (3×100 mL) for 30 min with intermittent shaking at room temperature. The extracts were combined and filtered through a 0.45 µm Nylon membrane filter. After The crude extracts stored at 4 °C in storage vials for the determination of phytochemicals and antioxidant activities.

### Phytochemical screening

Phytochemical screening of Thai red rice seed extracts were carried out on the three extracts, total phenolic flavonoids and anthocyanin contents.

#### Total phenolic contents

The total phenolic contents of crude seed extracts from Thai red rice were determined by spectrophotometric method using Folin–Ciocalteu’s phenol reagent as described earlier with some modifications [8]. The crude extract in ethanol (0.5 mL) was placed in a test tube and was diluted to 5.0 mL with a glass of distilled water. Folin–Ciocalteu’s phenol reagent (5.0 mL) was added, and the contents of the test tube were mixed thoroughly. After 3.0 min, 5 mL of 10% sodium carbonate solution was added, and the mixture was allowed to stand for 1 h with intermittent shaking. The absorbance of the blue color was measured in a Shimadzu UV-2101PC Spectrophotometer (Bio-Tek Instrument INC, Canada) at 750 nm. The concentration of total phenolic compounds was determined using the gallic acid equation (mg/g extract) obtained from the standard gallic acid calibration curve. This experiment was carried out three times, and the results were averaged for the different fractions in the Thai red rice varieties.

#### Total flavonoid contents

The total flavonoid contents of crude seed extracts from Thai red rice were determined by spectrophotometric method using the aluminum chloride colorimetric method [9]. Pipette crude extracts in ethanol (250 µL) was placed in a test tube, mixed with 1.25 mL of distilled water, Shake well. Add 75.0 µL of 5% NaNO<sub>2</sub> solution to shake well. Then set aside at room temperature for 5 minutes, and add 150 µL of 10% aluminum chloride (AlCl<sub>3</sub>). Shake the mixture well and allowed to stand for 6 min. Afterward, 500 µL of 1 mol/L NaOH solution were added, and the final volume of the mixture was brought to 10 mL with double-distilled water. The mixture was allowed to stand for 15 min, and absorbance was measured in a Shimadzu UV-2101PC Spectrophotometer (Bio-Tek Instrument INC, Canada) at 510 nm. The total flavonoid content

was calculated from a calibration curve, and the result was expressed as mg quercetin equivalent per 100 g of sample

#### Total anthocyanin contents

The total anthocyanin content (TAC) was determined by the pH-differential method [10]. Pipette crude extracts solution 1 mL into 10 mL volumetric flask for preparing two dilutions of the sample, one adjust volume with 0.025 M potassium chloride buffer, pH 1.0, and the other with 0.4 M sodium acetate buffer, pH 4.5, diluting each. Let these dilutions equilibrate for 15 min. Measure the absorbance of each dilution at the 510 and 700 nm, against a blank cell filled with ethanol. Results are expressed as micrograms of cyanidin 3-glucoside equivalents (Cy3-GE)/ 100 g of dry weight. The anthocyanin content was calculated as follows:

$$\text{The total anthocyanin content } \left( \frac{\text{mg}}{\text{L}} \right) = \frac{A \times \text{MW} \times \text{DF} \times 1000}{\epsilon \times 1} \quad (1)$$

Where

$$A = (A_{510\text{nm}} - A_{700\text{nm}})_{\text{pH} 1.0} - (A_{510\text{nm}} - A_{700\text{nm}})_{\text{pH} 4.5}$$

MW = molecular mass cyaniding-3-glucoside (449.2)

DF = dilution factor

ε = molar absorptivity of cyanidine-3-glucoside (26,900)

#### Antioxidant activities

##### 1,1-Diphenyl-2-picryl-hydrazyl (DPPH) assay

The radical scavenging activity of crude seed extracts from Thai red rice measured using the 1,1-diphenyl-2-picryl-hydrazyl (DPPH) assay, as described earlier with some modifications [9]. The crude extract (0.01-10.0 mg/mL) of 1 mL was placed in a test tube, mixed with 3.0 mL of 0.1 mM DPPH (2,2-diphenyl-1-picrylhydrazyl) in ethanol. The mixture was shaken vigorously and was left to stand for 30 min at room temperature in the dark. The absorbance was measured in a Shimadzu UV-2101PC Spectrophotometer (Bio-Tek Instrument INC, Canada) at 517 nm. The control reaction contained all reagents except for the crude samples. The radical scavenging effect was calculated by the following equation:

$$\text{Scavenging effect (\%)} = \left[ \frac{A_c - A_s}{A_c} \right] \times 100 \quad (2)$$

where A<sub>c</sub> is the absorbance of the control at 517 nm, and A<sub>s</sub> is the absorbance of the extract/standard at 517nm. This experiment was repeated thrice, and the results were averaged for the different fractions in the crude extracts.

### Ferric Reducing Antioxidant Power (FRAP) assay

Ferric Reducing Antioxidant Power FRAP assay was performed according to the methods of [11] with slightly modification. The FRAP reagent was freshly prepared by adding 10 mM of 2,4,6-Tris (2-pyridyl)-1,3,5-triazine (TPTZ) (dissolved in 40 mM of HCl), 20 mM of FeCl<sub>3</sub> in water and 300 mM of acetate buffer (pH 3.6) in the ratio of 1:1:10. The crude extract 10mg/mL (100  $\mu$ L) were mixed with 3 mL FRAP reagent in test tubes, mixed with 300  $\mu$ L of distilled water and undergoes vortex. Both samples and blank were incubated for 4 minutes at 37°C. The absorbance was measured in a Shimadzu UV-2101PC spectrophotometer (Bio-Tek Instrument INC, Canada) at 593 nm. The values obtained were expressed as  $\mu$ M of ferrous equivalent Fe (II) per 100 gram of sample.

### Statistical analysis

Results obtained were reported as mean  $\pm$  SD of triplicate measurements. Significance differences for multiple comparisons were determined by Turkey's Honest Significant Difference (HSD) at 0.05 probability level.

## RESULTS AND DISCUSSION

Phytochemical screening of Thai red rice seeds from different cultivated areas revealed the present of total phenolic and flavonoid contents in all the extracts, but no anthocyanin.

### Total Phenolic Compounds

Total phenolic content (TPC) of Thai red rice seeds from different cultivated areas was measured by the Folin-Ciocalteu reagent method using gallic acid as the standard. A linear calibration curve of gallic acid resulted with a linear regression equation of calibration curve ( $y = 1.939x + 0.048$ ,  $R^2 = 0.975$ ) This linear equation was used to determine the total phenolic compounds in the seed extracts from Thai red rice at different area. The average quantity of the total phenolic compounds found in the seed extracts is shown in **Table 1**. The amount of total phenolics content of the seed extracts were in the range of  $113.04 \pm 27.20$  -  $278.88 \pm 58.05$ mg GAE/100g Sample. Among the seed extract from rice Táptim-Chumphae at, NET 1 present the highest amount of TPC. Generally, phenolic compounds are the main constituents in plants and characterized by having at least one aromatic ring with one or more hydroxyl groups attached.

### Total Flavonoids Compounds

Total flavonoids content of Thai red rice seeds from different cultivated areas was determined by the aluminum chloride colorimetric method using quercetin as the standard. A linear calibration curve

of quercetin resulted with a linear regression equation of calibration curve ( $y = 1.939x + 0.048$ ,  $R^2 = 0.975$ ) This linear equation was used to determine the total flavonoids compounds in the seed extracts from Thai red rice at different area. Flavonoids are polyphenolic which are the most numerous of the phenolic compounds that found throughout the plant kingdom. The average quantity of the total flavonoids c compounds found in the seed extracts is shown in **Table 1**. The amount of total flavonoids content of the seed extracts were in the range of  $238.55 \pm 21.83$ -  $980.13 \pm 55.93$  mg GAE/100g Sample. Among the seed extract from Thai red rice seeds at, NET 1 present the highest amount of TFC.

**Table 1.** The total phenolic and flavonoids contents of Thai red rice seeds from different cultivated areas by total phenolic and flavonoid contents (n=5)

Red rice from different cultivated areas	TPC (mg GAE/100g Sample)	TFC (mg Quercetin/100 g Sample)
CRT 1	119.00 $\pm$ 19.32	871.64 $\pm$ 54.64
CRT 2	190.50 $\pm$ 21.13	811.69 $\pm$ 60.68
CRT 3	226.58 $\pm$ 53.13	912.30 $\pm$ 40.45
NET 1	278.88 $\pm$ 58.05	980.13 $\pm$ 55.93
NET 2	233.82 $\pm$ 37.44	657.36 $\pm$ 74.27
NET 3	231.55 $\pm$ 20.69	497.98 $\pm$ 55.32
ST 1	117.68 $\pm$ 17.74	727.06 $\pm$ 85.61
ST 2	119.75 $\pm$ 12.32	643.10 $\pm$ 48.29
ST 3	112.46 $\pm$ 14.78	519.47 $\pm$ 49.21
ET 1	149.29 $\pm$ 24.15	763.98 $\pm$ 11.52
ET 2	123.03 $\pm$ 26.74	713.49 $\pm$ 27.83
ET 3	133.56 $\pm$ 19.46	737.58 $\pm$ 39.45
WT 1	211.68 $\pm$ 22.83	829.95 $\pm$ 49.79
WT 2	199.03 $\pm$ 16.83	774.05 $\pm$ 28.91
WT 3	208.46 $\pm$ 18.73	805.89 $\pm$ 40.06
NT 1	113.04 $\pm$ 27.20	238.55 $\pm$ 21.83
NT 2	140.19 $\pm$ 27.02	278.79 $\pm$ 21.33
NT 3	164.85 $\pm$ 17.34	303.06 $\pm$ 79.04

NT means Northern Thailand, NET means Northeastern Thailand, CRT means Central Region Thailand, ET means Eastern Thailand, ST means Southern Thailand, WT means West Thailand

### Antioxidant Activities

Antioxidant activity of the seed extracts from Thai red rice at different area were measured by DPPH-radical-scavenging and FRAP assay (Table 2). The radical-scavenging activity of each crude seed extracts were measured by using the DPPH assay. When the DPPH radical was scavenged by an antioxidant through the donation of H<sup>•</sup> to form the reduced DPPH-H, the color changed from purple to yellow. In this study, the scavenging activity was amplified with the increased concentration of all the

rice antioxidants in the range of 0-40 mg/mL, and it was constant at concentration above 15 mg/mL. In the DPPH radical-scavenging assay, the concentrations of BHA, ascorbic acid and seed extract of Thai red rice at different area, at which the DPPH radicals were scavenged by 50 % (IC<sub>50</sub>), the lower the IC<sub>50</sub>, the higher the antioxidant activity. The average quantity of the DPPH and FRAP value in the seed extracts were shown in **Table 2**. The NET 1 extract showed the highest activity (IC<sub>50</sub> = 3.26 ± 0.23mg/mL). In addition, the NET 1 had the highest of FRAP value (2350.41 ± 360.42 mM Fe(II)/100 g Sample), too.

**Table 2.** The antioxidant activities of Thai red rice seeds from different cultivated areas by FRAP and DPPH assay (n=5)

Red rice from different cultivated areas different area	FRAP (mM Fe(II)/100 g Sample)	IC <sub>50</sub> (mg/mL)
CT1	1200.56 ± 124.07	4.41 ± 0.18
CT2	1324.03 ± 198.69	5.08 ± 0.18
CT3	1731.05 ± 113.44	4.45 ± 0.15
NET1	2350.41 ± 360.42	3.26 ± 0.23
NET2	1902.42 ± 121.45	3.31 ± 0.07
NET3	2002.78 ± 196.82	3.57 ± 0.46
ST1	658.04 ± 79.97	5.72 ± 0.32
ST2	712.39 ± 84.69	5.32 ± 0.31
ST3	729.04 ± 85.14	5.41 ± 0.28
ET1	510.50 ± 74.16	8.63 ± 0.59
ET2	521.40 ± 76.39	7.95 ± 0.48
ET3	553.08 ± 75.99	8.23 ± 0.44
WT1	1497.69 ± 283.80	4.66 ± 0.17
WT2	1538.95 ± 249.56	4.75 ± 0.22
WT3	1501.58 ± 263.01	4.72 ± 0.23
NT1	1089.65 ± 113.77	4.66 ± 0.28
NT2	1219.52 ± 208.10	4.20 ± 0.08
NT3	1352.20 ± 127.11	3.91 ± 0.32
BHA	-	0.0085 ± 0.00
Ascorbic acid	-	0.0071 ± 0.00

NT means Northern Thailand, NET means Northeastern Thailand, CRT means Central Region Thailand, ET means Eastern Thailand, ST means Southern Thailand, WT means West Thailand

## CONCLUSION

The results presented in this study showed that Thai red rice seeds from different cultivated areas is one of good sources of phytochemical compounds and antioxidant activities. The Thai red rice seeds from Northeastern Thailand had the highest amount of nutrients. It may be from soil, fertilizer, air etc. Therefore, the Thai red rice seeds from different

cultivated areas is a potential source of anti-oxidative phytochemicals and is a useful ingredient for nutraceutical, food industry, health products or functional food products.

## ACKNOWLEDGEMENTS

The authors wish to thanks to Mr. Ronnachai Changsri, The Chumphae Rice Research Center in Khon Kaen province, Thailand for supporting the Thai red rice seeds from different cultivated areas, Department of Chemistry, Faculty of Science, Department of Agricultural Technology, Faculty of Technology, Mahasarakham University, Mahasarakham 44150, Thailand for a partial support of some chemicals.

## AUTHOR'S CONTRIBUTIONS

The experiments were conducted in majority of the conception, design, acquisition, analysis and interpretation of data and drafting the article by Muntana Nakornriab. Critical reviewing and final approval of the version to be submitted were supported by Jiraporn Krasaetep, Maratree Plainsirichai and Sisikka Wannajun.

## ETHICS

This article is original work and not under consideration for publication in any other journal. There are not conflict interests on this paper.

## REFERENCES

- [1] Juliano, B. O., Rice in Human Nutrition. The International Rice Research Institute (IRRI), Laguna, and Food and Agriculture Organization of the United Nations (FAO); Rome; (FAO Food and Nutrition Series; Vol 26). 1993.
- [2] Artht, K., Apichart, N., Somdej, I. Lek, C. Evaluation of Nutritional Values in Colored Rice. Agric Sci. J. 40: 1 (Suppl.), 2009, pp. 345-348.
- [3] Suttajit, M., Immark, S., Teerajan, S., Suttajit, S., Chiyasut, C., Antioxidative activity and polyphenol content in different varieties of Thai rice grains. Proceedings of Asia Pacific Clinical Nutrition Society. Joint 8<sup>th</sup> ISCN and 5<sup>th</sup> APCNS conference 2006. [Online], [http://www.healthy\\_eating\\_club.com/APJCN/Volume15/Vol15\\_apcns.htm](http://www.healthy_eating_club.com/APJCN/Volume15/Vol15_apcns.htm). [June 21, 2007].
- [4] Sookwong P., Nakagawa K., Murata K., Kojima Y. and Miyazawa T, Quantitation of Tocotrienol and Tocopherol in various rice

- brans. J. Agric. Food Chemistry. 55, 2007, pp. 461- 466.
- [5] Shen Y., Jin L., Xiao P. and Bao, J., Total phenolics, flavonoids, antioxidant capacity in rice grain and their relation to grain color, size and weight. *Cereal Science*. 49, 2009, pp. 106-111.
- [6] Waltera M., Marchesana E., Sachet Massonia P.F., Silvab .PL., Sarzi Sartoria G.M. and Ferreira R.B., Antioxidant properties of rice grains with light brown, red and black pericarp colors and the effect of processing *Food Research International*. 50, 2013, pp. 698–703
- [7] Ling, W. H., Wang , L. L., Ma, J., Supplementation of the black rice outer layer fraction to rabbits decreases atherosclerotic plaque formation and increases antioxidant status. *J. Nutr*. 132, 2002, pp. 20-26.
- [8] Kotsaeng, N., Nakornriab, M. Total phenolic contents and antioxidant activity of some fresh Thai curry. *International Journal of GEOMATE*, 28, 2016, pp.2906-2909
- [9] Krasaetep, J., Total Phenolic Contents and Antioxidant Activities from Thai Glutinous Rice Leaves Extracts. Master's thesis of Science degree in Chemistry, Department of Chemistry, Faculty of Science, Mahasarakham University. Mahasarakham, 2012.
- [10] Giusti, M.M., Wrolstad, R.E. in *Current protocols in food analytical chemistry*, Anthocyanins: Characterization and measurement with UV-visible spectroscopy, ed Wrolstad R.E. (Wiley, New York), 2001, pp. F1.2.1–1.2.13.
- [11] Benzie I.F.F. and Szeto Y.T., Total antioxidant capacity of teas by the ferric derucing/ antioxidant power assay. *Agricultural and Food Chemistry*. 47, 1999 ,pp. 633-636.

# A STUDY ON PROPERTIES OF MORTAR WITH FLY ASH REMOVED UNBURNED CARBON BY FLOTATION METHOD

Rika Oie<sup>1</sup>, Koji Takasu<sup>2</sup>, Hidehiro Koyamada<sup>3</sup> and Hiroki Suyama<sup>4</sup>

<sup>1</sup>The University of Kitakyushu Graduate School of Environmental Engineering, Japan

<sup>2</sup>The University of Kitakyushu Faculty of Environmental Engineering, Japan

## ABSTRACT

In study of the past, we developed the device removing unburned carbon from the fly ash by flotation method and examined the performance of the device by experiments. In this study, we divided a modifying class of the fly ash into five. The loss on ignition of class 1 is the lowest. For various fly ash, such as fly ash conformed Japanese Industrial Standards (JIS) and Japanese Industrial non-Standards (non-JIS) are targeted, we confirmed the properties of mortar with fly ash controlled the modifying levels. As a result, quantity of AE agent addition to satisfy target air content decreased by increase modifying levels. The correlation was confirmed between the mortar flow value and the BET specific surface area. The BET specific surface area was able to reduce by flotation method. Thus, it was confirmed that it led to the improvement of the mortar flow level. It was thought that it was cause of cleaning effect of particle for the fine grain. It tended to compressive strength was to improve by increase modifying levels, but compressive strength of mortar with class 2 was the highest in. It was thought it was cause of that fine particle content had been extremely lost.

**Keywords:** Fly Ash, Slurry, Flotation Method, Unburned Carbon

## INTRODUCTION

In study of the past, when we use fly ash as admixture for concrete, the chemical admixture such as AE agents was adhered to Unburnt Carbon which fly ash contains, and a problem to adversely affect air entraining and a fresh property has it pointed out. Therefore we examined a quality improvement by flotation method and the development of the quality stabilization technique to make the low quality fly ash admixture for concrete and to do the use expansion, and developed the device removing Unburned Carbon. However, it is necessary to repeat examination because there are few examination data which used fly ash modified by flotation method as admixture. In this study, the mortar properties of the modified fly ash were compared, and the influence of the change in the modifying level on the fresh and mechanical properties was confirmed.

## EXPERIMENTAL PROGRAM

### Materials and Mix proportions

Table 1 shows the physical properties of the fly ash. Table 2 shows the physical properties of the materials. For the admixture, the fly ash prepared in this report 1 was used. The mix proportions are shown in Table 2. For fly ash of Class 8 or higher, the effect of the AE agent was not obtained and it was impossible to secure the target air volume. Therefore, a total of 18 mixture up to Class6 were tested. The unit water amount was set to 180 kg/m<sup>3</sup>, and the water

Table 1 Properties of fly ash

Fly ash	Modification	Modified strength [Class]	Ignition loss [%]	Density [g/cm <sup>3</sup> ]	BET specific surface area [m <sup>2</sup> /g]	Blaine's specific surface area [cm <sup>2</sup> /g]	Specific surface area [cm <sup>2</sup> /cm <sup>3</sup> ]
FA-A	×	-	11.78	2.27	13.54	3890	10509
	○	10	9.64	2.24	8.45	4150	11262
		8	8.48	2.25	7.56	4180	17053
		6	6.42	2.26	6.55	4220	16924
		4	3.61	2.27	4.54	4560	18087
		2	2.04	2.26	5.27	4280	20027
		Max	0.49	2.23	3.27	4830	22205
FA-B	×	-	11.95	2.13	17.52	3320	10438
	○	10	10.14	2.18	11.10	3390	14957
		8	8.33	2.19	8.57	3330	16246
		6	5.64	2.18	8.21	3410	12817
		4	4.18	2.21	5.67	3800	21161
		2	2.38	2.20	5.86	3740	17505
		Max	0.62	2.20	5.01	3640	17699
FA-C	×	[10]	9.16	2.29	6.22	3190	7461
	○	8	8.28	2.26	7.46	3260	8440
		6	6.24	2.29	6.59	3240	14367
		4	3.93	2.27	5.78	3370	15056
		2	1.80	2.28	4.88	3480	13417
		Max	0.70	2.28	5.23	3690	17937
		FA-D	×	[4]	3.37	2.25	3.44
○	2		2.24	2.22	1.71	3560	7878
	Max		0.56	2.24	1.54	3610	9663
FA-E	×	[2]	1.32	2.36	2.42	4910	17891
	○	Max	1.01	2.33	2.17	4700	12328

Table 2 Materials

Item	Type	Properties	Mark
Cement	Ordinary Portland cement	Density 3.16g/cm <sup>3</sup>	C
Water	Tap water	-	W
Fine aggregate	Sea sand (Kitakyushu Iwataya offshore)	Surface dry density	S
		2.60g/cm <sup>3</sup>	
		Water absorption rate	
		1.36%	
AE agent	AE Water reducing agent	Actual rate	AE
		61.5%	
		Coarse particle fraction	



Table 3 Mix proportions and Experimental

Symbol	Water-Cement ratio	Water-Powder ratio	sand-total aggregate ratio	Unit Content kg/m <sup>3</sup>					Fresh test		Compressive strength N/mm <sup>2</sup>		Modulus of static elasticity ×10 <sup>4</sup> /mm <sup>2</sup>	
				W	C	FA	S	G	Flow Value cm	Air value%	7days	28days	7days	28days
FA-A6	50	35	45	180	360	150	693	883	15.2	5.3	38.2	49.6	2.16	2.83
FA-A4							693	884	15.4	5.3	38.5	51.7	2.42	2.87
FA-A2							693	883	15.9	7.2	38.1	52.8	2.26	2.45
FA-AMax							692	882	18.2	7.1	34.6	44.7	2.07	2.57
FA-B6							690	880	14.8	5.3	32.9	47.3	2.04	2.35
FA-B4							691	881	14.9	6.2	38.5	48.8	2.67	2.78
FA-B2							691	880	15.4	5.2	38.6	52.0	2.08	2.61
FA-BMax							691	880	18.6	7	35.7	48.6	2.01	2.38
FA-C6							694	884	16.2	6	30.1	45.5	1.78	2.41
FA-C4							693	884	16.35	5.2	34.3	48.0	2.65	2.58
FA-C2							694	884	17.3	6	37.0	49.4	2.11	2.56
FA-CMax							694	884	18.35	8	32.2	41.8	1.90	2.40
FA-D4							693	883	18.35	6.6	35.6	49.0	2.30	2.62
FA-D2							692	881	18.45	7	41.0	56.4	2.56	2.61
FA-DMax							692	882	20.4	7.2	33.3	45.0	2.68	2.54
FA-E2							696	887	19.85	6.4	39.3	54.0	2.53	2.59
FA-EMax							695	886	19.9	7.1	31.3	44.6	1.97	2.31

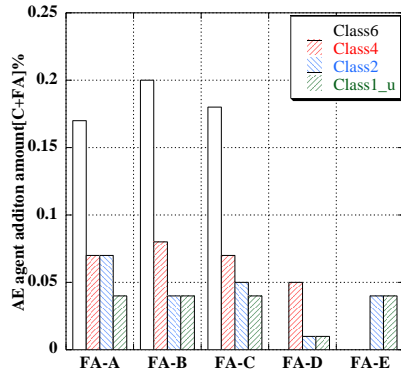


Fig.1 AE agent addition amount

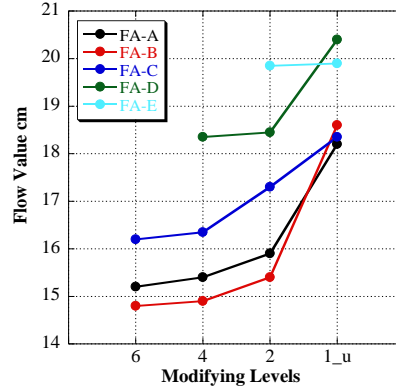


Fig.2 Flow value

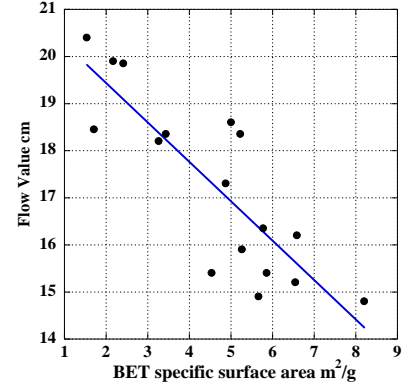


Fig.3 Relationships between Flow value and BET specific surface area

cement ratio was kept constant at 50% for all mixture. As part of fine aggregate, fly ash amount was 150 kg/m<sup>3</sup>. In addition, when the modified fly ash is used as an admixture in a slurry state. The concentration of slurry fly ash adjust 50-60%. Fly ash slurry was stirred in speed 400rpm in ten minutes. For mixing, a mortar mixer was used.

In the specimen preparation method, after mixing cement, water and fly ash slurry for 30 seconds, sea sand was added and mixing was carried out in the range of 4 -6 minutes. When adding fly ash slurry, the shortage of water was added so as to satisfy the unit water quantity. We adjusted quantity of AE agent addition with target of 6% of air volume.

### Test methods

Compressive strength tests, modulus of static elasticity and drying shrinkage were done according to JIS for each test.

## EXPERIMENTAL RESULTS

### Fresh properties

Fig. 1 shows a graph of the amount of AE agent added in each ash. In FA-A,B,C, the amount of AE agent that must be added changes greatly between Class 6 and Class 4. It was found that the unburned carbon in the fly ash adsorbs a large amount of AE agent if the ignition loss is about 6% or more; therefore, in performing the modification treatment by flotation, the amount of additional AE agent can be greatly reduced by reducing the ignition loss to 4% or less. The amount of additional AE agent generally decreases as the modification level is increased, but it was confirmed that there was no marked difference between Class 2 and Class 1\_u therefore, the amount of additional AE agent can be minimized by bringing the ignition loss down to less than 2%. Fig.2 shows the relationship between the reforming level and the flow value. Flow values tended to increase as modifying levels increased in all ashes. It is believed that the



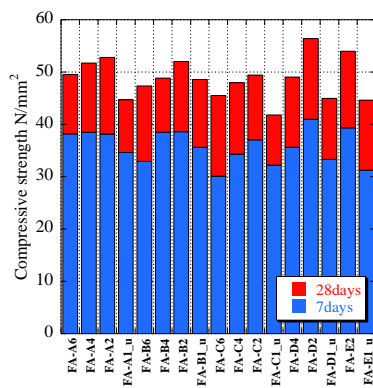


Fig.4 Compressive strength

flow value is increased by the flotation method because unburned carbon is removed and the particle surface is cleaned. Regarding the mortar flow value, FA-A, FA-B, FA-C tended to be low, and FA-D, FA-E tended to increase. It was confirmed that the flow value could not be simply evaluated by the ignition loss. Except for with ash E, the increase of flow value from Class 2 to Class 1\_u was the largest. In modifying the fly ash by flotation, the primary difference between maximum modification and other modification levels is that unburned carbon may possibly be reduced to the limit. This suggests that a classifying effect is produced by the maximum modification, because fine particles are separated from the fly ash (since fly ash contains unburned carbon and other fine particle components). Therefore, it is considered that the flow value from Class 2 to Class 1\_u has greatly improved. FIG. 3 shows the relationship between the BET specific surface area and the flow value. It has been reported<sup>1)</sup> that in fly ash with a BET specific surface area of 3.60 m<sup>2</sup>/g or more, the greater the BET specific surface area, the more strongly adverse effects on fluidity are exhibited. Similar results were also obtained in this experiment, and this tendency was observed even when the BET specific surface area was 3.60 m<sup>2</sup>/g or less. It was confirmed in the previous section that the BET specific surface area decreases as the modification level is increased, indicating that a higher modification level leads to an improved flow value.

### Compressive strength

Fig. 4 shows the temporal change in compressive strength. Compressive strength tended to increase with progress of age in all preparations. Fig. 5 shows the relationship between the removing level and compressive strength at 7 days and 28 days of age. In FA-A FA-D of up to Class 2, the compressive strength increased somewhat at the material age of 7 days, and decreased from Class 2 to Class 1\_u. At a

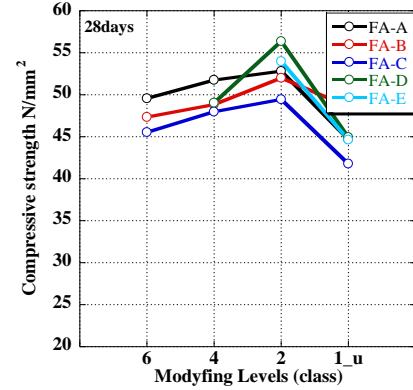
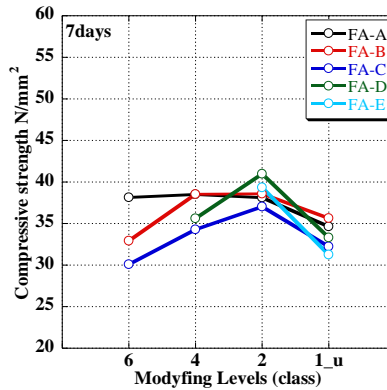


Fig.5 Compressive strength and modifying levels

material age of 28 days, just as at a material age of 7 days, the Class 2 formulation showed the highest compressive strength in all ashes. Also, except for FA-B, Class 1\_u showed the lowest compressive strength in all Classes. The change in observed trend between Class 2 and Class 1\_u is similar to that observed in the mortar flow, and the ability to evaluate the compressive strength through the presence or absence of the fine particle component, mentioned before, was confirmed. In this experiment, we expected that the compressive strength of the fly ash fully modified by flotation would decrease due to the excessive loss of fine particles in the case of the fly ash substitution of 150 kg/m<sup>3</sup> of fine aggregate. Different amounts of substitution are to be studied in the future.

### Modulus of static elasticity

Fig. 6 shows the relationship between the removing level and the modulus of static elasticity at 7 days and 28 days of age. At a material age of seven days, FA-A, B, C showed the largest static elastic modulus in Class 4, while the static elastic modulus became smaller beyond Class 4, and Class 1\_u and Class 6 showed similar values. In addition, the static elastic modulus of ash D increased with modifying level, while the static elastic modulus of ash E tended to decrease with modification level. At 28 days of material age, the static elastic modulus of Class 4 tended to be the largest, just as at 7 days of material age. As for ash C, the static elastic modulus tended to decrease as the modification level became stronger, at 28 days of material age. Comparing the material ages of 7 days and 28 days, it was confirmed that the static elastic modulus varies to a lesser extent when the material is 28 days of age. Fig. 7 shows the relationship between the compressive strength and the static elastic modulus at 7 days and 28 days of age, NEW-RC formula<sup>2)</sup>. In the relational expression in the figure, the coefficient  $k_1$  is set to 1.0,  $k_2$  is set to 1.1, and the unit volume mass  $r$  is assumed to be 2.27. This tended the coefficient  $k_1$  is set to 1.0,  $k_2$  is set to

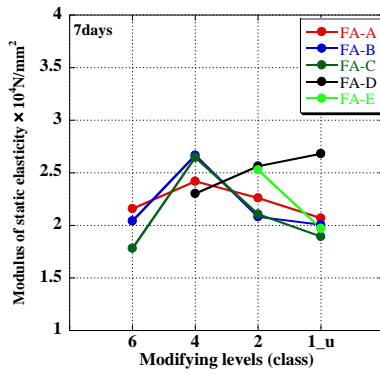


Fig.6 Removing class and Modulus of static elasticity

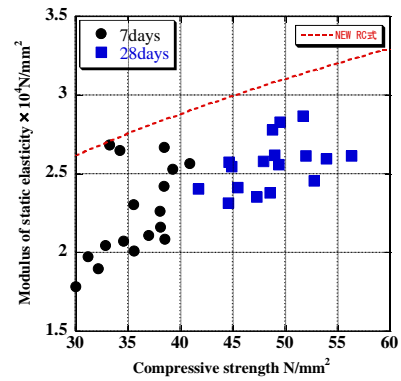
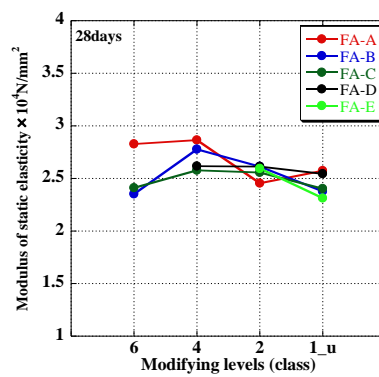


Fig.7 Relationships between the Compressive strength and Modulus of static elasticity

1.1, and the unit volume mass  $r$  is assumed to be 2.27. This tended to be lower than the value of the NEW-RC formula in all formulations used in this experiment. This experiment was carried out using mortar; when using concrete, the static elastic modulus should be evaluated appropriately.

### Drying shrinkage

Fig. 8 shows the change over time of drying shrinkage. At approximately 28 days of material age, Class 6 fell below (and Class 2 surpassed) the level of approximately  $-1500\mu$  of the length change rate. It became clear that strengthening the modification level has the effect of suppressing drying shrinkage. Focusing on Class 6 and Class 4, the length change rate is larger in Class 4. In contrast, between Class 2 and Class 1\_u, the length change rate is generally smaller in Class 1\_u. This is thought to be due to the adsorption of water by unburned carbon, suggesting that drying contraction has a strong influence due to unburned carbon. One possibility is that dry shrinkage can be evaluated by the modification level only when the ignition loss is 4% or less. Though d4 ash has not undergone a modification treatment, as mentioned earlier, it can be evaluated for modification level by using ignition loss as an index, as in the case of the modified fly ash. In this experiment, differences dependent on ash species were not found.

### CONCLUSIONS

The findings obtained below are shown.

1-1) For fresh mortar, the amount of additional AE agent needed to achieve the target air volume decreased sharply between Class 6 and Class 4. As for mortar flow, the amount became larger as the modification level was increased. The rise rate was greatest between Class 2 and Class 1\_u, possibly due to the detachment of fine particles and the cleaning effect of particles at the maximum modification level. In addition, a negative correlation was observed

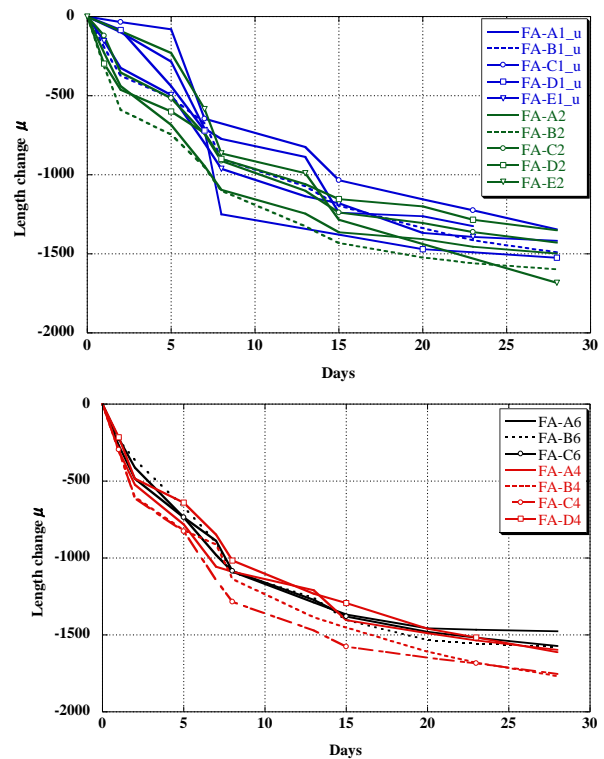


Fig.8 Drying shrinkage

between BET specific surface area and mortar flow, indicating that strengthening the modification level reduced the BET specific surface area, leading to the improved flow value.

1-2) The compressive strength of Class 2 was the highest in all ashes, while Class 1\_u showed the lowest compressive strength among the 28-day strengths. This is thought to be due to the excessive reduction of the fine particle component at the maximum modification level of fly ash.

1-3) In the moduls of static elasticity, a moduls of static elasticity of Class4 showed the tendency that became highest with all fly ash class.

1–4) In terms of drying shrinkage, we confirmed that modification intensified suppression of drying shrinkage due to modification.

#### **ACKNOWLEDGMENTS**

The materials were provided by Nippon Steel and Sumitomo Metal Corporation. The experiment was supported by Eiji Mikura, Saori Itanami, YutoMurakami, Yuta Nimura. We show gratitude to them.

#### **REFERENCES**

- [1]Akira Yoshino, The influence that a property of the fly ash gives to quantity of addition of the additive Vol.27, No.1, pp.175-180, 2005.6
- [2] Architectural Institute of Japan: Building works standard specifications, 5 commentary JASS steel reinforced concrete construction
- [3] Japan Standards Association: 2009 JIS handbook soft concrete

## A STUDY ON PROPERTIES OF WITH FLY ASH REMOVED UNBURNED CARBON BY FLOTATION METHOD

Yuto Murakami<sup>1</sup>, Koji Takasu<sup>2</sup>, Hidehiro Koyamada<sup>2</sup> and Hiroki Suyama<sup>2</sup>

<sup>1</sup> The University of Kitakyushu Graduate School of Environmental Engineering, Japan

<sup>2</sup> The University of Kitakyushu Faculty of Environmental Engineering, Japan

### ABSTRACT

In study of the past, when we use fly ash as admixture for concrete, the chemical admixture such as AE agents was adhered to Unburnt Carbon which fly ash contains, and a problem to adversely affect air entraining and a fresh property has it pointed out. Therefore we examined a quality improvement by flotation method and the development of the quality stabilization technique to make the low quality fly ash admixture for concrete and to do the use expansion, and developed the device removing Unburned Carbon. However, it is necessary to repeat examination because there are few examination data which used fly ash modified by flotation method as admixture. We had changed the loss on ignition of modified fly ash for an index at degree of the modifying by flotation method and confirmed the change of fly ash properties. The fly ash did not conform to the demand value of the Japanese Industrial Standardized class 1 only by removing Unburnt Carbon by flotation method. We were revealed that it influenced other properties by the characteristic of the fly ash.

*Keywords: Fly Ash, Slurry, Flotation Method, Unburned Carbon*

### INTRODUCTION

In study of the past, when we use fly ash as admixture for concrete, the chemical admixture such as AE agents was adhered to Unburnt Carbon which fly ash contains, and a problem to adversely affect air entraining and a fresh property has it pointed out. Therefore we examined a quality improvement by flotation method and the development of the quality stabilization technique to make the low quality fly ash admixture for concrete and to do the use expansion, and developed the device removing Unburned Carbon. However, it is necessary to repeat examination because there are few examination data which used fly ash modified by flotation method as admixture. In this study, we had changed the loss on ignition of modified fly ash for an index at degree of the modifying by flotation method and confirmed the change of fly ash properties. The degree of modifying by fly ash flotation method was changed by using loss on ignition as an index, and the change of fly ash physical properties was confirmed.

### EXPERIMENTAL DETAILS

#### Materials

The particle size distribution was measured using a laser diffraction / scattering type particle size distribution measuring apparatus. For SEM image analysis, an SEM image was taken using a probe electron microscope. For the BET specific surface area, the BET specific surface area was measured using an automatic specific surface area pore distribution measuring apparatus, and for the

Table 1: Fly ash

Fly ash	Modification	Modified strength [Class]	Ignition loss [%]	Density [g/cm <sup>3</sup> ]	BET specific surface area [m <sup>2</sup> /g]	Blaine's specific surface area [cm <sup>2</sup> /g]	Specific surface area [cm <sup>2</sup> /cm <sup>3</sup> ]
FA-A	×	-	11.78	2.27	13.54	3890	10509
	○	10	9.64	2.24	8.45	4150	11262
		8	8.48	2.25	7.56	4180	17053
		6	6.42	2.26	6.55	4220	16924
		4	3.61	2.27	4.54	4560	18087
		2	2.04	2.26	5.27	4280	20027
		Max	0.49	2.23	3.27	4830	22205
	×	-	11.95	2.13	17.52	3320	10438
FA-B	○	10	10.14	2.18	11.10	3390	14987
		8	8.33	2.19	8.57	3330	16246
		6	5.64	2.18	8.21	3410	12817
		4	4.18	2.21	5.67	3800	21161
		2	2.38	2.20	5.86	3740	17505
		Max	0.62	2.20	5.01	3640	17699
FA-C	×	[10]	9.16	2.29	6.22	3190	7461
	○	8	8.28	2.26	7.46	3260	8440
		6	6.24	2.29	6.59	3240	14367
		4	3.93	2.27	5.78	3370	15056
		2	1.80	2.28	4.88	3480	13417
FA-D	×	[4]	3.37	2.25	3.44	3480	7867
	○	2	2.24	2.22	1.71	3560	7878
		Max	0.56	2.24	1.54	3610	9663
FA-E	×	[2]	1.32	2.36	2.42	4910	17891
	○	Max	1.01	2.33	2.17	4700	12328

measurement of the particle size distribution, the SEM image analysis and the BET specific surface area, all the fly ash had raw powder and 24 hours or more fly ash dried in an 105°C electric furnace was used. The flow value ratio and the activity index were performed in accordance with JIS A 6201 Annex 2 "Test method of flow value ratio and activity index by mortar of fly ash". Table 1 shows the properties of the fly ash used. In this experiment, we use five types of fly ash A supplied from different producers. FA-A,B,C,D is ash from a power generation plant. FA-E

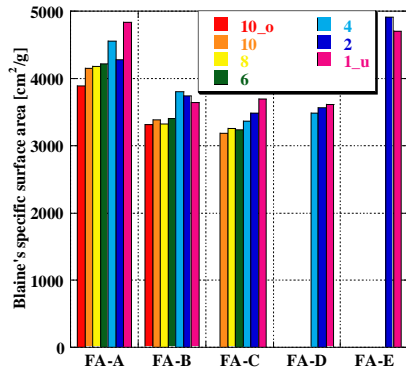


Fig.1: Blaine's specific surface area

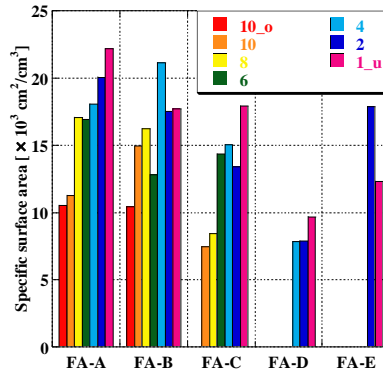


Fig.2: Specific surface area

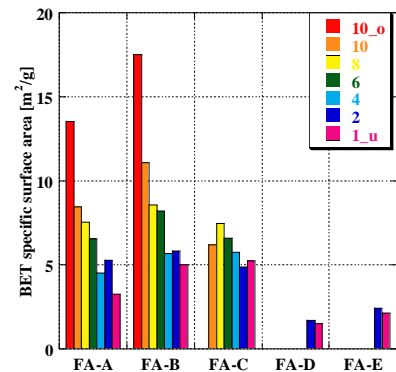


Fig.3: BET specific surface area

is JIS-II certified. As a method of preparing these samples, when modifying raw ash with a device, the modification level (Preprocessing time, Amount of foaming agent, Flotation method time, Amount of trapping agent) was weakened or strengthened by controlling the processing level, and multiple types of modified ashes with different ignition loss were made from one kind of raw ash; additionally, the modification level was set more finely by mixing, using the ignition loss to characterize the modified ash. As a measure of the modification level of each ash (using ignition loss as an indicator), the modification level of FA-A~C was varied in steps of 2%, and FA-D in steps of 1%, with minimum modification levels of 10% for FA-A, 10% for FA-B, 8% for FA-C, and 2% for FA-D. The error in the index of ignition loss of each sample was  $\pm 0.5\%$  for FA-A~C and  $\pm 0.25\%$  for FA-D. Note that Class10\_o of FA-A, Class10\_o of ash B, Class10 of FA-C, Class4 of FA-C, and Class2 of FA-E are all raw powders, and are not subjected to modifying treatment.

## Measurement

Samples in which the 25 reforming levels shown in Table 1 were operated were used to confirm their properties. In order to decrease the influence of precipitated fly ash when the modified slurry ash is cast as an admixture, a fly ash slurry is prepared with a fly ash concentration of 65%; for the samples that did not become slurry, water was further added to increase the concentration to 50% or more, and a pre-stirring procedure was used for 10 min, using a stirrer rotating at 400 times per minute. After casting the fly ash slurry, the lack of water was compensated so as to satisfy the unit water quantity of the preparation before mixing.

## RESULTS AND DISCUSSION

### Fresh properties

Fig. 1 shows the raw powder of each ash and the Blaine's specific surface area for each reforming level. Every ash, except for ash E, resulted in high Blaine's

specific surface area when modification was carried out by flotation. For FA-A(11.78%) in which the ignition loss of the raw powder was high, when the maximum modification(0.49%) was carried out, a change of about 1000  $\text{cm}^2/\text{g}$  (from 3890  $\text{cm}^2/\text{g}$  to 4830  $\text{cm}^2/\text{g}$ ) was observed in the Blaine specific surface area. In contrast, for FA-B(11.95%) in which the ignition loss of the raw powder was high, a change of only about 300  $\text{cm}^2/\text{g}$  (from 3320  $\text{cm}^2/\text{g}$  to 3640  $\text{cm}^2/\text{g}$ ) in the Blaine specific surface area was observed in the case of the maximum modification(0.62%). Also, in the case of the FA-D(3.37%), in the case with a low ignition loss of raw powder, a change of only about 500  $\text{cm}^2/\text{g}$  (from 3190  $\text{cm}^2/\text{g}$  to 3690  $\text{cm}^2/\text{g}$ ) was observed in the Blaine specific surface area, even in the case of the maximum modification(0.56%). It was found that the relation between the decrease in ignition loss and the improvement in Blaine specific surface area varied with the ash species.

Fig. 2 shows the raw ash powder and the specific surface area for each reforming level. The specific surface area for FA-A changed by about 12000  $\text{cm}^2/\text{cm}^3$  (from 10509  $\text{cm}^2/\text{cm}^3$  to 22205  $\text{cm}^2/\text{cm}^3$ ) when the maximum modification of the raw powder was made, but the change for FA-B was only about 7000  $\text{cm}^2/\text{cm}^3$  (from 10438  $\text{cm}^2/\text{cm}^3$  to 17699  $\text{cm}^2/\text{cm}^3$ ) after the modification of the raw powder. In FA-D as well, a change of only about 2000  $\text{cm}^2/\text{cm}^3$  (from 7461  $\text{cm}^2/\text{cm}^3$  to 9663  $\text{cm}^2/\text{cm}^3$ ) was observed.

Fig. 3 shows the values of BET specific surface area for each ash raw powder and each reforming level. The value of BET specific surface area decreases if any ash type, except FA-C, is modified by flotation, and tends to decrease as ignition loss decreases. In the case of FA-C, the BET specific surface area was higher than that of the raw powder when it was modified to Class10, and the BET specific surface area tended to decrease as the modification level was strengthened. In Fig. 4, a positive correlation was confirmed, with a coefficient of determination of 0.73 in the relationship between BET specific surface area and ignition loss. With a high ignition loss of the base ash powder, the BET

specific surface area of FA-A and FA-B show relations that differ from the aforementioned relation: the BET specific surface area of the raw powder was not consistent with the assumption of a correlation between ignition loss and BET specific surface area. Also, no clear correlation was found for the relation with the BET specific surface area when the ignition loss was 4% or less, and the BET specific surface area varied within the range of 5.0 m<sup>2</sup>/g or less.

Photo 1 shows SEM images of raw powder of FA-A, B, C ash and fly ash at maximum reforming. Relative to the original powder, in all the fly ash, unburned carbon adhering to the fly ash particles is peeled off from the tail ash, indicating that the particle surface is cleaned; specifically, while the particle surface is completely cleaned in FA-A when the change in the Blaine's specific surface area is large, complete cleaning is not achieved in FA-B and FA-D, in which the change in the Blaine specific surface area is small. Although it has been reported in earlier studies that unburned carbon cleaning is apparent despite the increase in ignition loss, this experiment shows that residual substances remain in FA-B, as seen in the SEM image, and cannot be removed from the particle surface despite the ignition loss of 0.62% at the maximum modification. Horiuchi et al. reported that immersing and leaving fly ash in water for 1 day decreased strength decreased and generated reactants on the particle surface. Because we measured the samples dipped in water (except for the raw powders), reaction products may have been created in water. Reaction products other than unburned carbon are generated, adhering to the fly ash surface during the modification by flotation, and there are ash types that can be cleaned and those that cannot. It is possible that the cleaning condition influences the Blaine specific surface area and the specific surface area; therefore, detailed study is necessary in future.

Fig. 5 shows the change in the particle size distribution of raw FA-A,B,C raw powder and samples with different reforming levels. FA-A shows median diameters of modified ash smaller than those of the raw powders; it is thought that the fly ash particle diameter is decreased by flotation. As for FA-D, there was hardly any difference in particle size between the raw powder and the modified ash. If the most common particle size of the raw material was around 10 µm, then the most common particle diameter was hardly changed from that of the raw powder, even with modification by flotation. This clarifies the removal of unburned carbon by flotation has an influence on the particle size distribution, and that this influence varies with the fly ash. In all ashes except for FA-D, ash modified by flotation has a peak at a particle diameter of about 10 µm, and the frequency in the vicinity of 10 µm intensifies as the modification level is raised or the ignition loss is decreased. It is considered that there is a classification effect in reforming fly ash by flotation method, so it

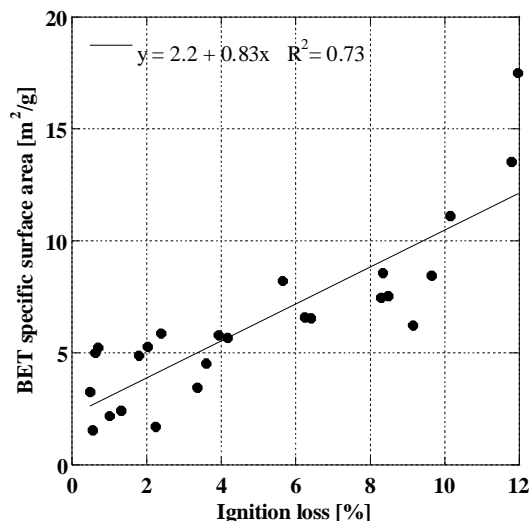
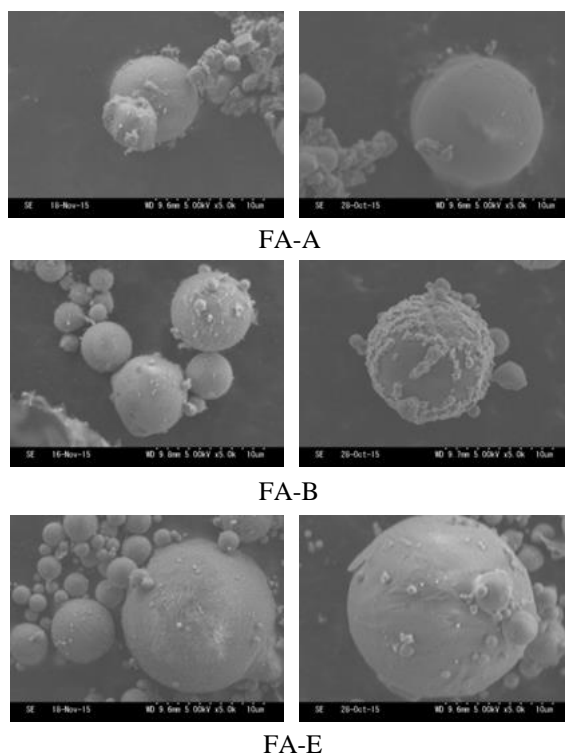


Fig4: BET specific surface area and Ignition loss



※ Left: Raw powder Right: maximum modified

Photo1: SEM images (magnification:5000 times)

is necessary to verify in detail in the future.

### Flow value ratio and Activity index

Fig. 6 shows the results of the flow value ratio. Comparing the raw powder and the ashes of various modification levels, a tendency can be seen: the flow value ratio rises sharply as the modification level is strengthened for FA-A and FA-C. FA-A with an ignition loss of 4% or less and FA-C with an ignition loss of 2% or less meet the JIS-I reference value of 105% for flow value ratio. For FA-D and FA-

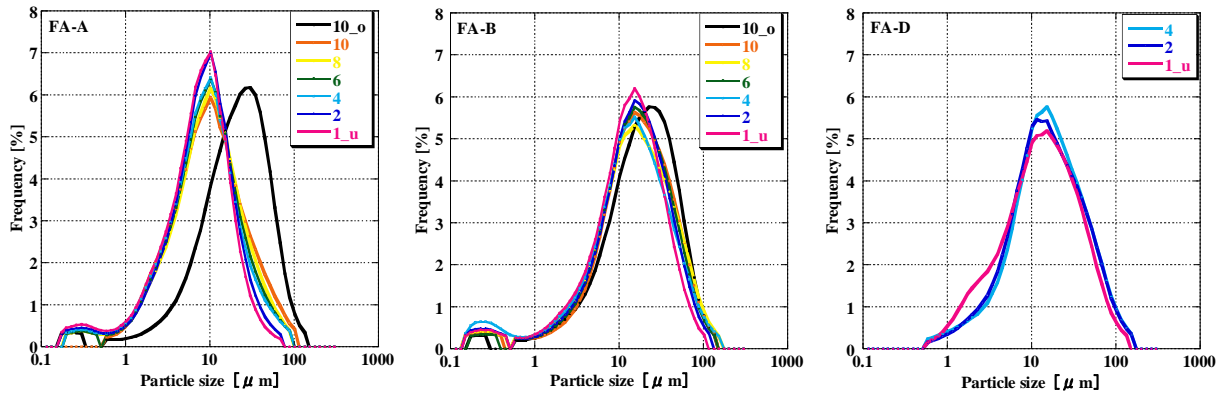


Fig5: Particle size distribution

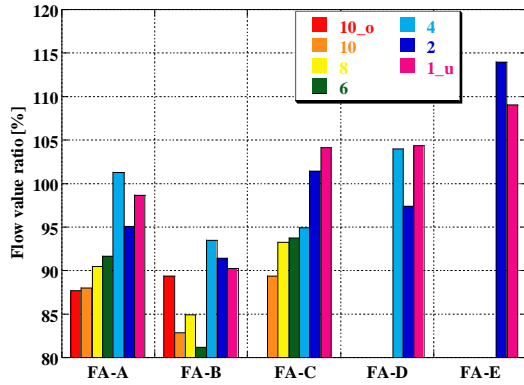


Fig6: Flow value ratio

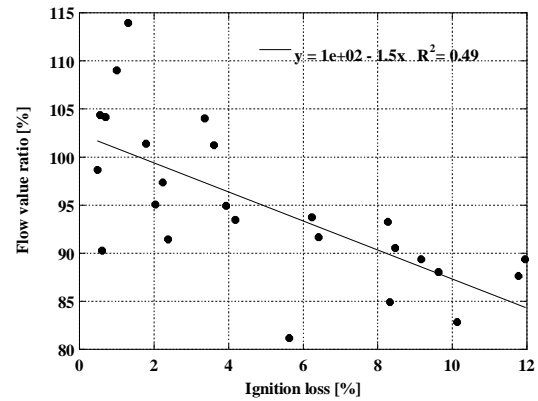


Fig7: Flow value ratio and Ignition loss

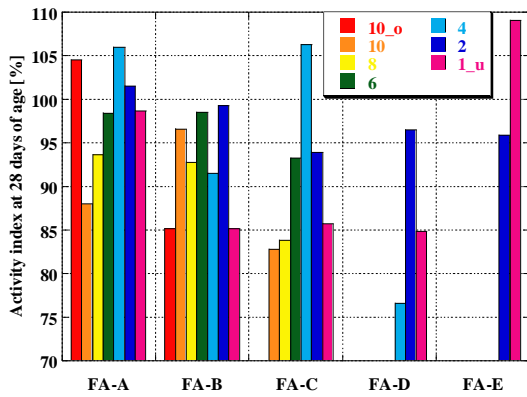


Fig8: Activity index at 28 days of age

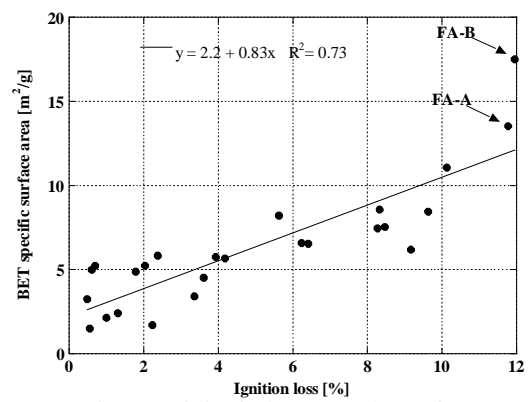


Fig9: Activity index at 28 days of age and BET specific surface area

E, the raw powders satisfied the reference values of JIS-II and JIS-I, at 95% and 105% for flow value ratio, respectively; note that the flow value ratio tended to be equal to or lower than that of the raw powder after the modification. FA-B did not show any remarkable tendency and did not satisfy the flow value ratio of 95%—the reference value of JIS-II for both raw powder and modified ash. With the flow value ratios in this experiment, most of the ash with an ignition loss of 4% or less satisfies the JIS-II reference value of 95%; however, because unburned carbon is an influence on ash with an ignition loss of 4% or more, it is recommended the ignition loss be brought down to 4% or less to improve the flow value ratio.

Fig. 8 shows the results of the activity index at 28

days of age. In the cases of FA-A and FA-C, the flow value ratio clearly increased as the modification level was strengthened. FA-A with an ignition loss of 4% or less and FA-C with an ignition loss of 2% or less meet the flow value ratio of the JIS-I reference value of 105%. For FA-D and FA-E, the flow value ratios of 95% and 105%, which are the reference values of JIS-II and JIS-I, respectively, were satisfied in the raw powders; note that the flow value ratio tended to be equal to or lower than that of the raw powder after the modification. The FA-B did not show a clear tendency and did not satisfy the flow value ratio of 95%, the reference value of JIS-II, for both raw powder and modified ash. In the flow value ratio in this experiment, most of the ash with an ignition loss



of 4% or less satisfies the JIS-II reference value of 95%. Because unburned carbon in ash with an ignition loss of 4% or more seems to influence the outcome, it is recommended that the ignition loss be brought down to 4% or less to improve the flow value ratio by modification.

## CONCLUSIONS

The findings obtained below are shown.

- 1-1) Regarding the BET specific surface area, there was a correlation between ignition loss and BET specific surface area, except that the BET specific surface area converged to a value of about 5 m<sup>2</sup>/g or less when the ignition loss was 4% or less.
- 1-2) As the modification level was increased, the Blaine specific surface area and the specific surface area increased, but the rise rate depended on ash species. Furthermore, even when the ignition loss was low, there were areas in the scanning electron microscope images where the substances were not well separated.
- 1-3) For ash with a frequency peak at a particle size for the raw powder of larger than 10 µm, the frequency peak drops to around 10 µm after the modification. Meanwhile, for ashes in which the peak frequencies are around 10 µm in the raw powder, the frequency peak remains at around 10 µm even after the modification. Taken together, in all ashes, the modified ash tended to have a frequency peak at a particle diameter of 10 µm, with the peak becoming more pronounced as the modification level is strengthened. The classification effect is made more apparent by modification of the fly ash by flotation.
- 1-4) The flow value ratio tended to increase and the fluidity improved when the modification level was strengthened.
- 1-5) In ash A, the 28-day activity index surpassed the JIS-I reference value of 90% when the ignition loss was 10% or less. As for ash B, the JIS-I reference value of 90% was met when modified, except at the maximum modification level.

## ACKNOWLEDGMENTS

The materials were provided by Nippon Steel & Sumitomo Metal Corporation. The experiment was supported by Eiji Mikura, Saori Itanami, Rika Oie, Yuta Imuran and Shoma Takegawa. We show gratitude to them.

## REFERENCES

- [1] Koji Takasu, Experimental Study on Removal of Unburnt Carbon in Fly Ash by Flotation Method and Properties of Concrete with the Fly Ash Slurry, Architectural Institute of Japan, pp331-340, Japan(2014)
- [2] Yosuke Tihara, A Basic Study on Removing Unborn Carbon in Fly Ash by Ore Flotation, Part7 The Change in The Composition and Physical Properties Between The Original Fly Ash and The Removed Fly Ash, Architectural Institute of Japan, (52), pp33-36, 2013.3
- [3] Sumiob Horiuti, A Study on strength characteristics of fly ash, Shimizu Corporation Research Report (39), pp.1-9, 1984.4

# CHARACTERIZATION OF CERIUM OXIDE-CHITOSAN NANOCOMPOSITE-MODIFIED SCREEN PRINTED CARBON ELECTRODE AND APPLICATION IN MELATONIN DETERMINATION

Pachanuporn Sunon<sup>1</sup>, Porntip Wongkaew<sup>2\*</sup>, Jeffrey Johns<sup>1</sup>, Nutjaree Johns<sup>1</sup>

<sup>1</sup>Division of Clinical Pharmacy, Faculty of Pharmaceutical Science,  
Khon Kaen University, Khon Kaen 40002, Thailand

<sup>2</sup>Division of Plant Pathology, Faculty of Agriculture, Khon Kaen University, Khon Kaen 40002, Thailand

## ABSTRACT

A simple and effective modification of the working screen printed carbon electrode (SPCE) surface has been developed with a mixture of chitosan biopolymer and nano cerium oxide at 1:1 composition for the detection of melatonin, a circadian rhythm regulation hormone. The fabricated electrode was characterized by scanning electron microscopy (SEM), energy dispersive X-ray spectrophotometer (EDS), electrochemical impedance spectroscopy (EIS) and cyclic voltammetry (CV). Electro-oxidation behaviors of melatonin were extensively observed by differential pulse voltammetric (DPV) analysis. The experimental results demonstrated that the modified cerium oxide-chitosan screen printed carbon electrode (SPCE-Chi-CeO<sub>2</sub>) exhibited satisfactorily improvement in the electrochemical current sensitivity. A linear calibration curve for melatonin was obtained in the concentration range from 0-10 µg/ml with a detection limit of 0.18 µg/ml based on DPV measurement. Good selectivity was also obtained in an interference study with some other closely structural related compounds such as tryptophan and serotonin. Thus this modification strategy was proved to be a suitable tool for the simple, fast, sensitive and selective determination of melatonin.

*Keywords: SPCE-Chi-CeO<sub>2</sub>, SEM and EDS, EIS and CV, melatonin, DPV analysis*

## INTRODUCTION

Melatonin (N-acetyl-5-methoxytryptamine) is an important hormone that is synthesized in the pineal gland. It is also recognized as ubiquitous among living organisms, including humans, animals, plants, bacteria, fungi, and algae [1]. It is responsible for regulating sleep and circadian rhythms in mammals, and is used to counteract the effects of jet-lag or to aid sleep. Principally, it is used for the diagnosis and remedy of insomnia, hypomnesia and of the cerebrum and is used to treat some diseases such as Alzheimer and cancer. Melatonin is biomarker of circadian dysregulation, and measurement melatonin levels in saliva and blood, and the melatonin metabolite 6-sulphatoxymelatonin in urine are useful to evaluate problems related to circadian rhythms and sleep. The development of rapid, simple, easy to use, real-time detection, low cost and portable detection of melatonin in animal tissues and fluids emerges as imperative. The biosensor is methodologies employed for qualitative and quantification detection of melatonin in cells, animals and human products.

Although many methods have been applied in the qualitative and quantitative determination of low levels of melatonin in samples such as enzyme linked immunosorbent assay (ELISA) and

radioimmunoassay (RIA), high-performance liquid chromatography (HPLC) and capillary electrophoresis; but they are expensive and time consuming methods and are confined to the laboratory. ELISA and RIA provide a stable calibration curve, reasonable speed and small sample volume with specificity, sensitivity and precision [2], but they have some limitations and disadvantages by their high cost and laborious time requirement. Moreover, a special lab in radiochemistry is needed in RIA analysis and the radioactive tracer is toxic as well. Recently, electrochemical biosensors have expanded their attractive attributions that offer new challenges of analytical methodology and a possibility of miniaturization and portability, sensitivity, selectivity, a wide linear range, energy saving, minimal space, and cost effective usage.

Screen printed carbon electrode (SPCE) in combination with suitable surface modification and a proper electrochemical technique has been shown applicable in various electrocatalytic studies. Previous works on the fabrication of an effective and affordable electrochemical implement via a route of this SPCE modification have provided a possibility for the development of a potent biosensor [3]. The versatile chitosan biomaterial has been employed as main structural scaffold for a wide variety of biosensor due to its robust properties especially an ionic binding of biomolecules including DNA and

proteins [3, 4, 5]. In addition, many types of nanoparticles such as metals and metal oxides have provided an ideal remedy for enhancing the sensing performance of the sensors. Cerium oxide ( $\text{CeO}_2$ ) is one among the metal oxides mostly introduced for biosensor fabrication due to its excellent properties, including a good biocompatibility, high chemical stability, excellent electronic conductivity and huge electroactive surface. A composite matrix construction based on chitosan and  $\text{CeO}_2$  for an immobilization of single stranded DNA probe has also been reported for effective sensing of cancer gene [6].

In the present study, modification of SPCE with a combination of chitosan and  $\text{CeO}_2$  is organized to fabricate an electrochemical sensor for melatonin determination via differential pulse voltammetry (DPV). Techniques in scanning electron microscopy (SEM), energy dispersive X-ray spectrophotometer (EDS), electrochemical impedance spectroscopy (EIS) and cyclic voltammetry (CV) are utilized to investigate the modified SPCE performance. An appreciable sensitivity of SPCE-Chi- $\text{CeO}_2$  in the detection of melatonin is expected from the inheritance of advantageous chitosan and  $\text{CeO}_2$  properties as well.

## MATERIALS AND METHODS

### Materials and instruments

Chitosan (85% degree of deacetylation) with a molecular weight of 0.28 kDa was obtained from Bioline Lab, Co., Thailand. Cerium oxide ( $\text{CeO}_2$ ) nanoparticles (50 nm), tryptophan and serotonin were gained from Sigma-Aldrich Co. LLC, USA. Melatonin (GMP 99.96%) was acquired from HuanggangSaikang Pharmaceutical Co., Ltd, Hubai, China. Other chemicals for reagent preparation were purchased from Ajax Finechem Pty, Ltd., Australia. Buffer solutions and reagents were made up using organic free ultrapure water from an Elga DV25 Purewater OptionQ system with resistivity (25 °C)  $>18.18 \text{ M}\Omega\cdot\text{cm}$ . Screen printed electrode DS-150 strip made of carbon as working area (4 mm diameter) with a counter electrode made of platinum, a reference electrode made of silver and an electric contact made of silver was provided by DropSens, ParqueTecnológico de Asturias, S.L. Llanera (Asturias) Spain. A scanning electron microscope (SEM) LEO1450VP was from Hurley, UK and an energy dispersive X-ray spectrophotometer (EDS) was from Technai G2 20, FEI; Thermo Fisher Scientific, Oregon, USA. Electrochemical performances were acquired with a potentiostat/galvanostat model PGSTAT 302N of ECoChemieAutolab (MetrohmAutolab B.V., Utrecht, The Netherlands) incorporated with Nova system software.

### Modification of working electrodes

Fabrication of the modified SPCE-Chi- $\text{CeO}_2$  electrode was done using a DS-150 screen printed carbon electrode (SPCE) as the basal platform. The  $0.25 \text{ cm}^2$  working surface area of the SPCE was cleaned by ultrapure water rinsing for 3 times prior to a modification. Chitosan solution was made by a mixing of chitosan powder with 1% acetic acid at 1% by weight per volume. Afterward, the nano-cerium oxide ( $\text{CeO}_2$ ) particles were added up at 1% (w/v) and sonicated for 15 min at room temperature. Later, a 5  $\mu\text{L}$  of this Chitosan- $\text{CeO}_2$  solution was embedded onto the  $0.25 \text{ cm}^2$  SPCE working surface and left drying in clean air environment overnight. Then it was rinsed with ultrapure water and allowed to dry again for the ready use.

### Structural and electrochemical characterization

Surface morphological characteristics of the modified SPCE-Chi- $\text{CeO}_2$  in comparison to its basal SPCE were acquired through scanning electron microscopy (SEM). Three replicates of each were sputter coated with gold and  $0.25 \text{ cm}^2$  working electrode areas were investigated using  $10,000\times$  magnifications. A structural profiling of the elements was consequently investigated by energy dispersive X-ray spectrophotometer (EDS) in couple with the SEM. Electrochemical performance were done via Autolab PGSTAT 302N controlled with the Autolab Nova software. An electrolyte 0.1 M phosphate buffer saline (PBS) at pH 7.0 solution containing 1.0 mM of  $\text{K}_3\text{Fe}(\text{CN})_6$  as a model electrochemical probe was employed for the electrochemical characterization. Electrochemical impedance spectroscopy (EIS) was carried out by applying a potentiostatic state of 0.01 V AC potential and 0.17 V bias potential with 10 mV amplitude in the frequency range from 0.01 to  $10^5$  Hz. Cyclic voltammograms were obtained over the potential scan range from -0.6 to 1.2 V at a varied scan rate of 25, 36, 81, 144 and 255 mV/s. Subsequent measurement of electrochemical response of SPCE-Chi- $\text{CeO}_2$  to a function of melatonin concentration (0-10  $\mu\text{g/ml}$ ) was set up using differential pulse voltammetric (DPV) technique at 50 mV/s scan rate.

## RESULTS AND DISCUSSION

### Morphological and structural characterization of modified SPCE-Chi- $\text{CeO}_2$

The surface morphologies and atomic components of SPCE-Chi- $\text{CeO}_2$  in comparison to the basal SPCE at different mixing molar percentage were characterized by SEM and EDS. The SEM image in Fig. 1A presents homogeneous carbon platelets containing in SPCE working surface,

whereas the modified SPCE-Chi-CeO<sub>2</sub> surface has uniform granular porous morphology attributed to the homogeneous dispersion of CeO<sub>2</sub> nanoparticles in chitosan network as seen in Fig. 1B. Seemingly, a stable surface cover could be obtained following the modification by this highly adhesive nanocomposite. Fig. 2 represents atomic fingerprints from EDS investigation that signify the differences between SPCE (Fig. 2A) and SPCE-Chi-CeO<sub>2</sub> (Fig.2 B). The bare SPCE has shown its dominant containing elements as carbon, chlorine and oxygen. The carbon is presented as the major constituent of SPCE, and chlorine is present as a constituent of the binder or solvent, whereas the presence of oxygen is due to any hydrophobic contamination.

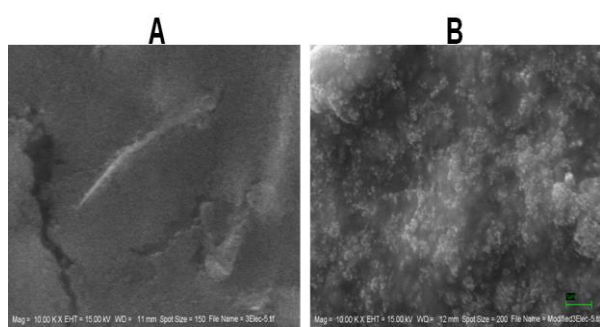


Fig. 1 SEM images observed from working surface of bare SPCE (A) and SPCE-Chi-CeO<sub>2</sub> (B).

In view of the modified SPCE-Chi-CeO<sub>2</sub>, many more types of atoms are presented such as fluorine, nickel, sodium, technetium, gadolinium and gold as well as cerium component in Chi-CeO<sub>2</sub> matrix. The carbon in this case is assumed as a constituent of the chitosan and electrode, the presence of oxygen is due to any hydrophobic contamination and from chitosan, fluorine, nickel, sodium and technetium maybe from electrode plastic basement and contamination, while gold is from gold coating electrode for EDS in couple with SEM analysis. The percentage of atomic and weight by element and total compound in SPCE-Chi-CeO<sub>2</sub> are as displayed in Table 1. The atomic percentage of carbon is present as 23.68% in chitosan constituent and 33.92% in the electrode basement. While the atomic percentage of CeO<sub>2</sub> molecules and total chitosan molecules are 20.42 and 3.95, respectively. Considering the weight percentage by compound, it has been stated that the carbon content is about 8.5%, the CeO<sub>2</sub> molecules are 73.35% and total chitosan molecules are 12.77%. Thus, it can be concluded that in SPCE-Chi-CeO<sub>2</sub> the major constituent by atomic percentage is carbon and by weight percentage is cerium.

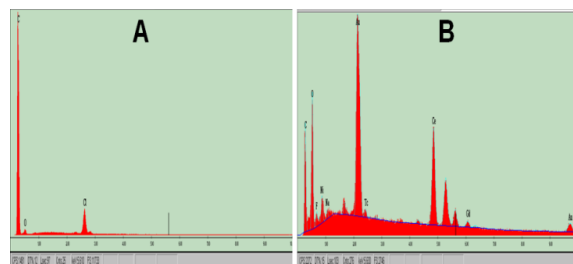


Fig. 2 Atomic fingerprints of bare SPCE (A) and SPCE-Chi-CeO<sub>2</sub> (B) components by EDS analysis.

Table 1 Percentage of atomic and weight by element and total compound in SPCE-Chi-CeO<sub>2</sub> from EDS analysis.

Components	Atom (%)	Weight(%)
<u>Elements</u>		
C	57.60	-
O	29.40	19.82
F	2.27	1.81
Ni	2.42	5.99
Na	1.09	1.06
Tc	0.37	1.54
Ce	6.81	40.18
Gd	0.07	0.47
<u>Compounds</u>		
Total chitosan molecules	3.95	12.77
CeO <sub>2</sub> molecules	20.42	73.35
C in chitosan	23.68	-
C in SPCE basement	33.92	8.50

### Electrochemical characterization of modified SPCE-Chi-CeO<sub>2</sub>

EIS analysis has provided information about the changes on interface properties between the basal SPCE and the modified SPCE-Chi-CeO<sub>2</sub> as illustrated by Nyquist plots in Fig. 3. The semicircle diameter represents the electron charge-transfer resistance ( $R_{ct}$ ) character which controls the electron transfer kinetics of the redox probe ( $K_3Fe(CN)_6^{3-/4-}$  in this experiment) at the electrode interface [7]. The bare SPCE showed a large semicircle diameter with  $R_{ct}$  value about 8,000  $\Omega/cm^2$  (Fig.3 curve a), whereas the modified SPCE-Chi-CeO<sub>2</sub> produced almost half size smaller with the  $R_{ct}$  value down to about 3,000 $\Omega/cm^2$  (Fig.3 curve b) implying less charge transfer resistance and hence about 2.7 times better electron transfer ability. An extreme faster in electron transfer obtained following the modification of SPCE with CeO<sub>2</sub>-chitosan nanocomposite probably due to the robust positive charges containing in this composite that offer electrostatic anchors for negative charges of the probe to accelerate the electron transfer at the interface. The fast electron transfer property of SPCE-Chi-CeO<sub>2</sub>

could also be affirmed by CV testing, as shown in Fig. 4. It can be seen that typical current peak curves for the oxidation and reduction versus potential applied were arisen in all performing scan rate of 25, 36, 81, 144 and 255 mV/s. The current peaks slide apart a bit with increasing scan rate as a characteristic of quasi-reversible reaction of the electrode against the  $K_3Fe(CN)_6^{3-/4-}$  redox probe (Fig. 4A). The peak potential ( $E_p$ ) of oxidative and reductive currents was about 0.2 and 0.04 V, respectively. The peak separation was about 0.09 V with a potential window from -0.2 to 1.2 V, while the anodic and cathodic peak current responses were linearly proportional to the square root of the investigated scan rate with the regression coefficient about 0.9 (Fig. 4B). Thus the modified SPCE-Chi-CeO<sub>2</sub> is certified satisfactory efficient for further use in electrochemical sensing according to its approved linear diffusion control mechanism and fast electron transfer ability [8].

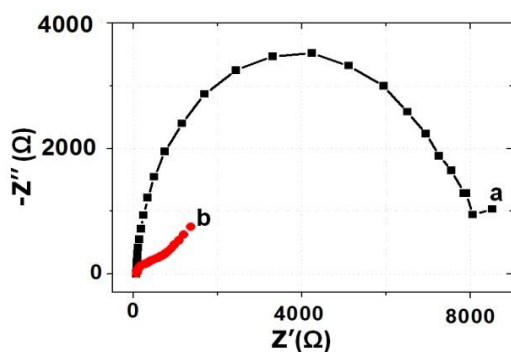


Fig. 3 Nyquist plot of electrochemical impedance spectra from bare SPCE (a) and SPCE-Chi-CeO<sub>2</sub> (b).

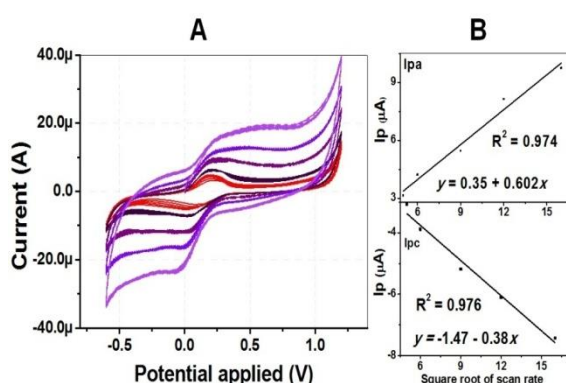


Fig. 4 Cyclic voltammograms of SPCE-Chi-CeO<sub>2</sub> in response to an electrochemical probe  $K_3Fe(CN)_6^{3-/4-}$  accounted by curves from inner to outer corresponding to 25, 36, 81, 144 and 255 mV/s scan rates, respectively (A), with their coordinate linear relationship of anodic and cathodic peak current vs. square root of scan rate (B).

### Electrochemical oxidation of melatonin

An electrochemical oxidation of melatonin on the screen printed carbon electrode before and after surface modification with cerium oxide-chitosan nanocomposite was investigated using DPV analysis. Fig. 5 shows the DPV of bare SPCE in the absence (curve a) and the presence (curve b) of melatonin at 1  $\mu$ g/ml in 0.1 M PBS pH 7.0 electrolyte as a sample at the scan rate of 50 mV/s, meanwhile the DPV of SPCE-Chi-CeO<sub>2</sub> in this absence and presence of melatonin is shown up by curve c and d, respectively. The current curves in the presence of melatonin produce one oxidation peak at  $E_p$  around 0.5-0.6 V with peak height ( $I_p$ ) about 0.1  $\mu$ A from bare SPCE and 1.6  $\mu$ A from SPCE-Chi-CeO<sub>2</sub>, whereas almost none peak current is exhibited in the absence of melatonin. Obviously higher response and well defined melatonin oxidation peak has been obtained in the case of SPCE-Chi-CeO<sub>2</sub> indicating an efficiently improvement by this working surface modification.

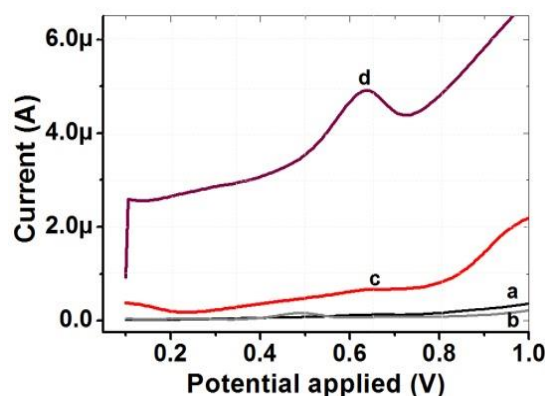


Fig. 5 Differential pulse voltammetric responses of bare SPCE and modified SPCE-Chi-CeO<sub>2</sub>: (a) bare SPCE at 0  $\mu$ g/ml melatonin, (b) bare SPCE at 1.0  $\mu$ g/ml melatonin, (c) SPCE-Chi-CeO<sub>2</sub> at 0  $\mu$ g/ml melatonin, and (d) SPCE-Chi-CeO<sub>2</sub> at 1.0  $\mu$ g/ml melatonin, all in PBS pH 7.0 based electrolyte.

### Quantitative determination of melatonin

Quantitative melatonin determination performance of the SPCE-Chi-CeO<sub>2</sub> was further examined by DPV with reference to its high current sensitivity and a small noise contribution from previous experiment. The peak current tended to increase with the increase of melatonin concentration. A linear relationship between peak current and melatonin concentration was obtained in the range from 1 to 10  $\mu$ g/ml in measurement by bare SPCE with the regression equation of

$$y = 2.067 + 0.44x$$

where  $y = I_p$  in  $\mu$ A,  $x$  = concentration in  $\mu$ g/ml,

and a correlation coefficient ( $R^2$ ) = 0.99 (Fig. 6A). Much lower concentration range down to 0.1 to 1.0  $\mu\text{g/ml}$  could be measured by the SPCE-Chi-CeO<sub>2</sub> with the regression equation of

$$y = 1.484x - 0.074, \text{ and } R^2 = 0.96 \text{ (Fig. 6B).}$$

The limit of detection, calculated by three times the standard deviation of the linear regression ( $S_{y/x}$ ) divided by the slope value (b), was 1.07  $\mu\text{g/ml}$  from the use of SPCE and 0.18  $\mu\text{g/ml}$  from SPCE-Chi-CeO<sub>2</sub>. Much higher sensitivity was achieved with SPCE-Chi-CeO<sub>2</sub> in consideration of the slope value and LOD results due to a better affinity of CeO<sub>2</sub>-chitosan nanocomposite for melatonin molecules that enhanced an electrochemical response performance. The relative standard deviation (RSD) of each calibration experiments was less than 10% indicating acceptable reproducibility. Although it seems that this LOD is not as low as some other recent reports such as the LOD of 0.02  $\mu\text{M}$  (0.005  $\mu\text{g/ml}$ ) by CV measurement with multi-walled carbon nanotube (MWCNT) modified glassy carbon electrode [9], the LOD of 0.1  $\mu\text{M}$  (0.025  $\mu\text{g/ml}$ ) by square wave voltammetry (SWV) with boron-doped diamond microelectrode [10], and the LOD of 0.004  $\mu\text{M}$  (0.001  $\mu\text{g/ml}$ ) by DPV on carbon ionic liquid electrode modified with MWCNT and cobalt hydroxide nanoparticles [11], but the ease of preparation and a facile operation for the prompt use with considerable lower cost in comparable to satisfactory detection range for the onsite practical use has made the SPCE-Chi-CeO<sub>2</sub> enduring attraction.

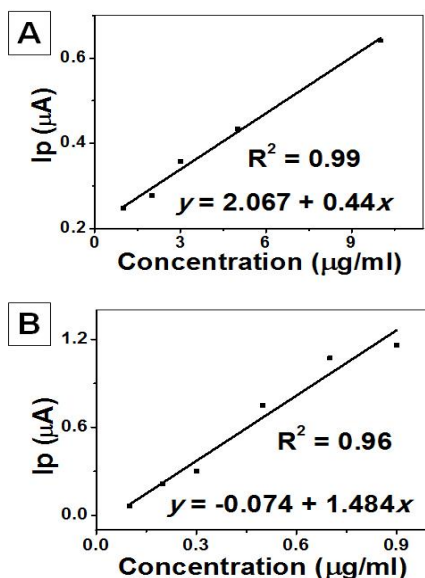


Fig. 6 Calibration plots for melatonin determination from DPV responses with bare SPCE (A) and with SPCE-Chi-CeO<sub>2</sub> (B).

### Selectivity in terms of interference study

To examine the relative reactivity and selectivity of the fabricated SPCE-Chi-CeO<sub>2</sub> toward melatonin detection, the electrochemical DPV were performed with 0.1 M PBS (pH 7.0) supporting electrolyte containing a fixed amount of 10  $\mu\text{g/ml}$  melatonin in the presence of other two closely structural related biological indoles as tryptophan and serotonin, adding at similar concentration. Usually, direct measurement of melatonin in presence of indole compounds especially of tryptophan would be impossible due to the proximity of the potentials of their oxidation peaks [12]. However, successful discrimination among them has been testified with SPCE-Chi-CeO<sub>2</sub> as displayed in Fig.7 by the DPV response in a mixture of melatonin with tryptophan (curve a), and the mixture of melatonin, tryptophan, and serotonin (curve b). A well separate oxidation peak of melatonin from that of tryptophan can be observed as shown in curve a, in which the typical oxidation peak of melatonin occurs at  $E_p$  around 0.53 V (peak 1), whereas the tryptophan's peak has placed at the next  $E_p$  of 0.65 V (peak 2). Slightly shift in  $E_p$  is apparent in the mixture of melatonin and its two precursors, tryptophan and serotonin which probably due to the competition in the diffusion rate to the electrode surface. The current peak concerning to melatonin exhibits at  $E_p$  of 0.56V and tryptophan originated peak appears at  $E_p$  around 0.69 V, meanwhile the oxidation peak corresponding to serotonin at  $E_p$  of 0.23 V is evident (peak 3). This phenomenon suggests that melatonin could still be selectively determined in the presence of both indolic precursors. In addition, the modified SPCE-Chi-CeO<sub>2</sub> has also allowed feasibility for effective simultaneous detection of these compounds.

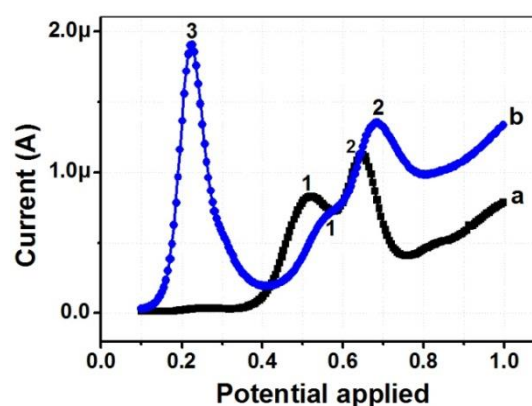


Fig. 7 Differential pulse voltammograms of SPCE-Chi-CeO<sub>2</sub> in 0.1 M PBS (pH 7.0) supporting electrolyte containing melatonin in the presence of tryptophan (a), and in the presence of tryptophan and serotonin (b) at 10  $\mu\text{g/ml}$  of each compound.



## CONCLUSION

An effective working electrode SPCE-Chi-CeO<sub>2</sub> was fabricated based on a combination of SPCE and cerium oxide-chitosan nanocomposite for rapid detection of a circadian rhythm regulation hormone, melatonin. Signified characteristics of the fabricated electrodes were morphologically and electrochemically manifested through SEM, EDS, EIS and CV analyses. A prominent improvement in electrochemical response signal was obtained in comparison to the original bare SPCE. Satisfactory working performances in melatonin inspection with rapid response and considerably low detection limit and reproducibility as well as good selectivity have also been verified by quantitative DPV and interference testing with its structural related tryptophan and serotonin. Melatonin detection by this electrode via DPV has shown simple and easy to operate, providing great potential application for practical use. Moreover, this system has allowed simultaneous speciation analysis of these three related indole compounds within the same time, as well as a tool extensible for elaboration of an easy and direct electrochemical determination of melatonin and other hormones in pharmaceutical preparations.

## ACKNOWLEDGEMENTS

The authors gratefully acknowledge Khon Kaen University's Division of Research and Technology Transfer Affair for partial funding to both individual and research group (KKU-56-57) and KKU Research Instrument Center for laboratory facilities.

## REFERENCES

- [1] Tan DX, Zheng X, Kong J, Manchester LC, Hardeland R, Kim SJ, Xu X, Reiter RJ, "Fundamental issues related to the origin of melatonin and melatonin isomers during evolution: relation to their biological functions" *Int. J of Molecular Sciences*, Vol.15, Sep. 2014, pp. 15858-15890.
- [2] Chegini S, Ehrhart-Hofmann B, Kaider A, Waldhauser F, "Direct enzyme-linked immunosorbent assay and a radioimmunoassay for melatonin compared", *Clinical Chemistry*, Vol. 41, Mar. 1995, pp. 381-386.
- [3] Wongkaew P, Poosittisak S, "Atomic force microscopic and electrochemical characterization of the modified screen printed carbon electrode by self assembled deposition of chitosan and activated carbon", *Int. J. of GEOMATE*, Vol. 11, Aug. 2016, pp. 2356-2362.
- [4] Wongkaew P, Poosittisak S, "Electro-affinity of SCWL-dsDNA on different high deacetylation degree chitosans deposited glassy carbon electrode", *Advances in Developing Affordable In-Vitro Molecular Diagnostics*, Puri CP, Abidi N, Bhanushali, P, Pere A, Gupta SK, Eds. Mumbai: Yashraj Research Foundation, 2012, pp. 249-258.
- [5] Wongkaew P, Poosittisak S, "Diagnosis of sugarcane white leaf disease using the highly sensitive DNA based voltammetric electrochemical determination", *Amer. J. of Plant Sciences*, Vol.5, Jul. 2014, pp. 2256-2268.
- [6] Feng KJ, Yang YH, Wang ZJ, Jiang JH, Shen GL, Yu RQ, "A nano-porous CeO<sub>2</sub>/chitosan composite film as the immobilization matrix for colorectal cancer DNA sequence-selective electrochemical biosensor", *Talanta*, Vol.70, Oct. 2006, pp. 561-565.
- [7] Orazem ME, Tribollet B, *Electrochemical Impedance Spectroscopy*. New York: Wiley, 2008, pp. 1-459.
- [8] Nicholson RS, "Theory and Application of Cyclic Voltammetry for Measurement of Electrode Reaction Kinetics", *Analytical Chemistry*, Vol. 37, Apr. 1965, pp.1351-1355.
- [9] Qu W, Wang F, Hu S, Cui D, "Electrocatalytic properties and voltammetric determination of melatonin at a nanostructured film electrode", *Microchimica Acta*, Vol. 15, Jun. 2005, pp. 150-109.
- [10] Levent A, "Electrochemical determination of melatonin hormone using a boron-doped diamond electrode", *Diamond & Related Materials*, Vol. 21, Jan. 2012, pp. 114-119.
- [11] Babaeia A, Taheria AR, Farahanic IK, "Nanomolar simultaneous determination of levodopa and melatonin at a new cobalt hydroxide nanoparticles and multi-walled carbon nanotubes composite modified carbon ionic liquid electrode", *Sensors and Actuators B: Chemical*, Vol. 183, Jul. 2013, pp. 265-272.
- [12] Radi A, Bekhiet GE, "Voltammetry of melatonin at carbon electrodes and determination in capsules", *Bioelectrochemistry and Bioenergetics*, Vol. 45, May 1998, pp. 275-279.



## COMPARISON OF HEART RATE VARIABILITY BETWEEN PATIENTS WITH MAJOR DEPRESSIVE DISORDER AND NORMAL SUBJECTS

Warangkana Chompoopan<sup>1</sup>, Sipanut Silaket<sup>2</sup>, Wichai Eungpinichpong<sup>3</sup>, Suwanna Arunpongpaisal<sup>4</sup> and Niramol Patjanasootorn<sup>5</sup>

<sup>1</sup>Sirindhorn College of Public Health, Khon Kaen, Thailand <sup>2</sup>Faculty of Associated Medical Sciences, Khon Kaen University, Khon Kaen, Thailand; <sup>3</sup>Research Center in Back, Neck, Other Joint Pain and Human Performance, Khon Kaen University, Thailand; <sup>4</sup> Faculty of Medicine, Khon Kaen University, Khon Kaen, Thailand

### ABSTRACT

Major Depressive Disorder is one of major mental health problems that affect quality of life of the patients. The reduced heart rate variability (HRV) and elevated heart rate that associated with depression have been found as risk factors for cardiac mobility and mortality. These patients should be assessed regularly on HRV parameters and compare with those of normal subjects. This study aimed to compare heart rate variability between patients with major depressive disorder and normal subjects. This study was conduct at a psychiatric department in Khon Kaen University, Srinagarind hospital, Khon Kaen province, Thailand. A cross sectional analytic study design was used. Forty patients diagnosed with major depressive disorder (who had been treated with antidepressants) were matched according to age, gender with 40 normal subjects participated. They were assessed on HRV for time domain (standard deviation normal to normal: SDNN, and the root mean square of successive differences: RMSSD) and frequency domain (High frequency: HF, low frequency: LF, and LF/HF ratio) using SA 3000P Digital. The results shown that The HRV in the patients and in the normal subjects were found with SDNN 28.60, 31.44; RMSSD 23.78, 26.73; HF 4.70, 5.04; LF 4.46, 5.01; and LF/HF 1.16, 1.35 respectively. However, No significant difference in the HRV variables between MDD and normal subjects except LF. Findings in this study show that HRV in the treated patients with major depressive disorder seem to be a little lower than the normal subjects. This may be due to the effects of well treated with antidepressants. It is suggested that HRV may be one of outcome measures for this patient population.

*Keywords: Major depressive disorder, Heart rate variability, Time domain, Frequency domain*

### INTRODUCTION

Major depressive disorder (MDD) is the most common illness psychiatric problem and will be one of the most disabling medical conditions by 2020. It has a large prevalence worldwide, with an estimated 350 million people affected. [1] MDD has been found around 2.4% in Thai population from epidemiological study of Mental Disorders National Survey in 2008. [2] It could be one of the risk factors for developing ischemic heart disease and has been found to elevate mortality rate of cardiovascular diseases that sudden death can occur after cardiac infarction. [3] Depression and stress were initially associated with the sympathetic activities and then were found to correlate with parasympathetic activity. [4] The reducing heart rate variability (HRV) and elevated heart rate were associated with Depression [5] which have been known to be risk factors for cardiac mobility and mortality. [6] Several evidence also suggest that depression is associated with altered brain function

and elevated sympathetic activity, which may lead to cardiovascular dysregulation.

Interactions of central nervous system increased sympathetic tone, decreased parasympathetic tone to the heart will also reduce heart rate variability. However, the effects of sympathetic and parasympathetic activities on interaction between stress and depression of the autonomic nervous system remains were unclear. [7] HRV is an electrocardiograph-based technique developed to assess the relative influences of sympathetic and vagal branches over heart's beat-to-beat activity. [8] It may be a trait – maker for MDD which can be used for evaluating and classifying the severity of symptoms in these patients. This study aimed to compare heart rate variability between patients with major depressive disorder and normal subjects.

### METHODS

#### Design and setting

A cross-sectional analytical design was used in this study.

## Participants

Forty patients, aged 18-64 years, who were diagnosed with MDD, were recruited at the psychiatry outpatient clinic of Srinagarind hospital, Khon Kaen University, Khon Kaen province, Thailand.

## Procedure

The study proposal was approved by the Khon Kaen University Ethics Committee for Human Research with reference number HE581192. The objective and design of the study were explained to all participants before they gave informed consent at the psychiatric clinic of Khon Kaen University, Srinagarind hospital. Diagnostic and Statistical Manual of Mental Disorders, Fifth Edition (DSM-5) was conducted to ensure the diagnosis of MDD by a licensed psychiatrist.

The process of data collection consisted of three steps. The first step included demographic data (sex, age). The second step included physician-assessment measure were assessed by the Hamilton rating scale for depression and structured clinical interview for Mini International Neuropsychiatric Interview (MINI). It was used to determine depression and to rule out other similar psychiatric disorders such as bipolar disorder, schizophrenia, and psychotic disorder. The third step, all subjects were asked to have early meal at least 2 hours prior to participate in the measurements. They were also instructed to refrain from alcohol or caffeinated consumption 24 hours before participation. To control for diurnal variation, HRV was measured between 10.00 a.m. and 2 p.m. by using SA-3000P (Medi-core, Seoul, Korea). Each of the subject was comfortably seated on a chair, then the probe was placed on his/her left index finger to measure HRV for 3 minutes. During HRV measurement the subject was guided to breathe naturally in order to obtain accurate HRV data.

## Measurement equipment

All variables were calculated as indicators of ANS function. Time domain variables included: (1) the standard Deviation of all normal to normal intervals (SDNN) as an estimate of overall HRV, and (2) the Root Mean Square successive differences of normal to normal interval (RMSSD) which indicate mostly parasympathetic activity.

Frequency domain variables included: (1) High Frequency power expressed as normalized units (HF nu; 0.15-0.4 Hz); (2) Low Frequency power expressed in normalized units (LF nu; 0.04-0.15 Hz). The LF- band is associated with both sympathetic and parasympathetic activity, while the HF band can be interpreted as a specific measure of parasympathetic control; and (3) LF/HF display for sympathovagal balance of HRV.

## Statistical analyses

Data were performed using IBM SPSS 19.0 software (IBM Corp. Released 2010. IBM SPSS Statistics for Windows, Version 19.0. Armonk, NY: IBM Corp) (Licensed of Khon Kaen University). Frequency (percent), mean, and standard deviation were presented for quantitative variables, respectively. The Kolmogorov-Smirnov test was tested to verify normal distribution of the data. For analysis of HRV data that exhibit non-normal distribution of the data, the median (with Quartile 1 and Quartile 3) was presented. All HRV variable were then compared between sex and age-matched groups.

## RESULTS

### Demographic features

The demographic variables based on age, sex were balanced between the case (MDD) group and the control group. Forty depression patients [11 males and 29 Female; Mean age (SD) = 43.35 (14.37) years] participated.

For the control group, age and sex matched healthy volunteers were recruited from university students, teacher, hospital workers, and people in the community. They were chosen after excluding those with psychiatric and physical disorder by a psychiatrist (Table 1).

Table 1 Demographic data between patients with major depression and normal controls

Parameters	Depression Patients (n=40)	Normal Control (n=40)
Sex		
Male	11(27.50)	11(27.50)
Female	29(72.50)	29(72.50)
Age		
18-30	9(22.50)	9(22.50)
31-40	5(12.50)	5(12.50)
41-50	11(27.50)	11(27.50)
51-60	10(25.00)	10(25.00)
61+	5(12.50)	5(12.50)
Total	40(100.00)	40(100.00)
Mean	43.35	43.10
S.D.	14.37	14.50

No significantly differences in the demographic variables (sex, age) between the control and depression groups were observed.

The comparison between the frequency domain and time domain of HRV in the two group was shown in Table 2. The Mean and standard deviation of HR, SDNN, RMSSD, LF, HF and LF/HF ratio in the depression patients were 79.40(12.62) beat/min, 28.60(15.84)ms<sup>2</sup>, 23.78(15.87)ms<sup>2</sup>, 4.46(1.50) ms<sup>2</sup>,

4.70(1.37)ms<sup>2</sup>, 1.16(1.01) and in the normal subjects were 79.32(13.79) beat/min, 31.44(16.58) ms<sup>2</sup>, 26.73(15.28)ms<sup>2</sup>, 5.01(1.10) ms<sup>2</sup>, 5.04(0.91)ms<sup>2</sup>, 1.35(1.09) respectively.

No significant difference in the HRV variables between MDD and normal subjects except LF. However, it was noted that mean of all variables in the MDD group seemed to be lower than those in normal group.

Table 2 Comparison on HRV data between MDD and the control groups.

Parameters	MDD (n=40)	Control (n=40)	p-value
	Mean (S.D.)	Mean (S.D.)	
HR	79.40(12.62)	79.32(13.79)	0.98
SDNN	28.60(15.84)	31.44(16.58)	0.37
RMSSD	23.78(15.87)	26.73(15.28)	0.40
LF	4.46(1.50)	5.01(1.10)	0.01
HF	4.70(1.37)	5.04(0.91)	0.14
LF/HF	1.16(1.01)	1.35(1.09)	0.43

HRV variables in patients with different degree of depression were also compared. No statistically significant difference in median HR, frequency domain and time domain (Table 3).

Table 3. HR, HRV in patients with depression Level

HRV	No depression Median (n=8)	Mild Depression Median (n=9)	Less than MDD Median (n=10)	Mild MDD Median (n=10)	Severe MDD Median (n=3)	p-value
HR	76.50 (23.50)	74.00 (17)	90.00 (15)	86.00 (12.5)	78.5 (12.5)	0.49
SDNN	21.40 (15.83)	24.75 (17.20)	30.98 (24.79)	16.71 (10.48)	31.05 (15.80)	0.37
RMSSD	16.61 (12.01)	20.18 (16.83)	19.87 (23.81)	13.59 (14.54)	18.39 (12.25)	0.44
LF	3.60 (2.22)	4.74 (1.57)	4.96 (2.89)	3.57 (2.06)	4.70 (1.60)	0.16
HF	3.74 (1.40)	5.18 (2.33)	5.23 (3.42)	4.04 (1.72)	4.92 (1.07)	0.22
LF/HF	1.68 (1.56)	1.00 (1.40)	0.56 (1.30)	0.44 (0.66)	0.84 (0.85)	0.79

Kruskal-Wallis equality-of-population rank test  
No depression (0-7), Mild (8-12), Less than MDD (13-17)  
MDD (18-29) and severe (30<sup>+</sup>)

HRV and HR data were also compared by mean of different medications for treatment. The only TCA was significant difference in HRV. Furthermore, we found no difference on Serotonin and norepinephrine reuptake inhibitor (SNRI), Selective serotonin reuptake inhibitors (SSRIs) and there was significant increase on HR and decrease HRV associated with Tricyclic antidepressants (TCA) (*p*-value 0.003), SDNN (*p*-value 0.0009), RMSSD (*p*-value 0.008), LF (*p*-value 0.0009), HF

(*p*-value 0.008) and LF/HF (*p*-value 0.02). According for the results on anti-depressants, patients treated with TCA has relatively low HRV as compared with other antidepressants (Table 4).

Table 4. Comparison of HR, HRV and difference of Drug

SNRI: Serotonin and norepinephrine reuptake inhibitor  
SSRIs: Selective serotonin reuptake inhibitors  
TCA: Tricyclic antidepressants

HRV	SNRI			SSRIs			TCA		
	Yes	no	p-value	yes	no	p-value	Yes	no	p-value
	Median (IQR)	Median (IQR)		Median (IQR)	Median (IQR)		Median (IQR)	Median (IQR)	
HR	75.5 (15)	78 (20)	0.56	76 (20)	84.5 (18)	0.09	93 (9)	76 (15)	0.003
SDNN	23.04 (20.73)	26.33 (25.85)	0.91	26.33 (15.96)	18.42 (24.17)	0.10	11.11 (0.05)	26.93 (15.96)	0.0009
RMSSD	19.03 (19.47)	19.47 (10.32)	0.82	20.02 (19.19)	16.57 (9.27)	0.09	10.59 (2.15)	19.87 (17.99)	0.008
LF	4.42 (1.85)	4.69 (2.20)	0.84	4.69 (1.92)	3.91 (2.93)	0.26	2.23 (1.05)	4.70 (1.97)	0.0009
HF	4.49 (2.95)	4.74 (1.31)	0.93	4.81 (1.47)	3.65 (2.16)	0.06	3.05 (.077)	4.85 (1.82)	0.008
LF/HF	0.82 (1.50)	0.84 (1.35)	0.69	0.64 (1.38)	1.34 (1.41)	0.20	0.5 (0.35)	1.09 (1.50)	0.02

## DISCUSSION

Depression is an affective disorder of patients who are suffering to daily life. Prolonged depression they may lead to the risk of have heart diseases. Previous studies, MDD patients were found to have a decreased in HRV as compared to the non-depressed group. [9]-[10] Conversely, our findings did not find significant difference in HRV between MDD and normal subjects except Low frequency (LF). This could be due to small sample size of the current study. With a trend of having lower HRV in the MDD as compare to the normal indicate that a large sample size may show a larger power for statistical analysis. Another reason may be that the patients in the MDD group of this study have been on medication for a while where their conditions may be getting near normal. Further study on new case of MDD that have not started any medication may provide a clearer result.

## CONCLUSION

Based on the results of the study, HRV variables in the treated patients with MDD seemed to be a little lower than those in the normal subjects but no statistical significance. This may be due to the effects of well treated with antidepressants and small sample size of the study. Further study with a larger sample size is needed to explore the different in HRV between the MDD and normal subjects.

## ACKNOWLEDGEMENTS

This study would not have been possible without kind cooperation of Khon Kaen University, Srinagarind hospital and the 80 participants. More importantly, the Research Center in Back, Neck, Other Joint Pain and Human Performance, Khon Kaen University as well as Sirindhorn College of Public Health where have funded this study.

## REFERENCES

- [1] World Health Organization, Sixty-fifth world Health: <http://www.who.int/mediacentre/factsheets/fs369/en/>. assrmby 2012.
- [2] Kongsuk T, Pengjuntr W, Kittirattanapaiboon P, Kenbubpha K, Arunpongpaian S, Sukawaha S. The prevalence of major depressive disorders in Thailand: results from the Epidemiology of Mental Disorders National Survey 2008. 2013.
- [3] Glassman AH, Bigger J, Jr, Gaffney M. Psychiatric characteristics associated with long-term mortality among 361 patients having an acute coronary syndrome and major depression: Seven-year follow-up of sadhart participants. Archives of general psychiatry. 2009; 66(9):1022-9.
- [4] Lin H-P, Lin H-Y, Lin W-L, Huang AC-W. Effects of stress, depression, and their interaction on heart rate, skin conductance, finger temperature, and respiratory rate: sympathetic-parasympathetic hypothesis of stress and depression. Journal of Clinical Psychology. 2011; 67(10):1080-91.
- [5] van der Kooy KG, van Hout HP, van Marwijk HW, de Haan M, Stehouwer CD, Beekman AT. Differences in heart rate variability between depressed and non-depressed elderly. International journal of geriatric psychiatry. 2006; 21(2):147-50.
- [6] Robert M, Carney P, Kenneth E. Freedland, and Richard C. Veith, Depression, the Autonomic Nervous System, and Coronary Heart Disease. Psychosomatic Medicine 67. 2005;1: 529-33.
- [7] Shinba T, Kariya N, Matsui Y, Ozawa N, Matsuda Y, Yamamoto K-i. Decrease in heart rate variability response to task is related to anxiety and depressiveness in normal subjects. Psychiatry Clin Neurosci. 2008; 62(5):603-9.
- [8] Foerze T. Heart rate variability standards of measurement, physiologic interpretation, and clinical use. Circulation. 1996; 97(5):1043-65.
- [9] Carney RM, Blumenthal JA, Stein PK, Watkins L, Catellier D, Berkman LF, et al. Depression, Heart Rate Variability, and Acute Myocardial Infarction. Circulation. 2001;104(17):2024-8.
- [10] Yiming Wang XZ, Adrienne O'Neil, Alyna Turner, Xingde Liu and Michael Berk. Altered cardiac autonomic nervous function in depression. BMC psychiatry. 2013; 13.

## **EFFECT OF ARM SWING EXERCISES ON CARDIOVASCULAR RESPONSE AND BALANCE OF OLDER WOMEN**

Worawut Chompoopan<sup>1</sup>, Piyathida Kuhirunyaratn<sup>2</sup>

<sup>1</sup>Faculty of Medicine, Khonkaen University, Thailand.

<sup>2</sup>Research Center in Back, Neck, Other Joint Pain and Human Performance,  
Khon Kaen University, Thailand.

### **ABSTRACT**

The purpose of this study was to assess the effect of arm swing exercises (ASE) on cardiovascular response and dynamic body balance of older women. 4 villages were randomly selected. The total population was 128 participants divided into 63 older women from two villages in the experimental group, another 65 older women from another two villages in the control group. The experimental group participated in the evening ASE program, five days a week, lasted for six months. The ASE program began with warming up for 5 minutes, swinging arms for 30 minutes, and gradually cooling down for another 5 minutes. Data collection consisted of pre and post-data collection before and after six months of the ASE program exercise. The collected data were validated by the experienced researcher. An independent t-test was used to compare the mean of both groups before participating in the ASE program. An intention-to-treat analysis was used for last observation carried forward missing data. Analysis of Covariance (ANCOVA) was used to compare the mean of both groups and Paired t-test within the group. After 6 months of exercising, the cardiovascular response and body balancing of both groups were measured. The results showed that the systolic blood pressure and diastolic blood pressure of participants in the experimental group were declined at 5.64 and 6.72 mmHg, respectively while there was only slightly changed in the control group of which statistically was not significant. In addition, the resting heart rates of the participants in the experimental group declined to 6.76 beats /minute and their body balancing has improved. Therefore, the ASE program can be effective to improve BP, HR, and body balancing of older women.

*Keywords: Older, Arm-swing exercise, Blood pressure, Resting heart rate, Balance.*

### **INTRODUCTION**

An increase of ageing society has globally been an issue of discussion and challenges for many countries. More than a half of the ageing population (414 million) is in Asia and Europe (161 million). China was reported to have the most older people (209.24 million), India was the second (116.55 million) and Japan had 41.85 million. Indonesia and Brazil had almost the same amount (21.19 and 24.39 million). [1]

Thailand is one of the countries where the ageing population has increased to 10.73 million and has a tendency to increase each year. [2] Health problems also occur. These older people have to encounter not only their health problems, but also the other aspects of their living like high blood pressure, chronic diseases, unexpected non-communicable diseases, more dangerously body balancing. [3] Physiological changes in the older people can be very dangerous, particularly cardiovascular system. For instance, the reduction of Cardiac function, the inflexibility of blood vessel. [4] These can cause hypertension and heart disease. [5]

Regular exercises have benefit towards cardiovascular health, increase cardiovascular endurance, decrease heart disease, or any factors associated to heart diseases. [6]

In China, Arm-swing exercise (ASE) has been performed and very popular among older people for more than thousand years and has been proved very safe for them. [7] It is non-equipment involved. No cost is concerned. People can do everywhere and any circumstances. It is very easy to remember. The only condition is that it has to be done continuously at certain period of time.

The study involving Arm-swing exercise (ASE) related to the effect of cardiovascular system and body balancing of older people has been limited. This study aims to assess the effect of Arm-swing exercise on cardiovascular response and balance of older women.

### **METHODS**

#### **Participants**

Four villages were randomly selected and divided into an experimental and a control group. 128 healthy older women, age more than 60 years old from the

four villages were randomly recruited and grouped accordingly to the inclusive criteria (have been living in the village more than a year and have to live in the village more than a year) to participate in the study. The exclusive criteria include regular exercise, disability, and having dynamic body balance problems.

#### Design and setting

This study employed a parallel two-arm cluster randomized control trial (CRT). A Block of 2 was used for randomization. (4 villages were equally divided.) The size of each village was required to have similar geographically characteristics such as similar number of older women, similar size of the community, and each village has to be a distance apart. The study was conducted at one of the districts in Khon kaen province, from October 2014 to March 2015.

#### Intervention

All 63 participants from the two selected villages in the experimental group followed the ASE program in the evening, five days a week lasted for six months. All participants from each village did the exercise together at the same time. The ASE program started by warming up for five minutes, after that they followed the steps of the ASE program by standing on feet as wide as their shoulder width, swinging both arms forwards at thirty degrees and backwards at sixty degrees in a second. They had to repeatedly do this sixty times per minute, lasted for thirty minutes each day. Since the exercise had taken a bit of time, to avoid the boringness, local music was included throughout the exercise. All participants were allowed to walk or dance while swinging their arms. The exercise was gradually cooled down for five minutes.

All participants were suggested not to perform any other exercises apart from the ASE program during the period of this study.

#### Procedure

Firstly, the research proposal was required to be approved by the Khon Kaen University Ethics Committee. Eventually the research was registered for Human Research, coded HE571237. The objectives and the study design were described to all the participants for both the experimental and control groups. The consent form was read and signed at the Health Promoting Hospital. The appointment was arranged right after the consent form was acknowledged and signed for self-risk assessment. Those who were initially screened, the steps of the program were introduced. Every participant was provided with a recording-book to sign every time participated in the exercise.

Normally, the exercise was performed in the village meeting point center nearby where was convenient and older people had fun.

Village health volunteers and Health Promoting Hospital officers followed up whether the ASE program had been regularly performed. All the participants were encouraged to regularly participate accordingly to the study design. The researcher and research assistants regularly visited and interviewed the participants. After 6 months of the ASE program, another appointment was made at the Health Promoting Hospital in the morning to measure blood pressure (BP), resting heart rate (HR), and dynamic body balance.

#### Measurement equipments

Blood pressure (BP) and resting heart rate (HR) were measured by a digital sphygmomanometer (Omron® Japan) at the right arm. The participant rested for 10 minutes after the arrival at the Health Promoting Hospital. The measurement was repeated 3 times for each participant and recorded. If the results of the systolic or diastolic blood pressure varied more or less than 10% of the previous measurement, the participant was advised to sit down for a 10 minutes rest. All the three times measurement was averaged.

A timed up and go test (TUG) was used to measure the dynamic body balance (Podsiadlo & Richardson, 1991) purposely to assess the balance, walking ability, and fall risk in older women. Participants were suggested to wear their regular footwear. The procedure of TUG measurement began with the advice for the participants to sit on a chair, waited for the signal from the researcher to get up and walk along the three meters line, then went back to their seat. The duration of this performance was timed and recorded.

#### STATISTICAL ANALYSES

Shapiro-Wilk test was used to verify the normal distribution of continuous variables. Data were analyzed through using SPSS Version 19 (IBM Corp. Released 2010. IBM SPSS Statistics for Windows, Version 19.0. Armonk, NY: IBM Corp.) Under licensed by Khon Kaen University. An intention-to-treat analysis was also used for last observation carried forward missing data. The Independent t-test was used to compare the averaged results from blood pressure, resting heart rate and dynamic body balance of both groups before participating in the ASE program. The intention-to-treat analysis for last observation carried forward missing data was also used. Subsequently, an analysis of covariance (ANCOVA) was employed to compare the averaged results from blood pressure, resting heart rate, and dynamic body balance of both groups after the ASE program, followed by a paired

t-test to compare the mean within the experimental and control group. A difference at the level of  $p < 0.05$  was considered statistically significant.

## RESULTS

Before participating in the ASE program, all participants ages, systolic blood pressure (SBP), diastolic blood pressure (DBP), resting heart rate, (HR), and dynamic body balance were compared to find out any obvious differences. There was not statistically different except the systolic blood pressure of the experimental group was higher than the control group and it was statistically significant. (As shown in Table 1)

Table 1 Base line characteristics before experiment

Variables	ASE	CON	p-value
Age	67.32±5.95	67.94±6.58	0.58
SBP	124.23±12.82	125.19±14.15	0.81
DBP	75.76±10.05	70.98±8.94	0.01
HR	79.10±10.59	77.22±8.11	0.26
Balance	9.60±3.34	10.45±3.11	0.14

Present Mean±SD., Independence t-test

After 6 months of the ASE program, the results of systolic blood pressure (SBP), diastolic blood pressure (DBP), resting heart rate (HR), and dynamic body balance of the experimental group were improved more than the control group. (As shown in Table 2)

Table 2 Comparison between ASE and CON group

Variables	ASE	CON	p-value
SBP	118.60	123.12	0.005
DBP	67.71	71.87	0.003
HR	71.75	75.86	0.005
Balance	8.78	10.62	<0.001

Present Mean, ANCOVA mean adjust baseline as covariate

A comparison within the experimental group after 6 months of the ASE program, the results of systolic blood pressure and (SBP) diastolic blood pressure (DBP), and resting heart rate (HR) were reduced, while the dynamic body balance was significantly improved. (As shown in Table 3)

Table 3 Comparison with in ASE group

Variables	Before	After	p-value
SBP	124.23±12.82	118.59±12.47	0.001
DBP	75.18±10.05	68.46±6.41	<0.001
HR	79.10±10.59	72.34±7.70	<0.001
Balance	9.60±3.34	8.75±2.40	0.028

Present Mean±SD., paired t-test

A comparison within the control group after 6 months of the ASE program, the results of systolic blood pressure and (SBP) and resting heart rate (HR) were reduced, but statistically no difference, while there were no significantly changes for dynamic body balance and diastolic blood pressure (DBP) (As shown in Table 4)

Table 4 Comparison with in CON group

Variables	Before	After	p-value
-----------	--------	-------	---------

SBP	125.19±14.15	123.83±11.54	0.436
DBP	70.98±8.94	71.02±9.62	0.974
HR	77.22±8.11	75.33±9.04	0.070
Balance	10.45±3.11	10.72±3.32	0.179

Present Mean±SD., paired t-test

## DISCUSSION

The results of the ASE program for older women in the villages could help reduce blood pressure and resting heart rate, similarly to several studies. Vitro reported that 12 weeks of low intensity exercise in older men and women found affected the reduction of resting heart rate. [8] Similarly to the study of healthy older men and women, after 6 months of low and high intensity exercise, it was found that the low intensity exercise group developed lower blood pressure comparing to the high intensity exercise group. [9] Another study of borderline diabetic mellitus older people, after 12 weeks of low intensity exercise training, their blood pressure was also reduced. [10]

The potential based on mechanism of reducing the blood pressure can be explained by the effect of sympathetic nerve activity. During the exercise recovery period, the sympathetic nerve activity is decreased. This also happens to the signal transduction from sympathetic nerve activation into vasoconstriction. The local vasodilator mechanisms decrease the arterial blood pressure, apparently found after the exercise. [11]

As far as the dynamic body balance is concerned, the results of the ASE program affected similarly to several studies. A home exercise program for 78 years old people, the results showed that their dynamic body balance has improved. [12] Similarly to another study done on three month exercise program for older men and women and followed up after 12 months, the finding demonstrated that the exercise program significantly improved their dynamic body balance measurement of which the same type of tool used for this study (timed up and go test (TUG)). [13] Consequently, the potential based on mechanism increased the dynamic body balance due to the peripheral sensation improved by the ASE program.

## CONCLUSION

Regular exercising of older women in the villages by Arm-swing, 5 times a week lasted for 6 months, may reduce blood pressure, resting heart rate and improve the dynamic body balance. This kind of activity can contribute a lot to the communities where there are a lot of older people in terms of health promotion, opportunities for social gathering, having fun as well as no-money costing. Any older people with any social status can perform this exercise program. More importantly older people could use their leisure time worthwhile for their



lives. This activity can certainly economically reduce the medication cost of the country.

## ACKNOWLEDGEMENTS

This study would not have been possible without the generous cooperation of the Health Promotion hospital officers, community health care volunteers, and the 128 participants. The researcher is thankful for Siridhorn College of Public Health, Khon Kaen to provide proportion of study funding and the financial support from the Research Center in Back, Neck, Other Joint Pain and Human Performance, Khon Kaen University for paper publication.

## REFERENCES

- [1] United Nations. Department of Economic and Social Affairs. Population Division. Current Status of the Social Situation, Wellbeing, Participation in Development and Rights of Older People Worldwide. New York 2011.
- [2] United Nations. Department of Economic Social Affairs. Population Division. World population prospects the 2015 revision. New York: United Nations; 2015.
- [3] World Health Organization. Global health and aging. Bethesda, MD: National Institute on Aging; 2011.
- [4] Strait JB, Lakatta EG. Aging-associated cardiovascular changes and their relationship to heart failure. *Heart Fail Clin*. 2012;8(1):143-64. Epub 2011/11/24.
- [5] Lakatta EG, Levy D. Arterial and cardiac aging: major shareholders in cardiovascular disease enterprises part ii: the aging heart in health: links to heart disease. *Circulation*. 2003;107(2):346-54.
- [6] Williams AD, Almond J, Ahuja KD, Beard DC, Robertson IK, Ball MJ. Cardiovascular and metabolic effects of community based resistance training in an older population. *Journal of science and medicine in sport / Sports Medicine Australia*. 2011;14(4):331-7. Epub 2011/03/29.
- [7] Ladawan S. Effects of arm swing exercise on metabolism and heart rate variability in type 2 diabetes mellitus: Khon Kaen University; 2008.
- [8] De Vito G, Hernandez R, Gonzalez V, Felici F, Figura F. Low intensity physical training in older subjects. *The Journal of sports medicine and physical fitness*. 1997;37(1):72-7.
- [9] Seals DR, Hagberg JM, Hurley BF, Ehsani AA, Holloszy JO. Endurance training in older men and women. I. Cardiovascular responses to exercise. *Journal of applied physiology: respiratory, environmental and exercise physiology*. 1984;57(4):1024-9. Epub 1984/10/01.
- [10] Hua LP, Brown CA, Hains SJ, Godwin M, Parlow JL. Effects of low-intensity exercise conditioning on blood pressure, heart rate, and autonomic modulation of heart rate in men and women with hypertension. *Biol Res Nurs*. 2009;11(2):129-43. Epub 2009/01/20.
- [11] Floras JS, Sinkey CA, Aylward PE, Seals DR, Thoren PN, Mark AL. Postexercise hypotension and sympathoinhibition in borderline hypertensive men. *Hypertension*. 1989;14(1):28-35. Epub 1989/07/01.
- [12] Brown M, Sinacore DR, Ehsani AA, Binder EF, Holloszy JO, Kohrt WM. Low-intensity exercise as a modifier of physical frailty in older adults. *Archives of physical medicine and rehabilitation*. 2000;81(7):960-5.
- [13] Arai T, Obuchi S, Inaba Y, Shiba Y, Satake K. The relationship between physical condition and change in balance functions on exercise intervention and 12-month follow-up in Japanese community-dwelling older people. *Archives of gerontology and geriatrics*. 2009;48(1):61-6.

## PLASTIC FLOW HETEROGENEITY AND FAILURE OF BIMETAL MATERIAL

Svetlana Barannikova<sup>1</sup>, Lev Zuev<sup>2</sup> and Yulia Li<sup>3</sup>

<sup>1</sup> Institute of Strength Physics and Materials Science, SB RAS, 2/4 Akademicheskii Ave., Tomsk, 634055,  
Russia

### ABSTRACT

The aim of this paper was to display the kinetics of Lüders band (LB) propagation of bimetallic material on the yield plateau at the microscale level. The localization patterns of plastic deformation in the process of uniaxial tension were obtained by noncontact method of recording the fields of displacement vectors. Microstructure of the interfaces with the using results of optical, atomic force and scanning microscopy showed that in the direction of the pearlite steel to the austenitic form there are structural components: the weakened zone of the ferrite layer; hardened section of the ferrite layer dark-pickling layer from the side of austenitic steel. Plastic deformation of a bimetal began from the nucleation of the Lüders band on the boundaries of the bimetal on stress raisers with higher hardness due to the diffusion effect. In the main layer the Lüders band was limited to a pair of fronts moving in opposite directions along the bimetal axis with different velocities. The cladding layer did not suppress the formation of Lüders bands, led to an increase in the propagation velocity of Lüders band fronts in the base layer.

*Keywords: Lüders band, localization of plastic deformation, DIC, steel, bimetal*

### INTRODUCTION

Unstable plastic deformation of metals and alloys at the macroscopic level is manifested in the form of a sharp yield point, neck formation and discontinuous deformation [1-3]. The bands of macrolocalized deformation accompanying jumps of deformation and/or stresses impair the industrial products surface quality, cause their premature corrosion and increase the probability of sudden destruction. Studies of the nonuniformity of materials deformation had been previously made in detail on specimens of pure metals and alloys [4-6]. This paper considers the deformation behavior of a corrosion-resistant bimetal – carbon steel - stainless steel – which is used in chemical engineering for the manufacturing of reaction columns, autoclaves, reactors and heat exchangers [7-10]. The main requirement for a bimetal is to ensure the strength and ductility of the compound, its continuity and stability of its properties over the entire contact surface. In this connection, it is necessary to improve knowledge about the processes of joining dissimilar metals and their joint deformation on micro-, meso- and macroscale levels.

### RESEARCH MATERIALS AND METHODS

The studied samples of bimetallic compounds were cut from a strip produced according to the following procedure: between the sheets of cladding metal put into the mold box - 321 AISI as a parent metal steel of A 283 Grade C was poured ( $t = 1500^{\circ}\text{C}$ ), followed by hot rolling of the

obtained three-layer sheet at  $t = 1200 \div 1400^{\circ}\text{C}$ . Along the outer edge of the sample on both sides  $\approx 750$  microns thick cladding layer of 321 AISI steel is located; in the center  $\approx 6.7$  mm thick layer of the base metal of A 283 Grade C.

Sample preparation of the bimetal for metallographic studies and visualization of zones of large deformation localization was carried out according to the standard procedure for steels and alloys: grinding on abrasive cloths of various grades: 50H 865, M50 L219, P120; polishing using diamond paste ACM 1/0 on a felt base. Chemical etching of the sample was carried out with reagents to reveal structures of stainless and low-carbon steels.

Pre-prepared samples in the form of a double dog bone with the dimensions of the working section  $42 \times 8 \times 2$  mm were extended at  $T = 300\text{K}$  at a rate of  $6,67 \times 10^{-5} \text{c}^{-1}$  on LFM-125 test machine.

Visualization of the localized plastic deformation bands and registration of their proliferation kinetics was carried out at the working portion of the sample by the length of 42 mm by two non-contact methods: the method of digital image speckle correlation and the method of digital statistic speckle photography [11,12]. When these methods were implemented, the extended sample was illuminated with coherent light of a semiconductor laser with a wavelength of 635nm and a power of 15W. The strained sample images obtained in this light and superimposed with speckle patterns were recorded with PixelLink PL-B781 digital video camera at the frequency of 10Hz and the resolution of 15.114 microns/pixel, digitized and stored as files. The idea of the method of digital correlation of speckle images is in possibility to

determine displacement fields with a high accuracy by tracking changes in the material surface and comparing the digital images recorded during stressing. In the method of digital statistical speckle photography, a count sequence for each picture point of a speckle image structure was formed characterizing the time course of its brightness, variance and the expectation were calculated and the ratio between them was used for mapping zones of plastic deformation localization.

## RESULT AND DISCUSION

The study of the microstructure by optical metallography has allowed to establish that after rolling of a three-layer sample, the interfaces of dissimilar materials are clear and thin, pores and nonmetallic inclusions are absent, which indicates continuity and high quality of the engagement.

Examination of the bimetal conjugation area using the LEO EVO 50 scanning electron microscope (Carl Zeiss, Germany) with the Oxford Instruments attachment for X-ray dispersion microanalysis (NANOTECH Center of the Institute of Theoretical and Experimental Physics affiliated with SB RAS) yielded data on the quantitative content of elemental composition of steels in the conjugation area in the course of a step-by-step approximation to the boundary, as, for instance, shown in Fig. 1.

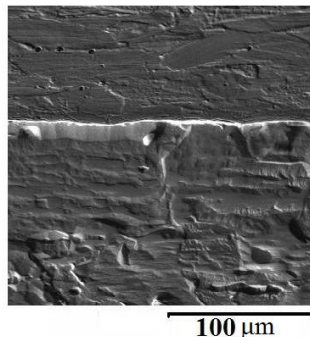


Fig. 1 Bimetal areas for dispersive microanalysis (5 μm distance to the conjugation boundary).

The results of the study of the quantitative elemental composition of steels in the conjugation area showed a chromium content in steel of 321 AISI, the concentration of which increases from 0.18 to 0.39 (wt.%) in the direction of the conjugation boundary between 25 and 5 μm. At the same time, in the stainless steel, in the direction of the conjugation boundary between the two steels, the chromium content decreases, due to the diffusion of chromium from stainless steel in 321 AISI. Since carbon belongs to chemical elements with a low sequence number, in this case, only its qualitative assessment is possible. Analysis of the carbon content in

stainless steel at the depth of 10 μm from the conjugation boundary between the two metals has showed an increase of 0.32 (wt.%). At the same distance and less than 10 μm from the conjugation boundary, carbides are formed as a result of diffusion of alloying elements from steel A 283 Grade C into 321 AISI, which explains the increased hardness of structural steel in the conjugation area.

The results of the investigation of the microhardness distribution along the thickness of the bimetallic compound are shown in Fig. 2. Thus, the microhardness at the conjugation was significantly higher than the microhardness of the base metal (321 AISI) and the cladding layer (A 283 Grade C) outside the conjugation area. Such a change in the microhardness along the width of the conjugation zone can be explained by the manifestation of two competing effects due to the presence of directed flows: carbon from low-carbon steel 321 AISI into stainless steel A 283 Grade C, and alloying elements Cr and Ni in the opposite direction. The first stream leads to softening and formation of a ferrite structure in the border sections of 321 AISI, which originally had a perlite structure, and the second, on the contrary, leading to their hardening.

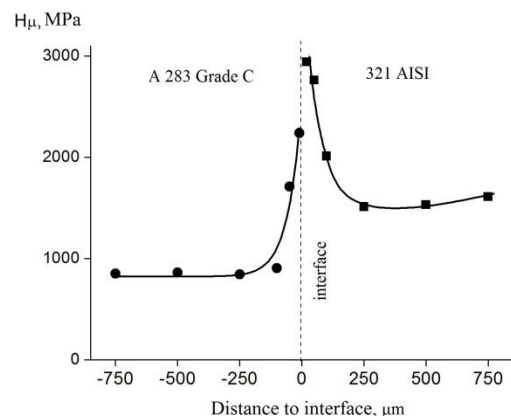


Fig. 2 Distribution of microhardness in the area of conjugation of steels 321 AISI and A 283 Grade C.

In steel 321 AISI the basis is ferrite, and in steel A 283 Grade C it is austenite (Fig. 3) [3].

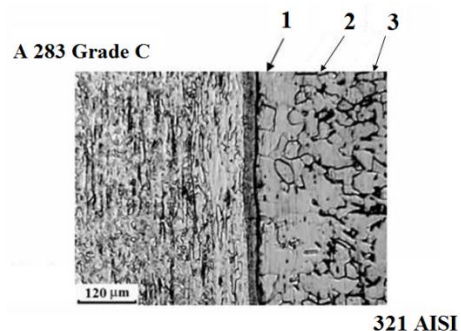


Fig. 3 Optical metallography of bimetal in the conjugation area: (1) – the decarbured layer – the

conjugation area; (2) – the zone of partial decarburization; (3) – structure of the base metal (321 AISI).

Fig. 4 (a-c) shows atomic force microscopy scan images taken when examining the structure of the base metal of 321 AISI, with successive approximation to the boundary of conjugation with the cladding layer of stainless steel on an atomic force microscope. Thus in Fig. 4a the image of the structure of the base metal 321 AISI is obtained at the distance of  $\approx 2$  mm from the conjugation boundary and represents a matrix of ferrite with perlite colonies, which is a typical picture for low-carbon steels. A successive approximation to the conjugation boundary at a distance of about  $200\text{ }\mu\text{m}$  makes it possible to detect an area of partial decarburization, which is transitional from the structure of the base metal to the ferrite structure (see Fig. 4b).

Further in Fig. 4c directly shows the conjugation boundary between the two metals. It is clearly seen that a decarburized layer consisting entirely of ferrite grains is formed on the side of the base metal of 321 AISI. That means that a structure of pure ferrite was formed.

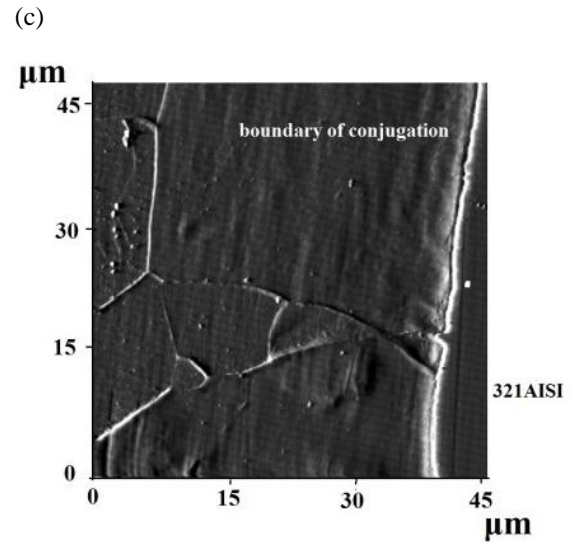
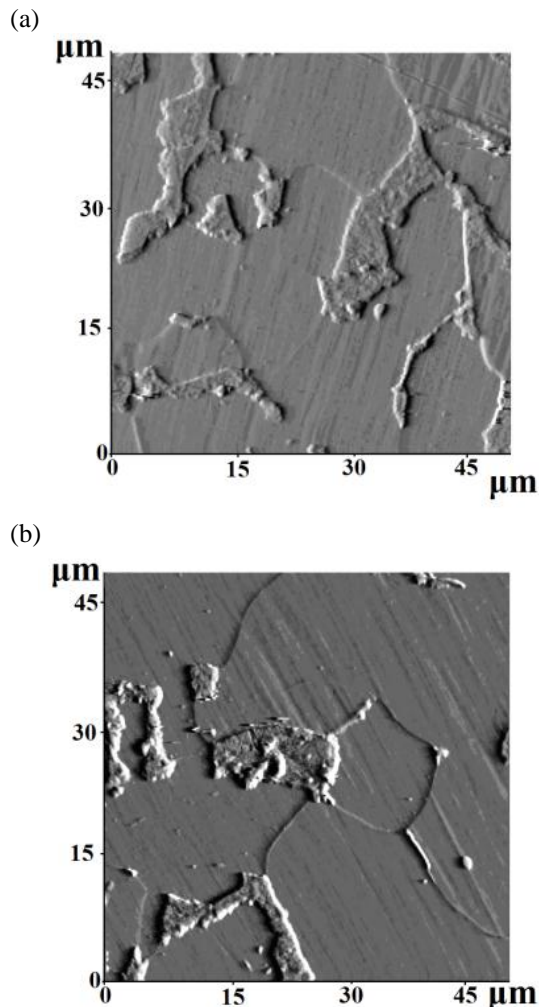
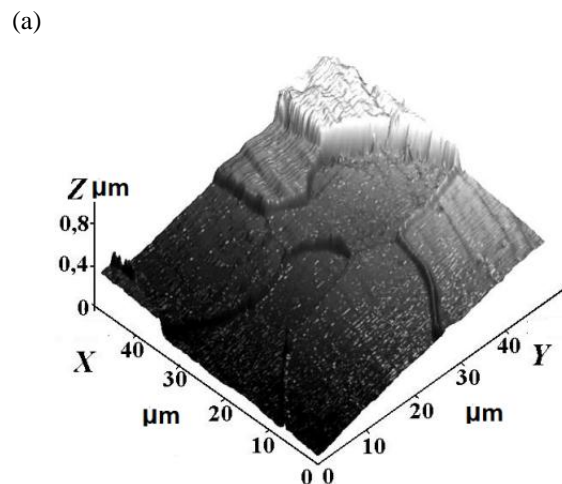


Fig. 4 An atomic-force image of the bimetal structure in the conjugation area: (a) the base metal structure; (b) the zone of partial decarburization; (c) the decarburized layer - the conjugation area.

Let us consider in more detail the zone of partial decarburization of the structure of 321 AISI steel in the case of the AFM analysis. From the scan images (Fig. 5a) it follows that along the boundaries of the ferrite grains there are small spots of perlite, which is located between the grains of ferrite in the form of separate inclusions or interlayers. Studies have shown that the perlite cementite in 321 AISI is represented with thin, parallel plates, alternating with ferrite plates. Fig. 5b shows the fragmented structure of a pearlitic grain. It is shown that the cementite plates have an intermittent appearance, which may indicate a heterogeneous release of cementite within a single grain, and they can be unequal in thickness and curved.



(b)

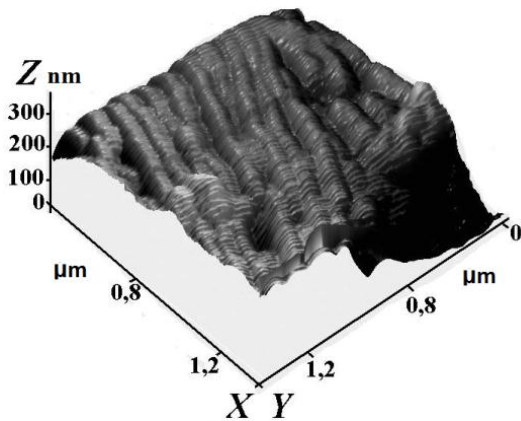


Fig. 5 An atomic-force image of the bimetal structure in the zone of partial decarburization; (a) a 3D image; (b) features of perlite structure.

It should be noted that the results shown in Fig. 3-4 were obtained directly by observing the surface of a metallographic section made by means of traditional methods without the manufacture of special preparations (foils) required for electron microscopy by the method of AFM [13].

Loading curves of flat samples of bimetal, and the samples equal in size made separately from steels 321 AISI and A 283 Grade C are presented in Figure 6.

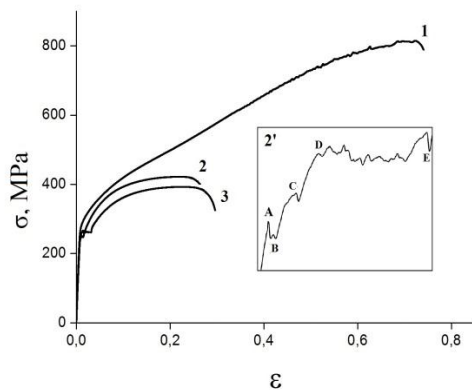


Fig. 6 Loading curves: 1 - A 283 Grade C; 2 - bimetal; 3 - 321 AISI; 2' is the yield surface of curve 2 for the bimetal.

They cover the areas of elastic and large deformations, and the area of fracture. The bimetal curve after the yield point in the area of large deformations is located between the curves for its components (20 samples from each material were tested). On the loading curves for 321 AISI and the bimetal, the pronounced tooth and the yield plateau are visible, on which the oscillations of the deforming stress are noticeable (Fig. 6). The presence of a cladding layer of stainless steel leads to a reduction in the duration of the yield plateau, an

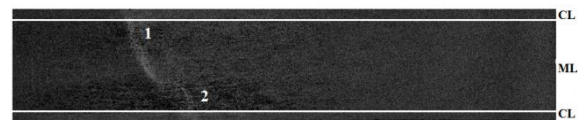
increase in the strength limit, and a decrease in the ductility of the base metal (321 AISI). For complete coverage of the processes of nucleation and development of Lüders bands (LB) in the bimetal, during the experiments, the registration of speckle images began at a voltage lower than the yield strength and ceased at the completion of the yield plateau and transition to the stage of strain hardening.

As the experiment showed, the large deformation in the bimetal sample is localized first in the form of a LB nuclei, which appears on the yield drop (point A in the inset of Figure 6), i.e., at the stage of microlarge deformation. Fig. 7a shows that the Lüders band front (1) arises at the upper conjugation boundary of the cladding layer, the main layer of the bimetal, and germinates in the base layer of 321 AISI. Along with this (Fig. 7b), at the lower conjugation boundary of the cladding layer (the main layer of the bimetal) the second Lüders band front (2) is generated (point B in the inset of Figure 6). At the bimetal flow plateau (inset of Fig. 6), the growth of the embryo of the strip across the sample corresponds to the formation of the ascending branches of the BC for the front of the Lüders band (1) and the CD for the Lüders bands (2). At the moment when both embryos cross the entire section of the bimetal, the formation of the Lüders band ends and its expansion begins. In the bimetal expansion diagram, this process corresponds to the DE area of the yield plateau. The generated Lüders band is limited by a pair of fronts moving in opposite directions along the axis of the sample at velocities  $\pm V_f$ , and gradually transferring the bimetal from the elastic to the plastic state.

(a)



(b)



(c)

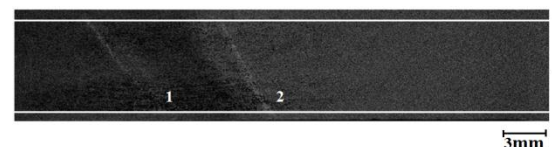


Fig. 7 Origin of the Lüders band fronts of the bimetal at the plateau: (a)  $\epsilon = 0.0081$ ; (b)  $\epsilon = 0.0084$ ; (c)  $\epsilon = 0.0099$ .



An important characteristic of the process is the speed of motion of the LB fronts. It was found out that when the LB starts, its two fronts move in the main layer of 321 AISI in opposite directions with different velocities  $V_1 = 0.8 \cdot 10^{-4}$  m/s and  $V_2 = 2.3 \cdot 10^{-4}$  m/s (Fig. 8a). Since the deformation is due to the more complex resistance of the bimetal to the loading compared to its components, the plastic flow at the initial stage is effected by means of propagation of the LB front in the basic soft metal, while the stronger cladding layer of stainless steel is deformed even more elastically. Then, the base layer and the cladding layer of the bimetal are deformed plastically. As a result, in the upper cladding layer of the material A 283 Grade C only the Lüders band front (2) propagates with velocity  $V_2 = 2.4 \cdot 10^{-4}$  m/s (Figure 8b), and two Lüders band fronts (1) and (2) propagate in the lower cladding layer (A 283 Grade C) in opposite directions with velocities  $V_1 = 0.7 \cdot 10^{-4}$  m/s,  $V_2 = 2.3 \cdot 10^{-4}$  m/s (Fig. 8c).

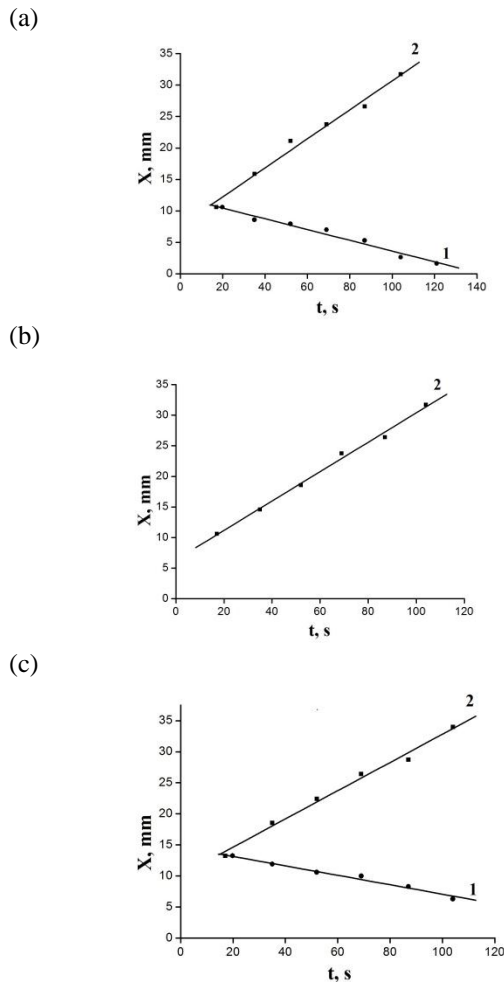


Fig. 8 Propagation of Lüders bands fronts in the bimetal at the yield plateau: (a) in the main layer of 321 AISI (ML), (b) in the upper cladding layer (CL), (c) in the lower cladding layer of A 283 Grade C.

To compare the data, note that when analyzing the patterns of localization of large deformation of samples of 321 AISI low-carbon steel under tension, the following was revealed. The generation of LB fronts corresponds to the stress of the upper yielding tooth and occurs in the area of the base stress concentrator near the mobile gripper of the test machine (Fig. 9a). As a result, one LB front propagates throughout the yield plateau with the velocity  $V_2 = 1.1 \cdot 10^{-4}$  m/s (Fig. 9b).

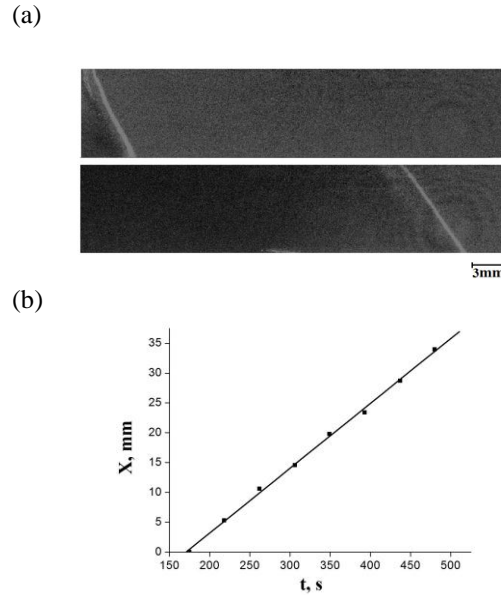


Fig. 9 Origin of the Lüders band front at the yield plateau of 321 AISI: (a)  $\varepsilon = 0.008$  and  $\varepsilon = 0.028$ ; (b) propagation of the CLB front at the yield plateau of 321 AISI

The parabolic reveals plastic flow localization in the form of a stationary system of the plastic flow centers through the specimen length with the distance  $\lambda = 4$  mm between them (Fig. 10).

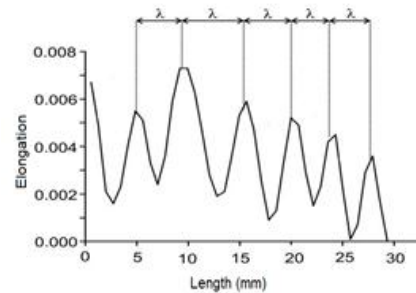


Fig. 10 The distribution of local elongation  $\varepsilon_{xx}$  along the axis of extension during of parabolic work hardening stage.

At the prefracture stage, the immobile zones of plastic strain localization started moving consistently

with a tendency to merge into a high-amplitude focus of localized straining, where a neck-like narrowing of the sample cross section was formed. This maximum forms at the place of occurring damage. The peculiarity of damage of the bimetal is related to the heterogeneity of plastic deformation in the intermediate layer of the metal.

Fragmentation of the specimen determines the fracture pattern of bimetal composite. Two macro bands of localized plastic deformation are formed at the stage of the shoulder effect in the area of stress macro concentrator. They propagate along conjugated directions of maximum shear stress across the whole section of the sample, forming trihedral prisms on the macro level on the bond interface of the bimetal. The cracks are nucleated in the area of parent metal at the trihedral prism tip, gradually merged passing across the whole section of the metal sample (Fig. 11).

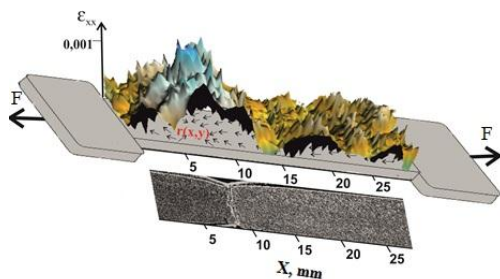


Fig. 11 Bimetal fracture patterns and distribution of local extensions at the prefracture stage under deformation 0.24.

## CONCLUSION

The research conducted allowed to identify the main patterns of proliferation of LB in the main layer material. It is revealed that the LB is limited to a pair of fronts moving in opposite directions along the bimetal axis with different propagation velocities. The cladding layer does not suppress the formation of LB, leading to an increase in the propagation speed of the LB fronts in the main layer. Metallographic studies have shown that at extension of bimetallic samples of A 283 Grade C + 321 AISI a decarbonized layer is formed in bimetal at the side of A 283 Grade C steel, and at the side of 321 AISI steel a carburized layer is formed. On the boundary of conjugation of bimetal layers an intermediate layer (carbide) is found, by the depth of up to 50μm.

## ACKNOWLEDGEMENTS

The work was supported by the Russian Science Foundation (project No. 16-19-10025).

## REFERENCES

- [1] Orlova D, Barannikova S, Zuev L, "On the kinetics of localized plasticity domains emergent at the pre-failure stage of deformation process", AIP Conf. Proc. 2016, Vol.1783, pp. 020168.
- [2] Danilov V.I, Barannikova S.A, Zuev L.B, "Localized strain autowaves at the initial stage of plastic flow in single crystals", Tech. Phys. 2003, Vol. 48, pp. 1429-1435.
- [3] Zuev L. B, Barannikova S. A, "Experimental study of plastic flow macro-scale localization process: Pattern, propagation rate, dispersion", 2014, Int. J. Mec. Sci. Vol. 88, pp. 1-7.
- [4] Acarer M, Gulenc B, Findik F, "Investigation of explosive welding parameters and their effects on microhardness and shear strength", 2013, Mater.Des. Vol. 24, pp. 659-664.
- [5] Venkateswara N, Madhusudhan G, Nagarjuna S, "Weld overlay cladding of high strength low alloy steel with austenitic stainless steel – Structure and properties", 2011, S. Mater. Des. Vol. 32, pp. 2496-2506.
- [6] Findik F, Yilmaz R, Somyurek T, "The effect of heat treatment on the microstructure and microhardness of explosive welding", 2011, Acad. J. Vol. 6, pp. 4141-4151.
- [7] Guobin L, Jianjun W, Xiangzhi L. Guiyun L, "The properties and application of bi-metal hot-forging die", 1998, J. Mater. Proc. Technol. Vol. 75, pp. 152-156.
- [8] Mehnen L, Pfutzner H, Kaniusas E, "Magnetostrictive amorphous bimetal sensors", 2000, J. Magn.Magn. Mater. Vol. 215, pp. 779-781.
- [9] Nakano J, Miwa Y, Tsukada T, Kikuchi M, Kita S, Nemoto Y, Tsuji H, Jitsukawa S, "Characterization of 316L(N)-IG SS joint produced by hot isostatic pressing technique", 2002, J. Nucl. Mater. Vol. 307, pp. 1568-1572.
- [10] Akramifarid H.R, Mirzadeh H, Parsa M.H, "Cladding of aluminum on AISI 304L stainless steel by cold roll bonding: Mechanism, microstructure, and mechanical properties", 2014, Mater. Sci. Eng. Vol. A 613, pp. 232-239.
- [11] Sozen S, "Determination of displacement distributions in welded steel tension elements using Digital image techniques", Steel Comp. Str. Int. J., Vol. 18, pp. 1103-1117.
- [12] Sokoli D, Shekarchi W, Buenrostro. E, Wassim M, "Advancing behavioral understanding and damage evaluation of concrete members using high-resolution digital image correlation data", 2014, Earthquakes and Structures An Int'l Journal, Vol.7, pp.609-626.
- [13] Barannikova S., Shlyakhova G., Zuev L., Malinovskiy A. "Microstructure of superconducting cable components", Int. J. Geomate, 2016, Vol. 10, Is. 21, pp. 1906-191.



## SEARCHING OF NEW ANTIVIRAL COMPOUNDS OF SUDAN EBOLAVIRUS GLYCOPROTEIN BASED ON FLAVONOID COMPOUNDS USING IN SILICO METHODS

Rendy Pramuda Putra<sup>1</sup>, Ahmad Husein Alkaff<sup>2</sup>, Mochammad Arfin Fardiansyah Nasution<sup>3</sup> and  
Agustinus C. B. Kantale<sup>4</sup>, and Usman Sumo Friend Tambunan<sup>5\*</sup>

<sup>1</sup>Bioinformatics Research Group, Department of Chemistry, Faculty of Mathematics and Natural Science,  
Universitas Indonesia, Indonesia.

### ABSTRACT

Ebola hemorrhagic fever is a viral disease from *Ebolavirus* genus and lethal to primates, including humans. The case fatality rate is 30%-90%. Until now, no vaccines nor drugs that could effectively combat Ebola hemorrhagic fever. Sudan ebolavirus (SEBOV), which is classified into *Ebolavirus* genus, is the second deadliest species after *Zaire ebolavirus*, with a fatality rate of SEBOV is 50-70%. In Ebola life cycle, glycoprotein (GP) is crucial for mediating *Ebolavirus* entry into the host cell. Thus, molecules that could inhibit glycoprotein activity has a potential to become an ideal therapeutic compound of Ebola hemorrhagic fever. Flavonoid compounds are potential because of its antiviral properties. In this research, we utilized *in silico* method to investigate the potency of flavonoid compounds as an inhibitor of SEBOV GP through molecular docking and computational ADME test. Moreover, the oral bioavailability and toxicity prediction of the flavonoid compounds were performed as well to get the best flavonoid compounds. In this research, about 1479 flavonoid compounds and 3D structure of EBOV GP were retrieved from ZINC15 database and RCSB PDB, respectively. Moreover, MOE 2014.09 software was used as the main operating software. Furthermore, we utilized Toxtree v2.6.13, Osiris Data Warrior, and Swiss ADME as the software for conducting computational ADME test. In the end, we found Cyanidin-3-(p-Cuomaro) and Prurin 6''-O-gallate have the potential as an inhibitor of EBOV GP because they have the best binding affinity to SEBOV GP and have the excellent ligand properties.

**Keywords:** Sudan ebolavirus, glycoprotein, *in silico*, molecular docking, ADME test

### INTRODUCTION

*Ebolavirus* is a genus of virus that causes the deadly Ebola hemorrhagic fever (EHF). Case fatality rate of EHF is between 30-90% [1]. Ebola is classified in group V ((-) ssRNA), *Mononegavirales* order, *Filoviridae* family, and *Ebolavirus* genus. There are five species of *Ebolavirus*: Ebola virus (*Zaire ebolavirus*, EBOV), Sudan virus (*Sudan ebolavirus*, SEBOV), Tai Forest virus (*Tai Forest ebolavirus*, once *Côte d'Ivoire ebolavirus*, CIEBOV), Bundibugyo virus (*Bundibugyo ebolavirus*, BEBOV), and Reston virus (*Reston ebolavirus*, REBOV). *Reston ebolavirus* only infects primate nonhuman. Until now, no medicine nor vaccine can effectively cure EHF.

SEBOV outbreak occurred for the first time in 1976 at Nzara and Maridi, Sudan with 284 people is being infected and 153 people lost their life. The species got it is from the country it first identified. The biggest outbreak occurred in 2000-2001 at Gulu, Masindi, and Mbarara, Uganda which infected 425 people and 224 people died. Another case of Sudan Ebolavirus happened in England at 1976; Uganda at 2011, 2012, and 2013, Sudan at 1979 and 2004 [2]. Look at the long list of the outbreak; it is important to find a therapeutical compound for treating SEBOV infection.

Glycoprotein (GP), nucleoprotein (NP), RNA-polymerase (L), VP35, VP30, VP40, and VP24 are

the protein existed in SEBOV. The most important protein for penetration of host cells is a glycoprotein. Glycoprotein core is GP<sub>1</sub>-GP<sub>2</sub> [1]. Glycoprotein mechanism to penetrate host cell is attached to host cell surface, open its core by changing conformation, and penetrate by endocytosis pathway. The inhibitor can disrupt conformation change [3]. Any disruption in glycoprotein core could devastate Ebola life cycle [1].

Flavonoid is the biggest phytonutrient group in a natural product. It is very abundant in various plants, fruits, and vegetables. It has low toxicity, high bioavailability, antioxidant activity, free radical activity [4]. They have the potential to become therapeutical medicine of SEBOV by inhibiting glycoprotein [5].

### RESEARCH METHODOLOGY

This research utilized some online and offline software such as Molecular Operating Environment (MOE) 2014.09, Osiris DataWarrior, Toxtree v2.6.13, and Swiss ADME. Additionally, the ChEMBL database, RCSB PDB (Research Collaboratory for Structural Bioinformatics Protein Data Bank) and NCBI BLAST (National Center for Biotechnology Information Basic Local Alignment Search Tool) were used as the primary sources of our experimental data. The general pipeline in this research referred to the previous research that has

been validated and approved [6]–[8].

First, the flavonoid compounds were retrieved from ChEMBL database [9], [10]. Thus, a total of 1358 flavonoid compounds were obtained and saved in .sdf file format. RCSB PDB (Research Collaboratory for Structural Bioinformatics Protein Data Bank) is the source for *Sudan Ebolavirus* glycoprotein database. NCBI BLAST (National Center for Biotechnology Information Basic Local Alignment Search Tool) is used to sequence the glycoprotein. Molecular Operating Environment (MOE) 2014.09 [11], [12] software was used to perform molecular docking simulation.

Before glycoprotein is ready, we need to look at glycoprotein similarity with standard Ebola Glycoprotein. Next unwanted amino acid chain, solvent, and ligand should be removed. Protonate 3D is important to add explicit hydrogen. Energy minimization to lowering glycoprotein local energy. AMBER99 is chosen for forcefield because of it is compatible with protein and nucleic acid. Solvation is a gas phase which means the simulation does not include solvent solvation for calculation. Root mean square gradient is 0,05 kcal/Å.mol, which mean energy minimization will be stopped when RMS Gradient is below 0,05 kcal/Å.mol since it is compatible with protein [13]. In chase of the active site, number two is chosen because of its similarity with Endosomal Receptor Niemann-Pick C1 [14]. Tether function is to limit atom shifting from the original position.

In preparation of flavonoid database need to screen up to make sure there is no same ligand to be calculated in docking phase. Wash is to repair flavonoid imperfect structure such as strong acid deprotonation, strong basic protonation, and add explicit hydrogen. MMFF94 (modified) method is chosen specifically for its compatible with small organic molecule when selecting ligand partial charge. RMS Gradient value is 0,001 kcal/Å.mol since its compatible with a small molecule.

In this study, 'Triangle Matcher' was used as the

placement method. The function of the 'Triangle Matcher' is orienting ligand to the active site based on charge group and spatial fit. The role of 'London dG' scoring is to calculate Gibbs energy for binding for certain conformation or pose to allow orientation analyzing and ligand position as an inhibitor of the protein [13], [15].

A toxicology test is needed to accurate measure data such as ADME (Absorption, Distribution, Metabolism, Excretion) and Carcinogenicity for every compound that will be tested to human. Before going to in vitro test, flavonoid will be tested by three software. They are Osiris Data Warrior, Toxtree v2.6.13, and Swiss ADME. Osiris Data Warrior and Toxtree v2.6.13 are offline software, but SwissADME is online software.

## RESULT AND DISCUSSION

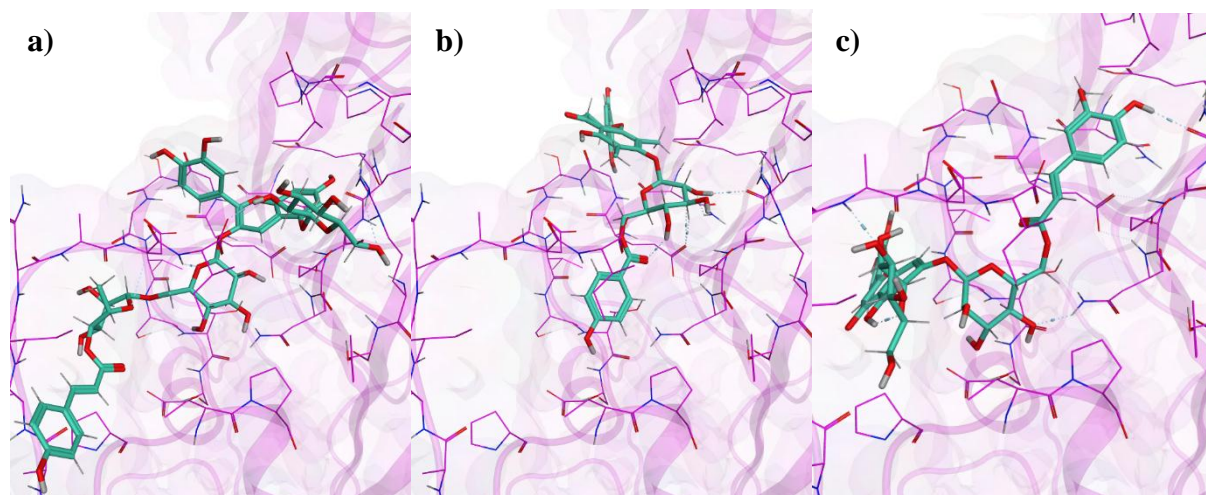
Before docking can be started the flavonoids and glycoprotein must be prepared. We used 1358 flavonoid ligands. In addition, the selected SEBOV glycoprotein was obtained by employing Swiss Model. The result itself can be seen in **Figure 1**. Glycoprotein from the database does not attach with any unwanted amino acid, solvent, or water molecule.

Docking flavonoid-glycoprotein complexes process resulting in the seven best ligand that has a potential to become an alternative medicine for Ebola. Then the result is selected to become 553 by removing all ligand with rms\_define above 2. Then selected again by stronger than standard attachment to the glycoprotein. The result is seven ligand.

Based on the interaction of flavonoid-glycoprotein complexes, the flavonoid is attached strongly to a polar group such as a hydroxyl group with aspartate. In this research, we utilized neplanocin A, 3-deazaneplanocin A, toremifene, and clomiphene 1 as the standard ligands [16].



**Figure 1. Similarity of Sudan Ebolavirus with standard Ebolavirus (99,6%)**



**Figure 2. Binding pattern of SEBOV GP and (a) cyanidin-3-(p-coumaroyl)-rutinoside-5-glucoside, (b) myricitrin V, and (c) 7-O-(6-feruoylglucosyl)isoorientin**

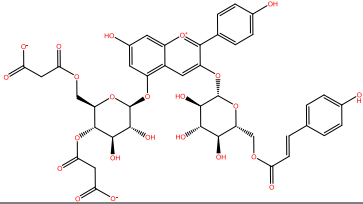
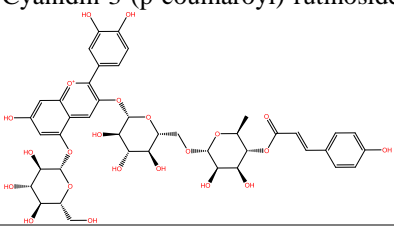
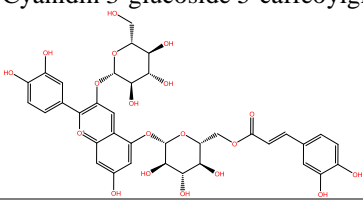
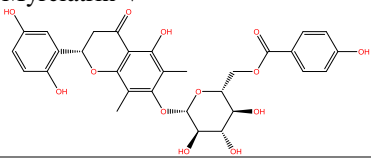
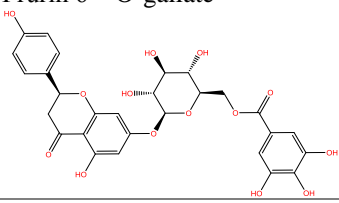
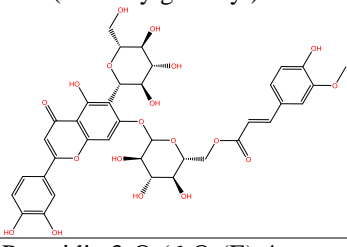
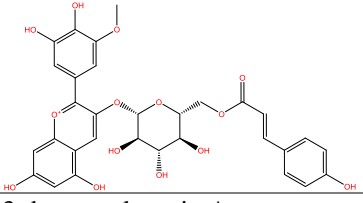
The molecular docking simulation was performed by using MOE 2014.09 software. This simulation determines the binding affinity of the selected ligands in the binding site of the protein/enzyme by knowing the Gibbs free binding energy ( $\Delta G_{\text{binding}}$ ) value, inhibition constants, molecular interaction in the respective binding site. Moreover, the interaction between the ligand and the key residues that play a crucial role in the protein/enzyme is also observed. If the selected ligand has lower  $\Delta G_{\text{binding}}$  value and higher inhibition constants than the standard ligand and may bind with the key residues at the binding site of the protein/enzyme, then the selected ligand has better chance to be a drug candidate than the standard ligand. In this study, about 1358 flavonoid compounds underwent docking simulation against SEBOV GP. After the docking simulation was conducted, we found out that there were seven ligands, namely monardaein, cyanidin-3-(p-coumaroyl)-rutinoside-5-glucoside, cyanidin 3-glucoside 5-caffeoylglucoside, myricitrin V, prurin 6''-O-gallate, 7-O-(6-feruoylglucosyl)isoorientin, and petunidin 3-O-(6-O-(E)-4-coumaroyl-beta-D-glucoside), which have lower  $\Delta G_{\text{binding}}$  value than the four standards that we tested in the simulation as well. Moreover, we also figured out that cyanidin-3-(p-coumaroyl)-rutinoside-5-glucoside has the lowest  $\Delta G_{\text{binding}}$  value among all with -8,5716 kcal/mol. Followed by myricitrin V and 7-O-(6-feruoylglucosyl)isoorientin, with a  $\Delta G_{\text{binding}}$  value of -9,1728 kcal/mol and -9.0058 kcal/mol, respectively. These are much lower than the lowest  $\Delta G_{\text{binding}}$  value among all of the standard ligands (clomifane), which has a  $\Delta G_{\text{binding}}$  value of -7.5146 kcal/mol. The results of molecular docking simulation in this study are shown in **Table 1**.

In addition, we also take molecular interaction between the ligands and the protein into account in determining the best ligand. Cyanidin-3-(p-

coumaroyl)-rutinoside-5-glucoside forms three hydrogen bond interactions, two with Ile285 and one with Arg136. In addition, the positively charged oxygen from the ligand forms an ion contact with the side chain of Glu71. 19 residues from the protein interact with the ligands through van der Waals interaction. On the other hand, myricitrin V, the ligand with the second lowest  $\Delta G_{\text{binding}}$ , interact with Glu71 and Gly72 through side chain hydrogen bond and Trp104 through backbone hydrogen bond. Moreover, the ligand also interacts with 18 protein residues by van der Waals interaction. 7-O-(6-feruoylglucosyl)isoorientin forms three hydrogen interactions with a backbone of Trp104 and Ala283, also side chain of Asn107. In term of van der Waals interaction, this ligand interacts with 24 residues. From the molecular interaction, we can assume that 7-O-(6-feruoylglucosyl)isoorientin has the finest interaction. The molecular interaction of the selected flavonoid ligands with SEBOV GP is displayed in **Figure 2**.

Finally, the root mean square deviant (RMSD) score is also considered for determining whether the ligand pose that created during the docking simulation is acceptable and can be replicated during the real interaction when the ligand acts as the drug or inhibitor for the respective protein. The acceptable value for each docking pose is below 2.0 Å [17]. In this research, we found out that four out of the seven best ligands have RMSD score below 2.0 Å, namely monardaein (1.6116 Å), myricitrin V (1.8359 Å), Prurin 6''-O-gallate (1.8922 Å), 7-O-(6-feruoylglucosyl)isoorientin (1.8618 Å). It means that these ligands pose which were generated during the docking process is acceptable and can be considered as a model for the real interaction that may happen during the inhibition process of the respective ligands into the SEBOV GP.

Table 1. Molecular docking simulation result

No	Molecule Name (with Molecular Structure)	$\Delta G_{\text{binding}}$ (kcal/mol)	RMSD
1	Monardaen 	-8,5716	1,6116
2	Cyanidin-3-(p-coumaroyl)-rutinoside-5-glucoside 	-9,6941	3,1720
3	Cyanidin 3-glucoside 5-caffeoylglucoside 	-8,1407	2,3497
4	Myrciatrin V 	-9,1728	1,8359
5	Purpurin 6''-O-gallate 	-8,4739	1,8922
6	7-O-(6-feruoylglucosyl)isorientin 	-9,0058	1,8618
7	Petunidin 3-O-(6-O-(E)-4-coumaroyl-beta-D-glucoside) 	-8,6197	2,1168
S1	3-deazaneplanocin A	-6.0057	1,2494
S2	Clomifane	-7.5146	1.6039
S3	Neplanocin A	-6.1226	1.7294
S4	Toremifene	-7.3515	1.6344

**Table 2. Molecular properties of the selected ligands by Osiris DataWarrior**

Ligand	Druglikeness						Druglikeness
	MW	clogP	clogS	H-acceptor	H-Donor	PSA (Å <sup>2</sup> )	
1	903,813	-4,9096	-5,286	23	8	357,92	-16,498
2	598,555	-1,3391	-4,887	22	13	344,67	-11,851
3	786,690	-0,7744	-4,384	19	12	305,98	-9,7867
4	625,557	2,0912	-4,202	13	7	212,67	0,79392
5	911,749	1,0577	-3,218	14	8	232,9	0,76076
6	586,500	-0,5711	-3,531	19	11	312,05	-3,3256
7	773,671	1,4906	-4,812	14	8	215,83	-5,5318
S1	262,268	-0,8991	-0,433	7	4	219	1,7618
S2	406,975	3,7701	-4,147	2	1	353	-2,5935
S3	263,256	-1,1785	-1,069	8	4	215	1,7618
S4	406,975	3,5829	-4,798	2	1	356	-3,4787

In this research, we also conducted the computational ADMET prediction to determine the molecular properties of the best ligands and also predict their toxicity potency. Two software were deployed to calculate their properties, namely Osiris DataWarrior and SwissADME. These software were used to calculate the toxicity potency based on the structure and the fragments that contained in the respective ligands.

The molecular properties, druglikeness, and toxicity of the ligands and the standards are predicted using Osiris DataWarrior. Following the Lipinski's Rule of Five, all the ligands have molecular weight more than 500 g/mol, H-acceptor more than 10, H-donor more than 5, and TPSA greater than 140 Å<sup>2</sup> [18]. However, the Lipinski's rule of five doesn't take into account because it cannot be applied to the natural product compound [19]. On the other hand, the standards have the molecular properties which mostly acceptable according to Lipinski's Rule of Five. The result of druglikeness score showed that only ligand 4, ligand

5, standard 1, and standard 3 that have the score below zero. It means the four molecules have a better potential to act as a drug. In the toxicity test, the ligands perform well in all parameters, i.e. mutagenic, tumorigenic, reproductive effective, and irritant, while two standards showed a high probability to have tumorigenic and reproductive effective probability. Only standard 2 demonstrated a high probability of being mutagenic.

In SwissADME test, all flavonoid ligands have low GI absorption. On the other hand, three out of four standards have high GI absorption, except neplanocin A. Only cyanidin-3-(p-Cuomaro) and prurin 6''-O-gallate, flavonoid have zero PAINS alert. All standards also have zero PAINS alert. Brenk prediction shows that only ligand 2 and 6 produced one alert. Overall, based on the result of our computational ADMET tests, it is possible to make flavonoid compound as a drug that orally available for the body.

**Table 3. Toxicity and absorption prediction by Swiss ADME and OSIRIS DataWarrior**

Ligand	LE & Tox			Pharmacokinetics		Medicinal Chemistry	
	Mutagenic	Tumorigenic	Reproductive Effective	Irritant	GI Absorption	PAINS	Brenk
1	No	No	No	No	Low	1 alert: catechol_A	3 alerts: catechol, charged_oxygen_sulfur, michael_acceptor_1
2	No	No	No	No	Low	0 alert	1 alert: hydroquinone
3	No	No	No	No	Low	1 alert: catechol_A	2 alert : catechol, Michael_acceptor_1
4	No	No	No	No	Low	1 alert: catechol_A	3 alerts: catechol, charged_oxygen_sulfur, michael_acceptor_1
5	No	No	No	No	Low	0 alert	4 alerts: beta_keto_anhydride, charged_oxygen_sulfur, michael_acceptor_1, more_than_2_esters
6	No	No	No	No	Low	1 alert: catechol_A	1 alert: catechol
7	No	No	No	No	Low	1 alert: catechol_A	3 alerts: catechol, charged_oxygen_sulfur, michael_acceptor_1
S1	No	No	No	No	High	0 alert	1 alert: isolated_alkene
S2	High	High	High	No	High	0 alert	1 alert: stilbene
S3	No	No	No	No	Low	0 alert	1 alert: isolated_alkene
S4	Low	High	High	No	High	0 alert	2 alert: alkyl_halide, stilbene

## CONCLUSIONS

The result of the current study shows flavonoid is still potential impressive for combating SEBOV by inhibiting its glycoprotein. Flavonoid such as Cyanidin-3-(p-Cuomaro), myricitrin V, and 7-O-(6-feruoylglucosy) have the lowest Gibbs energy binding ( $\Delta G_{\text{binding}}$ ), but when looking at Swiss ADME test myricitrin V, and 7-O-(6-feruoylglucosy) resulting alert in PAINS (false alarm). However, it can be said that all best seven ligand is still relatively safe, look at data such as carcinogenicity, mutagenic, tumorigenic, reproductive effective, and irritant.

## ACKNOWLEDGEMENTS

Usman Sumo Friend Tambunan supervised this study, Agustinus C.B. Kantale and Rendy Pramuda Putra worked on the experimental details and wrote the research reports, while Mochammad Arfin Fardiansyah Nasution and Ahmad Husein Alkaff wrote the manuscript and analyzed the experimental data. The authors would like to thank Directorate of Research and Community Engagement (DRPM) Universitas Indonesia for granting us Hibah Publikasi Internasional Terindeks Untuk Tugas Akhir Mahasiswa (Hibah PITTA) 2017 with No: 693/UN2.R3.1/HKP.05.00/2017. Moreover, the authors declare that there is no conflict of interests and competing financial interests.

## REFERENCES

- [1] G. Chen *et al.*, "Synthetic antibodies with a human framework that protect mice from lethal Sudan ebolavirus challenge," *ACS Chem. Biol.*, vol. 9, no. 10, pp. 2263–2273, 2014.
- [2] Centers for Disease Control and Prevention (CDC), "Ebola (Ebola Virus Disease)." 2016.
- [3] E. H. Miller *et al.*, "Inhibition of Ebola virus entry by a C-peptide targeted to endosomes," *J. Biol. Chem.*, vol. 286, no. 18, pp. 15854–15861, May 2011.
- [4] P. M. Dewick, *Medicinal Natural Products: A Biosynthetic Approach: Third Edition*. 2009.
- [5] U. Raj and P. K. Varadwaj, "Flavonoids as multi-target inhibitors for proteins associated with Ebola virus: in-silico discovery using virtual screening and molecular docking studies," *Interdiscip. Sci.*, pp. 1–10, 2015.
- [6] U. S. F. Tambunan, A. A. Parikesit, Y. C. Unadi, and D. Kerami, "Designing Cyclopentapeptide Inhibitor of Neuraminidase H5N1 Virus Through Molecular and Pharmacology Simulations," *Tsinghua Sci. Technol.*, vol. 20, no. 5, pp. 431–440, 2015.
- [7] U. S. F. Tambunan, R. Bakri, A. A. Parikesit, T. Ariyani, R. D. Puspitasari, and D. Kerami, "In silico modification of Zn 2+ binding group of suberoylanilide hydroxamic acid (SAHA) by organoselenium compounds as Homo sapiens class II HDAC inhibitor of cervical cancer," *Mater. Sci. Eng.*, vol. 107, no. 1, p. 12054, 2016.
- [8] U. S. F. Tambunan, A. A. Parikesit, V. C. Adam, M. A. F. Nasution, R. D. Puspitasari, and D. Kerami, "Virtual Screening of Commercial Cyclic Peptides as  $\beta$ --OG Pocket Binder Inhibitor in Dengue Virus Serotype 2," *Int. J. GEOMATE*, vol. 13, no. 37, pp. 60–68, 2017.
- [9] A. Gaulton *et al.*, "ChEMBL: A large-scale bioactivity database for drug discovery," *Nucleic Acids Res.*, vol. 40, no. D1, pp. 1100–1107, 2012.
- [10] A. P. Bento *et al.*, "The ChEMBL bioactivity database: An update," *Nucleic Acids Res.*, vol. 42, no. D1, 2014.
- [11] S. Vilar, G. Cozza, and S. Moro, "Medicinal chemistry and the molecular operating environment (MOE): application of QSAR and molecular docking to drug discovery," *Curr. Top. Med. Chem.*, vol. 8, no. 18, pp. 1555–1572, Jan. 2008.
- [12] "Molecular Operating Environment (MOE) 2014.09." Chemical Computing Group Inc., Montreal, QC, Canada, 2015.
- [13] D. D. Ben, M. Buccioni, C. Lambertucci, A. Thomas, and R. Volpini, "Simulation and comparative analysis of binding modes of nucleoside and non-nucleoside agonists at the A 2B adenosine receptor," *Silico Pharmacol.*, vol. 1, no. 24, pp. 1–14, 2013.
- [14] H. Wang *et al.*, "Ebola Viral Glycoprotein Bound to Its Endosomal Receptor Niemann-Pick C1," *Cell*, vol. 164, no. 1–2, pp. 258–268, 2016.
- [15] A. M. Manikrao *et al.*, "Presuming the Probable Anti-inflammatory Mechanism of Ursolic Acid: a plant derived pentacyclic triterpenoid, using molecular docking," *Library (Lond.)*, vol. 1, no. 2, pp. 9–13, 2011.
- [16] L. M. Johansen *et al.*, "FDA-Approved Selective Estrogen Receptor Modulators Inhibit Ebola Virus Infection," *Sci. Transl. Med.*, vol. 5, no. 190, p. 190ra79–190ra79, 2013.
- [17] J. W. Liebeschuetz, J. C. Cole, and O. Korb, "Pose prediction and virtual screening performance of GOLD scoring functions in a standardized test," *J. Comput. Aided. Mol. Des.*, vol. 26, no. 6, pp. 737–748, 2012.
- [18] P. J. Lipinski, C.A.; Lombardo, F.; Dominy, B.W.; Feeney, "Experimental and computational approaches to estimate solubility and permeability in drug discovery and development setting," *Adv. Drug Deliv. Rev.*, vol. 64, pp. 4–17, 2012.
- [19] C. W. Murray and D. C. Rees, "The rise of fragment-based drug discovery," *Nat. Chem.*, vol. 1, no. 3, pp. 187–192, 2009.



# NEW ESTIMATION IN AR MODELS WITH EXPONENTIAL WHITE NOISE BY USING REVERSIBLE JUMP MCMC ALGORITHM

Suparman<sup>1</sup>

<sup>1</sup>Department of Mathematics Education, Ahmad Dahlan University, Indonesia

## ABSTRACT

A white noise in an autoregressive (AR) model is often assumed to be normally distributed. In application, the white noise usually does not follow a normal distribution. This paper aims to estimate a parameter of AR model that has an exponential white noise. A Bayesian method is adopted. A prior distribution of the parameter of AR model is selected and then this prior distribution is combined with a likelihood function of data to get a posterior distribution. Based on this posterior distribution, a Bayesian estimator for the parameter of AR model is estimated. Because the order of AR model is considered a parameter, this Bayesian estimator cannot be explicitly calculated. To resolve this problem, a method of reversible jump Markov Chain Monte Carlo (MCMC) is adopted. The result is an estimation of parameter AR model that can be simultaneously calculated.

*Keywords: AR Model, Exponential White Noise, Bayesian, Reversible Jump MCMC*

## INTRODUCTION

Autoregressive (AR) with normally white noise is a time series model that is often used in many fields. For example, it is used in the field of economics [1]. But there are so many applications where white noise is not normally distributed. A LSE of AR model with heavy-tailed G-GARCH(1,1) noises is studied [1]. A class of non parametric tests on the Pareto tail index of the innovation distribution in the linear autoregressive model is proposed [2]. A study of the autoregressive model with exponential white noise can be found in the literature (see [3]-[8]). A form of time series models where marginal distributions are in fact exponential distributions is presented in [3]. A Bayesian analysis of threshold AR model with exponential noise is developed in [4]. A robust of the bayesian estimation of an AR model with exponential innovation to obtain optimal bayesian estimator is analyzed [5]. A bayesian method to estimate the coefficient of the AR(1) model is proposed [6]. Generally, the order of the autoregressive is known and must be estimated by the data.

If the AR model with white noise is fitted to the data, the order and coefficient of model will be generally unknown. Let  $x_t$  be a time series with  $t=1,2,\dots,n$  and  $n$  be a number of samples. An AR(p) with exponential white noise can be expressed as:

$$x_t = \sum_{i=1}^p \phi_i x_{t-i} + z_t \quad (1)$$

where  $p < n$  and the  $z_t$  ( $t=1,\dots,n$ ) are

independently and identically exponential random variables with parameter  $\lambda$ , written  $z_t \sim \text{Exp}(\lambda)$ .

For example, Figure 1 shows the graph of the autoregressive model with and  $\lambda = 5$ .

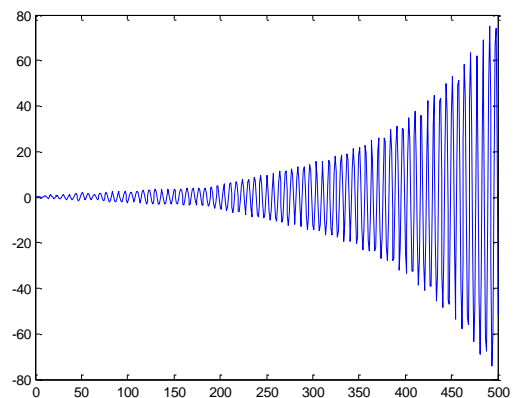


Figure 1 AR(3) with exponential white noise

Suppose that  $\phi^{(p)} = (\phi_1, \dots, \phi_p)$  is coefficient vector.

Let  $\theta$  be the above autoregressive model. Then this parameter  $\psi$  can be written as

$$\psi = (p, \phi^{(p)}, \lambda)$$

Suppose that is a data. This data is taken from a population having a autoregressive model with exponential white noise. Based on this data, the main problem is how to estimate the parameter  $\psi$ . This paper aims to estimate this parameter  $\psi$ .



## METHOD

The parameter  $\psi$  is estimated by using Bayesian method. For this, a likelihood function is determined.

### Likelihood Function

Because the random variabel  $z_t$  has an exponential distribution with parameter  $\lambda$  for  $t = 1, 2, \dots, n$ , the density function of  $z_t$  is

$$f(z_t | \lambda) = \lambda \exp - \lambda z_t \quad (2)$$

The variable transformation

$$x_t = \sum_{i=1}^p \phi_i x_{t-i} + z_t \quad (3)$$

is used. Then  $z_t = x_t - \sum_{i=1}^p \phi_i x_{t-i}$  and  $\frac{dz_t}{dx_t} = 1$ . Let  $x = (x_1, x_2, \dots, x_n)$  be a realization vector of AR(p) with exponential error. Thus, the density function of  $x_t$  is

$$f(x_t | \psi) = \lambda \exp - \lambda (x_t - \sum_{i=1}^p \phi_i x_{t-i}) \quad (4)$$

for  $t = 1, 2, \dots, n$ .

Suppose that  $y_0 = (x_1, x_2, \dots, x_p)$  and  $y = (x_{p+1}, x_{p+2}, \dots, x_n)$ . Then the likelihood function of  $x$  can be approximated by:

$$L(y | \psi) = \lambda^{n-p} \exp - \lambda \sum_{t=p+1}^n g(t, p, \phi^{(p)}) \quad (5)$$

where

$$g(t, p, \phi^{(p)}) = x_t - \sum_{i=1}^p \phi_i x_{t-i} \quad (6)$$

for  $t = p+1, 2, \dots, n$ , with a initial value  $y_0$ . Let

$S_p$  be a stationary region and  $r^{(p)} = (r_1, r_2, \dots, r_p)$  be a sample partial autocorrelation vector. By using a transformation

$$F: \phi^{(p)} \in S_p \rightarrow r^{(p)} \in [-1, 1]^p \quad (7)$$

then the AR(p) model is stationary if and only if  $r^{(p)} \in [-1, 1]^p$ . Finally, the approximated likelihood function of the  $x$  can be written by:

$$L(y | \theta) = \lambda^{n-p} \exp - \lambda \sum_{t=p+1}^n g(t, p, F^{-1}(r^{(p)})) \quad (8)$$

where  $\theta = (p, r^{(p)}, \lambda)$  and  $F^{-1}$  is a inverse transformation of  $F$ .

### Prior Distribution

Before obtaining a posterior distribution, a prior distribution must be selected. The prior distribution is taken as follows. A binomial distribution is choosen for a number of order  $p$  ( $p = 1, 2, \dots, p_{\max}$ )

$$\pi(p | \varphi) = C_p^{p_{\max}} \varphi^p (1 - \varphi)^{p_{\max} - p} \quad (9)$$

where  $p_{\max}$  is a maximum of  $p$  and  $\mu$  is an hyperparameter. A uniform distribution is choosen for a coefficient vector  $r^{(p)}$

$$\pi(r^{(p)} | p) = U(0, 1)^p \quad (10)$$

Also, a uniform distribution is choosen for a parameter  $\lambda$

$$\pi(\lambda) = U(0, 1) \quad (11)$$

Furthermore, a hyperprior distribution for  $\varphi$  is a uniform distribution.

Let  $\pi(\theta, \varphi)$  be a prior distribution for  $(\theta, \varphi)$ . Because the distribution of  $\theta$  given  $\varphi$  is

$$\pi(\theta | \varphi) = \frac{\pi(\theta, \varphi)}{\pi(\varphi)}, \text{ the prior distribution for } (\theta, \varphi) \text{ can be written as follows:}$$

$$\pi(\theta, \varphi) = \pi(\theta | \varphi) \pi(\varphi) \quad (12)$$

### Posterior Distribution

Let  $\pi(\theta, \varphi | y)$  be a posteriori distribution for  $(\theta, \varphi)$ . According to the Bayesian Theorem the posterior distribution for  $(\theta, \varphi)$  is given as follows

$$\pi(\theta, \varphi | y) \propto f(y | \theta) \pi(\theta, \varphi) \propto f(y | \theta) \pi(\theta, \varphi) \pi(\varphi) \quad (13)$$

Unfortunately, the Bayesian estimator cannot be determined analytically because the posterior distribution of parameter  $\theta$  has a complicated form. To overcome these problems, reversible jump MCMC Algorithm [9] is used.

### Reversible Jump MCMC

Suppose that  $M = (\theta, \varphi)$ . An MCMC method for the simulation of a distribution  $\pi(\theta, \varphi | y)$  is a method producing an ergodic Markov chain  $M_1, M_2, \dots, M_m$  whose stationary distribution  $\pi(\theta, \varphi | y)$ . This Markov chain  $M_1, M_2, \dots, M_m$

can be considered as a random variable whose distribution is  $\pi(\theta, \phi | y)$ . Furthermore, the Markov chain  $M_1, M_2, \dots, M_m$  is used to estimate the parameter  $M$ . To realize this, the Gibbs sampling algorithm is adopted. It consists of five steps:

- Simulate  $\phi \sim B(p+1, p_{\max} - p + 1)$
- Simulate  $\lambda \sim G(\alpha, \beta)$  with  $\alpha = n - p + 1$  and

$$\beta = \sum_{t=p+1}^n (x_t - \sum_{i=1}^p F^{-1}(r_i) x_{t-i})$$

- Simulate  $(p, r^{(p)}) \sim \pi(p, r^{(p)} | y, \lambda, \phi)$

Unfortunately, the distribution  $\pi(p, r^{(p)} | y, \lambda, \phi)$  is not an explicit form. The exact simulation is not possible to be done. Since the value  $p$  is not known, the MCMC algorithm cannot be used to simulate  $\pi(p, r^{(p)} | y, \lambda, \phi)$ . Here, reversible jump MCMC algorithm [9] is adopted.

Let  $\omega = (p, r^{(p)})$  be an actual point of the Markov chain. There are 3 types of transformations are used, namely: a birth of the order, a death of the order and a change of the order. Furthermore, let  $N_p$  be the probability of transformation from  $p$  to  $p + 1$ , let  $D_p$  be the probability of transformation from  $p + 1$  to  $p$ , and let  $C_p$  be the probability of transformation from  $p$  to  $p$ .

### Birth/Death of the Order

A transformation of the birth of the order will change a number of coefficients, from  $p$  to the  $p + 1$ . Suppose that  $\omega = (p, r^{(p)})$  is a current point and  $\omega^* = (p+1, r^{(p^*)})$  is a updated point. The birth of the order from  $\omega = (p, \phi^{(p)})$  to  $\omega^* = (p+1, r^{(p^*)})$  is defined in the following way. Set  $p^* = p+1$  and choose a random point  $v \sim U(-1, 1)$ . Next, create a new point  $\omega^* = (p+1, r^{(p^*)})$  with

$$r_1^* = r_1, \dots, r_{p^*-1}^* = r_p, r_{p^*}^* = v$$

Otherwise, the transformation of the death of the order will change the number of coefficients, from  $p+1$  to  $p$ . Suppose that  $\omega = (p+1, r^{(p+1)})$  is a

current point and  $\omega^* = (p+1, r^{(p^*)})$  is a updated point. The death of the order from  $\omega = (p+1, \phi^{(p+1)})$  to  $\omega^* = (p, r^{(p^*)})$  is defined in the following way. Set  $p^* = p$  and create a new point  $\omega^* = (p, r^{(p^*)})$  with

$$r_1^* = r_1, \dots, r_{p^*}^* = r_p$$

Suppose that  $a_n$  and  $a_d$  are respectively a probability of acceptance for birth of order and death of order. The probability of acceptance for birth is as follows:

$$a_n(\omega, \omega^*) = \min \left\{ 1, \frac{\pi(\omega^* | \phi, y) q(\omega, \omega^*)}{\pi(\omega | \phi, y) q(\omega^*, \omega)} \right\}$$

While the probability of death is as follows:

$$a_d(\omega, \omega^*) = \min \left\{ 1, \frac{1}{a_n(\omega^*, \omega)} \right\}$$

where

$$\frac{\pi(\omega^* | \phi, y)}{\pi(\omega | \phi, y)} = \frac{D_{k+1}}{N_k} \frac{(\beta^*)^{n-p}}{\beta^{n-p+1}} \frac{1}{n-p} \frac{p+1}{p_{\max} - p}$$

and

$$\frac{q(\omega^*, \omega)}{q(\omega, \omega^*)} = 1$$

### Change of the Coefficients

The transformation of the change of order will not change the number of coefficients. This transformation makes to change the value of coefficients. Suppose that  $\omega = (p, r^{(p)})$  is a current point and  $\omega^* = (p, r^{(p^*)})$  is a updated point. The change of the coefficient from  $\omega = (p, \phi^{(p+1)})$  to  $\omega^* = (p, r^{(p^*)})$  is defined in the following way. Set  $p^* = p$ , choose a random point  $i \in \{1, 2, \dots, p\}$ , and choose a random point  $u \sim U(-1, 1)$ . Then a new point  $\omega^* = (p, r^{(p^*)})$  is created with

$$r_1^* = r_1, \dots, r_{i-1}^* = r_{i-1}, r_i^* = u, r_{i+1}^* = r_{i+1}, r_p^* = r_p$$

Let  $a_p$  be a probability of acceptance to a change of coefficient. Then the probability of acceptance for change is as follows:

$$a_p(\omega, \omega^*) = \min \left\{ 1, \frac{\pi(\omega^* | \phi, y)}{\pi(\omega | \phi, y)} \frac{q(\omega_*, \omega)}{q(\omega, \omega^*)} \right\}$$

where

$$\frac{\pi(\omega^* | \phi, y)}{\pi(\omega | \phi, y)} = \left( \frac{\beta^*}{\beta} \right)^\alpha$$

and

$$\frac{q(\omega_*, \omega)}{q(\omega, \omega^*)} = 1$$

## RESULTS AND DISCUSSIONS

The transformation in equation (7) is used in order to get a stationary conditions for AR model. First result of this paper is a AR model that is obtained is always stationary. The hierarchical Bayesian is adopted to estimate the order of AR model, the coefficient of AR model, the variance of the white, and its hyper parameter. The second result of this paper is both the order of AR model and the coefficient of AR model can be estimated simultaneously.

## CONCLUSION

The purpose of this paper was to estimate the parameters of AR model with exponential white noise when the order is unknown. The parameters cannot be estimated by Markov chain Monte Carlo algorithm, because the order of AR model is unknown.

The reversible jump Markov chain Monte Carlo algorithm is one of the new methods that can be used to estimate the parameters of AR models although an order of AR is unknown. The advantage of this method is both the order of AR and the coefficient of AR can be estimated simultaneously.

## ACKNOWLEDGEMENTS

The author would like to thank the program of foreign seminar aid (BSLN), the General Directorate

of research strengthening and development, Indonesian Ministry of Research and Higher Education (Kemenristekdikti), that has given the grant to present in this international conference. The author would also like to thank the Ahmad Dahlan University (UAD) that has supported the grant for this research.

## REFERENCES

- [1] Zhang R and Ling S, Asymptotic Inference for AR Models with Heavy-Tailed G-GARCH Noises, *Econometric Theory*, 2015, 880-890.
- [2] Jureckova J, Koul HL, and Picek J, Testing the tail index in autoregressive models, *Annals of the Institute of Statistical Mathematics*, 2009, 579-598.
- [3] Novkovic M, On Exponential Autoregressive Time Series Models, *J. Math*, 1999, 97-101.
- [4] Pereira IMS and Amaral-Turkman MA, Bayesian prediction in threshold autoregressive models with exponential white noise, *Test*, 2004, 45-64.
- [5] Larbi L and Fellag H, Robust Bayesian Analysis of an Autoregressive Model with Exponential Innovations, *Afr. Stat.*, 2016, 955-964.
- [6] Ibazizen M and Fellag H, Bayesian Estimation of an AR(1) process with exponential white noise, *A Journal of Theoretical and Applied Statistics*, 2003, 365-372.
- [7] Suriyakit W, Areepong Y, Sukparungsee S, and Mititelu G. On EWMA Procedure for AR(1) Observations with Exponential White Noise. *International Journal of Pure and Applied Mathematics*, 2012, 73-83.
- [8] Shi Z and Aoyama H, Estimation of the Exponential Autoregressive Time Series Model by Using The Genetic Algorithm, *Journal of Sound and Vibration*, 1997, 309-321.
- [9] Green PJ, Reversible Jump MCMC Computation and Bayesian Model Determination, *Biometrika*, 1995, 711-732.

## **ECOLOGY AND CONSERVATION OF INDIAN HORNBILL WITH PARTICULAR REFERENCE TO NARCONDAM HORNBILL (*ACEROS NARCONDAMI*) OCCURRING ON NARCONDAM ISLAND OF ANDAMAN& NICOBAR ISLAND ARCHIPELAGO**

Hafiz S.A. Yahya

Department of Wildlife Sciences, A.M.U. Aligarh, India  
E-mail: has.yahya@gmail.com

### **ABSTRACT**

Hornbills are old world birds with pan tropical distribution. Out of 54 species of hornbills found in different parts of the world, only two species of South Africa are ground dwellers. Hornbills are mainly fruit eating birds but during breeding season feed varieties of animal matters to their nestlings and to the confined females inside the natural tree holes, entrance of which is sealed by the pair all along except a thin slit through which males provide food and females drop out the fecal matter. On account of rapid decline of their suitable foraging and nesting habitats, most Indian species of hornbills are facing various categories of threats. During my almost four decades of observations on avian communities in India I have opportunities of studying the hornbills at various sites, more particularly on ecology and biology of Narcondam Hornbills occurring only on a small island (6.8 sq. km) in the Andaman archipelago. Although their present population density is good, they are quite vulnerable to any anthropogenic or natural catastrophe such as tsunami. This paper entails accounts of ecology, distribution and conservation issues of Indian hornbills with especial reference to Narcondam Hornbill.

**Key words:** *Indian Hornbills, Narcondam Island, Ecology and Avian Conservation*

### **INTRODUCTION**

By virtue of encompassing large tract of land, diversified bio-geographical zones and varied climates, India's biodiversity vis-à-vis avian diversity is very rich. The hornbills are a prominent group of birds well adapted in variety of habitats and providing immense ecological services. Out of 54 species found in Asia and sub-Saharan Africa (el Hoyo et al 2001), 10 species are found in India. According to Kemp (1995), the hornbills are most recognizable group of all birds belonging to Order Coraciiformes under the Family Bucerotidae with 14 Genera, 54 species and 78 Taxa. Although their phylogeny is rather established, according to new taxonomic arrangement some changes in nomenclature and arrangement may be inevitable in many avian groups of birds (Jente et al 2016) as well as in hornbills. The Hornbills are largely arboreal birds (Sub-Family Bucerotinae) but a few African species are ground dwelling too (Sub-Family Bucorvinae). The hornbills chiefly consume fruits and berries and help in seed dispersal; they also eat variety of animal matters - insects, small vertebrates and a few even scavenge

on large animal carcass. Most hornbills possess large bills with remarkable casque that makes them unique in the avian community. Only toucans of South America possess such massive bills. Hornbills are mostly sedentary, move only locally in search of food, at times to considerable distances. The breeding habits of the hornbills are also unique. They nest in natural tree holes and the females confined themselves by plastering the opening of the hole. Only a small slit is left through which the males keep feeding the female and the nestlings. After the nestlings are able to fly, the opening is broken for fledging of the occupants.

### **DISTRIBUTION OF INDIAN HORNBILL**

Indian Hornbills are widely distributed (Table 1). Being large and conspicuous birds their morphology, distribution, general habits and habitat have been described variously (Ali 1941, Ali & Ripley 1974, Mundappa 2000, Baker 1927, Datta 2000, Kannan & Douglas 1997, Grimmett et al 1998, Ranjit et al 2011, etc.).

## Narcondam Hornbill

Narcondam is a small island in Bay of Bengal (130.27 N& 94.17 E; Fig.1) comprising about 6.8 sq.km; 114 KM from Port Blair towards Myanmar; the Coco Island of Myanmar is only about 40 KM from Narcondam. From defense point of view, the Island is quite strategic and hence a party of 15 policemen camp on the island while the Indian Coast Guard keep constant vigil in the vicinity. The Island is lofty peak rising out of deep waters of the sea with the highest peak of about 900 meters. Generally, it is an evergreen type of forest lashed by heavy rains during two monsoons (SW & NE), temperature varying 22 to 27 degree Celsius. It was declared as Narcondam Bird Sanctuary under Wildlife Protection Act 1972 and an Important Bird Area in 2004 by Birdlife International.

## METHODS OF STUDY

Observations on feeding habits, group structure, nest feeding, population density and other behavioral aspects of the Narcondam Hornbill were made in Feb- March 2000. Line transect and point count methods were adopted to estimate population density and program TRANSECT was used for the analysis of data. Nest feeding by breeding males (Fig. 2 & Fig. 3) were observed in 3 shifts of 4 hours daily to cover the entire day at three nests. Foods items were identified directly on the fruiting trees and indirectly by collecting the debris of the seeds thrown down by the females. Density of fruiting and nesting trees were estimated by Point Circular Quadrant method. The vegetation at Narcondam island is quite thick comprising large trees, thorny bushes and climbers. A herbarium of main trees and shrub were collected and identified with the help of botanists at the Botanical Survey of India Office at Port Blair.

Active nests were located by following the breeding male hornbills and by checking tall trees with natural tree holes. Like the study of breeding biology of barbets (*Megalaima* spp; Yahya 2001), at times food begging calls of the nestlings while feeding by male hornbills also helped in locating active nests. A lofted hide was made at nest number 2 for regular observations and photography. Feeding and other activities of the group of non-breeding hornbills were also recorded during the study period (Table 1).

## RESULTS AND DISCUSSION

Among other 23 avian species recorded on this Island, Narcondam Hornbill is the most populous and vociferous bird. The second most common species is Andaman Koel (*Eudynamis scolopacea adolosa*) but it is an intrigue that how this brood parasitic bird is flourishing on this island where none of the 23 resident birds (Yahya & Zarri 2000) look like appropriate host for the Koel; neither any such species can visit the Island for breeding due to its remoteness and inaccessibility.

In comparison to other hornbills, the Narcondam Hornbill has been least observed because of the inaccessibility to the Narcondam Island and difficulties in obtaining the permission to visit the island. Therefore, so far only a few ornithologists have contributed meaningfully on ecology and biology of Narcondam Hornbills (Abdul Ali 1976, Cory 1902, Hussain 1984, RaviSankar&Vijayan, 1998, Vivek&Vijayan 2003, Yahya&Zarri, 2000 & 2002 and Yahya 2012). Details of our observations as given in Reference section; a summary is given below:

As per our observation the population of the N. Hornbill was 423, whereas Vivek and Vijayan (2003) estimated their number about 300. Such number is though stable considering the small area, it is not viable in long term survival because of possible inbreeding and confinement to a single habitat. We collected considerable qualitative and quantitative data on nest feeding, foraging and other behavioral traits of the hornbills (Table 2). A total of 20 pairs were recorded nesting while detail observations were carried out at 3 nests. Natural large holes in tall trees were preferred between 5 and 35 m heights. Nest feeding started as early as 0440 hours and with an average of 2.5 visits per hour continued until late afternoon (1840 hrs.). Most feeding was recorded in morning session. The males carry 45 to 70 fruits in its throat and feed the female and nestling by regurgitation. It is a laborious work, especially during raining when clinging to nest opening is very difficult.

The non-breeding hornbills often gather in large numbers on fruit trees and besides feeding, perform a number activities such as calling, fighting, chasing, preening and aerodynamics (Table 2). The Narcondam hornbills roosted in foliage of large trees and various pre- and post-roosting activities such as loud calling and movement in group on fixed route were performed. The breeding males were often observed chasing

the White-bellied Sea eagle (*Haliaeetus leucogaster*), that could be a potential predator of fledgling hornbills. Watching hornbills performing aerodynamics mostly in overcast weathers was spectacular scenes. So far I have not observed such behavior in other Indian hornbills.

## CONCLUSION

### Conservation of Indian Hornbills

Owing to rapid decline in content and quality of habits, like other groups of birds, the population of most hornbills is declining in the country except the Narcondam Hornbill. However, the future of this endemic and endangered species is also quite vulnerable because about 300-400 birds occur only on a small island and any catastrophe, such as a tsunami, may be detrimental to their survival. The Narcondam Island is close to Indonesia which falls in severe seismic zone. During 2004 earthquake and subsequent tsunami biodiversity of several islands of Andaman and Nicobar archipelago has been dented. I have given some specific recommendations for the conservation of Narcondam Hornbill earlier (Yahya 2012): Besides other measures, the most important step to safeguard the future of this important bird is captive breeding and introduction of the species to some ecologically similar and uninhabited island so that alternate population is established.

To restore the habitat and reduce increasing anthropogenic pressures, it is desirable that a long term study is conducted to ascertain present status of all Indian hornbills. Based on the data thus gathered, the conservation efforts could be prioritized. Forming a separate project – SAVE INDIAN HORNBILLS – should be launched by the Ministry of Environment, Forests and Climate Change with the collaboration of Birdlife International. For sustainable future of Indian biodiversity vis-à-vis avian diversity increase from only 4% land to at least 14% land under Protected Area coverage is imperative.

## ACKNOWLEDGEMENTS

While information on other hornbills were gathered during my several ornithological expeditions, for the study on Narcondam Hornbill I am grateful to the British Ecological Society, U.K. for funding. I am also indebted to officials of Ministry of Defense, Ministry of Home Affairs, Ministry of Environment & Forests and Inspector General of Police, Port Blair for the needed permissions. I am obliged for the assistance of Dr. Ashfaq Zarri, the then research scholar of our

Department and cooperation of the Police party deputed at Narcondam Island during the study.

## REFERENCES

- [1] Abdul Ali, H. 1976. "The fauna of Narcondam Island. Part 1 Birds." *JBNHS* 71(3): 496-505
- [2] Ali Salim. 1941. "Book of Indian Birds". Bombay Natural History Society.
- [3] Ali, S. & Ripely, S.D. 1970. "Handbook of the Birds of India and Pakistan ." Vol 4. Oxford University Press, Bombay, London
- [3] Baker, E.C. 1927. "Fauna of British India. Birds." Vol. 4. Taylor and Francis London
- [4] Cory, C.P. 1902. "Some further notes on Narcondam Hornbill." *JBNHS* 14(2): 372
- [5] Datta, A. 2000. "Seed dispersal by Hornbills in tropical forest in Arunachal Pradesh." Report XIV. Wildlife Institute of India, Dehradun, India.
- [6] Jente, Ottenburhs, Pim van Hooft, Spike E. van, Ronal C Yenbergh and Herbert, H.T. Prins. "Birds in a bush: Toward an avian phylogenetic network." *The Auk*: 133. 2016, Pp577-582.
- [7] Kanan, R. an, R. & A.J. Douglas. 1997. "Breeding biology of Great Pied Hornbill (*Bucerosbicornis*) in the Anamali Hills of south India." *JBNHS* 94 (3)
- [8] Kemp, A C. 1995. "The Hornbills". Oxford University Press, Oxford.
- [9] Mundapa, D. 2000. "Breeding biology of Malabar Grey Hornbill, in Southern Western Ghats, India." *JBNH* 97(1): 15-24.
- [10] delHoyo, J., Elliott, A. and Sargatal, J. (2001) "Handbook of the Birds of the World. Vol. 6: Mousebirds to Hornbills." Lynx Edicions, Barcelona
- [11] Ranjeet, M., J.C. Daniel & Nikhil Bhopale. "Birds of the Indian Subcontinent." *A Field Guide*. Bombay Natural History Society & Oxford University Press, New Delhi.
- [12] Sankar, R. and Lalith, V. 1993. "The avifauna of Andaman & Nicobar islands." In A. Verghese, S. Sridhar and A.K. Chakravarthy (eds). *Bird Conservation and Strategies in the Nineties and Beyond*. Ornithological Society of India, Bangalore.
- [13] Yahya, H.S.A. & Zarri, A. A. 2000. "Status and Behavior of Narcondam Hornbill at Narcondam Island." Technical Report. 58 Pp.

- Dept. of Wildlife Sciences, A. M.U. Aligarh, India.
- [14] Yahya, H. S. A. & Zarri, A. A. 2002. "Status, ecology and behaviour of Narcondam Hornbill (*Acerosnarcondami*) in Narcondam Island, Andaman and Nicobar Islands, India." *J BNHS Bombay* 99(3): 418-433.
- [15] Yahya, H.S.A. 2001. "*Biology of Indian Barbets*." Authorspress, New Delhi, The Netherlands.
- [16] Yahya, H.S.A. 2012, "Ecology and Conservation of Narcondam Hornbill, *Acerosnarcondami* in Andaman & Nicobar Islands. In *Ecology of Faunal Communities on the Andaman & Nicobar Island*." Edited by : K. Vendataraman, C. Raghunathan W & C. Sivaperuman, Springer Heidelberg, New York, London. Pp.263 - 272

**Table 1: Distribution of Indian Hornbills**

SN	Common Name	Scientific Name	Distribution	Remark
1	Indian Grey Hornbill	<i>Ocyerosbirostris</i>	Widely spread, forests and gardens; almost throughout subcontinent	Seen individually or in small groups. Population declining due to loss of habitat
2	Malabar Grey Hornbill	<i>Ocyerosgriseus</i>	Endemic to Western Ghats	Population declining due to habitat loss
3	Great Hornbill	<i>Bucerosbiornis</i>	Mainly from Uttrakhand east through Himalayas to Arunachal Pradesh, N E India & Western Ghats	Sporadically common in forests and well wooded areas
4	Brown Hornbill	<i>Anorrhinustickelli</i>	North east India; mainly upper Barhamputra valleys, also in Bangladesh	Populations declining due to local poaching and loss of forests
5	Rufous-necked Hornbill	<i>Acerosnepalensis</i>	North east India, east Nepal to Arunachal Pradesh, also in Bangladesh	Locally common in Bhutan; occasional in Chittagong Hill tracts; rare in Nepal
6	Wreathed Hornbill	<i>Acerosundulates</i>	Locally fairly common in low foothills west Bengal to Arunachal Pradesh	Population stable in Indian territories but declining in earths while ranges
7	Narcondam Hornbill	<i>Acerosnarcondami</i>	Endemic to Narcondam Island.	Flagship species on the Island. 423 birds estimated in 2000. See text.
8	Plain-pouched Hornbill	<i>Acerossubruficollis</i>	Earlier common in Margherita area in Assam, now rare.	Globally threatened.
9	Oriental Pied Hornbill	<i>Anthracocerosalbirostris</i>	Resident from Nepal foothills to Arunachal Pradesh, Bhutan and Bangladesh	Locally common; keeps in small groups and pairs
10	Malabar Pied Hornbill	<i>Anthracoceroscoronatus</i>	Resident, subject to local movement.	Common; use same nest holes' year after year; at times fly in large groups; flight frighteningly noisy.



**Table. 2. Group structure and activities of Norcondum Hornbill, March 2000**

Date March 2000	Time of observation			Number	Male	Female	Activity
	Start	End	Total (min)				
09	1650	1726	36	32	19	13	Calling preening moving
10	0510	0543	33	15	08	07	branch to branch (Hop-
11	1200	-	-	04	02	02	Hop-Move)
12	1437	1500	23	14	05	09	Post-roosting feeding &
13	1645	1705	20	50	24	26	displays
14	1103	1121	18	04	03	01	Flew across the valley
15	0600	0645	45	06	05	01	Actively feeding
15	0725	0728	03	04	02	02	Pre-roosting displays
15	1517	1529	12	05	02	03	frequent movements less
16	0940	0945	05	04	-	-	feeding calling
18	1610	1700	50	37	19	18	Feeding actively
20	1615	1633	08	05	02	03	Feeding & aerial displays
22	1530	1610	40	06	-	-	Aerial displays
23	1530	1700	90	22	14	08	Active calling + Feeding
24	1612	1620	08	05	03	02	Flying high across valley
25	0615	0620	05	07	-	-	Pre-roosting activities
25	1215	1230	15	19	-	-	Pre-roosting activities
25	1515	1542	37	19	10	09	Parachute like dropping in
26	0542	0724	96	18	-	-	mid air about 60-70m
26	0905	0910	10	06	-	-	high
26	1150	1203	13	11	05	06	Aerodynamics +Pre-
27	0545	0630	45	48	22	26	roosting activities
27	1340	1445	65	16	09	07	Mobbing the White-
28	0900	0910	10	18	-	-	Bellied Sea Eagle
28	1600	1630	30	34	20	14	Mobbing the White-
29	1500	1620	80	22	12	10	Bellied Sea Eagle
30	0555	0558	03	04	02	02	Aerial Movements
							Feeding & Aerodynamics
							Feeding & Aerodynamics
							Crossed valley after rain
							Active Feeding
							Feeding + aerial
							movements
							Feeding + calling
							Flew across valley
							Pre-roosting activities
							Pre-roosting activities
							Aerodynamics



Fig. 1. An enchanted view of Narcondam Island, eastern side



Fig.2. A male NH about to feed



Fig.3. A Male NH removing fecal matter from the rim of the nest.

# **THE IMMEDIATE EFFECTS OF FOOT MASSAGE WITH COCONUT SHELL ON PRESSURE PAIN THRESHOLD AND FOOT GRIP STRENGTH IN HEALTHY SUBJECTS: A PILOT STUDY**

Laojeenwong P<sup>1</sup>, Eungpinichpong W<sup>2\*</sup>

<sup>1</sup>Division of Exercise and Sport Sciences, Graduate School, KhonKaen University.  
Muang, KhonKaen 40002, Thailand

<sup>2</sup>Back, Neck, and other Joint Pain and Human Performance Research Center, KhonKaen University.  
Muang, KhonKaen 40002, Thailand, \*e-mail wiceun@yahoo.com

## **ABSTRACT**

Feet are very important parts of the body because they carry almost all of the body weight and contribute on human locomotion. Daily works in prolonged standing position may cause foot pain and fatigue easily. Currently, foot massage with coconut shells has been practiced in some eastern countries to relieve foot pain and fatigue for long time without sufficient scientific evidence. This study aimed to preliminarily determine the immediate effects of a foot massage with coconut shell on pressure pain threshold and foot grip strength in healthy subjects. Thirteen healthy volunteers, who worked in standing position mostly, participated in the study and received a 5-minute session of foot massage using coconut shells. Pressure pain threshold and foot grip strength were measured before and 2 minutes after the foot massage. The results showed that foot massage with coconut shells could increase pressure pain threshold and foot grip strength significantly ( $P < 0.05$ ). We suggested that foot massage with coconut shells may raise pressure pain threshold of the feet and provide better effort on foot muscles contraction. Further study with a randomized controlled trial was recommended to verify these effects.

**Keywords:** Coconut shells, Foot massage, Pressure pain threshold, Grip strength

## **INTRODUCTION**

Feet are major organs of the body that support the weight of the whole body. They are always tired or fatigue and pain after long hours of working in weight bearing positions such as standing and walking. A study found prolonged standing may decrease pressure pain threshold of the feet (Messing K, Kilbom A, 2001). Untreated foot discomfort and pain may lead to abnormal gait and prone to have injury and falls especially in the elderly people. Foot massage is one of commonly used treatments for relieving foot fatigue and pain. Moreover, based on the theory of foot reflexology, foot massage on specific zone on the feet may reflect to normalize the functions of the remote organs on the body such as heart and brain. It has been found that foot massage may be helpful in maintaining health by reducing muscle fatigue (Kim OJ and Kim IS, 2012) and balancing the autonomic nervous system (Guan L et al., 2014). Some studies found foot massage may have a positive effect on type 2 diabetes and exert a beneficial effect on lowering blood pressure and incontinence (Song, 2015), (McCullough, 2014). Foot massage using coconut shells has been practiced in many countries in Asia for relieving foot fatigue and reduce pain in lower extremities. However, the effects of foot massage using coconut shells have not been reported.

The current study aimed to preliminary determine study on the immediate effects of the foot massage using coconut shell on pressure pain

threshold and foot grip strength in healthy subjects.

## **Methodology**

### **Sampling site**

Subjects who met the criteria were recruited from students and staff at Prince of Songkhla University, Thailand

### **Inclusion criteria**

Subjects were included if they were healthy and aged between 20-35 years.

### **Exclusion criteria**

Subjects were excluded if they met one of the exclusion criteria:

- Physical fatigue or fever
- Pregnant women
- Having menstruation
- Hyper sensitive to pressure massage
- An open wound in the foot

### **Measurement instruments and procedures**

- Pressure pain threshold (PPT)

A calibrated pressure algometer (WE Algometer, Thailand) was used to measure PPT of the feet. A research assistant marked the ten locations on plantar surface of the feet for measurement of the PPT. (figure 1). Each of the subjects was rested in prone lying position and carried a control switch of PPT in a hand. Then, the research assistant carried the handle of the algometer and gradually applied

perpendicular pressure through the probe on each marked location. When the subject had a sensation of pain distinct from pressure or discomfort (Fischer AA, 1987) on the applied pressure location, he/she pushed the stop button and got the reading of PPT. At this point, the algometer pressure was immediately released. The measurement was done twice and the average of the readings was recorded.

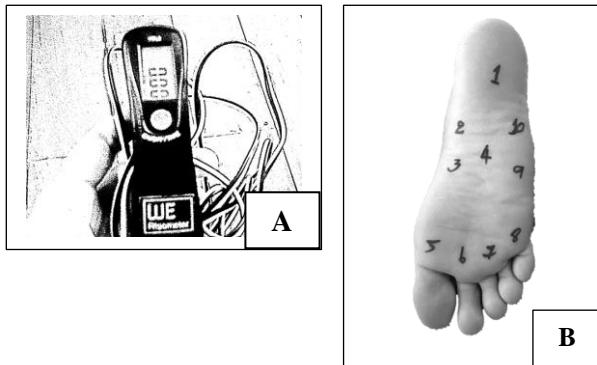


Fig. 1 Measurement of PPT. (A). Plantar surface of the foot with the 10 marked at the locations for measurement of PPT10 test locations (B).

#### ●Foot grip strength

Isometric measurement of foot grip strength was performed using a Toe Grip Dynamometer (TAKEI SCIENTIFIC INSTRUMENTS CO., LTD, Japan). Each of the Subjects was instructed to stand upright on the measuring plate where both feet were placed shoulder-width apart. The handle of the force meter or grip bar was set underneath the 1st metatarsophalangeal joint and the heel stopper was adapted to fit the heel of the participant. When, the subject was ready to start, the dynamometer was set to zero. Then the subject was asked to squeeze and pull the grip bar with the toes as hard as possible and get the reading. After the adequate number of practice and rest, the actual toe grip strength was measured twice, each time maintained the maximal force about 3 seconds and rested 10 seconds between times, the mean value of the foot grip strength was calculated (Uritani et al., 2014; Uritani et al., 2015). Using this method of measurement, Uritani et al. (2012) reported that the interrater reliability of foot grip strength was high in young adult and middle-age adult (ICC=0.76-0.95).

#### Procedure

After the participants underwent screening procedures by interview, they gave informed consent.

After the baseline were measured each subject received 5 minutes of self-foot massage using coconut shells and followed by 2 minutes rest on a chair. To perform self-foot massage, the subject stood on one foot while placing another foot of a prepared half-sized coconut shell and gradually increasing pressure to the plantar surface of the foot until he/she felt a little discomfort then releases the pressure. This procedure of self-foot massage had been repeated for 2.5 minutes and ensures to cover the whole area of plantar surface of the foot and then swabbed to massage on another foot for 2.5 minutes. After 2 minutes of rest on a chair, the subject was measured again. The procedure of data collection was summarized in figure 2.

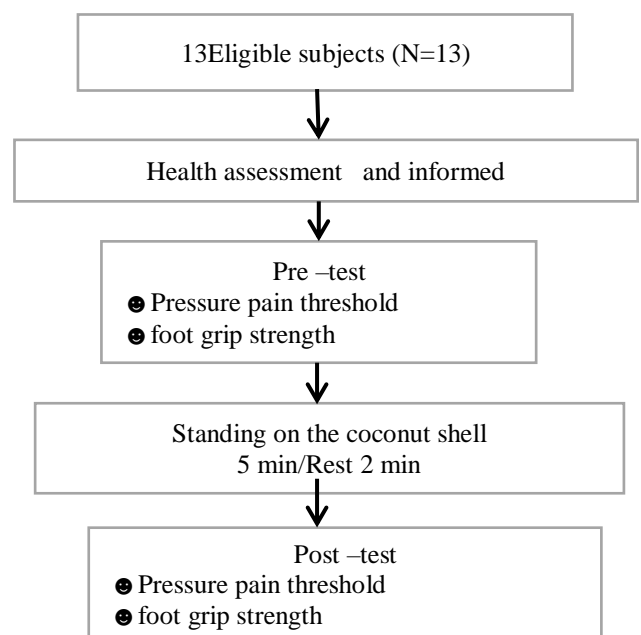


Figure 2 A diagrammatic representation of data collection procedure.

#### Data analysis

All data were expressed using descriptive statistics as the means and the standard deviation (mean  $\pm$  SD). Pair t-test was used to compare outcome measures between baseline and after the treatment. All p-values were two-tailed, and the level of significance was set at 0.05. All statistical analysis was performed with IBM SPSS statistics 20 software (SPSS Inc., Chicago, IL, USA)

#### RESULTS AND DISCUSSION

Demographic data of the subjects was presented in Table 1. Most of the subjects were females, aged ranged 20-30 years, and had normal range of body mass index.

Table 1 Characteristics of healthy subjects.

Item		N=13	Percentage
<b>Sex</b>	Female	8	62
	Male	5	38
<b>Age</b>	20 – 25	3	23
	26 - 30	10	77
	41 -50	5	38
	51-60	3	23
	61-70	3	23
<b>Weight (Kg)</b>	71-80	1	8
	81-90	-	-
	91-100	1	8
	141-150	1	8
	151-160	8	62
<b>Height (cm)</b>	161-170	2	15
	171-180	2	15
	< 18	1	8
	18.5– 23.4	8	62
	23.5– 28.4	3	22
<b>Body mass index (kg/cm<sup>2</sup>)</b>	28.5– 34.9	1	8
	35.0– 39.9	-	-
	> 40	-	-

The results of the paired t-test revealed a significant changes in PPT mostly after the treatment ( $P < 0.05$ ) (Table 2). PPTs of the left leg were increased at Seven out of ten locations ( $p \leq 0.5$ ) whereas three locations were decreased. The low PPT at location P1, P3, P4 after foot massage may be due to over pressure during procedure of applying foot massage using the coconut shells. For the right foot, almost all the locations (9 out of 10) were found with significantly increased in PPT after having foot massage. It was noted that at P5 the PPTs were not significantly increased for both feet. This may be due to the location of P5 that was underneath the first metatarsal joint and has less muscle mass than the others. The response to foot massage was lower than the locations with relatively more muscle mass in the foot. The intrinsic muscles of the feet that were prone to get fatigue during stance may respond to massage quicker than the area with less muscles. Although, the results of the current study were in line with those of previous studies, it was also noted that the overall changes in PPT after foot massage were less than 1 kg/cm<sup>2</sup>. The effect size was relatively small which may be due to a single session of foot massage may provide small effect. If more sessions of foot massage were administered, more effect size may be occurred. The algometer being used to measure (PPT) in this study had high precision with two decimals of digital

reading and well calibrated, it was unlikely that the small effect sizes were due to the instrumental error.

Table 2 Pressure pain threshold (PPT) measured on the plantar surface of the foot with at the 10 test locations.

		Mean PPT (kg/cm <sup>2</sup> )			
		Baseline	Post	Difference	p-value
Location					
Left (Kg/ cm <sup>2</sup> )	P1	5.44 ± 1.98	5.12 ± 1.67	-0.32	0.001*
	P2	4.45 ± 1.70	4.55 ± 1.96	0.1	0.001*
	P3	4.49 ± 1.89	4.16 ± 1.83	-0.33	0.001*
	P4	4.90 ± 1.91	4.71 ± 1.78	-0.19	0.001*
	P5	4.77 ± 1.58	4.82 ± 1.72	0.05	0.001*
	P6	5.04 ± 2.04	5.25 ± 1.98	0.21	0.001*
	P7	5.07 ± 2.29	5.29 ± 1.95	0.22	0.001*
	P8	5.17 ± 2.42	5.28 ± 1.99	0.11	0.001*
	P9	4.81 ± 2.21	5.13 ± 2.02	0.32	0.001*
	P10	4.99 ± 2.20	5.23 ± 1.95	0.24	0.001*
Right (Kg/ cm <sup>2</sup> )	P1	5.60 ± 2.19	6.25 ± 1.99	0.65	0.003*
	P2	5.05 ± 2.39	5.29 ± 1.92	0.24	0.005*
	P3	4.58 ± 1.94	4.86 ± 1.74	0.28	0.008*
	P4	5.18 ± 2.21	5.38 ± 1.53	0.2	0.004*
	P5	5.03 ± 1.84	5.21 ± 1.59	0.18	0.082
	P6	5.24 ± 2.11	5.59 ± 1.94	0.35	0.021*
	P7	5.30 ± 2.12	5.74 ± 2.03	0.44	0.001*
	P8	5.31 ± 2.35	5.70 ± 2.18	0.39	0.001*
	P9	5.16 ± 2.31	5.53 ± 2.04	0.37	0.002*
	P10	5.47 ± 2.31	5.80 ± 2.05	0.33	0.006*

\*sig  $p < 0.05$

The result from paired t –test of foot grip strength revealed significantly different after foot massage. ( $p < 0.05$ ) (Table 3). The higher score of foot grip strength after foot massage reflected that less fatigue

so that the subjects could exert more forces than those of baseline.

Table 3 Foot grip strength.

Mean foot grip strength				
Location	Baseline	Post	Difference	p-value
Left	12.74±4.32	13.79±2.80	1.04	0.001*
Right	13.12±4.42	15.54±4.57	2.33	0.001*

\*sig p<0.05

The purposes of this study preliminarily determined the immediate effect of a foot massage with coconut shell on pressure pain threshold and foot grip strength in healthy subjects. To our knowledge, this is the first study on the effect of a foot massage with coconut shell on plantar surface muscles after immediate. This study showed a significant increase in pressure pain threshold, and foot grip strength after treatment compared with score. The increase in nearly PPT after foot massage may be a sign of recovery from muscle fatigue and let the subject exert more muscle power than baseline and have more foot grip strength on both feet. The findings of this study were consistent with the study of Eungpinichpong W et al (1999) which found that foot massage increased blood circulation, reduce the tension and pain of the muscles, and increases the skin temperature in area being massaged. Some limitations of this study were noted. First, this was only a pilot study in 13 healthy volunteers. Small sample size may provide limitation on conclusion. Second, the pre-post study design in this study could not provide a definite conclusion. However, results of this study could provide a clue that foot massage with coconut shell may result in immediately increased pressure pain threshold, and foot grip strength. Finally, we also do not know the long-term effects.

## CONCLUSION

Based on the results of this study, we conclude that the foot massage with coconut shells may increase the (PPT) and foot grip strength. Further study with a larger sample size and randomized controlled trial is needed.

## ACKNOWLEDGEMENTS

This project is supported by Traditional Thai Medicine Hospital, Faculty of Traditional Thai Medicine, Prince of Songkla University, Thailand.

## REFERENCES

- [1] Messing K, Kilbom A. Standing and very slow walking: foot pain-pressure threshold, subjective pain experience and work activity. *Appl Ergon.* 2001 Feb;32(1):81-90
- [2] Kim JO, Kim IS. [Effects of aroma self-foot reflexology massage on stress and immune responses and fatigue in middle-aged women in rural areas]. *J Korean Acad Nurs.* 2012 Oct;42(5):709-18.
- [3] Guan L, Collet JP, Yuskiv N, Skippen P, Brant R, Kissoon N. The effect of massage therapy on autonomic activity in critically ill children. *Evid Based Complement Alternat Med.* 2014;2014:656750
- [4] Fischer AA (1987) Pressure algometry over normal muscles. Standard values, validity, and reproducibility of a pressure threshold. *Pain.*30:115–126.
- [5] McCullough JE, Liddle SD, Sinclair M, Close C, Hughes CM (2014) The physiological and biochemical outcomes associated with a reflexology treatment: a systematic review. *Evid Based Complement Alternat Med.*2014:502123.
- [6] Song HJ, Choi SM, Seo HJ, Lee H, Son H, Lee S (2015) Self-administered foot reflexology for the management of chronic health conditions: a systematic review. *J Altern Complement Med.*, 21(2), 69-76.
- [7] Uritani D, Fukumoto T, Matsumoto D, Shima M (2015) Associations between toe grip strength and hallux valgus, toe curl ability, and foot arch height in Japanese adults aged 20 to 79 years: a cross-sectional study. *J Foot Ankle Res* 8(1): 1-6
- [8] Uritani D, Fukumoto T, Matsumoto D (2012) Intrarater and interrater reliabilities for a toe grip dynamometer. *J Phys Ther Sci* 24: 639–43.
- [9] Uritani D, Fukumoto T, Matsumoto D, Shima M (2014) Reference values for toe grip strength among Japanese adults aged 20 to 79 years: a cross-sectional study. *J Foot Ankle Res* 7: 1-6.
- [10] Eungpinichpong W, Montri N(1999) Basic physiological effects of modified foot massage. *J Med Tech Phys Ther* 11: 98-105.

## MOCAF TEMPEH DATES BISCUIT FOR THE IMPROVEMENT NUTRITIONAL STATUS OF UNDERWEIGHT CHILDREN

Fatmah<sup>1</sup>

<sup>1</sup>Public Health Nutrition Department, Faculty of Public Health, Universitas Indonesia, Depok City, West Java  
Province, Indonesia

### ABSTRACT

The prevalence of PEM (Protein Energy Malnutrition) in toddlers in Indonesia has increased due to lower macro-nutrient intake and exposure to infectious diseases. Therefore, it is necessary to intervene with supplementary feeding in the form of highly nutritious food products, such as biscuits made from flour enriched from mocaf from soybean and date jam. The effects of mocaf tempeh dates biscuits were investigated in villages within the Cinere District and the Pancoran Mas District in Depok City. The study was conducted to assess the effects of consumption of mocaf tempeh dates biscuits with the nutritional status of KEP toddlers. **Approach:** Randomized Controlled Trial (RCT) with pre-post tests were used with 70 subjects, divided into 3 groups: 27 subjects in the treated group (mocaf tempeh dates biscuits), 26 subjects of control group 1 (tempeh dates biscuits), and 17 subjects in control group 2 (placebo biscuits). The intake of energy, protein, and fat, along with haemoglobin (Hb) examination and blood albumin were collected pre-post intervention. **Results:** A change in weight of 0.4 kg was found in the intervention group. The highest increase in height was found in control group 1 (1.7 cm). An increase in blood hemoglobin levels of 0.1 points were found in the intervention group and the control group 1. The albumin was decreased by 0.3 points in the intervention group. Weight gain in the intervention group was influenced by macro-nutrient intake. Intake of vitamin A, Fe, and Zn affected blood hemoglobin levels in post-intervention with the intervention group. **Conclusion:** Mocaf tempeh dates biscuits can be consumed by underweight children as an alternative food of Nutritional Supplementation Program.

*Keywords: Mocaf Tempeh Dates Biscuits, Weight, Height, Hemoglobin, Albumin*

### INTRODUCTION

The lack of energy/calories and protein in the nutrition of toddlers increases morbidity and mortality and is a significant public health concern in Indonesia. In developing countries, approximately 60% of deaths occur in children under five years' old due to malnutrition [1]. In general, KEP in toddlers presents higher levels of hemoglobin (Hb) and lower albumin due to a decrease in protein content in the blood and body tissues [2]. One of the preventive efforts is through supplementary feeding recovery (PMT). The PMT food form preferred by children is a biscuit and PMT for toddlers in this form proved to be quite effective and significantly improve nutritional status [3-7]. Other studies have also shown an increase in the nutritional status of children under five with an increase in weight and height of 1.3 kg and 0.7 cm, respectively over four weeks through the supplementation of tempeh dates biscuits [8]. Similar studies on malnutrition in children under five who suffered from Tuberculosis (TB) in Depok and in East Jakarta show an increase of weight and

height of 0.7 kg and 1.7 cm, and 0.4 kg and 2.4 cm, respectively [9-10]. Further, there are significant differences between the consumption of biscuits in the study that spanned six weeks in Ease Jakarta on the change of weight and height of toddlers. Referring to the findings of the above study, it is clear that a study of the development of local food products in Indonesia that are easily available at affordable prices is warranted. One possibility is the use of the base material of mocaf biscuits since it is widely used as an additional food product in PMT for malnourished toddlers in Indonesia. This study has developed a biscuit made from a flour mixture of mocaf with tempeh and date jam. Mocaf is derived from extracts/cassava extract, which is chosen as the base material of biscuits because it has become a favorite food of Indonesian people, especially in Java. Tapioca processed foods from cassava (one of the staple food in Indonesia) should be consumed with complimentary foods due to its lower protein content and the presence of phytic acid that inhibits iron (Fe) and zinc (Zn) absorption. Excessive consumption of tapioca without consuming other nutrients will cause



the body to become deficient in several nutrients [11]. Therefore, tapioca must be balanced with other foods that are high in protein, such as soybean flour, and iron and zinc, such as dates, in order to prevent severe anemia in KEP toddlers. Malnourished toddlers generally have low hemoglobin levels so that there is an interaction between the low nutrient status with infectious diseases [12]. This study was conducted in the district and sub-district of Cinere and Pancoran Mas, Depok City, which have the largest PEM toddler prevalence in Depok (10.6%). A prevalence of greater than 10% is considered a significant public health issue [13]. Moreover, the proportion of children under five (KEP toddlers) in this district in Depok has exceeded 5.31% [14]. It was hypothesized that there would be effect of supplementation with protein-enriched mocaf biscuits from soybean flour and iron and vitamin C levels from date jam to changes in anthropometry weight/age (W/A) and the biochemistry of blood (hemoglobin and albumin) in KEP toddlers three months post-intervention.

## MATERIALS AND METHODS

A Randomized Clinical Trial (RCT) was used in this study with 70 samples in Depok that have a prevalence of PEM (W/A) in toddlers, of which the largest was in Depok with 10.6% [14]. Nutritional interventions were conducted for three months from May-July 2014. Ethical Clearance was obtained from the Research Ethics Committee of Research and Development Agency for Health Care Ministry of Health of the Republic of Indonesia. Initial screening of nutritional status was done through anthropometric measurements of body weight (BW) in 100 KEP toddlers based on the integrated health post (*posyandu*) data of toddlers in April 2014. The sample size was determined by the formula mean difference test two independent groups with weight gain samples from a previous study of 0.4 kg [8]; significance level ( $Z\alpha$ ) by 1.96; and strength test ( $Z\beta$ ) of 0.84. The minimum sample in each group was therefore determined to be 15 toddlers. Participants were selected through appropriate data from calendar notes of *posyandu* cadres of the weighing results from the previous month. Inclusion criteria for the study were male and female children aged between 12–56 months, a status of malnutrition (W/A) with a Z-score between  $-3$  to  $-2$  SD, not suffering from a chronic or acute infectious disease and not currently participating in the (PMT) Recovery and Counseling Program either from the government (*posyandu*, community health center, hospitals, and others), private organizations, or local or international NGOs.

A total of 70 samples were divided into three groups (mocaf tempeh date biscuits, tempeh dates biscuits, placebo biscuits). 75 samples were originally enrolled at the beginning of the study; however, five did not continue in the second week of the study for a variety of reasons, including the toddler not wanting to eat the biscuits, out of town travel or moving without providing a forwarding address. The use of indicators of weight/age (W/A) in this study was based on the indicators of malnutrition status. Each subject received 50 grams of biscuits per day for 12 weeks. The children were differentiated into three groups: the treatment group (mocaf tempeh dates biscuits) and two control groups (tempeh dates biscuits and placebo biscuits, respectively). Height and weight as well as any presence of illness were monitored every two weeks. Anthropometric measurements were collected twice and daily recordings of food consumption were collected by enumerators through home visits as many as 24 times during the study. Nutritional counseling was conducted twice by investigators with the mothers of the sample in the village office simultaneously with *posyandu* with the monitoring of the nutritional status in the form of anthropometric measurements of samples. The distribution of mocaf tempeh dates biscuits, tempeh dates biscuits, and placebo biscuits were achieved through home visits by a team of researchers and toddlers cadres every three days at which time daily food record forms (24 hours food recall) were also collected. At the end of the intervention, weight, height, and blood samples were taken again. Weight anthropometric data were measured using a digital scale (SECA) by trained field workers. An indicator Z-score of weight/age of less than  $-2$  SD was used to determine the status of children under five who had malnutrition [13]. Basic data (baseline survey) were collected at the beginning and at the end of the study through direct interviews with a structured questionnaire administered with the mothers. The independent variables were toddlers' weight before research and the dependent variable was their weight after the intervention. Confounding variables in this study included demographic characteristics of mothers and toddlers, mothers' knowledge about nutrition and intake of macro and micro nutrients. The measurements for independent and confounding variables were obtained once before the study. The mothers' knowledge of nutrition and height were assessed before and after the study based upon mean scores. The educational background of mothers were divided into categories of low and moderately long, an indicator of being educated for at least nine years. Weight anthropometric data samples were analyzed by WHO Anthroplus software Version 02 of 2009.

based upon indicators of W/A [13]. Food consumption data to assess the adequacy of intake of energy and protein with Nutri Survey were analyzed and then compared to Nutritional Adequacy Rate in toddlers aged 12–59 months (14). Univariate and bivariate data analyses were performed using SPSS version 13. Test paired t-tests were used to assess changes in the mean intake of energy, protein, fat, vitamin A, vitamin C, calcium (Ca), zinc (Zn), ferrous (Fe), weight, height, albumin and Hb pre- and post-intervention in each group. ANOVA test was used to assess the mean differences between variables based on the group (among groups).

## RESULTS

### Contents of Nutrition of Three Types of Biscuits

Table 1 describes the contents of macro-nutrients (energy, carbohydrates, protein, and fat) and micronutrients (Na, Zn, Fe, and vitamin A) in three kinds of biscuits. Mocaf tempeh dates biscuits contain the most energy, fat, and vitamin A compared with the other types of biscuits. The placebo biscuits contained the highest amount of carbohydrates. Tempeh dates biscuits contained protein, Fe, and Zn in larger amounts than the mocaf tempeh dates biscuits and placebo biscuits. By consuming 50 grams of mocaf tempeh dates biscuits per day, the energy sufficiency of a toddler aged 1–3 years would be met with a fat content of between 22 % and 27%.

### Toddler Nutritional Status Change

Gender distribution of toddlers involved in this study was almost equal between males and females, 54.3% and 45.7%, respectively. The largest number of children were between the ages of 12–23 months (38.6%) followed by 24–25 months of age (28.6%). Changes in nutritional status of toddlers in anthropometric and biochemical are illustrated in Table 2. The increase in weight of toddlers was slightly larger in the intervention group (0.4 kg) than the other two control groups (0.2 kg for control group 1 and 0.3 kg for control group 2). Weight before and after the intervention showed significant differences in all three groups ( $p = 0.05$ ). Changes in body height of 1.7 cm in toddlers who consumed the tempeh dates biscuits and the placebo biscuits group are slightly higher than the toddlers who consumed mocaf tempeh dates biscuits (1.3 cm). Toddlers in the intervention and control group 1 initially had lower nutrition status at the end of the normal nutritional intervention based upon Z-score of W/A. Significant differences were found on these indicators in both

groups, except the control group 2 ( $p = 0.142$ ). Further, the mean measurement of Hb increased by 0.1 at the end of the intervention in the intervention group and the control group 1. The albumin in intervention group decreased by 0.3 after three months of ingesting mocaf tempeh dates biscuits. The toddlers in control group 1 did not show increased levels of albumin and the toddlers in control group 2 showed an increase of 0.1 at the end of the study. Mean albumin levels is significantly different in all groups, unlike the case with the mean change in Hb level. A significant difference in nutrient intake at the end of the study was found in the intervention group and control group 1. Table 3 illustrates the differences in nutrient intake of macro and micronutrients among groups. There are significant differences in both macro-nutrient intakes of energy, carbohydrate, fat, and protein and micronutrients. This is in contrast with the current post-study in which the intake of energy and carbohydrates are different among groups ( $p < 0.05$ ). The intervention group has energy intake, fat, protein, and carbohydrate levels that are large compared with the control groups. Whereas, the intake of Fe, vitamin A, and zinc were the most widely consumed by the control group 2. The intake of energy and carbohydrate were significantly different at all the groups after the intervention ( $p < 0.05$ ).

### The Knowledge of Toddlers' Mother about Nutrition

The mothers' knowledge concerning nutrition was assessed by the following indicators: the composition of a healthy diet; the benefits of eating a variety of food sources, including carbohydrates, protein, and fruit; the definition of healthy food; the meaning of balanced nutrition; the meaning of weight of toddlers that remains the same or decreases and understanding its cause; and the efforts that should be made by the mother to increase the toddler's weight. Most mothers could describe the composition of a healthy diet, which consists of a source of protein, vitamins and minerals, but only few mention sources of carbohydrates, such as rice, noodles, bread, etc. as part of a healthy diet composition. The mother's knowledge about the meaning of balanced nutrition is still very low as 17% of respondents rate that the "4 healthy 5 perfect" (*4 sehat 5 sempurna*) as the slogan of healthy food was the same as balanced nutrition. When asked whether or not mothers weighed their babies regularly every month, almost all said it was important (95.7%). However, 25% of women stated that the cause of their toddler's static weight or weight loss was because the toddlers were often ill

and had low food intake. Approximately one-third of the mothers (37.1%) gave their child vitamins or an appetite enhancer when their toddlers' weight was low or did not increase. Therefore, this study concluded low levels (58.6%) and sufficient levels (41.4%) of nutritional knowledge of mothers at the end of the KEP study. Upon further analysis, no effect of changes in anthropometric and biochemical nutritional status with the level of nutrition knowledge of mothers was found at the end of the study ( $p > 0.05$ ). Nonetheless, mothers with toddlers who had sufficient levels of nutritional knowledge in all three groups were more likely to see their underweight children reach a normal weight after the study intervention. Changes in the nutritional status of children under five in the intervention group were based on the indicators of weight/age which was affected by the intake of energy, protein, and fat ( $p < 0.05$ ). This indicator changed for toddlers in control group 1, which was affected by the intake of carbohydrates and Fe ( $p < 0.05$ ) and in control group 2, which was affected by the intake of vitamin A, Fe, and Zn. Further, the intake of vitamin A, Fe, and Zn affected the hemoglobin levels post-intervention in the intervention group ( $p < 0.005$ ). Meanwhile, an influence on the intake of macro and micro nutrients on changes in Hb levels at the end of the study in control groups 1 and 2 was not found ( $p > 0.05$ ). The same is also found concerning the influence of intake of macro and micronutrients to changes in blood albumin levels post- intervention ( $p > 0.05$ ).

## DISCUSSION

The total energy needs of children aged 1-3 years can be fulfilled by 24.25%, 20% of carbohydrates nutritional adequacy rate and 16.9% of protein nutritional adequacy rate, if the toddlers consume 50 grams of tempeh dates biscuits per day. The most rapid change in weight was experienced by the children who consumed tempeh dates biscuits (control group 1). The rapid increase in weight in the intervention group of mocaf tempeh dates biscuits was caused by the intake of carbohydrates, which was the greatest in this group compared to the two control groups. The high intake of carbohydrates can be obtained from the content of glucose and fructose in the dates that can be digested by the body and directly changed into energy. Fulfilling the needs of carbohydrates by 20% is derived from dates jam consumption in toddlers 1 years' old and 15% carbohydrates in toddlers 4-5 years' old. The toddlers who consumed mocaf tempeh dates biscuits showed an increase in height greater than the other two groups. The height increase in tempeh dates

biscuits groups (control group 1) is affected by the increase mothers' knowledge on nutrition and TB disease. Mothers' knowledge on nutrition and TB may be affected the level of tempeh dates biscuits consumption, which affect on the height of the most rapid increase in this group. This latter finding is consistent with a similar study conducted in East Jakarta [10] and studies in Sragen [15] and Ghana [16]. Mothers' knowledge about nutrition was significantly associated with the nutritional status of her children. Specifically, the intervention of nutrition education with families with children underfive has shown to change the behavior of the mother and the family in terms of feeding the child resulting in improvements in the nutritional status of children [17]. The highest weight gained in the group of mocaf tempeh dates biscuits in this study is in line with the three previous studies [18-19, 10]. The first study proved that there are significant differences in weight and height through the provision of biscuits from potato flour for undernourished children in India over the course of months. The second study was conducted with children underfive years' old who had malnutrition in Depok, which found a weight gain of 1.3 kg in the group consuming tempeh dates biscuits over four weeks. The third study proved that a multi-micronutrient in toddlers who had malnutrition can improve the weight of toddler in four months.

## CONCLUSION AND RECOMMENDATION

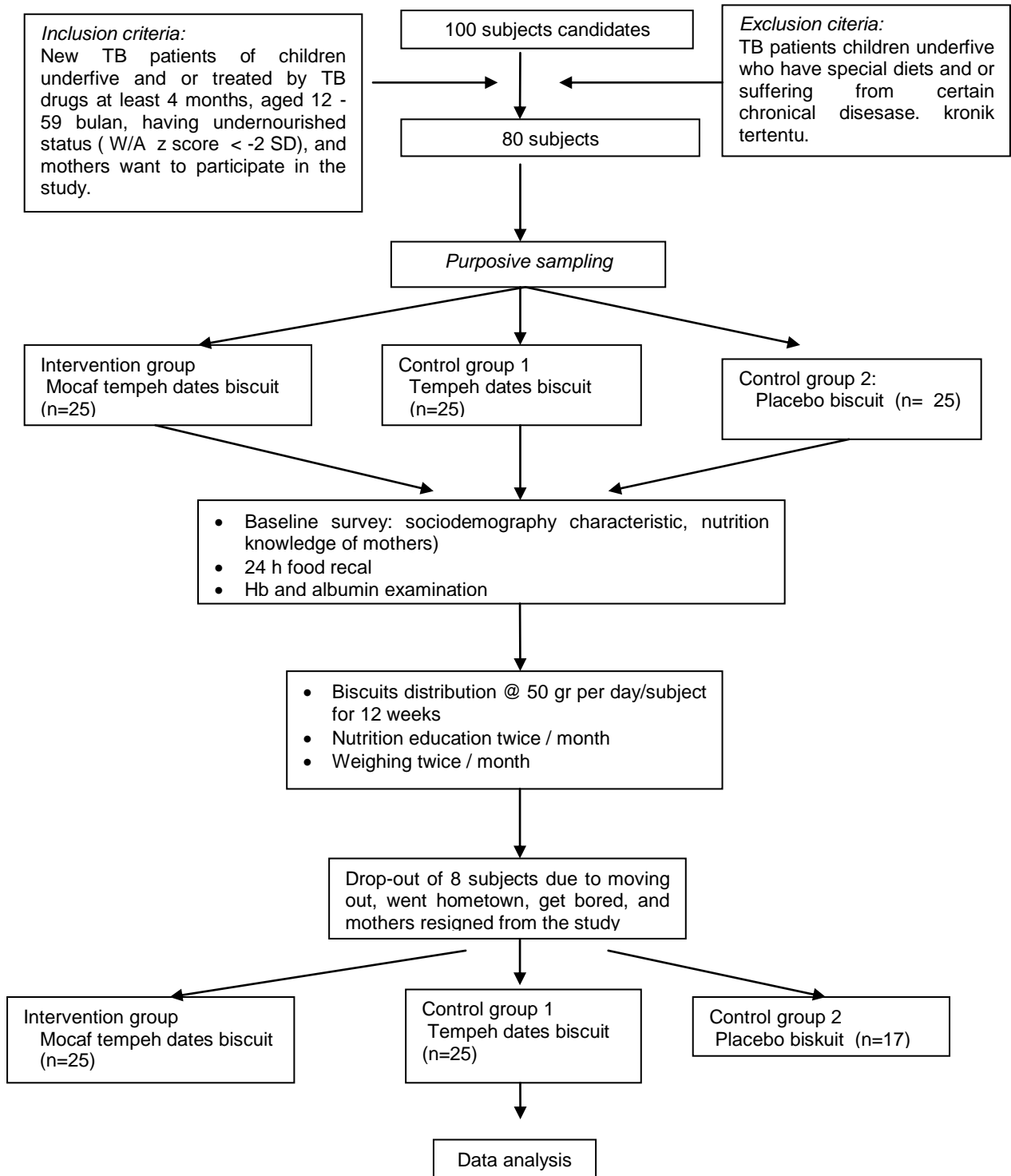
The greatest weight gain (0.4 kg) was found in toddlers who consumed mocaf tempeh dates biscuits, while the largest increase in height (1.7 cm) was found in toddlers who consumed tempeh dates biscuits. It is recommended that mocaf tempeh dates biscuits can be consumed by toddlers as an alternative food for PMT recovery for undernourished children in Depok.

## ACKNOWLEDGEMENT

Our appreciation is extended to DP2M Higher Education of Ministry of Education and Culture (DIKTI KEMENDIKBUD) for the funding of these activities through the Research Grants of PUPT 2014 and also for Program Overseas Seminar of Directorate General of Research and Development Reinforcement 2017.

## REFERENCES

- [1] Faruque et al. Nutrition: basis for healthy children and mothers in Bangladesh. *Health Popul Nutr.* 26 (3), 2008: 325–339.
- [2] Muller O. & Krawinkel M. Malnutrition and health in developing countries. *CMAJ* 173 (3), 2005: 279-286.
- [3] Fitriyanti. et al. Effect of recovery supplementary feeding for undernourished children underfive. *Scripton*. Semarang: Public Health Faculty, University of Diponegoro, 2012.
- [4] Kandarina J.I. et al. Effectivity of Giving Cassava Flour fortified with ferrous among elementary school children at Bantul District: effort to overcome micronutrient deficiency local food based. Final report of National Strategic Fund Year 2010. Yogyakarta: LPPM UGM, 2010
- [5] Kurnia P. et al. Ferrous and zinc fortification effect on biscuits made from tempeh and bran combination to increase albumin level of anemic and undernourished children underfive *Explanation* 5 (2), 2010: 10-23.
- [6] Rivera J.A. & J.P. Habitch. Recovery of Guatemalan children with mild to moderate wasting: factors enhancing the impact of supplementary feeding. *Am J Public Health* 86 (10), 1996: 1430-1434.
- [7] Maleta et al. Feeding patterns of underweight children in rural Malawi given Supplementary fortified spread at home. *Matern Child Nutr* 4 (1), 2008: 65-73
- [8] Fatmah et al. Tempeh-dates biscuits effect on the gained weight of moderate underweight children. *International Journal of Medicine and Medical Sciences* 2 (8), 2012: 165-172
- [9] Fatmah. The intervention of tempeh dates biscuit on the improved nutritional status of tuberculosis preschoolers patients. *The Indonesian Journal on Clinical Nutrition* 9 (4), 2013: 147-154
- [10] Fatmah. Effect of tempeh dates biscuit on nutritional status of preschool children with tuberculosis. *Malaysian Journal of Nutrition* 19 (2), 2013: 173-184
- [11] Astawan M. Cassava flour, benefit, and its procedure <http://www.aremaipb.wordpress.com>, 2010.
- [12] Sulaeman A., Deddy Muchtadi. The nutrient quality of children underfive food products made from cassava flour and banana flour enriched with fish flour and tempeh flour *Media Gizi dan Keluarga* 27(2), 2003: 77-85.
- [13] World Health Organization. Physical Status: Uses and Interpretation of Anthropometry. WHO Technical Report Series, Report No. 854. Geneva, Switzerland: World Health Organization, 1995
- [14] Depok District Health Office. Report of The Nutritional Status of Children Underfive Year Depok: Depok DHO, 2011
- [15] Munthofiah S., 2008. The association between knowledge, attitude, and practice of mothers with the nutritional status of children underfive. Thesis. Solo: Postgraduate Faculty of Sebelas Maret University.
- [16] Appoh LY, Krekling S. Maternal nutritional knowledge and child nutritional status in the Volta region of Ghana. *Maternal Child Nutrition* 1(2), 2005: 100-10.
- [17] Frost MB, Forste R, Haas DW. Maternal education and child nutritional status in Bolivia: finding the links. *Soc Sci Med* 60(2), 2005: 395-407.
- [18] Vasantha M, Gopi PG & Subramani R. Weight gain in patients with tuberculosis treated under directly observed treatment short-course (DOTS). *The Indian Journal of Tuberculosis*, 56 (1), 2009: pp.5-9.
- [19] Mursalim, Juffrie M., Sri Mulyani N. Multimicronutrient fortification affecting the growth of poor family children underfive. *The Indonesian Journal on Clinical Nutrition* 8 (2), 2011: 69-80.



**Figure 1. Research scheme****Table 1. Nutrient value per 100 gr biscuit**

Type	Energy (cal)	Carbohydrate (gr)	Protein (gram)	Fat (gram)	Na (mg)	Fe (mg)	Zn (mg)	Vitamin A (IU)
Tempeh dates	490	61.8	9.62	22.7	267	1.9	1.9	139
Mocaf tempeh dates	495	61.8	5.80	23.8	460	1.3	0.9	155
Placebo	462	70.4	5.03	17.8	-	0.6	1.3	< 0,5 IU

Source: BBIA Laboratory, 2014

**Table 2. Mean change of subject's antropometric and biochemical assessment**

Indicator	Group								
	Intervention (n=26)		p	Control 1 (n=25)		p	Control 2 (n=17)		p
	Pre	Post		Pre	Post		Pre	Post	
Weight (kg)	11.0 ± 2.1	11.4 ± 2.2	*0.001	9.1 ± 1.0	9.3 ± 1.6	0.001	9.3 ± 1,6	9.6 ± 1.5	*0.013
Height (cm)	86.1 ± 8.3	87.4 ± 8.1	*0.001	76.7 ± 4.3	78.4 ± 4.3	0.001	81.0 ± 8,3	82.7 ± 7.9	*0.001
W/A (kg/m2)	- 2.0 ± 1.3	-1.5 ± 1.4	*0.007	- 2.1 ± 1.4	-1.4 ± 0.8	0.001	-2.5 ± 0.9	-1.9 ± 0.9	0.142
Hb	11.8 ± 1.1	11.9 ± 1.0	*0.001	11.9 ± 0.9	12.0 ± 0.9	0.001	11.6 ± 0.7	11.5 ± 0.9	0.114
Albumin	4.4 ± 0.3	4.1 ± 0.3	*0.003	4.3 ± 0.4	4.3 ± 0.4	0.036	4.2 ± 0.2	4.3 ± 0.3	0.013

\*p &lt; 0,05

**Table 3. Mean macro-micronutrients intake of subject**

Type of nutrient	Group			p
	Intervention	Control 1	Control 2	
	Mean ± SD	Mean ± SD	Mean + SD	
<i>Pre-intervention:</i>				
Energi (cal)	1360.3 ± 335.2	932.2 ± 420.6	1184.1 ± 426.3	*0.000
Karbohidrat	187.7 ± 50.2	122.5 ± 58.7	144.1 ± 50.1	*0.000
Protein (gr)	43.5 ± 13.2	35.1 ± 14.7	40.9 ± 17.9	*0.003
Fat (gr)	47.8 ± 18.7	33.6 ± 15.8	48.9 ± 20.8	*0,000
Vitamin A (IU)	1027.9 ± 515.1	1172.8 ± 1270,5	939.5 ± 541.4	0.757
Fe (mg)	14.5 ± 7.7	13.1 ± 9.1	12.0 ± 9.6	0.468
Zinc (mg)	10.0 ± 6.5	8.4 ± 7.7	9.9 ± 6.8	0.179
<i>Post-intervention:</i>				
Energy (cal)	1755.7 ± 479.4	1081.9 ± 381.2	1258.2 ± 351.1	*0.032
Carbohydrate (gr)	231.1 ± 61.1	144.4 ± 47.8	160.4 ± 64.5	*0.025
Protein (gr)	58.2 ± 17.9	37.3 ± 15.5	43.0 ± 13.5	0.265
Fat (mg)	66.4 ± 26.2	38.5 ± 17.2	52.1 ± 18.2	0.053
Vitamin A (IU)	1076.6 ± 682.7	1301.5 ± 1242.2	1183.6 ± 59.9	0.557
Fe (mg)	18.2 ± 13.9	16.2 ± 15.7	14.3 ± 9.7	0.828
Zinc (mg)	13.7 ± 7.3	9.8 ± 7.4	11.0 ± 7.0	0.843

## SPATIAL VARIATION OF WATERBIRDS IN PALLAI AND THADDUVANKODDY IN THE NORTHERN PROVINCE, SRI LANKA

G. Kandasamy<sup>1\*</sup>, D. K. Weerakoon<sup>2</sup>, and A. Sivaruban<sup>3</sup>

<sup>1</sup>Department of Zoology, University of Jaffna <sup>2</sup>Department of Zoology, University of Colombo, Sri Lanka  
vadhana.gk@gmail.com

### ABSTRACT

The Jaffna Peninsula is one of the main entry and exit points for migratory birds that use the Central Asian Flyway. However, ornithological studies and Avitourism have been rare in the Jaffna Peninsula as the study area was inaccessible for three decades due to the armed conflict. The present study was done to determine spatial variation of water birds in two selected locations, Pallai wind farm in the Pachchilappalli DS division and Thadduvankoddy in the Kandavalai DS division in the Kilinochchi district, Sri Lanka. Thadduvankoddy area lies close to Chundikulam National park (24 km). The bird counting was done once a month, by walking along three counting blocks of approximately 500 m x 500 m in each study site. Altogether 50 bird species belonging to 15 families were recorded in the study area, of which 47 species were recorded in Thadduvankoddy while 35 species recorded in Pallai. Out of the 50 bird species recorded, 32 species were shared between the two sites, 15 species were recorded only in Thadduvankoddy while three were recorded only in Pallai. A higher water bird diversity was found in Pallai (Shannon Diversity Index: 2.41; Shannon Evenness Index: 0.68) compared to Thadduvankoddy (Shannon Diversity Index: 2.13; Shannon Evenness Index: 0.55). A high number of *Anas penelope* (1682 individuals) and *Phoenicopterus ruber* (1567 individuals) were observed in Thadduvankoddy while *Calidris minuta* (303 individuals) and *Phoenicopterus ruber* (120 individuals) were the dominant species recorded in Pallai during the study period. It can be concluded that Thadduvankoddy is an excellent place for the development of Avitourism in the Northern Province, Sri Lanka due to the presence of large number of migrant bird species.

*Keywords: Spatial, Pallai, Thadduvankoddy, waterbirds*

### INTRODUCTION

Waterbirds play an important role in energy fluxes between aquatic and terrestrial ecosystem [05]. According to the Ramsar convention on Wetlands, the term “waterbirds” is defined as species of birds that are ecologically dependent on wetlands [4] for variety of activities such as foraging, nesting, resting and roosting [22]. Migratory waterbirds are important indicators of the ecological condition and productivity of wetland ecosystem [16]. Sri Lanka is blessed with 441 species of birds including 239 resident and 202 migratory birds, of which, 155 (35 %) are waterbirds [26]. According to Wetland International, 21 out of 33 families of waterbirds are represented in Sri Lanka [6].

Sri Lanka is divided into six avifaunal zones based on the distribution of the resident bird species. The Northern avifaunal zone shares many similarities with south Indian Avifauna [27]. Migratory birds that use the Central Asian flyway, use five main entry and exit points, of which three are located in the Northern Province of Sri Lanka namely, the Jaffna Peninsula, the Adam's Bridge/Mannar region and the Devil's Point [14]. As Sri Lanka is located in the Central Asian Flyway, it is the final destination point for majority of birds

migrate from northern latitude, during winter in the northern hemisphere [26]. Most of the ducks, birds of prey, and waders, reach southern tip of the India along the eastern coastline, cross Indian Ocean and enter Sri Lanka [14]. Certain pelagic species migrate from southern regions, during their winters, to the Indian Ocean, within the oceanic limits of the country [26]. Six species of off-shore bird species are summer visitors in Sri Lanka [12].

The high environmental heterogeneity of coastal lagoons provide habitats for waterbirds. In Sri Lanka, most of the coastal waterbirds are migrants [26]. The numerically largest migratory groups are the waders, ducks and coastal birds [14], where 42 of 47 species belonging to Family Charadriidae, 11 of 14 species belonging to Family Anatidae and 15 of 19 species belonging to Family Laridae are migrants in Sri Lanka [14]. Altogether, 54 species of seabird species belonging to Order Ciconiiformes were recorded in Sri Lanka [12]. Northern coastline is the longest coastline in Sri Lanka, which extends from Mannar to Mullaitivu [23] and consists of rich habitat heterogeneity, mangroves, marshland, sand dunes, tidal flats and coastal lagoons [28], which provide stopover habitats for migratory water birds.



Tropical coastal lagoons are the most threatened ecosystem due to multiple disturbances including, habitat fragmentation, habitat alterations, climate change and various forms of anthropogenic activities [25]. Although wind power is an ideal alternative renewable energy option in Sri Lanka, it negatively impacts migrant bird population arriving the country in many ways, including collision, displacement and disbursement, barrier effect and habitat change and loss [9] [15] [18] [20]. This may lead to disruption of ecological links between feeding, breeding and roosting sites [15].

However, a few ornithological studies have been done in the Northern Province of Sri Lanka due to three decades of armed conflict [21] [29] [10] [11]. Long term monitoring of waterbirds provide crucial information on conservation of waterbirds and their wetland habitats [4]. The present study was done to explore habitats which were inaccessible for several decades and to determine spatial variation of waterbird species in two selected locations, Pallai wind farm and Thadduvankoddy located in the Northern Province, Sri Lanka.

## MATERIALS AND METHODS

### Study Area

Pollupallai wind farm (Figure 01) is located in the Pachchilapalli DS division in Kilinochchi District, Northern Province of Sri Lanka ( $9^{\circ} 35' 59''$  N and  $80^{\circ} 18' 60''$ ). This wind farm consists of 16 turbines which are placed 400 m apart in a single row, facing the Jaffna lagoon. This is the first-ever windfarm constructed in the Northern Province [30]. Pallai wind farm is surrounded by true mangrove species such as *Exoecaria aggalocha*, *Pemphis acidula* and *Lumnitzera racemosa*, and other plant species, salt marshy vegetation such as *Suaeda maritima*, mangrove associate *Pandanus* sp., and Dry and arid species such as *Aloe vera*, *Borassus flabillifer*, *Annua* sp. *Opuntia* sp. etc.

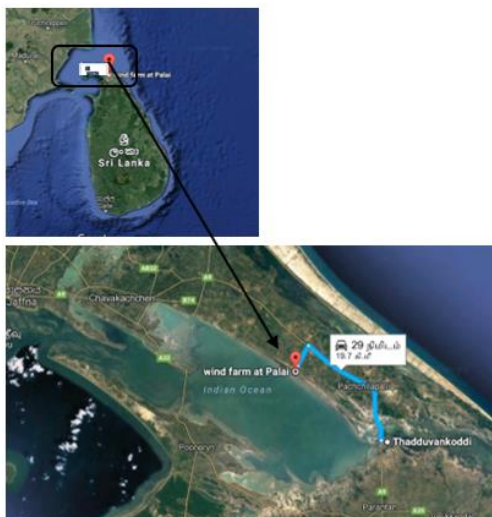


Fig. 01: Location of two study sites

Fig. 01: Pallai windfarm

Fig. 02: Thadduvankoddy

Thadduvankoddy (Fig. 02) situated in the Kandavalai DS division in Kilinochchi district, Northern Province, Sri Lanka ( $9^{\circ} 30' 0''$  N and  $80^{\circ} 25' 0''$ ) and it lies close to the Chundikulam National Park (24 km away from the NP). The site can be described as a marsh with salt marsh species such as *Suaeda maritima* along with other plant species such as *Volkameria inermis*, *Dopatrium cinerea*, *Heliotropium supinum*, *Ipomoea pes-caprae*, *Calotropis gigantea* etc.



A line transect was established in each study site, the entire transect belt was divided into three counting blocks of 500 m x 500 m, each block was separated at least by 500 m to avoid double counting as most were open areas. Three blocks established in Pallai site are designated 1, 2 and 3 while the three blocks established in Thadduvankoddy are designated as 4, 5 and 6. Counting of waterbirds was done during dawn, noon or dusk on alternate months to capture temporal variations, by walking along the transect line of each block. Waterbirds were identified and counted using binoculars (10 x 50) and telescope (60 x) in the three counting blocks in each study site, once a month from December, 2016 to February, 2017.

## DATA ANALYSIS

Diversity Indices such as Shannon's diversity Index, Shannon Evenness Index, Inverse of Simpson's Index, Margalef's richness index and Berger-Parker Index were used to compare the two study sites. The percent occurrence was compared for families of waterbirds recorded in the study area.

### Defining the Foraging Guilds

The foraging guild is a group of waterbirds that exploit the same set of food resources in similar way but not necessarily closely related taxonomically [22]. In this study, Waterbird species were categorised into 10 main guilds according to morphological characteristics, taxonomic groupings based on different habitat requirements, following [2][3][17][19].

1. Dabbling: ducks and gallinules;
2. Stalking: comprising herons, egrets and bitterns.
3. Fishing: pelicans
4. Diving waterbirds: comprising cormorants, darters and grebes
5. Coots: Common coot, Common moorhen, white-breasted Waterhen and Purple Swamphen
6. Flamingoes, storks and spoonbills: comprising flamingoes, storks, ibises and spoonbills
7. Terns
8. Gulls
9. Shorebirds: The Shorebird guild was further subdivided on the basis of the shorebird's sensory mechanism of food detection, and feeding style.
  - a. Visual surface foraging shorebirds: Thick-knee, Plovers, Lapwings, Common Sandpiper, Whimbrel, Wood sandpiper and Common Redshank
  - b. Tactile surface foraging shorebirds: Curlews, Godwits and Stints
  - c. Pelagic foraging shorebirds: Stilts and Marsh Sandpipers

Euclidean distances were measured for abundance of waterbird communities for each foraging guild to create dendrogram to find similarities among three blocks in Pallai and three blocks in Thadduvankoddy using Minitab, version 17.

## RESULTS AND DISCUSSION

Altogether 50 species of waterbirds belonging to 15 families were recorded in the study area, of which 47 species were recorded in Thadduvankoddy which 35 species recorded in Pallai. Out of the 50 bird species recorded, 32 species were shared between the two sites, 15 species were recorded only in Thadduvankoddy while three were recorded only in Pallai.

According to Shannon Wiener diversity Index, a higher waterbird diversity was recorded in Pallai compared to Thadduvankoddy (Table. 01). Shannon Evenness was higher in Pallai compared to Thadduvankoddy. Thadduvankoddy was dominated by Eurasian Wigeon, *Anas penelope* (1682 individuals) and Greater flamingoes, *Phoenicopterus ruber* (1567 individuals). However, Species richness and Margalef's Richness Index were higher in Thadduvankoddy compared to Pallai (Table 01). That might be due to habitat heterogeneity and availability of food in Thadduvankoddy. In general, wetland birds are heterogeneous in their feeding habits [1]. Birds might be displaced into less favourable feeding areas due to the development of windfarm [24].

Table 01: Comparison of species richness and diversity indices in two study sites

	Pallai	Thadduvankoddy
Species Richness	35	47
Shannon diversity index	2.41	2.13
Shannon Evenness Index	0.68	0.55
Inverse Simpson Index	5.27	4.77
Margalef's Richness Index	5.11	5.38
Berger Parker Index	0.39	0.32

Of all, family Scolopacidae was dominated with nine waterbird species, representing 47.61 % of percent occurrence in Pallai and Thadduvankoddy was dominated by Anatidae with five waterbird species, representing 43.88 % of percent occurrence. Thadduvankoddy is an excellent place to observe Greater Flamingo (*Phoenicopterus ruber*) and Migratory ducks such as Northern Pintail (*Anas acuta*), Eurasian Wigeon (*Anas penelope*), Northern Shoveller (*Anas clypeata*) and Garganey (*Anas querquedula*) during the migratory season.

Table 02: Status of families of waterbirds recorded in Pallai and Thadduvankoddy

Sr. No.	Family Name	No of Spec	Percent occurrence	Percent occurrence Thadduvank
---------	-------------	------------	--------------------	-------------------------------

		ies	Pallai	oddy	and 6 represent Blocks 01, 02, 03 in Pallai and Blocks 04, 05 and 06 in Thadduvankoddy respectively).
01	Podicipedidae	01	0.78	0	
02	Pelicanidae	01	1.55	0.27	
03	Phalacrocoracidae	02	1.42	6.16	
04	Anhingidae	01	0	0.15	Table 03: Checklist of waterbird species recorded in the study
05	Ardeidae	09	8.54	1.85	
06	Ciconiidae	02	0.13	0.10	
07	Threskiornithidae	03	2.07	1.37	
08	Phoenicopteridae	01	15.52	30.19	
09	Anatidae	05	1.68	43.88	
10	Rallidae	04	0	0.06	
11	Recurvirostridae	01	1.94	3.06	
12	Burhinidae	01	0.78	0.06	
13	Charadriidae	07	14.75	3.02	
14	Scolopacidae	09	47.61	6.67	
15	Laridae	02	4.01	3.01	

When Euclidean distance based on the abundance of waterbirds is considered, sampling sites, Block 04 in Thadduvankoddy was distinct from other sampling sites (Fig. 03) due to the presence of unique species with relatively high abundance. This site was dominated by Family Anatidae and Phoenicopteridae. This Block in Thadduvankoddy is close to Chundikulam Bird sanctuary, (around 24 km), in the Northern Province, Sri Lanka. It seems that is an excellent place for bird watching during migratory season. Further studies are important to confirm this observation in Thadduvankoddy in the Northern Province. Other two blocks in Thadduvankoddy were clustered together due to the habitat homogeneity near the causeway. However, Block 05 was dominated by family Anatidae while Block 06 was dominated by Family Phalacrocoracidae. Block 01 was distinct from Block 02 and 03 in Pallai at about 20.83 % level of similarity due to the presence of unique shorebird species in the other side of the turbines near the shoreline. However, Block 02 and 03 show similarity at about 57.99 % due to habitat homogeneity near wind turbines.

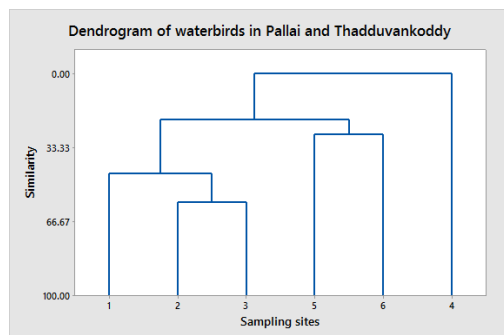


Figure 03: Dendrogram of the Euclidean distance showing similarity among three blocks in Pallai site and three blocks in Thadduvankoddy, based on the abundance of waterbird communities in each foraging guild. (In the Figure, Numbers, 1, 2 3, 4, 5

Family name	Common Name	Scientific Name	Guild
Podicipedidae	Little Grebe	<i>Tachybaptus ruficollis</i>	4
Pelicanidae	Spot-billed Pelican	<i>Pelecanus philippensis</i>	3
Phalacrocoracidae	Indian Cormorant	<i>Phalacrocorax fuscicollis</i>	4
Phalacrocoracidae	Little Cormorant	<i>Phalacrocorax niger</i>	4
Anhingidae	Oriental Darter	<i>Anhinga melanogaster</i>	4
Ardeidae	Grey Heron	<i>Ardea cinerea</i>	2
Ardeidae	Purple Heron	<i>Ardea purpurea</i>	2
Ardeidae	Great Egret	<i>Casmerodius albus</i>	2
Ardeidae	Intermediate Egret	<i>Mesophoyx intermedia</i>	2
Ardeidae	Little Egret	<i>Egretta garzetta</i>	2
Ardeidae	Cattle Egret	<i>Bubulcus coromandus</i>	2
Ardeidae	Indian Pond Heron	<i>Ardeola grayii</i>	2
Ardeidae	Striated Heron	<i>Butorides striatus</i>	2
Ardeidae	Yellow Bittern	<i>Ixobrychus sinensis</i>	2
Ciconiidae	Painted Stork	<i>Mycteria leucocephala</i>	6
Ciconiidae	Asian Openbill	<i>Anastomus oscitans</i>	6
Threskiornithidae	Black-headed Ibis	<i>Threskiornis melanocephalus</i>	6
Threskiornithidae	Glossy Ibis	<i>Plegadis falcinellus</i>	6
Threskiornithidae	Eurasian Spoonbill	<i>Platalea leucorodia</i>	6
Phoenicopteridae	Greater Flamingo	<i>Phoenicopterus ruber</i>	6
Anatidae	Lesser Whistling Duck	<i>Dendrocygna javanica</i>	1
Anatidae	Eurasian Wigeon	<i>Anas penelope</i>	1
Anatidae	Northern Shoveller	<i>Anas clypeata</i>	1
Anatidae	Northern	<i>Anas acuta</i>	1

Anatidae	Pintail Garganey	<i>Anas querquedula</i>	1
Rallidae	White-breasted Waterhen	<i>Amaurornis phoenicurus</i>	5
Rallidae	Purple Swamphen	<i>Porphyrio porphyrio</i>	5
Rallidae	Common coot	<i>Fulica atra</i>	5
Rallidae	Common Moorhen	<i>Gallinula chloropus</i>	5
Recurvirostridae	Black-winged Stilt	<i>Himantopus himantopus</i>	10c
Burhinidae	Great Thick-knee	<i>Esacus recurvirostris</i>	10a
Charadriidae	Yellow-wattled Lapwing	<i>Vanellus malabaricus</i>	10a
Charadriidae	Red-wattled Lapwing	<i>Vanellus indicus</i>	10a
Charadriidae	Pacific Golden Plover	<i>Pluvialis fulva</i>	10a
Charadriidae	Common Ringed Plover	<i>Charadrius hiaticula</i>	10a
Charadriidae	Kentish Plover	<i>Charadrius alexandrinus</i>	10a
Charadriidae	Mongolian Plover	<i>Charadrius mongolus</i>	10a
Scolopacidae	Black-tailed Godwit	<i>Limosa limosa</i>	10b
Scolopacidae	Whimbrel	<i>Numenius phaeopus phaeopus</i>	10a
Scolopacidae	Eurasian Curlew	<i>Numenius arquata</i>	10b
Scolopacidae	Common Redshank	<i>Tringa tetanus</i>	10a
Scolopacidae	Common Greenshank	<i>Tringa nebularia</i>	10c
Scolopacidae	Marsh Sandpiper	<i>Tringa stagnatilis</i>	10c
Scolopacidae	Wood Sandpiper	<i>Tringa glareola</i>	10a
Scolopacidae	Common Sandpiper	<i>Actitis hypoleucos</i>	10a
Scolopacidae	Little Stint	<i>Calidris minuta</i>	10b
Laridae	Great Black-headed Gull	<i>Larus ichthyaetus</i>	8
Laridae	Brown-	<i>Larus</i>	8

Laridae	headed Gull	<i>brunnicephalus</i>	
Laridae	Whiskered Tern	<i>Chlidonias hybridus</i>	7
Laridae	Gull-billed Tern	<i>Gelochelidon nilotica</i>	7
Laridae	Caspian Tern	<i>Hydroprogne caspia</i>	7
Laridae	Little Tern	<i>Sterna albifrons</i>	7
Laridae	White-winged Tern	<i>Chlidonias leucopterus</i>	7
Laridae	Lesser-Crested Tern	<i>Thalasseus bengalensis</i>	7

## CONCLUSION

It can be concluded Thadduvankoddy is an excellent place for the development of bird-related tourism in the Northern Province, Sri Lanka due to the presence of large number of migrant bird species while Pallai wind farm has comparatively lower abundance and diversity of waterbirds might be due to the impact of noise and motion of the wind turbines.

## RECOMMENDATION

Further studies are needed to know about the temporal variation and the ecological requirements of waterbirds in both study sites.

## ACKNOWLEDGEMENTS

Financial assistance provided by the University Grants Commission (Grant No. UGC/DRIC/PG/2015(iii)/UJA/01) to carryout this study is gratefully acknowledged. And we like to thank Mr. A. Sumanapala and Mr. H. Jayasinghe for field survey and identification of vegetation and Miss. N. Mohanachandran for her support during field survey.

## REFERENCES

- [1] Ali S., and Ripley SD. Handbook of the birds of India and Pakistan. Compact edition. Delhi: Oxford University Press, 1983.
- [2] Bellio M, Kingsford RT, Alteration of wetland hydrology in coastal lagoons: Implications for shorebird conservation and wetland restoration at a Ramsar site in Sri Lanka. *ELSEVIER*, 167, 2013, pp. 57-68.
- [03] Bellio MG, Kinsford RT, Kotagama SW, The importance of artificial habitats to migratory waterbirds within a natural/artificial wetland mosaic, Yellow River Delta, China. *ELSEVIER*, 146, 2009, pp. 3076-3085.

- [04] Delany S, Guidance on waterbird monitoring methodology: Field protocol for waterbird counting . *Wetlands International Black Sea programme*, 2011, pp. 64 .
- [05] Gregory RD, Vorisek P, Noble DG, Van Strien A, Klvaova A, Eaton M, Meyling AWG, Joys A., Foppen, RPB, Burfield IJ, The generation and use of bird population indicators in Europe. *Bird Conservation International*, 18, 2008, pp. S223–S244.
- [06] Henry GM, A Guide to the Birds of Sri Lanka. Third edition, revised by T W Hoffmann, D Warakagoda & U Ekanayake. KVG de Silva and Sons (Kandy) & *Oxford University Press*, 1998.
- [07] Grimmett R, Inskipp T, Birds of the Indian Subcontinent. Christopher Helm (Publishers) Ltd, London, 1998.
- [08] Harrison J, A Field Guide to the Birds of Sri Lanka. *Oxford University Press*, 1999.
- [09] Hettiarachchi K, Perera M, Stiff winds hit Mannar Island wind turbine project. *Sunday Times*, October, 02, 2016.
- [10] Kandasamy G, Wijesundara C, Sivaruban A, Comparison of avifaunal diversity in different habitats in the Jaffna Peninsula. *Peradeniya University Research Proceedings*, 2016, pp. 362.
- [11] Kandasamy G, Weerakoon DK, Sivaruban A, Spatial variation of water birds in Kapputhu and Nagarkovil in the Jaffna Peninsula. *40 Years of Bird Research – Field Ornithology Group of Sri Lanka, FOGSL symposium, Faculty of Science, University of Colombo*, 2017.
- [12] Kotagama SW, De Silva RI, Wijayasinha AS, Abeygunawardane V, Avifaunal List of Sri Lanka. *The Fauna of Sri Lanka*, 2006, pp. 164-203.
- [13] Kotagama SW, De Silva RI, The Taxonomy and Status of Offshore Birds (Seabirds) of Sri Lanka: *The Fauna of Sri Lanka*, 2006, pp. 288-293.
- [14] Kotagama S, Ratnavira G, *An Illustrated Guide to the Birds of Sri Lanka. Field Ornithology Group of Sri Lanka*, 2010.
- [15] Langston RHW, Pullan JD, Windfarms and birds: an analysis of the effects of wind farms on birds, and guidance on environmental assessment criteria and site selection issues. *BirdLife International to the Council of Europe, UK*, 2003, pp. 1-58.
- [16] Li ZWD, Mundkur T, Monitoring waterbirds in the Asia-Pacific region. Waterbirds around the world. Eds. G.C. Boere, C.A. Galbraith & D.A. Stroud. *The Stationery Office, Edinburgh, UK*, 2006, pp. 339-342.
- [17] Li D, Chen S, Lloyd H, Zhu S, Shan K, Zhang Z, The importance of artificial habitats to migratory waterbirds within a natural/artificial wetland mosaic, Yellow River Delta, China. *Bird Conservation International*, 23, 2013, pp. 184-198.
- [18] Marques AT, Batalha H, Rodrigues S, Costa H, Pereira MJR, Fonseca C, Mascarenhas M, Bernardino J, Understanding bird collisions at wind farms: An updated review on the causes and possible mitigation strategies. *ELSWIER*, 2014, pp. 40-52.
- [19] Ntiamoa-Baidu Y, Piersma T, Wiersma P, Poot M, Battley P, Gordon C, Water depth selection, daily feeding routines and diets of waterbirds in coastal lagoons in Ghana. *Ibis*, 140(1), 1998, pp. 89-103.
- [20] Powlesland RG, Impact of windfarms on birds: A Review. Publishing team, Department of Conservation, New Zealand, 2009, pp. 1-49.
- [21] Rajkumar P, Wijesundara C, Preliminary observations on migratory birds of the Island of Mandaitivu, Jaffna, Sri Lanka. *Proceedings of the Peradeniya Univ. International Research Sessions, Sri Lanka, Vol. 18*, 2014, pp. 30.
- [22] Rajpar MN, Zakaria M, Bird abundance and its relationship with microclimate and habitat variables in open area and shrub habitats in Selangor, Peninsular Malaysia. *The Journal of Animal and Plant Sciences* 25 (1), 2015, pp. 114-124.
- [23] Silva EIL, Katupotha J, Amarasinghe O, Manthirithilake H, Ariyaratna R, Lagoons of Sri Lanka: from the origins to the present. Colombo, Sri Lanka: International Water Management Institute, 2013, pp. 122.
- [24] Stillman RA, West AD, Caldow RWG, Dit Durell SEA, Le V, Predicting the effect of disturbance on coastal birds. *Ibis*, 149 (Suppl. 1), 2007, pp. 73–81.
- [25] Tavares DC, Guadagnin DL, Moura F, Siciliano S, Merico A, Environmental and anthropogenic factors structuring waterbird habitats of tropical coastal lagoons: Implications for management. *ELSVIER*, 2015, pp. 12-21.
- [26] Warakagoda D, Sirivardana U, Status of Waterfowl in Sri Lanka. *The Fauna of Sri Lanka*, 2006, pp. 204-215.
- [27] Weerakoon DK, Gunaeardena K, The Taxonomy and conservation status of Birds in Sri Lanka. In: The National Red List 2012 of Sri Lanka; Conservation Status of the Fauna and Flora. Weerakoon, D.K. & S. Wijesundara Eds., Ministry of Environment, Colombo, Sri Lanka, 2012, pp. 114-133.
- [28] Gunatillake N, Pethiyagoda R, Gunatillake S, Biodiversity of Sri Lanka. *Journal of National Science Foundation*, 36, 2008, pp. 25-62.
- [29] Wijesundara CS, Chathuranga D, Hettiarachchi T, Perera N, Rajkumar P, Wanniarachchi S, Weerakoon G, Avifaunal diversity in Vallai and Thondamanaru areas in Jaffna: Potential for Ecotourism. *Proceedings of the Peradeniya University International Research Sessions, vol, 19*, 2015, pp. 302.
- [30] www. Renewgen.lk, Jan, 2017.

## FACTORS RELATED TO SELF-CARE ABILITY AMONG ELDERLY WOMEN IN SEMI-URBAN COMMUNITIES, KHON KAEN, THAILAND.

Kanchana Nimsuntorn<sup>1</sup>, Piyathida Kuhirunyaratn<sup>2</sup> and Kanaporn Tansriprasiri<sup>3</sup>

<sup>1,2</sup> Faculty of Medicine, Khon Kaen University, Thailand

<sup>3</sup> Kanchanabhishek Institute of Medical and Public Health Technology, Nonthaburi, Thailand

### ABSTRACT

This research study aims to describe factors related to self-care ability among elderly women in semi-urban communities around Khon Kaen, Thailand. A cross-sectional study was conducted on individuals elderly woman who were over 60 years old in the Banped Municipality of Khon Kaen, Thailand. The total of elderly woman 268 valid questionnaires were received from 317 participants who were recruited by a simple random sampling method. Study measurements or interview questionnaire constructs included self-care ability, demographics, chronic disease, health status and mental health. Descriptive statistics i.e., frequency, percentage, mean, standard deviation (S.D.), median and inter quartile range (IQR) were conducted to describe initial results. Furthermore, inferential statistics for bivariate analysis: chi-square, odds ratio and multivariate analysis using multiple logistic regression were performed. The self-care ability level of all individual participants was assessed by Self-care Ability Scale for the Elderly (SASE). The individual's mental health level was assessed by Thai Geriatric Depression Scale-15 (TGDS-15). After analyzing the results with the SASE, 166 elders were found to have a high level of self-care ability while 102 elders had the low level of self-care ability. Self-care ability was found to be highly associated with demographics, chronic disease, health status and mental health. Factors that were statistically proven to be related to a high level of self-care ability included age, chronic disease, perceived health status and mental health: depression ( $p$ -values  $< 0.05$ ).

*Keywords: Factors, Self-care ability scale for the elderly, Elderly women, Semi-urban communities*

### INTRODUCTION

Global aging situation is arisen. The number of world population aged 65 and older is projected to grow from an approximately 524 million in 2010 to nearly 1.5 billion in 2050, with most of the increment in developing countries [1]. In Asia, over the next 30-year period, this number will increase very fast. For instance, the proportion of Chinese aged 60 and over is estimated to be sharply increased from 12.4 to 28.1 percent [2].

Thailand has a faster growing aged population rate than other countries in South East Asia. As the growing rate of Thai elders rapidly increase, Thai society is rapidly becoming an aging society. The proportion of elderly in Thailand has risen from 10.5% in 2005 to 11.2% in 2009 and will be close to 30% in 2050. Additionally, Thailand's oldest aged population group ( $> 80$  years old) will sharply increase from approximately 12.7 percent to almost 20 percent in 20 [3].

This rapid aging population is changing the social structure from socio-economic and health status to the labor force, the employment sector and the dependency of the senior population on the working age group due to the social condition change and decreased family size [4].

Several studies found that the growing rate of elder population could become both social and public health problems. Almost half of the elders had an insufficient income and only two third of

them were a health status in a moderate level. The most common disorders were back pain, rheumatoid arthritis, high blood pressure, gastritis and heart disease. Furthermore, these health problems resulted in the lower income of these elders. Specifically, most of these elders had to live alone or apart from their couple due to this lower income [5].

Many people in Thai society consider those who enter their aging period to have a poor health or to be commonly ill with a little contribution to their community and should not work. This tends to be a result from a Buddhism-based belief about gratitude, particularly for parents, grandparents including elder family members. In other words, descendants have to take care of older people in their family. With this ideology, even some elders who have an ability to take care of themselves expect their descendants to take care of them in order to avoid the criticism from the society. This lack of support for self care may be a major cause of self-care ability declining in some elders.

There are few studies focus on self-care ability in elderly. The study found that studying abroad is mainly a study of Self-care ability among home-dwelling older people.[6] Self - care ability Scale for the elderly (SASE) [7] In international the level of self - care ability was categorized by group of age 65 – 74 years equal 73.89 75- 84 years equal 66.55 85 years above equal [8] and a mean SASE score of 78.[9] Those who had higher self-care ability had a mean SASE score of 77.8 and those who had lower

self-care ability had a mean SASE score of 57.4.[10]

In Thailand not found a study about increasing Self-care ability in elderly. Unable to assess self-care ability. Therefore this study than to identify level of the SASE and factor related among community elderly. In addition most of study show only self-care behavior [11]. There is no study self-care assessment. For that reason. A study was conducted to assess the self-care ability of the elderly among the elderly women. This reason show the elderly should have self-care ability.

## OBJECTIVE

The aim of this study was to describe factors related to self-care ability among elderly women in semi-urban communities of Khon Kaen, Thailand.

## METHODS

### Design

A cross-sectional study was conducted on individuals who were over 60 year-old in Banped Municipality of Khon Kaen, Thailand.

### Population and Sample size

The total number of elder women in target population from all twenty-three villages was 3000 people. A simple random sampling method was used to select 350 elder women who registered for healthcare at Banped Health Promoting Hospital were from the four villages of the twenty-three villages under the supervision of Banped Municipality; Moo 1, Moo 2, Moo 3, and Moo 18 in 2014 to be a research participant. Sample size of elder women calculate by WinPepi. Assumed proportion = 0.79 [10]. Required sample size 317 (Inflate to compensate for a loss of 15% of subject). Response rate was  $268/317 = 84.50\%$ . Total of sample size was 268 elder women.

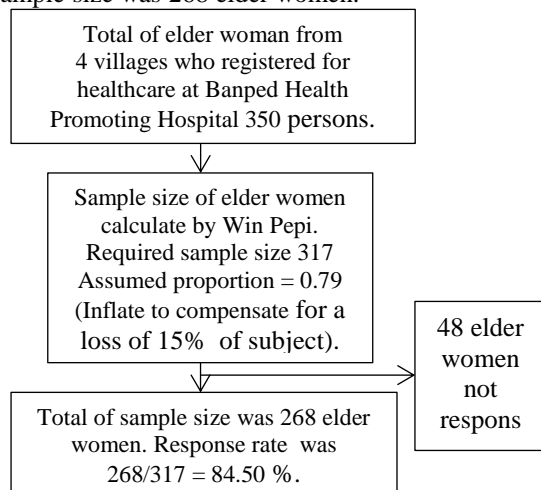


Fig. 1 Sample size Diagram.

## Research instrument

Study measurements or interview questionnaire constructs included self-care ability, demographics, chronic disease, health status and mental health. The self-care ability level of all individual participants was assessed by Self-care Ability Scale for the Elderly (SASE) [6]. Whereas the individual's mental health level was assessed by Thai Geriatric Depression Scale-15 (TGDS-15).

## Data collection

Data were collected by trained interviewers between February and March, 2015. Face-to-face interviews were conducted in a comfortable environment for each individual participant, mostly at their home.

## Data analysis

After collecting the data, all forms and data were checked for completeness. All data was entered twice and validated in EPI INFO for DOS before transferring in to SPSS application for Windows as a preparation for data analysis. Data were analyzed through using SPSS version 19 (IBM Corp. Released 2010. IBM SPSS for Windows version 19.0. Armon, NY:IBM Corp. Under Liciensed by Khon Kaen University). Descriptive statistics i.e., frequency, percentage, mean, standard deviation (S.D.), median and inter quartile range (IQR) were conducted to describe initial results. Furthermore, inferential statistics for bivariate analysis: chi-square, odds ratio and multivariate analysis using multiple logistic regression were performed. Only a probability ( $p$ -value) less than 0.05 was considered to be a statistically significant.

## Ethical issues

An ethical approval for this study was issued by Khon Kaen University, Thailand. Participants gave a written consent prior to their participation in the study.

## RESULTS

### Study sample

The study sample included 268 elder women ( $n = 268$ ), ranging in age between 60 and 95 years old, with a median age of 67 years old.

### Demographic characteristics

This study response rate was 84.50 %. A median age of participants was 67 years old ( $IQR \pm 11$ ). The highest education of most participants was



a primary school. The majorities of participants were widows (48.9%) and married (42.9%). Most participants worked, had a caregiver, stayed connected with close friend(s) and joined religious activities. More than half of participants received home visits.(As shown in Table1)

Table 1 Demographic characteristics of the sample.

Characteristics	(n= 268)	Percentages (100)
Age		
60 – 69	157	58.6
70 – 79	80	29.9
80 above	31	11.6
Median	67	
IQR	11	
Max – Min	95 - 60	
Education	1	0.4
Bachelor	1	0.4
Secondary school	10	3.7
Primary school	264	91.8
No school	6	2.2
Marital status		
Single	22	8.2
Married	115	42.9
Widow	131	48.9
Working		
Yes	196	73.1
No	72	26.9
Caregiver		
Yes	223	83.2
No	45	16.8
Close friend		
Yes	233	86.9
No	35	13.1
Joined religious activities		
Yes	223	83.2
No	45	16.8
Home visits		
Yes	153	57.1
No	115	42.9

### Self-care ability

After measuring the self-care ability of participants using a SASE, the results indicated that an average score of the total 268 study participants was 72.4 points (S.D. = 10.9). When dividing the participants into two groups, this study showed that

102 participants (38.10%) had a low level of self-care ability and 166 (61.90%) had a high level of self-care ability. The low-level self-care ability group (with scores ranged from 50 to 85 points) had a statistically significant relationship with more advanced age participants. (As shown in Table 2)

Table 2 Proportion of SASE among the elderly

SASE	(n = 268)	Percentages (100)	95%CI
Low level	102	38.10	
High level	166	61.90	70.50- 73.64
Mean score = 71.82		SD = 10.94	

### Self-care ability and health-related variables

Results showed that self-care ability levels were related to many health variables i.e., Age 70-79 y.o., Age 80 y.o. and above, Marital status, Having caregiver, Living arrangement, Having close friend, Joining religious activities, Received home visits, Having professional care, Perceived good health, Perceived poor health, Having chronic disease, Had a fall (in the last 6 months), Time Up & Go (TUG) test, and Thai Geriatric Depression (TGD) test (suspected depression). (As shown in Table 3)

Table 3 Factors related to SASE

Factors related SASE	Higher SASE Scores > 69 (n = 102)	Low SASE Scores ≤ 69 (n = 166)	P
Age			
60-69	46(45.1)	111(66.9)	
70-79	38(37.3)	42(25.3)	0.006
80 above	18(17.6)	13(7.8)	0.002
Education			
In school	101(99.0)	161(97.0)	0.280
No school	1(1.0)	5(3.0)	
Marital status			
Single	67(65.7)	86 (51.8)	0.026
Married	35(34.3)	80(48.2)	
Working			
Yes	31(30.4)	41(24.7)	0.307
No	71(69.6)	125(75.3)	
Caregiver			
Yes	70(68.6)	153(92.2)	<0.01
No	32(31.4)	13(7.8)	
Living arrangement			
Yes	66(64.7)	153(92.2)	<0.01

Factors related SASE	Higher SASE Scores > 69 (n = 102)	Low SASE Scores ≤ 69 (n = 166)	P
No	36(35.3)	13(7.8)	
Close friend			
Yes	75(73.5)	158(95.2)	<0.01
No	27(26.5)	8(4.8)	
Joined religious activities			
Yes	76(74.5)	147(88.6)	0.003
No	26(25.5)	19(11.4)	
Home visit			
Yes	68(66.7)	85(51.2)	0.013
No	34(33.3)	81(48.8)	
Professional care			
Yes	45(44.1)	155(93.4)	<0.01
No	57(55.9)	11(6.6)	
Exercise adequate			
Yes	80 (78.4)	126 (75.9)	0.634
No	22 (21.6)	40 (24.1)	
Smoking			
Yes	3 (2.9)	4 (2.4)	0.791
No	99(97.1)	162(97.6)	
Perceive good health			
Good	50 (49.0)	95 (57.2)	
Moderate	42(41.2)	66 (39.8)	0.470
Poor	10(9.8)	5(3.0)	0.014
Chronic disease			
Yes	88 (86.3)	29 (17.5)	<0.01
No	14 (13.7)	137 (82.5)	
Fall (last 6 months)			
Yes	38(37.3)	28(16.9)	<0.01
No	64(62.7)	138(83.1)	
TUG			
Yes	91(89.2)	74(44.6)	<0.01
No	11(10.8)	92(55.4)	
TGDs			
Normal	26 (25.5)	161(97.0)	
Suspect	65 (63.7)	4 (2.4)	<0.01
Depress	11(10.8)	1(0.6)	<0.01

### Predictors for self-care ability

Among several health variables, five predictors emerged in this study's logistic regression equation. These five predictors included Age 70-79 y.o., Having chronic diseases, and Thai Geriatric Depression (TGD) test (suspected depression). (As shown in Table 4)

Table 4 Summary of multiple regression analyses for variables predicting SASE

Variable	P	COR	AOR	95%CI
Age				
70-79	0.03	0.46	0.42	0.20 - 0.93
Chronic disease	<0.01	0.03	0.04	0.02 - 0.09
TGDs				
Suspect	<0.01	0.01	0.01	0.00 - 0.03
Depression	0.01	0.01	0.01	0.00 - 0.18

The summarize of this result shows people in North East Thailand appreciate and interest in elderly care. The average score of the sample regarding self-care was high level, which shows that the woman people at average age of 67 years are capable to take care of their selves. There was predictors for self-care ability included Age 70-79 y.o., Having chronic diseases, and Thai Geriatric Depression (TGD) test (suspected depression).

### DISCUSSION

This research study aimed to describe factors related to self-care ability among elderly women in semi-urban communities. The outcome of the demographic data study confirmed the results of previous researches in Khon Kaen study [18] which shows that the main caregiver of the older people sample was a higher number than that of three ago. This result shows people in North East Thailand appreciate and interest in elderly care.

The results of the factors related to self-care ability among elderly women program in the villages, similarly to several studies. An SASE average score of this study's participants who resided in Khon Kean's semi-urban communities was in a high level which indicated that the participants, in general, manage well in performing self-care ability and relate to age average 67 years and exclude criteria older people with an acute or current medical or being confused and unable to provide information. This result was close to previous study Self-care ability among home dwelling older people in Norway people.[10][9] This corresponds with a study regarding self-care

behaviors of Thai elders that showed most elders perceived their own health status in a high level as a result from a decade of Thailand's health promotion policies under the healthcare reform following the enactment of the 2002 National Health Security Act and the 2003 National Senior Act [12].

This comparable result also appeared in among the seniors in the other country who used the same SASE instrument to assess elder self-care ability, Norway. In Norway, an average high level of self-care ability was 83.3% while an average low level of self-care ability was 16.7% with an overall average score of 78.2 points which was comparable with an overall average score of 78.4 points of the Banped Municipality's elders. The slight differences between these numbers may result from different demographic characteristics e.g., average life expectancy and a higher chronic illness rate of developed countries [13]. Additionally, Norwegian elders were received a regular health promotion that they could practically apply to their lifestyle. The same study showed that Norwegian 65 y.o. and above elders had enhanced their learning skills and appropriately adapted their lifestyle to be in harmony with their surrounding environment and social conditions.

Although Thai elders yielded a comparable result in terms of an overall average score, a high-level self-care ability proportion representing by the SASE scores of Thai elders was less than the same proportion of Norwegian elders. This lower proportion reveals that Thailand still has difficulties in enhancing senior learning ability to diminish the rising healthcare costs and challenges of aging population who tends to be a burden for their family. Therefore the development of a model for enhancing senior learning skills for increasing self-care ability is needed for Thai senior citizens.

Factors related to enhancing self-care ability in the over seventy years old group had a higher statistically effect as an obstacle for enhancing self-care ability than the same effect in the 60-70 years old group (OR= 0.42, 95% CI = 7 – 80,  $p$ -value < 0.05). This result can be interpreted as this higher age affects elder deteriorate body and lessening elder capacity during the progression of their aging process [14]. This supposition corresponds with the other two studies in 2001 and 2003 [15], [16]. Additionally, the self-care ability of elders is gradually decreased by emergent age numbers. Therefore, aging is a statistically significant impediment factor in maintaining self-care ability (OR = 0.946, 95% CI = 0.901– 0.993 in 2012[13] and  $R^2$  = 0.18,  $p$ -value < 0.001 in 2001 [16].

For elders with chronic diseases, having chronic diseases was a higher impediment factor for maintaining their self-care ability than those without chronic diseases (OR = 0.04, 95% CI = 0.02 – 0.09

,  $p$ -value < 0.001). This result was influenced by the lack of self-confidence in their own health from anxiety caused by physical illnesses and possible disease complications. As a result, these elders tend to overlook or lessen their own healthcare. Together with their dementia or partially skipping medications, elders with chronic diseases are more likely to have their illnesses worsening or developing into more complications and become more dependent on their caregiver than healthy elders. This corresponded with a study in 2009 which indicated that individuals in a good health who has no inherited disorders or chronic diseases are likely to have a high level of self-care ability ( $R^2$  = 0.356,  $p$ -value < 0.001) [17].

Furthermore, the results also showed that statistically depression was the worse significant impediment factor for elders with chronic diseases than for those without any (OR= 0.01, 95% CI= 0.00 - 0.03,  $p$ -value < 0.001). This corresponded with the other two studies in China and Sweden which concluded that depression caused by isolation was an impediment factor in maintain a proper self-care ability ( $r$  = -0.299,  $p$ -value < 0.001 in 2009 [17]. and  $R^2$  = 0.25,  $p$ -value < 0.001 in 2000) [8]. In other words, the loss of the loved one might be a significant cause of sorrow, self isolation, lack of social interaction, resulting in separation anxiety and depression and ultimately diminished self-care ability of individual elders.

## CONCLUSION

The findings of the study show that age, chronic disease, perceived health status and mental health i.e., depression had a greater impact on female elder self-care ability. Therefore more public awareness such as culturally appropriate policies and programs is needed to support senior women in coping with their challenges. Policies and programs should focus on preventing chronic diseases in this age group and address the methods for increasing self-care ability. In communities for basic information on health promotion. Strengthen and empowering the elderly to self-reliance. To reduce the cost of health care and reduce the burden of reliance on others. In addition control this factor can certainly economically reduce the medication cost of the country.

## ACKNOWLEDGEMENTS

We wish to acknowledge Ole and Ulrika Soderhamn, Professors at the Faculty of Health and Sport Sciences, University of Agder, Grimstad, Norway for a permission to use the SASE scale and the Faculty of Medicine, Khon Kean University for their financial support. We would like to thank Banped Health Promoting Hospital's staff members

and participants for their excellent support and cooperation.

## REFERENCES

- [1] United Nations. World population ageing 2013. [2013 Jan 14]. Available from: <http://www.un.org/en/development/desa/population/publications/pdf/ageing/WorldPopulationAgeing2013.pdf>.
- [2] X Zhu. Population Aging and Economic Growth. United Nations. . [2013 Jan 15]. Available from: [https://www.ruor.uottawa.ca/bitstream/10393/34168/1/Zhu\\_Xun\\_2015\\_researchpaper.pdf](https://www.ruor.uottawa.ca/bitstream/10393/34168/1/Zhu_Xun_2015_researchpaper.pdf)
- [3] United Nations. population age composition [2013 Jan 14]. Available from: [www.un.org/esa/population/publications/WPP2004/WPP2004\\_Vol3.../Chapter2.pdf](http://www.un.org/esa/population/publications/WPP2004/WPP2004_Vol3.../Chapter2.pdf)
- [4] National Statistical Office (NSO). (2014). The elderly population survey in Thailand 2007. Bangkok: Text and Journal Publication Co.,Ltd.
- [5] Vipap Prachuapmao. Health Promotion with the International Year of the Elderly in 1999. College of Population Studies Chulalongkorn University. (1999).
- [6] Soderhamn O, Ek, A.-C., Porn, I. The self-care ability scale for the elderly. *Scand J Occup Ther*, 1996, 3, pp. 69-78.
- [7] Soderhamn, O., Lindencrona, C., & Ek, A.-C. Validity of two self-care instruments for the elderly. *Scand. J. Occup. Ther.*, 1996. 3, 172–179.
- [8] Soderhamn O, Lindencrona C, Ek AC. Ability for self-care among home dwelling elderly people in a health district in Sweden. *International Journal of Nursing Studies*, 2000, pp. 361-368.
- [9] Sundsli, K., Söderhamn, U., Espnes, G. A., & Soderhamn, O. Ability for self-care in Urban living older people in southern Norway. *J Multidiscip Healthc*, 2012. 5, 85-95.
- [10] Bjorg Dale, Ulrika Soderhamn and Olle Soderhamn. Self-care ability among home-dwelling older people in rural areas in Southern Norway. *Scand J Caring Sci.*, 2012 26, pp. 113- 122.
- [11] Klainin, P., & Ounnapirok, L. A meta-analysis of self-care behavior research on elders in Thailand: an update. *Nurs Sci Q*, 2010, 23(2), pp. 156-163.
- [12] Jittapunkul, S., Wivatvanit, W. Panyacheewin, J., & Kangkanpanich, P.(2003).OlderPopulation and Health System: A profile of Thailand In World Health Organization (Ed.), *Developing Integrated Response of Health Care Systems to Rapid Population Ageing (INTRA) Thailand Survey Report (Draft 1)* Bangkok. Thailand: World health organization. 2003.
- [13] World population ageing 1950-2050 Population Division. DESA. [2013 Feb 10]. Available from:[http://www.un/esa/population/publications/world\\_ageing\\_1950-2050](http://www.un/esa/population/publications/world_ageing_1950-2050).
- [14] Nordenfelt, L. On the nature of health. An action-theoretic approach. Second revised and enlarged edition. Kluwer Academic Publishers; 1995.
- [15] Haveman-Nies, A., de Groot, L.C.P.G.M., van Staveren, W.A. Relation of dietary quality, physical activity and smoking habits to 10-year changes in health status in older Europeans in the SENECA study. *American Journal of Public Health*, 2003, 93, pp.318-323.
- [16] Soderhamn Olle and Christina Cliffordson. The Structure of Self-Care in a Group of Elderly People. *Nurs Sci Q*, 2001, pp. 55-58.
- [17] Yu-Ling Bai, Chou-Ping Chiou and Yong-Yuan Chang. Self-care behavior and related factors in older people with Type 2 diabetes. *Journal of Clinical Nursing*, 2009, 18(23), pp. 8-15.
- [18] Kuhirunyaratn, P., Prasomrak, P., & Jindawong, B. Factors related to falls among community dwelling elderly. *Southeast Asian jTrop Med Public Health*, 2013. 44(5), 906-915.

## IMMEDIATE EFFECTS OF THAI MASSAGE ON GAIT PARAMETERS IN NORMAL ADULTS: A PILOT STUDY

Nutthanun Tatchananusorn<sup>1</sup>, Wichai Eungpinichpong<sup>2</sup>, Uraiwan Chatchawan<sup>3</sup> and Donlaya Promkaew<sup>4</sup>

<sup>1</sup>Faculty of Associated Medical Sciences, Khon Kaen University.

<sup>2</sup>Research Center of Back, Neck, Other Joints Pain and Human Performance (BNOJPH), Khon Kaen University.

<sup>3</sup>Improvement of Physical Performance and Quality of Life (IPQ) research group, Khon Kaen University.

### ABSTRACT

The purpose of this study was to determine the short-term effects of Thai massage on gait parameters including stride length, step length, step width, and gait speed, and hamstring flexibility, trunk flexibility, and hip, knee and ankle range of motion while walking in normal adults aged 19-25 years. A randomized crossover trial was used. Thirty healthy subjects (17 females and 13 males) with tightness of hamstring muscles as indicated by a straight-leg-raising (SLR) ranged between 40 to 70 degrees participated. Each of them received a session of 1-hour Thai massage and a controlled condition of 1-hour resting on a bed with a 2-day washout period. Changes in the gait and flexibility parameters were assessed before and immediately after both conditions and analyzed using paired t-test. Crossover statistical analysis was performed by independent t-test. Significant differences were found between-group comparison in hamstring flexibility (4.88°; 95% CI, -8.23 to -1.52), trunk flexibility (2.35 cm.; 95% CI, -3.45 to -1.25), step length (1.94 cm.; 95% CI, -3.47 to -0.40), and stride length (4.77 cm.; 95% CI -7.41 to -2.12) ( $p < 0.05$ ). However, no differences were found in changes of gait speed, range of motion of hip, knee, and ankle. We concluded that one session of Thai massage could provide immediate effects for improving some of the gait parameters, body flexibility and hamstring flexibility.

*Key words: Thai Massage, Gait, Walk, Flexibility, Pilot Study*

### 1

Walking is ambulatory function of activity in daily life. There are many benefits of walking. A 30-minute walking affects to improve mental health and physical health. It may increase endorphin production to easing stress, tension, anger, fatigue, and confusion and improve sleep quality and cognitive performances [1]. Walking is also one of the best choices of physical activity to decrease and prevent risks of non-communicable diseases such as diabetes, heart diseases, osteoporosis, Alzheimer disease and cancer [2].

According to the lifestyle of people nowadays, they will easily have the abnormal sign of musculoskeletal systems such as muscle tightness and decreased of flexibility, by prolonged abnormal postures [3]. Furthermore, prolonged abnormal posture may lead to decrease walking performances because of some muscle get tightness and decreased flexibility. Muscles that mostly to be activated while walking are Hamstrings, Quadriceps, Gastrocnemius, Soleus, Tibialis Anterior, Hip Flexors and Hip extensors. Therefore, if these muscles become tightness, they will decrease the flexibility and affect walking performance such as short step length, decreased step width, decreased walking speed, and abnormal posture [4].

Recently, Thai massage has become a popular treatment of massage therapy for Thai people. Some studies suggested that Thai massage help improve body

### INTRODUCTION

flexibility and range of motion that is important for walking performance. However, there is no evidence on the effects of Thai massage to walking performance in normal adults. The present study aimed to investigate the effects of Thai massage to spatiotemporal gait parameters in normal adults.

### METHOD

#### Design and setting

A crossover design study was conducted at the Department of physical therapy, Khon Kaen University, Thailand. The study was approved by the ethical committee of Khon Kaen University.

#### Participants

Healthy participants with tightness of Hamstring muscle, aged 19-25 years, were recruited through flyers posted around Khon Kaen University. These recruitment announcements called for individuals who had experienced tightness in legs to volunteer to take part in the study. Participants for inclusion in this study were selected by a physical therapist who conducted a detailed physical examination and collected baseline data. Participants must not have evidence of underlying

disease or anatomical abnormalities. (e.g. malignancy, osteoporosis, spondylolisthesis, scoliosis, herniated nucleus pulposus, and spondylosis)

## Intervention

A session of whole body of Thai Massage used as intervention in this study. The 1-hour Thai massage protocol consisted of deep pressure massage and stretch on major muscles of the body. Firstly, therapist applied gently and deep thumb pressure massage along the meridian lines that covered head, neck, back, and upper and lower extremity consequently. Thumb pressure massage was maintained at each point on the meridian lines for 5-10 seconds per point and repeated 3 times. The intensity of thumb pressure was not exceeded pressure pain threshold of participants and was adjusted by the therapist. After massage session, the therapist applied gentle stretch for those muscles including calf, hamstring and quadriceps.

## PROCEDURE

### Randomization

Thirty participants who met the above inclusion/exclusion criteria were recruited and randomly allocated into one of the two groups using block-randomized allocation with block sizes of 2 and 4. The groups were assigned using a pre-generated random assignment scheme enclosed in envelopes, which resulted in a total of 15 participants per group.

### Treatment

Participants in group A received an hour Thai massage and took a rest in supine lying position after taking Thai massage 2 days later. Whereas, participants in group B took an hour rest in supine lying position and 2 day after they took a rest, they received one-hour Thai massage. The same pre-assessments and post-assessments were conducted on both groups.

In keeping with the recommendation of Khon Kaen University's ethical committee, all gave informed consent before participation in the study.

## ASSESSMENT

Prior to and following Thai massage and control sessions, all outcome measures were assessed by one physical therapist. Details of outcome measures and assessments are described below.

### Gait parameters

Gait parameters were assessed by inkmat footprint. Outcomes consisted stride length, step length and step

width. Reliability of data obtained with footprint was found to be high ( $r = 0.92$ ) [5].

### Body flexibility

A Sit-and-reach box was used to measure body flexibility. Body flexibility was measured three times. Reliability of data obtained with sit-and-reach box is reported to be moderate ( $r = 0.46-0.67$ ) [6].

### Range of motion and gait speed

Range of motion of the hip, knee, and ankle were measured by recording the video while walking. Prior to walking, markers were placed at shoulder joint, greater trochanter, lateral epicondyle, lateral malleolus and middle phalange of the participants. Kinovea program (version 0.8.15) was used to measure both parameters.

## STATISTICAL ANALYSES

Changes in spatiotemporal parameters for both Thai massage session and control session results were analyzed by paired t-test. Crossover statistical analysis was performed by independent t-test. All statistical analyses was calculated by Stata 10 software (StataCorp LP, 4905 Lakeway Drive College station, Texas 77845, USA), assuming no carryover effects. A P-value of less than 0.05 was considered statistically significant.

## RESULTS

Thirty-five potential participants responded to flyers, or word-of-mouth; 5 were excluded after screening for eligibility. A total of 30 adults met the inclusion /exclusion criteria and were randomly assigned to the treatment group and to the control group. A flow chart of participant progression through the trial is presented in Figure.1

Table 1. demonstrates the characteristic of the study population. There were 17 females and 13 males. The mean age was  $21 \pm 1$  years. The mean weight and height was  $57 \pm 9$  kilograms and  $166.10 \pm 9.26$  centimeters respectively

Outcome measures were found to be similarly distributed in both groups at baseline (Table 2)

Step length and stride length test showed significant improvement after Thai massage session, whereas only ankle plantar flexion ROM of toe off period showed improvements in the control period. SLR test showed significant improvement after both sessions; however, Thai massage session gave better results. (Table 2)

Independent t-test showed significant differences in Step length ( $P=0.015$ ), Stride length ( $P<0.001$ ), SLR ( $P=0.006$ ) and Sit and Reach ( $P<0.001$ ) test between groups. (Table 3)

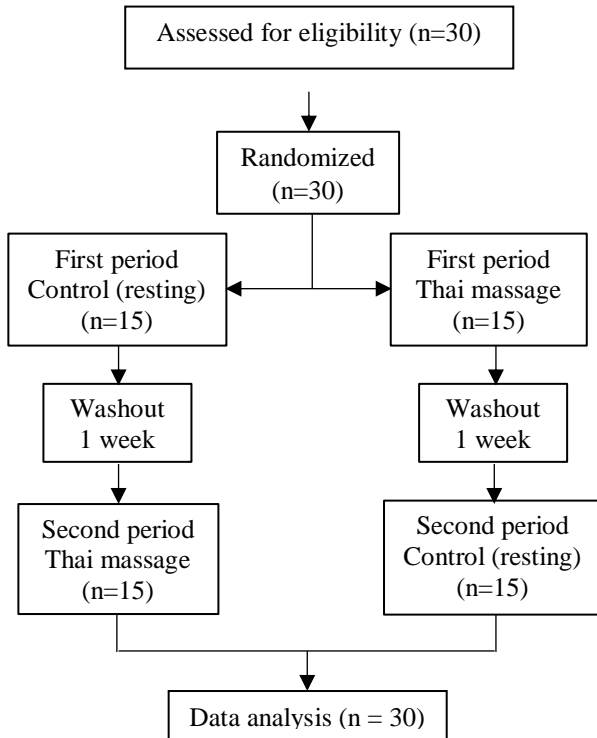


Figure 1. Diagram of study design and participants

Table 1 Characteristics of the study population

Participant Data	
Sex (Female/Male)	17/13
Age (year)	21 ± 1
Weight (kilogram)	57 ± 9
Height (centimeter)	166.10 ± 9.26

## DISCUSSION

This study showed that one session of whole body Thai massage could provide improvements on walking performance and flexibility, including step length, stride length, SLR and Sit and Reach, in normal adults with muscle tightness of hamstring muscles. Our result are consistent with previous studies reporting that Thai massage is able to improve lumbar flexibility and hamstring muscle length which tested by Sit and Reach and SLR test. This was because Thai massage, using deep pressure, followed by passive stretching, is applied along the meridian lines covers all taut bands of whole body. The potential of Thai massage are stimulation of Golgi tendon organ and send to the spinal cord. Within the spinal cord, an inhibitory interneuron will releases the neurotransmitter glycine than inhibits alpha motor neuron to inhibit stretch reflex and relieve muscle with tension, thus it affects to reduce pain, release the taut band in the tissues and help increase muscle length. This provides the muscles to have more flexibility [7], [8], [9]. Moreover, flexibility help improve step length and stride length [10].

Table 2. Evaluation of outcome measures (Mean±SD). Variables showing a significant interaction effects between groups have been signed with \*,\*\* and \*\*\* (*p*-value is 0.015, 0.006 and <0.001 respectively).

Parameters	Pre-A	Post-A	Pre-B	Post-B
Step length (cm.) *	65.51 ±5.53	65.41 ±5.45	65.34 ±5.23	67.18 ±5.17
Stride length (cm.) ***	131.41 ±10.93	130.84 ±10.50	129.89 ±9.83	134.09 ±10.29
Step width (cm.)	6.38 ±1.86	6.26 ±2.40	6.58 ±2.33	6.66 ±2.33
SLR (Degree) **	54.83 ±5.83	59.11 ±8.49	54.45 ±6.38	63.60 ±9.80
Sit and reach (cm.) ***	-1.56 ±8.73	-2.20 9.28	-1.79 ±9.32	-0.07 ±9.32
Heel strike (ROM)				
Hip Flexion (Degree)	22.66 ±2.88	22.37 ±3.17	22.50 ±3.46	23.14 ±3.87
Knee Flexion (Degree)	4.68 ±3.37	4.22 ±3.39	3.82 ±3.81	4.89 ±4.56
Ankle Plantar Flexion (Degree)	10.32 ±2.38	10.56 ±2.30	10.20 ±2.40	10.16 ±4.60
Toe off (ROM)				
Hip Flexion (Degree)	-7.57 ±3.38	-7.81 ±3.54	-8.41 ±3.03	-8.13 ±3.31
Knee Flexion (Degree)	41.62 ±4.30	41.62 ±4.26	40.44 ±3.36	41.03 ±4.17
Ankle Plantar Flexion (Degree)	24.92 ±3.48	27.09 ±4.97	24.70 ±3.47	26.01 ±3.69
Speed (m/s)	1.30 ±0.15	1.29 ±0.14	1.29 ±0.13	1.31 ±0.13

A: control session, B: Thai massage session

Table 3. Comparison of the mean change between control session and Thai massage session by independent t-test, where a significant interaction effects was found.

Parameters	Within-group difference		Between-group difference (95% CI)	<i>p</i> -value
	Control	Massage		
Step length	-0.10	1.84	-1.94 (-3.47 to -0.40)	0.015
Stride length	-0.57	4.20	-4.77 (-7.41 to -2.12)	0.001
SLR	4.28	9.16	-4.88 (-8.23 to -1.52)	0.006
Sit and Reach	-0.63	1.71	-2.35 (-3.45 to -1.25)	0.001

Although changings of range of motion while walking of hip, knee and ankle were not significant. Thai massage still provided little effects that relate to the due to Thai massage helps improve flexibility and lengthen muscle. [11], [12]. Moreover, when muscles were lengthen and reached the optimal resting length, it



could produce the maximal force and improve mobility [13].

Due to some unclear results, investigating the immediate effects could be the limitation of this study. Thus, further study should determine the effects of long-term treatment with follow-up.

## CONCLUSION

According to the results of this pilot study, we concluded that 1-hour Thai massage session may provide some improvement of spatiotemporal parameters and flexibility parameters, especially for step length, stride length, SLR and Sit-and-reach. In further study, a randomized controlled trial and a long-term treatment with follow-up are suggested. The other type of participants such as older adults also are suggested

## ACKNOWLEDGEMENT

The authors would like to thank the subjects who participated in this study. The study was supported by the Research Center of Back, Neck, Other Joint Pain and Human Performance of Khon Kaen University.

## REFERENCES

- [1] Johansson M., Hartig T. and Staats H. "Psychological benefits of walking: moderation by company and outdoor environment" *Applied Psychology: Health and Well-being*. Volume 3 No.3, 2011, pp. 261–80.
- [2] Cooper K. and Hancock C. "The Benefit of Regular Walking for Health, Wellbeing and the Environment – a review document by C3". C3 Collaborating for Health [serial online] 2012: [48 screens] Available from: <http://www.c3health.org/wp-content/uploads/2009/09/C3-report-on-walking-v-1-20120911.pdf>. Accessed June 8, 2015
- [3] DeLisa J. "Gait Analysis in the Science of Rehabilitation Industrial Biofouling". District of Columbia: Department of Veterans Affairs; 1998
- [4] Wilkinson MJ., Menz HB. "Measurement of gait parameters from footprints: a reliability study" *The Foot*. Volume 7, 1997, pp.19-23.
- [5] Mayorga-Vega D., Merino-Marban E., Viciano J. "Criterion-Related Validity of Sit-and-reach test for estimation hamstring and lumbar extensibility: a meta-analysis" *Journal of Sports Science and Medicine*. Volume 13, 2014, pp.01-14
- [6] Buttagat V., Eungpinichpong W., Chatchawan U., Kharmwan S. "The Immediate Effects of Traditional Thai Massage on Heart Rate Variability and Stress-related Parameters in Patients with Back Pain Associated with Myofascial Trigger Points" *Journal of Bodywork and Movement Therapies*. Volume 15 No.1, January 2011, pp. 15-23.
- [7] Srionla C. and Thong-iam R. "Effect of Thai Massage on Running Performance in Runner." (Thai) Thesis for Bachelor Degree of Science (Physical Therapy), Khon Kaen University. Khon Kaen: Khon Kaen University; 2003
- [8] Hongsuwan C, Eungpinichpong W, Chatchawan U, Yamauchi J. "Effects of Thai massage on physical fitness in soccer players". *Journal of Physical Therapy Science*. Volume 27 No.2, 2015, pp.505-508.
- [9] Barlow A. et al. "Effects of Massage of the Hamstring Muscle Group on Performance of the Sit and Reach Test". *British Journal of Sports Medicine*. Volume 38, 2004, pp.349-351.
- [10] Christiansen C. "The Effects of Hip and Ankle Stretching on Gait Function of Older People". *Archives of Physical Medicine and Rehabilitation* August. Volume 89, 2008 pp.1421-1428.
- [11] Zajac FE, Neptune RR, Kautz SA. "Biomechanics and muscle coordination of human walking. Part I: introduction to concepts, power transfer, dynamics and simulations". *Gait Posture*. Volume 16 No.3, Dec 2002, pp.215-32.
- [12] Brunner R, Rutz E. "Biomechanics and muscle function during gait". *Journal of Children's Orthopaedics*. Volume 7 No.5, 2013, pp.367-371.
- [13] Rassier DE, MacIntosh BR, Herzog W. "Length dependence of active force production in skeletal muscle". *Journal of Applied Physiological* (1985). Volume 86 No.5, May 1999, pp.1445-57.

## THAI MASSAGE COMBINED WITH MUSCLE ENERGY AND PASSIVE STATIC STRENGTHING TECHNIQUE COULD IMPROVE HEIGHT OF SEPAKTAKRAW SERVES

Apichat Deeminoi<sup>1</sup>, \*Dr.Wichai Eungpinichpong<sup>2</sup>, Dr.Maitree Pakarasang<sup>3</sup>, Dr.Thanarat Sripongngam<sup>4</sup>

<sup>1</sup> Exercise and Sport Sciences Program, Graduate School, Khon Kaen University, Thailand;

<sup>2</sup> Department of Physical Therapy, Faculty of Associated Medical Science, Khon Kaen University, Thailand;

<sup>3</sup> Department of clinical microbiology, Faculty of Associated Medical Science, Khon Kaen University, Thailand;

<sup>4</sup> Department of Health and Sport Science, Faculty of Education, Mahasarakham University, Thailand

### ABSTRACT

Flexibility of hamstring muscles is very important in the height of Sepaktakraw serves. The most beneficial type of stretching of lower limb muscles for this sport has not been verified. This study aimed to evaluate the effects of applied Thai massage combined with muscle energy technique (ATMMET) versus passive static stretching technique (PSST) on hamstring flexibility and the height of a Sepaktakraw serve. One hundred and eight healthy Sepaktakraw amateur athletes were randomly allocated to 3 comparison groups. Subjects in the ATMMET group and the PSST group received a 10 min session of corresponding intervention, whereas the subjects in the control group sat on a chair without intervention for the same period of time. Passive straight leg raise test (PSLR) and the height of Sepaktakraw serves were measured at 3 consecutive periods, consisting of pre-test, post-test, and 24 hour after intervention. An analysis of two-way repeated measures ANOVA found that there was a statistically significant difference in hamstring flexibility and the height of Sepaktakraw serves in both intervention groups but not in the control group. However, no significant differences were found between the three groups ( $p > 0.05$ ). We conclude that both ATMMET and PSST may improve hamstring flexibility and the height of a Sepaktakraw serve immediately.

*Keywords: Applied Thai massage, Muscle energy technique, Static stretching, Hamstring flexibility, Sepaktakraw serves*

### INTRODUCTION

Sepaktakraw is a popular sport in Southeast Asia. This sport has been competed in both the SEA Games and the Asian Games [1]. There are 5 players in each team (3 players on the court and 2 substitutes), and each player in the team has a different role, depending on their position. First, “the striker” is responsible for kick, jump kick, or head the Sepaktakraw ball over the net, to fall into the opponent’s area. Second, “the feeder” is responsible for set the Sepaktakraw ball near the net in their team’s area for the striker. Finally, “the server” has a duty to serve or kick the Sepaktakraw ball to go over the net and fall into the opponent’s area [2].

Serving skill is very important in the modern game of Sepaktakraw, as it is the main reason for attacking and scoring points. Serving with high efficiency helps to win the game easily which this requires the greatest flexibility of lower limb muscles. The main anatomical motion for the serving highest kicking consist of hip flexion, hip abduction, and knee extension [3]. In an earlier study, Rezaei et al. investigated lower limb motion in Sepaktakraw elite athletes, they found that the server players had a greater range of hip motion than did strikers and feeders [4]. In addition, the height of

the exposed balls was correlates with the Sepaktakraw serve speed [5]. Therefore, the flexibility of lower limb muscles is an important factor for increasing the efficiency of the serve.

Massage is one of the treatments used in sport medicine to increase the performance of the athlete through its mechanical, physiological, and psychological effects. Massage has been used in many cultures and has been employed in sports for a long time [6]. Techniques of massage therapy include acupressure, rubbing, friction, kneading and muscle stretching [7]. In Thailand, Traditional Thai massage (TTM) has been used for heal and relax the body since ancient times. TTM has the appearance of deep massage, with brief sustained pressure on the muscles. The TTM therapist use body weight to press down on the muscles through thumbs, palms, elbows, knees, and feet [8]. The therapist often uses feet to press on large muscles, such as the gluteus muscle group, gastrocnemius muscles, and hamstring muscles.

Moreover, muscle energy technique (MET) is another method that can be used in the treatment of shortened muscle, restricted joints, and weakened muscles [9]. Ballantyne et al. showed that 32 seconds of MET produced a significant immediate increase in passive knee extension. The prominent

point of TTM is that it provides muscle relaxation resulting from deep massage or pressure on muscle, whereas the prominent point of MET is to lengthen muscle within a short period of time. Therefore, the combination of two techniques may provide a better way to increase the flexibility of muscle as much as possible without any injury [10].

The most common technique is used to increase muscle flexibility is the static stretch. Rosario and Feletto compared 4 different static stretching treatments: 10 minutes of passive static stretching performed in 3 sessions over 3 consecutive days; 20 minutes' walking combined with 30 seconds of passive stretching; 10 minutes' warming of the hamstrings by microwave diathermy combined with 30 seconds of passive static stretching; and 30 seconds of passive static stretching. The results showed that 10 minutes of passive stretching performed in 3 sessions over 3 consecutive days was the most effective. However, there are relatively few studies on the acute effects of passive static stretching for 10 min in only 1 stretching session [11].

While static stretching has also been found to be an effective method to increase muscle flexibility but there is no scientific evidence about the most effective method for this purpose. Therefore, we aim to compare the effect of Thai massage in combination with muscle energy technique (ATMMET) with the passive static stretching technique (PSST) on both hamstring flexibility and the height of the Sepaktakraw serve.

## MATERIAL AND METHOD

### Design and Setting

The research design of this study was a randomized controlled trial with a blinded measurer, approved by the Khon Kaen University Ethics Committee for Human Research (approval number 582221).

### Participants

One hundred and sixty healthy college students aged between 18 - 25 years from Roi Et province, Thailand, were recruited in this study. Firstly, the participants had to complete a questionnaire providing general information, experience in Sepaktakraw sport, and history of injuries. After that, all the participants received a passive straight leg raise test (PSLR) [12]. The remaining participants consisted of one hundred and eight healthy college students because of 5 participants had played Sepaktakraw for less than 1 year, 10 participants had incurred hamstring muscle injuries within the last 3 months, and 37 participants had PSLR tests of equal or greater than 120 degree.

The remaining participants were randomly divided into 3 groups (using software at <http://randomizer.org>), 36 people in each group. The measurers were unaware about the groups' assignment to reduce bias (Fig. 1).

### Procedure

On the first day, all participants warm up before testing begins about 5 minutes by jogging without any stretch to prevent injuries. After that, they undertook the passive straight leg raise test (PSLR) [12] for measuring hamstring flexibility followed by the height of Sepaktakraw serve test (pre-test), which was recorded by a digital video camera and using a movement analysis program (Kinovea version 0.8.15) [13].

On the second day, the participants in ATMMET group received 8 min of ATM from an experienced trainer and then received 2 min of MET. The participants in PSST group received 10 min of PSST on both sides of their legs. And the participants in control group carried out activities of daily living without intervention. They sat on a chair for 10 min. Participants in all groups were received PSLR test and the height of Sepaktakraw serve test immediately after intervention (post-test1).

On the third day, 24 hours after intervention (post-test2), all participants were tested as well as pre- and post-test for determining chronic effects. All measurements were done at the same time of day between 08.00 AM and 12.00 PM.

### Interventions

#### *Applied Thai massage (ATM)*

The participants received 8-minutes of the ATM by using moderate foot pressure on the calf, the rear legs and the bottom area on both sides in the prone position by the experienced massage trainers which trained by professional Thai massage therapists and receive a certificate

#### *Muscle energy technique (MET)*

MET was performed in the supine position and hamstring muscles were stretched to the point of discomfort. And then they were instructed to contract muscles with moderate isometric contraction (approx. 75% of maximal) for 5 second in each 4 repetition and rest between repetition for 3 second [10].

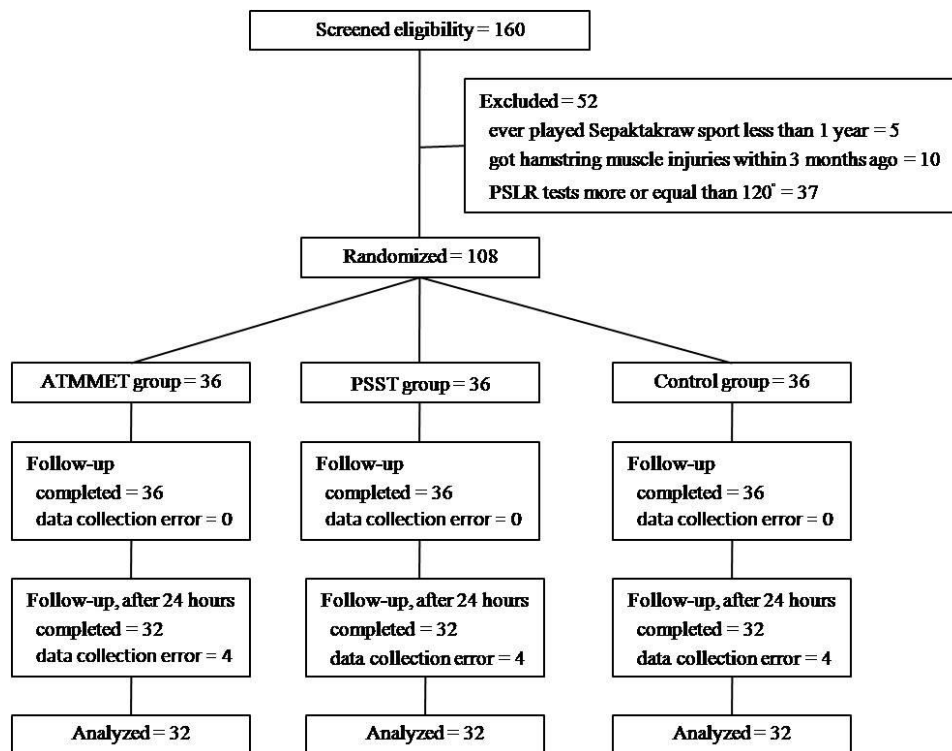


Fig. 1 Flow chart for study participation

#### *Passive static stretching technique (PSST)*

The subjects were placed in the supine position and hamstring muscles were stretched at below the pain threshold level by lifting one leg for 10 minutes [11].

#### **Outcome Measurements**

The height of the Sepaktakraw serve was measured by digital video camera recording and analyzed by using the software Kinovea version 0.8.15 [13] (Fig. 2). The reliability and criterion-related validity of the software are 0.95 and 0.99, respectively [14].

Hamstring flexibility was measured by PSLR [12]. The subjects were placed supine on the bed, and they raised one leg with knee extension and held it for 3 s. Subsequently, the goniometer pro application (trial version) on a smart phone was used to measure ROM of hip flexion (Fig. 3). In-house tests have shown tolerances of  $\pm 0.2^\circ$  and  $\pm 0.3^\circ$  depending on device [15].

Height of Sepaktakraw serves and hamstring flexibility were measured before, immediately after intervention, and 24 hours after intervention.

#### **Statistical Analysis**

The data were presented as mean  $\pm$  SD. Kolmogorov - Smirnov test was used to verify the

normality of the data. Kruskal Wallis test or one-way analysis of variance (ANOVA) statistics were used to compare outcome variables between the three groups in baseline characteristics. Friedman test or two-way repeated measures ANOVA by using the Bonferroni test were used to compare outcome variables within group and between groups. Significance level was set at the  $p \leq 0.05$ .

#### **RESULTS**

Kolmogorov test - Smirnov test showed that the data are distributed normally. There was no significant difference between the three groups in baseline characteristics. None of the subjects had sustained hamstring injuries in last 3 months. Four subjects in each group were excluded from this study because of data collection errors (Table 1). So, the remaining ninety six participants were used to analyze the data.

Within-groups comparison of the means between pre-test and post-test1 found that hamstring flexibility and height of Sepaktakraw serves were significantly increased in PSST and ATMMET groups ( $p < 0.05$ ). Comparison of the means between pre-test and post-test2 found that hamstring flexibility was significantly increased in PSST and ATMMET groups ( $p < 0.05$ ). Only height of Sepaktakraw serves was significantly increased in ATMMET group ( $p < 0.05$ ). But these parameters were not changed in the control group.

However, all parameters showed no significantly different between groups comparison (Table 2).

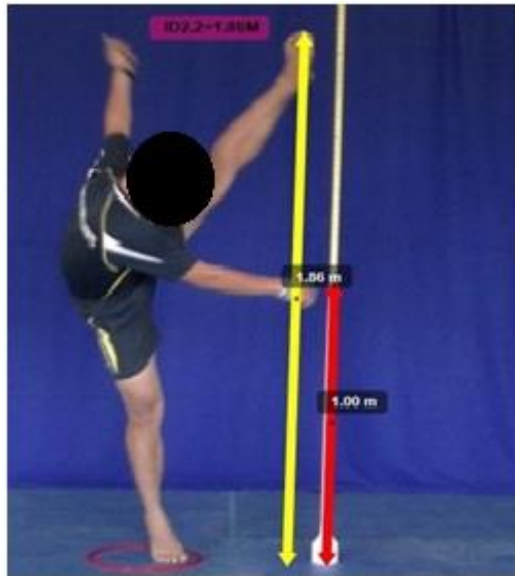


Fig. 2 The Sepaktakraw serve test by using the software Kinovea.



Fig. 3 Passive straight leg raise test (PSLR)

## DISCUSSION

The study showed that treatment with PSST and ATMMET for 10 min could increase hamstring flexibility and height of Sepaktakraw serves. The findings of this study correspond to previous studied, they found that stretching of soft tissue could increase tissue elasticity [7], [9], [11]-[12], [16]-[17] leading to increased hamstring flexibility. The effect of using multiple massage techniques on flexibility was studied. It found that Thai massage, deep massage and hand massage could increase the muscles flexibility [16]-[20]. Table 1 Baseline characteristics

Some previous study demonstrated that MET could increase hamstring flexibility [9], [21]-[22]. They concluded that MET affects shortened muscle, restricted joints, and weakened muscles. From this reasons, it can be concluded that both PSST and ATMMET could increase hamstring flexibility. Furthermore, this study found that both techniques could maintain hamstring flexibility for 24 hours after intervention (Fig. 4).

This study demonstrated that both techniques could increase the height of the Sepaktakraw serve as a result of increasing hamstring flexibility. After 24 hours post-intervention, the height of the Sepaktakraw serve with both techniques decreased continuously but only the ATMMET group still maintained the performance of the Sepaktakraw serve. It could be concluded that the ATMMET technique for 10 minutes could maintain the performance of the Sepaktakraw serve (Fig. 5).

However, there were no significant differences between the three groups in hamstring flexibility and the height of the Sepaktakraw serve. This might be because the subjects received only 1 intervention session, which may not be enough.

Our suggestion for further research is to add up the intervention session, increase the duration of intervention, and use more than one test for measuring hamstring flexibility and the height of the Sepaktakraw serve.

## CONCLUSION

In summary, the ATMMET and the PSST treatment could immediately significantly increase hamstring muscle flexibility. Moreover, 24 h post-intervention, both techniques could maintain hamstring flexibility.

Furthermore, the ATMMET and the PSST treatment could immediately significantly increase the height of the Sepaktakraw serve. At 24 h post-intervention, only ATMMET could maintain the height of the Sepaktakraw serve. No significant differences were found in the control group, both in hamstring muscle flexibility and the height of the Sepaktakraw serve.

## ACKNOWLEDGEMENT

The authors would like to thank the Research Center in Back, Neck, Other Joint Pain and Human Performance, KhonKaen University, Thailand, and Graduate School, KhonKaen University, Thailand for Financial supported. Special thanks to Assoc. Prof. Dr. Naruemon Leelayuwat for helpful comments

	Control Group (n=36)	PSST Group (n=36) <sup>a</sup>	ATMMET Group (n=36) <sup>b</sup>	p-Values <sup>c</sup>
Age (years)	21.28(0.70)	21.67(0.86)	21.89(1.63)	.076
Weight (kg)	64.69(11.95)	64.93(10.16)	64.71(10.45)	.994
Height (cm)	168.64(7.01)	170.94(6.55)	170.69(7.22)	.305
Playing Sepaktakraw (years)	2.56(1.48)	2.75(1.48)	2.89(1.43)	.626
SLR test (degree)	111.00(12.25)	106.56(11.23)	108.83(10.49)	.256
Past hamstring injuries (number)	0	0	0	
Data collection error (number)	4	4	4	

Note: <sup>a</sup> PSST, passive static stretching technique.

<sup>b</sup> ATMMET, applied Thai massage combined with muscle energy technique.

<sup>c</sup> One-way ANOVA

Table 2 Mean and Standard Deviation of PSLR test and Sepaktakraw serve test.

Group	Time	Sepaktakraw serve test	PSLR test	
			ROM (Degrees)	Torque (N.m)
Control	Pre-test	175(2.26)	115(2.13)	12.87(4.49)
	Post-test1	174(2.12)	116(2.01)	12.87(4.49)
	Post-test2	174(2.14)	116(2.01)	12.87(4.49)
PSST	Pre-test	178(2.26)	109(2.13)	12.22(4.73)
	Post-test1	180(2.12)*	115(2.01)*	12.30(4.85)
	Post-test2	179(2.14)	113(2.01)*,**	12.25(4.71)
ATMMET	Pre-test	176(2.26)	113(2.13)	11.87(3.88)
	Post-test1	179(2.12)*	120(2.01)*	12.70(3.79)
	Post-test2	178(2.14)*	119(2.01)*,**	12.17(3.78)

Note: \* The mean is significantly different compared between pre-test and post-test1 ( $P < 0.05$ ).

\*\*The mean is significantly different compared between pre-test and post-test2 ( $P < 0.05$ ).

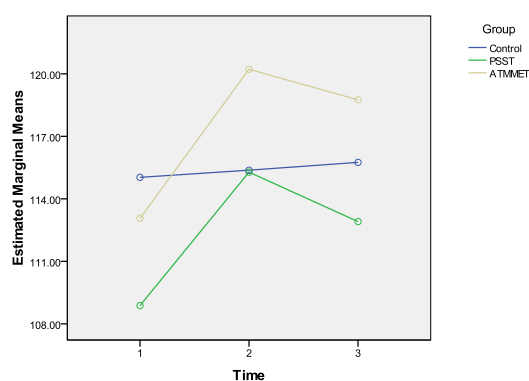


Fig. 4 Change in hamstring flexibility (degrees) by the PSLR test during pre-test, post-test1, and, post-test2.

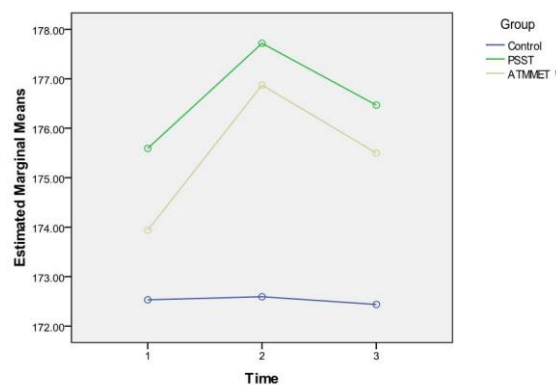


Fig. 5 Change in the height of Sepaktakraw serve (cm.) during pre-test, post-test1, and post-test2.

## REFERENCES

- [1] P. Mutalai. (February 19, 2014). History of Sepaktakraw. Available: <http://www.sepaktakrawworld.com/index.php/2014-01-17-04-10-40>
- [2] O. Sepaktakraw. (2014, 04 August). How to Play the Game. Available: <http://www.sepaktakraw.org/about-istaf/how-to-play-the-game/#.VAeRbfmSwgM>
- [3] K. I.-o. Suwat Sidthilaw, Chatchadaporn Pitaksathienkul, , "Biomechanical Analysis of Sepak Takraw Serves in 24th SEA GAMES," journal of Bureau of Sport Science, Office of Sport and Recreation Development, 2009.
- [4] M. Rezaei, M. Paziraei, M. Haghani, and S. Hariri, "The Comparison of some lower limb's motion range parameters in Sepaktakraw elite athletes with an emphasis on talent identification," *International Journal of Sport Studies*, vol. 4, pp. 1462-1465, 2014.
- [5] E. S. a. B. W. Nadzrin Hamdan, "Factors Correlated With Sepak Takraw Serve Speed " in 30th Annual Conference of Biomechanics in Sports, Melbourne, Australia, 2012 pp. 413-416.
- [6] B. J. Hemmings, "Physiological, psychological and performance effects of massage therapy in sport: a review of the literature," *Physical Therapy in Sport*, vol. 2, pp. 165-170, 2001.
- [7] A. Calder. (1998, Recovery: Restoration and Regeneration as Essential Components within Training Programs. Available: <https://swimmingcoach.org/recovery-restoration-and-regeneration-as-essential-components-within-training-programs/>
- [8] S. Tapanya, *Traditional Thai Massage*. Bangkok, Thailand: Duang Kamol, 1993.
- [9] G. Fryer, "Muscle energy technique: An evidence-informed approach," *International Journal of Osteopathic Medicine*, vol. 14, pp. 3-9, Mar 2011.
- [10] G. F. F Ballantyne, P McLaughlin, "The effect of muscle energy technique on hamstring extensibility: the mechanism of altered flexibility," *Journal of Osteopathic Medicine*, vol. 6, pp. 59-63, 2003.
- [11] J. L. Rosario and A. Foletto, "Comparative study of stretching modalities in healthy women: heating and application time," *J Bodyw Mov Ther*, vol. 19, pp. 3-7, Jan 2015.
- [12] A. C. Toby M. Hall, Catherine McNee, Jeremy Walsh, "Effects of the mulligan traction straight leg raise technique on range of movement," *Journal of Manual and Manipulative Therapy*, vol. 9, pp. 128-133, 2001.
- [13] Kinovea. (2016, 3 August). Kinovea. Available: <http://www.kinovea.org/>
- [14] A. Deeminoi, "Reliability and criterion-related validity of 2d motion analysis system: Kinovea computer program for measuring the height of sepaktakraw serves in amateur athletes. A pilot study," in *International Conference 2016 "Ergogenic Aids and Nutritional Supplement for Health and Sports"*, Centara Hotel & Convention Centre, Khon Kaen, Thailand, 2016.
- [15] 5fuf5. (2015). Goniometer Pro (trial version) - Android app on Google Play. Available: <https://play.google.com/store/apps/details?id=com.FiveFufFive.GoniometerProPreview&hl=th>
- [16] V. Buttagat, W. Eungpinichpong, U. Chatchawan, and S. Kharmwan, "The immediate effects of traditional Thai massage on heart rate variability and stress-related parameters in patients with back pain associated with myofascial trigger points," *J Bodyw Mov Ther*, vol. 15, pp. 15-23, Jan 2011.
- [17] J. Forman, L. Geertsen, and M. E. Rogers, "Effect of deep stripping massage alone or with eccentric resistance on hamstring length and strength," *J Bodyw Mov Ther*, vol. 18, pp. 139-44, Jan 2014.
- [18] D. Hopper, M. Conneely, F. Chromiak, E. Canini, J. Berggren, and K. Briffa, "Evaluation of the effect of two massage techniques on hamstring muscle length in competitive female hockey players," *Physical Therapy in Sport*, vol. 6, pp. 137-145, Aug 2005.
- [19] C. Uraiwon, "Therapeutic effectiveness of deep massage (Traditional Thai massage) on patients with back pain associated with myofascial trigger points," Thesis (Ph D ), Public Health, Graduate School, Khon Kaen University, 2005., 2005.
- [20] U. Chatchawan, B. Thinkhamrop, S. Kharmwan, J. Knowles, and W. Eungpinichpong, "Effectiveness of traditional Thai massage versus Swedish massage among patients with back pain associated with myofascial trigger points," *Journal of Bodywork and Movement Therapies*, vol. 9, pp. 298-309, 10// 2005.
- [21] F. Ballantyne, G. Fryer, and P. McLaughlin, "The effect of muscle energy technique on hamstring extensibility: the mechanism of altered flexibility," *Journal of Osteopathic Medicine*, vol. 6, pp. 59-63, 2003/10/01 2003.
- [22] R. Mehdikhani and F. Okhovatian, "Immediate effect of muscle energy technique on latent trigger point of upper trapezius muscle," *Clinical Chiropractic*, vol. 15, pp. 112-120, 12// 2012.



## **A STUDY OF THE CORRELATION BETWEEN FOUR CLINICAL TRIALS FOR THE MEASUREMENT OF HAMSTRING MUSCLE FLEXIBILITY**

Apichat Deeminoi<sup>1</sup>, Dr.ThanaratSripongngam<sup>2</sup>

<sup>1</sup> Department of Physical Education, Faculty of Education, Roi Et Rajabhat University, Thailand;

<sup>2</sup> Department of Health and Sport Science, Faculty of Education, Mahasarakham University, Thailand

### **ABSTRACT**

Flexibility of hamstring muscles is very important in sports which can be measured in many tests. The relationship of each test for measuring on the hamstring muscles flexibility has not been verified. The aim of this study was to examine the correlation between the four tests. Ninety six participants were received four methods of hamstring muscles flexibility tests consist of sit and reach test (SR), stand and reach test (ST), passive knee extension test (PKE), and passive straight leg raise test (PSLR). Pearson product-moment correlation analysis was used to analyze relationship between four tests. This study demonstrated the high significant correlation between SR and ST ( $r=0.87$ ), moderate significant correlation between SR and PSLR ( $r=0.50$ ), moderate significant correlation between ST and SLR ( $r=0.46$ ), and low significant correlation between PKE and SLR ( $r=0.33$ ). We conclude that SR and ST were a high correlation in the measurement of hamstring muscle flexibility which can be used interchangeably.

*Keywords: Hamstring flexibility, Sit and reach test, Stand and reach test, Passive knee extension test, Passive straight leg raise test*

### **INTRODUCTION**

Flexibility of hamstring muscles is very important in sports which the reduction of hamstring flexibility is a risk factor for muscle injury [1]. Sit and reach test (SR), stand and reach test (ST), passive knee extension test (PKE), and passive straight leg raise test (PSLR) [2-5] were usually use to measured hamstring flexibility in the field test.

The previous study, Hopper et al. studied about the effect of two massage techniques on hamstring muscle length in competitive female hockey players by using PKE test and PSLR test for measured hamstring flexibility. The result showed that hamstring muscle length was significantly increased by using the PKE test but not the PSLR test [6].

Moreover, Chu, et al. [7] studied about EMG activities between the SR test and the ST test: a pilot study. The results showed that hamstring and low back muscles activities higher in ST test than SR test, but found no significant difference between the tests.

Furthermore, Bakirtzoglou, et al. [8] studied about hamstring flexibility by using two different measuring instruments, SR test and PSLR test, in athletes and non-athletes. They found that hamstring flexibility score was significant greater in

athletes than non-athletes when measured by PSLR test. That is hamstring flexibility could measure achievement by using PSLR test than ST test.

It can be seen that, using different instruments to measure hamstring flexibility achieved different results. Relationship of each test for measuring on the hamstring muscles flexibility has not been verified. The knowledge from this study can help the interested people choosing the appropriate measurement method.

### **MATERIAL AND METHOD**

#### **Design and Setting**

The research design of this study was the analytical research, one group with four parameters.

#### **Participants**

Ninety six healthy college students aged between 18 - 25 years from Roi Et province, Thailand, were recruited in this study. Each of them signed an informed consent and completed a questionnaire to provide general information and history of injuries before participating in this study.

## Procedure

All participants warmed up before the test begins for 5 minutes by jogging to prevent injuries but not received stretching the muscles. After that, all participants received the SR test [4], the ST test [3], the PKE test [2], and the PSLR test [5] which rest between the tests for 20 minutes. All tests were examined on the same day.

## Outcome Measurements

### *Sit and reach (SR) test*

The participants sit with straight leg, soles of the feet against the box, bent hip about 90 degrees, and then, the participants bent forward, without bending the knee and tried to reach out as much as possible and hold for 3 s., 3 repetitions. After that, record the values in centimeters which the highest value was used to statistical analysis. [4] (Fig. 1).



Fig. 1 Sit and reach test (SR)

### *Stand and reach (ST) test*

The participants stood on a box, which is placed on a chair. Then bend down, straight leg, without bending the knee and tried to reach the hands downward as much as possible and hold for 3 s., 3 repetitions. After that, record the values in centimeters which the highest value was used to statistical analysis [4] (Fig. 2).



Fig. 2 Stand and reach test (ST)

### *Passive knee extension (PKE) test*

The participants lay supine on the bed, bend one side of hip and knee joint 90° degree. Then, the examiner raised the tested leg straight up to the point of feeling tight and hold for 3 s., 3 repetitions [2]. The test used goniometer pro (trial version) program on smart phone, which was placed above the ankle for measured hamstring flexibility. Record the values in centimeters which the highest value was used to statistical analysis. In-house tests have shown tolerances of the device between  $\pm 0.2^\circ$  and  $\pm 0.3^\circ$ . [10] (Fig. 3).



Fig. 3 Passive knee extension test (PKE)

### *Passive straight leg raise (PSLR) test*

The participants lay supine on the bed and then raised the one leg without bending the knee to the point of feeling tight and hold for 3 s., 3 repetitions. The testing done by the examiners [5]. Hamstring flexibility was measured by using the goniometer pro (trial version) program on smart phone as same as PKE test [10] (Fig. 4).



Fig. 4 Passive straight leg raise test (PSLR)

## Statistical Analysis

The data were presented as mean  $\pm$  SD. Kolmogorov - Smirnov test was used to verify the normality of the data. Pearson product moment correlation coefficient was used to analyze relationship between four tests. Significance level was set at the  $p \leq 0.5$ .

## RESULTS

Ninety six participants (74 men, 22 women) aged average  $21.61 \pm 1.06$  years, weight average  $64.78 \pm 10.85$  kg., and height average  $170.09 \pm 6.93$  cm. None of them had sustained hamstring injuries in last 3 months. All participants were tested for all tests. In each test, the participants repeated 3 times and the highest value was used to statistical analysis. Mean and standard deviation of each tests showed in table 2.

The results of this study showed that the highest correlation was between SR and ST ( $r=0.87$ ,  $p<0.001$ ), the relationship between SR and PSLR ( $r=0.50$ ,  $p<0.001$ ), ST and SLR ( $r=0.46$ ,  $p<0.001$ ) found moderate correlation and low correlation was found between PKE and SLR ( $r=0.33$ ,  $p=0.001$ ). This study showed no correlation between SR and PKE ( $r=0.14$ ,  $p=0.17$ ), and ST and PKE ( $r=0.14$ ,  $p=0.19$ ) (Table 2).

Table 1 Mean and standard deviation of four tests

Test	Mean $\pm$ SD
SR (Cm.)	$14.32 \pm 6.33$
ST (Cm.)	$13.81 \pm 5.35$
PKE (Degrees)	$89.34 \pm 1.85$
PSLR (Degrees)	$112.32 \pm 12.19$

Table 2 Correlation between four tests

	SR	ST	PKE	PSLR
SR	1.00			
ST	0.87*	1.00		
PKE	0.14	0.14	1.00	
PSLR	0.5*	0.46*	0.33*	1.00

Note: SR=sit and reach test, ST=stand and reach test, PKE=passive knee extension test, PSLR=passive straight leg raise test

## DISCUSSION

This study found that SR and ST tests were the most correlated probably due to the both tests required flexibility of back and leg muscles which can be used interchangeably. However, Chu et al. [7] demonstrated that hamstring (semitendinosus and biceps femoris) and lumbar erector spinae had higher activity in ST test than in SR test. Therefore, ST test may not be suitable for some individuals, such as the elderly or who had a problem of the lower back muscle.

PKE test was only correlated with PSLR test because of the participants were similar in the test posture (hip flexion) which was an isolate the joint measurement.

PSLR test was correlated to all tests. May be due to the test posture was similar with PKE test

but PKE test performed by bend the hip joint at 90 degrees. The PSLR test could bend the hip joint more than 90 degrees until it feels tight which it involved lower back muscles as same as SR and ST tests.

## CONCLUSION

This study showed that SR and ST were significant relationships in a high correlation. The tests can be used interchangeably. PKE and PSLR were significant relationships in a low correlation. The moderate correlations were found between SR and PSLR, and ST and PSLR. PSLR had a correlated with all tests.

## ACKNOWLEDGEMENT

The authors would like to thank Department of Physical Education, Faculty of Education, Roi Et Rajabhat University, Thailand, and Department of Health and Sport Science, Faculty of Education, Mahasarakham University, Thailand, for financial supporting this study. Special thanks to Assoc. Prof. Dr. Wichai Eungpinichpong for helpful comments.

## REFERENCES

- [1] Witvrouw E, Danneels L, Asselman P, D'Have T, Cambier D, "Muscle flexibility as a risk factor for developing muscle injuries in male professional soccer players", *Am J Sports Med*, Vol. 31(1), 2003, pp. 41-46,
- [2] Gajdosik R, Lusin G, "Hamstring muscle tightness. Reliability of an active-knee-extension test", *Phys Ther*, Vol. 63(7), Jul. 1983, pp. 1085-1090.
- [3] Rich BSE, "ACSM's Health-Related Physical Fitness Assessment Manual", *Med Sci Sports Exerc*, 2004, pp. 1657.
- [4] Wells KF, Dillon EK, "The sit and reach—a test of back and leg flexibility", *Research Quarterly of the American Association for Health, Physical Education and Recreation*, Vol. 23, 1952, pp. 115-118.
- [5] Hall T, Cacho A, McNee C, Riches J, Walsh J, "Effects of the mulligan traction straight leg raise technique on range of movement", *J Man Manip Ther*, vol. 9, 2001, pp. 128-133.
- [6] Hopper D, Conneely M, Chromiak F, Canini E, Berggren J, Briffa K, "Evaluation of the effect of two massage techniques on hamstring muscle length in competitive female hockey players", *Phys Ther Sport*, Vol. 6(3), Aug. 2005, pp. 137-145.
- [7] Chu DPK, Luk TC, Hong Y, "EMG activities between sit-and-reach and stand-and-reach: a pilot study", *Proceedings of the 20<sup>th</sup> annual*

- conference of the IEEE engineering in medicine and biology society, Vol. 20(5), 1998, pp. 2448-2451.
- [8] Bakirtzoglou P, Ioannou P, Bakirtzoglou F, "Evaluation of Hamstring flexibility by using two different measuring instruments", Sportlogia, Vol. 6, 2010, pp. 28-34.
- [9] Barlow A, Clarke R, Johnson N, Seabourne B, Thomas D, Gal J, "Effect of massage of the hamstring muscle group on performance of the sit and reach test", Br J Sports Med, Vol. 38, Jun. 2004, pp. 349-351.
- [10] 5fuf5. (2015, 3 August). Goniometer Pro (trial version) - Android app on Google Play. Available: <https://play.google.com/store/apps/details?id=com.FiveFuffFive.GoniometerProPreviewAndroid&hl=th>

## EFFECTS OF *KAEMPFERIA PARVIFLORA* ON PHYSICAL AND PSYCHOLOGICAL STRESSES IN ADULTS

Wichai Eungpinichpong<sup>1</sup>, Uraiwan Chatchawan<sup>2</sup>, Bung-orn Sripanidkulchai<sup>3</sup>  
Suwanna Arunpongpaisal<sup>3</sup>

<sup>1</sup>Faculty of Associated Medical Sciences, Khon Kaen University

<sup>2</sup>Faculty of Pharmaceutical Sciences, Khon Kaen University

<sup>3</sup>Faculty of Medicine, Khon Kaen University, Thailand.

### ABSTRACT

Although *Kaempferia parviflora* (*K. parviflora*) has been known as one of health promoting herbs, a clinical trial is needed to confirm its beneficial effect on stress reduction. The aim of this study was to determine the effects of *Kaempferia parviflora* on the physiological and psychological stresses. Healthy adult participants with moderate stress level were divided into two groups; either ingested with *Kaempferia parviflora* at doses of 360 mg/day for 14 days (intervention group) or placebo tablets (control group). The results indicated both groups had significantly decreased stress based upon Hamilton Anxiety Rating Scale (HAM-A) and Suanprung Stress Test-20 (SPST-20). Heart rate variability measures exhibited non-significant between-group comparison, except HF, SDNN, RMSSD and LF of which the control group had significantly lower than the experimental group. This study suggests that *Kaempferia parviflora* may be useful for both physiological and psychological stress reduction.

**Keywords:** *Kaempferia Parviflora*, Stress, Clinical Trial, Heart Rate Variability

### INTRODUCTION

Currently, stress has been one of the health problems in the society and its consequences have affected daily living in a great deal, such as peptic ulcer, depressive syndrome, diabetes, and high blood pressure. The reaction of stress does affect not only physically, but also psychologically wellbeing, like having fears and trembling, obvious symptoms reacted by the autonomic nervous system; feeling a terrible headache, fatigue, nausea, vomiting, increased heart rate, and muscle tightness. [1] The long term physical stresses can arouse the sympathetic nervous system, increase blood pressure, heart rates, salivary cortisol secretion, and decrease heart rate variability.

*Kaempferia parviflora* (Thai Ginseng) is an herbaceous plant in the family *Zingiberaceae*, native in Thailand. It has been believed that it might contain substance that increases libido when consumed. A study found that it has inhibiting effect on the growth of microorganisms. In addition, it also be found to have beneficial effect for health such as anti-inflammatory effect. [2] reduce of blood sugar levels and lipid levels in mice, increase physical fitness, and reduce oxidative stress in elderly people, [3] increase blood flow to the muscles. [4]-[5] Since persistent stress affects the body cells to produces excessive oxidants which destroy biomolecules in cells and cause tissue cell degradation [6] and because of antioxidant mechanism of *Kaempferia parviflora*, we propose

that consuming optimum dose of extracted *Kaempferia parviflora* may reduce physical and psychological stresses in adult subjects.

### METHODS

#### Design and Participants

This study was a randomized controlled trial in 40 volunteers aged 25-45 years who had mild to moderate degree of psychological stress were screened by a psychiatrist to rule out for anxiety. The self-assessment form for anxiety symptoms was used for volunteers who were identified having slightly low level of anxiety. The exclusion criteria were as follows: Volunteers with a history of psychiatric illnesses, such as depression, schizophrenia, bipolar mood, or having taken any type of stress medication, have had musculoskeletal pain, postmenopausal women, functional abnormalities of liver and kidneys, lack of understandable communication, unable to follow the instructions, or having a disease that requires continuous treatment.

#### Research Setting

The data collection procedures were obtained at research room, Faculty of Associated Medical Sciences where is very quiet, no noise disturbing. Room temperature was controlled at 25 degrees Celsius

## Intervention and Procedure

All qualified volunteers were informed on research objectives and how they were expected to perform while participating in the study. Then they sign the consent form as well as answering the questionnaire relating to general information. Self-stress level was subsequently self-evaluated while the anxiety was assessed by the psychiatrist. Volunteers were randomly allocated either in the experimental group to take the extracted *Kaempferia parviflora* or in the placebo group.

The randomized volunteers took either extracted *Kaempferia parviflora* or placebo which were contained in similar capsules. The data collector did not know which group each volunteer belonged to until the data collection process was finished. The volunteers received either extracted *Kaempferia parviflora* (360 milligrams/day according to human-equivalent safety dose in a previous study [7]) or placebo after having blood test for assessing liver enzymes and kidney function (AST, ALT, ALK, BUN, Creatinine: Cr) to identify the normality. After that each volunteer took 2 tablets at a time before meal in the morning and evening meal lasted for 7 days. The blood test was repeated again after 7 and 14 days of taking the tablets to ensure that liver enzymes and kidneys function were within normal range. At the end of the study, the anxiety of all the volunteers were assessed by the Psychiatrists and self-assessment was also performed.

## Measurement Equipment

Variables used for stress assessment in the study were as follows. The first four variables reflected more physical than psychological stress whereas the last two reflected more psychological stress.

Stress index is a measure, sensitive to changes and reliable. It can be measured by a HRV detector. The results are as follows: 50-70 excellent, 71-90 good, 91-110 normal, 111-130 stressed (poor), 131-150 stressed (very bad)

Stress resistance refers to the adaptation of the body towards stress, used to evaluate the functioning of the autonomic nervous system. The same tools and methods of measurement were used as stress index, the results are as follows: 50-70 Bad, 71-90 Poor, 91-110 Normal, 111-130 Good, 131-150 Very good

Heart rate variability: heart rate variability includes the values of heart rate (HR), standard deviation of normal-to-normal intervals (SDNN), root of the mean squared of successive difference of normal RR intervals (RMSSD), high frequency (HF), low frequency; LF) and low frequency per high frequency ratio (LF/HF ratio).

Salivary  $\alpha$ -amylase levels (Salivary  $\alpha$ -amylase levels) were measured by inserting a test strip into the mouth and left underneath the tongue for 2 minutes. Then the strip results were read by Human Cocoa Meters (Nipro Co., LTD., Japan). The readings were interpreted as follows: 0-30 KU/L Normal, 30-45 KU/L High, 46-60 KU/L High,> 60 KU/L very high.

Psychological stress level was assessed by Suanprung Stress Test with 20 questions (SPST - 20), recommended by the Department of Mental Health. The Cronbach's alpha reliability coefficient was greater than 0.7.

The level of anxiety was assessed by Thai version of Hamilton Anxiety Rating Scale (HAM-A).

## STATISTICAL ANALYSES

Descriptive statistics was used to describe the characteristics of the volunteers. The results of all the continuous variables were compared within the group by using the Sign test statistic providing that the data were not normally distributed. To compare between the groups, the Wilcoxon Rank Sum statistic was used. Statistically significant was set at  $\alpha < 0.05$ . All statistics were analyzed using SPSS version 19 (Armonk, NY: IBM Corp. Under licensed by Khon Kaen University)

## RESULTS

Recruited participants were 80 volunteers (13 males and 67 females), aged 24-36 years, who met the inclusive criteria. The demographic data were balance between the *Kaempferia parviflora* and the placebo groups. (Table 1)

Table 1 Demographic data of the *Kaempferia parviflora* and control groups

Characteristics	<i>Kaempferia parviflora</i> (n=40)	Placebo (n=40)
Gender		
Male	33(82.50)	34(85.00)
Female	7(17.50)	6(15.00)
Age		
<36	24(60.00)	20(50.00)
36-45	15(37.50)	20(50.00)
>45	1(2.50)	0(0.00)
Mean $\pm$ SD	34.50 $\pm$ 6.12	34.15 $\pm$ 6.93

Note: n(%)

Results of volunteer at baseline demonstrate that all stress variable were not significantly different between the two groups (Table 2).

Table 2 Comparison of stress variables at baseline between the two groups.

Stress variables	<i>Kaempferia parviflora</i> Median(IQR)	Placebo Median(IQR)	p-value
Stress index	95(10.50)	98(18.00)	0.065
Stress resistance	97(11.50)	93(21.50)	0.109
SDNN	39.86(22.24)	32.74(24.10)	0.175
RMSSD	30.02(21.75)	24.52(18.69)	0.194
HF	5.79(1.55)	5.29(1.44)	0.155
LF	5.44(1.60)	5.44(0.99)	0.870
LF/HF	0.81(1.58)	1.21(1.81)	0.051
AMYLESS	74.50(55.00)	83.00(46.50)	0.299
HAM-A	19(10.00)	18(15.00)	0.751
SPST – 20	57(10.50)	60(13.50)	0.287

Stress variables after 14 days of taking either extracted *Kaempferia parviflora* or placebo were compared. The results demonstrate that most of the stress variables were not significantly different between the two groups except the RMSSD and LF/HF ratio (Table 3). Liver enzyme and kidney function were found to be normal for every volunteer even after 14 days of taking the tablets.

Table 3 Comparison of stress variables after 14 days of taking either extracted *Kaempferia parviflora* or placebo tablets

Stress variables	<i>Kaempferia parviflora</i> Median(IQR)	Placebo Median(IQR)	p-value
Stress index	95.5(14.50)	101.50(18.50)	0.117
Stress resistance	96(13.00)	91(20.00)	0.119
SDNN	38.16(17.19)	30.25(19.58)	0.090
RMSSD	29.30(17.41)	22.90(15.98)	0.033
HF	5.43(0.88)	5.12(1.70)	0.084
LF	5.36(1.31)	5.08(1.50)	0.403
LF/HF	0.88(0.91)	1.28(1.71)	0.036
AMYLESS	63(47.00)	69(53.50)	0.528
HAM-A	9.5(8.00)	9.50(11.00)	0.647
SPST – 20	48(16.50)	44.50(13.00)	0.158

## DISCUSSION

The purpose of the study was to determine the clinical effects of extracted *Kaempferia parviflora* on physical and mental stress in adults. Forty volunteers without any contra-indication underwent the randomized controlled trial although most of the stress variables were not significantly different between the two groups at the end of the trial, RMSSD was higher, and LF/HF ratio was lower in the treatment group than the control (Table 3). The results of these two variables revealed that 14 days of 360 mg/day of extracted *Kaempferia parviflora* could reduce physical and psychological stresses.

The results from Table 3, when compared on the stress index, the level of stress in the *Kaempferia parviflora* taken group was lower than the placebo group by about 6%. However, the difference between

the groups was not statistically significant. As far as the value of RMSSD was concerned, the vagal tone was increased and denoted stress relief. This study also found that the group taken the extracted the *Kaempferia parviflora*, the stress was statistically better than the placebo. The results of changing, the Alpha-amylase and HAM-A show similarity pattern as the others. Volunteers from the *Kaempferia parviflora* taken group had a significantly lower stress and anxiety than those in the placebo group although no statistically significant differences.

The results from other variables of HRV did not detect any differences after the completion of 14 days, except RMSSD, and LF only. Even though the placebo group showed a significant stress reduction compared with the *Kaempferia parviflora* taken group (Table 3), and the size of the difference was very small. This might be due to a relatively short period of taking extracted *Kaempferia parviflora* that exhibited small stress reduction effects. Further study might consider a longer period of intervention and higher dose of taking extracted *Kaempferia parviflora* so that the differences between the groups may be obviously shown. The results of this study correspond to the past research which found that the *Kaempferia parviflora* was effective in reducing the volunteers stress in older subjects. [3]

The volunteers in the current study did not drop out or quit. No serious adverse reactions were found during taking the extracted *Kaempferia parviflora*. It was reported that only one volunteer from the extracted *Kaempferia parviflora* taken group developed flatulence which was a slight symptom. This shows that the amount of the extracted *Kaempferia parviflora* taken is safe and suitable for the volunteers' ages.

## CONCLUSION

Based on the results of the study, we conclude that the extracted *Kaempferia parviflora* may reduce stress and anxiety in adults aged 25-45 years.

## ACKNOWLEDGEMENTS

The authors would like to thank the Agricultural Commercial Research Project where provided a support with research funding. More importantly, good cooperation from the volunteers is always valued. This research project was grateful from the help of various sources contributed their valuable time to enhance a better living of people in the communities.

## REFERENCES

- [1] Selhub EM, "Stress and distress in clinical practice: a mind-body approach" NutrClin Care, Vol. 5, 2002, pp. 182-190.



- [2] Rujjanawate C, Kanjanapothi D, Amornlerdpison D, Pojanagaroon S. "Anti-gastric ulcer effect of *Kaempferia parviflora*" *Ethnopharmacology*, Vol. 102, 2005, pp. 120–122.
- [3] Wattanathorn J, Muchimapura S, Tong-Un T, Saenghong S, Thukhum-Mee W, Sripanidkulchai B. "Positive modulation effect of 8-week consumption of *Kaempferia parviflora* on health-related physical fitness and oxidative status in healthy elderly volunteers" Evid Based Complement Alternat Med, Vol. 2012, Jul. 2012 Article ID 732816.
- [4] Wattanapitayakul S, Chularojmontri L., Herunsalee A, Charuchongkolwongse S, Chansuvanich N. "Vasorelaxation and antispasmodic effects of *Kaempferia parviflora* ethanolic extract in isolated rat organ studies" *Fitoterapia*, Vol. 79, 2008. pp. 214-216.
- [5] Chaturapanich G, Chaiyakul S, Verawatnapakul V, Pholpramool C, "Effects of *Kaempferia parviflora* extracts on reproductive parameters and spermatid blood flow in male rats" *Reproduction*, Vol. 136, Oct. 2008, pp. 515-22.
- [6] Pansarasa O, Bertorelli L, Vecchiet J, Felzani G, Marzatico F, "Age-dependent changes of antioxidant activities and markers of free radical damage in human skeletal muscle," *Free Radical Biology and Medicine*, Vol. 27, 1999, pp. 617–622.
- [7] Chivapat S, Chavalittumrong P, Attawish A, Rungsipipat A, "Chronic Toxicity Study of *Kaempferia parviflora* Wall ex. Extract", *Thai J. Vet. Med*, Vol. 40, 2010, pp. 377-383.

## DEVELOPMENT OF POLY (D, L-LACTIC ACID) WITH POLYBENZOXAZINE VIA SOLUTION BLENDING

Kansiri Pakkethati<sup>1</sup> and Yodthong Baimark<sup>2</sup>

<sup>1</sup>Biodegradable Polymer Research Unit, Department of Chemistry, Faculty of Science,  
Mahasarakham University, Thailand

### ABSTRACT

Polybenzoxazine was synthesized by using bisphenol A, formaldehyde and diamine as precursor via condensation reaction. Triethylenetetraamine was used as dianmine precursor. Polybenzoxazine was characterized by FTIR technique in order to confirm the obtained polybenzoxazine. The ratio of poly(D,L-lactic acid)/polybenzoxazine (Mw=10,000 and 20,000 g/mol) was 0:100, 1:99, 3:97 and 5:95, respectively. The poly(D,L-lactic acid)/polybenzoxazine films was characterized by using Scanning Electron Microscope (SEM). The results showed homogenous and smooth films. Thermal stability of poly(D,L-lactic acid)/polybenzoxazine films was better than pure polybenzoxazine film. Moreover, 3:97 ratio of polybenzoxazine mixed with poly(D,L-lactic acid) (Mw = 20,000 g/mol) film showed good tensile strength, because the stress at break was  $24.06 \pm 7.99$  when determined by Universal Tinting Machine. It was concluded that poly(D,L-lactic acid) improved the property of the polybenzoxazine film.

*Keywords: Biodegradable polymers, polybenzoxazine, poly(D,L-lactic acid)*

### INTRODUCTION

The research of biodegradable polymers has gained considerable momentum in latest years with the growing public attention to environment problems. Poly(lactic acid), a biodegradable polymer which can also be produced from annually renewable resources, has extended recently an increasing attention [1].

Lactic acid (2-hydroxy propanoic acid) is a hydroxyl acid containing an asymmetric carbon atom. The lactic acid exists in two optically active configurations: D- and L-lactic acids. These lactic acids are produced by fermentation using bacterial systems. However chemical process was used to produce a racemic or D,L-lactic acid. The poly(L-lactic acid) and poly(D-lactic acid) are semi-crystalline, while the poly(D,L-lactic acid) is amorphous. The mechanical and thermal properties of poly(D,L-lactic acid) are usually lower than poly(lactic acid) [2]. Moreover below  $T_g$  in the range of 50 – 60 °C, amorphous poly(D,L-lactic acid) is rigid and brittle having the elastic modulus about 3-3.5 GPa and low ability to plastic deformation. The transition from brittle to ductile behavior in the plasticized polylactide occurs when  $T_g$  is shifted to 35°C.

Polybenzoxazine is a new class of phenolic resins which is very accepted and useful in polymer research. There are three common types of chemical needed to synthesize polybenzoxazine, including various aromatic/aliphatic amines, mono/diphenols,

and formaldehyde. Accordingly, phenol and amine could be varied and this is one of the most advantages of polybenzoxazine in excellent molecular design flexibility. The preparation of polybenzoxazine is also easy and low cost. Moreover, polybenzoxazine has good properties in high glass-transition temperature ( $T_g$ ), high thermal stability, good mechanical properties, and low shrinkage upon polymerization thermal stability [3].

Polybenzoxazine precursors have been synthesized from various aromatic/aliphatic amines, mono/diphenols, and formaldehyde [3,4]. One approach was to synthesize polybenzoxazine from a low molecular weight monomer, using monofunctional amine, phenol, and formaldehyde as reactants [4]. However, polybenzoxazines obtained via this approach usually suffered from brittleness. Another method was the preparation of polybenzoxazine from high molecular weight oligomers from diamine, bisphenol-A, and formaldehyde [5]. The properties of the polybenzoxazines derived from these high molecular weight oligomers, especially brittleness, have been greatly improved when compared with cured films from the typical low molecular weight precursors. This enables polybenzoxazine to be an excellent candidate for flexible film applications. Therefore, combination of polybenzoxazine with poly(D,L-lactic acid) could improve the film properties when compare to the pure polymer.

## MATERIALS AND METHOD

### Materials

Analytical grade 1,4-dioxane (99%) was purchased from Sigma-ALDRICH. Bisphenol-A (BPA, 97 % purity) and Triethylenetetramine (TETA, 60% w/w) were obtained from Aldrich, Germany. Formaldehyde was gained from Ajax Finechem. D,L-lactic acid was purchased from Acros Organics. All chemicals were used as received.

### Synthesis of poly(D,L-lactic acid)

In a typical synthesis experiment in this work, approximately 200 g of D,L-lactic acid were added into a 500 mL round-bottomed flask which contained about 2 g of p-toluene sulfonic acid (PTSA) as catalyst (1% by weight). The flask was then heated at 170 °C in a conventional short-path distillation apparatus for 4 hours. The pressure of system was reduced (ca. -25 inch Hg) for 2 hours to facilitate further removal of water and to increase the polymer yield. The molecular weight of products was consisting of 10,000 and 20,000 g/mol.

### Synthesis of polybenzoxazine

The polybenzoxazine precursors were prepared by mixing bisphenol-A, TETA, and formaldehyde at a mole ratio of 1:1:4, respectively [6,7]. Firstly, bisphenol-A (6.84 g, 30 mmol) was dissolved in 1,4-dioxane (15 mL) in a 50 mL glass bottle and was stirred until a clear solution was obtained. A formaldehyde solution (9.73 g, 324 mmol) was then added to the bisphenol-A solution. The temperature was kept under 10 °C by using an ice bath. TETA was then added dropwise into the mixture while continuously stirring for approximately 1 hour until a transparent yellow viscous liquid was obtained [8]. The process of chemical precursor was shown in Fig.1

### Preparation of poly(D,L-lactic acid)/polybenzoxazine films

The benzoxazine precursors were mixed with poly(D,L-lactic acid) ( $M_w=10,000$  and  $20,000$  g/mol) with 100:0, 99:1, 97:3, 95:5 and 0:100 ratio cast on glass plates at room temperature. The membranes were dried at room temperature in air for one day, followed by drying at 80 °C in an air-circulating oven for 24 hours to remove excess solvent.

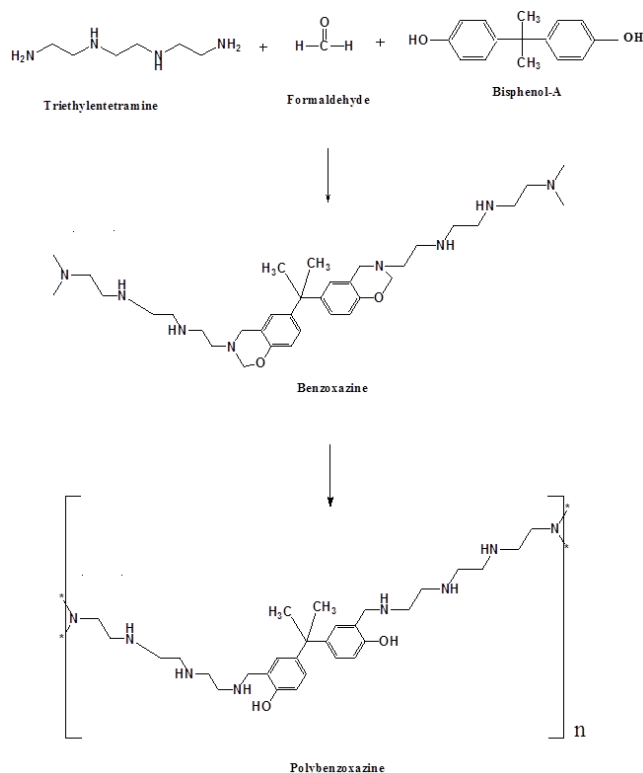


Fig.1 Synthesis of polybenzoxazine

### Characterization of poly(D,L-lactic acid)/polybenzoxazine

FTIR results were obtained by using Thermo Nicolet Nexus 670 (Vacuelli55) used to determine the chemical structure. The sample was mixed with KBr powder then it was compressed in sample preparation equipment to obtain the thin plate. The measurement wavelength was 500-4000  $\text{cm}^{-1}$ .

Morphological observations of poly(D,L-lactic acid)/polybenzoxazine films were performed using a JEOL JSM-6460LV scanning electron microscopy. The samples were sputter-coated with gold to produce a conductive coating and to prevent charging.

The thermal transition properties of the poly(D,L-lactic acid), polybenzoxazine and poly(D,L-lactic acid)/polybenzoxazine films were determined with a Perkin-Elmer Pyris Diamond differential scanning calorimeter (DSC) under a nitrogen flow. For DSC, samples of 5 – 10 mg in weight were heated at 10 °C/min over a temperature range of 0 to 250 °C to observe their melting temperature ( $T_m$ ) and glass transition temperature ( $T_g$ ). Thermogravimetric analyses (TGA) were done on TA-Instrument (TG SDT Q600) instrument from 30 to 800 °C using nitrogen. The heating rate was 10 °C/min.

Mechanical properties including stress at break, percentage Strain at Break and initial Young's modulus, of the poly(D,L-lactic acid),

polybenzoxazine and poly(D,L-lactic acid)/polybenzoxazine films were determined at 25 °C and 65% relative humidity with a Lloyds LRX+ Universal Mechanical Testing Machine. The film samples (80 x 10 mm) were tested with a gauge length of 25 mm and a crosshead speed of 10 mm/min. The mechanical properties were determined from the average of three measurements for each sample.

## RESULTS AND DISCUSSION

The photographs of poly(D,L-lactic acid) ( $M_w=10,000$  and  $20,000$  g/mol), polybenzoxazine and poly(D,L-lactic acid)/polybenzoxazine films were shown in Fig.2-3.

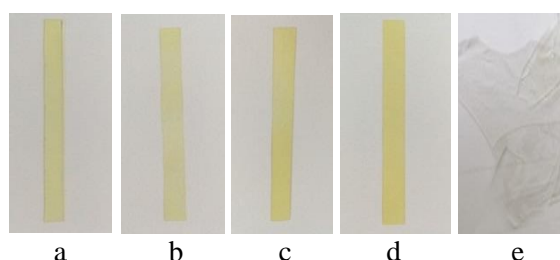


Fig. 2 The photographs of poly(D,L-lactic acid) ( $M_w=10,000$ g/mol)/polybenzoxazine films a=0PDLLA/100PBZ, b=1PDLLA/99PBZ, c=3PDLLA/97PBZ, d=5PDLLA/95PBZ and e =100PDLLA/0PBZ

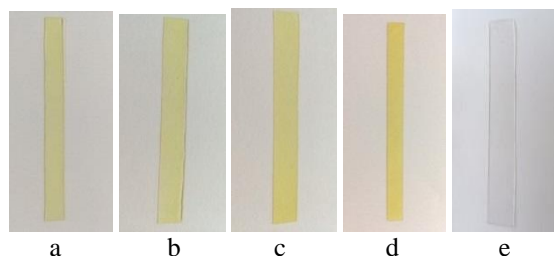


Fig. 3 The photographs of poly(D,L-lactic acid) ( $M_w=20,000$  g/mol)/polybenzoxazine films a=0PDLLA/100PBZ, b=1PDLLA/99PBZ, c=3PDLLA/97PBZ, d=5PDLLA/95PBZ and e=100PDLLA/0PBZ

The chemical structure of the prepared poly(D,L-lactic acid), polybenzoxazine and poly(D,L-lactic acid)/polybenzoxazine films were also confirmed using FTIR technique. The band of N-H stretching of the TETA was observed at around  $3400\text{ cm}^{-1}$ . The band at  $1502\text{ cm}^{-1}$  represents the stretching of the tri-substituted benzene ring. The out-of-plane bending vibration of C-H was observed at  $932\text{ cm}^{-1}$ . In addition, bands assigned to the asymmetric stretching of C-O-C and C-N-C were found at  $1233$  and  $1128\text{ cm}^{-1}$ , respectively. Furthermore, the  $\text{CH}_2$  wagging of the oxazine ring was also observed at  $1378\text{ cm}^{-1}$ . These FTIR results are in agreement with the study of Ning and Ishida [3], who also observed

the asymmetric stretching of C-O-C ( $1234\text{ cm}^{-1}$ ), the asymmetric stretching of C-N-C ( $1180$  to  $1187\text{ cm}^{-1}$ ), the  $\text{CH}_2$  wagging of oxazine ( $1325$  to  $1328\text{ cm}^{-1}$ ), the tri-substituted benzene ring ( $1502$  to  $1511\text{ cm}^{-1}$ ), and the out-of-plane bending vibrations of C-H ( $1502$  to  $1511\text{ cm}^{-1}$  and  $937$  to  $943\text{ cm}^{-1}$ ). The band of O-H and C=O of poly(D,L-lactic acid) was observed at around  $3500\text{ cm}^{-1}$  and  $1725\text{ cm}^{-1}$ , respectively as shown in Fig 5.

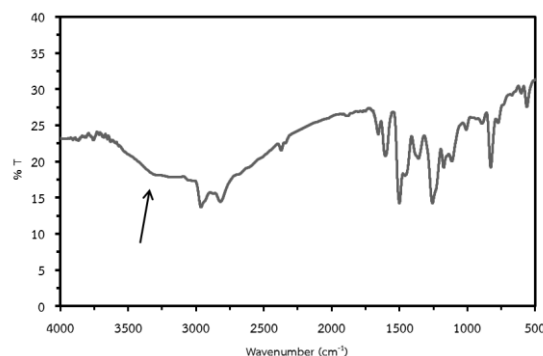


Fig. 4 The FTIR spectrum of polybenzoxazine

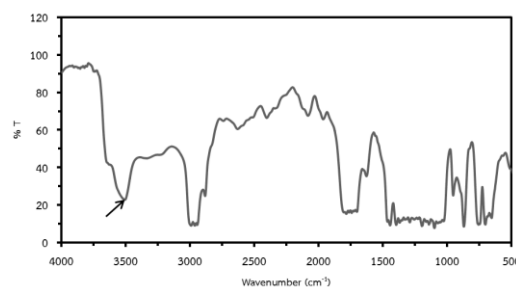


Fig. 5 The FTIR spectrum of poly(D,L-lactic acid)

## Morphology

Morphology of the blend films was studied from SEM images. Figure 6 and 7 show SEM images of poly(D,L-lactic acid)/polybenzoxazine films with ( $M_w=10,000$  g/mol) and ( $M_w=20,000$  g/mol), respectively. The blend films show smooth surface. The increasing ratio of poly(D,L-lactic acid) show the higher rough surface.

## Thermal transition properties

The thermal transition properties of the blend films were obtained from DSC thermograms to obtain melting temperature ( $T_m$ ) glass transition temperature ( $T_g$ ) as shown in Fig. 8-9. The  $T_g$  of the blend films were around  $30$ - $29\text{ }^{\circ}\text{C}$ . The raising  $T_g$  was gained with high molecular weight because the polymer chain was more disorder. Addition of poly(D,L-lactic acid) was also increase  $T_g$ . The formation of polymer chain affected to the thermal transition properties. The blend films with

3PDLLA/97PBZ and 5PDLLA/95PBZ show the  $T_m$  at around 117-143 °C according to some part of polymer chain was order formation to get crystallinity. The thermal stability of the poly(D,L-lactic acid), polybenzoxazine and poly(D,L-lactic acid)/polybenzoxazine was investigated using TGA as shown in Fig. 10-11. The blend films show 3 steps of degradation, 150-200 °C, 250-400 °C and 400-450 °C

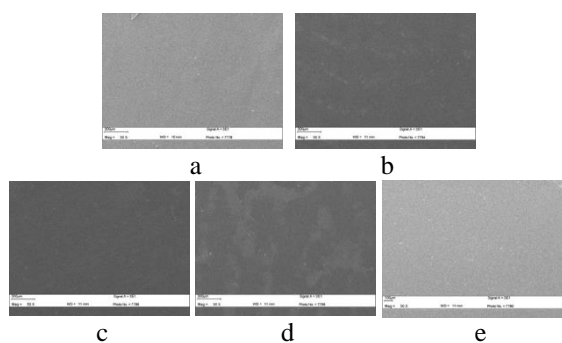


Fig. 6 The SEM results of polybenzoxazine (a), poly(D,L-lactic acid)( $M_w=10,000$  g/mol) /polybenzoxazine 99:1 (b), 97:3 (c), 95:5 (d) and poly(D,L-lactic acid) (e)

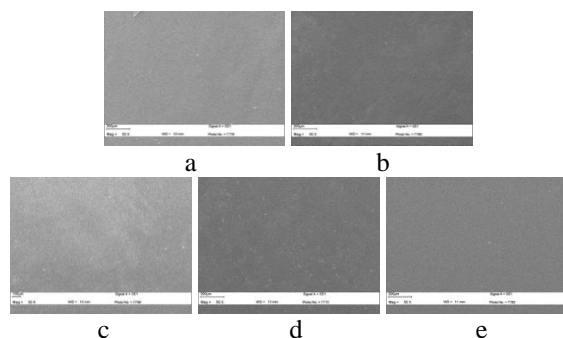


Fig. 7 The SEM results of polybenzoxazine (a), poly(D,L-lactic acid)( $M_w=20,000$  g/mol) /polybenzoxazine 99:1 (b), 97:3 (c), 95:5 (d) and poly(D,L-lactic acid) (e)

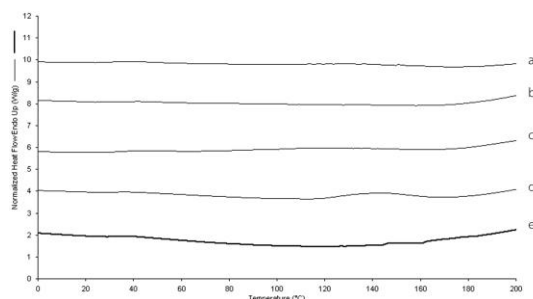


Fig. 8 The DSC results of polybenzoxazine (a), poly(D,L-lactic acid)( $M_w=10,000$  g/mol) /polybenzoxazine 99:1 (b), 97:3 (c), 95:5 (d) and poly(D,L-lactic acid) (e)

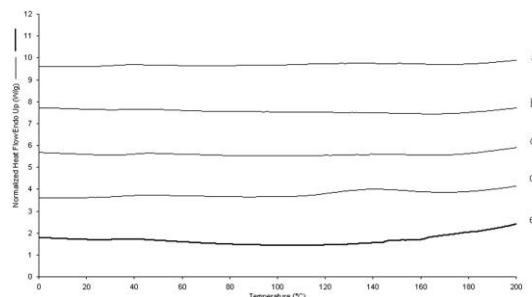


Fig. 9 The DSC results of polybenzoxazine (a), poly(D,L-lactic acid)( $M_w=20,000$  g/mol) /polybenzoxazine 99:1 (b), 97:3 (c), 95:5 (d) and poly(D,L-lactic acid) (e)

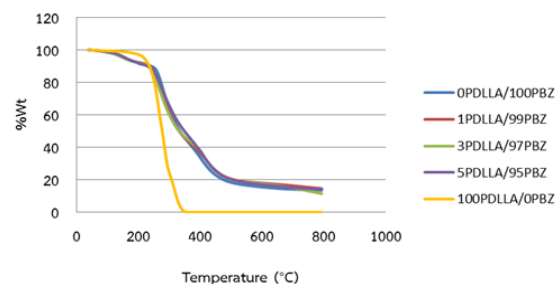


Fig. 10 The TGA results of poly(D,L-lactic acid)( $M_w=10,000$  g/mol), polybenzoxazine and poly(D,L-lactic acid)/polybenzoxazine.

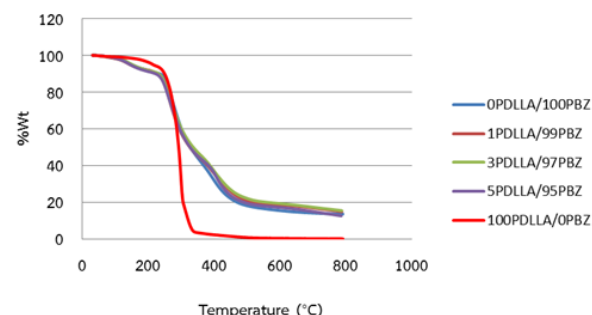


Fig. 11 The TGA results of poly(D,L-lactic acid)( $M_w=20,000$  g/mol), polybenzoxazine and poly(D,L-lactic acid)/polybenzoxazine.

### Mechanical properties

The mechanical properties, stress at break, percentage strain at break and Young's modulus, of poly(D,L-lactic acid), polybenzoxazine and poly(D,L-lactic acid)/polybenzoxazine were determined from tensile testing. The results of mechanical properties of the blend films were compared in Table 1-2 for stress at break, percentage strain at break and Young's Modulus, respectively. It can be seen that Young's modulus of blend films significantly increased as the poly(D,L-lactic acid) ratio increased. Especially 3PDLLA:97PBZ ratio showed high stress at break and good flexibility.

This due to the poly(D,L-lactic acid) can increase free volume of polybenzoxazine molecules. The tensile results suggested that poly(D,L-lactic acid) showed good potential for mix with polybenzoxazine.

Table 1 Tensile properties of poly(D,L-lactic acid)( $M_w=10,000$  g/mol), polybenzoxazine and poly(D,L-lactic acid)/polybenzoxazine.

Sample PDLLA : PBZ	Stress at Break (MPa)	Percentage Strain at Break	Young's Modulus (MPa)
0:100	12.69 $\pm 3.97$	77.82 $\pm 25.83$	374.53 $\pm 95.61$
1:99	10.52 $\pm 5.83$	45.90 $\pm 84.58$	352.49 $\pm 114.93$
3:97	9.05 $\pm$ 6.96	2.59 $\pm 1.55$	581.90 $\pm 128.10$
5:95	19.18 $\pm 6.25$	27.15 $\pm 37.06$	588.80 $\pm 153.21$
100:0	nd	nd	nd

nd = not detected

Table 2 Tensile properties of poly(D,L-lactic acid)( $M_w=20,000$  g/mol), polybenzoxazine and poly(D,L-lactic acid)/polybenzoxazine.

Sample PDLLA : PBZ	Stress at Break (MPa)	Percentage Strain at Break	Young's Modulus (MPa)
0:100	12.69 $\pm 3.97$	77.82 $\pm 25.83$	374.53 $\pm 95.61$
1:99	12.37 $\pm 6.44$	2.83 $\pm 1.36$	668.92 $\pm 106.60$
3:97	24.06 $\pm 7.99$	6.04 $\pm 3.72$	657.23 $\pm 137.45$
5:95	15.29 $\pm 2.79$	34.16 $\pm 17.49$	466.33 $\pm 67.39$
100:0	15.56 $\pm 4.89$	7.03 $\pm 2.98$	491.29 $\pm 81.41$

## CONCLUSIONS

In conclusions, it was successfully synthesized of poly(D,L-lactic acid) ( $M_w=10,000$  and  $20,000$  g/mol), polybenzoxazine and poly(D,L-lactic acid)/polybenzoxazine with 0PDLLA/100PBZ, 1PDLLA/99PBZ, 3PDLLA/97PBZ, 5PDLLA/95PBZ and 100PDLLA/0PBZ. It was found that the blend films showed better thermal properties than the pure polymer due to the good formation of polymer blend. The SEM images were confirmed well blending poly(D,L-lactic acid)/polybenzoxazine. Increasing the amount of poly(D,L-lactic acid) gave the film a more smooth and homogeneous. It was also approved by mechanical properties using tensile testing. The 5PDLLA/95PBZ ratio with poly(D,L-lactic acid)  $M_w = 10,000$  g/mol and 3PDLLA/97PBZ

ratio with poly(D,L-lactic acid)  $M_w = 20,000$  g/mol show the best flexibility compare with other ratio. It was concluded that a mixture of poly(D,L-lactic acid) with polybenzoxazine improved the performance of the blend film.

## ACKNOWLEDGEMENTS

This research was financially supported by Mahasarakham University, Mahasarakham, Thailand.

## REFERENCES

- [1] Jacobsen, S.; Degee, Ph.; Fritz, H.G.; Dubois, Ph.; Jerome, R. *Polym. Eng. Sci.*, 39, 1999, pp.1311-1319.
- [2] Celi, A. Scandola, M. *Polymer*, 33, 1992, pp. 2699-2703
- [3] Ning, X., and Ishida, H., *J. Polym. Sci.*, 32, 1994, pp. 1121-1129.
- [4] T. Takeichi, T. Kano, T. Agag, *Polymer*, 46, 2005, pp. 12172-12180.
- [5] T. Agag, T. Takeichi, *J. Polym. Sci. Part A: Polym. Chem.* 45, 2007, pp. 1878-1888.
- [6] P. Lorjai, T. Chaisuwan, S. Wongkasemjit, *J. Sol-Gel Sci. Technol.* 52, 2009, pp. 56-64.
- [7] P. Lorjai, T. Chaisuwan, S. Wongkasemjit, *Mater. Sci. Eng., A* 527, 2009, pp. 77-84.
- [8] T. Takeichi, T. Agag, *High Perform. Polym.* 18, 2006, pp. 777-797.
- [9] Y. Ikada, K. Jamshidi, H. Tsuji, S. H. *Macromolecules*, 20, 1987, pp. 904-906.
- [10] Z. Kulinski, E. Piorkowska, K. Gadzinowska, M. Stasiak, *Biomacromolecules*, 7, 2006, pp. 2128-2135.
- [11] H. Tsuji, S.H. Hyon, Y. Ikada, 1991. *Macromolecules*, 24, 1991, pp. 5651-5656.
- [12] G. Theryo, F. Jing, L. M. Pitet, M. A. Hillmyer, *Macromolecules*, 43, 2010, pp. 7394-7397.
- [13] Y. Hu, Y.S. Hu, V. Topolkaraev, A. Hiltner, E. Baer, *Polymer*, 44, 2003, pp. 5711-5720.
- [14] E. Piorkowska, Z. Kulinski, A. Galeski, R. Masirek, *Polymer*, 47, 2006, pp. 7178-7188.
- [15] H. Xu, C. Teng, M. Yu, *Polymer*, 47, 2006, pp. 3922-3928.

## BIOCHEMICAL CHANGES IN CHEMICAL INGRADIENTS OF SILK COCOONS UNDER ENVIRONMENTAL FACTORS

H.N.P. Singh<sup>1</sup>, Sunita Kumari<sup>2</sup> and M.M. Prasad<sup>3</sup>

<sup>1&3</sup>Post. Graduate Department of Biotechnology

<sup>1</sup>T.M. Bhagalpur University Bhagalpur-812007, Bihar, (India)

<sup>2</sup>S.M. Inter Girls School, Mirjanhat Bhagalpur

### ABSTRACT

Environmental factors like temperature, light and relative humidity greatly influence the damage and spoilage of agricultural, horticultural and sericultural products. Subsequently the quality of these sericultural products depend on temperature and relative humidity of storage centers at which they are stored. The healthy as well as infested lots of tasar and mulberry by three test fungi viz *Fusarium moniliforme*, *Aspergillus flavus* and *Penicillium citrinum* were stored under different RH i.e. 33, 55, 75, and 96 per cent. The results show that storage of infested tasar and mulberry cocoons at various RH for different intervals had pronounced effect on total protein and carotenoid contents. In general, there was an increase in the rate of degradation of chemicals with increase in RH values and incubation period. The results show that at all the relative humidities, maximum degradation in the chemical constituents was recorded in 60 days by all the *infested fungi*. Out of four variables (33, 55, 75, 96%), maximum degradation was observed at 96% RH in 60 days of storage period in tasar as well as mulberry cocoons. However minimum reduction was noted in 20 days of incubation in both types of tasar and mulberry cocoons in all test fungi.

**Keyword :** Biochemical, Silk Cocoons, Environmental Condition

### INTRODUCTION

The history of silk dates back to the origin of civilization. It has been named in legends, folklores. The superiority of silk as textile fibre has been recognized since time immemorial. The luxurious look, sleek feel, fine lusture and textiles of silk fabrics are unquestionably inimitable. However the chemical constituents of silk fibre changes due to fungi under environmental factors like RH. So the present investigation aims to study the biochemical changes in chemical constituent of silk cocoons under different relative humidities during fungal infestation.

### MATERIAL METHODS

The effect of different relative humidifies was studied following the method of [10]. To maintain different relative humidities viz, 33%, 55%, 75% and 96%, saturated solution of Magnesium chloride ( $\text{MgCl}_2 \cdot 6\text{H}_2\text{O}$ ), Magnesium nitrate  $\text{Mg}(\text{NO}_3)_2$  Sodium chloride (NaCl) and Potassium nitrate ( $\text{KNO}_3$ ) respectively were prepared and placed in sterilized desiccators. In order to study the bio

chemical changes in tasar and mulberry cocoons under infestation, 5gm of each healthy cocoons were surface sterilized by 0.1% mercuric chloride and followed by two successive washing with sterilized distilled water. These samples were infested separately and aseptically by the spore, suspension of fungi in sterilized distilled water. Standardization of spore suspension was done by dilution technique (about 200 – 250 spores / 0.5 ml)

Infested as well as control lots were incubated at room temperature ( $25 \pm 2^\circ\text{C}$ ) for 20 days, 40 and 60 days under various relative humidities. At the end of each incubation period sample were washed then oven dried and powdered. The powdered samples were taken for the estimation of total protein [4] and carotenoid and then estimated [1].

### RESULTS

#### *Protein*

The total protein (8.52%) of controlled tasar cocoons showed little fluctuation in their concentration during storage at various RH for



different intervals (Table-I) Infestation by all the fungi caused a gradual fall in the amount of total protein. The maximum decline in the amount of the total proteins were recorded at 96% RH by *F. moniliforme* (88.14%) followed by *A. flavus* (86.66%) and *P. citrinum* (85.18%), respectively in 60 days in case of tasar cocoons.

Mulberry cocoons exhibited the similar trend. The maximum degradation of total protein was noted at 96% RH due to all the three fungi where as minimum was observed at 33% RH in 20 days of storage (Table-II)

**Table I Level of total protein (mg/100 mg) in tasar cocoons under infestation at different RH**

	33%				55%		
	0	20	40	60	20	40	60
FUNGI	day	days	days	days	days	days	days
Control	8.52	8.52	8.52	8.10			
<i>F. moniliforme</i>		6.96	6.66	6.12	6.48	6	5.52
% Loss		18.3	21.83	24.44	23.94	29.57	1.85
<i>A. flavus</i>		7.32	6.96	6.48	6.66	6.12	5.64
% Loss		14.08	18.3	20	21.83	28.16	28.87
<i>P. citrinum</i>		7.5	7.14	6.66	6.84	6.48	5.64
% Loss		11.97	16.19	17.77	19.71	23.94	0.37

**Contd. Table I**

	75%			96%		
	20	40	60	20	40	60
days	days	days	days	days	days	days
4.56	1.44	1.08	2.04	1.32	0.96	
46.47	83.09	86.66	76.05	84.50	88.14	
4.68	1.92	1.32	2.46	1.74	1.08	
45.07	77.46	83.70	71.12	79.57	86.66	
5.04	2.34	1.44	2.88	2.16	1.20	
40.84	72.53	82.22	66.19	74.64	85.18	

**Table II Level of total protein (mg/100 mg) in mulberry cocoons under infestation at different RH**

	33%				55%		
	0	20	40	60	20	40	60
FUNGI	day	days	days	days	days	day	days
Control	14.10	14.16	14.16	13.95			
<i>F. moniliforme</i>		10.53	9	8.48	8.59	7.46	6.90
% Loss		25.63	36.44	40.11	8.89	7.46	51.27

<i>A. flavus</i>	11.25	10.60	10	9.51	8.46	8.75
% Loss	20.55	25.14	26.37	32.83	40.25	38.20
<i>P. citrinum</i>	10.66	10.23	10	10.10	9.79	9.32
% Loss	24.71	27.75	29.37	28.67	30.86	34.28

**Contd. Table II**

	75%			96%		
	20	40	60	20	40	60
days	days	days	days	days	days	days
6.4	5.85	5.28	4.74	4.40	4.10	
54.80	56.07	62.71	66.52	68.92	71.04	
7.18	7.80	6.22	6.86	6.40	5.90	
49.29	44.91	56.07	5.55	54.88	58.33	
8.93	8.52	7.50	7.00	6.50	5.58	
36.93	39.83	47.03	50.56	54.09	60.59	

**Table III Level of carotenoid (mg/100 mg) in tasar cocoons under infestation at different RH**

	33%				55%		
	0	20	40	60	20	40	60
FUNGI	day	days	days	days	days	days	days
Control	0.112	0.112	0.112	0.102			
<i>F. moniliforme</i>		0.111	0.111	0.171	0.068	0.065	0.058
% Loss		1.508	0.892	4.375	39.307	41.696	
47.946							
<i>A. flavus</i>		0.112	0.111	0.111	0.870	0.082	0.073
% Loss		0.354	0.714	0.714	22.448	26.696	
34.464							
<i>P. citrinum</i>		0.111	0.111	0.111	0.101	0.090	
0.064							
% Loss		1.419	0.535	0.803	10.204	19.642	
42.589							

**Contd. Table III**

	75%			96%		
	20	40	60	20	40	60
days	days	days	days	days	days	days
0.050	0.043	0.035	0.031	0.023	0.012	
55.456	60.803	68.392	72.315	79.107	88.750	
0.057	0.051	0.040	0.048	0.043	0.031	
49.157	54.285	64.017	56.699	61.428	71.964	
0.054	0.049	0.036	0.041	0.025	0.011	
51.286	55.535	67.50	62.821	76.964	90.178	

**Table IV Level of carotenoid (mg/100 mg) in mulberry cocoons under infestation at different RH**

FUNGI	33%				55%			
	0	20	40	60	20	40	60	
	day	days	days	days	days	days	days	days
Control	0.16	0.16	0.16	0.16				
<i>F. moniliforme</i>		0.141	0.12	0.109	0.116	0.11	0.10	
% Loss		11.87	20	25.62	27.50	31.25	37.50	
<i>A. flavus</i>		0.15	0.14	0.13	0.139	0.128	0.119	
% Loss		6.25	12.50	18.75	13.12	20	25.62	
<i>P. citrinum</i>		0.138	0.127	0.118	0.12	0.109	0.10	
% Loss		13.75	20.62	26.29	25	31.87	37.50	

Contd. Table IV

	75%			96%		
	20	40	60	20	40	60
	days	days	days	days	days	days
0.111	0.10		0.091	0.102	0.09	0.072
30.62	37.50		43.12	36.25	43.75	55
0.128	0.116		0.108	0.12	0.10	0.082
20	27.50		32.50	25	36.25	51.25
0.112	0.102		0.096	0.101	0.097	0.08
30	0.363		40	36.80	43.12	50

## CAROTENOID

It is obvious from the results (Table-III) that infestation of tasar cocoons by *F. moniliforme*, *A. flavus*, *P. citrinum* caused a considerable change in the carotenoid contents with the increase in the storage period as well as RH values. The maximum fall was recorded by *P. citrinum* (90.17%) which was subsequently followed by *F. moniliforme* (88.75%) *A. flavus* (71.96%) respectively in 60 days at 96% RH.

The controlled mulberry cocoons contained 0.162% of carotenoid under infestation by all the three test fungi was reduced to varying extent at different relative humidities. Maximum reduction of carotenoid was noticed at 96% RH due to *F. moniliforme* (55.00%) which in turn was followed by *A. flavus* (51.05%) and *P. citrinum* (50.00%) respectively in 60 days of storage. However the losses were observed minimum at 33 percent RH in 20 days of incubation by all the three test fungi (Table-IV).

## DISCUSSIONS

The present findings indicate that storage of infested tasar and mulberry cocoons at various relative humidities for different intervals had pronounced effect on their total protein and carotenoid contents. In general, there was an increase in the rate of degradation of protein and carotenoid with the increase in relative humidity as well as period intervals. The maximum loss in the concentration of protein and carotenoid was recorded in 60 days by *F. moniliforme* at 96% RH, however minimum degradation was observed at 33% relative humidity value in 20 days of storage. Greater loss in chemical constituents upon 96 percent relative humidity in the present investigation is supported by the results of [2, 3, 5, 7 and 9]. Such loss in cocoons could be firstly due to luxuriant growth of fungi between 75-96% relative humidity resulting into more utilizations of chemical constituents of silk fibres for growth and development of fungi. Secondly, it might be due to greater enzymatic activity by the colonizing fungi [6&8].

## CONCLUSIONS

On the basis of present findings we conclude that the environmental factor *i.e.* relative humidity is very important factors for the degradation of chemical constituents of silk cocoons due to different fungi and storage period. The relative humidity value of 96% as well as 60 days of incubation period are most suitable condition for growth and development of fungi and their metabolic activities. However maximum degradation was observed due to fungi so the farmers and tribal people of these regions are suggested to control the spoilage of cocoons by keeping the cocoons in safe and scientific storage centre in scientific way so that silk thread quality remains maintained along with good market value.

## ACKNOWLEDGEMENTS

I am highly thankful to P.G. Dept. of Botany and Biotechnology, T.M Bhagalpur University, Bhagalpur – 812007, Bihar (INDIA) for laboratory and library facilities as well as U.G.C, Government of INDIA for Financial supports. I am also grateful to my teacher Prof. A. K. Roy Vice Chancellor B. N. Mandal University Madhepura Bihar India for continuous inspirational supports.

## REFERENCES

- [1] Davis, B.H. (1976). Carotenoids. In Goodwin, T.W. ed. *Chemistry and Biochemistry of plant pigments Vd-2* London : Academic Press. 38-165.
- [2] Jolly, Dr. M.S., S.K. Sen., T.N. Sonwalkar and G.K. Prasad (1981). *Non Mulberry silk Food & Agriculture Organization of United Nations*, Rome, Italy.
- [3] Kumari Vineeta and A.K. Roy (1990). Biodegradation of embelia ribus seeds under the influence of different relative humidities. *Nat. Acad Sai. Letters* **13** (5) 167-169.
- [4] Lowry, O.H., N.J. Rosebrough, A.L. Farr and R.R. Randall (1951). Protein measurement with the folin phenol reagent *J. Biol. Chem* **193**, 265-275.
- [5] Prasad, M.M. and H.N.P. Singh (1995). Biodegradation on of chemical constituents in silk cocoons by some storage fungi. *National academy Science letters* Vol. **18**, (9&10), 163-164.
- [6] Prasad, M.M. and H.N.P. Singh (1995). Biodegradation of chemical constituents in tasar silk cocoons after infection with fungi *Letters in Applied Microbiolgy*. Vol. **21**, 235-236.
- [7] Prasad, M.M. and HNP. Singh (1998). *Screening of silk cocoons under storage for Microbial damage*. Proceeding volume phytodiversification and Human welfare (Eds A.K. Roy J.V.V. Dogra & S.K. Verma) M.D. Publications. New Delhi Page 47-51.
- [8] Prasad, M.M., HNP. Singh, A.K. Roy and R.K. Sinha (1995). *Microbial spoilage of silk cocoons in storage centres of Bihar and their control*. Final Technical Report UGC, Code No. F. 3-22/91 (RBB-I), Research Project Govt. of India, New Delhi.
- [9] Roy, A.K and Nilamy Choubey (1984). Changes in protein contents of bitter gourd at different relative humidities by two pathogenic fungi. *Indian Phytopath.* **37**, 179-181.
- [10] Wink, S.A. and G.R. Sears (1950) Instrumentation studies LVii equilibrium related humidities above saturated salt solutions at various *Tappi* **39** (9): 96 A-97.

## ACUTE EFFECTS OF TRADITIONAL THAI MASSAGE ON HEART RATE VARIABILITY, HEART RATE AND SALIVARY ALPHA AMYLASE

Jaruk Keawsod<sup>1</sup> Wichai Eungpinichpong<sup>2</sup>

1. Graduate school, Khon Kaen University, Thailand;

2 Research and Training Center for Enhancing Quality of Life of Working Age People, Khon Kaen University, Thailand;

\*Corresponding Author, Received: 00June 2017, Revised: 00 June 2017, Accepted: 00 0000 2017

**ABSTRACT:** Prolonged stresses always lead to autonomic nervous system (ANS) imbalance that causes physical and mental disorders. A session of 60 minute of Tradition Thai massage (TTM) can reduce stress and heart rate as well as improve heart rate variability (HRV). However changes in the HRV, an indicator of ANS balance during TTM has not been explored. The purposes of this study are to investigate the effects of TTM on HRV and other stress parameters including heart rate (HR) and Salivary alpha amylase (sAA). Across-over design was carried out in 18 healthy subjects who were recruited and randomly allocated into two groups receiving either TTM or Control (CT) for 60 minute in each session. HRV and HR were recorded every 5 minute while sAA was recorded at baseline and post-intervention sessions. The results showed that high frequency (HF) component of HRV was increased significantly at 20, 55 minutes and maintained until the end of session within TTM group ( $P<0.05$ ). Within the CT group, HF was significantly increased at 15, 20 and 40 minutes ( $p<0.05$ ), however it was significantly decreased close to baseline at post session. Between group comparison revealed that HF was significantly increased at 35, 55, 60 minutes and post session ( $P<0.05$ ). The HR within TTM group was decreased significantly at the first 5 minutes of having TTM and maintained until post session ( $p<0.01$ ) whereas within CT group, the HR was decreased significantly only at the first 15 minutes of session. The HR was also decreased significantly in TTM at 10 to 50 minutes when compared to CT. Salivary alpha amylase (sAA) level at post-session in TTM was slightly decreased as compare to baseline. However, it was decreased significantly at post session in TTM when compared to CT ( $p<0.01$ ). The results suggest that a session of 60 minutes of whole body TTM could increase HF, and thus improve HRV and decrease HR. A short duration of 20 minutes of TTM is sufficient to improve autonomic nerves system activity (ANS). Therefore, for the purpose of improving ANS activity or stress reduction in healthy individuals by mean of TTM, we suggest that practitioner may use a shorter duration (20 minutes) than 60 minutes.

*Keywords: Massage, Stress, Heart Rate Variability, Salivary alpha amylase*

### 1. INTRODUCTION

Sufficient stress can be effective against challenge such as competitive stress for athlete. It may drive someone to complete their goal in an excellent standard [1]. But if prolonged stresses persisted, for example over train athlete or over stressed office workers, SNS becomes over stimulated (even in the rest time that PNS should be more activated) and leads to ANS imbalance. This not only drop on performance of the athlete but also cause many health problems such as insomnia, anxiety, fatigue, headache and constipation [2]. In long term, expose to chronic stresses can increase cardiovascular risk [3].

Traditional Thai Massage (TTM) is one type of manual therapies using the hand or thumb to apply pressure to muscles of limbs and back along meridian lines and combine with stretching. TTM is a non-invasive and

non-pharmacological treatment that has been shown to reduce stress, pain, anxiety, increase blood circulation and muscle flexibility and promote relaxation [4]-[6]. A 30-minutues session of TTM in patients with back pain associated with myofascial trigger points can also increase HRV and improve stress-related parameters [7]. Although touch massage (TM) could lower the stress level and increase HRV using full therapy of 80 minutes, the researcher found that just only 5 minutes of TM could significantly increase HRV [8]. Similarly, duration of application using TTM always be 1-2 hours per session for promote relaxation or stress reduction. A shorter period on application using TTM has not been studied on this regard. The duration of time that affects the change in HRV resulting from TTM has not been investigated.

## 2. MATERIAL AND METHOD

This study was a crossover randomized controlled trial, approved by the Ethical Committee of Khon Kaen University, Thailand (HE592306). eight teen participants were recruited in this study but two of them dropped out during the washout period due to unable to come for data collection on the second visit second visit. The remaining participants consisted of six teen healthy participants including 16 with the average age of  $25.4 \pm 4.8$  years who completed all the procedures. They were randomly allocated into either a Traditional Thai massage group (TTM) group or a Control (CT) group after which they were swabbed to the other one with 2 weeks washed out period. Each of them gave written informed consent to participate in this study. The participants were excluded from the study if A history of having disease or disorder which may affect on heart rate variability (HRV), such as heart diseases, and hypertension or having disease or disorder that met contraindication to Thai massage, regular smoking or drinking alcohol within the past one year or regularly drinking coffee or beverage that contained caffeine more than 2 times per week.

### 2.1 Procedure and Protocol

After the participants underwent screening procedures using interview and subjective examination, they were asked to give inform consent and followed by having the sequence of the following interventions.

#### 2.1.1 Traditional Thai massage group

The participant was asked to rest in supine for 5 minutes then Salivary alpha-amylase baseline was collect by the participants put the edge of the test strip (saliva-collecting paper) into the mouth, and left it underneath the tongue (sublingual) for 2 minutes. After that HRV 5-min measurements were taken with a probe attached to the tip of the participant's left finger to collect the HF baseline. Then the participant received TTM session for 60 minutes in supine lying position. The session was divided into 10-minute sub-sessions for each of the body parts including the right leg, the left leg, the right arm, and the left arm (when massage the left arm part; the probe was attached to the tip of the

participant's right finger). When the TTM in supine lying position was completed (40 minutes) the participant changed to prone position and rest for 5 minutes before starting the massage for lower back and upper back (included neck) parts for 20 minutes. HRV were measured every 5 minutes during the 60-minute massage session. After the massage session was over, the participant was asked to rest in supine for another 5 minutes. Then the HRV and Salivary alpha-amylase were measured for post session data. The pressing technique employed in TTM was done by transferring the body weight of the massage therapist to apply gentle, gradually increasing, pressure through the therapist thumb, palm or elbow. The amount of pressure used was controlled by the therapist to be within the pressure pain threshold. Each of the pressure was maintained for 5 second. [9]. Massage session was performed by a 7-year experience full time physiotherapist. who has been certified and had good skills in performing Thai massage. For control group, the participants were received the same protocol as TTM group without massage.

### 2.3 Outcome measurements

#### 2.3.1 Heart rate variability (HRV)

All participants were asked to refrain from talking, falling asleep, exaggerated body movements and intentionally altering their respiration. They were carefully monitored to ensure there were no significant respiratory or postural changes during the session [10]. After resting in supine position for 5 minutes, baseline HRV was measured in a supine position with the APG UbioMacpa (HPLAN Co., Ltd., Busan, Busan-Gwangyeokshi). HRV data were measured every 5 minutes with a probe attached to the tip of the participant's left finger. This measurement was performed by the research assistant. Time domain analysis of HRV and power spectral analysis using the fast Fourier transformation were performed. Test measurements were taken in a temperature controlled room (25°C). During the massage HRV parameters were determined for every successive 5-min segment. HRV were calculated using frequency domains by APG UbioMacpa software, and the following parameters were calculated to yield high frequency power (HF) and mean heart rate. In this study, HF was the main parameter since it reflected the sole parasympathetic activity.

#### 2.3.2 Salivary alpha-amylase (sAA) levels

### assessment

Each of the participants was chewing cotton wool for 1 minute to induce excretion of saliva, participants put the edge of the test strip (saliva-collecting paper) into the mouth, and left it underneath the tongue (sublingual) for 2 minutes. After that, the test strip was fit into the handle sleeve and slid into the Cocoro meter (NiproCo., LTD., Japan).

## 2.4 Statistical Analysis

That data were present as mean  $\pm$  SD. Shapiro-Wilk test was used to test for normal distribution of each variable. ANOVA with repeated measures was used to analyze each of the variables before, during intervention, and follow up measurements. Paired sample t-test was used to test for differences in each measure between the groups. The statistical analyses were performed with SPSS software (version 17.0, SPSS Inc., Chicago IL, USA). And Statistical significance was set a  $p < 0.05$ .

## 3. RESULTS

High frequency (HF) was used as the main outcome measure for HRV. Paired T-test revealed that there were significantly higher HF values in TTM compare to CT at 35, 65 minute and post session ( $P$ -value  $< 0.01$ ) and at 70 minute ( $P$ -value  $< 0.05$ ) the data were present in Table 1

Table 1 Changes of High frequency (HF) between CT and TTM group at each time point (Mean  $\pm$  SD)

Time point (minutes)	High Frequency		
	CT	TTM	P value
Baseline	6.31 $\pm$ 0.59	6.26 $\pm$ 0.34	0.629
5	6.30 $\pm$ 0.50	6.29 $\pm$ 0.81	0.933
10	6.38 $\pm$ 0.35	6.48 $\pm$ 0.74	0.482
15	6.68 $\pm$ 0.29	6.36 $\pm$ 0.68	0.103
20	6.66 $\pm$ 0.34	6.53 $\pm$ 0.73	0.459
25	6.37 $\pm$ 0.63	6.33 $\pm$ 0.75	0.778
30	6.38 $\pm$ 0.61	6.56 $\pm$ 0.84	0.109
35 **	6.23 $\pm$ 0.65	6.49 $\pm$ 0.55	0.001
40	6.74 $\pm$ 0.54	6.39 $\pm$ 0.75	0.114
55	6.69 $\pm$ 0.68	6.71 $\pm$ 0.81	0.913
60	6.67 $\pm$ 0.63	6.61 $\pm$ 0.68	0.598
65 **	6.34 $\pm$ 0.73	6.73 $\pm$ 0.68	0.002
70 *	6.51 $\pm$ 0.65	6.80 $\pm$ 0.50	0.019
Post session**	6.39 $\pm$ 0.68	6.89 $\pm$ 0.37	0.001

Note: CT is control group, TTM is traditional Thai massage group, \* =  $p < 0.05$ , \*\* =  $p < 0.01$

significantly from 5 minutes to post session as compare to baseline ( $P$ -value  $< 0.05$ )

For mean heart rate (Mean HR), paired T-test comparing mean HR in CT and TTM at each time point revealed that there were significantly lower mean HR in TTM compare to CT from 10 to 60 minute

Salivary alpha-amylase (sAA) was found significantly increased in CT, whereas in TTM, it slightly decreases but no statistical significance. When compare sAA between TTM and CT group, the sAA at post session significantly lower ( $P$ -value  $< 0.01$ )

## 4. DISCUSSION

In the present study, TTM to whole body for 60 minutes is effective in increasing parasympathetic activity in healthy participant (Table 1). Even though the data in figure 1 revealed that HF began to change significantly at 35 minute of session, it increased slightly from 5 to 15 minute compare to baseline (6.29, 6.48 respectively). The change in HF as biphasic curve and tended to increase until the end of session. In control state at 15 and 20 minutes, the increase in HF might be due to the relaxation from resting position. Then it decreased to nearly close to baseline. However HF it became a peak again at 40 minute. This may be because of changing the probe site from an index finger of one hand to another one at 30 to 40 minutes of investigation according to the preset protocol. Changing the probe from left to right finger may affect the HRV recordings [11]. A decreasing in HR in this study also was in accordance with the study of Lindgren et al.,[8] that HR decrease significantly after 5 minutes of massage and lasting for 65 minutes. In the present study, HR decreased significantly after 5 minutes and lasted until post session of TTM. Even though the context of these study were different such as pressure, form of massage, and the duration of treatment or the control environment, the results showed a similar trend. These results support the theory that massage has an effect on parasympathetic nervous system [12]. Salivary alpha-amylase (sAA) was found significantly increased in CT, whereas it slightly decreased but no statistical significance in TTM. When compare sAA between TTM and CT group, The sAA at post session significantly lower. This finding supported the result of Sripongngam et al.,[13] that TTM could lower stress as indicated by the lower level of Salivary alpha-amylase in healthy

individual. Since we do not have stressor onto the participants, the changes in sAA might not be significantly different. Our protocol required that participants had to change position at 40 minute, and they laid in a certain position in order to measure the HRV correctly. This may lead to a decrease level of Salivary alpha-amylase (sAA) at post session in control group.

Even though APG Ubiomacpa can give the real time HRV data with only finger probe attach to participants' fingertips during assessment, the participant had to be carefully monitored to ensure there were no significant respiratory or postural changes during the session [10]. Thus we have to modify TTM to minimize the movement of body part when TTM was performed and even pause the assessment when change position to prone to wait for HRV to be stable and continue to the end of the protocol. This prolonged constrained condition may affect the feeling of the participants and the HRV results.

## 5. CONCLUSION

The results of this study suggested that a session of 60 minutes whole body TTM could increase HF, thus improve HRV and decrease mean HR. A short duration of 20 minutes of TTM was sufficient to improve autonomic nerves system activity (ANS). Therefore, we suggest that practitioner may use a shorter duration of TTM (20 minutes) for improving ANS in healthy individual.

## 6. ACKNOWLEDGEMENTS

The authors would like to thank the volunteers who participated in the study. Our special thanks go to Research and Training Center for Enhancing Quality of Life of Working Age People, Khon Kaen University for financially supporting this study.

## 6. REFERENCES

- [1] Yerkes RM, Dodson JD. "The relation of strength of stimulus to rapidity of habit-formation". *J comp neurolpsychol* 1908; 18: 459-482.
- [2] Carlson, Neil. *Physiology of Behavior*. Pearson 2013; 602-606.
- [3] Blascovich J., Spencer S. J., Quinn D. M., Steele C. M. "African Americans and high blood pressure: The role of stereotype threat". *Psychological Science* 2001; 13 (3): 225-229.
- [4] Tapanya S. *Traditional Thai massage*. Bangkok: DuangKamol; 1993.
- [5] Chaithavuthi J, Munagsiri K. *Thai massage the Thai way in theory and practice*. Bangkok: Nuntapun printing; 2005.
- [6] Eungpinichpong W. *Therapeutic Thai massage*. Bankok: Suweeriyasarn Printing Press; 2008.
- [7] Buttagat V, Eungpinichpong W, Chatchawan U, Kharmwan S. The immediate effects of traditional Thai massage on heart rate variability and stress-related parameters in patients with back pain associated with myofascial trigger points. *J Bodywork Mov Ther* 2011; 15(1): 15-23.
- [8] Lindgren L, Rundgren S, Winsa O, Lehtipalo S, Wiklund U, Karlsson M, Stenlund H, Jacobsson C, Brulin C. Physiological responses to touch massage in healthy volunteers. *j.autneu* 2010; 158(1-2): 105-10.
- [9] Chatchawan U, Thinkhamrop B, Kharmwan S, Knowles J, Eungpinichpong W. Effectiveness of traditional Thai massage versus Swedish massage among patients with back pain associated with myofascial trigger points. *Journal of Bodywork and Movement Therapies* 2005; 9(4): 298-309.
- [10] McCraty R, Atkinson M, Tiller WA, Rein G, Watkins AD. The effects of emotions on short-term power spectrum analysis of heart rate variability. *Am J Cardiol* 1995; 76(14): 1089-93.
- [11] Pishbin T, Firoozabadi SM, JafarniaDabanlo N, Mohammadi F, Koozehgari S. Effect of Physical Contact (Hand-Holding) on Heart Rate Variability. *International Journal of Advanced Computer Science* 2012; 2(12): 452-6.
- [12] Moyer CA, Rounds J and Hannum JW. A meta-analysis of massage therapy research. *Psychol Bull* 2004; 130(1): 3-18.
- [13] Sripongngam T, Eungpinichpong W, Sirivongs D, Kanpittaya J, Tangvoraphonkchai K, Chanaboon S. Immediate Effects of Traditional Thai Massage on Psychological Stress as Indicated by Salivary Alpha-Amylase Levels in Healthy Persons. *Med Sci Monit Basic Res* 2015; 21(5): 216-21.



***Engineering***

## SHEAR STRENGTH OF SOIL BY USING SHELL HUSKS WASTE AS RECYCLE AGGREGATE

Siti Hanggita Rachmawati<sup>1</sup>, Zakaria Hossain<sup>2</sup>  
<sup>1</sup>Graduate School of Bioresources, Mie University, Japan

### ABSTRACT

Every year in Japan, a large amount of shell husks waste is generated due to industry and household consumption. This amount of shell husk plays a negative impact not only on environmental but also on the economic problem because the disposal process costs. To solve this problem, the abandon shell husks are generally used as recycle aggregate for ground improvement and for protection of the natural resources of aggregates. In this study, shell husks are used as recycle aggregate for ground improvement. Soil is mixed with shell husk percentages of 0% (control), 10%, 20%, and 30% respectively. Specimens of soil-shell husk composite were tested under the triaxial consolidated-drained tests (CD tests). Test results in terms of deviatoric stress and axial strain are depicted. Results obtained showed that the addition of shell husk in soil leads to an increase in the deviatoric stress. The shear strength parameters were quantified in terms of cohesion and frictional resistances. It was observed that the angle of internal friction of soil-shell husks composite increased up to 30% shell husks. Interestingly, the cohesion of soil-shell husk composite was conspicuously increased with the increase of shell husk of up to 20% then decreased at 30% shell husk. Further addition of shell husk (30%) in soil altered the behavior of the composite leading to a reduction of shear strength.

*Keywords: Shell husks waste, Ground improvement, Principal stress difference, Axial strain shear strength*

### INTRODUCTION

Annually, enormous volume Seashell-By-Products (SBP) are produced in all over world. Burning and burying are most common way to treat those kinds of waste [1]. All those disposal process affected a serious problem in environment, and economic perspective. For example in Japan, an example of SBP is abandon shell husks which has total amount about 151,000 tons/year and nearly 32 million US\$ are being used for disposal. That budget is not expected event for developed country like Japan. In developing country, many illegally dumped are happened due to high cost of disposal waste. In long time, if this waste is untreated, could be causing the air pollution and other environmental problems. These circumstances motivate the development of technologies that using abandoned shell husk [1], [3].

Recently, the abandon shell husks are investigated widely as recycle aggregate in construction field. The utilization of abandon shell husk is expected solving mainly two environmental and economic aspects, such as: 1) waste storage problem and 2) protection of limited natural resources of aggregates [2]. From point of view the potency of shell husks, generally clam shell is composed mainly 95-99% (by weight) of  $\text{CaCO}_3$  that potentially convert to  $\text{CaO}$  for reinforcing the soil or binding the material[1], [4]. In previous study the shell husk is had been used as recycle aggregate for ground improvement. By using the direct shear

test, the result showed that certain amount of shell husk increased the shear strength of soil [5]

In this study, the abandon shell husks also are being used as the recycle aggregate for ground improvement. Ground improvement techniques are provided to increase the soil strength, reducing compressibility and enhance the performance under the load. The triaxial test has been performed to evaluate the shear strength of soil-shell husk composite with 0% (control), 10%, 20% and 30% shell husks percentage. The triaxial test is the most reliable methods available for determining shear strength parameters under different drainage condition [6]. The triaxial test provides information on the stress-strain behavior of the soil that the direct shear test does not. It also provides more uniform stress condition than the direct shear test does with it its stress concentration along the failure plane [7].

### MATERIALS AND METHOD

#### Properties of Soil

The soil sample was collected from Shiratsuka port, Tsu, Mie Prefecture, Japan. From the laboratory test which are based on Unified Classification System, revealed that sand has the highest part of this soil. Figure 1 illustrates the particle size distribution of sandy soil. Approximately 7 % is coarse gravel, 19% is pebble, 7% is granule, 10% is fine sand, 29% is medium

sand, 13% is coarse sand, 11% is silt and 4% is clay.

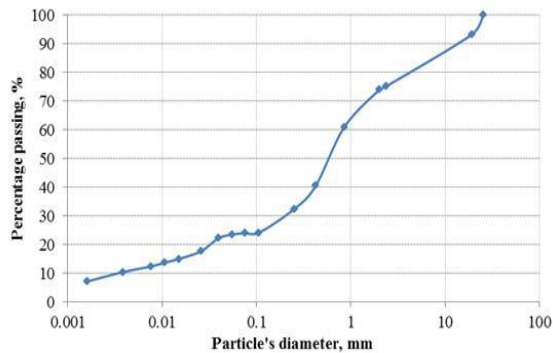


Fig. 1 Particle size distribution curve

The other properties of soil are shown in Table 1. It is revealed from plasticity chart shown in Figure 2, that this soil contains silt which caused higher permeability, higher compressive strength, higher dry density and low toughness.

**Table 1. Properties of soil**

Parameters	Values
Dry density ( $\rho_d$ )	1.80g/cm <sup>3</sup>
Optimum Water Content ( $W_{opt}$ )	13.29%
Specific gravity ( $\rho_s$ )	2.589
Cohesion ( $c$ )	1.52
Angle of internal friction ( $\phi$ )	23.23
Sand > 75 $\mu m$	85.00%
Silt > 5-75 $\mu m$	11.00%
Clay < 5 $\mu m$	4.00%
Liquid limit	39.00%
Plastic limit	26.80%
Plasticity Index	12.20%

### Properties of Shell Husk

The Mactridae shell husk waste was collected from the seashore closed to Mie University, Tsu city, Mie Prefecture, Japan. Then the shell husks were graded by performing sieve analysis. The fineness modulus and the maximum size of the abandon shell husks were 4.35 and 4.76 mm, respectively. The shell size distribution curve is shown in Figure 2 and the physical properties are given in Table 2.

**Table 2. Physical properties of shell husk**

Physical Properties	Values obtained
Water absorption	7.28%
Specific Gravity	1.75
Unit Weight (g/cm <sup>3</sup> )	1.57

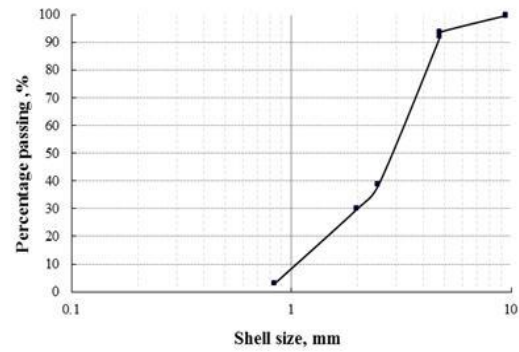


Fig. 2 Shell size distribution

### Methodology

The specimens were manually compacted inside the mold with 12.5cm in height and 5.0cm in diameter. The mixtures of soil-shell husk-cement were compacted in three layers using 4.9cm diameter hand-rammer with rammer mass 1.0 kg and falling height of 30 cm. Each layer was compacted by 20 blows.

The consolidated-drain (CD) test triaxial compression test was conducted using soil with shell husk percentages (0%, 10%, 20% and 30%). The triaxial chamber is assembled after soil specimen sealed by the rubber membrane. In the baseplate groove, the chamber cylinder is installed and thereafter the top plate is positioned on it. The three components of the triaxial chamber (i.e., baseplate, chamber cylinder and top plate) are clamped together by tightening the tie bars. The specimen cap has a circular indentation at the center and the position of loading piston should be aligned. It is achieved by pushing down the loading piston and verified precisely into the center of the specimen cap. Then the chamber is filled by the fluid from water channel and in the same time air release valve on top cap kept open. An axial stress ( $\Delta\sigma$ ) is applied through the loading piston and during the process the dial gauge which connected with piston and specimen recording vertical deformation. The hydrostatic chamber pressure is applied using the air channel on the top cap while the air release valve on top cap closed. The confining pressures in this research are 50kPa, 100kPa, 150kPa, 200kPa. During the test, water valve is kept open due to drained condition requirement in CD test.

## RESULT AND DISCUSSION

### Relationship Between Differential Stress ( $\sigma_a - \sigma_r$ ) and Axial Strain ( $\epsilon_a$ )

#### 0% shell husk

In Fig. 3, the relationship between axial strain ( $\epsilon_a$ ) and principal stress difference ( $\sigma_a - \sigma_r$ ) of soil composite with 0% shell husk are illustrated. This graph shows the increasing of axial strain ( $\epsilon_a$ ) also enhance the principal stress differences ( $\sigma_a - \sigma_r$ ). For confining pressure 200kPa, the 15% axial strain was define as the ultimate principal stress difference because the peak value has not achieved. On the other hand, under confining pressure 150kPa, 100kPa, and 50kPa the peak value was recognized at axial stress ( $\epsilon_a$ ) 7.05, 4.25, 3.8% respectively.

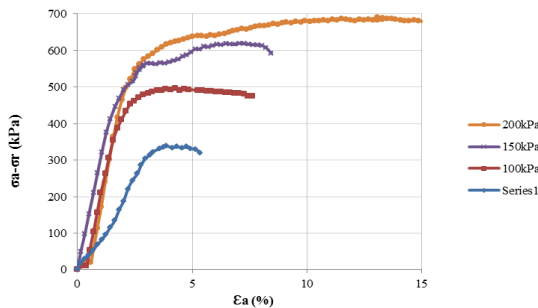


Fig. 3 Differential stresses versus axial strain (0% shell husk)

#### 10% shell husk

Fig. 4 depicts the axial strain ( $\epsilon_a$ ) and principal stress difference ( $\sigma_a - \sigma_r$ ) of soil composite with 10% shell husk. For confining pressure 200kPa and 150kPa, the ultimate peak value is 15% of axial strain. However, the principal stress difference under confining pressure 100kPa and 50kPa have peak value. For 100kPa the peak value at 3.5% axial stress. Then for 50kPa the peak value at 2.1% axial stress. From the graph also known that before peak value on 100kPa, the principal stress difference between 100kPa and 150kPa are slightly different.

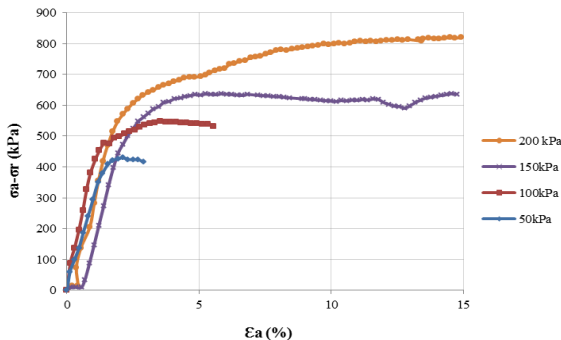


Fig. 4 Differential stresses versus axial strain (10% shell husk)

#### 20% shell husk

As shown in Fig. 5, under different confining pressure, for soil composite with 20% shell husk when the axial strain ( $\epsilon_a$ ) getting higher, the principal stress difference ( $\sigma_a - \sigma_r$ ) also increasing. Initially, axial strain 0-2%, between the principal stress under confining pressure 150 kPa and 200kPa are slightly different. The ultimate principal stress difference under confining pressure 150 kPa and 200kPa are decided at maximum 15% of axial strain. Then for maximum principal difference stress under confining pressure 100kPa and 50 kPa are obtained between 3.0%-4.9% axial strain.

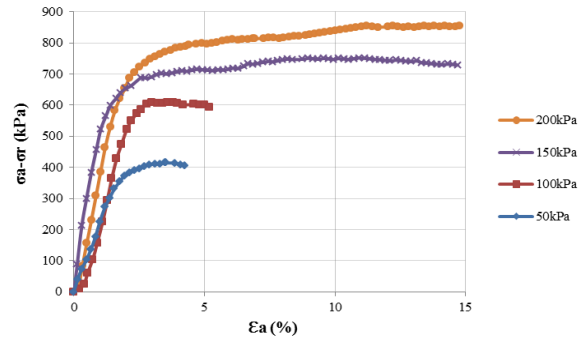


Fig. 5 Differential stresses versus axial strain (20% shell husk)

#### 30% shell husk

The curves of principal stress difference ( $\sigma_a - \sigma_r$ ) versus axial strain ( $\epsilon_a$ ) of composite with 30% shell husk under several confining pressure are given in Fig. 6. From this curve, could be seen only the ultimate principal stress difference under confining pressure 150kPa that decided until 15% axial stress. For the ultimate principal stress difference under confining pressure 200kPa is achieved at 10% axial stress then decreased. Then the maximum principal stress difference under confining pressure 50kPa and 100kPa are reached at axial stress 2.0% and 3.7% respectively.

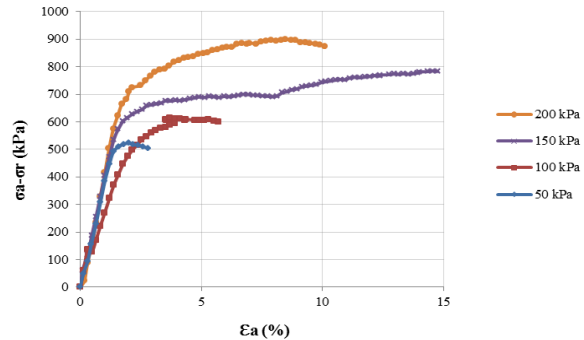


Fig. 6 Differential stresses versus axial strain (30% shell husk)

### Shear Strength of Soil Composition with Shell Husk Percentages

The shear strength of soil from triaxial test, internal friction ( $\phi$ ) and cohesion ( $C$ ) are obtained using the Mohr-Coulomb failure criterion. The triaxial test has failure surface that reflected the real stress-strain characteristic of samples compared to direct shear test. In triaxial test different conditions (drained, undrained, consolidation, and unconsolidated) can be simulated. It could be understood that the triaxial compression test has choose as the accurate and reliable method by many researcher [8].

The shear strength ( $\tau_f$ ) of a soil is combination of soil cohesion ( $c$ ) and internal friction angle ( $\phi$ ). The calculations are obtained by Mohr-Coulomb criterion as a linear function of the normal stress ( $\sigma_f$ ) on the plane at the same point which following by the equation [9]:

$$\tau_f = c + \sigma_f \tan \phi \quad (1)$$

The Mohr-Coulomb circles as representation of soil-shell husk composite according to triaxial test are presented on Fig. 7-Fig. 10. Internal friction is the measure of the shear strength of soils due to friction. Friction is attributed to displacement between soil particles and materials which combine soil and reinforcing materials together [8]. The internal friction comparison between percentages of soil-shell husks composite are shown in Fig. 11. This graph shows additional shell husk percentages increased the internal friction. The enhancement of internal friction along with the shell husk percentage increasing is assumed due to the irregular shape of shell husk particle which develop the frictional resistance between particles. The internal friction of soil composite with 0, 10, 20, and 30% shell husk are  $35^\circ$ ,  $37^\circ$ ,  $38^\circ$ , and  $40^\circ$  respectively.

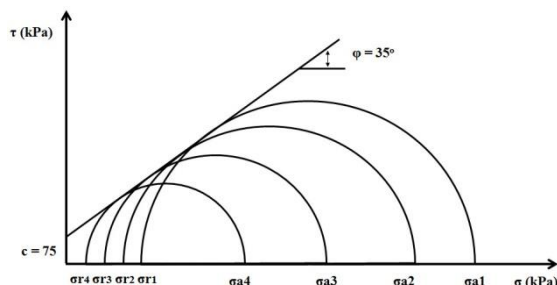


Fig.7 Mohr-Coulomb failure envelop for soil with 0% shell husk

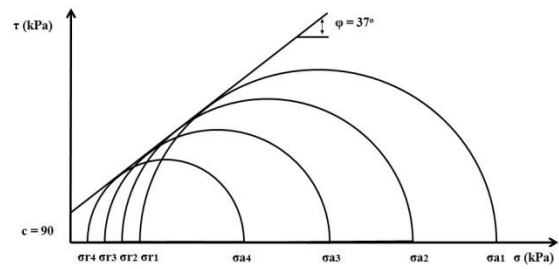


Fig. 8 Mohr-Coulomb failure envelop for soil with 10% shell husk

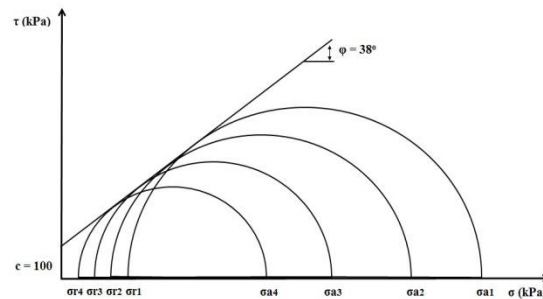


Fig. 9 Mohr-Coulomb failure envelop for soil with 20% shell husk

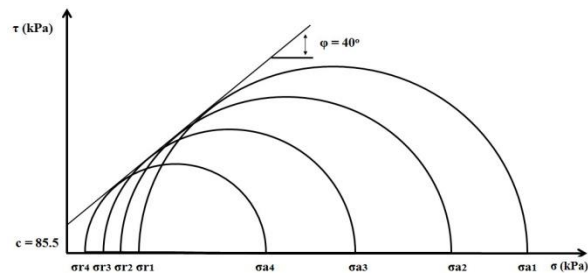


Fig. 10 Mohr-Coulomb failure envelop for soil with 30% shell husk

Cohesion holds the particles of the soil together in a soil mass and independent of the normal stress [6]. In Fig. 12 could be seen the cohesion of shell husks composite increasing up to 20% shell husk percentages then decrease at 30% shell husk percentage. The increasing of cohesion is assumed due to the interlocking mechanism between soil and shell husks particles. On the other hand, decreasing cohesion at 30% shell husk is assumed due to the integration limit between soil and shell husk particles. The cohesion ( $c$ ) of soil composite with 0, 10, 20, and 30% shell husk are 75, 90, 100, and 85.5 respectively. The trend of internal friction and cohesion were also occurred on previous research which observed the shear strength of soil with shell husk reinforcement using direct shear test [5].

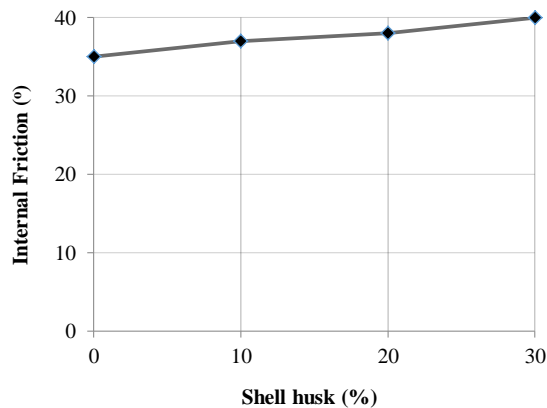


Fig. 11 Internal friction of soil-shell husks composite

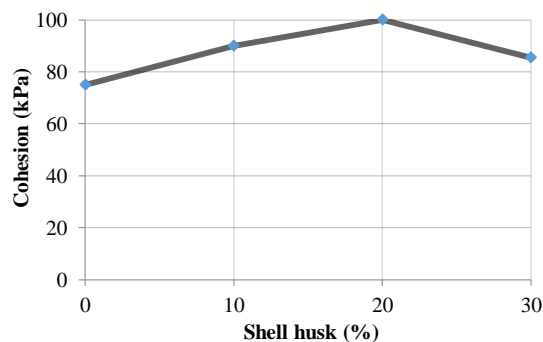


Fig. 12 Cohesion of soil shell husks composite

## CONCLUSION

The maximum differential stress ( $\sigma_a - \sigma_r$ ) of soil-shell husks composite were taken at 15% axial strain ( $\epsilon_a$ ) when there was not any softening behavior. It was observed that differential stress ( $\sigma_a - \sigma_r$ ) increased with the increasing of the confining pressure. Soil-shell husk composite with 20% shell husk percentages under confining pressure of 200 kPa showed the highest differential stress as compared to others.

From the triaxial tests, the shear strengths ( $\tau_f$ ) of soil-shell husks composite were quantified in terms of internal friction ( $\phi$ ) and cohesion ( $c$ ). It was observed that the shear strength of soil increased along with the shell husk percentage increasing up to 20% shell husk then decreased at 30% shell husk.

These types of behavior were attributed with soil-shell husk mixture under direct shear test. More research is needed to clarify this type of behavior of soil-shell husk mixture.

## ACKNOWLEDGEMENTS

This research was supported by Mie University, Japan and Sriwijaya University, Indonesia. Our gratitude also to Mr. Ito for assistance during the research.

## REFERENCES

- [1] Motamedi S, Shamshirband S, Hashim R, Petkovic D, Roy C, "Estimating unconfined compressive strength of cockle shell-cement-sand mixtures using soft computing methodologies", April. 2015, pp: 49-58.
- [2] Hossain, MZ, "Waste shell husks concrete: durability, permeability and mechanical properties". J. of Building Construction and Planning Research. Vol. 1, Sept. 2013 pp. 61-66.
- [3] Yoon G L, Yoon YW, Chae, KS, "Shear strength and compressibility of oyster shell-sand mixtures", J. Environmental Earth Science. Vol. 60, Oct. 2009, pp. 1701-1709.
- [4] Park K., Jun S, Kim D, "Effect of strength enhancement of soil treated with environment-friendly calcium carbonate powder", The Scientific World Journal, Feb. 2014, pp. 1-11.
- [5] Rachmawati SH, Zakaria MZ, "Utilization of waste shell husks for ground improvement", International Agricultural Engineering J., Vol. 26, March 2017, pp. 11-18.
- [6] Arora KR, Soil Mechanics and Foundation Engineering. Nai Sarak-Delhi: Standard Publishers Distributors. 1978, Ch. 13.
- [7] Das BM, Fundamentals of Geotechnical Engineering, Third Edition, United States: SI Cengage Learning, 2007, Ch: 3.
- [8] Zhang CB, Chen LH, Liu YP, Ji XD, Liu XP, "Triaxial compression test of soil-root composites to evaluate influence of roots on soil shear-strength", Ecological Engineering, Vol. 36, 2010, pp. 19-26.
- [9] Mouazen A M, Ramon H, Baerdemaker JD, "Effects of Bulk Density and Moisture Content on Selected Mechanical Properties of Sandy Loam Soil", Biosystem Engineering, Vol. 83, 2002, pp: 217-224.

## ANALYTICAL STUDY ON SINGLE PILE DESIGN FOR SOLAR FOUNDATIONS FOR SLOPING LAND.

Alex Otieno Owino<sup>1</sup>, Hossain, M.Z.<sup>2</sup>, Ojio C.<sup>3</sup>, Ozumi, S.<sup>4</sup>, Harada, H.<sup>5</sup> and Okuyama, S.<sup>6</sup>

<sup>1</sup>Graduate School of Bioresources, Mie University, Japan

<sup>2</sup>Cosmowinds Company Ltd., Nagoya, Aichi, Japan

<sup>3</sup>Beppu Construction Company Ltd., Yokkaichi, Japan

### ABSTRACT

In accordance to rising queries in the global environmental concerns, such as climate change, environmental sustainable development have become handy so as to rescue the environment from further degradation. Most researches being done today focus mostly on the development of solar cells, architectural design of various types of solar cells, reduction in size of the solar panels while improving the operation and energy tapping efficiency. This paper therefore focuses on the main framework on the installation process which is the foundation. This consists of a single pile composite foundation made from hollow steel pipe bonded to the ground by a thin layer of cement and sand mortar. The experiments done here aims at establishing the bearing capacity of single pile composite foundation with respect to pull out forces (uplift tension), compression (axial) forces and lateral forces acting upon the structure upon full foundation installation and loading setup. The tests show the analysis of the interaction of the forces. The tests include the axial compression test and the pullout test. The results shows that the pull out and the compressions loads applied are capable to hold the entire structure subject to natural environmental condition.

*Keywords: Solar Panels, Single Pile Foundation, Pullout/ Lateral/Compression Load –Deflection Relationship,*

### INTRODUCTION

Energy demand is at growing level worldwide by production industries and governments. With the influx in the commodity demand most of the attention is being driven in the production of green energy sources. Solar energy is a green energy source that utilizes the radiant heat from the sun and is harnessed using different technologies like solar heaters, photovoltaic cells, solar thermal energy absorbers and solar architecture innovations.

The large magnitude of solar energy available to the earth surface makes it a highly appealing and efficient source of energy. During the United Nations Development Program in 2000 based on World Energy Assessment, it was found that the annual potential of solar energy ranged from 1,575 to 49,837 exa-joules (EJ). This range was much higher than the total world energy consumption, which was 559.8 EJ in 2012. [1][2]

As at now much of the research being conducted are based on the innovation on a wide variety of the solar cells and the architectural design of different size, shape and structure of the solar harnessing material. In addition to the design parameters, Somekawa et al has done the research on the effects of the wind loading on the solar panels. This aims at establishing a strong foundation that will resist any horizontal loading subject to fluctuating wind speeds. With reference to Japan Architectural Society and Aihara et al. [3][4] the coefficients of wind load pressures can be obtained to design the foundation.

The most conventional way of laying the foundation have been the use of steel reinforced concrete as seen in most of the construction companies worldwide not bearing in mind the financial implications and cost- performance relations. Nevertheless, foundations are designed so as to withstand extreme environmental condition such as earthquakes, typhoons, cyclones, soil cohesion variability and any other natural or artificial calamity that may lead to structural failure.

This paper shows a simple composite foundation design taking in to account cost-performance relation, made from a hollow steel pipe and anchored to the ground by a cement- sand mortar. The steel pile channels the entire load to the ground while the sand – cement mortar improves the soil bearing capacity as well as bonding the foundation to the immediate soil structure thus provides adequate frictional resistances and improved cohesion owing to its relatively greater surface area and roughness as compared to conventional foundation. The objective of this paper is to determine the optimum permissible loading that the foundation can withstand with respect to tensional (pullout) loading, axial (compression) loading, lateral loading and load displacement tests. The failure modes of the tests are used to determine the foundation strength and the optimal structure loading specifications.



## METHODOLOGY

### Wind Load Calculations

Wind is one of the major forces that require load transmission to the ground. The maximum wind load is assumed to act at an angle of  $45^\circ$ , [6] when with pressure is applied to the panel surface. Wind speed is 40m/s/slope  $10^\circ$ .

Table 1 Wind load calculations

Item	Formula
Effective projection area	(Length * Width)
Wind load (kg/m <sup>2</sup> )	$\{1/16 * (\text{wind speed m/s})^2 * \text{Resistance coefficient}\}$
Wind load on effective area	(Effective projection area * Wind load)
Horizontal wind load	(Wind load on effective area * $\sin 45^\circ$ )
Right angle wind load	(Wind load on effective area * $\cos 45^\circ$ )
Horizontal wind load Force	$\{(\text{Horizontal wind load} * \sin 10^\circ) + (\text{Right angle wind load} * \cos 10^\circ)\}$

### Pillar Root Length Calculation Using Extreme Ground reaction Force Method

Ground reaction force (GRF) encompasses the toleration of the force exerted by the ground to the foundation pillar in contact with it. This acts as a baseline parameter in the calculation of foundation strength taking in to account the overhead load to be transmitted, the bending moment of the pile extension above the ground and the soil parameters as shown in Table 2 below.

Table 2 Forces and ground conditions

Item	Value
Working Load;	horizontal force, H
Applied Load	Moment Bending, M
Pile dim.	Width of column, D
	Unit vol. weight, $\gamma$
Ground Condition	Internal friction angle, $\phi$
	Wall friction angle, $\delta$
	Adhesive force, C

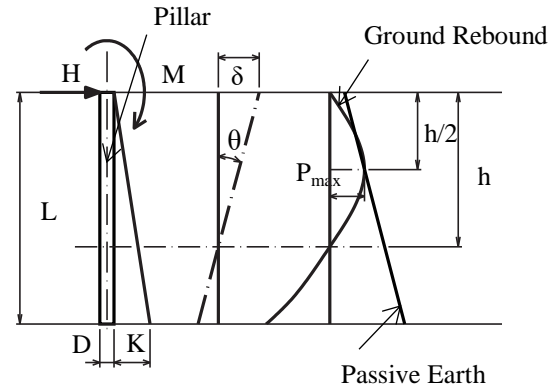


Fig. 1 Moment diagram

Engel method [8] shows that the root penetration length if the foundation is determined when the maximum ground reaction force ( $P_{\max}$ ) is less than or equal to the Passive soil pressure strength ( $P_p$ ). Considering a rigid foundation, taking into account the depth, bottom surface resistance and an increase of horizontal ground reaction force coefficient,  $K_h$  by first order then the rotation angle ( $\theta$ ) and the center depth ( $h$ ) is obtained by the following formula;

$$\text{Rotational angle } (\theta) = \frac{12 \cdot (3M + 2H \cdot L)}{K_h} \quad (1)$$

$$\text{Rotational center depth } h = \frac{L \cdot (4M + 3H \cdot L)}{2 \cdot (3M + 2H \cdot L)} \quad (2)$$

Maximum Ground reaction force occurs at  $h/2$ , hence;

$$P_{\max} = \delta K_h = \frac{1}{2} (h \cdot \theta) \cdot K_h \cdot (h/2L) \quad (3)$$

$$P_p = \frac{1}{2} \cdot h \cdot K_p \cdot \gamma + 2 \cdot C \cdot \sqrt{K_p} \quad (4)$$

$$K_p = \frac{\cos^2 \phi}{\cos \delta \left\{ 1 - \sqrt{\frac{\sin(\phi + \delta) \sin(\phi + \beta)}{\cos \delta \cos \beta}} \right\}}$$

When  $P_{\max}$  is equal to  $P_p$ ;

$$\frac{1}{2} (h \cdot \theta) \cdot K_h \cdot (h/2L) - \frac{1}{2} \cdot h \cdot K_p \cdot \gamma + 2 \cdot C \cdot \sqrt{K_p} = 0 \quad (5)$$

Substituting equation 1 and 2 into equation 5;

$$3 \cdot K_p \gamma \cdot D \cdot H \cdot L^4 + 4 \cdot D \cdot (K_p \gamma \cdot M + 4 \cdot C \cdot \sqrt{K_p}) \cdot H \cdot L^3 - 3(9 \cdot H^2 - 8 \cdot C \cdot \sqrt{K_p}) \cdot D \cdot M \cdot L^2 - 72 \cdot M \cdot H \cdot L - 48 \cdot M^2 = 0 \quad (6)$$

Resistance width of the pile is considered to be,  $D=3D$  according to Broms Method and the analytical method of piles, Eq. (6) becomes,



$$3.K_p \gamma.D.H.L^4 + 4.D.(K_p \gamma.M + 4.C.\sqrt{(K_p).H}).L^3 - (9.H^2 - 24.C.\sqrt{(K_p).D.M}).L^2 - 24.M.H.L - 16.M^2 = 0 \quad (7)$$

Replacing the coefficients of L with C1, C2, C3, C4 and C5 we have;

$$C1.L^4 + C2.L^3 - C3.L^2 - C4.L - C5 = 0 \quad (8)$$

### Solution and Graph of the Quartic Polynomial

From Eq. (8) the fourth order polynomial can be solved to obtain four values of L3 ranging between -1.3 to 1.4 with the most positive number as the desired value for pillar root length as shown in Fig. 2 below

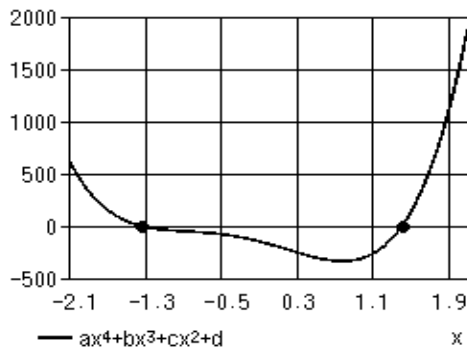


Fig. 2 Graphical representation of Pillar support insertion length

By solving the fourth order equation,  $L = 1.4\text{m}$  [14]

### Foundation Depth versus Pile Shaft Diameter

From Eq. (7), a relationship between the foundation depth and the pile shaft diameter can be analyzed.

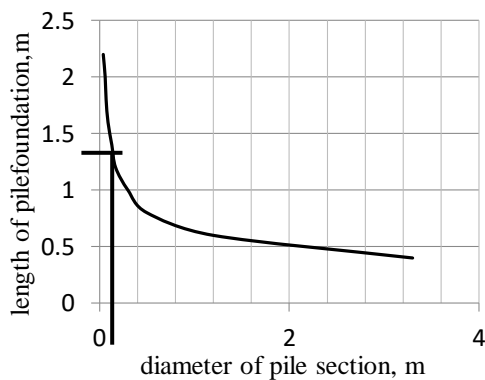


Fig. 3 Pile Shaft Diameter against Pile Length

### Pile Displacement Calculation; Theoretical Value

With reference to previous analytical models [4], horizontal pile bearing capacity can be analyzed with respect to the displacement that occurs at the

ground level. The allowable empirical horizontal displacements 10mm in normal situations and 15mm in the areas prone to seismic process such as earthquakes. Okahara et al [13] also states that the permissible horizontal displacement is the larger value of 1% of the pile diameter or 15mm in both areas of normal conditions and seismic activity prone areas. This was derived from the examination of piles subjected to horizontal loads and the observation of the elastic limits displacements on the load displacement curves.

The pile head displacement is a function of;  $y = \{Q_g, M, z, L, T, EI, kh\}$ . Where T is the relative stiffness factor, EI is the product of Modulus of elasticity and the Moment of Area of the pile material, Kh is the Unit modulus of subgrade reaction. Hence the following equations.

$$y = \{(Q_g T^3)/EI\} A_y \quad T = \sqrt{(5EI/kh)}$$

$A_y$  is the displacement coefficient at the top of the pile, 2.435

### Construction Material and Methods

The pillar supporting material used was a 76.3mm diameter steel pipe measuring 2m and sand-cement mortar mixed at a ratio of 2.1 with water-cement ratio of 2.1. The steel section was then anchored into the ground at a depth of 1.3m. A burrow was drilled using a precision drilling machine set at right angles to the ground. An additional 10cm was drilled to allow for the complete anchoring of the steel pipe to the ground as shown in Fig. 4 below.

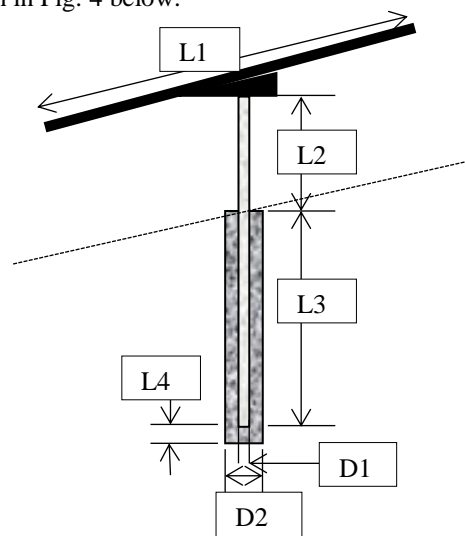


Fig. 4 Foundation set-up

### Work Flow Diagram

A comprehensive working procedure is

illustrated in the flowchart in Fig. 5 below.

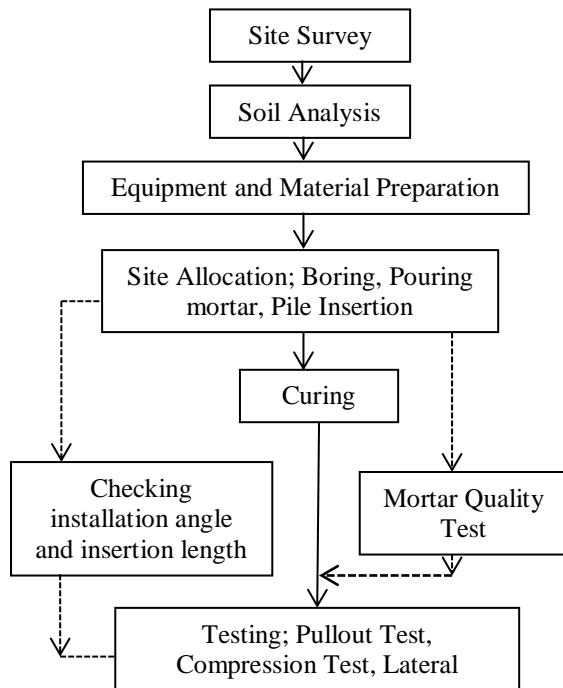


Fig. 5 Working procedure flow chat.

### Foundation Testing Methods

Once the foundation was fully cured it was subjected to pullout (tensile) test, axial compression test and the lateral displacement test. All the tests were carried out in accordance to the Japanese Geotechnical Society (JGS), 2014. Monitoring was done using the Linear Displacement Transducers (LDT) and readings recorded automatically with respect to loading variations. Experimental setup is as shown the Fig. 4 below.

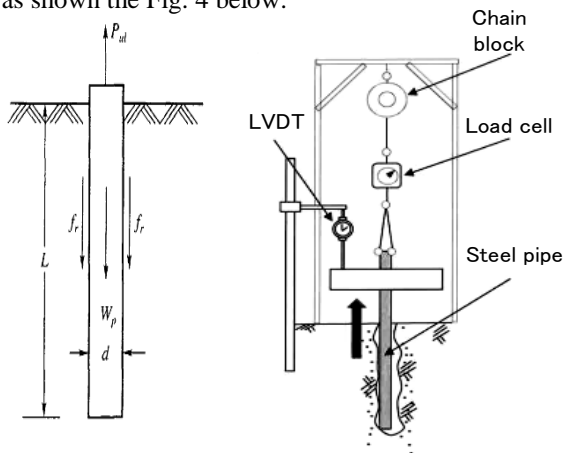


Fig. 6 Testing experimental setup.

### RESULTS AND DISCUSSIONS

From Fig. 7 it is evident that the pile

displacement increases with an increase in the pullout load. The graph is of a curvilinear shape with slow displacement from 3kN to 9kN for pile 2 then followed by a more linear relationship up to 15kN recording a displacement of 0.38mm. In Pile 1 the highest permissible load gives a displacement of 0.85mm, this is due to the cohesiveness variability of the soil [9].

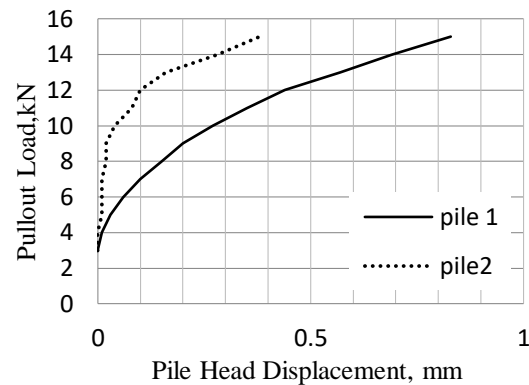


Fig. 7 Pullout load-pile displacement relationship

The result of compression loading shows a nonlinear relationship with both piles showing an increase in displacement as the compression load increases. Maximum displacement was recorded at 20kN with a minimal displacement of 0.7mm and 0.75mm for pile 2 and pile 1 respectively. This is more so evident in the theoretical value which shows linearity in the trend with minimum variations from the test data as shown in Fig. 8

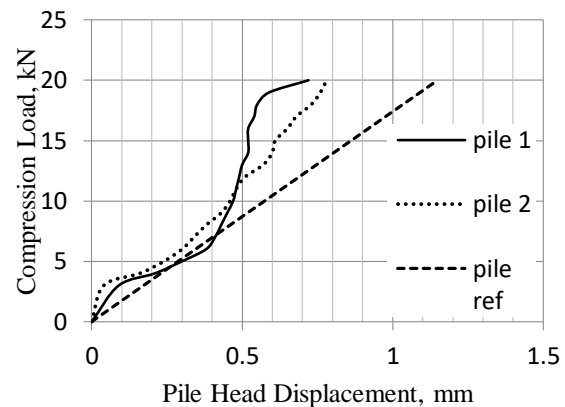


Fig.8 Compression load –pile displacement relationship

In Fig. 9, two phases of load- displacements relationship is evident. The first phase is a slow displacement phase from 0mm to 10mm as the load increases from 3kN to 13kN. The second phase shows a linear relationship of rapid displacement

from 13mm to 30 mm with 2kN increase in loading. Failure point is recorded at 14kN lateral loading.

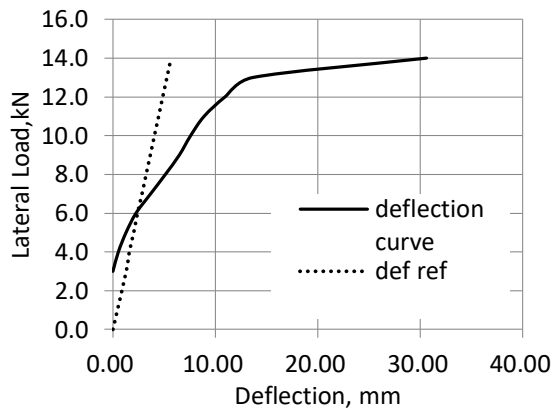


Fig.9 Lateral load- pile displacement relationship

## CONCLUSION

This research study shows that the design of composite foundation can be achieved using very simple techniques in the construction industry taking in to consideration the economic factors such as minimum cost evaluation and minimum material usage. The foundation is of high strength as it can withstand loads up to 20kN as evident during compression loading. This is with reference to the design loading of 3.28kN.

The Inclusivity of seismic loads to the working load in the foundation length design gives a clear indication of strength as it can withstand the design load of 3.28 kN and an additional 16kN. The pullout loading, compression loading and the lateral loading bearing capacity of the foundation shows that the foundation is able to withstand the wind loads at 40 m/s inclusive of the solar panels installation design weights without any risks of failure.

## ACKNOWLEDGEMENTS

I express my thanks to Japan International Cooperation Agency (JICA) for the financial assistance and cooperation in the entire design process.

## APPENDIX

$D1$	Width of strut, pile diameter.
$L3$	Pillar support insertion length
$Kh$	Horizontal ground reaction coefficient
$H$	Horizontal action force, Bending Moment.

$M$	Working Bending Moment.
$Kp$	Passive earth pressure coefficient
$\gamma$	Unit volume weight of soil (kN/m <sup>3</sup> )
$\phi$	Internal friction
$C$	Viscosity (kN/m <sup>2</sup> )
$\delta$	Wall friction angle
$\beta$	Ground surface inclination angle (degrees)
$L1$	Solar panel length
$D2$	Foundation diameter.
$L4$	Pile - wall clearance
$L2$	Pile height above ground

## REFERENCES

- [1] Somekawa D., Koizumi T., Taniguchi T. and Taniike Y.: Wind loads acting on the photovoltaic panels arrayed near ground, The 22nd Wind Engineering Symposium, pp.157-160, 2012
- [2] An Elastomeric Insole For 3-Axis Ground Reaction Force Measurement. 1st ed. Washington, D.C.: United States. National Nuclear Security Administration, 2012.
- [3] Engel, Michael W. Evaluation Of Barnes' Method And Kriging For Estimating The Low Level Wind. 1st ed.: Bibloscholar, 2012.
- [4] Honjo, Y. Foundation Design Codes And Soil Investigation In View Of International Harmonization And Performance Based Design. 1st ed. Lisse [u.a.]: Balkema, 2002.
- [5] Hamada, Masanori, and Takeshi Koike. Critical Urban Infrastructure Handbook. 1st ed. Boca Raton, Fla: CRC Press, 2015.
- [6] Reese, Lymon C, and W. F Van Impe. Single Piles and Pile Groups under Lateral Loading. 1st edition.
- [7] Okahara, M., Nakatani, S., & Matsui, K. 1991a. A study on vertical and horizontal bearing characteristics of piles, JSCE J. of Struct. Engrg. 37, 1453-1466. In Japanese.
- [8] Okahara, M., Takagi, S., Nakatani, S., & Kimura, Y. 1991b. A study on the bearing capacity of single piles and design method of column shaped foundations. Technical Memorandum of PWRI (2919), Public Works Research Institute. In Japanese.
- [9] Cosmo Winds Company Limited, <http://cosmowinds.jp/solar/studio/>
- [10] Beppu Construction Company Limited, <http://www.o-beppu.co.jp/>
- [11] "2014 Key World Energy Statistics" (PDF). [iea.org](http://www.iea.org). IEA. 2014. pp. 6, 24, 28. Archived

- from the original on 5 May 2014.
- [12] "Energy and the challenge of sustainability" (PDF). United Nations Development Programme and World Energy Council. September 2000. Retrieved 17 January 2017.
  - [13] JIS C8955: Japanese Industrial Standards, Design guide on structures for photovoltaic array, 2004.
  - [14] JIS C8917: Japanese Industrial Standards, Environmental and endurance test methods for crystalline solar PV modules, 2005.
  - [15] Aihara T., Asami Y., Nishimura H., Takamori K., Asami R. and Somekawa D.: An area correct factor for the wind pressure coefficient for cladding of hip roof —The case of square plan hip roof with roof pitch of 20 degrees— The 22nd Wind Engineering Symposium, pp.339-344, 2008.
  - [16] AIJ2004: Architectural Institute of Japan, Recommendations for Loads on Buildings, 2004.

## EXPERIMENTAL BEHAVIORAL INSPECTION OF COMPOSITE CONCRETE-OPEN WEB EXPANDED STEEL BEAMS EXPOSED TO STATIC LOADING

Nazar K. Oukaili<sup>1</sup> and Seezar Sh. Abdullah<sup>2</sup>  
<sup>1,2</sup>College of Engineering, University of Baghdad, Iraq

### ABSTRACT

The behavior of composite concrete – open expanded steel beams (castellated and cellular) under effect of flexure was studied experimentally. Two strengthening technics were implemented (strengthening by adding intermediate stiffeners only or strengthening by both external prestressing and intermediate stiffeners). The experimental program was designed in such way that six composite concrete- open web expanded steel specimens were tested, which are simply supported over a span of 2900 mm and divided to two main groups. Each group has three specimens, which designated according to the type of the strengthening technics, (reference specimens without strengthening, specimens with intermediate stiffeners, and specimens with external prestressing in addition to intermediate stiffeners). The bending moment was created by exposing the experimental specimens to two-point loads. Carrying capacity, load-deformation responses, and strain in both concrete and steel were recorded and analyzed. The experimental results show that the first strengthening technique improved the load carrying capacity by 26% for castellated specimens and 21.8% for cellular specimens, respectively. Meanwhile, the second strengthening technique enhanced the load carrying capacity by 186 % for castellated specimens and 134.3% for cellular specimens, respectively. It is worth to mention that, the first technique reduced the mid span deflection under service loads by 25% and 22% for castellated and cellular specimens, respectively. While the second technique decreased, the mentioned values by 56% and 61% for castellated and cellular specimens respectively.

*Keywords: Castellated, Cellular, Composite , Flexure, Strengthening, External Prestressing*

### INTRODUCTION

Open web expanded steel beam is a name commonly used for a specific type of standard hot rolled steel I-beam sections. It is made by cutting the web of the original steel beams in a regular pattern, separating into two halves, and rejoined by welding, (after offsetting one portion), to create a regular holes shape in the web such as castellated and cellular shapes [1].

The advantage of open web expanded steel beams coming from improving the strength due to increasing the section depth without increasing the self-weight. In some instances, the depth is increasing as much as 50%, and by these increasing, strong axis bending strength and stiffness is improving as the strong axis moment of inertia  $I_x$ , section modulus  $S_x$ , are increasing, more holes also allow plumbing pipelines and electrical conduits pass through them ultimately reducing the elevation of floor level [2].

With the development of buildings construction and the desire to make them capable to resist the applied loading with low cost, composite concrete – open web expanded steel beams have been use in various designs of structural buildings. They used

widely in multi-story buildings, hospitals, industrial, commercial, warehouse buildings and any structure with suspended floor, where the web-openings used for passage of the services, resulting in saving the height of the structure [3].

The existence of opening in the web alters the stress distribution within the member and influences its collapse behavior. Accordingly, the strength of these beams may be governed by the plastic deformation that occur due to moment and shear effects at openings.

The load carrying capacity of these types of beams will be reduced at the opening because of the reduction in the contribution of web to the moment capacity. This is not very significant, as usually the contribution of the web to the moment capacity is very limited. However, the reduction in shear capacity at the opening can be significant. Therefore the ultimate capacity under the combined action of moment and shear at the section where there is an opening will be less compared to that at the normal cross section without opening.

To restore the strength lost, strengthening with intermediate steel stiffeners, which should be welded to the web between openings, could be used. However, compared to such scheme, the use of post-

tensioned external tendons to strengthen these girders is relatively simple technique and economic method to employ also.

Few studies have been conducted on the behavior of composite concrete-open web expanded steel beams under flexure with or without strengthening technique. In the current study, the circular, and hexagonal castellation has been chosen to show the effect of different strengthening techniques on the global behavior of such configuration under the flexural effect.

The objective of this investigation was to examine experimentally the benefits of steel stiffeners and external prestressing as used in strengthening of composite concrete – open web expanded steel beams and to evaluate their effect on both the service load behavior and nominal carrying capacity.

## EXPERIMENTAL PROGRAM

Six composite concrete – open web expanded steel specimens divided into two groups according to castellation shape (cellular (CEB) and castellated (CB)) were fabricated and tested as simply supported over an effective span of 2900 mm. All specimens had the same cross – sectional dimensions where the total height of the beam was 360 mm, which divided into 60 mm concrete deck slab and 300 mm hot-rolled I-beam as the steel section.

The steel IPEA - section with overall height of 200 mm was chosen to fabricate the cellular and castellated steel section. Electric cutting was then used to split the web into two parts where one part was shifted half a pitch to obtain the shape of castellation. Finally, the steel section was assembled using continuous electric welding of 3 mm thickness on both sides, the end of the beam was then polished and the extra parts of castellation were cut to obtain a castellation section of total height of 300 mm and total length of 3000 mm.

The success of composite action depends on the shear resistance at the interface between the steel beam and the cast-in-place deck to allow full transfer of stresses. Thus, a good connection between the two components of the composite system is essential. To achieve full connection between the steel cellular or castellated I-section and the concrete deck slab, rigid shear connectors were used in form of channel section of total height of 40 mm and flange width of 30 mm. The thickness of the channel was constant for both web and flange and was equal to 3 mm, while its spacing was 150 mm perpendicular to the longitudinal axis of the beam.

The length of the channel was chosen as 50 mm centered above the upper flange. The concrete deck slab above the steel beam was 60 mm in thickness and 500 mm in width. It was reinforced in both directions by mild steel rods of 6 mm diameter which spaced 150 mm c/c.

For specimens subjected to external prestressing, two low - relaxation seven - wire steel strands, with 12.7 mm diameter, (Grade 270), were used and located at symmetrical distances of 100 mm from either sides relative to the longitudinal axis of the composite beam. The two strands were tensioned simultaneously from one end. Special care was exercised to balance the prestressing force in the strands to avoid biaxial bending of the specimens. The wedge anchored prestressing strands were supported directly on an 200 mm wide x 300 mm deep x 20 mm thick bearing plate attached to the ends of the beam, where two holes were formed to facilitate the application of the prestressing. Draped external tendon profile was adapted for the test specimens. Two deviators around the third points of the span consisted of 25 mm diameter cylindrical rod welded to the bottom surface of the steel section. The steel strands were stretched and anchored to the vertical steel bearing plate using Supreme Product anchorage chucks (grips). The prestressing force was transferred to the steel strand through the use of hydraulic jack of 20 tons capacity and a stroke of 150 mm. The target effective prestress  $f_{pe}$  in the external prestressing steel was 40% of the ultimate strength of the strand  $f_{pu}$ . The corresponding stress was monitored accurately using readings of the strain gauges attached to the surface of the prestressing strands along with the readings of the pressure gauge of the hydraulic jack used in the prestressing operation. Figure 1 shows details of the sections after castellation process. The longitudinal prestressing steel strands, welded wire fabric of slab reinforcement, and steel for web, flanges, stiffeners, and shear connectors had different mechanical properties which are summarized in Table 1.

The concrete mix was prepared using Type I cement, crushed stone of 10 mm maximum aggregate size and fine river sand. By weight the cement: sand: aggregate proportion was 1:1.5:3 with water/cement ratio of 0.45.

The concrete compressive strength was determined from three standard 150 x 150 x 150 mm cubes taken from each specimen, where the target value was 32 MPa. The concrete deck for all specimens was cast horizontally in wooden forms.

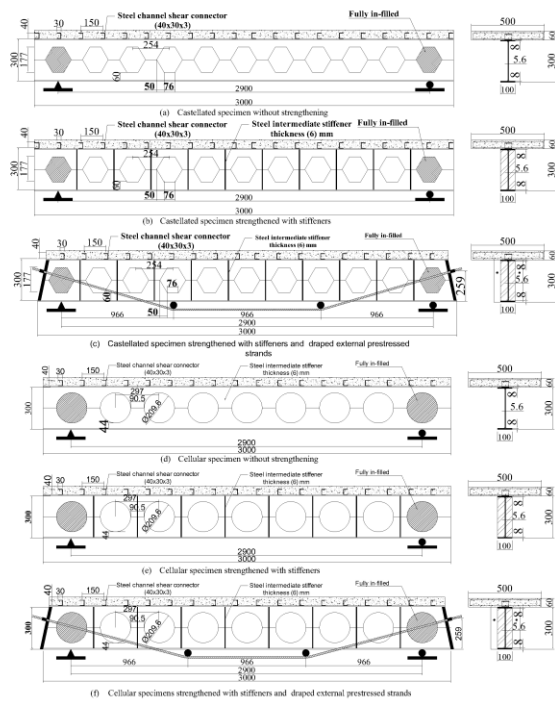


Fig. 1 Details of experimental specimens.

One day after casting, the standard cubes and the sides of the deck slab were stripped from the molds and covered in wet material. The deck slabs were covered until the seventh day, when the wet material was removed and the specimen allowed air-drying until testing.

Table 1 Mechanical properties of steel components

Component	Thickness (mm)	Yield Stress (MPa)	Ultimate Stress (MPa)
Plate for web	5.6	397.87	520.52
Plate for top and bottom flanges	8.0	378.95	519.80
Plate for shear connectors	3.0	246.14	332.79
Welded wire fabric	$\Phi = 6.0$	456.62	615.60
Prestressing steel strand	$\Phi = 12.7$	1675.00	1862.00

Each group has three specimens, which designated according to the type of the strengthening techniques used. The first specimen of each groups, (CEBR and CBR), has no strengthening and considered as a control specimen. The second specimen of each groups, (CEBS and CBS), was characterized by strengthening using vertical intermediate steel stiffeners at both sides of all web-

posts. While the third specimens, (CEBP and CBP), were subjected to external prestressing in addition to using vertical intermediate steel stiffeners. All specimens were strengthened at the end zone by filling the first castellation.

It should be mentioned that, the external prestressing was applied to the steel cellular I-section before pouring the concrete of the deck slab.

All specimens were loaded in four-point bending using two symmetrical concentrated loads applied at one-third the span length. The test was conducted using closed loop ram with 50 ton capacity actuator. Specimens were subjected to a monotonically increasing load to failure using a load control test.

All measurements, such as beam deflections, strains in concrete, steel strands and steel section were recorded twice, immediately after the application of the load and after 10 minutes later.

## EXPERIMENTAL RESULTS

Detailed analysis and comparison among the two groups have been conducted considering the following: mode of failure; carrying capacity; load-deformation responses.

Eight failure modes for castellated and cellular beams are known [4]: flexural mechanism; lateral torsional buckling; distortional buckling; web-post buckling due to shear force; web-post buckling due to compression force; Vierendeel or shear mechanism; rupture of welded joints; and ultimate deflection.

In the current investigation, the failure due to lateral torsional buckling was not happened due to the stiffness achieved by the concrete deck slab. As for the rupture of welded joints, this mode of failure was excluded as the welded joints were properly designed. Also, failure due to ultimate deflection could not have been possible to observe since the tested specimens were loaded until the complete collapse had occurred.

For the control cellular specimen (CEBR), the failure was characterized by local buckling of web-post, at section located directly under the concentrated load, due to shear force and Vierendeel mechanism. The remaining specimens (CEBS and CEBP) failed by a combination of failure modes such as flexural mechanism and Vierendeel or shear mechanism. In the same manner, for the control castellated specimen CBR, the failure was web post buckling, while specimens strengthening by adding intermediate stiffener (CBS) failed by flexural mechanism, finally specimen strengthening by external prestressing was failed by flexural mechanism caused compressive failure of concrete deck slab. Table 2 and Plate.1 show failure modes of all tested specimens.

Table 2 Failure modes of experimental specimens

Specimen designation	$P_u$ (kN)	Mode of failure
CEBR	160.0	Web-post buckling due to shear force plus Vierendeel mechanism
CEBS	195.0	Flexural mechanism
CEBP	375.0	Vierendeel or shear mechanism
CBR	115.0	Web-post buckling
CBS	145.0	Combined flexural and shear mechanisms
CBP	330.0	Vierendeel or shear mechanism

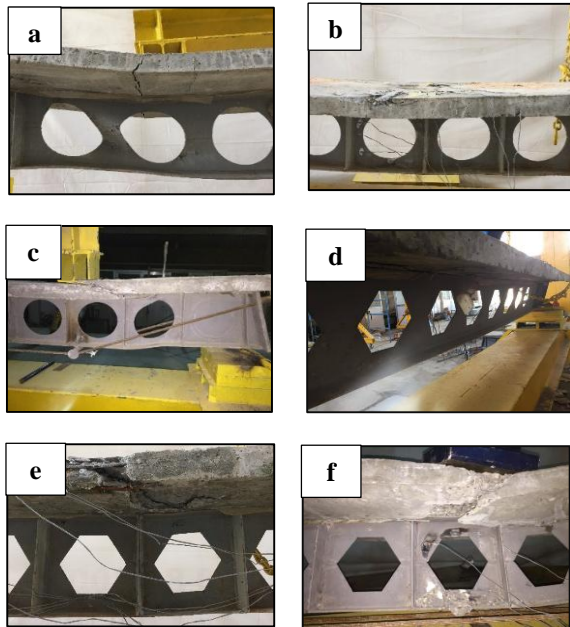


Plate 1 Failure modes of experimental specimens, (a) CEBR, (b) CEBS, (c) CEBP, (d) CBR, (e) CBS, and (f) CBP.

In term of ultimate load carrying capacity, it can be seen that, adding stiffeners to the web section as a first strengthening technique led to improve the load carrying capacity by 21.8% for cellular specimens, and 26% for castellated specimens, respectively. In the same manner, using external prestressing with intermediate stiffeners as a second strengthening technique enhanced the load carrying capacity by 134.3 % for cellular specimens and 186 % for castellated specimens, respectively. Figure 2 shows the effect of strengthening techniques on ultimate capacity of the tested specimens.

It is worth to mention that, the first technique reduced the midspan deflection under service loads by 22% and 25% for cellular and castellated specimens, respectively. While the second technique

decreased, the mentioned values by 61% and 56% for cellular and castellated specimens, respectively.

It was noted that, using these strengthening systems excluded certain failure modes, which are commonly happened with open web expanded beams. Figure 3 show load – deflection diagram of tested specimens.

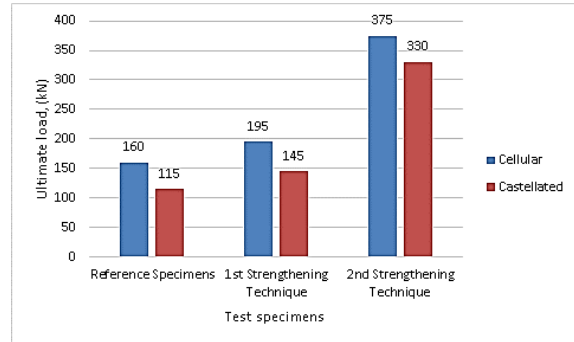


Fig. 2 Ultimate capacity of experimental specimens according to strengthening techniques.

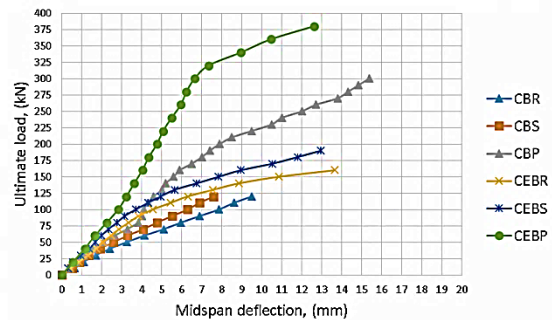


Fig. 3 Load -midspan deflection of all specimens.

The strain of the steel section and concrete deck slab were measured at each loading stage using different strain gages. These electrical strain gages were installed at different levels of the steel web, steel flanges, and at the extreme top and bottom concrete fibers of the deck slab, Fig. 4 – Fig. 9 show variations of strain across the section depth in variation and steel beam depending on the applied load level. The experimental results of cellular reference specimen (CEBR) show that strain in concrete fibers varied across the thickness of the deck slab from compression to tension which increased with the increasing of the applied load level approaching  $-1300 \times 10^{-6}$  in extreme top fiber and  $+169 \times 10^{-6}$  in extreme bottom fiber as the load attained the ultimate level. Meanwhile, the tensile strain values in extreme fibers of the bottom flange of the steel section reached  $+1248 \times 10^{-6}$  at ultimate load. It is noted that, using intermediate stiffeners produced rising of the load carrying capacity and decreasing of strains in concrete by 4.5% in extreme top fibers and 18% in extreme bottom fibers,



respectively, while the tensile strain in extreme fibers of the bottom flange increased by 16.5% in comparison with the above mentioned value of the reference beam. While for the specimen subjected to external prestressing with stiffeners, it was observed that, the strain decreased in extreme top and bottom concrete fibers by 24% and 34%, respectively. Meanwhile, the strain in the extreme fibers of the bottom flange was decreased by 9% in comparison with the reference beam (CEBR).

Moreover, results of castellated reference specimen (CBR) show that the strain in concrete fibers followed the same manner of changing across the thickness of deck slab with the excessive increasing of the applied load. Accordingly, at ultimate load the concrete strain attained  $-1225 \times 10^{-6}$  and  $+179 \times 10^{-6}$  in extreme top and bottom fibers, respectively. Also, the tensile strain in extreme fibers of the bottom flange approached  $+1560 \times 10^{-6}$ .

For the castellated specimen strengthened by intermediate stiffeners (CBS), strain in top and bottom concrete fibers of the deck slab decreased by 51% and 35%, respectively. While, strain in steel of the bottom flange decreased by 24%, in comparison with reference castellated specimens (CBR). In the same manner, for the specimen subjected to external prestressing with intermediate stiffeners, it was found that, the strain decreased in extreme top and bottom concrete fibers by 18% and 10%, respectively. Also, the strain in the extreme bottom flange fibers was decreased by 7.5% in comparison with the reference beam (CBR).

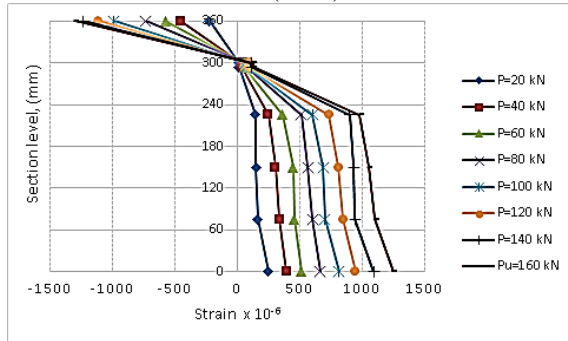


Fig. 4 Strain across section level of CEBR.

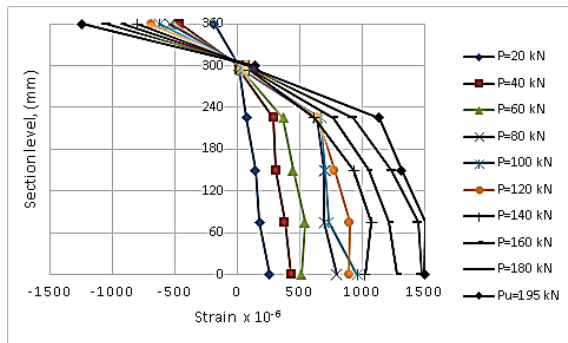


Fig. 5 Strain across section level of CEBS.

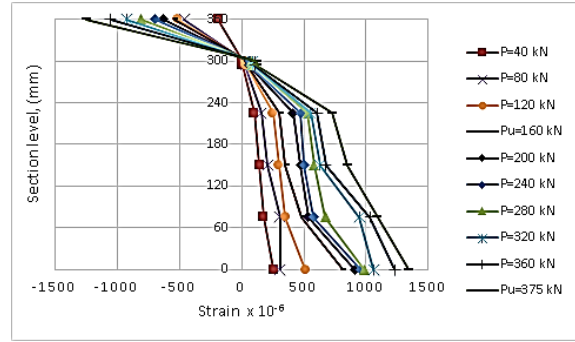


Fig. 6 Strain across section level of CEBP.

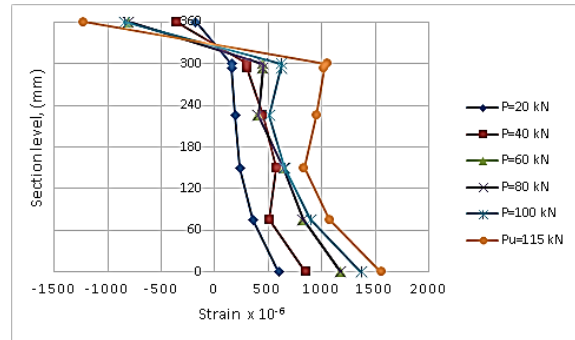


Fig. 7 Strain across section level of CBR.

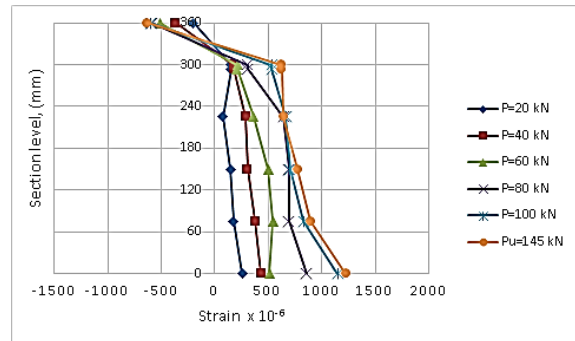


Fig. 8 Strain across section level of CBS.

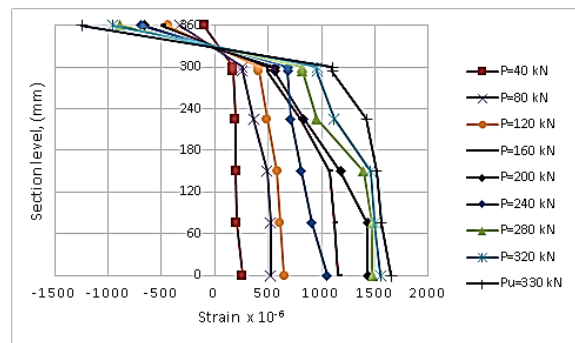


Fig. 9 Strain across section level of CBP.

The strain increment in the external prestressed strands due to applied loads in cellular specimen (CEBP) and castellated specimen (CBP) was indicated in Fig. 10, where these values attained at failure  $1526 \times 10^{-6}$  and  $1416 \times 10^{-6}$ , respectively.

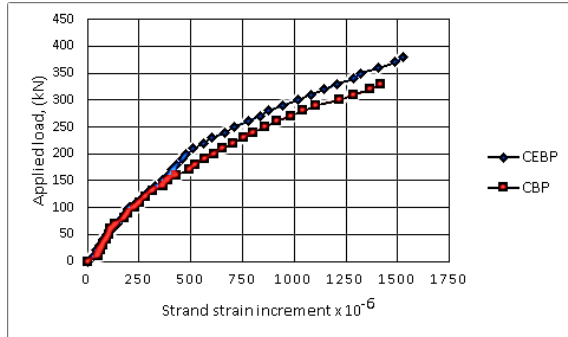


Fig. 10 Load – strand strain increment diagram.

## CONCLUSIONS

Based on the studied configuration of strengthening the composite castellated and cellular beams subjected to incremental monotonic static loading, the following conclusions can be drawn:

1. Adding vertical stiffeners at all web posts leads to increasing the ultimate capacity by 26% for castellated specimens and 21.8% for cellular specimens, respectively.
2. Using external prestressing in addition to vertical stiffeners leads to increase the ultimate load capacity by 186% for castellated specimens and 134.3% for cellular specimens, respectively.
3. The first technique reduced the midspan deflection under service loads by 25% and 22% for castellated and cellular specimens, respectively. While the second technique decreased, the mentioned values by 56% and 61%, respectively.
4. Applying external prestressing technique with intermediate stiffeners, led to more ductility in performance of specimens comparing with reference beams by decreasing strain over concrete and steel section with respect of high ultimate load carrying capacity.

## REFERENCES

- [1] Erdal, F. and Saka, M. P. "Ultimate load carrying capacity of optimally designed steel cellular beams" *Journal of Constructional Steel Research*, Vol. 80, No. 1, 2013, pp. 355–368.
- [2] Hosain, M., Cheng, W. and Neis, V. "Deflection analysis of expanded open-web steel beams" *Computers & Structures*, Vol. 4, No. 2, 1974, pp. 327–336.
- [3] Lorenc, W. and Kubica, E. "Behavior of composite beams prestressed with external tendons: experimental study" *Journal of Constructional Steel Research*, Vol. 62, No. 12, 2006, pp. 1353–1366.
- [4] Kerdal, D. and Nethercot, D. "Failure modes for castellated beams" *Journal of Constructional Steel Research*, Vol. 4, No. 4, 1984, pp. 298–315.

## RESIDENTIAL CUSTOMER DEMAND RESPONSE PROGRAM IN MICROGRID SYSTEM: A SURVEY LITERATURE

Ignatius Rendroyoko<sup>1</sup>, and Ngapuli I Sinisuka<sup>2</sup>

<sup>1</sup>School of Electrical Engineering and Information Technology - Institute Technology of Bandung, Indonesia; <sup>2</sup>Smart Grid Team PT PLN (Persero), Indonesia

### ABSTRACT

Electricity supply in microgrid power systems often faces limited power supply constraints. Besides to add more power generation, efforts to provide sufficient power in the power system can be made by controlling electricity load. A demand-side management (DSM) program can be done to regulate energy consumption and limit peak loads. The demand response (DR), as one of the DSM program, can be implemented to regulate the electric load to balance supply and demand. Residential customers demand response is a program that aims to reduce peak load by shifting or shedding residential electricity loads. This load reduction method has been used to control the peak load to be able to adjust to power supply conditions. This paper presents a literature survey of papers that address the application of DR for residential customers. The study uses the assumption that majority of electrical loads in microgrid systems are residential customers. It is expected that a balance between supply and demand for electricity in the power system can be achieved through demand response activities for residential customers. Here, a review of effective demand response methods is performed to precisely and accurately regulate the use of electricity by residential customers to limit peak load and control electrical energy consumption. In the end, this paper also discusses the possible implementation of demand response method for residential customers on a microgrid system.

*Keywords: Residential customers demand response, Load and power supply balancing, Electricity price, Incentives, Efficiency, Home energy management system*

### INTRODUCTION

In the development of micro grid power system to provide electricity supply for customers, often encountered constraints of a limited power supply of electricity. These problems are generally overcome by adding capacity of power plants, including RE generators, which is integrated into existing power systems to increase power capacity. Besides adding power generation, efforts to create a balance between supply and demand in power systems by controlling the electrical load. Here, the balance between the supply of electric power and variable load must be regulated and maintained [1].

On the demand side of a power system, controlling electrical loads and load scheduling can be done by using demand side management (DSM) method, with the aim to balance the load and electricity power supply. DSM is a method to regulate customer's demand load intelligently by reforming the load profile through efforts to change energy consumption patterns of electricity customers [2], [3]. Peter Palensky and D. Dietrich (2011) stated DSM could be used to intelligently influence the load, rather than building a new power plant [4]. The concept of DSM was first developed by utility with an aim to influence the customer's use of electricity [2]. In the report of EPRI (1993), utilities have load control programs that encourage the DSM programs.

Charles River Associates (2005) mentioned that the DSM has two main categories: energy efficiency and demand response (DR) [1]. The purpose of energy efficiency is a reduction of energy consumption, and the implementation of the DR refers to load profile adjustment, by implementing load shifting, shaving, and shedding, driven by market incentives [5].

DR scheme is an ability of an electric customer to reduce kWh usage or kW demand over a period or shift the usage to another period, in response to price or financial incentives [1]. Considering that the biggest part of electricity customers consist of residential customers, then DR program for residential customers may have a huge potential in electrical load controlling [6]. In electric power systems in remote areas or islands such as in Indonesia, where electricity supply is limited, DR schemes can be one of the appropriate ways to manage electricity loads, to be adapted to the electric power supply capability.

The proper design and scenario of DR implementation for residential customers will determine the successful implementation of intelligent electricity demand management to change the customer load profile. Therefore, some types of technology schemes, business models, and methods of implementation of the DR program for residential customers must be mastered and identified for the successful implementation of the program.

This paper presents a literature review of papers discussing the development, and implementation of DR program for residential customers. In general, discussions address the objectives, general concepts and technology schemes that are applied to residential customers. In particular, the review will focus on residential customer demand response optimization algorithms, control scheme mechanisms, program scheduling, and types of offers provided to motivate residential customers to participate in DR programs. Finally, it is discussed the implementation of DR schemes for residential customers on a microgrid power system to create a balance between demand and supply.

### DEMAND RESPONSE CONCEPT

The concept of demand response (DR) for residential customers can be described as a program to reduce peak load of electricity usage of residential customers by shifting or shedding electricity consumption, in response to power supply conditions.

### Main Objectives of the DR Scheme

Residential DR program refers directly to demand side management (DSM) which has main purposes as follows:

The first main purpose is the reduction of demand peaks of electricity usage in residential customers. Rajasekhar B. and Naran M. P. (2015) stated that the purpose of residential DR program is the reduction of electricity consumption by shifting, shaving and shaping electricity usage for residential customers, both individuals and customer groups [7].

The next purpose is to change the behavior of residential customers, so the load profile of residential customers may be modified into more adaptable load profile to electrical power system condition. Robin Roche (2012), mentioned that changes in residential customer load profiles could be done using new technologies and the function of DR aggregator [6]. As the load profile changes, DR can also reduce the possibility of overload conditions. Another important purpose is encouraging the reduction of large-capacity power generation [3]. When the load reduction can be carried out by DR scheme, it will directly reduce the need to operate the expensive power plants

### Work Mechanism of Demand Response

In implementing the DR scheme, one of the important things is how to make customers interested in participating in the program. This review on numbers of the mechanism of DR implementation will be a good reference for its practice on microgrid power system. Here, DR schemes can be classified according to the mechanism offered so that customers can be interested or willing to participate.

- DR Scheme based on the electricity price

Changes in the use of power and kWh consumption refer to electricity prices paid by customers, which consist of real-time pricing (RTP), critical peak pricing (CPC) and the time of use (TOU). When prices change, customer will react to adjust to changes in electricity rates according to the time so their consumption patterns will change. Peter Palensky (2011) describes that residential customers may join on DR activities by looking on real-time pricing and price signals [4]. P.T. Baboli et.al (2012) find that if the price gap between time periods are significant, customers will adjust the timing of their flexible loads to take advantage of lower price periods. Customers' reaction against implementing price-based DR is much important [8].

- DR schemes based on incentives

This scheme is provided by the utility or network operator. Here, customers will receive an incentive for any reduction in electricity usage. Some utilities also impose penalties when there are customers who already have a contractual obligation reduction in consumption but fail to comply. In their research on incentive-based DR program (IBDRP), James C Holyhead (2015) suggests that in the implementation of DR, especially on the incentive-based, optimal selection of customers must be performed, and be targeted to customers whose expected behavior leads to a reduction in the cost to the supplier [9].

- DR programs imposed by state or utility

The implementation of DR is done by requiring a particular group of residential customers to participate. In this way, the percentage of participation will be high, and the effect on the electrical system will be very influential.

Based on the above discussion, it is understood that the method to implement DR programs for residential customers will largely determine its success. Especially on how to give an explanation on residential customers about the importance of following the DR program with the option of competitive electricity prices or incentives offered. Here, the mindset change is required, where knowledge and awareness about energy management and efficiency also depend on customer engagement.

In the implementation of DR for residential customers, Rajasekhar B. and Naran M. P. (2015), states that residential customers tend to follow DR schemes based on the price offered. Depending on pricing scheme used, DR programs may operate in real-time, while others may work on a daily/hourly scheduling basis. For individual residential customers coordination of day-ahead scheduling and real-time DR need to be focused on optimization strategy of usage time. At the group of residential level, cooperative methods will result in greater impact on efficient and economical distribution network operations [7].

Meanwhile, P.T. Baboli et.al (2012), state that the successful implementation of the above two DR schemes depends on customer behavior. The results of research that have been implemented on a single customer and multi-customer give results that incentive-based DR schemes can be successful with a formation of customers habits. This is dependent on proper education and publicity programs [8].

Amir and Alberto (2010) presented on their study that although the price-based DR scheme has several advantages, it's limited due to the lack of automation systems (HEMS) and real-time pricing scheme cannot be executed manually. Therefore, scheduling the consumption of electrical energy for residential customers is proposed to be done automatically to provide more optimal results [10].

On coordination between systems and equipment in demand response, Bingnan Jiang and Yunsi Fei (2011), expressed about the concept of dynamic demand response and management of distributed generation (DG) for the implementation of DR in a residential community [11]. With conditions dynamically update mechanism, the DR will operate automatically according to the latest condition. Results show the effectiveness of this management system on the energy consumption cost reduction.

### Architecture and Components Framework DR Scheme

Architecture and components of the scheme of DR, described by Antimo Barbato and Antonio Capone (2014). Specifically, individual user methods are designed to manage users' electrical resources individually, while for cooperative consumers, users collaborate in determining their operating plans [12]. The frameworks for DSM are designed to be able to adjust its user's power source optimally, as shown in Figure 1 below.

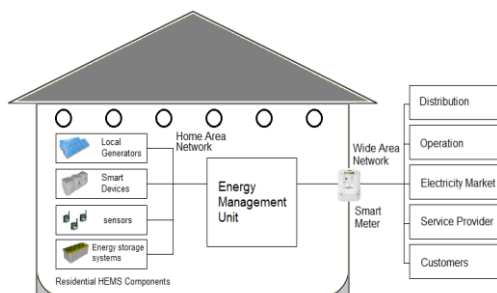


Figure 1 Frameworks architecture of DR

Figure 1 shows the basic components of DSM. It consists of power generation, power monitoring system, sensors, energy storage, and energy management unit (EMU). The EMU works as a device to exchange information with other devices in the system and manage resources electricity of the user based on demand response mechanism [12].

In another paper, M. Pipattanasomporn, Murat Kuzlu, and Saifur Rahman [13] states that the

concept of HEM system, proactively and effectively, able to control and manage the operation of household appliances to maintain overall electrical energy consumption to keep them under a certain limit. Here, HEMS has operated with priorities of both the load and customer comfort level settings.

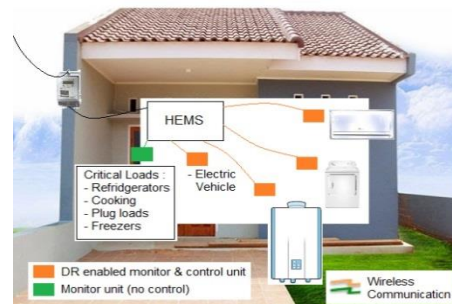


Figure 2 Architecture of HEM system

Both of the concepts above discuss the architectural scheme of DR for residential customers of an individual home. The resource management electricity of individual customer is managed separately by separating the operational plans of home appliances, energy storage systems, and renewable energy resources, as well as manage energy deals with the electricity system network.

### DR Method Based on the Decision Variable

DR methods can also be grouped by decision variables into two main groups: the first group refers to the DR program that decides when to activate the requested electrical load, while the DR program in the second group determines the amount of energy that can be allocated for each consumer, Vardakas et.al. (2015). In the method of DR with load scheduling, the most important thing is controlling the activation time of requested load [14]. In here, the load is divided into two types:

1. The type of load that must be operable and not allowed any failure or delay time of the entry load (such as lights and refrigerators).
2. Type of load that can be scheduled and may be discontinued, adjusted, or can be shifted to another time slot.

In the implementation of DR with decision variable, James C. Holyhead et.al. (2015) stated that the success of the program of acceptance of customers demand reduction could be improved by targeting a certain group of customers in the program. Evaluation of the algorithm against a classical approach that sees all customers within a group is targeted at reduced demand for a period with the use of maximum demand and indicates that solutions with targeting customers show greater peak reductions and increased cost savings [9].

Mohammad Rastegar et.al (2012), suggested in an article, an optimal framework for the implementation of commitments and an automatic

load of residential customers [15]. Here, the issue of load commitment (LC) is formulated with a purpose to determining the status on/off for responsive equipment. This formulation expanded to combine the capabilities of direct load control (DLC).

The importance of decision-making in the scheduling of operating equipment is also discussed by Alessandro et.al (2011), mentioned that in residential home, the problem occurs at the time of scheduling the operation of equipment, to be able to adjust with goals of cost savings and convenience related to the weather, and timeliness [16].

The second DR method is based on energy management by limiting or decreasing power consumption of specific loads, so the total power consumption in the peak load period will go down. This is implemented by controlling operation of domestic electrical appliances that will consume less power when the power capacity limitations in the power system [17].

## RESIDENTIAL DEMAND RESPONSE AND HOME ENERGY MANAGEMENT SYSTEM

In performing the DR scheme for residential customers, the key to successful implementation of the program may depend on the willingness of customers to participate in the program. For residential customers who are willing to follow the program this DR scheme, customers should also be able to implement energy management in each residential home (home energy management) [7].

Implementation of HEM can be done manually and automatically using auxiliary equipment of energy management. For manual implementation, HEM can be conducted by always informing customers not to operate household electrical appliances at peak periods. The implementation of HEMS can be done automatically by the algorithmic programming operation. Figure 3 shows the DR algorithm for residential smart home [7].

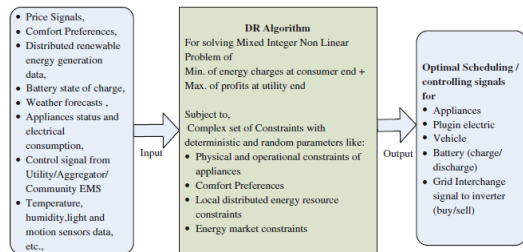


Figure 3 DR Algorithm for Smart Home Residential

Formulation of algorithms DR and load control strategies depending on the characteristics of the load consisting of types of loads, usage patterns, the duty cycle, consideration of the uncertainty, modeling behavior, technical obstacles and renewable energy generation and energy storage

facilities. Therefore, the potential of DR scheme for various home appliances needs to be assessed as a consideration in designing DR algorithms.

Adam Taylor et.al. (2014) delivered on the evaluation of several algorithms have been designed to include a variety of conditions on the application of DR [18]. It was concluded that the algorithm residential DR should be following the structure of the electricity network so that the compliance between the data acquisition and dissemination of control commands can be synchronized without any significant delay time.

In specific about the load profile, Sara Ghaemi and Gunther Brauner (2010) presented the results of an analysis of the stochastic model for generating customer load profile [19]. This model can allow for the assessment of potential energy savings through the replacement of energy-saving devices and changing the customer's behavior.

## OPTIMIZATION MODEL FOR RESIDENTIAL CUSTOMER DEMAND RESPONSE

In this section, a review of the optimization of several DR schemes : for single houses, and for a group of houses or communities. The optimization process is defined as a process of discovering the conditions that provide a maximum benefit or minimal cost of a process [7]. The research which is conducted on optimizing the DR program aimed at minimizing power consumption while maintaining a level of customer comfort.

### Optimization of DR Model for Single home

The problem of optimization of a DR model is to manage electricity consumption, generation, and customer's energy storage over a period, which is divided into some time slots from a few minutes to hour periods. The purposes of DR model optimization are as follows:

- 1) Minimizing the total cost of electricity
- 2) Minimize the discomfort experienced by customer of delay operation time
- 3) Maximizing network's power resources with electricity transactions from/to the network
- 4) Peak load reduction and ratio of PAR

An optimization model for the above purpose can be provided by the following formula [7]:

- 1) To minimize the cost of electrical power  
Focus on reducing the cost of electricity

$$\min \sum_{t \in N} (c_t \cdot y_t - d_t \cdot z_t)$$

When the reward parameter included in the calculation, then the formula becomes:

$$\min \sum_{t \in N} (c_t \cdot y_t - d_t \cdot z_t - (R_t^U \cdot a_t^U + R_t^L \cdot a_t^L))$$

Where  $c_t$ ,  $d_t$  are buying, selling cost of energy and  $y_t$ ,  $z_t$  are energy brought and injected into the grid at



time  $t$ .  $R_t^U$  can be reward paid/penalty collected depending on demand request satisfaction.

- 2) To minimize the inconvenience that perceived by customer. Here, the focus is on minimizing the inconvenience experience

$$\min \sum_{t \in N} (\alpha \sum_{s \in S} f_{st}^S \cdot x_{st} + \beta \sum_{e \in e^{CB}} f_{et}^{e^{CB}})$$

- 3) To maximize the energy from local generation

$$\max \frac{\sum_{n \in N} (\pi_t^{R,PV} - \pi_t^{net})}{\mu \cdot p_t^{TOT}}$$

Where  $\pi_t^{R,PV}$  is energy that generated by the PV panel at time  $t$  and  $p_t^{TOT}$  is total power and  $\pi_t^{net}$  is nett generation.

In the single home model, customers have four types of equipment that are distinguished by their control functions: fixed/critical, time and power shiftable, comfort base and local renewable energy generation and energy storage.

### Optimization of DR Model for group of homes or community Tables

In this condition, a group of individual residential customers will cooperate with an aggregator or Community Energy Management System (CEMS) to conduct electricity transaction management with electricity company or power system grid [7], [12]. The main purpose is to reduce total cost of electricity from a group of homes or communities by setting the schedule for the time allowed. The formula for calculating cost minimization is:

$$\min \sum_{u \in U} \sum_{t \in T} (c_t \cdot y_t^u - d_t \cdot z_t^u)$$

Where  $c_t \cdot y_t^u$  is energy received from system grid, and  $d_t \cdot z_t^u$  is selling cost of energy. The challenge remains the total peak load of users cannot exceed a total aggregate peak load customers. Cooperative methods of multiple residential homes have the potential to provide a greater influence on the efficiency of the system, when the settings are done with system-wide perspective.

Some papers also discuss the DR relationship with the electricity market. The influence of DR scheme can result from electricity price and options of incentive offered so that customers are interested in participating in the DR program. Several types of the tariff are available for determining the price of electricity : time of use (TOU), critical peak pricing (CPP) and real-time pricing (RTP) [12].

### LOAD CHARACTERISTICS IN INDONESIAN ISLAND MICROGRID SYSTEM

In this chapter, it is discussed load characteristics of microgrid systems in the island where the DR

scheme will be developed. The system has limited power supply, high electrical load during peak loads and loads, are dominated by residential customers.

Referring to an article from Tongam (2008), numbers of factors that may influence the demand for electrical energy in the residential sector are household income, prices or tariffs of electricity, electrical appliances, load characteristics, and other relevant variables [20]. These factors will affect load characteristics of the microgrid system, which is dominated by residential customers.

Characteristics of the electrical load in a microgrid system will greatly determine the strategies used to balance between the load profile and generation capacity.

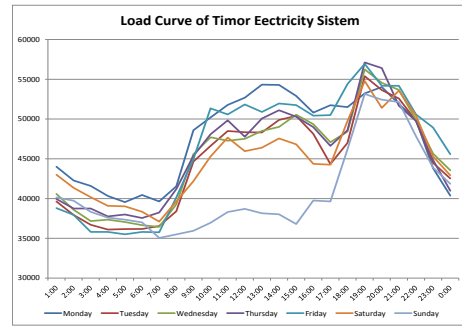


Figure 4 Load Curve of Timor Power System

Figure 4 shows the daily load curve of the Timor power system, in the period of 4 - 10 April 2016 (Monday-Sunday). It is shown a gap between peak load and off-peak load, about 23% of total power capacity in Timor electric power system.

At single residential homes in Timor electricity system, loading curve with details of energy consumption per equipment can be seen in Figure 5. It has a similar pattern to a study on residential demand response scheduling [20].

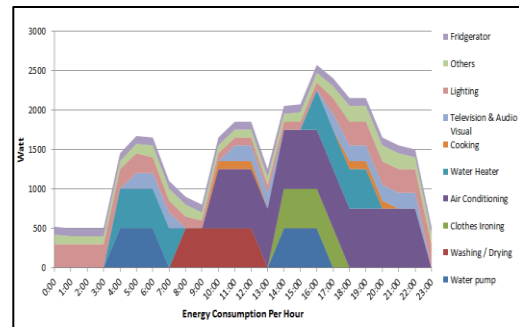


Figure 5 Energy consumption per hour for every household electrical appliances

The demand for electricity with characteristics, as shown in Figure 5 above, supplied by existing power plants, including renewable energy power plants that have intermittent characteristics. To maintain a balance between the power supply and the load, the implementation of demand response for residential customers need to be performed on the microgrid system such as in Timor power system.

## CONCLUSIONS

From discussions in the preceding paragraph, several conclusions can be drawn as a reference and valuable lesson that can be used to conduct further research in the future :

- 1) In general, the purpose of applying the demand response is to reduce the peak load, and it directly impacts the reduction of generating capacity to be operated and changes the customer behavior so that the load profile can be improved.
- 2) Optimization of DR scheme implementation are classified into individual customers and groups of customers that will define the architecture of the program and the success rate of implementation
- 3) Residential demand response has great potential to be used as a method of load balancing and power supply in microgrid systems in Indonesia

## REFERENCES

- [1] Charles River Associates, "Primer on Demand-Side Management", Tech. Rep. February, The World Bank, 2005
- [2] Gellings CW, "The concept of demand-side management for electric utilities", Proceedings of the IEEE 73(10):1468–1470, 1985
- [3] Barakat & Chamberlin, Inc. "Principles and Practice of Demand-Side Management", EPRI TR-102556, Palo Alto, California, August 1993
- [4] Peter Palensky, and Dietmar Dietrich, "Demand Side Management: Demand Response, Intelligent Energy Systems, and Smart Loads", IEEE Transaction on Industrial Informatics, Vol. 7, No. 3, August 2011
- [5] Qi Zhang and Ignacio E. Grossmann, "Planning and Scheduling for Industrial Demand Side Management: Advances and Challenges", Alternative Energy Sources and Technologies, pp 383-414, Springer, March 2016
- [6] Robin Roche, "Agent-Based Architectures and Algorithms for Energy Management in Smart Grids: Application to Smart Power Generation and Residential Demand Response," Ph.D. dissertation, Abbrev. Dept., UTBM, Belfort, France 2012.
- [7] Rajasekhar Batchu and Naran M. Pindoriya, "Residential Demand Response Algorithms: State-of-the-Art, Key Issues and Challenges," in *7th EAI International Conference on Wireless and Satellite Systems*, Bredford, Great Britain, 6-7 July 2015, pp. 18–32.
- [8] P.T. Baboli, M. Eghbal, dan M. Parsa Moghaddam and H. Aalami, "Customer behavior based demand response model," Power and Energy Society General Meeting, 2012 IEEE, San Diego, California, USA, Juli 2012
- [9] James C. Holyhead, Sarvapali D.R. and, Alex Rogers, "Consumer Targeting in Residential Demand Response Programmes," in *the ACM International Conference on Future Energy Systems*, Bangalore, India, 14 - 17 Jul 2015.
- [10] Amir-Hamed M., and Alberto L. G., "Optimal Residential Load Control with Price Prediction in Real-Time Electricity Pricing Environments Demand Response in an Isolated System with high Wind Integration," in *IEEE Transactions on Smart Grid*, Volume: 1, Issue: 2, Sept. 2010.
- [11] Bingnan Jiang and Yunsi Fei, "Dynamic Residential Demand Response and Distributed Generation Management in Smart Microgrid with Hierarchical Agents," in *Procedia ICSGCE 2011: 27–30 September 2011, Chengdu, China*.
- [12] Antimo Barbato and Antonio Capone, "Optimization Models and Methods for Demand-Side Management of Residential Users: A Survey," *Energies* 2014.
- [13] Manisa Pipattanasomporn, M. Kuzlu, and S. Rahman, "An Algorithm for Intelligent Home Energy Management and Demand Response Analysis," in *IEEE Transactions on Smart Grid*, Vol. 3, No. 4, December 2012.
- [14] John S. Vardakas, Nizar Zorba, and Christos V. Verikoukis, "A Survey of Demand Response Programs in Smart Grids: Pricing Methods and Optimization Algorithms", *IEEE Communication Surveys & Tutorials*, Vol. 17 (No. 1), 152-178.
- [15] M. Rastegar, M. Fotuhi-Firuzabad, and F. Aminifar, "Load commitment in a smart home," *Appl. Energy*, vol. 96, pp. 45–54, Aug. 2012.
- [16] Alessandro Agnetis, et.al., "Appliance Operation Scheduling for Electricity Consumption Optimization," in *50th IEEE CDC - ECC*, Orlando, FL, USA, December, 2011.
- [17] Q. Dong, L. Yu, W. Z. Song, L. Tong, and S. Tang, "Distributed demand and response algorithm for optimizing social-welfare in smart grid," in *Proc. 26th IEEE IPDPS*, Shanghai, China, May 21–25, 2012, pp. 1228–1239.
- [18] Adam Taylor, Ivana D., C. Harris, A. Marinescu, Edgar G.L., Fatemeh G., Siobhan C., and Vinny Cahill, "Self-Organising Algorithms for Residential Demand Response," in *IEEE Conference on Technologies for Sustainability (SusTech)*, 2014, Portland, USA, 24-26 July 2014, pp. 55–60
- [19] S. Ghaemi, and Günther Brauner, "Stochastic Model For Household Load Profile," in *11. Symposium Energieinnovation*, 10-12 February 2010, Graz/Austria
- [20] Tonggam Sihol Nababan, "Household Electrical Energy Demand (Case Study on Domestic Electricity Consumer Group Electrical PT PLN (Persero) in Medan), Ph.D. Dissertation, Doctoral Studies Program in Economics, University of Diponegoro, Indonesia, 2008.



# CRACKING AND DEFORMABILITY OF BONDED AND UNBONDED PRESTRESSED CONCRETE BEAMS UNDER MONOTONIC STATIC LOADING

Nazar K. Oukaili<sup>1</sup> and Mohammed M. Khattab<sup>2</sup>

<sup>1</sup>Professor, University of Baghdad, Iraq; <sup>2</sup>Ph.D. Candidate, University of Baghdad, Iraq

## ABSTRACT

This paper presents outcomes of the study undertaken on partially prestressed concrete beams with bonded and unbonded prestressing strands. In order to investigate the cracking and deformability of partially prestressed concrete beams, an experimental program has been conducted on 10 full-scale simply supported beams over a span of 3000 mm. The objective of this investigation was to examine experimentally the effect of varying partial prestressing ratio (PPR) and type of bond development between prestressing steel and surrounding concrete (bonded or unbonded) on cracking and deflection values. Accordingly, two specimens were fully reinforced concrete, three partially prestressed concrete with bonded strands, three partially prestressed concrete with unbonded strands and the remaining two were fully prestressed with bonded strands. All specimens were loaded up to failure in four-point bending using two symmetrical concentrated monotonic static loads applied at one-third of the span length. Measurements were made for strains in prestressed, nonprestressed steel and concrete, midspan deflections, crack spacing and crack widths at different loading stages. Theoretical analysis was also carried out using ACI Code to predict the cracking load, deformability, stress at failure in prestressing steel, and ultimate load of the specimens. Results of the theoretical analysis according to code methods have been found to be consistent with the experimental data.

*Keywords: Partial Prestressing, Bonded, Unbonded, Flexure, Deflection, Cracking*

## INTRODUCTION

In the last few decades, prestressed concrete has been widely used due to enormous development in the construction techniques. Now more than 50 percent of bridges in the world are constructed using prestressed girders [1]. The major disadvantages of using conventionally reinforced concrete beams is the corrosion of reinforcement which occurs due to the effects of cracks in the tension zone. In the other hand, the major defect of fully prestressed concrete beams, where no flexural tension allowed in the concrete under service load, is the low ductility. The ductility of fully prestressed concrete beams could be enhanced with the presence of nonprestressed reinforcement. Partial prestressing describes prestressed beams wherein limited cracking is permitted through the use of additional mild nonprestressed reinforcement to control the extent and width of cracks and to contribute with part of the ultimate flexural moment strength. Partially prestressed concrete beams, therefore occupies the complete spectrum between the two extremes. It permits cracking under service loads, but to satisfy the serviceability requirements, the maximum crack width and the maximum deflection should not exceed the code recommended limits on crack width and deflection.

The term Partial Prestressing Ratio (PPR) is the ratio of ultimate resisting moment due to the prestressing steel to the ultimate resisting moment due to the total tensile steel [2]:

$$PPR = \frac{A_{ps} f_{ps} d_p}{A_{ps} f_{ps} d_p + A_s f_y d_s} \quad (1)$$

Where:

$A_{ps}$  = area of prestressing steel;

$A_s$  = area of nonprestressed steel;

$f_{ps}$  = stress in prestressing steel at ultimate behavior;

$f_y$  = yield strength of nonprestressed steel;

$d_p$  = distance from extreme compressive fiber of concrete to centroid of prestressing steel;

$d_s$  = distance from extreme compressive fiber of concrete to centroid of nonprestressed steel.

Reinforced concrete beams always have to be designed as underreinforced to ensure ductile failure by yielding of the steel reinforcement. Prestressed beams can be either underreinforced using relatively small percentage of mild nonprestressed steel, leading to rupture of the tensile steel at failure, or essentially overreinforced, using a large percentage of steel, resulting in crushing of the concrete at the compression top fibers in somewhat less ductile failure [3].

According to ACI 318-2011 [4], the prestressed concrete beam sections can be classified into three types based on the tension – reinforcement area, such that when the beam reaches its nominal flexural strength, the net tensile strain in the extreme layer of tensile steel,  $\epsilon_t$ , as follow:

Tension - controlled section if  $\epsilon_t > 0.005$

Transition – zone section if  $0.002 < \epsilon_t < 0.005$

Compression - controlled section if  $\epsilon_t < 0.002$

## EXPERIMENTAL PROGRAM

The experimental program consists of testing ten full scale specimens with overall dimensions of (200x300x3300) mm, which were divided into four groups. The first group consists of two fully reinforced concrete specimens (FR). The second and the third groups, each consists of three partially prestressed concrete specimens (PP) with bonded and unbonded strands, respectively. The fourth group consists of two fully prestressed specimens with bonded strands (FP).

For all specimens concrete mix of target value of 40 MPa, cylinder compression strength at 28 days age, was used. Deformed steel bars with yield stress of 570 MPa and ultimate strength of 650 MPa was used for flexural nonprestressed and stirrups. All specimens were reinforced using closed stirrups of 10 mm diameter with spacing 100 mm c/c in shear spans of 1000 mm length and 3 stirrups were used in the pure bending moment zone (Fig. 1). Low - relaxation seven - wire steel strands, with 12.7 mm diameter, (Grade 270), has been used in all prestressed specimens.

To achieve the objective of the study, the experimental specimens were designed in such a way that to allow investigate the effect of partial prestressing ratio and type of bond development between prestressing steel and the surrounding concrete on the behavior of these members (Table 1).

Table 1 Details of experimental specimens

Group	Specimen	PPR	$\omega_p$	$\omega$	$\omega'$
1	FR-UN	0.000	0.000	0.043	0.043
	FR-MAX	0.000	0.000	0.244	0.045
2	PP-U-TC	0.743	0.157	0.043	0.043
	PP-U-TR	0.409	0.144	0.172	0.044
	PP-U-CC	0.339	0.138	0.224	0.044
	PP-B-TC	0.771	0.185	0.043	0.043
3	PP-B-TR	0.529	0.178	0.124	0.043
	PP-B-CC	0.358	0.169	0.259	0.045
4	FP-B-TC	1.000	0.187	0.000	0.049
	FP-B-CC	1.000	0.270	0.000	0.000

Note: UN = under - reinforced; MAX = maximum reinforced ( $\rho = 0.75 \rho_b$ ); U = unbonded; B = bonded; TC=tension - controlled; TR=transition - controlled; CC = compression - controlled;  $\omega_p, \omega$  and  $\omega'$  = the reinforcement index for tensile prestressing, tensile nonprestressed and compression nonprestressed reinforcement, respectively.

In all prestressed concrete specimens, except specimen (FP-B-CC), two strands were used with target initial prestress  $f_{pi}$  of  $0.7 f_{pu}$ . For specimen (FP-B-CC), three strands with  $0.6 f_{pu}$  initial prestress were applied. Strands were tensioned simultaneously from one end. Special care was

exercised to balance the prestressing force in the strands to avoid biaxial bending of the specimens. The corresponding stress was monitored accurately using readings of the strain gauges attached to the surface of the prestressing strands along with the readings of the pressure gauge of the hydraulic jack used in the prestressing operation.

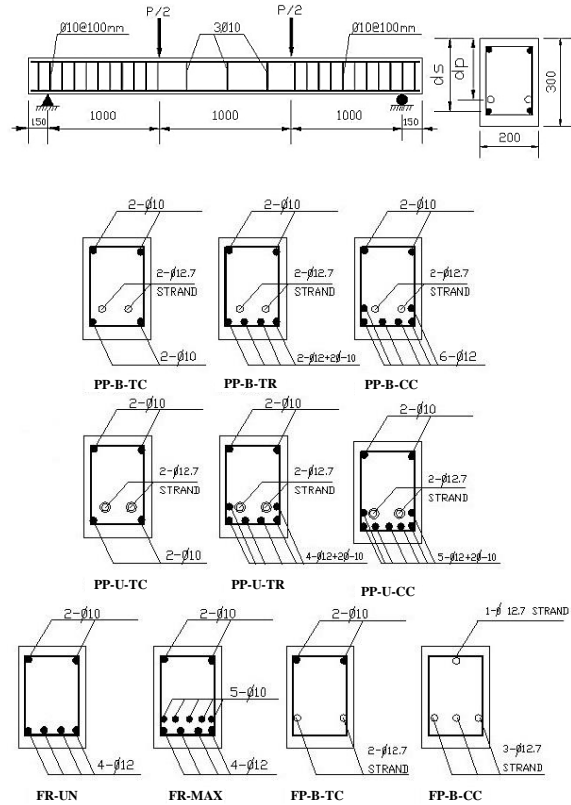


Fig. 1 Details of experimental specimens.

## TEST SETUP

All specimens were loaded in four-point bending using two symmetrical monotonic concentrated static loads applied at one-third of the span length. The test was conducted using closed loop ram with 50 ton capacity actuator. Specimens were subjected to a monotonically increasing load up to failure using a load control test. All measurements, such as beam deflections, strains in steel strands, strains in steel bars and strains in concrete were recorded twice, immediately after the application of the load and after 10 minutes later.

Deflection was measured at midspan using dial gage of 0.01 mm accuracy. Electrical strain gauges were used to measure the strains in prestressing steel, nonprestressing steel and concrete. Cracks were monitored along the span of the beams. Maximum crack width, number of cracks and average crack spacing were measured sequentially during loading.

## EXPERIMENTAL RESULTS

### Cracking load, Crack Width, Crack Number, and Average Crack Spacing

Flexural cracks in all specimens were initiated at the location of pure moment zone perpendicularly to the longitudinal axis of the specimen and extended up to the location of the tensile nonprestressed reinforcement. Table 2 illustrates experimental and theoretical cracking load as well as experimental and theoretical deflection at this loading stage. Theoretical cracking load was determined according to the following equations [5]:

$$M_{cr} = f_r \frac{I_t}{c_b} + f_{ps} A_{ps} \left( e_o + \frac{I_t}{c_b A_t} \right) \quad (2)$$

Where:

$M_{cr}$  = cracking moment;

$f_r$  = modulus of rupture;

$I_t$  = transformed moment of inertia;

$c_b$  = distance between centroid of section and bottom fiber of concrete;

$A_t$  = transformed area of concrete section;

$e_o$  = distance between centroid of prestressing reinforcement and centroid of section.

The following equation was used to calculate theoretical deflection at cracking load [5]:

$$\Delta_{cr} = \frac{P_{cr} b}{24 E I_t} (3l^2 - 4b^2) \quad (3)$$

Where:

$l$  = span between the supports;

$b$  = distance from support to point load, (Fig. 1).

Table 2 Experimental and theoretical cracking load and deflection

Specimen	Exp. $P_{cr}$ , (kN)	Theo. $P_{cr}$ , (kN)	Exp. $\Delta_{cr}$ , (mm)	Theo. $\Delta_{cr}$ , (mm)
FR-UN	20.0	23.0	1.10	0.75
FR-MAX	22.0	24.2	1.70	1.77
PP-U-TC	67.0	75.0	3.00	2.95
PP-U-TR	68.0	76.0	3.00	2.58
PP-U-CC	72.0	76.8	2.88	2.58
PP-B-TC	70.0	74.3	3.33	2.62
PP-B-TR	67.0	75.0	2.50	2.70
PP-B-CC	73.0	77.2	3.25	2.66
FP-B-TC	70.0	74.9	3.12	2.85
FP-B-CC	90.0	91.3	4.24	6.30

From Table 2, it was observed that the presence of prestressing steel has good contribution to delay the cracking appearance and increase the cracking load. For (FR) specimens, the cracking load was much less than that for (PP) and (FP) specimens. It was

also noted that, for (PP) specimens, increasing nonprestressed reinforcement, i.e. decreasing (PPR), slightly affected the cracking load. In the other hand, for (FP) specimens, increasing the area of prestressing steel in (FP-B-CC) led to increase the cracking load by about (29%) in comparison with (FP-B-TC).

Crack width, number of cracks and average crack spacing at failure were measured and recorded throughout the test (Table 3).

Table 3 Number of cracks, average crack spacing and crack width for experimental specimens

Specimen	Number of cracks	Average crack spacing, (mm)	Crack width, (mm)
FR-UN	24	120	1.30
FR-MAX	27	100	1.20
PP-U-TC	10	140	4.25
PP-U-TR	22	90	1.00
PP-U-CC	20	110	0.95
PP-B-TC	18	110	2.10
PP-B-TR	20	100	0.95
PP-B-CC	23	100	0.95
FP-B-TC	13	150	5.00
FP-B-CC	14	125	2.40

In (FR) specimens, the number of cracks was the highest among all specimens. For prestressing specimens with high nonprestressed steel area, i.e. low level of (PPR), more cracks were propagated and less crack spacing was observed (Plate 1). This is due to the better overall bond achieved by the tensile nonprestressed steel with the surrounding concrete which led to control the cracks in tension zone of the element.

### Load - Deflection Response

The load deflection curves for the tested specimens are shown in (Fig. 2). It can be seen that for specimens of (FR) and (PP) groups with tension - controlled and transition - controlled concrete sections, three distinctive points could be observed. These points are characterizing cracking, yielding and ultimate loads. However, for partially and fully prestressed compression - controlled concrete sections, only points which characterized cracking and ultimate loads can be observed. Thus, clear yielding point cannot be distinguished. Prior to cracking all specimens behaved in an elastic manner. After cracking, (FR) and (PP) specimens with low (PPR) developed approximately linear load-deflection response. All specimens experienced decreasing of stiffness after cracking, depending on the level of (PPR) and the reinforcement index. Increasing the area of tension reinforcement

produced stiffer specimen which led to low rate of deflection versus applied load.



Plate 1 Crack propagation of tested specimens.

It was observed that, specimen with highest stiffness before cracking suffered from highest stiffness reduction after cracking. Also, specimens with bonded strand were stiffer than the similar but with unbonded strand. Yielding of the nonprestressed steel occurred prior to prestressing steel for all the specimens. This is because of the location of reinforcing steel relative to neutral axis. (FR) specimens developed a well-defined yield point followed by a strain hardening stage prior to failure.

### Moment Capacity and Strain in Prestressing Reinforcement

The strain in prestressing strands has been measured using two electrical strain gauges per each strand which were fixed at midspan section. Accordingly, the stress was determined by using the actual stress-strain curve of the strand. This stress was compared with the stress determined according to the mentioned below empirical equations, which adopted by the ACI-318-2011 [4]:

For bonded strands

$$f_{ps} = f_{pu} \left[ 1 - \left\{ \frac{\gamma_p}{\beta_1} \rho_p \frac{f_{pu}}{f'_c} + \frac{d_s}{d_p} (\omega - \omega') \right\} \right] \quad (4)$$

$$\omega = \rho \frac{f_y}{f'_c} ; \omega' = \rho' \frac{f_y}{f'_c} \quad (5)$$

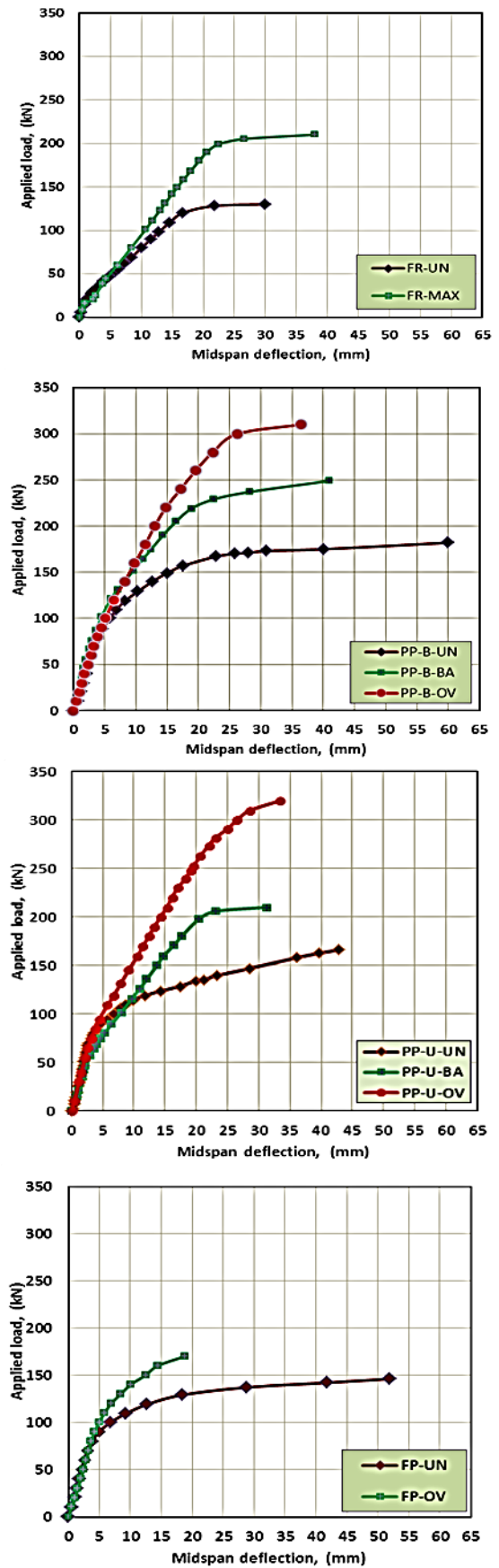


Fig. 2 Load-deflection response of tested specimens.

For unbonded strands

$$f_{ps} = f_{pe} + 70 + \frac{f'_c}{k\rho_p} \leq f_{pe} + c \quad (6)$$

Where:

$f_{ps}$  = stress in prestressing strand at flexural resistance of the section;

$f_{pu}$  = specific tensile strength of prestressing strand;

$f_{pe}$  = effective prestress;

$f'_c$  = specific compressive strength of concrete;

$\gamma_p$  = factor used for type of prestressing steel;

$\beta_1$  = factor relating depth of equivalent rectangular compressive stress block to depth of neutral axis;

$\rho_p$  = ratio of  $A_{ps}$  to  $b d_p$ ;

$\rho$  = ratio of  $A_s$  to  $b d_s$ ;

$\rho'$  = ratio of  $A'_s$  to  $b d_s$ ;

$k = 100$  and  $c = 414$  for span/depth ratio  $\leq 35$

$k = 300$  and  $c = 207$  for span/depth ratio  $> 35$

Table 4 shows experimental strain and stress and empirical stresses in prestressing strands for each prestressed specimens.

Table 4 Experimental and theoretical strain and stress in prestressing strands

Specimen	Exp. $\epsilon_{ps,exp}$	Exp. $f_{ps,exp}$ , (MPa)	Theo. $f_{ps,theo}$ , (MPa)	$\frac{f_{ps,exp}}{f_{ps,theo}}$
PP-U-TC	0.00820	1621	1414	1.146
PP-U-TR	0.00730	1449	1337	1.084
PP-U-CC	0.00740	1469	1284	1.144
PP-B-TC	0.01189	1722	1725	0.998
PP-B-TR	0.01042	1712	1662	1.030
PP-B-CC	0.00897	1661	1566	1.061
FP-B-TC	0.00863	1641	1745	0.940
FP-B-CC	0.00777	1540		

The concept of determining experimental ultimate load varies from one researcher to another. In this study, the load value corresponding to the maximum load on the load-deflection curve was taken as the ultimate load.

The theoretical nominal moment capacity of tension - controlled concrete rectangular section can be determined by the following equation [5]:

$$M_n = A_{ps}f_{ps} \left( d_p - \frac{a}{2} \right) + A_s f_y \left( d_s - \frac{a}{2} \right) + A'_s f_y \left( \frac{a}{2} - d'_s \right) \quad (7)$$

For compression - controlled concrete rectangular section

$$M_n = f'_c b d_e^2 (0.36\beta_1 - 0.08\beta_1^2) \quad (8)$$

$$d_e = \frac{A_{ps} f_{ps} d_{ps} + A_s f_y d_s}{A_{ps} f_{ps} + A_s f_y} \quad (9)$$

Table 5 illustrates the experimental and the theoretical load carrying capacities for each specimen.

Table 5 Experimental and theoretical ultimate load capacity

Specimen	PPR	Exp. $P_{u,exp}$ , (kN)	Theo. $P_{u,theo}$ , (kN)	$\frac{P_{u,exp}}{P_{u,theo}}$
FR-UN	0.000	130	121	1.074
FR-MAX	0.000	210	199	1.055
PP-U-TC	0.734	165	151	1.093
PP-U-TR	0.409	210	211	0.995
PP-U-CC	0.339	320	212	1.509
PP-B-TC	0.771	182	172	1.058
PP-B-TR	0.529	230	213	1.082
PP-B-CC	0.358	310	209	1.483
FP-B-TC	1.000	146	138	1.058
FP-B-CC	1.000	170		

The magnitude of ultimate load capacity was varied depending on the value of the reinforcement index. Almost experimental ultimate load results were greater than the theoretical values. The reason of this can be interpreted that the calculated stress in prestressing steel, according to equations (4) or (5), was smaller than the experimental values. In general, comparison of these results indicates good agreement between the experimental and theoretical results for all the specimens except the compression - controlled specimens ((PP-U-CC) and (PP-B-CC)). The experimental results of these specimens gave approximately 1.5 times the theoretical values. Thus, the ACI-code equation (Eq. 8) is not considering the impact of the presence of reinforcing steel on the moment capacity of compression - controlled sections. This equation also doesn't distinguish between bonded and unbonded strands in calculating the moment capacity of compression controlled sections.

Obviously, two modes of failure have been observed through the experimental tests. The first mode of failure is due to the crushing of concrete in compressive zone of the section, which resulted after yielding and excessive deformation of tension nonprestressed steel. This type of failure was occurred in (FR) and tension - controlled (PP) specimens. The second mode of failure which was observed is the crushing of concrete of the section compression zone before the yielding of the tension nonprestressed steel. This is primarily due to an excessively large quantity of tension reinforcement in the section. This type of failure was observed for (FR) as well as compression - controlled (PP) specimens. No slip between strand and concrete has been observed in any specimen through the experimental tests.

Table 6 summarizes strains in nonprestressed tension  $\epsilon_s$  and compression  $\epsilon'_s$  reinforcement and the strain at the top extreme concrete fibers  $\epsilon_c$ . It shows also, the ultimate deflection  $\Delta_u$  at midspan of the specimens. These results indicate that, for tension - controlled sections the tensile steel reached yielding point while for compression - controlled specimens the strains were below the yielding point.

Table 6 Strains in nonprestressed reinforcement, top extreme concrete fibers and ultimate deflection

Specimen	$\epsilon_s$	$\epsilon_c$	$\epsilon'_s$	$\Delta_u$ , (mm)
FR-UN	0.0055	0.00140	0.00024	41.4
FR-MAX	0.0053	0.00069	0.00023	32.8
PP-U-TC	0.0123	0.00154	0.00032	45.0
PP-U-TR	0.0157	0.00179	0.00144	35.0
PP-U-CC	0.0024	0.00211	0.00243	29.0
PP-B-TC	0.0063	0.00205	0.00108	56.0
PP-B-TR	0.0052	0.00170	0.00085	32.4
PP-B-CC	0.00383	0.00193	0.00195	34.0
FP-B-TC		0.00142	0.00044	38.0
FP-B-CC		0.00145		30.0

## CONCLUSIONS

The following conclusions can be drawn

- 1- For specimens with approximately the same (PPR), ultimate strain in bonded prestressing strands is higher than its counterpart of unbonded prestressing strand. Accordingly, the value of ultimate load capacity for specimens with bonded strands is significantly higher than that of the counterpart specimen with unbonded strands.
- 2- The appearance of first crack in (PP) as well as in (FP) specimens was delayed in comparison with (FR) specimens. This is due to the presence of prestressing force.
- 3- The first flexural crack initiated at load ranged 8.6% to 52.9% of the ultimate load.
- 4- In (FR) and (PP) specimens with small (PPR) value, the crack pattern was distributed along the pure bending moment zone with small crack width and large number. This is due to the presence of nonprestressing steel which controls the cracks in tension zone. In the other hand, for (FP) and (PP) specimens with high (PPR), small number of cracks were appeared with large crack width.
- 5- Failure modes for (FR) and tension – controlled (PP) specimens were more ductile than that of (FP) and compression - controlled (PP) specimens.

## REFERENCES

- [1] Collins, M. and Mitchell, D. “Prestressed Concrete Structures”, Prentice Hall, Engineering Cliffs (NJN, USA), 199, pp. 4-5.
- [2] Harajli, M.H. and Naaman, A. E. “Deformation and Cracking of Partially Prestressed Concrete Beams Under Static and Cycles Fatigue Loading” Report No. UMEE 84R1 Department of Civil Engineering, the University of Michigan, College of Engineering, 1984, pp. 21.
- [3] Nawy, E. G. “Prestressed Concrete: A Fundamental Approach”, Prentice Hall, 5<sup>th</sup> Edition, 2009, pp. 198 - 201.
- [4] ACI Committee 318-2011, “Building Code Requirements for Structural Concrete and Commentary” American Concrete Institute, Farmington Hills, Michigan, 2011.
- [5] Naaman, A. E., “Prestressed Concrete Analysis and Design”, 2<sup>nd</sup>, Techno Press 3000, Ann Arbor, Michigan, 2004, pp. 235-236.

## DISTRIBUTED MODEL OF HYDROLOGICAL AND SEDIMENT TRANSPORT PROCESS IN MEKONG RIVER BASIN

Zuliziana Suif<sup>1</sup>, Chihiro Yoshimura<sup>2</sup>, Nordila Ahmad<sup>1</sup> and Sengheng Hul<sup>3</sup>

<sup>1</sup>Department of Civil Engineering, Faculty of Engineering, National Defence University of Malaysia, Malaysia; <sup>2</sup>Department of Civil engineering, Tokyo Institute of Technology, Japan, <sup>3</sup>Institute of Technology Cambodia, Cambodia.

### ABSTRACT

Soil erosion and sediment transport have been modeled at several spatial and temporal scales, yet few models have been reported for large river basins (e.g., drainage areas > 100,000 km<sup>2</sup>). In this study, we propose a process-based distributed model for assessment of sediment transport at a large basin scale. A distributed hydrological model was coupled with a process-based distributed sediment transport model describing soil erosion and sedimentary processes at hillslope units and channels. The model was tested in Mekong River Basin (795,000 km<sup>2</sup>). The simulation over 10 years showed good agreement with the observed suspended sediment load in the basin. The average Nash–Sutcliffe efficiency (NSE) and average correlation coefficient (r) between the simulated and observed suspended sediment loads were 0.60 and 0.78 respectively. Sensitivity analysis indicated that the suspended sediment load is sensitive to soil detachability over land ( $K_d$ ) in the Mekong River Basin. Overall, the results suggest that the present model can be used to understand and simulate erosion and sediment transport in large river basins such as Mekong River Basin.

*Keywords: Soil Erosion, Sediment Transport, Hydrological Model, Mekong River Basin*

### INTRODUCTION

Sediment erosion, transport and deposition are complex natural processes strongly affected by human activities and leads to environmental damage through sedimentation, pollution and increased flooding. The sediment produced by soil erosion process is transported into rivers, reservoirs and ponds resulting in high sediment deposition rates and frequent dredging operations. Effective management of sediment in rivers is becoming increasingly important from an economic, social and environmental perspective. Sediment dynamics in a river basin can be estimate both quantitatively and consistently by using modeling tools [1]. Currently, there are many models was developed for a wide range of applications, over a range of scales from the plot based models to basin scale approaches for erosion and sediment transport. Basin scale process-based distributed approach is advantageous for modeling sediment delivery processes since eroded sediments are produced from different sources throughout a basin.

Despite of the fact that many of process-based sediment transport models have been developed over the past four decades, such as Water Erosion Prediction Project (WEPP) [2], European Soil Erosion Model (EUROSEM) [3] and Areal Non-point Sources Watershed Environment Response Simulation (ANSWER) [4], the application of these models to large basin scales (e.g drainage area > 100 000 km<sup>2</sup>) remained questionable. While to address the

problem, in this study we primarily consider the large basin scale in developing the process-based sediment transport model. Besides, some existing models application at these scale have borrowed heavily from smaller scale application. The existing models are either in-stream models, land surface models or, in some cases, have both land surface and in-river components. Basin scale prediction of sediment generation and transport requires consideration of land surface processes and in-river processes. The objectives of this study to check the feasibility of developed process-based model on simulating of sediment dynamic considering hillslope sediment and sediment in river system separately. The model was developed by integrating soil erosion-sediment transport process with the distributed hydrological model to estimate the soil erosion, deposition, transport and sediment yield in large river basin. The model has been calibrated and validate for Mekong River basin.

### STUDY AREA

The present study focused the Mekong River basin, which covers an area of approximately 795,000 km<sup>2</sup> (Fig.1). The basin consists of approximately 33 % of forests. Among major rivers of the world, the Mekong ranks 12th with respect to length (4880 km), 21st with respect to catchment's area. The wet season lasts from May to October when the average rainfall around 80-90% of the annual total. The dry season period starts from November and lasts until April.



The minimum annual rainfall is 1000 mm/year (NE of Thailand) and the maximum is 4000 mm/year (West of Vietnam).

The Mekong River Basin is populated with approximately 60 million people and is considered to be one of the most culturally diverse regions of the world. Agriculture, fishing and forestry provide employment for approximately 85% of the basin's residents. In this basin, Acrisols were found the dominant soil type, which are tropical soils that have a high clay accumulation in a horizon and are extremely weathered and leached. Their characteristics include low fertility and high susceptibility to erosion if used for arable cultivation. The rest of the areas are mixtures of deciduous and evergreen covers as well as woodland and shrubland with some undisturbed forest land.

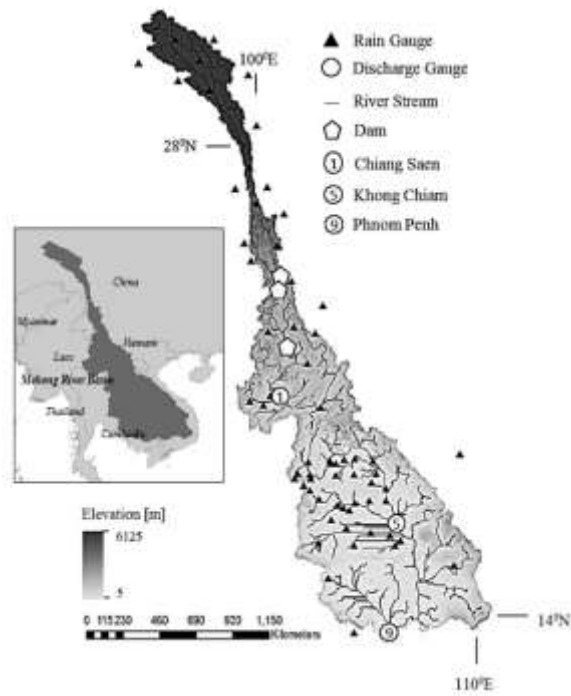


Fig.1 Mekong river basin map.

## METHODOLOGY

The important sediment dynamics (soil erosion, sediment transport and deposition) were modelled and integrated with a process-based distributed hydrological model (DHM). In sediment module, sediment dynamics on hillslope and river was modelled separately and linked to each other systematically.

### Hydrological Modelling

The distributed hydrological model used in this

study is a geomorphology based hydrological model (GBHM) developed at the University of Tokyo [5]. It solves the continuity, momentum and energy equations using two modules; hillslope model and river routing model. The GBHM uses a basin subdivision scheme, a sub grid parameterization scheme, a physically based hillslope hydrological simulation, and a kinematic wave flow routing in river network [6]. Further details can be described as in [5].

### Process based soil erosion and sediment transport model

#### Hillslope erosion process

Hillslope erosion is divided into two systems; detachment from raindrop and flow. In Eq. (1), soil eroded by raindrop is calculated with canopy ratio, rain intensity and surface water depth using the equation as follows [7].

$$D_R = (1 - C_g)k_r(KE)e^{-zh} \quad (1)$$

where,  $D_R$  is soil detachment by raindrop impact ( $\text{g m}^{-2} \text{s}^{-1}$ ),  $k$  is an index of the detachability of the soil ( $\text{g J}^{-1}$ ).  $KE$  is the total kinetic energy of the rain ( $\text{J m}^{-2}$ ),  $z$  is an exponent ranging between 0.9 and 3.1,  $h$  is the depth of the surface water layer (mm),  $C_g$  is the proportion of canopy cover in each grid.

In Eq. (2, 3), soil eroded by sheet flow on the surface occurs with when hydraulic shear stress is larger than critical hydraulic shear stress using the equation as follows [8].

$$D_F = K_f \left( \frac{\tau}{\tau_c} - 1 \right) \quad (\tau > \tau_c) \quad (2)$$

$$D_F = 0 \quad (\tau < \tau_c) \quad (3)$$

Where,  $D_F$  is overland flow detachment ( $\text{kg m}^{-2} \text{s}^{-1}$ ),  $K_f$  is an overland flow detachability coefficient ( $\text{kg m}^{-2} \text{s}^{-1}$ ), here  $10 (\text{mg/m}^2)$  is used,  $\tau_c$  is critical shear stress for initiation of motion, which is obtained from the Shield's curve ( $\text{N m}^{-2}$ ) and  $\tau$  is hydraulic shear stress ( $\text{N m}^{-2}$ ).

#### Sediment transport process

The eroded soil on each hillslope would flow into the main stream and get dissolved in suspended load. The detachment or deposition in the river is expressed using the equation as follows [9]. In Eq. (4), the process of deposition to the bed and detachment from bed is calculated by transport capacity concentration and SS concentration. If it is larger than  $C_s$ , entrainment occurs. If it is smaller than  $C_s$ , deposition occurs. However, bed load was ignored in this case.

$$DF_{river} = \beta_s w v_s (TC - C_s) \quad (4)$$

$$\beta_s = 0.79e^{-0.85J} \quad (5)$$

Where,  $DF_{river}$  is the flow detachment or deposition ( $m^3 s^{-1} m^{-1}$ ),  $C_s$  is sediment concentration in each flow-interval ( $kg m^{-3}$ ),  $TC$  is Transport capacity concentration ( $m^3 m^{-3}$ ),  $w$  is the width of the flow (m),  $v_s$  is the particle settling velocity ( $m s^{-1}$ ) and  $\beta_s$  is a correction factor to calculate cohesive soil erosion,  $J$  is soil cohesion (kPa).

#### Model setup

The input data for the model include weather data, topography data, soil properties, land cover. In this study, the GTOPO30, global Digital Elevation Model (DEM) data with a horizontal grid spacing of  $\sim 20 km^2$  (grid area:  $2 \times 2 min$ ) resolution was used to delineate the Mekong River Basin. The land cover and soil type for the basin, obtained from global land cover 2000 ([http://edc2.usgs.gov/glcc/eadoc2\\_0.php](http://edc2.usgs.gov/glcc/eadoc2_0.php)) and FAO soil map of the world [10] respectively. The elevation data were first aggregated to  $3.6 km \times 3.6 km$  resolution, and land cover and soil data were aggregated by reclassifying the land-use data for nine classes, and the soil data for eight classes. Daily precipitation and air temperature data from 65 station weather stations were obtained from the Mekong River Commission (MRC) in this river basin.

Annual records of discharge and suspended sediment concentration in the study are being extracted from the series of historical record published by the MRC. The publications tabulated measurements of water discharge, suspended sediment concentration (SSC), water quality and other physical characteristics of a series of gauging stations located along the Mekong River and its tributaries. In view of this study, flow and SSC records from three stations (Fig. 1) located in the mainstream were identified, of which records three stations were used to calculate the sediment load (Chiang Saen, Khong Chiam and Phnom Penh). The stations were selected based on their relative location from one another and the completeness of flow and sediment records for the station. Unlike discharge which was measured daily, measurements of SSC were relatively sporadic, sampling frequency is monthly and measurements of sediment concentration were not conducted at several gauging stations due to the political unrest in some of these areas. SSC samples were collected near the surface of the river (0.3 m depth) in the middle of the mainstream [11]. The estimation of suspended sediment load is challenging in the Mekong River, given that many gauging stations do not document relatively long-term sediment concentration

measurements. Hence it is acknowledged that the frequency of sampling does not ensure that all ranges of the flow were sampled. In this study, monthly observed sediment load was computed from the monthly measured of suspended sediment concentration and the measured water discharge.

#### Model calibration and validation

The model was simulated for 10 years from 1991-2000 and three stream gauge along Mekong are used for calibration and validation. The period of simulation is selected depends on the data availability. Taking into account the availability of data, the daily discharge and sediment data for periods 1991 to 1995 were used to calibrate discharge simulation. Meanwhile, 1996-2000 data were used for validation. The six parameters required for calibration were initialized with empirical values, and then adjusted according to the observed discharge at different river sections. The residual soil moisture (wrsd) and the saturated hydraulic conductivity (ksat1) are the only hydrological parameters calibrated by semi-automatic calibration method. While, the two parameters of soil detachability by raindrop ( $k$ ) and on overland flow ( $K_f$ ) and soil cohesion ( $J$ ) were initialized by empirical values [9], and then adjusted according to the observed sediment. Manual calibration was performed for soil detachment and transport parameters.

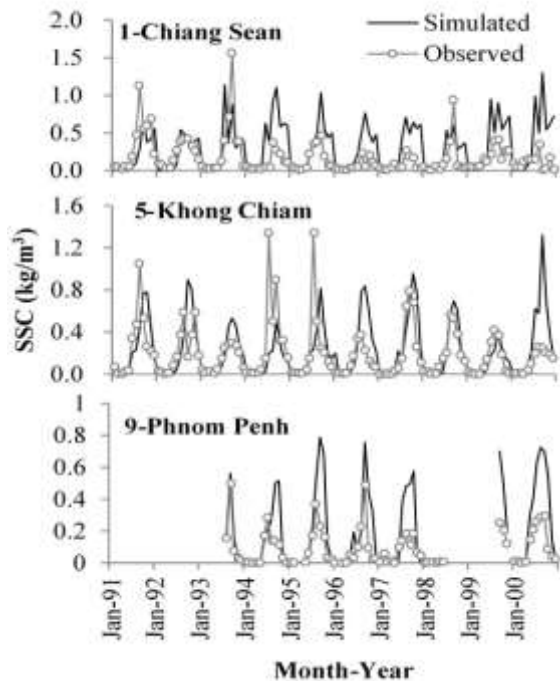
## RESULTS AND DISCUSSION

### Suspended sediment concentration simulation

To check the seasonal characteristics of suspended sediment in the river, the concentration was also simulated as shown in Fig. 2. Generally, a declining trend in mean monthly suspended sediment concentration (SSC) was observed along the entire length of the Mekong River since water quality measurement began in 1985 [12]. Figure 2 shows the monthly SSC simulation at stream gauging station for the period 1991 to 2000. The result reveals a decreasing trend in the SSC along the three regions from upstream to the downstream. This decrease trend was due to the decrease in the main stream water velocity, which increases the sediment deposition and the SSC become lower. The average monthly SSC was highest at the Chiang Saen station was estimated by  $0.9 kg/m^3$ . While, the average SSC at Phnom Penh were estimated to be  $0.25 kg/m^3$ . That was the lowest among the studied stations due to the sediment deposition behaviour in the Delta region, which decrease the SSC in the water. The model results also show the SSC was high in the rainy (July, August, September) season than the dry season at all three stations. That is due to the intensive soil erosion

coincident with heavier precipitation.

Fig. 2 Daily suspended sediment concentration (SSC) simulation at stream gauge stations for 1991-2000.



#### Suspended sediment load simulation

The annual sediment loads of the Mekong River were relatively stable in the past 40 years [13]. However, there is a significant seasonal change in the annual sediment loads among the year seasons. Changes in sediment loads of the Lower Mekong Basin have been analysed relying on the existing sediment data in many literatures [14], [15], [16], [17], [18]. Since the existing sediment data in the Mekong river basin have been collected by inconsistent method and had a low sampling frequency [18] studies reported different changing trends on sediment load in the Mekong River Basin. Figure 3 shows the simulated results of monthly suspended sediment load compared with measurements of upper, middle and lower monitoring stations cases from 1991-2000. The simulated results show in good agreement with observations, as reported in Table 1. The *NSE* result is greater than 0.6; 0.62, 0.62 and 0.64 for upper, middle, and lower station respectively (1991-1995) except the validation period for the Chiang Sean station (*NSE* = 0.51). A relatively highest simulation error at the Chiang Sean may have been caused by the effect of the reservoir on the upper basin of Mekong River. While, the linear correlation coefficient (*r*) between simulated and observed values was in the range of 0.80 to 0.86 for all three region stations. The model

simulation was underestimated at some point but generally, the suspended sediment load was fairly well simulated at the three stations. The results also indicate that the model simulates suspended sediment load with reasonable accuracy and describing the seasonal of suspended sediment load in the Mekong River Basin, which can be applied to estimate the future suspended sediment load. The lower values of *NSE* and *r* may attribute to limitations in terms of the continuity and length of the records. As [19] also reported the lower *NSE* and *r* values for the daily sediment calibration of the Nam Ou basin in Lao PDR for a similar reason – a limited number of sediment samples for calibration. This lack also highlights the need for further investigation in the quality of the observed sediment data reflected from the sampling process and the method of sediment analysis.

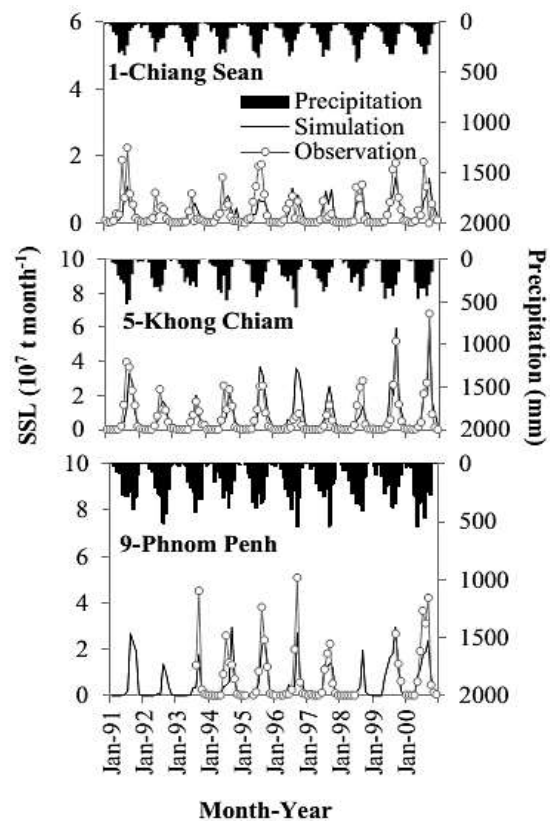


Fig. 3 Monthly suspended sediment load (SSL) simulation at stream gauge stations for 1991-2000.

In general, higher sediment load is expected during the wet season. The model results reveal that, for the entire period of 1991-2000, the average suspended sediment load a highest ( $76 \times 10^5$  t/day) at middle region. While the upper region had a lower average suspended sediment load calculated ( $27 \times 10^5$  t/day) compared to other study region. Moreover, the monthly suspended sediment load increased with increasing basin area from Chiang Saen and Phnom

Penh. The results reveal the increasing sediment load in the lower region due to deposition process. Thus, the suspended sediment load in the upper region of the Mekong River Basin was lower than the middle-lower region.

Table 2 Model performance indicators for daily river suspended sediment load simulation in Mekong River Basin from 1991 to 2000

Stations		Performance Indicators			
ID	Name	Calibration (1991-1995)		Validation (1996-2000)	
		NSE	r	NSE	r
1	Chiang Sean	0.62	0.85	0.51	0.65
2	Khong Chiam	0.62	0.86	0.62	0.83
3	Phnom Penh	0.64	0.80	0.64	0.87

### Suspended sediment yield simulation

The resulting spatial mean distribution of annual SS yield was simulated in 1991-2000 as the model output as shown in Fig. 4. The spatial pattern of SS yield categories has five ranges of SS yield values. Three qualitative categories have been chosen for the output SS yield classes: low (SS yield range, 0.0-14.36 t km<sup>-2</sup> yr<sup>-1</sup>), moderate (SS yield range, 14.36-91.80 t km<sup>-2</sup> yr<sup>-1</sup>), and high SS yield (SS yield range, 91.80-274.52 t km<sup>-2</sup> yr<sup>-1</sup>). This trend can be determined by coverage of land use, indicating severely eroded area locates at the region with poor vegetation cover and topographic of the basin.

Total annual SS yield range from 0.0 to 14.36 t km<sup>-2</sup> yr<sup>-1</sup> are scattered in all over the MRB area. This range occupying 60% of the study area in correspondence to low steepness slope, range from 0 to 5.98% in lower region Mekong basin, in Thailand and Cambodia part, and also some part in upper region. Sand and clay of these parts, have better permeability and highly resistant to runoff impact. This total annual SS yield also is related mainly to the protective role of forest and natural vegetation cover. While, the SS yield range from 14.36 to 91.80 t km<sup>-2</sup> yr<sup>-1</sup> class occupying 35% in this study scattered in the middle region near Vietnam and some parts near Myanmar and Lao PDR. This is due to cropland cover and higher average annually rainfall distribution. Furthermore, type of soil is highly contents silt and sand, easy to detach due to runoff. Small parts occupying 5 % with extremely high value of SS yield, 91.80 to 274.52 t km<sup>-2</sup> yr<sup>-1</sup> in upper, middle and lower region especially in the valleys with steep slopes and high rainfall-runoff factor between 7986-12,599 MJ

ha<sup>-1</sup> mm ha<sup>-1</sup>.

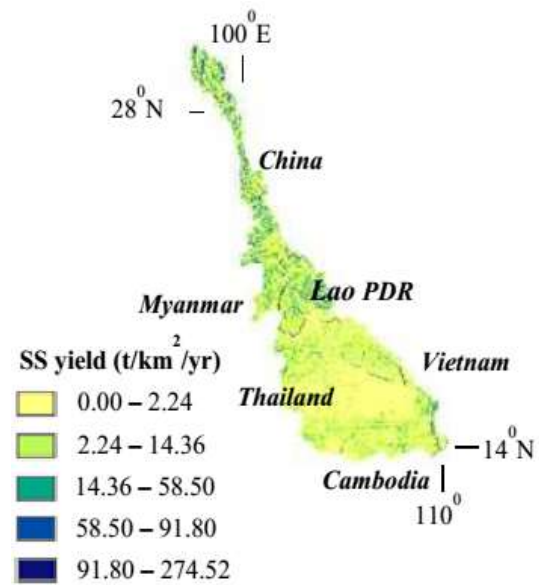


Fig. 4 Average suspended sediment (SS) yield (t km<sup>-2</sup> year<sup>-1</sup>)

### CONCLUSION

In this study, the sediment dynamic process was successfully assessed using integrated process-based model. The main findings were as followed.

1. Integrated process-based sediment dynamic model with targeting large basin in South East Asia showed the applicability to simulate sediment dynamic process, indicating the sufficient accuracy for long term simulation.
2. The simulated suspended sediment concentration is higher in the rainy (July, August, September) season than the dry season.
3. The sediment load in the lower region Mekong River basin showed an increase due to deposition process.
4. The results provide the spatial distribution of SS yield over the Mekong River basin. SS yield was the highest close to Vientiane and Nakhon Phanom due to highest annual rainfall records around this area. This can help us to identify the severe SS yield produced areas which deserve priority attention in basin management for soil and water conservation.

### ACKNOWLEDGEMENTS

This work was supported by Core-to-Core Program (B. Asia-Africa Science Platforms) of Japan Society for the Promotion of Science (JSPS). The part

of the modeling work was also supported by Asian Core Program of JSPS and Collaborative Research Program (CRA) of AUN/SEED-Net.

## REFERENCES

- [1] Bhattarai R and Dutta DUSHMANTA, "Analysis of Soil Erosion and Sediment Yield using Empirical and Process Based Models, Proceedings of the MTERM International Conference, AIT, 2005, pp. 215-226.
- [2] Nearing MA, Foster GR., Lane LJ and Finckner, SC, "A process-based soil erosion model for USDA-Water Erosion Prediction Project technology", Transactions of the American Society of Agricultural Engineers 32, 1989, pp. 1587-1593.
- [3] Morgan RPC, Quinton JN and Rickson RJ, "EUROSEM version 3.1 a user guide", Silsoe College, Cranfield University, Silsoe, Bedford, UK., 1993, pp.83.
- [4] Beasley DB, Huggins LF and Monke EJ "ANSWERS: A model for watershed planning", Transactions of the American Society of Agricultural Engineers 23, 1980, 938-944.
- [5] Yang D, Herath S, Oki T and Musiaka K, "Application of distributed hydrological model in the Asian monsoon tropic region with a perspective of coupling with atmospheric models", Journal of the Meteorological Society of Japan, 79,1B, 2001, 373-385.
- [6] Yang D, Oki T, Herath S and Musiaka K, "A geomorphology-based hydrological model and its applications", In: Singh, V. P. & Frevert, D. K. Eds. Mathematical Models of Small Watershed Hydrology and Applications, Water Resources Publications, Littleton, Colorado, USA, Chapter. 9, 2002, pp. 259-300.
- [7] Torri D, Sfalanga M and Delsette M, "Splash detachment: runoff depth and soil cohesion", Catena, Vol. 14 (3), 1987, pp. 149-155.
- [8] Habib-ur-Rehman DM and Akhtar EMN, "Development of regional scale soil erosion and sediment transport model; its calibration and validations", Pakistan Engineering Congress, Vol. 69th Annual Session Proceedings, 2006, pp. 231-245.
- [9] Morgan RPC, Quinton JN, Smith RE, Govers G, Poesen JWA, Auerswald K, Chisci G, Torri D, and Styczen ME, "The European soil erosion model (EUROSEM): a process-based approach for predicting sediment transport from fields and small catchments", Earth Surface Processes and Landforms 23, 1998, 527-544.
- [10] FAO, "The digital soil map of the world and derived soil properties", version 3.6, FAO/UNESCO: Rome, Italy, 2003.
- [11] Mekong River Commission, "Lower Mekong Hydrologic Yearbook", Mekong River Commission (MRC), 2000.
- [12] Lu XX and Siew RY, "Water Discharge and sediment flux changes over the past decades in the Lower Mekong River: possible impact of the Chinese dams", Hydrol. Earth Syst. Sci., Vol. 10, 2006, pp. 181-195.
- [13] Walling DE, "Evaluation and analysis of sediment data from the Lower Mekong River", Report to the Mekong River Commission, 61, 2005.
- [14] Fu KD, He DM and Li SJ, "Response of downstream sediment to water resource development in mainstream of the Lancang River", Chinese Science Bulletin, Vol. 51, 2006, pp. 119-126.
- [15] Kummu M and Varis O, "Sediment-related impacts due to upstream reservoir trapping, the Lower Mekong River", Geomorphology, Vol. 85 (3-4), 2007, pp. 275-293.
- [16] Walling DE, "The Changing Sediment Load of the Mekong River", Ambio, Vol. 37, 2008, pp. 150-157.
- [17] Walling DE, "Chapter 6 The Sediment Load of the Mekong River, In: The Mekong: Biophysical Environment of an International River Basin, Ian C. Campbell (eds.), New York: Elsevier Inc., 2009, pp. 113-142.
- [18] Wang JJ, Lu XX and Kummu M, "Sediment load estimates and variations in the Lower Mekong River", River Res. Appl., Vol. 27, 2011, pp. 33-46.
- [19] Shrestha B, Babel MS, Maskey S, Griensven AV, Uhlenbrook S, Green A, and Akkharath I, "Impact of climate change on sediment yield in the Mekong River basin: a case study of the Nam Ou basin, Lao PDR", Hydrol. Earth Syst. Sci., Vol. 1, 2013, pp. 1-20.

## EVALUATION OF PIER-SCOUR PREDICTIONS FOR WIDE PIERS USING FIELD DATA

Nordila Ahmad<sup>1</sup>, Bruce W. Melville<sup>2</sup>, Thamer Mohammad<sup>3</sup>, Zuliziana Suif<sup>1</sup>

<sup>1</sup>Faculty of Engineering, National Defence University, Malaysia; <sup>2</sup>Faculty of Engineering, The University of Auckland, Auckland; <sup>3</sup>Faculty of Engineering, Universiti Putra Malaysia, Malaysia

### ABSTRACT

Many studies have been conducted and equations developed to predict wide bridge-pier scour equation. However, most of these equations were developed using laboratory data and very limited equation that had been developed were tested using field data. The purpose of this paper is to evaluate the laboratory wide pier scour equation that proposed from the previous findings with field data set. Large amount of field data from the literature was extracted and it consist both live-bed and clear-water scour. A method for assessing the quality of the data was developed and applied to the data set. Three other wide pier-scur equations from the literature also used to compare the performance of each predictive method. Comparisons of computed and observed scour depths indicate that the equation from the previous publication produced the smallest discrepancy ratio and RMSE value when compared with the large amount of laboratory and field data.

*Keywords— Field Data, Local Scour, Scour Equation, Wide Piers*

### INTRODUCTION

Scour is the lowering of the level of the riverbed due to water erosion such that there is a tendency to expose the foundations of a bridge. The extent of this reduction below an assumed natural level is termed the *depth of scour* or *scour depth*. The basic mechanism that causes local scour around piers is the downflow at the upstream face of the pier and the formation of vortices at the base. The flow moves more slowly as it approaches the pier, coming to a rest at the face of the pier. The approach flow velocity is reduced to zero at the upstream side of the pier and this result in a pressure increase at the pier face. The associated pressures are highest near the surface, where the rate of decrease in velocity is greatest, and becomes lower the closer the flow is to the river bed [17]. As the velocity decreases the closer the flow is to the river bed, the pressure on the face of the pier also decreases accordingly, forming a downward pressure gradient. The pressure gradient hence forces the flow down the face of the pier, resembling that of a vertical jet. The resulting downflow creates an effect on the streambed and creates a hole in the vicinity of the pier base. The downflow impinging on the bed is the main scouring agent [17], [15], [11]. Fig. 1 shows the flow and scour pattern at a circular pier under the action of currents.

Actually, the flow field surrounding a pier structure is quite complex, even for simple pier structures such as piers with a circular shape. One of

the main characteristics of the local flow field is the formation of secondary flows called vortices. Many researchers [12], [13], [7] have proposed that these vortices are the most important mechanisms of local scour.

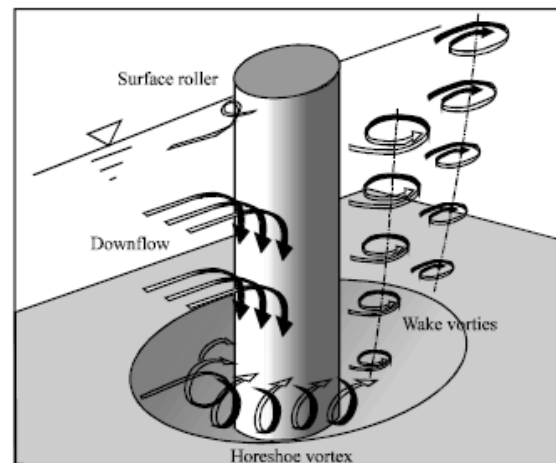


Fig. 1 The flow and scour pattern at a circular bridge pier

### PARAMETERS AFFECTING LOCAL SCOUR AROUND BRIDGE PIERS

In order to measure the relation between the depth of local scour at a bridge pier and its dependent parameters, a detailed discussion of the mechanics of local scour at bridge piers was presented. [6] presented the relation between the

depth of local scour at a bridge pier and its dependent parameters, which can be written as:

$$d_s = f[\text{Flood flow}(\rho, \nu, U, y, g), \text{Bed sediment}(d_{50}, \sigma_g, \rho_s, U_c), \text{Bridge geometry}(b, Sh, Al), \text{Time}(t)] \quad (1)$$

where  $\rho$  and  $\nu$  = fluid density and kinematic viscosity, respectively;  $U$  = mean approach flow velocity;  $y$  = flow depth;  $g$  = acceleration of gravity;  $d_{50}$  and  $\sigma_g$  = median size and geometric standard deviation of the sediment particle size distribution, respectively;  $\rho_s$  = sediment density;  $U_c$  = critical mean approach flow velocity for entrainment of bed sediment;  $b$  = pier width;  $Sh$  and  $Al$  = parameters describing the shape (including floating debris) and alignment of the pier, respectively;  $t$  = time; and  $f$  denotes “a function of”.

By assuming a constant relative density of sediment, for example by neglecting  $\rho$ , and  $\rho_s$ , and  $\nu$ , Eq. (2) can be written as:

$$\frac{d_s}{b} = f\left(\frac{U}{U_c}, \frac{y}{b}, \frac{b}{d_{50}}, \sigma_g, Sh, Al, \frac{Ut}{b}, \frac{Ub}{\nu}\right)$$

The first three parameters on the right-hand side of Eq. (2) are flow-related and represent, respectively, the stage of sediment transport on the approach flow bed (termed flow intensity), the depth of flow relative to the size of the foundation (termed flow shallowness), and the foundation size relative to the sediment median size (termed sediment coarseness). The last two terms is a time scale for the development of scour ( $Ut/b$ ) and the effect of viscosity ( $Ub/\nu$ ) based on the size of the foundation.

The rational of choosing that dimensionless parameters in this study is, all of those parameters were use in piers analyses.

## PREVIOUS FORMULAS FOR WIDE PIER LOCAL SCOUR

In terms of wide and long skewed piers, most empirical local scour prediction equations overestimate scour depths around structures that are wide compared to the water depths where they are located. The equations were derived using laboratory data from steady flow experiments. Due to the complexity of the flow and sediment transport associated with local scour processes, there are a number of dimensionless groups needed to fully characterise the scour. Many of these groups, such as the ratio of water depth to structure diameter ( $y/b$ ), can be kept constant between the laboratory model and the prototype structure. However, as there is a lower limit on the sediment particle size before cohesive forces become important, those groups

involving sediment size cannot be kept constant between the model and the prototype [1]. If the sediment-to-structure-length scales are not properly calculated for in the predictive equations, problems will occur when the equations are used in situations which differ from the laboratory conditions on which they are based. The problems will be related to the model not being able to maintain the proper scale between model and prototype sediment as the size of the prototype structure increases [1]. This condition always occurs in huge gravity structures such as in the case of large coastal and inland bridge piers.

The wide pier problem is usually considered to be a concern when the relative depth,  $y/b$ , is too small to allow the vortices to fully develop. Earlier investigations of the dependence of scour depth ( $y/b$ ) were performed with small piles and very small water depths [7]. [5] established an upper threshold at  $y/b = 3$  beyond which the scour depth is relatively independent of the relative depth. However, [1] conducted tests with large piers which indicate that the threshold should be closer to 2, although data below these thresholds are included in a number of empirical equations that overestimated prototype scour depths. There are various researchers who have attempted to deal with this problem.

HEC-18 [3] is the standard used by most highway agencies for evaluating scour at bridges. It was determined from a plot of laboratory data for circular piers. In the latest edition of HEC-18 [9], the HEC-18 pier scour equation (based on the CSU equation) is recommended for both live-bed and clear-water pier scour. The equation predicts maximum pier scour depths. Basic applications include simple pier substructure configurations and riverine flow situations in alluvial sand-bed channels. The new equation of HEC-18 [9] is shown in Eq. (3).

$$\frac{d_s}{b} = 2K_1K_2K_3\left(\frac{y}{b}\right)^{0.35} Fr^{0.43}$$

where

- $d_s$  = scour depth (m)
- $y$  = flow depth directly upstream of the pier, (m)
- $K_1$  = correction factor for pier nose shape
- $K_2$  = correction factor for angle of attack of flow
- $K_3$  = correction factor for bed condition
- $b$  = pier width (m)
- $Fr$  = Froude Number directly upstream of the pier,  $U/(gy)^{1/2}$ , where,  $U$ =mean velocity of flow directly upstream of the pier, (m/s)



Jones and Sheppard equations [1] include the structure-width-to-sediment-size ratio and thus should be directly applicable to large structures (wide piers). They concluded that the pier width impacts the equilibrium scour depth in two ways. First, the pier size to flow depth ratio ( $y/b$ ) is important and can best be represented by a hyperbolic tangent function, which makes the scour depth primarily a function of the pier size for relatively slender piers, but a function of the flow depth for relatively wide piers. Second, the pier size to sediment ratio ( $b/d_{50}$ ) can have an even greater impact on the prediction of scour. Moreover, they have shown that the maximum relative clear-water scour occurs when the  $b/d_{50}$  ratio is about 46, and that scour tends to diminish on both sides of this value for constant values of  $U/U_c$  and  $y/b$  (Fig 2). The equation produced by Jones and Sheppard is shown in Eq. (4).

$$\frac{d_s}{b} = c_1 \left[ \frac{5}{2} \left( \frac{U}{U_c} \right) - 1 \right]$$

where

$$c_1 = \frac{2}{3} k \quad \text{and}$$

$$k = \frac{\tanh \left[ 2.18 \left( \frac{y}{b} \right)^{0.66} \right]}{\left[ -0.279 + 0.049 e^{\left( \log_{10} \left( \frac{b}{d_{50}} \right) \right)} + \frac{0.78}{\log_{10} \left( \frac{b}{d_{50}} \right)} \right]}$$

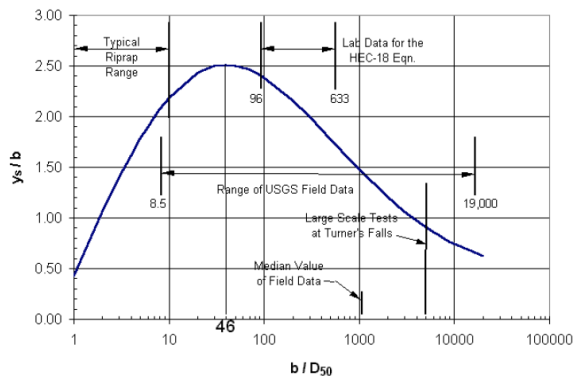


Fig. 2 Dependence of normalised scour depth on  $b/d_{50}$  for a circular pier. For the curve shown  $U/U_c=1$  and  $y/b>2$

Based on a recent publication, [10] have made an improvement in developing the best-performing equations. The recommended equilibrium local

scour equation resulting from their study is a combination of equations developed by [2] and [4], and is referred to as the Sheppard/Melville or S/M equation. [10] concluded that the predictive methods have improved in accuracy over the years, with those developed in recent years demonstrating the best performance. The Sheppard/Melville (S/M) method was found to be the most accurate of those tested and is recommended for use in design. The S/M equation is shown in Equation 2.27.

$$\frac{d_s}{b^*} = 2.5 f_1 f_2 f_3 \quad \text{for } 0.4 < U/U_c < 1 \quad (5)$$

where

$$f_1 = \tanh \left( \frac{y}{b^*} \right)^{0.4},$$

$$f_2 = \left\{ 1 - 1.2 \left[ \ln \left( \frac{U}{U_c} \right) \right]^2 \right\}, \text{ and}$$

$$f_3 = \left[ \frac{\left( \frac{b^*}{d_{50}} \right)}{0.4 \left( \frac{b^*}{d_{50}} \right)^{1.2} + 10.6 \left( \frac{b^*}{d_{50}} \right)^{-0.13}} \right]^4$$

where

$$b^* = b_p \phi$$

$b^*$  = effective pier width;

$b_p$  = projected pier width;

$\phi$  = 1.0 for a circular pier;

and

$$\phi = 0.86 + 0.97 \left[ \theta - \frac{\pi}{4} \right]^4$$

for a skewed pier

## EVALUATION OF LABORATORY-DERIVED CURVE ON FIELD DATA

[16] present the relationship between equilibrium local scour depth ( $d_s/b$ ) and sediment coarseness for large ranges of  $b/d_{50}$ . A least-squares regression analysis using a fitting criterion of mean square error was applied to all data in their study plus with laboratory data in the literature, and found the optimum coefficients which minimised the mean square error between the experimental and predicted values. The best fit relationship between  $d_s/b$  and  $b/d_{50}$  is described by this laboratory-derived curve in Eq. (6) and the graph can be shown in Fig. 3.

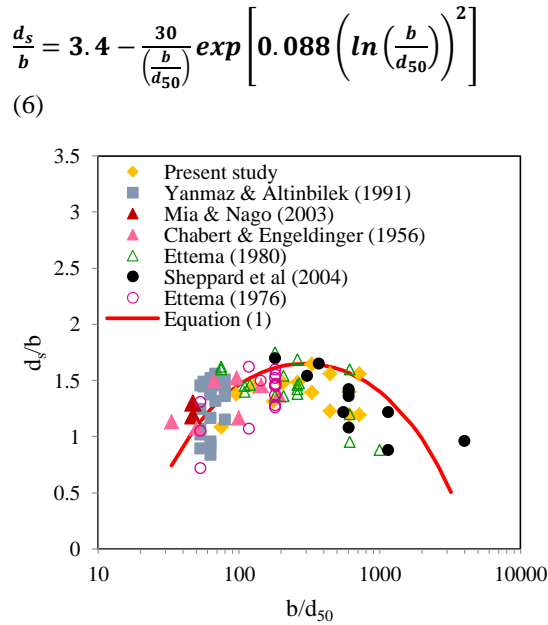


Fig. 3 Plot of  $d_s/b$  versus  $b/d_{50}$  from laboratory data [16]

In this study, the field measurements of [14] were used to test the applicability of Eq. (6) to field data. The measurements consist of both clear-water and live-bed data sets. Before the comparison was made, the field data were filtered from 493 to 45 data sets. This is because when the full data set is used, there is no relationship obtained between  $d_s/b$  and  $b/d_{50}$ . Therefore, several steps had been taken in choosing the field data. First, only a single pier type was selected. Second, data that  $b/d_{50} > 50$  were chosen [8]. Thirdly, the data points that have  $d_{50} < 0.1$  mm were eliminated in order to consider the cohesive effects from that sediment. Fourth, data that affected from debris accumulation around the bridge pier were also eliminated due to there being no definite relationship between the scour depth and debris accumulation. Fifth, if the scour depth was measured at the upstream and downstream of the bridge pier, only the maximum value of scour depth was preferred. Finally, if the scour depth was measured around the same bridge pier, only the maximum scour depth was chosen. This gives 15 data sets from clear-water scour conditions and 30 data sets from live-bed conditions. All of the filtered data are graphically shown in Fig. 4 along with the best fit curve from Fig. 3.

According to Fig. 4, most of the clear-water field data indicate reasonable agreement with the laboratory-derived curve when it is considered as an upper envelope curve. For those clear-water scour data sets below the curve, it may be that pier scour depth could not attain the equilibrium stage during the time in which the data were measured because of the short duration of the flood relative to the

equilibrium time. Regardless, it can be considered that uncertainty occurs during measurement of scour and it is never known whether the bed has attained an equilibrium stage during scour data measurements. Similar discrepancies can occur for scour data in live-bed conditions, but this may be for other reasons.

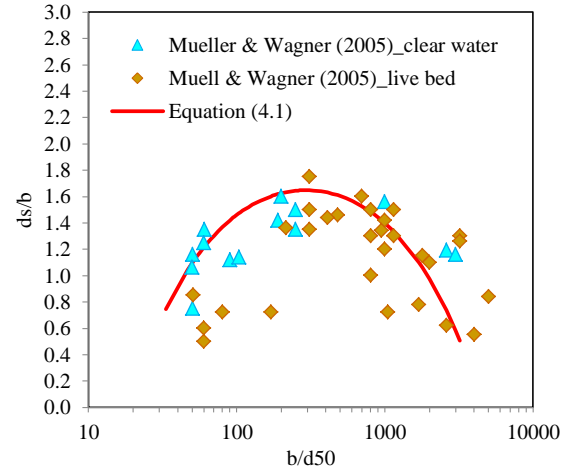


Fig. 4 Plot of  $d_s/b$  versus  $b/d_{50}$  for selected field data. (Source of data: [14])

Although the recorded scour depth can represent equilibrium scour conditions for live-bed scour, it is possible that the recorded scour depth was less than the equilibrium value because of the dynamic flow and sediment transport aspects around a bridge site like the transition of dunes through the scour hole. However, the combination of the laboratory-derived curve with the field data which have been filtered as demonstrated in Fig. 4 gives evidence that the normalised scour depth appears to be significantly reduced for the large values of  $b/d_{50}$  that are frequently found in the field. It was found that Eq. (6) can fit both data sets for clear-water and live-bed conditions. For extra safety, 25% can be added to the value obtained from Eq. (6) in order to consider the value of the maximum scour depth for the all data sets used.

## EVALUATION OF EXISTING EQUATIONS FOR PREDICTING MAXIMUM LOCAL SCOUR DEPTH AT WIDE PIERS

In this section, field data sets were used to validate the predicted maximum scour depth at wide piers using equations proposed by [1], HEC-18 [9], and [10]. Statistical analysis was carried out to assess the performance of each predictive equation. The discrepancy ratio ( $r$ ), the standard deviation of the discrepancy ratio ( $\sigma_r$ ), and the root mean square error (RMSE) were determined. The formulae for the statistical analysis are described below:

$$RMSE = \sqrt{\frac{\sum_{i=1}^N (d_s/b_{predicted,i} - d_s/b_{measured,i})^2}{N-1}} \quad (7)$$

$$r = \frac{(d_s/b)_{predicted}}{(d_s/b)_{measured}} \quad (8)$$

$$\sigma_r = \sqrt{\frac{1}{N-1} \sum_{i=1}^N (r_i - \bar{r})^2} \quad (9)$$

Where  $\bar{r}$  is the average of the discrepancy ratio. A value of unity for  $\bar{r}$  shows perfect agreement between the dimensionless scour depths of the predicted and measured values.  $\sigma_r$  represents an evaluation of the scatter in the predictions relative to the average value.

The statistical analysis using the predicted and field data sets is also shown in Table 1. It was found that all the tested equations over-predict the  $d_s/b$  values for field conditions. As stated previously, the probable reasons for this are that the field data contain non-equilibrium field scour conditions and discrete measurements rather than data based on measurements that were made continuously with time in the field. The lack of agreement with the field data sets can be attributed to the difficulty in measuring field data using flood-chasing or discrete measurement in time without being able to take into account the unsteady development of the scour hole itself. Therefore, it is likely that the proposed equation will produce the smallest discrepancy ratio and RMSE value when compared with the large amount of laboratory and field data. Visual comparison (scattergrams) is another method that can be used to evaluate the predictive equations using the predicted and measured scour depths at wide piers. Fig. 5 demonstrate the dimensionless scour depth for field data sets. The plot indicate how much the predicted values of normalised scour depth deviate from the line of perfect agreement. From the observation, the results obtained from applying Eq. (6) are found to be in agreement with the results obtained from applying the selected equations when field data sets are used.

Table 1. Summary of the discrepancy ratio,  $r$ , and root mean square error, RMSE, for each predictive equation

	Field data		
	$r$		
	$\bar{r}$	$\sigma_r$	RMSE
Jones and Sheppard (2000)	2.75	3.43	1.21
HEC-18 (2012)	6.26	7.95	4.22
Sheppard et al. (2014)	2.68	3.43	0.99

Present study                      2.54    3.01    0.80

$\bar{r}$  = average discrepancy ratio,  $\sigma_r^2$  = standard deviation of discrepancy ratio, RMSE<sup>3</sup> = root mean square error

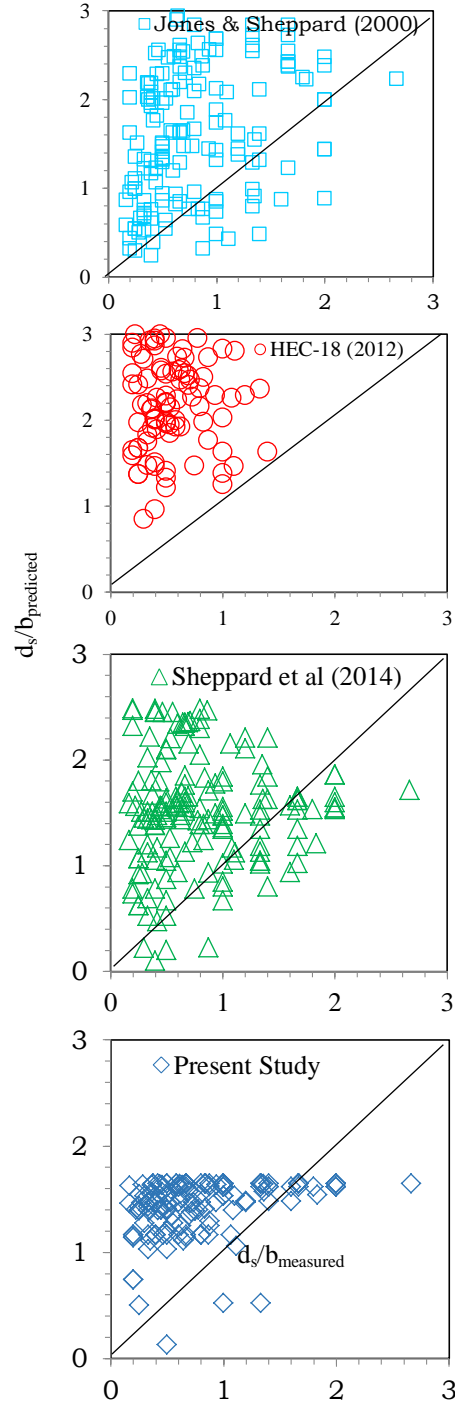


Fig. 5. Comparison of the predicted and measured normalised scour depths in the field [14] with selected existing scour depth predictive equations

## CONCLUSION

In order to show the effectiveness of the proposed equation from the previous findings [16] for predicting maximum scour depth around wide piers, several scour prediction equations were evaluated with field data. It was found that equations from [1], [9] and [10] mostly over-predict scour depth, as shown by the statistical analysis with the discrepancy ratio,  $r$ , and RMSE in Table 1. This evaluation was also supported by scattergrams, shown in Fig. 5. Equation (6) produces the smallest discrepancy ratio,  $r$ , and RMSE, and thus can be reliably used to predict scour depth at the prototype scale. As a factor of safety, 25% can be added to the value obtained from Eq. (6) in order to consider the value of the maximum scour depth for all data sets used. Meanwhile, it needs to be stressed that the applicability of Eq. (6) is limited to values of  $b/d_{50}$  from 50 – 4200, to skewed piers with angle of attack,  $\alpha < 45^\circ$ , to piers in shallow flows and to graded sediments with  $\sigma_g$  less than 7.

## ACKNOWLEDGEMENTS

The financial support from the Research University Grant Scheme (RUGS) given by University Putra Malaysia (Grant No. 05-01-10-0904RU) for this project is acknowledged. The experiments were conducted in the Hydraulic Laboratory in the National Hydraulic Research Institute of Malaysia (NAHRIM).

## REFERENCES

- [1] Jones, J. Sheppard, D. 2000, Scour at wide bridge pier. *Building Partnerships*, pp. 1–10.
- [2] Melville, B. W. (1997). "Pier and abutment scour: Integrated approach." *Journal of Hydraulic Engineering-ASCE*, 123(2), 125–136.
- [3] Richardson, E. V., and Davis, S. R. (2001). "Evaluating scour at bridges." Fourth Edition. Hydraulic Engineering Circular No. 18 (HEC-18), Federal Highway Administration, Washington, D.C.
- [4] Sheppard, D.M., Miller, W., 2006. Live-bed local pier scour experiments. *Journal of Hydraulic Engineering*, ASCE, 132(7), 635–642
- [5] Melville, B. W., and Sutherland, A. J. (1988). "Design method for local scour at bridge piers." *Journal of Hydraulic Engineering-ASCE*, 114(10), 1210–1226.
- [6] Melville, B.W., Coleman, S.E., 2000. *Bridge Scour*. Water Resources Publications, LLC, Colorado, U.S.A., 550 p.
- [7] Ettema, R., 1980. Scour around bridge piers. Report No. 216, University of Auckland, Auckland, New Zealand.
- [8] Sheppard, D. M. (2004). "Overlooked local sediment scour mechanism." *Transportation Research Record: Journal of the Transportation Research Board*, 1890, 107–111.
- [9] Arneson, L. A., Zevenbergen, L. W., Lagasse, P. F., and Clopper, P. E. (2012). Evaluating scour at bridges, 4th Ed. Hydraulic Engineering Circular No. 18 (HEC-18), Federal Highway Administration, Washington, DC
- [10] Sheppard, D. M, Huseyin, D. Melville. B. W. (2014). Evaluation of Existing Equations for Local Scour at Bridge Piers. *Journal of Hydraulic Engineering-ASCE*, 140(1), 14–23
- [11] Ibrahimy M. I. and S. M. A. Motakabber. Bridge Scour Monitoring by Coupling Factor Between Reader and Tag Antennas of RFID System. *International Journal of GEOMATE*, 8(2), 1328-1332
- [12] Shen, H. W., Schneider, V. R., and Karaki, S. (1966). Mechanics of local scour, U.S. Dept. of Commerce, National Bureau of Standards, Institute for Applied Technology, Fort Collins, CO.
- [13] Melville, B. W. (1975) "Local Scour at Bridge Sites." Rep. No.117, School of Engineering, The Univ. of Auckland, New Zealand.
- [14] Mueller, D. S., and Wagner, C. R. (2005). "Field observations and evaluations of streambed scour at bridges." Office of Engineering Research and Development, Federal Highway Administration, McLean, Virginia.
- [15] Dey, S. (1996). "Sediment pick-up for evolving scour near circular cylinders." *Applied Mathematical Modelling*, 20(7), 534-539.
- [16] Nordila A., Thamer A. M. and Zuliziana S. (2017). "Prediction of Local Scour around Wide Bridge Piers under Clear-water Conditions". *International Journal of GEOMATE*. 12(34), 135-139.
- [17] B.W. Melville, A.J. Raudkivi (1977). "Flow characteristics in local scour at bridge piers". *Journal of Hydraulic Research*, 15 (4) (1977), pp. 373-380

## MECHANICAL CHARACTERISTICS OF ARTIFICIAL STONE MADE FROM WASTE OF SILICEOUS TUFF

Hiroaki Shigematsu<sup>1</sup> and Shogo Hashimoto<sup>2</sup>

<sup>1</sup> National Institute of Technology, Ishikawa College, Japan; <sup>2</sup> Taisei Corporation, Japan

### ABSTRACT

In this study, in order to clarify the mechanical characteristics of the artificial stone made from waste of the siliceous tuff, a series of laboratory tests are carried out. The experiments involve unconfined compression test, bending test and needle penetration test. From experimental results, the in-situ applicability of the artificial stone as civil engineering materials is discussed. The following conclusions are obtained from present study: (1) Unconfined compressive strength of the artificial stone made from waste of siliceous tuff increases remarkably by extending the curing period. Also, the higher the density of the artificial stone is, the higher the strength of the artificial stone is due to pozzolanic reaction. (2) As siliceous tuff contains more silica and alumina than other soil materials, it has higher pozzolanic reactivity. (3) Unconfined compressive strength of the artificial stone can be estimated by two parameters of dried density and curing period. (4) By compacting artificial stone densely, the stiffness of the artificial stone becomes higher. (5) Sandy soil is unsuitable for base material of artificial stone. (6) Even though the flexural strength of the artificial stone is not as high as that of concrete, its strength increases remarkably by extending the curing period.

*Keywords: Siliceous Tuff, Artificial Stone, Strength Development, Deformation, Flexural Strength*

### INTRODUCTION

Siliceous tuff which belongs to Hokuriku layer group of Neogene period, around 23 million to 2.6 million years ago, is deposited thickly in Ishikawa Prefecture facing the Sea of Japan. The siliceous tuff is light and porous material, so it has been often used as a filtration material and a remover material for slug in an ore for a long time. However, the size of the crushed pieces of the siliceous tuff is required to be more than 0.25 mm in these uses. Others have been thrown away as waste. Therefore, the effective utilization of the waste discharged in crushing process of the siliceous tuff must be considered quickly. Fortunately, it contains much silica ( $\text{SiO}_2$ ) and alumina ( $\text{Al}_2\text{O}_3$ ) necessary for pozzolanic reaction in cement or lime soil stabilization. Authors have decided to use the waste as a base material of the artificial stone in these situations.

The artificial stone, called "Tataki" in Japanese, is soil compacted after mixed with lime and anti-freezing agent, and has high strength and hardness comparable to concrete [1], [2]. Being also low environmental load, its application in a wide range of fields will be expected in the future. Recently, strong points of the artificial stone and Japanese traditional technique have been reconsidered and reported by researchers and technicians. Tamayama et al. [3] reported that the artificial stone made by using the Japanese traditional technique can be utilized as pedestrian pavement materials. Iwasaki [4] introduced the Japanese traditional technique of

the artificial stone into the restoration work of Angkor heritage.

In this study, in order to clarify the mechanical characteristics of the artificial stone made from waste of the siliceous tuff, a series of laboratory tests were carried out. The strength development characteristics of the artificial stone are firstly discussed based on unconfined compression test results. Secondary, the deformation properties of the artificial stone are explained with attention to the modulus of deformation obtained from unconfined compression tests. Finally, the flexural strength characteristics of the artificial stone are described based on the results of bending test and needle penetration test.



Fig. 1 Sampling site for Siliceous tuff.

Table 2 Physical and chemical properties of base materials

	Ishikawa-Lite	Fujinomori soil	Ohta soil
Density of soil particle, $\rho_s$ (g/cm <sup>3</sup> )	2.443	2.689	2.629
Maximum dry density, $\rho_{dmax}$ (g/cm <sup>3</sup> )	1.402	1.601	1.698
Optimum moisture content, $w_{opt}$ (%)	25.7	22.9	15.3
Sand fraction (%)	9.0	12.7	62.8
Silt fraction (%)	74.2	76.9	26.4
Clay fraction (%)	16.8	10.4	10.8
Liquid limit, $w_L$ (%)	—	43.8	30.7
Plasticity limit, $w_P$ (%)	NP	21.0	NP
Plasticity index, $I_P$	—	22.8	—
Ignition loss, $L_i$ (%)	6.1	5.9	3.0
Activity, $A$ (%)	—	3.93	—

Table 1 Chemical composition of Ishikawa-Lite

Silicon dioxide (Silica), SiO <sub>2</sub> (%)	63.4
Aluminium oxide (Alumina), Al <sub>2</sub> O <sub>3</sub> (%)	17.1
Potassium oxide, K <sub>2</sub> O (%)	3.34
Iron(III) oxide, Fe <sub>2</sub> O <sub>3</sub> (%)	2.79
Sodium oxide, Na <sub>2</sub> O (%)	2.62
Calcium oxide, CaO (%)	0.86
Magnesium oxide, MgO (%)	0.66
Others (%)	9.23

Table 3 Mix proportion of specimen (Dried mass per 100g)

Base material	Hydrated lime	Magnesium chloride
$a$ (g)	$b$ (g)	$c$ (g)
65	30	5

## MATERIALS AND LABORATORY TESTS

### Materials

Base material of the artificial stone used for experiments are waste of the siliceous tuff and two kinds of soil samples. The siliceous tuff was taken at Tsuribe area of Kanazawa city in Ishikawa Prefecture, Japan, as shown in Figure 1. Based on the name of this area, the siliceous tuff is called “Ishikawa-Lite” from now on. Ishikawa-Lite was crushed, air-dried and then passed once through the 0.425 mm sieve. The tuff includes much silica and alumina as shown in Table 1. This means that the long term pozzolanic reaction increases the strength of the material. In this study, other two base materials were used. One is cohesive soil obtained at Fujinomori area of Kyoto city, Japan, and another is sandy soil taken at Ohta area of Tsubata town in Ishikawa Prefecture, Japan. These soils are named “Fujinomori soil” and “Ohta soil” respectively from

now on. Both of them were air-dried and then passed once through each sieve (Fujinomori soil: 0.425 mm, Ohta soil: 4.75 mm).

Physical and chemical properties of the base materials after passed through the sieve are shown in Table 2. From grain size distribution, both of Ishikawa-Lite and Fujinomori soil contains more than 70 percent silt, and Ohta soil includes more than 60 percent sand. Ishikawa-Lite is porous material, so density of its soil particle shows slightly lower value than that of Fujinomori and Ohta soils. This affects the maximum dry density of three base materials. Ishikawa-Lite and Ohta soil are also classified as “non-plastic” because the plastic limit could not be obtained.

Hydrated lime (Ca(OH)<sub>2</sub>) for stabilizer and magnesium chloride (MgCl<sub>2</sub> · 6H<sub>2</sub>O) for anti-freezing agent were used in a series of laboratory tests. Mix proportion of specimen was decided based on the dried mass of the whole sample with base material  $a$  (g), hydrated lime  $b$  (g) and magnesium chloride  $c$  (g), as shown in Table 3. Amount of water added  $d$  (g) was determined by the following equation (1),  $w_{opt}$  in it means optimum moisture content for each base material.

$$d = (a + b + c) \times \frac{w_{opt}}{100}$$

(1)

### Laboratory tests

In order to understand the strength development, deformation and flexural strength characteristics of the artificial stone, three different kinds of experiments were carried out. Figure 2 shows preparation method of the specimen for unconfined compression test and bending test. The diameter and height of the specimen used for unconfined compression test is 35 mm and 70 mm respectively, and those of the specimen used for bending test is 50



mm and 110 mm respectively. Dry density of each specimen is decided based on maximum dry density ( $\rho_{dmax}$ ) of each base material as shown in Table 2.

The specimen used for each experiment was static compacted after mixed with hydrated lime and magnesium chloride into each base material at predetermined ratio as shown in Table 3. After that, the cylindrical mold was used to prevent the expansion of the specimen for 24 hours. The specimen demolded was wet cured at a constant temperature for predetermined days. Curing periods of the specimen used for unconfined compression test are 1, 3, 7, 14, 28, 56 and 112 days, and those of the specimen used for bending test are 28, 56, 112 and 225 days.

## EXPERIMENTAL RESULTS

### Strength Development Characteristics

Unconfined compression test results of the artificial stones are shown in Figures 3 to 7.  $\rho_{d0}$  shown in those figures means the dry density after static compaction. Figure 3 shows the relationships between unconfined compressive strength ( $q_u$ ) and curing period for Ishikawa-Lite as base material. From experimental results,  $q_u$  of the artificial stone increases remarkably by extending the curing period. Strength development of lime-stabilized soil is generally divided into two phases. The first phase is a short period during which water absorption and ion exchange reaction take place. The second phase is a long period during which the pozzolanic reaction takes place. Artificial stone is the material that hardens due to pozzolanic reaction over a long period of time. Also, the higher the density of the artificial stone is, the higher the strength of the artificial stone is due to pozzolanic reaction as shown in Figure 3.

In order to investigate the influence of the difference of physical properties of base materials, Fujinomori and Ohta soils mentioned earlier were prepared as comparative soils. Figure 4 shows the relationships between  $q_u$  and curing period of the artificial stones for different base materials.  $\rho_{d0}$  of each specimen was set to make equal to the value of the maximum dry density of each base material. In the case of Ohta soil as base material,  $q_u$  is lower than the case of other base materials. Especially, the strength increase due to pozzolanic reaction in long-term curing for Ohta soil is much lower than that for other two base materials.  $q_u$  for Fujinomori soil as a base material is higher than that for Ishikawa-Lite in short-term curing. On the other hand,  $q_u$  for Fujinomori soil as a base material is lower than that for Ishikawa-Lite in pozzolanic reaction stage. The pozzolanic reaction is the phenomenon that the pozzolan with the silica and alumina as main components reacts with hydrated calcium slowly, as

the result, generates compound with binding ability. Therefore, Ishikawa-Lite with more silica and alumina than other soil materials indicates higher pozzolanic reactivity.

The strength  $q_u$  of the artificial stone can be predicted by two parameters of dry density ( $\rho_d$ ) and curing period.  $\rho_d$  means the dry density after curing for predetermined period. This is very useful for practical use. Figure 5 shows the relationships between  $\rho_d$  and  $q_u$  of the artificial stones at each curing period for Ishikawa-Lite as base material.  $\rho_d$  of each specimen is slightly lower than  $\rho_{d0}$ .  $\rho_d - q_u$  curve can be approximated by logarithm at each curing period. For example, the artificial stone of  $\rho_d = 1.43 \text{ g/cm}^3$  will reach to  $q_u = 6.5 \text{ MN/m}^2$  at 56 days of curing.

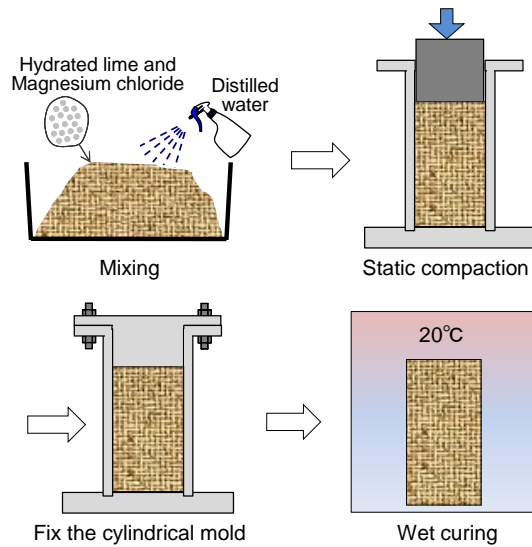


Fig. 2 Preparation method of specimen.

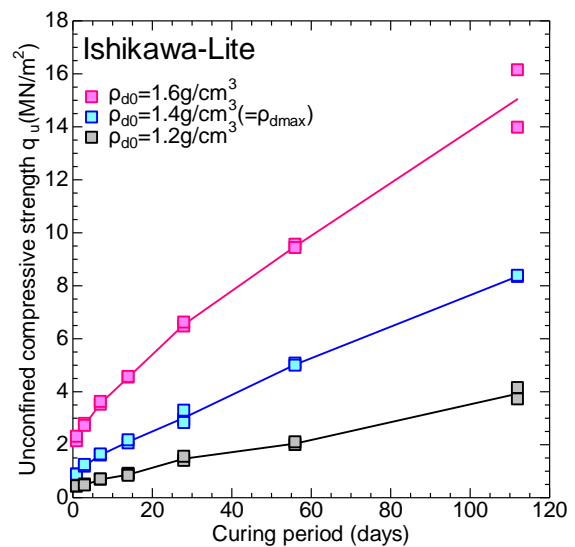


Fig. 3 Relationships between unconfined compressive strength and curing period of artificial stones for Ishikawa-Lite as base



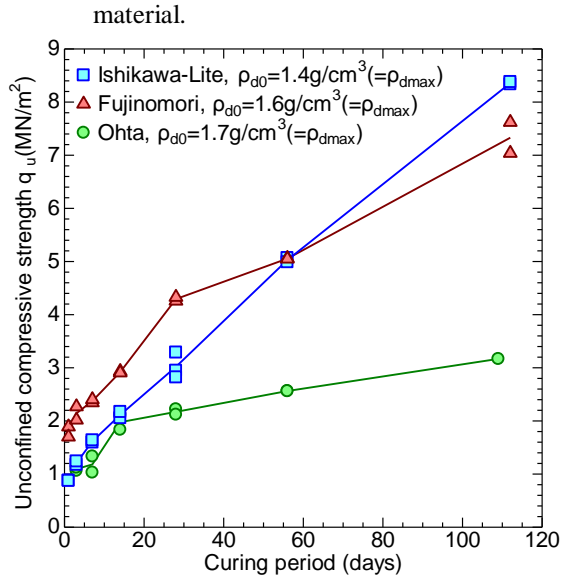


Fig. 4 Relationships between unconfined compressive strength and curing period of artificial stones for different base materials.

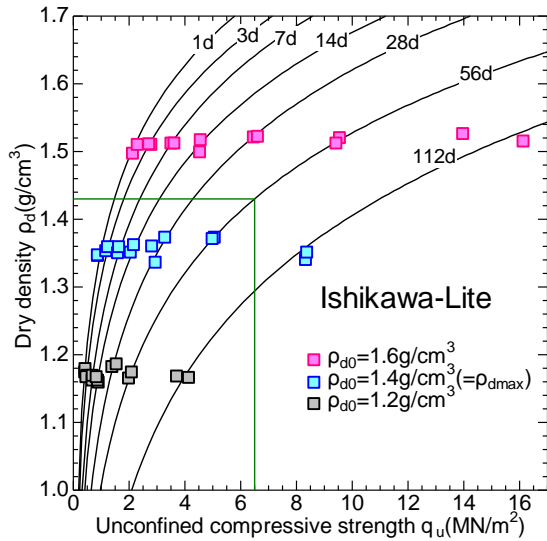


Fig. 5 Relationships between dry density and unconfined compressive strength of artificial stones for Ishikawa-Lite as base material.

### Deformation Properties

Figure 6 shows the relationships between  $E_{50}$  and  $q_u$  of the artificial stones at each dry density  $\rho_{d0}$  for Ishikawa-Lite as base material. Each  $E_{50}$  -  $q_u$  relation can be approximated by a linear function.  $E_{50}$  increases roughly proportionally with the increase of  $q_u$  at the same dry density  $\rho_{d0}$ . This tendency means that the deformation of the artificial stone becomes small with the increase of compressive strength. Consequently, the artificial stone becomes stiffer

material gradually. By compacting the material densely, the stiffness of the artificial stone becomes higher as shown in Figure 6.

Figure 7 shows the relationships between  $E_{50}$  and  $q_u$  of the artificial stones for different base material. The stiffness of artificial stone for Ohta soil as base material is not low as shown in Figure 7. However, the strength development of the artificial stone for Ohta soil is lower than the artificial stone for Ishikawa-Lite and Fujinomori soil. Consequently, sandy soil such as Ohta soil is unsuitable for base material of artificial stone.

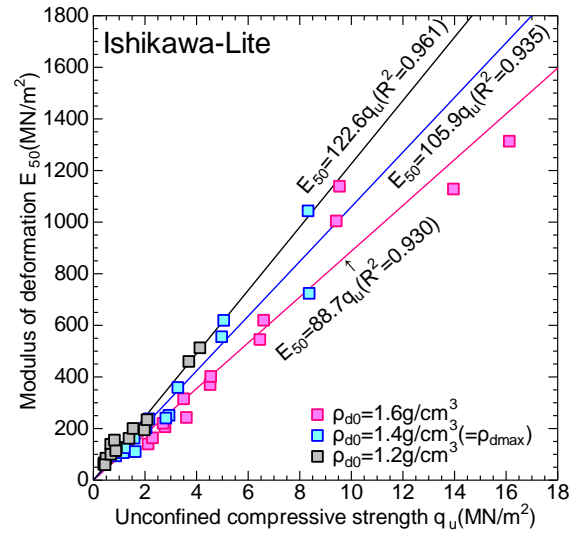


Fig. 6 Relationships between modulus of deformation and unconfined compressive strength of artificial stones for Ishikawa-Lite as base material.

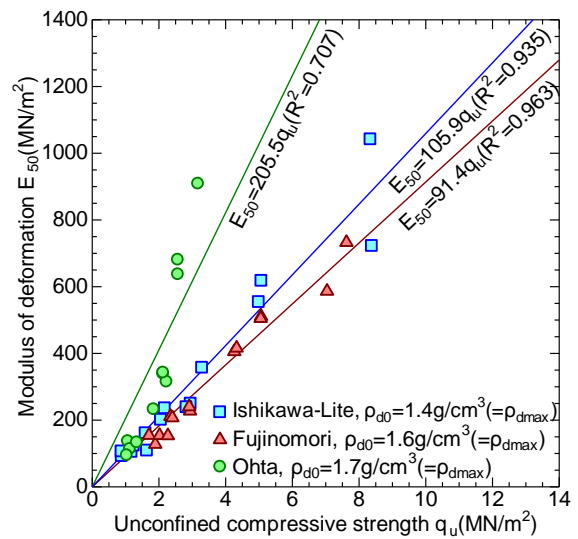


Fig. 7 Relationships between modulus of deformation and unconfined compressive strength of artificial stones for different base materials.

### Flexural Strength Characteristics

Artificial stone is expected to be widely used for construction work such as block pavement and the block for retaining wall in the future. Therefore, in order to clarify the flexural strength characteristics of artificial stone, bending tests based on civil engineering material experiment method were carried out as shown in Figure 8. Flexural strength ( $\sigma_b$ ) was determined by the following equation (2), in which  $I$  means moment of inertia.

$$\sigma_b = \frac{M}{I} y = \frac{\frac{P_{\max}}{2} \cdot \frac{l}{2}}{\frac{\pi D^4}{64}} \cdot \frac{D}{2} \quad (2)$$

Figure 9 shows the relationships between  $\sigma_b$  and curing period of the artificial stones at each dry density  $\rho_{d0}$  for Ishikawa-Lite as base material. Even though flexural strength  $\sigma_b$  of the artificial stones at each dry density  $\rho_{d0}$  is not so high as that of concrete using ordinary portland cement ( $\approx 7.0 \text{ MN/m}^2$ ), it increases remarkably by extending the curing period. The values of  $\sigma_b$  ( $\approx 1.4$  or  $2.5 \text{ MN/m}^2$ ) at 225 days of curing is found to be obtained nearly three times higher than  $\sigma_b$  ( $\approx 0.5$  or  $0.9 \text{ MN/m}^2$ ) at 28 days of curing as shown in this figure.

In order to investigate  $\sigma_b$  - compressive strength relation of the artificial stones, the needle penetration tests were carried out by using a piece of specimens after bending tests as shown in Figure 8. The conversion unconfined compressive strength  $q_u^*$  is calculated from the penetration resistance (N/mm). Figure 10 shows the  $\sigma_b$  -  $q_u^*$  relation of the artificial stones. The  $\sigma_b$  and  $q_u^*$  relation can be expressed by the following equation (3). The needle penetration test can be easily conducted without worrying time and place. Therefore, it is very useful for practical engineers if the flexural strength of the artificial stones is estimated by using equation (3). However, in order to make the  $\sigma_b$  -  $q_u^*$  relation clearer, more experiments of artificial stones are needed in the future.

$$\sigma_b = \frac{1}{5} q_u^* \quad (3)$$

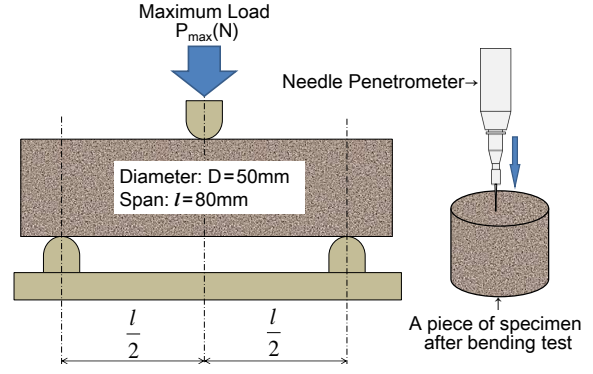


Fig. 8 Methods of Bending test and needle penetration test.

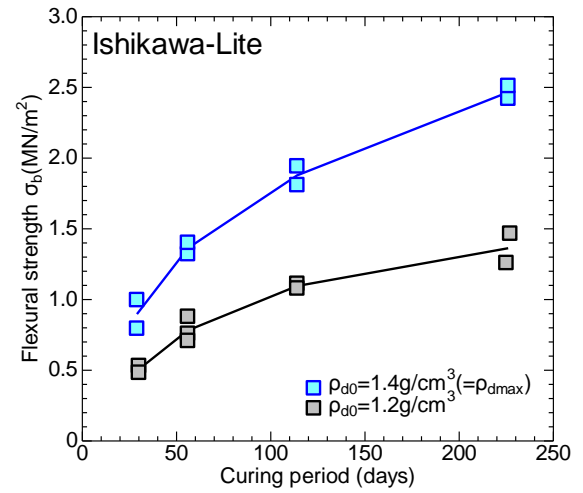


Fig. 9 Relationships between flexural strength and curing period of artificial stones for Ishikawa-Lite as base material.

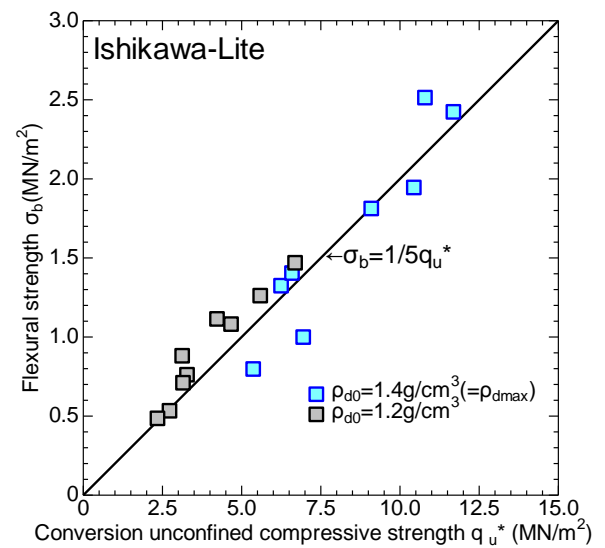


Fig. 10 Relationships between flexural strength and conversion unconfined compressive strength of artificial stones for Ishikawa-Lite as base material.

## CONCLUSIONS

The main conclusions obtained in this study are summarized as follows.

(1) Unconfined compressive strength of the artificial stone made from waste of siliceous tuff increases remarkably by extending the curing period. Also, the higher the density of the artificial stone is, the higher the strength of the artificial stone is due to pozzolanic reaction.

(2) As siliceous tuff contains more silica and alumina than other soil materials, it has higher pozzolanic reactivity.

(3) Unconfined compressive strength of the artificial stone can be estimated by two parameters of dried density and curing period.

(4) By compacting artificial stone densely, the stiffness of the artificial stone becomes higher.

(5) Sandy soil is unsuitable for base material of artificial stone.

(6) Even though the flexural strength of the artificial stone is not as high as that of concrete, its strength increases remarkably by extending the curing period.

## REFERENCES

- [1] Yoshida N., "Lime concrete observed at the foundation of old Osaka prefectural government building completed in 1874", General Building Research Corporation (GBRC), Vol.37, No.4, 2012, pp.29-37 [in Japanese].
- [2] Ishida S, "Research and Conservation on Industrial Heritage of Artificial Stone "TATAKI"", Journal of Historical Studies in Civil Engineering, Vol.11, 1991, pp.309-318 [in Japanese].
- [3] Tamayama Y, Iwashita T, Akagi T and Ito T, "The Environmental Properties of Artificial Stone Developed by Using the Method of Construction, "Tataki"", The Japanese Geotechnical Society, Vol.52, No.11, 2004, pp.23-25 [in Japanese].
- [4] Iwasaki Y., "Authenticity and Technical Transfer of Rammed Ground for Restoration Work of Angkor Heritage", The Japanese Geotechnical Society, Vol.62, No.4, 2014, pp.6-9 [in Japanese].

## **3 DIMENSION REAL TIME IMAGES OF RAINFALL INFILTRATION INTO UNSATURATED SOIL SLOPE**

Aniza Ibrahim<sup>1</sup>, Irfana Kabir Ahmad<sup>2</sup>, Hapsa Husen<sup>3</sup>, Jestin Jelani<sup>4</sup> and Mohd. Raihan Taha<sup>5</sup>

<sup>1</sup>Faculty of Engineering, National Defense University of Malaysia;<sup>2</sup>Faculty of Engineering, National University of Malaysia.

### **ABSTRACT**

Failure of soil slope is mainly due to infiltration of rainfall. The complexity of rain water path infiltrate soil slope can be predicted using commercial software, and volumetric moisture content at the infiltrated slope area can be measured by Time-Domain-Reflectometry (TDR). Prediction of rain water path is based on parameters obtained by laboratory works, and volumetric water content using TDR can only available at the point of insertion. In this research, an innovative method called Electrical Capacitance Volume Tomography (ECVT) was used in geotechnical engineering application in determining the real time imaging of rain water infiltration into unsaturated soil slope. This method also achieves permittivity value through the experiments and converted to volumetric water content using equation. A soil sample obtained from slope failure around National Defense University of Malaysia (NDUM) campus during monsoon season were used in the research. The results revealed real time 3 dimension (3-D) images of rain water infiltrated into soil slope were produced through image reconstruction method of ECVT. Volumetric water content were also achieved using permittivity value attained by ECVT result. Images which permittivity indicated the infiltration of rain water through soil slope were clearly shown in the results. This innovative technology is expected to improve the understanding of soil slope behavior especially in for rainfall infiltration that relates to soil stability.

*Keywords: Rainfall, Infiltration, Soil Slope, ECVY.*

### **INTRODUCTION**

Slope instability in tropical country such as Malaysia, normally triggered by the high seasonal rainfall event. [1], [2], [8]. This main reason is also caused by other activities such as construction development of hillside, and geological factors. As rainfall event started and for some times, infiltrate into unsaturated soil slope, and increase the negative pore pressure above groundwater table and moisture content. In the monsoon season, soil slope will vigorously subjected by high intensity and long duration of rainfall, and this cause rainfall- induced slope failure. [6].

The complexity of rainfall infiltration event into soil slope is due to non-linear of soil water characteristic and soil permeability [12]. The study of main parameters such as initial moisture content, soil water retention ability, soil porosity and others is vital for the understanding of soil behavior when subjected to various rainfall intensity and duration[3], [5],.

Current studies on the rainfall- induced involve laboratory work such as using soil slope flume equipped of apparatus to measure the parameters. The images of rainfall infiltration showing the real time infiltration is not available since all simulations were done by software. The prediction of soil moisture

content was determined by laboratory works and previous data to simulate rainfall infiltration into soil slope event.

This study is to introduce ECVT as a innovative technology used in geotechnical engineering research. ECVT is 3 dimensional real- time imaging system considered as “the most promising technique for dynamic flow imaging, which has a relatively high temporal resolution, up to few milliseconds, with reliable spatial resolution [4].

The used of tomography technique is widely known for medical field purposes such as Magnetic resonance imaging (MRI), X-ray micro tomography, Optical tomography, resistive tomography, Acoustic tomography, Positron-emission tomography (PET), Capacitance tomography, and others [11].

The principle of ECVT is based on forward and inverse problem electrical properties measurement [10].

Collection of capacitance data from electrodes to the data acquisition system is a forward problem, which the electrodes act as sensors are located at the perimeter of ECVT wall vessel. Next, inverse problem will retrieving the capacitance data.

Consequently, reconstructing the images is obtained through the measured data capacitance.

Earlier studies using ECVT are including gas distributor of single gas distributor of paraffin liquid, air, and glass beads as flow media [9] to ensure the moving object is detected by ECVT sensors and produce real time images. Research by [7] shows the successfully capturing water seeping in each layer and producing 3D real images using ECVT.

As mentioned earlier, rainfall – induced soil slope failure mechanism were complex and obtaining related parameters and images in this area currently were using previous laboratory studies and prediction were attained from software.

Therefore, the objective of this study is to capture 3 dimension real-time imaging along the experiment, and the capacitance data is then converted to evaluate volumetric water content for soil slope sample. Other than that the effect of rainfall intensity and duration to the image developed by ECVT and volumetric moisture content is also captured during infiltration process.

## MATERIALS AND METHOD

Samples for the purpose of experiment were obtained from a sites (Cadet Mess) around NDUM campus. These two sites experienced soil slope failure during monsoon season as high intensity and long duration of rainfall.

### Basic Soil Properties

Basic soil properties were obtained from laboratory for moisture content, porosity, bulk density and soil classification.

### Experiment Set Up

The experiments were conducted in the laboratory using flume apparatus and other apparatus were attached such as water supply system, tilted flume with ECVT sensors and water effluent system.

#### Water Supply system

Water pump to simulate rainfall were used in this experiment. Water flow regulator to simulate rainfall is manufactured by Cole-Parmer, model 07554-80 Masterflex L/S economy with variable-speed console and the speed are varies from 1 to 10.

#### Tilted Flume Apparatus

Tilted flume as soil slope model was used and ECVT sensors system was attached to it. ECVT system is including the 32 channel sensors and results were obtained through data requisition system (DAS) by personal computers.

Through laboratory experiment, DAS will capture the real time images using MATLAB software. Schematic diagram of tilted flume apparatus using ECVT system and sizes is shown in Fig 1 (a) and (b) respectively.

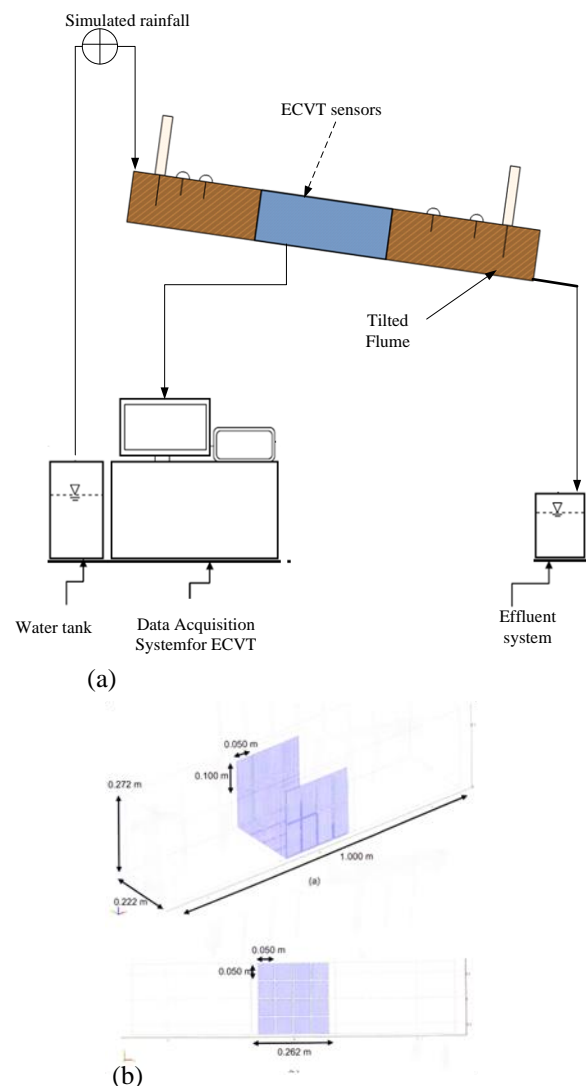


Figure 1: Schematic diagram of (a) tilted flume apparatus using ECVT system (b) sensors and sizes.

### Experiment Schedule

Rainfall infiltration tests were conducted with intensity of 50/240 mL/s flow rate, and duration for 30 and 60 minutes for all three samples. Schedule of experiments is shown in Table 1.

Table 1: Experiments schedule

Soil Sample	Experiment no	Rainfall duration (second)	Drying duration (second)
CADET	Calibration (Air)		300
MESS	Calibration (Soil)		300
	1	1800	1800
	2	5400	5400

### Images Reconstruction

In this research, 3 D real time images were obtained through images reconstruction after experiments were done using MATLAB software. The different script to run the software were used and all saved file will be retrieved and went through the process.

### Permittivity and Volumetric Moisture Content

Other than real time images, permittivity and volumetric water content were also obtained in this study. Permittivity data were retrieved from the data and converted to determine volumetric water content proposed by [7]. It is noted that the relative permittivity for air, water, residual soil, and saturated soil are 1, 80, 2-4, and 23-28 respectively. The equation is as follows:

Normalized permittivity,

$$\epsilon_N = \frac{\epsilon - \epsilon_{res}}{\epsilon_{sat} - \epsilon_{res}} \quad (1)$$

Volumetric water content,

$$\theta = \eta \left( \frac{\epsilon - \epsilon_{res}}{\epsilon_{sat} - \epsilon_{res}} \right)^{0.5} \quad (2)$$

where  $\epsilon_N$ ,  $\epsilon$ ,  $\epsilon_{res}$ , and  $\epsilon_{sat}$  are normalized, relative, residual, saturated permittivity respectively, and  $\eta$  is the porosity.

## RESULT AND DISCUSSION

### ECVT 3 D Images

3 D real time images for all samples were obtained as in Table 3. Selection of images were done through observation to present the significant changes to the images.

The result for the real time images shows the detection of rainfall infiltration into the soil but there are many images need to be selected in order to show the changes.

In this experiment, there are 1800 and 5400 images for experiment 1 and 2 respectively. It is noted that  $x$  frame in this experiment refers to real time images at the  $x$  second.

Results shown in Table 3 shows the 3 D Images of sample for axis XY, YZ and XZ for slices of 1, 9, 17, and 25, at frame 1, 1000, 3000, and 5000. Each frame has 32 slice images (for 32 channel sensors). Images shows the variation of color indication for permittivity from dark blue (lowest permittivity value), light blue, yellow, orange to red (highest permittivity value).

The results shows that water infiltration is clearly indicated though the images but only small variation shown. This is believed due to the lower intensity and short duration rainfall applied during the experiment.

### Permittivity and Volumetric Moisture Content (ECVT)

After images were obtained, the permittivity data were retrieved and converted to volumetric water content. Sample of average permittivity data and volumetric moisture content is shown in Figure 2 (a) and (b) for the frame of 5000 respectively.

The result of permittivity in Figure 2(a) indicated that the average volumetric moisture content of all frames during the experiment. The changes and increasing of permittivity during shows that the increasing of moisture content throughout the experiment.

This result are shown by a sample value shown in the Figure 2(b) which all 32 slices. The successful of using equation by [7] is observed for this experiment.

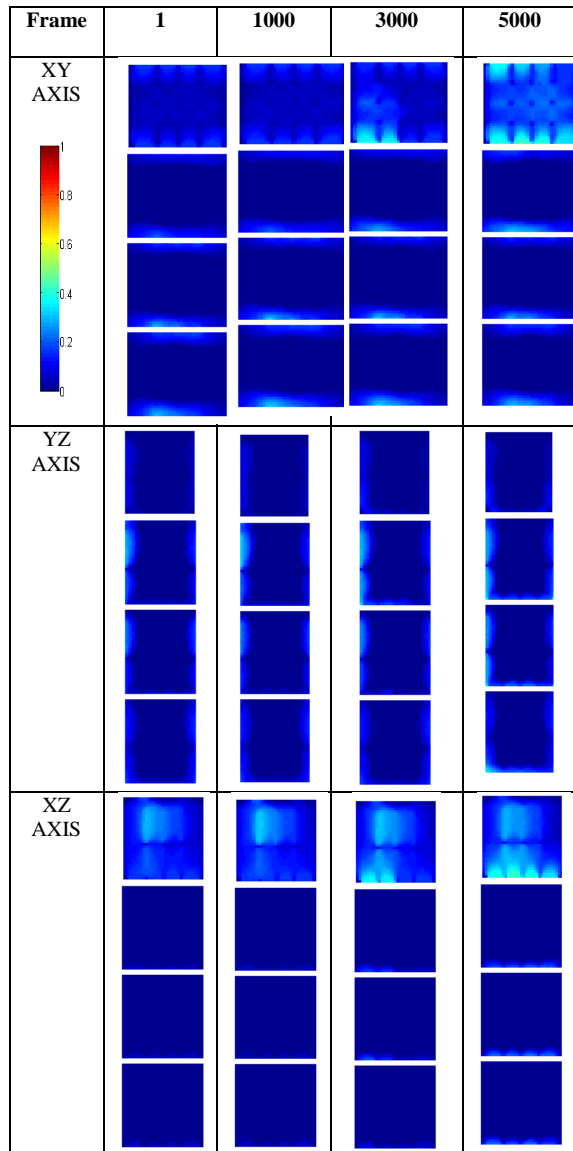


Table 3: 3 D Images of sample for axis XY, YZ and XZ for slices (a) 1 (b) 9 (c) 17 and (d) 25.

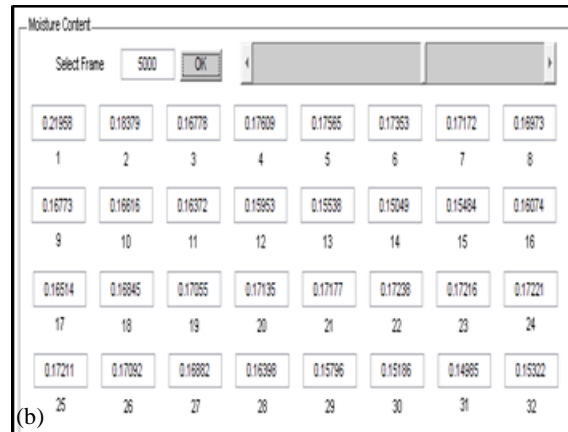
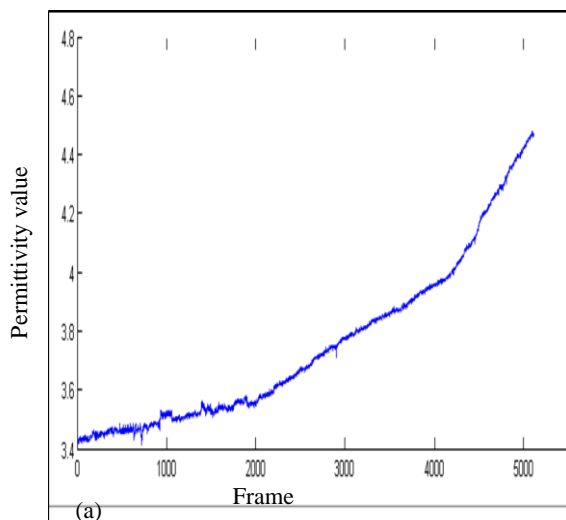


Figure 2: (a) Graph of average permittivity value and (b) average moisture content for each slice for frame 500.

## CONCLUSION

This research study is regarding the using of ECVT system to detect rainfall infiltration into soil slope. Through previous studies in geotechnical engineering field, moisture content can be obtained through this system but only small scale experiments were done. This experiment using indicated rainfall intensity and duration of wetting (rainfall) and drying (after rainfall) clearly shown the images of rainfall infiltration. Result of permittivity values also shown the changes of volumetric moisture content and proved that ECVT is appropriate to use to observed and study in soil slope rainfall infiltration. On the other hand, the small variation and changes in the 3D images indicate that the rainfall intensity may be too small. Therefore the author would like to suggest further experiments with higher rainfall intensity and longer rainfall duration for future.

## ACKNOWLEDGEMENTS

The authors would like to express their appreciation to the financial supports provided by National Defense University of Malaysia through RACE/F3/TK3/UPNM/10.

## REFERENCES

- [1] B. B.K, Ali F. H and Low T.H, "Water Infiltration Characteristics of Unsaturated Soil Slope and its Effect on Suction and Stability," Geotechnical and Geological Engineering, vol. 24, 2006, pp. 1293-1306.
- [2] Gofar N, Lee L. M, and Kassim A, "Instrumented Soil Column Model for Rainfall Infiltration Study," presented at the GEOTROPIKA 2008.



- [3] Lee L. M, Kassim A, and Gofar N, "Performance of Two Instrumented Laboratory Models for the Study of Rainfall Infiltration into Unsaturated Soils", *Engineering Geology*, vol. 117, 2011, pp. 78-89.
- [4] Marashdeh Q, Fan L.S, Du B, and Warsito W, "Electrical Capacitance Tomography - A Perspective," *Ind. Eng.Chem. Res.*, vol. 47, 2008, pp. 3708-3719.
- [5] Mukhlisin M, Kosugi K, Satofuka Y, and Mizuyama T, "Effects of Soil Porosity on Slope Stability and Debris Flow Runout at a Weathered Granitic Hillslope", *Vadose Zone J*, Vol 5, 2006, pp. 283-295.
- [6] Mukhlisin, M., and Taha, M.R., "Numerical Model of Antecedent Rainfall Effect on Slope Stability at a Hillslope of Weathered Granitic Soil Formation", *Journal Geological Society of India*, Vol 79, 2009, pp.525-531.
- [7] Mukhlisin M, Saputra A, El-Shafie A, and Taha M. R, "Measurement of Dynamic Soil Water Content Based on Electrochemical Capacitance Tomography," *Int. J. Electrochem. Sci.*, vol. 7, 2012, pp.5457-5466.
- [8] Rahardjo H, Ong T.H, Rezaur R. B, Leong E.C, and Fredlund D.G, "Response Parameters for Characterization of Infiltration," *Environment Earth Science*, vol. 60, 2010, pp. 1369-1380.
- [9] Van Genuchten M.TH, "A Closed-form Equation for Predicting the Hydraulic Conductivity of Unsaturated Soils", *Soil Sci. Soc. Am. Journal*, vol.44 (5), 1980, pp. 892-898.
- [10] Warsito W and Fan L.S, "Dynamics of spiral bubble plume motion in the entrance region of bubble columns and three-phase fluidized beds using 3D ECT", *Chemical Engineering Science*, vol. 60, 2005, pp.6073-6084.
- [11] Warsito W, Marashdeh Q, and Fan L-S, "Electrical Capacitance Volume Tomography", *IEEE Sensors Journal*, vol. 7, 2007, pp.525-535.
- [12] Willians R. A and Beck M. S., 'Introduction to process tomography', *Process Tomography: Principles, Techniques and Applications.*, 1 ed.: Butterworth-Heinemann, 1995, pp.3-10.

## STEREO ECHO CANCELLATION USING ADAPTIVE NON-LINEAR NETWORK FILTER FOR HOME THEATRE ROOM

Sunisa Kunarak

Department of Electrical Engineering, Srinakharinwirot University, Nakhonnayok, Thailand 26120

Email: sunisaku@g.swu.ac.th

### ABSTRACT

The Stereo Echo Cancellation (SEC) is a necessary process for reducing undesired noise in order that the audiences can receive the apparent sound signal. In this paper, we use the Adaptive Non-Linear Network Filter (ANNF) that is an algorithm based on Radial Basis Function Neural Networks (RBFNNs) in order to get rid the unwanted sound signal. The fully ANNF is used to model the room transfer function with the proper activation function as the Gaussian structure. We obtain the samples of the echo sound in home theater room and apply it as the input to the adaptive non-linear network filter. Furthermore, this method is implemented in MATLAB program. To ensure the clarity sound, the simulation results show that our proposed algorithm provided outperform the previous works as Adaptive Filter with Gain and Time-shift, Wiener Adaptive Filter and Feedforward Network in term of the Echo Return Loss Enhancement (ERLE) and Mean Square Error (MSE), respectively. We observe that the proposed approach can improve the ERLE around 10 dB and can reduce the MSE less than 0.001.

*Keywords: Adaptive Non-Linear Network Filter, Echo Return Loss Enhancement, Mean Square Error, Radial Basis Function Neural Networks, Stereo Echo Cancellation*

### INTRODUCTION

The echo is a phenomenon that is delayed and distorted of the original signal which is reflected back to the source as the voice signals. Stereo Echo Cancellation (SEC) is a common approach in removing the echo and noise path. The normalized least mean square (NLMS) algorithm is the most popular method since this one is a simple structure and lower computational time complexity. However, the performance of this algorithm is essentially deteriorated for correlated input speech signals [1-2].

To overcome in echo cancellation, the affine projection algorithm (APA) that reuses the input vector to accelerate the convergence speed in [3]. Unfortunately, the performance of this method is depend on the step size i.e. if the step size is small, the approach can get a smaller misalignment but has a slower convergence speed. In the other hand, when the step size is large, the algorithm can achieve a faster convergence but has a bigger misalignment.

Additionally, the frequency-domain adaptive filter [4-5] can reduce the distinction between the expected and actual output filter is also known as error signal but this method is not suitable for non-statistical information situation due to unpredictable environments. To enhance the performance, we propose the adaptive non-linear network filter that is based on radial-basis function neural networks. This proposed algorithm can control the tendency of mean square error (MSE) and echo return loss enhancement (ERLE).

This paper is organized as follows: the adaptive radial-basis function neural network filter is summarized in the next section. After that, the stereo echo cancellation using adaptive non-linear network filter is explained. Next, the simulation environment and simulation results is presented. The conclusion is finally given in the last section.

### ADAPTIVE RADIAL BASIS FUNCTION NETWORK FILTER

In this section, the radial-basis function neural networks (RBFNNs) is utilized the stereo echo cancellation (SEC) process as explained in Fig. 1. This approach is suitable for abundant non-linear sound signal. The three layers as input layer, hidden layer and output layer are gathered in the basic structure [6]. The speech voice that is direct sound, is sampled about 4,096 samples as the input nodes, the non-linear Gaussian are the transfer function in the hidden layer to connect them to all of the input nodes. Finally, the output layer consists of one node that is obtained by a linearly weighted sum of the outputs of the hidden units that are updated in the training procedure. The output of this network is the error that is minimized less than 0.001.

In order to adjust minimized the error, the network will find the optimal weight,  $\mathbf{w} = [w_1, w_2, \dots, w_N]^T$  is learned as the following steps [7].

1. Set the initial value of center  $(\mu_{ji})$  in the hidden

layer for the  $i^{th}$  input node and the  $j^{th}$  hidden node and the value of span  $(\sigma_j)$  in the  $j^{th}$  hidden node, respectively. Also, the initial weight vector which is distributed uniformly between 0 and 1.

2. Calculate the output of hidden layer as:

$$z = \exp\left(-\|\vec{x} - \vec{\mu}_{ji}\|^2 / 2\sigma_j^2\right) \quad (1)$$

where  $\mathbf{x} = [x_1, x_2, \dots, x_{i-1}, x_{5000}]^T$  represents the input vector.

3. Calculate the output of output layer as:

$$y_k = \sum_{j=0}^M w_{kj} z_j, \quad k = 1; M = 10 \quad (2)$$

4. Calculate the error of this network:

$$e_k = d_k - y_k \quad (3)$$

where  $d_k$  is the desired output.

5. Update the weight as:

$$w_{kj}(n+1) = w_{kj}(n) + \eta_w (e_k) z_j \quad (4)$$

where  $\eta_w$  is the learning rate of weight.

6. Update the center momentum with the learning rate of center as:

$$\mu_{ji}(n+1) = \mu_{ji}(n) + \eta_\mu \frac{z_j}{\sigma_j} (x_i - \mu_{ji}) \sum e_k w_{kj} \quad (5)$$

7. Update the span with the learning rate of span  $(\eta_\sigma)$  as:

$$\sigma_j(n+1) = \sigma_j(n) - \eta_\sigma z_j \frac{2}{\sigma_j} \ln z_j \sum e_k w_{kj} \quad (6)$$

In our implementation, the training process use 1000 samples of sound and 300 samples are used to test the network. The mean square errors of actual output and desired output are calculated in each simulating epoch.

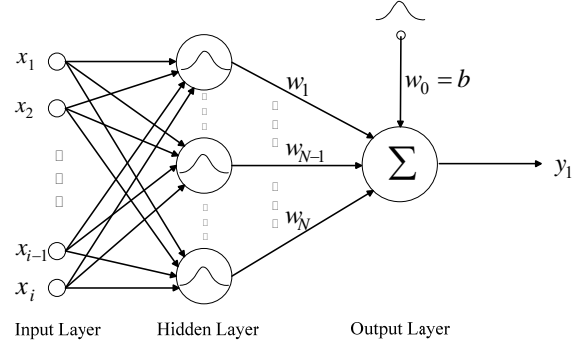


Fig. 1 Adaptive radial-basis function structure.

### STEREO ECHO CANCELLATION USING ADAPTIVE NON-LINEAR NETWORK FILTER

When the user speaks into a microphone is called the direct sound, the surroundings noise as a door, walls, furniture and so on in the room is added to the speech signal, and the resultant signal heard by audience would be of low quality. So, we would like to obtain a signal that contains the clarity speech voice, but not the surroundings noise. We can do this an adaptive non-linear network filter if we get a sample of the surroundings noise and apply it as the input to the adaptive non-linear network.

Here we adaptively train the non-linear network filter to predict the combined speech voice and environment signal as  $m$  from a surroundings noise as  $n$ . Notice that the surroundings signal does not tell the adaptive non-linear network filter anything about the speech signal contained in  $m$ . However, the direct sound signal does give the adaptive non-linear network filter information which it can use to predict the surrounding's contribution to the speech voice and environment signal as illustrated in Fig. 2.

The network will do its the best to adaptively output  $m$ . In this case, the network can only predict the surroundings interference noise in the speech voice and environment signal. The network error ( $e$ ) is equal to  $m$ , that means the speech voice and surroundings signal will be minus the predicted contaminating surrounding noise signal. Thus, the network error contains only the speech voice. Finally, the adaptive non-linear network filter adaptively learns to cancel the surroundings noise.

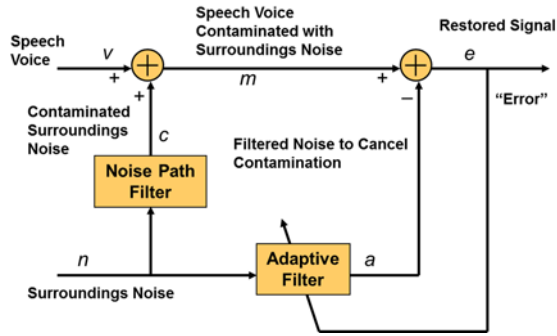


Fig. 2 Echo cancellation using ANNF process.

## SIMULATION

In this section is explained into 2 sub-section as the simulation environment and simulation results, respectively.

### Simulation Environment

The main disadvantages of the home theatre are reverberation and echo signal. In order to solve this problem, we propose an efficient methodology for get rid the echo signal. In this paper, the fundamental home theatre room feature has a width  $\times$  length  $\times$  height size is equal to 10 meter  $\times$  16 meter  $\times$  5 meter and compose 5 loudspeakers and 1 sub-woofer (SW) that is called 5.1. The position of loudspeakers are fixed in the center (C) of the audience and under the television, the front loudspeakers in the left hand side (FL) is angle 30 degree and the right hand side (FR) is angle 20 degree and finally, surround in the left hand side (SL) and surround in the right hand side (SR) are arranged in the audience's axis as shown in Fig. 3. The sound signal that is generated 30 seconds of music, is sampled 4,096 points for each input pattern with 16 kHz sampling frequency and stored to memory for off-line processing [10].

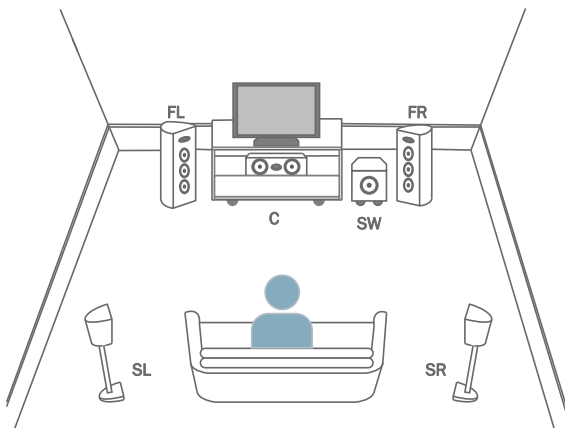


Fig. 3 Home theatre room characteristic.

## Simulation Results

In the simulation results, we observe that the Adaptive Non-Linear Network Filter (ANNF) which is a proposed method outperforms the other algorithms as the Wiener Adaptive Filter (Wiener) [8], Feedforward Network (FF) [9] and Adaptive Filter with Gain and Time-shift (AFGT) [11] in Mean Square Error (MSE) value as illustrated in Figs. 4-7. Figure 4 shows the speech voice or original signal (top), noise signal (middle) and restored signal (bottom) of the proposed approach that is nearly the speech voice. Also, it has a MSE equal to  $1.7496 \times 10^{-6}$  which is less than the Adaptive Filter with Gain and Time-shift, Feedforward and Wiener methods because the proposed approach is suitable in non-stationary systems and numerous non-linear signal while the Adaptive Filter with Gain and Time-shift is relatively stable systems as displayed in Fig. 5. The Feedforward network is a one type of neural networks but this algorithm is improper to distinguish the non-linear sound signal as illustrated in Fig. 6. Finally, the Wiener Adaptive Filter depends on the window size that is disadvantage of this one as shown in Fig. 7.

Accordingly, the coverage echo return loss enhancement (ERLE) of the ANNF algorithm is increased around 10 dB with comparing the other methods as the adaptive filter with gain and time-shift, feedforward network and Wiener adaptive filter. Furthermore, the proposed algorithm is not limited in high power i.e. the ERLE augments despite the high power owing that it has a recursive structure while the ERLE of the other algorithms are dropped at larger than 0.1 watt as depicted in Fig. 8.

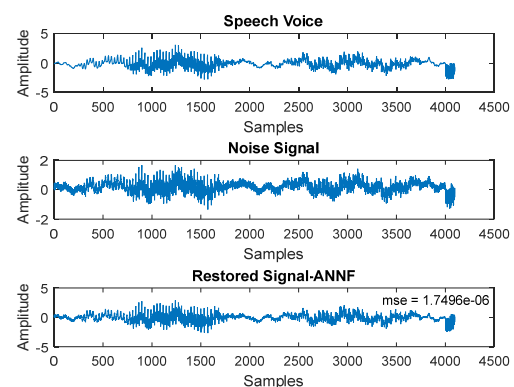


Fig. 4 Restored signal by adaptive non-linear network filter.

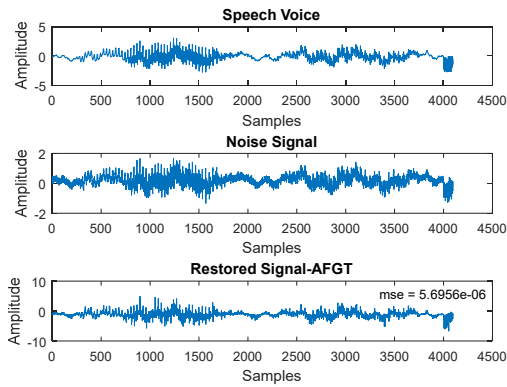


Fig. 5 Restored signal by adaptive filter with gain and time-shift.

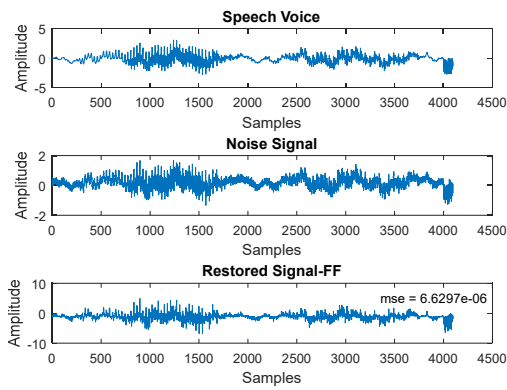


Fig. 6 Restored signal by feedforward network.

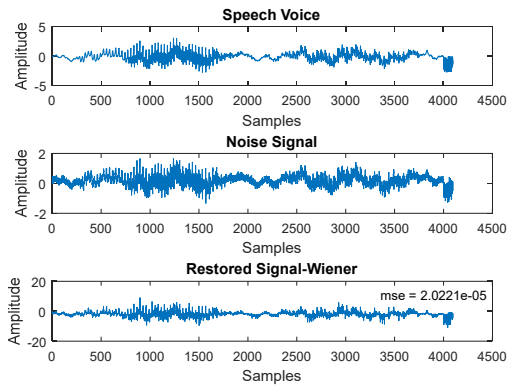


Fig. 7 Restored signal by Wiener adaptive filter.

## CONCLUSION

We proposed the Adaptive Non-Linear Network Filter (ANNF) that is an algorithm based on Radial Basis Function Neural Networks (RBFNNs) for home theatre room in 5.1 characteristic. The simulation results indicate the proposed algorithm that increases efficiency compared with the other three approaches in increasing the coverage echo return loss enhancement. Also, this algorithm can decrease the mean square error, respectively.

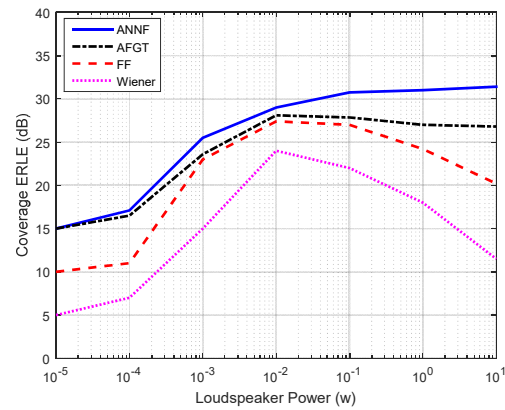


Fig. 8 Coverage ERLE versus loudspeaker power.

## REFERENCES

- [1] H. H. Qin and L. Zhang, "Adaptive feedback cancellation based on variable step-size affine projection for hearing aids", *The Journal of China Universities of Posts and Telecommunications*, Vol. 22, Feb. 2015, pp. 6-10.
- [2] F. Strasser, "Adaptive feedback cancellation for realistic hearing aid applications", *IEEE/ACM Transactions on Audio, Speech and Language Processing*, Vol. 23, Dec. 2015, pp. 2322-2333.
- [3] M. Zhu and L. Zhang, "APA with Evolving Order and Variable Step-size for Echo Cancellation", *IEEE Advanced Information Management, Communicates, Electronic and Automation Control Conference*, 2016, pp. 841-844.
- [4] N. Praveen, S. Ranjitha and H. N. Suresh, "A frequency-domain adaptive filter (FDAF) prediction error method and ARLS for speech echo cancellation", *2<sup>nd</sup> International Conference on Applied and Theoretical Computing and Communication Technology*, 2016, pp. 182-187.
- [5] S. Wu, X. Qiu and M. Wu, "Stereo acoustic echo cancellation employing frequency-domain preprocessing and adaptive filter", *IEEE Transactions on Speech and Audio Processing*, Vol. 19, Jun. 2011, pp. 614-623.
- [6] S. Haykin, *Neural Networks and Learning Machines*. New York: Prentice Hall, 2008, pp.68-73.
- [7] S. Kunarak, "Vertical Handover Decision based on RBF Approach for Ubiquitous Wireless Networks", *International Conference on Platform Technology and Service*, 2016, pp. 1-4.
- [8] I. J. Dahanayaka, P. K. Y. N. Kulasekara, M. N. F. Zihra and S. H. G. Chamindu, "Acoustic Echo Cancellation for Hands-free Applications using Adaptive Filters", *Annual Technical Conference 2010 of IET-YP Sri Lanka*, 2010, pp. 1-4.

- [9] A. N. Birkett and R. A. Goubran, "Acoustic Echo Cancellation for Hands-free Telephony using Neural Networks", Proceedings of the IEEE Workshop Neural Networks for Signal Processing, 2002, pp. 1-11.
- [10] M. Müller, J. Janský, M. Boháč and Z. Koldovský, "Linear Acoustic Echo Cancellation using Deep Neural Networks and Convex Reconstruction of Incomplete Transfer Function", IEEE International Workshop of Electronics, Control, Measurement, Signals and their Application to Mechatronics, 2017, pp. 1-6.
- [11] Z. Zhang and Z. Wu, "An Adaptive Filter with Gain and Time-Shift Parameters for Echo Cancellation", 10<sup>th</sup> International Symposium on Chinese Spoken Language Processing, 2016, pp. 1-5.

## FINITE ELEMENT ANALYSIS OF EWECS COLUMNS WITH VARYING SHEAR SPAN RATIO

Fauzan<sup>1</sup>, Ruddy Kurniawan<sup>2</sup> and Zev Al Jauhari<sup>3</sup>

<sup>1</sup> Department of Civil Engineering, Andalas University, Indonesia

### ABSTRACT

A new hybrid structural column system called Engineering Wood Encased Concrete-Steel (EWECS) was developed for low and high to seismic zones. Experimental studies on seismic behavior of EWECS composite columns with varying shear span to depth ratio (shear-span ratio) have been conducted by one of the authors. To complement and validate the experimental program, finite element analysis (FEA) on EWECS Columns with varying shear span ratio ranging 1.0 to 2.0 under constant axial load and lateral load are summarized. This numerical analysis was used finite element program, ANSYS APDL v.14, to investigate the structural performance of the EWECS columns, which was compared with experimental results. A detailed three-dimensional (3D) non linear FE model of three composite columns were performed. The FEA results showed that the shear span ratio was affect to the maximum shear strength and failure mode of the EWECS columns. The maximum strength of the columns increased with decreasing shear-span ratio. The stress distribution on the FE models representing the failure mode of the EWECS column specimens well. More damages on the columns were observed with decreasing shear-span ratio. Generally, the numerical results was able to accurately simulate the behaviour of the EWECS composite columns on experimental study.

*Keywords: Column, Composite Structure, Finite Element Analysis, ANSYS, and Seismic Performance*

### INTRODUCTION

It has been known that the composite steel-concrete columns such as Steel Reinforced Concrete (SRC) and Concrete Filled Tube (CFT) columns have been widely used in high-rise and long-span buildings. Based on the ideologies of SRC and CFT composite columns, a new hybrid structural column system called Engineering Wood Encased Concrete-Steel (EWECS) was developed for low and high to seismic zones [1]. This new composite material overcomes the limitation of the number of stories that can be constructed by utilizing wood as a material on its own. This column consists of concrete encased steel (CES) core wrapped with an exterior wood panel [2], as shown in Figure 1.

Some benefits of using wood panel as column cover in EWECS column include the improved structural behavior through its action to provide core confinement and resistance to bending moment, shear force and column buckling, environmentally friendly, and save time during construction. Therefore, EWECS column is possible to apply to actual structures as an alternative to SRC columns, which have weaknesses due to difficulty in constructing [3].

An experimental study on EWECS columns with varying shear span to depth ratio ranging from 1.0 to 2.0 under constant axial load and lateral load reversals was conducted by Fauzan et al. in the Laboratories of Toyohashi University of Technology

(TUT), Japan to obtain the effects of shear span to depth ratio on the seismic behavior of EWECS columns [4]. The results shows that the maximum flexural strength of the columns increased with decreasing shear-span ratio. However, more damages on the columns were observed with decreasing shear-span ratio.

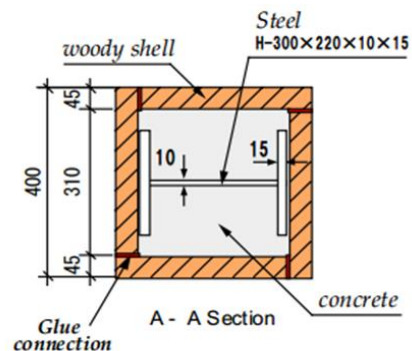


Fig. 1 Specimen Detail of EWECS Column

To complement and validate the experimental program, a 3D finite element (FE) model of EWECS composite columns with varying shear span ratio subjected to axial and lateral cyclic loads using ANSYS APDL 14.0 software was developed [5]. This software has proven its reliability in many benchmark studies and was considered suitable for the current task. The developed model takes into consideration the nonlinear behavior of material.



The results of the FEA were compared with the experimental test results. In this paper, the shear span to depth ratio hereafter referred to as “shear-span ratio”.

### THE GEOMETRY AND ELEMENT TYPE OF 3D FE MODEL

A total of three composite column models with varying shear-span ratios were performed in 3D FE model. The column cross-section was constant at 400 mm square section for all specimens and different shear-span ratios (1.0, 1.5 and 2.0) were achieved by varying the column height (800 mm, 1200 mm and 1600 mm). Details and named of the 3D FE models in terms of geometry of steel section, concrete, and wood panel are generated and described in Figures 2 and 3.

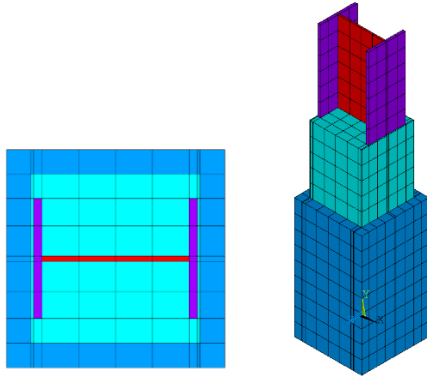


Fig. 2 The 3D FE Model of EWECs Column

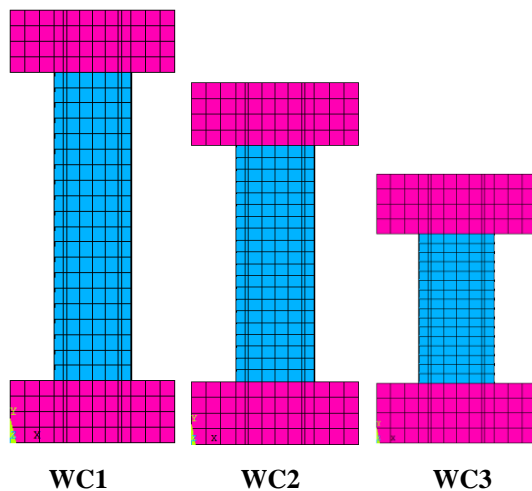


Fig. 3 Full Models of EWECs Column with Varying Shear Span Ratio

The steel encased in each column had a single H-section steel of 300 x 220 x 10 x 15 mm. The FE models are developed to accurately represent the geometrical configuration and dimensions of the test specimen. The full model EWECs composite columns with varying shear span ratio are modeled as illustrated in Figure 3. The concrete, steel, and

wood panels were modeled as block and solid cube with an equivalent length representing the total area of specimen.

Two types of elements are used in the modeling of steel H-section, concrete, and wood panel. ANSYS solid element, SOLID185 is used to modelling the steel section and wood panel, while SOLID65 is used to modelling the concrete of the EWECs column. The SOLID185 and SOLID65 elements are a 3D hexahedral element defined by eight nodes as shown in Figure 4. The elements have three translational degrees of freedom at each node in the nodal x, y, and z directions. The FE model in this study is considered perfectly-bonded for each material interfaces (steel-concrete and wood-concrete) in adjacent contact. This assumption is applied because based on the experimental results, the effect of slips and separations in each material are not much influence [6], so the interface modelling on the FE model is not performed.

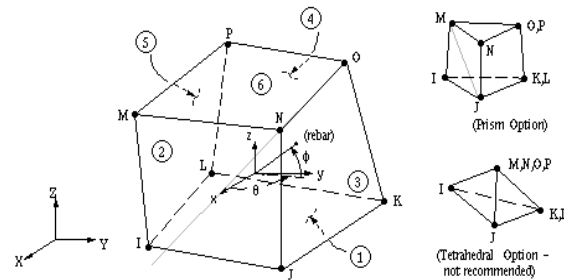


Fig. 4 Solid65 and Solid185 ANSYS Elements

### MATERIAL PROPERTIES, MESHING, LOAD, AND BOUNDARY CONDITIONS

#### Material Properties

##### Concrete

The compressive strength of concrete used in both specimens was 35 MPa. A peak concrete strain of 0.0025 was used in the analysis [7]. Figure 5 presents the tensile stress-strain curve used for the concrete. The stress-strain relationship in the rising region was designed on the model developed by Saenz [8], which was built in the program. In the softening region, the linearly decreasing model was adopted. The tensile relaxation (softening) was presented by a sudden reduction of the tensile strength to  $0.6f_t$  upon reaching the tensile cracking strain  $\epsilon_{cr}$ . After this point, the tensile response decreases linearly to zero stress at a strain of  $6\epsilon_{cr}$  as shown in Figure 6.

Additional concrete material data, such as the shear transfer coefficient  $\beta_t$  for open cracks and  $\beta_c$  for closed cracks are also needed for the concrete constitutive material data table. The shear transfer coefficients  $\beta_t$  and  $\beta_c$  control the amount of shear

transfer across the cracks. Typical shear transfer coefficients range from 0.0 to 1.0, with 0.0 representing a smooth crack (complete loss of shear transfer) and 1.0 representing a rough crack (no loss of shear transfer). A shear transfer model developed by Al-Mahaidi [9] was included in the analysis, with value of 0.75 and 0.9 was used in the FE model for  $\beta_t$  and  $\beta_c$ , respectively. The fracture criterion of concrete was applied with the adoption of the five parameter model of William-Warnke [10].

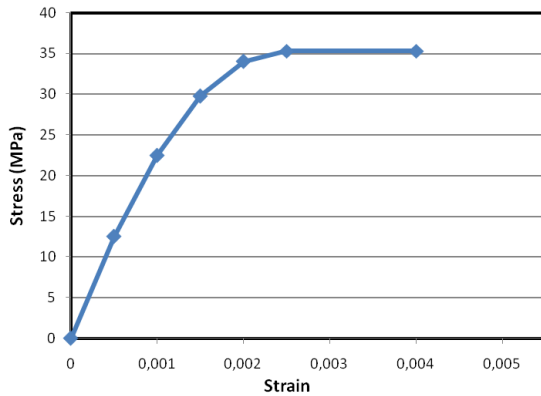


Fig. 5 Compressive stress-strain curve for concrete

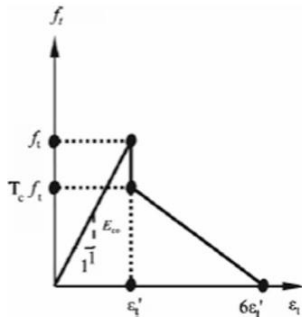


Fig. 6 Tensile stress-strain curve for concrete [11]

#### Steel Section

The yield strength of steel used in each models are 293.6 and 313.3 MPa for flange and web steel, respectively. The constitutive model of the steel used in this study is a perfectly elastic-plastic criterion. At first, this curve is elastic, then it assumed to be perfectly plastic (bilinear isotropic model), as shown in Figure 7. This curve is suitable for representing stress-strain characteristics of normal and high quality steel section.

#### Wood Panel

The compressive strength and modulus elasticity of wood are 46.2 MPa and 11200 MPa, respectively. The constitutive model of engineering wood panel is shown in Figure 8. Owing to the design to allow the force to be applied in the direction parallel to the annual growth ring of the wood, some existing concrete models built in the program by many researchers might be used in the analysis with some

modifications [7]. Stress-strain relationship in the rising region was modeled with the linearly increasing model. The fracture criterion of wood was adopted following the rule of the five parameter model of William-Warnke [10] for concrete with the input of wood material characteristic. The maximum tensile strength of the wood panel during the analysis was taken as 5 MPa. This value took into consideration the lower tensile strength in the direction perpendicular to the grain. The shear transfer model for concrete developed by Al-mahaidi [9] was included with the use of modified shear transfer coefficient  $\beta_c$  of 0.35 for wood.

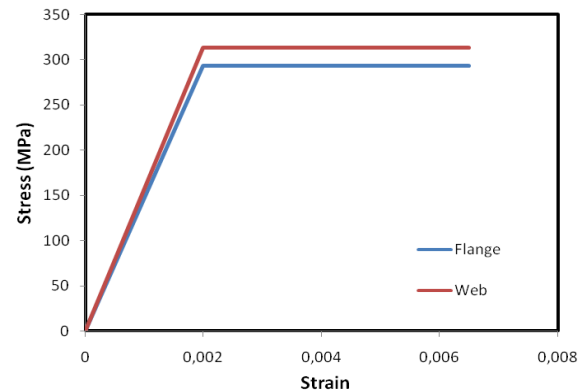


Fig. 7 Tensile stress-strain curve for steel

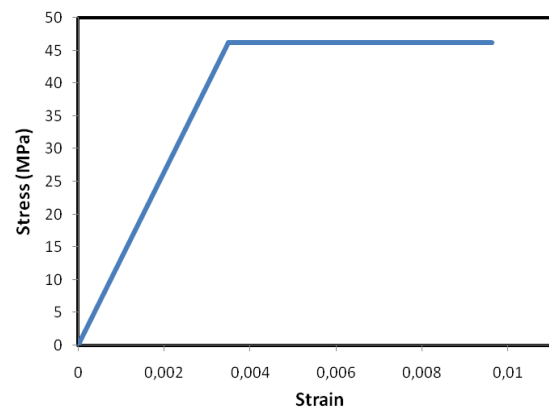


Fig. 8 Tensile stress-strain curve for wood

#### Meshing

The mesh density was chosen so that the elements aspect ratio is nearly equal to one. This provided adequate accuracy and fair computational time in modelling the steel columns. The total numbers of element used is 5095 elements. This is an adequate refinement for the constructed 3D FE model.

#### Boundary Conditions

The boundary conditions in FE models were corresponding to the experimental setup. An anchor Plate (700.700.400 mm) was used in the model at

the top and bottom of the column. Fixed at the bottom of the column and roller supported at the top of the column.

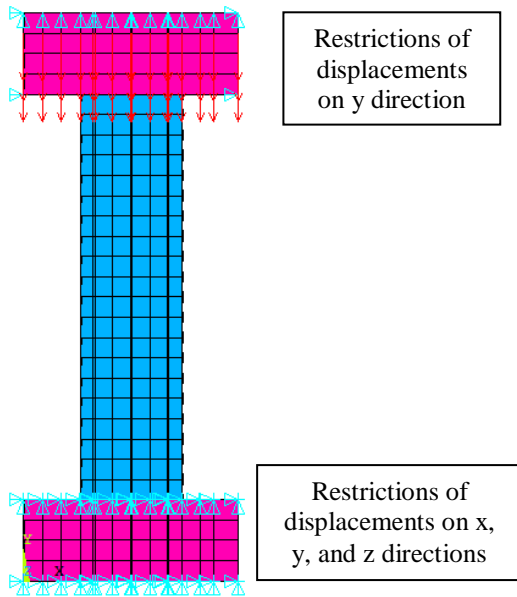


Fig. 9 Boundary Conditions of FE Model

Nodes at the bottom of the column are restrained in all translational degrees of freedom, and the top of the column is restrained in the vertical y direction. The lateral y direction is restrained since the column prevent any displacement in this direction. The nodes at the two edge lines of the column are coupled in the vertical y direction to ensure all the nodes associated with this line move together. The nodes located at the middle face of the column along the direction of the applied displacement are coupled in the horizontal x direction. It should be noted that the boundary conditions were the same for all loading cycles. The final boundary conditions of FE model is shown in Figure 9.

### Loads

The loading in the study was applied as follows: Constant axial load, approximately 1031 kN was applied to the top face column. This is represented in the FE model by applying a point pressure of 1.4 kN on the upper elements (steel plate) of a total nodal area of 717. The loading history for the model is based on story drift and is the one recommended for use in the experimental study [4]. This is represented in the FE model by applying the displacement in cycles of loading and unloading at the top edge of the column. The incremental loading cycles were controlled by story drift,  $R$ , defined as the ratio of lateral displacements to the column height,  $\delta/h$ . The lateral load sequence consisted of one cycle to each story drift,  $R$  of 0.5, 1, 1.5, 2, 3 and 4% followed by half cycle to  $R$  of 5%, as shown in Figure 10.

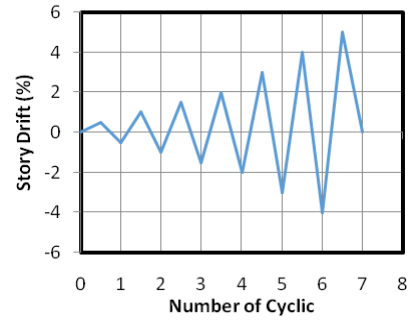
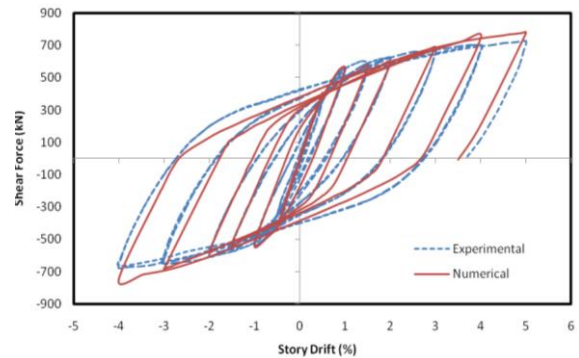


Fig. 10 Lateral Cyclic Load History

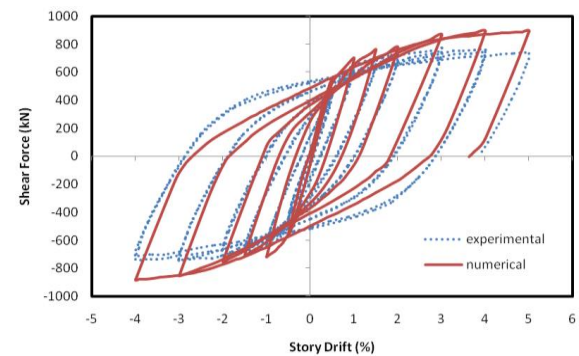
## RESULT AND DISCUSSIONS

### Hysteresis Characteristics

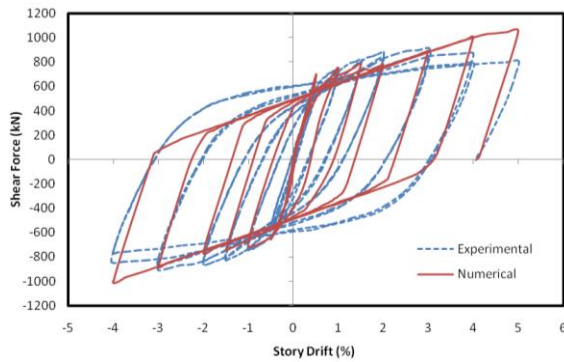
The comparison of shear versus story drift relationships between all specimens and FE model are plotted in Figure 11. The blue dotted and red lines drawn in these figures represent the measured hysteresis loops of the specimens and FE models of EWECS column, respectively. The yield and maximum strengths and the corresponding story drift for each specimen are listed in Table 1. The yielding of each specimen was assumed when the first yielding of steel flange and/or web at the top and bottom of the columns was observed, while the yielding of FE model was observed when the principal strain in the encased steel was reached by around 0.002, as seen in Figure 12.



(a) EWECS Column with SSR = 2



(b) EWECS Column with SSR = 1.5



(c) EWECS Column with SSR = 1

Fig. 11 Comparison of Hysteresis Loop between Experimental and Numerical Results

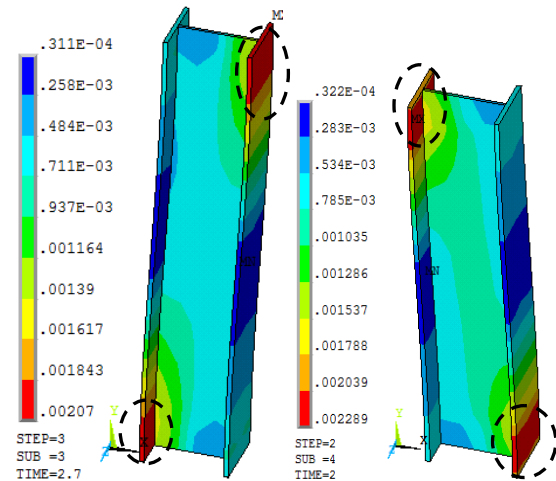
Table 1 Comparison of measured strength between experimental specimens and FE models

Model	Study	At Yielding		Max. Capacity	
		Qy (kN)	Ry (%)	Qmax (kN)	Rmax (%)
WC1	Exp.	386	0.5	728	5
	Num.	367	0.55	772	5
WC2	Exp.	423.1	0.5	771.9	3
	Num.	454	0.49	951	5
WC3	Exp.	666.2	0.64	916	3
	Num.	613	0.58	1022	5

In Specimen WC1 with a shear-span ratio of 2.0, the first yielding occurred on steel flange when the applied load was 386 kN and R of 0.5 %, while in the FE model, the first yielding occurred on steel flange at R of 0.55%. From Figure 11 (a), it can be seen that the specimen and FE models showed ductile and stable spindle-shaped hysteresis loops without degradation of load-carrying capacity until R of 5%. The maximum capacity of the specimen was reached in the last story drift of 725 kN, while the maximum capacity was 778 kN in the FE model. This was approximately 6.8% higher than the results obtained from the experiment. Good correlation exists in all stages of lateral cyclic loading. The FE and experimental results are almost the same in the each stages of cyclic loading, and the FE results are greater than those of the experimental results (within 5.5%) in the each stage of loading cycles.

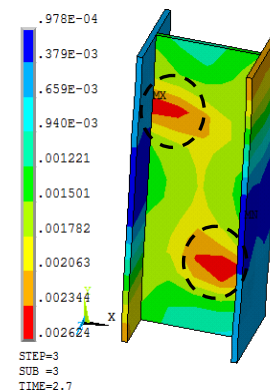
For Specimen WC2 with a shear-span ratio of 1.5, the first yielding also occurred on steel flange at shear force of 423.1 kN and R of 0.5%, while in the FE model, the first yielding occurred on steel flange at R of 0.49%. From Figure 11 (b), it can be seen that the FE model showed ductile and stable spindle-shaped hysteresis loops without degradation of load-carrying capacity until last story drift with maximum capacity of 972 kN, while the hysteresis loop of the

specimen have a little strength degradation after attaining the maximum capacity of 771.9 kN at R of 3%. This was approximately 6.8% higher than the results obtained from the experiment. Good correlation exists in all stages of lateral cyclic loading. The FE and experimental results are almost the same in the each stages of cyclic loading, and the FE results are greater than those of the experimental results (within 8.4%) in the each stage of loading cycles. The maximum capacity of Model WC2 was higher than that of Model WC1.



(a) WC1

(b) WC2



(c) WC3

Fig. 12 The principal strain at first yielding of the FE models

Specimen WC3 with the smallest shear-span ratio showed the highest maximum capacity among the tested specimens. However, the yielding location of this specimen was different from the other two specimens. The first yielding of the specimen occurred on the steel web at shear force of 666.2 kN at R of 0.64%, while in the FE model, the first yielding occurred on steel web at R of 0.58%. From Figure 11 (c), it can be seen that the specimen showed ductile and stable spindle-shaped hysteresis



loops, while the FE model showed pinching-shaped hysteresis loops without degradation of load-carrying capacity until story drift,  $R$  of 5%. The maximum capacity was reached at shear force of 916 kN and  $R$  of 3% in the specimen, while the maximum capacity of FE model was 1022 kN at  $R$  of 5%. The maximum capacity of Model WC3 was higher than that of other models. The FEA results are greater than those of the experimental results (within 11%) in the each stage of loading cycles.

### Failure Mode

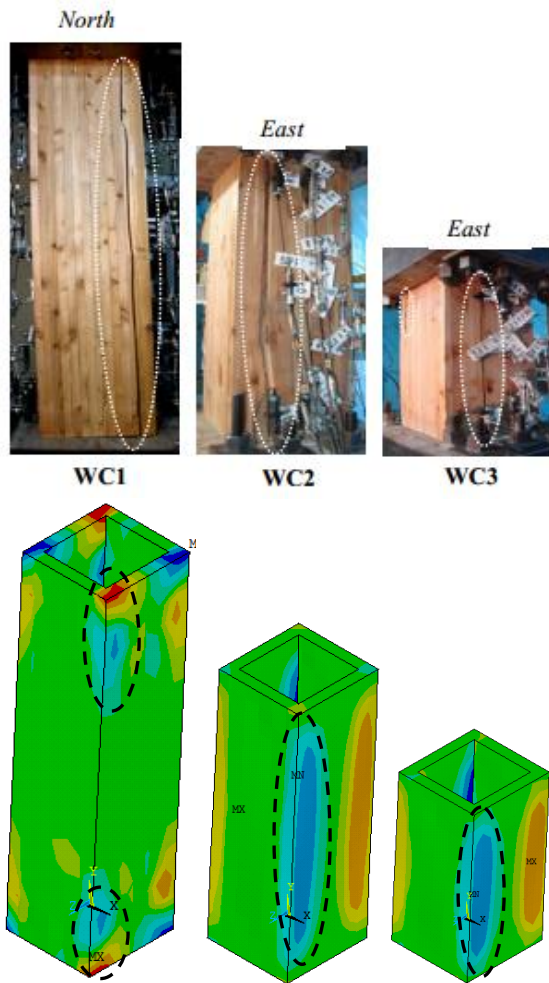


Fig. 13 Comparison of failure mode of wood panel between experimental and FE result

In Specimen WC1, within a drift ratio of 3 %, the first cracks in the wood panel occurred in the North side of the column face at around 30 cm away from the top of the column. This is also seen on the FE model, that the cracks on the wood is indicated by the principal shear stress in the wood was higher than the tangential shear strength of the wood suggested by Calderoni et al. [12] was averaged at 7.44 MPa at the location where the wood panel of the column were assembled together by using wood

glue, as seen in Figure 13 (a). Cracks also formed at the opposite side of the column, propagated along the column height.

For Specimen and Model WC2, the first cracks of wood panel occurred at  $R$  of 3% in the East side of the column. In FE model, the cracks occurred on the wood panel of the column at a shear stress of approximately 7.8 MPa, as shown in Figure 13 (b). Subsequently, the cracks extended along the column height with the increase of story drift.

In Specimen WC3, the first cracks of wood panel occurred at  $R$  of 2% in the East side of the column, while in the FE model, first cracks occurred at  $R$  of 3% as indicated by the principal shear stress in the wood approximately 7.3 MPa. The cracks extended along the column height with the increase of story drift.

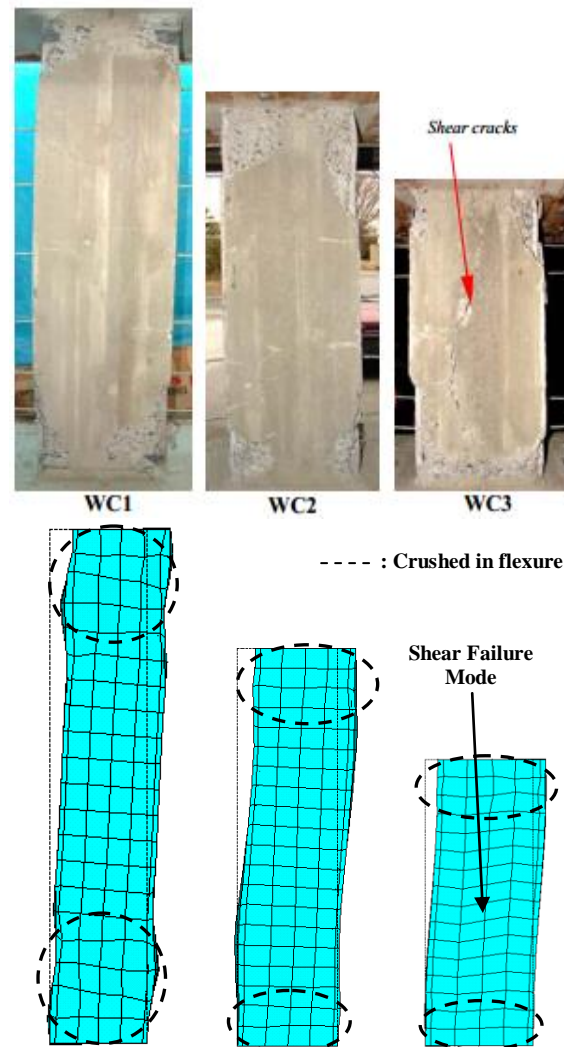


Fig. 14 Comparison of failure mode of concrete between experimental and FE result

From test results, it was found that the shear-span ratio also greatly affected the observed cracking patterns of the wood panel at the column

faces. The cracks extended with increasing story drift. Finally, the wood panel was split along the column height for all specimens. From the figure, it can be seen that Specimen WC3 with the smallest shear-span ratio had the most damages in which the cracks of the wood panel occurred in both East and North sides of the column. This indicates that the damage of wood panel becomes dominant with decreasing the shear-span ratio.

After the test of experimental, the wood panel was removed from the columns to visually inspect the damage. It was observed for all specimens and models that the in-filled concrete had crushed in flexure at both the top and bottom of the column, and no local buckling occurred at the encased steel. In addition, shear cracks occurred along the column height in Specimen WC3 and no shear cracks was observed for the other two specimens, as shown in Figure 14.

## CONCLUSION

- (1) The FE model proved to be effective in producing results that were in good agreement with the experimental results in the elastic and plastic ranges.
- (2) The response envelope from the FEA correlated fairly well with experimental results. Good correlation exists in all stages of cycling loading. Specifically, the FE results for the peak loads are smaller than the experimental results within 6.8%; 8.4%; and 11% in the each stages of cyclic loading for FE models WC1, WC2, and WC3, respectively.
- (3) A smaller shear-span ratio led to a higher shear force for the composite columns. The ultimate strength of EWECS columns increased with decreasing the shear-span ratio.
- (4) The stress distribution on the FE models representing the failure mode of the EWECS column specimens well. The damage of the columns in the wood panel and the CES core became dominant with decreasing the shear-span ratio.

## REFERENCES

- [1] Fauzan, Kuramoto, H., Shibayama, Y. and Yamamoto, T., "Structural Behavior of Engineering Wood Encased Concrete-Steel Composite Columns," Proceedings of JCI, Vol.26, No.2, 2004, pp. 295-300.
- [2] Fauzan, Kuramoto, H. and Kim, K-H., "Seismic Performance of Composite EWECS Columns using Single H-steel," Proceedings of JCI, Vol.27, No.2, 2005, pp. 307-312.
- [3] Fauzan, and Kuramoto, H., "Experimental and Analytical Study on Structural Performance of Engineering Wood Encased Concrete-Steel Composite Columns," Proceedings of the Third International Conference on ASEM, Seoul, Korea, September, 2004, pp. 1447-1459.
- [4] Fauzan, Kuramoto, H., Matsui, T., and Kim, K.-H. (2006). "Seismic behavior of composite EWECS columns with varying shear-span ratios." Proceedings of JCI, 28(2), 1357-1362.
- [5] ANSYS Version 14.0, User and Theory Reference Manual, 2004.
- [6] Meas, K., Fauzan, Matsui, T., and Kuramoto, H. (2006). "Seismic behavior of engineering wood encased concrete-steel composite structural systems, Part I: Effect of shear studs on behavior of EWECS columns." Proc., Architectural Institute of Japan, AIC, Tokyo, 1181-1182.
- [7] Kuramoto, H., Li, B., Meas, K., and Fauzan. (2011). "Experimental and Analytical Performance Evaluation of Engineering Wood Encased Concrete-Steel Beam-Column Joints". Journal of Structural Engineering ASCE, pp. 822-833.
- [8] Saenz, L. P. (1964). "Discussion of equation for the stress-strain curve of concrete." J. Am. Concr. Inst., 61(9), 1229-1235.
- [9] Al-Mahaidi, R. S. H. (1979). "Nonlinear finite element analysis of reinforced concrete deep members." Rep. No. 79-1, Dept. of Structural Engineering, Cornell Univ., Ithaca, NY
- [10] William, K. L., and Warnke, E. P. (1975). "Constitutive model for the triaxial behavior of concrete." Int. Association for Bridge and Structural Engineering, Proc., Vol. 19, IABSE, Zurich, Switzerland.
- [11] Hawileh, R.A. (2010). "Nonlinear finite element analysis and modeling of a precast hybrid beam-column connection subjected to cyclic loads". Journal Applied Mathematical Modelling Sciencedirect 34, pp. 2562-2583.
- [12] Calderoni, C., Matteis, G. D., Giubileo, C., and Mazolani, F. M. (2006). "Flexural and shear behavior of ancient wood beams: Experimental and theoretical evaluation." J. Struct. Eng., 28(5), 729-744.

## **EXPERIMENTAL INVESTIGATION ON BOX-UP COLD-FORMED STEEL COLUMNS IN FIRE**

Fadhluhartini Muftah<sup>1</sup>, Mohd Syahrul Hisyam Mohd Sani<sup>2</sup>, Ahmad Rasidi Osman<sup>3</sup>, Shahrin Mohammad<sup>4</sup>,  
Shek Poi Ngian<sup>5</sup>

<sup>1</sup>Faculty of Civil Engineering, Universiti Teknologi Mara Cawangan Pahang, 26400 Bandar Jengka, Pahang, Malaysia;

<sup>2</sup>Faculty of Civil Engineering, Universiti Teknologi Malaysia, 81310 Skudai, Johor, Malaysia

### **ABSTRACT**

Cold-formed steel (CFS) is a popular material with various advantages. Its easy production and assembly give engineer an option to speed the construction process. However, thinness relates to the major issue of buckling, especially when dealing with high temperature. The unprotected CFS behaviour under fire is expected to have a little strength as compared to hot-rolled steel. Information on such behaviour is still limited. Fire resistance testing on built-up box CFS column was presented in this paper. Two fire resistance tests were carried out under compression load. The Standard ISO 834 Fire Resistance Test under 50% and 70% degree of utilisation measured the temperatures at several points of the steel column surface by using surface thermocouple and axial column deformation. For reference purpose, one same static test at ambient temperature was carried out to assess the load bearing capacity. Results found that the failure temperature of built-up CFS could reach up to 515°C and 443°C within 8 minutes and 7 minutes resistant time for 50% and 70% degree of utilisation, respectively. Based on deformation analysis, buckling temperature of the column was 448°C and 394°C with critical time of 7 minutes for 50% and 70% degree of utilisation, respectively. This concluded that the higher degree of utilisation result in lower critical temperatures of the columns.

*Keywords: Cold-formed steel, Standard ISO 834 fire, buckling temperature, buckling time*

### **INTRODUCTION**

In the event of fire, much loss was identified, such as people injury, huge damage, loss of life, loss of capital, and production. Data from the Malaysian Fire and Rescue Department reported that Malaysia were facing with 5,248 fire cases in 2011. Housing was recorded as the highest cases at 2,761 and was dramatically increased from 2001 to 2007 [1]. Efficient method of construction involving innovate building material is the main considerations to support modern building design requirement. Hence, the use of cold-formed steel (CFS) as the main structure, i.e. column, is broadly significant due to its various advantages. The fire safety information about this material is still limited and somehow still unavailable in any practical design guideline. Usually the technical time is 20 minutes for other structure type, but it was unsuitable for the CFS type of structure. Moreover, CFS failure gives little or even no warning on unlike wood structure with cracking and moaning sounds [2].

Currently, the design of structure on fire is applied as fire safety factors that proposed based on fire testing such as for stainless steel column design under fire condition. Most CFS related research was done under elevated temperature, but not under direct fire, such as real fire stimulation [3] - [8]. This

research trend happened because the required information is on the performance of wall made up with an embedded CFS wall which may be covered with a fire retention material. Hence, information on elevated temperature is fairly enough. Moreover, the local buckling failure was observed as similarly as failure mode in ambient temperature [9]. Research on CFS at high temperature were broadly explored on the material strength models according to various parameters, such as thickness and steel grade by using CFS from different countries. Hence, the strength of CFS structure was predicted based on these models. Currently, the EN 1993-1-2: 2005 is meant for hot-rolled steel material is also practiced for CFS. The section always considered as Class 4 section. Annex E has stated the reduction factor material property for Class 4 section. The limiting temperature stated in National Annex is 350°C for all degrees of utilisation.

The ISO 834 fire curve is widely used to test the fire resistance of materials under the category "A" fire hazard, i.e. with the fire hazard rating based on the burning rate of general combustible building materials and contents. The study of cold-formed structural column under fire was conducted by [10] using stainless steel material. A fire design multiplier of 1.37 was used for design buckling resistance. It was valid for stainless steel hollow



column with utilising the buckling resistance design equation in EC3-1.2. The research on CFS under ISO 834 standard fire was conducted by [11]. The column section was open channel and built-up I (2C). It was loaded under compression and the heat was generated from an electric furnace. The exposed temperature was lower temperature from the Standard ISO 834 fire curve in the early fire state, might result column fail at longer duration. The results show that the CFS had lower resistant time and temperature and the exposed temperature was slightly lower. It has produced a conservative finding. Research conducted by [12] reported that the unprotected restrained column for section factor (F/V) of  $424.6 \text{ m}^{-1}$  experienced a temperature increase very quickly, almost the same as the atmosphere temperature. The buckling temperature is the temperature at which the axial deformation reaches a maximum value, while the column failure temperature is defined as the temperature at which the axial force in restrained column returns to its initial value.

Previous studies found very limited information of CFS column exposed to the Standard ISO 834 fire. This research evolution trend may be due to the thickness of CFS is thin and may fail due to various buckling modes which are unsuitable for column structure. However, adopting the current design guideline, which is mainly used for hot-rolled steel and has clearly different production method, this practice is barely inappropriate. A practical solution for this issue is by conducting a fire test on CFS column. The test was conducted in the Construction Research Centre (CRC) at Universiti Teknologi Malaysia in Skudai, Johor. The test involved a box-up column. Two columns with different degree of utilisation were studied. The column was supported on constant constrain. The objective of this study is to evaluate the temperature rise behaviour of CFS column when exposed with the Standard ISO 834 fire.

## MATERIALS AND METHODS

A channel with lipped column was supplied by a local manufacturer in Johor, Malaysia. The channel size is 200 mm depth, 73 mm width of flanges, 17 mm lipped size, thickness is 1.9 mm, round corner is 2.5 mm and centroid is 20.38 mm from the web. The column height is 3 m. Each column was constructed as a built-up section by using two identical lipped channel sections. Two of the channel sections were connected at their flanges by using self-drilling screws, at 400 mm c-c spacing along the length. It will form a box-up section with a self-drilling screw in the middle of the flange.

The end column was screwed to the two steel angles at both column webs. It used to restrain lateral movement of the column. A circular steel

plate was used to place the bottom and top end of the column. It is used to ensure the load was uniformly distributed over the column cross-section. Column top was attached in the same manner at the bottom. Meanwhile, fire test support was improved to prevent support expansion due to fire. All steel-end plates, angle and steel-based, were coated with 3 mm high temperature coating paint. 20 mm ceramic fibers, which were covered with steel-based and thermocouple were placed at the bottom of column to monitor the temperature. Temperature measured was less than  $100^{\circ}\text{C}$ . The rise of temperature data in the column was captured by a surface type K thermocouple. The thermocouple position along the length of the column and in the column section was according to BS EN 13381-4:2013 (E) recommendation. Figure 1 shows the of the thermocouples position on the column height and at the cross-section. Since the column is unrestrained, the axial deformation was allowed during fire exposure. The axial deformation of column was also monitored based on the actuator movement. The ambient and a series of fire tests were conducted under the same actuator and loading frame. At ambient test, the CFS column was loaded until it failed. During the fire test, the column was loaded till reach a constant load level for 5 to 10 minutes before the fire was introduced inside the furnace. The test was stopped until the load dropped, which was considered that the column had failed. A hydraulic jack loading system with maximum load of 1000 kN were used to load the column with loading rate of 0.25 kN/s.

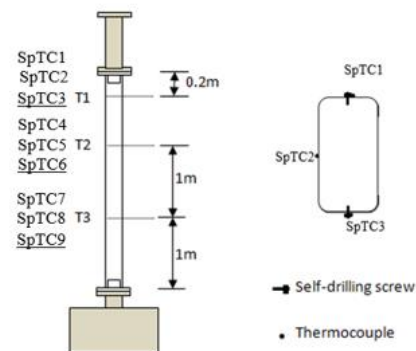


Fig. 1 Location of thermocouple on the column

ISO 834 standard fire curve and 15% percentage deviation (de) from a standard fire curve, as shown in Fig. 2(a), was according to BS EN 1363-1:2012 (E). The graph also plots the furnace average temperature curve for all samples during testing. The furnace consists of six blowers. 3 blowers located at left and right side of the furnace, which by location were at the top side, middle side and bottom side of the furnace. Furnace fire was produced by a gas furnace which transfers heat to the CFS through radiation and convection. Convection will cause the

air particles (gases) to spread out and become dense, causing a movement of gases. Cooler gas is dense and warmer gas is less dense and thus causes warmer gases to rise up. Radiation does not require a medium to transfer heat. The CFS shiny surface is poor in absorbing radiation heat.

The furnace pressure should be approximately 8.5 Pa per-metre height within  $\pm 5$  Pa after 5 minutes during fire, as recommended in BS EN 1363-1:2012 (E). Pressure inside the furnace was presented in Fig. 2 (b), which shows that the furnace pressure during the fire test was within an acceptable range.

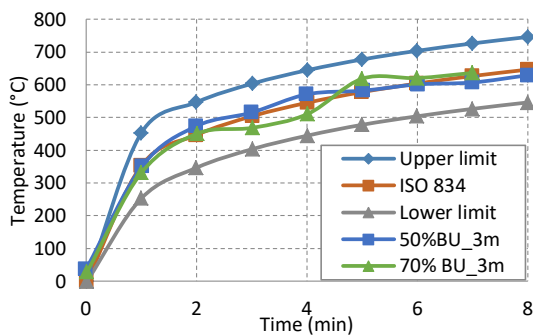


Fig. 2(a) Furnace average temperature during testing for Box-up column

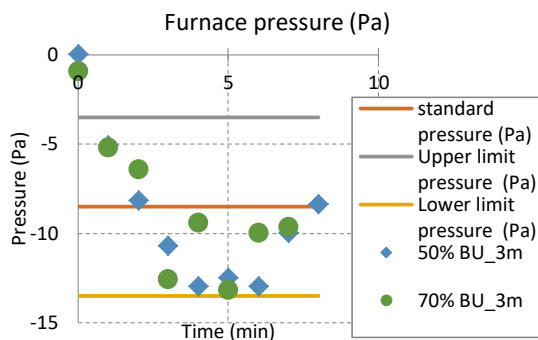


Fig. 2(b) Furnace pressure

## RESULTS AND DISCUSSION

### Compression Strength of CFS Column

The strength test of the column at ambient temperature results that the ultimate compression load is 170 kN. The calculation ultimate load prediction from EC3-1.3 is 162.34 kN. Loading for 50% and 70% degree of utilisation were 85 kN and 119 kN, respectively. It was calculated bases on normal strength test.

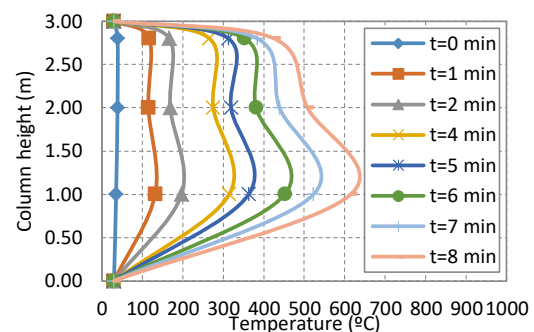
### Temperature Rise in CFS Column

Nine thermocouples gave reliable results, whereby the steel temperature rise over time of fire

exposure was observed. It was found that the CFS temperature rise was propositional to the fire exposure time for all stations. Thermocouples located at 200 mm from top support and loading were known as SpTC1–SpTC3. The rise of temperature at this location was lower the Standard ISO 834 fire for all degrees of utilisation until the column failed. The rate of temperature rise of 50% and 70% degree of utilisation was similar for all the thermocouples except for SpTC6. This may happen due to uneven fire blow during testing. The rate of temperature rise was also similar for different degrees of utilisation. It can be concluded that the rate of temperature rise of the BU CFS column was constant for CFS and independent to the degree of utilisation. It was found that rise of temperature at the bottom was faster as compared to the top. This may happen because the heat in the furnace was pressured to the bottom of the furnace and may be due to some heat losses from the ceramic fibre on top of the furnace. A technician can feel the temperature around the outer furnace top. The 70% load utilisation failed at lower temperatures as compared to the 50% load utilisation. In addition, the 70% load utilisation had a lower failure temperature than Standard ISO 834 fire curve in contrast with the 50% load utilisation, was failed when approaching the ISO 834 fire curve.

SpTC5, SpTC7, SpTC8, and SpTC9 for 50% degree of utilisation rose up to the Standard ISO 834 fire curve at failure while for 70% degree of utilisation, the column failed at lower temperatures.

SpTC7, SpTC8, and SpTC9 were temperatures at the lower column. SpTC5 was the temperature at 2m from the bottom, specifically at the web of the box-up CFS. SpTC4 and SpTC6 were located at the flanges which had double thickness, resulting in a lower failure temperature. The greater web thickness and thermal conductance between the two CFS profiles have caused these respective behaviours [11].



(a) 50% BU\_3m

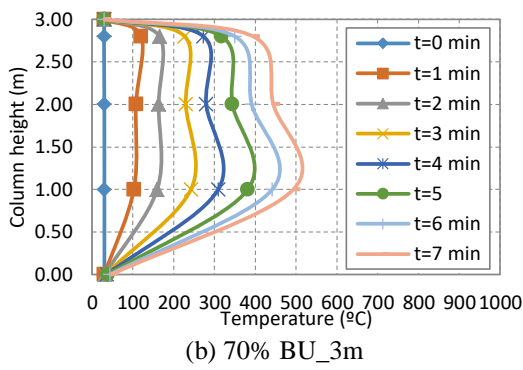


Fig. 3 Temperature evolution along the length of Box-up column

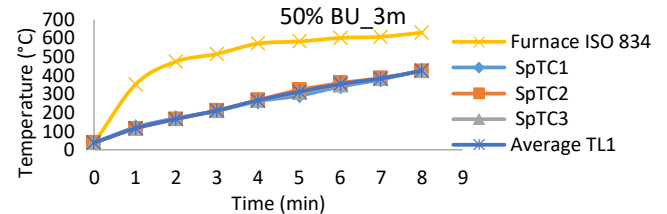
Fig. 3 shows the temperature evolution of CFS column due to different load utilisation. At the beginning of fire exposure until failure time both columns evolved at a uniform temperature and slightly higher temperature at the bottom. The evolution of temperature was independent to the degree of utilisation of the column.

### Mean Temperature

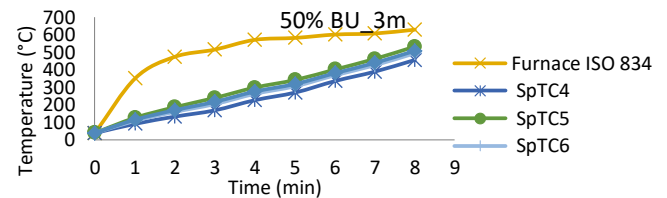
This section explains the analysis of a mean temperature for the column. The evaluation of mean temperature along the column was calculated by using the weightage area methods in which the temperatures recorded were multiplied to the area of column surface and divided by the total area of the column. This method was applied to account for the area coverage near the thermocouple that represented the flange and web surface temperature. Figure 6 and Figure 7 shows the temperature for 50% and 70% load utilisation, respectively.

Level T1 for 50% load utilisation recorded a similar value for all surfaces as in Fig 4(a). Hence, the average is directly determined by a simple average. As the lower side of the column was high in temperature at, a difference in temperature at respective levels was found. The temperature at web was higher than at the flanges due to the thicker thickness as in Fig 4 (b) and (c). However, the difference in temperature was less than 10%, hence the calculated simple average can be accepted. The analysis was continued with depth detail on the average TL for each column. TL3 resulted in a higher average followed by TL2 and TL1 as in Fig. 4(d). This behaviour was similar for the 70% degree of utilisation. All columns had the same temperature rise behaviour where the upper thermocouple registered a lower temperature until column failure. This may be caused by the thermocouple located nearer to the ceramic fibre which supported the column end. The heat was shielded by a ceramic fibre that restricted the conductance of heat to this position.

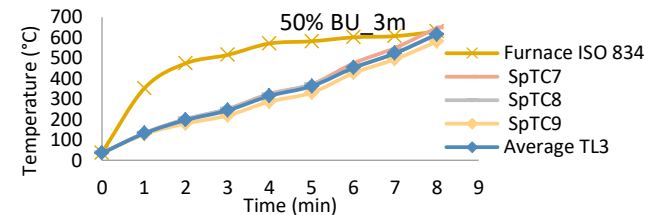
To select the appropriate mean temperature for the column, the minimum, maximum and average temperature for each level was plotted. Again, the difference between all values was small, hence the average value was selected. Table 1 shows the mean temperature for each degree of utilisation.



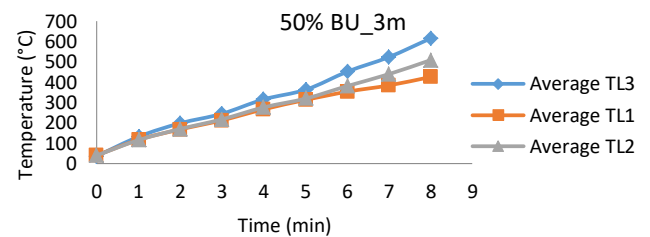
(a)



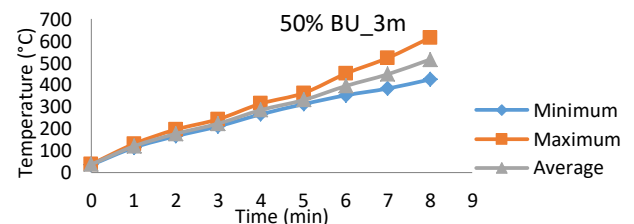
(b)



(c)



(d)



(e)

Fig. 4 Evaluation of mean temperature along the column for 50% degree of utilisation

Table 1 Mean temperature of the column

Time	Degree of utilisation (%)	
	50	70
0.0	30	30
1.0	121	110
2.0	177	162
3.0	224	233
4.0	285	287
5.0	331	347
6.0	395	394
7.0	448	444
8.0	515	-

### Failure Time and Failure Temperature

The consideration in fire safety design is concerned about preventing structural failed before resistant period. The evaluating of the critical temperature steel column is characterised as a uniform temperature all over the column surface. The critical temperature was determined by evaluating the results of the maximum temperature gain from the experiment, the highest values of the average temperature for each thermocouple level, and the highest value from the mean temperature. Figure 5 plots the temperature values against degrees of utilisation. Furthermore, the safe temperature value in selecting the critical limiting temperature, the smallest value was considered. As expected, the resistant time was decreased as the degree of utilisation was increased. Then, both the initial and average heating rates were calculated by using the temperature at the first 1 minute, meanwhile the value of the average heating rate was according to the temperature and time of the column at failure. The load applied on the column does not affect the heating rate of the column and this was also reported by [11]. The heating rate of 60°C/min was constant for all box-up columns. The initial heating rate of 84°C/min is higher at for the column due to rate of Standard ISO 834 was higher at 329°C/m at the first 1 minute. The critical temperature for box-up column was 515.95°C and 443.77°C and the critical time was 8 and 7 minutes for 50% and 70% degree of utilisation, respectively. The degree of utilisation was increased results in decreasing of critical temperature and time.

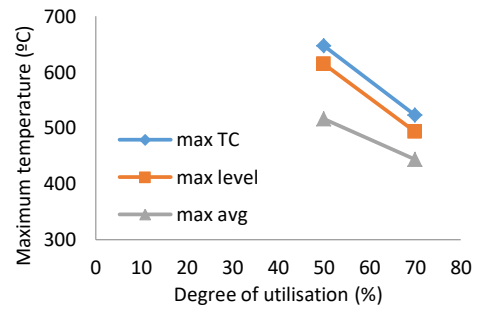


Fig. 5 Evaluation of critical temperature

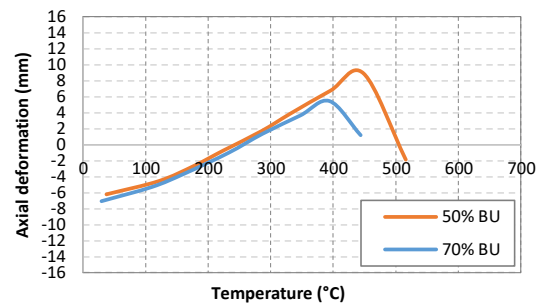


Fig. 6 Variation of axial deformation over the box-up CFS column means temperature.

The axial deformation of the column was analysed against the mean temperature rise of the column and the results were presented in Fig. 6. The column had an initial deformation due to load level application of 50% and 70% load utilisation. The axial deformation was accounted after the column was fired. According to the buckling temperature definition given by [12], the buckling temperature is considered at the maximum axial deformation of the column. It was found that the buckling temperatures of the column were 448°C and 394°C, with critical time of 7 minutes for 50% and 70% degree of utilisation, respectively. This concluded that the higher degree of utilisation resulted in lower buckling temperatures of the columns. Both values, critical temperature and buckling temperature, would be significant in predicting future CFS fire resistance design. Figure 7 shows the testing configuration and buckling failure of the CFS column under Standard ISO 834 fire exposure.



Fig. 7 (a) Test set-up (b) buckling of box-up column

## CONCLUSION

This paper found that the temperature rise in CFS is independent to the degree of utilisation for box-up CFS columns. According to the recorded analysis for all degrees of utilisation, it can be concluded that there was a constant rate of temperature rise of the box-up CFS column. The heating rate was 60°C/min and the initial heating rate was 84°C/min. The temperature behaviour of BTB column showed both degrees of utilisation, the flanges recorded a lower temperature as compared to the flange due to the greater thickness. It was found that critical temperature was 515.95°C and 443.77°C and critical time was 8 and 7 minutes for 50% and 70% degree of utilisation, respectively. While buckling temperature was 448°C and 394°C with critical time of 7 minutes for 50% and 70% degree of utilisation, respectively. Thus, findings concluded that the higher degree of utilisation resulted in lower critical and buckling temperatures of columns. The buckling resistance time was not dependent on the degree of utilisation.

## ACKNOWLEDGEMENTS

This research was funded by the Ministry of Higher Education Malaysia and Universiti Teknologi Mara (UiTM) through the Fundamental Research Grant Scheme grants. The technical support from the Laboratory of Structures and Materials, Faculty of Civil Engineering, Universiti Teknologi Malaysia and UiTM are greatly appreciated.

## REFERENCES

- [1] Salleh N and Ahmad A, "Fire safety management in heritage buildings: the current scenario in Malaysia, 1996 (Table 1)", (2009). Retrieved from <http://irep.iium.edu.my/1085/>.
- [2] Thompson KK, (2006), Retrieve at <http://www.fireengineering.com/articles/print/volume-159/issue-6/features/the-dangers-of-lightweight-steel-construction.html> (3/10/13).

- [3] Chen J and Young B, "Cold-formed steel lipped channel columns at elevated temperatures", *Engineering Structures*, Vol. 29(10), 2007, pp. 2445–2456.
- [4] Feng M, Wang Y and Davies J, "Structural behaviour of cold-formed thin-walled short steel channel columns at elevated temperatures. Part 1: experiments", *Thin-Walled Structures*, Vol. 41(6), 2003a, pp. 543–570.
- [5] Feng M, Wang Y, and Davies J, "Structural behaviour of cold-formed thin-walled short steel channel columns at elevated temperatures. Part 2: Design calculations and numerical analysis", *Thin-Walled Structures*, Vol. 41(6), 2003b, pp. 571–594.
- [6] Feng M, Wang YC and Davies JM, "Axial strength of cold-formed thin-walled steel channels under non-uniform temperatures in fire", *Fire Safety Journal*, Vol. 38(8), 2003c, pp. 679–707.
- [7] Kaitila O, "Imperfection sensitivity analysis of lipped channel columns at high temperatures", *Journal of Constructional Steel Research*, Vol. 58(3), 2002, pp. 333–351.
- [8] Ranawaka T and Mahendran M, "Distortional buckling tests of cold-formed steel compression members at elevated temperatures", *Journal of Constructional Steel Research*, Vol. 65(2), 2009, pp. 249–259.
- [9] Kankanamge ND, "Structural behaviour and design of cold-formed steel at elevated temperature", Thesis, (2010).
- [10] Gardner L, & Ng KT, "Temperature development in structural stainless steel sections exposed to fire", *Fire Safety Journal*, Vol. 41(3), 2006, pp. 185–203.
- [11] Craveiro HD, Rodrigues JPC, and Laím L, "Cold-formed steel columns made with open cross-sections subjected to fire", *Thin-Walled Structures*, Vol. 85, 2014, pp. 1–14.
- [12] Wang P, Wang YC and Li GQ, "A new design method for calculating critical temperatures of restrained steel column in fire", *Fire Safety Journal*, Vol. 45(6-8), 2010, pp. 349–360.
- [13] BS EN 13381-4: Test methods for determining the contribution to the fire resistance of structural members - Applied passive protection to steel members.
- [14] BS EN 1363-1: Fire resistance tests. General Requirements.
- [15] EN. 1993-1.3: Design of steel structures. General rules - Supplementary rules for cold-formed members and sheeting.
- [16] EN. 1993-1.1: Design of steel structures. General rules and rules for buildings. Brussels, Belgium: European Committee for Standardization (CEN); 2005.
- [17] EN. 1993-1.2: Design of steel structures. General rules. Structural fire design. Brussels, Belgium: European Committee for Standardization (CEN); 2005.



## **EXPERIMENTAL INVESTIGATION OF COLD-FORMED STEEL CHANNEL SECTION WITH NOTCH**

Mohd Syahrul Hisyam Mohd Sani<sup>1</sup>, Fadhluhartini Muftah<sup>3</sup>, Muhammad Isha Ismail<sup>4</sup>

<sup>1</sup>Faculty of Civil Engineering, Universiti Teknologi Mara Cawangan Pahang, Kampus Jengka, 26400 Bandar Jengka, Pahang, Malaysia

### **ABSTRACT**

Cold-formed steel (CFS) channel section is a construction material that often been used in the building and still in the research for utilising in structural element. The advantages of the CFS channel section such as lightweight, anti-corrosion and etc are becoming so interesting in selecting it as a roof purlin, roof truss system and storage rack. For having the structure element with strong, safe and stable condition, the study of the CFS with the notch is carried out to determine the behaviour. The parametric study is taking place to determine the suitability of notch pattern whether the notch depth and spacing is affecting the ultimate load of the CFS channel section column and beam. The study of the CFS channel section is divided into two parts, the first part is to examine the ultimate load of the column in varies of notch depth and the second part is to determine the ultimate load of the beam in varies of notch spacing. By referring the study of the notch depth on CFS channel column section, the result of the ultimate load is obtained to have the reduction about 19-80% of variation of notch depth when compared with normal section. Although, the CFS channel beam section with variation notch depth is influenced of approximately 4-14% when compared with CFS channel normal beam section.

*Keywords: Cold-formed steel, Notch, Ultimate load, Column, Beam*

### **INTRODUCTION**

Cold-formed steel (CFS) is a structural and building material that has been introduced broadly in construction such as a roof truss system, wall panel, storage pallet rack and etc. CFS with a lot of advantages in construction such as highest strength to weight ratio, impervious to termites, rot and mold, recyclable, non-combustibility, cost-effectiveness and anti-corrosion. Currently, CFS is shifted as a structural element rather than before, for only non-structural element. There is comprehensive information about the design of the CFS in the codes especially Eurocode 3 or American Iron and Steel Institute (AISI). However, there are having not clear information and design of the CFS as structural element, such as a column or beam with a notch or perforated.

The notch can be referred that steel structure is discontinuities in cross-sectional geometry as example v-shape, semi-circle shape square-shape and etc or non-uniformity of material [1]. Generally the steel notch is produced to provide some spacing to mechanical and electrical service activity in the building. The study of the steel notch is significant to certify the structure is could be utilised back if there are some failure happened on it. There are two types of the notch counting of V-notch and U-notch in the previous study. Additionally, fatigue of the steel structure is existed when the fatigue loading occurred at plastic strain and produced the surface defect such as a notch or cracking. The notch of the

steel is the main problem that always been discussed by researchers because of its fatigue issues. It is happened due to the localised or restricted changes of the steel structure with producing the concentration stress on the location of the notch and lastly growth of cracking. Reference [2] has explained about the fatigue design limit for conventional parts are acquired at stress cycles of  $10^7$  for determining and designing the allowable stress.

There are a lot of researchers studied about the notch which become popular for stopping the failure of the material and structure. Reference [3] has analysed the fatigue of complex notch that established from welded joints. Welded joint for industries purpose such as offshore, oil and gas, and building is used as a joint between structure member to provide safety and stability of the construction [3]. Reference [4] has clarified the tensile residual stresses from the welding activity for steel assemblies is combined with initial stress from steel component is lead to crack initiation. Others researchers that study on the notch made from welded joints are [5] and [6].

Reference [7] has reported the result of compression testing of the concrete filled steel tubular (CFST) short column with notch and the performance of the column when subjected to the material imperfection. So, the notch in the steel tubes is reacted as the material imperfection problem which must be solved to obtain the excellent in the structural integrity and also

extended their service life [7]. Besides, the notch length, orientation and location are proposed for determining the column performance and load-strain response. As the result, the ultimate load of the CFST short column is decreased with increasing of the notch length. Reference [8] has reported the mechanical behaviour of the circular concrete-filled steel tube short column subjected to axial concentrated load and also the impact of the steel tubes due to geometry imperfection.

Reference [9] has explored the crack growth resistance of a sharp notch of the high strength rail steels for their mechanical properties. There are three test specimens including smooth, short gauge and pre cracked single-edged-notched bending specimen that used in the railway industry [9]. Reference [10] explained the structural integrity of the structure is evaluated by assessing the defect condition or flaw assessment procedures derived from the mechanics of fracture approaches such as loading and temperature. Furthermore, many researchers are studied about the notch as a crack and defects of the section or material such as [11], [12], [13] and [14].

There is no information about CFS with notch for column and beam in design, standard and previous study. Besides, there are a lot of studies about steel notch as an imperfection, welding and cracking effect but no information about the steel notch as an initial work before being curve of the steel component. CFS is cut with same notch spacing and width but varieties of notch depth as a preliminary study to form CFS curved section. Cut-curved method is one of the methods that's been utilised in curving process and other method are cold-curved and hot-curved process. Cut-curved method is chosen due to the simple way of process and also avoids using the skill workers, high technology machine and high cost equipment. For producing the CFS curved section, the notch depth must be studied to determine the physical effect of the section before being curved, ultimate load and also the load-deformation behaviour. Reference [15] has stated that the mitred bends by cut-curved is produced the smooth bends for impractical circumstances such as uneconomical and limited space factor.

Usually, many studies are only emphasized on the tensile load either flat or coupon tensile specimen but for column and beam structure in actual size or small scale is still deficient. Additionally, there is no standard and experimental method that's been utilised in evaluating the performance of the structure with notch. Hence, the objective of the study is to investigate the mechanical behaviour especially the ultimate load of the CFS column and beam section with a variety of notch depth under concentrated load. Finally, the paper determines the behaviour of the CFS with

notch to propose some new information and understanding of production of the CFS cut-curved.

## SPECIMEN PREPARATION AND TEST SETUP

A CFS channel section with lipped and double intermediate web stiffener is chosen and clean. A CFS channel section with double intermediate web stiffener is selected to avoid the local buckling on early stage and as a reference of the cut limit. The cross-section and section dimension of the CFS channel section are tabulated in Fig. 1 and Table 1. Besides that, the section dimension of the testing specimen is taken because the section is easy to get from construction material suppliers. The initial geometric imperfection and residual stress of the section is ignored. The ratio between the section and element is tabulated in Table 1 for checking the appropriateness of the section dimension due to deformation ability and allowable stability.

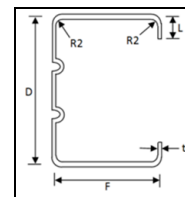


Fig. 1 The cross-section of the CFS channel section

Table 1 The section dimension and properties of CFS channel section

Section dimension			
Notes	Value	Notes	Value
Web, $D$	75 mm	Flange, $F$	34 mm
Lipped, $L$	8 mm	Thickness, $t$	1 mm
Area, $A$	148	Yield	550
	mm <sup>2</sup>	Strength, $\gamma_s$	MPa
Ratio			
$F/t = b/t$	34.0	$F/L$	4.25
$D/F = h/b$	2.21	$D/t = h/t$	75.0
$D/L$	9.38	$L/t = c/t$	8.0

The section is cut by using an electric saw with notch width of 3 mm and notch spacing which measured centre to centre of 100 mm as a constant value. There are two experiments is arranged, the first experiment is a column specimen with varies of notch depth and second experiment is still a variation of notch depth but for beam specimen. The first experiment is obtained three column specimens with difference notch depth and profile is illustrated in Table 2 and Fig. 2. The section is cut according to three parts of notch depth for column and beam specimens. First part, the section is cut from the bottom flange until bottom intermediate web stiffeners with 14 mm of notch



depth from the bottom of the CFS channel section. Second part, the section is cut to half of the total height of the CFS channel section with notch depth of 37.5 mm. The section is cut from the bottom flange until upper intermediate web stiffeners with notch depth of 60 mm for the last part. The notch depth of 14 mm, 37.5 mm and 60 mm are compared with an overall depth of the CFS channel section without notch is roughly about 81.3 %, 50 % and 20 %, respectively. The height of the column is 400 mm and the length of the beam is 250 mm.

Table 2 The profile of CFS with notch

Notes	Value Data
Notch width, a	3 mm
Notch spacing, c	100 mm
Notch depth, d	14 mm, 37.5 mm, 60 mm
Ratio	
a/t	3.0
c/t	100
d/D	0.19, 0.50, 0.80

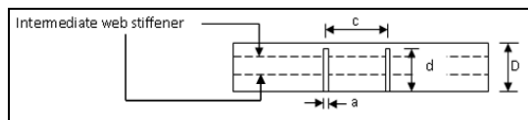


Fig. 2 The schematic diagram of CFS channel section with notch.

Table 3 is represented the specimen profiles and labels for column and beam specimen. The compression test of the CFS channel section of column and beam with the variety of notch depth is tested by using the Universal Testing Machine (UTM) with a capacity of 100 kN. The end support condition for column specimens are acknowledged as a semi-rigid end support which utilise the steel plate 6 mm that attached to the compression steel jigs. The column specimen is situated on the surface of the steel plate at the upper and bottom side of the support by using self-drilling screw and monitored the fixity of the specimen to avoid the movement. Two of the linear variable deformation transducers (LVDT) are placed in the middle of the column height of flange and web element, and one LVDT is located on the steel plate to measure the axial shortening of the specimen as shown in Figure 3 (a) and (b). The height of the CFS channel column section is 400 mm.

Meanwhile, the end support condition for beam specimens are also recognised as a semi-rigid end support condition. Two plates and one steel rod are used for every end support to avoid the movement. Two LVDTs are located on mid-span of the web beam and end of the flange beam. The 50 mm extensometer is also being used for determining the mid-span flange deformation as shown in Figure 4.

The length of the CFS channel beam section is stated of 250 mm. Both specimens are utilised the pace rate of the loading of the UTM is 1 mm/min. All LVDTs is connected to a data logger to acquire the value of the web and flange deformation.

Table 3 Specimen profile and label for a CFS channel section for both experiments

Specimen profile	Label
Experiment One - Column	
CFS without notch section	CFS-CC0
CFS with notch depth of 14 mm	CFS-CC1
CFS with notch depth of 37.5 mm	CFS-CC2
CFS with notch depth of 60 mm	CFS-CC3
Experiment Two - Beam	
CFS without notch section	CFS-CB0
CFS with notch depth of 14 mm	CFS-CB1
CFS with notch depth of 37.5 mm	CFS-CB2
CFS with notch depth of 60 mm	CFS-CB3

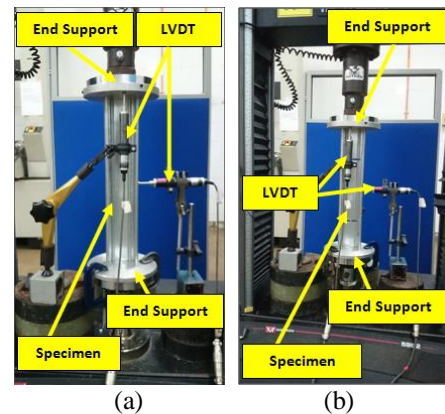


Fig. 3 The compression testing arrangement and setup of the CFS channel section column specimen (a) without notch and (b) with notch.

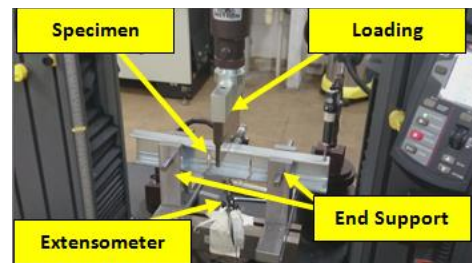


Fig. 4 The flexural testing arrangement of the CFS channel section beam specimen.

## RESULT AND DISCUSSION

The mechanical behaviour of the column and beam specimen is calculated and analysed.

### Mechanical Behaviour of CFS Channel Column Section with Difference Notch Depth

The result of the compression behaviour of a CFS channel column section especially ultimate load, axial shortening and failure mode shape is represented in Table 4. From the table, the CFS-CC1 is the largest value of ultimate load and lowest value of axial shortening at ultimate load when compared with other CFS-CC specimen with notch. The percentage different of ultimate load between CFS-CC1 with CFS-CC2 and CFS-CC3 is approximately 5.51% and 8.52%, respectively. The ultimate load of the specimen is decreased with increasing of the notch depth. The ultimate load of the CFS-CC specimen is not extensively affected and influenced even if the notch depth in a high percentage. The percentage difference of the ratio notch depth over the section web between CFS-CC without notch and CFS-CC1, CFS-CC2 and CFS-CC3 is 19%, 50% and 80%, respectively. 56.85% of the ultimate load percentage difference between CFS-CC0 with CFS-CC1 is recorded. Furthermore, the difference of axial shortening at ultimate load between CFS-CC0 with CFS-CC1, CFS-CC2 and CFS-CC3 in percentage is represented roughly 17.44%, 18.08% and 18.39%, respectively. The axial shortening at ultimate load for CFS channel section with the notch is not showing significant changes between all specimens. This is because the specimen is no longer having the compression deformation but the specimen is demonstrated to have the small rotation or known as distortional buckling. Besides, the notch depth is getting smaller when compression load is applied and the peak at both sides of the notch is touching each other. Lastly, the axial shortening at ultimate load is increased when the notch depth is increased. Failure mode shape for all specimens is reported having local and distortional buckling. All specimens is stated to meet the local buckling in early loading and finally shifted to distortional buckling with the movement of the both flange from the origin.

Table 4 Compression behaviour testing of CFS channel section with and without notch depth

Specimen	Ultimate Load (N)	Axial shortening (mm)	Failure mode shape
CFS-CC0	42,410.55	2.13	L & D
CFS-CC1	18,299.17	2.58	L & D
CFS-CC2	17,290.63	2.60	L & D
CFS-CC3	16,739.64	2.61	L & D

Note: L-Local buckling and D-Distortional buckling

The detail of the specimen from initial applied load to failure load with compression deformation

is illustrated in Fig. 5. The initial stiffness of CFS-CC0 is higher than other specimens and CFS-CC1 is higher than CFS-CC2 and CFS-CC3. CFS-CC2 and CFS-CC3 is illustrated having the same pattern of load-deformation behaviour because the notch depth is located more than 50% of the web depth and percentage difference of notch depth between them is 37.5%. Therefore, the initial stiffness is decreased when the notch depth is increased. Some example of the failure of the CFS-CC0 and CFS-CC3 is shown in Fig. 6. Circle line in the figure is shown the location of the critical failure which has proven the local and distortional buckling is existed. The flange element is more critical to deflect and buckle when compared to the web element. However, the CFS-CC channel section with the notch is capable to avoid the large deformation at the flange and cause the overall column structure to bend to weak axis.

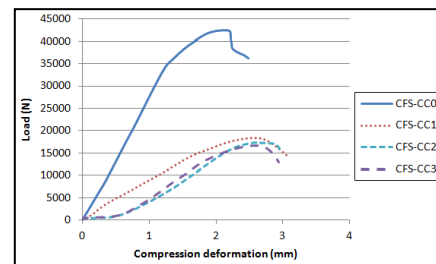


Fig. 5 Applied load versus compression deformation graph.

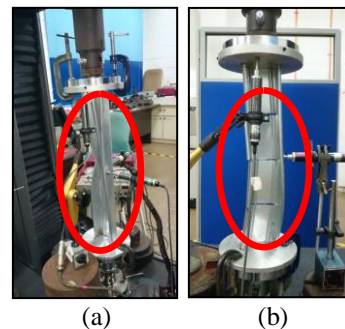


Fig. 6 The schematic diagrams of (a) CFS-CC0 (b) CFS-CC3 after fail.

### Mechanical Behaviour of CFS Channel Beam Section with Difference Notch Depth

The result of the flexural behaviour of a CFS channel beam section for instance ultimate load and the moment is tabulated in Table 5. The ultimate load of CFS-CB without notch is recorded to have 6,931.42 and the highest value of the ultimate load among of the CFS-CB with notch is 6,598.15. The percentage difference between them is expressed around 4.80%. It showed that the notch depth with less than 50% of the cut along the web depth is not

influenced the ultimate load and the moment of the section. This is because the beam is categorised as a short beam with less of deformation and bending condition when compared to slender beam. 16.93% and 35.14% of comparison percentage between CFS-CB1 with CFS-CB2 and CFS-CB3, respectively is reported. Additionally, the percentage difference between the CFS-CB0 with CFS-CB2 and CFS-CB3 is noted having 20.93% and 38.26%, respectively. Lastly, a summary that can be designated is that when the notch depth is increased, the ultimate load of the beam decreased.

The failure mode shape of the CFS-CB is tabulated in Table 5. All specimens are observed having a local buckling in the early stage of loading and shifted to distortional buckling in the middle period of loading. Table 5 also mentioned about the flexural deformation of mid-span flange at ultimate load and flexural deformation of the overall beam at mid-span under the applied load. The flexural deformation of mid-span flange is noted to have non uniform and uncertain data because of the location and depth of the notch. When the notch depth is not achieved the second web stiffener or middle of the section, the flexural deformation is still in a stable condition but if the notch depth is

reached the second web stiffener, the beam has lost its stability and strength. The percentage difference between the CFS-CB0 with CFS-CB1 and CFS-CB2 is recorded to meet about 4.14% and 11.90%, respectively. The load-flexural deformation graph at mid-span flange is illustrated in Fig. 7 and showed that the initial stiffness and line pattern of CFS-CB0 and CFS-CB1 is same. Meanwhile, the initial stiffness and stability of the CFS-CB is decreased with increasing of the notch depth. The percentage difference between CFS-CB3 with CFS-CB0 is 14.07%. In addition, the flexural deformation of overall bending at mid-span is increased when the notch depth is increased. The percentage difference between the specimen with the lowest value, CFS-CB3 and the specimen with the highest value is 99.31%. Fig. 8 is shown applied load versus the flexural deformation of overall bending at mid-span. From the figure, the initial stiffness of the CFS-CB without notch is higher when compared with CFS-CB with notch. This is because the CFS-CB has lost its stability, strength, toughness and stiffness if the section is cut vertically though small by following the direction of the applied load.

Table 5 The result of CFS channel beam section under three pinned bending

Specimen	Ultimate Load (N)	Moment (Nmm)	Flexural deformation at mid-span (mm)		Failure mode shape
			Flange at ultimate load	Overall bending	
CFS-CB0	6,931.42	433,213.75	5.80	0.05	L & D
CFS-CB1	6,598.15	412,384.38	5.56	0.85	L & D
CFS-CB2	5,480.94	342,558.75	5.11	2.40	L & D
CFS-CB3	4,279.27	267,454.38	6.75	7.26	L & D

Note: L – Local buckling and D – Distortional buckling

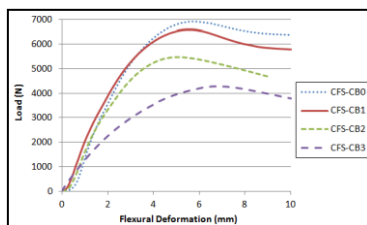


Fig. 7 Applied load versus flexural deformation of mid-span flange under load graph.

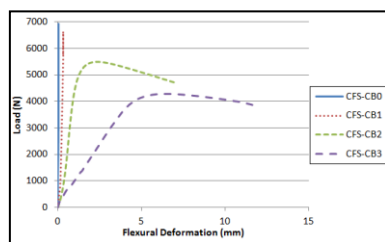


Fig. 8 Applied load versus flexural deformation of overall mid-span beam graph.

When the load is applied, the beam with higher notch depth is able to open in widespread, added more stress at the end of the notch and eventually cause the part to be torn. CFS-CB2 and CFS-CB3 are illustrated to have the additional gap of the notch width to 40-60%. From observation, the CFS-CB channel section with the notch is so flexible and elastic when load is applied, and form into large deformation. But, after the applied load is released, the beam is capable to form back to original shape with less deformation. The flange element at top side is more critical compared with bottom side. Whilst as, the web element for CFS-CB0 and CFS-CB1 are not critical when distinguished with CFS-CB2 and CFS-CB3 channel section. The failure of local and distortional buckling of the CFS-CB is less deformation compared with the CFS-CC specimen this is due to slenderness.

## CONCLUSION AND RECOMMENDATION

CFS-CC1 channel section which notch location below the web stiffener is a specimen that has a higher value of ultimate load and lower value of axial shortening at ultimate load when compared with other specimen with notch. Besides that, 56.85% and 17.44% of ultimate load and axial shortening at the ultimate load percentage difference between CFS-CC0 with CFS-CC1 is achieved. Consequently, the notch depth is increased and the ultimate load of the specimen decreased.

CFS-CB1 channel section is a specimen with the highest value of ultimate load among the specimen with notch and percentage difference when compared with specimen without notch is 4.80%. The failure mode shape of the specimen is recorded having local and distortional buckling. Initial stiffness of the CFS-CB1 is in a good result when compared with CFS-CB2 and CFS-CB3.

For further study, some experiment for several of cross-section and section dimension must be done to get the good relationship between the ultimate load and cross-section.

#### ACKNOWLEDGEMENTS

The authors gratefully acknowledge the financial support from Ministry of Higher Education, Malaysia under the Fundamental Research Grant Scheme for Universiti Teknologi Mara (UiTM) Pahang. Thanks are also extended to Faculty of Civil Engineering of UiTM Pahang, Kampus Jengka and Universiti Teknologi Malaysia (UTM) Skudai, Johor for providing laboratory equipment.

#### REFERENCES

- [1] Bader Q and Kadum E, "Effect of V notch shape on fatigue life in steel beam made of AISI 1037", *Qasim Bader Int. J. of Engineering Research and Applications*, Vol. 4 (6), 2014, pp. 39-46.
- [2] Akiniwa Y, Miyamoto N, Tsuru H and Tanaka K, "Notch effect on fatigue strength reduction of bearing steel in the very high cycle regime", *International Journal of Fatigue*, Vol. 28 (11), 2006, pp. 1555-1565.
- [3] Lagoda T, Bilous P and Blacha L, "Investigation on the effect of geometric and structural notch on the fatigue notch factor in steel welded joints", *International Journal of Fatigue*, Vol. 101, 2017, pp. 224-231.
- [4] Ibrahim OA, Lignos DG and Rogers CA, "A probabilistic approach for assessing discontinuities in structural steel components based on Charpy-V-notch test", *Engineering Structures*, Vol. 147, 2017, pp. 1-11.
- [5] Berto F and Fergani O, "A review of the notch rounding approach under in plane mixed mode loading", *International Journal of Fatigue*, Vol. 101, 2017, pp. 127-136.
- [6] Bilous P and Lagoda T, "Structural notch effect in steel welded joints", *Materials and Design*, Vol. 30, 2009, pp. 4562-4564.
- [7] Ding F, Fu L and Yu Z, "Behaviors of axially loaded square concrete-filled steels tube (CFST) stub columns with notch in steel tube", *Thin-walled Struct.*, Vol. 115, 2017, pp. 196-204.
- [8] Chang X, Fu L, Zhao H-B and Zhang Y-B, "Behaviors of axially loaded circular concrete-filled steel tube (CFT) stub columns with notch in steel tubes", *Thin-walled Struct.*, Vol. 73, 2013, pp. 273-280.
- [9] Yu F, Ben Jar P-Y and Hendry M, "Fracture behaviour at the sharp notch tip of high strength rail steels – influence of stress triaxiality", *Engineering Fracture Mechanics* Vol. 178, 2017, pp. 184-200.
- [10] Horn AJ, Sherry AH and Budden PJ, "Size and geometry effects in notched compact tension specimens", *International Journal of Pressure Vessels and Piping*, Vol. 154, 2017, pp. 29-40.
- [11] Torabi AR and Alaei M, "Mixed-mode ductile failure analysis of V-notched Al 7075-T6 thin sheets", *Engineering Fracture Mechanics*, Vol. 150, 2015, pp. 70-95.
- [12] Hassan AR and Radhi SH, "Effect of the crack geometry and notch on stress intensity factors in bonding of materials", *Academic Research International*, Vol. 4 (4), 2013, pp. 93-103.
- [13] Cicero S, Madrazo V and Garcia T, "The notch master curve: A proposal of master curve for ferritic-pearlitic steels in notched conditions", *Engineering Failure Analysis*, Vol. 42, 2014, pp. 178-196.
- [14] Aratani M and Knott JF, "The growth of short fatigue cracks ahead of a notch in high strength steel", *Engineering Failure Analysis*, Vol. 17, 2010, pp. 200-207.
- [15] Neilson R, Wood J, Hamilton R and Li H, "A comparison of plastic collapse and limit loads for single mitred pipe bends under in-plane bending", *Int. J. of Pressure Vessels and Piping*, Vol. 87, 2010, pp. 550-558.

## **A REVIEW OF UNEXPECTED LARGE SLOPE FAILURES**

Marthinus Sonnekus<sup>1</sup> and John Victor Smith<sup>2</sup>

<sup>1</sup>School of Engineering, RMIT University, Melbourne,  
Australia

### **ABSTRACT**

Significant advancements in the application of soil and rock mechanics have been achieved in managing the risk of large scale slope instability. In practice, however, unexpected slope failures do occur, sometimes with significant safety and economic implications for nearby communities, public infrastructure or the environment. This review focus on large slope failure case studies, considering the slope failure mechanisms and the effectiveness of the controls adopted in managing the geotechnical risk. The role of appropriate data collection and interpretation in underpinning analysis methods is investigated. The impact of levels of uncertainty of input data on different methods of analysis is addressed in the paper. In some instances, the slope failure mechanisms are not understood and can therefore not be incorporated into geotechnical models. It is also found in this review that the safety implications for communities located in the failure path were not initially evident, in some case, resulting in significant loss of life. A thorough understanding of the failure mechanism and triggers is essential for assessing slope stability conditions. In addition, reliable stability monitoring, geological and hydrogeological data are required for determining slope stability conditions. It is also evident from this review that time dependent behavior is likely to result in shear strength reduction and should be considered for long term slope stability.

*Keywords: Slope stability, slope failure, Southern Leyte, Guinsaugon, Vaiont, Yallourn Mine*

### **INTRODUCTION**

Large landslides can be highly complex in terms of failure mechanisms and movement history [1]. The examples reviewed here include a natural slope in a remote location, a natural slope in the vicinity of a large engineering project and a cut slope in an open pit mine. The role of geology, landforms and geotechnical conditions related to each failure are reviewed. Geotechnical issues include the failure mechanism, the role of progressive failure, geotechnical parameters and reliability and failure triggers. The lessons learned in each case and by comparison of the cases are identified.

### **GUINSAUGON LANDSLIDE**

A large slope failure occurred on 17 February 2006 at St Bernard, Southern Leyte province in the Philippines. The failure volume is estimated at between 20 to 25 million cubic meters with a runout distance of almost four kilometers [2]. The maximum velocity of the failure was estimated at between 120 to 130 m/s [3]. The failure resulted in the destruction of the Guinsaugon village with more than 1,000 people being killed and many more displaced.

### **Geology**

Leyte Island is in the central part of Philippine islands. The archipelago is in one of the most active geological settings on earth. The Philippine Fault Zone, NW-SE orientated 1,200km long fault system traverses the Leyte Island. The fault is actively moving with a mean slip rate of  $26 \pm 10$ mm/year at an azimuth of about N130°E [4].

The Geological Map of the Philippines indicates that the landslide developed in a succession of Upper Miocene-Pliocene interbedded sedimentary, volcanic and volcanoclastic rocks [5]. Field mapping undertaken in the Guinsaugon landslide area consist of sandstone, breccias and mudstones with faults and defect infill comprising smectite clay [6].

### **Natural landform**

The failure is bound at the crest of the 780 m a.s.l Mount Can-abag. This ridge is approximately 30 km long and is a geomorphic expression of the active Philippine Fault Zone. The pre-landslide topography was characterized by steeply dipping slopes that formed a wedge geometry. The slope release area is approximately 780 to 400 m a.s.l on the eastern slope of Mount Can-abag [3].





Fig. 1 Scar of the Guinsaugon landslide above intensively farmed plains (photograph by Christian Arnhardt, 2010).

## Geotechnical

### *Failure mechanism*

The Guinsaugon failure mechanism was structurally controlled with failure on defects that were continuous, slickensided and weathered with a smectite clay infill. The Philippine Fault Zone resulted in the weakening of the rock mass strength. Kinematic analysis suggests a wedge failure mechanism with a plunge towards the east [7].

It was proposed by [2] that the Philippine fault zone may have acted as a release surface i.e. the failure was initiated along the fault zone.

It is expected that high porewater pressure would have developed in the rock mass and along the defects due to heavy rainfall. It was found in a study by [3] that increasing pore water pressure significantly affected the calculated Factor of Safety (FoS) of the slope.

At the base of the slope the landslide debris spread out almost 3 km<sup>2</sup> over flooded paddy fields. The extensive spread is the result of reduced frictional resistance at the base of the debris mass sliding on the flat flooded rice paddies [2].

### *Progressive failure*

Post-landslide studies indicate that there are no slope movement and groundwater level monitoring data. There are also no records of inspections to identify cracks or other signs of slope instability. In addition, it would have been difficult to locate tension crack due to the dense tropical vegetation and difficult terrain. The absence of monitoring data makes it difficult to determine the progressive failure mechanism and to calibrate stability models.

If movement and piezometric data were available, it may have indicated the onset of the landslide. Residents observed small failures a few months and

days before the landslide. Other indications include cracking and muddy water flow of the Aliho Creek that flows down the mountain [2].

### *Geotechnical parameters and reliability*

There is very limited laboratory testing data available for the Guinsaugon landslide. Intact cored samples were obtained for Uniaxial Compressive Strength (UCS) testing with results ranging from 17.9 to 23 MPa [3]. The number of tests, rock type and reliability of test work are not known.

The calculated rock mass (and defect) cohesion range between 0.45 and 0.78 MPa and the angle of friction between 22.9° and 32.2° [3].

The shear strength of the clay infill is not known.

### *Failure triggers*

No direct triggers for the Guinsaugon landslide could be identified [2], [5], [7]. Heavy rainfall preceded the landslide and two minor earthquakes occurred the day of the failure.

The Leyte island is characterized by a total annual rainfall of approximately 3,640 mm. This has resulted in deep tropical weathering profiles [5].

During February 2006, 970.8 mm rainfall was recorded at the Otikon rainfall station. This was significantly more than the average rainfall of 275 mm for February. The heaviest recorded rainfall of 687.8 mm occurred from 8 to 16 February [2]. This rainfall would have resulted in significant pore water pressure buildup in the rock mass and along defects. There would have been relatively limited time for drainage.

Two minor earthquakes were recorded in Southern Leyte Island on the day of the landslide. There is uncertainty if the earthquakes induced the landslide. Some authors believe the magnitudes are well below the threshold that would be required to induce the landslide. It is also possible that the landslide itself could have caused the ground tremors [2], [5], [7]. It is possible that the occurrence of the earthquakes may not have any relationship with the Guinsaugon landslide.

## Lessons Learned

Practical monitoring methods such as the identification of tension cracks, changes in slope geometry, changes in creek flows and the reporting of small failures to authorities should be encouraged.

Slope movement and hydrogeological data is important in the development and calibration of stability models. In the case of the Guinsaugon landslide this data doesn't exist. There is also very limited geological, geotechnical and hydrogeological information available. Most of the data were only collected after the landslide and this make

geotechnical back analysis work difficult.

In landslide prone areas geotechnical mapping and drilling can be highly beneficial in understanding geotechnical conditions and obtaining samples for geotechnical testing purposes.

With technological advancements, it is possible to set up a very cost effective and accurate slope monitoring system. Groundwater levels can be monitored by drilling observation bores and installing piezometers.

Geological mapping of the pre-historic landslides in the Guinsaugon area will aid in the understanding of failure mechanisms, volumes, triggers and perhaps even the frequency of landslides. Authorities should continue to develop and implement a Landslide Risk Management Plan with alert levels for monitoring and evacuation of villages.

## VAIONT LANDSLIDE

The Vaiont valley is situated in the Italian Alps, approximately 90 km north of the city of Venice.

The Vaiont landslide occurred on 9 October 1963 with approximately 270 to 280 million cubic meters of material suddenly sliding from the northern slope of Mt. Toc into the Vaiont reservoir. The failure resulted in a 245 m high wave that overtopped the 260 m high double curved arced dam. The flood wave destroyed Longarone and nearby villages. It is estimated that more than 2,000 people were killed in the disaster [8], [9].

### Geology

The Vaiont valley slopes comprise of middle Jurassic limestone and overlain by upper Jurassic limestone with clay and Cretaceous limestone [9]. Multiple clay layers occur near the base of lower Cretaceous stratigraphic units [10].

### Natural landform

The 300 m deep valley was formed by glacial and fluvial action in an asymmetric syncline [9]. The deep and narrow gorge made it ideal for dam construction. The dam is located just above the junction of the Vaiont and Piave rivers.

There is evidence of the existence of an old landslide on the northern slope of Mt. Toc. Air photo studies identified evidence of the landslide that includes drainage pattern changes, bulges and depressions in the slope geometry [10].

### Geotechnical

#### *Failure mechanism*

Although numerous geotechnical studies have been published since the Vaiont landslide there is

still uncertainty on the failure mechanism.

The re-activation of an ancient landslide would have resulted in very low shear strength along the pre-existing sliding surface. The low shear resistance could have contributed to the high failure velocity of 20 to 30 m/s [11]. A residual friction angle as low as 5° may even be possible [12].

The presence and influence of clay beds in the landslide have been widely discussed. Some authors dismiss the presence of any clay beds while others have described the presence of these layers in the stratigraphy and even conducted laboratory testing on the clay beds [10], [13].

Some authors propose that sliding occurred along 5 to 15 cm thick bands of clay 100 to 200 m deep within the limestone mass. The clay layers are sub-horizontal near the gorge and further out dip at 35° towards the valley [9]. It is possible that persistent rainfall and raising the reservoir level resulted in increased pore water pressure [9], [10].

If a clay sliding surface is at sufficient depth, then the clay may exhibit brittle type behavior due to the formation of microscopic cracking. This may also explain the rapid failure that occurred [9].

Another recent study described a 30 to 60 m thick shear zone at the base of the landslide [8].

### *Hydrogeology*

Two aquifers are present in the northern slope of Mount Toc. The upper aquifer was mainly influenced by the reservoir level and the lower aquifer by both the reservoir and rainfall. The two aquifers may be separated by a continuous clay layer [12].

Limited groundwater level data was obtained from three boreholes with open standpipes. The standpipes only recorded the average groundwater levels for the different hydrogeological units encountered. In addition, the piezometers did not reach down to the sliding surface. The reliability of groundwater data is one of the biggest obstacles in understanding the effect the reservoir levels may have had on slope movements [12].

There is also evidence of karstic conditions at Mt. Toc, suggesting transmission of high groundwater pressures along a possible clay sliding surface [10].

### *Progressive failure*

Three cycles of raising and lowering of the reservoir water commenced in February 1960 until the landslide occurred. During the first cycles a small failure occurred on March 1960 and a 2 km long tension crack opened up. A second failure of 700,000 m<sup>3</sup> occurred on 4 November 1960. Displacement rates of up to 3.5 cm/day were recorded. During the third cycle movement velocities continuously increased with rates of up to



20 cm/day [12].

#### *Geotechnical parameters and reliability*

Direct shear test results on the clay material ranged between 5° and 22°. Back analyzed effective friction angle values calculated by various authors ranged between 17° to 39°. The back analyzed values are considerably higher than the direct shear results. The back analysis was complicated by not having reliable groundwater data [10].

#### *Failure triggers*

It is possible that rainfall and raising and lowering of the reservoir levels could have acted as triggers for the landslide [12]. It was difficult to correlate the piezometric levels with the rainfall and water level of the reservoir [11].

Seismic events were recorded from May 1960 until the landslide occurred. However, the seismic events could not be located with confidence as there was only one seismometer installed at the Vaiont dam [9].

#### **Lessons Learned**

It is very important to incorporate the correct failure mechanism into slope failure models. In the Vaiont landslide there still appears uncertainty on the failure mechanism and hydrogeological conditions that could have contributed to the landslide.

An adequately designed slope monitoring system can provide valuable insight into the failure mechanism and early warning of an impending landslide. Instrumentation such as borehole extensometers can be used to locate deep seated sliding surfaces.

Groundwater observation bores should be drilled to the correct depths and equipped to ensure reliable and representative readings are obtained for each hydrogeological unit. Modern grouting techniques have simplified the installation of vibrating wire piezometers.

Geological and geotechnical field investigation may include comprehensive mapping, drilling and laboratory testing programs. It is important that experienced geologists, hydrogeologists and geotechnical engineers manage these programs.

#### **YALLOURN LANDSLIDE**

A review and discussion of some of the key findings of the Mining Warden Yallourn Mine Batter Failure Inquiry [14] is provided. The authors of this paper are also familiar with the geotechnical aspects of the Latrobe Valley brown coal mines.

The Yallourn Mine is in the Latrobe Valley,

approximately 150 km east of Melbourne in the state of Victoria, Australia. The Latrobe Valley forms part of the Gippsland Basin that holds significant brown coal deposits [15]. The coal is used for power generation at the Yallourn Power Station.

On 14 November 2007, a large landslide occurred on the approximately 80 m high North-East slope of the Yallourn East Field Mine. The failure volume was estimated at approximately 6 million cubic meters. The landslide was sudden with a runout distance of approximately 250 m [14]. The Latrobe River that is behind the North-East slope flooded the mine after the landslide. The landslide resulted in significant damage to the environment and mine infrastructure. Fortunately, there was no loss of life.

#### **Geology**

The brown coals of the Gippsland Basin were deposited during the Eocene to Late Miocene. The coal forms part of a sequence of non-marine sands, clays and coals, comprising the Latrobe Valley Group. The Yallourn seam is mined at the Yallourn Mine. Pliocene sandy clays, sands and gravels form part of the Haunted Hill Formation. [15].

The Haunted Hill overburden thickness may range from 10 to 44 m overlying 50 to 88 m of the Yallourn brown coal seam. Below the Yallourn seam there is clay, sand and other coal seams [16].

#### **Natural Landform**

The Yallourn Mine is in a relative flat area. The Morwell river is west of the Yallourn East Field Mine and flows into the Latrobe river. The Latrobe river is north of the North-East slope. The Eastern Highlands is north of the mine and the South Gippsland Highlands towards the south [17].

#### **Geotechnical**

##### *Failure mechanism*

The Yallourn coal seam is highly jointed with continuous sub-vertical joints. The dominant joint set is striking west-northwest to east-southeast and form an acute angle with the North-East mine slope [14].

Due to the low density of the brown coal, the coal slopes are prone to movement and can fail if there is a sufficient increase in the slope groundwater levels.

The Yallourn landslide is a typical horizontal block sliding mechanism. The high groundwater pressure in joints that connected to the Latrobe river and along the interseam resulted in the failure. The planned buffer distance between the pit slope and the Latrobe river was only 150 m [14].

### *Hydrogeology*

A phreatic groundwater level is present in the Yallourn coal seam. This groundwater level can be affected by rivers or rainfall runoff into open joints.

Horizontal drainholes have historically been used at the Yallourn Mine to dewater and reduce the groundwater level in the coal slopes. A decision was made around 2003 to stop the drilling of horizontal drainholes [14].

Confined aquifers are present below most of slopes for the Latrobe Valley Mines. These aquifers can be very extensive [18].

Deep aquifer dewatering has historically been required at the Yallourn Mine to manage the risk of floor heave. After various studies, it was decided in 2004 to switch off the deep aquifer dewatering bores. Unfortunately, high porewater pressures remained in the interseam clays under the North-East slope [14].

### *Progressive failure*

The movement monitoring survey pins on the North-East slope indicated accelerated movement for years before the landslide occurred.

In general, the piezometer levels on the North-East slope reduced over time. However, a few months before the failure there was a significant increase in some of the bore levels. This sudden increase may indicate hydrogeological connectivity being established between the joints that formed the failure surface and the Latrobe river [14].

In the months before the failure large cracks started forming between the pit crest and the Latrobe river. This was followed with significant inflows of water from the Latrobe river until the failure occurred. There were also significant displacement of the conveyers and other infrastructure on the North-East slope the days and weeks before the failure.

### *Geotechnical parameters and reliability*

Movement of the North-East slope in the months and years before the failure would have resulted in residual shear strength conditions in the interseam clays below the base of the coal. A residual friction angle of  $16^\circ$  was used in back analysis / validation modelling by [14]. Based on experience in the Latrobe Valley mines the residual friction angle can be significantly lower than  $16^\circ$ .

### *Failure triggers*

Various factors contributed to the Yallourn landslide as previously discussed. It is possible that a rainfall event on 4 November 2007 could have acted as a trigger for the landslide to occur.

## **Lessons Learned**

There is a long history of the block sliding failure mechanism in the Latrobe Valley brown coal mines.

The use of horizontal drainholes and deep aquifer dewatering is required to reduce groundwater pressure in both the coal joints and along the interseam clays [14]. Removing these controls, and mining very close to the Latrobe river, resulted in a significant increase in the risk of slope instability.

## **CONCLUSION**

The three large slope failures reviewed share the following features. (1) The failure mechanisms are complex and have required significant detailed investigation. (2) No single trigger event could be identified as the 'cause' of the landslide. (3) Movement on pre-existing bedrock structures was involved thus generating the large volumes involved in the landslides. (4) Water movement and related water pressure was part of the problematic conditions associated with the failures.

Risk management planning is needed in excavations, engineering projects and for communities in the vicinity of slopes. In the case of excavations such as mining, every slope requires a management plan to assess stability. All engineering projects including dams, transport corridors and building construction also require assessment of slopes in the vicinity. In remote areas it may not be reasonable to assess and monitor the stability of every natural slope. However, every community should be aware of slopes that represent a potential hazard. Risk factors such as heavy rain periods and observations such as ground cracking or anomalous surface water behavior together with associated action plans should be known by local residents.

Significant advances have been made in regional assessments of susceptibility to shallow landslides [19] but the potential for larger, deeper landslides to occur remains difficult to assess on a regional scale.

## **REFERENCES**

- [1] Hungr O, Leroueil S, Picarelli L, "The Varnes classification of landslide types, an update", *Landslides*, Vol. 11, 2014, pp. 167-194.
- [2] Orense RP, Gutierrez MS, "2006 large-scale rockslide-debris avalanche in Leyte Island, Philippines", *Earthquake geotechnical case histories for performance-based design*, 2009, pp. 31-45.
- [3] Catane SG, Cabria HB, Zarco MAH, Saturay RM, Mirasol-Robert AA, "The 17 February 2006 Guinsaugon rock slide-debris avalanche, Southern Leyte, Philippines: deposit characteristics and failure mechanism", *Bull*

- Eng Geol Environ, Vol. 67(3), 2008, pp. 305-320.
- [4] Duquesnoy TH, Barrier E, Kasser M, Aurelio M, Gaulon R, Punongbayan RS, Rangin C, "Detection of creep along the Philippine Fault: First results of geodetic measurements on Leyte Island, central Philippine", Geophysical Research Letters, Vol. 21(11), 1994, pp. 975-978.
- [5] Evans SG, Guthrie RH, Roberts NJ, Bishop NF, "The disastrous 17 February 2006 rockslide-debris avalanche on Leyte Island, Philippines: a catastrophic landslide in tropical mountain terrain", Nat. Hazards Earth Syst. Sci., Vol. 7, 2007, pp. 89-101.
- [6] Futralan KM, Biscaro JRD, Saturay RM, Catane SG, Amora MS, Villafior EL, "Assessment of potential slope failure sites at Mt. Can-abag, Guinsaugon, Philippines, based on stratigraphy and rock strength", Bull Eng Geol Environ, Vol. 69, 2010, pp. 517-521.
- [7] Guthrie RH, Evans SG, Catane SG, Zarco MAH, Saturay RM, "The 17 February 2006 rock slide-debris avalanche at Guinsaugon Philippines: a synthesis", Bull Eng Geol Environ, Vol. 68, 2009, pp. 201-213.
- [8] Barla G, Paronuzzi P, "The 1963 Vajont Landslide: 50th Anniversary", Rock Mech Rock Eng, Vol. 46, 2013, pp. 1267-1270.
- [9] Kilburn CRJ, Petley DN, "Forecasting giant, catastrophic slope collapse: lessons from Vajont, Northern Italy", Geomorphology, Vol. 54, 2003, pp. 21-32.
- [10] Hendron AJ, Patton FD, "The Vaiont slide – A geotechnical analysis based on new geological observations of the failure surface", Engineering Geology, Vol. 24, 1987, pp. 475 – 491.
- [11] Semenza E, Ghirotti M, "History of the 1963 Vaiont slide: the importance of geological factors", Bull Eng Geol Environ, Vol. 59, 2000, pp. 87-97.
- [12] Genevois R, Tecca PR, "The Vajont Landslide: State-of the Art", J. Eng. Geol. Environ Vol. 6, 2013, pp. 15-39.
- [13] Müller-Salzburg L, "The Vajont Slide", Engineering Geology, Vol. 24, 1987, pp. 513-523.
- [14] Sullivan T, "Mining Warden Yallourn Mine Batter Failure Inquiry", Victorian Government Printer, No. 156, Session 2006 – 08, 2008.
- [15] Barton CM, Gloe CS, Holdgate GR, "Latrobe Valley, Victoria, Australia: a world class brown coal deposit", International Journal of Coal Geology, Vol. 23, 1993, pp. 193-213.
- [16] Wood WJ, Dugan K, Coulthard M, Rivalland J, "Deep Aquifer Shutdown Tests at Yallourn Mine", Fifth Large Open Pit Mining Conference, 2003, pp. 205-214.
- [17] Blackburn DT, Sluiter IRK, "The Oligo-Miocene coal floras of southeastern Australia", History of the Australian Vegetation: Cretaceous to Recent, 1994, p. 329.
- [18] Schaeffer J, "Scaling Point Based Aquifer Data for Developing Regional Groundwater Models: Application to the Gippsland Groundwater System", University of Melbourne, PhD Thesis, 2008, p. 42.
- [19] Rabonza ML, Felix RP, Lagmay AM, Eco RN, Ortiz IJ, Aquino DT. "Shallow landslide susceptibility mapping using high-resolution topography for areas devastated by super typhoon Haiyan". Landslides, Vol. 13, 2016, pp. 201-210.

## THE EFFECT OF STEEL FIBERS EXTRACTED FROM WASTE TYRE ON CONCRETE CONTAINING PALM OIL FUEL ASH

Fauzan<sup>1</sup>, Febrin Anas Ismail<sup>2</sup> and Rio Sandi<sup>3</sup>

<sup>1</sup>Engineering Faculty, University of Andalas, Padang City; <sup>2</sup>West Sumatera, <sup>3</sup>Indonesia

### ABSTRACT

Tyre production is increasing every year due to the increase of vehicle sales in the world. In Indonesia, more than 50 billion waste tyre was generated per year. The generation and disposal of waste are inherent to life itself and have presented very serious problems to the human community in Indonesia. Recently, some research has been devoted to the utilization of steel fibers extracted from waste tyre (SFEFWT) in concrete. This study is focusing on the use of SFEFWT with containing palm oil fuel ash (POFA) in concrete mix. Steel fibers was extracted from chips of waste tyres by manual cutting process and cut to 1 inch (25.4mm) length. Number of cylindrical specimen of steel fibers extracted from waste tyre (SFEFWT) with addition of 0%, 0.25%, 0.5%, 0.75%, 1% and POFA with addition 15% by cement weight were used in concrete mix to fabricated and tested. The experiment has been tested at 28<sup>th</sup> day. In particular, concrete containing POFA obtain by adding SFEFWT evidence a satisfactory improvement, mostly in cracking control, compressive strength, flexural strength and also splitting tensile strength. On the other hand, compressive, flexural and tensile strength was positively affected by the additions of SFEFWT on POFA concrete. The percentage of SFEFWT on concrete containing POFA will give high number of bonding in concrete to delay the crack growth.

*Keywords: Concrete; Steel Fiber; Waste Tyre; Palm Oil Fuel Ash; Compressive Strength; Flexural Strength; Splitting Tensile Strength; Cracking Control.*

### INTRODUCTION

Facts and figures show that concrete is very common and extensively used for construction as a favorable material all over the world. Even then, there are many deficit characteristics of concrete which limits its applications, as concrete has a low stiffness, low ductility and low energy absorption. Also when concrete is hardened, shrinkage cracks appears on its surface, therefore to improve these deficiencies in concrete, now a day's variety of fiber materials are being used in concrete to improve its applications for best services. The fibers such as steel, glass, polymeric, natural and plastic fibers mixed with concrete at particular cut length and specified aspect ratio and randomly distributed, can effectively be utilized to overwhelm such deficits. However, in developing countries like Indonesia the major problem to utilize steel fibers extracted from waste tyre (SFEFWT) produced from industry is inherent to life itself. In Indonesia, more than 50 billion waste tyre was generated per year.

The use of steel fibers extracted from waste tyre (SFEFWT) is day by day increasing in structural applications because of high stress resistance, toughness and long term strength. The fibers join together in a synchronized manner and become enmeshed to aggregates and substantially fibers tend to reduce the workability of mix, this phenomenon

of concrete mix makes it less liable to segregation due to increased cohesiveness.

The addition of fibers to concrete considerably improves its structural characteristics such as static flexural strength, impact strength, tensile strength, ductility and flexural toughness [1]. The inclusion of steel fibers in concrete considerably enhanced the engineering properties of mortar and concrete [2]. Using a little percentage of steel fibers efficiently improve the load-carrying capability of slabs on ground and significantly improve the slab ductility [3]. With the inclusion of hooked steel fibers with cut length of 6 cm and aspect ratio of 80 and replacement of cement with 0.5%, and 1% improved the mechanical properties of concrete [4]. The results of ultrasonic pulse velocity revealed that the using of small percentage of steel fiber in concrete improved the quality of concrete [5]. Sata et al., (2010) investigated that the strength development of POFA concretes with w/c ratios of 0.50, 0.55, and 0.60 tended to be in the same direction. At early ages, concretes containing POFA as a cement replacement of 10, 20, and 30% had lower strength development than control concretes while at later age 28 days, the replacement at rates of 10 and 20% yielded higher strength development [6]. Hussin et al., (2008) discovered that inclusion of 20% POFA would produce concrete having highest strength as compared to any other replacement level [8]. Ahmad et al., (2008) studied that one of the potential

recycles material from palm oil industry is palm oil fuel ash which contains siliceous compositions and reacted as pozzolans to produce a stronger and denser concrete [9]. In this paper, the effect of steel fibers extracted from waste tyre on concrete containing palm oil fuel ash was studied.

## MATERIALS AND METHODS

### Materials Used

#### Cement

Ordinary Portland Cement (OPC) commonly available in market was used.

#### Fine and Coarse Aggregate

Locally available aggregates were used; fine aggregate with size retained on 200 number sieve and passing from 4.75 mm. The specific gravity and fineness modulus of fine aggregate was 2.57 respectively. The coarse aggregate used was locally available quarry having two different sizes; one fraction is passing through 20 mm sieve and another fraction passing through 10 mm sieve. The specific gravity of 20 mm and 10 mm aggregates are 2.70 and 2.60 respectively.

#### II.1.3 Water

Potable tap water was used in mix preparation.

#### Steel Fiber Extracted From Waste Tyre

Waste tyres in Indonesia are the low-priced, economical and in abundance available material. In Indonesia there is a lack of appropriate recycling industry of waste tyres, manually a huge amount of Steel fiber are being taken out which includes a little quantity of rubber particles on their surfaces. In this study, the steel fibers taken out from waste tyres are used in the concrete mix to form a composite fibrous material. Steel fibers waste tyre were extracted from chips of waste tyres by manual cutting process (Figures 1 and 2) and cut to 1 inch (25.4 mm) length (Figure 3) and average diameter of fiber was 0.28 mm keeping aspect ratio 90. As waste tyres steel fibers are uniformly and randomly distributed in different proportions from (0-1%) with increment of 0.25% by the weight of cement to prepare the different concrete matrix. The chips of waste tyres available in local market; normally they sell those as scrap to scarp industry.



Fig. 1. Cutting Process From Waste Tyre to Obtained Steel Fiber Extracted



Fig. 2. Steel Fiber Extracted From Waste Tyre



Fig. 3. Steel Fiber in 1 Inch Cut Length

#### II.1.5 Palm Oil Fuel Ash

Palm Oil Fuel Ash (POFA) is the product of burning palm oil husk and palm kernel shell in the palm oil mill. POFA obtained from PT. Sawit, Sangir in Dhamasraya was used in the electrical energy. The specific gravity of palm oil fuel ash was 1.65. The chemical composition of POFA was tested at Indarung II, PT. Padang Cement Indonesia and the results is given in Table 1. Figures 4 and 5 show the Palm Oil Residues and Palm Oil Fuel Ash.



Fig. 4. Palm Oil Residues



Fig. 5. Palm Oil Fuel Ash

Table 1. Chemical Composition of POFA

Chemical Composition	Formulae	Content (%)
Silicon Dioxide	SiO <sub>2</sub>	62.84
Aluminium Trioxide	Al <sub>2</sub> O <sub>3</sub>	2.19
Iron Oxide	Fe <sub>2</sub> O <sub>3</sub>	0.00
Lime	CaO	9.57
Magnesium Oxide	MgO	3.48
Potassium Oxide	K <sub>2</sub> O	-
Loss of Ignition	LOI	-

## EXPERIMENTAL STUDY

### Mix Proportions of Concrete

The concrete mix is designed as Indonesian Nasional Standar (SNI) for the normal concrete. The grade of concrete adopted is M35 with a water cement ratio of 0.52. Five mixture proportions were made. First was control mix (with palm oil fuel ash, without steel fiber), and the other four mixes is steel fiber with percentage of 0.25%, 0.5%, 0.75%, 1% contained POFA. Cement was replaced with POFA by weight. The proportions of cement replaced 15%. The ingredients of concrete were thoroughly mixed in a mixer machine till uniform consistency was achieved. Mix proportions are given in Table 2.

Table 2. Mix Proportions

Sample ID	C	SF 0%	SF 0.25 %	SF 0.50 %	SF 0.75 %	SF 1%
<b>Cement (kg/m<sup>3</sup>)</b>	391	332.35	332.35	332.35	332.35	332.35
<b>Water (kg/m<sup>3</sup>)</b>	205	205	205	205	205	205
<b>F.A. (kg/m<sup>3</sup>)</b>	725.6	725.6	725.6	725.6	725.6	725.6
<b>C.A. (kg/m<sup>3</sup>)</b>	108	108	108	108.4	108	108
<b>SFEF WT (kg/m<sup>3</sup>)</b>	-	-	0.976	1.955	2.933	3.910
<b>POFA (kg/m<sup>3</sup>)</b>	-	58.650	58.650	58.650	58.650	58.650

### Casting of Specimens

Total 27 cylinders were casted, for compressive, tensile and flexural strength test. Cylindrical specimens of length 300 mm and diameter 150 mm and beam specimens of length 500 mm, wide 100 mm, high 100 mm casted with adding 0%, 0.25%, 0.5%, 0.75% and 1% of used waste tyre steel fibers extracted.

### Testing of Specimen

Compressive, splitting tensile and flexural strength tests were conducted on cylindrical specimens and beam specimens using Universal testing machine (UTM) in the concrete laboratory of PT. Semen Padang as per SNI 1974:2011, ASTM C 496-86 and ASTM C 293-08, respectively. Figures 6, 7 and 8 show the specimens under compressive, splitting tensile and flexural testing in the laboratory.



Fig. 6. Compressive Test on Cylindrical



Fig. 7. Splitting Tensile Test on Cylindrical



Fig. 8. Flexural Test on Beam

## RESULT AND DISCUSSION

### Compressive Strength

The results of the tests for compressive strength performed on the samples are shown in table 3.



Table 3. 28 Days Compressive Strength of Cylinder Specimen

No.	Palm Oil Fuel Ash Content (%)	(SFEFWT) Content (%)	Compressive Strength (N/mm <sup>2</sup> )
1	15	0	26.40
2	15	0.25	27.60
3	15	0.50	28.40
4	15	0.75	29.10
5	15	1.00	29.70

\*SFEFWT : Steel Fiber Extracted From Waste Tyre

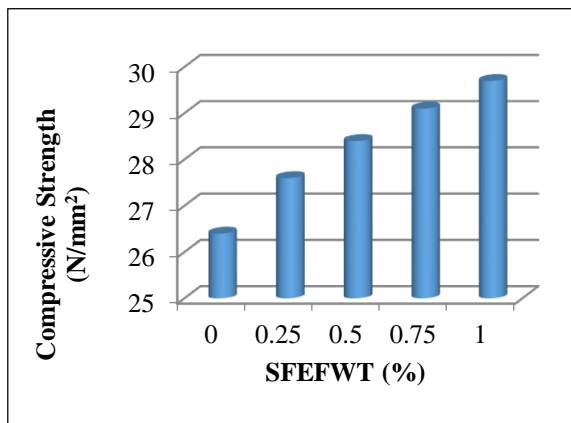


Fig. 9. Comparison of Compressive Strength of Ordinary and SFEFWT POFA Concrete

Compressive strength of POFA concrete mixes made with SFEFWT was determined at 28 days. The results presented in Table 3 and Figures 6 and 9, that the compressive strength of POFA concrete reinforced with SFEFWT slightly increases with the increase of SFEFWT content. The maximum 13% increase i.e. 29.70 N/mm<sup>2</sup> as compared to without SFEFWT concrete; at addition of 1.0% SFEFWT.

#### Splitting Tensile Strength

The results of the indirect tensile strength tests performed on the samples are shown in Table 4.

Table 4. 28 Days Indirect Tensile Strength of Cylindrical Specimen

No.	Palm Oil Fuel Ash Content (%)	(SFEFWT) Content (%)	Splitting Tensile Strength (N/mm <sup>2</sup> )
1	15	0	2.32
2	15	0.25	2.50
3	15	0.50	2.61
4	15	0.75	2.71
5	15	1.00	2.85

\*SFEFWT : Steel Fiber Extracted From Waste Tyre

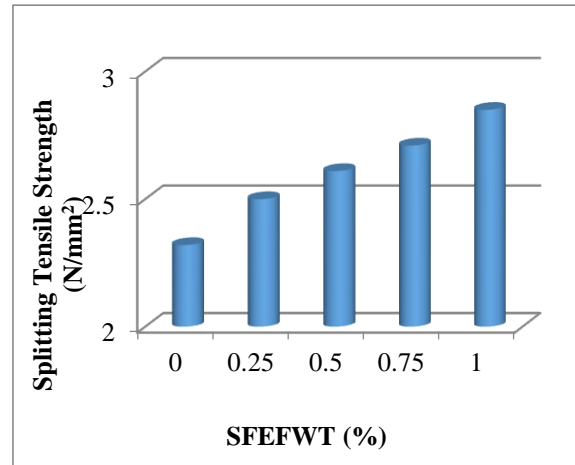


Fig. 10. Comparison of Splitting Tensile Strength of Ordinary and SFEFWT POFA Concrete

The results of splitting tensile strength of POFA concrete mixes with SFEFWT measured at 28 days are given in Table 4 and Figures 7 and 10. Test results indicate that the tensile splitting strength increases as the percentage of the SFEFWT on POFA concrete increases from 0% to 0.5%, 0.75% and 1%. The maximum splitting tensile strength with the addition of 1.0% of SFEFWT is 2.85 N/mm<sup>2</sup>, which is 23% increment as compared to conventional concrete.

#### Flexural Strength

The results of the tests for flexural strength performed on the samples are shown in Table 5.

Table 5. 28 Days Flexural Strength of Cylinder Specimen

No.	Palm Oil Fuel Ash Content (%)	(SFEFWT) Content (%)	Flexural Strength (N/mm <sup>2</sup> )
1	15	0	4.19
2	15	0.25	4.46
3	15	0.50	5.06
4	15	0.75	5.32
5	15	1.00	5.50

\*SFEFWT : Steel Fiber Extracted From Waste Tyre

Flexural strength of POFA concrete mixes made with SFEFWT was determined at 28 days. The results presented in Table 5 and Figures 8 and 11, that the flexural strength of POFA concrete reinforced with SFEFWT increases with the increase of SFEFWT content. As can be seen that, the maximum 31% increase i.e. 5.50 N/mm<sup>2</sup> as compared to without SFEFWT concrete; at addition of 1.0% SFEFWT on POFA Concrete.



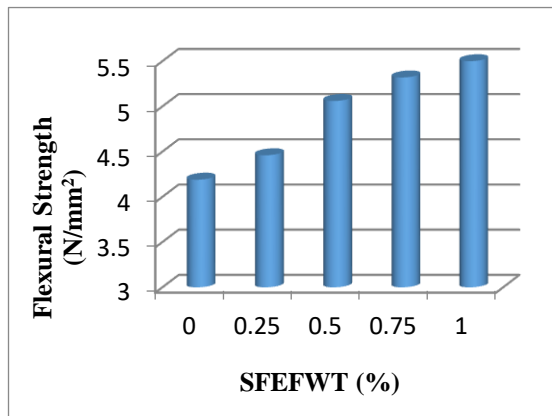


Fig. 11. Comparison of Flexural Strength of Ordinary and SFEFWT POFA Concrete



Fig. 12. Crack Growth in Concrete

The results presented in Figure 12 show that the percentage of SFEFWT on POFA concrete given high number of bonding in concrete to delay the crack growth.

## CONCLUSION

The following conclusions could be arrived at from the study:

- Compressive strength, Splitting tensile strength and Flexural strength of POFA concrete specimens with steel fiber extracted from waste tyre (SFEFWT) were found to be stronger than those of without SFEFWT.
- By inclusion of SFEFWT on concrete containing palm oil fuel ash, the compressive strength increases slightly, at addition of 1.0% SFEFWT, maximum compressive strength, 29.70 N/mm<sup>2</sup> i.e. 13% increase as compared to POFA concrete without SFEFWT is observed.
- With addition of 1% SFEFWT on POFA concrete, the maximum splitting tensile strength was 2.85 N/mm<sup>2</sup>, which is 23%

increase compared to the POFA concrete without SFEFWT.

- Results suggest that 1% SFEFWT on POFA concrete could be the optimum level for the maximum flexural strength; 5.50 N/mm<sup>2</sup> i.e. 31% increase as compared to POFA concrete without SFEFWT.

## ACKNOWLEDGEMENTS

The authors wish to acknowledge the staffs of the Laboratory of Material and Structure in Andalas University and the Laboratory of Concrete in Padang Cement Factory for their support.

## REFERENCES

- [1] Mohammadi Y, Singh SP, Kaushik SK. "Properties of steel fibrous concrete containing mixed fibers in fresh and hardened state". *Constr Build Mater* 2006; doi:10.1016/j.conbuildmat.2006.12.004.
- [2] Yet, T.C., Hamid, R. and Kasmuri, M. "Dynamic Stress-Strain Behavior of Steel Fiber Reinforced High-Performance Concrete with Fly Ash" *Hindawi Publishing Corporation, Advances in Civil Engineering* vol. 2012, Article ID 907431, 6pages. (2012)
- [3] Luca G. S., Meda, A. and Giovanni, A. P. "Steel Fiber Concrete Slabs on Ground: A Structural Matter" *ACI Structural Journal*, Vol 103. pp 551-558 (2006)
- [4] Nili, M. Afroughsabet, V. "Combined effect of silica fume and steel fibers on the impact resistance and mechanical properties of concrete" *International Journal of Impact Engineering*, Vol 37, pp 879-886. (2010)
- [5] Nataraja, M.C., Nagaraj, T.S. and Basavaraja. S.B. "Reproportioning of steel fibre reinforced concrete mixes and their impact resistance" *Cement and Concrete Research*, Vol 35, pp 2350 – 2359. (2005)
- [6] Vanchai Sata., Chai Jaturapitakkul., & Chaiyanunt Rattanashotinunt., "Compressive Strength and Heat Evolution of Concretes Containing Palm Oil Fuel Ash", *Journal of Materials in Civil Engineering*, Vol. 22, No. 10, October 1, 2010. ©ASCE, ISSN 0899-1561/2010/10-1033–1038.
- [7] Mohd Warid Hussin., Mohamed A. Ismail, Ahmed Budiea., & Khairunisa Muthusamy., "Durability of high strength concrete containing palm oil fuel ash of different fineness", *Malaysian Journal of Civil Engineering*, Vol.21 (2), 2009, pp.180-194.
- [8] Ahmad M. H., Omar R. C., Malek M. A., Noor N & Thiruselvam S., "Compressive Strength of Palm Oil Fuel Ash Concrete", *ICCBT 2008 - A - (27) – pp297 – 306*.

## **ACCURACY OF CENTRALIZED AND DECENTRALIZED MANUFACTURING SYSTEMS TOWARDS AN INDUSTRY 4.0'S PERSPECTIVE**

Poonpakdee, P.<sup>1</sup>, Koiwanit, J.<sup>2</sup>, Yuangyai, C.<sup>3</sup>

<sup>1</sup>Department of Industrial Engineering, Faculty of Engineering, King Mongkut's Institute of Technology  
Ladkrabang, Bangkok 10520, Thailand

### **ABSTRACT**

With significantly improving the overall manufacturing operations commonly known in smart factory practices, vertical and horizontal integrations of various components are introduced throughout the entire value chain. The proliferation of smart factory practices introduce the fourth industrial revolution called Industry 4.0. Industry 4.0 creates new challenges and the application of networked manufacturing systems is one of the important features required to handle the systems in an efficient way by communicating and processing information to each other. Distributed systems provide coordination to allow the global information to be available for a better decision making and consequently achieving high efficiency. This connectivity helps for a better decision making and therefore achieve high efficiency. However, the evaluation on the accuracy of global information between different architectures of distributed systems (centralized systems and decentralized systems) has little work mentioning in the state of current manufacturing systems under the conception of Industry 4.0. As a result, this research will fill the gap by providing an accuracy of the decentralized system over the centralized system together with their sensitivity analysis.

In this study, the decentralized system is built based on the concept of Epidemic protocols or Gossip-based protocols, while the centralized system is a simple client-server. Epidemic protocol is a bio-inspired communication paradigm that imitates the behavior of virus when the outbreak is occurred in a community. The accuracy in both systems has been monitored by mean of simulations. The effects of message loss to the accuracy of centralized and decentralized systems are studied. By comparing the system accuracy between both systems, it was found that the accuracy of decentralized system is generally more accurate when the system is used for a long period. The accuracy tends to be lower down especially when the information is not completely distributed, while the accuracy of centralized system receive an excessive suffer from message loss.

*Keywords: Industry 4.0, centralized systems, decentralized system, accuracy*

### **INTRODUCTION**

The proliferation of smart factory practices introduces the fourth industrial revolution called Industry 4.0. Industry 4.0 creates new challenges and the application of networked manufacturing systems is one of the important features required to handle the systems in an efficient way by communicating and processing information to each other. Distributed systems provide coordination to allow the global information to be available for a better decision making and therefore achieve high efficiency.

The basic architecture of distributed systems, which is a part of smart factory systems, can be categorized into two major groups: centralized systems and decentralized systems. The most familiar form of topology is centralized systems, whose structure is typically similar to the client-

server. A server aims to centralize all function and information taken from clients by directly connecting to the clients. Clients share their resources by sending and receiving the information to a server [1]. In contrast, decentralized systems are similar to peer-to-peer systems where all peers communicate symmetrically and equally in roles. A well-known example of decentralized systems is Gnutella, the practical decentralized systems with only a centralized function for starting a new host [1]. In this study, Epidemic protocols or Gossip-based protocols, which is bio-inspired communication paradigm for information dissemination in extreme scale network systems, are used to construct the decentralized system.

In general, the convergence speed of centralized systems is faster than decentralized systems because the complete set of data is stored and managed within a hub that does not exist in decentralized

systems. However, many circumstances such as message loss and node failure in centralized systems can cause data missing which can skew the results of the global aggregation. This introduces an inaccuracy in the decision making [2]. Unlike centralized systems, decentralized systems allow data from each node to be distributed to its neighbors [3]. This results in the networked infection over the whole system as the time goes by. Several works related to the accuracy of the global information in distributed systems have been reviewed. Reference [4] studied on the accuracy of failure detection in distributed system Reference [2] explored the accuracy analysis of data aggregation for distributed network monitoring. Reference [5] analyzed the convergence in decentralization in a specific problem. Reference [3] studied the accuracy of the epidemic spreading over a network. However, the literature review reveals that little work has been done under the concept of Industry 4.0 particularly focusing on the accuracy of global aggregation between both systems. As such, this paper presents how accuracy decentralized systems is evaluated against centralized systems in the context of manufacturing.

The rest of the paper is organized as follows. Section 2 gives the detail of Epidemic aggregation protocols and some of the related works. Application case study is presented in Sections 3. The experimental scenario and their results are presented and analyzed in Section 4 and 5, respectively. Finally, Section 6 draws some conclusions and provides possible directions of future work.

## EPIDEMIC AGGREGATION PROTOCOLS

An epidemic protocol or a gossip-based protocol aims to solve problems in an extreme-scale distributed system. The definition of an epidemic protocol is generally a bio-inspired communication and computation, which takes over the concepts of a virus-spreading mechanism and the gossip manners of human. The characteristics of the protocol are robustness and scalability with respect to a global communication paradigm based on a deterministic interconnection network [6]. Epidemic protocols use randomized communication as the principle mechanism in order to achieve these characteristics.

A number of applications based on epidemic protocols have been proposed to serve different purposes in different environments. Examples of these applications are: Peer-to-Peer (P2P) overlay networks [7], distributed computing [8], mobile ad hoc networks (MANET) [9]-[11], failure detection [12],[13], exascale high performance computing [14]-[16], data mining [17]-[18], data aggregation [19]-[22], and wireless sensor networks (WSN) [23]-[25].

Several epidemic protocols have been proposed

to solve data aggregation problems because highly distributed systems such as P2P or large-scale network systems have currently become more popular and enabled for a broad range of applications [26],[22]. Due to these systems, the information of data aggregation over the network is often more important than the information of an individual node [19], so tools that can compute significant system properties of a network are necessary [27]. A monitoring system is an example where the system administrator would be more interested in the aggregation information about the average of measured values from all sensors in an area than the individual measured value of a single sensor. More details about the utilizations of epidemic aggregation protocols are given in the next section.

## APPLICATION CASE STUDY

A case study of the monitoring system using epidemic aggregation protocol related to urban environmental aspects is studied to illustrate their use of the distributed systems in manufacturing. The interesting aspect is the urban flooding that occurs when an urban drainage system (UDS) becomes overloaded during an extreme rainy condition. As a result, the wastewater treatment plant (WWTP) is not able to treat the wastewater. This problem causes sewer flooding and combined sewer overflows in an urban environment, which are a potential risk to human life, economic asset, and the environment. In general, the UDS is managed by a real-time control (RTC) system that requires the network to be embedded with sensors and actuators permitting the network to be monitored real-time and regulated to adapt to the different rainfall events.

Many previous works of RTC are based on centralized systems that introduce several problems due to the large amount of data to be read, managed, and processed. The drawbacks of centralized systems include: 1) a complex mathematical model of network is required, 2) the central unit needs to be connected with all physical parts, and 3) a single failure in any part of the system, especially the central unit, can compromise the entire system.

In order to solve these drawbacks, a decentralized system is considered Reference [28] developed an urban drainage network of the city of Cosenza in Italy, which adopts the decentralized real-time control (DRTC) system based on a distributed agent-based architecture and specifically an epidemic protocol, which exhibits good performance, and fault tolerance properties. The characteristics of the systems are shown as follows:

- **Autonomy:** Each agent is self-aware and has a self-behavior. It observes the environment, cooperates with others, and plans its execution

autonomously.

- **Local views:** None of the agents have a full global view of the whole environment. However, its performance is solely based on the quality of local information.
- **Decentralization:** There is no master agents controlling the others, but the system is built from the interaction of peer agents.

The results are generated by using the Storm Water Management Model (SWMM), an open-source computer model for the simulation of hydrodynamic water and pollutant transport in sewer systems. The process to balance the water level throughout the conduits is simulated as the main contribution in their work. The water balancing process consists two tasks: 1) Computing the average water level in the generated network accomplished by epidemic protocol and, 2) Triggering the gate in order to bring the water level closer to its average value.

Reference [28] confirms that epidemic protocol is able to support UDS to control water level successfully, ensuring a full utilization of the actual storage capacity of the system.

## EXPERIMENTAL SCENARIO

The experiments in this study have adopted the scenario from the case study mentioned in the previous section. The simulated scenarios are shown in the context of Industry 4.0, specifically in manufacturing systems under smart factory practices, where all the work units are connected. Machines, sensors, mobile devices, computers, laptops, and servers are some of the examples of the work units in smart factory practices. The simulation presents the activity in the manufacturing systems in terms of monitoring the system status in order to perform system maintenance. The goal of the experiments is to evaluate the accuracy of a global aggregation computation in different network environments: decentralized and centralized systems by mean of simulation. Fig. 1 presents two different architectures of simulated scenarios, which include centralized systems and decentralized systems.

In this study, the systems consist of two classes of work units: a base station and sensors. The base station's objective is to monitor the status of the system based on the data from the sensors. In centralized systems, a base station will compute the global aggregation by processing all of local data sent by every sensors in the system. In general, a base station is a hub of data in centralized systems whereas decentralized systems do not have any hubs. Each of the sensor is distributing its local data to the system while processing the global aggregation locally. A base station aims to monitor and provide the global aggregation by obtaining the information

from gateways, which are sensors that communicate with the base station.

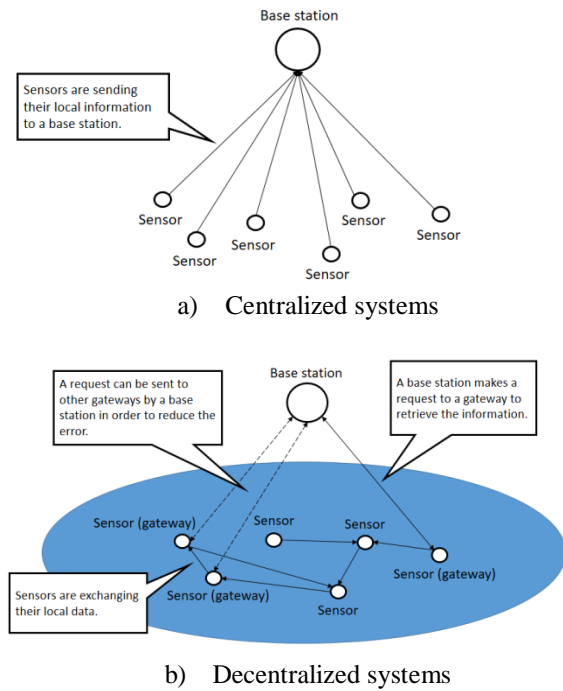


Fig. 1 Architectures of simulated scenarios.

In comparison with the case study, each sensor represents as an agent that maintains the measured value as local data. The differences between the case study and the simulation are that the global aggregation in the case study is the average of the measured values, whereas the global aggregation in the simulation is represented in terms of a maximum value.

## EXPERIMENTAL RESULTS

The experimental results and their analysis are presented in this section. The simulations have been completed in PeerSim [29], a discrete-event based Peer-to-Peer simulator developed in Java. The simulations are based on an asynchronous network model with a network latency. Each sensor contains the local data initialized with uniformly distribution between 1 and 100,000, and the base station will monitor the system by computing the maximum value among the local data. Message loss is also introduced and included as one of the main parameters in the simulations. The value of the parameter indicates the possibility of message loss in percent.

For decentralized systems, the global aggregation is executed by an epidemic aggregation protocol. The protocol is based on push-only gossip-based communication modified from the SI model, one of the epidemic dissemination algorithms [30].

Algorithm 1 presents the mechanism of epidemic aggregation protocol where  $v$  is local data and  $j$  is a remote sensor. Every sensor uses the protocol to estimate and distribute the global aggregation. When the base station requires the global aggregation, it will send a request message to a gateway of the system, and then the gateway will reply its current estimated maximum value to the base station. In this work, the base station will make a request to a single fixed gateway.

For the centralized systems, the base station will collect the local data from every sensor to find the maximum value.

---

**Algorithm 1** Epidemic Aggregation Protocol

---

```

1: procedure SENDPUSHMESSAGE
2:    $j \leftarrow$  get a random node
3:   send a push message to  $j : m_{\rightarrow}(v)$ 
4:
5: procedure RECEIVEPUSHMESSAGE( message  $m_{\rightarrow}$ )
6:   if  $m_{\rightarrow}.v > v$  then
7:      $v \leftarrow m_{\rightarrow}.v$ 

```

---

The general configuration of a simulation is based on the evaluation criterion and the objectives of this study. The total number of work units using in this study is 1,000, which includes a single base station and 999 sensors. The initial topology depends on the models of simulated scenarios. For centralized systems, the initial topology is similar to a client-server architecture: a server (base station) contains a completed list of work units while clients (sensors) contain only a connection to the server. In contrast, the initial topology for decentralized systems is similar to a random graph that all sensors are randomly connected while a base station can only communicate with a gateway.

In decentralized systems, an epidemic membership protocol is required in this scenario. Epidemic membership protocols offers mechanisms intended to maintain the connectivity of the systems in terms of overlay topology [33]. Each sensor holds the local cache containing the connections to 20 random sensors. As a result, each sensor will recognize approximately 2% of other sensors. In each cycle, one-fourth of the connections in the local cache will be exchanged with other sensors due to the mechanism of an epidemic membership protocol. As a result, the structure of the system is continually rewired in every cycle. On the other hand, centralized systems are not required rewiring the structure, thus epidemic membership protocols are not taken into account.

The results can be categorized in two sets and presented in the following sections. First, the convergence speed of epidemic application in decentralized systems is examined, specifically the intention of the results showing how message loss affects the convergence speed. Second, the performance of base station is evaluated in both

systems. The performance index is presented as the accuracy of the global aggregation.

### Convergence Speed

This section shows how fast sensors can distribute the information across the system when different percentages of message loss occur. The results were collected from five trials with five different random seeds to avoid any experimental biases. The standard deviation of local estimated maximum value at each sensor is used to determine the convergence speed.

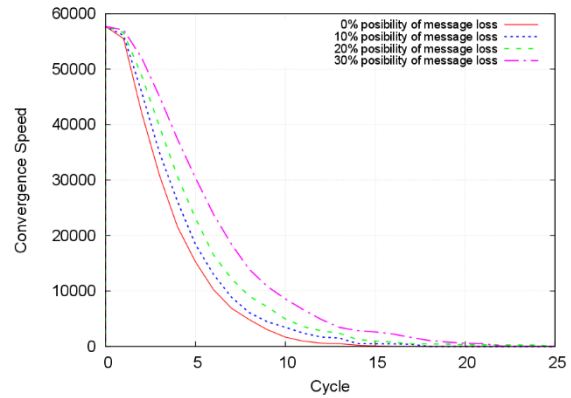


Fig. 2 Convergence speed with different possibility of message loss.

The effect of message loss to the convergence speed can be observed from the results. Fig. 2 shows the average standard deviation of the local estimated maximum over five trials. The y-axis is the standard deviation and the x-axis is the number of cycles. A curve in the chart indicates a convergence to the target value.

At the beginning of the simulation, it is expected that the standard deviation is high because there is no sensors that is able to determine the maximum value. After the first cycle, the standard deviation is decreasing which shows that each sensor is starting to generate the maximum value. Different possibilities of message loss including 0%, 10%, 20%, and 30%, were simulated for the evaluation. Without message losses in the network, Epidemic protocol provides the fastest convergence speed and it will be slower with a higher possibility of message loss.

### System Accuracy

This set of simulations aims to evaluate the accuracy of the systems between decentralized and centralized systems when message loss occurs. Each simulation was run for 100, 300, and 700 cycles and was repeated five times with different random seeds in order to compute an average number of

inaccuracies. The base station will compute the maximum for once at a cycle.

Table 2 Average number of inaccuracies from the base station

Message Loss	Centralized Systems			Decentralized Systems		
	100 cycles	300 cycles	700 cycles	100 cycles	300 cycles	700 cycles
0%	0	0	0	7.6	7.6	7.6
10%	11	30.4	72.2	11.8	11.8	11.8
20%	19.6	61.8	146.6	12.4	12.4	12.4
30%	32.2	92.4	206	16.8	16.8	16.8

Table 2 shows that message loss has a correlation to the accuracy. The number of inaccurate estimations is increasing with the higher possibility of message loss. The best result comes from centralized systems which claims that the estimation of the base station are seamless regardless to message loss; however, the systems also receive a great suffer when message loss is considered. The system usage during a long period will lead to higher number of inaccuracies. In contrast, the long usage of decentralized systems does not affect an increase in the number of inaccuracies because they will only occur when the system is not completely distributed with the information. Nonetheless, a delay of information distribution is a necessary for decentralized systems. Figure 3 and table 2 show that there is a relationship between the convergence speed and the number of inaccuracies in decentralized systems. The systems with the fastest convergence speed have the lowest number of inaccuracies.

## CONCLUSION

Within the Industry 4.0's context, one of the smart manufacturing features is to focusing on the establishment of the high-tech communication between not only humans but also machines in order to reach the goal of the smart factory practices. Industry 4.0 promises increased networking of these machines, which can be highly accurate and consequently customized to manufacture individual outcomes.

Centralized systems that are currently used in any industries require a single control center or hub to collect all required data to create a global information that can potentially suffer from being inaccurate, especially when messages are missing. This consequently results in poor decision making and most importantly, leading to an organization's future irreparably. Decentralized systems, however, redesign the networking system to allow each working unit to contain a global information without using any hubs.

This work has investigated the effect of systems architectures, centralized systems and decentralized systems, to the accuracy of global aggregation. The characteristics of these architectures are also mentioned in this study. Epidemic aggregation protocols are used as the key for information distribution in the decentralized systems. The main task of these protocols is to provide a service to disseminate and generate the global information. The sets of results were produced under message loss conditions. By evaluating the accuracy of the decentralized systems over the centralized systems, the results show that message loss have negative effect to the accuracy of the system and it is interesting to notice that the long period of system usage does cause higher inaccuracies in the centralized systems when message loss occurs, but not in decentralized systems. In addition, when there is no message losses, centralized systems run perfectly without any such inaccuracies while decentralized systems still have some error at the beginning of the simulations. These results can draw the conclusion that decentralized systems are suitable under the condition that the messages can be missing. On the other hand, centralized systems should be selected when the messages are guaranteed to be delivered.

In order to achieve the practical implications, further study on distributed systems in a real world manufacturing systems, e.g. node churn, information retrieval from multiple gateways and sub base stations, are required for future work. Another aspect to consider is how to improve the convergence speed of epidemic aggregation protocols under the context of Industry 4.0 with the variety of environmental conditions and case studies.

## REFERENCES

- [1] O'Reilly Media, Inc., "Distributed Systems Topologies", O'Reilly Network: Distributed Systems Topologies, 2004.
- [2] Sofra N, He T, Zerfos P, Ko B J, Lee K, and Leung K K, "Accuracy Analysis of Data Aggregation for Network Monitoring", in Proc. 2nd Annual Conf. of the International Technology Alliance, London UK, September 2008.
- [3] Qu B, and Wang H, "The Accuracy of Mean-Field Approximation for Susceptible-Infected-Susceptible Epidemic Spreading", in Proc. of the 5th International Workshop on Complex Networks and their Applications, 2016.
- [4] Gupta I, Chandra D T, and Goldszmidt G S, "On scalable and efficient distributed failure detectors" in Proc. PODC'01, 2001, pp. 170-179.
- [5] Yuan K, Ling Q, and Yin W, "On the Convergence of Decentralized Gradient



- Descent”, in *SIAM Journal on Optimization*, vol. 26, no. 3, 2016, pp. 1835-1854.
- [6] Poonpakdee P, and Di Fatta G, “Connectivity Recovery in Epidemic Membership Protocols”, in *IDCS*, Springer, 2015, pp. 177 - 189.
- [7] Tang S, Jaho E, Stavrakakis I, Koukoutsidis I, and Van Mieghem P, Modeling gossip-based content dissemination and search in distributed networking, in *Comput. Commun.*, vol. 34, 2011, pp. 765 - 779.
- [8] Di S, Wang C L, and Hu D H, “Gossip-based dynamic load balancing in an autonomous desktop grid,” in *Proc. of the 10th International Conference on High Performance Computing in Asia-Pacific Region*, 2009, pp. 85-92.
- [9] Vahdat A, and Becker D, “Epidemic Routing for Partially-Connected Ad Hoc Networks”, *Duke Tech Report CS-2000 – 06*, 2000.
- [10] Ma Y, and Jamalipour A, “An epidemic P2P content search mechanism for intermittently connected mobile ad hoc networks”, in *IEEE GLOBECOM*, 2009, pp.1-6.
- [11] Novotny P, “Fault Localization in Service-Based Systems hosted in Mobile Ad Hoc”, Ph.D. thesis, Imperial College London, UK, 2013.
- [12] Van Renesse R, Minsky Y, and Hayden M, “A Gossip-Style Failure Detection Service”, in *Middleware’98 Proc. of the IFIP Int. Conf. on Distributed Systems Platforms and Open Distributed Processing*, Springer-Verlaq, 2009, pp. 55- 70.
- [13] Ahn J H, and Kim C Y, “Gossip-Pull System-based Dissemination Protocol Satisfying Message Causality Condition”, in *2nd Int. Conf. on Advances in Computer Science and Engineering (CSE 2013)*, Atlantis press, 2013, pp. 323 325.
- [14] Strakov H, Niederbrucker G, and Gansterer W N, “Fault tolerance properties of gossip-based distributed orthogonal iteration methods”, in *Proc. Int. Conf. on Computational Science*, vol. 18, 2013, pp. 189 - 198.
- [15] Soltero P, Bridges P, Arnold D, and Lang M, “A gossip-based approach to exascale system services”, in *Proc. of the 3rd Int. Workshop on Runtime and Operating Systems for Super computers*, ser. ROSS 13. ACM, 2013.
- [16] Katti A, Di Fatta G, Naughton T, and Engelmann C, “Scalable and Fault Tolerant Failure Detection and Consensus”, in *Proc. of the 22nd EuroMPI*, 2015.
- [17] Di Fatta G, Blasa F, Cafiero S, and Fortino G, “Epidemic K-Means Clustering”, in *Proc. of the IEEE Int.l Conf. on Data Mining Workshops*, 2011, pp. 151 158.
- [18] Mashayekhi H, Habibi J, Voulgaris S, and van Steen M, “GoSCAN: Decentralized scalable data clustering”, in *Computing*, vol. 95, no. 9, 2013, pp. 759- 784.
- [19] Kempe D, Dobra A, and Gehrke J, “Gossip-Based Computation of Aggregate Information”, in *’FOCS’*, IEEE Computer Society, 2013, pp. 482-491.
- [20] Jelasity M, Montresor A, and Babaoglu O, “Gossip-based aggregation in large dynamic networks”, in *ACM Trans. Comput. Syst.* vol. 23, no. 3, 2005, pp. 219-252.
- [21] Boyd S P, Ghosh A, Prabhakar B, and Shah D, “Randomized gossip algorithms”, in *IEEE Transactions on Information Theory* 52 (6), 2006, pp. 2508-2530.
- [22] Blasa F, Cafiero S, Fortino G, and Di Fatta G, “Symmetric push-sum protocol for decentralised aggregation”, in *Proc. of the Int.l Conf. on Advances in P2P Systems*, 2011, pp. 27-32.
- [23] Dimakis A, Kar S, Moura J, Rabbat M, and Scaglione A, “Gossip algorithms for distributed signal processing”, in *Proc. of the IEEE*, vol. 98, no. 11, 2010, pp. 1847 - 1864.
- [24] Ragusa C, Liotta A, and Pavlou G, “An adaptive clustering approach for the management of dynamic systems,” in *Selected Areas in Communications*, *IEEE Journal on*, vol. 23, no. 12, 2005, pp. 2223 - 2235.
- [25] Galzarano S, Savaglio C, Liotta A, and Fortino G, “Gossiping-based aodv for wireless sensor networks,” in *Systems, Man, and Cybernetics (SMC)*, 2013 IEEE Int. Conf., 2013, pp. 26-31.
- [26] Bawa M, Garcia-molina H, Gionis A, and Motwani R, “Estimating Aggregates on a Peer-to-Peer Network”, *Technical Report*. Stanford InfoLab, 2003.
- [27] Jesus P, Baquero C, and Almeida P S, “Dependability in Aggregation by Averaging”, in *CoRR abs/1011.6596*, 2010
- [28] Garofalo G, Giordano A, Piro P, and Spezzano G, “A distributed real-time approach for mitigating CSO and flooding in urban drainage systems”, in *Journal of Network and Computer Applications*, vol. 78, 2017, pp. 30-42
- [29] Montresor A, and Jelasity M, “PeerSim: A scalable P2P simulator,” in *Proc. of the 9th Int. Conference on Peer-to-Peer (P2P’09)*, 2009, pp. 99–100.
- [30] Jelasity M, “Self-Organising Software: From Natural to Artificial Adaptation”, *Natural Computing Series*, Springer, 2011, pp. 139-162, DOI: 10.1007/978-3-642-17348-6\_7
- [31] Poonpakdee P, Di Fatta G, “Robust and Efficient Membership Management in Large-Scale Dynamic Networks”, in *Future Generation Computer Systems*, 2017, DOI:10.1016/j.future.2017.02.033



# NUMERICAL ANALYSIS OF NONLINEAR MODEL OF SFRC SLAB AND NONLINEAR SUBSOIL MODEL IN INTERACTION

Jana VASKOVA<sup>1</sup>, Radim CAJKA<sup>2</sup>

<sup>1,2</sup> Faculty of Civil Engineering VŠB-Technical university of Ostrava, Czech Republic

## ABSTRACT

Experimental measurements of concrete slab in interaction with subsoil are compared with numerical analysis based on Finite Element Method FEM. Experimental measurements are conducted with using of experimental device constructed at the Faculty of Civil Engineering VSB – Technical University of Ostrava. In this article several types of nonlinearities enters into FEM analysis. Subsoil-structure interaction requires an iterative solution procedure - and therefore structural nonlinearity. Material nonlinearity was used in the numerical model of slab. This model also allows the creation and development of cracks in concrete - similar as during the experimental load test. Material nonlinearity was also used in the numerical model subsoil - to ensure of apposite subsoil behaviour. The purpose of this paper is to compare resulting deformation of the slab with values observed during experimental loading test.

*Keywords: Foundation Structure, Experimental Measurement, Soil – Structure Interaction, Interaction Models, FEM Calculation.*

## INTRODUCTION

With the beginning and subsequent development of computer technology, numerical methods have also been used to solve the interactions between base and subsoil. The most well-known numerical methods are Boundary Element Method (BEM) and Finite Element Methods (FEM). Currently (and also in the past) many experts have been dealt with numerical model based on Finite Element Method (FEM) – eg. Zienkiewicz a Taylor [1], Králík, Jendželovský [2], Kolář, Němec [3]. The most widely used software, which solve interaction tasks, are Scia Engineer, Ansys, Trimas, MKPINTER, RFEM a RF-Soilin and Plaxis. Despite many commercial software and non-commercial software, a computational model was not still found to accurately capture the behavior in interaction of the foundation structure and subsoil. The difficulty of designing an accurate static design of foundation structures lies in several aspects, for example the influence of physical-nonlinear behavior of the structure or the uncertainty associated with the description of the properties and behavior of the foundation soil, because it is natural material and its properties cannot be determined unambiguously. Despite these uncertainties in input parameters, Finite Element Method (FEM) is an excellent computing method for a whole range of tasks, including interaction tasks. The Finite Element Method (FEM) allows solution of a so-called complete interaction system including "subsoil - foundation structure - upper structure". Complete interaction system is more demanding to compute, but provides more accurate results than a simplified

interaction system "subsoil - foundation structure". However, the question is, how accurate is input data and parameters entering the calculations. Both, 2D and 3D finite elements, can be using to solve of numerical analyzes of the complete interaction systems and also simplified interaction systems.

## EXPERIMENTAL LOADING TEST

A combination of experimental tests, laboratory tests, field tests and numerical modelling is optimal to obtain reliable results of analyses of subsoil-structure interaction. Combination of all the foregoing approaches was also used in this paper. In 2016, experimental loading test of concrete slab was realized using the experimental facility built in campus of Faculty of Civil Engineering, VŠB - Technical University of Ostrava in the Czech Republic, see Fig. 1. For this experimental loading test, numerical analyses have been done in the program Ansys, Plaxis, Scia Engineer, MKPInter, all based on the finite element method (FEM).



Fig. 1 Experimental equipment, called Stand



Fig. 2 Experimental loading test

The concrete was mixture of C 25/30 XC2. It was concrete with consistency S3, with the limit value of the minimum content of cement (CEM I 42.5 R VL) of  $280 \text{ kg/m}^3$  and for the maximum grain size to 16 mm. A modulus of elasticity of concrete was obtained with laboratory tests, which were conducted in the day when the slab was loaded. The modulus of elasticity was  $E = 19.75 \text{ GPa}$ . Poisson's ratio of concrete was  $\mu = 0.2$ . Compressive strength of concrete  $f_c = 20.03 \text{ MPa}$  was also obtained by laboratory tests. The slab dimensions were  $2.00 \times 2.00 \times 0.15 \text{ m}$ . The slab model was loaded by hydraulic press in the slab center, see Fig. 2. The load area was  $400 \times 400 \text{ mm}$ . The subsoil had these properties – Poisson coefficient  $\mu = 0.35$ , modulus of deformability  $E_{\text{def}} = 12.5 \text{ MPa}$ . A load step method was used at  $25 \text{ kN}/30 \text{ minutes}$ . Loading was carried out up to the load during which the experimental load test of slab was failed ( $345 \text{ kN}$ ). A load of  $345 \text{ kN}$  applied on the loading area ( $400 \times 400 \text{ mm}$ ) was also used in numerical analyses.

### NONLINEAR NUMERICAL MODEL OF INHOMOGENEOUS HALF-SPACE

Soil is naturally and heterogeneous material. Because of it, its properties differ from idealization of linear elastic, isotropic and homogeneous material. That's the reason why the calculated values of settlement differ from the actual settlement. This can be appropriately dealt with using the inhomogeneous half-space [4]. In inhomogeneous half-space the modulus of deformability of the subsoil varies continuously with the increasing depth. In the inhomogeneous half-space there is a different concentration of the vertical stress in the axis of the foundation than that in the homogeneous half-space. The Equation (1) based on the minimum of deformation work was derived by Frölich [5].

$$E_{\text{def}} = E_0 z^m \quad \text{where} \quad m = \frac{1}{\mu} - 2 \quad (1)$$

where

$E_0$  – modulus of deformability at the surface

$z$  –  $z$ -coordinate (depth)

$m$  – coefficient depending on Poisson's ratio  $\mu$

Value of modulus of deformability  $E_{\text{def}}$  continuously increases with increasing depth according to the formula (1) in an inhomogeneous half-space. When the subsoil model is created as inhomogeneous nonlinear continuum, results are significantly less affected by the selected geometry subsoil model than subsoil model created as a linear homogeneous continuum. Inhomogeneity of the numerical model of the subsoil was created by dividing into separate layers (Fig. 3), in which the modulus of deformability grew in layers.

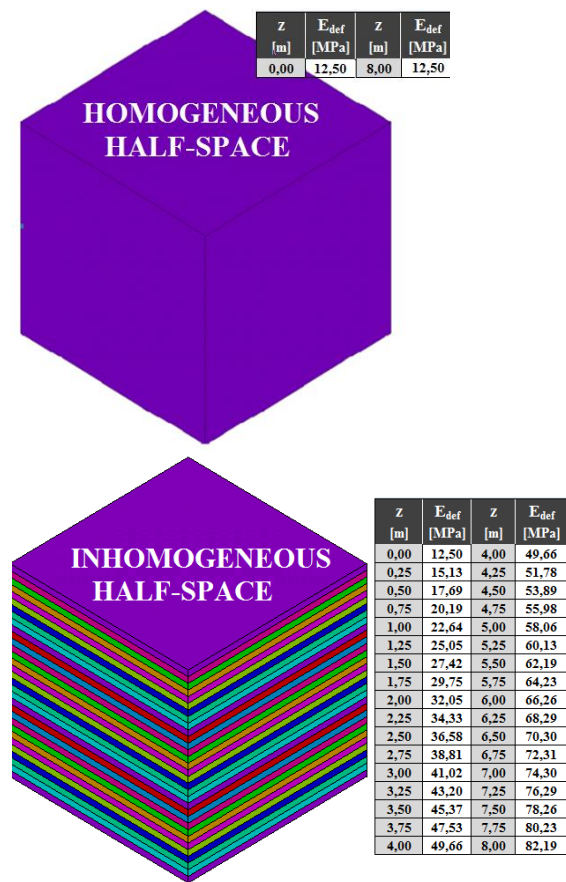


Fig. 3 Homogeneous half-space model and inhomogeneous half-space model, ANSYS

### NUMERICAL ANALYSES IN ANSYS

3D numerical model was created in ANSYS. The input data were taken over the experimental loading test. Subsoil model was created as a three-dimensional model using 3D finite element SOLID 45. Subsoil model was created as homogeneous half-space and also as inhomogeneous half-space, see Fig. 3. Based on a parametric studies [6], [7], [8], area representing the subsoil was  $8.0 \times 8.0 \times 8.0 \text{ m}$ .

Physical nonlinearity associated with material properties was used. Nonlinear material model was performed by Drucker-Prager model. SOLID 65 was used for spatial modelling of experimentally loaded slab. It was necessary in the numerical model to take into account the influence of nonlinearities and cracks in concrete (occurring during the continuous loading of the concrete slab). These were taken into account by the use of the finite element SOLID 65. SOLID 65 enables non-linear calculation of concrete structures by Willam - Warnke criterion. This model of behavior of quasi-brittle material considers both tensile damage (forming cracks) and pressure damage (crushing the material). Fracture properties of concrete are also described eg. [9].

If spatial numerical model is created using 3D finite element, results are largely dependent on the chosen parameters entering into the calculation. It has been proven by parametric analysis in author's articles, eg. [6], [8]. Important parameters influencing the results of numerical analysis are, among other, the size of the modelled area representing the subsoil, the choice of boundary conditions or mesh size.

#### NUMERICAL ANALYSES IN PLAXIS 3D FOUNDATION

Model in the PLAXIS 3D FOUNDATION program, despite the title, it is not a full 3D model of the subsoil because the spatial model is created by stretching the cut to depth. In PLAXIS 3D FOUNDATION, therefore, a concrete slab was created as a 2D linear model, which was also computed for ANSYS for comparison purposes (above).

PLAXIS 3D FOUNDATION is primarily used to solve geotechnical problems. In this computing system is a specialized module designed to analyze subsoil-structure interaction. The 3D numerical model in PLAXIS 3D FOUNDATION was created with the same geometry of the subsoil model as in numerical analyses in ANSYS - in order to compare the results obtained by numerical analysis in ANSYS. The area representing the subsoil model was 8.0 x 8.0 x 8.0 m. The subsoil model is created as a homogeneous half-space and inhomogeneous half-space, as in ANSYS including the same values of the modulus of deformability. All input parameters are the same as input parameters in numerical analyzes in ANSYS and therefore according to experimental load test. The boundary conditions are automatically created in the PLAXIS 3D FOUNDATION and cannot be changed. The boundary conditions prevent by horizontal shifts of the nodes in the walls of the subsoil model and the vertical and horizontal shifts of the nodes in the lower base of the subsoil model. No boundary conditions prevented the nodes shifting in the upper

base of the subsoil model, because it represented the terrain. The boundary conditions in numerical analysis in ANSYS were the same. The finite-element mesh was created automatically by 15 nodal finite elements. The Mohr - Coulomb material model was used for the subsoil and consequently, the difference between tensile and compressive strength can be described.

When the subsoil model was created as a homogeneous half-space (Fig. 4), the maximum calculated vertical deformation at the center of the slab was 13.23 mm.

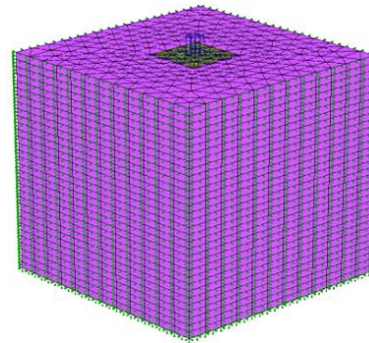


Fig. 4 Homogeneous half-space model, PLAXIS 3D FOUNDATION

The deformation measured during the experiment (using the sensor closest to the slab center) was 15.05 mm. In the inhomogeneous model of the subsoil (Fig. 4) the value of the modulus of deformability increased with the depth according to formula (1).

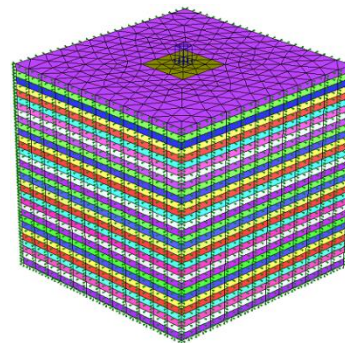


Fig. 5 Inhomogeneous half-space model, PLAXIS 3D FOUNDATION

In the PLAXIS 3D FOUNDATION the subsoil model was divided into 32 layers (Fig. 5). In these layers the value of the modulus of deformability gradually increased with the depth (as in ANSYS). When the subsoil model was created as the inhomogeneous half-space, the maximum calculated vertical deformation at the center of the slab was 9.68 mm (Fig. 4).



## NUMERICAL ANALYSES IN SCIA ENGINEER

Subsoil-structure interaction can also be solved using the SCIA ENGINEER, commercial software [10]. The results then was compared with the results obtained by the 3D numerical models created in the ANSYS, PLAXIS 3D FOUNDATION and with the experimental values.

In SCIA ENGINEER [10], the so-called standard model of subsoil according to ČSN 73 1001 [11] is applied, which is based on the theory of elastic half-space of modified structural strength of soil. If the design in the program is modeled according to Eurocode 7 [12], the value of the structural strength coefficient is automatically  $m = 0.2$  and is unchanged. It is a surface model of the subsoil, which is characterized by the parameters  $C_x$ ,  $C_y$ ,  $C_z$ . The properties of the modeling subsoil are inter alia entered through the parameters of the subsoil  $C_{1x}$ ,  $C_{1y}$ ,  $C_{1z}$ , and  $C_{2x}$ ,  $C_{2y}$  [10].  $C_{1z}$  is the compressibility parameter of the elastic subsoil in the z-axis direction, which represents the resistive elastic resistance against the vertical displacement  $w$ .  $C_{2x}$  and  $C_{2y}$  are shear deformation parameters that take into account the shear interaction of the subsoil.  $C_{1x}$  and  $C_{1y}$  are parameters of pliability of the subsoil in the x-axis direction, respectively y-axis direction, which represent resistance against horizontal displacement  $u$ , resp.  $v$  (shifts in the plane of the slab). The SCIA ENGINEER offers calculation module SOILIN to solve the interaction of foundations with the subsoil. SOILIN calculates the parameters of the subsoil  $C_{1z}$ ,  $C_{2x}$  and  $C_{2y}$ . Parameters  $C_{1x}$ ,  $C_{1y}$  are always specified by the user. The SOILIN module calculates the settlement based on the elastic half-space. Then subsoil parameters  $C$  are automatically calculated. Whereas the subsoil parameters  $C$  affect the contact stress, and this affects settlement, and all interdependencies are valid also conversely, it is an iterative calculation. The iteration cycle is finished when the calculated value of shift or calculated value of contact stress in two consecutive cycles is almost unchanged (use of quadratic norm). In the author's article [10] the dependence of the deformations calculated by the SOILIN module on the input values of the individual subsoil parameters was monitored and evaluated. Differences in deformations occur depending on the parameters  $C_{2x}$  and  $C_{2y}$ . If  $C_{2x} = C_{2y} = 0$ , these parameters do not enter the SOILIN iterative process and the influence of the surrounding soil environment is not taken into account in the calculations. If the parameters  $C_{2x}$  and  $C_{2y}$  are non-zero, they enter the iterative calculation and the influence of the surrounding soil environment is taken into account [10]. In calculation of the interaction of the subsoil with the slab loaded during the experiment, the SOILIN module was used. The input values of the parameters  $C_{2x}$  and  $C_{2y}$  are non-

zero, i.e. the influence of the surrounding soil environment has been taken into account.

The same values were entered in the calculation as in all previous programs in which this task was also solved (ANSYS and PLAXIS 3D FOUNDATION). Parameters of the geological profile were defined by the modulus of deformability  $E_{\text{def}} = 12.5$  MPa and the Poisson coefficient  $\mu = 0.35$ . In addition, the soil mass density  $\gamma = 20.0$  kN/m<sup>3</sup>, the structural strength coefficient  $m = 0.2$  (according to EC 7 [12]) and the layer thickness (defining the geological profile)  $h = 8.0$  m were given. In this model, the maximum calculated vertical deformation in the center of the slab was 6.26 mm (Fig. 6).

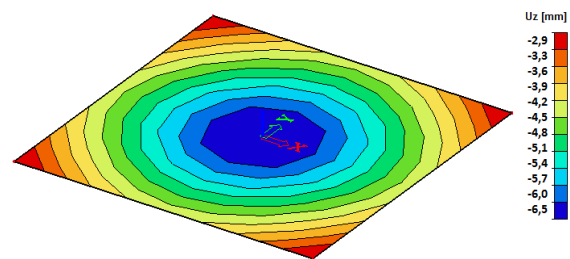


Fig. 6 Surface subsoil model, SCIA ENGINEER

## NUMERICAL ANALYSES IN MKPINTER

To compare the results of the solution of the interaction of the subsoil with the concrete slab, this task (with the same input values) was also analyzed in the non-commercial program MKPINTER [13], [14]. Calculation of the deformations and internal forces of the slab is done by the finite element method (FEM) using isoparametric plate elements with shear effect. The course of contact stress affects the deformation of the slab and of the subsoil too. To cause the contact stress of the same deformation of the slab and subsoil in this nonlinear interaction, this solution is performed by an iterative method. The calculation of stress, settlement and contact stress is solved by the universal method of calculation using Jakobian transformation. In MKPINTER, subsoil-structure interaction is solved using numerical integration calculations of stress and settlement of the modified elastic half-space by structural strength. For more information about MKPINTER see [13], [14].

## COMPARISON OF RESULTS

This article compares the resulting vertical deformations calculated in the software based on FEM - ANSYS, PLAXIS 3D FOUNDATION, SCIA ENGINEER, MKPINTER FEM, and also vertical deformations calculated according to recommended normative procedures.

In the graph (Fig. 7), the vertical deformations

calculated by the various computational programs and procedures are compared. The vertical deformations calculated by the solution of the interaction of subsoil with concrete slab in ANSYS, PLAXIS 3D FOUNDATION, SCIA ENGINEER and MKPINTER are compared. The settlement calculated according to the normative procedures recommended in ČSN 73 1001 [11] and Eurocode 7 [12] are also included in the chart.

The red full line indicates the slab deformation measured at the last loading test step, i.e. at a time when the slab was significantly damaged by cracks. The graph shows vertical deformation dependence on the depth of the 3D subsoil models created in ANSYS (yellow and green) and PLAXIS 3D FOUNDATION (blue). The light lines indicate vertical deformations calculated on the homogeneous model of the subsoil. The dark lines indicate the vertical deformations calculated on the inhomogeneous model of the subsoil in which the value of modulus of deformability increases with the depth. In tasks where the slab was modeled as a 2D linear model (without the impact of cracks), there was a very good accordance in the results from ANSYS (dark and light yellow dashed line) and PLAXIS 3D FOUNDATION (dark and light blue dashed lines). Due to the impact of the cracks in the concrete slab model is not taken into account, the vertical deformations calculated by the above mentioned models are less than the measured deformation of the already extensively damaged concrete slab. This is also valid for vertical deformation obtained in SCIA ENGINEER (purple) and MKPINTER (pink), in which the concrete slab was also created as a 2D linear model without the impact of cracks. There are the subsoil surface model based on the elastic half-space of the modified structural strength of soil (according to EC 7 [12],  $m = 0.2$ ) in programs SCIA ENGINEER and MKPINTER, in comparison with ANSYS and PLAXIS 3D FOUNDATION. It is a surface model of the subsoil and its results do not depend on the chosen depth of the area as it is with 3D models in ANSYS and PLAXIS 3D FOUNDATION. Using the procedure according to ČSN 73 1001 [11], the depth of the deformation zone was 4.15 m and the settlement was 6.55 mm for  $m = 0.1$  (brown dotted line with a cross). The value of the correction coefficient of overload  $m = 0.1$  was determined according to the table in ČSN 73 1001 [11]. According to Eurocode 7 [12], it is always  $m = 0.2$ , the depth of the deformation zone is 3.25 m and the settlement was 5.89 mm (black dotted line with a cross). For calculations of the depth of active zone according to the both above-mentioned recommended standards, it is clear from the graph that different models of subsoil and slab models (which are not uniquely specified in the standards) can obtain a large range of calculated deformation

values.

The calculations whose resulting vertical deformations were greater than the measured deformations of the damaged slab are marked by green lines. Specifically, this is the deformation calculated in the ANSYS, in which the concrete slab was created as a 3D non-linear model with influence of cracks. The highest values of the calculated deformations indicate that in the numerical analyzes performed in this way the influence of the cracks was taken into account, leading to a reduction of stiffness of the concrete slab model and its greater deformations. Of course, these deformations are also dependent on the subsoil model created as a homogeneous continuum (light green) and as an inhomogeneous continuum (dark green).

The average difference was about 66% - between the results of the 2D linear slab model without influence of cracks and the 3D nonlinear slab model with influence of cracks (in the comparison the deformations obtained from the ANSYS). The average difference between the calculated deformations in the homogeneous and inhomogeneous subsoil models was about 29%. The 3D nonlinear model of the subsoil has always been retained when comparing.

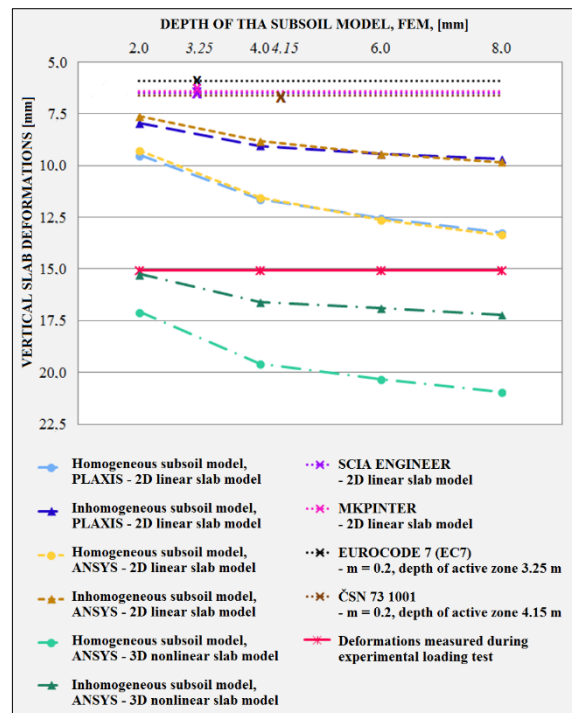


Fig. 7 Comparison of results – deformations

## CONCLUSION

This article compares the resulting vertical deformations calculated in the software based on FEM - ANSYS, PLAXIS 3D FOUNDATION, SCIA ENGINEER, MKPINTER FEM, and also vertical

deformations calculated according to recommended normative procedures.

A very good accordance was in the results from the ANSYS and PLAXIS 3D FOUNDATION - programs in which 3D finite elements were used, and from the SCIA ENGINEER and MKPINTER - programs, which in which 2D finite elements were used. A significant difference in the calculated deformations occurred when comparing the results from the ANSYS and PLAXIS 3D FOUNDATION with results from the SCIA ENGINEER and MKPINTER in which the subsoil-structure interaction is solved based on the theory of elastic half-space modified by structural soil strength. A significant difference in the calculated deformations occurred when comparing the results from the ANSYS and PLAXIS 3D FOUNDATION with results from the SCIA ENGINEER and MKPINTER in which the subsoil-structure interaction is solved based on the theory of elastic half-space modified by structural soil strength.

For calculations of the depth of active zone according to the recommended standards, it is clear that different models of subsoil and slab models (which are not uniquely specified in the standards) can obtain a large range of calculated deformation values.

Although it has been shown that the resulting deformation of the interaction of foundation structure and subsoil created as an inhomogeneous continuum model provide deformations to better delineate the real deformations, prudence is in place when creating a numerical model of subsoil created by spatial finite elements. By choosing the geometry of the solved area without previous experience with the aforementioned parameters, a numerical model can be created that would adversely affect the calculated deformations and lead to dangerous and unreliable results.

## ACKNOWLEDGEMENTS

This outcome has been achieved with the financial support of the project GACR No. 16-08937S „State of stress and strain of fiber reinforced composites in interaction with the soil environment“.

## REFERENCES

- [1] Zienkiewicz, O. C., Taylor, R. L., The Finite Element Method, Volume 2: Solid Mechanics, Oxford, Butterworth-Heinemann, 479 p, 2000.
- [2] Kralik, J., Jendzelovsky, N., Contact problem of reinforced concrete girder and non-linear Winkler foundations, Geomechanics 93, Ostrava, Pages 233-236, 1994.
- [3] Kolar, V., Nemec, I.: Modelling of Soil Structure Interactions, Prague, 336 p, 1989.
- [4] Feda, J., Tenseness of subsoil and calculation methods for calculation of final subsidence, ACADEMIA, 152 pages, 1974. (In Czech)
- [5] Frölich, O. K.: Druckverteilung im Baugrunde, Mit Besonderer Berücksichtigung der Plastischen Erscheinungen, Vienna, 1934.
- [6] Labudkova, J., Cajka, R., Numerical analyses of interaction of steel-fibre reinforced concrete slab model with subsoil, Frattura ed Integrita Strutturale, Volume 11, Issue 39, January 2017, Pages 47-55, 2017.
- [7] Cajka, R., Labudkova, J., Mynarcik, P., Numerical solution of soil - foundation interaction and comparison of results with experimental measurements, International Journal of GEOMATE, Volume 11, Issue 1, 2016, pp. 2116-2122.
- [8] Labudkova, J., Cajka, R., Application of an Inhomogeneous Halfspace for the Solution of Foundation-Subsoil Interaction based on the Finite Element Method, in Proceedings of the Fifteenth International Conference on Civil, Structural and Environmental Engineering Computing, Civil-Comp Press, Stirlingshire, UK, Paper 9, 2015. doi:10.4203/ccp.108.9
- [9] Sucharda O., Pajak, M., Ponikiewski T., Konecny P., Identification of mechanical and fracture properties of self-compacting concrete beams with different types of steel fibres using inverse analysis, Construction and Building Materials, 138, pp. 263-275, 2017, doi:10.1016/j.conbuildmat.2017.01.077.
- [10] Labudkova, J., Cajka, R., Numerical analysis of interaction of steel-fibre concrete slab with subsoil and comparison with values measured during experimental loading test. Proceedings of the International Conference FIBRE CONCRETE, Volume 2015-January, 2015, Pages 292-301, 8th International Conference Fibre Concrete 2015: Technology, Design, Application, FC 2015; 10 – 11 September 2015, Prague; Czech Republic;
- [11] Eurocode 7 - Geotechnical Design, Part 1: General Rules, European Committee for Standardization. EN 1997-1: 2004, Brussels
- [12] ČSN 73 1001. Foundation engineering. Foundation soils under flat foundations, Czech Standards Institute, Prague (in Czech).
- [13] Cajka, R., Analysis of Stress in Half-space using Jacobian of Transformation and Gauss Numerical Integration, Advanced Materials Research, Switzerland, p.178-186, 2013.
- [14] Cajka, R., Accuracy of Stress Analysis Using Numerical Integration of Elastic Half-Space, Applied Mechanics and Materials, Trans Tech Publications, ISSN: 16609336, Switzerland, p.1127-1135, 2013.

## **AN OVERVIEW OF THE IMPACTS OF SUSTAINABLE HOUSING DESIGN ON ENERGY EFFICIENCY OF THE AUSTRALIAN HOUSING**

Javad Asad Poor <sup>1,2</sup>; David Thorpe <sup>2</sup>; Yong Goh <sup>3</sup>

Javad.asadpoor@usq.edu.au; david.thorpe@usq.edu.au; Yong.Goh@usq.edu.au

Department of Architecture, Mashhad Branch-Islamic Azad University, Mashhad, Iran. <sup>1</sup>

School of Civil Engineering and Surveying, Faculty of Health, Engineering, and Sciences, University of  
Southern Queensland, Education City, Sinnathamby Blvd, Springfield Central QLD 4300, Australia. <sup>2</sup>

School of Psychology and Counselling, Faculty of Health, Engineering, and Sciences, University of Southern  
Queensland, Ipswich Campus, 11 Salisbury Rd, Ipswich, Queensland 4305, Australia

### **ABSTRACT**

The building industry has a substantial potential for short-run and cost-effective greenhouse gases emission mitigation with long-term positive sustainability impacts. However, the main problematic issue in the building industry is the existence of large number human-based factors, which makes the operation of the mitigation action plans very complicated and detracts from the outcomes of the implemented plans in this area of industry. The impacts of human-based factors are especially important in the area of small size residential buildings, where a variety of stakeholders play serious roles in the development of the industry. In Australia, the residential sector is the main component of the building industry and has a substantial responsibility in the energy consumption of the country. One critical human-based factor in the residential sector is the occupants' preferences, increasing substantially diversity and complexity of the dwelling units' physical characteristics. This paper intends to explain the role of feasibility assessment and design process in improving the energy performance of the Australian residential sector. In responding to this aim, an overview of spatial, functional, and physical characteristics of the Australian housing results in addressing the key characteristics of the Australian housing preferences. The analyses show that the typological monotony, the owner-occupied housing, alongside occupants' perceptual ability are a number of factors, facilitating the implementation of housing efficiency plans in the early stages of housing decision making. The direction of other characteristics, e.g. floor area, number of bedrooms, and number of people per dwelling units are somehow inefficient, stressing the designers' supervisory roles in enhancing the housing preferences toward more efficient choices. According to the analyses, the feasibility assessment and design process have potential to, directly and indirectly, impact the energy demand of the Australian housing by enhancing physical characteristics of the units, regulating the occupants' housing preferences, and simplifying their daily life activities.

*Keywords: Feasibility Assessment and Design Process; End-users' Environmental Perceptions and Preferences; Australian Housing; Energy Efficiency.*

### **INTRODUCTION**

A successful emission mitigation action plan requires a combination of bottom-up flexibility and top-down fixed rules, to achieve accountability and ambition by means of broad participation (Centre for Climate and Energy Solutions (C2ES), 2015). Based on the 2005 target mitigation baseline, Australia has a responsibility to cut down carbon dioxide (Co2) and greenhouse gas (GHG) emissions 26 percent by 2030 compared with the average global reduction rate of 36 percent (Hasham, et al., 2015).

However, in achieving the Australian target baseline, the building industry has a critical role, because of the responsibility of the industry in the energy consumption and the carbon emission. The

building sector is responsible for 40 percent of the total energy consumptions, and the generation of one-third of CO2 and GHG emission (United Nations Environmental Programme, Sustainable Buildings and Climate Change (UNEP SBCI), 2009). The sector also has exceptional potentials for cost-effective emission mitigation, so that it is possible to decrease up to 29 percent of the emission in the sector without any financial costs (Allwood et al., 2012; Desmarais, et al. 2013). In small size residential buildings, typological diversity of the products, the complexity and diversity of stakeholders, the direct impacts of occupants' attitudes and preferences, as well as the spread and magnitude of energy use activities detract from the effect of the mitigation actions plans (Cheng, 2010;



Levine et al., 2007).

In the residential sector, end-users are, indeed, the key driving forces in the development of the housing sector compared with the other industries. Therefore, improving the energy performance of the sector depends strongly on a proper attention to the bottom-up approach as the key concept in maximizing the occupants' participation parallel to taking into account the development of the efficiency rules alongside the investment on the technical aspects. This paper intends to explain the contribution of the housing design process in improving the energy performance of the Australian housing sector and in overcoming the challenges.

The spatial, functional, and physical characteristics of the residential buildings influence substantially the energy performance, and emission production of the sector (United Nations Environmental Programme, Sustainable Buildings and Climate Change (UNEP SBCI, 2009). The housing design process has a lot to contribute to the mitigation, not only by the direct effects on the dwelling units' physical characteristics, but also by the indirect effects on the occupants' environmental perceptions, attitudes, and housing choice behaviours (Levermore, 2008, Kwami et al., 2015). This paper makes initially an overview of the literature on the effects of the design process on the energy performance of the residential buildings, then explains the capacities of the housing design in enhancing the energy performance of the dwelling units in Australia.

## LITERATURE REVIEW

According to UNEP SBCI (2009), the main factors in the energy performance of the residential buildings are the building spatial and physical characteristics, along with the end-users' perceptions, attitudes, and behaviours. The study of Bawden & Williams (2015) also revealed that a number of housing characteristics, e.g. dwelling type, occupants' income, and household composition have substantial impacts on the energy consumption of the residential units. Australian Bureau of Statistics (ABS, 2013a) also indicated that the number of people and the number of bedrooms per dwelling unit affect significantly the energy consumption of the units. However, Richard (2014) believed that in the Australian residential sector, the current benchmark of the energy consumption in the residential buildings is substantially far from the sustainable level. However, it is believed that

regarding the emission mitigation in the residential sector, the feasibility assessment and design stages are highly responsible for improving the energy demands of the buildings for both embodied and operation energies (Allwood et al., 2012; Nasrollahi, et al., 2013; Sattary and Thorpe, 2016; UNEP SBCI, 2009).

In this regard, the study of Allwood et al. (2012) stressed that environmental sustainability relies substantially on developing a production process, which is capable of employing the efficient materials and reducing the demands, while the process has ability to retain the function and service qualities. In the housing production process, the decisions about spatial and physical characteristics, and the function and service quality are mostly made in the feasibility assessment and design process.

Sattary and Thorpe (2016) also stressed the necessity of replacing the conventional materials with the energy efficient materials in the production of the new houses to decrease the embodied energy of the buildings. Their study also highlighted the contribution of feasibility assessment and design stage in improving the sustainability of the housing industry. Sattary and Thorpe (2016) revealed that the sustainable usage of the building materials would make it possible to reduce the embodied energy of the buildings by up to 64 percent. Accordingly, the sustainable usage of the materials means the selection of the materials by considering the availability of the resources, the energy consumption of the mining and manufacturing process, the transportation, and the installation, alongside the possibility of employing reused or recycled materials, and the degree of environmentally friendly of the selected materials. The process of the material selection should be mainly developed in the early stages of the feasibility assessment and design process.

It is also evident that the energy-efficient architectural techniques and principles, e.g. orientation, courtyard, window to wall ratios, geographical location of windows, as well as cross ventilation and shading devices have serious contributions in improving the energy performance of the residential buildings during the operational phase (Nasrollahi, et al., 2013). Nasrollahi, et al., (2013) stated that an efficiently well-designed residential building is able to cut down the energy performance of the units up to 65 percent, which is substantially related to the decisions made during the design process.

The remaining question is the impacts of the physical, functional, and spatial characteristics, arrangement, structure, and organization, e.g. size, form, shape, depth, proportions, interconnections, openness, and interrelationships, flexibility, and complexity along with the occupants' housing behaviours in improving the energy performance of the residential buildings in the total lifecycle of the buildings including embodied and operation phases. The feasibility assessment and design stages are responsible not only for improving the buildings capacities for employing passive techniques through the implementation of the sustainable and efficient materials, technologies, and principles, but also for arranging the buildings spatial characteristics, structure, and organization, alongside regulating the end-users' choice behaviours toward more efficient energy consumption actions (Asad Poor 2014, 2012). Moving beyond this level, housing design has capability of improving end-users' sense of place by enhancing the congruity of the physical settings with the occupants' motivations; hence has particular role in improving their pro-environmental behaviours, enhancing the overall efficiency of the residential environment (Asad Poor, 2014, 2015; Morrison, 2011; Ramkissoon, 2013).

Although the housing design process has substantial responsibility for improving the energy performance of the residential buildings by improving the arrangement of the spatial layouts, and the end-users' preferences, so far the research works have paid proper little attention to this area. In the context of Australia, the current direction of housing development and the rapid growth of the number of new housing units are the main reasons for the rapid increase in the demands for energy in the residential sector; hence the direction of the housing development overrode the outcomes of the mitigation plans in the building sector (Beyond Zero Emissions (BZE), 2013). This paper, therefore, intends in explaining the contribution of the feasibility assessment and design stages in improving the energy performance of the Australian housing sector, possibly obtained by moderating end-users' housing preferences and energy demands, as will be discussed in the next sections.

## RESEARCH METHODOLOGY

It is believed that congruity between the outcomes of engineering and technological approach and occupants' choice behaviours alongside the

flexibility of energy efficiency rules is more beneficial for energy efficiency and emission mitigation than up-down fixed rules based on mere technological and engineering approach (BZE, 2013; C2ES, 2015). This research employs a down-up analytical model, stressing the potential contribution of individual housing units alongside the substantial role of occupants' preferences in enhancing the overall energy consumption of the residential sector.

In studying human perceptions from their choice behaviours, two possible methods are to look at people's revealed preferences based on their actual choices (secondary data) or stated preferences based on their intended choices (Collen & Hoekstra, 2001). Since the nature of stated preferences is hypothetical, referring to revealed preferences ensures the validity of analyses and the significance of findings if reliable actual data would be available (de Vaus, 2002; Opoku & Abdul-Muhmin, 2010). It is also believed that explaining occupants' housing preferences through an overview of the physical, functional, and spatial characteristics of their housing environments is a reliable methodology for explaining their perceptions (de Vaus, 2002; Asad Poor, 2014).

In Australia, a number of online databanks, e.g. Australian Bureau of Statistics (ABS) and Beyond Zero Emissions (BZE) provide reliable data related to the Australian housing characteristics, which are appropriate sources for tracking the Australian housing trends. This research, therefore, employs revealed preferences model and compiled the secondary data from these online sources. The analyses facilitate the representation of key characteristics of the Australian housing; hence, make it possible to explain the potential contribution of the design process in enhancing the energy performance of the residential sector. The analyses indeed explain the role of feasibility assessment and design process in improving spatial layout arrangements and physical characteristics of dwelling units, enhancing the energy performance of the sector through improving the overall efficiency of the buildings and facilitating the occupants's daily life activities.

Mapping the key characteristics by merging the compiled data through Microsoft Excel, the next section initially discusses the critical aspects of occupants' housing preferences. The section then makes a comparison between Australian residential and non-residential sector to explain the substantial role of energy performance of the housing sector in overall energy consumption of the building and construction industry in Australia. Referring to the Australian projected population (ABS, 2015b), the section also calculates a number of future trends of the Australian housing, representing the impacts of the current direction of housing development on future energy performance of the Australian

domestic sector. In final, addressing a previously conducted research work, a feasibility assessment is made to briefly estimate the potential contribution of the design process in enhancing the energy performance of the Australian housing. The section ends up with a brief discussion on the different components of sustainable housing design and the techniques related to each component.

## ANALYSES AND DISCUSSION

In discussing the responsibility of the feasibility assessment and design stages in facilitating the mitigation baseline of Australia, it is initially necessary to make an overview of the Australian housing characteristics.

In this section, the housing characteristics will be initially explained, and then a discussion on the impacts of these characteristics on energy performance improvement in the residential sector will be discussed. In the discussion, the main effort is to explain the impacts of end-users' preferences on the housing physical characteristics, and the impacts of these preferences on the housing units energy performance, and finally the contribution of the design process and feasibility assessment in enhancing energy performance of the Australian housing. Table 1 provides a brief picture of the key characteristics of the Australian housing, which reveals the rapid and dramatic increase in the demands for more spacious dwelling units with higher energy demands during the recent decades.

Table 1. Key Characteristics of Australian housing

No	Key Characteristics	Description
1	Housing Type	Separate house standing on its own block: 79% (2012).
2	Number of Rooms	3 or more bedroom house: 70.3% ((2012)). The number of rooms have increased from 2.8 to 3.1 (1976 – 2014).
3	Housing Size	Overall average floor area increased from 149 to 207 Square Metre (1984-2013). Average floor area of the separate housing increased from 162 to 241 Square Metre (1984-2013). Average floor area of the apartments increased from 99 to 134 Square Metre (1984-2013).
4	Owner-Occupancy	67% (2013-2014).
5	Mortgage	31% without mortgage, 36% with mortgage (using low-interest loan for other financial purposes) (2013-2014). The decrease in the outright owner-occupied housing from 42% to 31% (1994-2014).
6	Average Floor Area per Person	Almost 90 Square Metre (2012).
7	Number of Person per Household	Decreased from 3.1 to 2.6 (1976 – 2014).
8	Number of Bedroom per Person	Increased from 0.9 to 1.2 (1976 – 2014).
9	Spare bedrooms	Almost 80% of the households have more than 1 spare bedrooms (2013-2014).
10	Proportion of Lone Households	Almost 2,100,000 Households by 2011 (24.3%), estimated to be increased to almost 3,300,000 households by 2036 (the growth rate of 63% with high demands for separate housing) (2013-2014).

Source: ABS (2012, 2013b, c, 2015a), de Vaus & Qu, (2015)

One of the factors that assist in explaining the housing characteristics is the housing tenure and ownership. 67 percent of the Australian households live in owner-occupied houses, and from this population, 31 percent are without any mortgages, and the rest of them (36 percent) mostly uptake the mortgage for other financial purposes rather than the housing purchase (ABS, 2015a). According to ABS (2012), the proportion of owner-occupied houses in

separate houses is 88 percent of the total owner-occupied houses. This means that the owner-occupied separate houses are the most preferred accommodation destination of the Australian population, while they purchase the other housing types for non-accommodation purposes, e.g. to have income from the rental payments or other financial opportunities. It is also evident that the outright owner-occupation has been dropped from 42% to 31% in the period of 1994-95 to 2013-2014. The descending order of outright owner-occupied housing makes it evident that the current direction of housing development has been achieved with the cost of loaning and mortgaging.

In other words, an overview of the Australian housing shows that 3 or more bedroom separate houses are the most important part of the building sector in Australia, and has significant responsibility in the energy performance of the building sector in this country. However, there are a number of multiple barriers that make the implementation of the mitigation plans in the residential buildings quite complicated and practically difficult, one of which is the diversity and complexity of the building types and characteristics, and the other is the diversity of the stakeholders along with the absence of the end-users and the separation of and the distance between the costs paid by the owners and benefits received by the occupants (Cheng, 2010; Levine, et al., 2007; UNEP SBCI, 2009). These factors detract from the leverage of the mitigation action policies; hence, make it necessary to find out a practical solution for the problem. The most preferred housing type and tenure provide a suitable platform for eliminating a number of barriers preventing from the implementation of energy efficiency action plans in the Australian residential sector, one of which is the diversity of the stakeholders, the second is the absence of the end-users' in early stages of housing decision-making, and the third is the distance between costs and benefits.

Looking at the housing type and tenure characteristics, it is also necessary to consider some other characteristics related to the spatial organization and physical settings of the residential buildings. Monitoring the changes happened to the Australian housing characteristics over the last few decades makes it possible to explain the direction of housing development in the Australian context. The changes in the spatial and physical characteristics makes it evident that the average floor area has increased from 170m<sup>2</sup> to 241m<sup>2</sup> from 1985 to 2013 (ABS, 2013c). The average floor area per person has also increased in the separate houses from 50m<sup>2</sup> to 90m<sup>2</sup> over the same period. The changes in the average floor area of the separate dwelling units from 2003 to 2013 shows a significant increase in the average floor area of the separate houses (from 235m<sup>2</sup> to 241m<sup>2</sup>) comparing with the decrease in the

average floor area in the other housing types (from 142m<sup>2</sup> to 134m<sup>2</sup>) (ABS, 2013c). From 1976 to 2013-2014, the number of bedrooms per dwelling has increased from 2.8 to 3.14, while the number of persons per household has decreased from 3 to 2.4 (ABS, 2015a). 49.9 percent of 3 or more bedroom separate houses were occupied by less than two persons households, 16.9 and 33 percent respectively for lone person and two persons households (de Vause & Qu, 2015; ABS, 2012). The amount of lone person households has grown from 11 to 25 percent during the period of 1911 to 2011 (de Vause & Qu, 2015). The number of lone person households is also estimated to significantly increase from 2'100'000 households in 2011 to more than 3'300'000 households in 2036 (1'300'000 households with growth rate of almost 63% growth) (ABS, 2015b). According to ABS (2012), 79 percent of households had spare bedrooms.

Accordingly, the households mostly have enjoyed relatively spacious accommodations, and the housing units are mostly not fully utilized by accommodating a reasonable number of people, even though the spare spaces might be allocated for other functional purposes, e.g. study room, office room, play room, and store. The most popular housing type, the accommodation preferences, the demographic of lone person households, along with the average number of people per dwelling in 3 or more bedroom separate houses are also some pieces of evidence of lack of diversity of the Australian housing industry market in relation to the different lifecycle stages of the Australian populations. In this regards, the diversity and flexibility of the housing spatial structure have a strong responsibility in making the industry more compatible with the lifecycle requirements of the population. The necessity of paying attention to the flexibility and the diversity of the new dwelling units is more obvious when the ascending order in the proportion of lone person in the Australian projected population in the next two decades (2026 and 2036) would be considered (ABS, 2015b).

The most preferred housing type decreases the problem of housing diversity, as the majority of the households prefer 3 or more bedroom houses as their residential place. The housing tenure is also an evidence of the presences and availability of end-users during housing delivery, and also gives the costs and benefits to the same person. The presence of the end-users during the design process increase the opportunity for making more reliable decisions about the operation phases of the buildings as well. The most preferred housing type and tenure, along with size and economic performance of the housing units in Australia, highlight the socio-economic characteristics of the end-users, their ability, capacity, and power in joining to the mitigation action plans, their presence and availability during

different stages of housing delivery, and the substantial decrease in the complexity of decision-making provided by stakeholders diversity. These parameters all together provide higher opportunity for the implementation of the efficiency policies in the design stage of the Australian housing.

Some other aspects like the increase in the average floor area and the number of bedrooms, compared with the decrease in the number of people per household are some of the growing inefficient aspects of the housing preferences in Australia. However, although these characteristics might be somehow signs of the intensification of unsustainable attitudes and perceptions, they meaningfully address the end-users' level of perceptual ability and socio-economic characteristics. These characteristics show the critical responsibility of the housing design practitioners in enhancing the situation by a careful consideration of their substantial potential in impacting the people's daily life activities, behaviours, preferences, and perceptions.

Regarding the role of residential sector in the energy performance of the Australian building and construction sector, it is necessary to make a brief

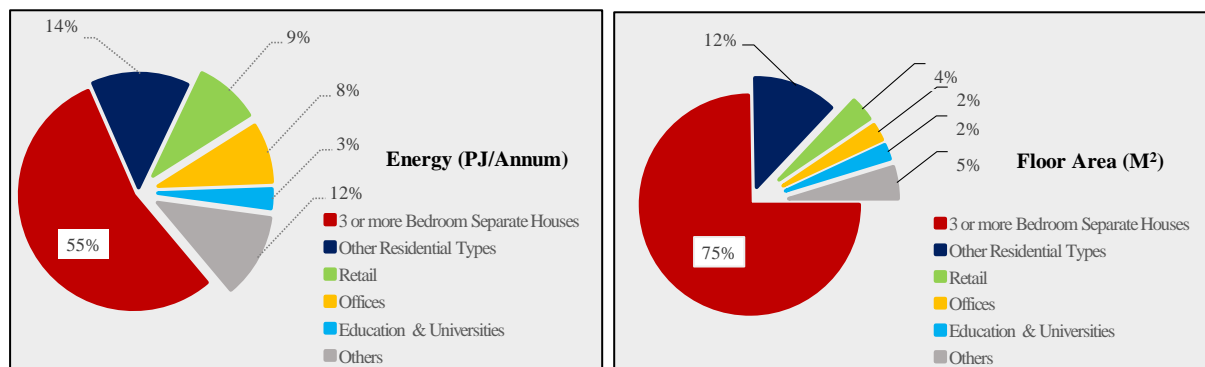
comparison between the residential sector and the whole building sector of Australia. Accordingly, a comparison has been made between the floor area and energy consumption of the residential buildings and non-residential buildings to visualise the substantial responsibility of the residential sector in energy performance of the building industry.

The floor area of the Australian residential buildings is almost 87 percent (Office 2.3 percent, Retail 3.3 percent) of the total building sector of the country (BZE, 2013, pp. 45-46; ABS, 2013b, c). The total floor area of separate houses standing on their own blocks is 79 percent, almost 75 percent of which are 3 or more bedroom housing units (ABS, 2013b, c). Regarding the energy consumption, the residential sector consume up to 69 percent of the total energy (office buildings 8 percent, and retail 9 percent), while most of this amount is consumed in 3 or more bedroom separate houses with the proportion of almost 55 percent of the total energy consumption of the building sector (Table 2; Figure 1) (BZE, 2013, pp. 45-46; ABS, 2013b, c).

**Table 2.** National residential and non-residential building characteristics

Building Category		Flor Area (m <sup>2</sup> )		Percentage (%)		National Energy Use (PJ/Annum)	
Residential	3 or more Bedroom Separate Houses	1 413 283 000	1 645 188 000	74.8	87	300 (54.5%)	375 (68.2%)
	Other Residential Units	231 905 000		12.2		75	
	Retail	67 134 855		3.55		49.4	
Non-Residential	Offices	47 232 731		2.5		46.0	
	Education & Universities	41 568 034	245 311 000	2.2	13	15.1	175 (31.8%)
	Others	89 457 986		4.75		64.5	
		1 890 500 000		100		550	

**Fig. 1.** National residential and non-residential building flat area and energy consumption



Source: BZE (2013); ABS (2013)b

The energy consumption of the 3 or more bedroom separate houses is more than 300 PJ/Annum (55% of the total building sector) and 114 PJ/Annum (38%) (The Government of South Australia: Department of State Development, 2015) consumes only for heating and cooling purposes. Addressing the findings of Nasrollahi, et al. (2013) study, an efficiently well-designed residential building is capable of improving the energy performance of the building up to 65%. Therefore, lack of attention to the design of efficient houses with respect to the energy required for heating and cooling would be substantially responsible for losing up to 74 PJ/Annum in the Australian housing sector, which is substantially higher than the total energy consumption of the non-residential, e.g. retails, offices, and education and universities.

The number of the Australian households is projected to be increased from 9'250'000 to 12'600'000 million in 2036 (3'350'000 or around 35 percent increase over the period of 2016-2036), while the Australia's population is estimated to increase by 33 percent in the same period, from 24'300'000 people to 32'400'000 people (ABS, 2015b). The projected population and household composition make evident the future demands for the new houses and the critical role and responsibility of the housing design process in enhancing the housing characteristics and regulating the end-users' preferences towards more efficient housing choice behaviours.

According to the projected number of households, during the next two decades (from 2016 to 2026 and 2036) more than 3'000'000 dwelling units should be constructed (an average of 1'500'000 units for each period) (ABS, 2015b), 2'250'000 (75%) of which would be from 3 or more bedroom separate houses. Accordingly, with assuming the average floor area of 240m<sup>2</sup>, the floor area of the 3 or bedroom dwelling units would be up to 550'000'000m<sup>2</sup>. The energy consumption of the projected dwelling units would be up to 2'300PJ (an average of 115PJ/Annum) over the period of these 20 years. Regarding the study of Nasrollahi et al. (2013), the potential the energy consumption reduction through the production of efficiently well-designed dwelling units with employing the bioclimatic architectural principles, just in the area of heating and cooling, would be up to 570PJ (an average of 28PJ/Annum).

The capacity of the reduction would be even far greater than this amount if the design process would be able to decrease the housing energy demands by

implication of bioclimatic architectural principles, e.g. using natural elements, e.g. vegetation and water features, cross ventilation, window to wall ratio and openings, shading devices, geographical orientation, external wall dimensions, building mass and density, height and 3D proportions. The second components of the sustainable design is the optimization of the building physical characteristics, e.g. floor area and the building size, as well as other physical characteristics, e.g. the number bedrooms, and other lateral facilities of the residential units. The architectural design is also capable of providing positive impacts on the occupants' choice behaviours by optimizing the spatial and functional structure and organization, improving the interior layouts arrangement of the dwelling units, along with enhancing the flexibility of the dwelling units in respect to the different lifecycle stages of the occupants, which has capability of reducing the overall energy demands of the dwelling units. The design process has also potential in improving the energy performance by facilitating the sustainable usage of the building construction materials by reducing the wasted materials, encouraging the consumption of the reusable and recycled materials alongside the usage of the materials that are environmentally friendly and more compatible with the climate and are efficient with respect to the availability of the resources, production and manufacturing process, transportation, and installation, which are capable of enhancing the embodied energy parallel to the operational energy of the dwelling units. Table 3 overviews briefly the application of architectural design in reducing the energy demands in the residential sector.

Regarding the housing spatial, physical, and functional characteristics and the direction of projected housing development, the design process has strong role and responsibility in enhancing the energy demands of the occupants, in improving the energy performance of the buildings, and in implementing the energy efficiency action plans. The designers are, also, responsible and have supervisory roles in improving the people's awareness, information, and knowledge, and to motivate them toward the selection of more efficient housing spatial and technological options. The designers should not be passive followers of their clients' preferences and market trends; they should have an active role in enhancing the sustainability of their housing design practices

**Table 3.** Key components of sustainable housing design

Different Components		Techniques	Advantages
1	Bioclimatic Architectural	Using natural elements, e.g. vegetation and water features	Improving the energy

	Principles		Cross ventilation		demands for heating and cooling
			Window to wall ratio and openings		
			Shading devices		
			Orientation		
			External wall dimensions and materials		
			Building mass and density		
			Height and 3D proportions		
2	Building Characteristics	Physical	Optimizing floor area and building size		
			Number of rooms		Enhancing the building energy performance
			Average floor area per person		
3	Interior Layouts Arrangement and Spatial Organization		Spatial and functional structure and organization		Improving the occupants' housing choice behaviours
			Interior layouts arrangement		
			Flexibility of the dwelling units in respect to the different lifecycle stages of occupants		
			Reducing the waste materials		
4	Sustainable Usage of the Building Construction Materials		Consumption of the reusable and recycled materials		Reducing the embodied energy of the residential buildings
			The material that are environmentally friendly and more compatible with the climate		
			Efficient materials with respect to the availability of the resources, production and manufacturing process, transportation, and installation		

### Conclusion

Regarding spatial, physical, and functional characteristics, housing preferences, and direction of housing development in Australia, the concept of sustainable housing design has substantial contributions for improving energy performance of the Australian housing. The responsibility of feasibility assessment and design process would be highly critical by considering the 2036 projected households and the future demands for new residential units. Although the literature mostly emphasized the responsibility of sustainable materials alongside bioclimatic architectural techniques and principles in improving the buildings energy performance, there are other components, e.g. physical characteristics of the buildings alongside interior layouts arrangements and spatial organization, impacting directly or indirectly the energy performance of the residential buildings. The employment of different components of housing design has direct impact on reducing the energy demand of the units by improving the physical characteristics of the buildings and has indirect impact by simplifying occupants' daily life activities. The implementation of the different components of housing design depends strongly on the interest and involvement of end-users. In this regard, the second level of indirect impacts of housing design is the supervisory role of the designers in enhancing end-

users' housing choice behaviours. The housing design is also responsible for paying higher attention to the diversity and spatial flexibility of housing products to improve the compatibility of the products with the different lifecycle stages of the Australian population. Improving the flexibility of the housing spatial structure in relation to the Australian end-users' lifecycle requirements and family composition changes is also applicable for the existing dwelling units. In sum, sustainable housing design has potential to impact the energy performance of the Australian residential sector directly through the enhancement of the spatial and physical characteristics of the housing units and indirectly through improving occupants' housing preferences and daily life activities; hence should gain centrality in the energy efficiency action plans.

### REFERENCES

- [1] Allwood, J. M., Cullen, J. M., Carruth, M. A., Cooper, D. R., McBrien, M., Milford, R. L., Moynihan, M. C., Patel, A. C. (2012). *Sustainable Materials: with both eyes open*. Citeseer.
- [2] Asad Poor, S. J. (2014). *Housing Needs and Preferences based on Maslow's Motivational Theory*. (Ph.D.), Universiti Teknologi Malaysia.
- [3] Asad Poor, S. J. (2015). Participation, Sense of



- Home, and End-users' Needs in Mass Housing. *Procedia - Social and Behavioural Sciences*, 201, 286-296. doi: <http://dx.doi.org/10.1016/j.sbspro.2015.08.177>. Retrieved from <http://www.sciencedirect.com/science/article/pii/S1877042815048259>.
- [4] Asad Poor, S. J., & Jusan, M. M. (2012). *Exploring Housing Attributes Selection based on Maslow's Hierarchy of Needs*. In *Procedia - Social and Behavioral Sciences* Retrieved from <http://www.sciencedirect.com/science/article/pii/S1877042812010774>.
- [5] Australian Bureau of Statistics, (2012). *Year Book Australia 2012, cat. no. 1301.0*. Canberra: ABS Retrieved from <http://www.abs.gov.au/ausstats/abs@.nsf/mf/1301.0>.
- [6] Australian Bureau of Statistics, (2013a). *Household Energy Consumption Survey, Australia: Dwelling characteristics: energy expenditure and consumption, cat. No. 4670.0*. ABS, Retrieved 31 May 2016, 2016 from <http://www.abs.gov.au/ausstats/abs@.nsf/web%20pages/Citing%20ABS%20Sources>.
- [7] Australian Bureau of Statistics, (2013b). *Housing Occupancy and Costs, 2011-12, cat. no. 4130.0*. Canberra: ABS Retrieved from <http://www.abs.gov.au/AUSSTATS/abs@.nsf/Lookup/4130.0Main+Features12011-12?OpenDocument>.
- [8] Australian Bureau of Statistics, (2013c). *Building Activity, Australia: Average floor area of new residential buildings, cat. no. 8752.0*. Canberra: ABS. Retrieved from <http://www.abs.gov.au/AUSSTATS/abs@.nsf/Previousproducts/8752.0Feature%20Article1Jun%202013>.
- [9] Australia Bureau of Statistics, (2015a). *Housing Occupancy and Costs, 2013-14, cat. no. 41340.0*. Canberra: ABS Retrieved from <http://www.abs.gov.au/ausstats/abs@.nsf/Lookup/by%20Subject/4130.0~2013-14~Main%20Features~Key%20Findings~1>.
- [10] Australian Bureau of Statistics, (2015b). *Household and Family Projections, Australia, 2011 to 2036, cat. no. 3236.0*. Canberra: ABS. Retrieved from <http://www.abs.gov.au/ausstats/abs@.nsf/Latestproducts/3236.0Main%20Features42011%20to%202036?opendocument&tabname=Summary&prodno=3236.0&issue=2011%20to%202036&num=&view=>.
- [11] Bawden, K., & Williams, E. (2015). Hybrid Life Cycle Assessment of Low, Mid and High-Rise Multi-Family Dwellings. *Challenges*, 6(1), 98-116.
- [12] Beyond Zero Emissions, (2013). *Zero Carbon Australia: Buildings Plan*. Melbourne: BZE, Melbourne Energy Institute, The University of Melbourne. Retrieved from <https://bze.org.au/buildings>.
- [13] Center for Climate and Energy Solutions, (C2ES). (2015). *OUTCOMES OF THE U.N. CLIMATE CHANGE CONFERENCE IN PARIS 21st Session of the Conference of the Parties to the United Nations Framework Convention on Climate Change (COP 21)*: C2ES. Retrieved 29/08/2016, from URL <http://www.c2es.org/international/negotiations/cop21-paris/summary>.
- [14] Cheng, C.-C. (2010). A new NAMA framework for dispersed energy end-use sectors. *Energy Policy*, 38(10), 5614-5624.
- [15] Collen, H. and Hoekstra, J. (2001). Values as determinants of preferences for housing attributes', *Journal of Housing and the Built Environment*, Vol. 16, No. 3, pp.285-306 (accessed 15 September 2012).
- [16] De Vaus, D. (2002). *Surveys in Social Research 5th Edition*. Taylor & Francis. Retrieved from <http://books.google.com.my/books?id=1IRDJEtBg48C>.
- [17] de Vaus, D., & Qu, L. (2015). *Demographics of living alone (Australian Family Trends No.6)*. (978-1-922038-98-2). Melbourne: AIFS, Australia Government, Australian Institute of Family Studies Retrieved from <https://aifs.gov.au/publications/demographics-living-alone>.
- [18] Desmarais, F., Lawson, M., & Owen, T. (2013). *Transparency in the Built Environment: Calculating and assessing embodied energy of construction materials*. Retrieved 01/05/2016.
- [19] Hasham, N., Bourke, L., & Cox, L. (2015). *Abbott government announces plan to cut emissions by 26 to 28 percent by 2030*. Retrieved 29/08/2016, from <http://www.smh.com.au/federal-politics>
- [20] Kwami, Husayn Idi, Che-Ani, Adi Irfan, Ibrahim, Nik Lukman Nik, & Abd-Razak, Mohd Zulhanif. (2015). Assessing students perceptions to sustainability practices at National University of Malaysia (UKM). *International Journal of Environment and Sustainable Development*, 14(2), 143-153. <http://www.inderscienceonline.com/doi/abs/10.1504/IJESD.2015.068603>.
- [21] Levermore, G. (2008). A review of the IPCC Assessment Report Four, Part 2: Mitigation options for residential and commercial buildings. *Building Services Engineering Research and Technology*, 29(4), 363-374.
- [22] Levine, M., Urge-Vorsatz, D., Blok, K., Geng, L., Harvey, D., Lang, S., Levermor, G., Mehlwana, A. M., Mirasgedis, S., Novikova, A., Rilling, J., Yoshino, H., (2007). Residential

- and commercial buildings. Climate change 2007; mitigation. Contribution of working group III to the fourth assessment report of the IPCC Cambridge University Press, Cambridge, United Kingdom and New York, NY, USA.
- [23] Morrison, N. (2011). *The Carbon Reduction Challenge: Motivating households to act*. Paper presented at the 23rd ENHR Conference, Toulouse, France.
- [24] Nasrollahi, F., Wehage, P., Shahriari, E., Tarkashvand, A., & Schäfer, R. (2013). *Energy Efficient Housing for Iran: Pilot Buildings in Hashtgerd New Town*. Univ.-Verlag der TU. Retrieved from [http://www.dmsw.net/downloads/YoungCities\\_Vol4.pdf](http://www.dmsw.net/downloads/YoungCities_Vol4.pdf).
- [25] Opoku, R. A., & Abdul-Muhmin, A. G. (2010). Housing preferences and attribute importance among low-income consumers in Saudi Arabia. *Habitat International*, 34(2), 219-227. Retrieved from <http://www.sciencedirect.com/science/article/B6V9H-4XFNCM2-1/2/1a380b8987f00c3361d7ff5ab0cf1bab>.
- [26] Ramkissoon, H., Weiler, B., & Smith, L. D. G. (2013). Place attachment, place satisfaction and pro-environmental behaviour: a comparative assessment of multiple regression and structural equation modeling. *Journal of Policy Research in Tourism, Leisure, and Events*, 5(3), 215-232. Retrieved from [http://www.tandfonline.com/doi/abs/10.1080/19407963.2013.776371#.V0u\\_snF96M8](http://www.tandfonline.com/doi/abs/10.1080/19407963.2013.776371#.V0u_snF96M8).
- [27] Richard. (2014). *A Rough Carbon Budget For Buildings*. eTool, Retrieved 26 May 2016, Retrieved from <http://etoolglobal.com/category/eblog/energy>.
- [28] Sattary, S., & Thorpe, D. (2016). Potential carbon emission reductions in Australian construction systems through bioclimatic principles. *Sustainable Cities and Society*, 23, 105-113. doi: <http://dx.doi.org/10.1016/j.scs.2016.03.006>. Retrieved from <http://www.sciencedirect.com/science/article/pii/S2210670716300373>.
- [29] Steg, L., & Vlek, C. (2009). Encouraging pro-environmental behaviour: An integrative review and research agenda. *Journal of Environmental Psychology*, 29(3), 309-317. doi: <http://dx.doi.org/10.1016/j.jenvp.2008.10.004>. Retrieved from <http://www.sciencedirect.com/science/article/pii/S0272494408000959>
- [30] The Government of South Australia: Department of State Development, (2015). *How energy is used in the home*. Retrieved 30 May 2016, 2016 from <https://www.sa.gov.au/topics/water-energy-and-environment/energy/saving-energy-at-home/check-and-reduce-your-energy-use/energy-use-at-home>.
- [31] UNEP SBCI, United Nations Environmental Programme, Sustainable Buildings, and Climate Change. (2009). *Buildings and Climate Change: Summary for Decision Makers*: United Nations Environment Programme. Retrieved from <http://www.unep.org/SBCI/pdfs/SBCI-BCCSummary.pdf>.

## **VULNERABILITY ASSESSMENT OF SURIGAO METRO WATER DISTRICT UNDER SEISMIC HAZARD**

Sheena I. Better<sup>1</sup> and Lessandro Estelito O. Garciano<sup>2</sup>

<sup>1</sup>Undergraduate student, De La Salle University - Manila, Philippines; <sup>2</sup>Associate Professor, De La Salle University - Manila, Philippines

### **ABSTRACT**

Earlier this year, Surigao Del Norte, a province in the Philippines experienced a 6.7 magnitude earthquake. The severe ground movement caused some of the buried pipelines to be pulled-out from their supports. This type of failure occurs when the ground strain during extreme seismic excitation exceeds the strain capacity of the buried pipe. The failure of the pipes resulted to the loss of water that was vital for post-earthquake recovery efforts. In this regard, there is a need to re-assess the vulnerability of the buried pipes of the water network. In this paper, a probabilistic seismic hazard analysis (PSHA) was employed to estimate the seismic hazard within the concession area. Past seismic data that can significantly affect the target structure is used for this purpose. The buried water lifeline system of Surigao Metro Water District (SMWD) was chosen as the target lifeline. An appropriate ground motion prediction equation (GMPE) was used to develop the uniform hazard response spectra for the site. To assess the vulnerability of the pipes three damage states were considered: major, moderate and minor. The probability of major, moderate and minor damage for each pipe was determined using Monte Carlo simulation. Subsequently, fragility curves were obtained.

*Keywords: Buried Pipelines, PSHA, Damage States, Fragility Curve, Monte Carlo Simulation*

### **INTRODUCTION**

Earthquakes are one of the most damaging natural hazard to a built environment. Countries located along the “Pacific Ring of Fire” such as the Philippines experience more earthquakes than any other part of the world. In recent years, there have been three earthquakes in the country that caused damage to lives and property, e.g. Bohol Earthquake in 2013, Batangas Earthquake in 2017 and the Surigao Earthquake in 2017. These earthquakes caused damage to bridges, schools, hospitals and historical structures (Garciano and Taclibon 2013), and power supply system (Crismundo, 2017).

Aside from potential damage to building and bridges, severe ground movement can trigger damage to buried utility lifelines that can stop the operation of the entire lifeline system. Previous works by Hamada, 2014, Sahoo et. al, 2014 O'Rourke and Liu, 1999, Tromans, 2004 discussed the seismic risks of buried water lifelines, as well the behavior of buried water lifelines.

The problems posed by the lack of potable water supply for post-seismic recovery operations after a destructive earthquake is therefore an important issue. Considering the vulnerability of our buried utility lifelines to extreme environmental events, there has been a change from a passive to a more pro-active stance by various government agencies to study, document, design mitigation measures, and to retrofit structures for the reduction of the effects of these

hazards. This paper is a contribution to these efforts. The purpose therefore of this study is to estimate the damage of the buried lifeline network of the Surigao Metro Water District (SMWD) and provide additional information on the effect of seismic ground motion to the buried steel pipes. The main outputs of this research are fragility curves of buried main water pipelines during extreme seismic events that can be used to develop risk management strategies.

The paper is organized into the following: first, assessing the site-specific seismic hazard using a probabilistic approach. In this step the peak ground acceleration (pga) at bedrock as well as the uniform hazard response spectra at the ground surface is established. Second, the performance criteria as a function of pipe and ground strains due to an earthquake are defined as well as the damage states criteria, i.e. minor, moderate and major damage were calculated. The results are summarized by fragility curves and are developed based on models developed by Koike (2009).

### **TARGET AREA**

Surigao City is the capital city of Surigao del Norte. It is situated in the northeastern part of Mindanao, Philippines. It has a total land area of 245.3 square kilometers (PSY 2010) with 17 municipalities and 335 barangays. Surigao City has a population of about 140,540 and is composed of three barangays namely: Washington, Taft and San Juan as shown in Figure 1.



(source: [www.zamboanga.com](http://www.zamboanga.com))

Fig.1 Study area

### Water Lifeline of SMWD

A schematic network diagram is shown in Fig. 2. This figure shows the span and location of the nodes of the lifeline system. It covers the whole city of Surigao with extensions to farther towns and municipalities. The system is composed of 8 different steel pipes. These pipes make up the trunk and distribution lines of the system. Their main function is to circulate water from one point to another. Trunk lines have a diameter of 35 cm to 40 cm that varied in length. Distribution lines have a diameter of 5 cm to 25 cm. Properties of steel pipes are considered on the pipe strain analysis. SMWD have two water sources, several control facilities that include tanks, reservoirs and pumping systems, and demand nodes. These are all connected to the distribution and service lifeline networks.

## METHODOLOGY

### Probabilistic Seismic Hazard Analysis (PSHA)

To estimate the seismic hazard at the site a PSHA was employed in the study as it can capture uncertainties in the estimation of the  $p_g$ . The uncertainties include but not limited to the identification of the seismic sources that exposes the area to significant ground motion, uncertainties in the fault parameters, historical data of the seismic events, distribution of the source-to-site distances, epicenter approximations, soil thickness and composition variations, local SPT results and the choice of an appropriate GMPE.

Uniform hazard response spectra for both spectral acceleration and velocity are developed for the estimation of the probability of failure for each pipe diameter and are followed by the

probability of damage for each pipe.

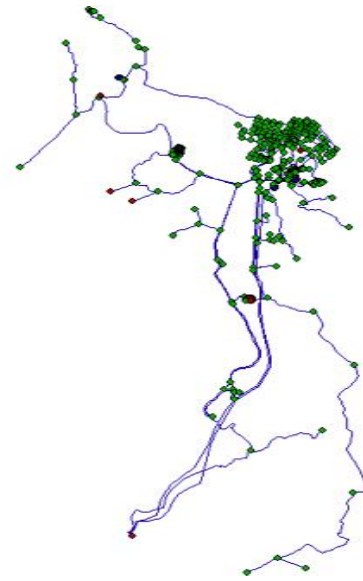


Fig. 2 SMWD pipe network system

### 3.1.1 Seismic Sources Identification

Surigao Del Norte is susceptible to frequent earthquakes due to the geologic setting of the province. Large earthquake occur within 150 km of the province. Three active seismic sources namely Surigao, Central Leyte and Bohol faults are within the 150 km radius from the target area. Surigao fault is the nearest seismic source to the target area.

Table I Properties of Seismic Sources near SMWD

Fault name	Tectonics	Style	Length (m)
Surigao	Crustal	Strike-slip	153
Central Leyte	Crustal	Strike-slip	116
Bohol	Crustal	Strike slip	38

Among the three seismic source, the Philippine Fault Zone: Surigao Segment (see Fig. 2) has the higher potential to cause damage to the target area. The 6.7 magnitude earthquake that affected Surigao City last February 10, 2017 is a case in point. According to National Disaster Risk Reduction and Management Council (NDRRMC) site report, 8 persons lost their lives while 249 were injured. More than 10,645 homes were damaged, 555 were totally damaged and 10,090 were partially damaged. The total cost of damage was estimated to be around US\$ 14

million.

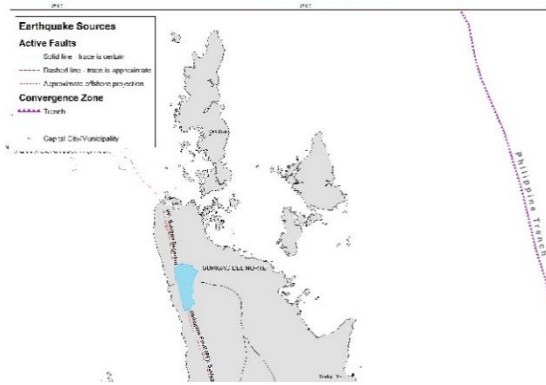


Fig. 3. Active Faults / Trenches near Surigao

### 3.1.2 Seismic Events Modeling

Historical data of the past earthquakes within the 150-km radius were obtained from the Philippines Institute of Volcanology and Seismology (PHIVOLCS). The records include the date, location, magnitudes and depths of the seismic events from 1952 to 2014. Only main shocks were considered in the analysis and aftershocks were removed. Moment magnitude less than 5.2 were removed as these were assumed not capable of triggering any damage. Historical surface, body and live wave magnitudes were all converted into moment magnitudes (Giacomo et. al. 1990) to conform to the GMPEs used. Due to the scarcity of the data from third-party resources uncertainties on fault parameters cannot be avoided.

### 3.1.3 Attenuation models and pga estimation

The Gutenberg-Richter recurrence law was adapted in the study to determine the distribution of the seismic magnitude for each seismic source. It conveys the relationship between the number of earthquakes for each magnitude group interval in comparison to the total number of earthquakes of the target area.

$$\log(\lambda_m) = a - bM \quad (1)$$

where  $a$  and  $b$  are constants derived from the regression analysis of the region while  $M$  is the earthquake moment magnitude. Total average exceedance rate for a given period is given by this model.

$$\lambda_{y*} = \sum_{i=1}^{N_s} \sum_{j=1}^{N_m} \sum_{k=1}^{N_r} v_i P[Y > y^* | m_j, r_k] P[M = m_j] P[R = r_k] \quad (2)$$

The probability distribution of the magnitude,  $P(M)$  is based on the function shown below (Kramer, 1996).

$$P[M_l \leq m \leq m_u] = \int_{M_l}^{M_u} f_m(m) \approx f_m\left(\frac{m_l + m_u}{2}\right) (m_u - m_l) \quad (3)$$

The attenuation model of Fukushima and Tanaka (1990) shown below was used to estimate the mean peak horizontal acceleration (PHA) for a 10% in 50 years probability (MRI = 475 years).

$$\log A = 0.41M - \log(R + 0.03 \times 10^{0.41M}) - 0.0034R + 130 \quad (4)$$

$A$  is the PHA mean value (in  $g$ ). A summary of the PSHA process through a total probability theorem (Thenhaus and Campbell, 2003) is shown below.

$$\lambda[X \geq x] \approx \sum_{\text{sources } i} v_i \int_{M_{\min}}^{M_{\max}} \int P[X \geq x | M, R] f_m(m) f_{R|m}(r|m) dr dm \quad (5)$$

### Uniform Hazard Response Spectra

The estimated acceleration experienced by the water pipelines during earthquake can be estimated by determining the spectral acceleration. This study adapted the GMPE of McGuire (Sen, 2009) to estimate the corresponding spectral acceleration for the following periods ( $T$ ) 0.1, 0.2, 0.3, 0.5, 1.0, 2.0, 3.0, and 4.0.

$$S_a = b'_1 10^{b_2 M} (R)^{-b_3} \quad (6)$$

$S_a$  is the spectral acceleration value (in  $g$ ).

Table 2. McGuire's GMPE values

Period ( $T$ )	$b'_1$	$b_2$	$b_3$	cov, $S_a$
0.1	1610	0.233	1.341	0.651
0.2	2510	0.226	1.323	0.577
0.3	1478	0.290	1.416	0.560
0.5	183.2	0.356	1.197	0.591
1.0	6.894	0.399	0.704	0.703
2.0	0.974	0.466	0.675	0.941
3.0	0.497	0.485	0.709	1.007
4.0	0.291	0.520	0.788	1.191

In conformity with the models of for damage estimations, spectral acceleration values are converted to response velocity spectrum,  $S_v$  (in/sec)

$$S_v = \frac{P}{2\pi} S_a \quad (7)$$

### Vulnerability Assessment of a Lifeline Network

#### 3.3.2 Damage functions

The damage estimation for this study adapted the models of Ogawa and Koike, 2001. The damage estimation of pipe is divided into three categories such as (a) major damage curve wherein



the structural reliability of the material considered exceeds the critical or allowable level for the major damage state or ultimate limit state under seismic loading;

$$P[\text{major damage}] = P[\epsilon_{cr}^{maj} - \epsilon_p < 0] \quad (8)$$

(b) moderate damage curve wherein the structural reliability of the material considered exceeds the moderate damage state seismic loading; and

$$P[\text{moderate damage}] = P[\epsilon_{cr}^{mod} - \epsilon_p < 0] \quad (9)$$

and (c) minor damage wherein the structural reliability of the material exceeds the minor damage state or the serviceability limit state under seismic loading.

$$P[\text{minor damage}] = P[\epsilon_{cr}^{min} - \epsilon_p < 0] \quad (10)$$

Where  $\epsilon_{cr}^{major}$ ,  $\epsilon_{cr}^{mod}$ ,  $\epsilon_{cr}^{min}$  are the critical strains for the different damage states and  $\epsilon_p$  is the actual pipe strain.

The models above are used to generate fragility curves which is expressed as the probability of damage occurrence of material conditioned on the pga as shown in Fig 4.

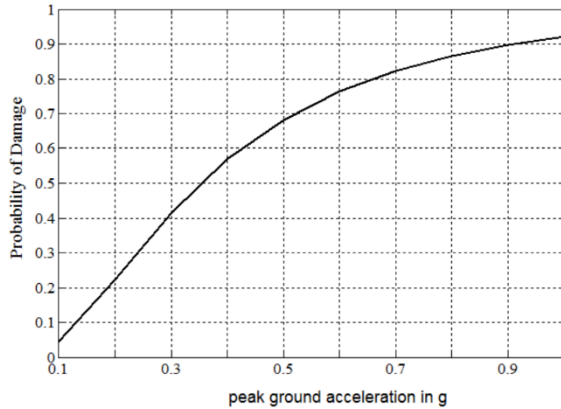


Fig. 4. Sample Fragility Curve

### Pipe Strain and Ground Strain

The seismic response analysis of buried pipeline is evaluated using ground response displacement (cm)  $U_h$  (JWWA, 1997) as shown in Eq. 11. The free field displacement of soil particles is based on spectral velocity, period of the ground surface, thickness of the ground surface and the distance of the pipeline to the ground.

$$U_h = \frac{2}{\pi^2} S_v T \quad (11)$$

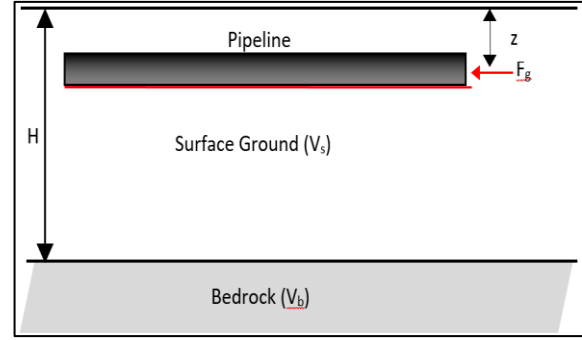


Fig. 5. Diagram of Buried Pipeline

The actual pipe strain is the product of the free field ground strain  $\epsilon_g$  and the  $\alpha_o$  (see Eq. 12)

$$\epsilon_p = \alpha_o \epsilon_g \quad (12)$$

$$\epsilon_g = \frac{2\pi}{L} U_h \quad (13)$$

The conversion factor  $\alpha_o$  is determined using Eq. 14 below

$$\alpha_o = \frac{1}{1 + \left(\frac{2\pi}{\lambda L}\right)^2} \quad (14)$$

$$\lambda = \sqrt{\frac{K}{EA}} \quad (15)$$

where  $L$  is the horizontally travelling wavelength (cm),  $K$  is the axial stiffness between the surrounding soil and pipe (N/m),  $E$  is the modulus of elasticity (Mpa),  $A$  is the cross-sectional area of the pipe ( $\text{mm}^2$ ).

## RESULTS AND ANALYSIS

### Probabilistic Seismic Hazard Analysis

The result of PSHA is summarized through the generation of seismic hazard curve and seismic hazard map for the province of Surigao Del Norte where the concession area of SMWD is located. The generated map provided the probability of exceedance of each points considered for a Design Basis Earthquake (DBE).

#### 4.1.1 Distribution of the Radius $R$

Seismic sources are considered linear source with distance  $L$ , based on the notion that point sources are not capable of generating earthquakes with magnitude 5.8 and above. The mathematical technique of triangulation is used to determine the shortest distance from any point of linear source. The calculated distances are divided by 10 km then

normalized to determine their source-to-site distribution.

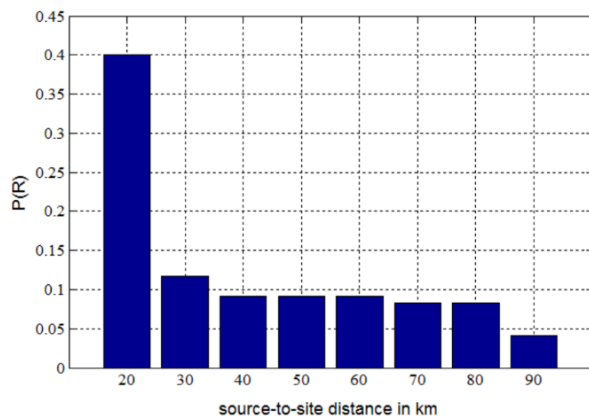


Fig. 6.  $P(R)$  for 6.4 - 6.9  $M_w$

It can be seen in figure 6 that the likelihood for a seismic event with a moment magnitude of 6.4 to 6.9 to occur with 3 km away is estimated to be around 53% from the site.

#### 4.1.2 Annual Rate of Occurrence and Probability Distribution of EQ Magnitudes, $P(M)$

The annual rate of occurrence is the likelihood of an earthquake with a corresponding magnitude to occur for a year. Values for each seismic source are plotted to determine the equation and slope of line. The equation and slope serves as the seismic constants,  $a$  and  $b$ , that is used for the determination of probability distribution of earthquake magnitude  $M$ ,  $P(M)$ .

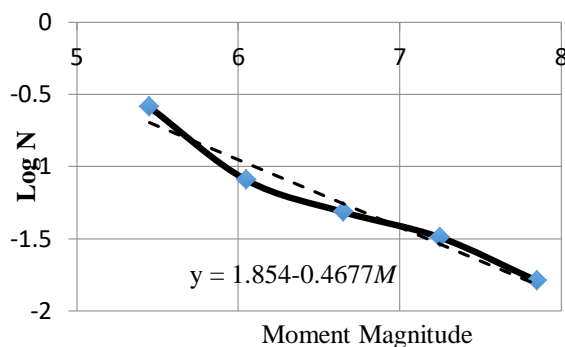


Fig. 7. Annual Rate of Occurrence of Surigao Fault

Figure 8 shows the likelihood of the seismic events with greater magnitudes to have longer return periods than events with smaller magnitude. Earthquakes with magnitude within 5.2 to 5.7 have a distribution of about 49.6% while earthquake

with magnitude 7.6 to 8.1 have distribution of around 3%.

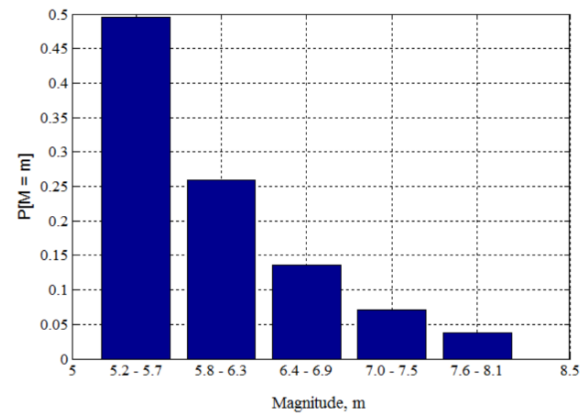


Fig 8. Annual Rate of Occurrence of Surigao Fault

#### 4.1.3 Seismic Hazard Curve and Map

The seismic hazard curve is based on the mean value for all magnitude-distance pairs. Figure 9 shows that for 0.0021 chance of occurrence for a DBE of 0.7g for PFZ: Surigao Segment. It must be noted that this even is likely to occur within 5km of the fault itself. The acceleration for all points considered is plotted on the map as seen the Figure 10.

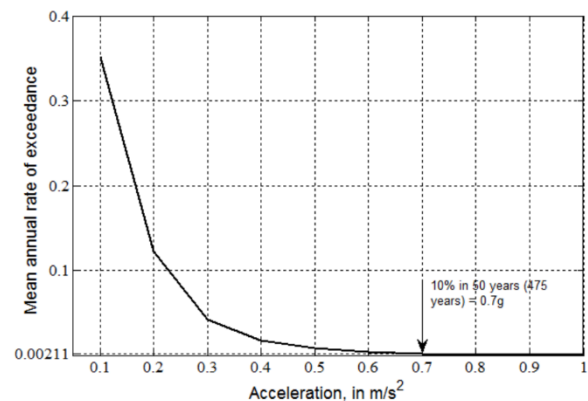


Fig. 9. Probability of Exceedance

#### 4.1.4 De-aggregation

De-aggregation is the summary of possible location magnitudes for each mean distance range. The graph below shows that as the distance range increases, the probability of each magnitude decreases that the likelihood of earthquake with mean magnitude of 7.9 has a 0.005 probability of occurrence within 5 km of the source.



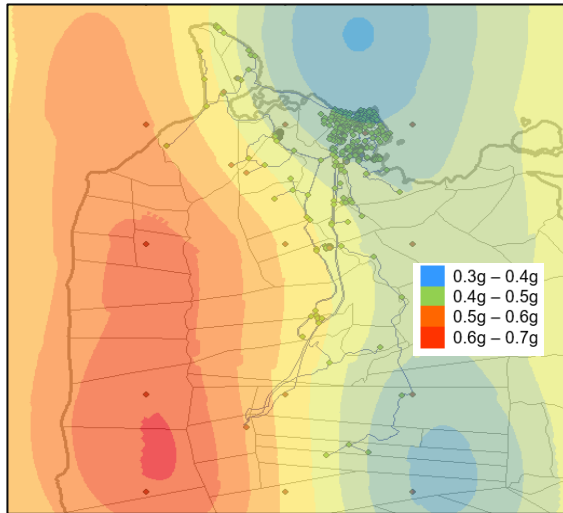
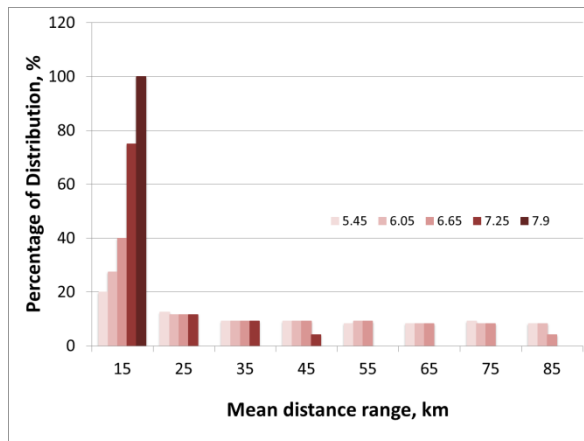


Fig. 10. Seismic Hazard Map of Surigao Del Norte

Fig. 11. De-aggregation of PSHA results  
**Uniform Hazard Response Spectra and Spectral Velocity Curve**

The figure below provides the uniform hazard response spectra for Surigao Del Norte. The spectral acceleration at sudden ground motion gradually increases until it reaches its peak movement. It slowly decreases as the period increases.

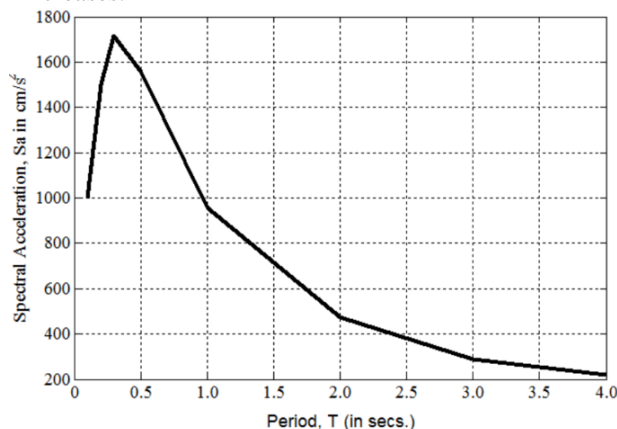


Fig. 12. Uniform Hazard Response Spectra

### Vulnerability Analysis of SMWD

The fragility curves for this study are developed using Monte Carlo Simulation. The figure below shows the fragility curves for minor, moderate and major damage states given the pipe diameter of 10 cm.

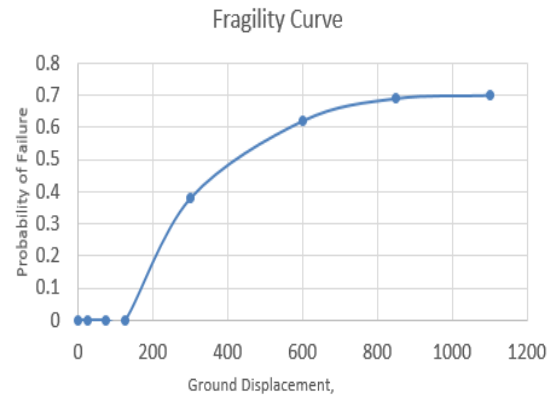


Fig. 13. Fragility curve for Major Damage State

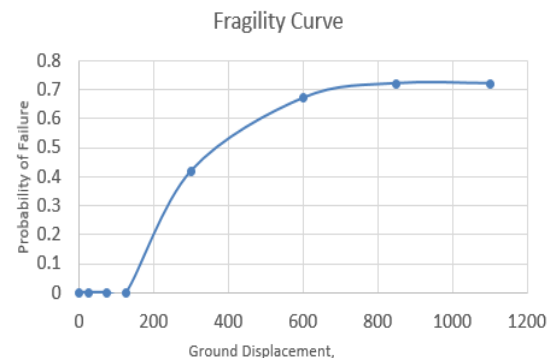


Fig. 14. Fragility Curve for Moderate Damage State

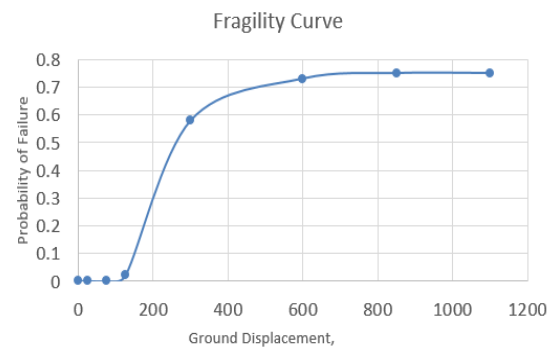


Fig. 15. Fragility Curve for Minor Damage State

Figure 16 shown below shows the summary of the probability of damage for major, moderate and minor damage state of all pipe diameters. Probability of minor damage is higher for all pipe sizes in comparison to major damage state.

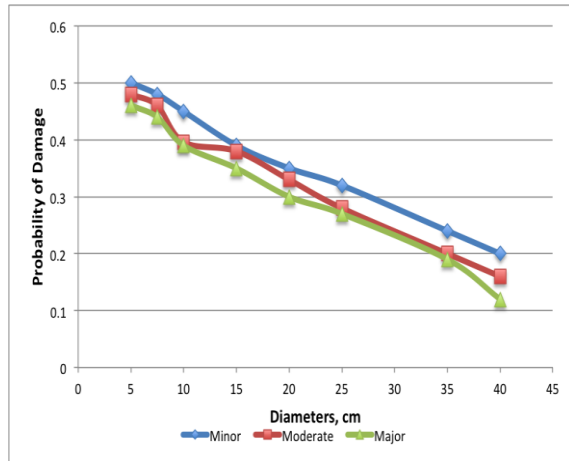


Fig. 16. Damage States for all pipe diameters

## CONCLUSION

Monte Carlo simulation is used to produce the fragility curves for each damage states. The fragility curves provided for three different damage states showed that the probability of failure for the pipe for period around 0.1 to 0.5 secs are around 0 to 10%. Aside from that, it can be seen that damage probability increases as period increases. It proves that the pipe strain is relative with the ground displacement and period of the seismic event. Major damage state is expected about 70% for longer earthquake period.

## ACKNOWLEDGEMENTS

The authors would like to thank Prof. Takeshi Koike as well as to SMWD and PHIVOLCS for their valuable assistance.

## REFERENCES

- [1] Garciano, L. E. and Taclibon, P. The October 15, 2013 Bohol Island, Philippines earthquake and its damaging effects: An investigative report, Journal of Disaster Factsheets, <http://committees.jsce.or.jp/disaster/FS2013-D-0004>, Dec. 2013.
- [2] Crismundo, M. Panic grips Surigao; Strong aftershocks, water shortage keep quake-affected residents on edge. Manila Bulletin, 2017.
- [3] Hamada, M. Critical Urban Infrastructure Handbook, 2014, CRC Press.
- [4] Sahoo, S., Manna, B., and Sharma, K. G. Seismic Behaviour of Buried Pipelines: 3D Finite Element Approach, Journal of Earthquakes. Vol. (2014), 2014.
- [5] O'Rourke, M. and Ayala, G. Pipeline Damage Due to Wave Propagation. Journal of Geotechnical Engineering, 119 (9), 1993, pp. 1490 - 1498.
- [6] Tromans, I. Behavior of Buried Water Supply Pipelines in Earthquake Zones. Doctorate Thesis, Imperial College of Science, Technology and Medicine, London. 2004.
- [7] Koike, T. Seismic Risk Assessment of a Water Supply Lifeline System in Baku. Conference Proceedings. In Proc. Reliability Engineering Conference, Azerbaijan. 2009.
- [8] The Philippine Statistical Yearbook (PSY), National Statistical Coordination Board (NSCB), 2010.
- [9] NDRRMC (National Disaster Risk Reduction and Management Council). SitRep No. 18 re: Effects of Magnitude 6.7 Earthquake in Surigao City, Surigao Del Norte. July 3, 2017 from <http://www.ndrrmc.gov.ph>.
- [10] PHIVOLCS (Philippines Institute of Volcanology and Seismology). Seismicity Map and Catalogue of Surigao Del Norte Earthquakes Magnitude 2.0 and above. 1952-2014.
- [11] Giacomo, D., Bondar, I., Storchak, D. A., Engdhal, E.R., Bormann, P., Harrus, J., "ISC-BEM: Global Instrumental Earthquake Catalogue (1900-2009), Physics of the Earth and Planetary Interiors, 2014.in of the Seismological Society of America. 1990.
- [12] Kramer, S. Geotechnical Earthquake Engineering. New Jersey: Prentice Hall. 1996.
- [13] Fukushima, Y., & Tanaka, T. A new attenuation relationship for peak horizontal acceleration of strong earthquake ground motion in Japan. Bulletin of the Seismological Society of America. 1990.
- [14] Thenhaus, P., & Campbell, K. Seismic Hazard Analysis. W. Chen Earthquake Engineering Handbook. 2003.
- [15] Sen, T. Fundamental of Seismic Loading on Structure. PSHA. John Wiley & Sons. 2009.
- [16] Ogawa, Y. and Koike, T., Structural Design of Buried Pipeline for Severe Earthquakes. Soil Dynamics and Engineering, 2001.
- [17] JWWA (Japan Waterworks Association). Seismic Design Guideline for Waterworks Pipeline and Facilities, 1997.

# A COMPARISON OF ESTIMATED SHEAR STRENGTH OF SOUTH-EAST QUEENSLAND RESIDUAL SOIL USING FIELD AND LABORATORY TESTING

Darren Newell<sup>1</sup> and Choo Yong<sup>2</sup>

<sup>1</sup>School of Engineering, Griffith University, Queensland, Australia

## ABSTRACT

Undrained shear strength of soil is an interpreted value that is typically used when undertaking geotechnical engineering analyses. There is a suite of laboratory and in situ tests readily available to engineering practitioners that can be used to estimate undrained shear strength of a soil. This paper compares estimates of the short term undrained shear strength of a sandy clay using laboratory (undrained triaxial, oedometer) and in situ (cone penetrometer) tests. The interpreted undrained shear strength derived from laboratory and in situ tests displayed significant variation. These differences in the estimated strength parameters for the subject clay highlight the importance of not relying on one type of test in isolation when assessing soil strength parameters.

*Keywords: Undrained Shear Strength, Triaxial Test, Cone Penetrometer Test, Oedometer Test, Fine Grained Soils, Over Consolidation Ratio*

## INTRODUCTION

Laboratory and in situ testing was undertaken on a sandy clay material obtained from a site in Yatala, Queensland (a suburb of the City of Gold Coast). The objective of this testing was to characterize the strength parameters of this material in order to estimate its short term undrained shear strength.

The short term undrained shear strength ( $s_u$ ) of soils is typically a critical value that must be interpreted in geotechnical engineering. There is no one value for the undrained shear strength of a soil; the value depends on various factors including the rate of loading, the in situ stress, stress history and test method. There is a suite of laboratory and in situ tests readily available to engineering practitioners that can be used to estimate the undrained shear strength of a soil.

Triaxial tests are widely recognized as an accurate laboratory test to determine the engineering properties of a soil, such as the angle of internal friction and cohesion from which  $s_u$  can be estimated. There are several variations of the test that relate to the way in which the sample is consolidated and drained. In this research, isotropically consolidated, undrained triaxial compression tests (CU) were used to estimate the strength parameters of the clay under investigation.

In situ testing was also undertaken at the site using the Cone Penetrometer Test (CPT). Since the inception of the CPT in the early to mid-1930s there has been continuous development and understanding of CPT technology, making it a widely accepted method for assessing soil strength parameters (see, e.g. [1]).

## SITE DESCRIPTION

Regional geological mapping of Yatala, where the subject clay is located [2], indicates that the area is comprised of soil and rock of the Neranleigh Fernvale beds that are typically characterized by greywacke, argillite, quartzite, chert, shale, sandstone and greenstone.

Geotechnical investigations on this site have been undertaken to assess subsurface ground conditions utilizing undisturbed sampling (rotary wash boring, 52 mm nominal dia.) and CPT techniques. Subsurface conditions were found to be comprised of three distinct layers, described as: engineered fill; residual clay (approx. 2.0 m deep); and meta-siltstone rock. Ground water was not encountered in any of the boreholes, which is consistent with the surrounding topography and elevation of the site (approximately 17.75 m AHD).

## TEST RESULTS AND INTERPRETATION

Various laboratory tests were conducted on undisturbed samples of the subject clay obtained from boreholes at the site. At each borehole, a CPT sounding was also undertaken. Test results and an interpretation of the soil strength follow.

### Laboratory Testing

Laboratory tests using undisturbed samples from a total of seven boreholes were undertaken to determine the engineering characteristics of the clay layer between depths of 1.2 and 2.6 m.

These tests included: Atterberg Limit, particle size distribution, oedometer and triaxial tests.

#### Atterberg limits and sieve analysis

Atterberg Limit tests indicate that the clay layer has varying plasticity. Of the ten tests performed on the subject clay, the average liquid limit (LL) and plasticity index (PI) was 46 percent and 30 percent, respectively. Particle size distribution tests show that more than 50 percent of the material has a particle less than 0.075 mm. The tested clay can be generally categorized as a Sandy Clay with medium plasticity (a CI material under the USCS system).

#### Over consolidation ratio from oedometer test

Oedometer tests were carried out on three undisturbed samples recovered from depths of 1.8, 2.8 and 3.4 m. Using the graphical method proposed by [3] the estimated Over Consolidation Ratio (OCR) for these samples was 1.0, 2.0 and 2.5, respectively, indicating a normal to lightly overconsolidated clay.

#### Undrained shear strength from triaxial tests

A total of seven CU tests were performed on undisturbed clay samples (recovered from depths between 1.2 and 2.6 m) to determine the material's effective cohesion ( $c'$ ) and angle of internal friction ( $\phi'$ ) (Table 1). These values were interpreted from Cambridge p-q plots (critical soil state theory developed by [4]). Using these values, the in situ  $s_u$  was estimated using the Mohr-Coulomb criterion, where for an in situ horizontal stress ( $\sigma'_{ho}$ ), the vertical ( $\sigma'_f$ ) and shear ( $\tau_f$ ) stress at failure are:

$$\sigma'_f = \frac{2 c' \cos \phi' + \sigma'_{ho}(1 + \sin \phi')}{1 - \sin \phi'} \quad (1)$$

$$s_u = \tau_f = \frac{1}{2} (\sigma'_f - \sigma'_{ho}) \cos \phi' \quad (2)$$

where ( $\gamma'_s$  is unit soil weight,  $z$  is depth),

$$\sigma'_{ho} = K_o \sigma'_{vo} \quad (3)$$

$$\sigma'_{vo} = \gamma'_s z \text{ (effective vertical stress, } \sigma'_{vo}) \quad (4)$$

For over consolidated soils the coefficient of earth pressure ( $K_o$ ) can be estimated using various methods. One of the most commonly used is that proposed by [5] where:

$$K_o = (1 - \sin \phi') OCR^{\sin \phi'} \quad (5)$$

The estimated  $s_u$  values were calculated using Eqs (1) – (5) at depths corresponding to those from which the specimens were recovered and assuming  $OCR=2$  (Table 1).

Based on these results the consistency of the subject clay can be generally described as Firm.

Table 1: Strength parameters from CU tests

$z$ m	$c'$ kPa	$\phi'$ degrees	$s_u$ kPa
1.45	12	17	25
1.59	13	18	27
1.80	22	23	47
2.15	20	21	43
2.25	12	17	31
2.29	10	24	39
2.50	20	23	51

#### Evaluation of shear strength from laboratory tests

Due the variability that can be encountered in estimating  $s_u$  there has been considerable research on the subject, see [6], [7] and [8]. From this published research an assessment of  $s_u$  can be made through various means. For an overconsolidated soil with a low to moderate PI, where  $\sigma'_{vc}$  is the effective preconsolidation stress, the normalized shear strength can be expressed as [8]:

$$\frac{s_u}{\sigma'_{vc}} = 0.23 \pm 0.04 OCR^{0.8} \quad (6)$$

Table 2: Normalized shear strength from CU tests

$z$ m	$s_u$ kPa	$\sigma'_{vc}$ kPa	$s_u / \sigma'_{vc}$	Upper Limit $s_u / \sigma'_{vc}$	Lower Limit $s_u / \sigma'_{vc}$
1.45	25	64	0.39		
1.59	27	70	0.39		
1.80	47	79	0.60		
2.15	43	95	0.45	0.47	0.33
2.25	31	99	0.32		
2.29	39	101	0.38		
2.50	51	110	0.46		

Normalized shear strengths were calculated using  $s_u$  values from Table 1 and assuming an  $OCR$  of 2 (Table 2). Generally, these values fall within the limits defined by Eq. (6) (Fig. 1). As noted by [9], a better fit of data can result if the exponent in Eq. (6) is varied between 0.75 and 0.85.

#### In Situ Testing

CPTs were undertaken close to each borehole so that a comparison could be made between laboratory and in situ estimates of soil strength parameters. Three of the seven CPT soundings were performed using a piezo-cone (CPTu) so that pore water pressure measurements could also be taken.

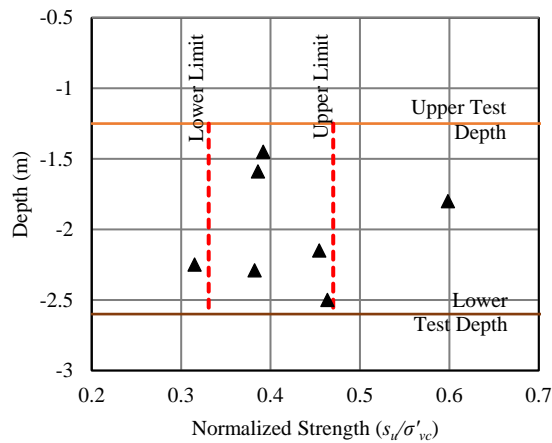


Fig. 1 Depth versus normalized shear strength

#### Over consolidation ratio from CPTu

A commonly used method to estimate the *OCR* of fine grained soils is outlined in [9] using the normalized cone resistance ( $Q_t$ ), which is a function of the cone resistance corrected for pore water pressure ( $q_t$ ) and, the total ( $\sigma_{vo}$ ) and effective ( $\sigma'_{vo}$ ) vertical stresses, expressed as:

$$OCR = k Q_t = k \frac{q_t - \sigma_{vo}}{\sigma'_{vo}} \quad (7)$$

The variable  $k$  in Eq. (7) is a preconsolidation cone factor that [10] suggests can be expected to range from 0.2 to 0.5 with an average value of 0.33. Higher values of  $k$  correspond with aged and heavily over consolidated clays. According to [10], estimating the *OCR* using Eq. (7) is not strongly influenced by soil sensitivity.

CPTu soundings were analyzed across the depth range where all undisturbed samples were recovered from (1.2 to 2.6 m deep). Using Eq. (7) with  $k = 0.33$  resulted in estimated *OCR* values greater than 10. These estimates appear far greater than would be expected based on laboratory tests and the qualitative assessment of the clay's consistency. Similarly, estimates of the *OCR* for CPTu soundings over the entire tested depth also resulted in values greater than 10.

#### Undrained shear strength from CPT and CPTu

CPT soundings were undertaken adjacent to each borehole that have been used to estimate  $s_u$  using Eq. (8) [1].

$$s_u = \frac{q_t - \sigma_{vo}}{N_{kt}} \quad (8)$$

From Eq. (8) it can be seen that an accurate estimate of  $s_u$  is limited by the adopted value of the empirical cone factor ( $N_{kt}$ ). Research indicates a range for likely values of  $N_{kt}$  of between 10 and 20 in clays

[1]. However, published ranges of between 4.5 and 75 have also been reported [11].

Assuming that the clay investigated is a lightly overconsolidated clay, [12] suggests a value of 19, which has been used in Eq. (8) to estimate  $s_u$  values (Table 3). When  $s_u$  is normalized by  $\sigma'_{vc}$  the resulting values (Table 3) exceed the upper limit given by Eq. (6). When a value of 75 (as in [11]) is chosen for  $N_{kt}$  normalized values were still found to exceed the upper limit.

Table 3: Normalized shear strength from CPT tests

$z$ m	$s_u$ kPa	$\sigma'_{vc}$ kPa	$s_u / \sigma'_{vc}$	Upper Limit $s_u / \sigma'_{vc}$	Lower Limit $s_u / \sigma'_{vc}$
1.45	168*	64	2.6		
1.59	136	70	1.9		
1.80	251	79	3.2		
2.15	251	95	2.7	0.47	0.33
2.25	267*	99	2.7		
2.29	366*	101	3.6		
2.50	213	110	1.9		

\* CPTu test, value adjusted for pore pressure.

## CONCLUSIONS

Comparative estimates of  $s_u$  and *OCR* for the same clay are shown to vary substantially between laboratory and in situ test methods. Laboratory testing was undertaken by two independent laboratories and gave very similar results. Similarly, CPT soundings were also undertaken by two independent contractors, one using CPT and the other using CPTu, yielding similar results.

With reference to laboratory testing, it is widely accepted that sample disturbance can influence test results. This influence is a function of the soil sensitivity, which is the ratio of the tested  $s_u$  for an undisturbed and remolded sample. However, [13] notes that sensitivity does not appear to influence normalized estimates of  $s_u$ .

Whilst sensitivity cannot be ruled out, it appears unlikely to be the cause of the large variance observed between the laboratory and in situ tests.

Based on normalized shear strength, CU tests appear to provide an estimate with the expected  $s_u$  range using Eq. (6). However, this relies on an accurate measurement of the *OCR*. Therefore, it cannot be concluded that the laboratory estimates of  $s_u$  are, or are not, accurate from this alone.

Therefore, the discrepancy in the estimated values of  $s_u$  from laboratory and in situ tests is likely to hinge on the *OCR* value for the investigated clay. To resolve this, additional oedometer tests will be undertaken in an endeavor to confirm the accuracy of the *OCR* value used to derive  $s_u$  for the tested clay.

Additional  $s_u$  tests (such as direct simple shear and field vane) may also be undertaken. Finally, testing information will be sought for similar clays in the area in order to benchmark estimated values.

The variance in the estimated strength parameters for the subject clay highlights the importance of not relying on one type of test in isolation when assessing soil strength parameters.

## REFERENCES

- [1] Robertson P and Cabal K, Guide to cone penetration testing for geotechnical engineering, 5th edition ed. California: Gregg Drilling and Tesing Inc., 2012.
- [2] Whitaker WG and Green PM, "Murwillumbah 1:100,000 Geological Series 9541 Geological Survey of Queensland", ed. Brisbane, Queensland: Department of Natural Resources and Mines, 1980.
- [3] Casagrande A, "The determination of the pre-consolidation load and its practical significance", in Proceedings of the International Conference on Soil Mechanics and Foundation Engineering, 1936, pp. 60-64.
- [4] Schofield A and Wroth P, Critical state soil mechanics. New York: McGraw-Hill, 1968.
- [5] Mayne PW and Kulhawy F, "Ko - OCR Relationships in Soil", Journal of the Soil Mechanics and Foundations Division, vol. 108, pp. 851-872, 1982.
- [6] Ladd CC and Foott R, New Design Procedure for Stability of Soft Clays. Massachusetts: Department of Civil Engineering, Massachusetts Institute of Technology, 1973.
- [7] Mesri G, "A reevaluation of using laboratory shear tests", Canadian Geotechnical Journal, vol. 26, pp. 162-164, 1989.
- [8] Jamiolkowski M, "New development in field and laboratory testing of soils", in Proceedings of the 11th International Conference on Soil Mechanics and Foundation Engineering, San Francisco, 1985, pp. 57-153.
- [9] Kulhawy FH and Mayne PW, "Manual on estimating soil properties for foundation design", Electric Power Research Inst., Palo Alto, CA (USA); Cornell Univ., Ithaca, NY (USA). Geotechnical Engineering Group 1990.
- [10] Robertson P, "Interpretation of cone penetration tests—a unified approach", Canadian Geotechnical Journal, vol. 46, pp. 1337-1355, 2009.
- [11] Djoenaidi WJ, "Compendium of soil properties and correlations", M. Eng. Sc. Thesis, University of Sydney, Sydney, 1985.
- [12] Look BG, Handbook of geotechnical investigation and design tables. Leiden, The Netherlands: CRC Press, 2014.
- [13] Larsson R, "Undrained shear strength in stability calculation of embankments and foundations on soft clays", Canadian Geotechnical Journal, vol. 17, pp. 591-602, 1980.

## **STUDY ON LANDSLIDE CATEGORY BASE ON TEMPORAL– SPATIAL CHARACTERISTIC DISTRIBUTION IN NORTHERN VIETNAM USING SATELLITE IMAGES**

Thuy Thi Thanh LE<sup>1</sup> and Seiki KAWAGOE<sup>2</sup>

<sup>1</sup>Department of Symbiotic Systems Science Fukushima University, JAPAN

### **ABSTRACT**

North Vietnam mountainous area is considered as one of the most landslide generate region in Vietnam. Landslides in this area often occurs under the influences of heavy rainfall or tropical storms, steep slopes on mountainous sides and human activities such as road or house constructions. Heavy rainfall events are estimated by climate change in the future. Therefore, it is necessary to understand landslide characteristic due to rainfall variation. This paper applied Landsat satellite images and calculated Normalized Difference Indexes to evaluate the condition of vegetation, soil and water and detected 87 landslide points in North Vietnam. As result, three typical types of landslides are classified as i) landslide caused by rainfall on construction sites, ii) landslide caused by rainfall on natural slopes, and iii) landslide caused by rainfall and water drawdown on banks of reservoirs or streams. Considering the Landsat result type 2 and type 3 consist larger proportions (48.3 % and 36.8 %) compared to those in historical data (11.7 % and 1.53 %). This means that many landslide would occur in mountainous areas that far from residential or road are-as (type 1). This paper thus would provide initial assessment for further studies on landslide problems on the bank of water sites such as reservoirs or streams.

*Keywords: Landslide type, Landsat 8, Digital geographic information, Climate change*

### **INTRODUCTION**

Vietnam is a tropical nation that is often hit by several typhoons and tropical cyclones every year. As the influence of climate change, abnormal weather phenomenon such as cyclones and severe typhoons have been occurring with more frequencies and higher intensities. During the period from 2014-2016 many strong tropical storms and heavy rains occurred in this country and led to disaster in many regions across Vietnam. According to a national study of the Vietnam Geography academy study in 2004<sup>[1]</sup>, North Vietnam is the most prone region to landslide. Sixteen out of twenty five provinces there are listed as provinces obtaining high hazard of landslide occurrences. In accordance with topographic and geology condition, landslides in this area often occurs under the influences of heavy rainfall or tropical storms, steep slopes on mountainous sides and human activities such as road or house constructions. Detecting landslides occurrences thus becomes necessary approach for landslide susceptibility regions there.

According to Dieu<sup>[2]</sup> and Metternicht et al<sup>[3]</sup>, four major classes for landslide susceptibilities are inventory, statistical, deterministic and heuristic approaches. Inventory map is based on satellite images, ground survey and historical data-base of landslide occurrence. It would give spatial distribution of past landslides and does not provide prediction of landslide susceptible areas. Statistical method would provide pre-diction of landslide in region that might not have landslide in the past basing

on statistical analysis of landslide ground characteristics. However it needs a large amounts of data collection and suitable for medium scale prediction. Deterministic approach requires physical processes. However, since the data availability is one of the difficulties, the limitation of this approach is shown. Heuristic, which requires long-term landslide data and causative parameters, estimates potential landslide from preparatory variables. It is an expert driven approach that depends on the knowledge and experiences of scientists in deciding degree and type of landslide risks. The report of Bui Tien Dieu<sup>[4]</sup> in 2012 also pointed that landslide inventory maps provide great importance input data in landslide hazard and susceptibility analysis. The inventories can be divided into two sub classes including historical landslide inventories and landslides with triggering factors. The application of inventory thus would give information of locations, types and causative factors of past landslides.

In case of Vietnam, lacking of continuous information about past occurrences of landslide hinders the landslide assessment. It also leads to difficulties in data integration with land use plan and management task in landslide hazard regions. As a one of the most vulnerable nation to climate change, such external hazard risk is estimated to increase significantly in Vietnam. It therefore requires substantial demand in acquiring comprehensive information of landslide in order to obtain adequately adaptive measurements and mitigations for landslide prone areas. Considering the data unavailability (long-term landslide data and its related factors), in



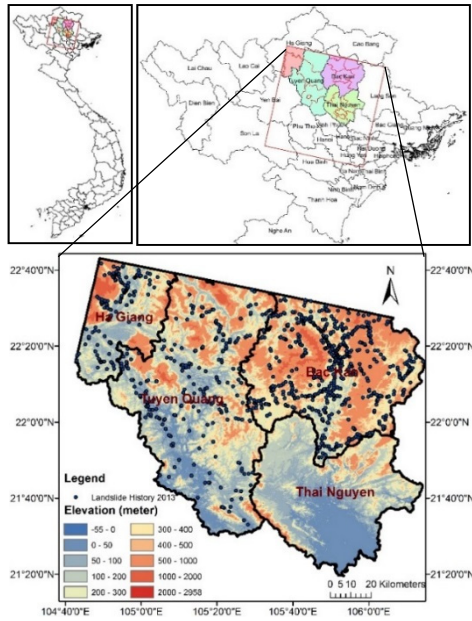


Fig. 1 Elevation classification in the study area

this paper, we apply the inventory approach to assess the landslide map based on the satellite images in a relationship with historical database of landslide occurrences [3],[5]. We also utilized Landsat satellite images and calculated Normalized Difference Indexes to evaluate the condition of vegetation, soil and water and detect land degradation in some areas in the North Vietnam. The outcomes would support further study on the landslide hazard prediction under the influence of climate change when considering additional triggering parameters such as heavy rainfall even and water drawdown.

## STUDY AREA

Study areas are Bac Kan (BK), Thai Nguyen (TN) and Tuyen Quang (TQ), and Ha Giang (HG) in North Vietnam (Fig 1). These four provinces are considered as having hazard of landslide occurrence in the North Vietnam. The elevation in this studied area varies from 0 to 2958 m covering both mountainous and midland region with complicated terrain characteristics. There are two major types of directions in mountain ranges: northwest to southeast and arc curve turning eastward Gam mountain ranges in HG and TQ, and Ngan Son range in BK and TN.

According to report of Vietnam academy of Water Resources Planning about monthly rainfall [7] from 1960 to 2015 in TQ and from 1960 to 2011 in other provinces, this area has considerably high annual rainfall with the ranges from 2467 to 4735 mm in H G and from 1342 mm (BK) to 1988 mm (TN) in others. Rainy season in this area often starts in late April and ends in October with average precipitation from 300 to 750 mm in HG and from 150 to 300 mm in BK, TN and TQ(Fig. 2). June to August is the heaviest rainfall time in rainy season with the

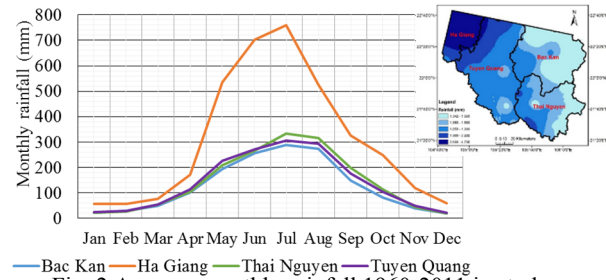


Fig. 2 Average monthly rainfall 1960-2011 in study

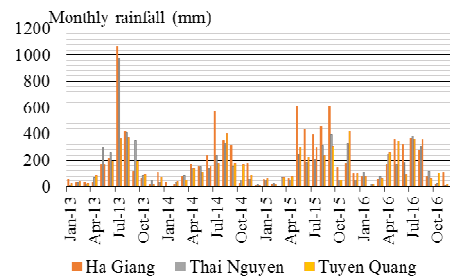


Fig. 3 Monthly rainfall 2013-2016 at 3 stations

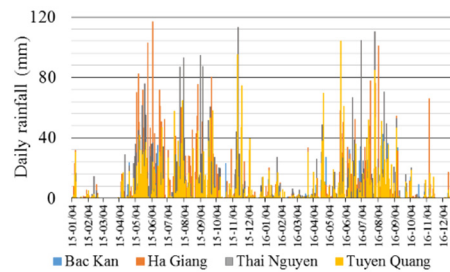


Fig. 4 Daily rainfall 2015-2016 in four provinces (Spatial average value)

maximum daily rainfall is greater than 100mm [8].

## DATASET AND METHODOLOGY

### Dataset

We tried to obtain landslide characteristic to relationship between landslide geomorphic information and rainfall condition. Therefore, we used actual landslide distribution data as landslide analysis. Satellite images and Landslide history data were used to landslide distribution characteristics. And geomorphic digital information was used to confirm to landslide factor characteristics. Rainfall data show timely incitement as temporal event characteristics.

#### a) Satellite image

We utilized Landsat 8 satellite images from USGS website (<http://earthexplorer.usgs.gov/>) to examine the land surface changes in area of four given provinces in northeast Vietnam. The Landsat 8 released the first image in the re-search site on 2013/04/22. It is used as the base image to compare the changes in surface condition in this area. With the 16-day-circle, from April 2013 to March 2017 among 94 images, the number of good quality images in

2013, 2014, 2015 and 2016 are 2, 3, 3 and 2, respectively. Looking at the rainfall data from 2013 to 2016 in some stations, we found that the year 2015 obtained the heavier monthly rainfall than that in 2014 and 2016 (Fig. 3). Comparing daily rainfall data in the last two years, we found that the number of rainy days in 2015 are higher than those in 2016 (Fig. 4). As rainfall is one of the most important triggering factor of landslide occurrence, in this paper, we choose year 2015 as the computing year to evaluate the changes of land surface in this studied region. Regarding to the image quality as well as the occurrence of heavy rainfall, we select the Landsat 8 data on 2015/07/01 as the comparative image for land degradation analysis.

#### b) Landslide history data

In 2012, the government released the national project "Investigation, assessment and zonation of landslide hazards in mountainous area in Vietnam". Phase I (2012-2015) conducted in 13 provinces in the north and 1 province in the north central Vietnam. Twenty-three remaining provinces in the north (4) and other areas (19) will be investigated in the second phase from 2016-2020. The output of this project is the landslide occurrences regarding to investigate time. In this study area, 1049 landslide points in three provinces BK, HG and TQ were recorded with brief information of observed locations, estimated sliding volume and repeated time. The observation routes were implemented along road lines and near residential areas in 2013

#### c) Other data

Rainfall data in this paper was adopted from the Academy of Water Resources Planning<sup>[7]</sup> (monthly rainfall from 1960-2011), the Directorate of Water Resources<sup>[11]</sup> (daily rainfall 2015-2016) and from the Institute of Meteorology in Vietnam (daily rainfall data at some stations). The terrain data was extracted from a digital elevation model (DEM) from the Open Mekong Development<sup>[6]</sup> with the grid cell size of 30m × 30m. Geology information data was collected from US Geological Survey (USGS). Land use data was extracted from Japan Aerospace Exploration Agency (JAXA)<sup>[12]</sup> with the resolution of 15m × 15m in north area in 2015.

## METHODOLOGY

#### a) Landsat dataset

Basing on the land cover mapping, the Landsat images would support the inventory of land degradation. It would visualize and map the past degradation of land surface including soil erosion, landslide, vegetation removal or land use changes<sup>[14]</sup>. In order to evaluate the changes in vegetation state and density by the satellite image instruments, a vegetation index is often utilized. This index

describes the greenness of surface throughout the reflection of light waves by land surface. Among wavelengths of light being gathered from satellite sensors, the red light's wave-lengths(VIS) are strongly absorbed by photo-synthetically active leaves, and the leaves reflect strongly the near-infrared (NIR) light's wave-lengths. In cases of death or stressed vegetation and non-vegetated surfaces they reflect less near-infrared light and more red light. The near-infrared and red light waves thus are applied to transform raw satellite data into Normalized Difference Vegetation Index (NDVI) (Equation 1).

$$NDVI = \frac{NIR - VIS}{NIR + VIS} \quad (1)$$

Unlike vegetation factor, water has stronger absorption capacity within the NIR wave range. It also has lower reflectance regarding to the higher wavelength. The Normalized Difference Water Index (NDWI), which is calculated basing on the NIR and Short wave infrared (SWIR) in order to evaluate the water amount in vegetation canopies, can therefore distinguish the vegetation and water<sup>[15]</sup> (Equation 2).

$$NDWI = \frac{VIS - SWIR}{VIS + SWIR} \quad (2)$$

In addition, the condition of soil moisture on the ground surface could be observed by applying the SWIR wavelength. The Normalized Difference Soil Index (NDSI) therefore would reflect the soil water content when using SWIR as a spectral signature in a relationship with the NIR wavelength (Equation 3)

$$NDSI = \frac{VSWIR - NIR}{VSWIR + NIR} \quad (3)$$

#### b) Landslide inventory approach

The occurrence of landslide is often in a close relationship with two main factors namely triggering and conditioning factors. According to Dieu<sup>[4]</sup>, triggering factors include heavy rainfall events, snow and earthquakes. States of slope, soil, geology and land use are some examples of conditioning factors. The former factors could lead to quick changes of slope condition while the latter factors refer to slowly processes. In this study, we consider four main conditioning parameters: slope, elevation, geology and land use. Historical landslide data and Landsat 8 calculated data are thus mapped and combined with DEM, slope, geology and land use data.

## RESULT

### Landsat analysis result

With the purpose of determining threshold value for land use change area, we first calculated the NDVI in pre event (2013/12/02) and post event (2015/07/01) (Fig. 5) and difference of NDVI between those two periods. The NDVI differences between pre and post event are grouped into 11 major land use categories, which are adopted from USGS database. They are Evergreen Broadleaf Forest (EBF), Mixed Forests (MF), Closed Shrub lands (CS), Open Shrub lands (OS), Woodley Savannas (WS), Savannas (Sa), Grassland (Gr), Permanent Wetland (PW), Croplands (Cr), Urban and Build-up (UB) and Cropland/Natural Vegetation on Mosaic (Cr/VM). The average NDVI value of NDVI in each land use type varies from -0.2223 to -0.1486. Standard deviations and its multiple values (said 2SD and 3SD) were calculated and subtracted from average values to obtain threshold NDVI values. NDVI values that below the given base lines are mapped as the first trial of land surface changes detection in the studied area (Fig. 7).

In case of land degradation, especially in the forest related area, the application of NDSI and NDWI would support the detection of soil-exposed area in post event. The NDSI thus will increase when it illustrates the changes in water content (absorption of SWIR) and chlorophyll of leaves (reflection of NIR). In addition, NDWI is a vital index that reflects liquid water content. Positive NDWI values typically present in open water area and negative ones refer to non-water region. According to Gao<sup>[15]</sup>, most bare soil provides negative NDWI values. Study of Takeuchi in 2004<sup>[16]</sup> showed the results of NDVI, NDSI and NDWI values for eleven land cover types (Fig.6). The results point that NDWI obtains the lowest values in conifers (-0.6), broadleaf forest (-0.64) and grass (-0.65) and varies from -0.34 to -0.12 in soil. Water and snow provide positive values. NDSI increases from vegetation cover type (-0.47 to -0.35) to soil cover group (-0.11 to 0.11). In the study of Deng et al. in 2015<sup>[17]</sup>, they tested the potential band combination of Landsat TM5 to calculate NDSI. The NDSI output show the critically low value of around -0.37 for vegetation surface for the combination of Shortwave infrared band (SWIR1) and Near Infrared band (NIR) while positive values are shown in impervious surface area and soil surface for all other band combinations (0.06 for soil with the SWIR1 and NIR combination).

In this study, we calculate and set up the relationship between NDVI, NDSI and NDWI in the selected pixels in the first trial map to evaluate the threshold for landslide detecting areas. In case of dead weak or removal of vegetation during the landslide occurrence, the soil will be exposed as a result. The NDSI and NDWI hence would increase comparing to the case of vegetation cover to the positive or near positive values (around zero). The results show the ranges of NDSI and NDWI are from -0.5 to -0.1 and from -0.38 to 0.14, respectively. Since positive

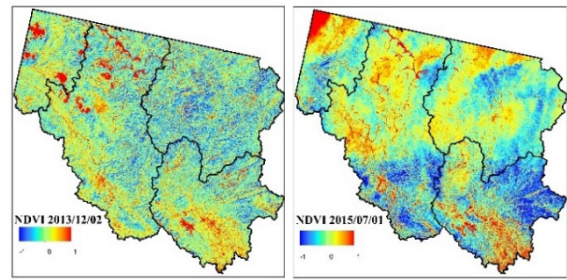


Fig. 5 NDVI calculation in study area (left:2013/12/02 and right: 2015/07/01)

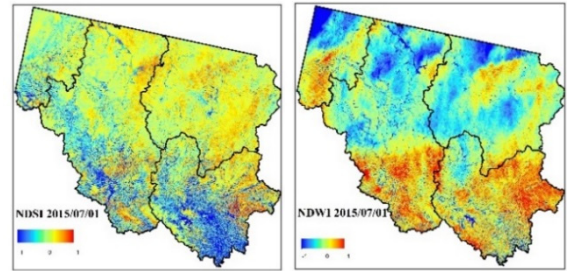


Fig. 6 NDSI (left) and NDWI (right) on 2015/07/01

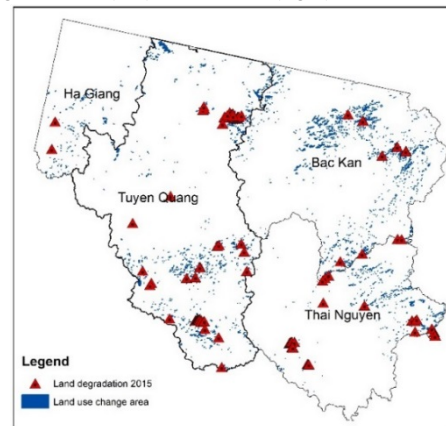


Fig. 7 Land use change area and land degradation area detecting from Landsat calculation

NDWI values come with low NDVI data in post even, it thus may refer to water or impervious surface. NDWI that less than -0.32 obtains high NDVI (greater than 0.5) so that it would reflect the vegetation type cover. The threshold of -0.32 therefore is primary set for NDWI value. NDSI bellowing -0.3 obtains NDVI values of around 0.4 and above. It also refers to vegetation cover area. Low values of vegetation index (reduction in green surface area) locate in the NDSI range from 0 to -0.2. In this case, -0.2 is set as NDSI threshold value. We will locate pixels obtaining NDSI that is higher than -0.2 and NDWI that is higher than -0.32 as landslide detection area (Fig. 7). In this detecting area, average values of NDVI and NDWI are 0.338 (from -0.04 to 0.48) and -0.199 (from -0.32 to 0.14), respectively.

### Inventory approach

In this part, we applied the land use map, which was released by JAXA in September 2016 to



demonstrate land cover situation in North Vietnam in the year 2015. In this version, land use cover includes 9 categories namely: water site(1), urban and built up (2), rice paddy(3), crops(4), grassland(5), orchards(6), bare land (7), forest (8) and mangrove (9) (Fig. 8). There are 9 main geology categories in this study area: Carboniferous/Permian(CP), Cambrian/Ordovician(CmO), Devonian(D), Jurassic/Cretaceous(JK), Ordovician/Silurian(OS), Permian/Triassic(PTr), Proterozoic/Cambrian(PtCm), Quaternary(undivided) (Q), and Silurian/Devonian(SD) (Fig. 9). The slope angle were divided into six sub-classes: i)  $<10^\circ$ , ii)  $10-20^\circ$ , iii)  $20-30^\circ$ , iv)  $30-40^\circ$ , v)  $40-50^\circ$ , vi)  $>50^\circ$ . The elevation is also grouped into six subclasses: i)  $<100$  m, ii)  $100$  m-  $200$  m, iii)  $200$  m –  $300$  m, iv)  $300$  m –  $400$  m, v)  $400$  m –  $500$  m and vi)  $>500$  m.

#### a) Historical landslides and its causative factors

We analyse 1049 historical landslide events in 2013 when combining with causative factors such as slope angle, elevation, geology and land use. The analysis results show that landslide density is the highest (27.5%) in the slope class iii ( $20-30^\circ$ ), following by class ii ( $25.8\%$ ) and class iv ( $21.9\%$ ). The numbers of landslide events decrease when the slope angle increase from group iii ( $20-30^\circ$ ) to group 6 ( $>50^\circ$ ). This overall trend is similar in all three provinces BK, HG and TQ. In general, landslide density concentrates in the elevation range from  $100\text{m}-300\text{m}$  (48.23%). The most common elevation class in landslide occurrence site in BK, HG and TQ is iii ( $200\text{m}-300\text{m}$ ), ii ( $100\text{m}-200\text{m}$ ) and i ( $<100\text{m}$ ) in respectively (Fig.10 & Fig.11). The susceptible geology type in landslide sites in BK area D and PTr while Devon dominates landslide areas in HG and TQ. Among 9 land use classes, historical landslides occurs mainly in forest (BK and HG) and crops (TQ). In all area, grassland also perform in intermediate level (16-26%) (Fig. 12).

#### b) Landslide classification

According to Chandrasekaran, et al [18]. Internal and external causes are two main types of landslide causes. Internal causes include seepage erosion, weathering and progressive failure. Some illustrations of external causes are slope geometry changes, slope toe under loading, slope crest loading, water regime changes or drawdown as well as vibrations and shocks. The external causes can also be divided into two sub categories: natural cause and human cause. For the case of North Vietnam, regarding to the external mechanism, the natural cause for landslide often relate to slope undercutting by wave strength and stream erosion, heavy and prolonged rainfall events, critical groundwater fluctuation and upper slope loading by dense vegetation. The human cause can be seen from some main activities such as slope overloading, slope cutting activities for houses and road constructions,

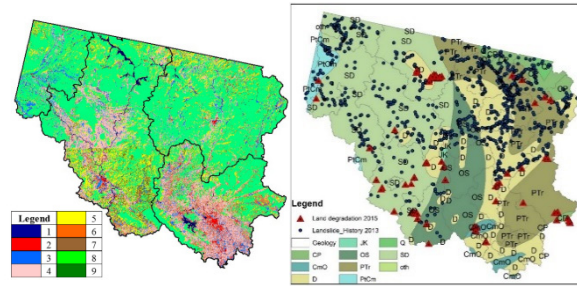


Fig. 8 Land use map

Fig. 9 Geology map

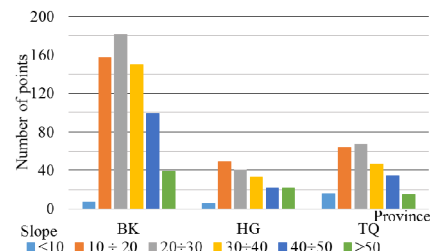


Fig. 2 Slope classification in historical landslide 2013

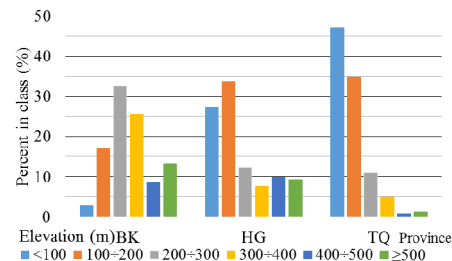


Fig. 11 Elevation classification in historical landslide

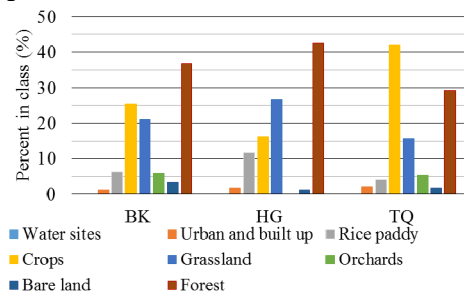


Fig. 2 Land use classification in history landslide 2013

cultivation activities (vegetation removal) and quarrying or mining activities. Our study in 2016 about the regional precipitation distribution in Vietnam [8] showed that an average annual rainfall in the studied site (1975-2006) is about 1997 mm (1762 mm in the North). Rainfall fluctuates significantly around the year. Approximately 80% of total rainfall occurs during summer time. This area has high dense of streams and rivers. The main river systems in North Vietnam [19] appear high density. With regards to geomorphic condition, mountain regions in this area are heavily divided and eroded by thick dense of tributaries so that erosion and sliding activities become more seriously, especially under the influence of heavy rainfall the main landslide triggering factor here. Considering the climatic, hydrological and geomorphic conditions as well as human-related activities in North Vietnam, in this

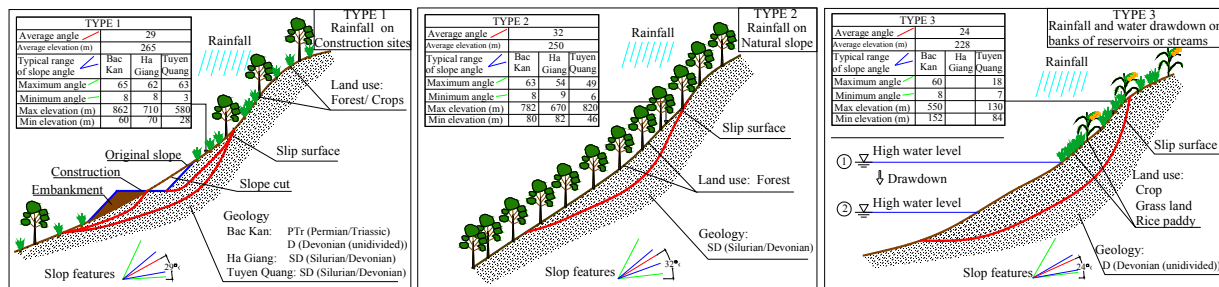


Fig. 13 Illustration of three landslide types

study, we divide the landslides into three major causing types: i) Type 1: Rainfall on construction sites, ii) Type 2: rainfall on natural slope, and iii) Type 3: Rainfall and water drawdown on banks of reservoirs or streams (Fig.13). Type 1 refers to landslide on artificial slopes that are resulted mainly from road and house constructions after heavy or prolonged rainfall events. Type 2 belongs to the case that slopes are not significantly modified by human activities<sup>[20]</sup> under the influences of rainfall triggering factors. In type 3, water fluctuation especially rapid drawdown in a relationship with rainfall event thus are major attributions to landslides that occur on the slope facing water sites such as rivers, ponds and reservoirs. Regarding to historical landslide data in 2013, only 1.34 % and 7.54% of landslide events are classified in type 3 and type 2, respectively. Type 1 dominates in all three provinces (from 83.7 % in HG to 94% in BK).

## DISCUSSIONS AND CONCLUSIONS

Above discussions lead to our consideration for further study on the landslide issues in upper stream regions in Vietnam. However lacking information of landslide scales (height, depth and area) throughout surveys are main limitations of this study. Outputs of this paper, which are mainly based on historical data in a relationship with Landsat instrument, would be considered as initial assessment results of landslide issue in those four provinces in North Vietnam. Further studies should be implemented with requirements of site surveys for position and scale verification and landslide hazard mapping as well as training model for rainfall induced land-slide and water level simulations.

## ACKNOWLEDGMENT

This research was supported by the Social Implementation Program on Climate Change Adaptation Technology (SI-CAT) of MEXT, Japan.

## REFERENCES

- [1] Hue, T. T.: Research on crack and subsidence hazards in mountainous region in North Vietnam, Vietnam Geogr Acad., 2004.
- [2] Tien. Bui. D, Owe, L., Inge, R. and Dick, O.: Landslide susceptibility analysis in the Hoa Binh province of Vietnam using statistical index and logistic regression, Nat Hazards. , Vol. 59, pp. 1413-1444, 2011.

- [3] Metternicht, G., Hurni, L. and Gogu, R.: Remote sensing of landslides: An analysis of the potential contribution to geo-spatial systems for hazard assessment in mountainous environments, Remote Sens Environ., Vol. 98, No. 2-3, pp. 284-303, 2005.
- [4] Dieu, T. B.: Modeling of rainfall-induced landslide hazard for the Hoa Binh province of Vietnam, Nor Univ Life Sci. , 2012.
- [5] Behling, R., Roessner, S., Golovko, D. and Kleinschmit, B.: Derivation of long-term spatiotemporal landslide activity-A multi-sensor time series approach, Remote Sens Environ. , Vol. 186, pp. 88-104, 2016.
- [6] ODM.: Digital Elevation Model (DEM) of Vietnam, Open Dev Mekong., 2016. Available at <https://data.opendevopmentmekong.net/vi/dataset/digital-elevation-model-dem>
- [7] AWRP.: Monthly rainfall in North Vietnam, Acad Water Resour Planning, Minist Agric Rural Dev Vietnam, 2016.
- [8] Thuy, T. T. Le, Kawagoe, S. and Suzuki, K.: Study on the variation of regional precipitation characteristics based on meteorological spatial data in Vietnam: Relationship between GCMs output and historical data, Vietnam-Japan Work Estuaries, Coasts, Rivers 2016, Ho Chi Minh City, Vietnam, 2016.
- [9] RCFEE.: Forest ecological stratification in Vietnam, Res Cent For Ecol Environ Vietnam., 2011.
- [10] USGS.: Landsat 8, US Geol Surv., 2015. Available at <http://landsat.usgs.gov/landsat8.php>
- [11] DWR.: Management of Hydraulic system in Vietnam, Dir Water Resour Minist Vietnam Agric Rural Dev, 2016.
- [12] JAXA.: High- Resolution Land Use and Land Cover Map of Northern Region of Vietnam (Released in Sep.2016/Version 16.09), Adv L Obs Satell – ALOS Res Appl Proj EORC, JAXA., Available at [http://www.eorc.jaxa.jp/ALOS/en/lulc/lulc\\_vnm.htm](http://www.eorc.jaxa.jp/ALOS/en/lulc/lulc_vnm.htm)
- [13] Broxton, P. D., Zeng, X., Sulla, M. D. and Troch, P. A.: A Global Land Cover Climatology Using MODIS Data, J Appl Meteorol Climatol., Vol. 53, No. 6, pp. 1593-1605, 2014.
- [14] Mwaniki, M. W., Agutu, N. O., Mbaka, J. G., Ngigi, T. G. and Waithaka, E. H.: Landslide scar/soil erodibility mapping using Landsat TM/ETM+ bands 7 and 3 Normalised Difference Index: A case study of central region of Kenya, Appl Geogr., Vol. 64, pp. 108-120, 2015.
- [15] Gao, B. C.: NDWI - A normalized difference water index for remote sensing of vegetation liquid water from space, Remote Sens Environ., Vol. 58, No. 3, pp. 257-266, 1996.
- [16] Takeuchi, W. and Yasuoka, Y.: Development of normalized Vegetation, soil and water indices derived from satellite remote sensing data, J Japan Soc Photogramm Remote Sens. , Vol. 43, No. 6, pp. 7-19, 2004.
- [17] Deng, Y., Wu, C., Li, M. and Chen, R.: RNDISI: A ratio normalized difference soil index for remote sensing of urban/suburban environments, Int J Appl Earth Obs Geoinf. , Vol. 39, pp. 40-48, 2015.
- [18] Chandrasekaran, S. S., Senthilkumar, V. and Maji, V. B.: Landslides in Nigiris: Causal factors and remedial measures, Indian Geotech Conf IGC 2016, 2016.
- [19] Hue, T. T.: Research on evaluation of the river bank sliding hazard in mountainous region in the North Vietnam, Vietnam Geogr Acad, 2004.
- [20] Ko, F. W. Y. and Lo, F. L. C.: Rainfall-based landslide susceptibility analysis for natural terrain in Hong Kong - A direct stock-taking approach, Eng Geol. Vol. 215, pp. 95-107, 2016.
- [21] VIGMR.: Geology hazard and natural disaster warning program, Vietnam Inst Geosci Miner Resour, 2014.

## **THE QUALITY ANALYSIS OF BICYCLE ROUTES FOR SUSTAINABLE URBAN MOBILITY IN THE WESTERN ZONE OF RIO DE JANEIRO**

Guilherme Marins Pessanha<sup>1</sup>, Jaime Massaguer Hidalgo Jr<sup>2</sup>.

Urban and Environmental Engineering<sup>1</sup>, Pontifícia Universidade Católica do Rio de Janeiro / Technische  
Universitat Braunschweig, Brazil

### **ABSTRACT**

In order to be an example of active urban mobility using bicycles, the city of Rio de Janeiro in Brazil, has developed the program "Rio de Janeiro, urban capital of mobility by bicycle", a program to increase the cycle infrastructure that preceded the mega events; 2014 World Cup and the 2016 Olympic Games. This article aims to apply bicycle model analysis criteria and to promote the discussion about quality of bicycle facilities in the west of Rio de Janeiro and its structure legacy. The bicycle lanes and cycle paths of the Santa Eugênia Road in Paciência neighborhood and the Padre Guilherme Decaminada avenue in Santa Cruz neighborhood were measured in order to highlight the real problems that are currently being faced in the specific spaces for bicycle use. For the analysis of local conditions and the cycle paths, field trips were made by bicycle. The methodology used has ten benchmarking criteria. The collected results point to good operating conditions but a lack of compliance with some minimum requirements for signaling, lighting and maintenance of bicycle ways pavement. Thus, this study contributes to the analysis of the quality of cycle routes in the city by encouraging sustainable urban mobility and its urban infrastructure itself.

*Keywords: Urban Planning, Bicycle Facilities, Mobility.*

### **INTRODUCTION**

In the last decades, the use of urban mobility policies by bicycles has gained prominence in the Brazilian scenario, especially in Rio de Janeiro. The history of the Rio de Janeiro cycle routes began in 1991, when the first cycle routes were built from a program to redevelop the seafront known as "Rio Orla" (Rio Seaboard). The program has built 23 km of bicycle lanes designed mainly for leisure. Since 1993, and with the influence of ECO92 (United Nations Conference on Environment and Development), which the city of Rio de Janeiro has hosted, the Municipal Environment Secretariat was created. The city government has incorporated the program "Rio, urban mobility capital by bicycle" into the urban mobility plan of the city as an alternative transportation and as a modal element of transport for short distances with the ability to integrate BRT systems (Bus Rapid Transport), trains and subway. The bicycle plan of the city of Rio de Janeiro had the goal of expanding its extension from 150 km in the year 2009 to 450 km by the end of 2016, a period in which the city received the Mega events such as World Cup 2014 and the 2016 Rio

Olympic Games. However, a cycling programme is not only sustained by its extension, and a set of socio-spatial criteria is necessary for its effectiveness. The Mobility Plan for Bicycles in Cities, (Ministry of Cities, 2007), states that the connection with different transport systems is a key factor for bicycles to be adopted by the population in their movements, the urban infrastructure of cities must adapt to modal and adaptations should and can be made. As a sample of existing bicycle infrastructure, the Santa Eugênia Road cycle paths were chosen in the Paciência neighbourhood and Padre Guilherme Decaminada Avenue in the Santa Cruz neighbourhood, both in the western zone of Rio de Janeiro. The west zone of Rio de Janeiro is represented as AP-5 (planning area 5) and comprises five administrative regions with 21 districts distributed in an area of 609.50 km<sup>2</sup> occupying about 42% of the city's territorial area (IPP, 2013 ). It is an area of great real estate expansion of the city, where the land use and occupancy patterns are predominantly horizontal and the use of the bicycle is frequent between residents and merchants.

**Padre Guilherme Decaminada Avenue**

The bicycle system of Av. Padre Guilherme Decaminada is 3.60 km long (Mobility and Culture, 2016), composed of a shared bicycle path in the sidewalk of the neighbourhood functioning as an axis between the train station of Santa Cruz and Avenida Brasil, Paracycles, lighting and signage. It has an intense flow of people due to the services and schools in the surroundings. The flow of cyclists and pedestrians is intense in the cycle path as well as the flow of private vehicles in the neighbourhood.

### Santa Eugenia Road

The cycle path of the Santa Eugenia Road has similar characteristics, with a 6.00 km extension (Mobility and Culture, 2016) divided between a shared cycle path on the sidewalk and the cycle path. It is located along the intense chain of services, schools and hospitals and goes to the train station of Patience and the station of BRT Santa Eugenia.

The Santa Eugenia Bus Rapid Transport (BRT) station is one of the many stations that make up a segregated collective transportation road that runs through the western zone of Rio de Janeiro implemented for the 2014 World Cup and 2016 Olympics Games. Bicycle as a means of transport in the west of Rio de Janeiro is a common practice, due to local economic conditions and precarious access to public transportation. For the reasons presented, the cycling systems cited were chosen for the application of the evaluation criteria of a bicycle system proposed in the “Caderno das Ciclovias”.

### METHODOLOGY

The present article makes a qualitative analysis of the bicycle paths and bicycle lanes of two important routes for the displacement of the local population. Based on this diagnosis, a critical analysis is carried out in these two routes and their connections with the public transport, focusing on the compliance with the criteria of the Caderno das Ciclovias, nonconformities and suggestions for improvements. To do this, maps and photos of the research scope were compiled. After this survey of documentation, a search was made for bibliographic references that indicated temporal results of the goals and actions proposed, from the period of 2013 to 2016 by the public and private partnerships in the period of the works.

From the observed references, the total route of bicycle route was divided into 2 distinct sections with the objective of a specific evaluation for each cycleway analysed.

In the figures below, we observe the geographic maps and studied in this article.

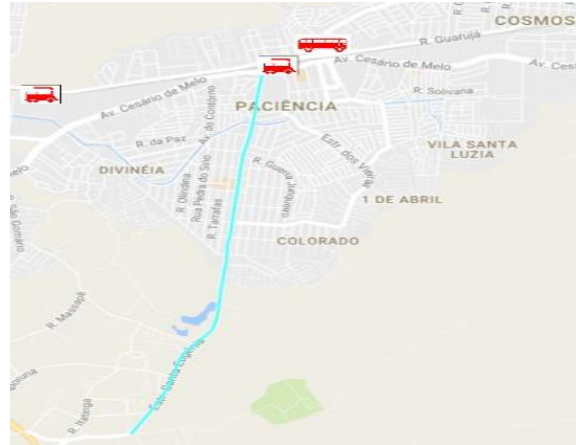


Fig. # 1: Padre Guilherme Decaminada Avenue  
Designed by co-author

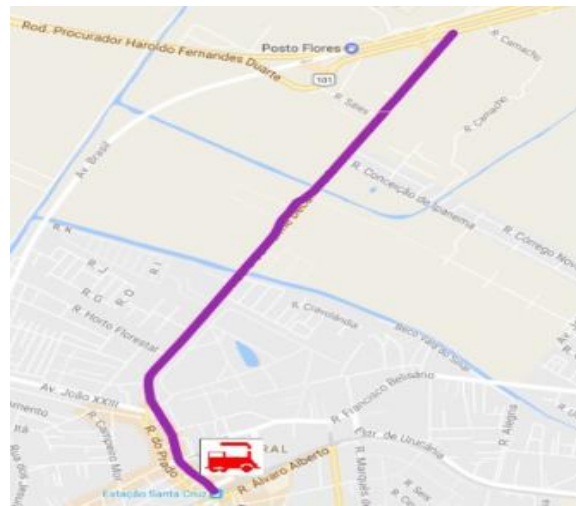


Fig. # 2: Santa Eugenia Road. Designed by co-author

### Study of the route and section markings

In possession of the aforementioned maps of the two avenues, the bicycle paths and their facilities were marked with a purple and light blue line. Each extension of the bicycle paths was evaluated as well as small sections due to different conditions along the two avenues.

### Method and Measurement Criteria's

Based on the research carried out in the theoretical references, it was defined that the "Brazilian Bicycle Mobility Program" and its "Reference Notebook for the elaboration of: Mobility Plan by Bicycle in Cities" indicates the criteria for the elaboration of the collection table for Data and metrics appropriate to a bicycle system. The main purpose of such table is to raise the situation of these cycle routes following minimum criteria and suggest improvements to expand the connectivity and meet the criteria required in the Brazilian Bicycle Mobility Program.



The table was divided into two topics. The first topic relates the Basic Elements for Projects with the purpose of detailing the criteria for evaluating the quality of the cycle paths of this research. This topic was divided into 10 questions with the objective of evaluating the following criteria: 1 - Geometric Project; 2 - Cyclist Useful Space; 3 - Traffic Moderation - measures for the humanization of the city; 4 - Runs and Tracks of Cyclists; 5 - Intersections and Crossings; 6 - Paving; 7 - Drainage; 8 - Lighting; 9 - Parking for Bicycles; 10 - Bicicletário. The second topic aimed to analyze the integration of the bicycle with the collective modalities in the following points: 1 - bicycle and bus; 2 - bicycle and train; 3 - bicycle in BRT; To measure, the following criteria were adopted:

- a) The criteria receive a score for each Section. The possible punctuation are : Not Conformity (zero point up to 0,59 points), In Conformity, need improvements (0,60 points up to 0,79 points) e In Conformity (0,80 points up to 1,00 point);
- b) If the sum of the points attributed to a certain section of cycling route is  $<0.60$  it is considered Non-Conforming the use of bicycles in this place because it does not contemplate 60% of the analyzed criteria; If the sum of the points attributed to a particular section of cycle path is  $\geq 0.60$  and  $< 0.80$ , it is considered Partially According to the use of bicycles in this section, since it presents more than 60% of the analyzed criteria, and in this way, there is The need for improvements in order to have the perfect state of use and its connections with the public transport systems evaluated; And if the sum of the points assigned to a given section of cycling track is  $> 0.8$  and  $\leq 1.00$ , the use of bicycles as In Conformity is adopted, since it can reach 80% to 100% of the criteria assessed.

These evaluation criteria were applied during the month of February 2017 in 2 field visits during the morning, afternoon and evening periods. At each start and end point, the bicycles were parked for the appropriate notes. With the notes, it was possible to calculate the BCI (Bicycle-Rate Conformity Index) of each of the small sections and then add them using a simple average formula that we will see. Thus we will have different notes for each short section evaluated and a general note for each scope of each cycle of the survey, giving an overview of

the conforming and nonconforming conditions of that urban space of the city of Rio de Janeiro.

### Adoption of a Bicycle Conformity Index – BCI

With possession of the notes of each section, by avenue and relating all evaluation criteria, we decided to adopt an Index of Compliance with the Brazilian Bicycle Mobility Program with the necessary adaptations for an adequate assessment. The adapted weighted average formula was chosen to facilitate readers' understanding and is also applied to large works contracts in Brazil and the city of Rio de Janeiro, and is accepted by fiscal audit courts.

**BCI** =  $\{(\sum \text{Basic Project Elements Criteria Applicable}) \times 8 + (\sum \text{Integration Criteria with collective modals Applicable}) \times 2\} / 10$

### The Evaluation Criteria

The selected criteria were taken from the Brazilian Bicycle Mobility Program in chapters 3 and 4. The topic lists the Basic Elements for Projects has the following criteria:

Geometric design - the arrangements and dimensions of bicycle spaces will always depend on five factors, namely: the minimum dimensions required for the safe circulation of bicycles; The remnants of spaces or the rearrangements of parts or all of the existing roads, converting to the bicycles a slice of the road system; The creativity of designers by combining techniques with existing opportunities in urban spaces, adapting them to the needs of cyclists.

Useful space of the cyclist - the standard bicycle in Brazil has a longitudinal dimension of about 1.75 m. The width of 1.00 m results from the width of the handlebar (0.60 m), plus the space required for the movement of the arms and legs (0.20 m on each side). The template to be adopted, however, for safety measures, shall be higher by 0.25 m in height and on each side, in order to maintain the cyclists' balance. (Brazilian Bicycle Mobility Program, page 99.) See figure 2 the useful space of the cyclist in centimetres.

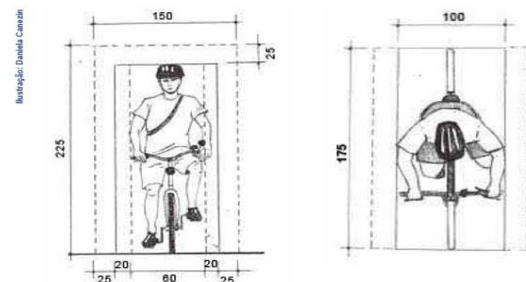


Fig. # 3: Cyclist parameters in Brazil

Source: Programa Brasileiro de Mobilidade Por Bicicleta, page. 99.

*Traffic moderation* - measures for humanization of the city As a measure of moderation of traffic directed to the circulation of bicycles, it is recommended to use cycle paths near the bed of the collecting ways. Corner radius reduction; • Change of texture and color of the lining of the cycle lane; • Adoption of central islands separating flows; • Demarcation of crosswalk;

*Cycle lanes and lanes* - Cycle lanes are dedicated to the exclusive circulation of bicycles, separated from the other runways by embankment, with a minimum of 0,20 m of unevenness, which is usually higher than the car lane Motorized. In the road system, it can be located along the central bed or on the sidewalks. Bicycle lanes is the space destined to the circulation of bicycles, contiguous to the raceway of automotive vehicles, being separated of it by painting and / or devices limited denominated of tacks by the Brazilian Transit Code.

*Intersections and crossings* - Will be evaluated in the crossings: the Circulation Channelized in Crossings with Ample Side Space, Circulation with Little Side Space, Shared Circulation, Upper Crossings. Rotary - Roundabouts are considered by many experts dangerous for pedestrians and cyclists. However, this concept has to be relativized, according to their sizes and positions in the territory of a city or region. Rotates with inclusion of special spaces for the bicycle In Brazil it is still not common.

*Paving* - The basic requirements for a bicycle lane in relation to the pavement are as follows: the rolling surface must be regular, waterproof, non-slip and, if possible, pleasant in appearance. Due to the close proximity of the bicycle lane with the pedestrian walk, it is desirable that the surface of the bicycle lane and that of the lane be visually differentiated so that there is no invasion of the bicycle path by the pedestrian as well as the invasion of the ride by the cyclist. Cycle paths are not subjected to great efforts, Requiring a larger structure than that used for pedestrian routes.

*Drainage* - The drainage of the bicycle lanes should be as natural as possible, taking advantage of the topography of the site, thus avoiding the installation of sophisticated networks for the drainage of rainwater. When there is greater freedom of tracing (especially on leisure cycle routes), cuts and embankments should be avoided, as soil movements always create some drainage problems that imply erosion or need for clearing. The position of the lobes in the mouth of a wolf is an important aspect regarding the safety of the cyclists, referring to the

drainage in cycle paths, cycle paths or routes where there is bicycle traffic. Considering that the size of adult bicycle wheels is greater than 0.60m, the space between the closing transverse bars being less than 0.50m will prevent their falling into the drainage area.

*Illumination* - When using poles of the existing electrical network, it is recommended to place metal rods in a lower position than is normally used for illumination of the entire track. The height should be between 2.60m and 3.20m, making access to the luminaire difficult for anyone without the use of stairs or other elements that raise their height.

*Parking for bicycles* - Two bicycles are inscribed in a rectangle of approximately 1.70m x 1.60m.

*Bicycles* - Bicycles are characterized as long-term parking lots, large number of seats, access control, whether public or private.

The topic related to the integration of the bicycle with the collective modes has the following criteria:

*Bicycles and buses* - bus shelter with paracycle, containing eight places for bicycle parking. The project was awarded in competition in Finland at the National Bicycle Year in that country in 1996. The project was part of a paper presented by Maija Rahka at the Velocity Congress in September 1997 in Barcelona.

*Bicycles and trains* - There are bicycles in the vicinity of the train stations near the section evaluated.

*Bicycles and BRT* - evaluated the existence of parking for bicycles on weekdays, in the vicinity of BRT stations near the evaluated section.

## EVALUATION OF RESULTS

Cycle routes and cycle routes of the Santa Eugênia Road in the Paciência neighbourhood, BCI = 0.61 STATUS = In Conformity, with suggestions for improvements.

Table 1 - BCI Santa Eugenia Road

<b>Santa Eugênia Road divided into sections</b>	<b>BCI = 0,61</b>
Section 2.1	0,63
Section 2.3-2.5	0,67
Section 2.6-2.13	0,66
Section 2.14	0,67
Section 2.15	0,59

Source: Own authorship

## Comments and results of the criteria

## . Geometric Design

Average = 1.0 - Conformed

Technical comment: Safe circuits and allow the visualization of the section to be covered.

## . Useful space of the cyclist

Average = 0.75 - Conformity, needs improvement.

Technical comment: The minimum dimensions of 1.20 required for circulation are respected, but in some cases the pedestrian walkway suffers bottlenecks

## . Traffic moderation

Average = 0.60 - Conformity, needs improvement.

Technical comment: There is a lack of elements for the reduction of the turning radius of corners and signalling on the bicycle lane. As well as a more objective demarcation in relation to the pedestrian range

## . Cycle tracks and tracks

Average = 0.60 - Conformity, needs improvement.

Technical comment: There are excerpts where the boundary between cyclist and sidewalk lanes are not well delimited.

## . Intersections and crossings

Average = 0.60 - Conformity, needs improvement.

Technical comment: In Brazil it is still not common crossings with satisfactory safety conditions for the rider. In the evaluated sections they are restricted to the end of the pivot radius.

## . Paving

Average = 0.65 - Conformity, needs improvement.

Technical Comment: Paving is either precast concrete or concrete block, both suitable. But the conservation is irregular. Leveling for crossing is the most critical point

## . Drainage

Average = 0.62 - Conformity, needs improvement.

Due to the irregular state of conservation of the pavement, imperfections and unevenness, the water flow is compromised creating areas and allowing the growth of unwanted vegetation.

## . Lighting

Average = 0.60 - Conformity, needs improvement.

Technical comment: illumination is interrupted or compromised by existing vegetation

## . Bicycle parking

Average = 0.61 Conformity requires improvement.

Technical comment: Bicycle stands are public and can be found mainly near public buildings or near corners. Along the stretches there is no presence of bicycle lifts

## . Connectivity to public transport

Average = 0,38 - Not in conformity

Technical comment: Not all train stations are prepared to receive the cyclist, in some of them it is necessary to go up or down a ladder carrying the bicycle. In the trains the schedules allowed for the bicycles are reduced and there is no such integration with the BRS.

See in the table below the results found for each Section of the cycle ranges and an integral evaluation of the whole cycle cycle:

Table 2 – BCI Padre Guilherme Decaminada

<b>Padre Guilherme Decaminada Avenue divided into sections</b>	<b>BCI = 0,67</b>
Section 1.1	0,74
Section 1..2	0,82
Section 1.3	0,77
Section 1.4	0,78
Section 1.5-1.6	0,76
Section 1.7	0,84
Section 1.8	0,77
Section 1.9	0,75
Section 1.10	0,60

Source: Own authorship

**Comments and results of the criteria**

## . Geometric Design

Average = 1.0 - Conformed

Technical comment: Safe circuits and allow the visualization of the section to be covered.

## . Useful space of the cyclist

Average = 0.78 - Conformity, needs improvement.

Technical comment: The minimum dimensions of 1.20 required for circulation are respected, but in some cases the pedestrian walkway suffers bottlenecks

## . Traffic moderation

Average = 0.67 - Conformity, needs improvement.

Technical comment: There is a lack of elements for the reduction of the turning radius of corners and signalling in the sections in bicycle-band

## . Cycle tracks and tracks

Average = 0.65 - Conformity, needs improvement.

## . Intersections and crossings

Average = 0.64 - Conformity, needs improvement.

Technical comment: In Brazil it is still not common crossings with satisfactory safety conditions To the cyclist. In the sections evaluated, they are limited to the distance at the end of the turning radius of the pavement

## . Paving

Average = 0.80 - Conformity.

Technical Comment: Paving is either precast concrete or concrete block, both suitable. But conservation is irregular.

## . Drainage

Average = 1.0 - Conformity.

The blocking paving in some sections works with a drainage element.

## . Lighting

Average = 0.75 - Conformity, needs improvement.

Technical comment: Crossings have irregular lighting

. Bicycle rental

Average = 0.65 In Compliance, you need improvements.

Technical comment: Bicycle stands are public and can be found mainly near public buildings or near corners. Along the stretches there is no presence of bicycle lifts

. Connectivity to public transport

Average = 0.43 - Nonconforming.

## CONCLUSION

By the methodology applied, the bicycle system of the Estrada Santa Eugenia reached an BCI = 0.61 and the Padre Guilherme Decaminada Avenue an BCI = 0.67. Both are compliant with the applicables criterias, but need improvements mainly in connectivity with modal systems and safety of crossings. It is necessary to adapt the train stations for the handling of bicycles, and to create bicycle stands with an infrastructure that can attend to the cyclist needs and secure the bicycle. The parameters established for analysis are physical and infrastructure and establish direct influence on the choice of the bicycle as an element of mobility. The results presented in this article highlight the need to broaden the research on the public policies adopted in the City of Rio de Janeiro to transform the bicycle into a complementary system and integrated with the other modes of public transport in the city.

## REFERENCES

- [1] BRASIL. Lei nº 12.587 de 2012. Institui as Diretrizes da Política Nacional de Mobilidade Urbana. Available on: <[https://www.planalto.gov.br/ccivil\\_03/\\_ato201](https://www.planalto.gov.br/ccivil_03/_ato2011-2014/2012/lei/112587.htm)

1-2014/2012/lei/112587.htm>. Acess on: 10/03/2017.

- [2] BRASIL. Lei nº 9.503 de 1997. Código de Transito Brasileiro. Available on: <[www.planalto.gov.br/ccivil\\_03/leis/L9503.htm](http://www.planalto.gov.br/ccivil_03/leis/L9503.htm)>. Acess on: 15/02/ 2017.
- [3] Ministério das Cidades (2007) Programa Brasileiro de Mobilidade por Bicicleta – Bicicleta Brasil. Caderno de referência para elaboração de plano de mobilidade por bicicletas nas cidades. Brasília: Ministério das Cidades. Available on: <[www.cidades.gov.br](http://www.cidades.gov.br)>. Acess on: 15/02/2017.
- [4] Inatti,G “Mobilidade e Cultura de bicicleta no Rio de Janeiro”,ed.1 Vol. 1, Rio de Janeiro Ed. Transporte Ativo, 2016
- [5] IPP-Instituto Pereira Passos “Cadernos do Rio de Janeiro, 2013”. Available on: [http://www.armazemdedados.rio.rj.gov.br/arquivos/3295\\_religiao.PDF](http://www.armazemdedados.rio.rj.gov.br/arquivos/3295_religiao.PDF) . Acess on 02/05/2017
- [6] Programa Brasileiro de Mobilidade por Bicicleta – Bicicleta Brasil; Caderno de referência para elaboração de Plano de Mobilidade por Bicicleta nas Cidades. Brasília: Secretaria Nacional de Transporte e da Mobilidade Urbana, 2007
- [7] Programa Cicloviário do Distrito Federal: Sistema Cicloviário Intermunicipal, Integrado com outros modais de Transporte e ação educativa - ABCP – Associação Brasileira de Cimento Portland. Programa Soluções para Cidades.

## COMPARATIVE ANALYSIS OF PAVEMENT FRICTION PREDICTION MODELS

Luciana Omar<sup>1</sup>, Karim Ismail<sup>2</sup> and Abd El Halim O. Abd El Halim<sup>3</sup>

<sup>1</sup>Faculty of Engineering and Design, Carleton University, Canada

### ABSTRACT

Pavement friction is an important operational variable that affects the safety and efficient operation of highways. Pavement friction measurement is a relatively complex and resource-intensive process, thus limiting data availability. This is especially problematic when studying extensive road networks such as inter-jurisdictional highways in North America. Other measurements of pavement conditions, however, are readily available through automated techniques using road analyzer vehicles that can potentially travel at free-flow speed along highways. This study explores the prediction of pavement skid number measured using a locked-wheel tester on provincial highways in Ontario, Canada. The study compares different model structures: multivariate regression and structural equation modelling. The explanatory variables available for all sites were: pavement age, traffic and loads, and macrotexture, which was measured using an instrumented vehicle that laser scanners pavement surface. A subset of these sites had mix-design information available and is considered in a separate analysis with more explanatory variables, but a more limited sample size.

*Keywords: Skid Resistance, Macrotexture, Multivariate Regression Model, Structural Equation Model*

### INTRODUCTION

Pavement skid resistance, or *friction*, refers to the force that resists the relative motion between a vehicle's tire and the pavement surface. Pavement friction is considered one of the most important indicators of road safety [1]. In general, driver control is related to the friction available at the tire-pavement interface; the higher the levels of friction, the greater the vehicle control [1]. Pavement friction is a function of pavement surface texture that combines two scales of surface texture properties: microtexture (texture wavelength range from 1  $\mu\text{m}$  to 0.5 mm and vertical amplitude less than 0.2 mm) and macrotexture (texture wavelength range from 0.5 mm to 50 mm and vertical amplitude between 0.1 mm and 20 mm) [1] [2].

In North America, friction field measurements are usually taken using a device called ASTM E-274 Brake Force Trailer; however, these tests are laborious, as is the data entry into a Pavement Management Systems (PMS). As a result, road agencies may not fully implement and integrate the data into existing performance models. These performance models also receive pavement condition information from field data collected using a state-of-the-art device called an Automatic Road Analyzer (ARAN), a high-speed road analyzer. Despite its strengths, ARAN is not readily used in conducting a comprehensive evaluation of pavement surface friction. There is an overall need to explore alternative approaches to identifying friction deficiencies. To address this need, the present study

aims to develop and compare multivariate statistical models of pavement friction prediction using field data collected by ARAN, mix design and operational characteristics of the roads. The results will contribute to a comprehensive knowledge base to guide transportation agencies in decision-making regarding maintenance services and highway safety.

### BACKGROUND

Previous studies have suggested that it is possible to estimate friction using statistical models that correlate pavement textures with other variables related to aggregate properties, mix parameters, and road characteristics (e.g., traffic, loads, road design, and environmental conditions). Reference [3] developed a method that can be used in models for predicting changes in asphalt pavement skid resistance as a function of aggregate texture, mixture properties, and environmental condition. Reference [4] and [5] developed models for estimating friction deterioration that incorporated aggregate characteristics and mixture gradation. Reference [5], for instance, developed a model that correlated skid resistance, initial and terminal, for asphalt pavements based on multiple mix design, aggregate characteristics, and traffic level.

Reference [7] developed models for estimating friction for asphalt concrete pavements using mixture and aggregate gradation, cumulative Annual average daily traffic, and equivalent single axle load. Reference [7] also demonstrated that the percentage of aggregates passing in different sieves were

significant predictors of pavement friction.

Reference [8] developed a model for predicting skid number (SN) and mean profile depth macrotexture (MPD) using mix design properties and aggregate gradation. The results indicated that SN could be estimated using mix design properties and macrotexture.

In a recent study, [9] attempted to develop models to predict SN that correlates MPD measurements collected using a laser mounted in a vehicle travelling at high speed (100 km/h). The models exhibited a positive correlation between SN and MPD when the MPD was less than 0.75 mm, and a negative correlation when the MPD was more than 0.90 mm. The authors also proposed reduction factors for SN to account for cumulative traffic volume.

## STUDY SITES AND DATA COLLECTION

The datasets used in this research were obtained from the Ministry of Transportation of Ontario (MTO) for 109 road sections of asphalt surface course within a variety of functional classes of rural roads (divided and undivided, single and multiple lanes) with speed limits of more than 80 km/h. The field data, skid resistance (SN) and macrotexture (MPD), were collected in the between April and October of the years 2012 to 2015.

Information about pavement and operational segment. The skid tests were performed on the left wheel path of the outsider lane in both directions of travel. In total, 1,544 tests were performed in different regions of Ontario's road network. On average, 14 skid tests were performed per road section, within a maximum of 33 tests in the longest segments and a minimum of four tests in the shortest segments.

Macrotexture measurements occurred in 87 road sections using a high-speed road analyzer (ARAN). ARAN is an example of a multi-purpose and multi-sensor data collection vehicle that employs cameras, sensors, and an advanced laser scanner to survey pavement distress, macrotexture, smoothness, and other relevant attributes. The ARAN laser measurement system is based on regular contactless scanning of longitudinal profile that computes average depths in intervals of 20 meters long of the pavement surface macrotexture. To determine the macrotexture level for each road section the macrotexture measurements were computed as the average of the MPD readings for each road section.

## METHODOLOGY

For prediction purposes, this study uses two approaches: multivariate analysis and structural modeling.

characteristics of each road section were also obtained from MTO. Pavement and operational characteristics include information regarding years of service of the pavement after the most recent maintenance or rehabilitation (pavement age), traffic, loads (ESAL), number of lanes, lane distribution factor, type of asphalt mix, and mix design parameters. The years of service of the 109 road sections ranged from two to nine years of service. Mix design information was available for 68 road segments.

The 109 road sections were divided into seven types of asphalt surface courses: one road section of recycled hot mix 40 (RHM40), one road section of hot mix HL type 1 (HL1), seven road sections of hot mix HL type 4 (HL4), 11 road sections of Stone Mastic Asphalt (SMA), 44 road sections of Superpave 12.5 (SP 12.5), 23 road sections of Superpave 12.5 FC1 (SP 12.5 FC1), and 22 road sections of Superpave 12.5 FC2 (SP 12.5 FC2).

Skid resistance measurements occurred in the field using a Locked-Wheel Friction Tester (LWT), ASTM E-274 Brake Force Trailer, ASTM E274-97, with a standard ribbed tire, ASTM E 501-97. The weighted trailer was connected to a standard fleet truck and travelled along wetted surfaces at a constant speed of 65 km/h. The average of skid resistance was generated over 20 to 30 meters of road

## Multivariate Regression

Multivariate regression using ordinary least square (OLS) is the most widely and adaptable statistical technique used to investigate the relationships between a single dependent variable (SN) and several independent variables [10]. The objective of multivariate regression is to use independent variables whose values are known to predict the single dependent variable. In the regression analysis each independent variable is weighted by the regression. The weights ( $\beta$ ) denote the relative contribution of each independent variable to the overall prediction [10]. For each variable added to the model, several measures were analysed to determine their contribution to the overall model fit regarding the increase in the coefficient of determination ( $R^2$ ), decrease of standard error (SE), the significance of the partial correlation (p-value), and the effects of collinearity. Usually, the threshold value for excluding variables from the equation is set at a p-value of 0.05 to 0.10. The effects of multicollinearity were assessed using the Variance Inflation Factor (VIF) with a threshold of five [10].

## Structural Equation Modelling

The structural models involve processing and

testing a structural equation model (SEM). The hypothesized model can be tested statistically in the simultaneous analysis of the entire system of variables to determine if the goodness-of-fit of models is satisfactory for the proposed relations within the variables [11].

SEM is a statistical technique for multivariate analysis similar to multivariate regression [10]. Reference [11] listed four main differences between SEM and other multivariate techniques:

1. SEM takes a confirmatory technique for data analysis, while other techniques are descriptive and exploratory in nature.
2. SEM is a technique for testing hypotheses about relationships among observed and unobserved (latent) variables. Other multivariate techniques are exclusively based on observed variables.
3. SEM is also capable of dealing with multivariate relations and estimating direct and indirect effects of variables.
4. SEM gives estimates of error variance parameters. In other techniques, these errors are ignored, which may lead to incorrect conclusions due to misleading regression estimates.

Another important difference between SEM and other multivariate techniques is the impact of sample size. While in the other multivariate the effects of sample size are directly related to the probability of detecting statistical power ( $R^2$ ) at a specified level of significance, in SEM these parameters are not the only consideration. SEM requires sufficient number of cases for the model to converge without improper estimate parameters [10] [14]. Estimate parameters include weights, covariances, variances, means, and intercepts.

SEM is more sensitive to sample size than other multivariate techniques because some statistical algorithms used by SEM are unreliable with small samples [10]. Generally, the more complex the model the larger sample size is required. Small sample size affects the ability of the model to estimate correctly error estimation. Larger samples reduces the variability of the model and increases the stability of the model. [10] [12].

As with the OLS multiple regression model, SEM cannot be used to prove causality; rather, SEM is a model-testing procedure used for evaluating hypotheses of relationships among variables.

The most common types of structural equation models are: path analytic models (PA), confirmatory factor analysis models (CFA), structural regression models (SR), and latent change models (LC) [12]. The main difference between the models is that PA models account for observed variables only, while the other three models account for the relationship between observed and latent variables. This research focus on development of a PA model for testing correlations between observed variables and

goodness-of-fit of the proposed model

In a PA model, observed variables are represented as rectangles. Direct effects between variables are indicated using a single directional arrow. The single arrow indicates directionality and does not imply causality. Curved double-headed lines between variables indicate correlations. Independent variables are called *exogenous* and dependent variables are called *endogenous*. Finally, each endogenous variable has an error term, denoted by a circle pointing towards the specific endogenous variable. The error term captures the unexplained variance of the variable, which corresponds to the assumption that the variable was measured with some degree of error [12].

The goodness-of-fit of the model is based on the difference between the observed and the model-implied variance-covariance matrices [13]. The most common indicators are Chi-square, the goodness-of-fit (GIF), the adjusted goodness-of-fit index (AGFI), and the root mean square of approximation (RMSEA) [12].

This research employed the software IBM SPSS 23 and IBM SPSS AMOS for multivariate and SEM analyses, respectively.

## Data preparation

For modelling purposes, all of the independent variables used in this study were graphically analysed to meet three assumptions: normal distribution, homoscedasticity, and linearity. The frequencies of the data were plotted to verify whether data distribution followed a Gaussian distribution. Linearity was examined using bivariate plots. The independent variables that violated these assumptions were transformed using logarithm function. Outliers were identified and removed by calculating the median absolute deviation (MAD).

## RESULTS

This section presents the modelling process to develop friction prediction models using multivariate regression. The SN was used as the dependent variable and 11 independent variables that were tested as potential predictors. The 11 predictors: MPD, a set of variables related to operational characteristics and a set of variables related to mix design characteristics.

The set of operational characteristics included pavement age (Age) and annual ESAL per lane (AESAL). Additionally, a variable was created to capture the effect of accumulated traffic loads over time by multiplying the age of pavement by the annual ESAL (AgeAESAL). When the variable AgeAESAL was tested in the models, Age and AESAL were not included.

The variables related to mix design



characteristics included nominal aggregate size (NMA), percentage of voids in the mineral aggregate (VMA), percentage of air voids (VA), percentage of asphalt content (AC), percentage of aggregates retained sieve 4.75 mm (Co), percentage of aggregates passing sieve 4.75 mm (Fi), and the percentage of aggregates passing sieve 2.36 mm (FFi). In addition, one variable was created to combine fine and coarse aggregates by dividing the percentage of the percentage of aggregates passing sieve 2.36 mm by the percentage of aggregates retained sieve 4.75 mm (FFi / Co).

### Multivariate Regression

The process of selecting variables to build the model started by selecting the independent variables that exhibit the highest correlation with SN in the Pearson correlation matrix. After testing the 11 variables, only four contributed to the increase of  $R^2$  and remained statistically significant. For models 1 to 3, the first variable entered in the model was the AESAL because it exhibited the highest bivariate correlation with the SN. This variable explained 0.349 percent of the variation ( $R^2$ ) of SN. The second variable added in the model was MPD, which contributed to an increase of  $R^2$  to 0.401. The third variable added in the model was the FFi/Co that contributed to an increase of  $R^2$  to 0.524.

Unpredictably, the variable Age did not exhibit statistical significance for inclusion in the regression model, despite theory stating that friction is affected by the polishing effect of traffic over time.

Table 1 displays a summary of regression models and their principal measures of overall fit for multiple regression analysis using a stepwise approach. In this approach, independent variables were added or removed based on their statistical significance. All of the predictor variables in the models exhibited p-values less than 0.10 and the VIF was lower than 1.5.

Table 1 Summary of models

Model	$R^2$	SE	Model Specification
1	0.349	4.929	$\beta_0 - \beta_1 \log \text{AESAL}$
2	0.401	4.778	$\beta_0 - \beta_1 \log \text{AESAL} - \beta_2 \text{MPD}$
3	0.524	4.304	$\beta_0 - \beta_1 \log \text{AESAL} - \beta_2 \text{MPD} + \beta_3 \text{FFi/Co}$

Note: SE = Standard error of the estimate.

The equation for SN prediction with unstandardized coefficients and intercept is depicted in Eq. (1).

$$\text{SN} = 75.09 - 4.98 \log \text{AESAL} - 4.61 \text{MPD} + 11.9 \text{FFi/Co} \quad (1)$$

### Structural Equation Model

Figure 1 shows a diagram of one of several attempts to specify a PA model. The initial PA diagram was based on hypothesized relationships within variables and derived from the same Pearson correlation matrix used in the multivariate OLS regression. As in OLS regression analysis, the exogenous variables were assumed to be correlated. By correlating these variables it was possible to assess the direct influence of exogenous variables (FFi/Co, VMA, NMA, AESAL, Age, and MPD) on the endogenous variable (SN). In addition, it was possible to assess the indirect influence of mix design and operational characteristics on SN through MPD by using MPD as a mediator.

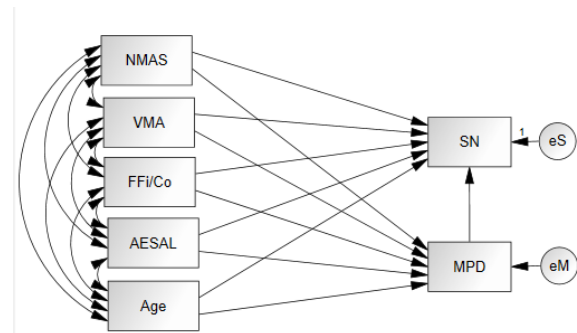


Fig. 1 Initial PA model specification

The initial PA model exhibited an  $R^2$  of 0.536 with model fit of Chi-square and degrees of freedom equal to zero, which indicated that the model is saturated. In other words, the model has too many parameters and some goodness-of-fit indicators could not be identified. Thus, the initial PA model needed to be modified by eliminating non significant parameters, or parameters that exhibited a p-value above 0.1.

The correlations between MPD and NMA, VMA, FFi/Co, AESAL, and Age did not exhibit statistical significance. MPD exhibited a statistically significant correlation with SN only. SN exhibited a statistically significant correlation with two variables, FFi/Co and AESAL.

As in the OLS regression analysis, the correlation of Age and SN was not statistically significant. However, Age was kept in the SEM model for further analyses of its correlation with other variables, and direct and indirect effects on SN.

Figure 2 displays the modified PA model and regression results after excluding all non-significant parameters except the variable Age.

In the modified PA model FFi/Co, AESAL, MPD accounted for the variance ( $R^2$ ) of 0.52 of SN. The goodness-of-fit indexes calculated for the modified model indicated reasonably good fit. The

model exhibited Chi-square of 1.2, degree of freedom (df) of 2 and p-value of 0.543, which indicated nonsignificant Chi-square. A nonsignificant Chi-square is required for the goodness-of-fit of the model and indicates that the two matrices, observed and variance-covariance, are similar. In other words, it indicates that the theoretical model reproduces the sample variance-covariance relationships [13].

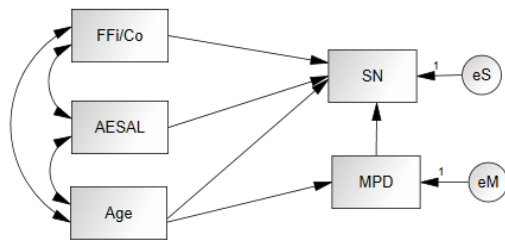


Fig. 2 Modified PA model

The other indicator (GFI, AGFI and RMSEA) also performed around the acceptable range of model fit with a GFI of 0.991, AGFI of 0.93, and RMSEA of 0.000.

Table 2 displays the estimated regression results. The unstandardized coefficients represent the amount of change in the endogenous and mediator variables for each unit in changing in the *exogenous* variable. The unstandardized coefficients are equivalent to the OLS regression coefficients. The standardized coefficients are used to assess the contribution, or importance, of each predictor variable to each outcome variable. The value of unstandardized and standardized coefficients indicated that the parameter related to mix design (FFi/Co) and the parameter related to the operational condition of the roads (AESAL) exhibited significant influence on SN prediction. MPD exhibited minor influence on SN. Age exhibited a positive and nonsignificant influence.

Table 2 Regression estimates

Variable	Estimate		Std. Error	p-value
	Unsta.	Stand.		
SN_FFi/Co	11.884	0.411	3.243	0.001
SN_AESAL	-4.987	-0.438	1.180	0.001
SN_MPD	-4.614	-0.176	2.495	0.070
SN_Age	0.152	0.062	0.254	0.549
MPD_Age	0.002	-0.024	0.014	0.862

The PA models provided estimates for each relationship in the model. These estimates are displayed in Table 3. The estimated correlation and

covariance determine the weight of direct and indirect effects on SN. The results indicated that there is a negative relationship between the pairs FFi/Co and Age, and FFi/Co and AESAL. This result suggests that the mix design parameters have an influence on the other variables.

Table 3 also displays the variances for each parameter in the model. The variances, also called *error term*, indicate unexplained variance on the variables due to the influence of factors that were not contained in the specified model. All the variables in the model exhibited significant levels of variance. The variance related to SN (eS) indicated that there is a measurement error of SN that was not explained by the model.

Table 3 Variance and Covariance

Variable	Estimate	Std. Error	p-value
	Covariance		
FFi/Co_Age	-0.143	0.068	0.036
AESAL_Age	0.004	0.180	0.984
FFi/Co_AESAL	-0.041	0.016	0.009
Correlation			
FFi/Co_Age	-0.307		
AESAL_Age	0.003		
FFi/Co_AESAL	-0.393		
Variance			
FFi/Co	0.038	0.007	0.001
AESAL	0.285	0.056	0.001
Age	5.784	1.145	0.001
eM	0.054	0.011	0.001
eS	16.977	3.362	0.001

Table 4 displays the results of the analysis of the total, direct, and indirect effects of Age on MPD and SN.

Table 4 Total, direct and indirect effects

	Age		
	Total	Direct	Indirect
MPD	-0.002	-0.002	0.000
SN	0.163	0.152	0.011

Results indicate that Age exhibited insignificant direct effect on MPD, and positive direct effect on SN. Age exhibited a slight indirect effect on SN using MPD as mediator.

#### Model Modification

The theoretical model included four explanatory variables that resulted in an  $R^2$  of 0.52. The regression weight for Age was positive and

statistically nonsignificant. Therefore, Age was excluded from the model. The model without Age exhibited fit measures (variances, covariances, correlations, standard errors, and p-values) similar to the previous model. The equation for SN prediction with unstandardized coefficients and intercept is depicted in Eq. (2).

$$SN = 75.10 - 4.98 \log AESAL - 4.61 MPD + 11.88 Fi/Co \quad (2)$$

## CONCLUSION

This study compared two multiple regression approaches, multivariate regression (OLS) and structural equation model (SEM), for development of models for pavement friction prediction. The results indicated that OLS and SEM exhibited comparable predictive models in terms of coefficient of determination,  $R^2$ , despite of limited sample size used in SEM analysis.

The SEM approach allowed statistical analysis that could not be measured using OLS. SEM allowed to assess correlation, covariances of pairs of predictors, and direct and indirect effects on SN. The assessment of covariance and correlation analysis within predictors indicated a negative correlation and covariance between FFi/Co and Age, and between FFi/Co and AESAL. Assessment of the direct and indirect effects of Age on MPD and SN indicated a positive direct effect of Age on SN and an insignificant indirect effect on MPD.

The models showed that SN can be predicted with a fair coefficient of determination using variables related to traffic and loads, macrotexture, and mix gradation. The variables AESAL and MPD exhibited negative correlation with SN, while the variable FFi/Co exhibited positive correlation with SN.

This research used limited data to develop the models; new field data are planned to be acquired to validate the models. Further research is needed to explore the influence of mineral hardness, physical and geometrical characteristics (e.g., angularity, shape, and texture), and abrasion of aggregates on SN. There is also a need to develop models employing skid resistance measured with LWT and with a smooth tire, because a smooth tire is more sensitive to macrotexture than a ribbed tire and the results might differ from those presented in this study.

## ACKNOWLEDGEMENTS

This research was supported by the Ministry of Transportation of Ontario, Highway Infrastructure Innovation Funding Program and the Natural Science and Engineering Research Council of Canada.

## REFERENCES

- [1] W. Hall, K. L. Smith, L. Titus-Glover, J. C. Wambold, T. J. Yager and Z. Rado, "Guide for Pavement Friction", National Cooperative Highway Research Program, Washington, 2009.
- [2] AASHTO, Guide for Pavement Friction, Washington: American Association of State Highway and Transportation Officials, 2008.
- [3] M. A. Ahammed and S. L. Tighe, "Long Term and Seasonal Variations of Pavement Surface Friction", In Proceeding of the 2008 Annual Conference of the Transportation Association of Canada, Toronto, 2008.
- [4] D. A. Noyce, H. U. Bahia, J. M. Yambo and G. Kim, "Incorporating Road Safety into Pavement Management: Maximizing Asphalt Surface Friction for Road Safety Improvements", Midwest Regional University Transportation Center, Wisconsin, 2007.
- [5] E. Kassem, A. Ahmed, E. A. Masad and D. N. Little, "Development of Predictive Model for Skid Loss of Asphalt Pavements", Journal of the Transportation Research Board, vol. 2372, 2013, pp. 83-96.
- [6] A. Rezaei, "Development of a prediction model for skid resistance of asphalt pavements", 2010.
- [7] G. S. Awoke, "Estimating The Friction Performance of Hot Mix Asphalt Pavements Based on Aggregate Properties and Route Characteristics: Analysis, Modelling and Validation," College Park, 2011.
- [8] M. Rajaei, N. R. Sefidmazgi and H. Bahia, "Establishment of Relationship Between Pavement Surface Friction and Mixture Design Properties", Transportation Research Board, vol. 2457, 2014, pp. 114-120.
- [9] J. N. Meegoda and S. Gao, "Evaluation of pavement skid resistance using high speed texture measurement", Journal of Traffic and Transportation Engineering, vol. 2, no. 6, 2015, pp. 382-390.
- [10] J. F. Hair, W. C. Black, B. J. Babin and R. E. Anderson, Multivariate Data Analysis, New Delhi: Pearson Educational Limited, 2015.
- [11] B. M. Byrne, Structural Equation Modeling With Amos: Basic Concepts, Applications and Programming, New York: Routledge, 2016.
- [12] M. S. Khine, Application of Structural Equation Modelling in Educational Research and Practice, Rotterdam: Sense Publishers, 2013.
- [13] R. E. Schumacker and R. G. Lomax, "A Beginner's Guide to Structural Equation Modelling", New York, NY: Taylor & Francis Group, 2010.
- [14] R. B. Kline, Principles and practice of structural equation modeling, vol. 2, New York: Guilford Press, 2005.

# APPLICATION OF MEMETIC ALGORITHM FOR SOLVING THE VEHICLE ROUTING PROBLEM WITH TIME WINDOWS

Chaowalit Hamontree<sup>1</sup>, Jiraporn Chuenjai<sup>2</sup> and Nawaporn Chamnanketgorn<sup>3</sup>

<sup>1</sup>Department of Industrial Engineering, Faculty of Engineering

<sup>2</sup>King Mongkut's Institute of Technology Ladkrabang,

Thailand

**ABSTRACT**

Most importantly, vehicle routing problem is one of logistic problems that impact on the economy which includes in business and industry. It is very important to manage the transportation system properly. This research is proposed the Memetic Algorithm (MA) to solve vehicle routing problems with time windows (VRPTW) and also capacity of vehicles constrains. The objective of this research is to find the minimize travel distance, and number of vehicles. A memetic algorithm has been developed to solve VRPTW by combining a genetic algorithm based on suitable encoding and genetic operators, with a local search procedure. Therefore, the experimental result shows that the memetic algorithm contributes a new good solutions and performs better than genetic algorithm but unable to get to the best results. However, for better analysis of the results, the sensitivity analysis is performed in order to investigate the effect of parameters, which are crossover rate, mutation rate, and population on the total distance criteria.

*Keywords: VRPTW, Memetic Algorithm, Genetic Algorithm, Local Search*

## INTRODUCTION

The Vehicle Routing Problem (VRP) is a general class of problems in which a fleet of vehicles based at one or several depots needs to be routed for a certain number of customers located in different places to minimize the number of routes, total travelling time and distance between all vehicles. VRP with time windows (VRPTW) is a generalization of VRP with additional restrictions, where each customer must be supplied within a specific time interval. The delivery of all vehicles dispatched from the single depot should satisfy the demand of all customers within their required time. Vehicle routes should be designed in such a way that each customer can only be visited once and the total demand of all customers in any particular route should not exceed the capacity of the vehicle. Meanwhile, each vehicle route must begin and end at the depot.

VRPTW has already been proven to be an NP-hard problem [7]. Many researches proposed exact methods and heuristics to solve this type of problem. Kolen et al. [5] developed a branch and bound approach to solve the VRPTW. Desrochers et al. [1] proposed a column generation approach that solved the Solomon's benchmark instances. Fisher et al. [2] proposed a K-tree relaxation approach to solve two of Solomon's benchmark instances. Instead, various heuristic or metaheuristic methods are applied to these types of problems. Compared to the traditional optimization approaches, heuristic and metaheuristic methods cannot guarantee optimal solutions,

although they can find near-optimal, or in some cases optimal, solutions much faster.

The main objective of this research is to find a set of routes that will minimize the total travelling distance of all vehicles in a VRPTW with Memetic Algorithm (MA). MA is a class of stochastic global search heuristics in which Evolutionary Algorithms based approaches are combined with local search heuristics techniques.

The organization of this paper presents the memetic algorithm for solving the VRPTW. In the first section, problem definition is described. In the second section, memetic algorithm and local search are illustrated. Then, computational results are conducted to evaluate the performances. Finally, conclusion is explained in the last section.

## PROBLEM DEFINITION

In this section, the study focused on the vehicle routing problem with time windows. The center node is called the depot with a set of customer  $N$  to be visited. The depot node is denoted as 0. Each arc in the network represents a connection between two nodes and also indicates the direction it travels. Each route starts from the depot, visits customer nodes and then returns to the depot. The number of routes in the network is equal to the number of vehicles used. One vehicle is dedicated to one route. A cost  $c_{ij}$  and a travel time  $t_{ij}$  are associated with each arc of the network.

This assumption makes the problem simpler,

because numerically the travel cost  $c_{ij}$ , the travel time  $t_{ij}$  and the Euclidean distance between the customer nodes equal each other. Each customer in the network can be visited only once by one of the vehicles. Every vehicle has the same capacity  $C$  and each customer demand  $d_i$ , must be equal to the summation of all demands on the route travelled by vehicle  $k$ , which means that no vehicles can be overloaded. The time windows constraint is denoted by a predefined time interval, given an earliest arrival time and latest arrival time. The vehicles must arrive at the customers not later than the latest arrival time. Each customer also imposes a service time to the route, taking consideration of loading and unloading time of goods. Moreover, vehicles are also supposed to complete their individual routes within a total route time, which is essentially the time window of the depot. VRPTW can be stated and solved by mathematical programming models [8] as shown in follows.

Decision Variables:

- $t_i$  = arrival time at customer  $i$ ;
- $w_i$  = waiting time at customer  $i$ ;
- $X_{ijk}$  = if there vehicle  $k$  travels from customer  $i$  to customer  $j$ , and 0 otherwise. ( $i \neq j$ ;  $i, j = 0, 1, \dots, N$ ).

Parameters:

- $V$  = total number of vehicles
- $N$  = total number of customers
- $c_i$ , = customer  $i$  ( $i = 1, 2, \dots, N$ )
- $c_0$  = delivery depot
- $c_{ij}$  = traveling distance between customer  $i$  to customer  $j$ ;
- $t_{ij}$  = travel time between customer  $i$  and customer  $j$ ;
- $m_i$  = demand of customer  $i$ ;
- $C$  = capacity of homogeneous vehicles;
- $e_i$  = earliest arrival time at customer  $i$ ;
- $l_i$  = latest arrival time at customer  $i$ ;
- $f_i$  = service time at customer  $i$ ;
- $r_k$  = max route time allowed for vehicle  $k$ ;

Minimize

$$\sum_{i=0}^N \sum_{j=0}^N \sum_{k=1}^V C_{ij} X_{ijk} \quad (1)$$

Subject to

$$\sum_{i=0}^N \sum_{k=1}^V X_{ijk} = 1 \text{ for } j \in \{1, \dots, N\}, \quad (2)$$

$$\sum_{i=0}^N \sum_{k=1}^V X_{ijk} = 1 \text{ for } i \in \{1, \dots, N\}, \quad (3)$$

$$\sum_{i=0}^N \sum_{k=1}^V X_{ijk} \leq V \text{ for } i = 0, \quad (4)$$

$$\sum_{j=1}^N X_{ijk} = \sum_{j=1}^N X_{jik} \leq 1 \text{ for } i = 0, k \in \{1, \dots, V\}, \quad (5)$$

$$\sum_{i=0}^N d_i \sum_{j=0}^N X_{ijk} \leq C \text{ for } k \in \{1, \dots, V\}, \quad (6)$$

$$\sum_{i=0}^N \sum_{j=0}^N X_{ijk} (t_{ij} + f_i + w_i) \leq r_v \text{ for } k \in \{1, \dots, V\}, \quad (7)$$

$$t_0 = w_0 = f_0 = 0, \text{ for } i = 0, \quad (8)$$

$$\sum_{k=1}^V \sum_{i=0}^N X_{ijk} (t_i + t_{ij} + f_i + w_i) \leq t_j \text{ for } j \in \{1, \dots, N\}, \quad (9)$$

$$e_i \leq (t_i + w_i) \leq l_i \text{ for } i \in \{1, \dots, N\}, \quad (10)$$

The objective function of this model is to minimize the total travelling distance by all vehicles to satisfy the demands of all the customers. The constraint in Eq. (2) and (3) ensure that exactly one vehicle enters and departs from each customer as well as from the depot. For each vehicle, the number of visits must be equal to the number of departures from each customer. There are at most  $V$  routes going out of the depot shown in Eq. (4). The constraint in Eq. (5) specifies only one vehicle leaves from and returns to the depot. The constraint in Eq. 6 imposes an upper bound which is the vehicle's capacity to the accumulated demand of each route. The constraint in Eq. (7) is the maximum travel time constraint. Finally, constraint in (8) to (10) ensures schedule feasibility and time windows are respected.

## MEMETIC ALGORITHM

The Memetic Algorithm nomination was first introduced by Moscato [6]. MA belongs to the larger class of evolutionary algorithms that use techniques inspired from natural evolution. It is a combination of genetic algorithm (GA), first introduced by Holland [4], and local search procedures that intensify the search. GA mimics the natural selection and natural genetic selection process concurrent with artificial system for optimizing problems. GA is inspired from the biological evolution, whereas MA mimics cultural transmission based on the meme concept analogous to the gene in GA. It is also called hybrid genetic algorithm or genetic local search algorithm. Since then, MA has been used in

several works and has proved its efficiency to solve VRP. In the following sections, we present the procedures used in the MA as shown in follows.

**Step 1 Initialize.** Construct the first generation of solutions. To produce a solution we use a constructive heuristic.

**Step 2 Improve the solutions.** We use a local search method to improve the initial solution and eliminate duplicate solutions.

**Step 3 Create the next generation.** Use reproduction, crossover, and mutation from genetic operators to produce the non-optimized next generation. Each of the genetic operators selects parent solutions from the previous generation. The length of a solution is used as the evaluation function.

**Step 4 Improve next generation.** Use a local search procedure to replace each of the current generation solutions except the reproduced ones by the local optimum. Eliminate duplicate solutions.

**Step 5 Evolve.** Repeat Steps 3 and 4 until a termination condition is reached.

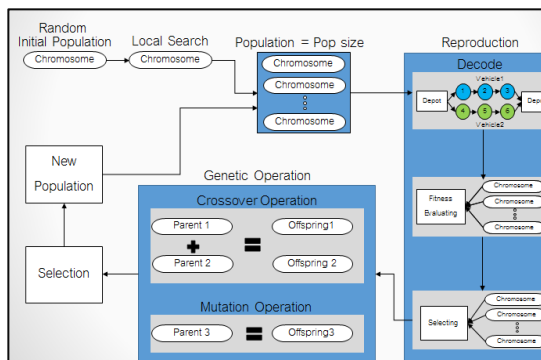


Fig. 1 Memetic algorithm

The proposed MA for VRPTW is described in detail and steps as shown in Fig. 1.

### Initial population

The initial chromosomes are randomly generated by randomly assigning customer numbers to the genes. First, an equal probability is assigned to every customer. A random number is then created to determine which customer is chosen for the next gene in the chromosome. After one customer is settled in the chromosome, all of the remaining customers are again assigned the same probability and are selected by generating another random number.

### Reproduction

For the VRPTW problem, the encoding of a candidate has to deal efficiently with the two level information of the multiple trip solution. Allocation of routes to vehicles, and the delivery order for each route. In the adopted representation, the chromosome (individual) contains several trips; the term “trip” is used for the genetic representation to designate a complete journey of a vehicle. Each route is composed by an ordered subset of customers.

### Crossover

In this part, two chromosomes are selected as parents to crossover by means of the crossover rate which is the probability of crossover. A random number between 0 and 1 is then generated. If the random number is smaller than the crossover rate, two chromosomes will undergo reproduction to generate new members as offspring that may be included in the next generation. Otherwise, the offspring will be the same as the parents.

### Mutation

Mutation is another important role, which brings more variation to the population to explore diversified solutions and prevent the premature local convergence. The mutation rate measures the probability that mutation is applied to a gene in the offspring. If a randomly generated number between 0 and 1 is smaller than the mutation rate, the gene undergoes the mutation process. Otherwise, the mutation does not take place for that gene.

### Selection

In MA, an appropriate selection method should be applied to select the fittest chromosomes from the current population to the next generation. The memetic progresses to find the optimal or near-optimal solution.

### LOCAL SEARCH

For each solution generated for the initial population, we use a local improvement procedure. The proposed local search uses exchange method for VRPTW. The procedure works as follow:

- Exchange: swaps one or two consecutive customers pertaining to one or two trips

## COMPUTATIONAL RESULTS

There are three data sets from the Solomon's VRPTW instances including of customer size 25, 50, and 100 customers, all distances are represented by Euclidean distance, and the speed of all vehicles is assumed to be unity. The locations of the stores are expressed using the (x, y) coordinates on the Euclidean plane. The problem has been solved by using two methods including of genetic and memetic algorithms.

The memetic parameters are very important for the success of a memetic algorithm, as well as for the representation of the individuals, the initial population and the genetic operators. Based on preliminary computational experiments, we set the following genetic parameters:

- The population size is set to 1000 individuals that are enough to guarantee a large search space.
- The crossover probability is set to 0.7 and the mutation probability is set to 0.1.
- The maximum number of generations in our algorithm is set to 50,000.

Table 1 The best solution of Solomon's published

(The best solution)			
Problem	No. customer	No. vehicle	Distance
R101.25	25	8	617.1
R101.50	50	12	1044.0
R101.100	100	20	1637.7

Table 2 The result of genetic algorithm

Problem	No. customer	No. vehicle	Distance
R101.25	25	8	625.48
R101.50	50	12	1157.1
R101.100	100	20	2001.1

Table 3 The result of memetic algorithm

Problem	No. customer	No. vehicle	Distance
R101.25	25	8	618.3
R101.50	50	12	1115.5
R101.100	100	20	1910.8

Table 4 Comparison performance measurement between the published best solution and our solution

Problem	Published best	% Deviation	
		GA	MA
R101.25	617.1	1.35%	0.19%
R101.50	1044.0	10.83%	6.84%
R101.100	1637.7	34.40%	16.67%

The computational experiments show that memetic algorithm can generated a good solution to minimize the total distance. Table 4 shows the percentage of deviation of the MA solutions against the best solutions in the literature. It demonstrates the position of MA is given a good solutions which better than GA for all instances. For instance R101.25, MA can give the good solution near the optimal solution but slightly different for instance R101.50 and also far away from the best solution for instance R101.100. However, it cannot generate the best solution for all instances.

## CONCLUSION

This work presents a memetic algorithm for solving the classical vehicle routing problem with time window. MA provides a very interesting approach to solve problems where an exact method cannot be applied. However, it is a bid disappointed that MA took many generations to find a solution, and unable to get to the best results.

## REFERENCES

- [1] Desrochers, M., Desrosiers, J., and Solomon, M., "A new optimization algorithm for the vehicle routing problem with time windows," *Operations Research*, vol. 40, 1992.
- [2] Fisher, M., Jornsten, K., and Madsen, O., "Vehicle routing with time windows: Two opt algorithms," *Operations Research*, 1997.
- [3] Goldberg, D.E. "Genetic algorithms in search, optimization, and machine learning. Boston": Addison-Wesley Pub. Co. 2004.
- [4] Holland, John H. "Adaptation in Natural and Artificial Systems. Ann Arbor": University of Michigan Press. 1975.
- [5] Kolen, A. W. J., Kan, A. H. G.R., and Trienekens, H. W. J. M., "Vehicle routing with time windows," *Operations Research*, 1987.
- [6] Moscato, P., 1989, On evolution, search, optimization, genetic algorithms and martial arts: Towards memetic algorithms, Caltech Concurrent Computation Program, C3P Report.
- [7] Savelsbergh, M. Local search for routing problems with time windows. *Annals of Operations Research*, 1985.
- [8] Tan, K. C., Lee, L.H., and Ou, K., "Artificial intelligence heuristics in solving vehicle routing problems with time window constraints," *Engineering Applications of Artificial Intelligence*, 2001.



## THE EFFECT OF MODEL DOMAIN SIZE FOR UNSUPPORTED PLAIN STRAIN TUNNEL HEADINGS IN UNDRAINED CLAY

Jim Shiau<sup>1</sup>, Fadhil Al-Asadi<sup>2</sup>

<sup>1</sup>School of Civil Engineering and Surveying, University of Southern Queensland, Australia

### ABSTRACT

This paper examines the effect of model domain size for unsupported plain strain tunnel headings in undrained clay. The tunnel heading models for different soil parameters (depth ratio  $C/D$  and strength ratio  $S_u/\gamma D$ ) are studied using the finite element limit analysis and strength reduction technique to determine the ideal geometric parameters  $X/C$ ,  $L/C$ , and  $B/C$  of established numerical models. The upper and lower bound limit solutions are presented alongside finite difference results for validation. A thorough comparison between these two methods finds a very good agreement. Design charts are established for a broad range of practical scenarios using dimensionless ratios, similar to the traditional slope stability design chart. Typical examples are presented to illustrate the usefulness for practicing engineers.

*Keywords: Model Domain Size, Plain Strain Heading, Undrained Clay, Strength Reduction Method, Limit Analysis, Design Chart*

### INTRODUCTION

The research of tunnel heading stability was initiated with [1] who studied the plastic flow of clay soil in vertical openings such as sheet pile walls and drew comparison to the stability of a tunnel heading face. Following this work, numerous studies were completed on centrifuge models by [2]. The work was culminated by [3] who investigated the experimental and theoretical undrained collapse of three-dimensional cylindrical tunnel headings in normal consolidated kaolin under different geometry and gravity regimes. [4 and 5] built further on the stability ratio by using upper and lower bound solutions using the classical limit theorems for tunnel collapse in undrained cohesive conditions.

With the development of computers over the last two decades, numerical modelling has become a useful “must-have” technique for engineering problem resolution [4]. A number of papers were achieved in the numerical area of tunnel stability and settlement prediction by [6-13]. In particular [6] extended the limit analysis theory on tunnel heading by investigating a three-dimensional multiblock failure mechanism for frictional and cohesive soil by the use of a spatial discretization technique. Authors in [7-9] recently developed a pressure relaxation method and automatic mesh generation by making use of *FLAC* script to conduct parametric studies conveniently. Besides, both numerical and physical modelling have also been introduced recently in geotechnical education by [10-13].

This paper utilises the finite element limit analysis (*OptumG2*) and the strength reduction method to study the effect of finite element model domain size. The strength reduction analysis is proceeded by computing a strength reduction factor

by which the material parameters need to be reduced in order to attain a state of incipient collapse [14 and 15]. A factor greater than one thus implies a stable system while a factor less than 1 implies that additional strength is required to prevent collapse.

For Tresca material in this study, the strength reduction factor can be viewed as a factor of safety (*FoS*) value shown in Equation (1).

$$FoS = \frac{S_u}{S_c} \quad (1)$$

Where  $S_u$  is the ultimate undrained shear strength of the soil, and  $S_c$  is the undrained shear strength of the soil at collapse. This is a similar approach used in Taylor's design charts for slope stability analysis [16].

In general, the FE model domain size has to be large enough to validate the assumption of an infinite soil, but small enough to obtain accuracy without large numerical CPU times. Over allowance of the model domain would decrease the solution accuracy in any numerical analysis, as more elements would need to cover the entire soil area [17-18]. Although this problem is of considerable analytical interest, particularly in regard to the stability of tunnels, there is no current literature stating the guideline in preparing the design model so that the boundary conditions do not affect numerical solutions.

This paper presents a comprehensive analysis for the geometric parameters to generate precise plain strain heading model in an unsupported excavation in green-field conditions. Based on these modified geometric parameter ratios, strength reduction technique using *OptumG2* is used to determine the factor of safety in cohesive soils over a wide

parametric range. Numerical results are compared with the strength reduction technique using *FLAC* and stability charts presented for practical uses.

## STATEMENT OF PROBLEM

Figure 1 shows the problem definition of an idealised tunnel heading. The problem is a two-dimensional plane strain tunnel heading. The soil medium is considered as undrained and is modelled as a uniform Tresca material, which is the same as a Mohr-Coulomb material with no internal friction angle. The undrained shear strength ( $S_u$ ) and the saturated unit weight ( $\gamma$ ) are soil properties used, whilst the tunnel has diameter ( $D$ ) and cover depth ( $C$ ) above its crown, as shown in Figure 1.

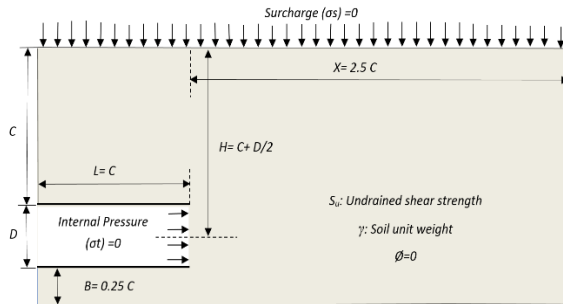


Fig. 1 Problem Definition

The other unknown geometric parameters are the distance away from the face of the tunnel heading ( $X$ ), the length of the tunnel inside the model ( $L$ ) and the depth between the base of the tunnel and the

base of the model ( $B$ ). For any model the geometric parameters ( $L$ ,  $X$ , and  $B$ ) have to be defined to ensure that the analysis results are not affected by the boundary conditions.

In this paper, numerical result based on strength reduction technique is represented by factor of safety ( $FoS$ ) that is a function of the depth ratio ( $C/D$ ) and strength ratio ( $S_u/\gamma D$ ).

$$FoS = f\left(\frac{C}{D}, \frac{S_u}{\gamma D}\right) \quad (2)$$

These dimensionless ratios allow the results of this study to be used in scenarios that are physically different, but where the soil strength ratio and the depth ratio still fall in the parametric domain. To cover all possible realistic ranges, the parameters used in the study include  $S_u/\gamma D = 0.1 - 2$  and  $C/D = 1-6$ . This would ensure that the design charts produced can be applied to many different tunnel design and analysis problems, which are useful for practical design purposes.

Figure 2 shows a typical finite element mesh of the problem in this study. The boundary conditions shown in Figure 2 are important to define the domain boundary of the model. The smooth rigid lining above and below the soil excavation is restrained in the vertical ( $y$ ) direction to reproduce the nature of the tunnel linings and mining supports. The base and sides of the model are restrained in the  $x$  and  $y$  directions.

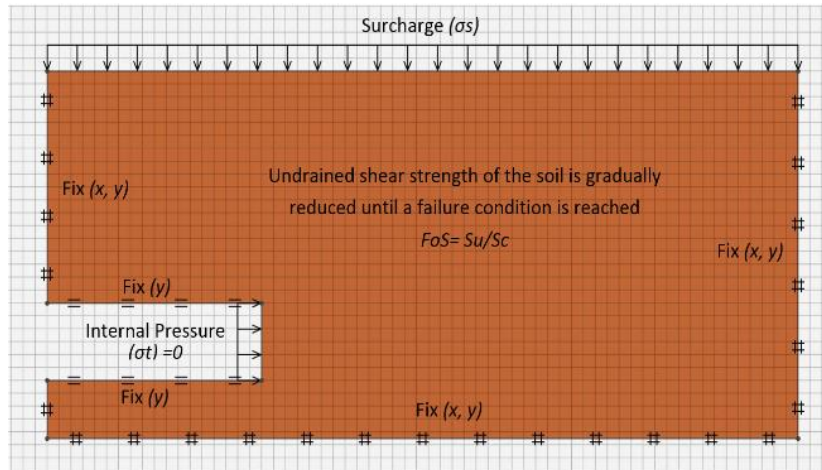


Fig. 2 Typical Mesh and Boundary Condition

Stability of plane strain tunnel heading models were investigated using a factor of safety approach. Factor of safety values were commuted in *OptumG2* using *FELA* with strength reduction and were compared with *FLAC* results. This method has been widely used for slope stability analysis but is rarely used for tunnel stability analysis. This strength reduction technique will yield a factor of safety

( $FoS$ ), which is not unfamiliar with practicing designers.

Such a method involving factors of safety has been described by [19] for slope stability. The factor of safety is defined as a ratio of the strength necessary to maintain limiting equilibrium with the soil's available strength. The shear strength of the material is reduced until the limiting condition is

found. This can be compared to the studies originated from [1] where the uniform surcharge pressure is increased until the limiting condition is found. If failure occurs initially, the shear strength of the soil is increased by amplifying the cohesion and friction angle until limiting equilibrium or failure state is reached. Once the actual and critical strength are known, the factor of safety can then be calculated.

## PARAMETRIC STUDIES

As shown in Figure 1,  $X$  represents the distance away from the face of the tunnel heading,  $L$  denotes the length of the tunnel inside the model while  $B$  is the distance between the base of the tunnel and the base of the model. The effects of dimensionless ratios  $X/C$ ,  $L/C$  and  $B/C$  on the obtained results are examined in this paper.

Using the strength reduction technique within the finite element limit analysis program *OptumG2*, factor of safety ( $FoS$ ) values were obtained for a range of parameters for an unsupported tunnel heading in undrained soil. The two dimensionless parameters used in the studies are the depth ratio ( $C/D$ ) and the strength ratio ( $S_u/\gamma D$ ). It is important to compare the finite element limit analysis, upper bound and lower bound with another numerical investigation. Using the finite difference technique, factors of safety have been calculated using *FLAC* over the same parametric ranges. The numerical procedures used in *OptumG2* are based on the limit theorems of classical plasticity [15].

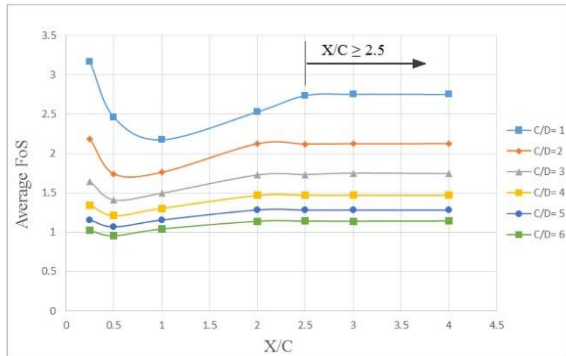


Fig. 3 Geometric Parameter Ratio  $X/C$

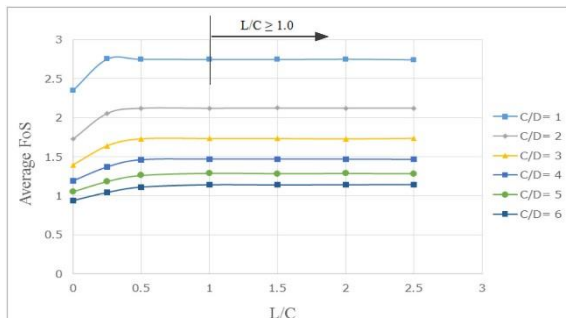


Fig. 4 Geometric Parameter Ratio  $L/C$

Numerical results of averaged  $FoS$  from upper and lower bound solutions are shown in Figures 3-5 for various values of  $X/C$ ,  $L/C$ , and  $B/C$ . In general it can be concluded that the  $FoS$  values remain constant for  $X/C \geq 2.5$ ,  $L/C \geq 1.0$ , and  $B/C \geq 0.25$ . The constant  $FoS$  results indicate an optima domain size for the problem in hand and ensure the boundary conditions have very little effect on the results.

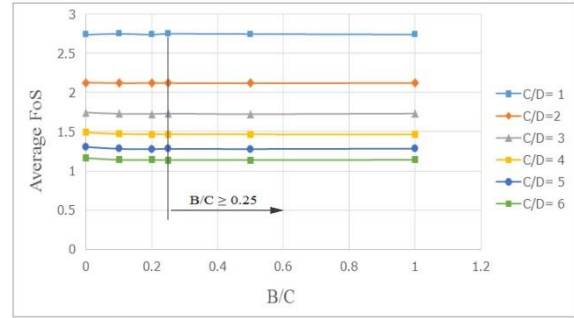


Fig. 5 Geometric Parameter Ratio  $B/C$

Dimensionless stability charts showing the numerical results obtained in this study are presented in Figures 6 and 7. In Figure 6,  $FoS$  increases linearly as the strength ratio  $S_u/\gamma D$  increases. The finite element upper bound solutions *OptumG* are in good agreement with the finite difference results *FLAC*. Also note that the rate of  $FoS$  increase is different for each  $C/D$  value. The gradient of the line is greater for smaller  $C/D$  values.

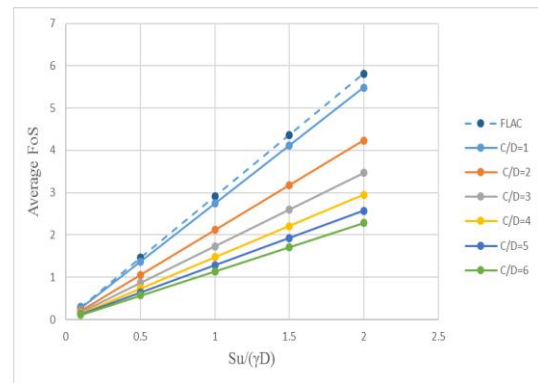


Fig. 6 Comparison of  $FoS$  results with respect to  $S_u/\gamma D$  for various values of  $C/D$

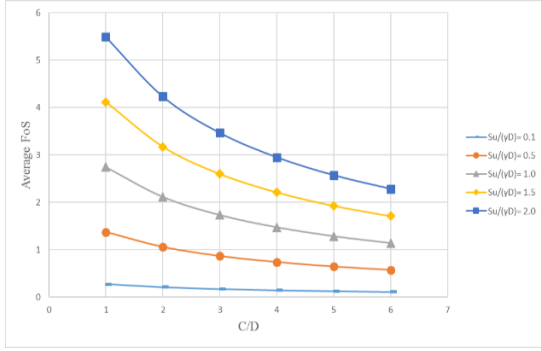


Fig. 7 Comparison of  $FoS$  results with respect to  $C/D$  for various values of  $S_u/\gamma D$

Figure 7 shows that the  $FoS$  decreases nonlinearly with increasing depth ratio  $C/D$  for all strength ratios defined as  $S_u/\gamma D$ . The finite element upper bound solutions are in good agreement with the finite difference results. Note the strength ratio is normalised with respect to the tunnel excavation depth ( $D$ ), and therefore the undrained shear strength ( $S_u$ ) remains constant throughout the increasing depth ratios. Owing to the increasing overburden pressure with the increasing of ( $C/D$ ) and the constant undrained shear strength ( $S_u$ ), it therefore results in  $FoS$  values decreasing. This is in contrast to the common belief that an increase to  $C/D$  always results in an increase to  $FoS$ .

A simple observation can be made from Figure 1, where the active force is the weight of soil and the resisting force is given by the shear strength of the soil. For two proposed tunnels in the same cohesive soil but at different depths, the tunnel with the smaller active force ( $\gamma C$ ) will have a higher probability of stability. This observation may not be true in a soil with internal friction angle ( $\phi \neq 0$ ) due to the additional shear strength ( $\sigma \tan \phi$ ) and geometrical arching effects. In purely cohesive soils, the latter still occurs, but its effect is not enough to overcome that subsequent increase in active force.

### EXTENT OF FAILURE SURFACE

Collapse of unsupported tunnel heading or vertical trapdoor inevitably lead to soil deformation of the ground surface. The extent ( $E$ ) and mechanism of such failure can be explained by observing some graphical outputs from *OptumG2* such as the plots for power dissipation in shear.

In reality the deformation trough would be three dimensional, but with the assumptions made, the largest extent of plastic deformation in the heading cross-section can be reasonably estimated. This information of failure extent is important as it will assist practicing engineers in the decision making in monitoring ground movements.

Figure 8 presents the surface failure ratio plot where the surface failure ratio is a function of the depth ratio. Regression of the chart gives the following approximate linear equation.

$$E/D = 0.9133(C/D) + 1.297 \quad (3)$$

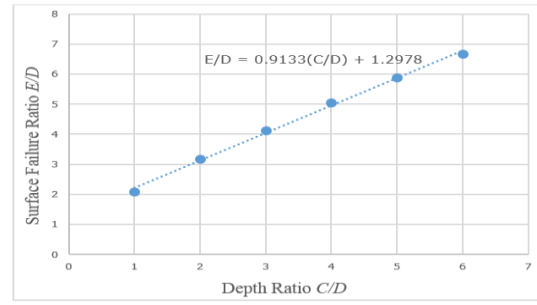


Fig. 8 Surface Failure vs. Depth Ratio

**Example:** For an unsupported green-field tunnel, determine the maximum extent of failure surface. Parameters are given as  $C = 10$  m, and  $D = 2.5$  m.

1. For  $C/D = 4.0$ , Eq. 3 gives an  $E$  value of 12.38 m.
2. For  $C/D = 4.0$ , Figure 8 gives an approximate  $E/D$  of 5.1 and therefore  $E$  value of 12.5 m.

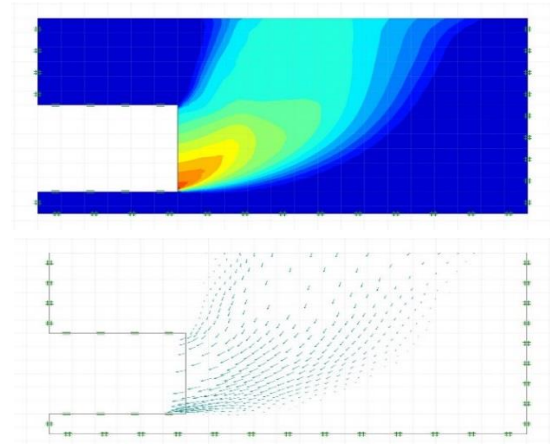


Fig. 9 Total displacements and displacement vectors for  $C/D=1$  and  $S_u/\gamma D=2.0$

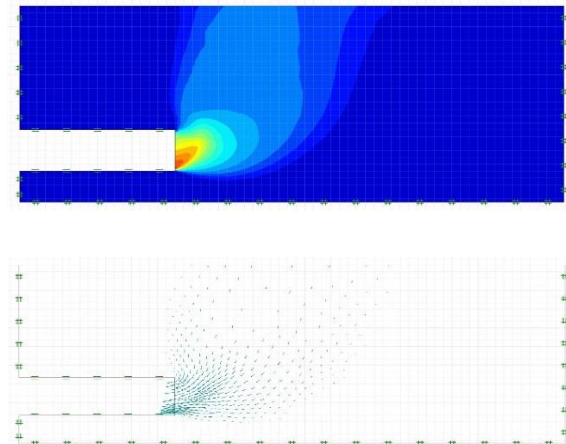


Fig. 10 Total displacements and displacement vectors for  $C/D=3$  and  $S_u/\gamma D=2.0$

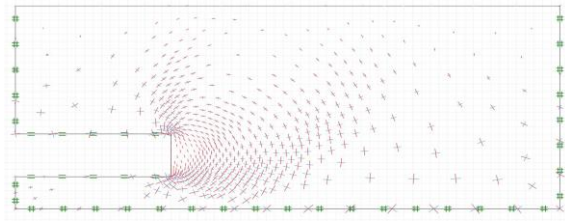


Fig.11 Principle elemental stresses at collapse for  $C/D = 3$  and  $S_u/\gamma D = 2.0$

Figures 9-10 show that the strength ratios have minimal effect on the appearance and the area of the failure, while the extent of the surface failure increase with large values of depth ratios. Figures 11 shows typical tensor plots for principal stresses. The blue vectors indicate the major principle stresses, whilst the red vectors indicate the minor principle stresses. For all cases, the vector fields are similar. Vertical stresses are shown in the major external failure zone just below the surface.

### USING THE STABILITY CHARTS

The stability design charts are best demonstrated through a number of examples. The numerical results have been used to produce design contour charts for factors of safety in Figure 12. A designer will use the chart to relate the depth ratio ( $C/D$ ), soil strength ratio ( $S_u/\gamma D$ ) and factor of safety for the particular tunnel heading. This process would predominantly be used in the initial design procedure.

Figure 12 presents the design chart where the factor of safety is a function of the depth ratio and strength ratio. Regression of the chart gives the following relationship with  $r^2 = 0.99$ .

$$FoS = 3 \left( \frac{S_u}{\gamma D} \right) \left( \frac{C}{D} \right)^{-0.50} \quad (4)$$

#### Examples

Using both the design chart and the regressed design equation, practical examples are presented for either analysis or design purposes.

##### Analysis of an existing unsupported tunnel

An existing mining excavation having no internal heading pressure and no surcharge pressure, determine the factor of safety for operations to

continue. Parameters are given as  $S_u = 50$  kPa,  $\gamma = 18$  kN/m<sup>3</sup>,  $C = 10$  m, and  $D = 2.5$  m.

- Using  $C/D = 4.0$ ,  $S_u/\gamma D = 1.11$ , Eq. 4 gives a  $FoS$  of 1.62.
- Using  $C/D = 4.0$ ,  $S_u/\gamma D = 1.11$ , Figure 12 gives an approximate  $FoS$  of 1.66.

An actual computer analysis of this particular case gives a  $FoS$  of 1.64.

##### Analysis of a temporary unsupported tunnel heading

During the construction of a tunnel in soft soil, a factor of safety of 3 is targeted for a shallow tunnel maintenance job. While the machine requires maintenance, it will be unable to apply pressure to the tunnel face for a short period. A decision needs to be made whether stability will be maintained during this period. Parameters are given as:  $S_u = 30$  kPa,  $\gamma = 18$  kN/m<sup>3</sup>,  $C = 20$  m and  $D = 5$  m

- Using  $C/D = 4.0$ ,  $S_u/\gamma D = 0.33$ , Eq. 4 gives a  $FoS$  of 0.5.
- Using  $C/D = 4.0$ ,  $S_u/\gamma D = 0.33$ , Figure 12 gives an approximate  $FoS$  of 0.52.

An actual computer analysis of this particular case gives a  $FoS$  of 0.49. Therefore, in this case, a failure to supply heading pressure would result in collapse. Ground improvement is needed to increase the soil strength.

##### Design of an unsupported tunnel heading

The soil properties are known at the tunnel project site, and the diameter is specified. A target factor of safety is chosen, and the designers need to specify a maximum cover depth that will satisfy the target  $FoS$ .

Parameters are given as:  $S_u = 100$  kPa,  $\gamma = 18$  kN/m<sup>3</sup>,  $D = 5$  m, and the target  $FoS = 2$

- Using  $FoS = 2$  and  $S_u/\gamma D = 1.11$ , Eq. 4 gives a  $C$  value of 13.86 m.
- Using  $FoS = 2$  and  $S_u/\gamma D = 1.11$ , Figure 12 gives an approximate  $C/D$  value of 3 and therefore  $C$  value of 13.5 m.

An actual computer analysis for this particular case ( $C$  value of 13.5 m) gives a  $FoS$  of 2.03

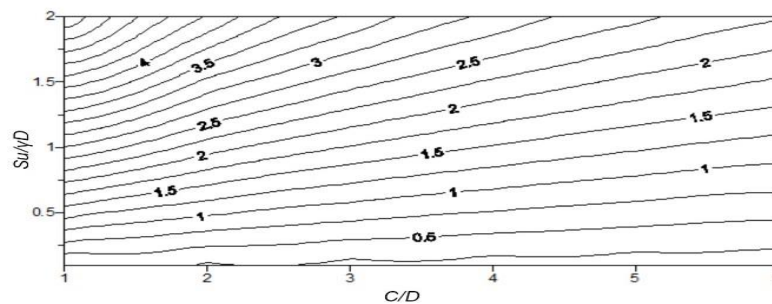




Fig.12 Stability chart for  $FoS$  with respect to  $C/D$  and  $S_u/\gamma D$

## CONCLUSION

The effect of tunnel heading models for different parameters (depth ratio  $C/D$  and strength ratio  $S_u/\gamma D$ ) were studied in this paper using a factor of safety approach with the strength reduction technique. It was found that results ( $FoS$  results and the extent of surface failure) are the most accurate when the models have the geometric parameters:  $X/C \geq 2.5$ ,  $L/C \geq 1.0$ , and  $B/C \geq 0.25$ .

Numerical results were obtained using both the finite element software OptumG2 and the finite difference software FLAC. Based on these modified results design equation and charts were produced aligned with examples to determine the stability of excavated heading depths, such as idealised tunnel headings and long wall mining excavations as well as the extent of failure surface. The factor of safety approach to plain strain heading stability is a useful approach to the initial design stage as it always provides direct information and understanding of tunnel stability.

## REFERENCES

- [1] Broms, BB & Bennermark, H 1967, 'Stability of clay at vertical openings', Journal of the Soil Mechanic & Foundations Division, Proceedings of the American Society of Civil Engineers, vol. 93, pp. 71- 93.
- [2] Atkinson, JH, & Cairncross, AM 1973, 'Collapse of a shallow tunnel in a Mohr-Coulomb material', In Proceedings of the Symposium on the Role of Plasticity in Soil Mechanics, Cambridge, UK, 13-15 September 1973. pp. 202-206.
- [3] Mair RJ 1979, 'Centrifugal modelling of tunnel construction in soft clay', PhD thesis, University of Cambridge.
- [4] Davis, EH, Gunn, MJ, Mair, RJ & Seneviratne, HN 1980, 'The stability of shallow tunnels & underground openings in cohesive material', Geotechnique, vol. 30, pp. 397-416.
- [5] Sloan, SW, Assadi, A 1994, 'Undrained stability of a plane strain heading', Canadian Geotechnical Journal, vol. 31, no. 3, pp. 443-450.
- [6] Mollon, G, Dias, D & Soubra, AH 2010, 'Face stability analysis of circular tunnels driven by a pressurized shield', Journal of Geotechnical & Geoenvironmental Engineering, Vol: 136, pp. 215-229.
- [7] Shiau, J. S. and Kemp R. J. (2013). Developing a numerical model for the stability design of tunnel heading. Third International Conference on Geotechnique, Construction Materials and Environment, Nagoya, Japan, Nov. 13-15, 2013.
- [8] Shiau, J. S., Sams, M. S., Zhang, J., & Kemp, R. J. (2014). Settlement analyses of underground circular tunneling in soft clay. In Geotechnical Aspects of Underground Construction in Soft Ground, Seoul, 347-352.
- [9] Shiau, J. S., Sams, M. S., & Kemp, R. J. (2014). Physical modelling and PIV analyses of an underground tunnel heading. In Geotechnical Aspects of Underground Construction in Soft Ground, Seoul, 61-66.
- [10] Shiau, J. S. and Buttlng, S. and Sams, M. (2016) Developing a project based learning assignment for geotechnical engineering. Electronic Journal of Geotechnical Engineering, 20(18): 10113-10121.
- [11] Shiau, J. S., Sams, M. S., & Lamb B. (2016). Introducing Advanced Topics in Postgraduate Geotechnical Engineering Education – Tunnel Modelling. International Journal of Geomate, 10(1): 1698-1705.
- [12] Shiau, J. S., Lamb B., & Sams, M. S.. (2016). The use of sinkhole models in advanced geotechnical engineering teaching. International Journal of Geomate, 10(2): 1718-1724.
- [13] FLAC 2003, Fast Lagrangian Analysis of Continua, Version 5.0, Itasca Consulting Group, Minneapolis, Minnesota, USA.
- [14] OptumG2 2016, Optum Computational Engineering, Standard Version, Newcastle, Australia.
- [15] Taylor, DW 1937, 'Stability of earth slopes.' Journal of the Boston Society of Civil Engineers, vol. 24, no. 3, pp. 197-246.
- [16] Shiau, J, Sams, M & Chen, J (2016) Stability design charts for unsupported wide rectangular tunnels. Electronic Journal of Geotechnical Engineering, 21(1): 139-150.
- [17] Shiau, J, Sams, M & Chen, J (2016) Stability charts for a tall tunnel in undrained clay. Electronic Journal of Geotechnical Engineering, International Journal of Geomate, 10(2), Japan: 1764-1769.
- [18] Bishop, AW 1955, 'The use of slip circle in the stability analysis of slopes', Geotechnique, vol. 5(1), pp. 7-17.

## APPLICATION OF HEC-RAS AND ARC GIS FOR FLOODPLAIN MAPPING IN SEGAMAT TOWN, MALAYSIA

Noor Suraya Romali<sup>1</sup>, Zulkifli Yusop<sup>2</sup> and Ahmad Zuhdi Ismail<sup>3</sup>

<sup>1</sup>Faculty of Civil Engineering and Earth Resources, Universiti Malaysia Pahang, Gambang, Malaysia;

<sup>2</sup>Centre for Environmental Sustainability and Water Security, Universiti Teknologi Malaysia, Skudai, Malaysia; <sup>3</sup>Faculty of Civil Engineering, Universiti Teknologi Malaysia, Skudai, Malaysia.

### ABSTRACT

Nowadays, a risk-based flood mitigation concept has received more attention rather than the conventional flood control approach in reducing the impacts of flooding. With the intention to assist in the management of flood risk, flood modeling is useful in providing information on the flood extend and flood characteristics. This paper presents the application of HEC-RAS model to the development of floodplain maps for urban area in Segamat town in Malaysia. The analysis used Interferometric Synthetic Aperture Radar (IFSAR) as the main modelling input data. Five distribution models, namely Generalized Pareto, Generalized Extreme Value, Log-Pearson 3, Log-Normal (3P) and Weibull (3P) were tested in flood frequency analysis to calculate extreme flows with different return periods. Using Kolmogorov-Smirnov (KS) test, the Generalized Pareto was found to be the best distribution for the Segamat River. The peak floods from frequency analysis for selected return periods were input into the HEC-RAS model to find the expected corresponding flood levels. Results obtained from HEC-RAS model were used in ArcGIS to prepare floodplain maps for different return periods. The results indicated that most of the inundated areas in the simulated 100 year return period were also affected by 2011 historical floods. For 100 years flood simulation, the inundated area was almost 5 times larger than the simulated 10 years' flood.

*Keywords: Floodplain Mapping, HEC-RAS, ARC GIS, Frequency Analysis, Segamat*

### INTRODUCTION

In recent years, the conventional flood control approach that focusing on structural flood mitigation measures have been shifted to a risk-based flood mitigation concept [1]-[3]. Flood risk is related to two elements i.e. flood hazard and flood vulnerability [4]. Flood hazard is the probability of a flood event to take place, while flood vulnerability is the potential flooding impacts to community and assets which is normally associated with the assessment of property damages [4]-[5]. In most studies i.e. [2], [3], [6], [7], the estimation of flood damage was obtained using the combination of flood characteristics, flood exposure and flood damage function curve.

Flood modelling is important for the assessment of flood hazard to show the magnitude of flood to a certain exceedance probability [4], while its function in vulnerability assessment is to provide hydrological characteristics for damage modelling. The existing literature on flood hazard assessment is extensive and focuses particularly on flood mapping (for example, [8]-[11]). Montane et al. [8] developed a numerical floodplain model to map extreme flood of Meurthe River in France. The model used hydrogeomorphological observations and LiDAR DEM data to produce water depth mapping.

Meanwhile, Cunha et al. [9] applied land morphology approach to map the flood risk of mainland Portugal. There is also a considerable volume of published studies describing the role of flood modeling in the flood vulnerability assessment. In literatures [12]-[14], flood modeling is used to provide hydrological and hydraulics information for flood damage modeling.

HEC-RAS is one of the most widely used model to analyze channel flow and floodplain delineation [10]. Khattak et al. [10] applied HEC-RAS and ArcGIS in their study to map a floodplain of Kabul River that lies in Pakistan. Similarly, Ullah et al. [11] in their flood forecasting study of Kalpani River, Pakistan used a combination of remote sensing, geographical information system (GIS), HEC-RAS (1D), and HEC-Geo RAS. HEC-RAS model was found to give good performance where the simulated results for both studies showed a close agreement with observed water surfaces. Several other applications of HEC-RAS model can be observed in [15]-[17].

In Malaysian, the implementation of flood risk management approach that is supported by modeling tools is still new [18], [19]. However, several flood modeling studies have been carried out during the last few years. Ab. Ghani et al. [19] had developed a flood mapping of 2007 Pahang River flood. In the



study, a digital elevation model (DEM) was produced using a combination of digital topography maps and satellite image. A few studies have applied HEC-RAS and GIS techniques in flood modeling (e.g. [20]-[22]). Shahriparsa et al. [20], [22] had applied HEC-RAS to simulate flood zoning in Kota Tinggi district in Johor state and Maka River district in Kelantan state.

Flood modeling is an important tool in the assessment of flood risk for both hazard and vulnerability. Hence, this study aimed at developing a floodplain map showing the extent of flood and providing related flood characteristics information for flood risk assessment purpose. The application of HEC-RAS modeling for the selected study area in Malaysia is presented.

### Study Area

The study area is Segamat River Basin, Johor which is located in the southern part of Peninsular Malaysia. The aim is to provide flood mapping for frequently flood affected areas in the Segamat town. Segamat town is a medium size town located at the center of the Segamat district with an approximate area of 12,875 hectares and 80,000 residents. The town center is divided into two, which is Bandar Atas (uptown) and Bandar Seberang (Crosstown). Both neighborhoods are separated by Segamat River. Bandar Atas is the original town center of Segamat while Bandar Seberang is located at the other side across Segamat River [23]. Figure 1 shows the Segamat River that flows through the Segamat town. Segamat River is located in 102° 49" E and 2° 30.5' N. With a length of 23 km, the average width of Segamat River is 40 m and is 14 m above sea level. Segamat River is the tributary of Sungai Muar that flow in Segamat town [24].

A series of major floods have occurred in the last few decades along the Segamat river. According to historical records, Segamat experienced flooding during the 1950s, 1984 and more recently in 2006 and 2011. The flood disaster had caused severe damages and inconvenience to the local community.

### METHODOLOGY

The research methodology generally follows the steps shown in Fig. 2. The flood model is a combination of four elements i.e., hydrologic model, hydraulic model, a tool for floodplain mapping and visualization and the extraction of geospatial for use in model [11]. A digital elevation model (DEM) was applied to provide the essential information. The DEM refers to a topographic map which contains terrain elevation properties. The DEM was used in order to set up 2D models for processing the results of flood progression. DEM can be represented by a raster map (grid) or as a triangular model network

(TIN). The DEM data used in this study was the Interferometric Synthetic Aperture Radar (ISFAR) obtained from the Drainage and Irrigation Department (DID) Malaysia.

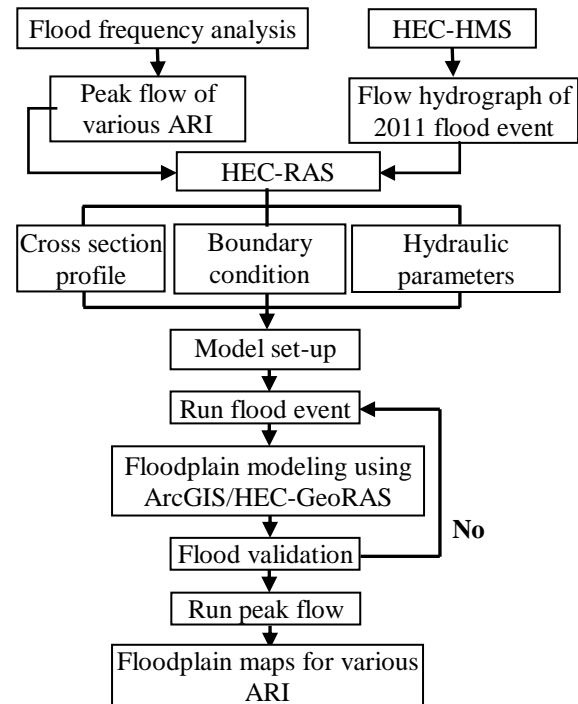


Fig. 2 Methodology flowchart of floodplain mapping

The initial step in developing flood plain maps is to provide peak flows for selected flood event and different return periods [10]. The peak flows for 10, 25, 50, 100, 200, 500 and 1000 average recurrence interval (ARI) were obtained by conducting flood frequency analysis. While the peak flood of 2011 flood used in this study is 1238.2 m<sup>3</sup>/s, obtained from hydrological modeling analysis using HEC-HMS. The steps followed with the hydraulics modeling to translate the discharges into water levels, and the final step is the determination of the inundated extent areas for discharges corresponding to different return periods.

### Flood Frequency Analysis

EasyFit software was used to select the best flood distribution model to calculate peak flows of various ARIs. We used 52 annual maximum flow data of Sg. Segamat gauging station (Site 2528414) for the water years between 1960 and 2011, provided by DID. Five flood distribution models were tested, namely Generalized Pareto (GP), Generalized Extreme Value (GEV), Log-Pearson 3 (LP3), Log-Normal (LN) (3P) and Weibull (3P). The goodness of fit test (GOF) of Kolmogorov-Smirnov (K-S) was used to evaluate and estimate the best-

fitted distribution. K-S at 5% level of significant ( $p < 0.05$ ) was used to define the best fit ranking. The

detailed description of flood frequency analysis is described in [25].

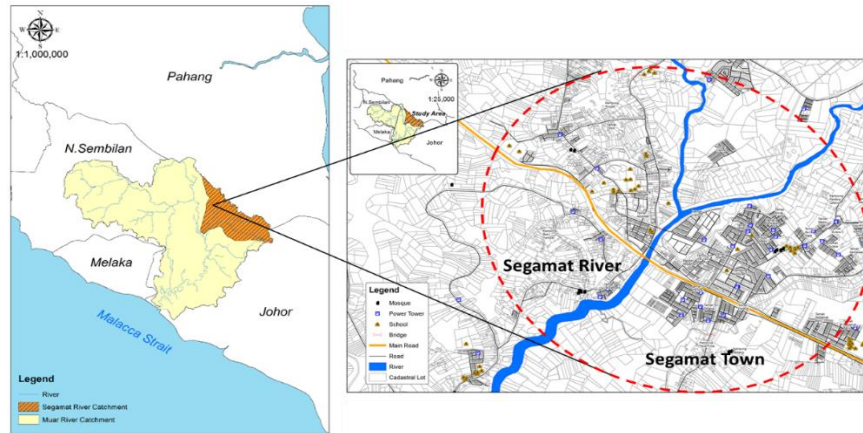


Fig. 1 Location of the study area

### HEC-RAS Modeling

As illustrated in Figure 2, a schematic geometry model that consists of river cross section profile and banks is required in a HEC-RAS model set up. The hydraulic parameters required manning  $n$  values for the land cover. Then the boundary condition was set up to a condition of the river. In the next step, the year 2011 floodplain was simulated in 1D result. The 1D result was converted into 2D using HEC-GeoRAS software. The simulated floodplain was verified with the 15 observed flood marks at various location. Once the simulated floodplain is verified, the HEC-RAS was applied to simulate flood inundated area for various return periods [26].

In HEC-RAS, the data input requirement consists of three main parts which are plan data, geometry data and flow data. Those requirements have to be fulfilled before running the simulation. The plan data is the first step in performing a simulation. The plan data will identify which geometry and flow data to be used as well as provide a description and short identifier for the simulation. If the geometry and flow data do not exist, the simulation will not run. It also includes the flow regime in the simulation option. Cross sections are required at representative locations along the stream and at locations where changes occur in discharge, slope, shape, and roughness [26].

## RESULT AND DISCUSSION

### Flood Frequency Analysis

The peak flows for 10, 25, 50, 100, 200, 500 and 1000 return periods, calculated using GP, GEV, LP3, LN (3P) and Weibull (3P) distributions are shown in Table 1. It's found that the predicted maximum flood using GEV is the highest, followed by LP3

and GP. The smallest values were obtained by Weibull distribution.

Table 1 Maximum flood for various return periods based on GP, GEV, LP3, LN (3P) and Weibull (3P) distributions

Return Period (Years)	Estimated flood discharge ( $m^3/s$ )				
	GP	GEV	LP3	LN (3P)	Weibull (3P)
10	541	830	616	666	176
25	943	1415	1099	1375	297
50	1362	2071	1563	2195	404
100	1914	2997	2112	3342	523
200	2642	4308	2755	4917	653
500	3971	6915	3280	6624	840
1000	5354	9861	4651	10877	993

Table 2 GOF K-S ranking results for GP, GEV, LP3, LN (3P) and Weibull (3P) distributions

Distributions	Kolmogorov Smirnov	
	p-value	Ranking
GP	0.832	1
GEV	0.678	2
LP3	0.673	3
LN (3P)	0.452	4
Weibull (3P)	0.294	5

Table 2 shows the performance ranking based on K-S GOF test. GP is ranked the first in terms of performance, followed by GEV, LP3, LN (3P), and the least for Weibull (3P). The ranking is based on the p-value. A p-value closer to one indicates a better-fit distribution. The highest p-value is 0.832 for the Generalized Pareto and the lowest is 0.294 for Weibull (3P). Based on the results, the estimation of peak flows using GP distribution was

used as the input into HEC-RAS model. The estimated peak flows for 10, 25, 50, 100, 200, 500 and 1000 years ARI are 541 m<sup>3</sup>/s, 943 m<sup>3</sup>/s, 1362

m<sup>3</sup>/s, 1914 m<sup>3</sup>/s, 2642 m<sup>3</sup>/s, 3971 m<sup>3</sup>/s and 5354 m<sup>3</sup>/s respectively.

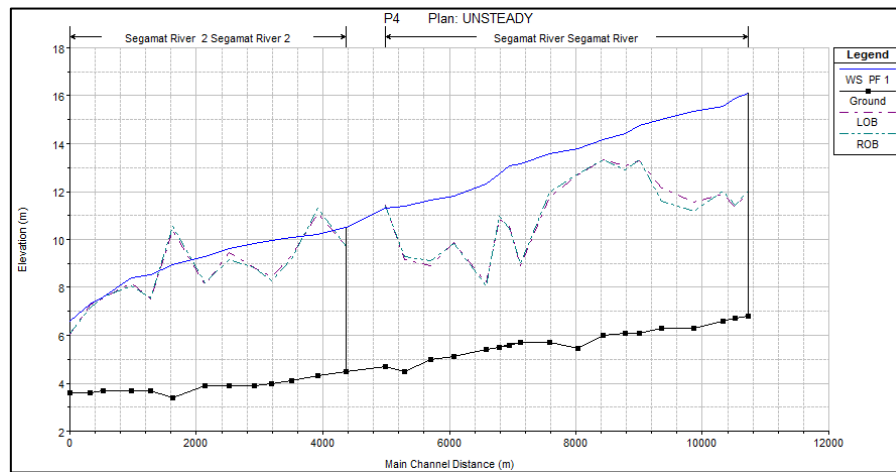
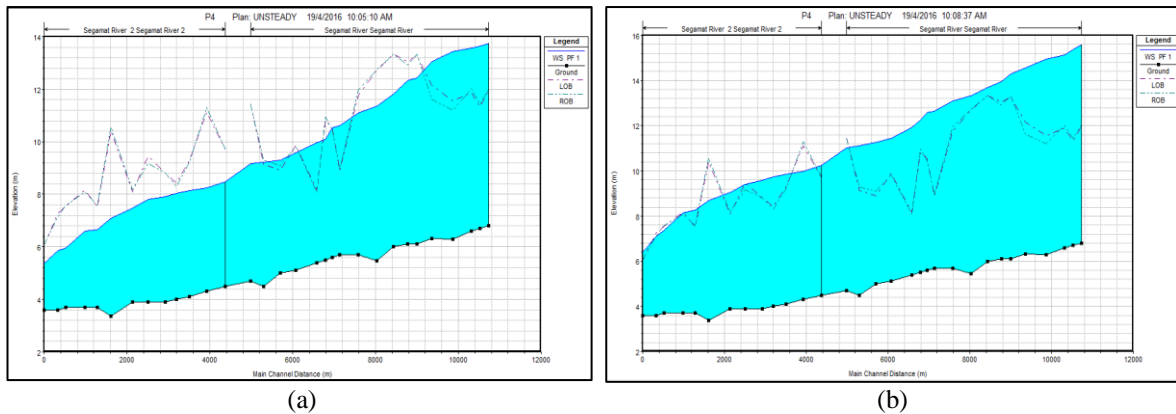


Fig. 3 Water surface profile for 2011 flood



Note: — = WS PF 1, - · - · = Ground, - · - · = LOB, - · - · = ROB

Fig. 4 Water surface profile for return period (a) 10 years (b) 100 years

### Floodplain Mapping

A HEC-RAS hydraulic modeling set-up was created to generate the water level due to the 2011 flood and subsequently the flood map for various return periods. The comparison between the simulated 2011 flood and the simulated 10 and 100 years return periods are presented. The cross section of water surface elevation for 2011 flood is shown in Fig. 3. The blue line shows the level of water surface (WS), while the dotted black line indicates the ground level. The purple and blue dotted line represent the left of bank (LOB) and right of bank (ROB) respectively. The water level produced by 2011 flood are higher than those simulated for 10 and 100 years return period floods, as shown in Fig. 4(a) and Fig. 4(b) respectively. This indicates the extreme situations of 2011 flood.

The results of HEC-RAS model were then exported to HEC-GeoRAS for flood map generation. The simulated inundated areas for 2011

flood, 10 and 100 years return period are shown in Fig. 5, Fig. 6 and Fig. 7 respectively. The blue color shows the extent of flooded area for depth between 0 to more than 1.2 meters.

Figure 5 shows that almost 45% of Segamat town was affected during 2011 flood where 66% of the area is inundated with more than 1.2 meters' depth (dark blue area). Most of the affected area were located at Bandar Seberang (crosstown) which is at the other side across Segamat river. The residential and commercial properties located at the center of the crosstown area i.e. Bandar Seberang, Jalan Sia Her Yam, Jalan Ros and Jalan Genuang experienced flood depth up to 2 meters. Kampung Abdullah and Kampung Jawa were severely affected during 2011 flood with flood depth more than 3 meters.

The simulation results for 10 years return period (Fig. 6) indicate that only 7.43 km<sup>2</sup> of the Segamat town area was affected by flood. The most affected area with flood depth more than 1.2 meters was

Kampung Chabong, Taman Pawana and Taman Pemuda. On the other hand, the simulation of 100 years return period (Fig. 7) shows that almost 40 km<sup>2</sup> of the area was affected by flood, which is 5 times larger than the simulated 10 years' flood. The results also indicate that most of the areas inundated by the 100 years' flood were also affected by 2011 historical floods. Kampung Abdullah and Kampung Tengah were most affected with flood depth more than 4 meters in certain parts of the area.

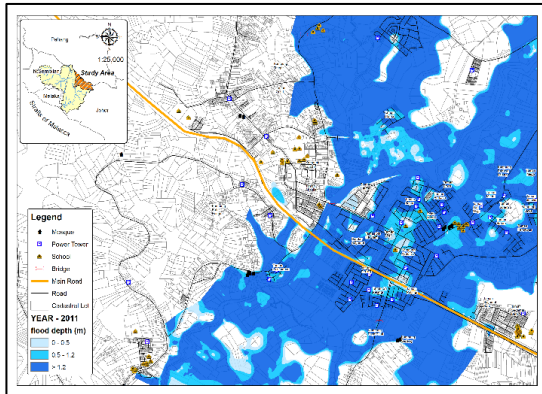


Fig. 5 Floodplain map of 2011 Segamat flood event

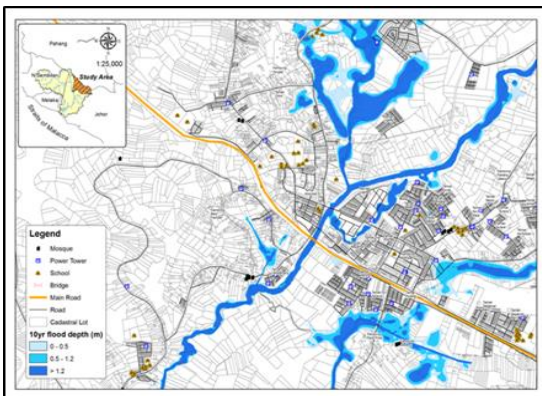


Fig. 6 10 years' floodplain map of Segamat town

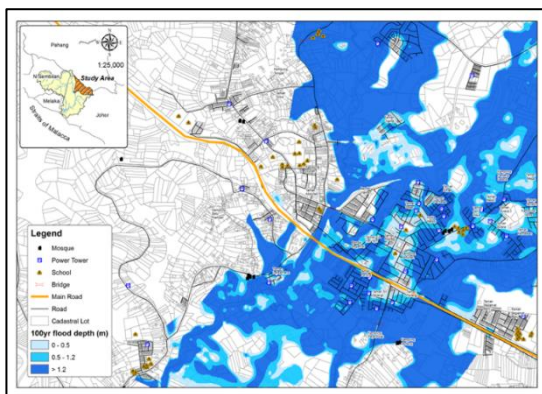


Fig. 7 100 years' floodplain map of Segamat town

The results were validated by comparing the simulated flood against the observed value at 15 stations for 2011 flood event. As shown in the 1:1 graph in Fig. 8, flood simulated flood depths are acceptable with more than 91% accuracy compared to the observed values. The simulated flood boundary is also close to actual flood boundary.

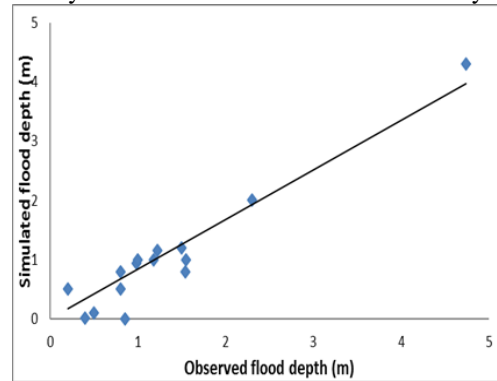


Fig. 8 Observed and simulated flood depth of 2011 Segamat flood

## CONCLUSION

HEC-RAS model was applied to map the inundated area of Segamat town during the 2011 flood and simulate flood map under various return periods. The modelling accuracy was validated against observed flood marks of 2011 event. The simulated flood depth is acceptable with more than 91% accuracy. It's found that Generalized Pareto is the best fit distribution model for peak discharge. The estimated peak flows of Segamat River for 10, 25, 50, 100, 200, 500 and 1000 ARIs are 541 m<sup>3</sup>/s, 943 m<sup>3</sup>/s, 1362 m<sup>3</sup>/s, 1914 m<sup>3</sup>/s, 2642 m<sup>3</sup>/s, 3971 m<sup>3</sup>/s and 5354 m<sup>3</sup>/s respectively.

The simulation suggests that most of the inundated areas of 100 years' flood were also affected by the 2011 historical floods. For 100 years flood simulation, the inundated area was almost 5 times larger than the simulated 10 years' flood.

## ACKNOWLEDGEMENTS

The authors would like to acknowledge Universiti Malaysia Pahang and Universiti Teknologi Malaysia for the financial support through research grant Institut Inovasi Strategik Johor (IISJ) Vot 15H00 and Department of Irrigation and Drainage (DID) Malaysia for providing data and relevant information.

## REFERENCES

- [1] Merz B, Kreibich H, Schwarze R, and Thielen A, "Review article "Assessment of economic



- flood damage”, *Natural Hazards and Earth System Science*, Vol. 10, 2010, pp. 1697-1724.
- [2] De Moel H, and Aerts JCJH, “Effect of uncertainty in land use, damage models and inundation depth on flood damage estimates”, *Nat. Hazards*, 58(1), 2011, pp. 407–425.
  - [3] Ward PJ, De Moel H and Aerts JCJH, “How are flood risk estimates affected by the choice of return-periods?”, *Nat. Hazards and Earth Syst. Sci*, 2011, pp. 3181–3195.
  - [4] Apel H, Merz B, and Thielen AH, “Quantification of uncertainties in flood risk assessments”, *International Journal of River Basin Management*, 6(2), 2008, pp. 149–162.
  - [5] Apel H, Thielen AH, Merz, B., and Blöschl, G. 2006. “A probabilistic modelling system for assessing flood risks”, *Natural Hazards*, 38(1-2), 2006, pp. 79–100.
  - [6] Meyer V, and Messner F, *National Flood Damage Evaluation Methods - A Review of Applied Methods in England, the Netherlands, the Czech Republic and Germany. FLOODsite*, 2005, (November).
  - [7] McGrath H, Stefanakis E, and Nastev M, “Sensitivity analysis of flood damage estimates: A case study in Fredericton, New Brunswick”, *International Journal of Disaster Risk Reduction*, 14, 2015, pp. 1–9.
  - [8] Montane A, Buffin-Belanger B, Vinet F, and Vento O, “Mappings extreme floods with numerical floodplain models (NFM) in France”, *Applied Geography*, Vol 80, March 2017, pp. 15-22.
  - [9] Cunha NS, Magalhaes, MR, Domingos, T, Abreu MM and Kupfer C, “The land morphology approach to flood risk mapping: An application to Portugal”, *Journal of Env. Management*, Vol 193, 15 May 2017, pp. 172-187.
  - [10] Khattak MS, Anwar F, Saeed TU, Sharif M, Sheraz K, Ahmed A, “Floodplain mapping using HEC-RAS and ARCGIS: A case study of Kabul River”, *Arab J Sci Eng*, 41, 2016, pp. 1375-1390.
  - [11] Ullah S, Farooq M, Sarwar T, Tareen MJ, Abdul Wahid M, “Flood modeling and simulations using hydrodynamic model and ASTER DEM-A case study of Kalpani River”, *Arab J Geosci*, 9, 2016, pp. 439.
  - [12] Dutta D, Herath S, and Musiake K, “A mathematical model for flood loss estimation”, *Journal of Hydrology*, 277(1-2), 2003, pp 24–49.
  - [13] Qi H and Altinakar MS, “Simulation-based decision support system for flood sensing and census block information”, *Nat. Hazards*, 59, 2011, pp. 1125-1143.
  - [14] Vozinaki AEK, Karatzas GP, Sibetheros, IA, and Varouchakis EA, “An agricultural flash flood loss estimation methodology: the case study of the Koiliaris basin (Greece), February 2003 flood”, *Nat. Hazards*, 79(2), 2015, pp. 899–920.
  - [15] Gul GO, Harmancioglu N, and Gul A, “A combined hydrologic and hydraulic modeling approach for testing efficiency of structural flood control measures”, *Nat. Hazards*, 54, 2010, pp. 245-260.
  - [16] Pistocchi A and Mazzoli P, “Use of HEC-RAS and HEC-HMS Models with ArcView Risk Management,” *iEMSs2002 Congress Proceedings*, Lugano, 2002.
  - [17] Haghizadeh A, Shui LT, Mirzaei M, and Memarian H, “Incorporation of GIS based program into hydraulic model for water level modeling on river basin”, *Journal of Water Resource and Protection*, 4, 2012, pp. 25-31.
  - [18] Chan NW, “Impacts of disasters and disasters risk management in Malaysia: The case of floods”, *Economic and Welfare Impacts of Disasters in East Asia and Policy Responses.*, December 2012, pp. 503–551.
  - [19] Ab. Ghani A, Chang CK, Leow CS, and Zakaria NA, “Sungai Pahang digital flood mapping: 2007 flood”, *International Journal of River Basin Management*, 10:2, 2012, pp. 139-148.
  - [20] Shahriparsa A, Heydari M, Sadeghian MS, and Moharrampour M, “Flood zoning simulation by HEC-RAS model (Case study: Johor River-Kota Tinggi region)”, *Journal of River Engineering*, Volume x1, Issue 1, 2013.
  - [21] Mina F and Ying TP, “GIS techniques for flood modeling and flood inundation mapping”, *EJGE*, Vol. 20, 2015, Bund. 16.
  - [22] Shahriparsa A, Noori M, Heydari M, and Rashidi M, “Floodplain zoning simulation by using HEC-RAS and CCHE2D models in the Sungai Maka River”, *Air, Soil and Water Research*, 2016:9, 2016, pp. 55-62.
  - [23] Segamat District. In Wikipedia. Retrieved May 11, 2017, from [https://en.wikipedia.org/wiki/Segamat\\_District#Segamat\\_District\\_Facts](https://en.wikipedia.org/wiki/Segamat_District#Segamat_District_Facts)
  - [24] Gasim MB, Surif S, Mokhtar M, Toriman ME, Abd Rahim S, Bee CH, “Sains Malaysiana 39(3), 2010, pp. 353-361.
  - [25] Romali NS and Yusop Z, “Frequency analysis of annual maximum flood for Segamat River”, *MATEC Web of Conferences* 103, 04003, 2017.
  - [26] Ismail Z, “Effect of tide on flood modeling and mapping in Kota Tinggi”, Master thesis, Universiti Teknologi Malaysia, 2015.

## EFFECT OF SATURATION ON STRENGTH BEHAVIOR OF SOAPSTONE

Ravikant R Singh<sup>1</sup>, Darga Kumar Nandyala<sup>2</sup> and Faijal Ali<sup>3</sup>

School of Building and Civil Engineering, College of Engineering Science and Technology,  
Fiji National University, Fiji Islands.

### ABSTRACT

Soapstone samples of standard size prepared from same location, for unconfined compression stress (UCS) test are placed in a water tub for one-day saturation and it is seen that these samples had experienced different failure patterns. Samples 2, 4 and 5 have experienced hairline cracks and samples 3, 6, 7 and 8 have experienced complete separation diametrically. Sample 1 is not subjected to saturation and it showed 4500 kPa of UCS, i.e., 4.5 MPa. Whereas the samples failed due to soaking were rejoined with cement coating and air-dried for one day and tested for UCS showed reduction in UCS. Though these samples were subjected to saturation for 24 hours, it was noticed that hardly 1 to 2% increase in water content. The liquid limit of soapstone is 55% and its plastic limit is negligible, i.e., non-plastic. The collapse potential of soapstone under 200kPa effective normal stress is 7.5% and 1% respectively for dry samples in disturbed and natural state. The free swell index is found to be 18%, which indicates non-swelling nature of soapstone. The dry unit weight of soapstone is 12.5 kN/m<sup>3</sup>. The UCS variations of cracked samples coated with cement and air dried for one-day are presented and discussed.

*Keywords: Soapstone, strength, saturation, collapse potential, dry unit weight.*

### INTRODUCTION

Soapstone is a natural metamorphic rock. Fiji is a country located in the south pacific and has got abundant soap stone in its land mass. In Fiji, soapstone is used as a backfilling material and also as subbase in the civil engineering construction. Soapstone is heat resistant, has high heat capacity and is very easy to work even with wood carving tools. The colour of soapstone varies from dull gray to bluish, greenish and brownish or reddish in general. The qualities of soapstone as is the case for all other stone types depend on those of its basic components, the minerals. Some minerals are hard and some are soft; some can endure extremely high temperatures, whereas others remain stable only up to 100°C.

Soapstone would include a considerable amount of talc, but the proportions and types of other minerals may vary considerably. In addition to talc, the main mineral components of the most typical types of soapstone include mica, chlorite, amphibole, pyroxene, and serpentine minerals. Based on its mineral content, soapstone can be categorized as a type with mica content, one with chlorite content, and so on. Variants including magnesite are quite rare as soapstone goes, but magnesite has, nevertheless, a significant role in increasing the heat storage capacity of the soapstone. The soapstone is characterized by intercalating soft carbonate rich and relatively hard, carbonate poor soapstone (Storemyr, 1996; Heldal and Storemyr, 1997).

Soapstone encompasses various talc-rich schists and that the major weathering problems are related to loss of carved detail along foliation planes at exposed places, and heavy crumbling when great amounts of soluble salts are present in sheltered or partly sheltered locations. There are major gaps in understanding of soapstone weathering. The influence of petrography on weathering at places exposed to direct precipitation, frost and biological agents are not properly understood. Moreover, the relative importance of frost, crystalizing salts and other agents, especially related to weathering at partly exposed places, should be investigated more carefully, as should the weathering mechanisms when soapstone is affected by alkaline salts (*Per Storemyr et al, 2000*).

Soapstone can be used as a building material because this was the first rock on the surface to be quarried and used for construction such as churches, roads, retaining walls, masonry walls which were completely built of soapstone. Most of the ca.200 Medieval baptismal fonts in Norway were made of soapstone (Solhaug, 2001). The use of different varieties of soapstone is almost universal in different building tradition. Soapstone artisan workshops produce a large quantity of powder (approximately 10-15% rock recovery), which is discarded carelessly, often causing environmental problems (Rodrigues and Lima, 2012). The specific gravity of soapstone powder collected from the artisan

workshop in the Bandeiras region varied from 2.73 to 2.83 (Rodrigues, 2010).

Many rocks show a significant strength decrease with increasing moisture content. In some cases, such as montmorillonite clay shales, saturation destroys the specimens completely. More typically, strength losses of 30-100% occur in many rocks as a result of chemical deterioration of the cement or clay binder (Broch [2]). Samples which have been left to dry in a core shed for several months, can give a misleading impression of the rock strength. Laboratory tests should be carried out at moisture contents which are as close as possible to those which occur in the field (Broch, 1974). Rock Quality Designation (RQD) based empirical relations are most commonly employed in determination of rock deformation modulus and unconfined compressive strength (Aydan & Dalgic, 1998; Barton, 2002; Zhang, 2016). The uniaxial compressive strength of rock mass varies by a factor of about 5, depending upon the direction of loading. Evidence of the behaviour of this graphitic phyllite in the field suggests that the rock mass properties are dependent upon the strength parallel to schistosity rather than that normal to it (Salcedo, 1983). Medhurst and Brown (1996) have reported the results of laboratory triaxial tests on samples of 61, 101, 146 and 300 mm diameter samples of a highly cleated mid-brightness coal from the Moura mine in Australia and showed that there is a significant decrease in strength with increasing sample size.

## EXPERIMENTAL INVESTIGATION

### Tests Conducted

To understand the behavior of soapstone, a basic laboratory study is carried out aiming geotechnical characteristics such as plasticity characteristics, free swell index, unconfined compression stress (UCS) and collapse potential. A block of soapstone sample was brought to the laboratory from Derrick campus of Fiji National University, Suva, Fiji. The soapstone collected was dry and whitish in colour. The dry unit weight of soapstone is  $12.5 \text{ kN/m}^3$ . From this block of soapstone, required number of samples of standard size 76 mm long and 38 mm diameter are dressed neatly for UCS test (Figs.1 and 2).

All the tests are carried out as per the standard test procedures of testing of soils (AS 1289.0 - 2014). Soapstone samples of standard dimension were prepared and tested them for unconfined compression strength with one-day saturation and without saturation. Samples had gone through different crack pattern as shown in Fig.1 due to one-day saturation. These cracks were joined with cement paste and air dried for one -day before

testing them for UCS (Fig.2).

The index properties of soapstone which were tested in the laboratory are presented in Table.1. The collapse potential of undisturbed and disturbed samples is presented in Fig.3. The samples unit weight maintained during test are  $12.5 \text{ kN/m}^3$ .

Table 1 Properties of Soapstone

Property	Value
LL	55%
PL	NP
FSI	18%
CP <sub>1</sub>	7.5 %
CP <sub>2</sub>	1 %
$\gamma_d$	$12.5 \text{ kN/m}^3$

Note: LL = Liquid Limit, PL = Plastic Limit, FSI = Free swell Index, CP<sub>1</sub> = Collapse Potential disturbed sample, CP<sub>2</sub> = Collapse Potential undisturbed sample,  $\gamma_d$  = dry unit weight.



Fig. 1 Samples cracked under one-day saturation.



Fig. 2 Cracked samples joined with cement paste.



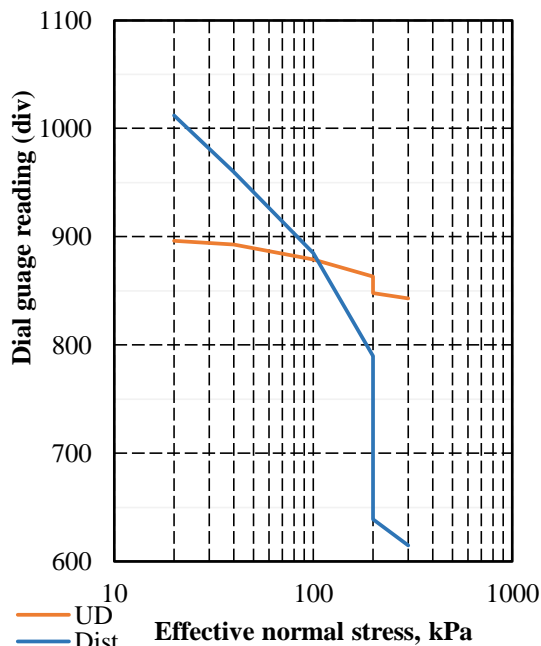


Fig. 3 Collapse Potential for Undisturbed and disturbed at 200 kPa.

## DISCUSSION OF RESULTS

The UCS test results of cement coated soapstone samples are presented in Figs. 4 to 11 for various failed samples due to one-day saturation (Fig.1). Figure 4 presents the compression stress-strain plot for the soapstone dry sample tested without subjecting to the one-day saturation. The sample has reached a peak compression stress at 1% strain and the corresponding UCS noticed is 4500 kPa. From this plot it is understood that the soapstone is failing at lower strain and it clearly shows brittle failure.

Figure 5 presents the stress – strain plot for sample 2 (Fig.1). Sample 2 is not affected due to 1-day saturation and it is almost same as the unsaturated sample as per the size is concerned. But, due to one-day saturation of sample, it is noticed that there is an increase in water content by 2%. As the sample 2 is intact, the specimen is tested without cement coating and corresponding UCS noticed is 950 kPa. This reduction in UCS as compared to the sample tested without saturation is attributed to the weakening of internal structure because of saturation.

Figure 6 presents the compression stress variation with strain for sample 3 (Figs.1 and 2). Due to one-day saturation the sample had horizontal cut at the middle. This sample is joined by gluing with cement and was kept for one-day air drying before testing for unconfined compression stress. From figure 6, the UCS of cement glued sample is noticed as 1245 kPa corresponding to a strain of 1.5%. From this result, it is noticed that the

soapstone can perform better in terms of bearing stress even after failure, if it had treated or glued with cement appropriately.

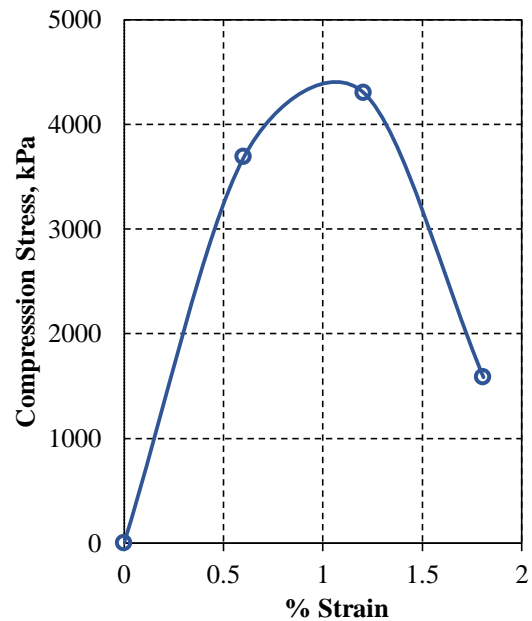


Fig. 4 Sample 1 UCS test zero day's saturation.

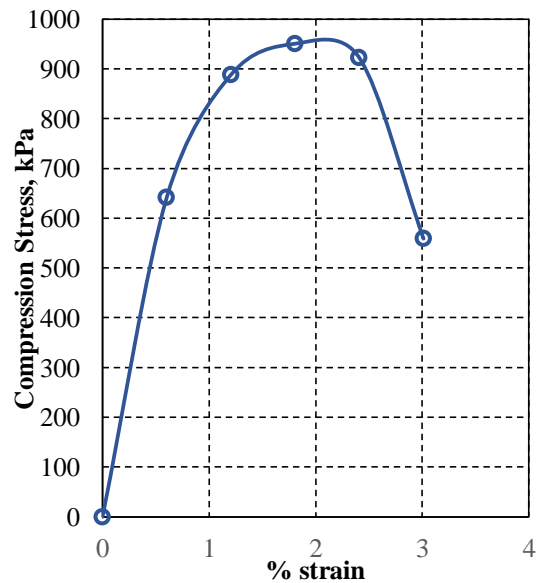


Fig. 5 Sample 2 UCS test one day's saturation with cement paste.

Figure 7 presents the compression stress variation with strain for sample 4 (Figs.1 and 2). Sample 4 shows the very minute level hairline cracks diametrically along the periphery of the sample due to 1-day saturation. These minute hairline cracks are glued with little cement and tested for UCS after one-day drying. The UCS of the sample noticed is about 445 kPa. The sample 2 and sample 4 are not experienced any major cracks, but

there is an influence of saturation towards reduced UCS.

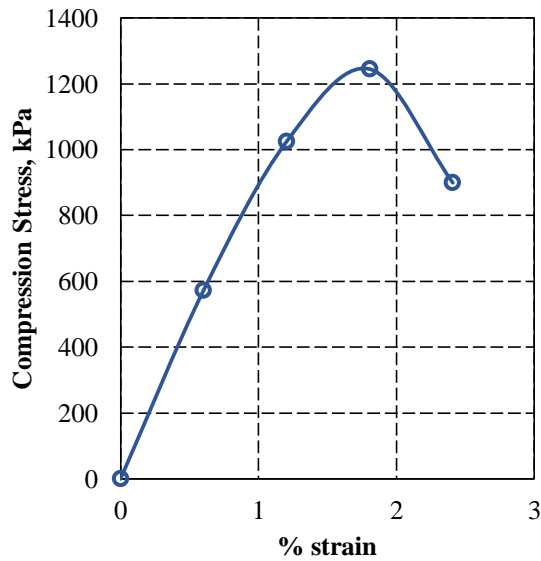


Fig. 6 Sample 3 UCS test one day's saturation with cement paste.

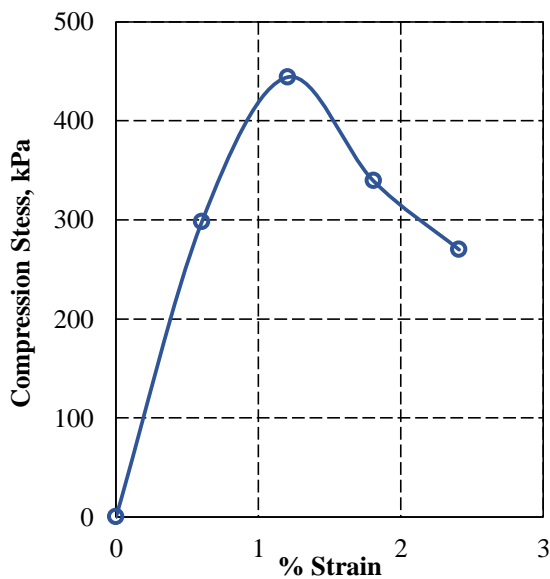


Fig. 7 Sample 4 UCS test one day's saturation with cement paste.

Figure 8 shows the UCS test plot for sample 5 (Fig.1) which has hairline crack diametrically at its middle portion. This hairline crack was glued with cement and kept for one-day air drying before testing for UCS (Fig.2). The UCS of sample 5 is noticed as almost 800 kPa corresponding to a failure strain of 1.7%.

Sample 6 (Figs .1 and 2) UCS plot is presented in Fig.9. The failure pattern due to saturation noticed is almost similar for the samples 3 and 6. The UCS of sample 6 when cement glued and tested is noticed

as 1175 kPa. This higher UCS of the sample is attributed to presence of more glued cement around the failure area of the sample. The sample is failed at about 2% strain.

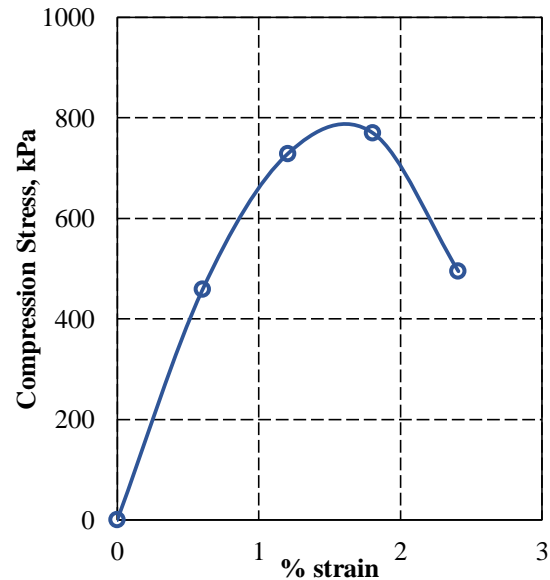


Fig. 8 Sample 5 UCS test one day's saturation with cement paste.

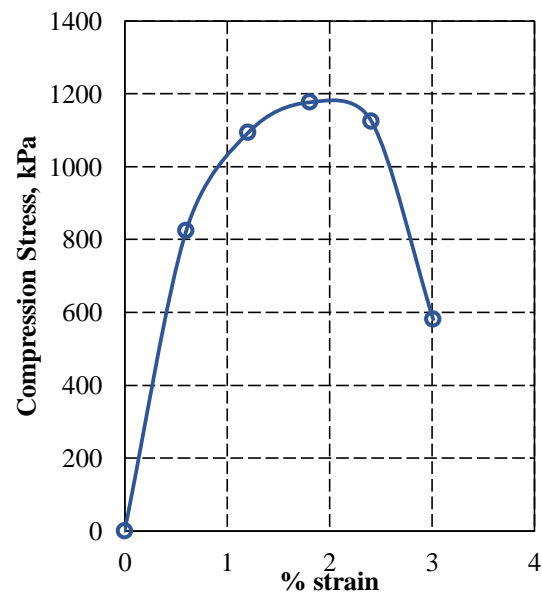


Fig. 9 Sample 6 UCS test one day's saturation with cement paste.

Similarly, for sample 7 and sample 8 the stress-strain plots are presented in Figs. 10 and 11. The sample 7 experienced the failure almost very close to the edge and sample 8 experienced the failure diametrically and almost at the middle of the sample height. The UCS of cement glued sample 7 (Fig.10) is noticed as 785 kPa and whereas for cement glued sample 8 (Fig.11), the UCS noticed is 1280 kPa.

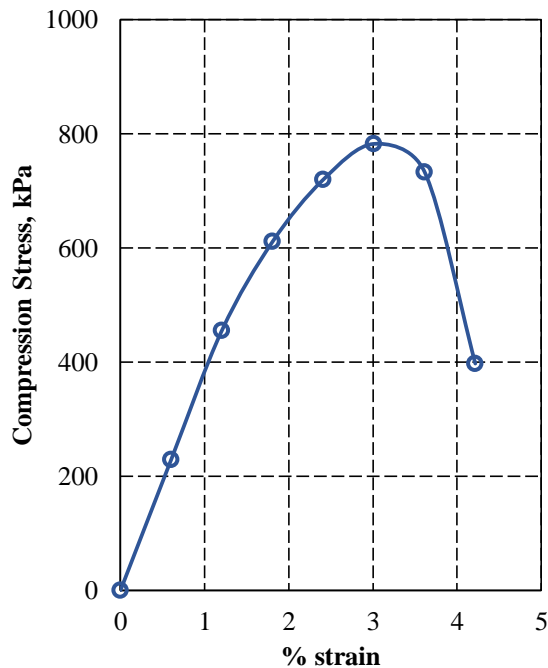


Fig. 10 Sample 7 UCS test one day's saturation with cement paste.

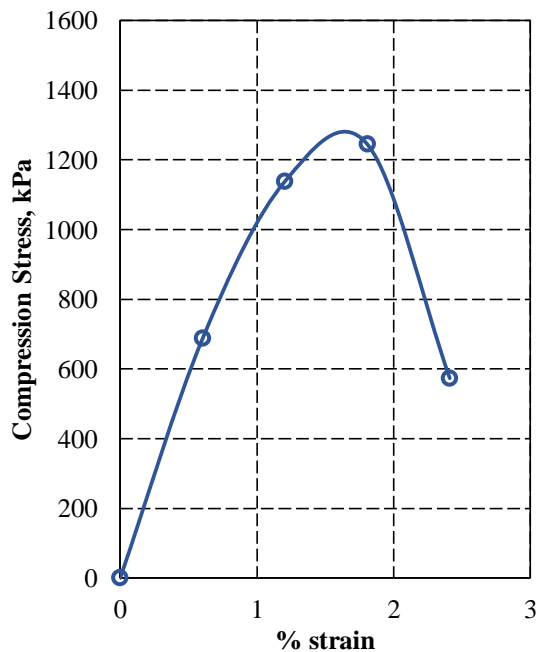


Fig. 11 Sample 8 UCS test one day's saturation with cement paste.

A typical failure pattern of cement pasted soapstone sample is presented in Fig.12. From this figure, it can be noticed that the most of the failure is concentrated at the bottom of the sample, where cement paste was not applied. It means that the soapstone samples when treated with cement and air dried can improve the strength and controls the failure in a sustainable way. Soapstone can be very

well utilized as a building material.



Fig.12 Typical failure of cement joined sample

## CONCLUSION

Interesting points are brought out from the above discussion. The UCS of samples 2, 4 and 5 is 950 kPa, 445 kPa and 800 kPa respectively. The low value of UCS in case of sample 4 is attributed to multiple hairline cracks diametrically close to top and bottom edges and also at the middle. The UCS of samples 2 and 5 is almost in the same range as it is evidenced that similar kind of crack pattern. The samples 3, 6, 7 and 8, though they were diametrically separated, but no hairline cracks are noticed. The UCS values of samples 3, 6, 7 and 8 are 1245 kPa, 1175 kPa, 785 kPa and 1280 kPa respectively. Though the failure pattern is same for the samples 3, 6, 7 and 8, it is noticed that UCS of sample 7 is low compared to samples 3, 6 and 8. It is attributed that the failure is occurred diametrically close to the edge in sample 7, whereas for the samples 3, 6 and 8, the failure is occurred at middle of the sample height.

Also it is interesting to note that the soapstone as long as it is dry, possesses reasonable strength, and when subjected to water saturation, its internal structure gets disturbed causing failure patterns such as cracks and separation. Cement coating can effectively join the failed soapstone to make the system intact and provide required minimum strength for serviceability point of view of civil engineering constructions on the soapstone.

Also the collapse potential of undisturbed and disturbed soapstone samples showed different values.

The collapse potential of undisturbed sample was 7.5% and whereas for disturbed sample it is 1%.

## FUTURE SCOPE OF THE WORK

From the limited work carried out in the laboratory, it is realized that there is a much scope to further carry out research on soapstone. In Fiji, there are three different varieties of soapstone available and these are stiff, very stiff to hard in nature. As most of the constructions are taking place on soapstone, it is required to understand effect of saturation on failure patterns, influence of cement on strength of joined specimens, physico-chemical behavior of soapstone and soapstone sustainability behavior with respect to various loading and environmental considerations.

## REFERENCES

- [1] AS 1289.0 - 2014. Methods of Testing Soils for Engineering Purposes, Australian Standard.
- [2] Aydan, O and Dalgic, S (1998). Prediction of deformation behavior of 3-lanes Bolu tunnels through squeezing rocks of North Anatolian fault zone (NAFZ), Proceedings of Regional Symposium on Sedimentary Rock Engineering, Taipei, China (1998), pp. 228–233.
- [3] Barton, N (2002). Some new Q-value correlations to assist in site characterization and tunnel design, International Journal of Rock Mechanics and Mining Sciences, 39 (2) (2002), pp. 185–216
- [4] Broch E (1974). The influence of water on some rock properties. Proc. 3rd Congress, ISRM, Denver 74(2), Part A, 33-38.
- [5] Heldal, T and Storemyr, P. (1997). Geologisk undersøkelse og arkeologisk registrering av de middelalderske steinbruddene ved øye, Klungen og Huseby I Sor-Trondelag. Norwegian Geological Survey, Report No.97: 149.
- [6] Kavvas M., Hewison L. R., Lastaratos P. G., Seferoglou C. and Michalis I (1996). Experience in the construction of the Athens Metro. Proc. Int. Symp. Geotechnical Aspects of Underground Construction in Soft Ground (Edited by Mair R. J. and Taylor R. N.), 277-282. City University, London.
- [7] Medhurst T. P. and Brown E. T. (1996). Large scale laboratory testing of coal. In Proc. 7th ANZ Conf. Geomech. (Edited by Jaksa M. B., Kaggwa W. S. and Cameron D. A.), pp. 203-208. IE Australia, Canberra.
- [8] Per Storemyr, Eberhard Wendler & Konrad Zehnder (2000). Weathering and Conservation of Soapstone and Greenschist used at Nidaros Cathedral Brief Summary of Investigations 1999-2000, Report Raphael I Nidaros Cathedral Restoration 98/034198 Project 68.
- [9] Rodrigues, M.L.M. (2010). Caracterização tecnológica de resíduos de pedra-sabão de oficinas de artesanato em pedra-sabão da região de Ouro Preto. Ouro Preto: Programa de Pós-Graduação em Engenharia Mineral, Universidade Federal de Ouro Preto (Master dissertation). p. 120.
- [10] Rodrigues, M.L.M & Lima, R.M.F. (2012). Cleaner production of soapstone in the Ouro Preto region of Brazil: a case study, Journal of Cleaner Production, 32, 149-156.
- [11] Salcedo D. A. Macizos Rocosos (1983). Caracterización, Resistencia al Corte y Mecanismos de Rotura. Proc. 25 Aniversario Conferencia Soc. Venezolana de Mecánica del Suelo e Ingeniería de Fundaciones, Caracas. 143-172.
- [12] Solhaug, M. (2001). Middelalderens døpfonter I Norge, Acta humaniora 89, Ph.D Thesis, University of Oslo, Unipub, 1999.
- [13] Storemyr, P. (1996). A study on the weathering of Norwegian greenchist, In J.Riederer (ed.), 8<sup>th</sup> International congress on Deterioration and conservation of Stone: Proceedings, I: 185-200, Berlin.
- [14] Zhang, L (2016). Determination and applications of rock quality designation (RQD), Journal of Rock Mechanics and Geotechnical Engineering, Volume 8, Issue 3, June 2016, Pages 389–397.

## MEASUREMENT ACCURACY OF ORIENTATION CODE MATCHING FOR SLOPE DEFORMATION MONITORING

Takeshi YAMAMOTO<sup>1</sup>, Keigo KOIZUMI<sup>2</sup>, Kazuhiro ODA<sup>3</sup>, and Yoshio FUKUDA<sup>4</sup>

<sup>1</sup>Graduate School of Engineering, Osaka University, Japan; <sup>2</sup>Earth Watch Institute, Inc., Japan

### ABSTRACT

Orientation code matching (OCM) is an image sensing technique and has already been used for the remote and accurate measurement of rainfall-induced slope deformation in the laboratory test. However, the influence of rainfall and differences in target patterns on the measurement accuracy have not yet been verified. In order to verify the influence, the displacement of target panels attached to a height gauge was measured. Comparing the measurement results of two target panels with different patterns confirmed that the displacement could be measured accurately by using a target with the same texture size as the camera pixel size. In addition, comparing the measurement results under rainfall and non-rainfall conditions confirmed that the displacement could be detected with an accuracy of 0.1 mm, although rainfall did influence the measurement accuracy. A model slope experiment was carried out to confirm that accurate measurements could be taken under rainfall conditions. Measurements could be taken without target panels when the slope surface pattern was the same size as the camera pixel size.

*Keywords: Slope Deformation, Image Sensing, Measurement Accuracy, Slope Failure*

### INTRODUCTION

Rainfall-induced slope failure can damage people and the economy. Therefore, an accurate remote slope monitoring system is required. A slope deformation monitoring system that utilizes orientation code matching (OCM) was developed [1]–[4]. Representations for an object image are constructed from corresponding gray images such that each pixel represents an orientation code that is obtained by quantizing the orientation angle at the corresponding pixel position in the gray image. The orientation code represents the steepest ascent orientation evaluated from the pixel neighborhoods and is measured with respect to the horizontal axis. The orientation codes are a function of the texture and shape of the object. Hence, they are essentially invariant to object translation and the effects of shading, background, and illumination variations [5].

In a previous study, it was confirmed that a positive correlation between the camera pixel size and measurement error under non-rainfall conditions using only one target pattern. However, in order to monitor the slope deformation, the system needs to be able to measure displacement under rainfall conditions. In addition, differences in target patterns may affect the measurement accuracy.

In this study, in order to verify the influence of rainfall and differences in target patterns, the displacement of two target panels with different patterns were measured under rainfall and non-rainfall conditions. A model slope experiment was carried out in order to confirm that the slope surface displacement can be measured accurately under rainfall conditions.

### INFLUENCE OF THE TARGET PATTERN ON THE MEASUREMENT ACCURACY

#### Target Patterns

When using OCM to measure the displacement, the influence of noise from low-contrast pixels needs to be reduced. Therefore, this method ignores low-contrast pixels.

Figure 1 shows the target pattern (pattern A) used in the previous study [6]. In this pattern, pixels except for those around the borders of the black and white areas were ignored. Because the number of ignored pixels was high, the influence of noise on the measurement accuracy should increase. If pixels can be effectively used over the whole target, the measurement would be more accurate. Therefore, in order to verify the influence of differences in target patterns on the measurement accuracy, the displacements of two target patterns were measured and compared. Figure 1 also shows the new target pattern (pattern B).

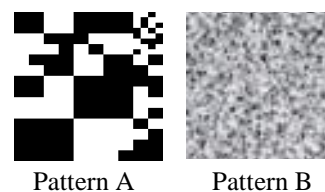


Fig. 1 Target patterns.

## Experimental Outline

In the laboratory, two target panels with patterns A and B (Fig. 1) attached to a height gauge (Mitutoyo HD30AX) were set facing the camera (Point Grey, Flea3 1.3M) lens (Edmund Optics, 9–90MM), as shown in Figs. 2 and 3. The instrumental error of the height gauge was  $\pm 0.02$  mm. The camera captured images with a  $1280 \times 1024$  pixel resolution at an 8-bit grayscale and rate of 50 frames per second. The lens was adjusted so that the pixel could be the specified value. The value varied from 0.20 to 1.00 mm/pixel in increments of 0.10 mm/pixel. After the camera started, target panels were moved 0.10 mm upward in the vertical direction by the handle drive device of height gauge. After the movement, OCM was used to measure for 10 s. The above procedure was carried out for every pixel size.

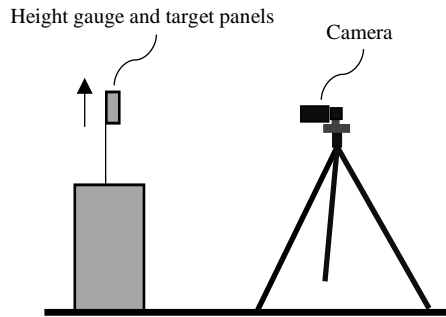


Fig. 2 Schematic diagram of the experiment.



Fig. 3 Height gauge and target panels.

## Experimental Results

Generally, the standard deviation  $\sigma$  or  $3\sigma$  is used as an evaluation index of the dispersion when the measurement results have a normal distribution. In this experiment, the Shapiro–Wilk test [7] was performed to determine if the measurement results followed a normal distribution. The p-value was 0.05 or more in every case, and the null hypothesis was rejected. In other words, the measurement results followed a normal distribution with a significance level of 5%. Therefore,  $3\sigma$  was used as the evaluation index. The accuracy  $\varepsilon_\mu$  was defined as equation (1) and measurement error  $\varepsilon$  was defined as equations (2):

$$\varepsilon_\mu = \mu - 0.10 \quad (1)$$

$$\varepsilon = |\varepsilon_\mu| + 3\sigma \quad (2)$$

where  $\mu$  is the mean of the measurement results.

Table 1 presents the measurement results for patterns A and B at every pixel size. For pattern A,  $3\sigma$  increased with the pixel size. In addition,  $\varepsilon_\mu$  was 0.04 mm when the pixel size was 0.80 mm/pixel and 0.08 mm when it was 1.00 mm/pixel. This showed that the displacement could not be accurately measured. For pattern B,  $\varepsilon_\mu$  was 0.06 mm or less when the pixel size was from 0.02 to 1.00 mm/pixel and 0.03 mm or less when it was greater than 0.06 mm/pixel. However,  $3\sigma$  increased suddenly when the pixel size was 0.90 mm/pixel or greater. Figure 4 shows the relation between the pixel sizes and  $\varepsilon$ .  $\varepsilon$  of pattern B was less than that of pattern A except when the pixel size was 0.90 mm/pixel. This demonstrates that the measurement results were more accurate with pattern B than with pattern A.

Table 1 Measurement results of patterns A and B

Pixel size (mm/pixel)	Pattern A			Pattern B		
	$\varepsilon_\mu$ (mm)	$3\sigma$ (mm)	$\varepsilon$ (mm)	$\varepsilon_\mu$ (mm)	$3\sigma$ (mm)	$\varepsilon$ (mm)
0.20	0.00	0.01	0.01	0.00	0.02	0.00
0.30	-0.01	0.01	0.02	-0.01	0.01	0.02
0.40	-0.02	0.01	0.03	-0.01	0.01	0.02
0.50	0.01	0.03	0.04	0.00	0.04	0.01
0.60	0.00	0.03	0.04	0.00	0.02	0.02
0.70	0.00	0.09	0.09	-0.02	0.04	0.06
0.80	-0.04	0.05	0.08	0.02	0.03	0.05
0.90	0.00	0.03	0.03	-0.02	0.12	0.14
1.00	-0.08	0.09	0.17	0.03	0.10	0.12



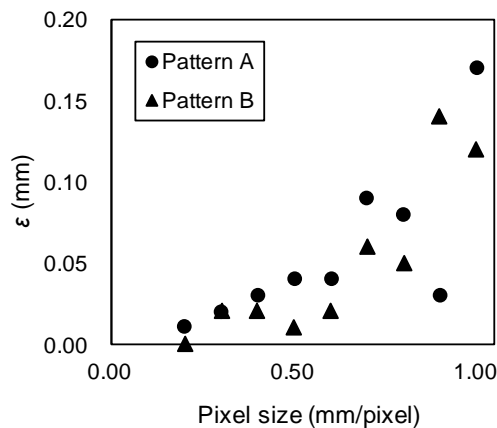


Fig. 4 Relationship between the pixel size and  $\varepsilon$ .

### Discussion

The measurement results were more accurate for pattern B than for pattern A except when the pixel size was 0.90 mm/pixel. Pattern B may be more robust against noise than pattern A because it has more effective pixels. In other words, the displacement could be measured accurately by using a target with the same texture size as the camera pixel size.

For the pattern B results,  $3\sigma$  increased suddenly when the pixel size was 0.90 mm/pixel or greater. Figure 5 shows camera images of the target patterns when the pixel sizes were 0.20 and 0.90 mm/pixel. When the pixel size was large, the image of the target pattern was unclear, and the contrast was low. Thus, pattern B was not robust when the pixel size was greater than the texture size of the target.

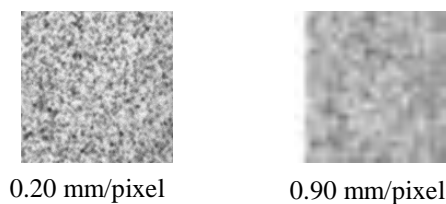


Fig. 5 Images of target panels.

### INFLUENCE OF RAINFALL ON THE MEASUREMENT ACCURACY

#### Experimental Outline

In the laboratory, a target panel with pattern B (Fig. 1) was attached to the height gauge (Mitutoyo HD30AX) at  $35^\circ$  with the horizontal axis. The height gauge was set facing the camera (Point Grey, Flea3 1.3M) and lens (Edmund Optics, 9–90MM), as shown in Figs. 2 and 3. The height gauge's instrumental error was  $\pm 0.02$  mm. The camera captured images with a  $1280 \times 1024$  pixel resolution, 8-bit grayscale, and rate of 50 frames per second.

The lens was adjusted so that the pixel size could be the specified value. The value was increased from 0.20 to 0.50 mm/pixel in increments of 0.10 mm/pixel. After water was sprayed (intensity of 180 mm/h) from above the target to simulate measurement under rainfall conditions, the camera was started. The target panels were moved 0.10 mm upward in the vertical direction with the handle drive device of height gauge. After they were moved, OCM was used to measure for 10 s. The above procedure was carried out for every pixel size.

### Experimental Results

Table 2 presents the measurement results for pattern B with every pixel size under non-rainfall and rainfall conditions. Under the non-rainfall condition,  $\varepsilon$  was 0.02 mm or less when the pixel size was from 0.20 to 0.50 mm/pixel. On the other hand, under the rainfall condition,  $\varepsilon$  was 0.03 mm when the pixel size was from 0.20 to 0.40 mm/pixel, and  $\varepsilon$  was 0.08 mm when the pixel size was 0.50 mm/pixel. Figure 6 shows the relation between the pixel size and  $\varepsilon$ . As a result,  $\varepsilon$  was smaller under the non-rainfall condition than under the rainfall condition. These results show that rainfall reduced the measurement accuracy. This may be because there were water drops between the target and camera, which changed the target pattern from the initial one. However, when the pixel size was 0.40 mm/pixel or less,  $\varepsilon$  was less than 0.05 mm. This means that a measurement accuracy with the order of 0.1 mm was realized. For the model slope experiment discussed in the next section, the pixel size was adjusted to 0.30 mm/pixel.

Table 2 Measurement results under rainfall conditions

Pixel size (mm/pixel)	Non-rainfall			Rainfall		
	$\varepsilon_\mu$ (mm)	$3\sigma$ (mm)	$\varepsilon$ (mm)	$\varepsilon_\mu$ (mm)	$3\sigma$ (mm)	$\varepsilon$ (mm)
0.20	0.00	0.00	0.00	0.11	0.02	0.03
0.30	-0.01	0.01	0.02	0.08	0.01	0.03
0.40	-0.01	0.01	0.02	0.08	0.01	0.03
0.50	0.00	0.01	0.01	0.14	0.04	0.08



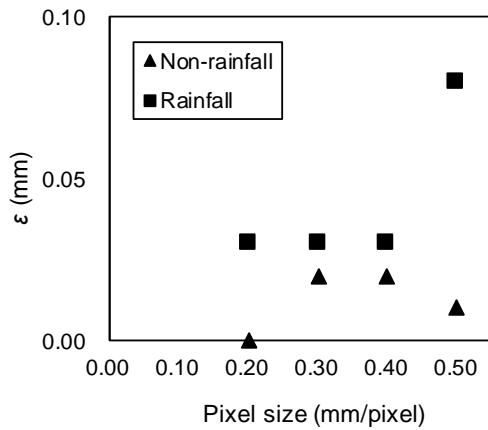


Fig. 6 Relationship between the pixel size and  $\varepsilon$  under rainfall conditions.

## MODEL SLOPE EXPERIMENT

### Experimental Outline

Figure 7 shows a schematic of the model slope used in this experiment. It was 30 cm wide, 83 cm long, and 54 cm high. The surface layer thickness was 10 cm, and the gradient of the slope was  $35^\circ$ . The surface layer was made of Masa, as given in Table 3. The slope was divided into five layers in the vertical direction, and the soil was compressed for a void ratio of 0.60.

A clay layer was arranged under the surface layer and acted as an impermeable layer. Measurement points (A-G) were at the middle of the slope surface, as shown in Fig. 7. Target panels were at A, C, F and G, but not at B, D, and E. The sand of the slope surface was also used as the target. The camera captured images with a resolution of  $1280 \times 1024$  pixels, 8-bit grayscale, and rate of 10 frames per second. The lens was adjusted so that the pixel size could be 0.30 mm/pixel. The measurement started with rainfall (intensity of 180 mm/h), and stopped when none of the targets could be recognized in the camera image.

### Experimental Results

Figure 8 shows the displacement time histories, and Fig. 9 shows partially expanded histories indicating where each measurement point began to displace. At 580 s after the experiment began, the displacement gradually increased at A-E. After 600 s, the displacement rapidly increased, and the slope finally failed. At F and G, the displacement gradually increased after 580 s and rapidly increased after 640 s before the slope finally failed. Figure 10 shows the slope after 640 s. Cracks were confirmed below F and G. Therefore, the displacement behaviors at A-E and at F and G were different.

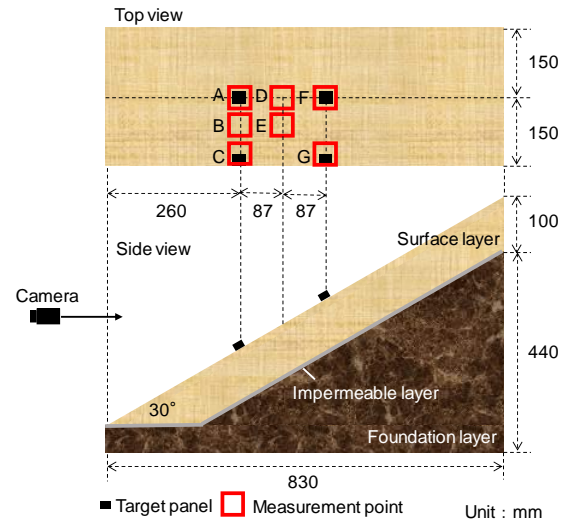


Fig. 7 Schematic diagram of the model slope.

Table 3 Soil sample properties

Soil samples	Masa	
Density of soil particles ( $\rho_s$ )	g/cm <sup>3</sup>	2.607
Water content ( $\omega$ )	%	5.0
Dry density ( $\rho_d$ )	g/cm <sup>3</sup>	1.629
Maximum dry density ( $\rho_{dmax}$ )	g/cm <sup>3</sup>	1.766
Void ratio ( $\rho_s$ )	-	0.6
Permeability ( $\rho_s$ )	cm/s	$1.21 \times 10^{-2}$

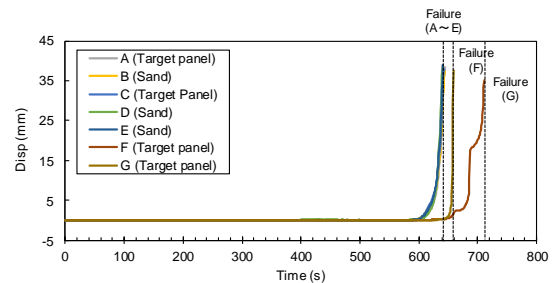


Fig. 8 Displacement time histories.

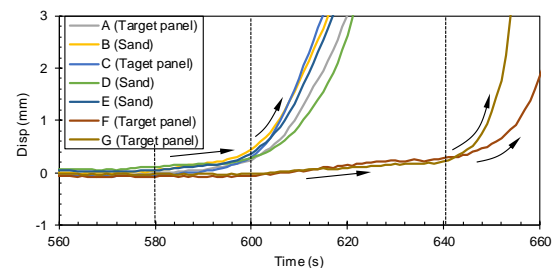


Fig. 9 Displacement time histories (partially expanded).

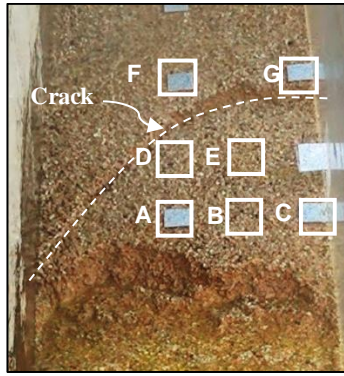


Fig. 10 Slope (after 640 s).

## DISCUSSION

At every measurement point, the displacement behavior could be measured from a small displacement to slope failure. There were no target panels at B, D and E, and the sand of the slope surface was used as the target directly. However, the displacement behavior at B was like that at A and C. If a mass of soil under the crack is displaced in one body, it is reasonable to assume that the displacement behavior at D and E was like that at A and C.

The displacement could be measured as accurately without target panels as with them. This is because the sand showed a high contrast, and its pattern was as rough as that of the target panel as shown in Fig.11. However, if sand is used as the target, the pattern could change from the initial one with slope deformation, which may reduce the measurement accuracy. Therefore, measurements without target panels must be a supplementary method.

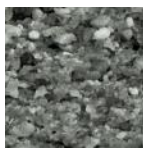


Fig. 11 Images of sand of surface (at B).

## CONCLUSIONS

A series of experiments was carried out to verify influences on the accuracy of measurements with OCM. The major findings and conclusions are presented below:

(1) The displacement can be measured more accurately by using a target with the same texture size as the camera pixel size.

(2) The displacement can be measured with an accuracy of the order of 0.1 mm even under the rainfall condition.

(3) In the model slope experiment, the surface displacement was measured as accurately without target panels as with them.

## ACKNOWLEDGMENTS

This research was partially supported by JSPS-LIPI Bilateral Research Projects and JSPS KAKENHI Grant Number 16H03154.

## REFERENCES

- [1] F. Ullah and S. Kaneko, Using orientation codes for rotation-invariant template matching, *Pattern Recognition*, Vol. 37, No. 2, pp. 201–209, 2004.
- [2] F. Ullah, S. Kaneko, and S. Igarashi, Orientation code matching for robust object search, *IEICE Trans. Inf. Syst.*, Vol. E84-D, No. 8, pp. 999–1006, 2001.
- [3] Y. Li · H. Takauji · S. Kaneko · T. Tanaka and I. Ohmura, Robust focusing using orientation code matching, *Electronic Letters on Computer Vision and Image Analysis*, Vol. 7, No. 3, pp. 101–114, 2008.
- [4] Y. Narita, Remote and robust displacement measurement based on picture matching, M.S. thesis, Hokkaido University, Japan, 2010.
- [5] S. Kaneko · I. Murase and S. Igarashi, Robust image registration by increment sign correlation, *Pattern Recognition*, Vol. 35, No. 10, pp. 2223–2234, 2002.
- [6] Y. Fukuda, K. Koizumi, T. Yamamoto, S. Kobashi, K. Oda, K. Sakuradani and M. Feng, Experimental study on slope deformation measurement utilizing a image sensing technology, *Kansai Geo-Symposium2016*, pp.243-248, 2016.
- [7] S. S. Shapiro and M. B. Wilk, An Analysis of Variance Test for Normality (Complete Samples), *Biometrika*, Vol. 52, No. 3/4, pp.591-611, 1965

# NANOSTRUCTURAL CHARACTERIZATION OF GLUTATHIONE-S-TRANSFERASE IMMOBILIZING CHITOSAN MODIFIED SCREEN PRINTED CARBON ELECTRODE BY ATOMIC FORCE MICROSCOPY

Buddhapala Wongkaew<sup>1</sup>, Porntip Wongkaew<sup>2</sup>, Panupong Thanutong<sup>3</sup> and ChitsanuphongThanutong<sup>4</sup>

<sup>1</sup>Metropolitan Waterworks Authority, Bangkok 10210, Thailand;

<sup>2</sup>Department of Plant Science and Agricultural resources, Faculty of Agriculture,  
KhonKaen University, KhonKaen 40002, Thailand;

<sup>3</sup>Office of The Secretary Permanent, Ministry of Digital Economy and Society, Bangkok 10210, Thailand.

## ABSTRACT

Immobilization of a bio-recognition element to the surface of a functional working electrode is fundamental for effective biosensor development. In this study, the enzyme glutathione-s-transferase (GST) that constitutes a protein superfamily involving various distinct chemical transformations was introduced as a versatile tool for the sensing of environmental toxicants. Functional electrode surface was made by self-assembly of a great bioscaffold chitosan onto screen printed carbon electrode surface concerning to its excellent covalent bonding binding of biomolecules. To enhance the enzyme proximity, glutaraldehyde was employed as an assisting bifunctional cross-linker. The self assembled chitosan layer and the GST immobilizing nanostructural features were explored by morphological imaging and several quantitative analyses such as surface grain size and distribution, power spectrum density (PSD) algorithm, fractal dimension character and other important surface roughness parameters via atomic force microscopy (AFM). Vertical aggregation of the successive layer was clearly verified in all quantitative approaches. Exceedingly, a better understanding in the direction of aggregation along with the growth mechanism was obtained by PSD analysis and the fractal dimension values gained around 2.27 for modified chitosan surface and 2.02 for GST immobilized chitosan modified screen printed carbon electrode. This could thus imply for the diffusion limited model in this growth mechanism.

*Keywords: Immobilization · Glutathione-s-transferase · Chitosan · Biosensor development · Atomic Force Microscopy*

## INTRODUCTION

Recently, researches based on electrochemical biosensor have been attractively considered as potential successors to the development of new methodologies for economical and real time monitoring of environmental pollutants and also for prevention of toxic materials in the environment [1]. The main functional activity is belonged to the oxidising and reducing ability of the selective bio-recognition elements that make a high throughput screening of analytical target possible in a reliable manner within a fraction of seconds. Therefore a critical step for development of biosensor is the selection of a proper bio-recognition element and the immobilization of this element to the surface of a working platform. Although there have been a wide range of bio-molecular recognition elements suggested, enzymes are historically the first molecular recognition elements included in former biosensors and continue to be the basis of data for newly biosensor development and application [2, 3]. Enzymes provide several advantages due to their excellent selectivity for the targeted substrate and high catalytic activity. In addition, a relatively high reaction rate with enzyme operation is commonly

achieved at mild conditions of temperature, pressure and pH which makes substantial process energy savings and reduced manufacturing costs. Moreover they are natural substances being mostly biodegradable proteins and peptides that can be easily withdrawn from contaminated environment without disposal problems.

Immobilization of the enzymes onto suitable platforms is crucial for maintaining their catalytic activity and long term stability, and also for biosensor development. In pesticide determination studies, the main in use enzymes are acetylcholinesterase, butyrylcholinesterase, cholinesterase, acid phosphatase, ascorbate oxidase, acetolactate synthase, urease, aldehyde dehydrogenase and glutathione-s-transferase [4]. On the other hand, it is necessary to choose a suitable platform that provides good support for demand in both catalytic and non catalytic activities including productivity, rapidity, selectivity, separation, control, and down streaming process. A natural material chitosan is one among nanomatrix choices in our attention because of its biocompatibility altogether with its prompt availability and inexpensive productivity which allows a wide array for application on environmental engineering [5,6]. Our

previous study on the modification of a screen printed carbon electrode by surface incorporation with chitosan has demonstrated one among potent application for obtaining an effective and affordable electrochemical implement [1]. With reference to such excellent advantages, it was further used to achieve another successful immobilization of enzyme in this present work to gain an effective specific biosensor.

According to the recent advance in nanotechnological science, many more sophisticated techniques have been developed for the analysis of interfacial events at micro and nanoscale. Among various instrumentations that enable imaging, atomic force microscopy (AFM) is the only empowered technique for material surface visualizing at sub-nanometer accuracy. In comparison to standard scanning (SEM) and transmission Electron (TEM) microscopy, the AFM not only offers the capacity to visualize nanometric features in two and three dimensions but also the physicochemical characteristics including its spatial distribution mapping of surfaces and the permissibility to perform an observation in several environments for example in air, vacuum and liquid environments with little or even no sample preparation requirement. The correlation between the physicochemical properties of biomaterials and the resulting biological response can also be resolved significantly. Inferably, the AFM allows superlative tool for imaging, quantifying, manipulating and other analyses of inspection materials at nanometer level without perturbation of the native characteristics. The fact that nanotopographical surfaces influence charge density and electric field strength, quantitative characterization of surface morphology is thus very important. To date, AFM has been employed progressively for exploring the surface morphological features especially in the research area of surface engineering [1, 7].

In the present study, an enzyme glutathione-S-transferase (GST) was chosen as a model for immobilization onto chitosan modified screen printed carbon electrode (SPCE) prepared according to our previous report [2]. Accomplishment of this immobilization event was then deeply evaluated through high resolution AFM imaging and important interfacial parameters analyses.

## MATERIALS AND METHODS

### Materials

Chitosan (85% degree of deacetylation) with a molecular weight of 0.28 kDa was obtained from Bioline Lab. Co., Thailand. Glutathione-S-transferase from equine liver was purchased from Sigma-Aldrich Co. LLC, USA. Other chemicals for experimental reagent preparation were bought from

Ajax Finechem Pty, Ltd., Australia. Solutions and reagents were prepared using high purity deionized water of 18.2 MΩ from Milli-Q RG system (Millipore Corporation, MA, USA). Screen printed carbon electrode DRP-150 was provided by DropSens, Parque Tecnológico de Asturias, S.L.Llanera (Asturias) Spain.

### Preparation of chitosan modified electrode platform

The chitosan modified electrode platform was made by self-assembling onto SPCE according to our previous report [2].

### Immobilization of GST enzyme

To form a better support condition for enzyme immobilization, the chitosan modified working surface was to be activated by an incorporation of glutaraldehyde (GA) covalent attachment. This working surface spot was treated with a 5 µl drop of 2.5% glutaraldehyde for 30 minutes at room temperature and rinsed with deionized water afterward to remove an excess of its particle. Preparation of 3 U GST enzyme solution was done in 0.05 M PBE that formulated from 0.05 M Phosphate buffer saline at pH 6.5 containing 0.05 M EDTA and 0.1 M KCl [8]. Immobilization of GST was then performed by adding a 5 µl drop of this enzyme solution onto the GA-activated chitosan modified working surface and incubated at room temperature for 2 hours. It was then washed down inordinate molecules with deionized water.

### AFM imaging and analysis

Nanostructural imaging of surface characteristics was carried out by an atomic force microscope model XE-120 (Park Systems Corp., Suwon, Korea) through a true non contact mode. Observation was done in non contact mode under ambient conditions with standard PPP-NCHR silicon cantilever consisting a < 10 nm tip radius (Nanosensors TM, Neuchâtel, Switzerland) with a spring constant of 42 N/m force constant and resonant frequency of 320 kHz. An x-y accessible 1×1 µm area at 0.5 Hz scan rate was inspected with XEP software for data acquisition and XEI software for image processing and quantitative analysis of the surface topography. Important parameters such as an average roughness  $R_a$  (nm), root mean square or standard deviation of the height value  $R_q$  (nm), height different or peak-to-valley ( $R_{pv}$ ), ten point height ( $R_z$ ), mean spacing average ( $R_{sm}$ ), skewness ( $R_{sk}$ ), kurtosis ( $R_{ku}$ ), power spectrum density (PSD) algorithm, fractal dimension and grain aggregation were then successively identified.

## RESULTS AND DISCUSSION

### AFM imaging of surface morphology

A creation of GST enzyme immobilization on working chitosan platform was sighted up by AFM imaging. Remarkable changing in surface morphology could be seen following the modification of screen printed carbon spot area of the SPCE with chitosan and the immobilization of GST enzyme onto chitosan modified platform with the aid of GA bifunctional covalent as shown in Fig.1. Morphological feature at nanometer scale of the scanned surface within a projection area of  $1 \times 1 \mu\text{m}$  has been revealed in 3D illustration for the screen printed carbon basement of SPCE in Fig. 1A, the chitosan modified SPCE (SPCE-Chi) in Fig.1B and the GST immobilized chitosan modified SPCE (SPCE-Chi-GST) in Fig. 1C, respectively. The different feature appearance from each other among these obtaining images, thus, is likely an indication of a progress in the surface modification.

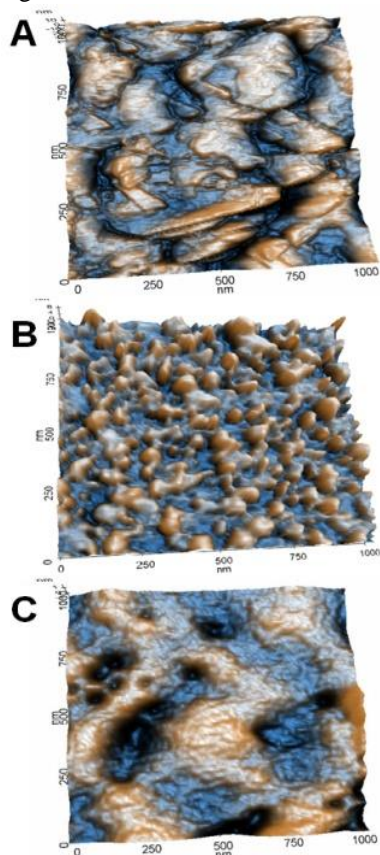


Fig. 1 Three-dimensional AFM nanoscale surface images of (A) SPCE, (B) SPCE-Chi, and (C) SPCE-Chi-GST.

### Surface grain profile

As the AFM nanostructural images have shown a wavy surface texture containing various ripples against a background. These ripples can be detected as grains by watershed algorithm with a software-based image processing. In this observation, the XEI software of Park System was used in quantitative analysis of the surface grain profile to provide comparative information related to the success of SPCE modification with chitosan and GST immobilization onto chitosan modified SPCE. Table 1 presents the measured surface grain information in average of grain area, volume, perimeter and peak-to-valley via level 2.5 filter of watershed algorithm by the XEI software. Differences among the surface natures could be demonstrated in this grain size quantification. Much larger in area, length and perimeter but smaller in volume and peak-to-valley value of the grains from SPCE-Chi and SPCE-Chi-GST than the original SPCE surface were obtained in this determination. With reference to these values, the surface look after chitosan modification and GST immobilization became rather slightly wrinkle taper smear on top of screen printed carbon basement in consent to our previous report [2].

**Table 1** Surface grain structure estimation of bare SPCE, SPCE-Chi and SPCE-Chi-GST at  $1 \times 1 \mu\text{m}$  AFM scan size.

Parameters		Bare SPCE	SPCE-Chi	SPCE-Chi-GST
Area ( $\text{nm}^2$ )	Mean	2.215	4.185	3.165
	Std.	3.385	1.029	3.792
Volume ( $\text{nm}^3$ )	Mean	1.882	0.037	1.063
	Std.	2.943	0.089	1.307
Length (nm)	Mean	67.544	83.854	89.109
	Std.	43.259	82.999	64.534
Perimeter (nm)	Mean	205	273	252
	Std.	155	335	179
$Rpv$ (nm)	Mean	10.212	6.942	5.683
	Std.	5.995	3.164	3.777

Note:  $Rpv$  = peak-to-valley, Std = root mean square or standard deviation

Statistical information on groups of these grains could also be evaluated to define distribution of the grain size. Quantitative scoring for the grain size distribution through histogram plots are shown in Fig. 2. Distinction in grain size distribution is also manifested among these surfaces, thus exemplify



asymmetric growth evidence following chitosan deposition and GST immobilization process.

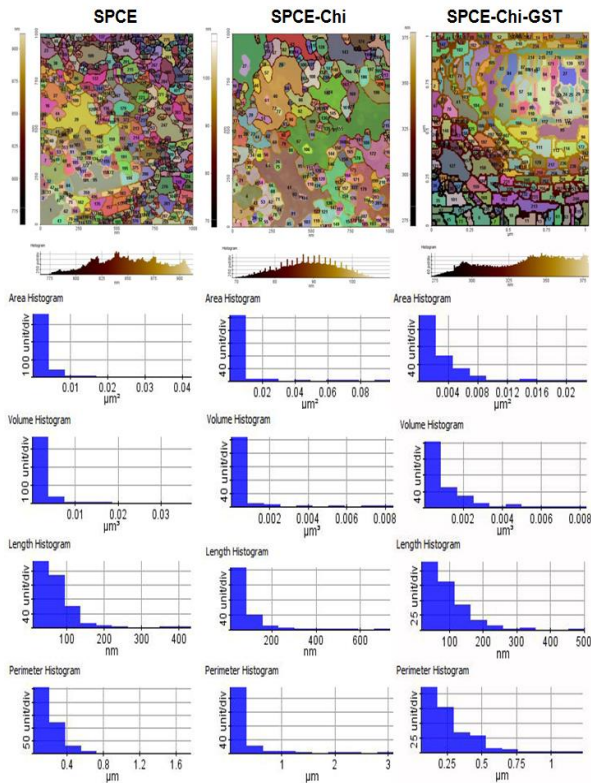


Fig. 2 Grain size distribution histogram of SPCE, SPCE-Chi and SPCE-Chi-GST at 1x1  $\mu\text{m}$  AFM scan size.

### Power spectrum density (PSD) and fractality

Further analysis of surface feature was performed by power spectral density (PSD) which is one of important parameters in surface roughness representation. PSD of the loaded image is obtained from Fourier Transform (FT) of the image and reflects the root mean square ( $Rq$ ) roughness of the sample surface. according to the relation:  $\text{PSD} = \text{FT}^2 = Rq^2$ . Information given from PSD graph provides not only roughness status but also the contribution of each frequency components to the total roughness of the surface [9]. The curves depicted in Fig. 3 show the PSD function of the waveguide evaluated along a line in the AFM image of each working surface acquired via 1x1  $\mu\text{m}$  scan size. The contribution of each spatial frequency to the line profile versus frequency is represented. The most outstanding peak with the highest frequency intensity in each curve at 2, 3 and 1  $\mu\text{m}^{-1}$  was delivered from SPCE, SPCE-Chi and SPCE-Chi-GST working surface, respectively. In spite of these low spatial values, the curves indicate that the spatial periodicity of resist molecular aggregates existed in the surfaces is

varied following the modification with chitosan and the immobilization with GST.

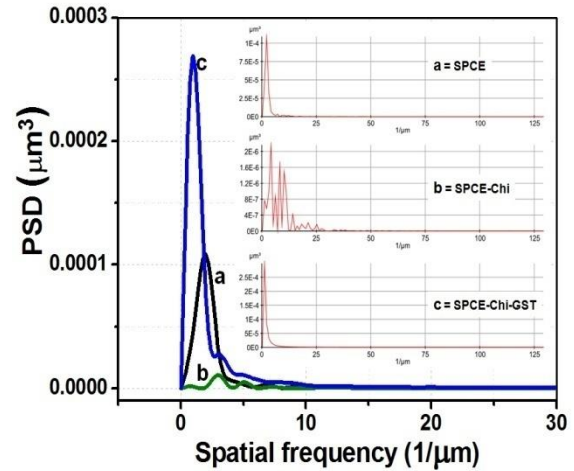


Fig. 3 Power spectral density (PSD) function of the waveguide analyzed along a line in the AFM image via 1x1  $\mu\text{m}$  scan size: (a) bare SPCE, (b) SPCE-Chi and (c) SPCE-Chi-GST.

Fig. 4 displays 2D isotropic power spectral in a log-log plot of PSD and frequency of each working surface in comparison to their relevant slopes for an estimation of the fractal dimension by triangulation method included in the XEI software. All the 2D PSD plots show quite similar in the slope pattern that gradually decreasing from lower to higher spatial frequencies but with a bit different in their waviness concerning to their relative waveguide profile in Fig. 3. These PSD plots also reflect the roughness contribution in their correlative surface. Moreover a condense description in term of fractal dimension of the surface can be quantified based on this PSD function in a more sample-independent manner according to the inverse power law decay [10]. Generally, the fractal model provides more detail on rough surface morphology considering the concepts of scale and the symmetry elements. In another words, fractal objects can be characterized by morphological invariance under scale variance in a restricted range of the spatial scales and allow determination of surface morphology by scale laws [11]. The calculated fractal dimensions in this study are 2.12, 2.27 and 2.02 for SPCE, SPCE-Chi and SPCE-Chi-GST working surface, respectively (Table 2), suggesting a small but markedly difference among each surface texture in subsequent to the layer-by-layer deposition process due to their distinct attribution in the fractal figure occupied along these investigated 3D images.

The higher value of fractal dimension in SPCE-Chi working surface represents a higher level of fractality and a more continuous irregular feature of

the surface roughness than the others while the smaller value represents a smoother top surface [12]. The lowest value obtained in the case of SPCE-Chi-GST thus infers a smoothing flow of successive GST immobilization. This evidence also indicates a vertical growing of the filling GST on the basal chitosan modified screen printed carbon surface.

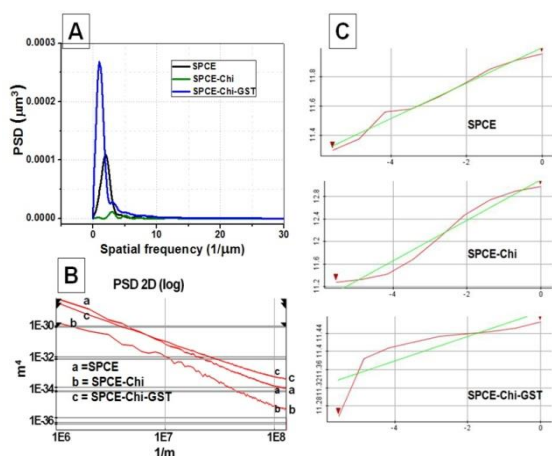


Fig. 4 Two dimensional (2D) isotropic power spectral plots of log PSD and frequency of the working surface of SPCE, SPCE-Chi and SPCE-Chi-GST at 1x1  $\mu\text{m}$  AFM scan size in comparison to their relevant slopes for an estimation of the fractal dimension by triangulation method.

### Surface roughness characteristics

The surface roughness characteristics of the chitosan modified layer both before and after GST immobilization in comparison to a screen printed carbon basement layer were measured from the obtained AFM images by important statistical parameters such as average roughness ( $R_a$ ), root mean square roughness ( $R_q$ ), peak-to-valley ( $R_{pv}$ ), ten point height ( $R_z$ ), mean spacing average ( $R_{sm}$ ), skewness ( $R_{sk}$ ), kurtosis ( $R_{ku}$ ), and mean spacing average ( $R_{sm}$ ). Table 2 displays the estimated values which explicitly show trends in their layer by layer topping relation. The  $R_a$  and  $R_q$  similarly describe overall height distribution profile as a result of the mean height and the standard deviation of the profile height hence imply the top surface wavy roughness characteristics which seem to be remarkably increase over one order of magnitude in SPCE-Chi platform, in consent to our previous report [2]. Simultaneously, these surface roughness parameters appear to be highest in the SPCE-Chi-GST working surface due to the succession of GST oriented assembling. The values gained in  $R_{pv}$  and  $R_z$  clearly explain a differentiation in spike depth among the

figuring surface profiles that is fluctuate from a high plateau of SPCE to a shallow top up layer in SPCE-Chi and an up level of the dept again in the following SPCE-Chi-GST. In cases of the  $R_{sk}$  and  $R_{ku}$  representing the shape and sharpness of the height distribution, on the other hand, the porosity and load carrying capacity, are decreased in SPCE-Chi from the value of the basal SPCE working surface thus suggesting a growing of valleys and cavities appropriate to groove the enzyme molecules. While an increasing of these value are scored in the working surface of SPCE-Chi-GST, on contrary, suggesting a growing of peaks rather than cavities by virtue of the fill up GST immobilization process. Measurement of the  $R_{sm}$  shows values down from 0.39  $\mu\text{m}$  in SPCE to 0.11 and 0.08  $\mu\text{m}$  in SPCE-Chi and SPCE-Chi-GST. These values similarly indicate a decreasing of lateral adjacent peak spaces following a diffusive topping aggregation in the corresponding stepwise manipulation. All the parameters determined thus definitely assure the progression of desirable environmental sensor based on the selective GST enzyme.

Table 2 Surface profile exploration from AFM micrographs at 1x1  $\mu\text{m}$  scan size of bare SPCE, SPCE-Chi, and SPCE-Chi-GST.

Analysis parameters	SPCE	SPCE-Chi	SPCE-Chi-GST
$R_a$ (nm)	18.69	21.74	26.72
$R_q$ (nm)	24.49	25.15	33.17
$R_{pv}$ (nm)	157.23	111.62	143.38
$R_z$ (nm)	155.24	108.88	142.81
$R_{sk}$	-0.19	-0.18	0.59
$R_{ku}$	3.32	1.96	2.67
$R_{sm}$ ( $\mu\text{m}$ )	0.39	0.11	0.09
Fractal (triangular)	2.14	2.27	2.02

Note:  $R_a$  = roughness average,  $R_q$  = root mean square roughness or standard deviation of the height value,  $R_{pv}$  = peak-to-valley,  $R_z$ = ten point height,  $R_{sk}$  = skewness,  $R_{ku}$  = kurtosis,  $R_{sm}$  = mean spacing average.

### CONCLUSION

A fundamental step in enzyme biosensor development is to get success in the immobilization of a selected enzyme onto suitable platform. In this study, a SPCE was chosen as a convenient basement for a self assembled modification with biocompatible chitosan polymer, afterward the enzyme GST was immobilized onto a working surface of this SPCE-Chi using glutaraldehyde as a crosslinker. To gain valuable information for a progress achievement of immobilization, a nanoscale imaging and several analysis strategies via AFM were employed. The obtaining 3D AFM



images have illustrated a clear distinction in morphological appearance among SPCE, SPCE-Chi and SPCE-Chi-GST working surfaces. Statistical parameters and fractal geometry were used as two main analysis approaches with an XEI software assistance for describing the surface roughness and complexity of irregular nanostructures. Determination of the surface grain size and distribution has denoted the asymmetric planar growth in grain area and parameter of SPCE-Chi and SPCE-Chi-GST working surface. One of the most important parameters as power spectral density (PSD) curves was performed and proved capable to reflect differences among the roughness and its contribution on these surfaces. Fractal dimension character of each surface could be calculated with reference to this PSD function and an indicative value for diffusion limited manner was gained from both SPCE-Chi and SPCE-Chi-GST as a result from surface modification with chitosan and subsequent immobilization with GST. Several other quantitative statistical roughness parameters were also assessed and all indicate the complete layer by layer development in the SPCE-Chi and SPCE-Chi-GST. The outcome AFM images as well as surface topographical delineation of these prepared surfaces have revealed a surface dependent characteristic and consequently, a successfulness of the proposed simple direct self assembling stepwise processing for well done enzyme immobilization. Fabrication of desirable biosensor for real time monitoring of specific environmental pollutants based on the selective GST enzyme shall be thus possible.

## ACKNOWLEDGEMENTS

The authors gratefully acknowledge the financial support provided by Division of Research and Technology Transfer Affair, KhonKaen University (KKU-56-57) and the KKU Research Instrument Center for technical supports.

## REFERENCES

- [1] Wongkaew P, Poosittisak, S. "Diagnosis of sugarcane white leaf disease using the highly sensitive DNA based voltammetric electrochemical determination", *Amer. J. of Plant Sciences*, Vol. 5, Jul. 2014, pp. 2256-2268.
- [2] Wongkaew P, Poosittisak, S. "Atomic force microscopic and electrochemical characterization of the modified screen printed carbon electrode by self assembled deposition of chitosan and activated carbon" *Int. J. of GEOMATE*, Vol. 11, Aug.2016, pp. 2356-2362.
- [3] Aminea A, Mohammadia H, Bourais I, Palleschi G, "Enzyme inhibition-based biosensors for food safety and environmental monitoring" *Biosens. Bioelectronics*, Vol. 21, Mar. 2006, pp. 1405-1423.
- [4] Krajewska B, "Application of chitin- and chitosan-based materials for enzyme immobilizations: a review", *Enzyme and Microbial Technology*, Vol. 35, Aug. 2004, pp. 126-139.
- [5] Wongkaew P, Poosittisak, S, 2012. "Electro-affinity of SCWL-dsDNA on different high deacetylation degree chitosans deposited glassy carbon electrode", *Advances in Developing Affordable In-Vitro Molecular Diagnostics*, Puri CP, Abidi N, Bhanushali P, Pere A, Gupta SK, Eds., Yashraj Research Foundation, Varun Enterprises, 2012, pp. 249-258.
- [6] Singh RP, "Prospects of Organic Conducting Polymer Modified Electrodes: Enzymosensors", *Int. J. of Electrochemistry*, Vol. 2012, Jan. 2012, pp. 1-14.
- [7] Variola F, "Atomic force microscopy in biomaterials surface science", *Phys. Chem. Chem. Physics*, Vol. 17, Feb. 2015, pp. 2950-2959.
- [8] Singh RP, Kim YJ, Oh BK, Choi JW, "Glutathione-S-transferase based electrochemical biosensor for the detection of captan", *Electrochem. Communications*, Vol. 11, Jan. 2009, pp.181-185.
- [9] Gavrilă R, Dinescu A, Mardare D, "A power spectral density study of thin films morphology based on AFM profiling", *Rom. J. Inform. Sci. Technology*, Vol. 10, Sept. 2007, pp.291-300.
- [10] Church EL, "Fractal surface finish", *Appl. Optics*, Vol. 27, Apr. 1988, pp. 1518-1526.
- [11] Stach S, Cybo J, "Multifractal description of fracture morphology: theoretical basis", *Mater. Characterization*, Vol. 51, Aug. 2003, pp. 79-86.
- [12] Țălu S, Stach S, Ikram M, Pathak D, Wagner T, Nunzi J-M, "Surface roughness characterization of ZnO: TiO<sub>2</sub>-organic blended solar cells layers by atomic force microscopy and fractal analysis", *Int. J Nanoscience*, Vol. 13, Jun. 2014, No. 03, 12 pp.

# **COLUMN BASED INFILTRATION EXPERIMENT FOR CONSIDERING INITIAL QUASI-SATURATED VOLUMETRIC WATER CONTENT DUE TO DIFFERENCES OF WATER SPRAY INTENSITY AND GRAIN SIZE DISTRIBUTION**

Hiroshi Kita<sup>1</sup>, Keigo Koizumi<sup>2</sup> and Kazuhiro Oda<sup>3</sup> and Mitsuru Komatsu<sup>4</sup>

<sup>1</sup> Graduate School of Engineering, Osaka University, Japan;

<sup>2</sup> Graduate School of Environmental and Life Science, Okayama University, Japan

## **ABSTRACT**

Rainfall-induced slope failure has been increasing in recent years in Japan. In this study, it was hypothesized that displacement on a model slope would not occur unless the initial quasi-saturated volumetric water content was exceeded. This prediction was based on a slope failure experiment using a scale-down slope model. However, in order to apply the initial quasi-saturated volumetric water content as an early warning index for slope failure monitoring, it is necessary to understand the relationship between the initial quasi-saturated volumetric water content and following two factors that affect water infiltration behavior. One is rainfall intensity. The other is soil physical properties. As the first try to understand the factors, two types of fundamental laboratory experiments were conducted; a column experiment for understanding the relationship with the water intensity; a column experiment for understanding the relationship with grain size distribution. As a result, a positive correlation between the initial quasi-saturated volumetric water content and a rainfall intensity was confirmed through the vertical one-dimensional infiltration experiment using a water spray and a column soil tank. Second, a result of evaluating the relationship between grain size distribution and the initial quasi-saturated volumetric water content, it was confirmed that the value of the initial quasi-saturated volumetric water content differed according to grain size distribution. Considering these results, it is expected that the initial quasi-saturated volumetric water content can be utilized for a forecast of the rainfall-induced slope failure by identifying them with multi-monitoring points on the target slope.

*Keywords: Volumetric Water Content, Rain Intensity, Grain Size Distribution, Slope Failure*

## **INTRODUCTION**

In recent years, rainfall-induced slope failure has been frequently occurring in Japan. In order to predict slope failure, on-site monitoring [1], laboratory-scale slope experiment and seepage analysis etc. are carried out [2]–[4].

The authors clarified the relationship between volumetric water content and displacement (shear deformation), as shown in Fig. 1, using a small model slope as a basic experiment for grasping rainwater infiltration. As this schematic diagram indicates, volumetric water content when the rate of rise initially decreases is defined as the initial quasi-saturated volumetric water content. After the initial quasi-saturated state appears, shear deformation that triggers the slope failure begins. Figure 2 shows the change in volumetric water content due to sprinkling water in a column experiment. The soil sample is not fully saturated by water infiltration from above, and it temporarily equilibrates at a certain volumetric water content. Owing to the subsequent rise of the saturation zone from the bottom of the column, volumetric water content again rises. The volumetric water content at the time of equilibrium in the

column experiment is the same as the initial quasi-saturated volumetric water content in the model slope when performing the sprinkling-water experiment on the column and the model slope under the same physical-property condition [5].

Koizumi et al. (2017) defined the initial quasi-saturated volumetric water content as the state at which the infiltration and drainage in the vicinity of the sensor are balanced under the infiltration process from the upper part. Based on the fact that deformation does not occur unless the initial quasi-saturated volumetric water content is exceeded, Koizumi et al. (2017) suggested that an initial quasi-saturated volumetric water content will be an index to forecast rainfall-induced slope failure in advance [6].

However, in order to apply the initial quasi-saturated volumetric water content as an early warning index for slope failure monitoring, it is necessary to understand the relationship between the initial quasi-saturated volumetric water content and following two factors that affect water infiltration behavior. One is rainfall intensity. The other is soil physical properties. As the first try to understand the factors, following fundamental relationships were

evaluated:

- 1) Relationship between the water spray intensity and initial quasi-saturated volumetric water content
- 2) Relationship between the grain size distribution and initial quasi-saturated volumetric water content

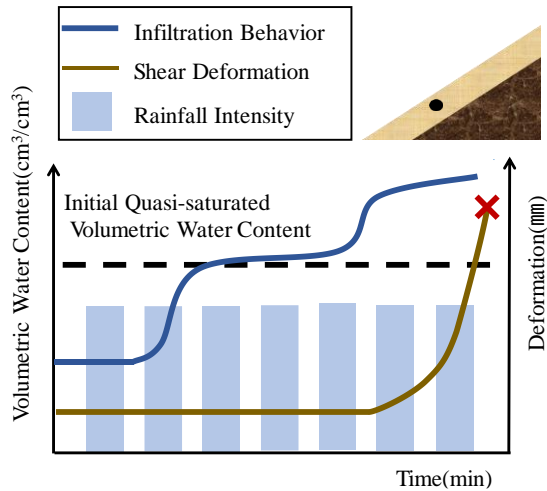


Fig. 1 Volumetric water content and slope deformation on model slope as functions of time

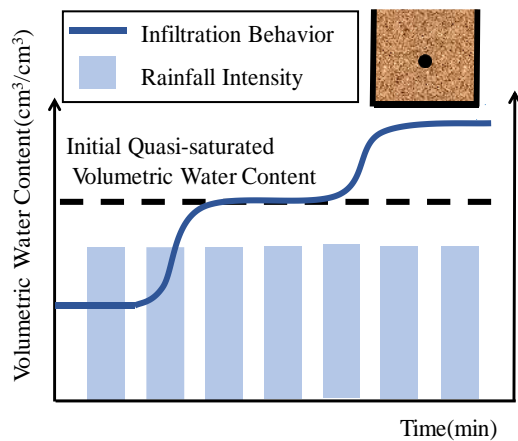


Fig. 2 Volumetric water content observed during water spray experiment on the column as a function of time

## COLUMN EXPERIMENT METHODS

In this study, in order to compare and evaluate the relationship between the water spray intensity and initial quasi-saturated volumetric water content, experiments were conducted using a water spray intensity of 60 mm/h and 100 mm/h. Additionally, in order to compare and evaluate the relationship between the grain size distribution and initial quasi-saturated volumetric water content, we focused on sandy soil, using sandy soil dominated by sandy fraction (A sample) and sandy soil dominated by silt fraction and clay fraction (B sample).

Table 1 outlines the experimental conditions,

Table 2 details the physical properties of the soil samples, Table 3 details the grain size fraction for each soil sample, Fig. 3 shows the grain size distribution, and Fig. 4 illustrates the column soil tank. The total number of cases in the experiments is three, which are referred to as Case-60 A, Case-100 A, and Case-100 B, respectively. The numbers 60 and 100 refer to the water spray intensity, whereas A and B refer to the soil sample. Using an acrylic column, a soil tank was prepared under the experimental conditions described in Table 1. Regarding the B sample, because the soil samples taken at the site were naturally dried in separate vats for the upper and lower parts, the initial water content was different. Thirty-two air holes each with a diameter of 2 mm were provided on the side of the column, thereby suppressing the occurrence of pore air pressure within the column and confirming the groundwater level via outflow of water from the air holes. However, once confirming the water level at the bottom of the column, all air holes were sealed with putty. To measure the volumetric water content, a soil moisture sensor, EC-5 (Decagon Co.; measurement accuracy:  $\pm 3.0\%$ ), was installed and implemented at depths of 50 mm (upper) and 150 mm (lower). The measurement interval was 1 min., and the sensor was installed horizontally because the soil moisture sensor should not obstruct the water path. In all cases, when the water reach the bottom and groundwater re-rise to the top of the soil tank, the experiment was finished.

Table 1 Experimental conditions

Case	Case-60A	Case-100A	Case-100B
Water Spray Intensity(mm/h)	60	100	100
Boundary Condition	Top	Opening(Water Spray)	
	Side	Impermeable Side(Air Hole)	
	Bottom	Impermeable Face	

Table 2 Physical properties of soil samples

Case	Case-60A	Case-100A	Case-100B
Samples	A Sample	A Sample	B Sample
Soil Particle Density( $\rho_s$ ) (g/cm <sup>3</sup> )	2.607	2.607	2.911
Initial Water Content (w) (%)	Upper	Upper	Upper
	Lower	Lower	Lower
Setting Dry Density( $\rho_d$ ) (g/cm <sup>3</sup> )	1.629	1.629	0.970
Maximum Dry Density( $\rho_{dmax}$ ) (g/cm <sup>3</sup> )	1.766	1.766	1.422
Void Ratio(e)	0.6	0.6	2.0
Hydraulic Conductivity(k) (cm/s)	$1.21 \times 10^{-2}$	$1.21 \times 10^{-2}$	$4.65 \times 10^{-3}$

Table 3 Soil sample grain size fractions

Samples	Gravel Fraction(%)	Sand Fraction(%)	Silt Fraction(%)	Clay Fraction(%)	Soil mark
A Sample	24.6	70.2	5.2		SG-Cs
B Sample	16.8	43.3	17.6	22.3	SCsG

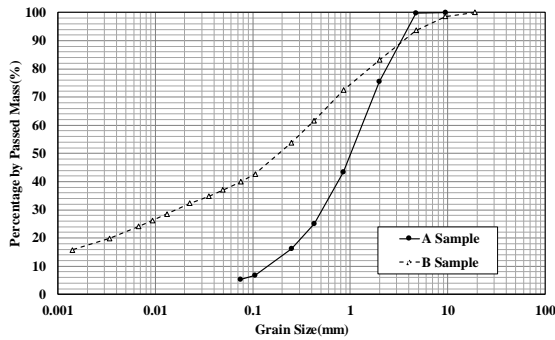


Fig. 3 Grain size distribution

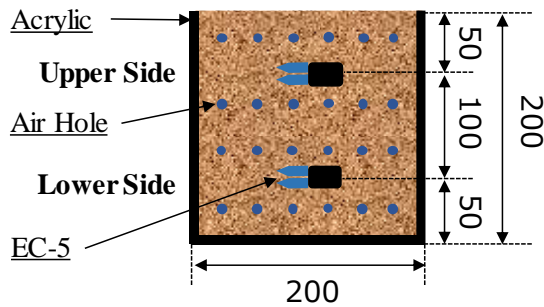


Fig. 4 Column soil tank

## RELATIONSHIP BETWEEN THE WATER SPRAY INTENSITY AND INITIAL QUASI-SATURATED VOLUMETRIC WATER CONTENT

### Experimental Results

Fig. 5 show relationships between the volumetric water contents and the elapsed times of Case-60A and Case-100A, respectively. After sprinkling water, the volumetric water content increased in order from the upper depths to the lower depth. An equilibrium state with values between 0.16 and 0.18 was observed in the case of Case-60A, and values between 0.19 and 0.20 in the case of Case-100A. Subsequently, the volumetric water content at the lower depth re-increased before re-increasing at the upper depth. Secondary equilibrium states of volumetric water content with values between 0.30 and 0.31 in the case of Case-60A and a value of approximately 0.30 in the case of Case-100A were observed.

### Discussion

Here, the relationship between the water spray intensity and the initial quasi-saturated volumetric water content, which is shown in Fig. 6, will be discussed. This figure shows that a positive correlation exists between the water spray intensity and the initial quasi-saturated volumetric water content. It indicates that this relationship should be considered as a fundamental property when the initial quasi-saturated volumetric water content is discussed.

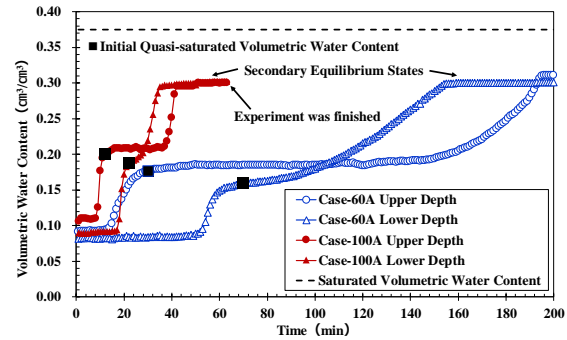


Fig. 5 Volumetric water content for different water spray intensities at upper and lower depths

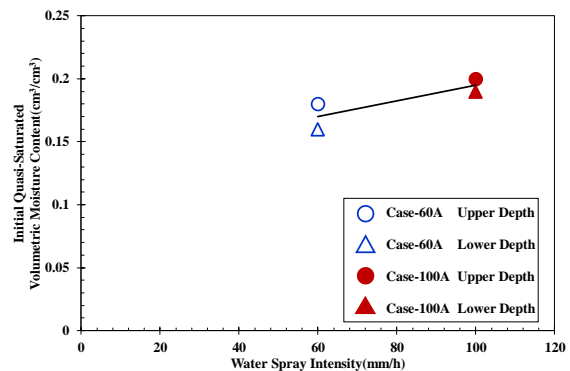


Fig. 6 Relationship between the water spray intensity and initial quasi-saturated volumetric water content

## RELATIONSHIP BETWEEN GRAIN SIZE DISTRIBUTION AND INITIAL QUASI-SATURATED VOLUMETRIC WATER CONTENT

### Experimental Results

Fig. 7 shows the time series change in each volumetric water content for Case-100A and Case-100B which are different grain size distributions. After sprinkling water, the volumetric water content increased in order from the upper depths to the lower depth. An equilibrium state with values between 0.19 and 0.20 was observed in the case of Case-100A, and values between 0.37 and 0.40 in the case of Case-100B. Subsequently, the volumetric water content at the lower depth re-increased before re-increasing at the upper depth. Secondary equilibrium states of volumetric water content with value of approximately 0.30 in the case of Case-100A, and values between 0.63 and 0.65 in the case of Case-100B were observed.

### Discussion

Here in Fig.7, the relationship between grain size distribution and the initial quasi-saturated volumetric water content will be discussed. It was confirmed that the value of the initial quasi-saturated volumetric water content differed according to grain size distribution. Fig. 8 shows the relationship

between the initial quasi-saturated volumetric water content and the degree of saturation for Case-100A and Case-100B. The degree of saturation was calculated from the relationship between the saturated volumetric water content and the volumetric water content. The saturated volumetric water content was calculated from the void ratio on the experimental condition. Although the initial quasi-saturated volumetric water content of each sample was different, the degree of saturation was ranging from 50% to 60%.

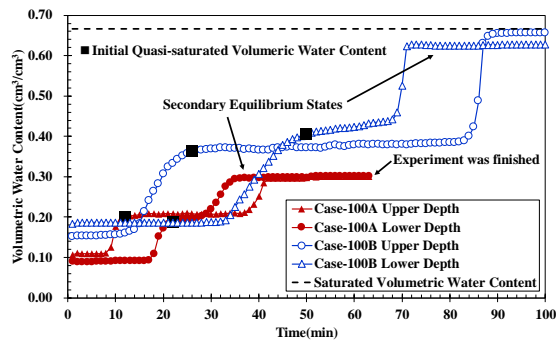


Fig. 7 Change in volumetric water content for different grain size distributions

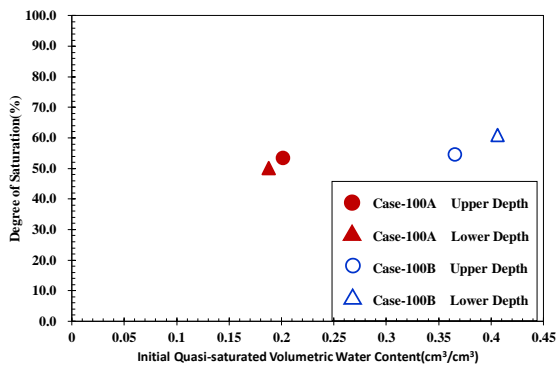


Fig. 8 Relationship between initial quasi-saturated volumetric water content and degree of saturation

## CONCLUSIONS

First, As a result, a positive correlation between the initial quasi-saturated volumetric water content and a rainfall intensity was confirmed through the vertical one-dimensional infiltration experiment using a water spray and a column soil tank. Second, a result of evaluating the relationship between grain size distribution and the initial quasi-saturated volumetric water content, it was confirmed that the value of the initial quasi-saturated volumetric water content differed according to grain size distribution.

Considering these results, it is expected that the initial quasi-saturated volumetric water content can be utilized for a forecast of the rainfall-induced slope failure by identifying them with multi-monitoring points on the target slope.

## ACKNOWLEDGEMENTS

This research was partly supported by Grant-in-Aid for Scientific Research (17K00615). We express our gratitude.

## REFERENCES

- [1] Koizumi K, Konishi T, et al., "Improvement of slope warning system with ubiquitous communication environment", in Proc. Kansai Geo-Symposium 2014, 2014, pp. 141–144.
- [2] Iida T, Fujimoto M, et al., "A method to judge slope failures using soil moisture characteristics", International Journal of GEOMATE, June, 2016, Vol. 10, Issue 22, pp.2094-2100
- [3] Sasahara K, Sakai N, "Shear deformation development and the increase of pore pressure due to rainfall infiltration in sandy model slope under different inclination", Int. J. of GEOMAT, Oct. 2011, Vol. 1, No. 1 (Sl. No. 1), pp., 64-70
- [4] Ito S, Oda K, Koizumi K, Usuki Y, "Identification of slopes with higher risk to slope failures based on information processing techniques", Int. J. of GEOMATE, June, 2015, Vol. 8, No. 2 (Sl. No. 16), pp. 1226-1231
- [5] Ohnishi T, Koizumi K, Oda K, Adrin T, "Grasp of water infiltration behavior up to shallow landslides in miniature slope", in Proc. Kansai Geo-Symposium 2014, 2014, pp. 213–216.
- [6] Koizumi K, Sakuradani K, Oda K et al., "Fundamental research on advancement of regulation standard for expressway management against rainfall-induced surface failure", J. of Japan Society of Civil Engineers, Ser. C (Geo-engineering), Vol. 73, No. 1, 2017, pp. 93–105.

## **ENVIRONMENTAL RISK ASSESSMENT AND MANAGEMENT OF BIOMASS POWER PLANTS FOR SUSTAINABILITY IN THAILAND**

Manutchanok Jongprasithporn<sup>1</sup>, Adisak Martsri<sup>2</sup>, Supapat Phuangkaew<sup>3</sup>, Wannapong  
Yeamma<sup>4</sup>, and Nantakrit Yodpijit<sup>5</sup>

<sup>1</sup>Department of Industrial Engineering, Faculty of Engineering, King Mongkut's Institute of Technology  
Ladkrabang, Thailand

<sup>2</sup>Center for Innovation in Human Factors Engineering and Ergonomics, Department of Industrial  
Engineering, Faculty of Engineering, King Mongkut's University of Technology North Bangkok, Thailand

### **ABSTRACT**

The environmental impact of electricity generation is becoming more critical as electricity consumption continues to increase. It is because the world's population is growing very fast and modern communities use large amounts of electric power. This paper presents the assessment and management of environmental risk of 7.5 and 9.9 MW biomass power plants in Thailand. Three environmental factors (air, transportation) have been examined in this research project. In the environmental analysis, comparisons of measured environmental data from the sites and environmental standards by USEPA (United States Environmental Protection Agency) and Thailand's PCD (Pollution Control Department) are performed. This research project focuses on sustainability that impacts economic, social, and environment aspects by communities, companies, and individuals. The sustainable development of the research project can lead to a coherent and long-term balance between these three aspects. Recent findings from the environmental monitoring system revealed that quality levels of all three environmental factors are under the standards. It is implied that these two biomass power plants do not negatively affect the environment and satisfy the essential needs of humanity.

Keywords: Environmental risk, Biomass power plant, Sustainability

### **INTRODUCTION**

Today electricity is an important energy. Electricity is used for daily life, activities and economic development. The demand for electricity in Thailand increases every year due to the economic growth and population growth as shown in Figure 1.

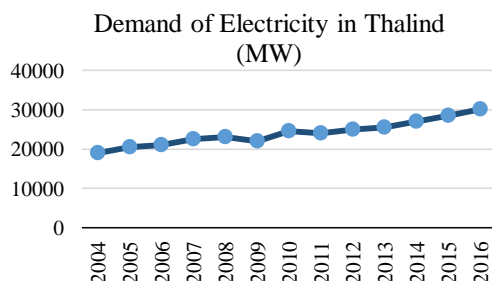


Fig. 1 Demand for electricity in Thailand [1]

The trend of the demand for electricity in Thailand is rising. Therefore, increasing the electrical capacity and constructing more power plants to solve the energy shortage problem in the

future is of importance. Moreover, the power plants should use renewable resources when generating electricity.

Renewable energies are becoming very important to economic development [2,3]. The thermal power plant and combined-cycle power plant are the most used in Thailand. Burning fossil fuels such as coal oil and natural gas has releases greenhouse gases and other pollutants into the atmosphere [4-6]. So a few renewable energy such as wind, solar, biogas, biomass energy are now used to produce electricity instead of fossil fuels and coal. Because Thailand has a lot of biomass resources, biomass power plants are a good choice to solve the energy shortage problem.

Previously, there were a lot of problems when constructing a power plant. They were opposed by the community due to the fear of various power plant issues which could affect the community. Especially, the environmental impact from the power plant was the main problem. The environmental impact has brought many complaints and has a negative impact on the surroundings. Therefore this research analyzes and manages the environmental risks of power plants. The risk affects the power plant safety and the people in the



community around the power plant [7]. In addition, risk assessments and opportunities for factor analysis as well as a recommendation hedging measure for the future.

## RESEARCH METHODS

This research has two steps as follows:

1. Study the power plant processes.
2. Study of environmental conditions and measurement of environmental factors in power plant areas.

### Study the Power Plant Processes

The power plants in this research are biomass power plant with a capacity of 9.9 MW and 7.5 MW. The fuel for biomass power in this research is rice husk. The rice husk is used as a combustion fuel to generate electricity. Location of both biomass power plants are at Suphan Buri-Uthaithani Road (Highway 333), U-Thong district, Suphan Buri. The process of a biomass power plant used in this research are shown in Figure 2.

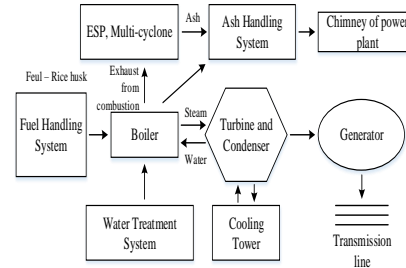


Fig. 2 The biomass power plants process used in this research

The process of generating electricity from a biomass power plant starts with the rice husk which is stored in the silo as a combustion fuel to heat the boiler. Until a high pressure steam is sent to the steam turbine to make the turbine rotate. The generator is connected to the shaft of the steam turbine. The generator will then rotate to produce electricity. The waste gasses from these processes are sent to the waste gas treatment plant and the ash removal machine before the gas is discharged through the plant's waste flue. The steam that goes through the steam turbine will be sent to the cooling tower to condense the hot steam into the water for reuse in the boiler. The machines and equipment found in a biomass power plant are listed in table 1.

Table 1 The machine and equipment of the biomass power plant

Machine	Number of Machines	Power (HP)	Total Power (HP)
Bucket Elevator	7.5	4	30
Belt Conveyor	7.5	2	15
Belt Conveyor	5.0	4	20
Husk Feeder	7.5	4	30
F.D Fan	125.0	1	125
F.D Fan	75.0	1	75
Spreader Fan	55.0	1	55
I.D Fan	270.0	1	270
Boiler and Pump	270.0	2	540
Electrostatic Precipitator	55.0	1	55
Air Compressor	15.0	2	30
Drum	3.0	1	3
Screw Conveyor Dust Collector	3.0	1	3
Screw Conveyor Dust Collector	3.0	1	3
Screw Conveyor Under ESP	2.0	2	4
Chain Conveyor	7.5	2	15
Pump to Clarify	30.0	2	60
Pump to Softener	20.0	2	40



Table 1 continued

Machine	Number of Machines	Power (HP)	Total Power (HP)
Pump to Sand Filter	20.0	2	40
Pump to R.O	5.0	2	10
Pump to Mixed	5.0	2	10
Pump to De-aerator	7.5	2	15
Pump to Cooling Water	20.0	2	40
Cooling Fan	50.0	4	200
Cooling Fan	270.0	3	810
Condensate Pump	15.0	2	30
Diesel Generator	1,610.0	1	1,610
Steam Turbine Generator	12,750.0	1	12,750
Etc.	67.00	1	67
Total		56	16,955

### The Study of Environmental Conditions and Measurements of Power Plant Area

In this process, the environmental impacts to the area of both biomass power plants were studied. Moreover, air quality and transportation are also measured.

#### Air quality

The risk of pollution in the air will be assessed to investigate if Biomass power plants have negative impact on the environment or not. The measured value will be compared with the standard values. The standard values have been set by environmental departments such as the United States Environmental Protection Agency (USEPA) and Thailand's Pollution Control Department (PCD) [8,9]. The measured value must not exceed the standard values, [2,3,7]. The air pollution should be composed of Total Suspended Particulate (TSP), Sulfur Dioxide (SO<sub>2</sub>), Nitrogen Dioxide (NO<sub>2</sub>), and Carbon Monoxide (CO). The area around both of the biomass power plants will be measured.

#### Transportation

Transportation is an important factor when developing economically [10]. If the power plant has a good transportation system, economics of the power plant are better because the transportation costs would be cheaper [11]. Both biomass power plants in this case study are located at U-thong district Suphan-buri province.

### RESULTS

In this section, the results of the implementation are covered. The environmental factors are air quality and transportation. Measurements of value were collected from both of the biomass power plants. The area of this research covers 5 km around the biomass power plants. The results of implementation are as follows.

#### Air quality

The value of environmental pollutants in the atmosphere were measured and collected. The results are shown in Tables 2 and 3.

The air pollutants measurement was a 1-hour average of Sulfur Dioxide (SO<sub>2</sub>), Nitrogen Dioxide (NO<sub>2</sub>), Carbon Monoxide (CO), and 24-hours average Total Suspended Particulate (TSP). The results show the air pollutants in the atmosphere of two biomass power plants. The quality of air quality was within the standard. Except total suspended particulate at the power plant (9.9 MW) in day 1 and 2 because of agency maintenance of the road surface in those two days. Therefore, total suspended particulate was higher than the other days.

Table 2 Air Monitoring (Power Plant 9.9 MW)

Measured Date	Pollutant Concentration			
	SO <sub>2</sub> (ppm)	NO <sub>2</sub> (ppm)	CO (ppm)	TSP (mg/m <sup>3</sup> )
1	0.0053	0.0165	0.58	0.52
2	0.0047	0.0106	0.62	0.45
3	0.0044	0.0086	0.53	0.25

Table 2 continued

Measured Date	Pollutant Concentration			
	SO2 (ppm)	NO2 (ppm)	CO (ppm)	TSP (mg/m <sup>3</sup> )
4	0.0028	0.0057	0.43	0.19
5	0.0030	0.0061	0.36	0.20
Standard*	0.30	0.17	30	0.33

Table 3 Air Monitoring (Power Plant 7.5 MW)

Measured Date	Pollutant Concentration			
	SO2 (ppm)	NO2 (ppm)	CO (ppm)	TSP (mg/m <sup>3</sup> )
1	0.0024	0.0149	0.49	0.13
2	0.0021	0.0132	0.63	0.16
3	0.0025	0.0129	0.42	0.18
4	0.0035	0.0136	0.55	0.15
5	0.0029	0.0140	0.54	0.13
Standard*	0.30	0.17	30	0.33

\*The standard values. Reference from criteria air pollutants USEPA and act of legislation of pollution control Department [5-6]

#### Air quality assessment

The result shows that Sulfur Dioxide (SO<sub>2</sub>) was low, this is because rice husk have a low sulfur compound. Controlling the temperature, heat and oxygen in the boiler helped to handle Nitrogen

Dioxide (NO<sub>2</sub>) and Carbon Monoxide (CO) within the standards [12]. The removal particular system in both of biomass power plants used Multi-Cyclone separators and Electrostatic Precipitator (ESP). Therefore, total Suspended Particulate (TSP) in the surrounding area of the biomass power plants were within the standards. The pollutant from the chimney of the biomass power plant is shown in Table 4.

Table 4 The pollutant from the chimney of the biomass power plants

Pollutant	SO2 (ppm)	NOx (ppm)	TSP (mg/m <sup>3</sup> )
power plant (9.9MW)	<0.10	106.41	28.22
power plant (7.5 MW)	<0.10	150.86	20.64
Standard*	60	200	320

\*The standard values. Reference from act of legislation from the factory Ministry of Industry [13]

#### Transportation

Due to the biomass power plants having rice husk deliveries every day, it is necessary to consider the effect of density on the roads. Database of Bureau of Traffic Safety, Department of Rural Roads, Ministry of Transport [11,14] shows the average daily traffic on the road that are used to transport rice husks. Traffic volumes are 6,400-10,000 per day. The detail of traffic volumes on the highway are shown in Table 5.

Table 5 Traffic volumes on highway [11, 14]

Vehicle	Traffic volumes on highway (per day)			
	No. 321	No. 333	No. 3342	No. 3472
Car < 7 persons	671	3,045	1,298	1,158
Car > 7 persons	1,636	1,001	2,658	789
Small Bus	51	227	424	395
Medium Bus	85	95	156	183
Large Bus	120	238	224	229
Small Truck	1,521	1,027	890	1,766
Medium Truck	522	497	882	1,158
10 Wheel Truck	401	514	658	512
Trailer	376	318	509	210
Hybrid Trailer	30	167	178	95
Motorcycle	964	1,432	2,204	1,817

Table 5 continued

Vehicle	Traffic volumes on highway (per day)			
	No. 321	No. 333	No. 3342	No. 3472
Total Truck	2,850	2,523	3,117	3,741
Total Vehicle	6,377	8,561	10,081	8,312

From table 5, the traffic volume on the highway no. 321, 333, 3342 and 3472 can calculate the proportion of car volume. Each type of vehicle can

adjusted to PCU (Passenger Car Unit)[14] as shown in Table 6.

Table 6 Traffic statistics on highway [14]

Vehicle	PCU	Expectation of traffic volumes on highway (per day)			
		No. 321	No. 333	No. 3342	No. 3472
Car < 7 persons	1	671	3,045	1,298	1,158
Car > 7 persons	1	1,636	1,001	2,658	789
Small Bus	1	51	227	424	395
Medium Bus	1.5	127.5	142.5	234	274.5
Large Bus	2	240	476	448	458
Small Truck	1.5	2,281.5	1,540.5	1,335	2,649
Medium Truck	2	1,044	994	1,764	2,316
10 Wheel Truck	2	802	1,028	1,316	1,024
Trailer	2	752	636	1018	420
Hybrid Trailer	2	60	334	356	190
Motorcycle	0.25	241	358	551	454.25
Total Vehicle	-	7,906	9,782	11,402	10,128

The standard values of traffic capacity in each type of road are set by department of highways [14] as shown in Table 7. Four highways (321, 333, 3342, and 3472) have the capability to support 2,000 PCU per hour as follows

Table 7 Traffic capability by road type [15]

Road type	Traffic volumes (PCU per hours)
2 lanes	2,000
3 lanes	4,000
4 lanes	2,000 per lane

The traffic capabilities in Table 7 with the traffic statistics on highway in Table 6 were compared. The ratio is as follows.

1. Highways No. 321 have the traffic volumes at 40 percent.
2. Highways No. 333 have the traffic volumes at 49 percent.
3. Highways No. 3342 have the traffic volumes at 57 percent.
4. Highways No. 3472 have the traffic volumes at 51 percent.

The ratio implies that, the volume of four highways traffic is moderate and does not affect either of the biomass power plants.

### Measures to Prevent Environmental Impacts

Environmental factors can change at any time.

The measured values may change for many reasons such as of the deterioration of a machine in the power plant when used for a long time or the expansion of a community near to the power plant. Therefore, the guidelines and prevention measures to solve problems that may arise in the future are proposed in this paper.

#### Air Pollution Prevention Measures

1. Define a maintenance schedule to monitor the condition and operation of machines to reduce the pollution from them.

2. Define regularly measured pollution from the power plant's chimney to control the pollutant within standard values.

3. Use water around the power plant's area to reduce the dust around the power plant.

4. Preventive maintenance should be used to prevent machine failure in the power plant.

5. Provide protection cloth and glasses to employees to prevent health problems because of the internal combustion has a large amount of dust from the rice husk processing.

#### Transportation Performance Measures

1. Control the pathway for the power plant's trucks.

2. The truck's speed must be limited by regulation. Cover trucks with burlap to prevent dust from spreading.
3. Avoiding rush hour. (7.00-9.00 am and 4.00-6.00 pm).
4. Define the traffic lanes in the biomass power plant and define traffic signs.
5. Set an employee to control the traffic in and out of the biomass power plant.
6. Provide adequate parking.

## CONCLUSIONS

This research has presented the environmental impact (air and transportation) from a biomass power plant. This research was defined into two steps 1. Study the power plant processes. 2. Study the environmental conditions and measurement of environmental factors in power plant areas. The air monitoring points were established for a village and community near the power plants to study the air quality. The relevant government departments also collaborated to study the traffic volume and statistic relevant to routes for transportation. Results of this research found that the pollutant (Sulfur dioxide, Nitrogen dioxide, Carbon monoxide and total suspended particulate) were within the standards and the volume of traffic on the four highways (321, 333, 3342, 3472) were at 40, 49, 57 and 51 percent. The result implies that the impact of both biomass power plants does not affect air or transportation. Measures to prevent environmental impacts to air and transportation were also presented. Although this research did not clearly conclude that the biomass power plants have an environmental impact or not, in future it would be necessary to study various environmental impacts such as water noise etc to fully confirm that the biomass power plant does not affect the environment.

## ACKNOWLEDGEMENTS

Research project was conducted at the Center for Innovation in Human Factors Engineering and Ergonomics, Department of Industrial Engineering, Faculty of Engineering, King Mongkut's University of Technology North Bangkok.

## REFERENCES

- [1] Electricity Generating Authority of Thailand. Electrical Capacity in Thailand. (Nov. 2016), [https://www.egat.co.th/index.php?option=com\\_content&view=article&id=80&Itemid=116](https://www.egat.co.th/index.php?option=com_content&view=article&id=80&Itemid=116)
- [2] Koornneef, J., Ramírez, A., Turkenburg, W., & Faaij, A. "The environmental impact and risk assessment of CO<sub>2</sub> capture, transport and storage—an evaluation of the knowledge base." *Progress in Energy and Combustion Science*, 38(1), 2012, 62-86.
- [3] Mishra, U. C. "Environmental impact of coal industry and thermal power plants in India." *Journal of environmental radioactivity*, 72(1), 2004, 35-40.
- [4] Singh, G., Kumar, S., Singh, M. K., & Mohapatra, S. K. "Environmental impact assessment of ash disposal system of a thermal power plant." *international journal of hydrogen energy*, 41(35), 2016, 15887-15891.
- [5] Malek, A. A., Hasanuzzaman, M., Rahim, N. A., & Al Turki, Y. A. "Techno-economic analysis and environmental impact assessment of a 10 MW biomass-based power plant in Malaysia." *Journal of Cleaner Production*, 141, 2017, 502-513.
- [6] Wang, Z., Pan, L., Li, Y., Zhang, D., Ma, J., Sun, F., ... & Wang, X. "Assessment of air quality benefits from the national pollution control policy of thermal power plants in China: A numerical simulation." *Atmospheric Environment*, 106, 2015, 288-304.
- [7] Deborah, P., Francesca, V., & Giuseppe, G. "Analysis of the environmental impact of a biomass plant for the production of bioenergy." *Renewable and Sustainable Energy Reviews*, 51, 2015, 634-647.
- [8] United States Environmental Protection Agency. Criteria Air Pollutants.1 (Nov. 2016), <https://www.epa.gov/criteria-air-pollutants>
- [9] Thailand's Pollution Control Department. Act of legislation for controlling pollutions. 1 (Nov. 2016), [http://www.pcd.go.th/info\\_serv/test\\_regulation5.cfm](http://www.pcd.go.th/info_serv/test_regulation5.cfm)
- [10] Leboireiro, J., & Hilaly, A. K. "Biomass transportation model and optimum plant size for the production of ethanol." *Bioresource technology*, 102(3), 2011, 2712-2723.
- [11] Ben-Iwo, J., Manovic, V., & Longhurst, P. "Biomass resources and biofuels potential for the production of transportation fuels in Nigeria." *Renewable and Sustainable Energy Reviews*, 63, 2016, 172-192.
- [12] Kanokporn Jangsawang. 1999. *Environmental Impact Assessment*. 2nd ed. Thai wattana panich publisher.
- [13] Ministry of Industry. Act of legislation for Environmental of factory. 25 (Nov. 2016), <http://www.diw.go.th/hawk/content.php?mode=laws&tabid=1&secid=3&subid=1>
- [14] Department of Highways. The traffic volumes on highways in Thailand 2016. 10 (Feb. 2017), <http://bhs.doh.go.th/download/traffic>

## **THE DESIGN OF AN ALTERNATIVE ENERGY DATABASE IN THAILAND**

Manutchanok Jongprasithporn<sup>1</sup>, Supapat Phuangkaew<sup>2</sup>, Siravitch Atipatha<sup>3</sup>, and Nantakrit Yodpijit<sup>4</sup>

<sup>1</sup>Department of Industrial Engineering, Faculty of Engineering, King Mongkut's Institute of Technology Ladkrabang, Thailand

<sup>2</sup>Center for Innovation in Human Factors Engineering and Ergonomics, Department of Industrial Engineering, Faculty of Engineering, King Mongkut's University of Technology North Bangkok, Thailand

### **ABSTRACT**

Energy is a critical factor for the global economy and development. Fossil fuels (ie, coal, oil, and natural gas) are expensive and linked to health problems. In Thailand, the management of strategic national energy plan is very challenging, especially for alternative energy. Alternative energy is any energy resource that does not consume fossil fuels. Recently, the Ministry of Energy in Thailand launched an Energy Efficiency Plan (EEP) 2015 indicating that 30% of total energy used in Thailand must come from alternative energy. As such, energy plans should rely on informative energy data. The purpose of this research project is to design a database management system for alternative energy in Thailand. The current design of the database management system focuses on seven resources of alternative energy: biomass, biogas, solar power, hydropower, wind, waste, and bio-fuel. Four major user sectors of energy sources are determined for national EEP, including industry, transportation, agriculture, and residential/commercial buildings. However, the use of energy sources for agriculture and transportation (ground and water) are still unclear. Limitations and future work for this research project are also discussed.

*Keywords: Alternative energy, Database, Energy Efficiency Plan (EEP)*

### **INTRODUCTION**

Energy is an important factor that directly affects all people, and fluctuations of energy prices can be high. Therefore, people are interested in researching and understanding energy deeply. Fuels used in energy production are mostly fossil fuels such as oil, natural gas, and coal. Fossil fuels are recognized as the main source of energy for electricity generation, but these fuels tend to run out. Therefore, the idea of supplying an alternative energy sources has been taken into considered. Alternative energy in Thailand today is of high interest because the royal Thai government announced a government policy to use more alternative energy: main energy 30:70 by the year 2070.

Data from alternative energy in Thailand is stored in many departments/offices. Each department has related data from many missions, but data of each department sometimes do not match and finding the central alternative energy database can be hard. Therefore, this research aims to create a system to manage alternative energy databases. The central alternative energy database will be created by data from related departments/offices. This research also presents a web service for users to modify or change data in the central alternative energy data

system.

### **METHODOLOGY**

#### **Database system**

The database system consists of many information structures that are used in a variety of systems, including a system where users can manipulate data, such as adding, modifying, deleting and retrieving information. A reliable database is the key to reducing operation costs[1,2].

#### *Relationship*

Relationship refers to the relationship between entities which can be divided into three types: [5]

1. One-to-One Relationships (1: 1) represents a relationship of information in an entity that is related to information in another entity.

2. One-to-Many Relationships (1: M) represents the relationship of data in one entity that is related to multiple data in another entity.

3. Many-to-Many (M:M) represents the relationship of two entity group data.

#### *Database management system*

Management Information Systems [6] are widely recognized in the globalization era as they facilitate the rapid, efficient and effective business process. One of the information systems that will assist in data management is the database management system [7]. The database management system defines the data in the database and facilitates to record data into the database. The database management system also determines user access level.

### Establish energy database

The steps in this research to create an alternative energy database are shown in Figure 1.

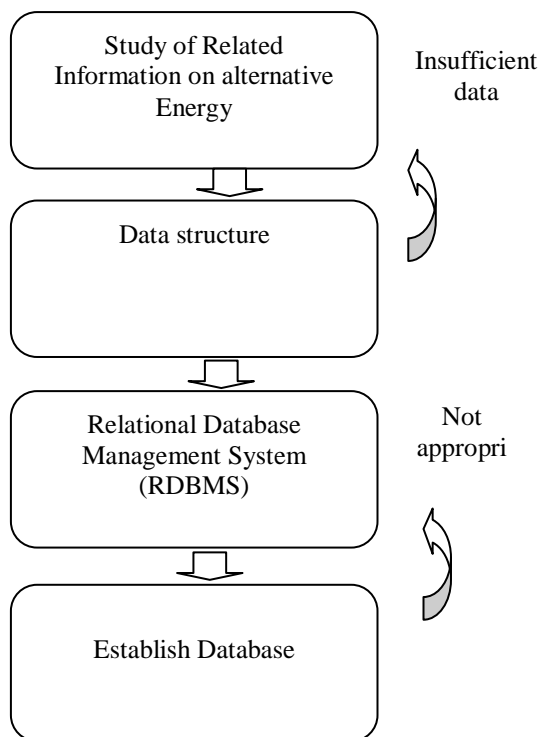


Fig. 1 Operation diagrams.

### Study of Related Information on alternative Energy

This research is incorporation with the royal Thai government ministries to identify all data that related to alternative energy in Thailand. The ministries of Thailand participated in this research included:

1. Ministry of Defence
2. Ministry of Agriculture and cooperative
3. Ministry of Digital Economy and Society
4. Ministry of Commerce
5. Ministry of Finance

6. Ministry of Natural Resources and Environment
7. Ministry of Industry
8. Ministry of Interior
9. Ministry of Energy

The data from 9 ministries was collected to create an alternative energy database.

### Data structure

The Thai energy sector has five key components. The five key components are energy source, energy requirement, regulation and relevant law, related departments/offices, processed. This research set uses the five key components as entity and defines an attribute for each entity. The Entity Relationship Diagram (ER Diagram) is used to explain structure and relation of alternative energy database. Components of ER Diagram are shown in table 1.

Table1 Symbol of components in ER diagram	
Components	Symbol
Entity	
Attribute	
Relationship	

This research has set the Attribute for each entity in this study as follows.

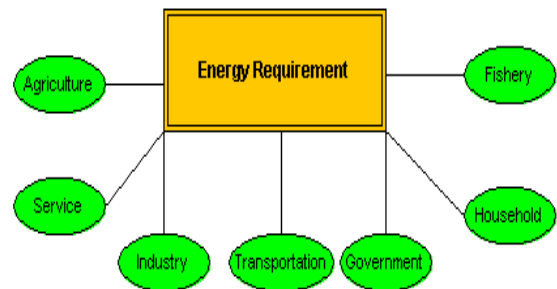


Fig. 2 Attribute of energy requirement

Figure 2 shows attribute of energy requirement. This entity includes seven attributes (Agriculture, Service, Industry, Transportation, Government, Household and Fishery).

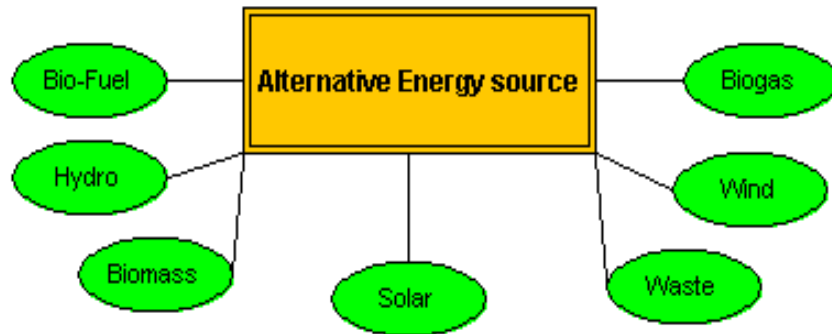


Fig. 3 Attribute of energy source

Alternative energy sources in Thailand are bio-fuel, hydro, biomass, solar, waste, wind and biogas as shown in figure 3. As part of the processes, we studied the process of each department/office and found that the main activates were setting up a board and defining a host. Therefore, an attribute for processes entity was defined as set up board and host as shown in figure 4.

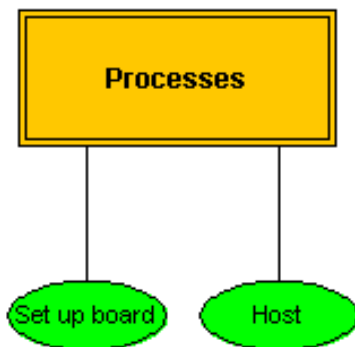


Fig. 4 Attribute of processes

Related departments/offices entities have various departments. The related data from 9 ministries were studied. The results found that related departments/offices totaled 29 departments from 9 ministries and state enterprises. Therefore, this research defined attribute as 2 major attributes (Government ministries and State enterprise).

Regulation and relevant law are a difficult part of this alternative energy database because this entity has lots of details. Moreover, each department has a regulation and relevant law, each relevant law was studied. Moreover, we also compiled an alternative energy database. There entity of regulation and relevant law in this study has two attribute as shown in figure 6.

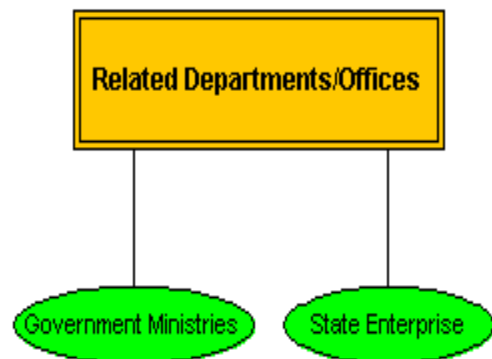


Fig. 5 Attribute of related departments/offices

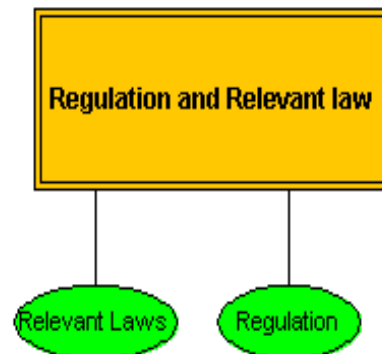


Fig. 6 Attribute of regulation and relevant law

#### *Relational Database Management System (RDBMS)*

The data was collected by the same database in steps 1 and 2. In this step, the relational database management system (RDBMS) was created [8]. The entity relationship diagram (ER Diagram) was used to design the relationship of each entity. Figure 7 shows the relationship between energy requirement and related departments/offices entity. The relationship of entities is one to many relationships (1: M).



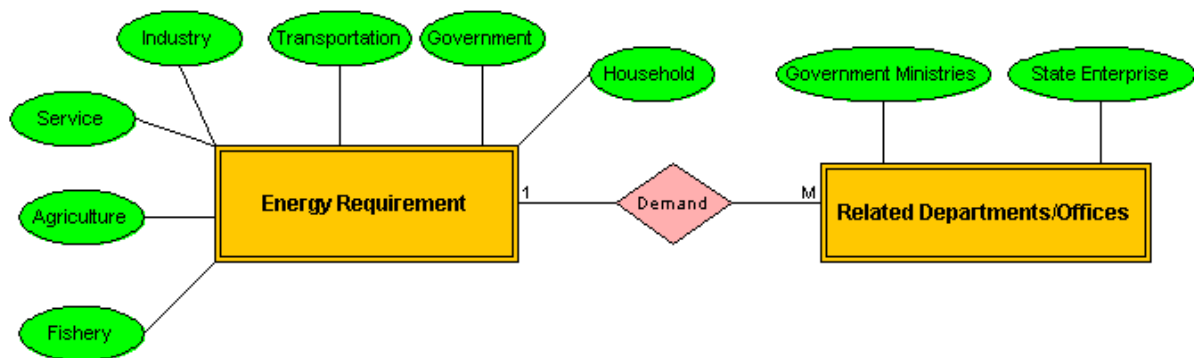


Fig. 7 Relationship of entities

### Establish Database

The operation in Steps 1-3 is complicated because the data linkage cannot be done directly [9]. Therefore, a registration number is used to identify data. Moreover, this defines registration number for all factories [10]. The registration number will be used

as the primary key in the database management. The alternative energy database was then created by dividing this into five groups (alternative energy source, regulation and relevant law, process, energy demand and related departments/offices). Details of the alternative energy database are shown in the ER Diagram in Figure 8.

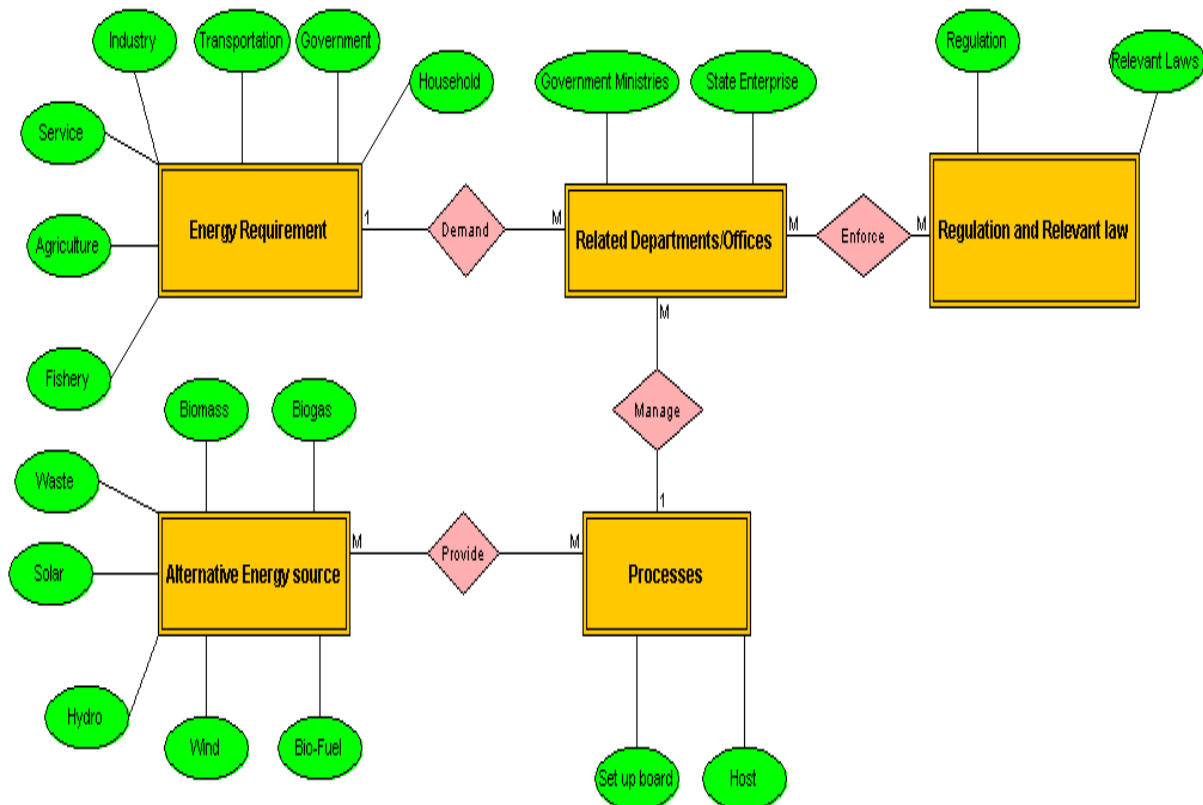


Fig. 8 Entities Relationship Diagram

## RESULTS

The results of this research includes an alternative energy database and networking for web services.

### Alternative energy Database

This research collected data from every entities/attributes from the ER diagram in Figure 8 to create a central alternative energy database. The

central alternative energy data base collect data form  
29

departments from 9 ministries. An example of the data in the central alternative energy database is shown in figure 9.

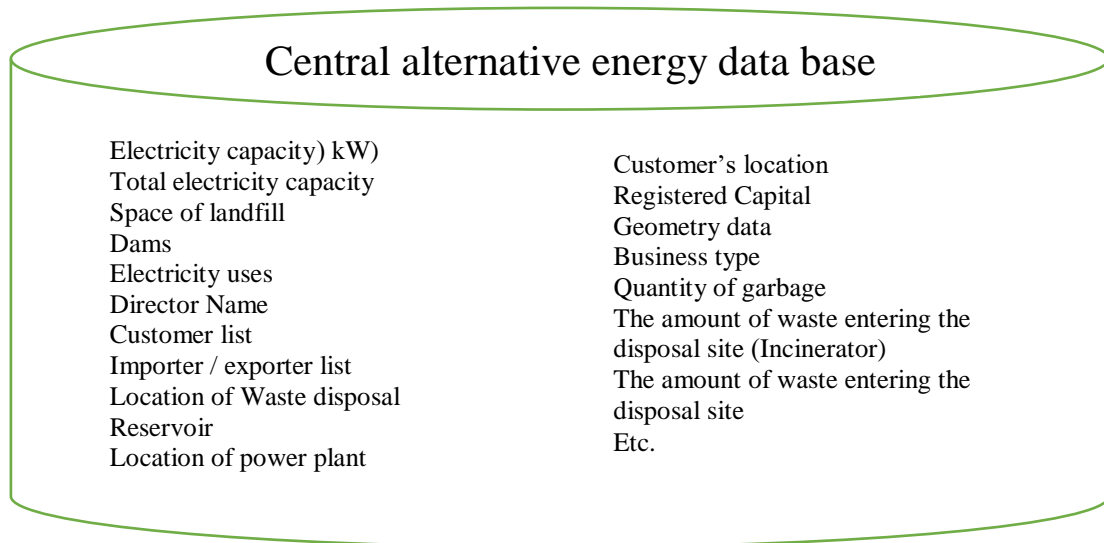


Fig. 9 Example data in energy data base

### Networking for web services

Networks from entities related in figure 8 were linked to create the web services. Users of the central alternative energy data base come from 11 departments/offices. Users can log in to the database

through the web service as shown in figure 10. Users can modify or change data in the central alternative energy database according to the level of the user. The level of user is defined by the admin of the central alternative energy data base.

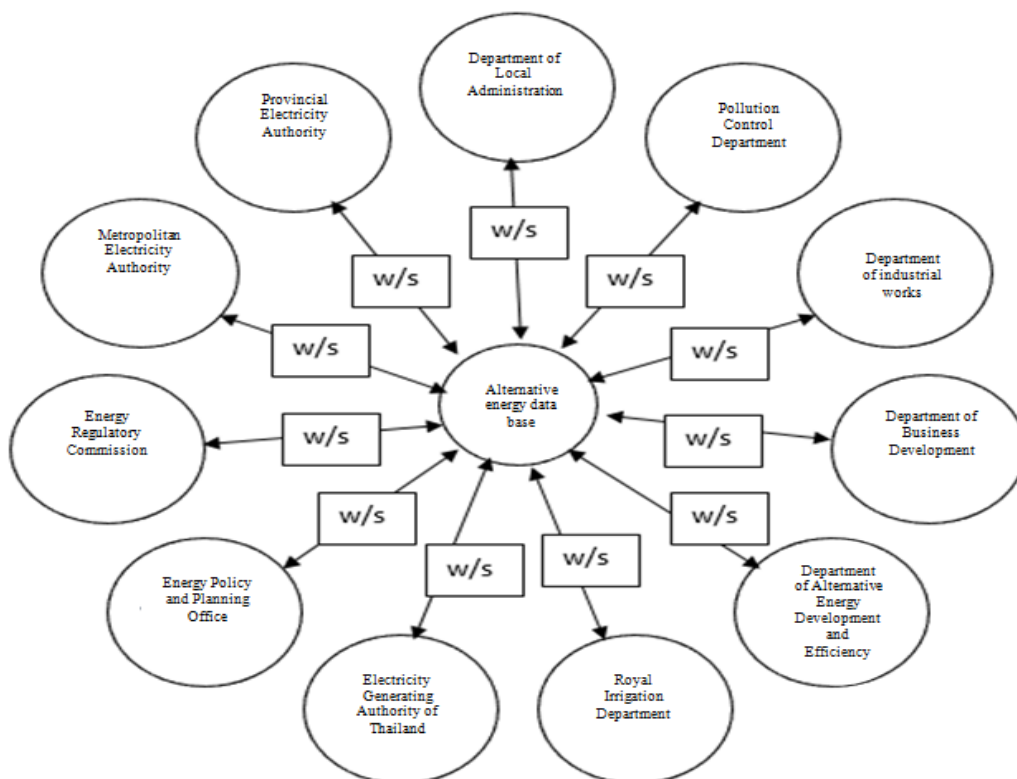


Fig. 10 Web service network diagram.

## CONCLUSIONS

This research has studied the alternative energy situation in Thailand. Relevant data was collected from 9 government ministries and concluded that the 5 core areas are: process, energy demand and related departments/offices. Therefore, we focused on studying in detail each core of data and set the core data as the entities in the database, and also set the detail in each core data as attribute. Then the relationship of each entity was created by the ER diagram. This research established the central alternative energy database by the data from relationship of each entity. The central alternative energy database connects to the databases from various departments/offices, which is defined by a registration number for each part of data. Therefore, all databases will be matched. This research also created a web service to access the central database. The central alternative energy database was connected to 11 departments/offices. The users were given the ability to edit, view, search and modify. The ability of a user was defined by the central admin. The result of this research was a database which is always up to date and matches. In conclusion, the central alternative energy database is an efficient method to manage energy in Thailand especially for the country's alternative energy efficiency plan (EEP).

## ACKNOWLEDGEMENTS

Research project was conducted at the Center for Innovation in Human Factors Engineering and Ergonomics, Department of Industrial Engineering, Faculty of Engineering, King Mongkut's University of Technology North Bangkok.

## REFERENCES

- [1] Lin, M., Wierman, A., Andrew, L. L., & Thereska, E. "Dynamic right-sizing for power-proportional data centers." *IEEE/ACM Transactions on Networking (TON)*, 21(5), 2013, pp.1378-1391.
- [2] Zhou, Y., Taneja, S., Qin, X., Ku, W. S., & Zhang, J. EDOM: Improving energy efficiency of database operations on multicore servers. *Future Generation Computer Systems*, 2017.
- [3] Hernández, J., Gyuk, I., & Christensen, C. "DOE global energy storage database—A platform for large scale data analytics and system performance metrics." In *Power System Technology (POWERCON)*, 2016 IEEE International Conference on (pp. 1-6). IEEE.
- [4] Haas, S., Arnold, O., Scholze, S., Höppner, S., Ellguth, G., Dixius, A., ... & Schiefer, S. "A database accelerator for energy-efficient query processing and optimization." In *Nordic Circuits and Systems Conference (NORCAS)*, 2016 IEEE (pp. 1-5). IEEE.
- [5] Amornsiraphachai, P., & Deejing, K. "THE PERFORMANCE OF UPDATING XML IN TRADITIONAL DATABASES." Nakhon Ratchasima Rajabhat University, Thailand.
- [6] Peeraphatchara, C., & Thalang, S. P. N. "Competitive technological database development project to support technology transfer on internet: Thai cuisine from four regions web database." In 45. Kasetsart University Annual Conference, Bangkok (Thailand), 30 Jan-2 Feb 2007.
- [7] Pho, N., & Prakancharoen, S. "Accuracy Comparison of Waveform Database Generator Data Set Imputation Estimation Using Structural Equation Modeling and Multiple Regression Analysis." *Information Technology Journal*. 13, 2011, 33-39.
- [8] Chutimaskul, W., & Chankham, S. "Distributed Relational Database Management System on PVM." *KMUTT Research and Development Journal*, 23(2), 2000, 47-58.
- [9] Trumpy, E., & Manzella, A. "Geothopica and the interactive analysis and visualization of the updated Italian National Geothermal Database." *International Journal of Applied Earth Observation and Geoinformation*, 54, 2017, 28-37.
- [10] McQueen, J., & Boss, R. W. "Sources of machine-readable cataloging and retrospective conversion." *Library technology reports*, 21(6), 1985, 597-732.

## NUMERICAL INVESTIGATION OF 2D TRAPDOOR STABILITY

Jim Shiau<sup>1</sup>, Mohammad Mirza Hassan<sup>2</sup>

<sup>1</sup>School of Civil Engineering and Surveying, University of Southern Queensland, Australia

### ABSTRACT

This paper investigates numerically the stability of trapdoor problem that is similar to a 2D sinkhole stability analysis. The shear strength reduction technique in the finite difference element software *FLAC* is used to determine factors of safety. The *FLAC* results are then verified by comparing with rigorous upper and lower bound limit analysis results using *OPTUM G2*. Numerical results presented are for various depth ratios in dimensionless forms to establish design charts like in Taylor's slope stability chart. Examples are provided to demonstrate the use of the design chart and table.

*Keywords: Sinkhole, Trapdoor, Stability, Strength Reduction Method, FLAC, OPTUM G2, Design Chart*

### INTRODUCTION

Sinkholes are as old as the age of the earth. The size of sinkholes can be as large as 100 meter or as small as meter or less. Whether it is big or small, it can be deadly and destructive [1]. Office of the internal auditor reported that the program fund in Sinkhole Managed Repair Program (SMRP) has increased from \$50 million in 2015 to \$250 Million in 2016, and this budget is only for in the United States [2].

Sinkholes can be natural or cause by human activities. Natural sinkholes can form by rise of the underground water surface, decrease the underground water piezometric level in the rocks below the surface or frequent fluctuation of the water table beneath. Human activities such as mining and drilling can also expedite the formation of the sinkholes [3].

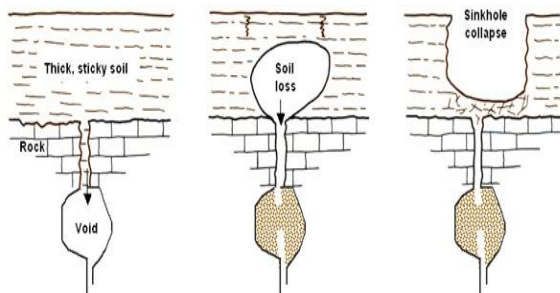


Fig.1 Sinkhole formation [4]

It is well known that sinkhole failure is an extremely difficult situation to investigate, such as the causes of the failure and the actual depth of it [5]. Therefore, researcher are working on the models to simulate, predict and estimate the stability of the sinkholes.

Abdulla [6] tested stability of 51 model through

the centrifuge modelling and developed failure envelope design chart. Broms and Bennermark [7], through the laboratory experiments and the field data collections, proposed the stability number (N). They concluded that the opening will be unstable the overburden pressure  $\gamma H$  is greater than 6~8 times of undrained shear strength of the soil.

Shiau [8] investigated the cause of sinkhole formation and used strength reduction method to analyze factor of safety and failure mechanism of sinkholes by making use of different depth ratios. Besides, both numerical and physical modelling have also been introduced recently in geotechnical education by [15-16]. Tao [9] in laboratory investigated the formation of sinkhole and verified his work by simulating in *FLAC*. The importance of pressure changes in confining layer for sinkhole prediction were discussed by the authors. Yang [10] developed a simplify method to evaluate the stability of the soil in karst and stated that the stability should evaluated with two different conditions. Augarde [11] used finite element limit analysis to obtain the upper bond and lower bond values for loading parameters. Shiau [12-14] extensively studied the pressure relaxation method and created automated mesh generation system using *FISH* programing language in *FLAC* [22-23].

Many researches were conducted on formation and prediction of sinkholes. However, most of those researches are limited to investigation on the cause of formation, failure mechanism or limited to specific geological site, yet there is little research done in producing the dimensionless design chart, which assist the engineers in field to evaluate the stability of the ground and decide whether it is safe regardless of the geographical location. This paper will investigate the stability of the sinkhole by using strength reduction method and presenting the results in form of Factor of Safety. Design charts will be presented dimensionally, just like in Tylor's slope

stability design chart [19]. This will simplify the problem and assist the engineers in making decision with required parameters in the field.

## PROBLEM DEFINITION

Figure 2 shows a schematic diagram of the 2D sinkhole problem and its associated failure surface. For simplicity, this study assumes that no surcharge load acting on the soil surface and the problem can be stated as a Greenfield unsupported condition as in [15].

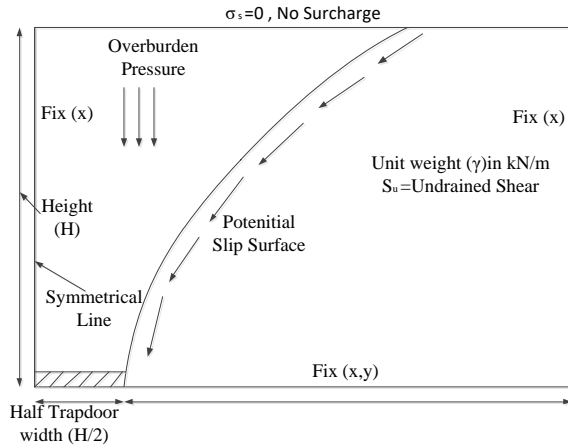


Fig.2 An idealized sinkhole problem.

The soil structure is modelled as uniform Tresca Material, which behaves the same as the Moher-Columb material when the soil friction angle is zero. For this material, the shear strength reduction factor can be represented by a factor of safety that is the ratio of ultimate undrained shear strength ( $S_u$ ) over the undrained shear strength at collapse ( $S_c$ ). This is shown in equation (1).

$$FoS = \frac{S_u}{S_c} \quad (1)$$

In Figure 2,  $W$  indicates the width of cavity opening whilst the depth of sinkhole is denoted by  $H$ . The depth ratio is represented by  $(H/W)$  and the strength ratio ( $SR$ ) of the soil can be defined as  $(S_u/\gamma W)$ . The solutions of factor of safety is therefore a function of the depth ratio and the soil strength ratio.

$$FoS = f\left(\frac{H}{W}, \frac{S_u}{\gamma W}\right) \quad (2)$$

In addition to the *FLAC* program, *OPTUM G2* [20] will be utilized to validate the obtained results. The finite element program *FLAC* and the *OPTUM G2* both has built-in shear strength reduction method to determine the *FOS*. This technique is widely used

in slope stability problem; however it has rarely used to analysis the sinkhole stability. *OPTUM G2* has ability to refine the mesh size by using the mesh adaptively feature or by increase the number of element in mesh to improve the accuracy of the upper bond and lower bound results.

## FLAC MODELLING

Figure 3 shows a typical half mesh adopted for all analyses in this paper using *FLAC*. To allow the downward movement of soil particles under overburden pressure ( $\gamma H$ ), both left and right side boundaries of the model have been restrained in X direction. This is particular important for the symmetrical boundary condition for the left side boundary.

In lower boundary except where the trapdoor opening is, both vertical and horizontal movement of soil particles are prevented. No surcharge has been considered in this paper, and therefore failure occurs only due to overburden pressure.

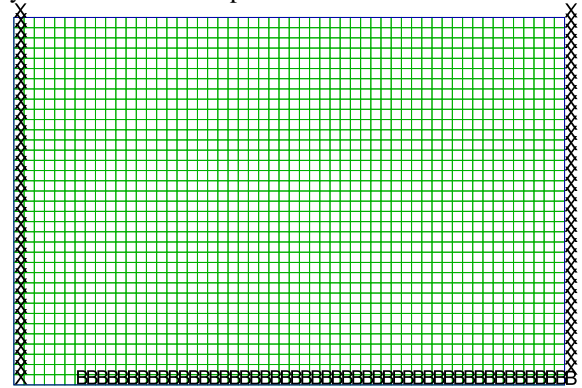


Fig.3 Typical half mesh and boundary condition

A *FISH* script has been developed to generate the mesh in *FLAC* environment and solve for the solution automatically. Using the script, parametric studies can be conducted efficiently and effectively with quick change of material input.

To solve the problem numerically, shear strength reduction method in finite different program *FLAC* has implemented to obtain the factor of safety for undrained clay soil. Using this method, the critical slip failure surface will be located automatically based on the stress failure in finite elements, therefore shear strength failure is appropriate to be used to assist in solving the stability problem [21].

The finite difference *FOS* results obtained from *FLAC* are compared with the rigorous lower bound and upper bound from *OPTUM G2*.

## RESULTS AND DISCUSSION

Based on the previous problem definition, the depth ratio  $H/W$  used in this study ranges from 1 to 10 and the strength ratio  $S_u/\gamma w$  used in this paper

ranges from 0.2 to 2. These parameters will cover most practical cases that practical engineers might face in field.

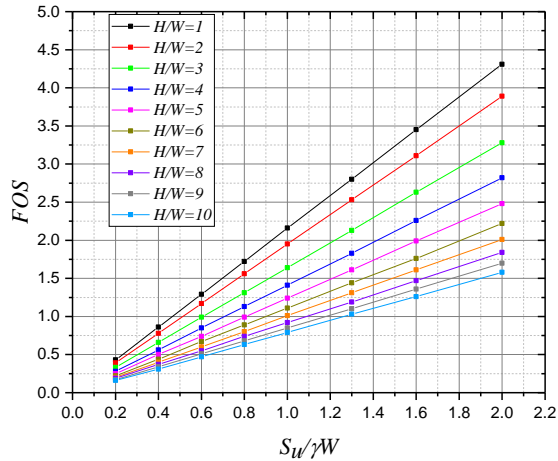
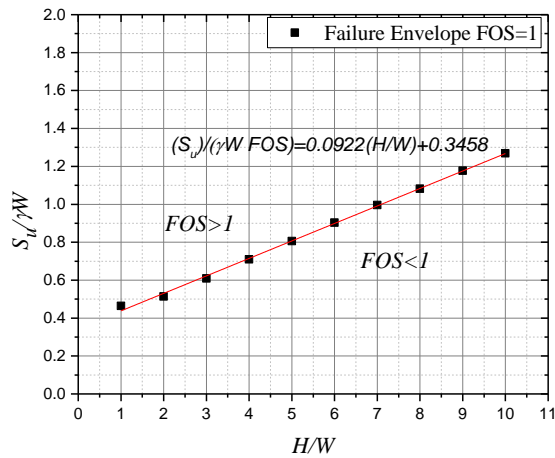


Fig.4 FOS vs shear strength ratio

Figure 4 shows the relationship between factor of safety (*FOS*) and strength ratio  $S_u/\gamma W$  for various depth ratios  $H/W$ , ranging from 1 to 10. It can be seen that the *FOS* increases linearly as the strength ratio increases. Note that the rates of increase are different for various  $H/W$  ratios. The gradient is much small for the deep case  $H/W=10$  than the shallow case  $H/W=1$ . By increasing the soil strength for deep cases is not as effective as that for



shallow cases.

Fig.5 Critical strength ratio – failure envelope

Owing to the linear response in Figure 4, the critical strength ratio  $(S_u)/(\gamma W FOS)$  is shown in Figure 5 for depth ratios of 1-10. This figure highlights the failure envelope for *FOS* of 1. When *FOS*=1, it reduces to a chart similar to Taylor's slope stability design chart where  $(S_u)/(\gamma W FOS) = (S_u)/(\gamma W)$ . The values below the failure envelope indicates an unsafe design where *FOS* < 1, whilst values above the failure envelope categorizes the stable condition which has *FOS* > 1.

$$(S_u)/(\gamma W FOS) = 0.0922 (H/W) + 0.3458 \quad (3)$$

This failure envelope can be represented by equation (3) for practical design purpose. It can be used to determine the critical depth  $H$ , as well as to calculate the critical strength ratio or where the *FOS* is 1.

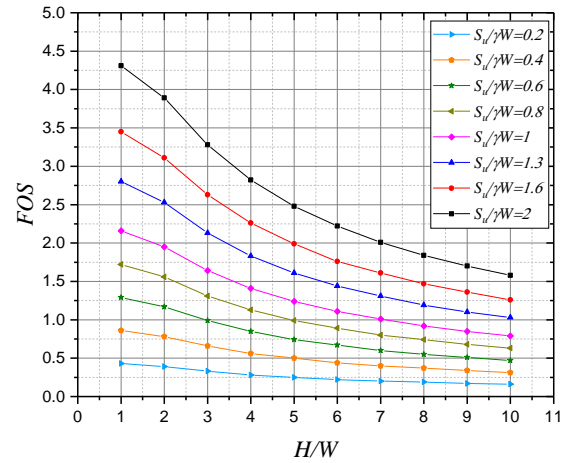


Fig.6 FOS vs. depth ratio

For a given strength ratio  $S_u/\gamma W$ , Figure 6 shows that the *FOS* value decreases non-linearly as the depth ratio ( $H/W$ ) increases. This figure highlights the effect of over burden pressure ( $\gamma H$ ) in these cohesive cases. Given the same strength ratio  $S_u/\gamma W$ , the larger the depth ratio, the larger ( $\gamma H$ ) it is. There is very little arch support for these cohesive cases. This finding is in agreement with Shiau's [22-23], showing the same effect on *FOS*.

Figure 7 shows a typical output plot of shear strain rate (*ssr*) for  $H/W=3$  and  $SR= S_u/\gamma W=1$ . The shear strain rate plot is used to display the possible collapse mechanism. It represents the zone of plastic deformation for the soil particle of such a perfectly elastic-plastic soil model where the actual strain cannot be determined.

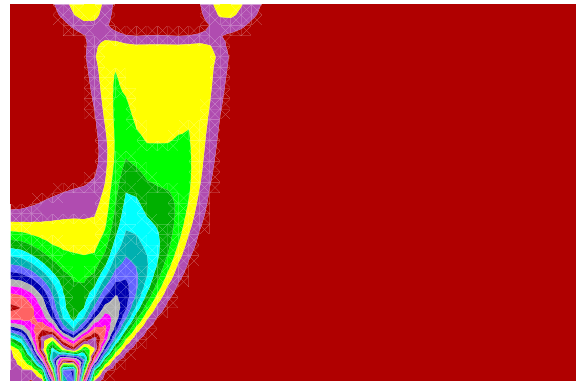


Fig.7 Shear strain rate plot for  $H/W=3$  and  $SR=1$

Figure 8 shows a typical vector plot showing the velocity field. The chosen case is for a depth ratio of 3, where the shear strength ratio  $S_u/\gamma W=1$ .



Velocity vector indicates the movement of soil particles. Vector path shows the direction as well as the magnitude of particle movements. This velocity plot can also be used to determine the overall failure mechanism.

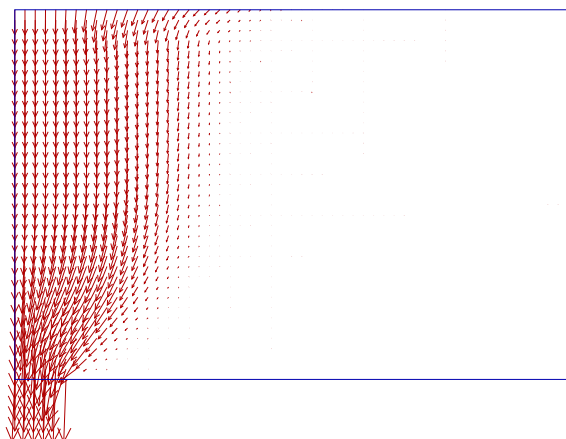


Fig.8 Velocity vector plot for  $H/W=3$  and  $SR=1$

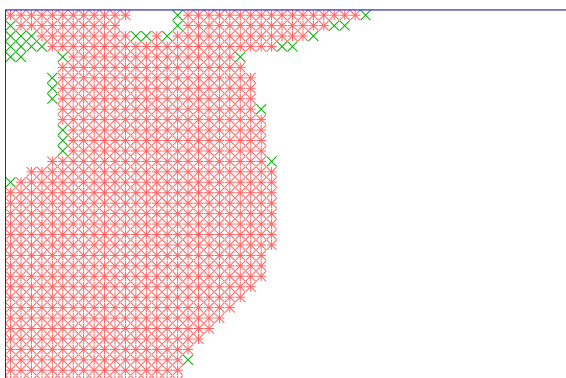


Fig.9 Plasticity indicator plot for  $H/W=3$  and  $SR=1$

Figure.9 presents a typical plot for plasticity indicators. This plot is for a depth ratio  $H/W$  of 3 and  $S_u/\gamma W=1$ . The area shown in (\*) presents the yield zones of soil particles, where the area shown in (x) possessed plasticity in the past but is currently in an elastic state. This typical plot can also be used to determine the likely zones of failure and therefore can be useful for engineering design.

Table.1  $FOS$  results for  $FLAC$ ,  $G2 UB$  and  $G2 LB$  (Strength Ratio;  $SR=1$ )

$H/W$	$G2 LB$	$G2 UB$	$FLAC$
1	1.92	1.976	2.05
2	1.8	1.846	1.89
3	1.546	1.587	1.64
4	1.341	1.378	1.41
5	1.187	1.214	1.24
6	1.061	1.088	1.11
7	0.964	0.988	1.01

8	0.878	0.906	0.92
9	0.811	0.838	0.85
10	0.753	0.779	0.79

## RESULTS VERIFICATION

To improve the confidence in  $FLAC$  results, a comparison is made with those obtained from  $OPTUM G2$  [20] using lower and upper bond analyses.

Table 1 shows the summarized  $FOS$  values obtained from  $FLAC$  and rigorous upper bound and lower bound for the case  $S_u/\gamma W = 1$  and  $H/W = 1$  to 10. Comparison of the two methods reveals that  $FLAC$  produces results that are consistently 3% to 4% higher than upper bound. These results are also shown graphically in Figure 10 for better observation of the comparison trend.

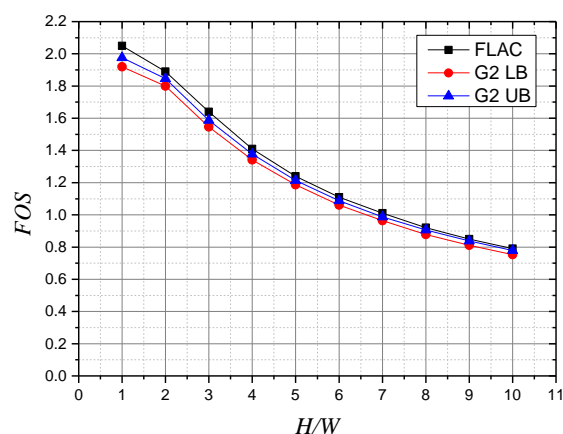


Fig.10 Comparison of  $FOS$  value for  $FLAC$  and  $G2 UB$  and  $LB$

This comparison has successfully validated the usefulness of  $FLAC$  results, and design charts can therefore be produced with high level of confidence in the next section.

## STABILITY DESIGN CHART

In addition to Figures 4-6 where the  $FOS$  can be estimated with input values of  $S_u/\gamma W$  and  $H/W$ , a design chart in form of the contour map is also provided in Figure 11. This chart can be best demonstrated practicality through the number of examples.

### Example of using the stability chart

*Example 1. To determine the factor of safety*

The following data has been provided to geotechnical engineer:  $H=10m$ ,  $W=2m$ ,  $\gamma= 18 KN/m^3$  and  $S_u=50 kPa$ . It is required from the



engineer to determine the factor of safety for such a given system.

1. Given  $H/W=5$ ,  $S_u/\gamma W = 1.39$ , Figure 11 returns approximately a value of  $FOS$  of 1.74. Using Figure 4, the value is 1.73.
2. Using equation 3, a value of  $FOS=1.72$  is obtained.

Actual computer analysis of this case returns the  $FOS$  of 1.76. Based on the results of the above analysis, this trapdoor is potentially stable and no further ground improvement requires.

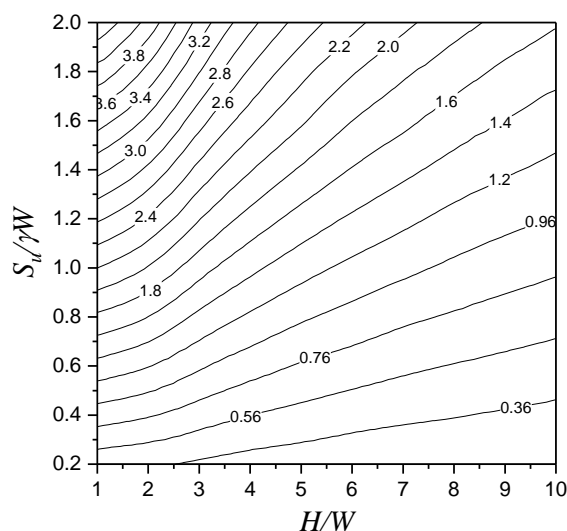


Fig.11 Stability design chart

#### Example 2. Evaluation of the sinkhole depth

Council requires further investigation after heavy rain to estimate the depth of a sinkhole. The following properties are available from previous investigation:  $S_u = 54$  kPa,  $W=3$ m,  $\gamma = 18$  KN/m<sup>3</sup> and  $FOS = 1.5$ .

Using  $S_u/\gamma W = 1$  and  $FOS=1.5$ , equation 3 gives the  $H/W=3.48$ , and the resulting depth  $H = 3.48 \times 3 = 10.44$  m.

#### Example 3. Estimation of Undrained Shear Strength

Geotechnical engineer is required to estimate the undrained shear strength of the soil for a sinkhole. The following data are available:  $FOS=1$ ,  $\gamma = 18$  KN/m<sup>3</sup>,  $H=18$ m and  $W=3$ m.

1. Using equation 3 where  $FOS=1$ , the critical strength ratio  $(S_u)/(\gamma W FOS)$  is 0.622.
2. Undrained shear strength  $S_u$  can then be calculated as 33.61 kPa.

## CONCLUSION

The shear strength reduction method was used in this paper to evaluate the stability of trapdoors. The  $FOS$  results produced in *FLAC* were compared

with rigorous lower and upper bound using *OPTUM G2*. The comparison confirmed the accuracy of these solutions and it greatly enhanced the confidence in using these results.

Both the design charts and equation for the failure envelope were presented to estimate the stability of sinkholes. Examples were illustrated on how to use these design charts and equation. It is recommended that future work be conducted by implementing three dimension models for better understanding of failure mechanism. Other further work such as investigation of surface failure extent and the effect of surcharge loading would improve the study.

## REFERENCES

- [1] Olick, D. (2013). Sinkhole Damage Insurance Claims Are Increasing Significantly In Florida [Online]. Business Insider. Available: <http://www.businessinsider.com/sinkhole-damage-insurance-claims-are-increasing-significantly-in-florida-2013-8/?r=AU&IR=T> [Accessed June 9th 2017].
- [2] Atwood, B & Martins, F. J. (2016). Sinkhole Managed Repair Program. US: Office Of Internal Auditor
- [3] Sowers, G. F. (1996) Building on sinkholes: design and construction of foundations in karst terrain. New York. American Society of Civil Engineers.
- [4] Wisconsin, (2013), Wisconsin Geological & natural history survey, Karst and sinkholes Available: <https://wgnhs.uwex.edu/water-environment/karst-sinkholes/> >. [Accessed 17th June 2017].
- [5] Lei, M., Gao, Y., Jiang, X. & Hu, Y. (2005). 'Experimental study of physical models for sinkhole collapses in Wuhan, China. Sinkholes and the Engineering and Environmental Impacts of Karst.
- [6] Abdulla, W. A. & Goodings, D. J. (1996). Modeling of sinkholes in weakly cemented sand. Journal of geotechnical engineering, 122, 998-1005.
- [7] Broms, B.B. & Bennermark, H. (1967), 'Stability of clay at vertical openings', Journal of the Soil Mechanic & Foundations Division, Proceedings of the American Society of Civil Engineers, vol. 93, pp. 71- 93.
- [8] Shiau, J. S., Lamb B., & Sams, M. S. (2016). The use of sinkhole models in advanced geotechnical engineering teaching. International Journal of Geomate, 10(2): 1718-1724.
- [9] Tao, X., Ye, M., Wang, X., Wang, D., Pacheco Castro, R. & Zhao, J. (2015). Experimental and Numerical Investigation of Sinkhole Development and Collapse in Central Florida.
- [10] Yang, M. Z. & Drumm, E. C. (2002) Stability evaluation for the siting of municipal landfills in karst. Engineering Geology, 65, 185-195

- [11] Augarde, C. E., Lymin, A. V. & Sloan, S. W. (2003). Prediction of undrained sinkhole collapse. *Journal of Geotechnical and Geoenvironmental Engineering*, 129, 197-205.
- [12] Shiau, J. S. and Kemp R. J. (2013). Developing a numerical model for the stability design of tunnel heading. *Third International Conference on Geotechnique, Construction Materials and Environment*, Nagoya, Japan, Nov. 13-15, 2013.
- [13] Shiau, J. S., Sams, M. S., Zhang, J., & Kemp, R. J. (2014). Settlement analyses of underground circular tunneling in soft clay. In *Geotechnical Aspects of Underground Construction in Soft Ground*, Seoul, 347-352.
- [14] Shiau, J. S., Sams, M. S., & Kemp, R. J. (2014). Physical modelling and PIV analyses of an underground tunnel heading. In *Geotechnical Aspects of Underground Construction in Soft Ground*, Seoul, 61-66.
- [15] Shiau, J. S. and Buttlng, S. and Sams, M. (2016) Developing a project based learning assignment for geotechnical engineering. *Electronic Journal of Geotechnical Engineering*, 20(18): 10113-10121.
- [16] Shiau, J. S., Sams, M. S., & Lamb B. (2016). *Introducing Advanced Topics in Postgraduate Geotechnical Engineering Education – Tunnel Modelling*. *International Journal of Geomate*, 10(1): 1698-1705.
- [17] Bishop, AW (1955), ‘The use of slip circle in the stability analysis of slopes’, *Geotechnique*, vol. 5(1), pp. 7-17.
- [18] FLAC (2003), *Fast Lagrangian Analysis of Continua*, Version 5.0, Itasca Consulting Group, Minneapolis, Minnesota, USA.
- [19] Tylor, D.W., (1937). Stability of earth slopes, *J Boston Soc Civil Eng*, XXIV (3) (1937), pp. 337-386
- [20] OptumG2 (2016), *Optum Computational Engineering*, Standard Version, Newcastle, Australia.
- [21] Matsui, T. & San, K.-C. 1992. Finite element slope stability analysis by shear strength reduction technique. *Soils and foundations*, 32, 59-70.
- [22] Shiau, J, Sams, M & Chen, J (2016) Stability design charts for unsupported wide rectangular tunnels. *Electronic Journal of Geotechnical Engineering*, 21(1): 139-150.
- [23] Shiau, J, Sams, M & Chen, J (2016) Stability charts for a tall tunnel in undrained clay. *Electronic Journal of Geotechnical Engineering*, *International Journal of Geomate*, 10(2), Japan: 1764-1769.

# INSTALLATION CONSTRAINTS OF SUCTION ASSISTED FOUNDATIONS AND ANCHORS FOR OFFSHORE ENERGY DEVELOPMENT

Kingsley Osezua Akeme<sup>1</sup>, Alireza Rezagholilou<sup>2</sup> and Meysam Banimahd<sup>3</sup>

<sup>1,2</sup>Petroleum Engineering Department, Curtin University, Australia; <sup>3</sup>Adjunct Research Fellow, University of Western Australia, Australia.

## ABSTRACT

The application of suction caissons have been increased over the last two decades for offshore energy developments. Their installation challenges in different seabed types affect their execution process and load bearing capacity. Hence, the identification of these challenges and understanding of their root causes are highly important. As such, this paper aims to review the recorded installation constraints due to different seabed conditions, discuss the various factors related to each of these constraints, and finally provide some suggestions to rectify each constraints and/or its relevant factors. To do so, the approach is to evaluate the geological (geophysical and geotechnical) conditions in multiple case studies and analyze the stability of suction caisson installation in different soil types. Results show that some factors such as: buckling, plug heave, soil piping, bottom resistance failure and high penetration resistance can exist in both homogeneous and heterogeneous seabed conditions, and the uncertainties of soil parameters or behavior, add more complexities into the above factors. Therefore, a good understanding of the seabed conditions and soil parameters before and during installation, as well as constant monitoring of the induced suction created with respect to the penetration depth is essential to mitigate the likely issues.

## INTRODUCTION

### Definition

Suction assisted caissons have been defined as large cylindrical steel structures of 5- 7m diameter opened at the base and closed by a lid at the top. The top contains a “valve controlled vent” which allows the escape of water from the caisson during installation (T. I. Tjelta 2001; Aubeny, Murf and Moon 2001; El-Sherbiny 2005). However in more detail, they are defined as foundation structures that are installed as a result of a differential pressure created within the caisson compartment through the application of a pump attached to the caisson top which reduces the internal pressure within the caisson compartment as shown in Fig 1.

Suction caissons are classified into two categories based on their application and function. By application, they are classified as: (1) Compression caisson foundations when they are used in shallow water applications as foundation supports, and as (2) Suction anchors when they are used in deep water applications as mooring and anchoring supports (Cao, et al. 2002; Tran, Airey and Randolph 2005).

In terms of their function, they are classified either as (1) an integrated foundation structure when they are attached to the base of a foundation structure e.g the Gullfak C platform, or as (2) a standalone structure when used for mooring and

anchorage support (M. N. Tran 2007). Some examples of other suction assisted foundation and anchors include: suction anchor, suction pile, bucket foundation, skirted foundation and skirt piles etc.



Fig 1 A Cluster of suction anchors (Adapted from M. N. Tran 2007)

### Installation Procedure

In general, suction assisted foundations and anchors have the same installation principle in which a suction induced force is required for their penetration into the seabed. Also, their installation process occurs in two-stages. *In the first stage*, they penetrate into the seabed by virtue of their self-weight. As the process occurs, the water displaced inside the caisson is evacuated through an open vent. The velocity of water that can be discharged

through the open vent with respect to the over pressure within the suction caisson is given by the following equation:

$$V = C \sqrt{\frac{2P}{\rho_{sw}}} \quad \text{when an Orifice is used} \quad (1)$$

$$V = \sqrt{\frac{2P}{\rho_{sw} \sum K_i}} \quad \text{when a piping system (valve) is used} \quad (2)$$

Where  $V$  = steady velocity of water flow,  $C$  = Coefficient of discharge ( $C=0.61$  for sharp edged orifice surface and  $C=$  for sharp edged orifice surface with short tube),  $P$  = over pressure in the suction caisson,  $\rho_{sw}$  = sea water density, and  $K_i$  = Resistance coefficient for the piping system ( $\sum K_i = 1.7 - 1.8$  for a 2 ft or 3 ft diameter butterfly valve system).

However, suction caisson would stop penetrating under its own weight when the soil resistance, including external and internal frictional resistances and tip resistance is equal to the weight of the suction caisson (Huang, Cao and Audibert 2003).

An important phenomenon in this stage is the formation of a *seal* between the seabed surface and the caisson. The importance of the seal is to prevent the formation of *localized piping and loss of suction* during penetration. It is thus important that the seal formed must be sufficient in order to guarantee suction assisted penetration. However, if an insufficient seal is formed this would result to failure of the entire installation process (Cao, et al. 2002; Sukumaran 1999).

The second stage consist of the later part of the penetration process of arriving at the design depth. This is achieved by the application of an additional installation force which is provided in the form of an under pressure or suction created by pumping water out of the caisson through a “submersible pump” attached to the top of the caisson (Cao, et al. 2002; Sukumaran 1999; Housby and Byrne 2005) as shown in Fig 2. The suction generated, is the total pressure difference between the caisson internal vacuum pressure and the external hydrostatic pressure. If the pressure difference created is relatively higher than the external hydrostatic pressure, the suction caissons may *buckle* during installation. Also, an excessive under pressure or suction created within the caisson compartment could result in the upward movement of the internal soil within the caisson which could lead to *plug failure*. Therefore, the amount of suction available for penetration ranges from a minimum value when the caisson internal pressure is at zero absolute pressure to a maximum value (*allowable suction*) which corresponds to the point

where the water within the caisson begins to vaporise. This maximum value is equal to sum of the atmospheric pressure and hydrostatic pressure outside the caisson. Once the design depth has been reached, the valve at the top is closed and a passive suction is generated within the caisson. This passive suction increases the holding capacity (pull-out resistance) of the caisson by engaging negative pore pressure from the soil plug inside and at the bottom of the caisson (Cao, et al. 2002; Sukumaran 1999; Cao, et al. 2003; Sparrevik 2002).

Generally, the allowable suction for caisson penetration before plug failure (Reverse end bearing failure) occurs can be calculated using the following equation:

$$P_{all} = F_{in} / A_{in} + Q_u / (A_{in} FS) \quad (3)$$

Where  $P_{all}$  = allowable suction,  $F_{in}$  = internal caisson wall frictional resistance,  $A_{in}$  = Caisson internal crosssectional area,  $Q_u$  = reverse end bearing over the all soil plug area at the caisson tip,  $FS$  = factor of safety (Huang, Cao and Audibert 2003).

Once the suction assisted foundation has been installed, a set up time is allowed to enable the surrounding soil regain some of its strength lost during installation before any load attachment is done. During this period the caisson remains unloaded. Set up time is mostly observed during mooring application (Tran, Airey and Randolph 2005).

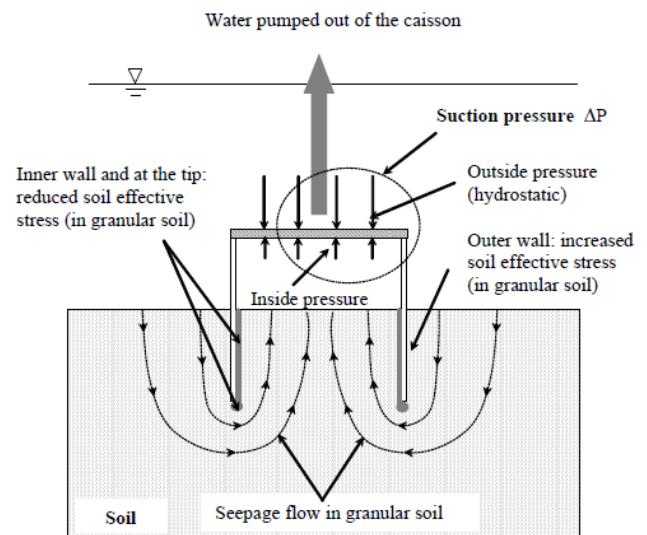


Fig 2 Suction installation process (Adapted from Tran MN 2007)

## METHODOLOGY

The approach adopted in achieving the

objectives of this paper is carried out in two parts. The *first part* is a review of the geological (geotechnical and geophysical) survey conducted before and during installation as well as the stability assessment of suction caisson during installation. While the *second part* is a comparative analysis of the installation issues of suction assisted foundations and anchors obtained from literature reviews and over 50 case study field reports

### Geological Properties of Soil That Affects the Installation and Load Bearing Capacity of Suction Caissons

Prior to the installation of suction caissons, a proper site investigation is conducted in order to select the right location for installation, and also to establish the geotechnical installation parameters needed for a successful installation campaign. To this end, a geotechnical survey involving in-situ and laboratory tests is conducted in order to obtain information about the soil properties such as: soil index properties, in-situ stresses and stress history, the soil shear strength profile (undrained and undrained conditions) etc.

The following geotechnical soil attributes below are considered very important during the installation of suction caissons at the design stage in order to accurately predict the likely installation issues that may be encountered during installation. These soil attributes are:

#### Set up/consolidation effects

This is a phenomenon due to the timely dissipation of excess pore water from the soil particles which results to an increase in the soil effective stress. The time of soil consolidation, need to be accurately predicted and monitored during installation in order to understand the soil strength conditions during penetration so as to regulate the rate at which suction is applied in order to avoid a *punch through* or *plug failure* during installation. For example, the soil strength gained during self-weight penetration takes much longer time than the soil strength gained during suction assisted penetration for different soil types. Also, the rate of soil strengths gained by soil particles outside the caisson wall is faster when compared to the soil strength gained by soil particles inside the caisson wall due to the differences in their drainage paths (Sukumaran 1999; Sharma 2005).

#### Soil permeability profile

The permeability of the subsurface soil and drainage paths determines the magnitude of suction the caisson can accommodate and sustain. The

more permeable the soil is, the faster the loss of suction under sustained tension loads. The permeability of the soil is very important especially in sand during installation so as to avoid *soil piping* and the possibility of having a *bottom resistance failure* (Huang, Cao and Audibert 2003).

#### Soil strength profile

This comprises of the drained and undrained shear strength profile of the soil from the mud line down to the seabed. This is very important to know especially in homogeneous clay soils and in layered structured soils in order to avoid *plug heave* and *punch through* during penetration (Huang, Cao and Audibert 2003).

#### Seabed topographical irregularities

The uneven nature of the seabed could cause problem during installation especially for suction caissons in cluster form where *cracks* are formed in the caisson walls during penetration. To overcome this challenge, an optimal levelling procedure of the suction caisson should be done immediately after self-weight penetration process but before the suction assisted penetration process begins. The levelling of the uneven section of the caisson should be carried out in small monitored steps (T. I. Tjelta 2001; Sukumaran 1999; Sharma 2005)

#### Penetration resistance

This is a measure of the soil shear strength conditions (drained and undrained conditions). The soil shear strength increases gradually with depth depending on the soil density profile. The soil penetration resistance is the sum total of the penetration resistance experienced during self-weight and suction assisted penetration(s). It comprise of the total internal and external caisson wall resistance and the caisson tip resistance altogether.

The following Eq. (4) – (7) shows the relationship between penetration resistance and the penetration depth that could be achieved during installation in clay and sand soils.

For self-weight penetration in clay soil

$$V' = h \alpha_o S_{u1} (\pi D_o) + h \alpha_i S_{u1} (\pi D_1) + (\gamma' h + S_{u2} N_c) (\pi D t) \quad (4)$$

For suction assisted penetration in clay soil before reverse bearing failure (plug failure) occurs

$$V' + N_c^* S_{u2} \frac{\pi D_i^2}{4} = h \alpha_o S_{u1} (\pi D_o) \left[ 1 + \frac{D_1^2}{(D_m^2 - D_o^2)} \right] (\gamma' h$$

$$+ S_{u2} N_c) (\pi D t) \quad (5)$$

For self-weight penetration in sand considering the effect of stress enhancement along the caisson walls and tip

$$V' = \int_0^h \sigma' v_o dz (K \tan \delta)_o (\pi D_o) + \int_0^h \sigma' v_1 dz (K \tan \delta)_i (\pi D_i) + \sigma'_{end} (\pi D t) \quad (6)$$

For suction assisted penetration in sand before reverse bearing failure (plug failure) occurs while considering the effect of stress enhancement along the caisson walls and tip

$$V' + S \left( \frac{\pi D_i^2}{4} \right) = \int_0^h \sigma' v_o dz (K \tan \delta)_o (\pi D_o) + \int_0^h \sigma' v_1 dz (K \tan \delta)_i (\pi D_i) + (\sigma' v_1 N_q + \gamma' t N_\gamma) (\pi D t) \quad (7)$$

Where  $V'$  = Effective vertical load,  $h$  = installed depth of caisson,  $\alpha_o$  = adhesion factor on outside caisson wall,  $\alpha_i$  = adhesion factor inside of caisson wall,  $S_{u1}$  = average shear strength over depth of skirt,  $S_{u2}$  = shear strength at caisson skirt tip,  $D_o$  = caisson diameter outside,  $D_i$  = caisson diameter inside,  $D$  = caisson diameter,  $t$  = caisson wall thickness,  $N_c$  = Bearing capacity factor (cohesion),  $\pi = 22/7$ ,  $N_c^*$  = Bearing capacity failure factor,  $\gamma'$  = effective unit weight of soil,  $D_m$  = caisson diameter as a result of enhanced stress,  $k$  = factor relating vertical stress to horizontal stress,  $\sigma' v_o$  = effective vertical stress outside the caisson,  $\sigma' v_1$  = effective vertical stress inside the caisson,  $\sigma'_{end}$  = effective vertical stress at the caisson tip,  $\delta$  = interface friction angle,  $s$  = suction within the caisson with respect to the ambient seabed water pressure,  $N_q$  = Bearing capacity factor (over burden),  $N_\gamma$  = Bearing capacity factor (self-weight) (Houlsby and Byrne 2004).

#### Soil sensitivity

This refers to the soil- stress conditions during penetration. It is very important during suction caisson installation. The sensitivity of the soil is critical in predicting the self-weight penetration depth of the caisson; and also in estimating the caisson's pull-out capacity immediately after installation (Huang, Cao and Audibert 2003).

#### Set down scour

This is an uneven seabed condition which could likely occur very rapidly as the caisson approaches the seabed during installation. During self-weight penetration, set down scour decreases the soil

resistance (soil strength) of the soil around the caisson where it occur. This could lead to *punch through failure* during penetration (Senders, Randolph and Gaudin 2007; Senders and Randolph 2009).

#### Soil stiffness

This parameter is used to analyze the horizontal displacement of suction caisson under loading conditions. Fig 3, demonstrates how large horizontal deflections are generated which alters the stress state of the soils around the caisson thereby leading to the formation of soil gaps around the back of the caisson. The gap created around the caisson could become a channel path for the flow of seawater into the caisson which could result into *soil piping or boiling failure*. Therefore, predicting accurately the caisson lateral displacement and the associated moment distribution along the caisson length is a critical factor in determining the suction caisson load bearing capacity (Huang, Cao and Audibert 2003).

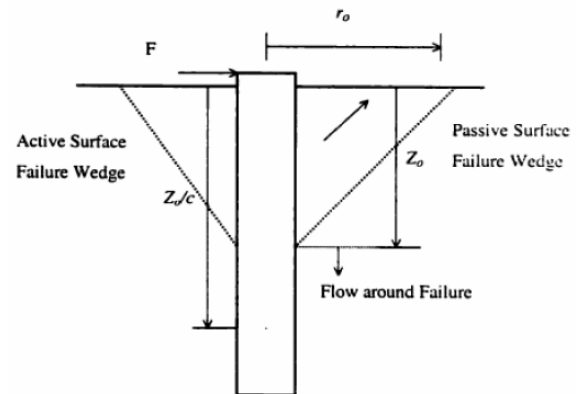


Fig 3 Failure mechanism and padeye optimization (Adapted from Tran MN 2007)

#### Load Bearing Capacity Factors

From the review of literatures and practical research works, some key factors that could affect the load bearing capacity of suction caisson were identified. These factors include:

##### Loading condition

Suction caissons are subjected to vertical, horizontal and moment loads during installation which may affect their load bearing capacity. These loads have different loading duration which produces different drainage conditions. Thus they require continuous monitoring of the load patterns during installation especially the hydrodynamic horizontal and moment loads (Huang, Cao and Audibert 2003).

*Suction caisson geometry- (Aspect ratio)*

*Aspect ratio (L/D)* is the limiting factor for the maximum penetration depth during installation (Sparrevik 2002). Suction caissons with high aspect ratios may be prevented from reaching the design penetration depth during installation when failure such as *plug heave* or *buckling* occurs. Another area of concern is the retrieval process where suction caissons with high aspect ratios are difficult to retrieve. It is therefore very important that during the installation process, the soil conditions are monitored and the rate of suction application is controlled (T. I. Tjelta 2001).

Table 1 below shows the aspect ratios for specific foundations systems and anchors with respect to the water depth, while Table 2 shows the range of Aspect ratios to be applied in different seabed locations as analyzed from the review of over 50 case study field reports

Table 1 Suction caissons applications vs aspect ratios from case studies reviewed from 1958 – 2014 (M.N Tran 2007, T.I Tjelta 2001)

Foundation System	Aspect Ratio	Water Depth (m)	Type of Suction Caisson	Platform
Foundation	0.3 - 1.7	25 - 220	Skirt foundation, skirt pile and bucket foundation	Fixed
Anchoring	0.71 - 5.3	20 - 1800	Suction Anchors and Suction Pile	Floater
Mooring	1.4 - 5.6	30 - 1920	Suction Anchors and Suction Pile	Floater

Table 2 Aspect ratio Vs seabed location from case studies reviewed from 1958 – 2014 (M.N Tran 2007, T.I Tjelta 2001)

Seabed Location	Soil types	Aspect Ratio	Water Depth (m)
Gulf of Mexico	Soft clay	5 - 5.6	1800 - 1920
West Africa	Soft clay	2.2 - 4	350 - 1400
North Sea	Soft Clay, Dense Sand, layered Clay (Soft Clay overlying Stiff Clay), Dense Sand overlying Stiff Clay, Soft Clay overlying Dense Sand	0.36 - 3	40 - 1050
South China Sea	Soft Clay	2	30
Japan	Layered Soil (Sand overlying Clay)*	0.3	25
Timor Sea	Carbonate (Soft clay overlying cemented soil layers)	2.4	400
Irish Sea	Sand (Dense Loose)*, Layered Soil (Clay overlying Sand)*	0.6	33
UK Lakes	Soft Clay	2.7	20 - 80
Baltic Sea	Clay overlying sand	2.1	357 - 384
Brazil	Soft Clay	1.7-3.6	720 - 1200
Adriatic	Layered Clay (Soft Clay overlying Stiff Clay)	3.2-3.6	850

\*= Not clearly stated

*Mooring/chain line attachment point (padeye)*

This is a very critical aspect during the installation of suction caissons when they are used as mooring or anchorage support. A mooring system under tension loads from a floating structure transfer the tension loads to the suction caisson via steel chains attached to the padeye. The padeyes are located along the caisson wall and they occupy about 5 to 10% or more of the caisson length. During installation, the padeyes alongside with the steel chain creates a groove in the soil as the suction caisson penetrates deeper into the soil. The groove created could also be a drainage path for soil piping failure to occur.

After the design penetration depth has been reached, the steel chain assumes the shape of a reverse catenary as a result of: (1) the tension loading on the steel chain, (2) the soil bearing resistance, (3) the frictional resistance along the embedded chain length, (4) the chain angle at the mud line, and (5) the chain weight during penetration.

To ensure that there is no rotational movement of the suction caisson during ultimate loading conditions, the mooring lines or chains should be attached to the padeye at the *optimal position*. This is important because, a larger amount of the ultimate load (weight of the floating platform + environmental loads) is transferred in the lateral direction to the caisson. This ensures that the caisson is operating at full capacity. However, if they are attached below or above the optimum load attachment point, the caisson will be operating at low capacity. This is because, more of the



foundation loads will be transferred in the vertical direction resulting in the vertical and rotational movements of the suction caisson. This would cause the caisson to buckle, or become unstable which may eventually reduce its load bearing capacity as shown in Fig 4 (T. I. Tjelta 2001, Sharma 2005, Randolph, et al. 1998), Huang, Cao and Audibert 2003).

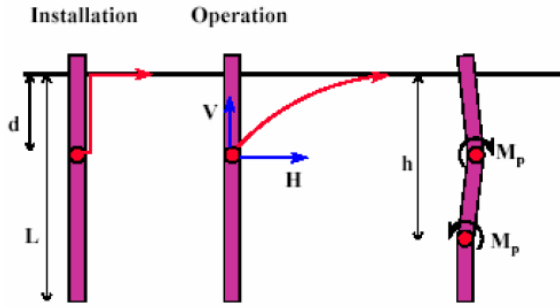


Fig 4 Buckling of anchor piles under tension loading (Adapted from Sharma 2005)

#### The “required suction” for penetration

This is the suction created within the caisson when water is pumped out through the pump during the suction assisted penetration stage. The amount of suction that can be accommodated and sustained during this process, greatly depends on the permeability of the sub surface soil and drainage paths. For example, highly permeable soils experience a higher suction decrease compared to less permeable soils. Thus, the required suction to install the caisson to the required depth is given by using the limit equilibrium equation:

$$P_{req} = (R - W_p) / A_{in} \quad (8)$$

Where  $P_{req}$  = required suction,  $R$  = soil resistance at different penetration,  $W_p$  = submerged suction caisson weight,  $A_{in}$  = suction caisson internal top cross sectional area (Huang, Cao and Audibert 2003).

As a rule of thumb, the *required suction* for penetration must be less than the maximum suction for all soil conditions. For example in soft clay soils, the ratio between the maximum suction and the required suction should be equal to at least 1.3 before failure occurs, but when failure occurs, the ratio should be greater than 1.3 (Sparrevik 2002).

#### The maximum allowable suction limit

This is a very critical aspect that is responsible for the installation of suction caissons and the

failure modes experienced during their installation. Zen (2016) derived the equations to calculate the limiting suction for plug heave in clay as shown in “Eq. (1)” and also an equation to calculate the critical suction for piping (boiling) in sand as shown in “Eq. (2)”.

$$P_{sc} = (d - \delta) \gamma' \quad (9)$$

$$P_{sc} = (2d - \delta) \gamma_w i_c \quad (10)$$

Where  $P_{sc}$  = Maximum suction or Plug heave suction,  $d$  = Diameter of the suction caisson;  $\delta$  = Displacement of the soil surface inside the foundation;  $i_c$  = Critical hydraulic gradient (mostly  $i_c = 1$ );  $\gamma'$  = Submerged unit weight of soil; and  $\gamma_w$  = unit weight of water (Zen and Hirasawa 2016).

#### Tilting/misalignment

The risk of misalignment of the caisson during installation could affect the load bearing capacity of the caisson due to the uneven load distribution as a result of the either the improper levelling of the caissons after touch down, buckling of the caisson, or attaching the steel chain or mooring lines to the padeye above or below the optimal position (Sharma 2005; Randolph and House 2002).

2005; Randolph and House 2002).

#### The type of installation used

The type of installation used (e.g. lift installed or launched installed) and their associated failure modes (e.g. fatigue and corrosion etc.) could reduce the stiffness and load bearing capacity of suction caissons (T. I. Tjelta 2001).

#### The pump requirement capacity

Identifying the right pump capacity for suction caisson installation in different soil types is very important. The pump capacity is very important in the installation process because it creates the suction required for penetration and also the penetration rate limiting factor.

Houlsby and Bryne (2004), proposed a formula for calculating the pumping requirement for caisson installation in clay refer to “Eq. (10)” and also in sand refer to “Eq. (11)”

$$Q = \frac{\pi D_i^2}{4} V \quad (11)$$

$$Q = \frac{\pi D_i^2}{4} V + F \frac{SKD}{\gamma_w}$$

(12)

Where Q= Pump capacity or required flow rate; V= Vertical penetration velocity; Di= Caisson internal diameter; D= Caisson outer diameter; F= Dimensionless quantity that depends on h/D (where h is the penetration depth), K is the sand permeability; s= suction within the caisson with respect to the ambient seabed water pressure, and  $\gamma_w$  = unit weight of water.

The above formula shows that the pumping requirement for sand is greater than that for clay due to the high seepage flow generated during caisson

Due to the high seepage flow generated during caisson installation in sand requirement for sand is greater than that for clay due to the high seepage flow generated during caisson installation in sand.

### Comparative Analysis of Suction Caisson Installation Issues, Their Causes and Possible Solutions in Different Seabed Conditions

From the review of suction caisson installation from literature reviews and 50 case study field reports, the results obtained are summarized in Table 3 and Fig 4.

**Table 3 Suction caisson installation issues in different seabed conditions (M.N Tran 2007, pp. 112, T.I Tjelta 2001, pp. 3, Colliat and Dendani 2002, Kolk, et al. 2001, Houlsby and Byrne 2004, Randolph and House 2002)**

Soil Density	Installation Issues	Seabed Location
Soft Clay	PH, B, SP, and BRF	Gulf of Mexico, West Africa, Brazil, North Sea, South China Sea and UK Lakes
Stiff Clay	IS, SP, BRF, and HPR	
Soft Clay Over Stiff Clay	HPF, BRF, SP, B and PH	North Sea and Adriatic Sea
Stiff Clay Over Soft Clay	HPR, BRF, IS, SP, and PTF	
Loose Sand	L, SP, B, PH and BRF	Irish Sea*
Dense Sand	SP, B, PH, BRF and HPR	Irish Sea* and North Sea
Loose Sand Over Dense Sand	L, SP, B, PH, HPR and BRF	Irish Sea* and North Sea*
Dense Sand Over Loose Sand	SP, B, PH, BRF, PT and HPR	
Loose Sand Over Soft Clay	PT F, PH, B, SP and BRF	Japan*
Soft Clay Over Loose Sand	SP, PH, B, BRF and HPR	Irish Sea* and Baltic Sea*
Dense Sand Over Soft Clay	PH, B, BRF, PT F, SP and HPR	Japan* and North Sea*
Soft Clay Over Dense Sand	HPR, BRF, PH B and SP	North Sea and Baltic Sea*
Stiff Clay Over Dense Sand	HPR, BRF, IS, SP, and PTF	
Dense Sand Over Stiff Clay	SP, B, PH, BRF and HPR	North Sea
Silt (Homogeneous/Layered)	HPR, SP, BRF, PH, B	
Soft Clay Over Cemented Soil	SP, B, PH, BRF and HPR	Timor Sea
Cemented Soil Over Sand/Clay Soil	HPR and PT F	

\* = Not clearly stated

PH= Plug Heave, B= Buckling, SP= Soil Piping, BRF= Bottom Resistance Failure, HPR= High

Penetration Resistance, IS= Insufficient Sealing, PTF= Plug Through Failure, L = Liquefaction

**Suction Caisson Installed in Different Seabed Conditions From 1958 - 2014**

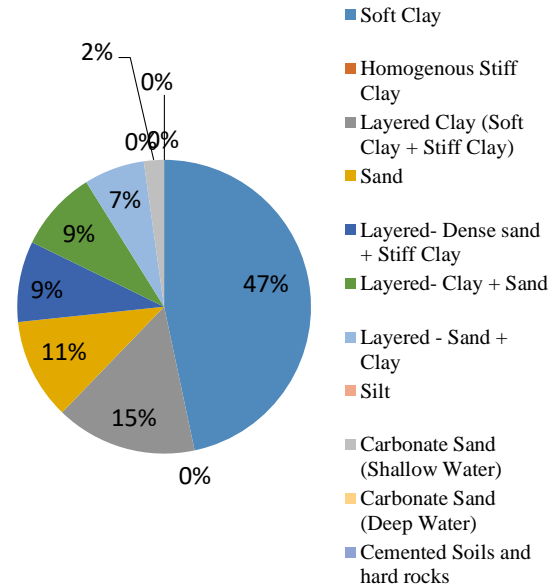


Fig. 5 Suction Caisson Installed in Different Seabed conditions from 1958-2014 (M.N Tran 2007, pp. 112, T.I Tjelta 2001, pp. 3)

These results highlights that, plug heave, soil piping and bottom resistance failure are the most common failure types amongst suction caissons. Plug heave contributes about 34% of the installation issues in both homogeneous clay soils and layered clay soils, soil piping and bottom resistance failure contribute about 24% and 20% respectively of the installation issues in both sand and layered sand soils, while high penetration resistance contributes about 27% of installation issues in layered soils. However, in spite of these installation issues, suction caissons are more widely used in clay soils (47%) among all other soil types.

### CONCLUSION

From the literature reviewed and analysis conducted, it was observed that the following installation issues such as: buckling, plug heave, soil piping, bottom resistance failure and high penetration resistance existed in both homogeneous and heterogeneous seabed conditions. These issues were caused by the amount of suction induced and the soil attributes exhibited during penetration. The amount of suction induced is dependent on the seabed condition and the soil attributes exhibited during penetration. Therefore, in order for these challenges to be mitigated, a good understanding of the seabed conditions and soil parameters before

and during installation, together with constant monitoring of the induced suction created alongside the penetration depth is essential.

## REFERENCES

- [1] Tjelta TL. "Suction Piles: Their Position And Application Today." International Society of Offshore and Polar Engineers, 2001
- [2] Aubeny CP, Murf JD, and Moon SK. "Lateral Undrained Resistance of Suction Caisson Anchors." International Journal of Offshore and Polar Engineering; ISOPE-01-11-3-211, 2001.
- [3] El-Sherbiny RM. "Performance of suction caisson anchors in normally consolidated clay [dissertation]." Austin, TX: The University of Texas at Austin, 2005
- [4] Cao J., Audibert JME, Al-Khafaji Z, Phillips R, and Popescu R. "Penetration Resistance of Suction Caissons In Clay." International Society of Offshore and Polar Engineers, 2002
- [5] Tran MN., David WA, and Randolph MF. "Study of Seepage Flow And Sand Plug Loosening In Installation of Suction Caissons In Sand." International Society of Offshore and Polar Engineers, 2005.
- [6] Tran MN. "Suction Caissons: A New Offshore Foundation Concept." Australian Geomechanics, 2007.
- [7] Sukumaran B. "Suction Caisson Anchors-A Better Option For Deep Water Applications." Rowan University, 1999
- [8] Solhjell E, Blaker O, Knudsen S, and Rahim A. Geotechnical Design and Installation of Suction Anchors for the Goliat FPSO, Offshore Norway. Offshore Technology Conference, 2014.
- [9] Housby GT, and Byrne BW. "Design procedures for installation of suction caissons in clay and other materials." Geotech. Eng 75-82, 2005
- [10] Bang S, and Karnoski S. "Field Retrieval of Suction Piles In Sand." Proceedings of the Seventeenth (2007) International Society of Offshore and Polar Engineers. International Society of Offshore and Polar Engineers, 2007
- [11] Cao J, Phillips R, Popescu R, Audibert JME, and Al-Khafaji Z. "Numerical analysis of the behavior of suction caissons in clay." International Journal of Offshore and Polar Engineering, 2003
- [12] Sparrevik P. "Suction Pile Technology and Installation in Deep Waters." Offshore Technology Conference, 2002
- [13] Dendani H. "Suction Anchors: Some critical aspects for their design and installation in clayey soils." Offshore Technology Conference, 2003
- [14] Sharma PP. "Ultimate capacity of suction caisson in normally and lightly overconsolidated clays. "Unpublished work but accepted (Thesis)" 2005.
- [15] Huang J, Cao J, and Audibert JME. "Geotechnical Design Of Suction Caisson In Clay." International Society of Offshore and Polar Engineers, 2003.
- [16] Senders M, and Randolph MF. "CPT-based Method for the Installation of Suction Caissons in Sand." Journal of geotechnical and geoenvironmental engineering 14-25, 2009
- [17] Senders M, Randolph MF, and Gaudin C. "Theory For The Installation Of Suction Caissons In Sand Overlaid By Clay." Society of Underwater Technology, 2007
- [18] Randolph MF, O'Neill MP, Stewart DP, and Erbrich C. "Performance of suction anchors in fine-grained calcareous soils." Offshore technology conference. Offshore technology conference, 1998
- [19] Zen K, and Hirasawa M. "Case History on the Penetration of Suction Foundation into Seabed." International Society of Offshore and Polar Engineers, 2016
- [20] Randolph MF, and House AR. "Analysis of Suction Caisson Capacity in Clay." Offshore Technology Conference, 2002
- [21] Houlsby GT, and Byrne BW. "Calculation procedures for installation of suction caissons." Report No. OUEL2268/04, University of Oxford, 2004
- [22] Colliat JL, and Dendani H. "Girassol: Geotechnical Design Analyses And Installation Of The Suction Anchors." Society of Underwater Technology, 2002
- [23] Kolk HJ, Kay S, Kirstein A, and Troestler H. "North Nemba Flare Bucket Foundations." Offshore Technology Conference, 2001.

## DIFFERENTIAL THERMAL ANALYSIS OF PMMA (POLY METHYL METHACRYLATE) - EXPERIMENTAL CONCERNS

Sam M Dakka<sup>1</sup>

<sup>1</sup>Department of Engineering and Mathematics, Sheffield Hallam University, United Kingdom

### ABSTRACT

Experimental concerns related to differential thermal analysis of 0.5mm PMMA particles are discussed with emphasis on experimental factors and sample characteristics impacting DTA trace signals. The experimental factors affecting recorded DTA signals are the heating rate and the shape of crucible while the major sample characteristics factors are size distribution, mass and tight packing. PMMA degradation results illustrated faster heating rate improved sensitivity, however slower heating rate improved resolution. Tight particle packing demonstrated a shift of PMMA decomposition to a higher temperature due to reduction in diffusion in and out of the reaction zones of the sample under investigation. The reaction terminated earlier for smaller diameter particles as compared with larger diameter particles. Furthermore, transformation of the DTA technique from qualitative to quantitative is illustrated by calibration factor obtained utilizing various melting metals. The results corroborate that DTA is a powerful investigative tool subject to strict implementation of experimental procedures and handling.

*Keywords: Thermal analysis, PMMA, Experimental concerns, Polymer*

### INTRODUCTION

Thermal degradation of PMMA has attracted great attention in various scientific fields in general and in particular in the aerospace industry [1], PMMA is used as a reference material in studies related to flammability of materials for the international space station cockpits and airline cabins [2]. Thermal degradation of PMMA particles via differential thermal analysis was investigated under various diluting environments ranging from pure Nitrogen to 79% nitrogen and 21% oxygen of the surrounding gas [2]. The main results revealed thermal degradation reaction in pure nitrogen can be described as one step reaction and the reaction is endothermic. As oxygen is introduced in the environment the reaction was transformed to exothermic. Furthermore, the heat of combustion also was determined in pure nitrogen environment utilizing a calibration factor. The following sections of this paper is focused on the experimental concerns implemented prior to acquiring the differential thermal analysis signals described above [2] in order to demonstrate that DTA is a powerful technique that should be considered seriously in any future investigation of thermal degradation samples subject to experimental concerns strict implementation. While the degradation discussed is for PMMA particles, the experimental DTA concerns are valid for any polymer particles

### EXPERIMENTAL APPARATUS

The experimental apparatus consist of thermogravimetric (TG) device Cahn Instruments, model 2131 [2, 3], the TG device is shown in Figure 1. The TG main components are a small furnace and a microbalance. A crucible inside the furnace is attached to the microbalance for weight loss and weight rate degradation studies.



Fig.1 TG device consists of small furnace.

For DTA experiments the crucible is replaced by a small plate with two small pans, a sample pan and a reference pan. This is illustrated in Figure 2 and 3. A Thermocouple located beneath the pans measured the temperature difference between the two pans,

after performing cold junction correction.



Fig. 2 Sample and reference quartz pans or crucibles utilized in the DTA measurements close view.



Fig. 3 Sample and reference quartz pans or crucibles utilized in the DTA measurements, remote view while the furnace is open (lowered).

## EXPERIMENTAL CONCERNS

Differential thermal analysis (DTA) is a method by which the temperature of a sample is compared to the temperature of thermally inert material. These temperatures are recorded for sample and inert material as the furnace is heated or cooled at a constant heating rate. The inert sample must have the same thermal mass as the sample under investigation with no occurrence of transformation reaction in the investigative range of temperatures. When transformation happens, it is either endothermic or exothermic, heat is absorbed or released respectively, Figure 4 illustrates a DTA signal of melting Zinc, in general, differential thermal analysis plots, describe the difference of temperature  $\Delta T$  as a function of time or temperature. As the sample undergoes a phase transformation as illustrated in Figure 4 the temperature of the sample will lag, since during melting the temperature holds steady until the transformation is completed, as compared to an inert sample, as illustrated the temperature of the sample is lower than the inert one, as the transformation is

completed the sample temperature will increase or decrease to catch-up with the inert temperature sample, in this case increases. For melting zinc the reaction is endothermic, the energy consumed to promote the phase transformation will result in a relative decrease in the temperature of the sample.

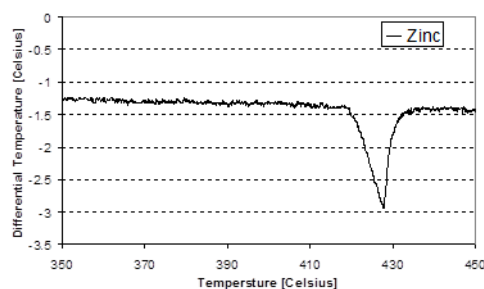


Fig.4 Typical DTA trace of melting Zinc

Large experimental factors can affect DTA curves. The shape, position and number of endothermic or exothermic curve peaks are crucial for qualitative analysis. In addition the furnace heating rate and furnace atmosphere content can alter the shape and position of the curves, therefore impacting quantitative analysis due to changes in the enclosed curve areas of the peaks. In general the DTA signal depends on two groups of factors instrument factor and sample characteristics.

## RESULTS AND DISCUSSION

### Heating Rate

The effect of heating rate on DTA curves is significant. Figure 5 and 6 illustrate the DTA signal shape-dependence on whether the horizontal axis is denoted by temperature or time. Also, the effects of heating rate on the onset temperature and the magnitude of the peak temperature for Zinc at 2°C/min and 4°C/min in pure nitrogen environment. By inspection of the curves carefully, the magnitude of the peak curves is slightly larger or higher for higher heating rate as compared with lower heating curves this is due to the fact that during melting the endotherm temperature of the sample is maintained constant while the reference temperature increases faster. Since less time is available for increase of one degree of temperature at higher heating rate, the time interval for the phase transformation to advance shorter, also since the rate of heat flow to the sample is higher the extent of reaction to proceed is narrower as illustrated in figure 6. Another observation is the onset of temperature is higher for higher heating rates due to larger temperature deviation between the sample interior and the



thermocouple junction.

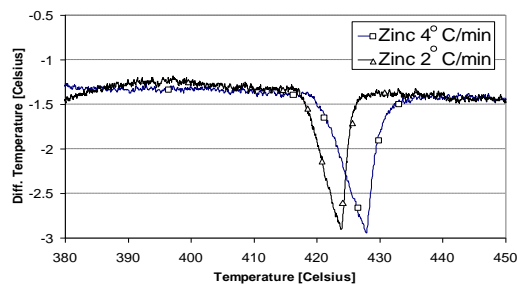


Fig. 5 The effect of heating rate on the melting endotherm of Zinc

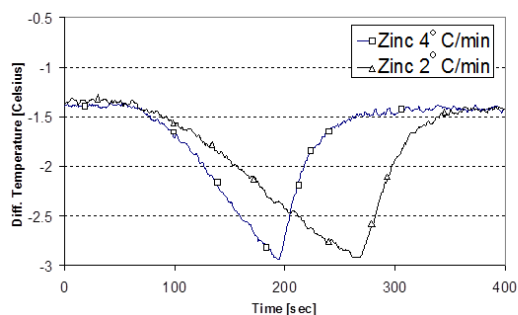


Fig. 6 The effect of heating rate on the shape of the DTA endotherm

As discussed and illustrated by figure 5 and 6 the heating rate has a large impact on the magnitude of the reaction peaks and the shape of the curves, narrow or wide. For example if the heating rate is too fast then some reaction will not be identified or recognized, as a peak of more than one reaction can be identified as one reaction. For accurate determination of the onset of temperature a slower heating rate should be exercised, in addition to discerning close adjacent reactions. On the other hand, too slow heating rate will cause the magnitude of the peak to be too small to be identified. To summarize the effect of the heating rate on PMMA degradation curves, slower heating rate yielded higher resolution, and faster heating rate higher sensitivity.

### PMMA Sample Characteristics

The reaction rates of the participating gases are influenced by how the sample particles are placed in the crucible [4]. Free diffusion in and out of the reaction zones will be reduced if the sample is tightly packed, hence heavier molecules such as carbon dioxide evolving from the sample will be convected slowly from the surface. To that end, tight packing will shift the decomposition to a higher

temperature. Figure 7 illustrates this effect by comparing the degradation weight loss rate of tight packed versus loosely packed PMMA particles as a function of temperature. As we can observe the tightly packed particle curve exhibit higher temperature due to reduced diffusion effects and the degradation curve is slightly broader.

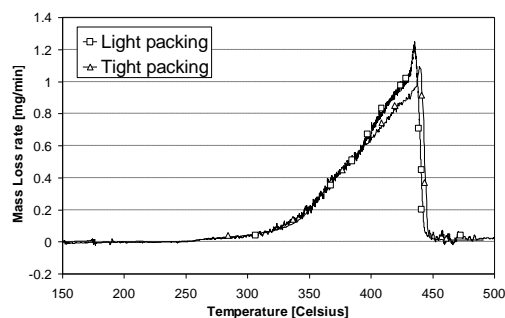


Fig. 7 The effect of packing on the weight loss rate of PMMA

The impact of the sample particle size was also considered, assuming spherical PMMA particles, in certain decompositions the surface to volume ratio increases as the inverse of the particle radius [4], hence the reaction will terminate earlier for smaller particles as illustrated in Figure 8. It is important to note, that, since the thermocouple is attached to the underside of the crucible, the larger the sample size, the larger the temperature gradients inside the sample, and therefore less sensitivity of the measurements. For example, for a large amount of powder, the upper side or the surface might melt first, while the lower part, in the vicinity of the thermocouple junction, may remain below the melting point. Thus, the melting of the upper surface will act as a heat sink, and promote endothermic deviation acquired by the DTA signal. This will yield a false DTA trace since the detected melting temperature will be lower. The geometric shape of the pan is important due to the fact that the transfer of heat to the sample should be uniform and efficient in order to reduce the temperature gradients within the sample. The sample preparation of the PMMA particles was obtained via shaving from large slab of PMMA. Packing is a factor that should be considered, light packing and tight packing would affect the TG curve. The maximum mass weight loss will increase for the tight packing due to less diffusion effects. In addition, for low-density packing the thermal conductivity is low due to the low conductivity of air between the particles. In these particular experiments the interest is in dense packing. For studying ignition of a PMMA slab, the interest is in relatively large bulk PMMA samples, therefore, emphasis in sample preparation and

handling in reducing the diffusion effects. Light sample packing, is achieved by placement the PMMA particles into the crucible with no any external interference. Dense packing involves an external procedure to reduce the pockets of environment gas between the particles, once the sample is placed in the crucible.

### Quantitative Aspects- Calibration

The ultimate goal is to determine the heat of reaction or transition or the mass of the reactive sample, this is accomplished from the area under the DTA curve by applying the simple relation  $\Delta H \cdot m = K \cdot A$ , where  $\Delta H$  is the heat of reaction,  $m$  is the mass of the sample,  $K$  is the calibration factor and  $A$  is the area under the peak. The application of DTA for determining the heat of reaction has been reviewed by [5, 6 and 7].

The calibration coefficient  $K$ , is determined by using compounds having a known heat of transition. These compounds must meet certain requirements such as chemical stability during transformation, low vapor pressure so that the heat of vaporization will be negligible and will not contribute to the heat effect. The melting of pure metals is the most common calibration method in DTA. Table 1 provides the type of metal, the transition temperature and the latent heat of transformation.

Table 1 DTA calibration of pure metals [4].

Metal Type	Transition Point [°C]	Heat of transition [J/g]
Indium	156.60	28.45
Tin	231.88	60.46
Lead	327.47	23.01
Zinc	419.47	108.37
Potassium Sulphate	585.0	33.26
Potassium Chromate	670.5	35.56

The calibration procedure used in this study included Indium, Lead and Zinc. These metals were chosen in order to cover the range of the decomposition reactions of PMMA. Two different tests were performed, one with emphasis on the dependence of the calibration factor on temperature and the other, on the effects of the mass of the sample tested on the calibration factor. More over the impact of the heating rate on the value of  $K$  was also evaluated.

Figure 8 shows the calibration DTA curves of different zinc weights as a function of temperature for the same heating rate of 4°C/min. The transition temperature of  $419.47^\circ\text{C} \pm 1^\circ\text{C}$  is consistent with table 1. In addition, the area and the maximum DTA trace are higher for larger mass; this is due to the fact that a larger amount of energy is needed to melt a larger mass compared to a smaller one. The differential temperature of the baseline is lower for 24 mgs since the sample experiences less temperature gradient inside the particles.

The area under the DTA curve is calculated via the equation listed in the beginning of this section. Figures 8 and 9 illustrate the values of the calibration factor versus temperature, for a variety of pure metals with different masses, and for 2°C/min and 4°C/min respectively.

Figures 9 and 10 indicate that the calibration factor indeed depends on the temperature; the value of  $K$  is higher for lower temperatures. The dependence on temperature can be approximated by linear relationship at 2°C/min

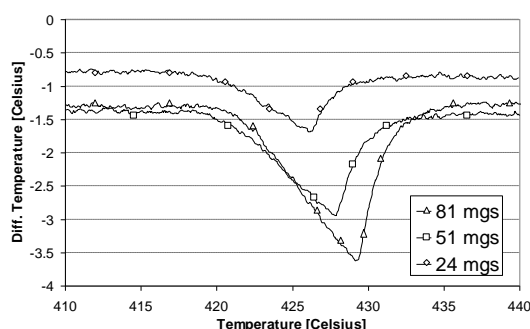


Fig. 8 The effect of packing on the weight loss rate of PMMA

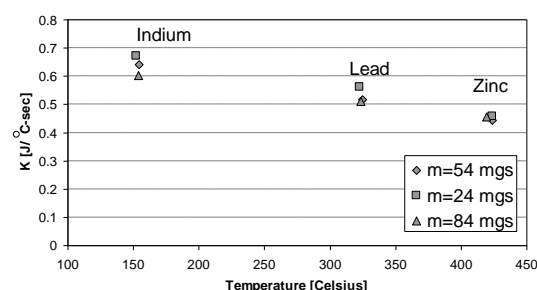


Fig. 9 Calibration factor as a function of temperature for various mass metals at a heating rate of 2°C/min.



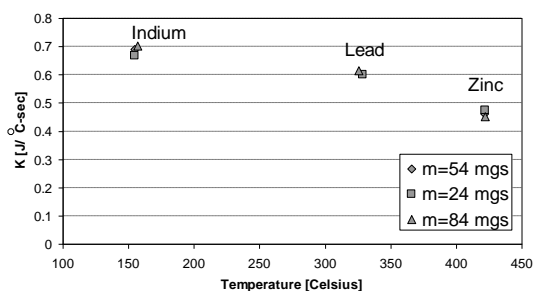


Fig. 10 Calibration factor as a function of temperature for various mass metals at a heating rate of 4°C/min

$$K = -0.0009T + 0.795 \quad , \quad \text{at } m = 54, 24, 84 \text{ mgs} \quad (1)$$

At higher heating rate 4°C/min, K can be approximated by a single relationship:

$$K = -0.0009T + 0.8595 \quad , \quad \text{at } m = 54, 24, 84 \text{ mgs} \quad (2)$$

Both figures imply that for higher heating rates the magnitude of K increases at lower temperatures. The suitable calibration factor, which depends on the decomposition temperature, must be used in the calculation of the DTA area trace.

Figure 11 shows the DTA trace as a function of different sample weights at 2°C/min and 4°C/min. The important conclusion from this figure is that the TG device provides more stable data for the calibration factor for higher temperatures. This is corroborated by the fact there is almost no scatter of data for the zinc, while the amplitude of the scattering for Indium, which melts at a lower temperature is much higher, and the scatter of lead is in between. This appears to be related to the TG device or furnace design; therefore, the importance of the calibration is crucial for obtaining accurate results to determine the heat of transition.

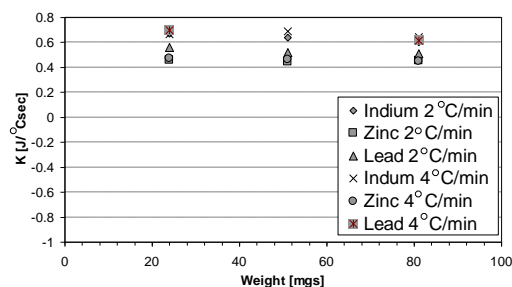


Fig.11 The calibration factor as a function of different weights of metals

## CONCLUSION

Differential thermal analysis experimental concerns related to 0.5mm PMMA particles degradation in a TG device was discussed. The main factors affecting the DTA traces are experimental factors and sample characteristics. The experimental factors affecting recorded DTA signals are the heating rate and the shape of crucible while the major sample characteristics factors are size distribution, mass and tight packing. PMMA degradation results illustrated faster heating rate improved sensitivity, slower heating rate improved resolution. The shape of the crucible is important in convection heavier molecules in and out of the surface of the sample. Tight particle packing shifted the decomposition to a higher temperature due to reduction in diffusion in and out of the reaction zones. The reaction terminated earlier for smaller particles as compared with larger particles. The larger the particle size or mass, the larger temperature gradients are experienced within the sample. Transforming the DTA measurements to a quantitative tool was demonstrated via a calibration factor. The methodology is based on calculating the area under or enclosed by the DTA trace signal. The above experimental consideration is vital to achieve a good quality and useful DTA traces.

## REFERENCES

- [1] Friedman R. Risks and Issues in Fire safety on the Space Station. NASA-TM-106430
- [2] Dakka SM., "TGA/DTA/MS of Poly(methyl methacrylate)-The role of the oxidative environment" Journal of Thermal Analysis and Calorimetry, Vol 73, 2003, pp. 17-24
- [3] Cahn instruments, Inc., Cerritos, CA.
- [4] Speyer R. F. Thermal analysis of materials. New York: Marcel Dekker; 1994
- [5] Brochard J. H., and Daniels F., "The application of differential thermal analysis to the study of reaction kinetics1", Journal of The American Chemical Society, Vol 79(1), 1957, pp.41-46
- [6] Bohon, R. L. Proceedings of the First Toronto symposium on Thermal Analysis. McAdie, H. G. Chemical Institute of Canada. Toronto; 1965. pp. 63.
- [7] Ozawa T., "A new method of quantitative differential Thermal Analysis", Bull. Chem. Soc. Japan, Vol 39, 1966, pp. 2071-2078

## INVESTIGATION OF CURING PERIOD OF CEMENTITIOUS ADHESIVE AND PERFORMANCE OF RUST PREVENTION

Yoichi Mimura<sup>1</sup>, Vanissorn Vimonsatit<sup>2</sup> and Isamu Yoshitake<sup>3</sup>

<sup>1</sup>Department of Civil and Environmental Engineering, National Institute of Technology, Kure College, Japan;

<sup>2</sup>Department of Civil Engineering, Curtin University, Australia;

<sup>3</sup>Department of Civil and Environmental Engineering, Yamaguchi University, Japan

### ABSTRACT

A steel-concrete composite structure needs generally mechanical shear connectors such as headed studs to ensure efficient load resistances. As an alternative to shear studs, a type of cementitious adhesives has been developed to connect a steel-concrete composite structure. The unique feature of this adhesive is the improved bond performance with fresh concrete which depends on the curing age of the adhesive. This paper presents the outcome of fifteen flexural tests of elemental steel-concrete composite beams with various curing ages of the adhesive to investigate the appropriate curing period. Shot blasting steel plate and the un-shot blasting steel plate were prepared to examine the bond performance from the surface condition of the steel plate. The result of the flexural tests indicates that the bond performance between the steel plate and the concrete is optimum when the curing periods are 7 - 14 days. The tests with longer curing age produce similar bond performances with the tests at 7 days. Use of steel plate without shot blasting may be undesirable for the composite structure using the adhesive. In addition to the flexural tests, 8 deformed bars with and without adhesive coating were exposed to a field condition to investigate the rust preventive performance of the adhesive. The deformed bars without the adhesive had already corroded at 5 days after exposure. The observation showed the deformed bar with the adhesive was hardly deteriorated after 200 days.

*Keywords: Cementitious Adhesive, Curing Period, Rust Prevention, Flexural Test, Field Exposure*

### INTRODUCTION

Steel-concrete composite structures are constructed by connecting concrete and steel, and have many advantages such as excellent fatigue durability and a reduced member size compared with non-composite sections. Interaction between concrete and steel affects performances (e.g. load carrying capacities, durability and rigidity) of composite structures. Various shear connectors such as headed studs, channels and T-connectors are currently available.

A new composite structural system using a cementitious adhesive has been developed in previous studies. The adhesive has been used in various structures as rust preventive materials. The previous study reports the composite beam using the adhesive had sufficient load carrying capacity [1] and fatigue durability [2]-[3]. Herein, it should be noted that the adhesive needs an appropriate curing term before casting of concrete. According to the previous report [1], the steel substrate sprayed with the adhesive was cured for 2 weeks. However, the curing period was not discussed sufficiently. Therefore, flexural tests using elemental composite beams cured in various terms were performed in order to investigate an appropriate curing period of the adhesive. In addition, the rust prevention

performance of the adhesive was examined using coated bars exposed to a field environment for 200 days.

### MATERIALS

#### Cementitious Adhesive

The carbon-fibre-blended cementitious adhesive developed in Japan consists of compound powder and liquid emulsion, as shown in Fig. 1. Table 1 and Table 2 give the components and properties of the adhesive [4]. The powder and liquid were manually mixed in the laboratory using a portable mixer at a weight ratio of 2.3 (powder/emulsion), as recommended by the manufacturer.



Fig. 1 Compound powder (left) and liquid emulsion (right)

Table 1 Components of the adhesive

	Component	Composition
Compound powder	White cement	36%
	Quartz sand	54%
	Carbon fibre	3%
	Additive	7%
Liquid emulsion	Water	73%
	Acrylic ester	27%
	Additive	<1%

Note: The manufacturer is Mighty-kagaku [4]

Table 2 Properties of fresh and hardened adhesive

Property	Value
Fluidity	>250 mm
Air permeability	476 cm <sup>3</sup> /m <sup>2</sup> (24 h)
	1455 cm <sup>3</sup> /m <sup>2</sup> (72 h)
Flexural strength	5.8 MPa (7 days)
	6.9 MPa (28 days)
Compressive strength	21.0 MPa (7 days)
	36.8 MPa (28 days)
Tensile strength	3.1 MPa (7 days)
	4.0 MPa (28 days)
Strain capacity	0.4% (7 days)
	0.4% (28 days)
Drying shrinkage	0.08% (7 days)
	0.13% (28 days)
Water permeability	0.4% (water pressure: 0.1 MPa)

Note: The manufacturer is Mighty-kagaku [4]

## Concrete

The Japan Bridge Association recommends the use of expansive concrete for composite slab to prevent cracks due to concrete contraction [5]. Table 3 gives the mixture proportion of the expansive concrete. The compressive strength and splitting tensile strength of concrete were obtained from the tests using the cylindrical specimen (100 mm diameter x 200 mm height). The concrete prisms (100 mm width x 100 mm height x 400 mm length) were used for the flexural strength. Table 4 provides the concrete strength at the age of 7 days.

## Steel Plate and Deformed Bar

Rolled steel for welded structure (Grade SM400A by JIS G3106 [6]) used in flexural tests had a yield strength of 245 MPa with Young's modulus of 200 GPa. The shot blasting steel plate (Type B) and the un-shot blasting steel plate (Type N) were prepared to examine the bond performance with a different surface condition of the steel plate. Fig. 2 shows steel plates used in this study. The steel

plate with shot blasting has rougher surface than the one without shot blasting, so the surface without shot blasting was shiny, as shown in Fig. 2. Steel plates were 100 mm width x 300 mm length x 3.2 mm thickness. The adhesive after mixing was sprayed on the steel plates by using a spray gun with a nozzle diameter of 4 mm as shown in Fig. 3. The amount of the adhesive sprayed on the steel plates was approximately 1.0 kg/m<sup>2</sup>. The adhesive was sprayed on all steel plates used in flexural tests at once as shown in Fig. 3.

Table 3 Mixture design of expansive concrete

Component	Quantity
Water-binder ratio	48.0%
Water	161 kg/m <sup>3</sup>
Ordinary Portland cement	316 kg/m <sup>3</sup>
Expansive additive	20 kg/m <sup>3</sup>
Fine aggregate	841 kg/m <sup>3</sup>
Coarse aggregate	980 kg/m <sup>3</sup>
Water-reducing admixture	2.69 kg/m <sup>3</sup>

Table 4 Strength of expansive concrete at the age of 7 days

	Strength
Compressive strength	39.1 MPa
Splitting tensile strength	3.30 MPa
Flexural strength	5.58 MPa



(a) Un-shot blasting steel plate



(b) Shot blasting steel plate

Fig. 2 Steel plates



Fig. 3 Steel plates sprayed with the adhesive

Eight deformed bars with a diameter of 13 mm were employed for field exposure. All bars (Grade SD345 by JIS G3112 [7]) had a yield strength of 345 MPa with Young's modulus of 200 GPa. Each reinforcing bar was 1940 mm long. The adhesive attached on the deformed bar was approximately 0.83 kg/m<sup>2</sup>. Fig. 4 shows the surface condition of the coated and uncoated deformed bars.



(a) Deformed bar without adhesive coating



(b) Deformed bar with adhesive coating

Fig. 4 Surface condition of the deformed bar

## FLEXURAL TESTS FOR ADHESIVE CURING PERIOD

### Test Detail

To examine the effect of curing time for the adhesive, flexural test was conducted by using the specimen shown in Fig. 5. The curing periods of the adhesive on steel plates (Type B and Type N) were 2, 7, 14, 28, 140 and 168 days before casting concrete. In addition, the flexural tests using the Type B steel plates cured for 3, 4 and 5 days were also performed to further explore the trend of the failure load at the initial age. After curing of the adhesive to a desired age, concrete was cast. The concrete formwork was removed at the concrete age of 1 day, and the concrete was cured in the water with a temperature of 20 degree Celsius. The side of the steel plate without adhesive was greased in order to prevent the rust during the water curing. The test age for concrete was 7 days for all test cases.

The load by using a universal testing machine was applied statically to the test specimen. The test was a 4-point loading system, as shown in Fig. 5. Two beam specimens were tested at each age. Strain of steel plate was measured at the mid-span of the beam.

### Experimental Results and Discussion

All specimens had a single line cracking due to the bending moment occurred at the loading span regardless the experimental conditions. After concrete cracking, the steel at the area from the

crack to the plate edge debonded from the concrete, as shown in Fig. 6.

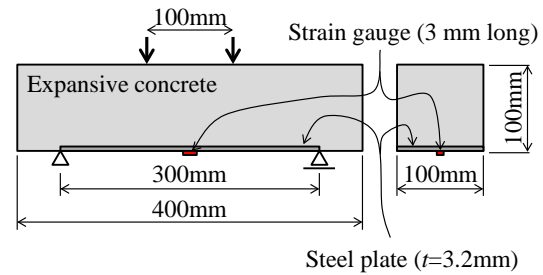


Fig. 5 Schematic of specimen and loading condition for flexural test

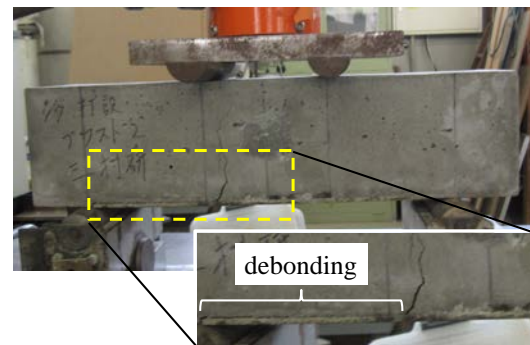


Fig. 6 Concrete cracking and debonding of steel plate

Fig. 7 presents the adhesive remaining on the steel plate after flexural test with 7 days curing of the adhesive. Little adhesive remained on un-shot blasting steel plate (Type N) because the un-shot blasting steel plate had a smooth surface. The surface of shot blasting steel plate (Type B) was rougher than Type N, more adhesive remained on Type B steel plate.

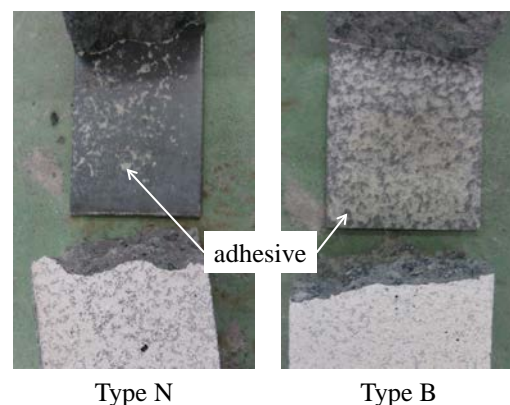


Fig. 7 Adhesive remaining on steel plate after test with curing period of 7 days

Fig. 8 presents a ratio of failure load (failure load



of elemental composite beam/load carrying capacity of concrete). The ratio of 2 days curing of Type N beams was almost 1.0, the adhesive cured for 2 days hardly had the bond performance with the un-shot blasting steel plate. In the test of Type B, the ratios at 28, 140 and 168 days were approximately equivalent to the ratio at 7 days. This result indicates that the bond performance between the steel plate and the concrete is optimum when the curing periods are 7 - 14 days. This appropriate curing is longer than one of typical adhesive such as epoxy resin. However, some procedures for casting concrete are needed after applying the adhesive, so the curing period of 7 - 14 days can be acceptable in actual construction. The tests with longer curing age, such as 140 or 168 days, produced similar bond performances with the tests at 7 days. A half year curing of the adhesive hardly affects the decrease in load carrying capacity of the composite beam. In the test of Type N, the ratio of the beam with 140 days curing was definitely smaller than the ratio of the one with 7 days curing. Use of steel plate without shot blasting may be undesirable for the composite structure using the adhesive.

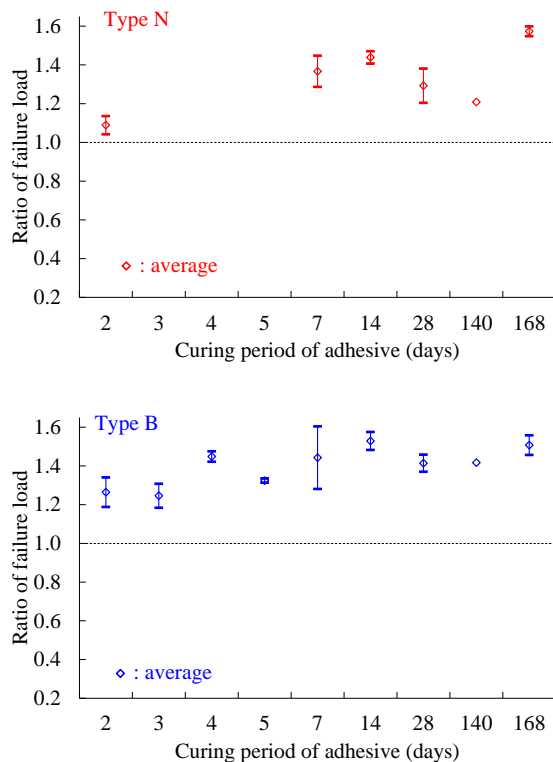


Fig. 8 Ratio of failure load

Fig.9 shows the relationship between load and strain of steel plate of Type B at the curing period of 5 days and 7 days. Both strain responses were similar up to the load of around 10 kN. Under the load of more than 10 kN, the strain of steel plate obtained from the specimen with 5 days curing was

smaller than steel strain from the specimen with 7 days curing. Such smaller strain was caused by the released strain due to the slip between concrete and steel plate, as evident in Fig. 6. Higher strain such as the elemental beam with 7 days curing was induced by the development of the bond performance of the adhesive.

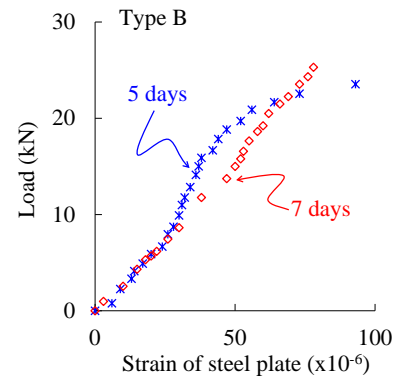


Fig. 9 Load - steel strain relationship

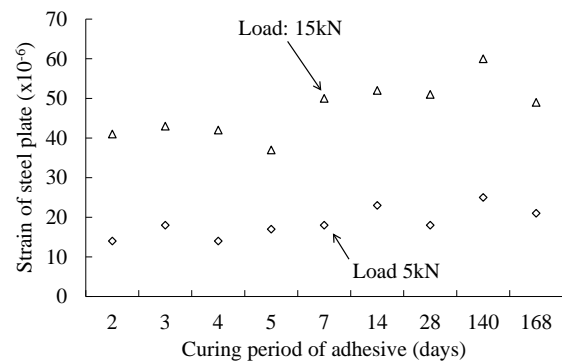


Fig. 10 Strain of steel plate at the load of 5 kN and 15 kN (Type B)

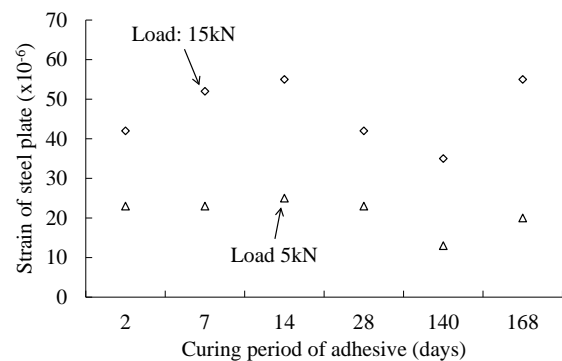


Fig. 11 Strain of steel plate at the load of 5 kN and 15 kN (Type N)

Fig. 10 shows the strain of steel plate in Type B at loads of 5 kN and 15 kN. Strains at 5 kN were from  $13 \times 10^{-6}$  to  $25 \times 10^{-6}$ , and almost equivalent at the ages of 2 - 168 days. At the load of 15 kN, the strains before 5 days and the strains after 7 days

were approximately  $40 \times 10^{-6}$  and  $50 \times 10^{-6}$ , respectively. Such smaller strains before 5 days mean a slip between the steel plate and the concrete. This result also indicates that the adhesive needs the curing period of more than 7 days.

The strains of the Type N beams are as shown in Fig. 11. The strain at a load of 15 kN tended to increase until 14 days of curing but decreased at 28 days of curing period, and at 140 days, the strain was less than that at 2 days due to the slip between the steel plate and the adhesive. Such a decrease in strain at these curing days was the same as the transition of the failure load ratio shown in Fig 8.

### FIELD EXPOSURE OF DEFORMED BARS COATED BY ADHESIVE

#### Test Detail

For applying the adhesive coating to steel bars, a roller and lysing gun can be used. However, with these ways, it is difficult to uniformly apply an appropriate amount of adhesive to the reinforcing bar. Therefore, in this study, a wood formwork with an inner dimension of 50 x 50 x 2000 mm as shown in Fig. 12 was used as a mould to hold the adhesive material inside. Reinforcing bars were then coated by immersing in the adhesive in this wood formwork. In the present test, each rebar was immersed for a few seconds, and after taking it out, it was manually rotated for about 30 minutes so that the adhesive was evenly applied to the rebar.



Fig. 12 Coating of the adhesive on the deformed bar

Table 5 shows the amount of adhesive applied. As a result of the application, the coating amount was  $0.38 \text{ kg/m}^2$ , and the adhesive could be applied only to the extent that a thin film was stretched over the surface of the reinforcing bar. Therefore, after the adhesive cured for around 30 minutes, the adhesive was again applied to the rebar with the same procedure. As a result of measuring the weight of the reinforcing bars after the second application of the adhesive, as shown in Table 5, the applied amount of the adhesive was 66 g on the average of 4 bars and the average coated amount per unit area was  $0.83 \text{ kg/m}^2$ .

Deformed bars were then exposed in a field condition to confirm the rust preventive effect of the adhesive, as shown in Fig. 13. The field exposure was performed at a site located 500 m from the seashore.

Table 5 Weight of the adhesive on the deformed bar

Bar	Bar weight (g)		Adhesive Weight (g)
	before	after	
1	1836	1899	63 ( $0.79 \text{ kg/m}^2$ )
2	1830	1897	67 ( $0.84 \text{ kg/m}^2$ )
3	1827	1892	65 ( $0.82 \text{ kg/m}^2$ )
4	1840	1910	70 ( $0.88 \text{ kg/m}^2$ )
Ave.	1833	1899	66 ( $0.83 \text{ kg/m}^2$ )



Fig. 13 Field exposure of the deformed bars

### Experimental Results and Discussion

Fig. 14 shows the corrosion of the deformed bars exposed for 0, 5 and 42 days. The deformed bars without the adhesive had already corroded at 5 days. The rust at 5 days appeared at some lugs and ribs of the deformed bars. After 42 days of exposure, most lugs and ribs had rusted, and the rust had expanded further to other areas of the bar. On the other hands, bars with the adhesive showed no sign of rusting.

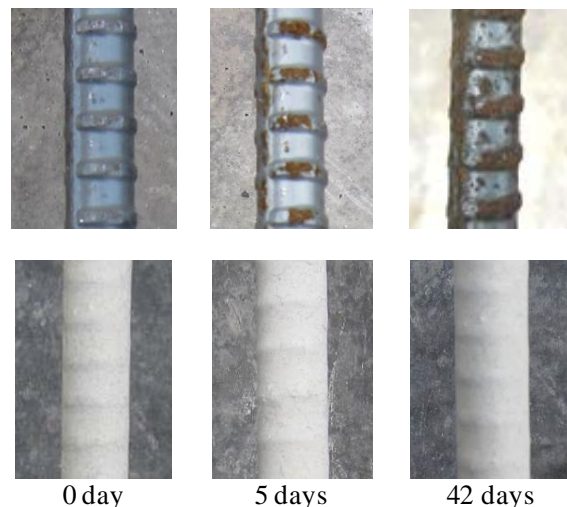


Fig. 14 Corrosion of the deformed bar at 0, 5 and 42 days

Fig. 15 shows the corrosion of the deformed bars exposed for 91, 136 and 200 days. The rust of the deformed bars without the adhesive expanded as exposure continued, and the whole of the bars deteriorated due to the rust when 200 days passed.

The deformed bars coated with the adhesive had some minor rust with the size of approximately 1 mm after 91 days exposure, as shown in Fig. 15. All such rust appeared like a pinhole at the lug which had locally thinner adhesive. The occurrence of this localized rust gradually increased with the increasing exposure period. In this study, although the bars were rotated until the adhesive hardened roughly, the uniform adhesive was not entirely applied around the lugs of the deformed bars. The application procedure and the amount of the adhesive required on a deformed bar need further studies to prevent the rust at the lug location. However, the local rust did not expand, and even after 200 days from the start of the exposure, the reinforcing bar was sound and no significant corrosion occurred.

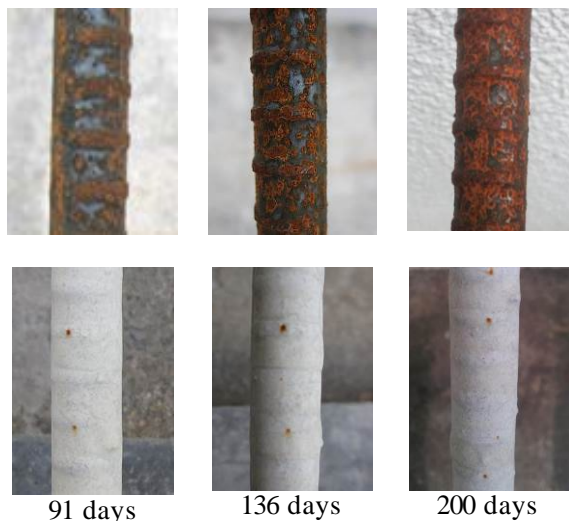


Fig. 15 Corrosion of the deformed bar at 91, 136 and 200 days

## CONCLUSION

This paper presents the investigations of the cementitious adhesive for a steel-concrete composite structure. Flexural tests using the elemental composite beams were conducted to obtain the appropriate curing period of the adhesive. Field exposure testing of deformed bars coated the adhesive was performed to confirm the rust prevention performance. Based on the test results in this study, it can be concluded as follows:

- (1) The appropriate curing period of the

cementitious adhesive can be recommended as 7 - 14 days based on the ratio of failure load and steel strain response obtained from flexural tests. In addition, the adhesive with longer curing age, such as 140 or 168 days has similar bond performances.

- (2) As a result of the field exposure test, the deformed bars without the adhesive had already corroded at 5 days, and the rust covered almost the whole surface area of the bar when 200 days passed. The deformed bar coated with the adhesive was sound and no significant corrosion occurred.

## ACKNOWLEDGEMENTS

The authors would like to thank Dr. Watada (Ube Machinery Co., Ltd.), Mr. Ikushima (Maeda Sangyo Co., Ltd.) and Mr. Shimoda (an advanced course student of National Institute of Technology, Kure College).

## REFERENCES

- [1] Yoshitake I., Ogawa A., Kim Y.J. and Mimura Y., "Development of a New Composite Slab System Using a Carbon Fiber-Blended Cementitious Adhesive", Journal of Structural Engineering, Vol.138, No.11, Nov, 2012, pp.1321-1330.
- [2] Yoshitake I., Ogawa A., Kim Y.J. and Ogami E., "Composite Deck Having Transverse Stiffeners Bonded with a Cementitious Adhesive Subjected to Moving-Wheel Fatigue", Journal of Bridge Engineering, Vol.18, No.9, Sep, 2013, pp.848-857.
- [3] Yoshitake I., Kuroda Y., Watada Y. and Kim Y.J., "Fatigue performance of steel-concrete composite slabs with a cementitious adhesive subjected to water leakage", Construction and Building Materials, Vol.111, Feb, 2016, pp.22-29.
- [4] Mighty-kagaku, Manufacturer's data sheet (in Japanese), <[www.mighty-kagaku.jp](http://www.mighty-kagaku.jp)> (accessed May.9, 2017)
- [5] Japan Bridge Association (JBA), 2007. (in Japanese)
- [6] Japanese Industrial Standards (JIS), JIS G3106: Japan Standard Association, 2008
- [7] Japanese Industrial Standards (JIS), JIS G3112: Japan Standard Association, 2010



## **REGIONAL DEPOSITION CHARACTERISTICS OF NANOPARTICLES IN A RAT NASAL CAVITY**

Yidan Shang<sup>1</sup>, Jingliang Dong<sup>2</sup>, Kiao Inthavong<sup>3</sup> and Jiyuan Tu<sup>4</sup>

<sup>1</sup>School of Engineering, RMIT University, PO Box 71, Bundoora, VIC 3083, Australia.

<sup>2</sup>Key Laboratory of Ministry of Education for Advanced Reactor Engineering and Safety, Institute of Nuclear and New Energy Technology, Tsinghua University, PO Box 1021, Beijing 100086, China.

### **ABSTRACT**

In this study, inhalation exposure to nanoparticles in a realistic rat nasal passage was numerically investigated by Computational Fluid-Particle Dynamics (CFPD) approach. The nasal passage was reconstructed from CT images of a 400g Sprague-Dawley rat, and moderate breathing condition was applied to produce laminar airflow field. Nanoparticle trajectories were calculated using Lagrangian one-way coupling method. Nanoparticles in the size of 1 to 200 nm were used and the effect of Brownian motion was considered. The simulation results showed the total deposition efficiency sharply decreased from 98.8% for 1 nm particles to 2.33% for 200 nm particles. The regional olfactory deposition efficiency peaked at 9.4% for particle size 5 nm. Particle flux distributions were plotted to identify the bulk particle flow at different cross-sectional planes. For 1 nm particles, the flux dominantly concentrated in the centre of the cross-section when exiting the vestibule region and no flux was shown in the olfactory region, whereas for 10 nm particles the flux was more uniformly distributed when exiting the vestibule and the particles travelling through the upper part led to the deposition in the olfactory region. This indicates that the rat nasal cavity retains a particle selective feature, which prevents high diffusive particles from entering the olfactory region but allows low diffusive nanoparticle to deposit in the olfactory region.

*Keywords: Rat, Nasal Cavity, Nanoparticle, CFPD*

### **INTRODUCTION**

Concerns about the health effects of inhaled nanoparticles on respiratory and central nerve system have been increased in recent years as the prosperity of nanotechnology has increased human's exposure to airborne nanoparticles. WHO [1] confirmed that inhalation hazards such as notorious asbestos cause severe health consequences. Previous investigations showed inhaled nanoparticles lead to increased risk of respiratory, cardiovascular and neurological disorders [2].

Recently, emerging evidences indicate the olfactory bulb and olfactory nerve play a vital role in brain uptake of neuro toxics [3, 4]. Oberdörster, et al. [5] used a confined compartment to study rats' exposure to carbon nanoparticles and found their translocation via neuron routes from olfactory mucosa to central nerve system.

Experiments on rats have been widely used to evaluate exposure risks to nanoparticles. However, it has been a challenge to extrapolate the experimental data from rats to humans due to various experimental limitations. For example, nanoparticles tend to agglomerate to micron in size before depositing and it is difficult to quantitatively measure regional particle deposition. With the rapid development of medical imaging technique and Computational Fluid Dynamics (CFD), simulations coupled with realistic rat nasal CAD models cost-

effectively bypass the challenges above with acceptable accuracy.

Previous CFD studies have investigated airflow characteristics and nanoparticle/gas deposition efficiencies in rats [6-8]. To estimate regional nanoparticle uptake, Schroeter, et al. [9] plotted the particle distribution and found the frontal part of the rat's nasal cavity was the major deposition region and it moved distally as the particle size increased. Furthermore, Shang, et al. [10] and Dong, et al. [11] revealed the detailed particle deposition patterns using a novel surface-mapping technique and compared between the rat and the human models.

The large olfactory to total nasal surface area ratio makes the rat olfactory region, a portal for nanoparticle translocation, vulnerable to even low toxic dosage level. Although the regional particle deposition in the rat nasal cavity has been intensively conducted, the exact mechanism of nanoparticle travelling from nostril to olfactory region remains unclear.

In this study, we performed 1-200 nm nanoparticle inhalation simulation under the moderate breathing condition (400 mL/min) in a realistic rat nasal cavity model (RNC01). Both total and regional (vestibule and olfactory) deposition efficiencies were calculated. 1 nm and 10 nm particle flux distributions were plotted on two cross-sections located posterior to the vestibule region and middle olfactory region. Combined with previous

studies, the cross-sectional particle distribution provides insights into the interaction between rat nasal structure and nanoparticle trajectories.

## METHOD

### Nasal Geometry and Particle Release Locations

The CAD model of a Sprague-Dawley rat labeled as RNC01 (Fig. 1) was reconstructed from CT-scan and was frequently used in authors' previous studies [10-12]. The model started from the rat's face/nostrils and ended at the exit of nasopharynx. The highly folded olfactory region, which occupied 52.4% of the total surface area [12], was highlighted at the posterior-dorsal part. Two cross-sections A and B located at the posterior vestibule and at the middle of olfactory region, respectively, were generated to reveal the particle flux patterns.

The particle releasing location, external facial features plays important roles on determining the fate of particles. Our previous study has demonstrated that the breathing zone was the key component that dominated particles trajectory [13]. In this study, nanoparticles were uniformly released from a spherical surface in front of the nose. Detailed governing equations of airflow simulation and Lagrangian particle tracking method can be found in the author's previous study [11].

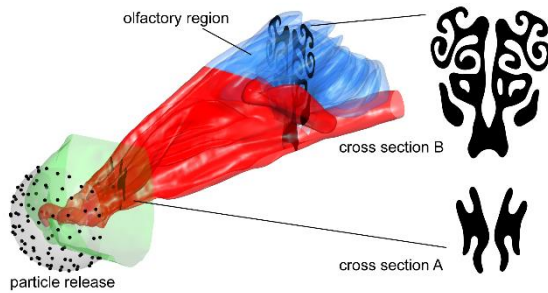


Figure 1. The rat nasal cavity with particle releasing locations. Two characteristic cross-sections, A and B, were used for particle transport analysis.

### Deposition Efficiency and Particle Flux

The deposition efficiency (*DE*) was defined as the ratio of number of particles deposited in a region to the total number entering the nasal cavity:

$$DE = \frac{\text{regional or total deposited particles}}{\text{total particles inhaled}}$$

The particle flux (*f*) was designed to assess the number of particles passing through an unit area on the cross-section. It was normalized by the number of particles inhaled into the nasal cavity, which

equals to particles passing through the nostrils. The definition was:

$$f(\vec{r}) = \frac{\text{particles per unit area}}{\text{particles passing through nostrils}}$$

Thus, the particle flux distribution can reveal the bulk movement of nanoparticles, and may shed a light on the mechanism of olfactory deposition.

For cross-sections at nostrils, the integral of particle flux is constantly 1,

$$\int_{\text{nostrils}} f(\vec{r}) dA = 1$$

Due to deposition on the nasal wall, the integral of particle fluxes on cross-section A and B were always less than 1,

$$\int_{\text{cross-section}} f(\vec{r}) dA < 1$$

## RESULTS

### Total Deposition Efficiency

Fig. 2 shows the total deposition efficiency against particle size between 1-200 nm. High deposition percentage (>80%) was found for particle smaller than 2 nm. The deposition efficiency sharply dropped to around 10% for 20 nm particles and then stabilized around 5% for 20-200 nm particles.

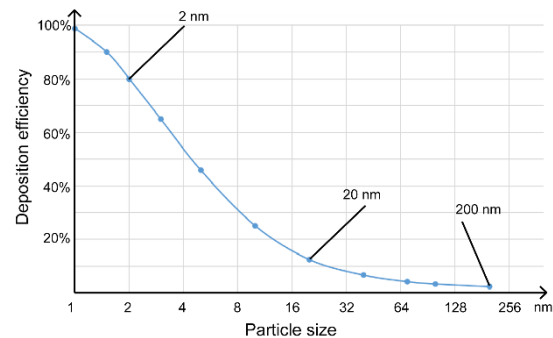


Figure 2. Particle deposition efficiency in the entire rat nasal cavity for particles range between 1 to 200 nm.

The data of the deposition curve was consistent with our previous paper [11]. Close agreements were found when comparing the trend of the curve to published relevant rat nasal deposition data [7, 9].

### Regional Deposition Efficiency

The vestibule region of rats serves a filtration function to avoid particles entering olfactory region and lung. The regional deposition efficiencies against particle size between 1-200 nm were plotted

for vestibule and olfactory regions in Fig. 3. The rat nasal vestibule showed strong filtration effect for particles smaller than 3 nm. It absorbed 20% of inhaled 3 nm particles and the filtration rate reached 60% for 1 nm particles. While for particles larger than 5 nm, the deposition in the vestibule region approached to the same level as in the olfactory, which kept below 10%.

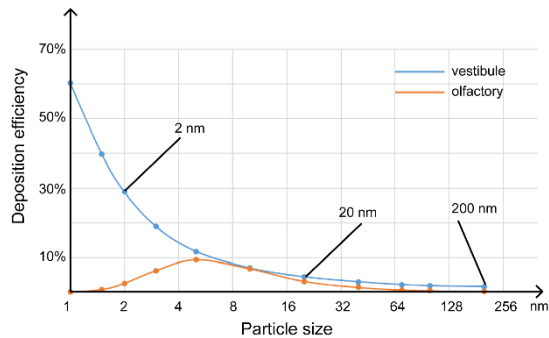


Figure 3. Regional particle deposition efficiency in the vestibule and olfactory regions.

Particles exited the vestibule region continued travelling to the deep nasal cavity and part of them deposited in the olfactory region. Different to the vestibule deposition, the olfactory deposition efficiency started from 0 and rose up gradually as the particle size increased. It peaked at 10% when particle size reached 5 nm and then smoothly decreased to 0% for 200 nm particles. This was consistent with previous study conducted by Schroeter, et al. [9].

### Particle Flux Distribution

Fig. 4 and Fig. 5 displayed the flux distributions of 1 and 10 nm particles at cross-sections A and B. The cross-section A was located at the posterior of vestibule and the cross-section B was located at the middle of main passage, with the upper part being included in the olfactory region. To have a complete view, the relative locations of two cross-sections in the nasal cavity remained unchanged and 3D-view was rotated. Nostrils and the exit of nasopharynx were also plotted.

Obvious preferential particle distributions were observed at the cross-section A for both 1 nm and 10 nm particles. Higher particle concentration were seen in the centre, where the mainstream of air flowed through as shown in the airflow patterns in Shang, et al. [10]'s study.

0 particle flux was observed at the top and bottom of cross-section A for the 1 nm case due to the strong filtration effect of the vestibule region. As seen in the Table 1, the integral of particle flux on cross-section A of 0.42 indicated that majority of inhaled particles were absorbed by the vestibule region and the particles at the margin of the cross-

section had larger chance to deposit. While for the 10 nm case, the resultant particle deposition was more broad. This is mainly because extremely low deposition occurred (merely 5%) in the vestibule region according to Fig. 3 and Table 1.

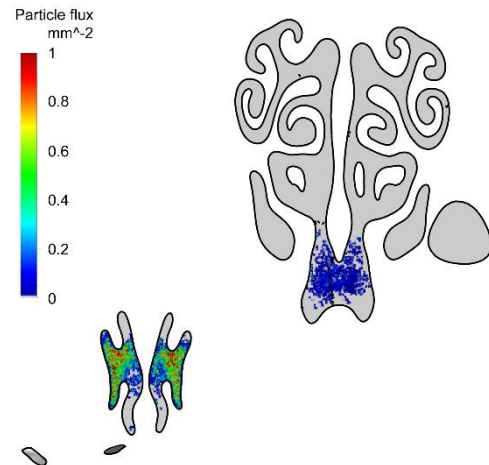


Figure 4. 1 nm particle flux on cross-sections A and B. Particles were concentrated in the middle when exiting vestibule and concentrated in the lower part of cross-section B without entering olfactory region (upper part).

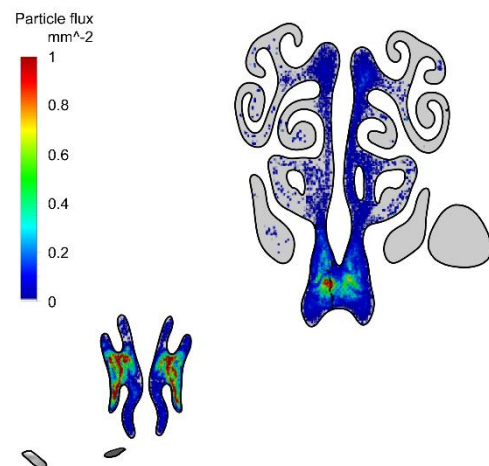


Figure 5. 10 nm particle flux on cross-sections A and B. Particles are more uniformly distributed when exiting the vestibule and significant amount of particles entered the olfactory region.

Table 1. Integrals of particle flux on nostrils, cross-section A and cross-section B.

	particle size	nostrils	cross-section A	Cross-section B
Integral	1 nm	1.00	0.42	0.03
of flux	10 nm	1.00	0.95	0.84

Particle size was seen clearly to affect particles

entering the olfactory region. The Table 1 also showed merely 3% of inhaled 1 nm particles reached the cross-section B and they were mostly concentrated in the lower part (Fig. 4), where the bulk streamlines flowed through. With less diffusivity, considerable amount of 10 nm particles entered the upper part of cross-section B, leading to high olfactory deposition. Comparing Fig. 4 and Fig. 5, it is reasonable to infer that the particles deposited in the olfactory region was travelled from the upper part of cross-section A.

## CONCLUSION

In this study, numerical results of 1-200 nm particles deposition in a Sprague-Dawley rat nasal cavity model under inhalation flow rate 400 mL/min were reported. The simulation results showed good agreement with previous experimental and numerical data.

The research findings demonstrate the particle size remain the key factor to determine particles' fate in the rat nasal cavity. The rat vestibule region posed strong filtration for high diffusive particles (1 nm) while it allowed low diffusive particles (10 nm) to travel through. The particle main mainstream was located at the centre when it exited vestibule and converted to the lower part when reaching the olfactory region. The particles exited in the upper part of the vestibule region may contribute to high deposition in the olfactory region.

## ACKNOWLEDGEMENT

This study was funded by the National Natural Science Foundation of China (Grant No.: 91643102) and Australian Research Council (Project ID: DP160101953).

**Corresponding Author:** Jiyuan Tu

**Email:** jiyuan.tu@rmit.edu.au

## REFERENCES

- [1] I. A. f. R. o. Cancer, I. A. f. R. o. Cancer, I. A. f. R. o. Cancer, and I. A. f. R. o. Cancer, "Asbestos (chrysotile, amosite, crocidolite, tremolite, actinolite, and anthophyllite)," *IARC Monogr Eval Carcinog Risks Hum. C*, vol. 100, pp. 219-309, 2012.
- [2] K. B. Knudsen, H. Northeved, P. K. Ek, A. Permin, T. L. Andresen, S. Larsen, et al., "Differential toxicological response to positively and negatively charged nanoparticles in the rat brain," *Nanotoxicology*, vol. 8, pp. 764-774, 2014.
- [3] R. Bai, L. Zhang, Y. Liu, B. Li, L. Wang, P. Wang, et al., "Integrated analytical techniques with high sensitivity for studying brain translocation and potential impairment induced by intranasally instilled copper nanoparticles," *Toxicology letters*, vol. 226, pp. 70-80, 2014.
- [4] W. K. Boyes, R. Chen, C. Chen, and R. A. Yokel, "The neurotoxic potential of engineered nanomaterials," *Neurotoxicology*, vol. 33, pp. 902-910, 2012.
- [5] G. Oberdörster, Z. Sharp, V. Atudorei, A. Elder, R. Gelein, W. Kreyling, et al., "Translocation of inhaled ultrafine particles to the brain," *Inhalation toxicology*, vol. 16, pp. 437-445, 2004.
- [6] J. S. Kimbell, M. N. Godo, E. A. Gross, D. R. Joyner, R. B. Richardson, and K. T. Morgan, "Computer simulation of inspiratory airflow in all regions of the F344 rat nasal passages," *Toxicology and Applied Pharmacology*, vol. 145, pp. 388-398, 1997.
- [7] G. J. Garcia and J. S. Kimbell, "Deposition of inhaled nanoparticles in the rat nasal passages: dose to the olfactory region," *Inhalation toxicology*, vol. 21, pp. 1165-1175, 2009.
- [8] J. Jiang and K. Zhao, "Airflow and nanoparticle deposition in rat nose under various breathing and sniffing conditions—a computational evaluation of the unsteady and turbulent effect," *Journal of aerosol science*, vol. 41, pp. 1030-1043, 2010.
- [9] J. D. Schroeter, J. S. Kimbell, B. Asgharian, E. W. Tewksbury, and M. Singal, "Computational fluid dynamics simulations of submicrometer and micrometer particle deposition in the nasal passages of a Sprague-Dawley rat," *Journal of Aerosol Science*, vol. 43, pp. 31-44, 2012.
- [10] Y. D. Shang, J. L. Dong, K. Inthavong, and J. Y. Tu, "Comparative numerical modeling of inhaled micron-sized particle deposition in human and rat nasal cavities," *Inhalation Toxicology*, vol. 27, pp. 694-705, 2015.
- [11] J. L. Dong, Y. D. Shang, K. Inthavong, J. Y. Tu, R. Chen, R. Bai, et al., "Comparative Numerical Modeling of Inhaled Nanoparticle Deposition in Human and Rat Nasal Cavities," *Toxicological Sciences*, vol. 152, pp. 284-296, 2016.
- [12] Y. Shang, J. L. Dong, K. Inthavong, and J. Y. Tu, "Computational fluid dynamics analysis of wall shear stresses between human and rat nasal cavities," *European Journal of Mechanics B-Fluids*, vol. 61, pp. 160-169, 2017.
- [13] Y. D. Shang, K. Inthavong, and J. Y. Tu, "Detailed micro-particle deposition patterns in the human nasal cavity influenced by the breathing zone," *Computers & Fluids*, vol. 114, pp. 141-150, 2015.

## SEGMENTATION OF PAP SMEAR IMAGES TO IDENTIFY AND DETECT CERVICAL CANCER

Vasundhara Acharya<sup>1</sup>, Preetham Kumar<sup>2</sup>

<sup>1</sup>Student, Dept. Of Information & Communication Technology, Manipal Institute of Technology, Manipal  
University, Manipal -576104, India.

<sup>2</sup>Professor, Dept. Of Information & Communication Technology, Manipal Institute of Technology, Manipal  
University, Manipal -576104, India.

### ABSTRACT

Cervical Cancer arises in the Cervix. It is caused due to Human Papillomavirus. The cancerous cells are located near transition area between the vagina and the uterus known as the squamo-columnar junction. Invasive cancer has the ability to spread to regional lymph nodes, the lungs, the liver, the bladder, the vagina, and the rectum. The cancer progresses slowly from normal stage to pre-cancerous stage and hence it provides an opportunity to diagnose it and prevent it. Visual inspection of the Pap smear is tedious and time consuming. Commercial systems for automated analysis are costly which makes it unaffordable for most hospitals. The main aim of this research work is to identify if the cervical cancer is Squamous cell carcinoma or Adenocarcinoma by segmenting the Pap smear images. Image Segmentation and Boundary detection techniques are utilised to clearly separate the nucleus from the cytoplasm. Automated cropping procedure is implemented to have one cell per image that allows to extract the cytoplasm features. The work extracts texture, shape and pixel value measurements to classify the cancer in to its respective categories. It also classifies Squamous cell carcinoma as Low-grade Squamous intraepithelial lesion (LSIL) or High-grade Squamous intraepithelial lesion (HSIL). It usually takes 3 weeks for the pathologists to generate the Pap smear results. The proposed work identifies the stage of the cancer within few seconds. It works for images with different stains and images with single cell and multiple cells. It achieved an accuracy of 98 percent when the results obtained were compared with the clinical results.

*Keywords: Cervical cancer, Pap smear, Squamous cell carcinoma, Adenocarcinoma. Automated cropping*

### INTRODUCTION

Cervical cancer is a cancer located in ectocervix, endocervix and transformation zone. Human Papilloma Virus is the root cause of cervical cancer. A recent survey says that, every seven minutes one woman loses her life because of cervical cancer and it is approximated to be one death in every 4.6 minutes by 2025. Initially precancerous changes are seen in the normal cells which later become cancerous cells. Effect of cancer can be warded off if it is detected in early stage since the growth of the cancer cells takes about 10-15 years. Cervical cancer can be detected by using a Pap smear, also called a Pap test. It identifies the abnormality present in the cells. Manual processes of analysis incur a lot of time and it is tiring to visualize millions of cells. The probability of sampling errors is high in this case. The analysis of Pap smear images of cervical region is based on distribution of the cell nuclei, shape and texture features of them. The research work intends to classify the instances in to two classes which are Squamous Cell Carcinoma and Adenocarcinoma. This approach uses MATLAB to analyze the Pap smear images. N/C ratio plays a vital role in diagnosis of cancerous cells. The nucleus is identified using Contrast adjustment and a number of morphological operations. The

Cytoplasm is obtained by using automated cropping technique with coordinates computed using the nucleus boundary detection. Binary Morphology is used to determine the cytoplasm area. The N/C ratio along with the other shape and texture features obtained from the image is analyzed using WEKA tool. An efficient data mining algorithm is used to classify the instances in to respective classes and the stage of cancer is identified. It also intends to predict the stage when a new patient data is given as an input based on the knowledge gained from the training phase.

### LITERATURE REVIEW

In [1] the author has used two hybrid steps approach to attain cell segmentation. Waterfall algorithm was used to construct the nested hierarchy. A Segmentation criterion was used to select the most appropriate hierarchy.

In [2] the author proposed a technique to classify the elements present in the Pap smear image using the Color intensity values. Variational Level Set Formulation of Curve evolution without reinitialization was used to determine the range of color intensity values of the cells. The normal cells had the color intensity between 122-150. The abnormal cells had in between 80-100.

In [3] the author proposed an unsupervised

technique to detect the overlapping cytoplasm of the cell. H-maxima transform was applied and the binary image was obtained using the regional maxima of the image. The cytoplasm was obtained using the distance regularized level set model.

In [4] the author proposed a technique to separate the normal cells from the inflammatory cells and classify them using the J48 algorithm. The algorithm considered only 8 features out of 11 for the construction of the rules. The classifications were performed along the different directions.

## LIMITATIONS IN THE EXISTING SYSTEM

Determination of stage of tumor at the earliest plays an important role in the field of medicine. Due to the complication of the disease it goes undiagnosed. Invasive cancer has the ability to spread to regional the lungs, lymph nodes, the bladder, the liver, the vagina, and the rectum. The delay in the diagnosis leads to further division of the stem cells which aggravate the condition. The present procedures incur a lot of cost and time and are imprecise. The accurate segmentation of the Pap smear images cannot be achieved using a single algorithm.

## METHODOLOGY

In the proposed work, the data mining technique is applied in the health sector. It intends to predict the stage of cervical cancer using Pap smear images. It identifies if the cell is a normal one or the cancer is a Squamous Cell Carcinoma or Adenocarcinoma. It further classifies Squamous Cell Carcinoma in to HSIL and LSIL. The manual procedure of detection of status of cancer involves a lot of effort and is error prone. The results will be highly dependent upon the physician's skills. A computer aided automated system would prove to be boon in this field.

### A. Description of Dataset

In this research work the data set is prepared by extracting features from the images using image segmentation algorithms. The Pap smear images are collected from public image database of Herlev University Hospital, Denmark with 917 images [5], Kasturba Medical Hospital, Manipal-India (6 images), International Agency for Research on Cancer [6] and DoveMed [7] (remaining images). The analysis is performed on 1000 images collected from the above data sources. The features extracted from the images is used to build the training data. The trained model is used to predict the stage of tumor in new cases. In the proposed work, 25 features are extracted. The features extracted are given in the Feature extraction section.

### B. System Description

The system development involves preparing the training data and classifying the new instances using the knowledge derived by the classifier from the training phase. The different classifiers like Naïve Bayes, Multinomial Logistic Regression, Decision tree, Support vector machine and Random Forest are used in the proposed work and the one with highest accuracy is chosen for further steps.

### C. Segmentation of Nucleus and Cytoplasm of White blood cell from Blood smear image with normal dimension and Feature Extraction.

The following steps are followed to achieve the goal of segmentation and feature calculation:

#### 1. Image Pre-Processing:

1.1 *Convert the Image to Gray scale:* "rgb2gray" function is used to convert the image to gray scale. It eliminates the hue and saturation information while retaining the luminance. The conversion is done as gray scale image is required for further processing.

1.2 *Adjust the contrast of the image:* In order to obtain accurate results with images stained with different stains like Haemotoxylin and Eosin and Papanicolaou stain, we have used four different types of contrast enhancement methods. They are mentioned below:

1.2.1. *Using Histogram Equalization:* The histogram of the image is equalized using the "histeq" function. The contrast of the resulting image is enhanced using the "imadjust" operation.

1.2.2. *Using the stretch limits:* The contrast of the image is adjusted using the "imadjust" function. The stretch limits used in this research falls in the range of 0.1 to 0.7. This step is undertaken to enhance the quality of the image.

1.2.3. *Addition of two channels:* The Red, Green and Blue channels of the RGB image are extracted individually. The contrast of Red and Green channel is enhanced using the "imadjust" operation with stretch limits in the range 0.3 to 0.5. The resulting images are added using the "imadd" operation. Histogram equalization operation is applied to the resulting image.

1.2.4 *Using Local Laplacian Filter:* The RGB image is filtered with an edge aware filter. Amplitude of the edges is given by the sigma and alpha does the controlling of smoothing of the details. In the proposed work sigma value is set as 0.2 and alpha is set as 2. Number of levels is set as 10 while applying the filter. The individual channels are extracted and green component is chosen for further processing.

#### 2. Image Segmentation

2.1 *Convert the image to binary to obtain the nucleus:* Based on the type of contrast adjustment technique chosen, the method to convert to binary is

opted. Case 1 is opted when the Histogram Equalization is used for contrast adjustment. Case 2 is opted when contrast is enhanced using the stretch limits. Case 3 is opted when the channels are added to improve the contrast. Case 4 is used when Local Laplacian filter is used to adjust the contrast.

2.1.1 *Case 1*: The image is converted to binary for further processing using a level value 0.37. The image is complemented to highlight the nucleus.

2.1.2 *Case 2*: The image is converted to binary using global Otsu's threshold. The image is complemented to highlight the nucleus.

2.1.3 *Case 3*: The image is converted to binary using a threshold value of 100. The image is complemented to highlight the nucleus.

2.1.4 *Case 4*: The image is converted to binary using a threshold value of 90. The image is complemented to highlight the nucleus.

## 2.2. Obtain the Cytoplasm:

In the proposed work two types of images are taken in to consideration. One with single cell per image and another with many cells. The work intends to extract the cytoplasm from Pap smear images using an automated approach. Previous works involved the manual cropping of the images to have one cell per image. But this work overcomes the drawback by automating the technique.

2.2.1. *Extract cytoplasm when one cell exists per image*: The Original image is converted to gray scale. The resulting image is applied with the contrast adjustment to enhance the quality. The image is converted to binary using the Otsu's threshold. The noise is filtered by applying a median filter value with 15\*15 neighborhood. The unwanted small particles in the image are separated by choosing a value of 4000. The values used for filtering of noise and morphological open operation are chosen after analyzing over a number of images.

2.2.2. *Image with Clustered cells*: In this research work an automated approach for cropping of the cells is specified. The procedure is specified below:

### Algorithm 2: Pseudo code for the extraction of Cytoplasm from Pap smear image

Input: Image of the Pap smear

Output: Extracted Cytoplasm.

1. Convert the RGB image to Gray Scale
2. Obtain the image of the nucleus obtained from the nucleus extraction stage.
3. Obtain the boundary of the image using the "bwboundaries" function.
4. for 1 to NumberOfBlobsdo
  - 4.1. Obtain the X and Y coordinate value.
  - 4.2. Compute the minimum value of x and y coordinate.
  - 4.3. Use the "imcrop" function with the cropping rectangle's x coordinate as minimum x value minus 10 and y coordinate as minimum value minus 15

with width and height as .

4.4. Adjust the contrast of the image using the "imadjust" function.

4.5. Equalize the image using the "histeq" function and convert it to binary with a level value of 0.65.

4.6. Fill the holes and use an area open function with value of 70.

### End For.

Area of extracted cytoplasm is calculated using the "regionprops" function.

### 3. Image Post-processing:

#### 3.1. Separate the touching objects using the Watershed transform:

The Nucleus extracted from the images will be touching each other. Touching cells if not separated generate inaccurate results. Watershed transform of the distance transform is calculated. The ridge lines obtained are used to segment the binary image. The existing Watershed algorithm faces the problem of over segmentation. So, we modify it. Tiny local minima are eliminated using the function "imextendedmin" . Distance transform is then modified so that no minima occur at the filtered out locations using the function "imimposemin" . Watershed is applied again to the resulting image. After the above operation, the touching objects will be clearly separated.

#### D. Feature extraction

The texture and shape features are calculated for the objects in the image using "region props" function. These features help the doctor to differentiate a cancerous cell from a non-cancerous one and also identify in to which category the tumor falls. The features extracted are as follows:

##### 1. Shape Features:

1.1 Eccentricity: It specified how much a shape of a nucleus deviates from being circular. The abnormal cells will have higher eccentricity due to abnormal bulging.

1.2 Centroid: Represents the center mass of the region.

1.3 Orientation: Angle between the x-axis and the major axis of the ellipse that has the same second-moments as the region.

1.4 Major Axis length: Gives the length of the major axis of the ellipse. The normal cells will a value below 30 and the abnormal cells will have a value above 30.

1.5 Area: Actual number of pixels in the region.

1.6 Solidity: Ratio between area and convex area.

1.7 Equivalent Diameter: Diameter of a circle with the same area as the region. The value for normal cells will be below 20. The cancerous cells will have a value above 20.

1.8 Perimeter: Specifies the distance around the boundary of the region. The perimeter of normal cells will be below 100. The cancerous cells will



have a value above 100.

1.9 Minor axis length: Gives the length of the minor axis. The normal cells will have a value below 20 and the abnormal cells will have a value above 20.

1.10 Form factor: The ratio between Area and perimeter. The Eq. (1) gives the Form factor value.

$$\text{Form Factor} = (4 * \pi * \text{Area}) / (\text{Perimeter} * \text{Perimeter}) \quad (1)$$

1.11 Roundness: Measure of how closely the shape of an object approaches that of a circle. Cancerous cells will have a roundness value above 12.

1.12 Radius: Measures the radius of the cells.

1.13 Elongation: Specifies the lengthening of a cell during the cell differentiation process. Cancerous cells will have an elongation value above 2.

1.14 Cytoplasm Area: Measures area of the cytoplasm which is used in calculating the N/C ratio.

1.15 N/C ratio: Specifies the ratio between the area of the nucleus and cytoplasm.

## 2. Pixel Value Measurements

2.1. Maximum Intensity: Specifies the value of the pixel with the largest intensity in the region. Normal cells will have a value below 200. Abnormal cells will have a value above 200.

2.2 Minimum Intensity: Specifies the value of the pixel with the smallest intensity in the region. Normal cells will have a value below 150. Abnormal cells will have a value above 150.

## 3. Texture Features

3.1 Entropy of the image: It measures the randomness that can be used to identify the texture of the input image. Cancerous cells will have a value above 1.

3.2 Contrast of the image: Measures the intensity contrast between a pixel and its neighbor over the whole image. Normal cells will have a contrast value below 0.1 and cancerous cells will have a value above 0.1

3.3 Correlation of the image: Returns a measure of how correlated a pixel is to its neighbor over the whole image. Normal cells will have a value above 0.5 and cancerous cells will have a value below 0.5.

3.4 Energy of the image: Specifies the uniformity of the image. Normal cells will be more uniform than the abnormal cells. Abnormal cells will be non uniform due to bulging. It is computed using the Eq. (2).  $P_i$  and  $P_j$  represent the marginal probabilities.

$$\sum \sum p(i,j)^2 \quad (2)$$

3.5 Homogeneity: Measures the closeness of the distribution of elements in the GLCM to the GLCM diagonal.

3.6 Contrast of the nucleus: It is the measure of the amount of local variations present in the image. Adenocarcinoma cells will have a value below 0.5 and Squamous cells will have a value above 0.5.

3.7 Difference Entropy: Returns the difference between the entropy values.

## 4. Fractal Dimension

4.1 Hausdorff Dimension: It is a quantity that indicates how completely a fractal appears to fill space. Box counting algorithm is used here. In box counting algorithms, the number of boxes covering a point set is a power law function of the box size. They indicate the roughness of the object. The Hausdorff dimension of a cancerous cell will be above 1. Normal cells will have a value below 1.

## E. Data Pre processing

Data preprocessing plays an important role in the data mining process. Usually the process of gathering data involves many errors, resulting in out-of-range values, impossible values. This stage plays a very important role in getting the accurate results.

## F. Feature Selection

Feature selection methods can be used to achieve efficient data reduction. In this research work, the subset of attributes is assessed using the InfoGainAttributeEval and the Ranker Search method is used. The attributes such as the cell id Centroid, Orientation which do not contribute to the classification are eliminated.

## G. Classification and Prediction of unknown class label

The classification algorithm is used to classify the data into groups. At the initial stage the training data set is used to train the classifier and then the test data is used to test the accuracy of the classifier algorithm. In this research work the classification algorithm classifies the instances of cervical cancer into Adenocarcinoma/Squamous carcinoma/Normal cell. In the proposed work, Random forest algorithm is used for classification. The accuracy of the algorithms is compared. It was found that Random forest outperformed other algorithms. It operates by constructing large number of decision trees at training time and predicts the unknown class labels at the prediction stage.

## RESULTS & DISCUSSION

The results obtained after the application of segmentation algorithm over the Pap smear images is discussed here. Table 1 shows the confusion matrix obtained using the Random forest algorithm. A indicates Adenocarcinoma instances. B indicates Normal instances. C indicates instances of High grade Squamous epithelial lesion. D indicates instances of Low grade Squamous epithelia lesion. Each instance indicates the cell present in the image. The Random forest classified the instances with 100 percent accuracy. Fig.1.–Fig.8. represents the images used to test the accuracy of the proposed work. Fig.4. represents the box plot. Test images are different from the images that are used for training. The features of the cells present in the image were

extracted and were given as input to Random forest algorithm for prediction. The input file was fed in form of ARFF (Attribute-Relation File Format). The Random forest algorithm predicted the stage by utilizing the knowledge gained from training model. The diagnosis done by the proposed system is compared with diagnosis done by experts. The evaluation done by experts is specified by DoveMed and International Agency for Research and Cancer (IARC). DoveMed is a health portal with medical content that is trusted by the physicians. IARC provides the classification of human tumors that helps in the cancer research. In the proposed work , a counter is set to count the number of cells falling under each category. This counter helps in identifying the final stage of tumor. The stage of tumor is declared to be in HSIL stage , if even one cell in the image is predicted as HSIL. It is done to prevent any risks as HSIL is dangerous. Fig.9. depicts the extraction of Cytoplasm from a normal Pap smear image when there is one cell per image. Fig .10. depicts the extraction of cytoplasm from an instances of High grade intra epithelia lesion by using the automated cropping technique. Second object is extracted from the labeled image obtained using case 1. Fig.11. Represents the cells extracted from the normal, Squamous cell carcinoma and Adenocarcinoma category. Significant feature values that helps in differentiating Normal, SCC and Adenocarcinoma is tabulated in Table 2.

Table 1. Confusion Matrix

Matrix	A	B	C	D
A	251	0	0	0
B	0	888	0	0
C	0	0	479	0
D	0	0	0	196

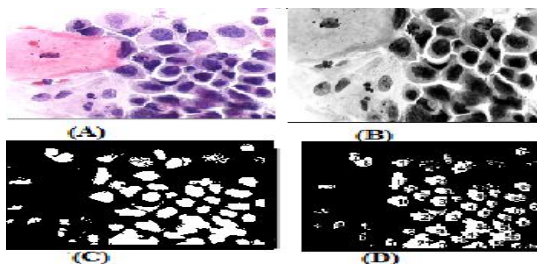


Fig.1. Img\_001 A. Input Image, B. Histogram Equalized Image, C. Binary Image, D. Image having nucleus after processing and labeling operation.



Fig.2. Imag\_002 A. Input image. B. Extracted and labeled nucleus.

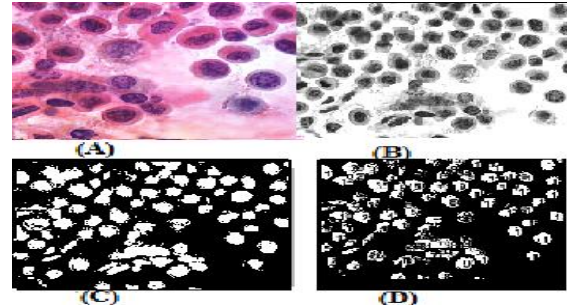


Fig.3. Img\_003 Depicts the image of the nucleus extracted from Squamous cell carcinoma using the contrast stretch operation with the stretch limits and binary conversion as in case 2.

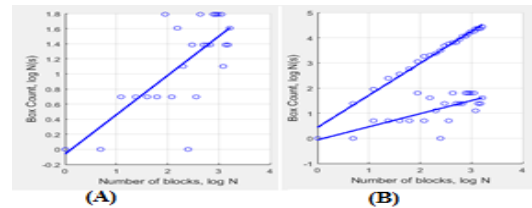


Fig.4. A. Box plot of Normal cell. B. Box plot of Cancerous cell

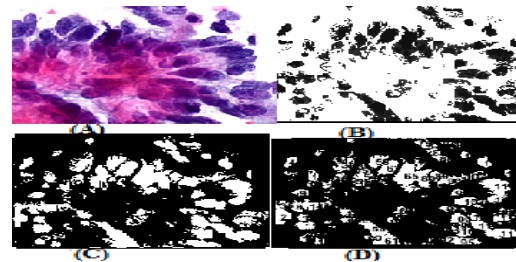


Fig.5. Img\_004 Depicts the image of the nucleus extracted from Adenocarcinoma using the addition of two channels and binary conversion as in case 3.

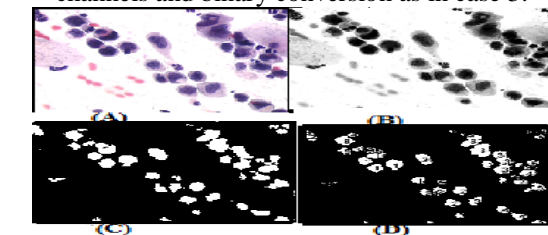


Fig.6. Img\_005 Depicts the image of the nucleus extracted from Squamous cell carcinoma using the Fast Laplacian filter and binary conversion as in case 4.

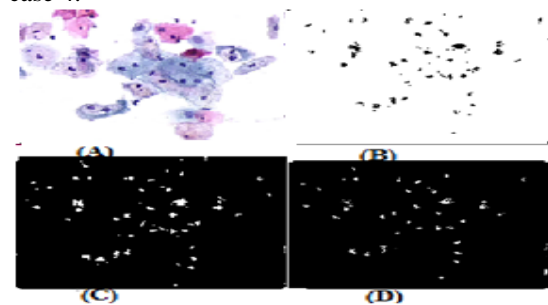


Fig.7. Img\_006 Depicts the image of the nucleus extracted from LSIL (Squamous Cell Carcinoma)

using the addition of two channels and binary conversion as in case 3.

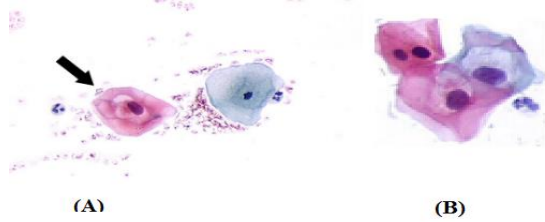


Fig.8. Img\_007 Depicts pap smear images of LSIL (Squamous Cell Carcinoma) .

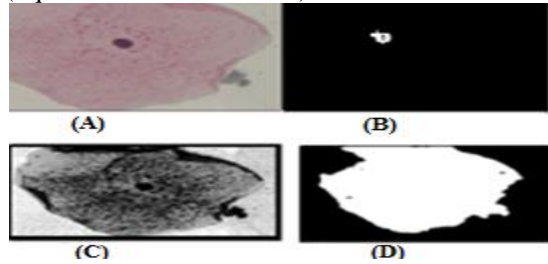


Fig.9. A. Input image. B. Labeled Nucleus. C. Contrast adjusted image. D. Extracted cytoplasm.

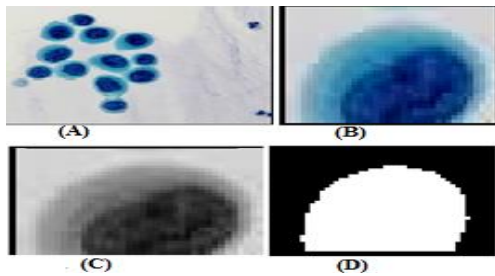


Fig.10. A. Input Image. B. Cropped Image. C. Contrast Adjusted Image. D. Binary Image of the Cytoplasm.

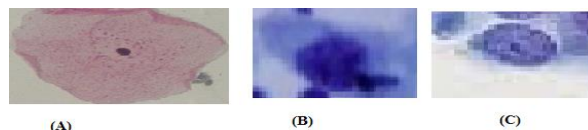


Fig.11. A. Normal cell. B. Squamous cell. C. Adenocarcinoma cell.

Table 2. Values of some significant features

Feature	Ncell	Scell	Acell
Eccentricity	0.64579	0.620864	0.70152
Form factor	1.00190	0.534535	0.86057
Elongation	1.50555	2.08796	4.02783
N/C ratio	0.21504	1.907773	0.61690
Diff Entropy	0.16504	0.37083	1.02441
Hausdorff	0.5125	1.1492	1.2122

Table 3: Count of cells present in the test images.

I	C	D	B	A	C5	C6
1	46	6	20	0	HSIL	HSIL [8]
2	0	0	1	0	Normal	Normal [5]

3	77	7	49	0	HSIL	HSIL [8]
4	0	0	78	54	Adeno	Adeno [9]
5	12	9	36	0	HSIL	HSIL [8]
6	0	38	2	0	LSIL	LSIL [10]
7A	0	1	1	0	LSIL	LSIL [10]
7B	1	1	2	0	HSIL	LSIL [10]

Table 3 gives the count value of the cells present in images used for testing. The stage predicted by the Random forest algorithm is compared with the ground truth. In the proposed work, one instance of LSIL is misclassified as HSIL (Img\_007B). C and D denote HSIL and LSIL. B and A denote normal cells and Adenocarcinoma cells. C5 denotes the prediction done by the system. C6 denotes ground truth. The misclassification is due to the minute error in the stage of segmentation. The LSIL cells have low grade changes that make it to look like a normal cell. In some cases, the LSIL cells will have a reactive change, which makes it to look like HSIL. The accuracy is computed by comparing the results predicted by the proposed system with the ground truth. The proposed work achieved an accuracy of 87.5 percent for these test images, as it misclassified one instance of LSIL as HSIL.

## CONCLUSION

The main aim of this work is to accurately segment the Pap smear image to obtain its components. After performing a survey, we identified that accurate segmentation of the image cannot be done with single segmentation algorithm. A combination of algorithms is required to achieve precise segmentation. Texture, shape and visual features are extracted to differentiate between different categories of cervical cancer and normal cell. A comparison is done between supervised learning algorithms and the one with highest accuracy. Random Forest was found to outperform other algorithms. The work achieved an accuracy of 87.5 percent in successfully identifying the stage of tumor in new patients when it was compared with clinical results (Ground truth).

## REFERENCES

- [1] Mingzhu Zhao, Lei Chen, L. B. J. Z. C. Y. and Zhang J., "Feature quantification and abnormal detection on cervical squamous epithelial cells," Computational and Mathematical Methods in Medicine, vol. 2015, no. 2015, 2014, pp.1–9.
- [2] Happy S. L., Chatterjee S., and Sheet D, "Unsupervised segmentation of overlapping cervical cell cytoplasm," CoRR, vol. abs/1505.05601, 2015.
- [3] Eko Supriyanto, Nur Azureen M. Pista, L. H. I. B. R. and Mengko, "Automatic detection system of cervical cancer cells using color

- intensity classification,” in Proceedings of the 15th WSEAS Int. conf.on Computers, 2011, pp. 303–307.
- [4] Dwiza Riana, D. H. W. and Mengko T. L., “Extraction and classification texture of inflammatory cells and nuclei in normal pap smear images, “in 4th Int. Conf. on Instrumentation, Communications, Information Technology, and Biomedical Engineering, November 2015, pp. 65–69.
- [5] Pap Smear dataset. [Online]. Available <http://mde-lab.aegean.gr/index.php/downloads>.
- [6] Pap Smear images.[Online]. Available: <http://screening.iarc.fr/atlascyto.php?lang=1>
- [7] Pap Smear images. [Online]. Available: <http://www.dovemed.com/diseasesconditions/squamous-cell-carcinoma-of-cervix/>
- [8] Diagnosis done by experts.[Online]. Available: [http://screening.iarc.fr/atlascyto\\_list.php?cat=F1c2&lang=1](http://screening.iarc.fr/atlascyto_list.php?cat=F1c2&lang=1)
- [9] Diagnosis done by experts.[Online]. Available: [http://screening.iarc.fr/atlascyto\\_detail.php?flag=0&lang=1&Id=cyto6185&cat=F2b](http://screening.iarc.fr/atlascyto_detail.php?flag=0&lang=1&Id=cyto6185&cat=F2b).
- [10] Diagnosis done by experts.[Online]. Available: [http://screening.iarc.fr/atlascyto\\_list.php?cat=F1b&lang=1](http://screening.iarc.fr/atlascyto_list.php?cat=F1b&lang=1)

***Environment***

## NUTRIENT LOADS AND SELF-REMEDICATION ASSESSMENT IN KHLONG RUNGSIT TAI, PATHUM THANI PROVINCE, THAILAND

Boontarika Thongdonphum<sup>1</sup>, Kittima Vanichkul<sup>2</sup>, Saming Champasri<sup>3</sup> and Jirapon Kulkham<sup>4</sup>

<sup>1</sup>Faculty of Agricultural technology, Rajamangala University of Technology Thanyaburi, Thailand

### ABSTRACT

The aim of this work was to investigate on the aquatic environmental factors and nutrients transfer patterns. The aquatic environmental impacts assessment was conducted based on analysis water quality of the Klong Rungsit Tai, Pathum Thani Province, Thailand of 6 sampling stations surveyed during September 2014 and March 2015. The results showed that aquatic environmental factors varied by season. The results indicated that ammonium-nitrogen ( $\text{NH}_4^+\text{-N}$ ), nitrite and nitrate-nitrogen ( $\text{NO}_2^- + \text{NO}_3^-\text{-N}$ ), and orthophosphate phosphorus ( $\text{PO}_4^{3-}\text{-P}$  or P) concentration ranged between 10.79-85.35  $\mu\text{M}$ , 56.70-135.79  $\mu\text{M}$  and 0.74-5.66  $\mu\text{M}$ , respectively. Analysis of the dissolved inorganic nitrogen (DIN) and P transfers patterns showed that self-remediation were rarely found in dry season. Levels of DIN and P load ranged between [5.05 and 0.40 tonne/day] and [5.12 and 0.32 tonne/day] in September 2014 and March 2015, respectively. The positive relative remediation efficiency ( $\text{EF}_\text{R}$ ) for DIN and P were highest in September 2014. The  $\text{EF}_\text{R}$  for DIN and P were [39.60%] and [12.82%], respectively. The negative  $\text{EF}_\text{R}$  were found in March 2015, indicating that input loads were higher than output loads. The whole results have revealed that water mass transfer direction and water drainage affected to self-remediation and accumulation of nutrients in the study area.

*Keywords: Nutrient loads, Self-remediation, Aquatic environmental factors, Dissolved inorganic nitrogen, Orthophosphate phosphorus*

### INTRODUCTION

Klong Rangsit Tai is the part of Klong Rangsit Prayurasakdi, as known Klong Rangsit or Rangsit canal, is located at Rangsit, Pathum Thani Province, in the eastern part of Chao Phraya River, centre of Thailand [1]. Runs from Thung Luang, Pathum Thani Province and flows toward into the Nakhon Nayok River. Klong Rangsit is approximately 54 kilometre in length [2]. Land utilization have been discussed as urbanization, agriculture, aquaculture, and industrial purpose [3]. Its has long been known that changes of river flow could impact biochemical composition, including nutrient loading, in the river and thereby phytoplankton abundance [4].

Here, the Klong Rangsit supports a resident population about 1,010,898 people (662.51 people per square kilometer) that related to the deterioration of water quality induced mainly by sewage, domestic discharges, and agricultural utilization [5]. In [6], reported that water quality in the urbanization area were deterioration. Increasing of urbanization, industrial and agricultural developments, and inadequate sewerage system had contributed material inputs in to the water resource [7].

Pollution problems can occur according to untreated municipal and industrial wastewater, eutrophication, trace metals contamination and petroleum hydrocarbon [8]. River water chemistry is controlled by natural factors, rainfall, and

anthropogenic factors such as land use, urbanization, sewage discharge, and nonpoint sources like storm water runoff and runoff from agricultural and urban areas [9]. Thus, this research aimed to assess the impacts of nonpoint sources nutrient loads, together with the nutrient transfer patterns in the impacted site. The findings could subsequently be used to establish a better management of water resources in this area.

### MATERIALS AND METHODS

#### Sampling sites

The surveys were conducted at 6 sampling stations (stn.) at Klong Rangsit Prayurasakdi, Rangsit, Pathum Thani Province, the stations of which nearly the residential areas, spanning from September 2014 to March 2015 (Fig.1). According to the rainfall patterns, Thailand is under the influence of monsoon winds [10]. The seasons can thus be divided into rainy season (May-September), winter season (October-February), and dry season (March-April). In addition, large amounts of water typically flow into the this area depends on the Chao Phraya River flows and is the head works of the South Rangsit Irrigation Office which diverts and distributes water to about 0.7 million rai (1 ha = 6.25 rai) [6]. Water samples from the 6 stations were collected during the two seasonal periods for the 2-



year interval such that all possible loading periods were taken into consideration.

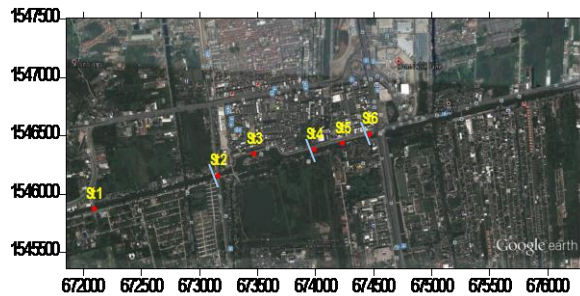


Fig. 1 Sampling stations (Stn. 1-6) and 3 cross-sectioned sites located at Klong Rangsit Prayurasakdi, Pathum Thani Province, Thailand.

### Sample collection and analysis

Temperature, dissolved oxygen (DO), salinity, and pH, were measured with a multi-parameter probe (YSI-6600 Sonde instrument) at the sampling sites. At each stations, surface water (30 cm deep) samples for nutrient analysis were pre-filtered through GF/F (Whatman) and then stored at 4°C before transporting to the laboratory. Ammonium ( $\text{NH}_4^+$ ), nitrite and nitrate ( $\text{NO}_2^- + \text{NO}_3^-$ ), and orthophosphate ( $\text{PO}_4^{3-}$ ) concentrations were determined using a SKALAR segmented flow analyzer.

### Nutrient transfer analysis

To assess nutrient transfer was conducted for 3 selected cross-sectioned sites (Fig 1), which were calculated with a two-dimensional Surfer model. Water mass and nutrient transfer were determined as dissolved inorganic nitrogen (DIN;  $\text{NH}_4^+ + \text{NO}_2^- + \text{NO}_3^-$ ) and orthophosphate phosphorus (P;  $\text{PO}_4^{3-}$ ) based on the nutrient balance method. The amount of nutrient loads were estimated using equation (1);

$$M_i = 8.64 \times 10^{-7} [\text{Conc}] A_i U_{hi} \Delta t_i \quad (1)$$

where:  $M_i$  = amount of each nutrient load (tonne/day),  $[\text{Conc}]$  = concentrations of DIN or P ( $\mu\text{g/L}$ ),  $A_i$  = cross-sectional area ( $\text{m}^2$ ) of section I,  $U_{hi}$  = flow velocity (cm/s) passing through section I, and  $\Delta t_i$  = time under a focus period (1 day) in section i [11].

### Data analysis

Comparisons of water quality in terms of temperature, salinity, DO, and pH between the sampling periods were performed using descriptive statistic as average levels and distribution characteristics. T-test was used for the

environmental variation comparison, and the level of confidence greater than 95% ( $p \leq 0.05$ ) was considered to indicate a statistically significant impact. The relative remediation efficiency ( $\text{EF}_R$ ) of each station was approximated using equation (2);

$$\text{EF}_R (\%) = [(\text{Input} - \text{Output}) / \text{Input}] \times 100 \quad (2)$$

where: Input and Output are amounts of DIN or P that transferred into and out of each section, respectively.

## RESULTS

Table 1 tabulates the results of water quality during study period. Water temperature and salinity varied slightly with seasons ( $p \leq 0.05$ ) and tend to decrease in dry season. The pH level was found to be relatively constant for the entire study area, while DO varied and markedly decreased to unsuitable levels ( $< 4 \text{ mg/L}$ ) in during study period. The levels of  $\text{NH}_4^+$  and  $\text{NO}_2^- + \text{NO}_3^-$  varied significantly ( $p \leq 0.05$ ) with seasons. The concentrations of  $\text{NH}_4^+$  and  $\text{NO}_2^- + \text{NO}_3^-$  varied from 10.79 to 85.35  $\mu\text{M}$  and 1.87 to 135.79  $\mu\text{M}$ , respectively. High of  $\text{NH}_4^+$  levels were recorded during the survey in September 2014, while  $\text{NO}_2^- + \text{NO}_3^-$  level were found during in March 2015.  $\text{PO}_4^{3-}$  levels ranged from 0.74 to 5.66  $\mu\text{M}$ .

Table 1 The water quality (mean $\pm$ SD) at Klong Rangsit Prayurasakdi during the study period.

Parameters	Study period	
	September 2014	March 2015
Temp ( $^{\circ}\text{C}$ )	31.43 $\pm$ 0.09 <sup>a</sup>	30.07 $\pm$ 0.05 <sup>b</sup>
DO (mg/L)	0.75 $\pm$ 0.35 <sup>a</sup>	2.90 $\pm$ 0.61 <sup>b</sup>
Salinity (psu)	0.27 $\pm$ 0.01 <sup>a</sup>	0.17 $\pm$ 0.01 <sup>b</sup>
pH	7.40 $\pm$ 0.12 <sup>a</sup>	7.50 $\pm$ 0.08 <sup>a</sup>
$\text{NH}_4^+$ ( $\mu\text{M}$ )	79.99 $\pm$ 4.33 <sup>a</sup>	27.73 $\pm$ 24.66 <sup>b</sup>
$\text{NO}_2^- + \text{NO}_3^-$ ( $\mu\text{M}$ )	5.21 $\pm$ 5.08 <sup>a</sup>	90.52 $\pm$ 29.42 <sup>b</sup>
$\text{PO}_4^{3-}$ ( $\mu\text{M}$ )	3.94 $\pm$ 1.37 <sup>a</sup>	2.20 $\pm$ 1.42 <sup>a</sup>

Note: The mean values in the same row with different superscript letters are significantly different ( $p \leq 0.05$ ).

Nutrient transport analysis was performed in the rainy and dry period for representing loading amounts in the area. Here, the water volume passed through 3 representative cross-sectioned sites and current velocities are shown in Table 2. The highest inflow volume and velocity were found at the stn. 4 of  $4.84 \times 10^6$  tonne/day and 50.31 cm/s, respectively. On the contrary, the lowest load and velocity of 0.91  $\times 10^6$  tonne/day and 10.06 cm/s, respectively, were found at the stn. 2.



Table 2 Water volume ( $\times 10^6$  tonne/day) and velocity (cm/s) of each section during rainy and dry period at the sampling site.

Station (Sectioned codes)	Section area ( $\text{m}^2$ )	Volume ( $10^6$ tonne/day)		Velocity (cm/s)	
		September 2014	March 2015	September 2014	March 2015
2 (R1)	105.24	2.68	0.91	29.44	10.06
4 (R2)	111.28	4.84	1.66	50.31	17.28
6 (R3)	98.61	2.81	3.49	32.95	40.95

Nutrient load estimation in the area indicated that DIN and P loads varied from 1.48 to 5.12 and 0.05 to 0.40 tonne/day, respectively. The highest of DIN was found at the R3 sectioned site during March 2015, while the highest of P load was located in R3 sectioned site during September 2014.

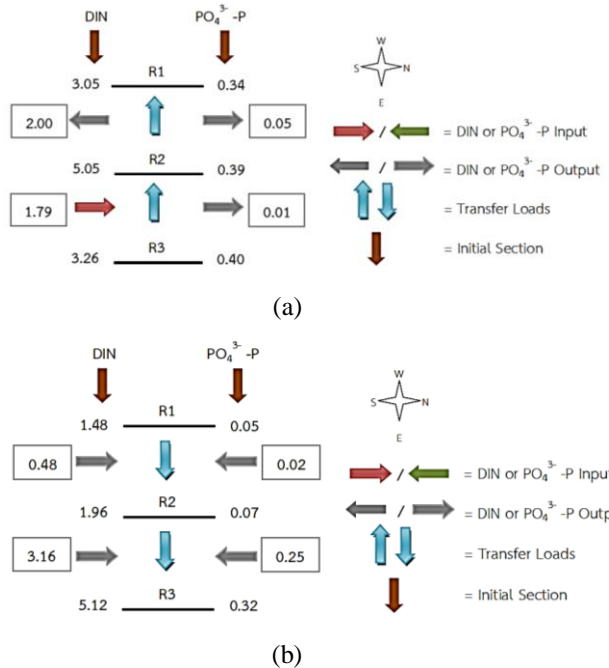


Fig. 2 DIN and P transport (tonne/day) in each cross-sectioned sites during (a) September 2014 and (b) March 2015.

Analysis of relative remediation efficiency ( $EF_R$ ) showed positive values only in the sections of R2 to R1 during rainy season. The  $EF_R$  in those area for DIN and P were [39.60%] and [12.82%], respectively. The other sectioned sites showed the negative values that reflected the level of Input loads were higher than the Output loads (Fig.3)

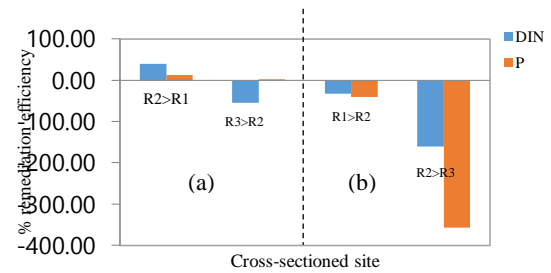


Fig. 3 The relative remediation efficiency (%) of DIN and P during (a) September 2014 and (b) March 2015.

## DISCUSSION

The general of water quality varied by season. Results showed the slightly changed of temperature, salinity, and pH, which were almost constant for the entire area. Freshwater inflow and precipitation-induced drainage influenced the level salinity [4]. Dissolved oxygen were low and showed the unsuitable levels ( $<4$  mg/l) for the living of aquatic animal [12], which was probably the result of bacterial decomposition of organic waste matter [4]. High nutrients concentration were apparent, reflected that the anthropogenic contamination because high population density and land use area are located near the water bodies. In [13], reported that nutrient loading in the river is controlled by natural and anthropogenic sources as runoff from urban areas, crop cultivation, and inflow through organic rich ground.  $\text{NH}_4^+$  is the important factor for water quality assessment that could be indicated the major anthropogenic and natural sources [14]. In [15], reported that  $\text{NH}_4^+$  levels in the water bodies should detect less than 1 mg/L (71.4  $\mu\text{M}$ ). Different nitrogen transformations may permanently occur in river floodplains and ecotones of the river bed and may involve several microbiological processes [16].  $\text{PO}_4^{3-}$  levels showed noticeably higher levels than the recommended level of 1  $\mu\text{M}$  that could cause eutrophication problems [4].

DIN and P loads revealed the impact of anthropogenic activity, water flow characteristics affected the water quality in the study area. Base water flow is a potential source of river nutrient, can provide dilution and enhance the transportation process through nutrient in base flow is from land use through leaching process, its efficiency could be significant physical function on self-remediation of the river ecosystem [11],[13]. Changes of land use could be leading to nitrogen enrichment in the river [17]. Relative remediation efficiency ( $EF_R$ ) analysis of the area were almost negative  $EF_R$ , indicating that

Input loads were higher than Output loads [11], reflected the high level of anthropogenic inputs from dispersed sources as fertilizers or point sources as wastewater facilities have altered the land-sea fluxes [18] and disturb the balance of the water ecosystem [19].

## CONCLUSION

The general of water quality, namely dissolved oxygen could be reflected to water resource deterioration in this area. Levels Of DIN and P loads were high in the rainy season, 5.05 tonne/day and 0.40 tonne/day, respectively. Based on  $EF_R$  estimation of DIN and P revealed that the level of Input loads were higher than the Output loads. The research finding showed that water mass direction effected to water drainage, nutrient dilution, and nutrient accumulation in the area.

## ACKNOWLEDGEMENTS

The authors would like to extend deep gratitude to the Faculty of Agricultural Technology, Rajamangala University of Technology, Thanyaburi (RMUTT) for the financial support.

## REFERENCES

- [1] Pathum Thani Office Center, "Development Plan of Pathum Thani Province", assessed : <http://www2.pathumthani.go.th/551017.pdf>. (April 3, 2017)
- [2] RIO 11, "Data project". South Rangsit Irrigation Project, Regional Irrigation Office 11, Royal Irrigation Department , Ministry of Agriculture and Cooperatives, assessed : <http://ridceo.rid.go.th/pathum/rangsits/Data.html>(Aug 22, 2012)
- [3] Thongkumpow J & Sumpunpanit P, "Water use patterns of the irrigation area in Klong Rung Sit Tai", Environmental research institute, Chulalongkorn university intellectual repository, 1997.
- [4] Thongdonphum B, Meksumpun S, Meksumpun C, Sawasdee B & Kasemsiri P, "The Predictive Model for Biochemical Component of Phytoplankton in the River and Estuary System of the Mae Klong River, Thailand", International Journal of Environmental and Rural Development, Vol. 4-1, 2013, pp. 13-18.
- [5] REO 6, "Environmental Status in the Western Report", 2011, Ministry of Natural Resources and Environment, Thailand.
- [6] RIO 11, "Data project". South Rangsit Irrigation Project, Regional Irrigation Office 11, Royal Irrigation Department , Ministry of Agriculture and Cooperatives, assessed : <http://ridceo.rid.go.th/pathum/rangsits/Data.html> (May 2, 2017)
- [7] Glibert PM, Mayorga E & Seitzinger S, "Prorocentrum minimum tracks anthropogenic nitrogen and phosphorus inputs on global basis: application of spatially explicit nutrient export models", Harmful Algae, Vol. 8, 2008, pp.33-38.
- [8] Cheevaporn V & Menasveta P, "Water Pollution and Habitat Degradation in the Gulf of Thailand", Marine Pollution Bulletin, Vol. 47, 2003, pp. 43-51.
- [9] David SE, Chattopadhyay M, Chattopadhyay S & Jennerjahn TC, "Impact of human interventions on nutrient biogeochemistry in the Pamba River, Kerala, India", Science of the Total Environment, Vol. 541, pp. 1420-1430.
- [10] TMD, "Climate of Thailand", Thai Meteorological Department, Thailand, assessed :<https://www.tmd.go.th/info/info.php?FileID=53> (April 4, 2017)
- [11] Thongdonphum, B, Meksumpun, S & Meksumpun C, "Nutrient Loads and their Impacts on Chlorophyll *a* in the Mae Klong River and Estuarine Ecosystem: An Approach for Nutrient Criteria Development". Water Science and Technology, Vol. 64(1), 2011, pp. 178-188.
- [12] Pollution Control Department, "Water quality standard", assessed : [http://www.pcd.go.th/info\\_serv/reg\\_std\\_water06.html](http://www.pcd.go.th/info_serv/reg_std_water06.html) (March 20, 2016)
- [13] Xia Y, Ti C, She D & Yan X, "Linking river nutrient concentrations to land use and rainfall in a paddy agriculture-urban area gradient watershed in southeast China", Science of the Total Environment, Vol. 566-567, 2016, 1094-1105.
- [14] Wang S, Lu A, Dang S & Chen F, "Ammonium nitrogen concentration in the Weihe River, central China during 2005-2015". Environmental Earth Science, Vol. 75, 2016, 512.
- [15] PHILMINAQ, "Water quality criteria and standards for freshwater and marine aquaculture. Mitigating impact from aquaculture in Philippines". assessed : <https://www.researchgate.net/file.PostFileLoader.html?id=571b93653d7f4b012861d0a1&assetKey=AS%3A354056255098880%401461424997739>. (Mar 2, 2016)
- [16] Kiedrzyńska E, Kiedrzyński M, Urbaniak M, Magnuszewski A, Skłodowski M, Wyrwicka A & Zalewski M, "Point source of nutrient pollution in the lowland river catchment in the context of the Baltic Sea eutrophication", Ecological Engineering, Vol. 70, 2014, 337-348.
- [17] Li R, Liu S, Zhang G, Ren J & Zhang J, "Biogeochemistry of nutrients in an estuary affected by human activities: the Wanquan River estuary, eastern Hainan Island", China, Continental Shelf Research, Vol. 57, 18-31.
- [18] Álvarez-Vázquez MA, Prego R, Ospina-Alvarez N, Caetano M, Bernárdez P, Doval M, Filgueiras AV & Vale C, "Anthropogenic changes in the fluxes to estuaries: Wastewater discharges compared with river loads in small rias", Estuarine, Coastal and Shelf Science, Vol. 179, 2016, 112-123.
- [19] Markogianni V, Varkitzi I, Pagou K & Dimitriou E, "Nutrient flows and related impacts between a Mediterranean river and the associated coastal area". Coastal Shelf Research, Vol. 134, 2017, 1-14.

## INFLUENCE OF ABIOTIC STRESS FACTORS ON BLACKCURRANT RESISTANCE TO PESTS

I.V. Mashkova<sup>1</sup>, T.G. Krupnova<sup>2</sup>, A.M. Kostryukova<sup>3</sup>

<sup>1</sup>Chemistry Department, South Ural State University, Russia

### ABSTRACT

Blackcurrant is one of the valuable berries of a temperate zone. *Lampronia Capitalla Cl.* is an extremely dangerous pest of blackcurrant in South Ural. Abiotic stress factors can significantly reduce blackcurrant resistance to *L. capitella Cl.* We studied blackcurrant in two areas and in laboratory. The first area is experimental and belongs to a horticultural selection station. It is situated close to the residential area, and a busy motorway is just 100 m from the selection station. The second area is presented by 5 private household plots in an environmentally clean area, far from the city and motorways. We noted that, in the horticultural selection station, *L. capitella Cl.* population explosion was often in three times more, than in the household plots. We registered the formation of specific complexes of leaf-eating micro-lepidopterans (entomocomplexes) in anthropogenically polluted air. The study of entomocomplexes is the framework of the research of the influence of temperature stress factors on blackcurrant resistance to *L. capitella Cl.* We compared the growth of *L. capitella Cl.* larvae in nature and in the laboratory at different temperatures. The experiment lasted for 7 days at +25 °C in the laboratory, and for more than 13 days at daily average temperatures of +9.7 °C, +14 °C, +15.1 °C private household plots. We discovered that larvae's harmfulness increases at the temperature lower than +25 °C.

**Keywords:** blackcurrant, *Lampronia Capitella Cl.*, Coefficient of Assimilation of Food, Abiotic Stress

### INTRODUCTION

Blackcurrant is rich in vitamins and bioactive substances [1–4]. It is one of the valuable berries of a temperate zone. Blackcurrants are an important berry crop in many European countries [5]. There is increasing demand for new and economically valuable blackcurrant cultivars suitable for organic production. In recent years, there have been significant changes in the methods of berries crops in some parts of Europe. Now, most blackcurrants are concentrated in central, east and south-eastern Europe where growing method relies on “traditional” open-field production systems [5].

Blackcurrant are attacked by a wide range of insect and mite pests that can reduce quality, yield or have phytosanitary implications in propagation and plant exports. Many of the insects and mites colonise specific to them small fruits. So, specific insect control strategies must be developed [5]. To date, research into insect pests blackcurrants has been fragmented, with little appreciation of how changes in climate and agronomic practices affect biology. It is very important to concentrate on enhancing natural plant resistance to some of important pests and diseases.

*Lampronia capitalla Cl.* is an extremely dangerous pest of blackcurrant in South Ural. Predicting how insect crop pests will respond to global climate change is an important part of

increasing crop production for future food security [6]. It was shown [7] that global climate change can accelerate the breakdown of crop resistance to insect pests. It is anticipated that global climate change could lead to increases in the incidence of blackcurrant through increased overwintering survival and longer seasonal activity *L. capitella Cl.*

There are scientific studies that allow us to evaluate varieties of black currant in respect of their yield, the quality of berries and resistance to pests [8]. Moreover, changes in management practices such as increased cropping densities and machine harvesting could lead to pest outbreaks through optimal microhabitats and increased susceptibility to pest colonization. It is important to consider future management options with an emphasis on integrated approaches to pest management, including s biocontrol and plant resistance enhancement through breeding [9].

The natural environment for plants is composed of a complex set of abiotic stresses and biotic stresses. Plant responses to these stresses are complex. While it is difficult to get accurate estimates of the effects of abiotic stress on crop production, it is evident that abiotic stress continues to have a significant impact on plants [10, 11]. The level and duration of stress (acute vs chronic) can have a significant effect on the complexity of the plants response [12, 13]

Abiotic stress is defined as environmental conditions that reduce growth and yield below optimum levels [14, 15]. With long-term stress, photosynthesis declines due to stomatal limitations for CO<sub>2</sub> uptake and increased photoinhibition from difficulties in dissipating excess light energy [13]. Abiotic stress factors can significantly reduce blackcurrant resistance to *L. capitella* Cl. There is little and very old published literatures on blackcurrant pest *L. capitella* Cl.

The aim of the present paper was to investigate the influence of abiotic stress on the resistance of blackcurrant to the pest *L. capitella* Cl.

## METHODS

### The Conditions of Blackcurrant Cultivation

Investigated in the present work, the blackcurrant were grown under three conditions: (1) laboratory, (2) natural conditions, area 1, (3) natural conditions, area 2. Area 1 is experimental and belongs to a horticultural selection station. It's situated close to the residential area, and a busy motorway is just 100 m from the site. Area 2 is presented by 5 private household plots in an environmentally clean area far from the city and motorways.

### Examining the Growth of *L. Capitella* Cl. Larvae

We compared the growth of larvae: (1) in nature and (2) in the laboratory at different temperatures.

In the nature we studied the growth of the larvae as follows. We made 5 frameless mesh cages-isolators on a branch of a currant, which was contained some of the kidneys. We placed 2 larvae in each mesh cage-insulator (in total, there are 10 larvae). Mesh cage did not allow the larvae to spread, but larvae could move from the kidneys to the kidney. Larvae took more than 13 days in natural conditions at the average day temperatures of +9.7 °C, +14.3 °C, +15.1 °C. The larvae were weighed when they left the buds, and therefore at the air temperature of +9.7 °C in natural conditions the second larval instars were weighed twice, not once, for the first two days of their development. When weighing the larvae, biology of *L. capitella* Cl., experimentally confirmed, was taken into account.

In the laboratory, we used 5 Petri dishes for each, and 2 larvae in a Petri dishes (total 10 larvae). The laboratory experiment was conducted for seven days at air temperature of +25 °C, air humidity of 70–75 % with a ten-hour daylight.

### Food Assimilation by *L. Capitella* Cl. Larvae

Larvae of *L. capitella* Cl. have 4 instars. According to the conventional approach, the number of instars equal to the number of molts. The

experiment did not consider the first larval instars as they feed in berries, and they have a direct impact on the black currant crop. For second, third and fourth instars larvae we studied food assimilation. We weighed the original amount of food, the remaining amount of food and excrements. The coefficient of food assimilation, C was calculated according to the equation:

$$C = \frac{(M_f - M_e) \cdot 100\%}{M_f},$$

where M<sub>e</sub> – larva excrement mass (mg), M<sub>f</sub> – mass of food eaten (mg).

## RESULTS AND DISCUSSION

The results of five years of research showed that the population of *L. capitella* Cl. increases faster in Area 1 (the horticultural breeding stations), where blackcurrant is a monoculture and grows under the influence of abiotic stress. In laboratory conditions, populations of *L. capitella* Cl. behaves the same. This is because in a laboratory population of *L. capitella* Cl. was kept on injured branches currant, who have reduced defense mechanisms. In Area 2 (private farms) the number and activity of the pest was much smaller than in Area 1, in conjunction with other types of plants. It is located in an ecologically clean area far away from cities and highways.

Insects are poikilothermal with their body temperature depending on that of the surroundings. Insects' activity rhythm is directly connected with the changes of the surroundings [16]. Their rhythm of life can differ in different points within the same space. Since they can differ in microclimatic conditions [17, 18]. For instance, temperature change influences the feeding intensity of insects including *Lampronia capitella* Cl. Further, feeding intensity should be researched to give a more detailed analysis of *L. capitella* Cl. harmfulness in various surroundings.

Basing upon the classification of insects according to their activity rhythm given by [19], *Lampronia capitella* Cl., according to our data, can refer to the insects whose feeding habits are equally intensive throughout the day. Primarily it is due to the fact that *L. capitella* Cl. develops in food abundance (in the food substratum: bud or berry). *L. capitella* Cl. nutritional adaptation is very important for identifying the researched characteristics. Numerous studies have shown that voracity of insects directly depends on the physiological state of a forage plant [20].

The experiment revealed that in the laboratory conditions the amount of food eaten by the larvae for the whole process of their development, i.e. of the second, third and fourth instars was 60.44 mg. In the

natural conditions at an average decade temperature of +12.4 °C the amount was 94.4 mg, which is 1.6 times more than in the laboratory.

Studying feeding intensity of the second, third and fourth larval instars separately the fourth instars are revealed to be the most active, and therefore they are more harmful than the second and third larval instars.

We understand uredospores as an indicator of yield reduction per plant is influenced by the life of one individual pest [21]. The mass of food eaten by the second instars larvae was 11.8 mg for the entire period of their development under laboratory conditions when the air temperature was +25 °C. Weight of food eaten by fourth instars larvae was 28.96 mg. It is 2.5 times more than in the laboratory. Similar patterns were observed in natural conditions. For example, in natural conditions over the period of full development, the second and fourth instars larvae destroyed 21.7 mg and 39.84 mg food, respectively. The third instars of *L. capitella Cl.* consumed 19.68 mg of food in the laboratory. In contrast, in natural conditions, this value was 33.86 mg when the air temperature was +13.9 °C.

Voracity coefficient for the fourth larval instars is found out to be 34.5 %; for the third – 25.4 %; for the second – 12.7 %. These findings suggest that the fourth larval instars are the most voracious. Table 1 illustrates larval voracity according to their instars in the natural and laboratory conditions.

Table 1 Mass of food eaten by *L. capitella Cl.* during their development

Larvae age	T <sub>a</sub> , °C	M <sub>f</sub> , mg	M <sub>e</sub> , mg	C, %
Laboratory				
II	+25	11.80±0.01	7.06±0.01	40.2
III		19.68±0.02	11.26±0.02	42.8
IV		28.96±0.03	17.44±0.03	39.8
Total	–	60.44±0.02	35.76±0.02	40.8
Nature (Area 1)				
II	+9.7	32.71±0.01	22.29±0.01	31.9
III	+14.3	45.76±0.03	31.43±0.02	31.1
IV	+15.1	51.48±0.03	37.13±0.03	27.9
Total	–	129.90±0.02	90.85±0.02	30.1
Nature (Area 1)				
II	+9.7	20.7±0.01	12.29±0.01	40.6
III	+14.3	33.86±0.03	20.53±0.02	39.4
IV	+15.1	39.84±0.03	27.13±0.03	31.9
Total	–	94.40±0.02	59.95±0.02	36.5

To monitor the influence of temperature on the voracity of *L. capitella Cl.* second, third and fourth instars, the amounts of food eaten daily by the larval instars at different air temperatures were compared. The evidence was found to state that the larvae feeding intensity increases with increasing temperatures (Table 2).

Thus, at the air temperature of +25 °C the second larval instars ate 7 mg of food in average, at +8.3 °C larvae of the same instars ate 5.7 mg of food daily. At the air temperature of +25 °C the third instars ate 10.52 mg of buds, while at +15.4 °C the amount of food eaten was 9.5 mg. The fourth larval instars ate 13 mg of food at +25 °C, while at +17.8 °C the mass of food eaten daily was 10.2 mg of buds.

Table 2 The mass of food eaten daily of larvae *L. capitella Cl.*

Larvae age	T <sub>a</sub> , °C	M <sub>f</sub> , mg	M <sub>e</sub> , mg	C, %
Laboratory				
II	+25	7.00±0.01	4.47±0.01	36.1
III		10.52±0.02	6.55±0.02	37.7
IV		13.00±0.02	7.78±0.02	40.2
Nature (Area 1)				
II	+8.3	6.90±0.02	4.68±0.01	32.2
III	+15.4	11.53±0.01	8.42±0.01	27.0
IV	+17.8	14.22±0.02	10.37±0.01	27.1
Nature (Area 1)				
II	+8.3	5.70±0.02	3.48±0.01	38.9
III	+15.4	9.55±0.01	6.40±0.01	33.0
IV	+17.8	10.20±0.02	7.47±0.01	26.8

The data characterizing the relationship between the second, third and fourth instars of *L. capitella Cl.* and air temperature are presented in Table 2.

When studying the dynamics of the digestion coefficient it was noted that in the laboratory conditions at the air temperature of +25 °C, air humidity of 70–75 % and a 10 hour daylight the digestion coefficient was slightly changing with the age, accounting for 40.2 % for the second instars, 42.8 % for the third and 39.8 % for the fourth. In the natural conditions at the average air temperature from 9.7 °C to 15.1 °C the digestion coefficient was declining from the second larval instars to the fourth being 40.6 %, 39.4 % and 31.9 % respectively (Tables 1, 2). These results indicate that the second larval instars digest food better.

In the whole, the digestion coefficient of the larvae brought up in the permanent laboratory conditions is higher (40.8 %) than that of those grown in varying natural conditions (36.5 %). Moreover, the digestion coefficient increases with age for the larvae grown in the laboratory conditions. In the natural conditions the coefficient declines with age. It means that at the air temperature of +25 °C nutrients are better digested, consequently the development cycle extends, and the harmfulness of *L. capitella Cl.* grows. Tables 1, 2 present how the digestion coefficient changes for the second, third and fourth instars daily and during their development.

The study of the food chains, voracity and harmfulness of *L. capitella Cl.* instars showed that

the most voracious are the fourth larval instars, the voracity coefficient is 34.5 %; the second instars are less voracious (12.7 %). But the digestion coefficient for the fourth instars is the lowest (31.9 %). The lower the air temperature is, the worse the larvae digest food.

## CONCLUSION

Comparison the conditions of blackcurrant cultivation is shown that the population of *L. capitella* Cl. increases faster in the Area 1 (breeding stations), where the blackcurrants are growing under the influence of abiotic stress. In the laboratory, population *L. capitella* Cl. was the same. In Area 2 (private farms) the number and activity of the pest was much smaller than in Area 1.

The food assimilation by *L. capitella* Cl. larvae was higher for larvae in constant laboratory conditions than larvae in a changing natural conditions.

## REFERENCES

- [1] Manganaris GA, Goulas V, Vicente AR, Terry LA, "Berry antioxidants: Small fruits providing large benefits", *Journal of the Science of Food and Agriculture*, Vol. 94(5), Mar. 2014, pp. 825-833.
- [2] Folmer F, Basavaraju U, Jaspars M, Hold G, El-Omar E, Dicato M, Diederich M, "Anticancer effects of bioactive berry compounds", *Phytochemistry Reviews*, Vol. 13(1), Mar. 2014, pp. 295-322.
- [3] Sava P, Calaras C, Tcaci V, Gherasimova E, Crivaia P, Vitelaru O, "Nutrients accumulation in fruits of berry species", *Fruit Growing Research*, Vol. XXXL, 2015, pp. 30-33
- [4] Kevers C, Pincemail J, Defraigne JO, Dommes J, "Antioxidant capacity of small dark fruits: Influence of cultivars and harvest time", *Journal of Berry Research*, Vol. 4, Jan. 2014, pp. 97-105.
- [5] Gordon SC, "Raspberry and currant entomology - The drivers for change in Europe", *Acta Horticulturae* 777, 2008, pp. 301-310.
- [6] Johnson SN, Barton AT, Clark KE, Gregory PJ, Mcmenemy LS, Hancock RD, "Elevated atmospheric carbon dioxide impairs the performance of root-feeding vine weevils by modifying root growth and secondary metabolites", *Global Change Biology*, Vol. 17(2), May 2011, pp. 688-695.
- [7] Martin P, Johnson S, "Evidence that elevated CO<sub>2</sub> reduces resistance to the European large raspberry aphid in some raspberry cultivars", *Journal of Applied Entomology*, Vol. 135(3), Jun. 2011, pp. 237-240.
- [8] Kahu K, Jänes H, Luik A, Klaas L, "Yield and fruit quality of organically cultivated blackcurrant cultivars", *Acta Agriculturae Scandinavica, Section B: Soil and Plant Science* Vol. 59(1), Jan. 2009, pp. 63-69.
- [9] Mitchell C, Brennan RM, Cross JV, Johnson SN, "Arthropod pests of currant and gooseberry crops in the U.K.: Their biology, management and future prospects", *Agricultural and Forest Entomology*, Vol. 13(3), Feb. 2011, pp. 221-237.
- [10] Cramer GR, Urano K, Delrot S, Pezzotti M, Shinozaki K, "Effects of abiotic stress on plants: a systems biology perspective", *BMC Plant Biology*, Vol. 11, 2011.
- [11] Lobell DB, Schlenker W, Costa-Roberts J, "Climate trends and global crop production since 1980", *Science*, Vol. 333(6042), 2011, pp. 616-620.
- [12] Tattersall EA, Grimplet J, DeLuc L, Wheatley MD, Vincent D, Osborne C, Ergul A, Lomen E, Blank RR, Schlauch KA, Cushman JC, Cramer GR, "Transcript abundance profiles reveal larger and more complex responses of grapevine to chilling compared to osmotic and salinity stress", *Functional & Integrative Genomics*, Vol. 7(4), Oct. 2007, pp. 317-333.
- [13] Pinheiro C, Chaves MM, "Photosynthesis and drought: can we make metabolic connections from available data" *Journal of Experimental Botany*, Jan. 2011, Vol. 62(3), pp. 869-882.
- [14] Skirycz A, Inze D, "More from less: plant growth under limited water", *Current Opinion in Biotechnology*, Vol. 21(2), Apr. 2010, pp. 197-203.
- [15] Cramer GR, "Abiotic stress & plant responses from the whole vine to the genes", *Australian Journal of Grape and Wine Research*, Vol. 16, Jan. 2010, pp. 86-93.
- [16] Bartel G.M., "Effect of temperature on development and survival of Argentine stem weevil (*List Incurvariidae*)". *Ber. naturwiss – med. Ver. Innsbruck*, 1987, pp. 197-205.
- [17] Shchelkanova VY, Mashkova IV, Shchelkanova EE. "Biotopical distribution of dasyhippus in south forest division of the Ural state reserve" In the collection: *People. The science. Innovation in the new millennium The collection of scientific papers of the International Youth Scientific and Practical Conference: in 2 parts*, 2015, pp. 103-108.
- [18] Mashkova IV., Krupnova TG., Kostyukova AM, Shchelkanova VY, "Landscape ecological distribution of diurnal butterflies of mixed forests in South forest division of Ilmen state reserve", *International Multidisciplinary Scientific GeoConference Surveying Geology and Mining Ecology Management, SGEM*, Book 1, Vol. 1, 2016, pp. 555-562.
- [19] Danilevsky AS, Kuznetsova IA, "Intraspecific adaptation of insects to climatic zonality" *Photopsychic adaptations in insects and mites*. Leningrad: Leningrad University, 1968, pp. 5-51.
- [20] Kozhanchikov IV, "Nutritional specialization and its significance in the life of insects" *Entomological review Moscow*, 1951, Vol.31, Issue. 4, pp. 324-335.
- [21] Tanskiy VI, "Biological basis of harmfulness of insects", *Moscow: Agropromizdat*, 1988, 182 p.

## USING BIRCH LEAVES TO INDICATE AIR POLLUTION

T.G. Krupnova<sup>1</sup>, I.V. Mashkova<sup>2</sup> and A.M. Kostryukova<sup>3</sup>

<sup>1</sup>Chemistry Department, <sup>2</sup>South Ural State University,  
Russia

### ABSTRACT

The present study investigated the utility of *Bétula pubéscens* L. leaves as a bioindicator of air pollution within an industrial Russian city. The study focused on the effects of air pollution on fluctuating asymmetry (FA) of leaves. *B. pubéscens* L. leaves (n=3800) were sampled from 190 trees growing at 38 different sites in Chelyabinsk. The relationship between the data was determined using Pearson's test with a significance level of 0.05. Correlations were observed between the integral index of fluctuating asymmetry (IIFA) and air pollutants such as suspended solids (P=0.527), nitrogen dioxide (P=0.313), sulfur dioxide (P=0.355), inorganic dust SiO<sub>2</sub> (P=0.790), and the air pollution index (P=0.607). The correlation was the highest for inorganic dust since dust clogs the stomata on the leaves of plants, affecting their photosynthesis and respiration. *B. pubéscens* L. could be considered as a bioindicator of air pollution of Chelyabinsk, Russia.

**Keywords:** *Fluctuating Asymmetry (FA), Bioindicator, Air Pollution, Leaves*

### INTRODUCTION

Fluctuating asymmetry (FA) consists of small, non-directional deviations from perfect symmetry in morphological characters. FA can be used as a handy indicator of stress experienced by organisms [1]–[10].

FA has been considered a marker of development instability for over half a century. FA is a nonspecific indicator of the conditions of development and a measure of random deviations in development. This gives us the opportunity to use it to assess the conditions of existence, both natural and artificial populations. It is believed that the stronger the external influence, than higher the FA [1]–[10].

Despite the fact that this method is widely used, including for monitoring the state of atmospheric air, it has been repeatedly criticized in the literature [11]–[14]. Recent works [15], [16] recommend this method under the following conditions: (1) using the blind method, where the person conducting measurements is not aware of the origin of samples being measured; (2) pay utmost attention to adequate and detailed description of data acquisition protocols, because all characteristics of instruments and methods need to be controlled to increase the quality and reproducibility of the data; (3) the measurements should be conducted with high accuracy from images of fresh or press-dried leaves.

*Bétula pubéscens* L. is most widely used as the object of FA studies [15].

The aim of the present work is to explore the nature of FA *B. pubéscens* L. leaves in different districts of Chelyabinsk and to explore the possibility of using this parameter to assess air pollution.

### METHODS

#### Study Area

38 sampling sites were selected for researching in different districts of Chelyabinsk (Fig. 1).

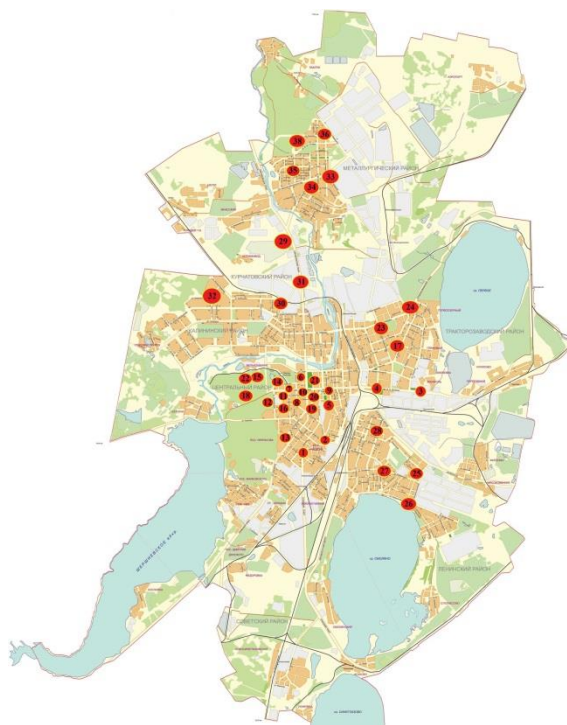


Fig. 1 The locations of sampling and air quality monitoring sites.



Chelyabinsk is a large industrial city. The air in Chelyabinsk is polluted by traffic, heavy industry (ferrous and nonferrous metallurgy, pulp production) and thermal power stations. The most dangerous pollutants are benzo(a)pyrene, formaldehyde, and nitrogen dioxide. Air quality is monitored at 24 monitoring sites.

In 2012 [16] the average concentration of benzo(a)pyrene, formaldehyde, and dioxide nitrogen exceeded the maximum allowable level of 3.9, 3.3, and 1.1 times, respectively. In addition, in 2012, disposable excess concentration of substances in the air was observed for Pb, Mn, Cd, suspended solids, H<sub>2</sub>S, NO<sub>2</sub>, phenol and formaldehyde [17].

### Leaf Collection

We collected birch leaves in July 2012. We chose July because leaf growth stops at this time. We collected leaves from 5 trees at each site, 20 leaves from each tree. The total number of leaves collected at each site was 100. A total of 190 *B. pubescens* L. trees were studied. We considered a few factors when we were selecting trees according to the recommendations of the literature [1]. First, it is important to determine that the plant belongs to the investigated species. *B. pubescens* L. is able to interbreed with other species of birches, and it forms interspecific hybrids which have characteristics of both species. To avoid errors, we chose trees with distinct characteristics *B. pubescens* L. Second, leaves should be collected from plants located in similar environmental conditions (it is necessary to consider the light level, moisture, etc.). We chose trees growing in open areas, because shading conditions are stressful for birch and significantly reduce the stability of plant development. Thirdly, the age of trees should be considered. We chose trees which had a generative age state.

We collected leaves from the maximum number of branches available evenly around the tree from the lower part of the crown. The leaves were collected only from short shoots. Leaf size was similar - the average for this plant. Damaged leaves were not used for the analysis [1].

56 students and teachers of South Ural State University participated in collecting and measuring leaves.

### Preparation and Storage of the Leaves

We made measurements of leaf immediately on the day of collection or kept short leaves 2–3 days in the refrigerator on the bottom shelf.

In addition, all leaves were dried according to standard Botanical methods for further measurements of the air-dried leaves blind. For this purpose the leaves were dried under standard Botanical press to air-dry state. Further, the leaves

from each plant were stored in separate envelope. We carefully marked envelope, indicating the place and date of leaf collection and has a number of the tree.

### Measurements of the Leaves

We made measurements of each birch leaf twice. The first time, we measured fresh leaves on the day of collection or within 2–3 days after collection. The second time, we measured the press-dried leaves. The second measurement was performed blindly with respect to the results of the first measurement.

For each leaf, we measured five parameters on the left and right sides (Fig. 2, 3):

- (1) the width of the halves of the leaf;
- (2) the length of the second order nerve that is the second from the base of the leaf;
- (3) the distance between the bases of the first and second nerves of the second order;
- (4) the distance between the ends of these nerves;
- (5) the angle between the main vein and the second from bottom nerve of the second order.

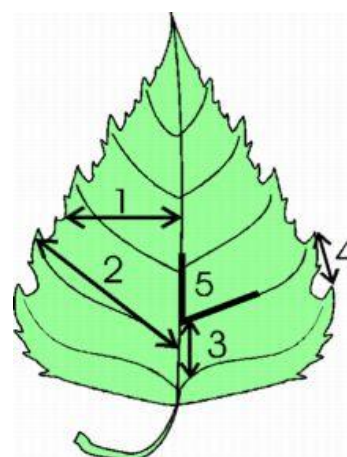


Fig. 2 Measurements of five parameters.

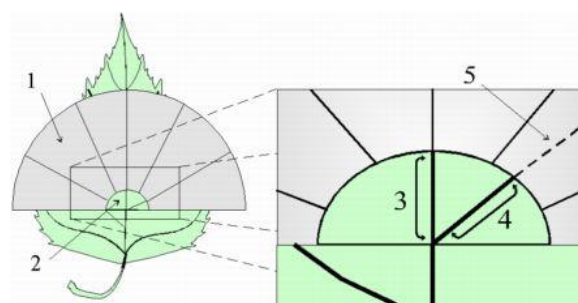


Fig. 3 Measurement methodology.

These measurements were performed with the use of a slide caliper, a ruler, and a protractor.

We used a scale (Table 1) to assess the degree of violation and consequently to assess disturbances in the ecosystem.

Table 1 Rating scale of comfort for living environment fluctuating asymmetry [1]

IIFA	Characteristics of the environmental condition of the territory
< 0,040	Conditionally clean
0,040–0,044	Disturbed
0,045–0,049	Considerably disturbed
0,050–0,054	Adverse
> 0,054	Extremely adverse

We calculated the integral index of fluctuating asymmetry (IIFA) using normalized difference algorithm [1]:

$$\bar{A}_1 = \frac{1}{m \cdot n} \sum_{i=1}^m \sum_{j=1}^n \frac{L_{ij} - R_{ij}}{L_{ij} + R_{ij}}, \quad (1)$$

where  $L_{ij}$  and  $R_{ij}$  are the values of the  $j$ -th character in the  $i$ -th leaf to the left and right side of the plane of symmetry and convolution of the functions, respectively, that in the form of finite sums can be represented by the following formula [18]:

$$\bar{A}_2 = 1 - \frac{1}{m} \sum_{i=1}^m \frac{2 \sum_{j=1}^n L_{ij} \cdot R_{ij}}{\sum_{j=1}^n (L_{ij}^2 + R_{ij}^2)}. \quad (2)$$

Statistical processing of the experimental data was performed with N.A. Plohinskiy methods [19] using the Microsoft Excel 2013 software suite.

### Air Pollution Index

We used data on service monitoring of urban air on 11 substances for the assessment of air pollution: suspended solids, carbon dioxide, sulfur dioxide, nitrogen dioxide, nitrogen monoxide, phenol, formaldehyde, sulfuric acid, inorganic fluorides, Mn, and inorganic dust  $\text{SiO}_2$ . We calculated the air pollution index (API) based on Chelyabinsk air monitoring by the standard method RD 52.04 186-89 [20], RD 52.04.667-2005 [21].

API shows the air pollution level characteristic of chronic, long-term air pollution [22].

API is calculated using the formula:

$$\text{API} = \sum_{i=1}^N \left( \frac{C_i}{\text{MPC}_i} \right)^{K_i}, \quad (3)$$

where  $C_i$  is an average  $i$ -substance concentration in  $\text{mg}/\text{m}^3$ ;  $\text{MPC}_i$  – the average daily maximum permissible concentration of  $i$ -substance in  $\text{mg}/\text{m}^3$ ;  $K_i$  – dimensionless constant depending on the substance hazard category,  $N$  – the number of contaminants considered.

$K_i$  values are equal to: 0.85 for substance hazard category 4; 1.0 for substance hazard category 3; 1.3 for substance hazard category 2; 1.5 for substance hazard category 1. The five substances with the highest index are used.

With an API of  $\leq 5$ , air pollution level is considered low. If  $5 < \text{API} \leq 7$ , then air pollution level is increased. If  $7 < \text{API} \leq 14$ , it is high, and if API is  $> 14$  it is very high.

### Data Processing

Microsoft Excel 2013, MapInfo Pro 15.0, and SPSS 24.0 software were used to organize and analyze the data. The Kolmogorov–Smirnov test was used to test data normality. The relationship between the data was determined using Pearson's test with a significance level of 0.05; the linear regression was considered significant.

### RESULTS AND DISCUSSION

The values of IIFA for the studied sites are presented in Table 2 and Figure 4.

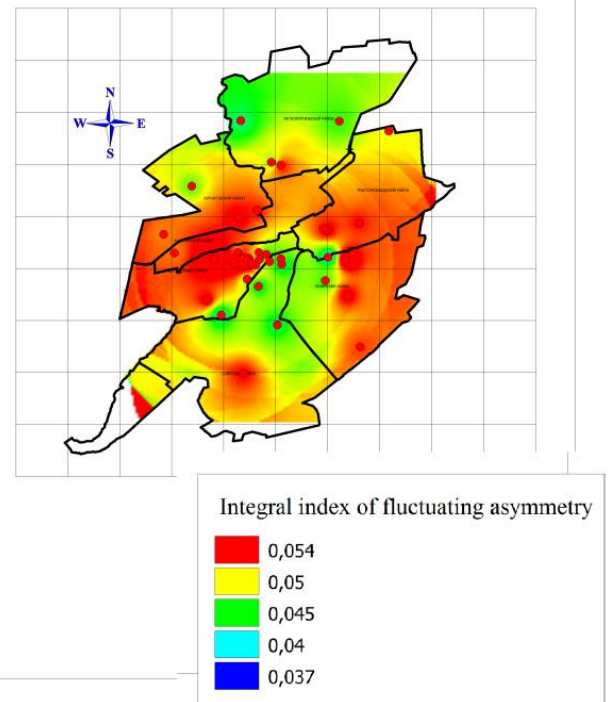


Fig. 4 Integral index of fluctuating asymmetry.

Table 2 IIFA in different sites

Site	IIFA
1	0.041±0.011
2	0.043±0.013
3	0.060±0.015
4	0.039±0.010
5	0.037±0.010
6	0.048±0.012
7	0.047±0.011
8	0.051±0.017
9	0.049±0.016
10	0.046±0.014
11	0.081±0.015
12	0.058±0.011
13	0.055±0.011
14	0.052±0.012
15	0.053±0.011
16	0.057±0.012
17	0.053±0.011
18	0.047±0.013
19	0.064±0.011
20	0.042±0.011
21	0.047±0.011
22	0.042±0.015
23	0.048±0.011
24	0.056±0.013
25	0.054±0.011
26	0.055±0.011
27	0.053±0.011
28	0.054±0.012
29	0.046±0.012
30	0.047±0.012
31	0.056±0.011
32	0.054±0.014
33	0.052±0.011
34	0.054±0.011
35	0.046±0.017
36	0.048±0.014
37	0.050±0.011
38	0.043±0.011

We observed only 2 sites with IIFA < 0.04. According to Table 1 and Table 2, there were 2 sites with a conditionally-clean environment, and 5 and 8 sites with disturbed and considerably-disturbed environment, respectively.

The remaining sites corresponded to the adverse (20 Sites) and the extremely adverse (5 Sites) environment level. Very high values are observed along highways that cross the entire central part of the city. In the central part of the area, the values of asymmetry were often higher than the values in the other areas. The maximum achieved value IIFA was 0.081 in Site 11.

A map of the air pollution of the city was built according to the calculation of API (Fig. 5).

Figure 5 shows that the sites with the greatest air pollution (maximum API) coincide with the areas

where the highest IIFA was obtained (Fig. 4).

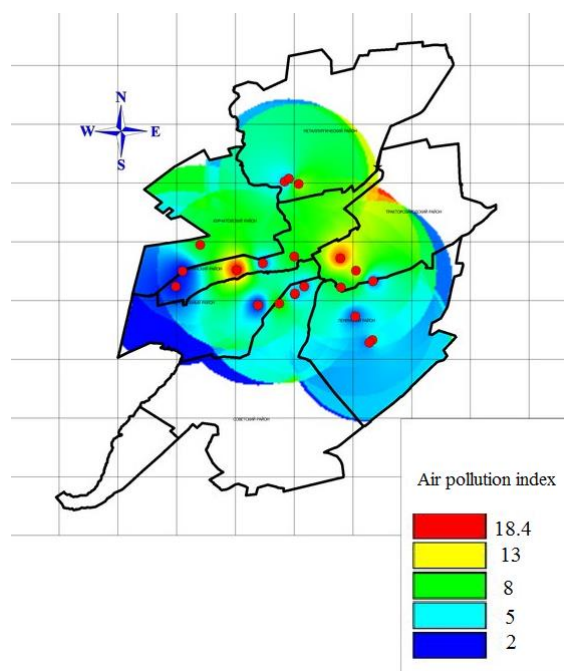


Fig. 5 Air pollution index.

Coefficients of correlation between IIFA and air pollutant were calculated to more accurate estimates (Table 3).

Table 3 Pearson's tests for different air pollutants

Pollutant	Pearson's test
Suspended solids	<b>0.527</b>
Carbon dioxide	0.242
Sulfur dioxide	<b>0.355</b>
Nitrogen dioxide	<b>0.313</b>
Nitrogen monoxide	—
Phenol	0.0006
Formaldehyde	0.203
Inorganic fluorides	—
Sulfuric acid	—
Mn	0.155
Inorganic dust $\text{SiO}_2$	<b>0.790</b>
API	<b>0.607</b>

Blank is insufficient data to calculate

Bold is significant value of correlation

The average value of API in July 2012 was 6.51. This corresponds to increased air pollution. The low degree of air pollution was observed only in the outskirts of the city away from the plants.

The values exceed the critical value of Pearson's tests 0.300 ( $n=38$ ,  $p=0.05$ ) for suspended solids ( $P=0.527$ ) nitrogen dioxide ( $P=0.313$ ), sulfur dioxide

( $P=0.355$ ), inorganic dust  $\text{SiO}_2$  ( $P=0.790$ ) and air pollution index ( $P=0.607$ ).

Correlation with sulfur and nitrogen dioxides was significant. Sulfur dioxide penetrates into leaves primarily in gaseous form through the stomata, although there is evidence for a limited pathway via the cuticle. Chronic damage results from long-term exposure to much lower concentrations of the gas and is essentially cumulative in nature, taking the form of reduced growth and yield and increased senescence, often with no clear visible symptoms or with some degree of chlorosis. Sulfur dioxide can also modify the response of plants to other environmental stresses, both biotic and abiotic, often exacerbating their adverse impacts. Nitrogen dioxide is the damaging component of photochemical smog. In the environment, excessive levels of nitrogen dioxide can rapidly inhibit photosynthesis per unit leaf area [22].

The highest correlation values were observed for suspended solids - inorganic dust  $\text{SiO}_2$  and API. It was found that dust accumulation on leaf surfaces induces water stress-like conditions, such as a reduction of stomata conductance, photosynthesis and transpiration, and increased leaf temperature [23].

## CONCLUSION

Analysis of fluctuating asymmetry of *Betula pubescens* L. leaves collected in July 2012 in the industrial city, Chelyabinsk, showed that:

- most sites have index deviations from its conditional standard;
- correlation coefficients between the fluctuating asymmetry and the concentration of pollutants in urban air are greater than the critical value.

In conclusion, it should be noted that, despite criticism of the method, fluctuating asymmetry of *B. pubescens* L. leaves can be used as a bioindicator of air pollution

## ACKNOWLEDGEMENTS

The authors wish to thank D. Uchaev (SUSU Nanotechnology ERC) for his XRF quantification measurements.

## REFERENCES

- [1] Zakharov VM, "Analysis of fluctuating asymmetry as a method of biomonitoring at the population level", Bioindications of chemical and radioactive pollution, Moscow: Mir Publishers and Boca Raton: CRC Press, 1990, p. 187-198.
- [2] Graham JH, Raz S, Hel-Or H, Nevo E, "Fluctuating asymmetry: methods, theory, and applications", Symmetry, Vol. 2, Mar. 2010, p. 466-540.
- [3] Bukharina IL, Povarnitsina TM, Vedernikov KE, "Ecological and biological characteristics of trees in urban environment", Izhevsk: State Agricultural Academy, 2007, pp. 5-215.
- [4] Vogel S, "Leaves in the lowest and highest winds: temperature, force and shape", New Phytologist, Vol. 183(1), Jul. 2009, p. 13-26.
- [5] Wilsey BJ, Haukioja E, Koricheva J, Sulkioja M, "Leaf fluctuating asymmetry increases with hybridization and elevation in tree-line birches", Ecology, Vol. 79(6), Sep. 1998, p. 2092-2099.
- [6] Wuytack T, Wuyts K, van Dongen S, Baeten L, Kardel F, Verheyen K, Samson R, "The effect of air pollution and other environmental stressors on leaf fluctuating asymmetry and specific leaf area of *Salix alba* L.", Environmental Pollution, Vol. 159(10), Oct. 2011, p. 2405-2411.
- [7] Moller AP, Swaddle JP, "Asymmetry, developmental stability, and evolution", Oxford: University Press, 1997, pp. 2-303.
- [8] Leamy L, "Heritability of directional and fluctuating asymmetry for mandibular characters in random bred mice", Journal of Evolutionary Biology, Vol. 12(1), Jan. 1999, p. 146-155.
- [9] Palmer AR, Strobeck C, "Fluctuating asymmetry: measurement, analysis, pattern", Annual Review of Ecology and Systematics, Vol. 17, Nov. 1986, p. 391-421.
- [10] Parsons PA, "Fluctuating asymmetry: a biological monitor of environmental and genomic stress", Heredity, Vol. 68, Apr. 1992, p. 361-364.
- [11] Klisarić NB, Miljković D, Avramov S, Živković U, Tarasjev A, "Fluctuating asymmetry in *Robinia pseudoacacia* leaves – possible in situ biomarker?", Environmental Science and Pollution Research, Vol. 21(22), Nov. 2014, p. 12928-12940.
- [12] Merilä J, Björklund M, "Fluctuating asymmetry and measurement error", Systematic Biology, Vol. 44(1), Mar. 1995, p. 97-101.
- [13] Lens L, van Dongen S, Kark S, Matthysen E, "Fluctuating asymmetry as an indicator of fitness: can we bridge the gap between studies?", Biological Reviews of the Cambridge Philosophical Society, Vol. 77(1), Feb. 2002, p. 27-38.
- [14] Rasmuson M, "Fluctuating asymmetry – indicator of what?", Hereditas, Vol. 136(3), Sep. 2002, p. 177-183.
- [15] Kozlov MV, Zvereva EL, "Confirmation bias in studies of fluctuating asymmetry", Ecological Indicators, Vol. 57, Oct. 2015, p. 293-297.

- [16] Kozlov MV, Cornelissen T, Gavrikov DE, Kunavin MA, Lama AD, Milligan JR, Zverev V, Zvereva EL, "Reproducibility of fluctuating asymmetry measurements in plants: sources of variation and implications for study design", *Ecological Indicators*, Vol. 73, Feb. 2017, p. 733-740.
- [17] "Report on the environmental situation in the Chelyabinsk region in 2015", Chelyabinsk, 2015.
- [18] Gelashvili DB, Chuprunov EV, Ludin DI, "Structural and bioindicative aspects of fluctuating asymmetry bilaterally symmetrical organisms", *Journal of General Biology*. Vol. 65(5), 2004, p. 433-441.
- [19] Plohinsky NA, "Biometrics", Moscow: Moscow State University, 1970, pp. 3-367.
- [20] RD 52.04 186-89, "Guidelines for air pollution", Russia, 1991, pp. 24-172.
- [21] RD 52.04.667-2005, "Documents on air pollution in cities for informing government and public. General requirements to the development, design, presentation and content", Russia, 2006, pp. 4-50.
- [22] "Air Quality Guidelines", WHO Regional Office for Europe, Copenhagen, Denmark, 2000.
- [23] Saravana KR, Sarala TD, "Effect of cement dust deposition on physiological behaviors of some selected plant species", *International Journal of Scientific & Technology Research*, Vol. 1(9), Oct. 2012, pp. 98-105.

## STUDY OF SYNANTHROPIC PLANTS OF THE SOUTH URAL

A.M. Kostryukova<sup>1</sup>, I.V. Mashkova<sup>2</sup>, T.G. Krupnova<sup>3</sup> and E.E. Shchelkanova<sup>4</sup>

<sup>1</sup>Chemistry Department, South Ural State University, Russia

### ABSTRACT

The present study aimed to assess the long-term dynamics of the synanthropic vegetation of the road and path network of the Ilmen State Reserve. The analysis of the synanthropic species spread among coenofloras of the elements of the road and path network revealed an increasing synanthropization index in the gradient of the stress factor for all forest types. Pine forest is the most resistant to the introduction of synanthropic species. The paper considers the element composition in the period before seed formation. 10 weeds most common in the central regions of Russia were analyzed. The studied weeds can accumulate metals in their green mass. Some wild plants are potentially resistant to metals, as they can grow on heavily dirty substrates. The analysis of the vegetational metals shows that most of the species do not translocate metals into their overground part, so they act as excluders. Due to the human-made impact on the natural landscape, synanthropic species of plants are taking a significant place in the structure of biodiversity.

*Keywords: Reserve, Synanthropic Plants, Anthropophytes, Apophytes, Metal Concentration*

### INTRODUCTION

There has always been increased interest in ruderal plants. The structure and composition of vegetative cover is irreversibly affected by human activity. Weeds strangle cultivated plants, absorbing large amounts of water and nutrients from the soil, discharging harmful substances from the roots, and blocking light. But the problem has not been studied comprehensively. Natural reserves are not the solution, as phytocoenosis can't but be affected by human activity even in a conservation area [1]. In economic and scientific activities, the main line used for preventing fires is connected with the process of invasion. The Ilmen State Reserve, which serves as a reserve for the gene and coenobank of South Ural region vegetation and a standard of common vegetation communities that, as part of environmental monitoring, may be compared with other territories' phytocoenosis under various human impact, is not an exception [1], [2].

The vegetation composition and structure on paths and roads are different. Species diversity and weed abundance are directly connected to their usage. Roads and paths are the place where "alien" species (or anthropophytes) invade the natural vegetation. As a result, separate species of native flora (apophytes), adapting to human-made impact, alter their coenotic positions. According to some researchers, these plants become dominant in new communities and oust common species [2]. Along with these transformations, synanthropization of the Reserve's vegetative cover occurs. The flora is degrading, derived communities are replacing the native, and phytocoenosis stability is declining. Since many synanthropic plants were reported to

accumulate heavy metals, the nature of soil is changing [3]. The problem of heavy metal accumulation by synanthropic plants is of current interest. Researchers all over the world have come to study heavy metal concentration in weeds. Some wild plants are potentially resistant to metals, as they can grow on heavily polluted substrates [4]. Both climate diversity and increasing human-made impact on natural ecosystems explain the high adaptability of synanthropic plants [5].

The growing interest of scientists in Russia and former Soviet republics in studying synanthropic flora is connected, first of all, to the increased role of synanthropic species of plants in the regional floras, secondly, to the influence of floristic schools of Central and Northern Europe that have achieved much in the sphere. Adventitious and synanthropic plants are well-studied in Primorsky Krai and some other regions [6]. There are some open questions concerning synanthropic species in phytogeography, ecology and phytocoenology.

The efficiency of monitoring the vegetative cover and tracking the natural (by anthropophytes) and cultivated (introduction) enrichment of local flora depends on working out the theory of synanthropization of the vegetative cover. Investigating these issues in the South Ural region seems to be important, as the territory is a complex structure of climatic, ecological, and phytocoenotic factors with a focus on the high ecological flexibility of species. This paper is aimed at studying heavy metal accumulation by the synanthropic vegetation in the road and path network of the Ilmen State Reserve and finding out the instances of the growth of their ecological and phytocoenotic positions.

The study of adaptability given human-made transformation of the vegetative cover is crucial for defining ecological and phytocoenotic positions of synanthropic species. It is important to identify the chemical and biological features of ruderal plants in a natural geographic habitat and in the newly developed territories of the road and path network of the Ilmen State Reserve.

## METHODS

### Study Area

The Ilmen State Reserve is located on the eastern South Ural macroslope between the latitude of 54° 58' 58" – 55° 20' 00" north and longitude of 60° 07' 00" – 60° 21' 00" east. It's a part of the South Ural physiographic region of the Ural highlands. The Reserve is a refuge for many endemic and extinct plants and for rare and protected species.

The complex history of the evolution of the South Ural fauna in the Quaternary Period and the Ilmen mountains unique borderline location between mountain (forest) and piedmont (forest-steppe) parts of the region allow the invertebrate animals, diverse in species and complex in composition, to evolve. In that context, the phenomenon of "rich local invertebrate fauna of the Ilmen mountains" is worth mentioning.

In the terrain analysis of Chelyabinsk region, the Ilmen State Reserve is a part of the erosion and denudation landscape of eastern foothills of South Ural that evolved on the eruptive rocks. The South forest division is located in the south terminal ridge of the Ilmen mountains, which is a mild terrace slope with a steep on the Ilmenskoye lake. The abundant flora and phytocoenosis diversity of the site is caused by the borderline location between steppe and forest-steppe zones, challenging landscape, various rock formations. The site's landscape is longitudinal-ridge-steep-sloping (400–300 m above sea level). According to the phytogeographical analysis, the South forest division is located in mixed forests of the preforest-steppe pine and birch forests subzone of the south taiga forests zone. On the west, the subzone borders on dark coniferous forests of dividing ridges, on the east – on forest-steppe of trans-Ural peneplain [7]. The variegated vegetative cover was formed under the challenging climate and landscape.

The data were gathered in 9 biotopes [7].

### Characteristic Features of Vegetation

The Ilmen State Reserve is 90 % covered by forests, which can be classified as South Ural preforest-steppe pine and leafed-pine forests. The main forest-forming species are pine and birch,

covering 56 % and 40 % of the territory of the Reserve, respectively. The territory of road and path vegetation is 6.4 % of all the Reserve's area [1].

Scotch pine (55 %) and European white birch (40 %) mainly constitute forests. Herb-grass, green moss, green moss-vaccinium (close to the original) and steppified biotopes are presented in the forests. Peat-bog and bog-moss pine forests are seen in the wetlands. European white birch and European aspen make young growth with herbs and grass at logging sites. Grass-pine and sedge-reed-sphagnum biotopes are seen in valleys, lakesides, and bogs. Such meadow herbs as various grasses (bluegrass, bentgrass, cocksfoot grass), many legume species, buttercups, globe-flowers, meadow cranesbills, snowdrops, etc. are found at the outskirts of the forest.

Being diverse and numerous, bogs don't cover large territories. Almost all of them appear at the sides of "aged" lakes or former bays thereof. Some of them occupied by reed-sedge formations still have the character of floating bogs. More developed bogs are characterized by the presence of sphagnum moss, bog low shrubs, and herbs specific for taiga bogs such as bog rosemary, swamp ledum, bog cranberry, moorberry, *Scheuchzeria palustris*, roundleaf sundew, mud sedge, whortleberry willow, white beak sedge, English sundew, cloudberry, and blueberry. Sometimes trees (birch, suppressed pine) are seen. Water and coastal water vegetation is rich and diverse. There are about 70 species of water macrophytes [1], [2]. Macrophyte vegetation is developing in shallow water in bays of the littoral zone of open shores.

### Research Methods

The research was conducted in 2015–2016. Standard methods were used to collect data. Sampling points were selected based on the landscape features, vegetation spread and human-made impact. Expedition trips were planned based on natural zone analysis, remote sensing of the earth (Landsat/ETM+ satellite images) with a landscape diversity assessment.

Road and path network with complexes of vegetation communities was chosen for analysis. 6 permanent sampling sites in glaucous-herb-gramineous birch forests and pleurocarpous moss herb-gramineous pine forests and 3 types of roads (unsurfaced road, forest road, and foot path) were described (Fig. 1). The coordinates of the sampling sites: site 1 – 55° 0'13.28"N, 60°10'26.98"E; site 2 – 54°59'57.00"N, 60°11'30.34"E; site 3 – 54°59'52.91"N, 60° 9'56.01"E; site 4 – 54°59'29.69"N, 60°10'29.14"E; site 5 – 54°59'21.32"N, 60°10'46.77"E; site 6 – 54°59'32.52"N, 60°10'54.98"E.

The routes cover 10 km in total. Geo-referenced data integration and correlation were completed with



a geographic information system (GIS). A total of about 100 plant samples were described. The area of the studied stations was more than 25m<sup>2</sup>.

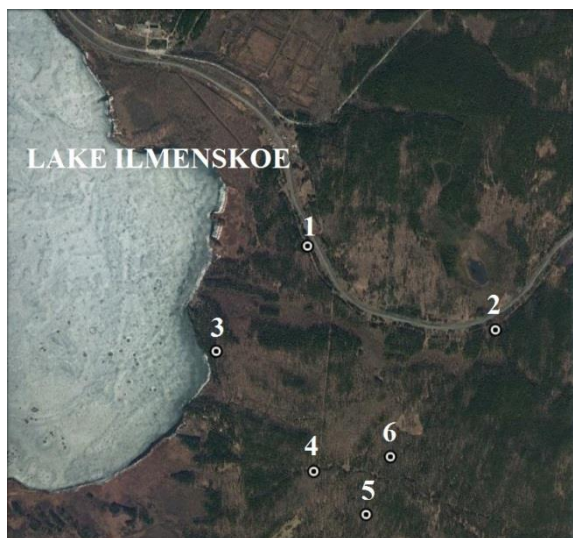


Fig. 1 Sampling sites: 1, 2 – unsurfaced roads, 3, 4 – forest roads, 5, 6 – foot paths.

The number of species, projective cover (%), species abundance (according to Drude), and share of synanthropic species were determined for every 10 m<sup>2</sup> structural unit of the road.

The level of phytocoenosis synanthropization was assessed based on the synanthropic species share (synanthropization index). An assessment scale of the synanthropization of vegetation communities [8] was used: I – human-made impact is low, synanthropic species up to 15 %; II – human-made impact is considerable, 16 % to 60 % synanthropic species; III – human-made impact is long-term and high, synanthropic species are dominant - 61 % to 100 %. Species grouped by coenotic and ecological similarity of ecotopes [9] and forming communities on separate parts of paths and roads are meant as coenoflora.

### Sampling and Determination of Metal Concentration

Sampling occurred in July 2016, when plants stopped in growth. To analyze the chemical content of ruderal plants and to minimize their individual distinctions, 5 samples of each plant species were gathered and air-dried. The air-dry samples of 5 plants were united into one mixed sample, they were then ashed at 550 °C for 5 hours. The ashed samples were ground in a mortar. The finely ground rock powder, mixed with a small amount of polyvinyl alcohol dissolved in water, was compressed using a hydraulic press into a pellet.

In the pellets, Cu, Zn, Mn, and Fe were measured using X-ray fluorescence (XRF) analysis. XRF

patterns were registered in the lab of Education and Research Center for Nanotechnology at South Ural State University. A Rigaku SuperMini XRF Spectrometer was used for XRF analysis. The relative standard results deviation was not more than 5 %.

### RESULTS AND DISCUSSION

The problem of synanthropic species is becoming more important not only for developed areas but also for reserves. Synanthropization significantly influences the flora of conservation areas. Synanthropic flora is heterogeneous. According to E.V. Dorogostayskaya [10], anthropophilic flora consists of some local species (apophytes) and species brought by man (anthropochores). The main factor for the growth of synanthropic plants is soil microclimate change made by man both deliberately and indeliberately or spontaneously. Anthropogenic plants are classified into native and adventive (anthropochores). Native species are divided into sedentary, indifferent, and apophytes. Apophytes fall into erosiophilous (in freshly exposed substrates) and nitrophilous-halophilous apophytes (in the dirty anthropogenic habitat). Adventive species (anthropochores) are classified into unnaturalized (accidental, permanently brought) and naturalized (growing only in the anthropogenic habitat; moving to the natural habitat). According to common classification [11], synanthropic plants are divided into local (or apophytes) and alien (or anthropophytes). Among synanthropic flora, S.G. Kudrin [12] distinguishes the following ecological-phytocoenotic groups: forest group (ruderal-forest element), meadow group (ruderal-meadow element), ruderal group (ruderal element with wide environment, brought or adventive element), and the cultivated group (food element, decorative element, introduced element).

The modern synanthropic flora of the Ilmen State reserve has increased by 45 species since 1986 [13], both apophytes (28 species) and anthropophytes (17 species). The synanthropization index has grown by 1.6 % (Table 1).

Our research revealed 51 species of synanthropic flora on the road and path network of the Reserve, 37 of which are apophytes and 14 - anthropophytes. It has been established that the number of synanthropic species has insignificantly increased in comparison with 2014 [14].

In the birch forests, the number of synanthropic species is larger (42–32) than in the pine forests (25–19), which may be explained by more favourable conditions for the growth of the herbal and suffruticose layer in the birch forests. A large number of published studies do not establish any differences in the parameters of the ecotopes of pine and birch forests, therefore the increasing number of

species in the synanthropic vegetation of the road and path network of the Reserve may be attributed to the anthropogenic factor. The study shows that with the increase of stress load, microclimate is slightly changing; humidity, trophicity, acidity, and nitrogen grow; and luminance in the pine and birch forests in all types of the main line is increasing [14].

Table 1 Dynamics of synanthropization of the Ilmen State Reserve flora according to the references

Plants groups	References	
	Gorchakovsky and et al., 2005 [1]	Gorchakovsky and Kozlova, 1998 [13]
Plants totally	953	841
Synanthropic species totally	265	220
Including apophytes	144	116
Including anthropophytes	121	104
Synanthropization index %	27.8	26.2
Apophytization index %	54.3	40.0

The quality of soil on the unsurfaced roads is lower than on the forest roads. Test planting is characterized by more xerophytic conditions, which may be explained by the drainage properties of the vegetative cover transpiring water surplus from organic-mineral substrate. Integrity disturbance of the herbal and suffruticose layer results in stagnation in tracks and the space between them, bogging, and acidification; increased nitrate is caused by polluting [14].

Analysis of synanthropic species distribution in the coenoflora of the elements of the road and path network revealed an increasing synanthropization index in the gradient of stress factor for all the forests. According to the assessment scale of

synanthropization level, the heaviest and most lasting impact is identified in the coenoflora of birch forests that belong to all the types of forest roads. In the pine forests, only unsurfaced and forest roads are affected.

The most coeno-stable populations were chosen to study heavy metal concentration in the ruderal plants of the Ilmen State Reserve species formation. Such metals as Zn, Mn, Fe, Cu, and Sr were found in the plants (Table 2).

Cuprum is an essential element playing a key role in a range of physiological processes such as photosynthesis, respiration, carbohydrate distribution, reducing nitrogen decline and fixation, protein metabolism, and cell wall metabolism. Many plants have cuprum. It also influences water permeability, and thus, governs water relationships. The most significant practical consequences of cuprum function for plants are attributed to its deficit and toxicity. Cuprum is a part of the disease resistance mechanism. Plant resistance to mycosis may be explained by an adequate cuprum supply. There is the evidence that plants with a rich cuprum concentration are more susceptible to some diseases.

Zinc is an essential microelement playing a key role as a specific activator of some ferments, such as carbonic anhydrase catalyzing the breakage of carbonic acid into water and carbon dioxide. It is easily absorbed as hydrated ion  $Zn^{2+}$ . Zn concentration in plants depends on the age and state of vegetation. A high concentration of Zn is usually seen in young plants, and it reduces with the age as a result of dilution. In general, plants can in large amounts of Zn without showing any instances of rejection with Zn concentration in soil being less than 500 mg/kg.

Iron is of great importance for the enzyme system and necessary for chlorophyll synthesis. It is part of the redox processes in plants, it can convert from oxidated form into protoxydic and vice versa.

Table 2 Heavy Metal Concentration in ash residue of ruderal plants, %

Plant	Zn	Mn	Fe	Cu	Sr
<i>Carduus crispus</i> L.	0.62	1.12	1.53	0.22	0.11
<i>Tanacetum vulgare</i> L.	0.45	1.42	1.65	0.24	0.12
<i>Trifolium montanum</i> L.	1.64	1.17	1.58	0.25	0.11
<i>Euphorbia esula</i> L.	0.49	2.04	2.10	0.26	0.11
<i>Leonurus quinquelobatus</i> GILIB.	1.12	2.52	2.13	0.21	0.10
<i>Linaria vulgaris</i> MILL.	0.65	1.54	1.79	0.25	0.12
<i>Artemisia vulgaris</i> L.	1.98	1.32	1.74	0.26	0.11
<i>Artemisia absinthium</i> L.	0.65	2.56	2.03	0.21	0.11
<i>Barbarea vulgaris</i> W.T.AITON	0.56	1.69	1.91	0.28	0.12
<i>Galeopsis ladanum</i> L.	0.48	1.23	1.65	0.22	0.10
<i>Capsella bursa-pastoris</i> (L.) MEDIK.	0.42	1.51	1.78	0.26	0.12

Manganese is a significant element used in the reduced form of  $Mn^{2+}$ . Like cuprum, manganese, being the part of ferments that enable these processes, plays an important role in the redox reaction in plants.

The most influential factor in the absorption of strontium by plants is Ca concentration in soil. Other factors are pH and organic matter concentration.

Accumulation of strontium by different organisms depends not only on their species but also on the interrelations of strontium, calcium and phosphorus in the environment. The total strontium concentration in soil is 0.035 % (in mass).

Strontium in adequate concentrations is favourable for plant metabolism [15].

Plant chemical composition reflects soil element composition. But this is affected by many factors. Therefore, heavy metal concentration in plants is very changeable and widely varies. This study found that motherwort and wormwood accumulate a high amount of manganese and may be used for drawing it out from soil in the process of phytoremediation. Phytoremediation is known as a relatively inexpensive method of soil reclamation [16, 17]. Clover and thistle accumulate more zinc and may be used for drawing it out from soil. Other plants accumulate iron ions and may be used for drawing out iron from soil.

## CONCLUSION

The study has identified 51 species of synanthropic plants on the road and path network of some parts of the Ilmen State Reserve. The plants cover ditches, quarries, embankments, wastelands, and the side of the roads. Rapidly growing annuals and perennials are dominant in such coenofloras, as they are not demanding of soil and grow well in sites lacking a humous soil horizon.

The paper analyzes the chemical composition of the metals Zn, Mn, Fe, Cu, and Sr for the most coeno-stable species. These elements are essential in low concentrations for plant metabolism and may be used for the phytoremediation of soil.

The obtained results indicate declining efficiency in the use of the current mainlines of the Reserve. But the road and path network of the birch forests is more frequently used than that of the pine forests, which are more resistant to the invasion of synanthropic species.

Climate and a growing human-made impact on the natural ecosystems explain the high adaptability of synanthropic plants. This study revealed the nonequivalence of different environmental factors for forming the adaptability of synanthropic species. Such parameters of the ecoarea as moisture variability, drainage, light, and anthropotolerance are gaining particular importance for increasing the ability to settle on various habitats.

## REFERENCES

- [1] Gorchakovskiy PL, Zolotareva NV, Koroteeva EV, Podgaevskaya EN, "Phyto-diversity of the Ilmen Reserve in the system of protection and monitoring". Ekaterinburg: Goschitsky Publishing House, 2005, pp 5-180.
- [2] Kulikov PV, "Additions to the flora of Ilmenski state reserve (South Ural)", Bulletin of Moscow Society of Testers of Nature. Department of Biology, Vol. 108(6), 2003, pp. 68-69.
- [3] Liang S-X, Gao N, Li Z-C, Shen S-G, Li J, "Investigation of correlativity between heavy metal concentration in indigenous plants and combined pollution soils", Chemistry and Ecology, Vol. 32(9), Jul. 2016, pp. 872-883.
- [4] González RC, González-Chávez MCA, "Metal accumulation in wild plants surrounding mining wastes", Environmental Pollution, Vol. 144(1), Nov. 2006, pp. 84-92.
- [5] Seledets VP, Mayorov IS, Syritsa MV, "The peculiarities of nature use in the coastal zone of the Russian far east seas: ecological ranges of sinanthropic plant species", News of the Samara Scientific Center of the Russian Academy of Sciences, Vol. 10(2), 2008, pp. 303-309.
- [6] Puzyrev AN, Baranova OG, "The study of adventive and synanthropic flora in the CIS: achievements and prospects", Adventive and Synanthropic Flora of Russia and Neighboring Countries: State and Prospects, in Materials of the III International Scientific Conference. Conference, 2006, pp. 3-4.
- [7] Mashkova IV, Krupnova TG, Kostyukova AM, Shchelkanova VY, "Landscape ecological distribution of diurnal butterflies of mixed forests in South forest division of Ilmen state reserve", in Proc. International Multidisciplinary Scientific GeoConference Surveying Geology and Mining Ecology Management, SGEM 16th., Vol. 1, 2016, pp. 555-562.
- [8] Gorchakovskiy PL, "Anthropogenic transformation and restoration of productivity of meadow phytocenoses". Ekaterinburg: Ekaterinburg Publishing House, 1999, pp. 3-150.
- [9] Yurtsev BA, "Monitoring of biodiversity at the level of local flora", Botanical Journal, Vol. 82(6), 1997, pp. 60-70.
- [10] Dorogostaiskaya EV, "Weed plants of the extreme North of the USSR". Leningrad: Science, 1972, pp. 3-170.
- [11] Kornas J, "Man's impact upon the flora: processes and affects", Memorabilia zoologica, Vol. 37, 1982, pp.11-30.
- [12] Kudrin SG, "Analysis of ecological and phytocenotic elements of the synanthropic part of the flora of the Hingemsky reserve", Adventive and Synanthropic Flora of Russia and

- Neighboring Countries: State and Prospects, in Materials of the III International Scientific Conference, 2006.
- [13] Gorchakovskiy PL, Kozlova EV, "Synanthropization of the vegetation cover under protected regime conditions", Ecology, Vol. 3, 1998, pp. 171-177.
- [14] Koroteeva EV, Kuyantseva NB, Chashchina OE, "Monitoring the composition and structure of synanthropic vegetation at Ilmen nature reserve", News of the Samara Scientific Center of the Russian Academy of Sciences, Vol. 16(1), 2014, pp. 1213-1217.
- [15] Kabata-Pendias A, "Trace Elements in Soils and Plants", 4th Edition. Boca Raton, FL: Crc Press, 2010, ch. 7.
- [16] Cuningham SD, Berti WR, "Remediation of contaminated soils with green plants: an overview", In Vitro Cellular & Developmental Biology - Plant, Vol. 29(4), Oct. 1993, pp. 207-2012.
- [17] Cuningham SD, Ow DW, "Promises and prospects of phytoremediation", Plant Physiology. Vol. 110(3), Mar. 1996, pp. 715-719.

## A STUDY ON THE EFFECTIVENESS OF LIQUID SMOKE PRODUCED FROM PALM KERNEL SHELLS IN INHIBITING BLACK POD DISEASE IN CACAO FRUIT IN VITRO

M. Faisal<sup>1</sup>, Tjut Chamzurni<sup>2</sup>, Hiroyuki Daimon<sup>3</sup>

<sup>1</sup>Department of Chemical Engineering, Syiah Kuala University, Banda Aceh, Indonesia; <sup>2</sup>Department of Agro Technology, Syiah Kuala University, Banda Aceh, Indonesia; <sup>3</sup>Department of Environmental and Life Science, Toyohashi University of Technology, Toyohashi, Aichi, Japan

### ABSTRACT

The effectiveness of liquid smoke made from palm kernel shells in inhibiting black pod disease (*Phytophthora palmivora*) in cacao fruit was studied. Palm kernel shells underwent pyrolysis in a slow-pyrolysis reactor at 280°C–400°C. The resulting liquid smoke was then distilled at a temperature of 200°C. The observed parameters were incubation period and spotting diameter. The experimental design was completely randomized, with a 4 × 6 factorial pattern having four repetitions and consisting of two factors. Both temperature and concentration significantly affected the incubation period of the fungi causing black pod disease. Additionally, the liquid smoke concentration had a strong influence on the spotting diameter. Phenolic compounds and acetic acid contained in the liquid smoke serve as antimicrobials and are bacteriostatic. Although the maximum phenol level was found at 280°C, the longest incubation period occurred in liquid smoke produced at a pyrolysis temperature of 360°C. Thus, 360°C was the optimum temperature for producing liquid smoke to inhibit black pod disease caused by *P. palmivora* in cacao.

**Keywords:** Liquid smoke, Pyrolysis temperature, Biopesticide, Cacao black pod disease, *Phytophthora palmivora*

### INTRODUCTION

A major developing industry in Indonesia is oil palm, which results in abundant biomass waste, including kernel shells, fronds and empty bunches. The potential of these waste products has not been utilized properly, even though Indonesia is an agricultural country with a large agriculture biomass. One method to utilize such potential is through pyrolysis to produce liquid smoke [1],[2]. Technology enables the processing of palm kernel shells into liquid smoke, which contains oxidized organic compounds, such as ketone, aldehyde, phenol, and carboxylic acid, resulting from the condensation of the pyrolysis vapor [3]. These compounds give liquid smoke its antioxidant and antibacterial properties, as well as its specific flavor [4]. Phenol and phenolic compounds possess bactericidal and bacteriostatic properties depending on the concentration used. Phenol and its derivatives function to denature proteins in bacterial cells and destroy cell membranes.

Because of the nature of some of its components, liquid smoke can also function as a plant-based insecticide and fungicide to inhibit disease-causing pathogens in agriculture. Previous studies on the effectiveness of liquid smoke in inhibiting anthracnose disease in chili plants have been conducted [1]. Liquid smoke made from palm kernel shells significantly influenced the incubation period

of anthracnose, halting the symptoms created by the disease. Thus, the use of liquid smoke in inhibiting plant disease is a step toward supporting the ‘go green’ organic program.

Presently, farmers still use chemical/synthetic pesticides that can harm the environment and are not suitable for human consumption. The damage caused by synthetic pesticides to soil microbiology has been intensively studied in the past [5],[6]. Plant-based pesticides are potential alternatives [7]. Cacao black pod disease is caused by the Straminipile genus of *Phytophthora* [8]. This fungus can rot the pods at any age and causes a total production loss of ~30% [9],[10]. The infected pods display brownish black spots, usually starting at the stem, middle or end of the pods. Under humid conditions, the spots spread rapidly on the surfaces of the pods, rendering them black and rotten. This pathogen’s spores are carried by wind and rain water, infecting other pods and spreading to other plant stems and branches.

This disease is difficult to control in a curative manner; therefore, preventive measures, such as fungicides, are used to stop its spread. Because of the phytopathogenic nature of this fungi, several of the biological agents used to combat its associated diseases are Trichoderma species, such as *T. asperellum*, *T. harzianum*, *T. polysporum*, *T. viride* and *T. virens* [11]–[14]. A few effective chemical compounds used to control/reduce cacao black pod

disease are metalaxyl- and copper-based fungicides [11],[15]. Additionally, chemical components containing essential oils, especially terpene, phenol and alcohol, are being considered for use as biopesticides because they have various biological activities [16],[17], such as insecticidal [18]–[20], antifeedant [21], repellent [22],[23], lure [24], insect growth inhibition [25], and antimicrobial [26],[27]. However, essential oils are mostly volatile, easily decompose, and are unstable when exposed to light and heat [28],[29]. Liquid smoke may serve as a better biopesticide because it is more stable, non-volatile and inexpensive.

Nonetheless, there has been nearly no in-depth research on the effectiveness of liquid smoke as a biopesticide. Research related to liquid smoke and its applications in agriculture are required to develop a sustainable agricultural industry. The utilization of waste and organic side products to produce liquid smoke will create an economic added value and an added social cultural value. This research studied the effectiveness of liquid smoke made from palm kernel shells as a plant-based fungicide against black pod disease caused by *Phytophthora palmivora* in cacao fruit (*Theobroma cacao*).

## RESEARCH METHODS

### Liquid Smoke Production

The slow-pyrolysis reactor made of stainless steel was 32 cm in diameter, 50 cm in height, and had a 5-kg capacity. This reactor was equipped with a tar container and temperature control. The upper temperature was 500°C. Samples of palm kernel shells were put in the reactor for a certain period of time and were pyrolyzed at temperatures ranging from 280°C to 400°C. The smoke was then condensed into liquid smoke using a stainless steel condensation unit (diameter of 50 cm and height of 60 cm), resulting in liquid smoke, Grade 3. This liquid smoke was then distilled at 190°C to become Grade 2. The complete process of liquid smoke production was previously published [1],[2]. The chemical compounds within the liquid smoke were identified using GC–MS based on a method developed by Guillen and Ibargoitia [30].

### Sampling of Cacao Pods

Cacao pod samples were obtained from the People's Plantation at Pidie Jaya, Aceh, Indonesia. The media used was 21 × 21-cm mica boxes, each containing one cacao pod and labeled based on the treatment received.

### Isolation and Cultivation of *P. palmivora*

The *P. palmivora* inoculum was isolated from

infected cacao pods before it was cultivated on healthy pods. *P. palmivora* was then inoculated into healthy pods by puncturing the surface of the pod once using a straight pin and then placing these pods into the mica boxes. The punctured sites were then inoculated with *P. palmivora* using a small 3-mm cork borer. These inoculated cacao pods were then incubated for 24 h before liquid smoke was applied in 2–10% concentrations.

### Liquid Smoke Application as Plant-based Fungicide in Cacao Pods

Liquid smoke was applied one day after *P. palmivora* inoculation by spraying the whole surface of the pods. The observed variables were (1) Incubation time: observations began one day after the inoculation of cacao pods with *P. palmivora* until the first symptoms appeared. (2) Spot diameter: Observations began two days after the inoculation of cacao pods with *P. palmivora* using a ruler and continued for the next five days. The data was statistically analyzed using the SPSS program for data in a completely randomized design, with a 4 × 6 factorial pattern having four repetitions and consisting of two factors. The first factor was temperature (T), T1 = 280°C, T2 = 320°C, T3 = 360°C and T4 = 400°C. The second factor was concentration (C), C0 = control, C2 = 2%, C4 = 4%, C6 = 6%, C8 = 8% and C10 = 10%.

## RESULTS AND DISCUSSION

### Chemical Composition of Liquid Smoke

Liquid smoke is a compound formed during the burning of cellulose, hemicelluloses and lignin. The pyrolysis of these component results in phenol and acetic acid, which can have antioxidant and antimicrobial characteristics. Phenolic compounds have antibacterial and antifungal effects [31] that can kill rot-causing bacteria that degrade proteins into amino acids, thereby preventing the foul smell. Liquid smoke also possesses strong bacteriostatic properties that inhibit bacterial growth, as well as fungicidal properties that inhibit fungal growth. Phenol itself functions as a bactericide because of its ability to increase the permeability of cell membranes, inactivating essential enzymes and destroying or inactivating functional genetic materials.

The pyrolysis of cellulose produces acetic acid and carbonyls, such as acetaldehyde, glucose and acrolein. The pyrolysis of lignin results in phenol, guaiacol and syringol, along with their homologs and derivatives. The numbers and types of

compounds contained in the resulting liquid smoke depend on the pyrolysis temperature and the raw materials used [1]. An analysis of the liquid smoke composition at T3 is shown in Table 1. The phenol and acetic acid contents of liquid smoke are shown in Table 2. The maximum phenol content occurred at the T1 pyrolysis temperature, while that of acetic acid occurred at T2.

Tabel 1 Liquid smoke composition at 360°C

Pe ak	R. Time	Area	Conc (%)	Name
1	5,70	182807746	28.0	Acetic acid (CAS)
	0	7	2	Ethyllic acid
2	6,11	451840165	6.93	Acetic acid (CAS)
	0			Ethyllic acid
3	7,05	792450881	12.1	Propanoic acid (CAS)
	8		5	Propionic acid
4	7,32	632271906	9.69	Acetic acid (CAS)
	2			Ethyllic acid
5	11,8	147795235	22.6	Benzenamine (CAS)
	77	4	5	Aniline
6	12,6	164876203	2.53	2-Cyclopenten-1-one, 2-hydroxy-3-methyl- (CAS) Corylon
	58			Phenol, 4-methoxy
7	13,0	280722335	4.30	
	95			
8	13,6	103445521	1.59	cis-1,3-Dideuterio-1,3- cyclohexandiamine
	40			
9	14,2	74541045	1.14	2-Methoxy-4- methylphenol
	58			
10	14,8	153070215	2.35	1,3-Benzenediol (CAS) Resorcin
	63			
11	15,1	44016691	0.67	Phenol, 4-ethyl-2- methoxy- (CAS) p- Ethylguaiaicol
	59			
12	15,2	67054314	1.03	3-Methoxy- pyrocatechol
	92			
13	15,9	195663312	3.00	Phenol, 2,6- dimethoxy- (CAS)
	25			2,6-Dimethoxyphenol
14	16,7	83136367	1.27	1,2,4- Trimethoxybenzene
	58			
15	17,8	175252398	2.69	1,6-Anhydro-beta-D- Glocopyranose
	87			

Tabel 2 The content of phenol and acetic acid in liquid smoke

No.	Pyrolysis temperature	Acetic acid (%)	Phenol (%)
1	280°C	1.29	0.73
2	320°C	2.06	0.62
3	360°C	1.20	0.31
4	400°C	1.86	0.36

Note : % = gr/100 ml

## Incubation Time

Incubation time was observed to establish the effectiveness of liquid smoke concentrations applied on the cacao pods to halt the fungal growth that causes black pod disease. Incubation periods were marked by the presence of brownish black spots on the surface of the pods, which will look clear under a magnifying glass. The application of liquid smoke produced at various temperatures and concentrations affected the incubation time differently. However, the temperatures and concentrations did not have visible interactions. The average incubation times of *P. palmivora* after the application of liquid smoke produced at different temperatures are shown in Figure 1.

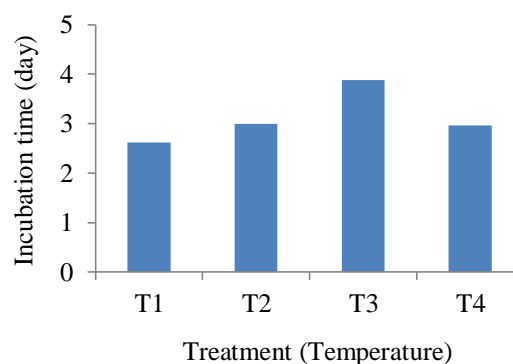


Fig.1 Average incubation time of *P. palmivora* after the application of liquid smoke (6%) produced at different temperatures.

The temperature with the longest incubation time of 3.88 days was T3. Meanwhile T1, T2 and T4 had similar incubation times, namely 2.62 days, 3.00 days and 2.96 days, respectively. Thus, T3 was effective in inhibiting the growth of *P. palmivora* as proven by the resulting longer incubation time, which is a criterion of resistance against pathogen infection. Longer incubation times mean that the symptoms are slow to appear because the pathogen's growth is inhibited.

The longer T3 incubation time was probably because of the chemical contents of the liquid smoke produced at T3. According to Lin *et al.* [32], liquid smoke's antifungal properties were influenced by its pyrolysis temperature. Similar results were shown on the effectiveness of liquid smoke in inhibiting *anthracnose* disease in chilies [1], and temperatures significantly affected the *anthracnose* incubation time.

Figure 2 shows the average incubation time of *P. palmivora* after the application of liquid smoke at several concentration levels. The highest concentration at C4 produced markedly different results from C0 and C2, but not significantly different from C6, C8 and C10, although the



incubation times at C2, C4, C6, C8 and C10 were markedly different from that of C0 (control). The lower incubation time at C0 occurred because no liquid smoke had been applied, leaving the pathogen free to infect the surface and the fruit of the cacao pods, resulting in the rapid display of symptoms. Thus, C4 should be used to control the disease because it inhibited black pod disease longer in cacao.

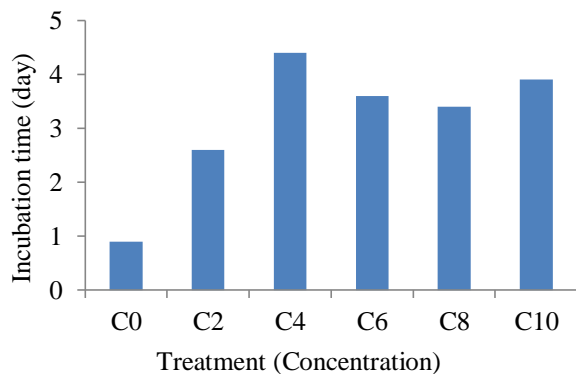


Fig. 2 Average incubation time of *P. palmivora* after the application of liquid smoke (from T3) at several concentration levels.

The high content of the functional components, phenol and organic acid, in C4 was able to destroy the fungal cell membranes, slowing its growth. The phenol compound increases the permeability of the fungal cell membranes, leading to the loss of nuclei, and the functional inactivation of genetic materials and essential enzymes [33].

### Spot Diameter

Diameter observation by consistently measuring the spots on the long side was carried out every day from the pathogen inoculation until infection symptoms began to show. The growth of *P. palmivora* was marked by mycelia that form brownish black spots or concave dry black spots on the surface of the infected cacao.

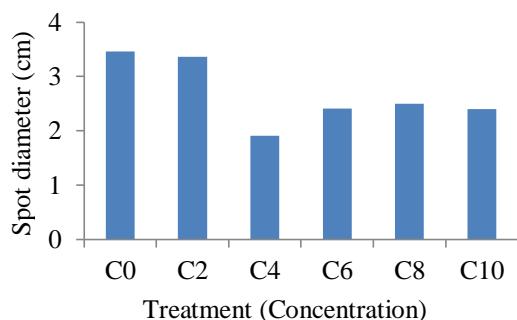


Fig. 3 Average spot diameters of the fungus after the application of liquid smoke at several concentration levels.

This pathogen can infect internal tissues of the fruit, causing the cacao seeds to wrinkle and change colors during infection [34]. An analysis of variance showed that several liquid smoke concentration levels produced significant effects on the spot diameter of the fungus that causes cacao black pod disease.

### CONCLUSION

Different temperatures and concentrations had significantly different effects on the incubation time of *P. palmivora*, the causal agent of black pod disease, and the concentration had markedly significant effects on the diameter of the spots. The phenol and acetic acid compounds contained in the liquid smoke have antimicrobial and bacteriostatic properties. The optimum conditions for inhibiting the spread of black pod disease in cacao were 360°C during liquid smoke preparation and the use of 4% liquid smoke.

### ACKNOWLEDGEMENTS

The Authors acknowledge the financial support provided by Syiah Kuala University and the Ministry of Research, Technology and Higher Education of Indonesia. The authors also thank Ms. Afriyani for help in the data analysis of this study.

### REFERENCES

- [1] Faisal M, Gani A, Husni, Baihaqi A, Daimon H, "Pyrolysis of oil palm kernel shell into liquid smoke and its application to control anthracnose disease on chili (*Capsicum annum* L.)", *J. of Eng. Appl. Sci.*, Vol.11, No. 12, Nov. 2016, pp. 2583-2587.
- [2] Gani A, Husni, Baihaqi A, Faisal M, "Potential development of liquid smoke from oil palm solid waste as biofungicides", *Int. J. of Sci. Eng.*, Vol.7, No.1, July 2014, pp.65-69.
- [3] Faisal M, Gani A, Husni, Daimon H, "A preliminary study of the utilization of liquid smoke from palm kernel shells for organic mouthwash", *Int. J. of GEOMATE*, Vol. 13, No. 37, Sept. 2017, pp. 116-120.
- [4] Saloko S, Darmadji P, Setiaji B, Pranoto Y, "Antioxidative and antimicrobial activities of liquid smoke nanocapsules using chitosan and maltodextrin and its application on tuna fish preservation", *Food Bioscience*, Vol 7, Sept.2014, pp. 71-79.
- [5] Imfeld G, Vuilleumier S, "Measuring the effects of pesticides on bacterial communities in soil: a critical review", *Eur. J. Soil Biol.*, Vol. 49, Apr. 2012, pp. 22-30.

- [6] Falkowski PG, Fenchel T, Delong EF., The microbial engines that drive earth's biogeochemical cycles", *Science*, Vol. 320, May 2008, pp. 1034-1039.
- [7] Ipsilantis I, Samourelis C, Karpouzas DG, "The impact of botanical pesticides on arbuscular mycorrhizal fungi", *Soil Biol. Biochem.*, Vol. 45, Feb. 2012, pp. 147-155.
- [8] Kroon LPNM, Bakker FT, Van den Bosch GBM, Bonants PJM, Flier WG, "Phylogenetic analysis of phytophthora species based on mitochondrial and nuclear DNA sequences", *Fungal Biol. Genet.*, Vol. 41, Aug. 2004, pp. 766-782.
- [9] Mbarga JB, Begoude BAD, Ambang Z, Meboma M, Kuate J, Schiffers B, Ewbank W, Dedieu L, Ten Hoopen GM, "A new oil-based formulation of *Trichoderma asperellum* for the biological control of cacao black pod disease caused by *phytophthora megakarya*", *Biol. Control*, Vol. 77, Oct. 2014, pp.15-22.
- [10] Akrofi AY, Amoako-Atta I, Assuah M, Asare EK, "Black pod disease on cacao (*Theobroma cacao*, L) in Ghana: Spread of *phytophthora megakarya* and role of economic plants in the disease epidemiology", *Crop Prot.*, Vol. 72, Jun. 2015, pp.66-75.
- [11] Tchameni SN, Ngonkeu MEL, Begoude BAD, Nana LW, Fokom R, Owona AD, Mbarga JB, Tchana T, Tondje PR, Etoa FX, Kuaté J, "Effect of *trichoderma asperellum* and arbuscular mycorrhizal fungi on cacao growth and resistance against black pod disease", *Crop Prot.*, Vol. 30, No. 10, Oct. 2011, pp.1321-1327.
- [12] Almeida FBR, Cerqueira FM, Silva RN, Ulhoa CJ, Lima AL, "Mycoparasitism studies of *Trichoderma harzianum* strains against *Rhizoctonia solani*: evaluation of coiling and hydrolytic enzyme production", *Biotechnol. Lett.*, Vol. 29, Aug. 2007, pp. 1189-1193.
- [13] Hermosa R, Rubio MB, Cardoza RE, Nicolás C, Monte E, Gutiérrez S, "The contribution of *Trichoderma* to balancing the costs of plant growth and defense", *Int. Microbiol.*, Vol.16, No. 2, Mar 2013, pp. 69-80.
- [14] Kaewchai S, Soyong K, Hyde KD, "Mycofungicides and fungal biofertilizers", *Fungal Divers*, Vol. 38, Sep. 2009, pp. 25-50.
- [15] Sonwa DJ, Coulibaly O, Weise SF, Adesina AA, Janssens MJJ, "Management of cocoa: Constraints during acquisition and application of pesticides in the humid forest zones of southern Cameroon", *Crop Prot.*, Vol.27 No.8, Aug. 2008, pp. 1159-1164.
- [16] Li H, Chen C, Cao X, "Essential oils-oriented chiral esters as potential pesticides: Asymmetric syntheses, characterization and bio-evaluation", *Ind. Crops Prod.*, Vol.76, Dec. 2015, pp.432-436.
- [17] Regnault-Roger C, Vincent C, Arnason JT, "Essential oils in insect control:low-risk products in a high-stakes world", *Annu. Rev. Entomol.*, Vol. 57, Jan. 2012, pp. 405-424.
- [18] Kumar P, Mishra S, Malik A, Satya S, "Insecticidal properties of *Menthaspecies*: a review", *Ind. Crops Prod.*, Vol. 34, Jul. 2011, pp. 802-817.
- [19] Machial CM, Shikano I, Smirle M, Bradbury R, Isman MB, "Evaluation of the toxicity of 17 essential oils against *Choristoneura rosaceana* (Lepidoptera:Tortricidae) and *Trichoplusia ni* (Lepidoptera: Noctuidae)", *Pest Manage. Sci.*, Vol. 66, Oct. 2010, pp. 1116-1121.
- [20] Maciel MV, Morais SM, Bevilacqua CM, Silva RA, Barros RS, Sousa RN,Sousa LC, Brito ES, Souza-Neto MA, "Chemical composition of eucalyptus spp. essential oils and their insecticidal effects on *Lutzomyialongipalpis*", *Vet. Parasitol*, Vol. 167, Jan. 2010, pp. 1-7.
- [21] Baskar K, Ignacimuthu S, Anti feedant, larvicidal and growth inhibitory effects of ononitol monohydrate isolated from *Cassia tora* L. against *helicoverpaarmigera* (Hub.) and *Spodoptera litura* (Fab.) (Lepidoptera: Noctuidae)", *Chemosphere*, Vol. 88, No. 4, Jul. 2012, pp. 384-388.
- [22] Zhang JS, Zhao NN, Liu QZ, Liu ZL, Du SS, Zhou L, Deng ZW, "Repellent constituents of essential oil of *cymbopogon distans* aerial partsagainst two stored-product insects", *J. Agric. Food Chem.*, Vol. 59, No. 18, Aug. 2011, pp. 9910-9915.
- [23] Mann RS, Tiwari S, Smoot JM, Rouseff RL, Stelinski LL, "Repellency andtoxicity of plant-based essential oils and their constituents against *diaphorinacitri kuwayama* (Hemiptera: Psyllidae)", *J. Appl. Entomol.*, Vol. 136, Feb. 2012, pp. 87-96.
- [24] Kendra P, Montgomery W, Niogret J, Schnell E, Deyrup M, Epsky N, "Evaluation of seven essential oils identifies cubeb oil as most effective attractant for detection of *Xyleborus glabratus*", *J. Pest Sci.*, Vol. 87, No.4, Dec. 2014, pp. 681-689.
- [25] Ketoh GK, Koumaglo HK, Glitho IA, "Inhibition of *Callosobruchusmaculatus* (F.) (Coleoptera: Bruchidae) development with essential oil extracted from *Cymbopogon schoenanthus* L. Spreng. (Poaceae), and the wasp *Dinarmus basalis* (Rondani) (Hymenoptera: Pteromalidae)", *J. Stored Prod. Res.*, Vol. 41, No.4, Dec. 2005, pp. 363-371.
- [26] Seow YX, Yeo CR, Chung HL, Yuk H-G, "Plant essential oils as active antimicrobial agents", *Crit. Rev. Food Sci. Nutr.*, Vol. 54, No. 5, Jan. 2014, pp. 625-644.

- [27] Dhara L, Tripathi A, "Antimicrobial activity of eugenol and cinnamaldehyde against extended spectrum beta lactamase producing enterobacteriaceae by in vitro and molecular docking analysis", *Eur. J. Integr. Med.*, Vol. 5, No. 6, Dec. 2013, pp. 527-536.
- [28] Wen H, Zhang Q, Cheng D, Zhang Z, Xu H, Song X, "Cassia oil as a substitute solvent for xylene for rotenone EC and its synergistic activities", *Pestic. Biochem. Phys.*, Vol. 105, No. 3, Mar. 2013, pp. 189-196.
- [29] Tong F, Bloomquist JR, "Plant essential oils affect the toxicities of carbaryl and permethrin against *Aedes aegypti* (Diptera: Culicidae)", *J. Med. Entomol.*, Vol. 50, No. 4, Jul. 2013, pp. 826-832.
- [30] Guillen MD, Ibargoitia ML, "Influence of the moisture content on the composition of the liquid smoke produced in the pyrolysis process of *Fagus sylvatica* L. Wood", *J. Agri. Food Chem.*, Vol. 47, Oct. 1999, pp. 4126-4136.
- [31] Aziz NH, Farag SE, Mousa LA, Abo-Zaid MA, "Comparative antibacterial and antifungal effects of some phenolic compounds", *Microbios.*, Vol. 93, No. 374, Dec. 1997, pp.43-54.
- [32] Lin HC, Murase Y, Shiah TC, Hwang GS, Chen PK, Wu WL, "Application of moso bamboo vinegar with different collection temperatures to evaluate fungi resistance of moso bamboo materials", *J. Fac. Agri.*, Vol. 53, No. 1, Feb. 2008, pp. 107-113.
- [33] Davidson MP, Alfred lary Branen, *Antimicrobial in Foods*, second edition, Marcel Decker Inc. New York. 1993.
- [34] Bowers JH, Bailey BA, Hebbar PK, Sanogo S, Lumsden RD, "The impact of plant diseases on world chocolate production", *Plant Health Progress*, Vol. 10, Jul. 2010, pp.1-15.

## HEAVY METALS IN MICROALGAE BIOMASS ADDED WITH DIFFERENT CONCENTRATION OF WET MARKET WASTEWATER

Radin Maya Saphira Radin Mohamed<sup>1</sup>, Najeeha Apandi<sup>2</sup>, Siti Nor Hidayah

Arifin<sup>3</sup>, A.A.S. Al-Gheethi<sup>4</sup> and Amir Hashim Mohd Kassim<sup>5</sup>

<sup>1, 2, 3, 4, 5</sup> Department of Water and Environmental Engineering, Faculty of Civil and Environmental Engineering, Universiti  
Tun Hussein Onn Malaysia, 86400 Parit Raja, Batu Pahat, Johor, Malaysia

### ABSTRACT

The aim of this study was to assess heavy metals content; arsenic (As), cadmium (Cd), lead (Pb) and mercury (Hg) in microalgae *Scenedesmus* sp. biomass cultivated with wet market wastewater. Microalgae *Scenedesmus* sp. added with wet market wastewater which contain high nutrient level has a potential for fish supplement product. However, it is depending on the level of heavy metals concentration. Different wet market wastewater was tested in the dilution of 10% (10SWM), 15% (15SWM), 20% (20SWM), and 25% (25SWM) during the cultivation to measure the potential by-product quality. Heavy metals for As, Cd, Pb and Hg in dry biomass of *Scenedesmus* sp. were measured by Inductively Coupled Plasma Mass Spectrometry (ICP-MS) and Mercury Analyser. Heavy metals content (ug/kg in ppb) in the *Scenedesmus* sp. were found in the range of As (182.5-7.74), Cd (0.985-2.111), Pb (4.95-2.375) and Hg (9.774-1.037). Arsenic was the highest trace metals (182.5 ppb) found in 25SWM and the lowest (0.311 ppb) was Cd (cadmium) from BBM (Bolt's Basal Medium) sample. The level of heavy metals in all microalgae biomass samples did not exceeded the maximum concentration set up by the European Commission Regulation. Therefore, the biomass from microalgae *Scenedesmus* sp. cultivated with wet market wastewater has acceptable concentration of As, Cd, Pb and Hg. Thus, make it a great potential for upcoming bio products such as fish feed and fish supplement.

**Keywords:** Heavy metals, *Scenedesmus* sp., Wet market wastewater, Heavy metals concentration

### INTRODUCTION

There are many markets available for buyers to get fresh foodstuff such as the wet market. Unfortunately, wet market wastewater which consists of variety components such as nitrogen and phosphorus commonly discharge directly to the drainage without any treatment [1]. In Malaysia, most of the wastewater will be channeled into the drainage and end up flowing into the river. This phenomenon escalates the pollution among Malaysian rivers. Thus, a river in Perlis, Malaysia, has been polluted with wastewater mostly coming from the effluent of food-based wastewater which includes wet market with a 58.30 (polluted), 61.87 (slightly polluted) and 41.64 (polluted) of water quality index [2]. Wastewater from wet market contains nutrient and heavy metals derived from the fresh foodstuff, waste scraps of seafood and fish entrails. The wastewater discharged contains various wastes such as organic materials, suspended solid, fat, and toxic compound such as heavy metals. The content of organic matter found in wastewater from wet market is three times more than in solid waste [3]. Although low concentration of heavy metal might give no harm to the living organisms, but high levels of it are potentially toxic.

For the past few years, a lot of research was carried out to study on the value potential of dual application of microalgae for wastewater treatment

and biomass production [4, 5]. Gani et al., [6] had studied the use of microalgae and had successfully removed up to 93.3% of total organic carbon from wastewater while the algae became a potential for biodiesel production. Wastewater treatment by using microalgae is eco-friendly and offers the advantage of a cost effective way of nutrient removal and biomass production [7]. Since microalgae have the ability to absorb nitrogen and phosphorus levels [8], instead of the nutrients being wasted; this will provide nutrients for the microalgae to grow which in turn become valuable biomass products [9-10]. Since microalgae has been recognized as a very favorable source of biomass, this can be applied in order to treat wastewater efficiently without involving high production cost. Microalgae are also the best candidate to decrease heavy metals concentration from ppm to ppb levels and known to be resilient to the contaminants of high concentrated wastewater [11].

There are few types of toxic heavy metals that may impact in human and animal diseases and mortality. The content of toxic heavy metals will lead the effect of the biomass quality. Heavy metals are dangerous because they tend to bioaccumulate the concentration of a chemical in a biological organism over time, compared to the chemical concentration in the environment [12]. Those four selected toxic heavy metals were Arsenic (As), Cadmium (Cd), Lead (Pb) and Mercury (Hg). To

evaluate and remove four toxic heavy metals (As, Cd, Pb and Hg) the process of bioremediation technology has been applied in this study [13]. The existence of heavy metals in the wastewater may affect the characteristic compound on the microalgae which automatically constitute negative impact to the main food source for bivalve mollusks at their growth stages (zooplankton; larvals stages of crustacean and fish species) [14]. Furthermore, these toxic metals in microalgae could be a threat to the ecosystem and public health and must be treated. Therefore, this study is to evaluate the heavy metals (As, Cd, Pb and Hg) contents from biomass that derived from different concentration of wet market wastewater.

## MATERIALS AND METHODS

### Wastewater Characterization and Experimental Procedure

Untreated wet market wastewater (WM) was collected from Pasar Borong Rengit, Batu Pahat, Johor, Malaysia (N 1° 40' 39.5144" E 103° 8' 43.7844"). Wet market wastewater has been taken by grab sampling according to the standard of APHA (2002) [15]. The main organic waste fraction was from seafood and fish entrails and market's activities operations. Wastewater was transported to the laboratory and went under sterilization using autoclave at 120°C for 15 minutes. Wet market wastewater sample was filtered with GF/C (Whatman) filter to remove suspended solids and diluted with distilled water into four concentrations 10%, 15%, 20% and 25% in triplicate to investigating the effect of different concentration in order to support microalgae growth. Bolt Basal Medium (BBM) was used as control media. The experiment was conducted in duplicate for each concentration. Physical and chemical parameters were analyzed according to the standard method given in APHA (2002) [15]. Samplings for parameters analysis were collected before and after the treatment. Total parameter removal efficiencies was calculated accordance with Eq. (1)

$$\text{Removal, \%} = \frac{\text{Initial conc. (mg/L)} - \text{Final conc. (mg/L)}}{\text{Initial conc. (mg/L)}} \times 100 \quad \text{Eq. (1)}$$

### Cultivations of *Scenedesmus* sp. Using Wet Market Wastewater

Microalgae *Scenedesmus* sp. was obtained from the culture collection of Faculty of Science, Technology and Human Development, Universiti Tun Hussein

Onn Malaysia. The inoculum of *Scenedesmus* sp. was maintained in Bolt's basal medium (BBM) prior to experiment. The experiment was carried out using 2L of Erlenmeyer flask containing 1.5 L of wastewater and Bolt's Basal Medium (BBM). BBM medium was used as control media. Microalgae were cultivated under outdoor sunlight with continuous aeration at 3.2 L/min to ensure the distribution of nutrients using atmospheric air from an aquarium pump through air spurger. The experiment flask was inoculated with the same initial microalgae cells of (106 cells/ml) at the starting day of the experiment. The biomass was harvested immediately after 12 days by centrifugation at 4000 rpm for 5 min. The sample was then kept and stored at -20 °C until further analysis. The cultivation batches were carried out in duplicate.

### Sample Preparation and Analysis

The frozen microalgae sample was melted individually and dried at 105°C to a constant weight. Dried microalgae were then finely crushed and homogenized using mortar and pestle and about 0.5g of the homogenized sample was digested in 10 ml of HNO<sub>3</sub> (nitric acid) at 160°. The solution was diluted with deionized water up to 50ml and analyzed for heavy metals content using Inductively Coupled Plasma Mass Spectrometry (ICP-MS) for As, Cd, Pb and Hg and Mercury Analyser for Hg [16].

## RESULTS AND DISCUSSION

### Wastewater Characteristics

Wet market wastewater remediated with *Scenedesmus* sp. was evaluated for the pollutants parameter removal of biochemical oxygen demand (BOD), chemical oxygen demand (COD) and turbidity. The percentage removal efficiency before and after the microalgae *Scenedesmus* sp. cultivation was shown in Table 1. The removal efficiency of BOD and COD of microalgae *Scenedesmus* sp. reached relatively high values; BOD (83.6%) from 25SMW, COD (94.7%) from 15SM. Comparing to the research data result from other study by Violeta et al., (2011) [17], this study achieved slightly high removal of BOD at 94.7% from wet market wastewater compared with Violeta et al., (2011) with a BOD removal of 92.12% from *Scenedesmus* sp. cultivation using sewage wastewater. The reduction of BOD and COD by microalgae cultivation because of the absorption of carbon dioxide since microalgae has the ability in converting BOD and COD concentration into their carbon sources of living [18-19]. As for pH parameter in each sample was slightly decreased and showed that the pH levels are not exceeding the

standard A & B [20]. Assimilation of photosynthetic activity reduce the pH levels due to the ammonia concentration react as a nitrogen source for microalgae to grow [9, 21].

### Heavy Metals Content in Microalgae Biomass

According to the Table 2, the highest concentration mostly dominated by the Arsenic (As) with the value of  $182.5 \pm 7.18$  ppb from the biomass of 25SMW. This amount may due to high concentration of wastewater medium (25% of wet market wastewater) during the microalgae cultivation process, compared to biomass from (7.74

$\pm 2.7$  ppb) and 10SMW ( $76.86 \pm 10.5$  ppb). The following metal value after mercury is Lead (Pb) with a total of  $4.95 \pm 4.82$  from 15SMW. Next, the lowest metal is Cadmium (Cd) with a total of  $0.985 \pm 0.124$  from the biomass of 20SMW. For BBM biomass shows that the total value of all metal are very low compared to others biomass sample directly verified that this microalgae *Scenedesmus* sp. are non-toxic algae straightly proved that this kind of microalgae are harmless. Low levels of trace metals in this study could be affected from the dilution due to low parameter content in the wastewater.

Table 1 Percentage Removal of Wet Market Wastewater Characteristic

Parameter	10SMW			15SMW			20SMW			25SMW		
	Before (MSC)	After (MSC)	%	Before (MSC)	After (MSC)	%	Before (MSC)	After (MSC)	%	Before (MSC)	After (MSC)	%
pH	7.36	7.0	-	7.41	6.4	-	7.49	6.18	-	7.52	6.79	-
BOD	349	74	78.8	375	78	79.2	512	87	83	566	93	83.6
COD	574	32	94.4	639	34	94.7	647	46	92.9	689	56	91.9

\*MSC: Microalgae *Scenedesmus* sp. Cultivation

Table 2 Heavy Metals Content in Microalgae Biomass Compared with the Maximum Content of the European Commission Regulation (2015)

Heavy Metals	Microalgae Biomass Concentration (ug/kg as in ppb)					Remarks	Max. content in ug/kg (ppb) (EU) No 186/2015
	BBM (control)	10SMW	15SMW	20SMW	25SMW		
Arsenic (As)	$7.74 \pm 2.7$	$76.86 \pm 10.5$	$107.7 \pm 3.68$	$117 \pm 11.98$	$182.5 \pm 7.18$	Low	25000
Cadmium (Cd)	$0.311 \pm 3.9$	$0.319 \pm 3.25$	$0.515 \pm 3.12$	$0.985 \pm 0.124$	$0.413 \pm 2.03$	Low	10000
Lead (Pb)	$2.695 \pm 5.1$	$3.36 \pm 0.343$	$4.95 \pm 4.82$	$3.195 \pm 1.57$	$2.375 \pm 5.59$	Low	200
Mercury (Hg)	$1.44 \pm 0.00$	$9.774 \pm 0.00$	$3.502 \pm 0.00$	$1.033 \pm 0.00$	$2.422 \pm 0.00$	Low	25000

The tests deduced that the microalgae *Scenedesmus* sp. biomass cultivation using four different mediums of wet market wastewater are harmless and non-toxic where all the values of heavy metal concentrations are below the limit based on the European Commission Regulation (2015) [22]. In order to protect public health, it is appropriate to refer the maximum levels of metal that are safe for human/animal exposure in foodstuffs [22, 23]. Upon to this achievement of evidence in proving the production of non-toxic algae biomass cultivated from wet market wastewater, this experiment can be great potential for upcoming bioproducts such as fish feed, food supplement for humans and animals and fertilizer.

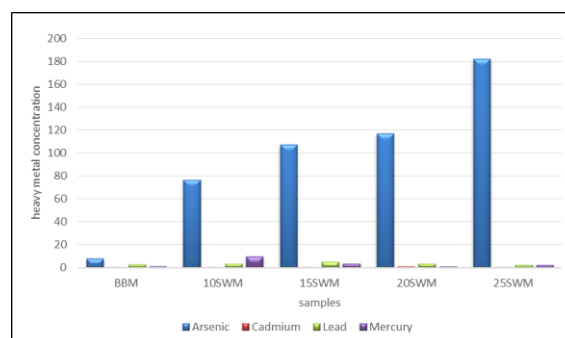


Fig 1 Heavy Metal Concentrations in Microalgae Biomass Sample BBM, 10SMW, 15SMW, 20SMW and 25SMW (ug/kg in ppb)

## CONCLUSION

The use of microalgae *Scenedesmus* sp. cultivation in wet market wastewater treatment is one of the alternative way in wastewater treatment before it can be discharged to the drainage. The result of metal concentration in dry biomass in each sample mostly acceptable under the regulation which are beneficial to make father experiment in producing bioproduct. It can be said that the microalgae *Scenedesmus* sp. has potential in absorbing pollutants that contain in wastewater. Although, levels of heavy metals in this study were below than the standard regulation (EU) No 186/2015) (Table 2), monitoring on more contaminated wet market wastewater should be continuously necessary since wet market wastewater has high nutrient and pollutants parameter when the sample is not dilute. Hence, the microalgae *Scenedesmus* sp. extracted from wet market wastewater in this study is non-toxic and risk-free to be consumed in producing as variety of bio products such as fish feed, fish supplement and much more.

## ACKNOWLEDGEMENTS

This research was funded under the FRGS (1574) and E-Science Fund project vot no: S029. Special thanks to Dr. Hazel Monica Matias-Peralta for providing the microalgae cell and any parties that involved in this project specifically Universiti Tun Hussein Onn Malaysia for providing the equipment and research facilities to carry out this project.

## REFERENCES

- [1] AY Maizatun, RMSR Mohamed, AA Al-Gheethi, MKA Hashim, "An overview of the utilisation of microalgae biomass derived from nutrient recycling of wet market wastewater and slaughterhouse wastewater," International Aquatic Research, 1-17 (2017).
- [2] W.A.Amneera, N.W.A.Z. Najib, S.R.Mohd Yusof, S.Ragunathan., "Water quality index of Perlis river, Malaysia", International Journal of Civil & Environmental Engineering IJCEE-IJENS, vol:13, no:02, 1312102-9595 (2013)
- [3] Santos, C., & Robbins, M. Low-Cost Innovative Solutions for Treating Public Market Wastewater in the Philippines: Deploying Hybrid Anaerobic/Aerobic Copeat Filtration Systems, 2011.
- [4] Rawat, I., Ranjith Kumar, R., Mutanda, T., & Bux, F, "Dual role of microalgae: Phycoremediation of domestic wastewater and biomass production for sustainable biofuels production," Applied Energy (88) 3411-3424 (2011).
- [5] NM Jais, R Mohamed, AA Al-Gheethi, MKA Hashim, "The dual roles of phycoremediation of wet market wastewater for nutrients and heavy metals removal and microalgae biomass production," Clean Technologies and Environmental Policy 19 (1), 37-52 (2017).
- [6] P. Gani, Norshuhaila Mohamed Sunar, Hazel Matias-Peralta, Siti Suhana Jamaian, and Ab Aziz Abdul Latiff, "Effects of Different Culture Conditions on the Phycoremediation Efficiency of Domestic Wastewater" Journal of Environmental Chemical Engineering, 2213-3437 (2016).
- [7] Wilkie AC, Mulbry WW, "Recovery of dairy nutrients by benthic freshwater algae." Bioresource Technology, 84:81-91 (2002)
- [8] Zhang, E., Wang, B., Wang, Q., Zhang, S., & Zhao, B., "Ammonia-nitrogen and orthophosphate removal by immobilized *Scenedesmus* sp. isolated from municipal wastewater for potential use in tertiary treatment," Bioresource Technology, 99(9), 3787-3793 (2008).
- [9] NM Apandi, RMSR Mohamed, N.A.A. Latiffi, N.F.M. Roslan, A.A.S. Al-Gheethi, "Protein and lipid content in biomass from microalgae *Scenedesmus* sp. grown in wet market wastewater," MATEC Web Conferences 103, 06011.
- [10] E.W Becker, Micro-Algae as a Source of Protein Biotechnology Advances 25(2): 207-10. (2007)
- [11] Latiffi, Nuratikah Ahmad, Radin Maya, Saphira Radin Mohamed, Najeeha Mohd Apandi, and Amir Hashim Mohd Kassim. "Application of Phycoremediation Using Microalgae *Scenedesmus* Sp . as Wastewater Treatment in Removal of Heavy Metals from Food Stall Wastewater." Applied Mechanics and Materials 773, 1168-1172 (2015).
- [12] Kulbat, E., Quant, B., Geneja, M., & Hauste, E. Heavy Metals Removal in the Mechanical-Biological Wastewater Treatment Plant " Wschód " in Gdańsk, 12(5), 635-641 (2003).
- [13] Muysen, B. T. a, & Janssen, C. R. "Zinc acclimation and its effect on the zinc tolerance of *Raphidocelis subcapitata* and *Chlorella vulgaris* in laboratory experiments," Chemosphere, 45(4-5), 507-514 (2001).
- [14] Wang, Ya et al. "Review of Arsenic Speciation, Toxicity and Metabolism in Microalgae." Reviews in Environmental Science and Bio/Technology 14(3):427-51



- (2015).
- [15] APHA “Standard Methods for the Examination of Water and Wastewater”, 22th edition. American Public Health Association American Works Association and Water Environment Federation USA, (2012).
- [16] Ogoyi, D. O., C. J. Mwita, E. K. Nguu, and P. M. Shiundu, “Determination of Heavy Metal Content in Water, Sediment and Microalgae from Lake Victoria, East Africa”, The Open Environmental Engineering Journal 4:156–61 (2011).
- [17] Violeta, Vaida Andrulevičiūtė, Virginija Skorupskaitė, and Jūratė Kasperovičienė, “Cultivation of Microalgae *Chlorella* Sp. and *Scenedesmus* sp. as a Potentional Biofuel Feedstock” 57(3): 21–27 (2011)
- [18] P Gani, N M Sunar, H Matias-Peralta, RMSR Mohamed, AAA Latiff, UK Parjo, “Extraction Of Hydrocarbons From Freshwater Green Microalgae (*Botryococcus* Sp.) Biomass after Phycoremediation of Domestic Wastewater”, International Journal of Phytoremediation, Taylors & Francis, 1, 679 (2017).
- [19] N.Abdel-Raouf, A.A.Al-Homaidan, I.B.M. Ibraheem, “Microalgae and wastewater treatment” Saudi Journal of Biological Sciences 19, 257-275 (2012)
- [20] Law of Malaysia Act 127, “Environmental Quality Act (1974)” (1975).
- [21] A Latiffi, N Atikah, R Mohamed, RM Saphira, NM Apandi, RM Tajuddin, “Experimental Assessment on Effects of Growth Rates Microalgae *Scenedesmus* sp. in Different Conditions of pH, Temperature, Light Intensity and Photoperiod,” Key Engineering Materials 744, 546-551 (2017).
- [22] Commission Regulation (EU) 2015/186 of 6<sup>th</sup> Feb 2015, Official Journal of the European Union L 31/11 (2015).
- [23] Radin Mohamed, Radin Maya Saphira, Haritharan Maniam, Najeeha Afandi, Adel Ali Saeed Al-Gheethi, Mohd Kassim, Amir Hashim, “Microalgae Biomass Recovery Grown in Wet Market Wastewater via Flocculation Method Using *Moringa oleifera*,” Key Engineering Materials 744, 542-545 (2017).

## **INFLUENCING PARAMETER OF SELF PURIFICATION PROCESS IN THE URBAN AREA OF CIKAPUNDUNG RIVER, INDONESIA**

Yonik Meilawati Yustiani<sup>1</sup>, Mia Nurkanti<sup>2</sup>, Neneng Suliasih<sup>3</sup> and Annisa Novantri<sup>4</sup>

<sup>1</sup>Dept of Environmental Engineering, Engineering Faculty, Pasundan University, Indonesia; <sup>2</sup>Faculty of Education, Pasundan University, Indonesia <sup>3</sup>Faculty of Engineering, Pasundan University, Indonesia

### **ABSTRACT**

Self purification process is an important process in the effort of recovering the river condition itself. This process usually takes place naturally. However, several inhibitions might disturb the process. It was indicated by the slow deoxygenation rate and unhealthy river condition. This research aims to identify the influence parameters responsible on the slow of self purification in the Cikapundung River, which is located in the urban area of Bandung City, Indonesia. The river water samples were taken and analyzed in the laboratory to obtain the water quality. The deoxygenation rate was also calculated based on the Slope Method after data was acquired from 10 days daily observation. Research showed that the value of urban river deoxygenation rate is relatively low. The low value of the rate of deoxygenation led to the difficulty in rivers to purify themselves. Pollutants inhibiting the process include phenol, detergent, and heavy metals, which are contaminating the river over the maximum standard. Biologically, the decomposer consists in the river is few. It leads to a slow organic degradation rate. The condition is representing the low capacity of self purification of the Cikapundung River which is caused mainly by chemical and biological parameters.

*Keywords: Self Purification, Deoxygenation Rate, Urban River, Water Quality*

### **INTRODUCTION**

Cikapundung River is a river that passes through Bandung. As the capital of West Java Province, Bandung City is a city with a large population, which is more than 2.4 million people. The rapid development of the population stimulates the growth of settlements on the banks of the Cikapundung River without adequate sanitation facilities. Cikapundung River becomes a place of disposal of liquid waste from the activity around the river banks.

Rivers in urban areas, including Cikapundung, have various functions, such as drinking water sources, recreational locations and main drainage canal [1]. The river is the main natural and ecological site from a water management perspective [2]. Some parameters are set in the quality standards to maintain the health of the river.

Organic pollutant can be removed naturally in rivers. The process is performed by microorganisms. Several physical, chemical and biological activities involves in the river water organic pollutant degradation. Many of these physical and chemical activities are influenced by the biological condition. The removal of pollutants from a water body without any artificial controls is called self purification, or natural purification [3].

Many urban rivers in Indonesia suffer with heavy pollution. Their capabilities to perform self purification appear relatively low and resulting the deterioration of the water quality, physically,

chemically and biologically.

Degradation of organic pollutants is primarily affected by the river water characteristic. Contaminants generated from industries can threat to river capability of self purification. Several indicators can be used to explain on how the natural remediation of river cannot be carried out. This research was conducted to investigate the influencing parameter of self purification process in the urban area of Cikapundung River. The result can be useful to track the pollutant sources and handle the issue from the initial causes.

BOD (biochemical oxygen demand) and COD (chemical oxygen demand) are 2 essential parameter of water quality to describe the organic pollutant condition of rivers. Thus BOD and COD are two widely used parameters for organic pollution measurement [4].

BOD (Biochemical Oxygen Demand) has a strong relationship with DO because it indicates the need for oxygen to decompose organic matter in the waters. Therefore, BOD becomes an important factor to evaluate the level of pollution of organic matter in the river [5]. Deoxygenation is the process of decreasing the amount of oxygen that occurs due to the use of oxygen by microorganisms to decompose pollutants into the aquatic bodies [6]. The deoxygenation process is an important process in the effort of the river to self purification process, i.e. degradation of bio-degradable organic pollutants to re-clean the water. The rate of the deoxygenation

process affects the sooner or later self purification takes place. The rate of deoxygenation rate is also an important tribe in the Streeter-Phelps equation which is always used to model the quality of river water. The rate of deoxygenation rate can be specific if it is in an area with different temperatures. In addition, the quality of the river, the presence of matter and pollutants in the river will affect the rate of deoxygenation. Research on deoxygenation is very rare in Indonesia.

The non-optimization of the work of decomposing microorganisms is also one of the factors that influence the process of self-purification in the river. Therefore, in this study the condition of decomposer microorganisms becomes one of the components to be studied.

## METHODOLOGY

### Research Location

Cikapundung River is chosen to represent the urban city river. Figure 1 shows the location of the Cikapundung River.

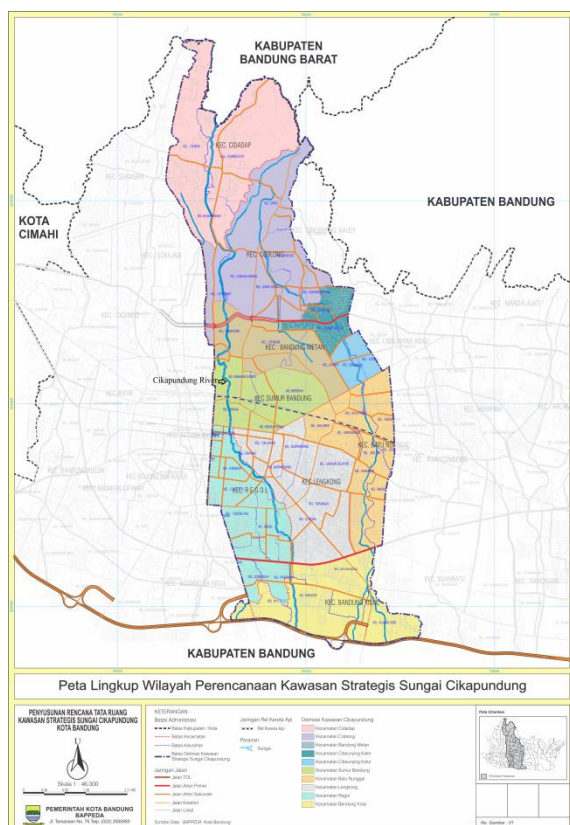


Fig.1 Research location and sampling points [10].

The rivers pass through Bandung City's most crowded area [7]. The Cikapundung river water quality suffers with the wastewater that being disposed directly without prior proper treatment. The condition stimulates the worse quality of the

river water. Not only polluted by the untreated wastewater, the river is also suffering from the solid waste. Cikapundung River plays a very strategic role as one source of water supply for Bandung, but its water quality decreased for several years [8]. Besides that, the Cikapundung river basin is one of the sub watershed Citarum that serves as the main drainage channel of Bandung [9].

### Data Collection

Data was collected from previous research and also from the government agency that perform periodic monitoring on the rivers. Measurement of river water quality is conducted regularly by the Environmental Protection Agency of Bandung City and West Java Province. Several points were appointed as sampling locations. The data were then being calculated to have average values.

Primary data was also obtained by laboratory analysis of the river water samples to investigate the type of microorganisms living in the water.

### Parameters

The investigated parameters to determine the self purification process in the urban river are including deoxygenation rate, BOD/COD ratio, heavy metals and surfactant concentration. The deoxygenation rate will indicate the degradation process of organic matter. BOD/COD ratio can describe the biodegradation capacity of the river [3]. Heavy metals and surfactant were considered as the inhibitors of decomposition process by microorganisms.

## RESULT AND DISCUSSION

### Deoxygenation Rates

Table 1 shows the deoxygenation rate of Cikapundung River water located in the upstream and downstream of Bandung City area.

Table 1 Deoxygenation rates of Cikapundung River

Year	Deoxygenation rate			
	Upstream		Downstream	
	Dry Season	Rainy Season	Dry Season	Rainy Season
2011	0.146	0.19	0.023	0.26
2012	0.016	0.1	0.08	0.01
2014	0.24	0.24	0.03	0.37
2015	0.13	0.12	0.19	0.29

The deoxygenation rate obtained from previous studies ranged from 0.010 to 0.26 per day. It was found that deoxygenation rate value was relatively low. This low rate of deoxygenation causes the slow recovery of organic pollution in the river. Seasons do not appear as an influencing factor for the deoxygenation rate value. Generally, there is no significant trend that differentiates between dry

season and rainy season [7].

Typical range of the deoxygenation rate for the surface water is 0.10-0.23 mg/L [11]. As comparison, the rates of deoxygenation of rivers outside Indonesia are found in the typical range such as Ravi River in Pakistan has 0.14-0.27 per day [12], and Gomti River in India has 0.45 per day [13].

Low rate of deoxygenation is typically found in the clean water without organic matter and microorganisms. The low of deoxygenation rate can also be caused by the turbulent condition of river flow [14].

### BOD/COD Ratio

The Fig. 2 depicts the calculation of BOD/COD ratio of Cikapundung River water during 2012-2014. The values were determined based on the periodical data of the river water quality.

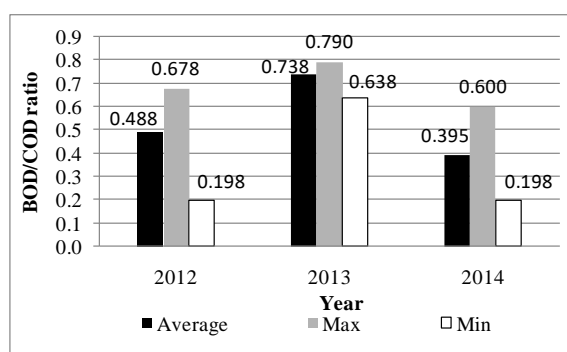


Fig. 2 BOD/COD ratio observed.

The range of BOD/COD ratio is 0.198-0.790. A value of more than 0.5 of BOD/COD ratio indicates rapid biodegradation; and a range of 0.2-0.4 specifies biodegradation only in favorable thermal condition [15]. The ratio of Cikapundung River water mainly denotes the rapid biodegradation process. It probably occurred in the anaerobic condition.

Considering the processes indicated by the deoxygenation rate, i.e. oxidation of organic material and aquatic plants respiration, the low value of the rate can probably denote a non-optimal condition of the processes. Decomposition of organic matter by the microorganism can be inhibited by several conditions, such as toxic material and heavy metals. The river quality data of Cikapundung show that several heavy metals were detected above the concentrations standard, i.e. Cr+6, Zn, Mn, Cu, and Pb. Research on the heavy metals impact on the biodegradation of organic matter are not generally explained, however the metals has potency on inhibiting biodegradation of pollutants under both aerobic and anaerobic conditions [16]. Heavy metals form complexes with protein molecules that causing inactivation of cells [17].

In the surface water, heavy metals consider as

toxic substances to the mixed culture of microorganisms responsible for the decomposition of organic matter [18]. The decomposing microorganisms play an important role in the self-purification of polluted river, thus heavy metals pollution might weaken the capability of river to purify itself.

Based on the laboratory analysis for identification of living decomposer microorganisms in the water, it was found that the only living bacterium was *Bacillus* sp type. This bacterium is the most active decomposer of organic matter in the river water. Consortiums of the *Bacillus* sp can effectively reducing organic pollutants [19]. *Bacillus* sp is non-pathogenic organisms [20]. Fungi that were existed include *Penicillium* sp, *Aspergillus* sp and *Cladosporium* sp. Several of the species in genus *Penicillium* and *Aspergillus* are known to produce mycotoxins in other substrates [21]. Those fungi are usually found in the treated and untreated water. *Aspergillus* and *Penicillium* spores are the most widespread aeroallergens in the world [22].

Activity of washing can also pollute the river, especially by the surfactant contaminant. It can affect the deoxygenation rate. An experimental substantiation was given to the potential environmental significance of the effect caused by the influence of synthetic surfactants on hydrobionts and the relationship between these effects and the hazard of anthropogenic impact on the processes of water self-purification [23]. Surfactants are diverse and amphiphilic compounds which can reduce surface and interfacial tensions [24].

### CONCLUSION

The deoxygenation rate of Cikapundung is quite low, indicating the slow process of self purification. However, the ratio of BOD/COD shows that the water has potential rapid biodegradation rate. The

The existence of heavy metals, synthetic surfactant, antimicrobial substances, indicate the unhealthy condition, especially in considering the self purification process. Toxic pollutants from various activities would inhibit the microorganism to live in the river water and to decompose the organic pollutants.

### ACKNOWLEDGMENT

This research was funded by the Ministry of Research, Technology, and Higher Education of the Republic of Indonesia.

### REFERENCES

- [1] Yustiani YM, Lidya L, "Towards an Information System of Modeling and Monitoring of Cikapundung River, Bandung,

- Indonesia”, *Procedia Engineering* 154, 2016, pp. 353-360.
- [2] Lincheva S, Todorova Y, Topalova Y, “Long-term assessment of the self-purification potential of a technologically managed ecosystem: the Middle Iskar cascade”. *Biotechnology and Biotechnological Equipment*, Vol. 28, No. 3, 2014, pp. 455-462.
- [3] Yustiani YM, Komariah I. “Investigation on the Biodegradation Capacity of Urban Rivers in Jakarta, Indonesia”. *International Journal of GEOMATE*, Vol. 12, Issue 34, June 2017, pp. 45-50.
- [4] Lee AH, Nikraz H, “BOD:COD ratio as an Indicator for River Pollution”, *International Proceeding of Chemical, Biological and Environmental Engineering* Vol. 88, 2015.
- [5] Siwiec T, Kiedrzyńska L, Abramowicz K, Rewicka A, Nowak P, “BOD measuring and modeling methods – review”, *Land Reclamation* No. 43 (2), 2011, pp.143-153.
- [6] Kumarasamy MV, “Deoxygenation and Reaeration Coupled hybrid mixing cells Based Pollutant Transport Model to Assess water Quality Status of a River”, *Int. J. Environ. Res.*, 9(1), 2015, pp. 341-350
- [7] Yustiani YM, “Determination of Deoxygenation Rate of Rivers Located in the Urban Areas to Characterized the Pollutants”, *Pollution Research*, 35(3), 2016, pp. 475-481.
- [8] Darul A, Irawan DE, Trilaksono NJ, Pratama A, Fitria UR, “Conceptual model of groundwater and river water interactions in Cikapundung riverbank, Bandung, West Java”, *IOP Conf. Series: Earth and Environmental Science* 29, 2016. doi:10.1088/1755-1315/29/1/012026.
- [9] Jatnika L, Rahardyan B, “Aplikasi Metode Valuasi Kontingen dalam Upaya Peningkatan Kebersihan Sungai Cikapundung Kota Bandung. (Application of Contingent Valuation Method in the Effort to Cikapundung River Quality Improvement)”, in *Indonesian. Majalah Ilmiah Globe*, Volume 17 No. 1, 2015, pp. 059-066.
- [10] Bappeda Kota Bandung, “Rencana Tata Ruang Kawasan Strategis Sungai Cikapundung Kota Bandung (Master Plan of Cikapundung River Strategic Area, Bandung City)” (in Indonesian), Project Report, 2011.
- [11] Peavy H.S., Donal R. Rowe, George Tchobanoglous 1985. *Environmental Engineering*. McGraw Hill, New York p. 43
- [12] Haider H, Al, W, “Development of Dissolved Oxygen Model for Highly Variable Flow River: A Case Study of Ravi River in Pakistan”, *Environmental Model Assessment*, Vol 15, 2010, pp. 583-599.
- [13] Jha R, Singh VP, “Analytical Water Quality Model for Biochemical Oxygen Demand Simulation in River Gomti of Ganga Basin, India”, *KSCE Journal of Civil Engineering* Vol 12 No.2 March 2008.
- [14] Hendriarianti, E. and Karnaningroem, N. 2015. Deoxygenation Rate of Carbon in Upstream Brantas River in the City of Malang. *Journal Applied Environmental and Biological Science*, 5 (12), 34-41.
- [15] Contreras S, Rodriquez M, Al Momani F, Esplugas S, “Contribution of the ozonation pre-treatment to the biodegradation of aqueous solutions of 2,4 dichlorophenol,” *Water Research*, 37, 2003, pp. 3164-3171.
- [16] Sandrin TR, Maier RM, “Impact of metals on the biodegradation of organic pollutants”, *Environ Health Perspect*, 111, 2003, pp. 1093-110.
- [17] Kim SJ, “Effect of Heavy Metals on Natural Population of Bacteria from Surface Microlayers and Subsurface Water”, *Marine Ecology*, Vol. 26, 1985, pp. 203-206.
- [18] Mala J, Maly J, “Effect of Heavy Metals on Self-Purification Processes in Rivers.” *Applied Ecology and Environmental Research* 7(4), 2009, pp. 333-340.
- [19] Safitri R, Priadie B, Miranti M, Astuti AW, “Ability of Bacterial Consortium: *Bacillus coagulans*, *Bacillus licheniformis*, *Bacillus pumilus*, *Bacillus subtilis*, *Nitromonas* sp. And *Pseudomonas putida* In Bioremediation of Waste Water in Cisirung Waste Water Treatment Plan” *AgroLife Scientific Journal*, Vol. 4(1) 2015, pp. 146-152.
- [20] Duru M, Nwanekwu K, “Physicochemical and microbialstatus of Nworie River, Owerri, Imo State, Nigeria”, *Asian Journal of Plant Science and Research*, 2012, 2 (4):433-436.
- [21] Pitt JI, Hocking AD. *Fungi and Food Spoilage*, 2nd edn. Aspen Publishers, Gaithersburg, MD., 1999.
- [22] Bandh SA, Kamili AN, Ganai BA, Saleem S, Lone BA, Nissa H, “First Qualitative Survey of Filamentous Fungi in Dal Lake Kashmir”, *Journal of Yeast and Fungal Research*, Vol 31(1), 2012, pp. 7-11.
- [23] Ostroumov SA, “The effect of synthetic surfactants on the Hydrobiological Mechanisms of Water Self-Purification”, *Water Resources*, Vol. 31, No. 5, 2004, pp. 502-510.
- [24] Chaturvedi AD, Tiwari KL, “Surfactants (surface-active agent) are diverse and amphiphilic compounds which can reduce surface and interfacial tensions by accumulating at the interface of immiscible fluids and increase the solubility, mobility, bioavailability and subsequent biodegradation of hydrophobic or insoluble organic compounds”, *Recent Research in Science and Technology* 2013, 5(5) pp. 12-16.

## THE PHYSICAL MICROHABITAT REQUIREMENTS OF FRESHWATER MUSSEL, *WESTRALUNIO CARTERI*, (BIVALVIA: HYRIIDAE) IN SOUTH-WESTERN AUSTRALIA

Le Ma<sup>1</sup>, Alan Lymbery<sup>2</sup>, Stephen Beatty<sup>3</sup> and David Morgan<sup>4</sup>

<sup>1</sup>Centre for Fish and Fisheries Research, School of Veterinary and Life Science, Murdoch University,  
Australia

### ABSTRACT

Freshwater mussels (Bivalvia: Unionoida) are important for maintaining the water quality. Carter's Freshwater Mussel, *Westralunio carteri*, is the only species of freshwater mussel in the south-west of Australia, and the only representative of *Westralunio* in Australia. Eighteen sites from thirteen rivers have been surveyed in this research for investigating the physical microhabitat requirements of *W. carteri*. Substrate type, debris size and water depth are believed to have significant impacts on the microscale occurrence of *W. carteri*. In channel, locations with shallow water, fine substrates and relative larger debris are most favored by freshwater mussels. Shadows of trees or bridges may have a less significant impact. Juvenile mussels are suspected to have a slightly different microhabitat requirements with adult mussels.

**Keywords:** *Westralunio*, *Bivalvia*, *Freshwater mussels*, *Ecology*, *Microhabitat*

### INTRODUCTION

Freshwater bivalves (Mollusca: Bivalvia: Unionoida) play significant roles for the balance of both freshwater ecosystems and development of human cultures [1], [2]. Freshwater mussels act as "ecological generalists" and benefit to the freshwater communities through the filter feeding function [3], [4]. Their presence further improves water quality through reducing the overall nutrient level [5] and the concentration of several chemicals [6], thereby reducing the probability of detrimental algal blooms and eutrophication. Unionoida is also key coupler, enhancing the links between benthic and pelagic systems through burrowing the sediment and releasing biological waste into water [7], [8]. After they dead, their shells may be occupied by other aquatic organisms as shelters and refuges [9], [10]. Additionally, they can be a source of mother-of-pearl and food for economy values [11], [12].

It is widely recognized that environmental features, especially stream characteristics, are able to influence the distribution of unionid species. [13] believed that microhabitat features are good predictors for investigating the distribution of bivalves. For instance, substrate sediment-type and hydrology are known to strongly influence the distribution of freshwater bivalves in waterways [14], [15]. Freshwater mussels tend to favor areas of increased flow stability, and in flood-periods rely on areas of reduced particle movement [16], with microhabitat preferences similar across life-stages [15], [17].

Carter's Freshwater Mussel, *Westralunio carteri*, is the only known Unionoida in the south-western

Australia and the sole representative of *Westralunio* present on the Australian continent [18]. A combination of drought, increasing salinity and nitrate-related pollution has led to a >60% decline in its extent of occurrence (EOO) over the past fifty years, resulting in its classification as a 'Vulnerable' species by both international and local conservation regulatory bodies [19], [20]. A map of *W. carteri*'s presence and distribution has been produced, however, detail concerning the living quality of this species is remaining unclear [18]. Investigation into the microhabitat requirements of *W. carteri* will help to reduce this knowledge gap and improve the conservation of this species.

This research firstly attempted to determine the distribution of *Westralunio carteri* in the rivers of south-western Australia from a microhabitat perspective. We hypothesized that the occurrence of *W. carteri* is affected by several selected stream characteristics.

### METHODS AND MATERIALS

#### *Survey sites*

Eighteen sites in thirteen rivers were selected based on the distribution of *Westralunio carteri* in previous records [18]. Gingin Brook, Yalyal Brook, Marbling Brook, and Ellen Brook, located to the north of Perth City, flow through agricultural areas from the east to the west. Bennett Brook and the mid-downstream part of Canning River, in the Perth Metropolitan Region, are situated in urbanised regions. To the east of Perth, Helena River and the upstream reach of Canning River originate in the

Darling Scarp, in areas largely covered by native vegetation. North Dandalup River and Collie River lie to the south of Perth in agricultural areas. Finally, Warren River, Fly Brook, Lefroy Brook and Smith Brook are located in the south-western corner of Western Australia. Sampling occurred between March and June 2016 (i.e. spring to early winter). The location of each site was recorded by GPS handset.

#### Mussel sampling

At each site, four to five transects were selected by channel accessibility and 10 random quadrats (each 25 cm × 25 cm) were taken at each transect. For each transect, surveys occurred in a downstream to upstream direction for a distance of up to 10 m of stream. Several selected in-stream environmental characteristics were recorded as shown in table 1. Mussels in each quadrat were searched by hand. Substrate was classified following the method used by [21]. Debris was classified as wood, leaves or other artificial debris. Current velocity was measured by a Hontzsch® HFA 711 series hand-held flowing meter at the water surface. Riverbed slope was measured by magnetic protractor. Finally, the condition of surrounding channel valley was roughly assessed following the method in [22] and recorded.

Table 1 Variables for modelling the micro-habitat requirements of *Westralunio carteri*

Variable Name	Mean ± s.e.	Range
Water Depth (m)	0.25±0.009	0.02-0.92
Streambed Slope (°)	7±0.4	0-49
Debris Type	Wood, Leaf and Artificial	
Debris Height (cm)	5±0.6	0-166
Debris Cover (%)	38±2.2	0-100
Current Velocity (m/s)	0.67±0.07	0-1.00
Substrate Grain Size*	3±0.1	0-10
Macrophytes Cover (%)	33±2.4	0-100
Distance to riverbank	1.0±0.04	0-3.9

\* the substrate grain size is converted to Sediment Particle Index following the method used by [21].

#### Statics

All collected data was processed by R software. The habitat requirements were analyzed through general liner regression model (glm) with binomial distribution. A decision tree was applied to find the most significant predictors for the occurrence of *W. carteri*.

## RESULTS

A total number of 604 mussels were recorded and examined from twelve sites in eight rivers. Mussel density ranged from 0 to 512 mussels/m<sup>2</sup> with half of the investigated quadrats having no mussels. The mean number of mussels/quadrat was 2 (±0.210) for all quadrats, and 3.67 (±0.331) for those quadrats with mussels present, while the median number is slightly lower, with 1 mussel per quadrat for all quadrats or 2 mussels per quadrat for the quadrats having living mussels. The quadrats-level mussel density distribution did not show significant difference (unpaired t-test, p=0.9535) with the transect-level in the analysis results as shown in fig 1. Living mussels were not detected in the selected reaches at Ellen Brook, Fly Brook, Lefroy Brook, Marbling Brook and Smith Brook.

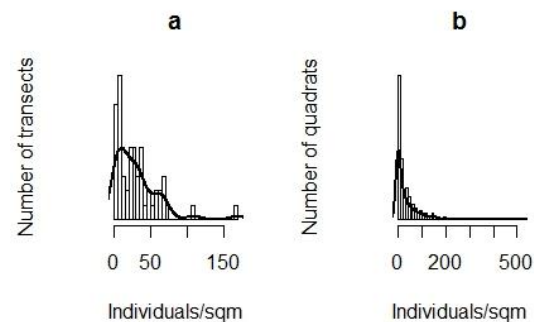


Fig. 1 Observed mussel density distribution at transect (a) and quadrat (b) level.

Mussels were found among a wide range of substrate types from silt to large rocks, while the majority of population inhabits fine silt. Channel width ranged from 2-33 m (7.19±0.880 m) with relatively narrower water width (5.94±0.736 m). Riverbanks at all selected locations were vegetated with grass and trees.

Table 2 Variables for modelling the micro-habitat requirements of *Westralunio carteri*

Variable Name	Estimate	P value
Water Depth (m)	0.465	0.522
Streambed Slope (°)	0.014	0.313
<i>Debris Height (cm)</i>	0.028	0.085
Debris Cover (%)	0.000	0.869
Current Velocity (m/s)	0.198	0.844
Substrate Grain Size (see methods for scale)*	-0.237	<0.001
Macrophytes Cover (%)	0.002	0.521
Distance to riverbank	-0.138	0.269

\* is the significant variable(s)

*Italic* is the near significant variable(s)



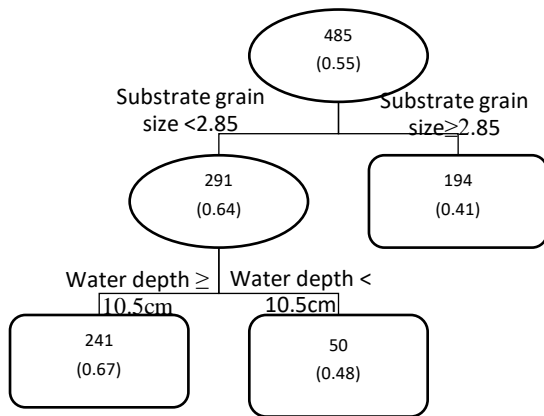


Fig. 2 Decision tree for the impacts of substrate and water depth on the presence of *W. carteri*. Rounded rectangles indicate terminal nodes. See method for the scale of substrates

General liner regression model only illustrated the significant negative impact of substrate grain size and a near significant relationship between the mussel occurrence and the debris height (Table 2). The decision tree analysis also indicated that substrate grain size is the most significant predictor for mussel occurrence, with water depth as the second level predictor (Fig. 2). The range and value of other variables did not show significant difference for the quadrats with and without living mussels (Fig. 3).

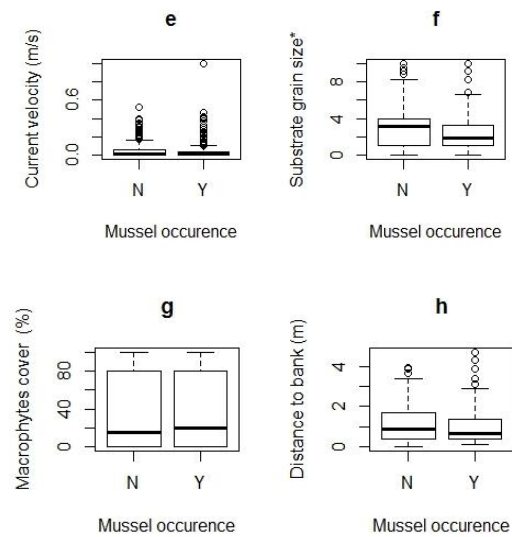


Fig. 3 Mussel presence (Y) and absence (N) coinciding with the water depth (a), riverbed slope (b), debris height (c), debris cover (d), water flow velocity (e), substrate grain size (f), macrophytes cover (g) and distance to riverbank (h), see methods for the scale of substrate grain size.

Transect analysis shown that mussel density was positively affected by canopy cover (estimate=0.005,  $p < 0.001$ ), and may be positively influenced by the occurrence of flat riverbed (estimate=0.327,  $p < 0.001$ ) and bank tree abundance (estimate=0.013,  $p < 0.001$ ) as shown in fig 4. No more relationship has been detected in this study.

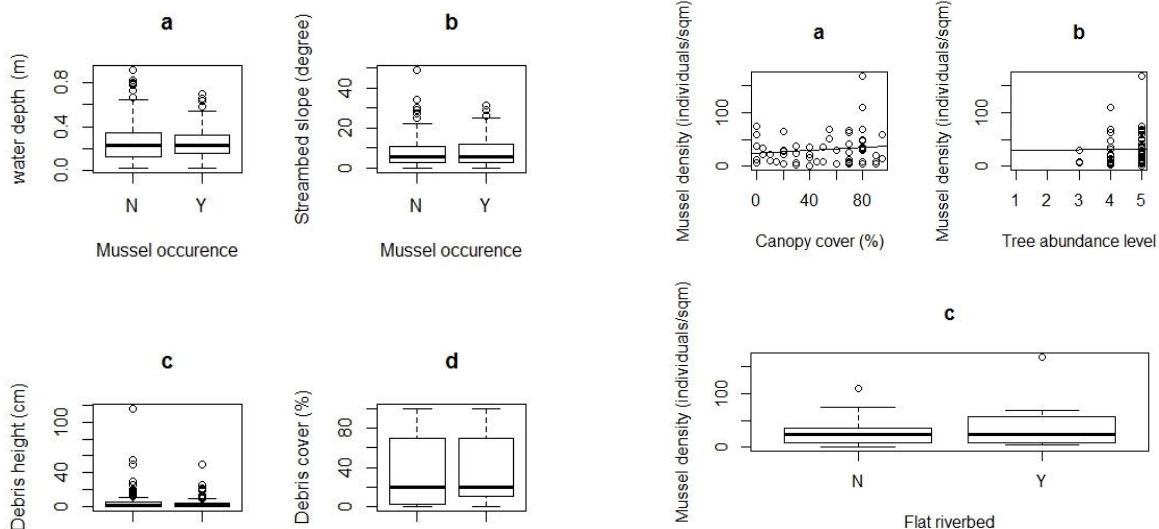


Fig. 4 The relationship between the transect level mussel abundance and canopy cover (a), the tree abundance level of riverbank (b) and flat riverbed (c). Scale of bank tree abundance level: 1 – no trees at the bank, 5 – bank is full with trees

## DISCUSSIONS

The assemblages of *Westralunio carteri* prefer to stay at the microhabitat with certain characters which matches our hypothesis. Locations with fine silt, shallow water and large debris in the rivers are likely to be preferred by *W. carteri*. In addition, shadows of the trees at the riverbank and flat riverbed may also be favored by the freshwater mussels.

Overall, substrate, water depth, canopy cover, streambed morphology are able to influence the presence of freshwater mussels, *Westralunio carteri*. The result generally matches other studies on Australian Hyriidae species and *Hyridella menziesi* in New Zealand [23], [24]. Respectively, researches in Asia [25], Northern America [13], [26] and Europe [17] also performed similar results. Thus, the hypothesis is believed to be true.

Substrate is believed to be the primary microhabitat environmental character, which respects the conclusions of almost all other studies for the same topic [17], [27]. In this study, *Westralunio carteri* requires fine and loose silt or sand. This fine substrate preference does not like its Australian relatives in the east, such as *Hyridella depressa* or *Hyridella australis*, which prefers coarse sand or sand [24]. Instead, the substrate preference of *W. carteri* is in some way similar with *Unio douglasiae nipponensis*, and *Lanceolaria grayana* in Japan [25]. It is probable because the streams in both Japan and Western Australia are relatively small, the normal flow is not able to create much turbulence with fine and loose substrate so mussels prefer to stay with those easy-burrowed sediments without being flowed away. In addition, *W. carteri* may find more food from fine silt due to the large amount of organic material within the silt. However, as indicated in [17], only substratum can never be a reliable predictor for mussels presence.

Water depth is the second primary predictor in the decision tree analysis and this result also matches a series of researches for other freshwater bivalves [28], [29]. The water depth must be neither too shallow nor too deep. The reason behind this result is not complicated, adequate water depth can provide both protection and dissolved oxygen. In the one hand, mussels will be easily seen and captured by their predators if the water is very shallow, especially in clean water. In the other hand, the dissolved oxygen of bottom water will be very low, which is not good for aquatic livings, if water depth

is too high. For the conditions above, an appropriate water depth is also required by freshwater mussels.

The next important microhabitat feature can be large debris. The debris may be in a relation with the stability of mussel bed as several researches claimed that the substrate stability is curial for freshwater mussels [30], [31]. As fine and loose silt is not as stable as boulders or coarse sands between boulders or rocks, stability adder may help to reduce the turbulence in water flow. In the south west of Western Australia, large pieces of debris (eg. wood log) may act as stability adders. It is suspected that several certain types of large aquatic vegetation, such as water lily or submerged water plants, may also act as the same role in the rivers while the statistical result did not illustrate a clear relationship in this study.

Furthermore, shear stress may also have impacts since a couple of past researches pointed out that shear stress is one of the most significant predictors of freshwater mussels [27], [30], [32]. High shear stress may remove both the suitable substrate and the mussels. It is believed that shear stress is determined by the substrate, riverbed morphology and water flow velocity [31]. Large pieces of objectives may create a shelter and reduce the shear stress by changing the nearby hydrological circumstance.

In addition, transect assessment suggested that flat channel bed, trees at the streambank and canopy cover are also able to positively affect the presence of mussels. The result can be reasonable. Flat bottom refers a generally stable flow velocity and even distributed shear stress. Trees at river bank can bring more shadow area in the channel. Canopy cover also can create shadows. Mussels may prefer to stay with shaded area as the temperature in summer is very high. In some very extreme events, for instance a long drought and the river dried, mussels may survive longer in shadow. However, the sample size of transect assessment is not enough and the transect assessment is not focused with this study, further research on larger scales might be help to improve the understanding of mussels' habitat requirements.

Finally, although there is no statistical result for juvenile *Westralunio carteri* in this study because the mussel searching method is biased to adult mussels with larger size. A few juvenile mussels were found in the places where large number of adult mussels were also found.

## CONCLUSION

This study firstly attempt to investigate the microhabitat of *Westralunio carteri* in the south western of Western Australia. Those freshwater mussels require fine substrate, large piece of stability adder in the habitat. Tree shadows and flat streambed may also contribute to the establishment of mussel bed. Further quantitative investigation on the mussels' microhabitat preference can help the conservation management of this endangered species.

## ACKNOWLEDGEMENTS

This research is part of PhD project at Murdoch University, we appreciate to all our volunteers for their help in our fieldwork. We thank the Holsworth Wildlife Research Endowment for funding the fieldwork. Special thanks to Ms. Suzanne Thompson and Ms Megan Sheehan from WA Department of Parks and Wildlife for her help in surveying Canning River, Helena River and Serpentine River. Many thanks to Holly Emery-Butcher, Nathan Beerkens and Tom J. Dimaline for their kind help in data collection and article editing. We also would like to thank all landowners for their permissions and assistances of working in their properties. All fieldworks are under licenses.

## REFERENCES

- [1] Strayer DL, Freshwater Mussel Ecology: A Multifactor Approach to Distribution and Abundance. Berkley, CA, USA: University of California Press, 2008.
- [2] Mackie GL and Claudi R, Monitoring and Control of Macrofouling Mollusks in Fresh Water Systems, 2nd ed.: CRC Press, 2009.
- [3] Caraco NF, Cole JJ & Strayer DL, "Top-down control from the bottom: Regulation of eutrophication in a large river by benthic grazing," *Limnology and Oceanography*, vol. 51, 2006, pp. 664-670.
- [4] Strayer DL, Caraco NF, Cole JJ, Findlay S & Pace ML, "Transformation of Freshwater Ecosystems by Bivalves," *BioScience*, vol. 49, 1999, pp. 19-27.
- [5] Howard JK & Cuffey KM, "The functional role of native freshwater mussels in the fluvial benthic environment," *Freshwater Biology*, vol. 51, 2006, pp. 460-474.
- [6] Barbiero RP, Tuchman ML & Millard ES, "Post-dreissenid increases in transparency during summer stratification in the offshore waters of Lake Ontario: Is a reduction in whiting events the cause?," *Journal of Great Lakes Research*, vol. 32, 2006, pp. 131-141.
- [7] Vaughn CC & Hakenkamp CC, "The functional role of burrowing bivalves in freshwater ecosystems," *Freshwater Biology*, vol. 46, 2001, pp. 1431-1446.
- [8] Strayer DL, "Understanding how nutrient cycles and freshwater mussels (Unionoida) affect one another," *Hydrobiologia*, vol. 735, 2014/09/01 2014, pp. 277-292.
- [9] Seed R, "Patterns of biodiversity in the macroinvertebrate fauna associated with mussel patches on rocky shores," *Journal of the Marine Biological Association of the United Kingdom*, vol. 76, 1996, pp. 203-210.
- [10] Jaramillo PQE & Pino M, "Macroinfaunal assemblages associated with mussel and clam beds in an estuary of southern Chile.," *Estuaries*, vol. 19, 1996, pp. 62-74.
- [11] Ray S, Ray M, Chakraborty S & Mukherjee S, "Immunotoxicity of environmental chemicals in the pearl forming mussel of India - a review," in *Mussels: Anatomy, Habitat and Environmental Impact*, L. E. McGevin, Ed., ed New York: Nova Science Publishers Inc., 2011, pp. 429-440.
- [12] FAO, The State of World Fisheries and Aquaculture 2014. Rome, 2014.
- [13] Strayer DL, "Macrohabitats of Freshwater Mussels (Bivalvia: Unionacea) in Stream of the Northern Atlantic Slope," *Journal of the North American Benthological Society*, vol. 12, 1993, pp. 236-246.
- [14] Box JB, Dorazio RM & Liddell WD, "Relationships between stream substrate characteristics and freshwater mussels (Bivalvia: Unionidae) in Coastal Plain streams," *Journal of the North American Benthological Society*, vol. 21, 2002, pp. 253-260.
- [15] McRae SE, Allan JD & Burch JB, "Reach - and catchment - scale determinants of the distribution of freshwater mussels (Bivalvia: Unionidae) in south - eastern Michigan, USA," *Freshwater Biology*, vol. 49, 2004, pp. 127-142.
- [16] Strayer DL, "Use of Flow Regfues by Unionid Mussels in Rivers," *Journal of the North American Benthological Society*, vol. 18, 1999, pp. 468-476.
- [17] Hastie LC, Boon PJ & Young MR, "Physical microhabitat requirements of freshwater pearl mussels, *Margaritifera margaritifera* (L.)," *Hydrobiologia*, vol. 429, 2000, pp. 59-71.
- [18] Klunzinger MK, Beatty SJ, Morgan DL & Lymbery AJ, "Distribution of *Westralunio carteri* Iredale, 1934 (Bivalvia: Unionoida: Hyriidae) on the south coast of south-western Australia, including new records of the species," *Journal of the Royal Society of Western Australia*, vol. 95, 2012, pp. 77-81.
- [19] Klunzinger MW, Beatty SJ, Morgan DL, Pinder AM & Lymbery AJ, "Range decline and conservation status of *Westralunio carteri* Iredale, 1934 (Bivalvia: Hyriidae) from south-

- western Australia," Australian Journal of Zoology, 2015,
- [20] Klunzinger M & Walker KF, "*Westralunio carteri*," in The IUCN Red List of Threatened Species Version 2014.3, ed, 2014.
- [21] Strayer DL, "Use of Flow Refuges by Unionid Mussels in Rivers," Journal of the North American Benthological Society, vol. 18, 1999, pp. 468-476.
- [22] Raven PJ, Holmes NTH, Dawson FH, Fox PJA, Everard M & Fozzard IR, "River Habitat Quality: the physical character of rivers and streams in the UK and Isle of Man," Scottish Environmental Protection Agency, Edinburgh 1998.
- [23] James MR, "Distribution, biomass and production of the freshwater mussel, *Hyridella menziesi* (Gray), in Lake Taupo, New Zealand," Freshwater Biology, vol. 15, 1985, pp. 307-314.
- [24] Brainwood M, Burgin S & Byrne M, "The role of geomorphology in substratum patch selection by freshwater mussels in the Hawkesbury-Nepean River (New South Wales) Australia," Aquatic Conservation-Marine and Freshwater Ecosystems, vol. 18, Nov-Dec 2008, pp. 1285-1301.
- [25] Nagayama S, Harada M & Kayaba Y, "Distribution and microhabitats of freshwater mussels in waterbodies in the terrestrialized floodplains of a lowland river," Limnology, vol. 17, 2016, pp. 263-272.
- [26] Layzer JB & Madison LM, "Microhabitat use by freshwater mussels and recommendations for determining their instream flow needs," Regulated Rivers: Research & Management, vol. 10, 1995, pp. 329-345.
- [27] Morales Y, Weber LJ, Mynett AE & Newton TJ, "Mussel dynamics model: A hydroinformatics tool for analyzing the effects of different stressors on the dynamics of freshwater mussel communities," Ecological Modelling, vol. 197, 8/25/ 2006, pp. 448-460.
- [28] Johnson PD & Brown KM, "The importance of microhabitat factors and habitat stability to the threatened Louisiana pearl shell, *Margaritifera hembeli* (Conrad)," Canadian Journal of Zoology, vol. 78, Feb 2000, pp. 271-277.
- [29] Parasiewicz P, Castelli E, Rogers JN & Plunkett E, "Multiplex modeling of physical habitat for endangered freshwater mussels," Ecological Modelling, vol. 228, 3/10/ 2012, pp. 66-75.
- [30] Zigler SJ, Newton TJ, Steuer JJ, Bartsch MR & Sauer JS, "Importance of physical and hydraulic characteristics to unionid mussels: a retrospective analysis in a reach of large river," Hydrobiologia, vol. 598, Feb 2008, pp. 343-360.
- [31] Morales Y, Weber LJ, Mynett AE & Newton TJ, "Effects of substrate and hydrodynamic conditions on the formation of mussel beds in a large river," Journal of the North American Benthological Society, vol. 25, 2006, pp. 664-676.

## EVALUATING THE EFFECTIVENESS OF VIRGINIA BUTTONWEED FOR EROSION CONTROL OF DAM RESERVOIR SLOPES IN JAPAN

Taizo Uchida<sup>1</sup>, Yuya Imamura<sup>2</sup>, Yoshifumi Kochi<sup>3</sup>, Mamoru Yamada<sup>4</sup>, Kunihiko Fukaura<sup>5</sup>, Aki Matsumoto<sup>6</sup>, William T. Haller<sup>7</sup> and Lyn A. Gettys<sup>8</sup>

<sup>1</sup>Graduate School of Engineering, Kyushu Sangyo University, Japan; <sup>2</sup>Fukuoka Prefectural Office, Japan; <sup>3</sup>K's Lab Co., Ltd., Japan; <sup>4</sup>SPTEC-YAMADA Inc., Japan; <sup>5</sup>Makino Green Corp., Japan; <sup>6</sup>Takino Filter Inc., Japan; <sup>7</sup>Center for Aquatic and Invasive Plants, University of Florida, USA

### ABSTRACT

Reservoir slopes of dams are typically bare or sparsely vegetated due to their steep inclination, long-term submergence, marked fluctuation of water levels and impact of waves, which promote soil erosion and cause water turbidity, deterioration of the landscape, and disrupt ecosystem functioning. Using plants to stabilize slopes and prevent erosion is difficult, and the introduction of plants for this purpose has been extensively debated. This study examined the effectiveness of Virginia buttonweed (Rubiaceae: *Diodia virginiana* L.) for stabilizing the exposed slopes of the Matsubara Dam in western Japan- *Diodia virginiana* was originally introduced to a 0.1-hectare experimental area on the dam slopes from 1994 to 1997. Since that time, *D. virginiana* flourished; in 2008 it was widespread around the dam, growing in harsh environments such as steep slopes and shoreline, and by 2016, the distribution and density of the species increased. These characteristics of *D. virginiana* growth mean that the species is well suited for use as a cover plant for preventing erosion on dam reservoir slopes.

**Keywords:** Cover plant, Dam, *Diodia virginiana*, Erosion control, Reservoir slope

### INTRODUCTION

Dams have a variety of functions, including the storage of water for drinking and agriculture, generating electricity, and providing habitats for wildlife. In addition, dams are important for mitigating floods in Japan, particularly in the rainy season in June and July, and the typhoon season in August and September. Dams used mainly for flood control exhibit marked fluctuations in water levels during the year as the water level of reservoirs is typically lowered artificially approximately two months before the onset of the rainy and typhoon seasons. Since these fluctuations in water levels can be in the order of dozens of meters, extensive reservoir slopes can be exposed when the water level is lowered (Photo 1).

These slopes are typically bare or sparsely vegetated due to their generally steep gradient, extended submergence and impacts of waves as well as marked fluctuation of water level, which have a negative effect on landscape appearance, ecosystem integrity and water quality [3], [6], [10], [11], [14], [16] (Photo 1). Although slopes can be stabilized using a variety of methods, the artificial introduction of cover plants for purposes of erosion control can be difficult.

It was previously reported that the reservoir slopes of some dams on Kyushu Island in western



Photo 1 Reservoir slopes exposed when the water level of dam was lowered before slope stabilization was attempted (reproduced from the River Bureau, Ministry of Land, Infrastructure and Transport [14]).

Japan had spontaneously become covered by Virginia buttonweed (Rubiaceae: *Diodia virginiana* L.); for example, Tsuruta Dam, Midorikawa Dam, and Ichifusa Dam [8], [10]. In 1994, therefore, test areas on the reservoir slopes of Matsubara Dam were stabilized with *D. virginiana* to prevent erosion and related problems [6], [10], [16]. Here we examine the current status of the slopes and discuss the utility of using *D. virginiana* as a cover plant for erosion control on reservoir slopes.

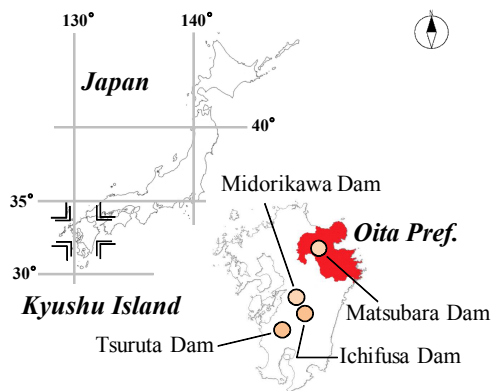


Fig. 1 Location of the study site, Matsubara Dam, in Oita Prefecture, and some dams the reservoir slopes of which are spontaneously covered by *Diodia virginiana*.

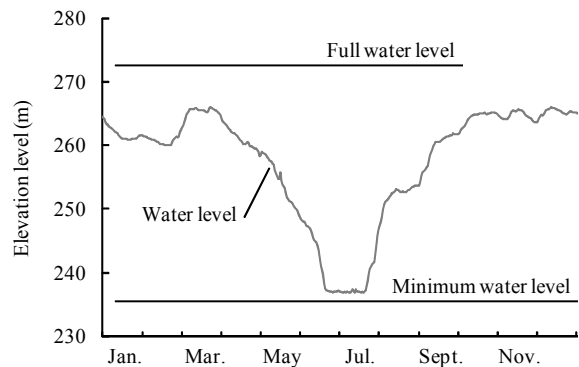


Fig. 2 Seasonal change of the average fluctuation in water level of reservoir of Matsubara Dam in recent years.

## METHODS

### Study Site

Matsubara Dam is situated in Oita Prefecture, Kyushu Island, in western Japan in an area that is dominated by andesite soils [9] (Fig. 1). This dam is located in the warm temperature zone where the mean annual temperature and annual precipitation for the last decade (2007-2016) ranged from 15.1 to 16.8°C and 1,561 to 2,481 mm, respectively [4].

Matsubara Dam, which was constructed in 1973 as a multipurpose dam for water supply, flood control and generation of electricity, is a concrete gravity-type dam with a wall measuring 83.0 m high (elevation level (meters above sea level): 192.0 - 275.0 m) and 192.0 m long [9]. The basin area, reservoir area and gross capacity are 491 km<sup>2</sup>, 1.9 km<sup>2</sup> and 54,600,000 m<sup>3</sup>, respectively [9]. Seasonal fluctuations in the water level of Matsubara Dam in recent years are shown in Fig. 2. The water level decreases most from the middle of June to the end of July, and the reservoir slopes are highly exposed in this period.

Introduction of *D. virginiana* to the reservoir slope was conducted on three occasions from 1994 to 1997 using seeds, rhizomes and seedlings. A total area of approximately 0.1-hectare was used for all trials [6], [10], [16].

### Vegetation Survey

Permission for the study on the reservoir slopes of Matsubara Dam was obtained from the Kyushu Regional Development Bureau, Ministry of Land, Infrastructure, Transport and Tourism. The steepest (steep slope) and gentlest (gentle slope) slopes were

selected for analysis in the permitted areas.

A transect was set up along the slope perpendicular to the dam shore in early July 2008 when the water level was lower than usual (at 237 m, see Fig. 2). After conducting a topographical survey along the transect, survey quadrats (1 × 1 m each) were placed on the transect at approximately 2-m intervals. The species composition of the plants in each quadrat was recorded using the Braun-Blanquet cover-abundance scale [1]. Vegetation on the slopes was classified by TWINSpan calculated using the PC-ORD statistical software package (ver. 4.0 for Windows, MjM Software Design, OR). The Braun-Blanquet cover-abundance scale (r, +, I, II, III, IV, and V) was transformed as follows: r and + were taken as 0.1%; I as 5.0%; II as 17.5%; III as 37.5%; IV as 62.5%, and V as 87.5%.

In addition, coverage of *D. virginiana* along the reservoir shoreline was also surveyed and mapped early in September 2008 and 2016 when the water level was 263 and 265 m, respectively; these surveys were conducted using a boat and Braun-Blanquet cover-abundance scale.

## RESULTS

### Reservoir Slope Vegetation

The reservoir slopes of Matsubara Dam were extensively vegetated (Photo 2 [A-H]). The vegetation was classified into six vegetation types (I, II, III, IV, V and VI) using TWINSpan (Fig. 3); Types I, II, III and IV were dominated by *D. virginiana*, which had been applied to the slopes as cover plant for erosion control, together with *Oenothera laciniata* Hill and *Cynodon dactylon* (L.) Pers. Types V and VI were dominated by *Xanthium occidentale* Bertoloni and *C. dactylon*. The former group was typically found on steep slopes and/or





Photo 2 Matsubara Dam from July to September.

near the top of both the steep and gentle slopes, which is where the shoreline is when the dam is full (Fig. 2), and the latter group was restricted to gentle slopes (Fig. 4).

#### ***Diodia virginiana* along the Reservoir Shoreline**

*Diodia virginiana* was observed over most of the dam slopes around the dam in 2008 (Fig. 5), and distribution and density of this species increased in 2016.

#### **DISCUSSION**

The effects of fluctuations in water level, extended submergence and wave action constitute

serious barriers to the colonization and establishment of plant species including cover plants [3], [11], [14]. The findings of this study showed that the stands of *D. virginiana* (2008) introduced approximately 10 years previously had expanded considerably beyond the 0.1 ha study plots to cover vast regions of exposed dam shore (Photo 2; Fig. 5), and that the distribution and density of this species had increased over time (2016) (Fig. 5). In addition, most of this growth was observed on steep slopes and along the shoreline, and the latter is vulnerable to wave impact (Fig. 4).

It appears that *D. virginiana* is suitable for use as a cover plant for stabilizing the reservoir slopes of dams. The success of this species for this purpose is considered to be due to the fact that the seeds of *D.*



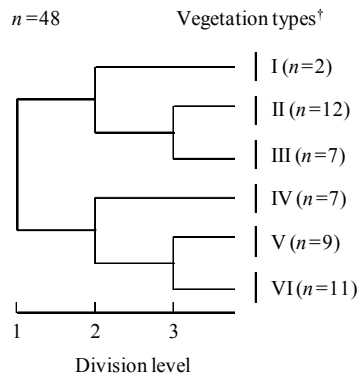


Fig. 3 Classification of vegetation on reservoir slopes by TWINSpan using species composition (coverage data, %).

<sup>†</sup>, on the basis of plant coverage size in each vegetation type (I-VI), it was defined as follows: I, *Diodia virginiana* - *Oenothera laciniata*; II, *Diodia virginiana*; III, *Diodia virginiana* - *Cynodon dactylon*; IV, *Cynodon dactylon* - *Diodia virginiana*; V, *Xanthium occidentale* - *Cynodon dactylon*, and VI, *Cynodon dactylon* - *Xanthium occidentale*.

*virginiana* contain suberin, which causes the seeds to float and spread widely [6] (Photo 2 [K]), and even young plants are remarkably resistant to inundation; according to Imamura *et al.* [3], several-month-old seedlings of *D. virginiana* can tolerate submergence for more than half a year.

It is also considered that the presence of other plant species, such as *O. laciniata*, *C. dactylon* and *X. occidentale*, on both types of slopes may have been facilitated by *D. virginiana*, which effectively bound the soil of the dam slopes and trapped the seeds of other grass species (Fig. 4). And furthermore, succession among species would have been promoted on the gentle slopes (Fig. 4).

## CONCLUSIONS

Given the importance of conserving landscapes and biodiversity, the application of cover plants for erosion control on slopes (e.g. Kondo *et al.* [7]; Uchida *et al.* [15]) has become preferable to civil engineering solutions. Under the circumstances, in this study it is considered that characteristics of *D. virginiana* growth are well suited for use as a cover plant on dam reservoir slopes (Figs. 4, 5). In addition, the dense carpets, attractive flowers and long rhizomes produced by this species (Photo 2 [I, J, L, M]), means it could be used to prevent erosion, increase aesthetic appearance, and promote soil binding in areas at risk of soil erosion. However, since *D. virginiana* is an alien species native to "North America", extensive growth of the species

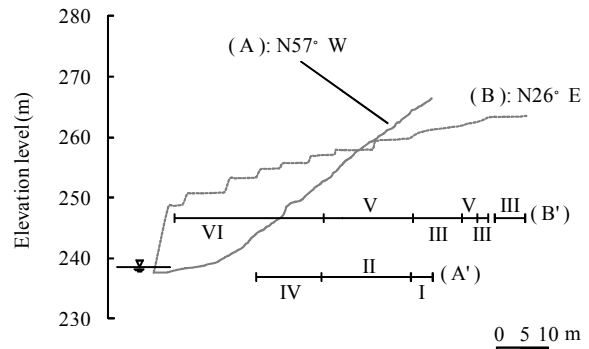


Fig. 4 Vegetation type on steep and gentle slopes. (A) and (B) indicate steep and gentle slopes, respectively. (A') and (B') indicate vegetation types on steep and gentle slopes, respectively. Vegetation types: See Fig. 3.

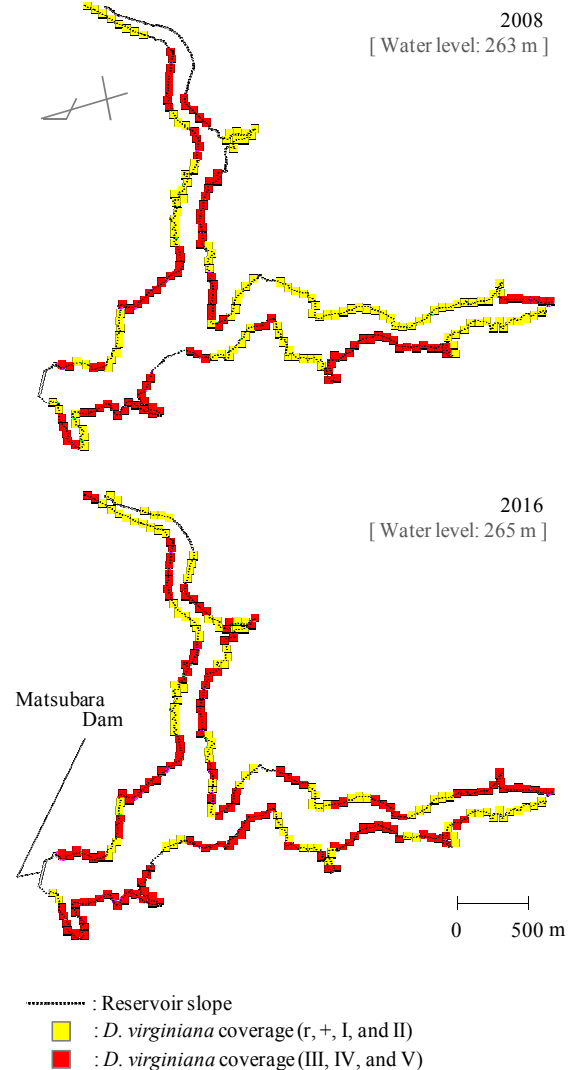


Fig. 5 Distribution of *Diodia virginiana* along the shoreline of Matsubara Dam.

could adversely affect ecosystem integrity and biological diversity. Indeed, *D. virginiana* is becoming increasingly troublesome weed even in the US, particularly in Alabama, Georgia, Mississippi, North Carolina, etc., where control using herbicides is currently being investigated [2], [5], [12], [13]. It is therefore necessary to overcome a trade-off between the application of *D. virginiana* as a cover plant and the potential negative effects of this species on biological diversity.

## ACKNOWLEDGEMENTS

We thank the Dam Joint Control Office of Chikugo-gawa River, Kyushu Regional Development Bureau for providing access to the experimental sites. We also thank Takeshi Goto, Hayato Yoshitsugu, Ryoji Zenmyou, Syuhei Yamawaki, Hisae Yonao, Kentaro Kondo and Yuki Tomoguchi at the Laboratory of Plant Ecology at Kyushu Sangyo University (KSU) for their assistance.

## REFERENCES

- [1] Braun-Blanquet J., 1964. Pflanzensozologie. Grundzüge der Vegetationskunde, 3rd ed. Springer-Verlag, Vienna. 865 pp.
- [2] Hutto K.C., Brecke B.J. and Unruh J.B., 2008. Comparison of flazasulfuron to pyridine herbicides for Virginia buttonweed (*Diodia virginiana*) control. Weed Technology 22, 351-353.
- [3] Imamura Y. and Uchida T., 2011. Seed germination and seedling growth of Virginia buttonweed- *Diodia virginiana* L. (Rubiaceae). LRJ 74, 479-482. *In Japanese*.
- [4] Japan Meteorological Agency, Ministry of Land, Infrastructure and Transport, 2017. Website of the AMEDAS <<http://www.jma.go.jp/jp/amedas/>>. *In Japanese*.
- [5] Kelly S.T. and Coast G.E., 2000. Postemergence herbicide options for Virginia buttonweed (*Diodia virginiana*) control. Weed Technology 14, 246-251.
- [6] Kochi Y., Matsumoto A., Mutsunobu K., Makino A., Yamada M. and Suzuki M., 2007. Application of *Diodia virginiana* L. as the revegetation plant on dam slope. J. Jpn. Soc. Reveget. Tech. 33, 171-174. *In Japanese*.
- [7] Kondo K., Uchida T., Hayasaka D., Tanaka J., Sato A. and Arase T., 2016. Vegetation succession on cut slopes covered with exotic grasses for erosion control, Mt. Sakurajima. Int. J. of GEOMATE 11, 2136-2142.
- [8] Konno R., 2003. Revegetation of reservoir slope of dam for environmental conservation, using *Diodia virginiana*. Mizutotuti 132, 29-35. *In Japanese*.
- [9] Kyushu Regional Development Bureau, Ministry of Land, Infrastructure and Transport, 2017. Website of the Dam Joint Control Office of Chikugo-gawa River <[http://www.qsr.mlit.go.jp/toukan/g\\_shokai/matsubara.html](http://www.qsr.mlit.go.jp/toukan/g_shokai/matsubara.html)>. *In Japanese*.
- [10] Matsumura M. and Fukuda K., 1996. Conservation of dam reservoir slope by Virginia buttonweed. Engineering for Dams 124, 42-50. *In Japanese*.
- [11] Miyake K. and Onishi A., 2005. Study on lake front planting within water level change area of dam reservoirs. Bull. of Water Resources Environment Technology Center, 50-56. *In Japanese*.
- [12] Ni H., Wehtje G., Walker R.H., Belcher J.L. and Blythe E.K., 2006. Turf tolerance and Virginia buttonweed (*Diodia virginiana*) control with fluroxypyr as influenced by the synergist diflufenzopyr. Weed Technology 20, 511-519.
- [13] Reed T.V., Yu J. and McCullough P.E., 2013. Aminocyclopyrachlor efficacy for controlling Virginia buttonweed (*Diodia virginiana*) and smooth crabgrass (*Digitaria ischaemum*) in tall fescue. Weed Technology 27, 488-491.
- [14] River Bureau, Ministry of Land, Infrastructure and Transport, 2006. Draft for revegetation of reservoir slope of dam. 96 pp. *In Japanese*.
- [15] Uchida T., Tanaka J., Kondo K., Hayasaka D., Tomoguchi Y., Arase T. and Okano T., 2017. Evaluating the dynamics of alien species (Poaceae) used for erosion control on Sakurajima volcano. Int. J. of GEOMATE 12, 114-120.
- [16] Yamamoto T., Makino A. and Yamamoto K., 1999. Bio-engineering technique with Virginia buttonweed on dam reservoir slope ( I ). Abstract of 30th Conference of Jpn. Soc. Reveget. Tech., 234-237. *In Japanese*.

# NANOCOMPOSITE WITH DUAL FUNCTIONALITY IN SIMULTANEOUS REMOVAL OF HEAVY METALS, DYE AND ANIONIC SURFACTANT FROM MULTICOMPONENT WASTEWATER

Maria Visa<sup>1</sup>, Nicoleta Popa<sup>1</sup>, Andreea Maria Chelaru<sup>1</sup>

<sup>1</sup> Transilvania University of Brasov, R&D Center: Renewable Energy Systems and Recycling Romania

## ABSTRACT

By means of the hydrothermal method, a new material was obtained from fly ash (FA) and tungsten oxide ( $WO_3$ ) with dual adsorbent and photocatalyst properties, which proved to be effective in removing the pollutants from wastewater. The characterization of the material by means of atomic force microscopy (AFM) analysis showed that the surface is rougher than that of raw FA and of  $WO_3$ . The energy dispersive X-ray detector (EDX) and X-ray diffraction (XRD) indicated the existence of nano- $WO_3$  on the FA surface. FT-IR spectroscopy measurements further illustrated that the alkali hydrothermal method causes not only the generation and anchorage of nano- $WO_3$  on ash surface but also the exposure of more hydroxyl groups on the ash surface; both proved able to adsorb heavy metals, dye and surfactant via the synergistic effect. Both activities of nanocomposite  $WO_3$ -FA were evaluated in the process of removing of  $Cu^{2+}$ ,  $Cd^{2+}$ , Methylene blue (MB) and of Sodium Dodecylbenzenesulfonate (SDBS) from mixture solutions. The adsorption capacity was improved up to 30.21mg/g cadmium cations and 90.09mg/g of copper cations in the removal process of the cations from complex pollutant systems.

*Keywords:  $WO_3$ , photocatalysis/adsorption, wastewater treatment*

## INTRODUCTION

Many branches of industry, especially the textile industry, generate great amounts of wastewater loaded with heavy metals, dyes, surfactants, which are all refractory and non-degradable. About 1-258 of the total world production of dyes is lost during the dyeing process and is released in the textile effluents [1]. Many physico-chemical methods have been developed for removing dyes, heavy metals and surfactants, for example: adsorption [2], coagulation [3], chemical precipitation, ion-exchange, reverse osmosis and nanofiltration membranes [4]. Adsorption technologies have many advantages: inexpensive equipments, easy operation, efficiency and the possibility of regenerating the adsorbents for the next cycle. Suitable adsorbents for dyes and/or heavy metal removal were reported to be modified FA, natural zeolite, clay, bentonite [5], [6], [7], [8], resins such as Dowex 11[9] or synthetic adsorbents represents a possible alternative for the simultaneous removal of the pollutants from wastewater. The advanced oxidation processes (AOPs), based on the generation of reactive species ( $\bullet OH$  radicals), are recommended for the degradation of organic pollutants [10], [11].  $WO_3$  is the semiconductor photocatalyst with a band gap of 2.8eV which can be activated by visible light but only with low photonic efficiency.

This paper reports the synthesis, characterization, adsorption and photocatalytic activity of the composite  $WO_3$ -FA, obtained by the alkaline fusing followed by hydrothermal treatment.

The enhanced photocatalytic activity of the nanocomposite was evaluated using synthetic pollutant systems loaded with  $Cd^{2+}$ ,  $Cu^{2+}$  cations, (MB) and anionic surfactant (SDBS) under UV and VIS light irradiation ( $h\nu > E_g$ ), as a new method for wastewater treatment.

## EXPERIMENTAL

### Materials and the Substrate's Preparation

Raw FA was collected from CET power plant in Brasov, Romania. This FA is type F, according to the ASTM standard C-618-2a [12].

The total percentage of major oxides ( $SiO_2$ ,  $Al_2O_3$ ,  $Fe_2O_3$ ) exceeds 70% and this type of FA will not aggregate during long contact with water, being suitable as substrate in adsorption of organic and inorganic pollutants [13].  $Ti_2O_3$  (1.07%),  $Fe_2O_3$  (8.97%) and  $MnO_2$  (0.08%) are important as possible participants in the photodegradation of dyes and surfactants. The composite substrate of FA and  $WO_3$  was obtained using FA, NaOH pellets and  $WO_3$  (99.8% purity) from Across Organics by alkali fusion at 500°C for 1h. The composite cooled with bi-distilled water was transferred in an autoclave

and stirred (300 rot/min) at atmospheric pressure and 100°C for 48h. Afterwards, the solid phase was further washed with ultrapure water until constant pH, followed by filtration and drying at 105-115°C. The new composite is noted FUS-WO<sub>3</sub>. Due to the synergistic effect of functional groups (-OH), ( $\equiv$ SiO<sup>-</sup>), ( $\equiv$ AlO<sup>-</sup>), ( $\equiv$ SiONa), this composite will exhibit good adsorption and photocatalytic ability in the wastewater treatment process.

### Adsorption and Photocatalytic Experiments

The pollutant systems were synthetically prepared using ultrapure water with resistivity of 18.23 MΩ cm<sup>-1</sup>, CuCl<sub>2</sub>·2H<sub>2</sub>O and CdCl<sub>2</sub>·2.5H<sub>2</sub>O (Scharlau Chemie S.A., c<983), MB (C<sub>16</sub>H<sub>18</sub>ClN<sub>3</sub>S) (Fluka AG, molecular weight (319.85g/mol) and anionic surfactant (SDBS) (C<sub>12</sub>H<sub>25</sub>C<sub>6</sub>H<sub>4</sub>SO<sub>3</sub>Na) with linear carbon chains having 983 purity (Sigma-Aldrich), with molecular weight (343.48g/mol). Experiments were done using solutions in the concentrations of c<sub>Cd</sub>=0..550mg/L, c<sub>Cu</sub>=0..300mg/L, c<sub>MB</sub>=0.03125mM and the initial concentration of SDBS=25mg/L being lower than the critical micelle concentrations (CMC<sub>SDBS</sub> =418mg/L), as evaluated based on conductivity measurements [14]. A series of experimental on adsorption and photocatalysis were done in solutions containing four pollutants:

- Adsorption under mechanical stirring denoted (A) with: Cd<sup>2+</sup>- Cu<sup>2+</sup>-MB-SDBS;
- Photocatalysis under UV irradiation, denoted (F-DV): Cd<sup>2+</sup>-Cu<sup>2+</sup>-MB-SDBS;
- Photocatalysis denoted with (F-VIS) under VIS irradiation: Cd<sup>2+</sup>- Cu<sup>2+</sup>-MB-SDB.

The kinetic adsorption parameters of cations, dye and surfactant were evaluated from batch experiments; in each experiment, the 0.1g FUS-WO<sub>3</sub> substrate was stirred at 20-23°C, with 50ml solution, at initial concentrations. For the kinetic studies, aliquots were taken at fixed moments (10, 15, 30, 45, 60, 90, 120, 150 and 180min.), when stirring was briefly interrupted and the supernatant was analyzed for evaluate the momentary concentration of pollutants. The concentrations of the metal in the aqueous solution were analyzed by AAS (analytic jena, zeenit700), at λ<sub>Cd</sub>=228.8nm, λ<sub>Cu</sub>=324.75nm, while MB and SDBS were analyzed by UV-VIS spectrometry on the calibration curve registered at the maximum absorption peaks of MB(λ=664nm), and of SDBS (λ=224 nm), respectively.

## RESULTS AND DISCUSSIONS

### Crystalline Structure of the Substrate

The novel WO<sub>3</sub>/SiO<sub>2</sub>Al<sub>2</sub>O<sub>3</sub> (aluminosilicates) heterojunction was obtained from fine FA and WO<sub>3</sub> via alkaline fusion followed by hydrothermal process. The X-ray diffraction was used in order to

investigate the crystal structures and phase composition of the composites, Fig.1.

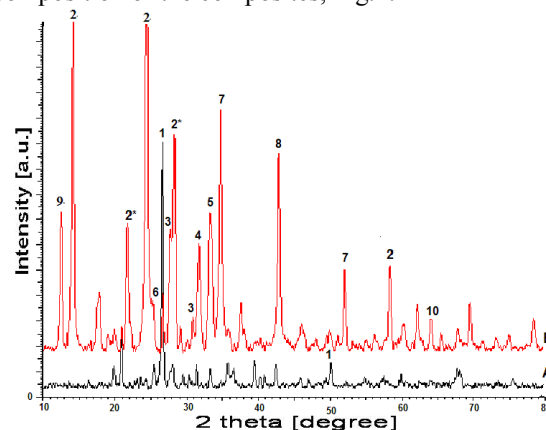


Fig.1.X-ray diffractograms of (A) FA; (B) FUS-WO<sub>3</sub>

In the FUS-WO<sub>3</sub>, the WO<sub>3</sub>(2) content is estimated at 52.58%, the alkaline tungsten oxides content at 8.54% and 38.88% aluminosilicates with adsorbent properties, mordenite (NaAlSi<sub>3</sub>O<sub>8</sub>·H<sub>2</sub>O) (6), faujasite-Na, (Na<sub>14</sub>Al<sub>12</sub>Si<sub>13</sub>O<sub>51</sub>·6H<sub>2</sub>O) (8), cancrinite syn(7), Na<sub>8</sub>(Al<sub>6</sub>Si<sub>6</sub>O<sub>24</sub>(OH)<sub>2,04</sub>(H<sub>2</sub>O)<sub>2,66</sub>, phillipsite (KNa)<sub>2</sub>(SiAl)<sub>8</sub>O<sub>16</sub>·4H<sub>2</sub>O (9) and albite Na(AlSi<sub>3</sub>O<sub>8</sub>). On the FUS-WO<sub>3</sub> diffractogram, the shape of the peaks (2, 2', 8) appears as overlapping, meaning that this substrate contains semiconductor oxides homogenously dispersed within the composite, which indicates the existence of a high number of contact aluminosilicates-WO<sub>3</sub>, Fig.1. The XRD data show that the new composite (FUS-WO<sub>3</sub>) has well embedded the WO<sub>3</sub> phases with crystallite size 132.3-184.4Å. The crystalline modifications are accompanied by a significant increase in the BET surface, from 6.14m<sup>2</sup>/g in FA to 39.753m<sup>2</sup>/g for FUS-WO<sub>3</sub>. Beside the diffraction lines corresponding to WO<sub>3</sub> triclinic, hexagonal and orthogonal, there appear other lines with high peaks, which were identified in crystalline structures of FUS-WO<sub>3</sub> proving the chemical restructuration of the FA together with WO<sub>3</sub> during the hydrothermal treatment. The formation of new compounds, such as, silicon tungsten (3), aluminum tungsten oxide silicate (5), sodium tungsten oxide (2'), potassium tungsten oxide (4), is the consequence of the dissolution/recrystallization processes followed by the partial transformation of the main components of the FA in alkaline media. The incorporation of WO<sub>3</sub> in the modified FA structure, along with the polymorphous transformation from monoclinic WO<sub>3</sub> to triclinic is also evidenced in the XRD pattern. The sharp peak at 2θ =27.203° corresponds to the formation of crystalline (Na<sub>6</sub>W<sub>4</sub>O<sub>6</sub>) and at 2θ=31.66° it corresponds to the (KW<sub>3</sub>O<sub>9</sub>), the specific tungsten oxide in strong alkaline media. All these processes lead to an increase of the overall crystallinity to 58.8% for the new synthesized composite.

### Surface Morphology of the Substrate

Information on the new substrate morphology/topography, respectively surface characteristics were obtained from the SEM micrographs and AFM. The highest roughness value (112.24nm) corresponds to the composite (FUS-WO<sub>3</sub>) which has more aggregates with different, almost round and stable shapes. The FA has a rough surface = 91nm with large pores, 12.33nm in diameter, while for WO<sub>3</sub> the diameter of the pores are 27.76nm, respectively. The adsorption efficiency depends not only on the pores' diameter, but also on the surface charge and the affinity of the pollutants molecules for the substrate.

The contact angles with water were very low (15-20), good surface wettability. With glycerol liquid the polar component was  $\sigma^p = 45.04\text{mN/m}$  and the dispersive component was  $\sigma^D = 8.69\text{mN/m}$ . The surface energy is 53.73mN/m such as the FUS-WO<sub>3</sub> composite has a predominant polar component, which indicates the hydrophilic character and wettability, thus making them a suitable composite with dual application (adsorbent and photocatalyst) in the process of simultaneous removal of pollutants from wastewater. The grains' dimension is affected, varying from the large domain for FA (27.6...100  $\mu\text{m}$ ) to narrower grains/agglomerates of 8...60  $\mu\text{m}$  diameter, for the FUS-WO<sub>3</sub>, as shown in Fig. 2.

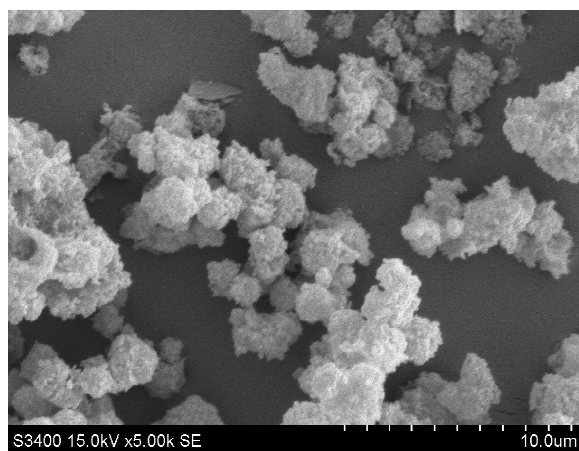


Fig.2. SEM images of the FUS-WO<sub>3</sub>

The SEM image of FUS-WO<sub>3</sub> shows a high degree of homogeneity. The elemental EDX analysis of the FUS-WO<sub>3</sub> shows a high intensity signal for the atoms: Si(14.51%), O(59.95%), W(1.09%), Al(10.13%) before adsorption and confirms the Cd(2.46%), S(3.59%), Cl(5.35%) percents on the surface scanned after the adsorption processes.

#### 3.2.1. FT-IR spectra analysis of the substrate

The FT-IR spectra of FUS-WO<sub>3</sub> before and after adsorption of cations were conducted to investigate the vibration frequency changes of the functional

groups in the adsorbent, which represent the number of adsorption bonds that identify the type of chemical bonds (functional groups), indicating the complex nature of the adsorbent as shown in Fig.3.

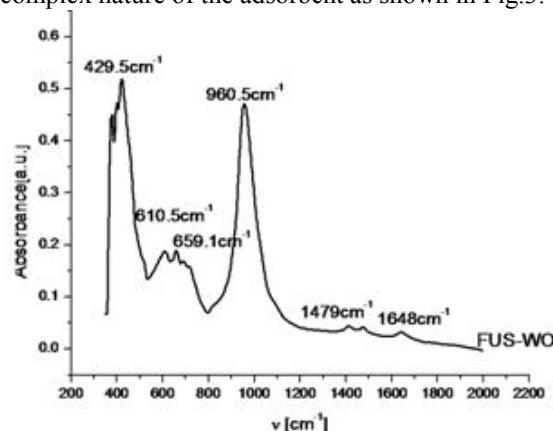


Fig. 3. IR spectrum FUS-WO<sub>3</sub> and FA-CET

The FT-IR spectra provided further insight into the structure of the composite synthesized by the hydrothermal method at 100°C. The peak located at 1648cm<sup>-1</sup> is indexed at O-H, bonding the water molecules associated with ions or molecules. This peak exists only at FUS-WO<sub>3</sub> after treating the FA-CET. The FT-IR spectrum shows a sharp peak at 909R cm<sup>-1</sup>, which is attributed to the symmetric stretching mode of terminal WW=O from all types of tungsten trioxide hydrates. The broad band around 610-657 cm<sup>-1</sup> is characteristic of the stretching of O - W-O modes [10]. The sharp absorption bands recorded at 429R 04 cm<sup>-1</sup> in the FUS-WO<sub>3</sub> spectrum and at 440 cm<sup>-1</sup> in the FA-CEET spectrum may result from their superposition with the symmetric stretch of Al-O and Si-O bonds, also represented in the zeolite structures [11].

### ADSORPTION AND PHOTOCATALYSIS

(a) Adsorption. The poor adsorption capacity of the raw FA and the negative efficiency for cadmium removal on WO<sub>3</sub> can be explained by the formation of new species of meta-wolframates, correlated with low surface area and, respectively, with low surface charge [16]. Heavy metals at low concentrations (as in the wastewaters from the textiles industry) can also be efficiently removed by adsorption; however, the efficiency of adsorption processes decreases when applied to wastewaters with a complex pollutants load (heavy metals, dyes and surfactants), as concurrent reactions may occur, thus decreasing the overall removal efficiency of the pollutants. Therefore, the employment of more processes may represent a feasible path, each process being highly efficient for one pollutant type [17].

The adsorption is implemented in systems with four pollutants: Cd<sup>2+</sup>+Cu<sup>2+</sup>+MB+SDBS/FUS-WO<sub>3</sub>,

the results being presented in Fig.4. The adsorption efficiency was evaluated based on the initial and equilibrium concentrations  $c_{M/D/S}^i$ ,  $c_{M/D/S}^e$  of the metal (M), dye (D) or surfactant (S), Eq. (1):

$$\eta = \frac{(c_{M/D/S}^i - c_{M/D/S}^e) \times 100}{c_{M/D/S}^i} \quad (1)$$

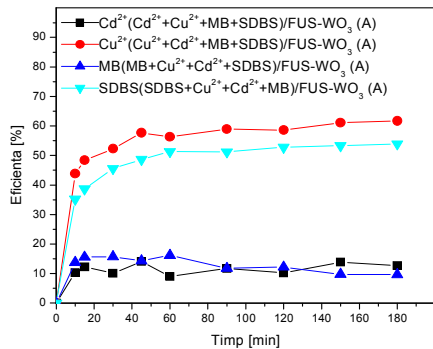
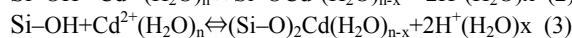


Fig.4. Adsorption efficiency vs. time for system  $\text{Cd}^{2+} + \text{Cu}^{2+} + \text{MB} + \text{SDBS}$

The optimal adsorption time can be estimated as 90min. when the adsorption equilibrium starts to settle for system and was set at this value in all further experiments. The adsorption efficiency of  $\text{Cd}^{2+}$  ions (11.73%) and of the MB molecules (11.79%) is very close, see Fig.4; the adsorption of  $\text{Cu}^{2+}$  ions (58.63%) and of SDBS molecules (51.22%) increases, in the same way, Fig. 4. This approach can be explained by interactions between heavy metal cations and ionic groups of organic molecules (MB and SDBS).

In systems containing two or more pollutants and the substrate, several adsorption processes occur:

a) The  $\text{Cd}^{2+}$  and  $\text{Cu}^{2+}$  cations can be absorbed by the silanol group ( $\text{Si}-\text{OH}$ ) of the layer, but with lower efficiency (eqs.2, 3):



b) The adsorption of heavy metals onto NaP1 zeolite has a cation exchange capacity over 2.7meq/g. Three different stages are observed in the ion + exchange adsorption of the heavy metals: fast adsorption on the zeolite microcrystal surfaces during the first 30 min; then the inversion stage has a short+time prevalence of the desorption process, connected with the diffusion flow from the zeolite microcrystal's [18], [19]. The amount of FUS+WO<sub>3</sub> in adsorption was optimised, considering the pollutants mixture ( $\text{Cd}^{2+}$ ,  $\text{Cu}^{2+}$ , MB, SDBS). Based on the experimental results, the optimal amount is 0.4g FUS+WO<sub>3</sub> in 50mL solution, Fig.5. By increasing the amount of substrate, the surface area as well as the number of the pores and of the cations+surface interactions will increase. The adsorption efficiency of the  $\text{Cu}^{2+}$  cations is higher than that of the  $\text{Cd}^{2+}$  cations.

Overall efficiency has increased, since the number of active centers, the number of pores able to host ions and molecules of pollutants has increased.

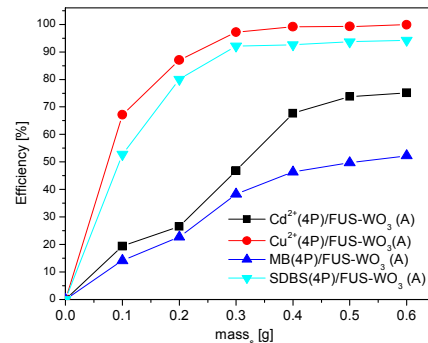
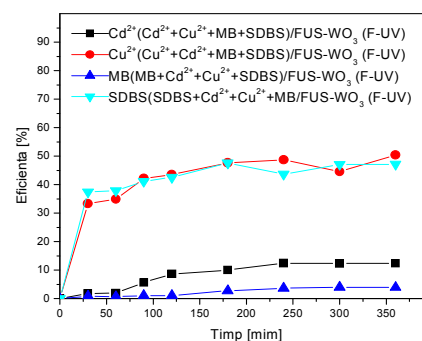


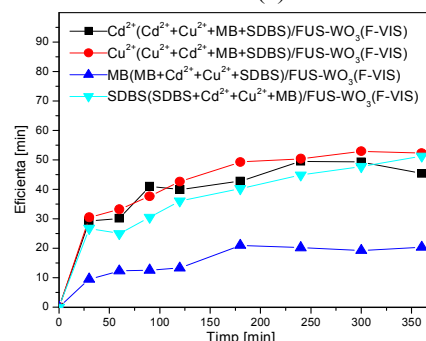
Fig.5. Adsorption efficiency vs. mass of substrate.

The reason may be the higher mobility to pores and the lower volume of the hydrated complexes of the cations in aqueous solution (hexacomplexes for Cd and tetra-coordination for Cu), as well as other processes at working pH=8.22.

(b) Photocatalysis. The active species generated by photo-irradiation will attack the organic pollutants, provided they are in the very close vicinity of the substrate. The most active photocatalytic components of the composite are WO<sub>3</sub> triclinic and silicon tungsten ( $\text{Si}_{0.043}\text{WO}_{2.839}$ ) with band gaps of 2.8 eV, active under both UV and VIS radiation. The influence of contact time in UV and VIS decomposition is presented in Fig.6 (a) and (b).



(a)



(b)

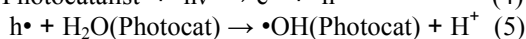
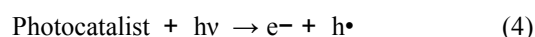
Fig.6. Photocatalysis efficiency vs. time: (a) (F-UV and (b) F-VIS for system

Under VIS irradiation the efficiency after 6h is

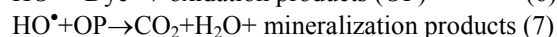
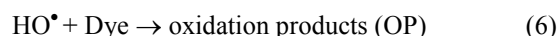


higher than in experiments, where the irradiation source is UV light, as in Fig. 6(b) ( $\text{Cd}^{2+}$  = 45.4%;  $\text{Cu}^{2+}$  = 52.33%; MB = 20.39% and SDBS = 51.29%). By coupling two or more semiconductors with suitable electronic band ( $\text{SiO}_2$ ,  $\text{TiO}_2$ ,  $\text{WO}_3$ , the photocatalytic activity under UV or VIS irradiation can be improved. The composite FUS- $\text{WO}_3$  with  $E_g$  = 4.41 eV is more active in visible light and it can involve other compounds from the substrate at working pH. This path is also valuable, with a view to upscaling as, by coupling UV-active with VIS active semiconductors; the costs of the process can be reduced.

Once formed the electron-hole pair was formed, the most common mechanisms involves the holes for hydroxyl radical production. In alkaline media several other reactions are possible [20], [21] involving the  $\text{O}_2/\text{HO}^\bullet$ ,  $\text{O}_2/\text{HOO}^\bullet$ .



These are powerful oxidizing species, able to degrade the dye and surfactant molecules (adsorbed on the catalyst or in solution, near the photocatalyst surface) to smaller fragments less colored, Eqs. (6,7), probably with similar dimensions/charges which can be further by adsorbed onto the active sites of substrate or can be further degraded up to mineralization [22].



## ADSORPTION KINETICS MODELING

### Adsorption Kinetics Models Analysis

The amount of pollutants adsorbed,  $q_t$  [mg/g] at time  $t$  was calculated from the following Eq. (8).

$$q_t = \frac{(c_{M/D/S}^i - c_{M/D/S}^e) \times V_{sol.}}{m_s} \quad (8)$$

The kinetics models are fitted to experimental data by nonlinear regression analysis. To determine the uptake kinetic mechanisms of pollutants ( $\text{Cd}^{2+}$ ,  $\text{Cu}^{2+}$ , MB, SDBS) from systems three kinetic models were investigated: pseudo-first order (Lagergren equation), pseudo-second order and intraparticle diffusion. The pseudo-second order kinetic (Eq.9) is the model which best describes the adsorption of the pollutants on the composite FUS- $\text{WO}_3$ .

$$\frac{t}{q_t} = \frac{1}{k_2 q_e^2} + \frac{t}{q_e} \quad (9)$$

Where:

$k_2$ - the equilibrium rate constant for the pseudo-second order adsorption ( $\text{g} \cdot \text{mg}^{-1} \cdot \text{min}^{-1}$ ),  $q_e$ - the adsorption capacity ( $\text{mg} \cdot \text{g}^{-1}$ ).

Table 1 Kinetic parameters of the processes

Pollutant process	Pseudo-second order		
	$k_2$ [ $\text{g} \cdot \text{mg}^{-1} \cdot \text{min}^{-1}$ ]	$q_e$ [mg/g]	$R^2$
$\text{Cd}^{2+}/\text{Ads.}$	0.183	30.21	0.961
$\text{Cu}^{2+}/\text{Ads.}$	0.06	90.09	0.999
MB/Ads.	5.384	0.134	0.992
SDBS/Ads	5.619	0.845	0.999
$\text{Cd}^{2+}/\text{F-UV}$	3.127	43.67	0.957
$\text{Cu}^{2+}/\text{F-UV}$	1.204	70.92	0.981
MB/ F-UV	1354.20	0.007	0.922
SDBS/F-UV	10.987	0.786	0.994

For the photocatalysis process, the Langmuir-Hinshelwood mechanism simplified for low concentration as a pseudo first order kinetics was tested, Eq. (10):

$$\ln c/c_0 = -kt \quad (10)$$

The kinetic parameters and the correlation coefficients calculated from the linear form of the kinetic laws are presented in Table 1 and kinetic plots are given in Fig.7.

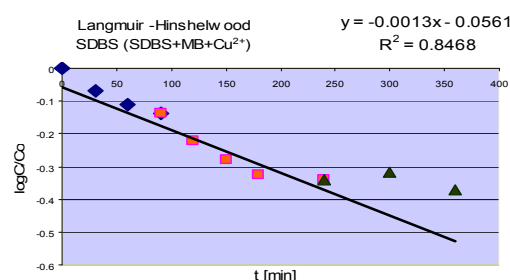


Fig.7. Langmuir – Hinshelwood

Parallel kinetic mechanisms may occur, especially inter-particle scattering, due to bulky cation adsorption in the pores of the substrate. As in previous cases, the maximum adsorption capacity values are associated with the species of cations, while the organic components associated with MB and SDBS are characterized by low values of maximum adsorption capacity.

## CONCLUSIONS

This paper investigates the removal of MB, SDBS,  $\text{Cu}^{2+}$ ,  $\text{Cd}^{2+}$  cations from synthetic solutions loaded with four pollutants by adsorption and photocatalysis, using FUS- $\text{WO}_3$  nanocomposites with dual activity.

The tungsten oxide imbedded on fly ash surface by the alkaline fusing and hydrothermal process, developed the new composite to be more effective in simultaneous processes of adsorption and of photocatalysis.



The results show that the adsorption efficiency significantly depends on the surface properties, while the process kinetics is mainly influenced by the type of cations and by the molecular structure of the surfactant and of MB.

Considering the adsorption processes, the data indicate that a large volume of MB allows the rapid adsorption of the cations, leading to higher rate constants, as compared to cadmium.

The pseudo-second order kinetic is the model that governs the entire process of removing pollutants from complex systems, while the parallel mechanisms of pseudo-first-order kinetics and inter-particle diffusion affect the complex processes of simultaneous adsorption and photocatalysis to a negligible extent.

The presence of more pollutants in aqueous solutions may adversely affect the adsorption process of other pollutants:  $q_e$  of the cadmium removal from systems with four pollutants is 30.21mg/g, in the case of copper cations removal is 90.09mg/g.

The reason may be the higher mobility and lower volume of the hydrated complexes of the cations in aqueous solutions (hexa-complexes for Cd and tetra-coordination for Cu).

The photocatalytic experiments proved various paths for the removal of SDBS and MB: independent adsorption and photocatalysis.

## REFERENCES

- [1] Konstantinou I. K, Albanis T. A, J. Appl. Catal. B- Environ, Vol.49, Nov. 2004, pp. 1-14.
- [2] Visa M, Duta A., Environ Eng Manag J. Vol. 7, Jul 2008, pp. 373-37A.
- [3] Patel H, Vashi R.T, J. of Chemistry, Vol. 7, Feb. 2010, pp. 1468-1476.
- [4] Bowen R.W, Welfoot J.S, J. of Chem. Eng. Sci, Vol. 07, 2002, pp.1393-1407.
- [5] Visa M, Bogatu C, Duta A, J. Appl. Surf. Sci, Vol. 206, Jun. 2010, pp. 0486-5471.
- [6] Wang S, Boyjoo Y, Choueib A, Zhu Z.H, J. Water Res, Vol. 39, Jan. 2000, pp. 129-138.
- [7] Perić J, Trgo M, Medvidović N.V, J of Water Res, Vol. 38, Apr. 2004, pp. 1893-1899.
- [8] Jiang M.Q, Jin X.Y, Lu X.Q, Chen Z.L, J. Desalination, Vol. 202, Nov. 2010, pp. 33-39.
- [9] Munesh, Swati, Sindal R.S., Meena R.C. J.of Basic and Appl,Chem. Sci., Vol. 2. March 2012, pp. 23-30
- [10] Wols B. A, Hofman-Caris C.H.M, J. Water Res, Vol. 46. Mar.2012, pp. 2810-2A27.
- [11] Visa M, Andronic L, Duta A, Environ Eng Manag J. Vol.8, Jul.2009, pp. 633-63A.
- [12] Ramme B. W, Tharaniyil M. P, Coal Combustion Products Utilization Handbook, 2<sup>nd</sup> Ed., of America. 2000.
- [13] Duta A, Visa M, J. of Photochem. Photobiol, Vol. 306, Jun. 2010, pp. 21-30.
- [14] Visa M, Duta A, J. Chem. Eng, Vol. 223, May. 2013, pp. 860-A6A.
- [15] Yaakob Z, Pudukudy M, Rajendran R, J. Der Pharma Chemica, Vol.0, 2013, pp. 208-2012.
- [16] Visa M, Duta A, J.of Optoelectronics and Advans. Mater., Vol. 12, Feb. 2010, pp. 406-410.
- [17] Visa M, Pricop F, Duta A, J. Clean Techn. Environ. Policy, Vol. 13, Dec. 2011, pp. 800- 861.
- [18] Sprynskyy M, Buszewski B, Terzyk A.P, Namiesnik J, J. Colloid Interf. Sci., Vol. 304, Dec. 2006, pp.21-2A.
- [19] Visa M, J. Powder Technology, Vol. 294, Jun. 2016, pp. 338-347.
- [20] Coronado J. M, Fresno F, Hernandez -Alonso M.D, Portela R, Springer, ISSN 1860-3537 (electronic) 2013, pp.12- 13.
- [21] Hsu L.J, Lee L.T, Lin, C.C, Chem. Eng. J. Vol. 173, Apr. 2011, pp. 698-705.
- [22] Ho Y. S, Mc Kay G., J. Chem. Eng. Vol. 76 1998, pp. 822.

## EFFECT OF WATER ACTIVITY ON ENZYMES ADSORBED ON BIOMASS CHARCOAL IN ORGANIC MEDIA

Hidetaka Noritomi<sup>1</sup>, Jumpei Nishigami<sup>2</sup>, Nobuyuki Endo<sup>3</sup>, Satoru Kato<sup>4</sup> and Katsumi Uchiyama<sup>5</sup>

<sup>1</sup>Department of Applied Chemistry, Tokyo Metropolitan University, Japan; <sup>2</sup>EEN Co., Ltd., Japan

### ABSTRACT

We have found that the organic solvent-resistance of  $\alpha$ -chymotrypsin ( $\alpha$ -CT) is enhanced by adsorbing  $\alpha$ -CT onto bamboo charcoal powder (BCP), which is obtained by pyrolyzing bamboo waste under nitrogen atmosphere, and is markedly dependent on the thermodynamic water activity ( $a_w$ ) in organic solvents. When BCP-adsorbed  $\alpha$ -CT was immersed in acetonitrile at an appropriate water activity, it effectively enhanced the transesterification of *N*-acetyl-L-tyrosine ethyl ester (*N*-Ac-Tyr-OEt) with *n*-butanol (BuOH) to produce *N*-acetyl-L-tyrosine butyl ester (*N*-Ac-Tyr-OBu), compared to the hydrolysis of *N*-Ac-Tyr-OEt with water to give *N*-acetyl-L-tyrosine (*N*-Ac-Tyr-OH). When the water activity was 0.28, the initial rate of transesterification catalyzed by BCP-adsorbed  $\alpha$ -CT was about sixty times greater than that catalyzed by free  $\alpha$ -CT. Regarding the reaction selectivity which is defined as a ratio of the initial rate of transesterification to that of hydrolysis, BCP-adsorbed  $\alpha$ -CT was much superior to free  $\alpha$ -CT. The catalytic activity of BCP-adsorbed  $\alpha$ -CT was markedly dependent on the reaction temperature. Furthermore, concerning the thermal stability at 50 °C, the half-life of BCP-adsorbed  $\alpha$ -CT exhibited 3.8-fold, compared to that of free  $\alpha$ -CT.

**Keywords:** Biomass charcoal, Adsorption, Enzymatic activity, Thermal stability, Water Activity

### INTRODUCTION

The utilization of biomass wastes, which are carbon neutral, for energies and functional materials is one of the most important challenges to reduce greenhouse gas emissions [1], [2]. However, almost all forestry residues have hardly been used. Accordingly, the development in the high value-added application of forestry residues has been desired to provide the multiple effective utilization system of forestry residues.

On the other hand, environmentally benign processes such as biotransformation, biosensor, biofuel cell, and so on have recently been developed by using enzymes as a kind of proteins, since enzymes exhibit their outstanding biological activity under mild conditions [3]-[5]. However, enzymes are gradually denatured and inactivated under various physical and chemical stresses such as heat, organic solvents, and so on, although they are generally stable in a cell [6]. To enhance the stress resistance of enzymes, enzymes have been modified chemically and genetically [3], [7]. As a chemical modification, enzyme immobilization and stabilizers have been developed, and molecular engineering has been carried out as a genetic modification. Among these enzyme modifications, an enzyme immobilization system has widely been studied due to following advantages [3]: 1. Concentration of substrate can be increased. 2. Recycled enzymes can be used many times. 3. Separation of the products is straight forward. 4. Stability of the enzyme to change under stress is increased. Especially, the adsorption of

enzymes onto various carriers has been widely used from the laboratory scale to the industrial scale because of the simplest and most economical method of stabilizing enzymes [8], [9]. The physical and chemical surface properties of carriers strongly affect the performances of adsorbed enzymes such as the catalytic activity, the specificity, and the stability. Thus, it is probably that the stress resistance of enzymes is enhanced by selecting an appropriate carrier.

As a part of our ongoing research efforts aimed at utilizing forestry residues, we have so far examined the usefulness of biomass charcoal powder, which is prepared from forestry residues by pyrolysis, as a enzyme carrier. We have found that enzymes are effectively adsorbed onto biomass charcoal powder [10], [11], and biomass charcoal powder imparts high heat stress resistance to enzymes through the adsorption [12]-[15]. Furthermore, we have reported that the adsorption of enzymes onto biomass charcoal powder can sufficiently improve the organic solvent resistance of enzymes in hydrophilic organic solvents [16]. When solid enzymes are at moist air, the catalytic activity of enzymes strongly depends on the thermodynamic water activity ( $a_w$ ), which is the ratio of water partial pressure to vapor pressure of pure water [17]. Likewise, since adsorbed enzymes are solids in hydrophilic organic solvents containing low water content, it is probably that the catalytic activity of adsorbed enzymes is influenced by the water activity. However, there have been few reports regarding the relation between the water activity in

hydrophilic organic solvents and the performance of adsorbed enzymes.

In our present work, we have assessed how the water activity affects the organic solvent resistance of enzymes adsorbed onto biomass charcoal powder in hydrophilic organic solvents. We have used bovine pancreas  $\alpha$ -chymotrypsin ( $\alpha$ -CT) as a model protein since it is well investigated regarding its structure, functions, and properties [18].

## MATERIALS AND METHODS

### Materials

$\alpha$ -Chymotrypsin (EC 3.4.21.1 from bovine pancreas) (type II, 52 units/mg solid) ( $\alpha$ -CT) was purchased from Sigma-Aldrich Co. (St. Louis, USA). *N*-Acetyl-L-tyrosine ethyl ester (*N*-Ac-Tyr-OEt) and *N*-acetyl-L-tyrosine (*N*-Ac-Tyr-OH) were also from Sigma-Aldrich Co. (St. Louis, USA). Acetonitrile of guaranteed grade was obtained from Kanto Chemical Co. (Tokyo, Japan). Before acetonitrile was used as a reaction solvent, it was dried by storing it over dry 0.3 nm molecular sieves (Wako Chemical Co.) for at least 24 h.

### Preparation of Bamboo Charcoal Powder

To prepare bamboo charcoal, under nitrogen atmosphere, bamboo waste was dried at 180 °C for 2 hr, was pyrolyzed at 450 °C for 2 hr, was carbonized at 350 °C for 3 hr, and then was cooled at 100 °C for 1 hr by pyrolyzer (EE21 Pyrolyzer, EEN Co. Ltd., Japan). Bamboo charcoal powder (BCP) was obtained by grinding the resultant bamboo charcoal with jet mill (100AS, Fuji Sangyo Co. Ltd., Japan).

### Characterization of Bamboo Charcoal Powder

The SEM micrograph was obtained using a scanning electron microscope (JSM-7500FA, JEOL, Japan) operating at 15 kV. The sample for SEM was prepared on a carbon tape without vapor deposition.

All samples were outgassed at 300 °C for 8 h prior to the nitrogen adsorption measurements. The specific surface area of BCP was calculated with the use of the Brunauer-Emmett-Teller (BET) method using a micropore system (BELSORP-mini II, BEL JAPAN, INC.).

The surface of BCP was analyzed by X-ray photoelectron spectroscopy (XPS) (Quantum-2000, ULVAC-PHI Co. Ltd.) operating at an x-ray beam size of 100  $\mu$ m.

### Adsorption of $\alpha$ -Chymotrypsin onto Bamboo Charcoal Powder

As a typical procedure, 5 mL of 0.01 M

phosphate buffer solution at pH 7 containing 300  $\mu$ M  $\alpha$ -CT and 3 g/L BCP was placed in a 10-mL test tube with a screw cup, and was incubated at 25 °C and 120 rpm for 24 h. After adsorption, the mixture was filtrated with a membrane filter (pore size: 0.1  $\mu$ m, Millipore Co. Ltd.). The amount of  $\alpha$ -CT adsorbed onto BCP was calculated by subtracting the amount of  $\alpha$ -CT included in the supernatant liquid after adsorption from the amount of  $\alpha$ -CT in the aqueous solution before adsorption. The amount of  $\alpha$ -CT was measured at 280 nm by UV/vis spectrophotometer (UV-1800, Shimadzu Co. Ltd.).

### Measurement of Catalytic Activity of $\alpha$ -Chymotrypsin

The standard reaction for transesterification was carried out as follows: Three milliliter of acetonitrile containing a certain amount of water, 10 mM *N*-Ac-Tyr-OEt, 1000 mM *n*-butanol, 1 mM acetanilide, and free  $\alpha$ -CT or BCP-adsorbed  $\alpha$ -CT (30  $\mu$ M) was placed in a 4 mL screw-cap vial, and was incubated at 120 rpm and 25 °C. The amounts of the reaction components were periodically determined with HPLC (Shimadzu LC-10A) (Shimadzu Co., Kyoto, Japan) using a TSK-GEL ODS-80TM column (Tosoh Co., Tokyo, Japan) eluted with water-acetonitrile (6:4 by volume) at 0.5 mL/min with detection at 270 nm. Acetanilide was used as an internal standard.

### Measurement of Remaining Activity of $\alpha$ -Chymotrypsin

In order to assess the thermal stability of free  $\alpha$ -CT and BCP-adsorbed  $\alpha$ -CT, the activity of free  $\alpha$ -CT or BCP-adsorbed  $\alpha$ -CT was measured at the water activity of 0.15 after free  $\alpha$ -CT or adsorbed  $\alpha$ -CT was stored in acetonitrile at 50 °C for appropriate time, and then was cooled at 25 °C for 30 min. The remaining activity was obtained by Equation (1).

$$\text{Remaining activity (\%)} = \frac{\text{Activity after heat treatment}}{\text{Activity before heat treatment}} \times 100 \quad (1)$$

### Measurement of Fourier Transform Infrared (FTIR) Spectroscopy

FTIR measurements of free  $\alpha$ -CT and BCP-adsorbed  $\alpha$ -CT were carried out using a Jasco FT/IR spectrometer model FT/IR-4100. A KBr pellet containing 0.5 mg of free  $\alpha$ -CT or BCP-adsorbed  $\alpha$ -CT powder per 100 mg of KBr was prepared, and the measurements were performed using 512 scans under 4.0  $\text{cm}^{-1}$  resolution.

## RESULTS AND DISCUSSION

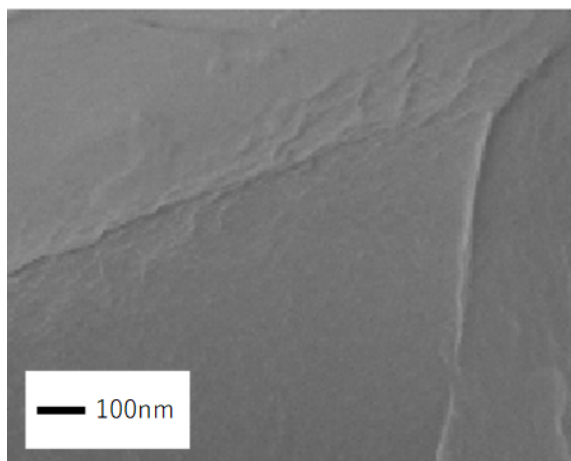


Fig. 1 SEM images of bamboo charcoal powder (BCP).

Table 1 Characteristics of BCP.

Textural property	Experimental value
Specific surface area ( $\text{m}^2/\text{g}$ )	294
Pore volume ( $\text{cm}^3/\text{g}$ )	0.041
Pore diameter peak (nm)	Less than 2.6

Table 2 Elemental ratio of BCP measured by X-ray photoelectron spectroscopy.

Element	Atomic percentage (%)
Carbon	80.7
Nitrogen	0.8
Oxygen	15.9
Other	2.6

### Characterization of Bamboo Charcoal Powder

We have pyrolyzed bamboo waste at low temperatures under nitrogen atmosphere to produce functional groups, which were used as a binding site for the adsorption of enzymes. The fine bamboo charcoal powder was obtained by grinding the resultant bamboo charcoal with jet mill. The mean diameter of BCP was  $7 \mu\text{m}$ .

Table 1 shows the characteristics of BCP. The surface area of BCP was one order of magnitude lower than that of activated carbon, which is used as an adsorbent, and was the pore volume of BCP was low as well. Moreover, the pore diameter peak was much smaller than the size of  $\alpha$ -CT since the size of  $\alpha$ -CT is  $5.1 \times 4.0 \times 4.0 \text{ nm}$  [18].

Figure 1 shows the scanning electron micrograph of BCP. The surface of BCP was almost smooth. It is probably that micropores were not observed under the magnification measured in the present work since the pore size was several nanometers or less.

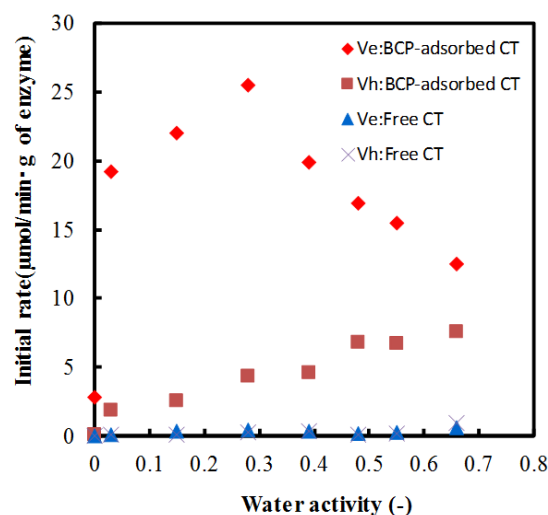


Fig. 2 Effect of water activity on the initial rate ( $V_e$ ) of transesterification and the initial rate ( $V_h$ ) of hydrolysis in acetonitrile. The enzyme was added into acetonitrile containing 10 mM *N*-Ac-Trp-OEt, 1000 mM *n*-butanol, and 1 mM acetanilide at an appropriate water activity, and the resulting mixture was shaken at 120 rpm and  $25^\circ\text{C}$ .

To estimate the chemical property of the surface of BCP, BCP has been measured by X-ray photoelectron spectroscopy (XPS). As shown in Table 2, carbon atom was the main element, oxygen atom was also located on the surface of BCP to some extent, and nitrogen atom was detected at a small ratio. Furthermore, by the measurement of narrow scan spectra of XPS, C-C, C-H, C-O, O-C-O, C=O, COOH, and C-N were detected as a chemical state of carbon.

BCP-adsorbed  $\alpha$ -CT was obtained by dispersing BCP in the buffer solution at pH 7 containing  $\alpha$ -CT, and the amount of  $\alpha$ -CT adsorbed onto BCP was  $9.8 \mu\text{mol}/\text{g}$ . The charge of  $\alpha$ -CT is positive in the buffer solution at pH 7 since the isoelectric point of  $\alpha$ -CT is 9.1 [18]. On the other hand, the  $\zeta$ -potential of BCP is negative at pH 7 in the buffer solution at pH 7 [10]. Accordingly, the electrostatic interaction between  $\alpha$ -CT molecules and BCP mainly contributes to the adsorption of  $\alpha$ -CT onto BCP.

### Dependence of Catalytic Activity of BCP-Adsorbed $\alpha$ -CT on Water Activity in Acetonitrile

An enzymatic reaction in hydrophilic solvents has the advantage of the solubility of a variety of substrates, including amino acid derivatives, which are poorly soluble in hydrophobic solvents [19]. However, when a hydrophilic solvent is used as a reaction medium, the enzyme molecule directly comes in contact with the solvent, and thereby its catalytic activity is strongly influenced by the nature of the solvent [20], [21]. Moreover, the catalytic

Table 3 Ratio of the absorbance at 1650  $\text{cm}^{-1}$  to the absorbance at 1630  $\text{cm}^{-1}$  ( $\text{ABS}_{1650}/\text{ABS}_{1630}$ ) of BCP-adsorbed  $\alpha$ -CT provided by the FTIR measurement.

Water activity (-)	$\text{ABS}_{1650}/\text{ABS}_{1630}$ (-)
0.03	1.3
0.28	1.3
0.55	1.3
0.73	1.3

activity of enzymes tends to be reduced since hydrophilic solvents tear water from enzymes. Water bound to enzymes is essential for enzymes to maintain their mobility for catalysis [22]. Accordingly, it is considered that the performance of enzymes is strongly influenced by the water activity in hydrophilic solvents. To assess the effect of water activity on the catalytic activity of BCP-adsorbed  $\alpha$ -CT in acetonitrile, we have examined the relationship of initial rates of transesterification and hydrolysis with the water activity in acetonitrile. The water activity was prepared by adding an appropriate amount of water to acetonitrile [23]. Figure 2 shows the plots of the initial rate ( $V_e$ ) of transesterification and the initial rate ( $V_h$ ) of hydrolysis against the water activity in acetonitrile at 25  $^{\circ}\text{C}$ . The inherent enzymatic hydrolysis of *N*-acetyl-L-tyrosine ethyl ester (*N*-Ac-Tyr-OEt) with water was inhibited by low water activity, while the enzymatic transesterification of *N*-acetyl-L-tyrosine ethyl ester (*N*-Ac-Tyr-OEt) with *n*-butanol (BuOH) was promoted. The initial rates of transesterification catalyzed by BCP-adsorbed  $\alpha$ -CT and free  $\alpha$ -CT were strongly dependent on the water activity, and displayed a bell-shaped curve. The initial rate of transesterification catalyzed by BCP-adsorbed  $\alpha$ -CT was about sixty times greater than that catalyzed by free  $\alpha$ -CT when the water activity was 0.28, at which the maximum initial rates of transesterification of free  $\alpha$ -CT and BCP-adsorbed  $\alpha$ -CT were obtained. On the other hand, the initial rates of hydrolysis catalyzed by free  $\alpha$ -CT and BCP-adsorbed  $\alpha$ -CT increased with an increase in the water activity. The relationship between the catalytic activity of enzymes and the water activity in organic solvents tends to exhibit bell-shaped curve. The optimal water activity results from the balance between the kinetic rigidity of enzyme structures and their thermodynamic stability [20], [23]. The kinetic rigidity decreases with increasing water activity, while the native enzyme structure gradually changes through thermodynamic stability. Accordingly, the catalytic activity of enzymes increases with an increase in the flexibility of rigid enzyme structures, and then decreases with an increase in the disturbance of enzyme structures. On the other hand, since the increase of water activity results in the increase of overall water concentration,

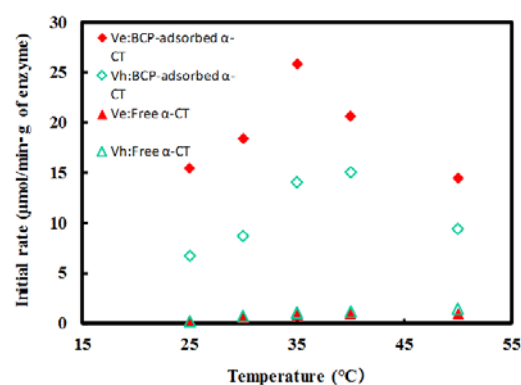


Fig. 3 Temperature-dependence of the initial rate ( $V_e$ ) of transesterification and the initial rate ( $V_h$ ) of hydrolysis in acetonitrile. The enzyme was added into acetonitrile containing 10 mM *N*-Ac-Trp-OEt, 1000 mM *n*-butanol, and 1 mM acetanilide, and the resulting mixture was shaken at 120 rpm and appropriate temperature.

the hydrolysis is enhanced by the increase of water activity. Regarding the reaction selectivity, which was the ratio of the initial rate ( $V_e$ ) of transesterification to the initial rate ( $V_h$ ) of hydrolysis, BCP-adsorbed  $\alpha$ -CT was much superior to free  $\alpha$ -CT.

Table 3 shows the ratio of the absorbance at 1650  $\text{cm}^{-1}$  to the absorbance at 1630  $\text{cm}^{-1}$  ( $\text{ABS}_{1650}/\text{ABS}_{1630}$ ) of BCP-adsorbed  $\alpha$ -CT. The bands at ca. 1650 and 1630  $\text{cm}^{-1}$  are assignable to  $\alpha$ -helix and intramolecular  $\beta$ -sheet, respectively [24]. The higher absorbance ratio, the higher secondary structure. Since the absorbance ratio ( $\text{ABS}_{1650}/\text{ABS}_{1630}$ ) of BCP-adsorbed  $\alpha$ -CT was independent on the water activity, the secondary structure of BCP-adsorbed  $\alpha$ -CT was not influenced by the water activity. Thus, the secondary structure of BCP-adsorbed  $\alpha$ -CT is firmly maintained through the adsorption. The absorbance ratio ( $\text{ABS}_{1650}/\text{ABS}_{1630}$ ) of BCP-adsorbed  $\alpha$ -CT is higher than that of free  $\alpha$ -CT [16]. The results indicate that the water activity effectively affects the catalytic activity of BCP-adsorbed  $\alpha$ -CT having a high second structure, compared to that of free  $\alpha$ -CT.

#### Temperature Dependence of Catalytic Activity of BCP-Adsorbed $\alpha$ -CT in Acetonitrile

Figure 3 shows the plots of initial rate ( $V_e$ ) of transesterification and the initial rate ( $V_h$ ) of hydrolysis in acetonitrile against reaction temperature when the water activity was 0.55 at 25  $^{\circ}\text{C}$ . The initial rate of transesterification catalyzed by BCP-adsorbed  $\alpha$ -CT exhibited a maximum around 35  $^{\circ}\text{C}$ , and then decreased with an increase in temperature, while that catalyzed by free  $\alpha$ -CT slightly increased with increasing temperature. The initial rate of transesterification catalyzed by BCP-adsorbed  $\alpha$ -CT

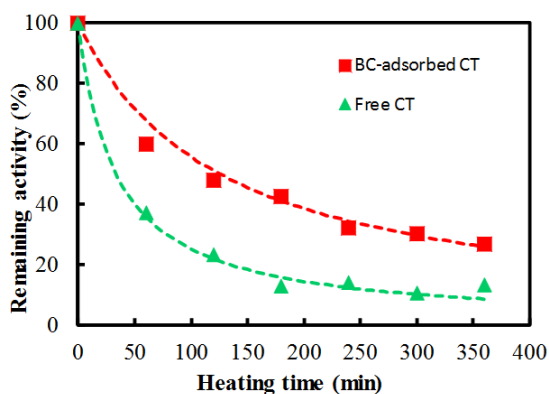


Fig. 4 Time course of remaining activities of free  $\alpha$ -CT and BCP-adsorbed  $\alpha$ -CT through the heat treatment at 50 °C. The activity of free  $\alpha$ -CT or BCP-adsorbed  $\alpha$ -CT was measured after free  $\alpha$ -CT or adsorbed  $\alpha$ -CT was stored in acetonitrile at 50 °C for appropriate time, and then was cooled at 25 °C for 30 min.

exhibited 30-fold, compared to that catalyzed by free  $\alpha$ -CT at 35 °C. On the other hand, the initial rate of hydrolysis catalyzed by BCP- adsorbed  $\alpha$ -CT showed a maximum around 40 °C, and then decreased with an increase in temperature, while that catalyzed by free  $\alpha$ -CT showed a slight increase with increasing temperature, as well as the case of transesterification. The initial rate of hydrolysis catalyzed by BCP-adsorbed  $\alpha$ -CT was thirteen times greater than that catalyzed by free  $\alpha$ -CT at 40 °C. Enzymatic reactions obey the Arrhenius correlation between the reaction rate constant and the reaction temperature as well as chemical reactions [25]. Thus, the initial rate becomes higher at higher temperatures. However, since the thermal denaturation of enzymes proceeds with increasing temperature due to the disruption of weak interactions in enzymes including ionic bonds, hydrogen bonds, and hydrophobic interactions, which are prime determinants of enzyme tertiary structures. On the other hand, the water activity is influenced by temperature [26]. Consequently, it is probably that the optimal temperature of the catalytic activity of BCP-adsorbed  $\alpha$ -CT was observed due to these factors. The result indicated that the catalytic activity of  $\alpha$ -CT is sufficiently enhanced by adsorbing  $\alpha$ -CT onto BCP since the initial rate of transesterification catalyzed by BCP- adsorbed  $\alpha$ -CT was about fifteen times greater than that catalyzed by free  $\alpha$ -CT even at 50 °C.

#### Thermal Stability of BCP-Adsorbed $\alpha$ -CT in Acetonitrile

Heating time directly enhances the denaturation of enzymes [25]. Figure 4 shows time course of remaining activities of free  $\alpha$ -CT and BCP- adsorbed  $\alpha$ -CT through the heat treatment at 50 °C when the water activity was 0.15 at 25 °C. Free  $\alpha$ -CT in acetonitrile, where  $\alpha$ -CT was dispersed as the solid

state, was unchanged during the heat treatment, although enzymes dissolved in an aqueous solution immediately form the aggregation of thermally-denatured enzymes [12]. Likewise, the enzyme aggregation and the cohesion among BCP- adsorbed  $\alpha$ -CT were not observed in acetonitrile during the heat treatment. However, the remaining activities of free  $\alpha$ -CT and BCP-adsorbed  $\alpha$ -CT gradually decreased with heat time. As seen in the figure, the relationship of the remaining activities of free  $\alpha$ -CT and BCP-adsorbed  $\alpha$ -CT with heat time could be correlated by first-order and second-order kinetics, respectively. The half-lives of inactivation of free  $\alpha$ -CT and BCP-adsorbed  $\alpha$ -CT calculated from the fitting curves in the figure were 33 and 125 min, respectively. Thus, the half-life of BCP- adsorbed  $\alpha$ -CT exhibited 3.8-fold, compared to that of  $\alpha$ -CT. On the other hand, we have reported that the half-lives of inactivation of BCP- adsorbed  $\alpha$ -CT is 15 min in an aqueous solution at 45 °C [14]. Thus, the thermal stability of BCP-adsorbed  $\alpha$ -CT in acetonitrile was much superior to that of BCP- adsorbed  $\alpha$ -CT in water. The result indicates that the adsorption is strengthened in acetonitrile by the electrostatic force, which mainly contributes to the adsorption of  $\alpha$ -CT onto BCP, and stabilizes  $\alpha$ -CT since the dielectric constant of acetonitrile is much lower than that of water [27].

#### CONCLUSION

We have demonstrated that the water activity affects the catalytic activity of  $\alpha$ -CT in acetonitrile. The catalytic activity of BCP-adsorbed  $\alpha$ -CT was more effectively enhanced by changing the water activity than that of free  $\alpha$ -CT. The catalytic activity of BCP-adsorbed  $\alpha$ -CT was strongly influenced by reaction temperature. The catalytic activity of BCP-adsorbed  $\alpha$ -CT exhibited the optimum temperature, and was much greater than that of free  $\alpha$ -CT. The thermal stability of  $\alpha$ -CT was markedly improved by adsorbing  $\alpha$ -CT onto BCP, and the half-life of BCP-adsorbed  $\alpha$ -CT exhibited 3.8-fold, compared to that of  $\alpha$ -CT.

#### REFERENCES

- [1] Ho YC, Show KY, "A perspective in renewable energy production from biomass pyrolysis-challenges and prospects", *Current Organic Chem.*, Vol. 19, 2015, pp. 423-436.
- [2] Straathof AJJ, "Transformation of biomass into commodity chemicals using enzymes or cells", *Chem. Rev.*, Vol. 114, 2014, pp. 1871-1908.
- [3] Buchholz K, Kasche V, Bornscheuer UT, *Biocatalyst and Enzyme Technology* 2<sup>nd</sup> ed. Wiley-Blackwell, 2012.
- [4] Silwana B, Horst CVD, Iwuoha E, "Aerometric determination of cadmium, lead, and mercury metal ions using a novel polymer immobilized



- horseradish peroxidase biosensor system", *J. Environmental Sci. Health Part A*, Vol. 49, 2014, pp.1501-1511.
- [5] Leech D, Kavanagh P, Schuhmann W, "Enzymatic fuel cells: Recent progress", *Electrochimica Acta*, Vol. 84, 2012, pp. 223-234.
- [6] Bailey JE, Ollis DF, *Biochemical Engineering Fundamentals* 2<sup>nd</sup> ed. McGraw-Hill, 1986.
- [7] Cioci F, Lavecchia R, "Thermostabilization of proteins by water-miscible additives", *Chem. Biochem. Eng. Q.*, Vol. 12, 1998, pp. 191-199.
- [8] Elnashar MMM, "Review article: Immobilized molecules using biomaterials and nanobiotechnology", *J. Biomaterials Nanobiotechnol.*, Vol. 1, 2010, pp. 61-77.
- [9] Mateo C, Palomo JM, Fernandez-Lorente G, Guisan JM, Fernandez-Lorente R, "Improvement of enzyme activity, stability and selectivity via immobilization techniques", *Enzyme Microbial Technol.*, Vol. 40, 2007, pp. 1451-1463.
- [10] Noritomi H, Iwai D, Kai R, Tanaka M, Kato S, "Adsorption of lysozyme on biomass charcoal powder prepared from plant biomass wastes", *J. Chem. Eng. Jpn.*, Vol. 46, 2013, pp. 196-200.
- [11] Noritomi H, Hishinuma K, Kurihara S, Nishigami J, Takemoto T, Endo N, Kato S, "Adsorption of  $\alpha$ -chymotrypsin on plant biomass charcoal", *J. Surface Eng. Materials Adv. Technol.*, Vol. 3, 2013, pp. 269-274.
- [12] Noritomi H, Kai R, Iwai D, Tanaka H, Kamila R, Tanaka M, Muneki K, Kato S, "Increase in thermal stability of proteins adsorbed on biomass charcoal powder prepared from plant biomass wastes", *J. Biomedical Sci. Eng.*, Vol. 4, 2011, pp. 692-698.
- [13] Noritomi H, Ishiyama R, Kai R, Iwai D, Tanaka M, Kato S, "Immobilization of lysozyme on biomass charcoal powder derived from plant biomass wastes", *J. Biomaterials Nanobiotechnol.*, Vol. 3, 2012, pp. 446-451.
- [14] Noritomi H, Kurihara S, Endo N, Kato S, "Heat-resistant properties of  $\alpha$ -chymotrypsin adsorbed onto biomass charcoal powder", *J. Biomaterials Nanobiotechnol.*, Vol. 5, 2014, pp. 179-185.
- [15] Noritomi H, Kurihara S, Endo N, Kato S, Uchiyama K, "Effect of adsorption condition on thermal stability of proteins adsorbed onto biomass charcoal powder", *International J. GEOMATE*, Vol. 11, 2016, pp. 2123-2128.
- [16] Noritomi H, Nishigami J, Endo N, Kato S, Uchiyama K, "Organic solvent-resistant properties of proteins adsorbed onto biomass charcoal powder", *International J. GEOMATE*, Vol. 12, 2017, pp. 140-145.
- [17] Acker L, "Enzyme reactions in foods of low moisture content", Vol. 11, 1962, pp. 263-330.
- [18] Kumar A, Venkatesu P, "Overview of the stability of  $\alpha$ -chymotrypsin in different solvent media", *Chemical Reviews*, Vol. 112, 2012, pp. 4283-4307.
- [19] Kise H, Hayakawa A, Noritomi H, "Protease-catalyzed synthetic reactions and immobilization-activation of the enzymes in hydrophilic organic solvents", *J. Biotechnol.*, Vol. 14, 1990, pp. 239-254.
- [20] Klibanov AM, "Improving enzymes by using them in organic solvents", *Nature*, Vol. 409, 2001, pp. 241-246.
- [21] Noritomi H, Sasanuma A, Kato S, Nagahama K, "Catalytic properties of cross-linked enzyme crystals in organic media", *Biochem. Eng. J.*, Vol. 33, 2007, pp. 228-231.
- [22] Klibanov AM, "Why are enzymes less active in organic solvents than in water?", *Trends Biotechnol.*, Vol. 15, 1997, pp. 97-101.
- [23] Bell G, Janssen AEM, Halling PJ, "Water activity fails to predict critical hydration level for enzyme activity in polar organic solvents: Interconversion of water concentrations and activities", *Enzyme Microb. Technol.*, Vol. 20, 1997, pp. 471-477.
- [24] Surewicz WK, Mantsch HH, "New insight into protein secondary structure from resolution-enhanced infrared spectra", *Biochim. Biophys. Acta*, Vol. 952, 1988, pp. 115-130.
- [25] Volkin DB, Klibanov AM, "Minimizing protein inactivation", *Protein Function: Practical Approach*, Creighton Ed. IRL Press, 1989, pp. 1-24.
- [26] Reid RC, Prausnitz JM, Poling BE, *The Properties of Gases and Liquids* 4<sup>th</sup> ed. McGraw-Hill, 1987.
- [27] Reichardt C, *Solvents and Solvent Effects in Organic Chemistry* 2<sup>nd</sup> ed. Wiley-VCH, 1988, p. 408.



## **EVALUATION OF ENERGY EFFICIENCY AND ENVIRONMENTAL PERFORMANCE IN LOBLAW COMPANIES LIMITED IN CANADA**

Koiwanit, J.<sup>1</sup>, Chan, V. K.<sup>2</sup>, Piewkhow, L.<sup>3</sup>, Katipelly, N. D.<sup>4</sup>

<sup>1</sup>Faculty of Engineering, King Mongkut's Institute of Technology Ladkrabang, Bangkok 10520, Thailand

<sup>2</sup>Faculty of Engineering and Applied Science, University of Regina, Canada

### **ABSTRACT**

There is growing pressure to limit Global Warming Potential (GWP) as it is the most significant way to reduce serious threats to people. The increase of average temperature in the atmosphere causes adverse effects on the environment, and this is changing the way business operates. Loblaw Companies Limited, the largest food distributors in Canada, has put more concerns on environmental impacts and worked diligently to reduce greenhouse gas (GHG) emissions through actions such as improving energy efficiency reducing refrigerant leaks, and incorporating renewable energy sources. This study analyzed Loblaw's energy efficiency and environmental performance and provided suggestions in the applications of skylight improvement, geothermal, refrigeration systems, kinetic energy to electricity, and e-grocery shopping. The results showed that the environmental concerns were substantially decreased. However, types of lights and refrigerators, distance driven, vehicle types, fuel used in e-grocery shopping results in the different amount of emissions; consequently, the GHG emissions varied depending on these factors. By integrating more environmentally technology, Loblaw could further reduce their emissions and waste and become a more sustainable company.

*Keywords: Environmental performance; Greenhouse gas emissions; Energy efficiency; TRACI; GaBi 6*

### **INTRODUCTION**

With a supermarket chain of over 2,000 stores operating under Loblaw and over 17 million Canadians shopping at the stores every week, Loblaw is the largest food distributor in Canada [1] [2]. For over 50 years, Loblaw has supplied the Canadian market with innovative products and services through corporate, franchised and associated stores. These supermarket chains include Loblaws®, Provigo® and Zehrs® [3]. With environmental concerns, Loblaw plays a major role in energy usage over other food distributors. They have answered with many innovations like the introduction of the reusable shopping bag, new "green" products and even installing a wind turbine to generate renewable energy. Regarding power consumption, Loblaw has worked diligently to reduce greenhouse gas (GHG) emissions through improving energy efficiency, reducing refrigerant leaks, and other renewable energy initiatives. According to Loblaw Companies Limited Corporate Social Responsibility Report in 2015, Loblaw has been tracking their operations focusing on carbon emissions since 2010 [4]. The results showed that they achieved their target of reducing energy consumption in stores by 4%, by investing in new lighting, upgrading fleet and building fuel consumption, refrigerant releases and corporate travel, and using renewable energy technologies [4].

All of these showed that they take reducing carbon emissions and contributing to mitigating climate change as their priority.

The objective of this study is to analyze energy used by Loblaw and provide suggestions for improvement. The GHG impacts on the provided suggestion was evaluated using the Life Cycle Assessment (LCA) methodology. The GaBi software system and databases developed by PE International, Germany together with TRACI, a life cycle impact assessment methodology, were applied in this study to convert existing inventory data into GHG impacts. The broad range data sets of the GaBi cover many different industrial sectors including metals (steel, aluminum and non-ferrous metals), plastics, mineral materials, energy supply (steam, thermal energy, power grid mixes), transport, disposal, manufacturing, and electronics.

### **TECHNOLOGIES TO SAVE ENERGY AND IMPROVE EFFICIENCY**

Supermarkets have reduced their electricity consumption to improve energy efficiency and reduce their carbon emissions. Lighting, refrigeration system, and heating, ventilation and air conditioning (HVAC) system are key opportunities for energy saving upgrades in typical supermarkets and these are monitored and controlled by centralized building energy management systems [5]

[6]. Example of technologies for energy efficiency upgrades are shown as follows [5] [7]:

#### Lighting

- Occupancy sensors installation in the active storage, restroom, office zones, etc.
- Skylights usage in warm and hot climates

#### Refrigeration

- Using frozen food and ice cream refrigerated cases with vertical models with doors
- Using medium-temperature refrigerated display cases with doors

#### HAVC

- Highest efficiency HVAC installed throughout corporate offices, stores, etc.
- Using an active HVAC asset performance tracking program
- implementing ground source heat pumps, packaged variable air volume systems, radiant heating and cooling, etc.
- Solar thermal technologies usage for service water heating

### SUGGESTIONS FOR IMPROVEMENT

Loblaws has put in much effort into improving their environmental performances in energy efficiency; however, there is also some room for improvement. After visiting the Superstore in Regina East, Saskatchewan, Canada, this study showed five suggestions for Loblaws/Superstore to become more environmentally friendly. The suggestions were analyzed based on the follow:

- Reliability: the reliability of a suggested is measured by the quality of producing stable and consistent results. A high means the suggestions produce similar results under consistent conditions, medium means the suggestions produces somewhat the same results, and low means it is hard to be reproduced with similar results.
- Applicability: this indicator refers to a degree of being applied. The applicability criterion is evaluated high if Loblaws have a high potential to implement the suggestions, medium if Loblaws have potential to apply them but not immediately, and low if Loblaws are nearly unable to implement the suggestions.
- Cost: this refers to all direct and indirect costs required for the suggestion. The cost criterion is

evaluated high, medium, and low if Loblaws need to spend a lot of money, not much money, and very low amount of money for the suggestions, respectively.

- Knowledge: this knowledge refers to the knowledge required for each suggestion. Advanced knowledge is required when the criteria is high, intermediate level of knowledge is required for medium, and low skills are required for low criteria.

- Time to adopt: this is the amount of time spent on implementation. For example, the time to adopt the new refrigeration systems is for six months; this means that six months are required to make changes on the refrigeration systems.

- Parties involved: this category shows the people or organizations who are involved or interested in each suggestion.

- Public perception: this refers to the conscious understanding that people have of public and official issues. A high public perception means a high level of public beliefs in the suggestions, medium means the majority of people are agree with the suggestions, low means there are not many people who support Loblaws for the implementation.

- Ease of implementation: this refers to an assessment required of the ease or difficulty of implementing the suggestions. The criteria is evaluated high if the suggestions are allowed for easy to set up, medium if the suggestions are not too difficult to set up, and low if the suggestions are not easy to set up.

- Capacity to reduce emissions: this assessment refers to an ability of suggestions to reduce emissions. The criteria is evaluated high if the suggestions have a high capacity in emission reductions, medium if the suggestions are normal in emission reductions, and low if the suggestions are low in emission reductions.

- Administrative simplicity: This is to perform the task of simplification of administrative procedures. The simplicity criteria is high when the suggestions are difficult for administration, medium when the suggestions are in general for administration, and easy when the suggestions' determination are easy to understand and manage.

The analysis on the environmental performance of the visited store and suggestions for improvement is summarized in Table 1.

Table 1 Analysis of Suggestion of Improvement

	Suggestion points	Reliability	Applicability	Cost	Knowledge	Time to adopt	Parties involved	Public perception	Ease of implementation	Capacity to reduce emissions	Administrative simplicity
1	Sky-light	High	High	Medium	High	Now	- Loblaws - Con-	High	Medium	High	Easy

	im- prove- ment						struction company - City of Regina				
2	Geo- thermal (for new store)	High	High	High	High	3 – 5 years	- Loblaw - Con- struction company - City of Regina	High	Easy	Me- dium	Me- dium
3	Refrige- ration systems	High	High	Low – Me- dium	High	6 months	- Loblaw - Con- struction company - City of Regina	High	Easy to Me- dium	High	Easy
4	Kinetic energy to elec- tricity	Me- dium	Me- dium	Me- dium	Low	1 – 2 years	- Loblaw - Sup- pliers	High	Me- dium	low	Easy
5	E-gro- cery shop- ping system	High	Me- dium	Low	High	1 – 2 years	- Loblaw - Cus- tomers	High	Me- dium	High	High

All the above suggestions are explained in more details as follows. However, GHG emissions will be calculated using GaBi 6 software tool for suggestions that show high capacity to reduce emissions. The GHG impact results are generated based on the TRACI methodology implemented in the GaBi 6 software. The users enter all the inputs and outputs of the two scenarios into the GaBi 6 software. GaBi 6 then generates the GHG emissions based on the TRACI methodology.

### Skylight Improvement

Lighting makes up the second largest share of the energy use and electricity bill [8]. Based on this reason, installing skylights can help save supermarkets' energy since a well-designed building with a good spread of natural light will benefit from passive solar gain and a reduced requirement for artificial light. The combination of these factors means that including skylights can offer a dramatic reduction in a building's total energy consumption and the emissions of CO<sub>2</sub> associated with this energy use. A naturally-lit interior will save money, provide a more pleasant environment where people want to spend time, and contribute to the reduction of CO<sub>2</sub> emissions.

The Superstore in Regina (East) has skylights installed; however, the store also has lights installed beneath the skylights. During our visit to the store, there was enough natural light, but Superstore still kept their lights. An improvement Superstore can make is to combine the skylight design with an automated dimming control system will achieve substantial energy savings and improve the store

environment significantly during the day. Another option would be to simply switch off the lights.

The National Association of Rooflight Manufacturers (NARM) commissioned the Institute of Energy & Sustainable Development at Leicester's De Montfort University to undertake a study to investigate the effect skylights have on the annual CO<sub>2</sub> emissions which result from the use of energy needed to operate a building. Savings from daylighting can cut lighting energy use by 50 percent [9]. Based on the average supermarket's electricity consumption is 5,000 MWh per year [10] and the energy consumption of lighting is approximately 15% to 25% of the total consumption [11].

It can be seen from the results generated by TRACI that savings from daylighting could reduce the energy usage numbers from 1250 to 625 MWh per year. The main substances that contribute to the Global Warming Potential (GWP) are CO<sub>2</sub>, Methane (CH<sub>4</sub>), and Nitrous oxide (N<sub>2</sub>O), and the highest contributor to the GWP comes from CO<sub>2</sub>. CO<sub>2</sub> emissions emitted into the air could be substantially reduced by 50% from 789,026.66 to 394,513.33 kg CO<sub>2</sub>-equiv. per year. This study covers electricity produced, but no accounting will be made of the GHG effects associated with construction, transportation, and operation of the Superstore.

### Use Geothermal

Geothermal energy is defined as heat from the Earth. Geothermal energy can be utilized for electricity production, for commercial, industrial, and residential direct heating purposes, and for

efficient home heating and cooling through geothermal heat pumps. Heat pumps are reversible of refrigerator and can provide either heating or cooling to almost any space or location. In warm weather the geothermal unit acts like home refrigerator. It removes unwanted heat from the space being cooled and deposits that unwanted heat somewhere else, in this case to the earth. In cool weather the geothermal heat pump acts as a reverse refrigerator because it withdraws heat from the earth and transfers that earth heat into the space being heated such as building, home, mall, etc. Heat pumps use a vapor compression cycle to transport heat from one location to another. In heating mode, the cycle starts as the cold liquid refrigerant within the heat pump which passes through a heat exchanger (evaporator) and then absorbs heat from the fluid circulated through the earth connection. The refrigerant evaporates into a gas as heat is absorbed from the earth connection heat exchanger (evaporator). The gaseous refrigerant then passes through a compressor where it is pressurized, raising its temperature to over 180 degrees F. The hot gas then circulates through a refrigerant-to-air heat exchanger where the heat is removed and sent through the air ducts. When the refrigerant loses the heat, it changes back to a liquid. The liquid refrigerant cools as it passes through an expansion valve and the process begins again.

This application can achieve very important energy savings by decreasing primary energy consumption by 28% to 32%, energy for cooling by around 25% and energy for heating by around 40%. These combined can potentially reduce CO<sub>2</sub> emissions by 28% to 32% [12]. However, installing geothermal energy system would be costly for the current Superstore and would be more applicable to new stores in the future.

### Improve Refrigeration

Refrigeration is the largest single energy consumer in most supermarkets and has very high potential for savings. According to Loblaw Corporate Social Responsibility report from 2012, running the refrigeration system contributes to approximately 50% of a supermarket's energy consumption [1]. The most common practice is to have open freezers, which causes the following problems: (1) inefficient energy consumption, (2) cold aisles that causes discomfort to consumers, and (3) gaining temperature of food products more rapidly than the ones in freezers with doors [13]. To solve the above problems, supermarkets should consider installing doors on every refrigerated cabinet and use glass door displays instead of open displays.

In the Superstore in Regina East, there are a lot of open freezers. To reduce energy consumption and

increase comfort for consumers, Loblaw could consider replacing the open freezer units with units with doors. This change would not only reduce GHG emission significantly, it will also save a large portion of Superstore's electricity bill. The closed display cabinets consumed less energy by approximately 5.46 kWh/m<sup>2</sup> per day compared to the opened display cabinets [14] as summarized in Table 2.

Table 2 Electrical energy consumption of the closed freezers (modified from [14])

	Average
Energy consumption (kWh/m <sup>2</sup> /day)	12.675
Saving from closure (kWh/m <sup>2</sup> /day)	5.4575

The analysis from TRACI showed that the closed cabinets will cause a reduction of 30.1% in the impact category of GWP compared to the opened cabinets. CO<sub>2</sub> emissions emitted into the air were reduced from 31,974.74 kg to 22,388.37 kg CO<sub>2</sub>-equiv. per year. However, the analysis covered electricity produced, but not for the GHG effects associated with construction, transportation, and operation of the Superstore.

Another suggestion for Loblaw to reduce the energy consumption of the refrigeration system is that the store could have one enclosed area for all of the refrigerators in the store. By having all of the refrigerators in one area the cold air that escapes the refrigerator will be contained in the zone and will lower the cost of refrigerating the units in that zone. In addition, the new innovative refrigeration battery from Axiom Energy can store energy at night when it is inexpensive and this can be discharged during peak hours for electricity demands in the afternoon. The battery can retrofit to the exiting refrigeration systems in which any modifications are not required. This helps the Superstore to be able to turn off their refrigeration systems' compressors and condensers and save their electricity by up to 40% [15].

### Kinetic Energy to Electricity

Renewable energy options are constantly replenished and more environmentally friendly compared to coal, oil, and natural gas for generating energy [16]. These options have experienced explosive growth over the past decade [17]. For Loblaws, electricity can be generated from the footsteps of people by installing special piezoelectric floor tiles. These tiles could be installed in the supermarket to generate electricity for lights and refrigerators within the supermarket. Pavegen System is a company based in the UK and is currently the only that sells energy-harvesting piezoelectric floor tiles. The new Pavegen's V3 is known to be generating over 200 times more power

than the first version launched in 2009 [18]. Each footstep can generate up to 8 Watts of electricity [19].

This study did an observation on people visiting the Superstore in Regina and the results showed that during the busiest time on a Sunday, there are approximately 200 people entering the store hourly. Based on this, we can make an assumption that on hourly average of 200 people would enter the store from 9 am to 9 pm and 100 people would enter the store other period of times (store hours is 6am to 11pm), giving a total of 2,300 people entering the store daily. Assuming that Superstore has 8 tiles at the entrance and each person entering the store would step on 6 of them; that would give a total of 0.139 MWh per day. This gives a total of 50.808 MWh per year, saving 1% of the electricity (based on the previous assumption that an average supermarket consumes 5000 MWh of electricity per year). Based on 2.17 pound of CO<sub>2</sub> eq/kWh electricity generated by lignite [20], the GHG reduction per year would be approximately 984.3 gCO<sub>2</sub> eq.

Although the amount of electricity saved by the tiles is not as high as the wind turbine, the capital required is also much lower, which makes the feasibility much higher. Wind turbine generating 10 kw costs approximately \$48,000 – 65,000 to install [21]. Pavegen's V3 is easy to install with no maintenance costs. Even though the cost of this technology is currently not released to the media, cost of a standard square meter of used in a building would cost approximately \$1,170 [22]. Since there are no regulations and community restrictions on this project, it is mostly up to the company to execute this project. From planning to installing and running, this project should be able to execute within a year. This product should be popular among the public. The tile itself has a LED lighting, which lights up with it is being stepped on (uses 5% of the electricity it generates), this is not only visually attractive, but can also be a good source of education to the public about sustainable and clean energy.

### E-Grocery Shopping System

An online ordering and delivering service is becoming increasingly popular in any companies because of continued increases in mobile adoption and broadband penetration which result in its service convenience with time saving [23]. The idea of the E-Grocery shopping system is that Loblaw/Superstore provides an online grocery shopping system to consumers. However, instead of delivering individually to the customers, Superstore delivers to companies in which the consumers are. In other words, Superstore would have some arrangement with big companies and customers are "grouped" by the companies they are in. The

groceries are delivered by the Loblaw truck to the company at a certain time once or twice a week (depending on the demand). The coordinators from the company are responsible for distributing the groceries to employees in need.

As employees can take their groceries from the workplace directly home, the individual trips to grocery stores can be avoided and the vehicles' emissions can be greatly reduced. The applicability of this system should be high in Regina, since majority of the people are grouped in limited places for work and the system has high potential to reduce GHG emission reduction.

This study assumed that 100 employees from the University of Regina (U of R) join this program and their average traveling distance is 6 km one way (i.e. 12 km return). A typical car is assumed to have a luggage space with around 424 liters [24], whereas a cargo van is assumed to have a luggage space with 6,787 liters [25]. In addition, this study assumed that 1 customer will buy goods with their full of luggage space. As a result, Superstore will need to deliver their products to 100 customers for 7 rounds in total.

By delivering to the 100 employees to the U of R, the results from the TRACI method showed a 92.9 % reduction of the impact in the GWP category in the "E-grocery shopping" scenario compared to the "conventional shopping" scenario. However, this study covers transportation and gas produced, but no accounting will be made of the GHG effects associated with construction, operation of the Superstore.

### CONCLUSION

Over the years, supermarkets have been undergoing changes to be more environmentally friendly. Loblaw committed on creating a positive impact in the community being socially responsible by respecting the environment. They have taken big measures to reduce their emissions, such as cutting discharges from refrigeration units and implementing a new low temperature system, which reduces greenhouse gas emissions. In addition, this makes supermarkets substantially cost savings and consequently high returns of investment. In this study, the energy efficiency and environmental performance of Loblaw have been analyzed. It can be shown that Loblaw has put in a lot of effort to enhance their environmental performance.

However, there are some areas of improvement and this study has presented 5 suggestions for Loblaw's further improvement. This study paid a visit to the Superstore in Regina East to inspect the applicability of our suggestions. The results showed that the option that is the most reliable, cheap, and easy for an implementation is the skylight improvement. However, as online shopping is becoming more popular these days, e-grocery

shopping becomes an important option for Loblaw to be considered. The sensitivity analysis can be obtained as a future work to identify important parameters that affect the most of the results in each suggestion.

## REFERENCES

- [1] 2012 Loblaw Corporate Social Responsibility Report, "2012 Loblaw Corporate Social Responsibility Report? Respect the Environment" 2012, Retrieved from <http://www.loblaw-reports.ca/responsibility/2012/respect-the-environment/>.
- [2] Glen B, "Loblaw responds to customer survey", Jan 2017, Retrieved from <http://www.producer.com/2017/01/loblaw-responds-to-customer-survey/>
- [3] Smartcanucks, "Loblaws to close 52 stores across canada including Superstore, Provigo, Zehrs, & No Frills", July 2015, Retrieved from <http://smartcanucks.ca/loblaws-to-close-52-stores-across-canada-including-superstore-provigo-zehrs-no-frills/>
- [4] Loblaw Companies Limited, "The way we do business: 2015 corporate social responsibility report", Ontario: Loblaw Companies Limited, 2015.
- [5] Retail Industry Leaders Association, "Energy saving opportunities and tactics for retail", 2014, Retrieved from <https://www.rila.org/sustainability/RetailEnergyManagementProgram/Documents/EnergySavingOpportunities+TacticsforRetail.pdf>
- [6] Arias J, "Energy usage in supermarkets-modelling and field Measurements", 2005, PhD thesis, KTH, School of Industrial Engineering and Management (ITM), Energy Technology
- [7] Leach M, Hale E, Hirsch A, & Torcellini P, "Grocery store 50% energy savings technical support document", Colorado, National Renewable Energy Laboratory, 2009.
- [8] The Fraunhofer Gesellschaft (FhG), "Supermarkets: Energy-optimized", Feb 2013, Retrieved from <https://phys.org/news/2013-02-supermarkets-energy-optimized.html>
- [9] Research for Energy Optimized Building (EnOB), "Energy-efficient supermarket uses daylight and ground cooling", Mar 2017, Retrieved from <http://www.enob.info/en/pdf/new-buildings/project/details/energy-efficient-supermarket-uses-daylight-and-ground-cooling/>.
- [10] Natural Resources Canada, "RETScreen International RETScreen - Energy Efficient Arenas & Supermarkets", Mar 2017, Retrieved from [http://www.etscreen.net/ang/speakers\\_notes\\_arenas\\_supermarkets\\_project\\_analysis.php](http://www.etscreen.net/ang/speakers_notes_arenas_supermarkets_project_analysis.php).
- [11] Ge Y, Tassou S, Foster A, Evans J, & Maidment G, "Modelling and evaluation of supermarket energy use and emissions", 2016.
- [12] Garcia J, Coelho L, Cerdeira R, Sanner B, Lentz P, & Frechin N, "Application of ground source heat pump to a supermarket in Portugal", J. of Civil Engineering and Architecture, Vol. 5, No. 3, 2011.
- [13] Tyrewala AS, Nelson D, & Almanza B, "The effects of door opening and food placement on food temperature within the refrigerator when power is lost during a disaster", 2011, Retrieved from [http://scholarworks.umass.edu/cgi/viewcontent.cgi?article=1235&context=gradconf\\_hospitality](http://scholarworks.umass.edu/cgi/viewcontent.cgi?article=1235&context=gradconf_hospitality)
- [14] Ligthart F, "Closed supermarket refrigerator and freezer cabinets: A feasibility study", No. ECN-E-07-098, Petten: Energy research Centre of the Netherlands (ECN), 2017.
- [15] Maloney P, "Walmart, axiom exergy partner for refrigeration energy storage project", Nov 2016, Retrieved from <http://www.utilitydive.com/news/walmart-axiom-exergy-partner-for-refrigeration-energy-storage-project/430487/>.
- [16] Renewable Energy World, "Types of renewable energy", 2016, Retrieved from [http://www.etscreen.net/ang/speakers\\_notes\\_arenas\\_supermarkets\\_project\\_analysis.php](http://www.etscreen.net/ang/speakers_notes_arenas_supermarkets_project_analysis.php).
- [17] Myers T, "The experts: What renewable energy source has the most promise?", The Wall Street Journal, 2013, Retrieved from [http://www.etscreen.net/ang/speakers\\_notes\\_arenas\\_supermarkets\\_project\\_analysis.php](http://www.etscreen.net/ang/speakers_notes_arenas_supermarkets_project_analysis.php).
- [18] Ellis EG, "The best new green energy tech could be right underfoot", 2016, Retrieved from <https://www.wired.com/2016/06/best-new-green-energy-tech-right-underfoot/>
- [19] Fujimoto A, "Energy harvesting flooring", 2014, Retrieved from <http://large.stanford.edu/courses/2014/ph240/fujimoto1/>.
- [20] The U.S. Energy Information Administration (EIA), "How much carbon dioxide is produced per kilowatt-hour when generating electricity with fossil fuels?", Mar 2017, Retrieved from <https://www.eia.gov/tools/faqs/faq.php?id=74&t=11>.
- [21] Energy Wind Power, "Small wind turbines for homes & businesses", 2017, Retrieved from <http://bergey.com/wind-school/residential-wind-energy-systems>
- [22] Freddie D, "Pavegen wants to become the Tesla of walking", 2016, Retrieved from <https://www.forbes.com/sites/freddiedawson/2016/05/17/pavegen-wants-to-become-the-tesla-for-walking/#3d74fd1f57d9>
- [23] The Nielson Company, The Future of Grocery. Ontario: The Nielson Company, 2015.
- [24] Popular science, "Wrong-way wings: Give new agility to supersonic planes", Apr. 1980.
- [25] General Motor Fleet, "2016 GMC savana cargo dimensions", Mar 2017, Retrieved from <http://www.gmfleet.com/previous-model-year/gmc/savana-cargo-van/features-specs/dimensions.html>

## **AN EVALUATION FOR EFFECTIVE PUBLIC PARTICIPATION IN EIA IN THAILAND**

Chutarat Chompunth<sup>1</sup>

<sup>1</sup>School of Environmental Development Administration,

<sup>2</sup>National Institution of Development Administration, Thailand

### **ABSTRACT**

In Thailand, environmental conflicts and problems from project development are increasing vastly. Many development projects have been delayed or postponed. The public has lost confidence in the environmental monitoring and mitigation plans of the EIA system. Many ongoing projects cause severe environmental and social impacts. To solve this problem, public participation in the EIA system is considered as a vital theme to promote sound management of development projects. Although, public participation has become an essential element of environmental decision-making and has grown considerably in Thailand, it frequently fails to solve environmental conflicts. Thus, there is significant to evaluate public participation practice to consider whether the participation process is effective and what works or does not work in this manner. This research aimed to evaluate the effectiveness of public participation in the Thai EIA system. The evaluation is based on in-depth interviews with key stakeholders, review of EIA reports as well as observing public hearing forums. The evaluation of the selected case study presented an overall weakness of public participation practice. It was found that the public participation in Thailand was not completely effective when tested against the evaluation criteria. The affected people had no chance to present any comments at the very beginning. The public participation process started too late, after a decision had been made and conflicts among stakeholders already occurred. Public participation is not yet properly established in the Thai context. There is an urgent need to find an appropriate approach and conditions of public participation in Thailand.

*Keywords: Public Participation, Evaluation, EIA, Environmental Conflict*

### **INTRODUCTION**

Thailand's rapid economic growth and industrialization over the last five decades have led to significant environmental crisis. The Thai government recognizes the linkage between continued economic prosperity and the protection of the environment. Thus, the concept of public participation in the environmental decision-making process through a number of laws and legal requirements was established, and the public began to recognize their rights granted by laws. Although a foundation for involvement in the decision-making process is provided to the public, this is still in the early stage of implementation [1].

Public participation is a continuing challenge in Thailand. A number of development projects initiated either by the government or the private sectors frequently face strong public opposition and the public participation process itself is viewed as unsuccessful practice. The question of how to be sure that the participation process is effective and results in desirable outcomes seems to be vital [2]. A systematic evaluation of public participation is essential as a means to ensure the acceptance of the process and outcomes, and, importantly, to develop knowledge of how to improve the practice [3].

This study is important to Thailand because it highlights the significance of conducting public

participation in the implementation of development projects in Thailand and identifies the critical factors for effective practice of public participation. The public participation processes of the Khao Hin Son power plant was evaluated to provide evidence to answer the research questions of this study that is: How effective is public participation for managing environmental conflict management in development projects in the Thai contexts?

The research findings and recommendations are vital to improve the public participation practice in Thailand and to enable all stakeholders to effectively participate in the decision-making process.

### **A Conceptual Framework of Public Participation**

#### **What is Public Participation?**

The term public participation has numerous different meanings and definitions. Different academics have different meanings when defining the term 'public participation' depending on who the people are and what the setting is [4]. It is always viewed differently depending on its contexts and purposes. In the past, public participation was considered as being an opportunity to give comments in a public hearing, to vote in referendums, or just being a member of a social movement society. Frequently, public participation



related to participation at public hearings only, but, at present, this term refers to a diversity of procedures for facilitating members of the public to be effective participants in deliberations in decision-making processes [1], [5].

### Effective Public Participation

When a government or a private agency employs public participation in their activities, there is a substantial interest in determining whether or not their endeavors have been successful. To begin with, it is important to clearly verify and define what successful or effective public participation means. In general, the effectiveness can be defined as: "whether something works as intended or meets the purpose(s) for which it is designed". However, indeed, the definition of effectiveness is typically complicated because of a diversity of objectives and expectations for public participation processes and mechanisms. The definition and interpretation can vary depending on participants' and stakeholders' perspectives, contexts and situations. Specific political, social and economic contexts in each country typically have an influence on the effectiveness of public participation. For these reasons, developing a single universal definition of effective public participation is difficult.

In terms of process effectiveness, many scholars indicate that process effectiveness focuses primarily on means rather than ends [1], [4]. It is therefore, to examine a variety of procedural aspects of the participatory programs that add value to a decision making process. These factors include; procedural justice, accessibility to the decision making process, inclusiveness, diversity of views represented, opportunities for participation, information exchange, identification and integration of concerns, early involvement of stakeholders, number of options identified, number/types of participants, decision maker presence at meetings, availability and clarity of materials, etc..

For some practitioners, the success of a public participation endeavor can be judged in terms of results or outcomes. They proposed important outcomes in terms of; project/decision acceptability, mutual learning, improved understanding and conflict resolution [5]. However, in practice, it is difficult to facilitate public participation processes to achieve all desired elements.

Effective participation should be perceived as a means to enhance effective decision making through an opening-up of the decision process to public views. Through this approach, public participation could constitute accountability and transparency to the decision-making process. These elements should be used as an outline when the practitioner designs a public participation program [6]. Thus, for public

participation to be effective in any context, it requires the public to be well informed and kept aware of the possibility of participation.

Conclusively, the definitions of effectiveness are pretty much influenced by individual expectations and interpretations. Thus, it can be summarized that there is no single definition of effective participation processes.

### A Development of Evaluation Frameworks for Public Participation

Obviously, the existing evaluation approaches vary widely with regards to differences in concept, purpose, focus, scope, methodology and disciplinary perspective. Besides, different stakeholders may have different objectives and measurements. As a result, the evaluations in the participation field have been applied from a variety of theories such as public participation theory, communication theory, and democratic theory [2], [6]. Indeed, the approaches to public participation evaluations are primarily developed from the traditional evaluation that focused on whether public participation achieves either process or outcome goals [6].

Most acknowledged evaluation approaches of public participation are related to the effectiveness of the construction and implementation of the participation procedure, and the success of the outcome. The participatory process-based evaluation typically measures fairness and competence matters, interchanged information, inclusiveness and procedures. This includes the evaluation for how effective public participation is in democratic decision-making. The outcome-based evaluation uses indicators of how stakeholders influence decisions, their satisfaction with the final decisions, or an ability to reach a consensus. This approach is not only based on stakeholders' or users' goals, but it also includes social goals [7].

In order to make a rigorous evaluation of public participation processes and build generalizable conclusions, some consistency in theoretical frameworks is essential and needed. An evaluation model for the evaluation of the public participation process of this study is developed which includes process-based evaluation and outcome-based evaluation.

Process-based evaluation of participant activities aims at evaluating the characteristics of stakeholders focuses on an identification of stakeholders and the inclusiveness and adequate representativeness of the participants. Outcome-based evaluation focuses on an evaluation of impacts and influence of the participation process, resolving conflict and an integration of public values and concerns to the decision-making process [2], [4].

It can be seen that this evaluation framework

attempts to make more explicit the factors that should be considered when evaluating both the processes and outcomes of a public participation process. The framework facilitates a balanced evaluation that indicates not only effectiveness but also the factors instrumental to that effectiveness. The evaluation criteria also encompass substantial consideration of the participation processes and outcomes [3].

## METHODOLOGY

A single case study was adopted for this thesis in order to conduct an in-depth study of the public participation practices in the Thai context. To achieve broader and better data and results, mixed methods of data collection were carried out. The first method was a review of documents concerning the operations, activities and concepts of public participation process. Interviews were selected, including semi-structured and in-depth interviews with stakeholders. Stakeholders who held key positions or played important roles in the public participation process were identified and selected. All relevant data were reviewed to build up knowledge and framework about the case study and public participation process. These processes aimed to provide background on the rationale for public participation and the Thai EIA system.

## RESULTS AND DISCUSSION

### Process-Based Evaluation

#### *Inclusiveness and adequate representativeness* ]

In this study, inclusiveness of the participants was not achieved due to some constraints such as strong opposing ideas of the protestors or unclear practical guidelines. The authorities and the developers did not try enough to engage stakeholders, particularly the affected villagers, at the beginning of the project implementation. After the conflict occurred, a participation process was then initiated. Most protestors refused to take part in these programs run by either the authorities or the developers and made it difficult for the government to engage all parties in the participation process. Besides, there were problems in practice when selecting the right participants due to selection criteria not being clear. For example, the participants in the public hearing case were identified and selected by a top-down approach which seemed to engage all stakeholders; however, the authorities did not make clear who the stakeholders were and who should participate in the process. Thus, it was hard to say that the opinions and comments from the participation process represented the voice of all people affected by the project. The finding suggested that the authorities should give the first

priority to participate in the process to lay people in the impacted area who were directly impacted from the development project.

A similar finding was evident in other research [8], [9]. It was found that it was difficult to engage an appropriate and inclusive representative cross section of the entire community in a participation process. Local villagers and stakeholders who would be directly affected by, or benefit from the decision and were closer to the project, should have first opportunity to participate and present their concerns. Stakeholders who felt they were excluded from the decision-making process would mount strong opposition to the project or policy initiatives which could delay or cancel the implementation.

#### *Multiple and appropriate participation methods*

A number of participation techniques were used to engage and communicate with the public; nonetheless, they were not conducted at the early stage of the project, particularly after the conflict occurred. These techniques ranged from traditional methods on an education and information provision level, to a more interactive approach such as public meetings. However, the majority of them were traditional. The public did not have more opportunities to discuss the issue and manipulate the decision.

The selected participation methods, particularly a public hearing, seemed not to be appropriate to the situation and the involved parties. Indeed, the government usually used public hearings to solicit the public's opinions and solve conflict among stakeholders in development projects; however, more often the public hearing was not successful in solving the conflict in Thai society, as clearly presented in this project. Many affected villagers were frustrated with the participation process and their government because they felt that the process was not a participation process in which they could make any change to the decision or create appropriate dialogue.

Similarly, [10] and [11] found that, although traditional methods were being widely used, they focused on one-way transmission of information from the developer or the authority to the public, and the public had less opportunity to input into an early stage of the decision-making processes.

#### *Early Involvement*

When the Khao Hin Son power plant was first initiated, it was implemented without providing opportunities for the public to take part early enough in project development. The affected people had no chance to present any comments at the very beginning. The public participation process started too late, after a decision has been made and conflicts among stakeholders already occurred. Clearly, the

public had little power to influence the decision and nothing could be changed. It could be said that, in this study, a lack of public participation in the early stage of project implementation became the critical problem.

This issue is a critical problem in practice in many countries, such as the Czech Republic [12], Spain [13], Bulgaria [14], and Kenya [15]. The public participation taken place late, particularly when decisions have already been taken, could be ineffective and obstructed by the public. This was because it was too late for the public to make meaningful contributions and its voice might have less power to influence the decisions.

#### *Transparency*

In this study, the participation process seemed not to be open and transparent enough. All decisions were decided before an involvement of the public; thus the public could not see how the decisions were being made. For example, the contract was already signed and the construction had been approved before the public had any details about the project. The affected villagers did not have an opportunity to participate through the processes. After the public hearing, the committee could not clearly explain how the public input was incorporated into the decision-making process. The hearing report and conclusion was not widely publicized in order to communicate the results back to the participants. The finding showed that if the participation process was credible, transparent and legitimate, the project would be more accepted and increase public satisfaction with decisions or even be successfully implemented

There is considerable empirical evidence of a lack of transparency in many studies [8], [16], [17]. This research showed that the decision-making and public participation processes failed to be transparent. An integration of public inputs into the decision-making process was poor and hardly existed. In particular, the information circulated back to participants had little evidence of how the participation process had an impact on the final decision.

#### *Resource and information availability and accessibility*

In this study, provision of resources was insufficient and unsatisfactory. Most relevant information was difficult to access and not available to the public. The public had difficulty accessing all data and information related to the project, maintained either by the government or the project proponent. Besides, this information was inappropriate and incomprehensible for many participants since most of it was in English and had

many technical terms, such as the EIA report. There were also some mistakes in the EIA report. This led to mistrust in other information provided by the government and the developers. Additionally, the participation programs, particularly public hearings, were conducted on workdays which means a number of people were unable to attend.

From the research findings, it was found that receiving, sharing and exchanging precise, correct, and updated information about the project was critical for project implementation. The public required sufficient information which was relevant and accessible to increase their knowledge and understanding, and enable them to meaningfully participate in the process.

A number of scholars stated that people could not effectively evaluate the problems and alternatives unless they were provided with appropriate and sufficient information. These resources are important and must be provided to the public in order to achieve an effective participation process [4], [17], [18].

#### **Outcome-Based Evaluation**

##### *Impact and influence of participation*

In this study, it was clearly presented that in the traditional management style of the Thai government, the public was often excluded from the decision-making process and the public did not have any power over the decision. The public input hardly influenced the decision-making process of the government. The public were provided little opportunity to comment on, or contribute to, any aspect of the project in any participation programs. It might be said that the decision-makers did not want to distribute their power to the local people, or even the local government bodies. Importantly, they did not intend to promote public participation at any level.

When the impacted villagers found that their involvement was too late and could not impact on the decision or even make any change to the project, so they preferred not to participate in the government's or the project owner's participation processes and began their protest activities. Clearly, the public needed to have a genuine opportunity to be heard and influence the final decisions.

This problem also has been found in many countries, such as Bulgaria [14], India [17], and the UK [18]. It was found that the outcomes of the public participation process have failed to be reflected in the decision-making stage and the final decisions. While the public expected that they should have a real influence in decision-making, they had a marginal influence only on what really happened. Indeed, empowering was not only power sharing and free access to information, but also an efficient transfer of necessary competency to the

public.

#### *Incorporation of public values and concerns*

Clearly, in this study, the local villagers tried to add their knowledge and concerns into the process. However, there was no obvious evidence that the public input or the outcomes of the participation process were brought and soundly integrated into the decision-making process. The public input hardly influenced the decision-making process of the government. Although the project was cancelled, there was no official evidence presented that the public input influenced the final decision. The decision-making process remained with the government.

Indeed, the public hold specific and valuable information, particularly local geography, the local ways of life, environmental conditions or other relevant factors that can influence the operation and safety of the project. This knowledge was potentially valuable to the decision-making process and should not be overlooked. Integrating this local knowledge and values into the decision-making processes could assist in finding consensus which leads to more accountability and legitimacy that satisfies a broader public. Undoubtedly, this study found that the public needed to ensure that their viewpoints and concerns were meaningfully incorporated into the decision-making process.

The public participation process needed to be conducted carefully to ensure that all stakeholders were given opportunities to voice their ideas and concerns, and every interest was considered fairly. This would eventually lead to a better decision and conflict resolution [1], [12].

#### *Resolving conflict*

Conflicts of the Khao Hin Son case were serious which mainly resulted from a lack of public participation. Evidently, the public was excluded from the decision from the beginning, so they thought the project was not transparent and did not accept it. The public tried to make their voices heard but they were overlooked. Later, although there had been an attempt to resolve conflicts between the protestors and the developer, it proved to be too late. For example, the public hearing's function was often to communicate prior decisions to the attendees rather than to foster discussion and problem solving to reach consensus. The developers and the officers claimed that they tried their best to resolve the conflict while the villagers viewed that they were not willing to do so. These conflicts were too complicated and difficult to handle.

Similar finding was found in other studies that different stakeholders looked for different tactics to achieve their own concerns and interests. This point is hard to handle it since it was very difficult to

make everyone agree with a decision [4], [16]. Importantly, conflicts could not be solved if the process of decision making is perceived to be unfair or biased.

## **CONCLUSION AND RECOMMENDATION**

### **To Establish Effective Public Participation in Thailand**

Public participation processes seem to be a rational strategy for a developing country with a poor economy and struggling democracy like Thailand. However, in this study, it was found that public participation of Thai people did not comply with a real concept of public participation; people who were stakeholders in the project did not have an opportunity to be informed and to express their ideas from the very beginning, and their opinions were not considered in the decision-making process. It could be said that the public participation process was not yet properly established in the Thai context. Thus, there is an urgent need to find a working model and conditions of public participation which can assist in resolving environmental problems.

From this study, it is recommended that public participation should be considered as obligatory in any development project and local communities should be empowered as equal development partners who should participate in activities related to development projects, in particular, in the design, implementation, mitigation, and benefit sharing aspects. This confirms that public participation was more than a procedural obligation to comply with in development project implementation [8]. It can provide extensive advantages to the whole of society in particular preventing, minimizing and resolving conflicts, developing trust and co-operation among stakeholders, increasing acceptance in projects, establishing democratic involvement, and improving the environmental decision-making process and its outcome [5].

Principally, participation processes are highly influenced by prior experience with participation, cultural, institutional contexts [18]. According to the specific and dynamic context of governance in Thai society, public participation techniques should be carefully considered to be properly applied in this specific context. There is no consensus on a format for public participation. Different methods are particularly favored and suitable in different contexts and vary in their purposes which should be judged on how well they fulfill a particular purpose. This research recommends that, in practice, a combination of participation methods could be more fruitful than an application of only one specific technique for the reason that different public participation techniques can complement the limits of other(s). These participation mechanisms should be multiple and rigorously applied case by case in

order to achieve the effectiveness of public participation.

It could be implied that effective public participation is not a single event, but a carefully designed and planned process that applies a multiplicity of techniques suited to the situations, contexts and the communities involved. To achieve it, it is very important to plan and execute the process very carefully, allowing adequate time and resources [19]. The participation issues need to be clearly framed and communicated before the processes are commenced. The sessions should be employed in two-way communication and sufficient information should be exchanged.

If the development projects are to be effectively implemented, and the potential to resolve conflicts from their implementation succeed, the public must be appropriately involved in the decision-making process. Public participation is an effective mechanism for conflict resolution since the public's cooperation is fundamental to the successful implementation of any development projects. A full involvement of the public in the decision-making process make the consideration of the project more efficient and effective than would otherwise would be the case.

Finally, various assumptions discussed previously in this study could lead to a conclusion that public participation is the pre-eminent approach to achieve a balance desired between stakeholders from development projects or policy implementation. By providing public participation from the beginning through until the end of the process, it could: reduce strong opposition since the public could be involved before the decision has been made; resolve conflict and lessen anger from the public; and, enhance the trust and credibility of the authority or developer.

## REFERENCES

[1] Chutarat Chompunth (2017). "Role of Public Participation in Environmental Impact Assessment in Thailand." *International Journal of GEOMATE*. Vol. 12(33): 109-113.

[2] Rowe, G. and L. J. Frewer (2004). "Evaluating Public Participation Exercises: A Research Agenda." *Science, Technology and Human Values*. Vol. 29(4): 512-557.

[3] Charnley, S. and B. Engelbert (2005). "Evaluating Public Participation in Environmental Decision-Making: EPA's Superfund Community Involvement Program." *Journal of Environmental Management*. Vol. 77(3): 165-182.

[4] Creighton, J. L. (2005). *The Public Participation Handbook: Making Better Decisions Through*

*Citizen Involvement*. San Francisco, Jossey Bass.

[5] Shepherd, A. and L. Ortolano (1997). "Organizational Change and Environmental Impact Assessment at the Electricity Generating Authority of Thailand: 1972-1988." *Environmental Impact Assessment Review*. Vol. 17(5): 329-356.

[6] Chess, C. and K. Purcell (1999). "Public Participation and the Environment: Do We Know What Works?" *Environmental Science and Technology*. Vol. 33(16): 2685-2692.

[7] Beierle, T. C. and J. Cayford (2002). *Democracy in Practice: Public Participation in Environmental Decisions*. Washington, DC, Resources for the Future.

[8] Dungumaro, E. W. and N. F. Madulu (2003). "Public Participation in Integrated Water Resources Management: The Case of Tanzania." *Physics and Chemistry of the Earth*. Vol. 28(20-27): 1009-1014.

[9] Vantanen, A. and M. Marttunen (2005). "Public Involvement in Multi-Objective Water Level Regulation Development Projects-Evaluating the Applicability of Public Involvement Methods." *Environmental Impact Assessment Review*. Vol. 25(3): 281-304.

[10] Fiorino, D. J. (1990). "Citizen Participation and Environmental Risk: A Survey of Institutional Mechanisms." *Science, Technology, and Human Values*. Vol. 15(2): 226-243.

[11] Daniels, S. E. and G. B. Walker (2001). *Working Through Environmental Conflict: The Collaborative Learning Approach*. Westport, Praeger Publishers.

[12] Richardson, T., J. Dusik and P. Jindrova (1998). "Parallel Public Participation: An Answer to Inertia in Decision-Making." *Environmental Impact Assessment Review*. Vol. 18(3): 201-216.

[13] Palerm, J. R. (1999). "Public Participation in Environmental Impact Assessment in Spain: Three Case Studies Evaluating National, Catalan and Balearic Legislation." *Impact Assessment and Project Appraisal*. Vol. 17(4): 259-271.

[14] Almer, H. L. and T. M. Koontz (2004). "Public Hearings for EIAs in Post-Communist Bulgaria: Do They Work?" *Environmental Impact Assessment Review*. Vol. 24(5): 473-493.

[15] Okello, N., L. Beevers, W. Douven and J. Leentvaar (2009). "The Doing and Un-doing of Public Participation during Environmental Impact Assessments in Kenya." *Impact Assessment and Project Appraisal*. Vol. 27(3): 217-226.

[16] Furia, L. D. and J. Wallace-Jones (2000). "The Effectiveness of Provisions and Quality of Practices Concerning Public Participation in EIA in Italy." *Environmental Impact Assessment Review*. Vol. 20(4): 457-479.

[17] Diduck, A., J. Sinclair, D. Pratap and G.

- Hostetler (2007). "Achieving Meaningful Public Participation in the Environmental Assessment of Hydro Development: Case Studies from Chamoli District, Uttarakhand, India." *Impact Assessment and Project Appraisal*. Vol. 25(3): 219-231.
- [18] Bond, A., J. Palerm and P. Haigh (2004). "Public Participation in EIA of Nuclear Power Plant Decommissioning Projects: a Case Study Analysis." *Environmental Impact Assessment* Vol. 24(6): 617-641.
- [19] Tippet, J., B. Searle, C. Pahl-Wostl and Y. Rees (2005). "Social Learning in Public Participation in River Basin Management: Early Findings from Harmoni COP European Case Studies." *Environmental Science and Policy*. Vol. 8(3): 287-299.

## **ACHIEVING WATER SENSITIVE CITY CONCEPT THROUGH MUSRENBANG MECHANISM IN SURABAYA CITY, INDONESIA**

Eddy Setiadi Soedjono<sup>1</sup>, Nurina Fitriani<sup>2</sup>, Rifda Rahman<sup>3</sup>, I Made Wahyu Wijaya<sup>4</sup>

<sup>1,3,4</sup>Faculty of Civil Engineering and Planning, Institut Teknologi Sepuluh Nopember, Indonesia;

<sup>2</sup>Faculty of Science and Technology, Universitas Airlangga, Indonesia

### **ABSTRACT**

Water sensitive city is a very important issue for development of future cities. Water sensitive is a kind way of live for all communities in the city. Cities with low level of environment awareness would be difficult to implement the issue of water sensitive city. The aim of this study is to access how water sensitive city would be implemented in Surabaya. Observations and surveys using focus group discussion (FGD) and in-depth interview (IDI) were conducted to get real information for each musrenbang from kelurahan level, up to kecamatan and city level. The concept of water sensitive city is likely to be possible to be implemented in Surabaya. It is, however, not easy to be implemented as human basic needs are not discussed during musrenbang yet as an indicator to further discuss the issue of water sensitive city.

*Keywords: communities, e-musrenbang, water sensitive city*

### **INTRODUCTION**

Increase of urban water demand forces water stakeholders like government, academia, and communities to change their live especially towards water. One of the modified system has been introduced in the concept of water sensitive city which may change a city, give best practice to manage water, improve environment and its relevant institutions (Brown *et al.*, 2008). In the context of water sensitive city, a city must be resilient, liveable, productive, and sustainable. The resilient system consists of: (1) number of disturbance that can be absorbed and still remain at same state, (2) degree of capability to self organisation, (3) degree of capability and capacity to learn and adapt (Folke, 2006). Resiliency of system to disturbance in the environment was well understood and based on the approaches, the 'hydro-social contract' was found (Lundqvist *et al.*, 2001). The term of the concept is used to describe the pervading values and often implicit agreements between communities, governments, and business on how water should be managed.

According to Brown *et al.* (2009), steps to transform to a water sensitive city were initiated from a city which could manage its own water supply system as called water supply city. Then it would moved forward subsequently to sewerage city, drainage city, then waterways city before becoming to a

water sensitive city. The steps were not fixed but leap frogging was a leap from whichever step to become a water sensitive city. There are three main supports to come to a water sensitive city, i.e: stock of water, proper ecosystem, and community involvement (Wong dan Brown, 2009).

Water management in Indonesia has already been strongly supported by the government, communities, and academia (Moerwanto, 2011). Water governance is basically using a top-down approach where water policy from the central government must be implemented for the benefit of all citizens and communities via provincial and municipal government, in this case Jawa Timur Province and Surabaya City. Even within the city level, it goes down to Kecamatan (sub-district), Kelurahan (village-like), Rukun Warga (RW; community-like), and Rukun Tetangga (RT; neighborhood-like) level (Soedjono *et al.*, 2017). Different level of government boards and institutions which regulates water in this study are Jasa Tirta (central government), Dinas PU Pengairan (provincial government), BAPPEKO, Dinas PUBMP, Dinas LH, DKRTH, and PDAM (municipal government). In Indonesia, however, water governance may also introduced using a bottom-up approach where water related program could be proposed from the communities to the



municipal, provincial, and central government as called MUSRENBANG (Musyawarah Perencanaan Pembangunan). Musrenbang would result a annual work plan of city and province (RKPD) as the mandate from RPJMD (Soedjono *et al*, 2017, UU 25/2004, PP 23/2014, and Permendagri 54/2010).

Study on Musrenbang in Jawa Timur Province like in Probolinggo District showed that water and sanitation was not strongly discussed during Musrenbang (Rahman and Soedjono, 2016). Musrenbang at the level of village/kelurahan, kecamatan, district, province, and even at the level of national level mainly discuss about infrastructures like road, rain drainage, and other public facilities. Some municipalities in Jawa Timur Province like Bojonegoro District, however, has discussed water and sanitation in its musrenbang. With all background has been mentioned before, the aim of this research is to access how water sensitive city concept can be introduced in the musrenbang (using bottom-up approach) at different level in Surabaya City: kelurahan, kecamatan, and municipal level.

## METHODS

Primary data were collected through in depth interview (IDI) and focus group discussion (FGD). The respondents were common people and representatives from local government officers which conducted the Musrenbang in the kelurahan, kecamatan, and municipal level. Secondary data collections were mainly information regarding relevant regulations from the central government level like Indonesia Law or UURI down to kelurahan regulations. Then results of secondary data was compared with the primary data. The comparisons were used to improve the current regulations, especially improvements towards water resource management to achieve water sensitive city conditions. As Musrenbang Kelurahan was conducted simultaneously for all kelurahan in Surabaya, then Kelurahan Kenjeran was selected to join the MUSRENBANG in January 2017. Within kecamatan level, then Kecamatan Bulak and Kecamatan Semampir were selected for the Musrenbang and eventually it was the Musrenbang at the city level.

## RESULTS AND DISCUSSION

As regulated by Regulation of Ministry of Home Affairs no. 54/2010 regarding Musrenbang then musrenbang is started from Kelurahan level, then it is continued to musrenbang in sub-district, city, province, and even at national level. The following musrenbangs are to describe Musrenbang at Kelurahan Kenjeran, Musrenbang at Kecamatan Bulak and Semampir, Musrenbang at Surabaya City, and even Musrenbang at Jawa Timur Province.

### MUSRENBANG at Kelurahan Kenjeran

Musrenbang in Surabaya started at RW level which all proposals could be inputted online through a website of [bapeko.surabaya.go.id/musrenbang2017](http://bapeko.surabaya.go.id/musrenbang2017). Each RW in Surabaya was given user id and password to log into the website. Surabaya government called this system as e-Musrenbang. RW was not only entitled to input any next year program into the website, but was also entitled to give any comments and critics to the city government (Putri, 2015). Such system would ease the interaction between communities and the city government. Input from RW definitely would accommodate input from its RT. With this system then any input from RT, RW, Kelurahan, and finally from kecamatan could be easily known by the city government. In the system, however, RW was only allowed to select proposal which were already given in the website; not any proposal could be accommodated in the website. Each RW was only allowed to propose 2 proposal with 1 reserved proposal to accommodate future adjustment due to program priority of the city.

Kelurahan Government was entitled to edit all input from RWs during the Kelurahan Musrenbang. That was why the RW speakers should be properly selected to clarify any priority within its RW. Website of RW and Kelurahan was definitely different as Kelurahan regulated all its RWs. Besides, Kelurahan had a fixed budget from the city government for local development using top-down approach. Results of bottom-up approach of Musrenbang were called development priorities of kelurahan for next year program. This top-down must meet the bottom-up approach during Musrenbang. Development priorities within Kelurahan were then submitted to Kecamatan through the website as well.

### MUSRENBANG at Kecamatan Bulak and Semampir

As Kelurahan Kenjeran is located at Kecamatan Bulak, then Kecamatan Musrenbang was at Bulak as well as Semampir. The condition of Bulak Musrenbang was basically typical at any other Kecamatan Musrenbang in Surabaya. Kelurahan representatives had to attend the musrenbang at kecamatan level. Each kecamatan in Surabaya had its own website as well to submit its musrenbang development priorities to the city of Surabaya online. All priorities and reserved proposal from each kelurahan were evaluated together during Musrenbang kecamatan. Some priorities were definitely agreed while some others were rejected. Some reserved proposal could be accommodated as this reserved became priorities at several other kelurahans. All the agreed proposals would later surveyed by relevant cities agencies (SKPD) to be executed next year.

Probably the biggest challenge within Kecamatan Musrenbang was the littlenumber of participants. Even the quality of participants in term of discussing and debating to goal priority development in each kelurahan was not strong. Hence the Musrenbang seemed a kind of forum to conclude decision without strong arguments. Example of musrenbang participations is shown in Table 1 at Kecamatan Semampir in the last two years (Azhar, 2015).

Tabel 1 Musrenbang participants at Kecamatan Semampir

Kelurahan	Number of RW	2014	2015
Pegirian	11	22 persons	23 persons
Ujung	14	27 persons	29 persons
Wonokusumo	16	39 persons	32 persons
Ampel	17	34 persons	37 persons
Sidotopo	12	29 persons	33 persons

According to PTPM (2006), RW representatives would be 3 persons (one would be woman) or 5 persons (2 would be women). Based on Table 1, it showed that the total participants in each Kelurahan were less than ideal. This was not to discuss the capacity of the representatives and gender representative.

### MUSRENBANG at Surabaya City

Within the city level then BAPPEKO was the one incharge to collect all online input from each kecamatan at Surabaya City. City Musrenbang was usually opened by the mayor which invited all the kecamatan representatives and other relevants invitations like NGO, academia, industries, etc. BAPPEKO and any agencies within the city would have their own meeting to determine which priorities were selected and surveyed. Each agency basically had its own program priorities and budged (top-down approach) which should be inline with musrenbang bottom-up approach. When decisions were taken, the the rejected proposals had to be infomed back to the kecamatan and kelurahan via the website as well. This kind of e-musrenbang was claimed by the city government to give better public service and transparency.

As there were different musrenbang levels like kelurahan, kecamatan, municipalities, provinces, and national level, the kelurahan musrenbang was the most important moment to discuss the issue of water sensitive city. As musrenbang kelurahan was opened by representative from kecamatan as also a moment to inform any top-down program from the central government, issueing water sensitive sensitive city would be a huge challenge. With the assumption that water sensitive city (WSC) is already the national program, WSC could not only be implemented through opening ceremony during kelurahan musrencang, but would be more like way of living. Isueing this during musrenbang opening, however, was also important for next or future development program. There should be other program from the city government to introduce water sensitive program via other institutes to inform basic human needs especially any related issues of water to bring this discussion at kelurahan musrenbang. Water sensitive issues had to be discussed during pre-musrenbang at RW level in Surabaya. Musrenbang had to be attended by women representatives in order to bring important issues regarding basic human needs like health, environement, water, and sanitation.

Summary of musrenbang in each government level is shown in Table 2.

Table 2. Summary of Musrenbang

Musrenbang	Results
Kelurahan	<ul style="list-style-type: none"> <li>• Input from RT and RW to online system.</li> <li>• Top-down meets the bottom-up approach during Musrenbang.</li> <li>• The kelurahan musrenbang is the most important moment to discuss the issue of water sensitive city.</li> </ul>
Kecamatan	<ul style="list-style-type: none"> <li>• Each sub-district in Surabaya had its own website to submit its musrenbang development priorities to the city of Surabaya online.</li> <li>• RW representatives would be 3 persons (one would be woman) or 5 persons (2 would be women).</li> </ul>
City	<ul style="list-style-type: none"> <li>• City Musrenbang is usually opened by the mayor which invites all the kecamatan representatives.</li> <li>• BAPPEKO and any agencies within the city have their own meeting to determine which priorities to be selected and surveyed.</li> </ul>

### MUSRENBANG at Jawa Timur Province

Provincial musrenbang is basically to continue the musrenbang results from municipalities in Jawa Timur. The musrenbang is also online. This musrenbang level is so important when there is development priorities which is cross border among municipalities. As water related issue is always cross border in inland area like Surabaya City and its neighbor regencies, then the issue of water sensitive cities become crucial, especially in the condition where surabaya water is coming from its neighbors regencies. Water security is becoming a crucial issue for city like Surabaya with about 3 millions population at area of 330 km<sup>2</sup> with rain intensity of 2200

mm/year. Although the issue of water supply, wastewater, and drainage is the issue of city centred, but the raw water supply of Surabaya is coming from its neighbors regencies. This is obvious that the issue of water sensitive city is so important for Surabaya. This issue must be raised to the provincial musrenbang of Jawa Timur; even though the issue of water in Surabaya was already mentioned in the regional planning of the Province.

### Water sensitive city concept through MUSRENBANG

Musrenbang is a forum to discuss development priorities in a bottom-up approach in Indonesia development system. As it is a bottom-up approach, then the priorities is started from the lowest of government level up to the highest. Within Surabaya City, then it started from the Kelurahan Government, which then to be continued to Sub-district, city, and eventually to provincial level of Jawa Timur Province.

Within this water sensitive city concept, then the top-down approach was not discussed as it was assumed that the government from the national to local level was already understood the concept of water sensitive city as it could be assumed that water sensitive city was already become the policy of the government, at least at Surabaya City Government. The crucial thing was then how water sensitive city became the topic of discussion at musrenbang kelurahan in Surabaya.

Musrenbang results would the development plan for next year. Next year development priorities should be obtained from the current year of Musrenbang. Hence the representatives of Musrenbang Kelurahan were very crucial. According to Soedjono *et al* (2017) and PTPM (2006), musrenbang had to be attended by women representatives in order to discuss at least human rights needs like education, health, and water-sanitation. Men representative would create men dominated forum which discussed man's local development world like development of roads, irrigation facilities, and other infrastructures rather than to discuss human right needs. This is to say that to discuss water sensitive city in Musrenbang Kelurahan is likely possible as long as the representatives raise the issue. Again, this is to say that water sensitive city concept must relates to daily activities of communities. The concept of water sensitive city is not merely knowledge; it must be attitude and way of live of communities. Then the main issue would be how to bring the issue

of water sensitive city to be widely well known by public.

## CONCLUSIONS

Musrenbang kelurahan was a coordination forum basically between the Government as represented by the Kelurahan Government and the communities. On one hand, the Government was mainly using a top-down approach to implement its development targets. The communities, on the other hand, proposed development priorities they need in a bottom-up approach. As it was assumed that the concept of water sensitive city was already understood by the government from the central down to the kelurahan level, then the community representatives who attended the musrenbang kelurahan were very crucial to come to a water sensitive city discussion. These representatives had to understand well about the water sensitive city. This would be far beyond ideal as the representatives in the beginning were not women representation. It was a male dominated forum while basic human right were not discussed. Then the concept water sensitive city would not be discussed in the musrenbang forum. The concept of water sensitive city to be discussed in the musrenbang forum, however, was possible as long as the proposal from the communities must propose anything related to water sensitive city. This to say that the communities must fully understand the concept of water sensitive city. Water sensitive is not enough to be only taught as concept, it must be attitude of communities on their daily live to bring the city robust for water related issues.

## REFERENCES

- [1] Azhar, F. 2015. Partisipasi masyarakat dalam musyawarah perencanaan pembangunan (musrenbang) di Kelurahan Pegirian Kecamatan Semampir Kota Surabaya. *Kebijakan dan Manajemen Publik*, 3 (2), pp: 63-70.
- [2] Brown, R., Keath, N., Wong, T. 2008. Transitioning to water sensitive cities: historical, current, and future transition states. *11<sup>th</sup> international conference on urban drainage, Edinburgh, Scotland, UK*.
- [3] Brown, R., Keath, N., and Wong, T. 2009. Urban water management in cities: historical, current, and future regimes. *Water sciences & technology*, 59, pp: 847-855.
- [4] Folke, C. 2006. Resilience: the emergence of a perspective for social-ecological system analysis. *Glob. Environ. Change*, 16 (3), pp: 253-267.
- [5] <http://bapekko.surabaya.go.id/musrenbang> 2017.
- [6] Lundqvist, J., Turton, A., and Narain, S. 2001. Social, institutional, and regulatory issues. In: Maksimovic, C. and Tejada-Gulbert, J.A. *frontiers in urban water management: deadlock or hope*. IWA Publishing, London, pp: 344-398.
- [7] Peraturan Menteri Dalam Negeri Nomor 54 Tahun 2010 tentang Tahapan, Tata Cara Penyusunan, Pengendalian dan Evaluasi Pelaksanaan Rencana Pembangunan Daerah.
- [8] Petunjuk Teknis Penyelenggaraan Musrenbang (PTPM) Tahun 2006
- [9] Putri, N., P. 2015. Studi Eksplorasi Tentang Variabel Pendukung Keberhasilan Aplikasi Sistem E-Musrenbang di Bappeko Surabaya. *Kebijakan dan Manajemen Publik*, 3 (3), pp: 109-122.
- [10] Rahman, R. and Soedjono, E. S. 2016. Study on achieving sanitation governance through musrenbang mechanism in probolinggo city. *Joint workshop global engineer in asia*. 25-30 July 2016, King Mongkuts University of Technology Thonbur, Bangkok, Thailand.
- [11] Soedjono, E., Rahman, R., Wijaya, W., Fitriani, N., 2017. Study on Musrenbang Mechanism to Promote Sanitation. Environmental Engineering Department, Institut Teknologi Sepuluh Nopember, Surabaya (unpublished)
- [12] Undang-undang Nomor 25 Tahun 2004 tentang Sistem Perencanaan Pembangunan Nasional.
- [13] Undang-undang Nomor 23 Tahun 2014 tentang Pemerintahan Daerah.
- [14] Moerwanto, A. S., 2011. Strategi Penelitian dan Pengembangan Sumber Daya Air dalam mendukung Pengelolaan Sumber Daya Air berkelanjutan. Pusat Litbang Sumber Daya Air, Badan Penelitian dan Pengembangan Kementerian Pekerjaan Umum.
- [15] Wong, T.H.F., and Brown, R.R. 2009. The water sensitive city: principle for practice. *Water science & technology-WST*, 60 (3), pp: 673-682.

## THE STUDY ON MITIGATION METHOD OF BEACH EROSION USING THE CORAL CELLS

Sang Kil Park<sup>1</sup>, Hong Bum Park<sup>2</sup>, Kyeong Mo Lim<sup>3</sup>

<sup>1</sup>Department of Civil Engineering Pusan National University, <sup>2</sup>Busan Metro-City Hall

### ABSTRACT

Recently, an artificial submerged breakwater method has been installing to prevent the loss of shoreline at everywhere. Artificial submerged breakwater is made to minimize the loss of sand nourishment of beach erosion. For this reason, submerged breakwater has been indiscriminately constructed that is planned throughout the country. Despite of its purpose to keep the shoreline of the beach, it has a quite a few problems. In addition, the purpose of utilizing the space of the marine leisure users does not like that because of the disconnection of the sea using sea space. Therefore, in this study, we propose to develop a economical method of Coral cell model that can mitigate degree rate of beach erosion and improve costal environments without installing the submerged breakwater for the maintenance. In the one-dimensional topography variations, hydraulic model experiments by measurement of residual rate of nourishment sand and water quality, it demonstrated the effectiveness of prevention of loss of nourishment sand and improvement of water quality.

*Keywords: Nourishment Sand, Water Quality, Mitigation of Beach Erosion, Residual Rate of Nourishment Sand, Coral-cell Model*

### INTRODUCTION

Coastal erosion due to climate change is one of the world's worst disasters. In order to prevent this, we are indiscriminately installing submerged breakwater, ignoring use and environment of the coast. In Korea, a plan to minimize the erosion of shoreline was implemented by conducting artificial nourishment on the coast. At the center of the submerged breakwater, the deposition occurs, in contrast, both ends erode. This phenomenon causes the shoreline to be cusped, which not only provides inconvenience to the visitors, but also generates strong rip current and causes safety accidents. Since access is prohibited to small boats and surfing users, it is inadequate for marine recreational facilities. We want to prevent the erosion of the designated Gwangan beaches at Busan City South Korea and utilize the sea level space as a space for marine leisure. In short speaking, we are trying to prevent erosion by installing Coral cells on the erosion coasts. This method is to capture the nourishment sand with the Coral cells pockets and retain the nourishment sand in the pockets. The field installation method is to install Coral cells of a certain size on a wide and long underwater sea bottom. Two dimension hydraulic experiments were carried out to investigate the effects of wave damping and prevention of sand outflow. Coral cells weakened the rip current and reduced the loss of nourishment sand. We directly measured the movement of the sand by continuous wave action for 20 hours. Nourishment sands flowed

out to the deep water until 8 hours, but after 8 hours the sea bottom topography was very stable. We defined the residual rate of nourishment sand as the amount of nourishment sand remaining in a certain space divided by the total amount of sand. Therefore, the purpose of this study is to propose a Coral cell method to prevent coastal erosion without installing a submerged breakwater for maintenance of the beaches.

### HYDRAULIC EXPERIMENT

#### Fixed Bed Hydraulic Experiment

In order to carry out the two dimension hydraulic model experiment, we used the regular and irregular wave generation tank in the coastal laboratory of the Civil Engineering Department at Pusan National University. Fig. 1 is simple illustration of a water wave tank and a wave device. The specification of the wave tank is shown in Fig. 1, the length is 22.5m, height is 1.0m, width is 0.6m. Fig. 1 is the position of the wave gauge after installing the Coral cell. The wave height was measured at the required point to observe the effect of the wave reduction. Fig.1's 5<sup>th</sup> wave gauge is the point where the incident wave is measured, 7<sup>th</sup> wave gauge measured wave time series at nature slope where the Coral cell is not installed, and 8<sup>th</sup> wave gauge measured wave time series at the slope where the Coral cell is installed. Furthermore, the 7<sup>th</sup> and 8<sup>th</sup> wave gauges measured wave time series in which incident waves and reflected waves

are synthesized at the same depth. In order to check the wave attenuation state caused by the Coral cell, we observed wave series at slope behind the Coral cell. The size of the Coral cell used in the movable bed hydraulic experiments (the size of the lower sand capture and the upper wave damp device of the Coral cell) is 3 cm pocket cell (Pocket cell) and 3 cm ripple cell that forms complex structure. The shape of the Coral cell is circular type with a height of 6cm and a width of 3cm.

### Manufacture of Subsea Bottom Slope

Sea bottom slope without Coral cell was constructed by setting natural beaches with 1/10 slope. The subsea bottom slope with Coral cell was produced as an 1/10 erosion type of artificial subsea bottom slope. The natural bottom slope without Coral cell was made of standard grain size sand and the depth of the sandy beaches was made from 15cm to 26cm deep. Of course, a 60cm water tank was separated by an acrylic plate, 29 cm and 29 cm, in the same way as the fixed bed. The natural erosion coast was made on the glass surface, and Coral cell was installed at the center of the sea bottom slope of inside the glass surface. Both beaches were constructed to allow erosion of the shoreline by incident waves.

### Irregular Waves of Time Series Group

The time series of irregular wave used in the mobile bed experiment is as same as the time series analyzed in fixed bed model. The incident wave height is the 14cm of significant wave height, the period of wave is 0.98 sec of significant waves period, and the wave steepness is 0.093.

In mobile bed experiments, we examined the topography of beaches elapsed time by using irregular waves. In order to verify the occurrence of the sand bars of beaches, Nayak  $H_{1/3}/d_{50} = 280$  was used as an evaluation criterion of erosion and deposit.[1] Iwatani and Noda's sand bar occurrence limit formula was used as an evaluation criterion for sandy beaches, and this coastal sandy beach belongs to Johnson's storm beach.[2][3] The purpose of the mobile bed experiment is to change the erosion coast to deposit coast. In other words, the nourishment sand did not flow into the deep sea by Coral cell but was collected in the pocket of Coral cell. In this experiment, we can see that the erosion coast changes to a stable coast. This phenomenon is thought to be the result of wave height attenuation by Coral cells in the fixed bed experiment. Experimental progress of the mobile bed experiment is to verify the variation of topography according to elapsed time. In the mobile bed experiment, we focused on the variation of topography of sea bottom rather than the trend of the wave experiment. The experimental

purpose of Cases1 was to perform a hydraulic experiment to test the pocket function of Coral cell. In this case, the topographic variation is summarized as a photograph, and the capture function of the topographic variation for the Coral cell is confirmed in the hydraulic experiment. The purpose of Cases 2 is to compare and analyze the topographic variability for Coral cell installation and without installation. Bottom topography of variation elapsed time was measured at intervals of 4 hours. We tried to verify the two functions of the Coral cell, the capture rate and the sea bottom profile rate. Table 1 summarizes the conditions of the mobile bed hydraulic experiment.

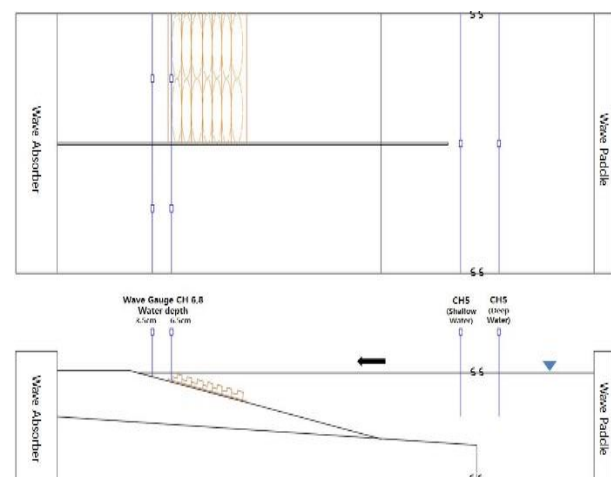


Fig. 1 Hydraulic experiment device

Table 1 Condition of mobile bed experiment

Case	Coral cell	Measuring Time	Observation
Case1	6cm pocket 6cm ripple	Every 2 hours total 8 hours	H.W.L. Height of sand
Case2	3cm pocket 3cm ripple	Every 4 hours (total 20 hours passed)	

### Model of Topographic Bed and Coral cell Installation

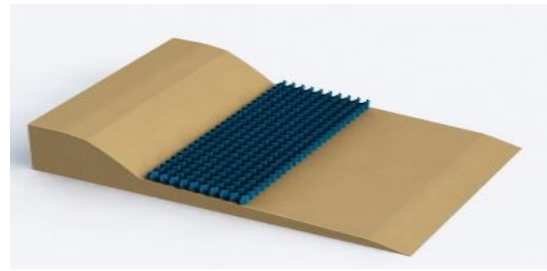
As mentioned above, table 1 shows the conditions of the mobile bed hydraulic experiment, and Case 1 and Case 2 have clearly different purpose for the mobile bed hydraulic experiment. For Case 2, we decided to measure the topography

variation and the nourishment sand of capture rate according to the elapsed time of hydraulic experiment. The purpose of estimating the capture rate is that nourishment sand does not flow into the deep sea by Coral cell but remains in the pocket to maintain stable beach of topography. Generally, the wave height is not measured in a two-dimensional mobile bed hydraulic model test. The geometric scale ratio was 1/20. Scale 1/20 is widely used for hydraulic model tests to show the reproducibility of the wave and sea bottom of topography variation. Fig. 2's (a) shows a natural beach with a constant sea bottom slope for stabilization, and (b) shows a Coral cell type installed on an eroded beach to prevent erosion. Of course, fig. 2 present the beaches made of hybrid type of Coral cell with a 3cm pocket and 3cm ripple. Fig. 3 is figure of the Coral cell with a nourishment sand capture and a wave attenuator. In this figure, the direction of the arrow indicates the direction of incident wave and the main direction of nourishment sand out flow.

Fig. 3's (a) is a 30mm pocket type, (b) is a hybrid type of 30mm pocket and 30 mm ripple. The pocket is designed to have an elliptical shape, and the ripple is designed to have a half elliptical shape. The largest 120mm pocket type and ripple type is actually designed to have a wave damping effect and a nourishment sand capture type. The pocket is designed to have an elliptical shape, and the ripple is designed to have a half elliptical shape. Coral cell was made in the petrochemical products that are not harmful to the environment. To be honest, the larger the Coral cell of the pocket and ripple, the greater the wave reduction and the nourishment sand of capture rate.

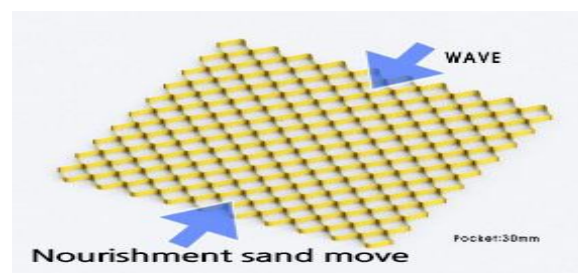


(a) Unstable beach form before coral cell installation

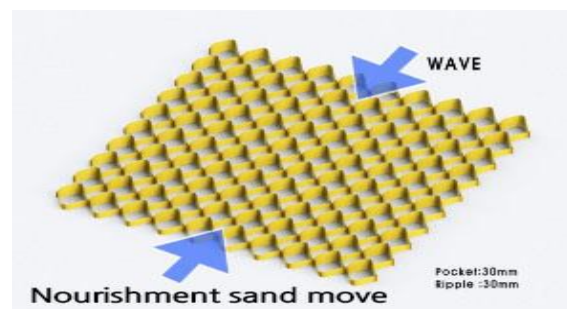


(b) Coral cell shape installed on erosion beach

Fig. 2 Beach with 3cm pocket and 3cm ripple of Coral cell



(a) 3cm pocket cell



(b) 3cm pocket and 3cm ripple cell

Fig. 3 Examples for cross-section of Coral cell

## EXPERIMENT ANALYSIS

### Situation of Nourishment Sand Movement by Coral cell

The mobile bed experiments were carried out to understand the movement of the nourishment sand in accordance with the elapsed time of the wave. Figure 4 shows the movement of the nourishment sand along with the elapsed time of wave after installing the Coral cell. In other words, we can see that nourishment sand is flowing into the Coral cell pocket and deposited. Fig. 4 shows the state in



which the Coral cell is buried by the movement of the sand. This phenomenon shows that the nourishment sand flows into the pocket of Coral cell and accumulates as the shoreline erode. The red line is the topography of original sea bottom.

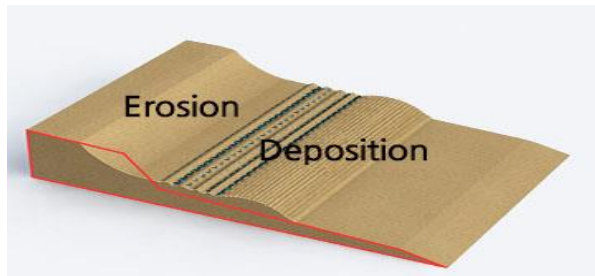


Fig. 4 View of bottom variation with Coral cell

Table 2 Wave condition for Pocket 3cm and ripple 3cm Coral cell

Elapse time (hours)	Maximum wave height			Significant wave height		
	deep sea	no cell	with cell	deep sea	no cell	with cell
4	26.4	7.2	6.5	14.6	4.3	4.1
8	26.8	7.5	7.0	15.7	4.5	4.3
12	19.0	5.6	5.0	15.7	5.3	4.3
16	26.9	7.2	6.9	15.4	4.5	4.0
20	25.8	7.0	6.8	14.7	4.8	4.0
Mean	25.0	6.9	6.4	15.2	4.7	4.2

#### Change of Sea Bottom Topography by Coral cell

Fig. 5 shows the sea bottom topography of variation according to elapsed time of wave action. The vertical axis is depth of the sand as unit of mm, and the horizontal axis is the length of location at each point as unit of which is indicating the change of water depth. In the figure, the upper side of 600mm is the point with the Coral cell and the lower side between 0mm ~ 600mm is the point without the installation of Coral cell. The thin black lines is subsea fixed slope, the red line is the sand depth of the initial sea bottom topography. The black line is the nourishment sand surface after elapsed time of 4 hours, the green line is the nourishment sand surface after elapsed time of 8

hours. The yellow line is nourishment sand surface after elapsed time of 12 hours, the blue line is the nourishment sand surface after elapsed time of 16 hours, and the pale purple line shows nourishment sand surface after elapsed time of 20 hours. In this picture, we can see three phenomena. Firstly, the installation of Coral cell can prevent the nourishment sand loss more than a certain value. Secondly, the nourishment sand on the steep slope can be collected in Coral cell to increase the residual rate, the sand that flows into the deep sea area flows into the pocket of Coral cell again and is deposited from the deep water depth of the Coral cell. Thirdly, the nourishment sand that flows out into the deep water area flows back into the Coral cell and accumulates from the deepest point.

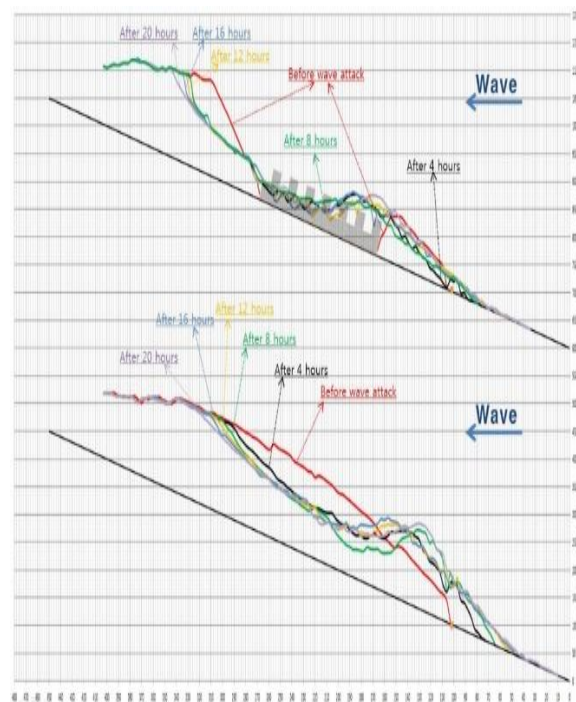


Fig. 5 View of bottom variation by elapsed time

#### Outflow Nourishment Sand Volume and Residual Amount by Coral cell

Fig. 5 is a figure for calculating the out flow and residual amount of nourishment sand. In order to calculate the amount of sand discharged into the deep sea, we assume that the cross-sectional shape of sand is triangular and rectangular. After calculating the cross-sectional area of the side surface in these shapes, the total nourishment sand volume was calculated by multiplying the width. Comparing the obtained values and the measured sand amount, it corresponded up to 95%. Table 3 and Table 4 summarize the residual amount or capture amount and outflow rate.

Table 3 Movement volume of nourishment sand before

Coral cell of installation accord to each depth

Category	Elapse time for wave generation(minute)				
	240	480	720	960	1200
Erosion quantity of beach	121.8	132.0	166.0	183.3	208.8
Sediment quantity of transition	102.5	111.4	101.2	122.4	139.2
Outflow quantity at deep sea	19.3	20.6	34.8	60.9	69.6

Table 4 Movement volume of nourishment sand after Coralcell of installation accord to each depth

Category	Elapsed time for wave generation(minute)				
	240	480	720	960	1200
Erosion quantity of Case	37.6	39.4	46.4	52.2	57.9
Sediment quantity of transition zone	33.5	32.2	37.0	39.9	43.4
Outflow quantity at deep sea	4.1	7.3	9.4	12.3	14.5

### Outflow Rate and Residual Rate by Coral cell

As a result, the residual amount of nourishment sand was summarized as shown in Table 5.

Table 5 Residual amount of natural beach with Coral cell

Category	Elapse time(minutes)				
	240	480	720	960	1200
Erosion quantity without	121.8	132.0	136.0	183.3	208.8
Erosion quantity with cell	4.1	7.3	9.4	12.3	14.5
Outflow rate	3.3	5.5	6.9	6.7	6.9
Residual rate	96.7	94.5	93.1	93.3	93.1

By installing coral cell, most of nourishment sand is

caught in Coral cell. In this case, the residual rate and the capture rate were defined to be the same mean. We found that installing the Coral cells can reliably capture the nourishment sand that flows into the deep water. Therefore, the total amount of sand outflow  $V_c$  which eroded by the wave, the elapsed time  $t$ , and the amount of deep water outflow  $\Delta V$  were calculated by following equation (1).

$$R = \frac{V_o - \Delta V}{V_o} \times 100(\%) \quad (1)$$

The amount of sand outflow rate and residual rate is illustrated from Fig.6 to Fig.10. Fig.6 shows the outflow of nourishment sand along the depth before the Coral cell installation

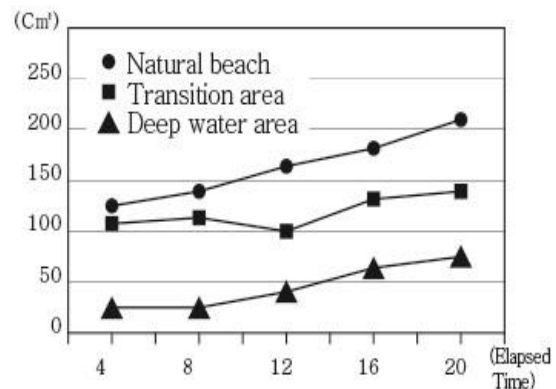


Fig. 6 Nourishment sand outflow amount with water depth before Coral cell installation

In this figure, we can see that the outflow of nourishment sand is very serious on the natural coast. Outflow phenomenon of nourishment sand is most severe in the surf zone.

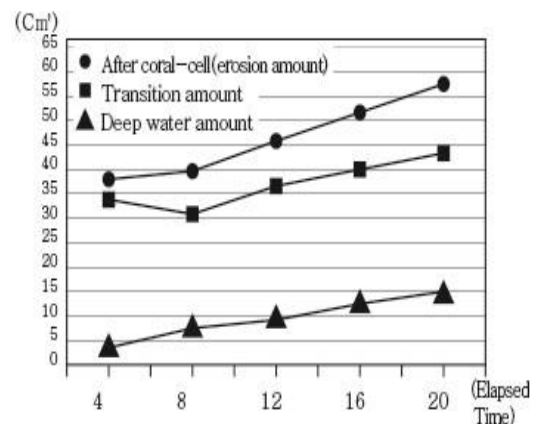


Fig. 7 Outflow quantity after installation of Coral cell

Fig. 7 shows the nourishment sand amount after coral cell installation. In this figure, we found that if the coral cell was installed on the sea bottom slope, the outflow amount would be very small. That is to say, Coral cells have a great effect of preventing outflow of nourishment sand.

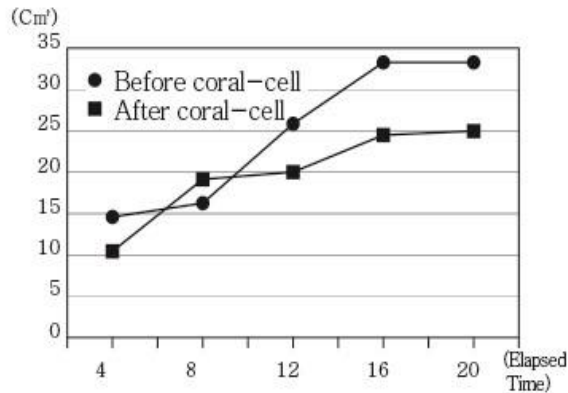


Fig. 8 Outflow difference between before and after Coral cell at deep water

Fig. 8 compares with outflow quantity of the nourishment sand for before and after the installation of the Coral cell accord to elapsed time at deep water. The tendency of the nourishment sand outflow is larger as the elapsed time of the wave becomes longer.

Fig. 9 shows the residual amount of nourishment sand for before and after the installation of Coral cell by equation (1). The residual amount of nourishment sand is increasing as the wave action elapsed time becomes longer.

Therefore, in this figure, we can say that installing a Coral cell is much more efficient than not installing it.

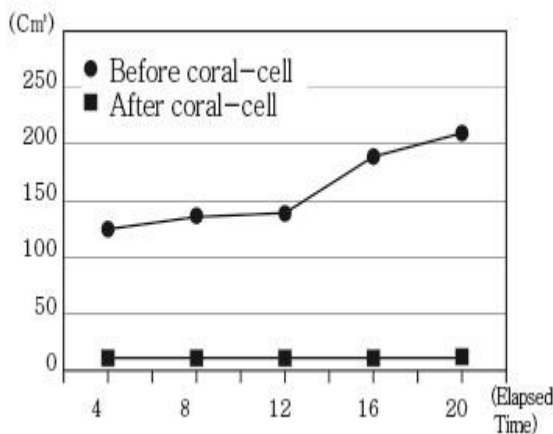


Fig. 9 Residual quantity of nourishment sand Coral cell for before and after installation

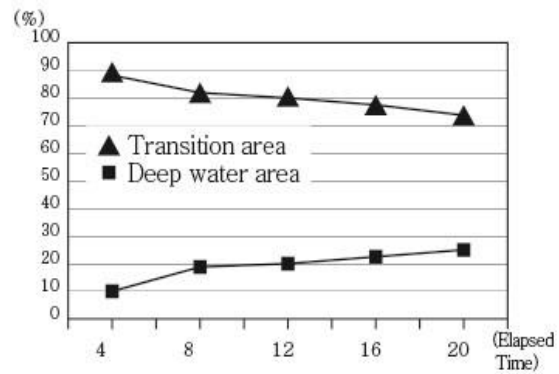


Fig. 10 Residual rate of sand under Coral cell

Fig. 9 shows the residual rate of nourishment sand for before and after the installation of Coral cell by equation (1). The residual rate in the transition depth is much larger than the residual rate in the deep water.

## CONCLUSION

It is a very difficult task to stabilize the coast by conducting nourishment sand on the erosive natural beach. The purpose of this study is to investigate the maintenance strategies to enlarge availability for artificial nourishment sand in Gwangsanri beach in Busan, South Korea. In other words, this research proposed an erosion prevention method using Coral cell as a customized method. As a results of the two dimensional hydraulic experimental model, this method was able to raise the residual rate of nourishment sand up to 70%. It is highly expected to have an economic value since its high residual rate.

## ACKNOWLEDGEMENT

This researches was supported by research fund of P.N.U. Small Business Incubator Center, Han Ocean Co.,Ltd and Green Land & Water Management Research Institute.

## REFERENCE

- [1] Nayak IV, "Equilibrium profiles of model beaches", Proc. 12<sup>th</sup> Int. Conf. on Coastal Eng., 1971 pp. 1321-1339.
- [2] Noda H, "Initial movement of sea bottom sand inception and generation sand ripples due to waves", Proc. 11<sup>th</sup> Conf. on Coastal Eng. in Japan, 1964, pp. 135-141.
- [3] Iwagaki Y, "Laboratory study of scale effects in two dimensional beach process", Proc. 8<sup>th</sup> Int. Conf. on Coastal Eng., 1963, pp. 194-210.

# THE DESCRIPTION OF LIGHTING ENVIRONMENTAL ON THE URBAN STREET

Shuto Takeuchi<sup>1</sup>, Kazunari Tanaka<sup>2</sup> and Shin Yoshikawa<sup>3</sup>

<sup>1</sup> Engineering, Osaka Institute of Technology, Japan; <sup>2</sup> Osaka Institute of Technology, Japan

## ABSTRACT

The purpose of this study is to visualize spatial illuminance for the street space at night. In the street space, it is necessary to consider the illumination effect in three dimensions, such as the direction and size of the light, as well as brightness and luminance of the surface. For example, depending on the brightness of the pedestrian's feet, chest, face, or the difference in the height of the light source, it is conceivable that the place or movement of people walking will affect the lighting. By grasping the characteristics of the light environment of each street, it is possible to confirm the role and function of the street. Furthermore, this information can be used to support the lighting design for streets at night-time. When designing a city, we should consider not only the implications for day-time, but also night-time. I will analyze the lighting environment of the street space utilizing three-dimension representation visuals from various angles.

*Keywords: Lightning Environmental, Urban Street, Calculation Method, Flat Surface Sources*

## INTRODUCTION

In Japan, the landscape law was enforced in 2004 to preserve, protect and create unique landscapes. Furthermore, night-time street lighting for pedestrians has increased, this includes the distance of streetlights by the number of pedestrians and soft light sources such as sodium lamps, and lighting for traffic direction has increased.

The influence of the light environment on pedestrian behavior and psychology in the night-time outdoor space is considerable. Various kinds of outdoor light exists such as; light for safety purposes to brighten a road like a street lamps, lights for visual purposes such as outdoor advertisements or signs, and indirect light leaking from building interiors etc.

Illuminating light which is effectively applied to an object such as light up is considered as an element for creating a nighttime landscape. For outdoor light, various kinds of light such as light for safety to brighten a road like a streetlight, light for making visually conspicuous such as an outdoor advertisement, light leaking from the indoor space exists. In addition, the light which is lit for advertisement such as a signboard light is being considered as a viewpoint of how easily it is perceived and as a factor interfering with a calm landscape.

In the commercial areas, stores and shops have their own unique designs to attract customers. Interior lighting is important because it is inviting and welcoming for potential customers to enter the building; signage also gives visual appeal. It is

thought that the lighting gives each street unique characteristics at night. In this research, attention is focused on the features of such streets, collection of basic data for surveying and analysis, and explanation of the results.

## PURPOSE

In this research, we aim to grasp the lighting environment in urban spaces and to concretize the method of describing and expressing it. This is done by trying to capture the night-time image in the street from the illuminance calculation point of view. In past studies, research on spatial illuminance in an indoor space and two-dimensional illuminance calculation in an outdoor space has been conducted, but there are limited studies for three-dimensional outdoor space. By expressing and grasping the spatial illuminance in the street space, we can see the personality and features of each street[1]. Furthermore, by describing and analyzing the light environment at night, it leads to the effective design and maintenance of lighting for urban streets.

## METHOD

A special light receiver is required that can measure spherical illuminance, hemispheric surface illuminance, cylindrical surface illuminance and half cylindrical surface illuminance. Furthermore, as a method of substituting the illuminance meter for ordinary planar illuminance measurement, a method of averaging measured values of illuminance in six directions or four directions is recommended. When



considering the light hitting a certain point in space, light is irradiated not only from one direction but from many directions. Therefore, it is difficult to accurately measure illuminance on-site (outside) from a single light source because there is light from various sources interfering. Taking this into account, the author opts to use a model in order to isolate a single light source, and measure the distance. This is done by calculating the illuminance corresponding to a box placed virtually in the street space and converted to spherical illuminance. As a result, it is possible to simply depict the nighttime light environment. Finally, the results of the lighting of each street are expressed on a map, creating a comprehensive night-time urban street map.

### Target area

Multiple factors were taken into consideration in choosing a target area such as the various lighting sources and features. The author chose Osaka-shi Chuo-ku, as the night-time pedestrian traffic here was also taken into consideration.



Fig.1 Chuo-ku, Osaka

### Calculation process

To calculate illuminance for this study; 1) Create a simple street model and measure the distance to the light source and 2) using illuminance calculation, obtain the value of the illuminance corresponding to the virtually rendered surface.

Previous studies analyzed the calculation formula of spatial illuminance from a planar light source of shapes and every tilted state using the same method; as in the case of horizontal illuminance by using an analytical system and applying the mediated perspective model[2].

In the mediated perspective model, in order to apply it to a stereoscopic light source such as an annular one, a perspective figure viewed from the calculation point is obtained on the screen, the perspective figure is regarded as a flat light source, and a deformation formula of boundary integration is applied. This can be applied to a flat light source

of arbitrary shape and arbitrary inclination via the method of obtaining horizontal plane illuminance, and can be applied to the calculation of various spatial illuminances.

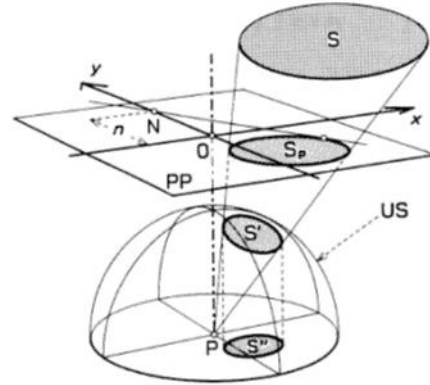


Fig. 2 Picture plane for via-perspective method

In this research, Autodesk's AutoCAD is used to create a simple model to portray the position of the light source. We then placed a rectangular parallelepiped 1.5 m in height vertically in the center of the target street, with pedestrians 1.8 m away on each side. Next, we measure the distance between the rectangular parallelepiped and the light source and use it for calculating illuminance.

### Calculation of hemispheric surface illuminance from horizontal plane light.

If the light source direction is vertical, the hemispheric surface illuminance of the horizontal surface light source can be obtained.

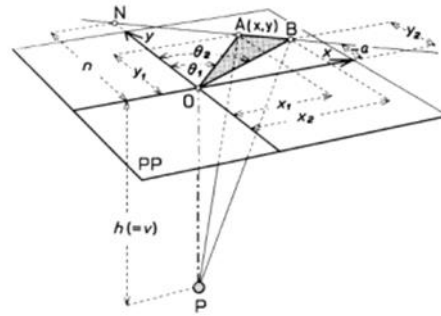


Fig.3 Spherical illuminance by means of a horizontal surface source

$$E_{hs} = \frac{L}{4} \int_{x_1}^{x_2} \left\{ \left( 1 - \frac{h}{\sqrt{x^2 + y^2 + h^2}} \right) + \frac{y}{2\sqrt{x^2 + y^2}} (A) \right\} \frac{n}{x^2 + y^2} dx \quad (1)$$

For example,

$$(A) = \tan^{-1} \frac{\sqrt{x^2 + y^2}}{h} - \frac{h\sqrt{x^2 + y^2}}{x^2 + y^2 + h^2} \quad (2)$$

### Half cylindrical surface illuminance from horizontal plane light.

In this calculation method, the light irradiated from a lateral direction hits the whole semi-cylindrical surface uniformly. The semi-cylindrical surface illuminance “Esc” is the average value of the vertical illuminance distributed on the small semi-cylindrical surface on the side facing the observation direction. It does not include illuminance distributed on top and bottom surfaces of the cylinder.

$$E_{sc} = \frac{L}{2\pi} \int_{x_1}^{x_2} \left(1 + \frac{y}{\sqrt{x^2+y^2}}\right) (A) \frac{n}{x^2+y^2} dx \quad (3)$$

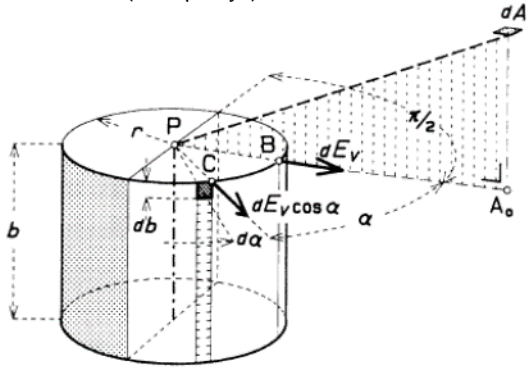


Fig.4 illuminated range on the minute cylindrical surface

### Relationship between the illumination range and observation range on a small cylindrical surface

$$E_s = \frac{L}{4\pi} \int_{x_1}^{x_2} \frac{y}{\sqrt{x^2+y^2+g^2}} * \frac{g}{x^2+g^2} dx \quad (4)$$

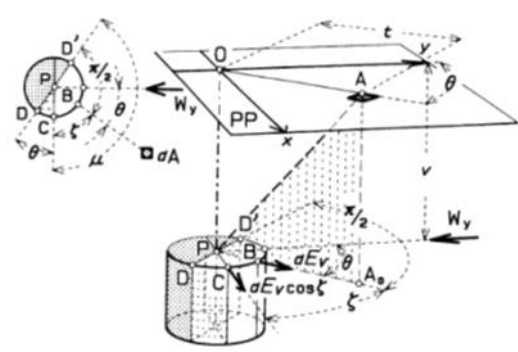


Fig.5 Geometrical relationship between an illuminated range and an observation range on a minute cylindrical surface.

The Fig.6 shows the output calculated by inputting the value of the target area into the formula.

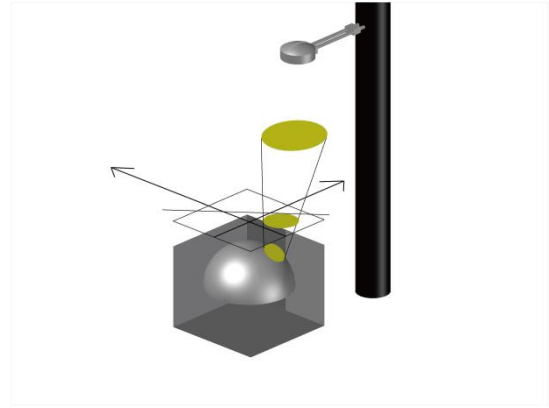


Fig.6 the output

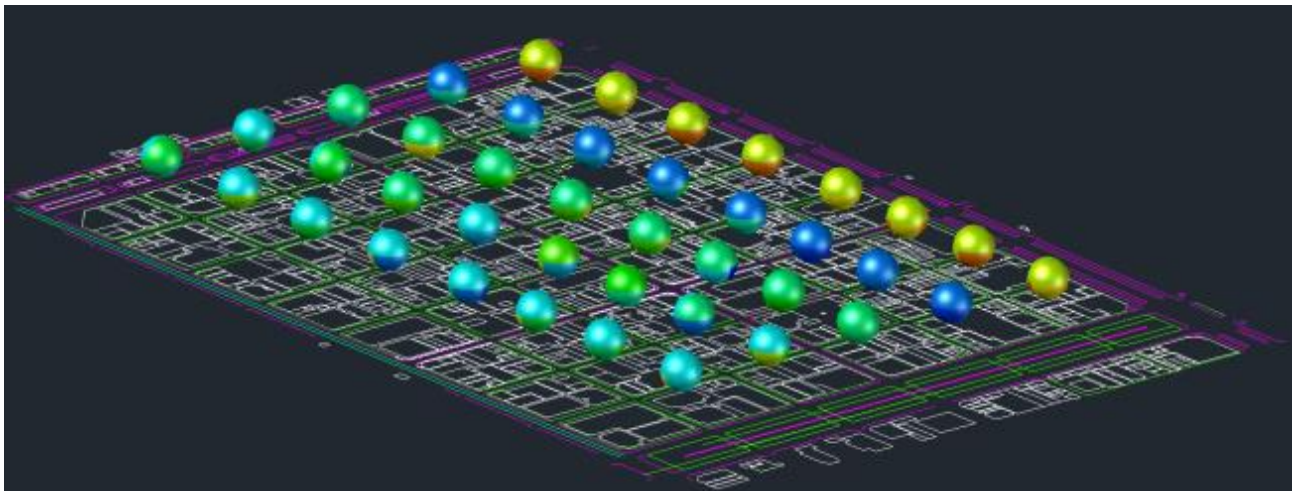


Fig.7 bird's-eye view

Fig.7 shows a depiction of the target area in a similar manner from a bird's-eye view. Analysis of streets by using simplified images as representations of the night-time landscape.

## CONCLUSION

In this research, as a means of better grasping the lighting environment in urban streets, we studied about modeling the light sources. In this example, we calculated the planar light source, but to get a more accurate analyzation, calculating the three-dimensional light source should be considered. Furthermore, we will also consider aspects such as appropriate shapes and sizes for modeling.

## References

- [1] Kamisaka Sho, "Calculation Method for Spacial Illuminances by means of Flat Surface Sources and Consideration for Rough Calculating Methods" J.Illum. Engng. Inst. Jpn., Vol.77 No.6 1993
  
- [2]Shuto Takeuchi, "Analysis on the Lighting Environment of the Urban Street Space" The 12th Conference for Architecture and Infrastructure Environment, JSCE. Jpn., No.12 2016



## **SOCIAL AND ENVIRONMENTAL RESPONSIBILITY IN DEVELOPING COUNTRIES: A THEORETICAL APPROACH OF REGULATION**

<sup>1</sup>Lindrianasari, <sup>2</sup>Mahatma Kufepaksi, <sup>3</sup>Yuztitya Asmaranti, and <sup>4</sup>Agrianti Komalasari,  
<sup>1</sup>Economics and Business Faculty, <sup>2</sup>Universitas Lampung, Indonesia

### **ABSTRACT**

This study aims to analyze and describe the social and environmental responsibility of companies listed on the stock exchange in three developing countries, namely Indonesia, Malaysia, and Thailand, before and after 2007. In 2007 chosen as the cut-off year of observation as we find in each country was issued significant environmental policy. By doing a differential test on a sample of 24.626 independent firms / years, the study found that four variables used in this study, overall showed a significant difference. Environmental costs, disclosure of environmental, social disclosure, and ESG that observed in three developing countries has increased significantly after 2007. However, we did not find significant increase in environmental costs in Indonesia. The findings of this study indicate that the theory of regulation, particularly for public interest theory, can explain clearly the reasons why the four variables research has increased after the environmental regulations issued.

*Keywords: Environmental accounting, accounting and social disclosure, developing countries, regulation.*

### **INTRODUCTION**

Scheme of government policies related to the environment in Indonesia has been demonstrated with the exclusion of some policies. The government policy was issued as Republic Act No. 17 Year 2004 on the Kyoto Protocol on Framework Convention of the United Nations on Climate Change; Republic Act No. 40 Year 2007 regarding Limited Liability Company; and Government Regulation No. 47 Year 2012 on Social and Environmental Responsibility (Social and Environmental Responsibility - TJSL) Company Limited. Implementation of Corporate Social Responsibility (CSR) in Indonesia has been strengthened and reinforced by the issuance of Government Regulation No. 47 Year 2012.

In other countries, Malaysia and Thailand, we also found that environmental policy was issued in 2007. The findings provide strong reasons for us to determine that 2007 be the year of the revival environmental issues in three developing countries, and then in 2007 became the cut-off on this research. This study aims to analyze and describe the social and environmental responsibility of companies listed on the stock exchanges of developing countries. The three countries intended are Indonesia, Malaysia and Thailand.

The study found that the cost of the environment, disclosure of environmental, social disclosure, and ESG observations in the three countries has increased significantly after 2007. Only in Indonesia we found no significant increase in environmental costs after 2007. The findings of this study indicate that the theory of regulation,

particularly for public interest theory, can explain clearly the reasons why the four variables research has increased after the environmental regulations issued.

### **LITERATURE REVIEW AND HYPOTHESIS DEVELOPMENT**

Theory of legitimacy and stakeholder theory is regarded as an influential theory in the domain of social and environmental accounting research [5]. In our previous studies, we also have used both of the theories ([1], [2], [3]). All of the above study refers to the opinion of [4] which explains that the theory of legitimacy and stakeholder theory are two theories that explain each other (overlapping theories). Both theories have differences in the level of perception and settlement, and not the conflicting theories. In other words, legitimacy theory and stakeholder theory can both explain and predict the relationship between the organization and the social environment, but with different approaches and decomposition [5]. However, both have profound benefits in providing understanding of the social and environmental accounting research.

The theory of legitimacy (introduced by Lindblom and Suchman) focus on the value system of society [(6), (7)]. So that the legitimacy theory predicts if the value system of an organization are congruent with the value system in the society around it, then the organization will survive. Therefore, organizations must be able to meet the expectations and subsequent revenues from the public. Meanwhile, stakeholder theory (introduced by R.

Edward Freeman, (see [8]) focused on the relationship between the organization and various stakeholders that form (affect) the environment. Stakeholder theory explains that each group of stakeholders has not the same impact on the environment. On the other hand, each stakeholder expectations are often at odds with each other [5].

This study re-examine whether there is a relationship regulations issued by the government on the actions of companies in environmental conservation. Corporate response that reflected their actions show their firm adherence to the regulator [9]. Although some have been inadequate disclosure quality and only limited social contract to meet the legitimacy to people around the company (Deegan, 2002; and O'Dwyer, 2003 in [1]). But the others research found a significant relationship between the regulations issued by the government to accountability on the environment by companies in Indonesia ([1], [2]). The findings of those previous studies indicates that the regulations issued by the government is very effective in encouraging compliance of company. If in earlier studies we have conducted investigations of companies in Indonesia related to compliance with the policies issued in Indonesia, then this study will conduct an empirical overview of the three developing countries which are relatively have similar cultures and economies, namely Indonesia, Malaysia and Thailand.

The management companies that do not have the basic laws of the government can run but without a clear direction [10]. Research conducted by Börzel and Risse also explained the importance of the role of a state in the making of rules and policies regarding corporate governance. Mandatory action in protecting the environment by the company can be seen as a gesture to the government that it is time for the regulation of an integrated environment in all activities seriously formulated.

This would greatly support by the earlier study in voluntary action taken by the companies (Haufler 2001 in [11]). The research found that the rules issued by the government for an entity would increase the compliance of these entities is greater than ever before. From the above, we establish the following research questions as below:

**RQ: how adherence of companies in developing countries on government regulation of social and environmental responsibility.**

## RESEARCH METHODS

The object of this research is Indonesia, Malaysia and Thailand. The reason is that these countries are at a relatively similar economic level, and are in the same region. 2007 became a cut-off because of that year in each important country.

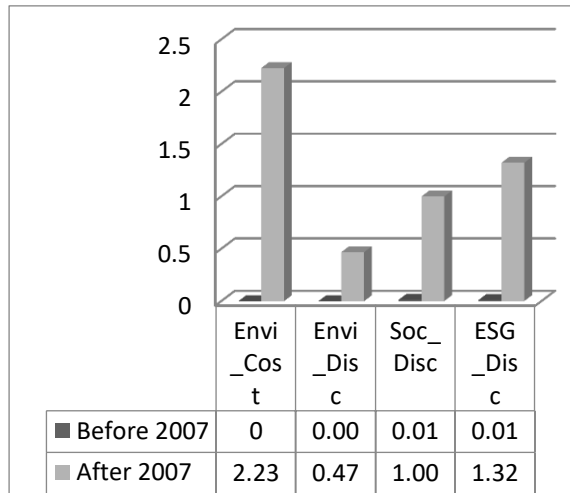
- a) Countries Indonesia issued Law No. 40 of 2007, which in Article 66 and Article 74 explained that companies are obliged to report on social and environmental activities of the company. This law is very revolutionary and very eagerly by the public.
- b) in 2007-2009 is the year where Malaysia issued a lot of environmental policies. Department of Environment, Ministry of Natural Resources and Environment (<http://www.doe.gov.my/eia/wp-content/uploads/2012/03/A-Guide-For-Investors1.pdf>).
- c) The Kingdom of Thailand passed the B.E.2550 Constitution in 2007. P This Constitution entitles communities to participate in the prevention and elimination of business acts that could damage natural resources and pollute the environment.

The data used is secondary data. Observations focused on the company's response on government policies related to social and environmental responsibility. Therefore, this study assesses how environmental performance before and after the issuance and promulgation of regulations related to the environment. The variables measured in this study are the environmental costs, the disclosure of environmental, social disclosure, and governance. Data obtained from Bloomberg database at Gadjah Mada University in 2016. Data were analyzed using Independent Sample test.

Data are obtained from Bloomberg database, the companies listed on the stock exchanges in Indonesia, Malaysia, and Thailand. The observation was conducted for 12 years ie period 2004-2015. The total sample is 24,626 years old. Table 1 shows the distribution of research samples.

## DISCUSSIONS AND ANALYSIS OF RESULTS

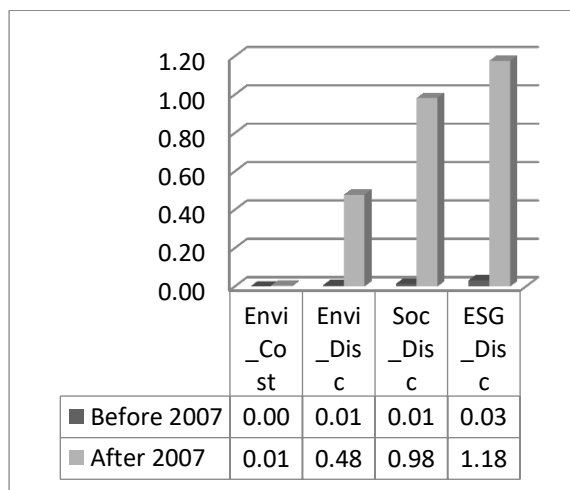
Figure 1 shows that before the Act No. 40 of 2007 was issued and applied in Indonesia, environmental and social performance in Indonesia is very low, even some variables worth null. But after it is issued and the enactment of Law No. 40 of 2007, environmental and social performance in Indonesia getting better, although there are still companies that do not respond properly government regulation. Nevertheless, it is generally seen that the regulations issued by the government have an impact on the preparation of the purpose of these regulations. This evidence also indicates that the regulations was issued related to this environment has been consistent with the public interest theory which predicts that the regulation should be made for the benefit of society



Source: Bloomberg, 2016.

Fig. 1 Environmental and Social Performance Before and After 2007 in Indonesia

The same condition also occurs in Malaysia and Thailand [see Fig. 2 and Fig. 3]. In the period prior to release and promulgation of regulations related to environmental and social performance of companies in each country do not show a good performance compared with after the enforcement of the regulations. From the three countries observed, changes in the allocation of environmental costs on average occurs in all countries, with the greatest increase occurred in Indonesia (relative to the value of the unit of measure) is from 0 before 2007 to 22270 after 2007. Next is Thailand, of the value

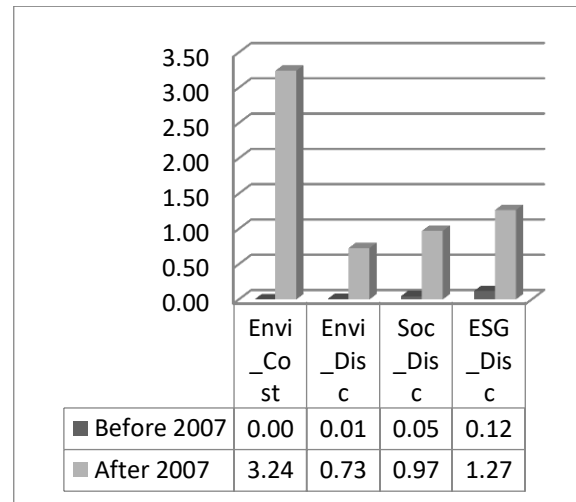


Source: Bloomberg, 2016.

Fig. 2 Environmental and Social Performance Before and After 2007 in Malaysia

To value environmental disclosure, Thailand experienced the greatest increase, from 0.0072 prior

to 2007, to 0.7278 after 2007. Meanwhile, Indonesia and Malaysia are in the same relative value changes. For social disclosure and disclosure of ESG, Indonesia showed the highest value of disclosure, then Malaysia and Thailand. However, the numbers change in each of these countries reached more than 95%.



Source: Bloomberg, 2016.

Fig. 3 Environmental and Social Performance Before and After 2007 in Thailand.

### Test of performance of Environmental, Social, and ESG

#### Environmental cost

Environmental costs are allocated in Indonesia, Malaysia, and Thailand on average increased from before and after it is issued and the enactment of regulations on the environment in these countries. From the test results of independent sample test found that there were significant differences in the allocation of environmental funds in Malaysia and Thailand, respectively at a significance level of 0.000 and 0.001. However, no significant differences were found for the allocation of environmental funds in Indonesia (P-value of 0.244) (see Table 1, Panel 1).

Investigations into the findings of the environmental cost allocation in Indonesia shows that no account name can be used to record and report the costs associated with managing an environmental company. The absence of the name of this account is suspected as the cause the level of lack environmental cost allocation found in the company's financial statements.

Table 1. Test of performance of Environmental, Social, and ESG

#### Panel 1. Environmental Costing

		<b>Sign.</b>	<b>F-value</b>	<b>t-value</b>
1	Thailand	0,001	10.956	-1.655
2	Malaysia	0,000	18.431	-2.144
3	Indonesia	0,244	1.357	-0.0585

---

Panel 2. Environmental Disclosure Score				
		<b>Sign.</b>	<b>F-value</b>	<b>t-value</b>
1	Thailand	0,000	128.646	-5.61
2	Malaysia	0,000	230.727	-7.545
3	Indonesia	0,000	123.284	-5.505

---

Panel 3. Social Disclosure Score				
		<b>Sign.</b>	<b>F-value</b>	<b>t-value</b>
1	Thailand	0,000	177.847	-6.561
2	Malaysia	0,000	336.522	-9.001
3	Indonesia	0,000	181.699	-6.617

---

Panel 4. Environmental, Social, and Governance Score				
		<b>Sign.</b>	<b>F-value</b>	<b>t-value</b>
1	Thailand	0,000	274.414	-8.117
2	Malaysia	0,000	533.08	-11.094
3	Indonesia	0,000	406.386	-9.786

#### *Environmental Disclosure Score*

Results of independent sample test showed a significant difference in the score disclosure of the company's concern the environment in Indonesia, Malaysia, and Thailand (see Table 1, Panel 2). Each level of significance obtained from the statistical test result is 0000 for all countries. Malaysia has a value F-value is higher (ie 230.727) compared to Thailand and Indonesia (which is 127.646 and 123.284).

#### *Social Disclosure Score*

On average, social disclosure made by the company increased before 2007 and thereafter. Social disclosure in Indonesia, Malaysia, and Thailand experienced a significant increase from before and after it is issued and the enactment of regulations on the environment in these countries. The test results of independent sample test showed significant difference at the level of 0000 in all countries. Respectively, Malaysia showed the highest increase, then Indonesia and Thailand (see Table 1, Panel 3).

#### *Disclosure of Environmental, Social and Governance (ESG) Score*

Results of independent sample test, showed a significant difference in scores ESG disclosure in Indonesia, Malaysia, and Thailand. Each level of

significance obtained from the statistical test result is 0000 for all countries. Malaysia has a value F-value is higher (which is 533.080) compared with Indonesia and Thailand, with each value of the F-value of 406.386 and 274.414. (see Table 1, Panel 4). These results indicate that the government's policy governing environmental, social and governance very effective in improving environmental awareness by companies.

## CONCLUSIONS

By doing independent sample t test on a sample of 24 626 firms / years, the study found that the cost of the environment, disclosure of environmental, social disclosure, and ESG observations in the three countries has increased significantly after 2007. In Indonesia was found no significant improvement only in environmental costs.

The findings of this study indicate that as predicted the theory of public interest that the existence of the policy should be aimed at the interest of the people is confirmed by this study. It is seen from the four variables were observed in this study as a whole showed a significant difference from before and after the issuance and implementation of policies in 2007. Each of the companies in the three countries that were observed in this study indicate compliance with the regulations issued on each country. In addition, the results of this study also indicate that the rules are mandatory (regulatory) much more real impact, than just voluntary, especially for developing countries.

## ACKNOWLEDGEMENTS

The research was funded by using a research grant from the Indonesian government, through the university of Lampung. We would like to thank for the financial support of this research. In addition, we would also like to thank our colleagues at the faculty of economics and business, university of gadjah mada, Indonesia to access the data.

## REFERENCES

- [1] Lindrianasari, "Hubungan antara kinerja lingkungan dan kualitas pengungkapan lingkungan dengan kinerja ekonomi perusahaan di Indonesia", Jurnal Akuntansi dan Auditing Indonesia, Vol. 11, No.2, 2007, pp.159-172.
- [2] Asmaranti, Y. and Lindrianasari, "Comparison of Greenhouse Gas Emission Disclosure Before and After Establishment of the Indonesian Act No. 17 of 2004", Issues In Social and Environmental Accounting (ISEA)

- Vol. 8, No. 3, 2014, pp. 225-234.
- [3] Lindrianasari and Asmaranti, Y., "Investigative studies on environmental disclosure and the costs of R&D as a compliance with government policy on corporate social responsibility in Indonesia", *International Journal of Environmental & Sustainability*, Vol. 5, No.2, 2016, pp. 61-71.
  - [4] Gray,R., R. Kouhy and S. Lavers, "Corporate Social and Environmental Reporting: A Review of the Literature and a Longitudinal Study of UK Disclosure", *Accounting, Auditing and Accountability Journal*, Vol. 81, No. 2, 1995, pp. 47-77.
  - [5] Chen, J. C. and Roberts, R. W., "Toward a More Coherent Understanding of the Organization–Society Relationship: A Theoretical Consideration for Social and Environmental Accounting Research", *Journal of Business Ethics*, Vol. 97, No. 4, 2010, pp. 651-665.
  - [6] Lindblom C. K., The of Implications Organizational Legitimacy for Corporate Social Performance and Disclosure. "Conference proceedings" in the Critical Perspective on Accounting Conference. 1994. New York.
  - [7] Suchman, "Managing Legitimacy: Strategi Approaches", *Academy of Management Review*, Vol. 20, No. 3, 1995, pp. 571-610
  - [8] Lindrianasari, Pemeriksaan kepatuhan terhadap pengelolaan lingkungan hidup pada perusahaan-perusahaan di Provinsi Lampung. "*Proceeding DepDikNas*", 2004.
  - [9] Freeman, R. Edward, *Strategic Management: A stakeholder approach*. Boston: Pitman. 1984.
  - [10] Börzel, Tanja A., and T. Risse. 2010. Governance without a state: Can it work?, *Regulation and Governance*, Vol. 4, No. 2, 2010, pp. 13–134.
  - [11] Potoski, Matthew and Aseem Prakash. 2005. Green Clubs and Voluntary Governance: ISO 14001 and Firms' Regulatory Compliance. *American Journal of Political Science*, Vol. 49, No. 2, 2005, pp.235–248.

## **ASSESSMENT OF URBAN CLIMATE CHANGE IN IPOH CITY, PERAK, MALAYSIA**

Mohd Hairy Ibrahim<sup>1</sup>, Mazlini Adnan<sup>2</sup>, Nor Kalsum Mohd Isa<sup>3</sup> & Kamarul Ismail<sup>4</sup>,

<sup>1</sup> Department of Geography and Environment, Faculty of Human Sciences, Sultan Idris University of Education, 35900 Tg. Malim, Perak.

<sup>2</sup> Department of Mathematics, Faculty of Science and Mathematics, Sultan Idris University of Education, 35900 Tg. Malim, Perak

### **ABSTRACT**

This paper focuses on the variation of changes of the urban climate parameters as a result of rapid expansion of human habitat in Ipoh City. The study found that long-term temperature trend Ipoh shows that the temperature has increased significantly between 1968 and 2010. Findings show that temperature increase in the industrial area has the value of  $r = 0.44$ , which indicates that the industrial area experiences temperature change in moderate strength. During all monsoon seasons, the trends of temperature change increase in low strength in the industrial area. The temperature variation increases significantly during the southwest monsoon and April monsoon transition seasons compared with during the northeast monsoon season. Urban climate change calls for cooperation of all parties in addressing the temperature change in preserving the urban ecosystem sustainability of Ipoh City. Urban climate change calls for cooperation of all parties in addressing the temperature change in preserving the urban ecosystem sustainability of Ipoh City.

*Keywords: Urban Climate, Human Habitat, Environmental Change, Ecosystem Sustainability*

## INTRODUCTION

Since the mid-1970s, global warming has accelerated at a rate of  $0.15^{\circ}\text{C}$  per decade [24] [14]. Due to rapid urbanization, urban warming has become a serious problem along with global warming [26] [27] [29]. Over 100 years ago, the average global temperature has increased by  $0.3^{\circ}$  to  $0.6^{\circ}\text{C}$  [14]. The situation arises due to expansion of human habitat via urbanization activities in the urban areas. Before we proceed, we need to discuss the expansion of human habitat in Malaysia in general.

The rapid expansion of human habitat through urbanization activities takes place mostly in Asian countries which experience rapid economic growth in the 19th century until 20th century. Malaysia is one of the fastest growing and urbanizing countries in Asia [12]. Urban development in terms of urbanization has caused a number of changes and transformation, including socio-economic and significant climate and weather changes [37]. Environmental changes in fast-growing urban areas can cause urban climate change, acid rain, and heat island which lead to increasing temperature and disruption of people's lives.

Most current research discusses environmental issues in relation to the rapid urban development and industrial factors which tend to alter natural patterns and temperature trends in urban environment [33]. As cities grow over time, the temperature also tends to increase and become higher [21]. Urban heat island has become a major problem associated with urbanization and industrialization of human civilization whereby temperature increases due to the urban heat island threaten human health. This makes the urban heat island a theme among climatologists and is documented in metropolitan areas around the world [28] [17] [3] [20] [30] [36] [4] [8] [19] [18].

Cities are vulnerable to climate change due to greenhouse gases and local effects of activities such as urban heat island. The process of urbanization definitely affects the urban environment. It is well known that urbanization creates a change in the morphology of the city, infrastructure, available facilities, increase in energy consumption, visible physical environmental conditions and also the number of population being accommodated [15]. Urban areas have different climatic conditions than the surrounding environment [27]. Urban heat island has become a major problem associated with urbanization and industrialization in which temperature increases due to the urban heat island threatens human health through thermal stress. This indicates problematic urban atmosphere or climate,

specifically urban heat island which is a major issue due to urbanization and industrialization.

This paper examines the increasing expansion of human habitat in Ipoh City, which is located in the Kinta Valley. The rapid expansion involves urbanization activities which alter the physical landscape in expanding cities and towns in Kinta Valley, such as Kampar, Gopeng, Batu Gajah, Seri Iskandar, Ipoh, Chemor, Bercham, Simpang Pulai, Lahat and Pengkalan, Kanthan, and Tanjong Rambutan. Development involving human activities in these areas has transformed the natural environment of Ipoh into a Kinta Valley metropolitan. The human activities have altered the landscape with opening of land for the purpose of urbanization, agriculture, mining and industrialization. From a well-known tin mining area in the past, Kinta Valley has largely been reclaimed by humans and transformed into residential, business and industrial areas. The hills in the east and north of Kinta Valley have been quarried for the precious marbles. These activities and changes have caused temperature change in Ipoh. As cities grow over time, the temperature also tends to increase and become higher [21].

## DATA AND METHOD

Malaysia's tropical climate is hot and humid. Data obtained from Malaysian Meteorological Department of a period of ten years shows that the external temperature is relatively uniform with an average temperature of between  $23.7^{\circ}\text{C}$  and  $31.3^{\circ}\text{C}$  during the day, with the highest recorded temperature of  $36.9^{\circ}\text{C}$  and an average relative humidity throughout the day between 67% and 95%. Generally, temperature increases in the rapidly developing cities with buildings and crowded with vehicles compared with suburban and rural areas.

All raw data are obtained from the Meteorological Department, Malaysia from its database. Meteorological data from the years 1970 to 2000 were gathered from Ipoh Airport Meteorological Station. Geographically, Ipoh is located at  $4.5975^{\circ}\text{N}$ ,  $101.0901^{\circ}\text{E}$ . Ipoh City is the third largest city in Peninsular Malaysia, and at a height of 75 meters above sea level based on the flat landing of both banks of Kinta River. The topology of the study area is low lands at a height of less than 180 meters above sea level. In the southwest of Ipoh is the Kledang Range, at a height of 600 meters above sea level acts as a permanent forest reserves and water catchment areas. In the south, the environment is littered with limestone hills about 160 meters high from Map of Peninsular Malaysia, Series 1307.



Time series data of mean maximum temperature, mean minimum temperature and mean annual temperatures from 1970 to 2000 (30 years) collected from Ipoh Airport meteorological station are used to determine the change in temperature of the metropolitan city of Ipoh. The data were analyzed in two parts by conducting linear regression and noting the anomalies of periods from 1968 to 2010. The linear regression is used to determine temperature changes in Ipoh, Perak. Temperature is used as a dependent variable, while the length of time as an independent variable. Temperature is used as: temperature =  $f(\text{time})$  and  $y = a + bx$ , where  $Y$  = mean temperature (minimum, maximum),  $X$  = period of time [31]. The analysis also shows the extent of relationship between the variables. The relationship between the minimum and maximum mean surface temperature, and annual time series (1968-2010) can assess the strength of the relationship between two variables as illustrated in Table 1 [1]. Trend analysis was carried out to show the mean temperature and time (in years). The trend given by the slope coefficient of the fitted linear regression line is tested for significance (95%).

Table 1: The strength of relationship between two variables

The value of coefficient $r$	Relationship
0.00 – 0.20	Nil
0.20 – 0.40	Low
0.40 – 0.60	Moderate
0.60 – 0.80	High
0.80 – 1.00	Very high

Source: [1] Alias Baba, 1999

## FINDINGS AND DISCUSSION

The temperature increase due to urbanization in Ipoh received a lot of attention from several researchers only in the early 1990s, but after 1993, the attention ceased. Preliminary studies have been carried out previously to understand changes in temperature [25] [13]. Temperature trends used in many of the studies is a popular way to assess trends of urban temperature changes due to urban warming [16] [9] [10] [5]. Analyzing the linear trend of change over the years and temperature changes in Ipoh had shown significant results (Fig. 1).

The study found that in the long-term, temperature change in Ipoh City shows a moderate and significantly positive temperature trend in the period between 1968 and 2010 (Table 3). The

average minimum temperature had a considerable increase compared with the average maximum temperature. Wind velocity had also undergone dramatic increase. At the same time, however, relative humidity only increased at a low level, and did not significantly influence temperature change.

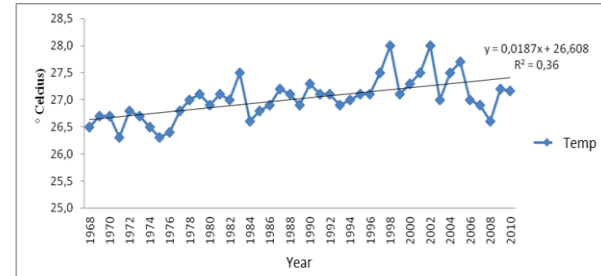


Figure 1: Trend of average temperature change in Ipoh from 1968 to 2010

The variation of urban climate parameters in Ipoh involves two areas, which are urban and industrial areas where the data of climate parameters from air quality station in Pengkalan Pegoh represents the urban area, while the air quality station in Tasek represents the industrial area. Research findings show that temperature increase in the industrial area has the value of  $r = 0.44$ , which indicates that the temperature change in the industrial area was positively increasing in moderate strength. Relative humidity also increased in moderate strength (Table 2).

Table 2: Result of Regression Analysis of Climate Parameter Change of Tasek (Industrial Area) in Ipoh

Field	Period	Industry	$r^2$	$r$	Trend	Strength of change
Temperature	1996-2010=14	$Y = 0.068x + 27.02$	0.193	0.44	Increase	Moderate
Relative humidity	2003-2010=7	$Y = 0.551x + 73.46$	0.724	0.85	Increase	Very high
Wind velocity	1996-2010=14	$Y = 0.069x + 146.4$	0.209	0.46	Decrease	Moderate
Ultraviolet	1996-2006=10	$Y = 3.002x - 582.3$	0.189	0.43	Increase	Moderate

\* Significance level: 0.0

Urban areas are experiencing temperature change which increases by  $0.085^\circ\text{C}$  per year in moderate strength, influenced by relative humidity which has increased in very high strength (Table 3). At the same time, wind velocity has decreased at moderate strength ( $r = 0.48$ ). The findings show that temperature change in the urban area is higher than in the industrial area.

Table 3: Result of regression analysis of temperature, relative humidity, rainfall and wind velocity in Ipoh (Urban) and Sitiawan (Suburbs)

Temperature	Period	Ipoh	r <sup>2</sup>	r	Trend	Strength	Sitiawan	r <sup>2</sup>	r	Trend	Strength
Annual (MAT)	1968-2010	$y = 0.0187x + 26.6$	0.36	0.6	Increase	Moderate	$y = -0.024x + 26.38$	0.54	0.7	Increase	High
Maximum (MMxT)	1968-2010	$y = 0.007x + 32.8$	0.08	0.3	Increase	Low	$y = 0.014x + 31.8$	0.21	0.5	Increase	Moderate
Minimum (MMiT)	1968-2010	$y = 0.0364x + 22.5$	0.66	0.8	Increase	Very high	$y = 0.0262x + 22.62$	0.66	0.8	Increase	Very high
Relative humidity	1968-2010	$y = 0.015x + 81.27$	0.03	0.2	Increase	Low	$y = 0.0588x + 85.89$	0.49	0.7	Increase	High
Rainfall	1968-2010	$y = 0.1813x + 2205.2$	0.18	0.4	Increase	Moderate	$y = 2.7186x + 1715$	0.03	0.2	Increase	Low
Wind velocity	1968-2009	$y = 0.0837x + 18.045$	0.52	0.7	Increase	High	$y = 0.08x + 15.46$	0.6	0.5	Decrease	Very high

\* Significance level: 0.05: MAT Mean Annual Temperature; MMxT Mean Maximum Temperature, and MMiT Mean Minimum Temperature (°C)

Field	Period	Urban	r <sup>2</sup>	r	Trend	Strength of change
Temperature	1998-2010=11	$Y = 0.085x - 144.5$	0.319	0.56	Increase	Moderate
Relative humidity	2003-2010=7	$Y = 0.824x - 1575$	0.781	0.88	Increase	Very high
Wind velocity	1999-2010=11	$Y = 0.0077x + 160.5$	0.233	0.48	Decrease	Moderate

Table 4: Result of Regression Analysis of Climate Parameter Change of Pegoh (Urban) in Ipoh

\* Significance level: 0.05

Table 5: Result of Regression Analysis of Temperature Change According to Monsoon Seasons of Industrial Area (Tasek) in Ipoh from 1998 to 2010

Field	Period	Urban	r <sup>2</sup>	r	Trend	Strength of change
Southwest Monsoon	1998-2010=11	$Y = 0.0047x - 18.733$	0.0003	0.02	Increase	Nil
April	1998-2010=11	$Y = 0.809x - 134.45$	0.38	0.62	Increase	Moderate
Northeast Monsoon	1998-2010=11	$Y = 0.0111x + 5.0547$	0.0053	0.07	Increase	Nil
October	1998-2010=11	$Y = 0.154x - 281.36$	0.1194	0.34	Increase	Low

\* Significance level: 0.05

Trends of increasing temperature change during all monsoon seasons are in low strength in the industrial area in Ipoh (Table 4). The industrial area (Tasek) experienced very high increase of relative humidity during the southwest monsoon ( $r=0.9$ ), April monsoon transition ( $r=0.7$ ), and northeast monsoon ( $r=0.9$ ), while it decreased during October monsoon transition ( $r=0.4$ ) (Table 5).

Table 6: Result of Regression Analysis of Temperature Change According to Monsoon Seasons of Urban Area (Pegoh) in Ipoh from 1998 to 2010

Field	Period	Urban	r <sup>2</sup>	r	Trend	Strength of change
Southwest Monsoon	1998-2010=11	$Y = 0.1224x - 217.7$	0.358	0.60	Increase	Moderate
April	1998-2010=11	$Y = 0.128x - 228.97$	0.4017	0.63	Increase	Moderate
Northeast Monsoon	1998-2010=11	$Y = 0.05727x + 78.753$	0.0865	0.30	Increase	Low
October	1998-2010=11	$Y = 0.0777x - 129.12$	0.0765	0.28	Increase	Low

\* Significance level: 0.05

Urban areas were experiencing positive increase of temperature change in moderate strength, influenced by an increase of relative humidity in very high strength (Table 6). At the same time, wind velocity had decreased in moderate strength ( $r=0.48$ ). The urban areas also experienced higher temperature change during the southwest monsoon and April monsoon transition seasons in moderate strength compared with during the northeast monsoon and October monsoon transition seasons (Table 6). Obviously, variations in temperature increase in the long term, but the strength of change is moderate. The temperature variation increases considerably during the southwest monsoon and April monsoon transition seasons compared with the northeast monsoon season. Urban climate change calls for cooperation of all parties in addressing variation of temperature change in preserving urban ecosystem sustainability of Ipoh City.

## CONCLUSION

In conclusion, the results of trend analysis show a positive temperature change in Ipoh between 1968 and 2000. The research findings are a sign of the need for feasible measures to protect the sustainability of urban environment so that urban temperature does not continue to rise and negatively affect the urban residents in the future. Therefore, sustainable planning and urbanization should continue to be strengthened to ensure that Ipoh becomes a sustainable city.

## ACKNOWLEDGEMENTS

Our appreciation to Malaysian Meteorological Department for generously contributing their data to this study.

## REFERENCES

- [1] Alias Baba, *Statistics of education and research in Social Sciences*. National University of Malaysia: Bangi, 1999. Ch.3.
- [2] Balling, R.C. & Cerverny, R.S., *Long-term associations between wind speeds and urban heat island of Phoenix*, Arizona. *Journal of Applied Meteorology and Climatology* Vol. 26, 1987, pp. 712–716
- [3] Böhm, R. *Urban bias in temperature time series - a case study for the city Vienna, Austria*. *Journal of Climatic Change*, Vol. 38, 1998, pp.113–128
- [4] Chung U, Choi J & Yun J. *Urbanization Effect on the observation change in mean monthly temperature between 1951-1980 and 1971-2000 In Korea*, *Journal Climate change*; Vol.66, 2004, pp.127-36
- [5] Figuerola PI, Mazzeo N. *Urban-rural temperature differences in Buenos Aires*. *International Journal of Climatology*; Vol.18:1, 1998, Pp. 709–1723.
- [6] Fujibe F. *An Increasing trend of extremely hot days in the inland of the Kanto Plain and its relation to urban effect*. *Tenki Journal Meteorology Society, Japan*, Vol.45, 1998a, pp. 643-653.
- [7] Fujibe F. *Time of the day dependence of long term temperature changes at urban meteorological stations in Japan*. *Journal Meteorology Society, Japan*, Vol.75, 1998b, pp. 1041-51.
- [8] Grimmond C.S.B, T.S. King, F.D. Cropley, D.J. Novak & C. Souch. *Local-scale fluxes of carbon dioxide in urban environments: methodological challenges and results from Chicago*. *Environmental Pollution* Vol. 116, 2002, pp. 243-254.
- [9] Hanafiah. N.H & Chan., N.W. *The occurrence Urban Heat Island and its effect human thermal discomfort in Penang*, National Conference of Human, Space and Environment, 16th and 17th November , Penang. 2011.
- [10] Hizam Mustafa. *Urbanization Impact On Air Pollution Concentration in Ipoh City*, Undergraduate Exercise, Not Published. National University of Malaysia, Bangi., 1993.
- [11] IPCC Third Assessment Report - Climate Change. Intergovernmental Panel on Climate Changes, GRID-Arendal. UNEP. 2001.
- [12] Jamaluddin Md. Jahi. *Impak Pembandaran Terhadap Persekitaran Atmosfera Bandar Dlm Jamaluddin Md. Jahi et. al. Prosiding Seminar Antarabangsa Habitat Manusia dan Lingkungan Hidup*, Universitas Riau dan Universiti Kebangsaan Malaysia: Bangi 2009. pp. 226.
- [13] Kato H. A. *A Statistical Method for separating urban effect trends from observed temperature data and its application to Japanese temperature record*. *Journal of Meteorology Society, Japan*, 1996, Vol.74, 1996. Pp. 639-53.
- [14] Katsoulis, B.D. & Theoharatos, G.A. *Indications of the urban heat island in Athens, Greece*. *Journal of Applied Meteorology and Climatology*, Vol. 24, 1985, pp. 1296–1302.
- [15] Kim, Y.H. & Baik, J.J. *Maximum urban heat island intensity in Seoul*. *Journal of Applied Meteorology and Climatology*, Vol. 41, 2002, pp. 651–659.
- [16] Klysik, K. & Fortuniak, K. *Temporal and spatial characteristics of the urban heat island of Łódź, Poland*. *Atmospheric Environment international Journal* Vol. 33, 1999, pp. 3885–3895.
- [17] Lee, D. *Urban warming? An analysis of recent trends in London's heat island*. *Weather* Vol. 47: 1992. pp.50–60.
- [18] Lisa Gartland. *Heat Islands: Understanding and Mitigating Heat In urban Areas*. Earthscan Pub.: London. 2009. Ch. 4.
- [19] Malaysian Meteorological Department. *Malaysian Climate Summary 2007*, Petaling Jaya. Selangor, 2007.
- [20] McCarthy, M. P., Best M.J. & Betts. R. A. *Climate change in cities due to global warming and urban effects*, *Geophysical. Research. Letter.*, 37, L09705, doi:10.1029/2010GL042845. 2010.
- [21] Normazidah Mohd Mokhtar. *Urbanization, patterns of temperature and comfort: Terms and Its Implications in Planning: A Study In Ipoh*. Unpublished master's thesis. Universiti Kebangsaan Malaysia, Bangi. 1990.
- [22] Nakagawa K. *Recent Trends of Urban Climatology Studies in Japan, with special emphasis on the thermal environments of urban areas*. *Geography Review, Japan*, Vol. 69-B, 1996, pp. 206-224.
- [23] Oke T.R). *Boundary Layer Climates*. 2<sup>nd</sup> ed. Routledge, 1987, pp. 435.
- [24] Oke, T.R. *City size and the urban heat island*. *Atmospheric Environment International Journal.*, Vol 7, 1973, pp. 769–779.
- [25] Rizwan, A.M. & Dennis YCL, Liu C. A *Review on The Generation, Determination and Mitigation of Urban Heat Island*, *Journal Environmental Science*; Vol. 20, 2008, pp. 120-128.
- [26] Saitoh, T.S., Shimada, T. & Hoshi, H. *Modelling and simulation of the Tokyo urban heat island*. *Atmospheric*

- Environment international Journal Vol. 30,  
1996. pp. 3431–3442.
- [31] S.H Sajjad, Babar Hussain, M. Ahmed Khan,  
Asif Raza, B. Zaman & Ijaz Ahmed. *On  
Rising Temperature Trends of Karachi in  
Pakistan*, Journal of Climate Change; Vol.  
96, Springer Science, 2009. Pp. 539-547,
- [33] Shaharuddin Ahmad, Hashim N.M & Jani  
Y.M. Urban Heat Island phenomenon and  
environmental issues in Kuala Lumpur.  
*GEOGRAFIA Online, Malaysian Journal of  
Society and Space*, Vol. 5, 2009, pp. 57 –  
67.
- [36] Yamashita, S. *Detailed structure of heat  
island phenomena from moving observations  
from electric tram-cars in metropolitan  
Tokyo*. Atmospheric Environment  
International Journal Vol. 30, 1996, pp. 429–  
435.
- [37] Zurawati Ismail. Trend Analysis: Climate and  
weather change in Kinta Valley, Perak,  
Proceedings of Environmental Science and  
Technology Conference (ESTEC2009)  
Kuala Terengganu, Malaysia, 7th-8th  
December, 2009. pp. 50-60.

## **TREND OF DAILY RAINFALL AND TEMPERATURE IN PENINSULAR MALAYSIA BASED ON GRIDDED DATA SET**

Chee-Loong Wong<sup>1</sup>, Zulkifli Yusop<sup>2</sup>, Tarmizi Ismail<sup>3</sup>

<sup>1</sup> Faculty of Civil Engineering, Universiti Teknologi Malaysia, 81310 Johor Bahru, Malaysia  
<sup>2</sup> Department of Irrigation and Drainage, Malaysia, Jalan Sultan Salahuddin 50626 Kuala

Lumpur, Malaysia

<sup>3</sup> Centre for Environmental Sustainability and Water Security, Research Institute for  
Sustainable Environment, Universiti Teknologi Malaysia, 81310 Johor Bahru, Malaysia

### **ABSTRACT**

A gridded data set with the size of 0.05 degree resolution (approximately 5.5km) which representing ground observations of daily rainfall and temperature of Peninsular Malaysia has been created over 1975-2006. The integration and processing of the variety of data sources and data assessment is also presented. The 32-year period of the daily gridded rainfall and temperature data set were assessed to see how the daily mean rainfall and temperature have changed over time and space. Northeast monsoon (NEM) contributes more rainfall over the country compare to southwest monsoon (SWM). The rainfall trend during NEM is found significantly increased at the 95% confidence level (7mm/season/year), meanwhile SWM rainfall does not pose any significant trends. Both NEM and SWM temperature trends show significant increasing trends at 95% confidence level at 0.32°C/decade and 0.31°C/decade, respectively over the 32-year period. A drastic increased of mean temperature (1.20°C) was found in Klang Valley over the 20-year period. The mean decadal temperature was found consistently decrease as it approached the northern, east coast and southern part of the country.

*Keywords: Rainfall trend, temperature trend, gridded data set, Peninsular Malaysia*

### **INTRODUCTION**

An accurate and complete hydrometeorological data source plays an important role in large scale models to simulate hydrological land surface conditions, especially in related to climate and water resources studies. Though the nature of each individual model varies due to the applied physics, the basic requirement is to acquire a complete data sources in terms of space and time. In many flood modeling applications, the simulations are dependent upon the availability of station data and the distance of the nearest station [1]. Because of the limited observation coverage, the selected nearest station data could be a few hundred kilometres away from the research area. The spatial distribution of stations or stations density in observation network and erroneous data in temporal aspects are the key problems for obtaining good hydrometeorological data within the study area [2]. Besides, the differences in customary observation practice, e.g. for rainfall measurements between countries [3,4], or differences in measurement methods or report timing between variables also limits the research works, especially affecting the modelling simulations (calibrations and verifications).

A current trend in achieving better hydrological modelling results, is turning to remote sensing as a possible means for quantifying e.g. variable rainfall

as an input in the hydrological models as explained by many researchers [5-8], particularly in areas with few rain gauges. However, few shortcomings of satellite data were identified e.g. short records of data, biases and discontinuities due to the disruptions of instruments or nature and frequent changes of algorithms causing lengthy calibration tasks [9,10]. Although the calibration methods are improved from time to time [10-12], gauge-based data remains as a primary data source for any hydrological and atmospheric models.

To overcome the spatial and temporal problems with the ground observations, gridded data sets become essential means for applications in hydrological research and climate studies. For examples, global and regional studies in hydrological cycles [1,13-17], water resources assessment in large river basin [15,18], hydrological extremes [19,20], flood forecasting [21,22], climate variability [23,24], climate change scenario projections [25,26] and high resolution climate model evaluation [27,28].

Motivated by the availability of long records and good quality of daily hydrometeorological gridded data set in Peninsular Malaysia [29], this study focuses on the trend assessment of the daily rainfall and temperature data set between 99.5°E to 104.5°E and 1°N to 7°N, with a 0.05° resolution. The study also covers the spatial and temporal variability

analysis of rainfall and temperature in Peninsular Malaysia.

## DATA COLLECTION

### Data Sources and Quality Control

The daily rainfall and temperature observation data used in this study has been extended from the previous study by Wong [29] to 2006. The data sources are based on the ground observations data of Malaysian Department of Irrigation and Drainage (DID), the publicly accessible Global Summary of the Day (GSOD) archive compiled from reports transmitted over the Global Telecommunication System of the World Meteorological Organisation (WMO-GTS) at the National Climatic Data Center of the National Oceanic and Atmospheric Administration (NOAA/NCDC), the Global Energy and Water Balance Experiment (GEWEX) research programme Asian Monsoon Experiment (GAME) archive, and the Malaysian Meteorological Department (MMD). Table 1 shows the data sources for the period 1975-2006.

Data sources	Variable		Duration
	Rainfall	Temp	
DID	152	-	1975-2006
MMD	5	5	2002-2006
GAME*	19	19	1997-2002
WMO-GTS**	87	87	1975-2006

\* from GEWEX Asian Monsoon Experiment (GAME)

\*\* retrieved from NOAA/NCDC

Fig. 1 shows the interpolation domain and distribution of the stations. For the purpose of interpolation, the station data includes several WMO-GTS stations in Thailand and Sumatra, which are located just outside of the grid as shown in Fig. 1.

The data quality control procedure follow that described by Wong [29]. Three levels of screening and filtering of data were conducted in order to obtain the most reliable and consistent data sources. The details were highlighted in gridded data set development by Wong [29]. The long-term MMD statistics become reference for the quality monitoring purpose. The quality control of WMO-GTS data was based on the quality flags in the data sources files. There are no additional quality checks on MMD and GAME data, assuming the data were checked by MMD.

Fig. 2 presents the number of available daily observations from the individual data sources and their combination for the period from 1975 to 2006. The total number of rainfall observations is relatively stable, except the lack of WMO-GTS observations during short periods. The combination

of three datasets has an average of 122 daily observations with a maximum of 167 for 2001 and 2003. Meanwhile, the average numbers of daily observations are 32 for temperature. The temperature records show a very small number of days were the number of observations significantly drops.

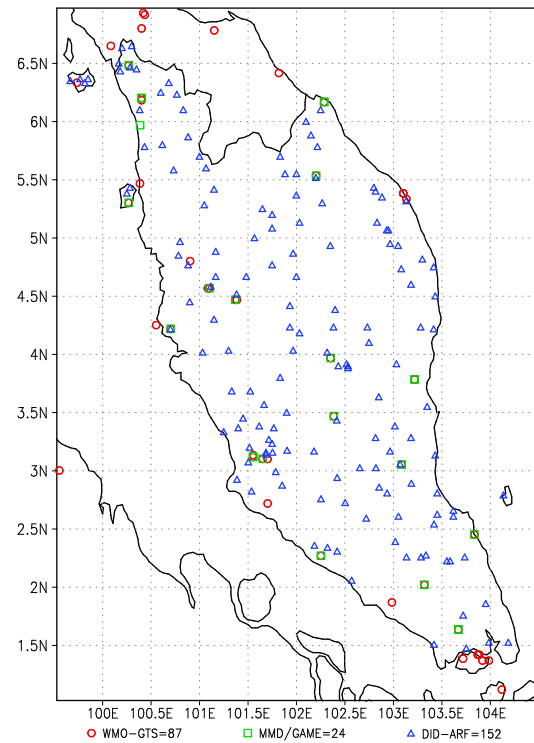


Fig. 1 Locations of the station in the study.

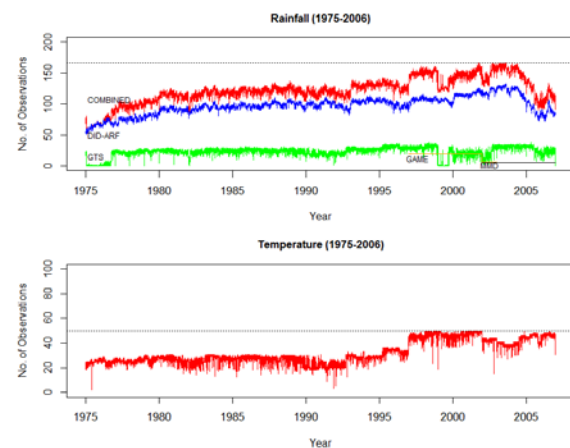


Fig.2 Number of daily observations during the record period, the dotted line shows the maximum number of observations for each variable.

### Terrain Data

Static data, i.e. terrain characteristics are constant over time. It is impossible to develop or operate

large-scale modeling without such data. Elevation data have been derived from the Shuttle Radar Topography (STRM 30) 1 km version 2 data set [30], and were averaged into the output grid resolution.

The dynamic terrain data are associated with the land cover properties in the study area. Land cover type data were obtained from MODIS MOD12Q1 annual V004 1 km data products for the period 2001-2004, using the International Geosphere-Biosphere Programme (IGBP) biome classification. The land cover data are used to obtain the effective momentum roughness length for wind speed interpolation by aggregating the roughness length values of all cover types within a grid box using a cover type fraction-weighted averaging scheme [31]. The relations between land cover types and roughness length are based on [32] and [33].

## METHODOLOGY

### Data Interpolation

The interpolation scheme is based on an adaption of Shepard's [34] angular distance weighting (ADW) procedure covers 32 years (1975 – 2006) period. Details description of the data set and gridding procedure are given in Wong [29]. In order to account for orography, interpolation of temperature are carried out on sea level equivalent values and then converted to grid box values using the derived DEM. Temperature is related to elevation, the temperature lapse rate formulations applied for the U.S. standard atmosphere [35] is used. There is no additional processing is carried out for rainfall, which is interpolated directly from point observation values. Since very few stations are available at higher altitude, it is not possible to identify clear orography effect on rainfall especially in daily time series.

The interpolation method requires an understanding of the spatial correlation structure of the station data as explained by Wong [29]. The inter-station correlations were investigated to determine the distances over which observed climate variables are related. This allows defining the distance weighting. The Pearson correlation coefficients between all pairs of stations for the variables are interpolated and plotting against distance. The spatial relationships between stations vary depending on the density of station coverage. In order to obtain daily spatial correlation coefficients for all pairs of rainfall and temperature stations, they were binned into separation distance intervals. In each bin, the mean and standard deviation of the correlation coefficient was calculated and an exponential curve was fitted through the mean distance-correlation points. The correlation decay

distance (CDD) then equals to the distance where the mean correlation coefficient drops to  $1/e$ .

In order to provide a measure of the expected accuracy, a jackknife cross-validation analysis has been carried out by repeated deletion and replacement of individual stations followed by a comparison of the grid box values with those of the deleted station. Overall daily error statistics for the entire area are computed in terms of mean absolute error (MAE) and bias. The results for temperature fields showed MAE is  $0.4\text{ }^{\circ}\text{C}$  with a bias of  $0.1\text{ }^{\circ}\text{C}$ . For rainfall a comparison at jackknifed grid box level resulted in a MAE of  $5.2\text{ mm/d}$  and a bias of  $-0.1\text{ mm/d}$  ( $-1.9\%$ ). These results show that interpolation on a daily basis is significantly more error-prone than for the long-term average. On short time scales, the largely convective rainfall exhibits a large amount of spatial variability over short distances. In some cases, multiple rainfall stations located in the same grid box and that are averaged by the interpolation scheme show distinct differences in daily rainfall.

### Trend detection

The annual and monsoon time series of rainfall of the climatic regions were analyzed using the Mann-Kendall nonparametric trend detection test [36,37]. The Mann-Kendall method has been widely used and tested as an effective method to evaluate a presence of a statistically significant trend in climatological and hydrological time series [18,38-40]. In the trend test, the null hypothesis  $H_0$  is that there is no trend in the series (the data are independent and identically distributed). The alternative hypothesis  $H_1$  is that a trend exists in the data. The Kendall  $S$ -statistic is obtained from comparison between all possible  $(x, y)$  pairs of data and is given by

$$S = \sum_{i=1}^{n-1} \sum_{j=i+1}^n \text{sgn}(x_i - x_j) \text{sgn}(y_i - y_j) \quad (1)$$

where, the sign function is defined (for any variable  $u$ ) as

$$\text{sgn}(u) = \begin{cases} -1 & \text{if } u < 0 \\ 0 & \text{if } u = 0 \\ +1 & \text{if } u > 0 \end{cases} \quad (2)$$

Under the null hypothesis, the statistic  $S$  is approximately normally distributed with zero mean and variance are given by

$$\text{Var}(S) = \frac{n(n-1)(2n+5) - \sum_{i=1}^n t_i i(i-1)(2i+5)}{18} \quad (3)$$

where  $t_i$  is the number of ties of extent  $i$  in either the  $x$  or  $y$  data. The summation term in the numerator is



used only if the data series contains tied values. The standardized test statistic  $Z$  is obtained as

$$Z = \begin{cases} \frac{S+1}{\sqrt{\text{Var}(S)}} & \text{if } S < 0 \\ 0 & \text{if } S = 0 \\ \frac{S-1}{\sqrt{\text{Var}(S)}} & \text{if } S > 0 \end{cases} \quad (4)$$

The test statistic  $Z$  is used to measure the significance of a trend. In a two sided test,  $H_0$  should be accepted if  $|Z|$  is greater than  $Z_{\alpha/2}$ , where  $\alpha$  represents the chosen significance level (e.g. 5% with  $Z_{0.025} = 1.96$ ) then the null hypothesis is rejected implying that the trend is significant. A positive  $Z$  value indicates an upward trend, whereas a negative  $Z$  value indicates a downward trend. If a significant trend is present, the average rate of increase or decrease can be obtained from the slope of a simple linear regression.

## DATA SET EVALUATION AND ANALYSIS

### Rainfall

An overview of rainfall distribution of Peninsular Malaysia as a whole is presented. The gridded data set at 0.05 degree resolution was used to analyze the monthly rainfall distribution in Peninsular Malaysia. The mean monthly areal rainfall data for entire Peninsular Malaysia is shown in Fig. 3.

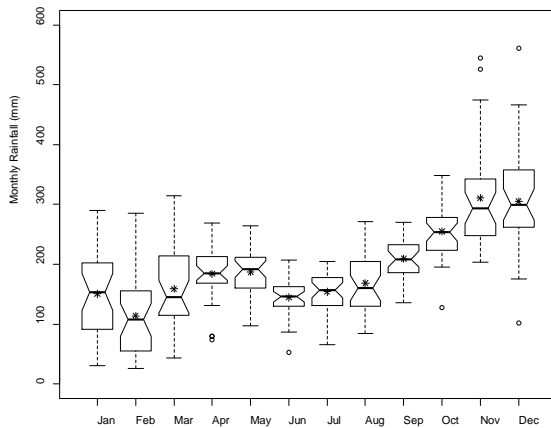


Fig. 3 Box and whisker plot of areal average mean monthly rainfall (1975-2006) in Peninsular Malaysia. The asterisk denotes the mean value, the solid line is the median, the height of the box is the difference between the third and first quartiles (IQR). Any data observation which lies 1.5 IQR lower than the first quartile or 1.5 IQR higher than the third quartile can be considered an outlier in the statistical sense, indicated by open circles.

The highest mean monthly rainfall of 311 mm is observed in November, equivalent to 13% of the

mean annual rainfall. The lowest mean monthly rainfall of 113 mm occurs in February, which contributes about 5% to the mean annual rainfall. It is noted that during the NEM from November to March both the maximum and minimum monthly rainfall are observed. A relative high rainfall variation is observed during the NEM than the Southwest Monsoon (SWM), which occurs from May to September. The result agrees with the findings by Moten [41], where maximum rainfall is observed near the end of the year during the Northeast Monsoon (NEM). A secondary maximum is found during the intermonsoon months (April or May).

Fig. 4 shows the distribution of annual average rainfall in Peninsular Malaysia. It is noted that the rainfall in the east coast region of Peninsular Malaysia is mostly influenced by the NEM, particularly during November or December [42,43]. The NEM influence was even reported to have more than 70% rainfall contribution over most parts of the Peninsular [41]. However, there is only 44% of annual rainfall throughout 32-year analysis occurred during the NEM. In this study, both monsoons contribute 81% of the total annual rainfall over the country as shown in Table 2. There is 37% of annual rainfall which occurred during SWM period. During the NEM, the dry northeasterly wind becomes wet during the passage over the South China Sea. The interaction between with the land along the east coast area creates deep convection clouds and rainfall [44].

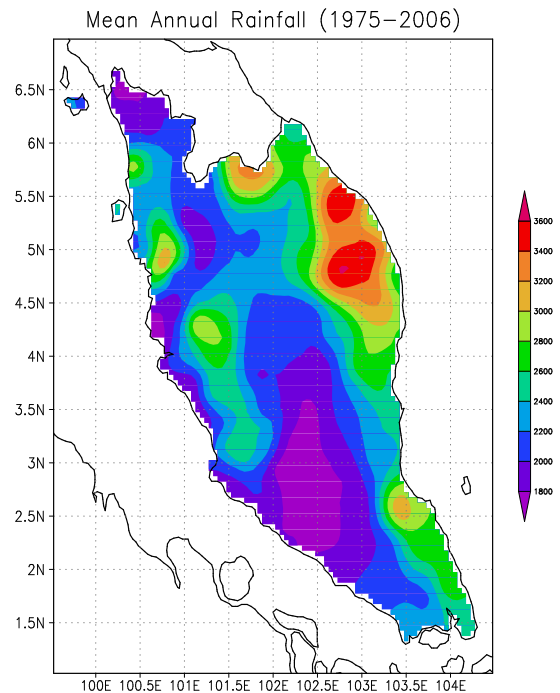


Fig. 4 Peninsular Malaysia rainfall distribution (1975-2006).

Table 2 Monsoons rainfall contributions in Peninsular Malaysia.

Annual Rainfall (mm)	NEM (Nov-Mar)		SWM (May-Sep)		Total Monsoons	
	Rainfall		Rainfall		Rainfall	
	mm	%	mm	%	mm	%
2343	1034	44	864	37	1898	81

The inland region received a relatively smaller amount of mean annual rainfall, i.e. 1950 mm/year as shown in Fig. 4. The reduction of rainfall amount in the inland is due to Titiwangsa mountain range forms the backbone of the Peninsula, from southern Thailand running approximately south-southeast over a distance of 480 km and separating the eastern part from the western part [42]. It appears to block the westward progression of the climatic system and therefore inhibits excessive rainfall over the inland areas [45]. The rainfall produced in this region is mainly due to local convection caused by intense heating of the land surface [46].

### Rainfall Trends

The annual and monsoons rainfall trends of Peninsular Malaysia are presented in Fig. 5. The mean annual rainfall shows minor increase trend (5 mm/year) over 32-year period, however it does not pose any significant increasing trends at the 95% confidence level under Mann-Kendall analysis.

For the mean NEM rainfall in the Peninsula, increasing trends of rainfall are significantly found at the 95% confidence level (7mm/season/year). It was probably due to the accumulation of increasing trend of other months though they are not significant at 95% confidence level. During SWM monsoon, Peninsular Malaysia shows  $-1.7$  mm/season/year of rainfall declining but it does not pose significant trends at the 95% confidence level. Generally, the trends of mean annual and monsoons rainfall are probably governed by the topographic characteristics and local or regional conditions that have an effect on the interannual rainfall variability, which is superimposed on the large-scale weather conditions.

### Temperature Trends

Fig. 6 shows the annual mean temperature trend of Peninsular Malaysia for 1975-2006. Significant increasing temperature trend at the 95% confidence level was found at about  $0.32^{\circ}\text{C}/\text{decade}$  for annual temperature in Peninsular Malaysia. This warming trend is comparable to those reported by Tangang *et al.* [47] where their results showed that the warming trend of between  $2.7$ – $4.0^{\circ}\text{C}/100$  years. The warming trend at  $0.30^{\circ}\text{C}/\text{decade}$  agrees with the simulated temperature increase range by MMD [48] and

NAHRIM [24] where the country will be warmer by about  $2^{\circ}\text{C}$  in the next 50 years. Both NEM and SWM temperature trends show significant increasing temperature trends at the 95% confidence level at  $0.32^{\circ}\text{C}/\text{decade}$  and  $0.31^{\circ}\text{C}/\text{decade}$ , respectively over the 32-year period (as shown in Fig. 6(b) and 6(c)).

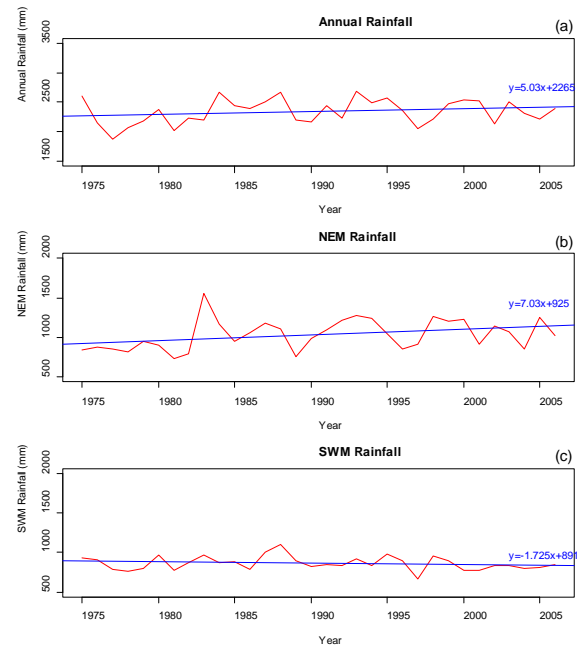


Fig. 5 Rainfall trends of Peninsular Malaysia (1975-2006).

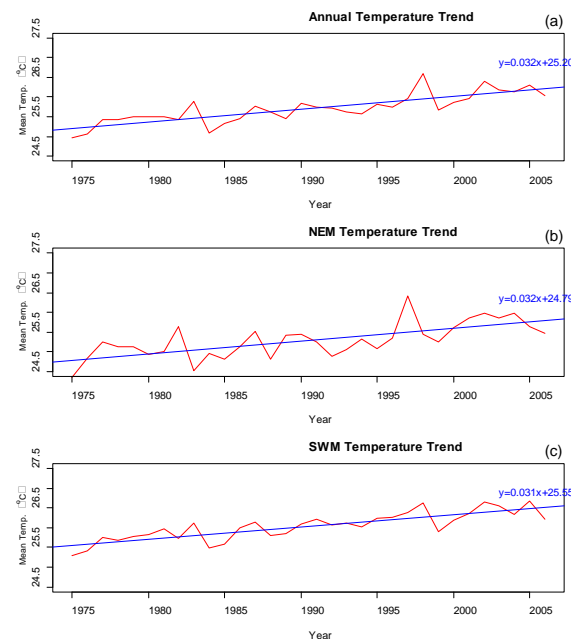


Fig. 6 Temperature trends of Peninsular Malaysia (1975-2006).

## Temperature Spatial Variation

To analyze the spatial variation of mean temperatures of Peninsular Malaysia, the 32-year of mean temperature gridded data was divided into three decades, i.e. 1975-1984, 1985-1994 and 1995-2006. The difference between the earlier and later decade was calculated to explore the spatial variation of mean monthly temperatures of Peninsular Malaysia as shown in Fig. 7.

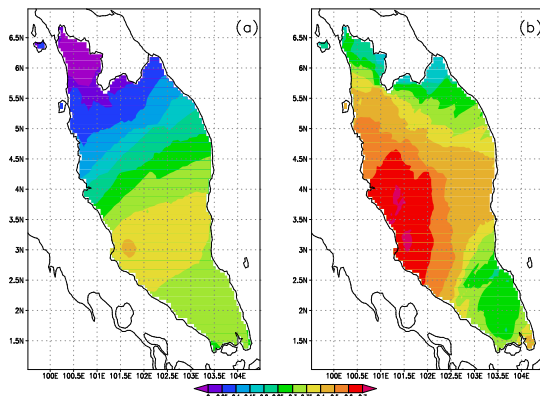


Fig. 7: Decadal temperature (a) differences between baseline (1975-1984) and intermediate decade (1985-1994) (b) differences between intermediate (1985-1994) and most recent decade (1995-2006) of Peninsular Malaysia.

The initial decade (1975-1984) was used as the baseline to compare with the intermediate decade (1985-1994) as shown in Fig. 7(a). It is noted that the inland region (especially Klang Valley) encountered higher degree of temperature between  $0.35^{\circ}\text{C}/\text{decade}$  to  $0.5^{\circ}\text{C}/\text{decade}$ . It dispersed towards northern and southern part of Peninsular Malaysia. The most northern part of the country has minima of differences mean temperature (less than  $0.05^{\circ}\text{C}/\text{decade}$ ) in terms of decade-to-decade comparison. Meanwhile, the southern of the country was at the range of  $0.3^{\circ}\text{C}/\text{decade}$  -  $0.35^{\circ}\text{C}/\text{decade}$  changes over 10 years period. Fig. 7(b) shows the difference of mean temperature between the intermediate decade (1985-1994) and the most recent decade (1995-2006). A drastic increased of mean temperature (more than  $0.6^{\circ}\text{C}/\text{decade}$ ) was noted in Klang Valley and west coast of Peninsular Malaysia. The mean temperature differences consistently decrease as it approached the northern, east coast and southern part of the country. The northern and southern part shows the approximately  $0.35^{\circ}\text{C}/\text{decade}$  or lesser of mean temperature differences. Majority of country area has an increased of mean temperature in the range of  $0.35^{\circ}\text{C}/\text{decade}$  between  $0.6^{\circ}\text{C}/\text{decade}$  over the latest decade-to-decade comparison. The mean temperature of Klang Valley areas was approximately  $1.2^{\circ}\text{C}$  warmer in 20-year period. This

may be caused by the urbanization and industrialization in the country [49]. For other parts of the country, the mean temperature is generally on significant increasing trend as discussed earlier. The reason for the rise of warming rates in the recent decade is the higher frequency of El Niño events [47,48].

## CONCLUSION

A high resolution, 0.05 degree gridded daily hydrometeorological data set was used to assess the rainfall and temperature variability in Peninsular Malaysia. The rainfall distribution of Peninsular Malaysia is generally influenced by two monsoons season, i.e. NEM and SWM. NEM has higher impact over the Study region compared to SWM. As most of the important rainfall trends may not be identified at the coarse time resolutions. A finer temporal scale is needed to investigate the rainfall trends in the future study.

Significant increasing trends ( $0.32^{\circ}\text{C}/\text{decade}$ ) at the 95% confidence level have been found in the mean temperature for the whole country. It was in line with the finding by other researchers [24,47,48]. The mean temperature of the country is generally spatially on increasing mode over the 32-year period. Klang Valley and west coast of Peninsular Malaysia encounter higher increase of mean temperature (the range of  $0.95^{\circ}\text{C}$  to  $1.2^{\circ}\text{C}$ ) between 1975-1984 and 1994-2006. In contrast, the northern and southern parts of the country were on slow increasing pace (less than  $0.35^{\circ}\text{C}/\text{decade}$ ) compared to other regions.

Future studies are likely to include the delineation of climatic regions using statistical analysis over the daily gridded data set in Peninsular Malaysia. It will be useful to further explore the regional characteristics of rainfall and temperature distribution through trend analysis and spatial rainfall and temperature variability analysis on different temporal resolution for different climatic regions in the country. It not only provides better understanding over the spatial and temporal climatology characteristics of Peninsular Malaysia, but also serve as the future fundamental for flood/hydrological research development in the country.

## ACKNOWLEDGEMENTS

The authors thank the Department of Irrigation and Drainage Malaysia (DID), Malaysia Meteorological Department (MMD), and NOAA/NCDC for providing the data.

## REFERENCES

- [1] Taesombat, W.; Sriwongsitanon, N. Areal rainfall estimation using spatial interpolation techniques. *Science Asia* 2009, 35, 268-275.
- [2] Tetzlaff, D.; Uhlenbrook, S. Significance of spatial variability of precipitation for process-orientated hydrological modelling: Results from two nested catchments using radar and ground station data. *Hydrology and Earth System Sciences* 2005, 9, 29-41.
- [3] Groisman, P.Y.; Legates, D.R. Documenting and detecting long-term precipitation trends: Where are we and what should be done. *Climatic Change* 1995, 31, 601-622.
- [4] Lanza, L.G.; Vuerich, E. The wmo field intercomparison of rain intensity gauges. *Atmospheric Research* 2009, 94, 534-543.
- [5] Nezhin, N.P.; Stein, E.D. Spatial and temporal patterns of remotely-sensed and field-measured rainfall in southern california. *Remote Sensing of Environment* 2005, 96, 228-245.
- [6] Droogers, P.; Kite, G. Remotely sensed data used for modelling at different hydrological scales. *Hydrological Processes* 2002, 16, 1543-1556.
- [7] Karimi, P.; Bastiaanssen, W.G.M. Spatial evapotranspiration, rainfall and land use data in water accounting - part 1: Review of the accuracy of the remote sensing data. *Hydrology and Earth System Sciences* 2015, 19, 507-532.
- [8] Kizza, M.; Westerberg, I.; Rodhe, A.; Ntale, H.K. Estimating areal rainfall over lake victoria and its basin using ground-based and satellite data. *Journal of Hydrology* 2012, 464-465, 401-411.
- [9] New, M.; Todd, M.; Hulme, M.; Jones, P. Precipitation measurements and trends in the twentieth century. *International Journal of Climatology* 2001, 21, 1899-1922.
- [10] Hou, A.Y.; Kakar, R.K.; Neeck, S.; Azarbarzin, A.A.; Kummerow, C.D.; Kojima, M.; Oki, R.; Nakamura, K.; Iguchi, T. The global precipitation measurement mission. *Bulletin of the American Meteorological Society* 2014, 95, 701-722.
- [11] Bergmann, H.; Scharzl, R.; Pozarnik, H.; Ruch, C.A.; Harum, T. Calibration of wether radar data in different space and time scales. In *Remote sensing and hydrology*, Owe, M.; Brubaker, K.; Ritchie, J.; Rango, A., Eds. Int. Assoc. Hydrol. Sci.: Wallingford, UK, 2000; pp 16-21.
- [12] Wood, S.J.; Jones, D.A.; Moore, R.J. Static and dynamic calibration of radar data for hydrological use. *Hydrology and Earth System Sciences* 2000, 4, 545-554.
- [13] Lohmann, D.; Raschke, E.; Nijssen, B.; Lettenmaier, D.P. Regional scale hydrology: Ii. Application of vic-2l model to the weser river, germany. *Hydrological Sciences - Journal - des Sciences hydrologiques* 1998, 43, 143-158.
- [14] Arnell, N.W. Climate change and global water resources. *Global Environmental Change* 1999, 9, S31-S49.
- [15] Yang, D.; Musiake, K. A continental scale hydrological model using the distributed approach and its application to asia. *Hydrological Processes* 2003, 17, 2855-2869.
- [16] Oki, T.; Kanae, S. Global hydrological cycles and world water resources. *Science* 2006, 313, 1068-1072.
- [17] Safeeq, M.; Mauger, G.S.; Grant, G.E.; Arismendi, I.; Hamlet, A.F.; Lee, S.-Y. Comparing large-scale hydrological model predictions with observed streamflow in the pacific northwest effects of climate and groundwater. *Journal of Hydrometeorology* 2014, 15, 2501-2521.
- [18] Yang, D.; Li, C.; Hu, H.; Lei, Z.; Yang, S.; Kususa, T.; Koike, T.; Musiake, K. Analysis of water resources variability in the yellow river of china during the last half century using historical data. *Water Resources Research* 2004, 40, W06502.
- [19] Alexander, L.; Zhang, X.; Peterson, T.C.; Caesar, J.; Gleason, B.; Klein Tank, A.M.G.; Haylock, M.; Collins, D.; Trewin, B.; Rahimzadeh, F., et al. Global observed changes in daily climate extremes of temperature and precipitation. *Journal of Geophysical Research* 2006, 111, D05109.
- [20] Donat, M.G.; Sillmann, J.; Wild, S.; Alexander, L.V.; Lippmann, T.; Zwiers, F.W. Consistency of temperature and precipitation extremes across various global gridded in situ and reanalysis datasets. *Journal of Climate* 2014, 27, 5019-5035.
- [21] Reed, S.; Schaake, J.; Zhang, Z. A distributed hydrologic model and threshold frequency-based method for flash flood forecasting at ungauged locations. *Journal of Hydrology* 2007, 337, 402-420.
- [22] Fowler, H.J.; Wilby, R.L. Detecting changes in seasonal precipitation extremes using regional climate model projections: Implications for managing fluvial flood risk. *Water Resources Research* 2010, 46, W03525.
- [23] Koster, R.D.; Suarez, M.J. Climate variability studies with a coupled land/atmosphere model. In *Macroscale modeling of the hydrosphere*, Wilkinson, B., Ed. Int. Assoc. Hydrol. Sci.: Wallingford, UK, 1993; pp 3-27.
- [24] NAHRIM. *Study of the impact of climate change on the hydrologic regimes and water resources of peninsular malaysia*; National Hydraulics Research Institute of Malaysia (NAHRIM): September 2006, 2006.

- [25] Meehl, G.A.; Washington, W.M.; Santer, B.; Collins, W.D.; Arblaster, J.M.; Hu, A.; Lawrence, D.M.; Teng, H.; Buja, L.E.; Strand, W.G. Climate change projections for the twenty-first century and climate change commitment in the ccs3. *Journal of Climate* 2006, 19, 2597-2616.
- [26] Roudier, P.; Ducharne, A.; Feyen, L. Climate change impacts on runoff in west africa: A review. *Hydrology Earth System Sciences* 2014, 18, 2789-2801.
- [27] Masson, V.; Champeaux, J.-L.; Chauvin, F.; Meriguet, C.; Lacaze, R. A global database of land surface parameters at 1-km resolution in meteorological and climate models. *Journal of Climate* 2003, 16, 1261-1282.
- [28] Platts, P.J.; Omeny, P.A.; Marchant, R. Africlim: High resolution climate projections for ecological applications in africa. *African Journal of Ecology* 2015, 53, 103-108.
- [29] Wong, C.L.; Venneker, R.; Jamil, A.B.M.; Uhlenbrook, S. Development of a gridded daily hydrometeorological data set for peninsular malaysia. *Hydrological Processes* 2011, 25, 1009-1020.
- [30] Farr, T.G.; Rosen, P.A.; Caro, E.; Crippen, R.; Duren, R.; Hensley, S.; Kobrick, M.; Paller, M.; Rodriguez, E.; Roth, L., *et al.* The shuttle radar topography mission. *Reviews of Geophysics* 2007, 45, RG2004.
- [31] Taylor, P.A. Comments and further analysis on effective roughness lengths for use in numerical three-dimensional models. *Boundary-Layer Meteorology* 1987, 39, 403-418.
- [32] Garratt, J.R. *The atmospheric boundary layer*. Cambridge Univ. Press: Cambridge, 1992.
- [33] Wieringa, J. Representative roughness parameters for homogeneous terrain. *Boundary-Layer Meteorology* 1993, 63, 323-363.
- [34] Shepard, D. In *A two-dimensional interpolation function for irregularly-spaced data*, Proc. 23rd National Conf. of the Association for Computing Machinery, Princeton, 1968; Princeton, pp 517-524.
- [35] NOAA. *The u.S. Standard atmosphere, 1976*; National Oceanic and Atmospheric Administration, National Aeronautics and Space Administration, United States Air Force: 1976.
- [36] Kendall, M.G. *Rank correlation methods*. Hafner: New York, 1948.
- [37] Mann, H.B. Non-parametric test against trend. *Econometrika* 1945, 13, 245-259.
- [38] Zhang, X.; Harvey, K.D.; Hogg, W.D.; Yuzyk, T.R. Trends in canadian streamflow. *Water Resources Research* 2001, 37, 987-998.
- [39] Liu, Q.; Yang, Z.; Cui, B. Spatial and temporal variability of annual precipitation during 1961-2006 in yellow river basin, china. *Journal of Hydrology* 2006, 361, 330-338.
- [40] Burn, D.H.; Hag Elnur, M.A. Detection of hydrologic trends and variability. *Journal of Hydrology* 2002, 255, 107-122.
- [41] Moten, S. Multiple time scales in rainfall variability. *Proc. Indian Acad. Sci. (Earth Planet. Sci.)* 1993, 102, 249-263.
- [42] Suhaila, J.; Jemain, A.A. Fitting daily rainfall amount in malaysia using the normal transform distribution. *Journal of Applied Science* 2007, 7, 1880-1886.
- [43] Tangang, F.T. Low frequency and quasi-biennial oscillations in the malaysian precipitation anomaly. *International Journal of Climatology* 2001, 21, 1199-1210.
- [44] Chang, C.P.; Harr, P.A.; Chen, H.J. Synoptic disturbances over the equatorial south china sea and western maritime continent during boreal winter. *Monthly Weather Review* 2005, 113, 489-503.
- [45] Juneng, L.; Tangang, F.T.; Reason, C.J.C. Numerical case study of an extreme rainfall event during 9-11 december 2004 over the east coast of peninsular malaysia. *Meteorology and Atmospheric Physics* 2007, 98, 81-98.
- [46] Nieuwolt, S. Diurnal rainfall variation in malaya. *Annals of the Association of American Geographers* 1968, 58, 313-326.
- [47] Tangang, F.T.; Juneng, L.; Ahmad, S. Trend and interannual variability of temperature in malaysia: 1961-2002. *Theoretical and Applied Climatology* 2006.
- [48] MMD. *Climate change scenarios for malaysia 2001-2099*; Malaysian Meteorological Department: 2009.
- [49] Shaharuddin, A. Urban climate research in malaysia. In *IAUC Newsletter*, Climate, I.A.f.U., Ed. International Association for Urban Climate: 2005; Vol. 12, pp 5-8.

## SPATIO-TEMPORAL ANALYSIS OF LAND USE AND LAND COVER CHANGES IN ARID REGION OF SAUDI ARABIA

Eman Albalawi<sup>1</sup>, Ashraf Dewan<sup>2</sup> and Robert Corner<sup>3</sup>

<sup>1,2,3</sup> Department of Spatial Sciences, Science and Engineering, Curtin University, Australia

<sup>1</sup>Department of Geography, Umm Al-Qura University, Makkah, Saudi Arabia.

### ABSTRACT

Changes in land use/land cover (LULC), are a major factor driving global environmental change, especially in arid and semi-arid regions. As a result, expansion of agriculture and urbanisation is occurring in ecologically fragile lands. This study analyses and detects land use/land cover changes in an agricultural centre Tabuk in Saudi Arabia. For LULC analysis, object-based classification technique using Landsat images for seven years (1985, 1990, 1995, 2000, 2005, 2009, and 2015) have been used. The urban growth type for Tabuk was measured using Urban Growth Analysis Tool (UGAT) within a GIS to analyse the pattern of urban growth that has occurred during the last three decades. The result showed a high level of accuracy, ranging from 85% to 97 %. The study found a significant increase in urban areas from 48 km<sup>2</sup> in 1985 to 315 km<sup>2</sup> in 2015. A remarkable increase of 61% in agricultural area, from the year 1985 (112 km<sup>2</sup>) to (577 km<sup>2</sup>) in 2015. This massive expansion is occurring at the expense of the bare land, indicating a loss of 768 km<sup>2</sup> bare land. The urban growth for Tabuk showed that 72% was determined to be of extension-type over the study period, with urban areas expanding in a direction towards the west and north-western areas. The LULC maps would assist government planners and decision makers to analyse and manage agricultural and urban growth.

*Keywords: Change detection; GIS; Land Use /land cover (LULC); OBIA; Remote sensing; Urban Growth Type*

### INTRODUCTION

Land use and land cover have been changed dramatically in Saudi Arabia over the last 30 years due to the high value of national petroleum revenues and rapid growth in urban population [1]. The arid climatic conditions in Saudi Arabia generate low and irregular rainfall, so that agricultural areas are dependent on groundwater. The Government has introduced plans and programs to increase agricultural productivity by augmenting agricultural areas to ensure consistent development of the country [2]. Tabuk is an important agricultural centre in Saudi Arabia and is highly susceptible to land degradation due to high aridity. An increase in agricultural activities around Tabuk city reflects the implementation of wheat subsidies, introduced in the 1980s. During that time, the Saudi government supported and encouraged new agricultural projects [3], with a view to enhance food self-sufficiency.

Reference [4] concluded that Tabuk is exposed to a high risk of environmental damage from 'desertification' due to rapid change in LULC as agricultural land use increased to about 68% over a 20-year period, from 1988 to 2008, into fragile areas. Inadequate planning, lack of awareness, and mismanagement of natural resources have led to massive changes in LULC and, therefore, hydrological processes [5]. Such changes have resulted in the further deterioration of the desert

ecosystem [3].

Migration plays an important role in population distribution between administrative regions of Saudi Arabia, and between rural and urban areas within the same region [6]. The imbalance of population distribution, however, has negative impacts for demands on resources and space [7].

Urban development together with human activities such as unsustainable agricultural practices, unplanned urbanisation, excessive use of groundwater and poor public policies in Tabuk have resulted in environmental problems across the city. A modelling study for Michigan USA, on the effects of urban growth on groundwater, predicted that urban growth dependent on ground water supply is not sustainable [8]. Such studies highlight the issues of urban expansion for cities, relying solely on groundwater. To prevent further damage in environment, land use change should be assessed [9].

Temporal and spatial observation of changes over a specific time period can provide reliable information for mapping and analysing LULC change at local, regional and global scales [10]. A variety of techniques have been used to detect changes in LULC, including post-classification comparisons. The selection of an appropriate classification method is essential for extracting reliable information from satellite data. Supervised and unsupervised classifications are two traditional pixel-based approaches to image classification [11].



Object-Based (or Object-Oriented) image analysis (OBIA) classification introduced by [12] has gained popularity in recent times. The key to OBIA is to exhibit features such as image textural; spectral and spatial information so an accurate analysis can be obtained [13]. Object-based classification provided higher accuracy than pixel-based classifications in urban classes. This technique was utilised spatial and spectral information for the mixed urban-agriculture arid region of Arizona [14]–[15]. Previous research applied remote sensing data for assessing and mapping urban sprawl, urban structures, sprawl direction, and urban growth pattern [16]–[17]–[18].

There is a need to accurately define LULC change using geospatial techniques to support environmental planning. To date, little attention has been paid to environmental and socio-economic stability in Tabuk region, which lacks spatial and temporal information about LULC changes. Assessing LULC change, therefore, can deliver essential information to aid environmental management and planning. The aim of this work is to assess land use and land cover changes in arid Tabuk from 1985 to 2015.

## MATERIALS AND METHODS

### Study Area

Tabuk has an area of 4212 km<sup>2</sup>, and is located at an altitude of 600–800 m above mean sea level: between 28°23' to 28°39' N and 36°35' to 36°57' E in the north-western region of Saudi Arabia (Fig. 1). The province is considered arid with an annual rainfall 40 mm, mostly occurring between Novembers and January with snowfalls every 2–3 years. The primary land use in Tabuk is agriculture. It is considered being the most important area in the country for commercial growers. Wheat, fruit, and export flowers (to Europe) are the main agricultural products in the study area.

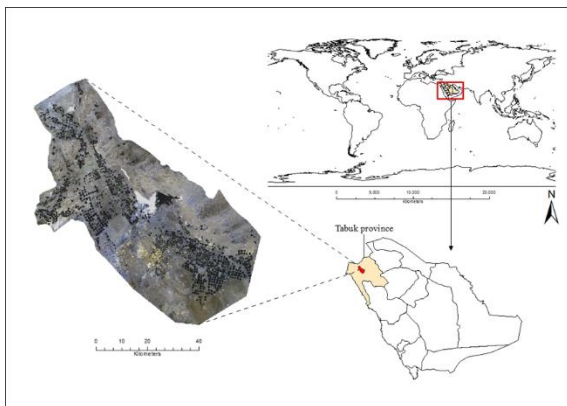


Fig. 1 Location of the study area Tabuk, within Saudi Arabia (Source: Landsat-8 image

2015)

### Dataset and Image Pre-processing

Landsat Multispectral Scanner (MSS), Thematic Mapper (TM), Enhanced Thematic Mapper (ETM+) and Operational Land Imager (OLI) (path 173 and row 40) for 1985, 1990, 1995, 2000, 2005, 2009 and 2015 were downloaded from Earth Explore. Images were selected during March and April of any given year to provide uniformity when detecting and assessing LULC change. Images were geometrically corrected and rectified to the Universal Transverse Mercator (UTM) coordinate system. Landsat images acquired at two or more different periods have different amounts of haze and dust in the atmosphere and required atmospheric correction to overcome these differences [19]. Dark object subtraction (DOS) used to correct Landsat imageries for atmospheric scattering.

### Image Segmentation

The land use/cover classification scheme from [20] was modified to account for local field knowledge and conditions of the study area to define four classes of land cover including Bare land, Urban areas, Agricultural land and Others (Table 1). ENVI software at scale level 10, merge level 97 and texture kernel size 3 was used to perform segmentation processes. An overlay procedure done using a GIS function with the help of available referenced data for all segmented images.

Table 1 Land use/cover classification scheme

NO	Class	Descriptions
1	Bare land	Desert sand, mountain, bare exposed rock,
2	Urban areas	Residential, commercial and industrial areas; settlements; and transportation infrastructure
3	Agricultural land	Cropland and pasture fields, grassland greenhouses, and fallow lands
4	Others	Dry salt flats and ponds

### Change Detection

Post-classification comparisons were used to detect the nature change of LULC by determining 'from-to' change by comparing classified images individually across different dates [21]. The nature of LULC change maps ('from-to') were for seven epochs, namely 1985–1990, 1990–1995, 1995–2000, 2000–2005, 2005–2009, 2009–2015, and 1985–



2015.

### Accuracy Assessment

Accuracy assessment measures the degree of closeness to true values. Error matrix is a common method in the accuracy assessment process, including overall accuracy, producer's accuracy, user's accuracy and kappa coefficient (which is a proportion of pixels that are classified correctly) [22]–[23]. Around 500 points distributed randomly were identified on the reference image and attributed to the four categories. Topographical map, high-resolution images, and field data were used as reference data to assess the image classification accuracy.

### Urban Growth Analysis Tool (UGAT)

The dataset of classified images was reclassified into urban and non-urban areas. Spatial metrics and statistics technique using UGAT was adopted [18], to analyse urban spatial growth and type of change over 30-year period. The municipality of Tabuk set as the Tabuk central area with 1 km<sup>2</sup> multi ring buffer implemented over the study area, using the average percentage of urban development for all built-up pixels. The direction of the urban growth for Tabuk city is presented. The result of urban development pattern for different periods described as 'extension, infill or leapfrog development, over open space.

## RESULTS

LULC maps showed a clear increase in irrigated agriculture and urban areas over a 30-year period (Fig. 2). Based on the classification results, change statistics in LULC in Tabuk are summarized (Table 2).

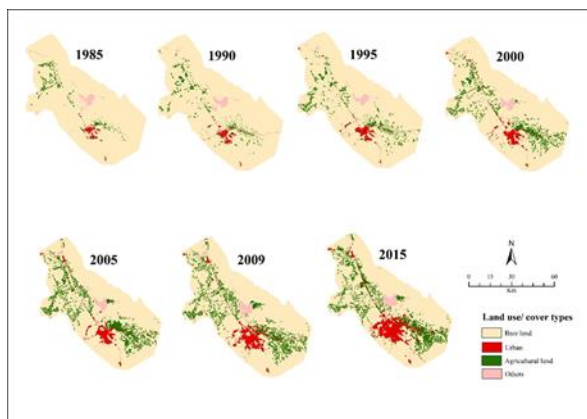


Fig. 2 Land use/land cover classification in Tabuk from 1985 to 2015

Table 2 Temporal change in land use/land cover for Tabuk (km<sup>2</sup>)

Year	Land Cover Categories			
	Bare	Urban	Agriculture	Others
1985	3986	48.3	112.5	66.1
1990	3927	64.4	152.3	68.8
1995	3840	88.1	226.7	57.3
2000	3652	122.1	357.8	80.3
2005	3465	145	528.3	73.7
2009	3405	203.6	524.4	78.9
2015	3218	315.1	576.6	102.9

The agricultural land for Tabuk in 1985 covered 112 km<sup>2</sup>, while in 2015 it covered 577 km<sup>2</sup>, an increase of 61 %. Urban land increased by 28% (from 48 km<sup>2</sup> in 1985 to 315 km<sup>2</sup> in 2015) (Table 2).

Both agriculture development and urbanisation have a similar trend over bare land (Fig. 3). From 1985 to 2015, around 767.75 km<sup>2</sup> of desert areas converted to agriculture land and built-up area.

In 2009, agriculture land had slight shrank (from 528.3 km<sup>2</sup> to 524.4 km<sup>2</sup>) of the total area, however, an increase in agriculture land by 52.2 km<sup>2</sup> was observed in 2015.

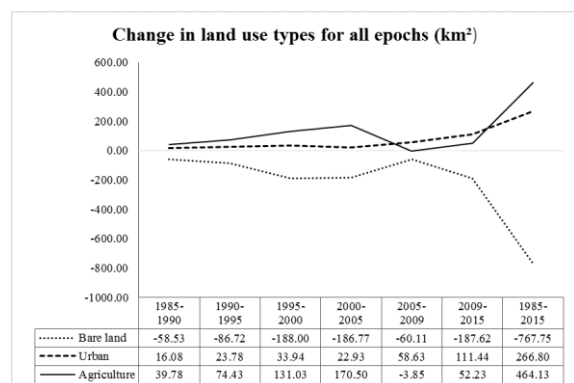


Fig. 3 Gain or loss of land use classes across seven epochs

Accuracy assessment for LULC classification generated an overall accuracy of > 92% across all image years (Table 3), which is the acceptable standard classification accuracy level of remotely sensed data for LULC [20].

In terms of producer's accuracy, vegetation and built up classes were over 76 %, and for bare land were above 97 %. Kappa coefficient of > 0.85 were obtained from the accuracy assessment for all images, while for the user's accuracy all classes were ranging from 87% to 100 %.

Table 3 User, Producers, Overall accuracy, and Kappa coefficient of LULC classification

Years	Classes	User accuracy	Producers accuracy	Overall Accuracy	Kappa coefficient
1985	Bare land	96	100	97	0.91
	Urban	100	95		
	Agriculture	100	75		
1990	Bare land	95	100	96	0.91
	Urban	100	92		
	Agriculture	100	78		
1995	Bare land	89	100	92	0.85
	Urban	100	79		
	Agriculture	100	82		
2000	Bare land	91	100	94	0.88
	Urban	100	84		
	Agriculture	100	84		
2005	Bare land	87	100	92	0.87
	Urban	96	77		
	Agriculture	100	90		
2009	Bare land	95	98	97	0.96
	Urban	96	96		
	Agriculture	100	97		
2015	Bare land	89	99	93	0.89
	Urban	90	98		
	Agriculture	100	85		

### Population Growth and Spatio-Temporal Analysis of Urban Growth

Urban expansion is based on the relationship between built-up area and population of an area. The latest demographic survey of Tabuk Province for 2016 revealed increase of population from 165 000 in 1985 to 890 922 in 2015 with an annual population growth rate 2.48.

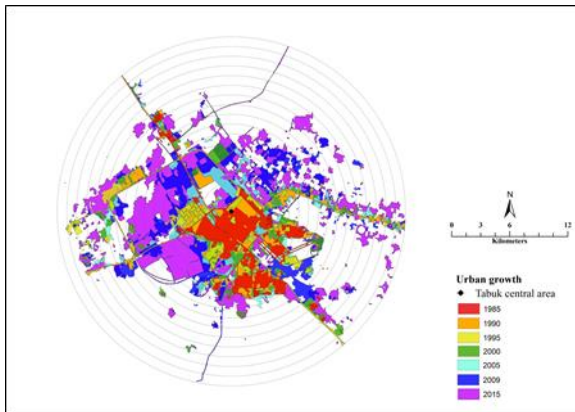


Fig. 4 The urban growth map for 30 years within 15 rings

The major urban growth was noticed in between time period (2009 to 2015) with around 112 km<sup>2</sup> had gained of built area (Fig. 4).

The urban type result of Tabuk in each epoch indicated that extension type development in Tabuk was the main urban growth type by 72%, whereas infill type growth only 11 %. The leapfrog type growth 17 % of total urban land (Table 4). The growth direction is clearly expanded towards the north-west and west of Tabuk city (Fig. 4 and Fig. 5).

Table 4 Area of urban growth attributed to each urban growth type

Epoch	Urban growth type (km <sup>2</sup> )		
	Extension	Infill	Leapfrog
1985 to 1990	31.64	4.22	7.33
1990 to 1995	31.28	9.73	8.73
1995 to 2000	41.99	6.98	16.09
2000 to 2005	58.96	7.49	8.82
2005 to 2009	91.97	3.96	19.97
2009 to 2015	133.19	25.68	30.47

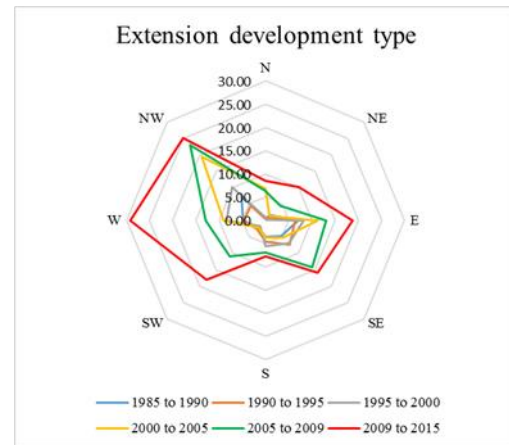


Fig. 5 Direction of urban growth for each epoch

## DISCUSSIONS

Quantitative results from OBIA classification allow us to understand spatio-temporal LULC change pattern. The view of [15], that OBA is suitable for assessing area under mixed urban agriculture in arid regions, is supported by the results found in this study. Social and economic change in Tabuk city over a 30-year period can be attributed to migration and increases in the military force leading to increased urbanisation that has changed the demography of the city. Reference [6] showed that migration in the Tabuk region for 1999 was the fourth largest after Riyadh, Makkah (Mecca), and Eastern regions. Many of the younger generation choose to leave the Nomadic way of life, drawn to the city by economic gain and social benefits [24]. People choose to move to Tabuk to gain better health service, education and increased job opportunities. The continued increase in population leads to a significant impact on the physical and economic infrastructure, and the spatial and social interaction within Tabuk city. [7]. Increasing population growth through migration impacts services for urban areas [25], while the additional pressure on limited natural resources and the subsequent rise in food insecurity [26].

Population size impacts the amount of agricultural land and water needed to grow food [27]. Rapid population growth and resource mismanagement can result in soil erosion and land degradation, causing imbalances in the environment [28].

Tabuk considered to be the largest producer of wheat, olives and grapes in Saudi Arabia, producing 200,000 tonnes of wheat annually [29]. A considerable increase of agricultural land and built-up areas in Tabuk attributed to increasing demand of land the growing population. The sharp increase in land use change to agriculture around Tabuk city reflects the implementation of wheat subsidies introduced in the 1980s [30]. The Saudi government encouraged agricultural projects, such as Astra farms and TADCO, with a view to increasing food self-sufficiency. In 2003, sustainable use of water for irrigation has been a top priority for Saudi Arabia, the government restructured agricultural policies to conserve natural resources and increase water use efficiency [30]. The loss of agricultural areas during 2005 to 2009 epoch coincidence with the government policy.

The trend for agriculture to expand to the northwest and southeast of Tabuk city is due to the accessibility of water from the Saq aquifer. Increased demand of water for agricultural and urban use coincided with decreasing groundwater levels of the Saq aquifer [5]. High demand of irrigation required for increased area of agriculture places immense pressure on valuable water reserves, being the most scarce resources in Saudi Arabia [31]. Agricultural land in Tabuk used pivot irrigation technique that exhibits relatively low efficiency for water usage in arid areas using fossil groundwater, which is not sustainable. More than 80% of the usable water for agriculture, industry and daily consumption is withdrawn annually to total

renewable supply in Saudi Arabia set the country in extremely high stress on its limited renewable water resources [32]. Desert climate and unsustainable human activity are creating stress on and depleting water resources in Saudi Arabia [33].

## CONCLUSIONS

Satellite data and GIS are complementary and have proven to be effective for providing information of agriculture and urban expansion. The high accuracy result showed OBIA can be an accurate LULC extraction method for Saudi Arabia and in other arid regions. Fast expanding agricultural and urban areas in Tabuk pose serious environmental threats that require urgent attention. Increasing agriculture and urban expansion that relies solely on groundwater resources is unsustainable and requires diligent management procedures. The expansion of Tabuk city is more

towards the west and north-western areas of the city, following the location of groundwater aquifer.

Several factors were identified in agricultural and urban area change that can contribute to the problems of land degradation in Tabuk city. Intensive crop irrigation of expanding agriculture across the Tabuk region, increases the risk of land degradation. Increasing population places additional pressure on the limited natural resources within this fragile, arid region. The result of this work would help government planners and decision makers to manage agricultural and urban growth in arid regions. This information is important for further prediction studies that can indicate potential impacts on natural resources and provide a spatio-temporal dynamics of LULC change.

## REFERENCES

- [1] F. A. Mubarak, "Urban growth boundary policy and residential suburbanization: Riyadh, Saudi Arabia," *Habitat International*, vol. 28, no. 4, pp. 567-591, 12// 2004.
- [2] M. S. Al-Shayaa, M. B. Baig, and G. S. Straquadine, "Agricultural extension in the Kingdom of Saudi Arabia: Difficult present and demanding future," *J. Anim. Plant Sci*, vol. 22, no. 1, pp. 239-246, 2012.
- [3] K. Al Harbi, "Discovering and detecting agricultural change in Eastern Tabuk - Saudi Arabia, using remote sensing technique.," *Kuwaiti Geographic Society*, vol. 283, 2003.
- [4] K. Al-Harbi, "Monitoring of agricultural area trend in Tabuk region-Saudi Arabia using Landsat TM and SPOT data," *The Egyptian Journal of Remote Sensing and Space Science*, vol. 13, no. 1, pp. 37-42, 2010.
- [5] M. E. Al-Ahmadi, "Hydrogeology of the Saq Aquifer Northwest of Tabuk, Northern Saudi Arabia.," *Journal of King Abdulaziz University: Earth Sciences*, vol. 20, pp. 51-66, 2009.
- I. A. Al Humaidi, "Internal Migration in Saudi Arabia: Its Magnitude and Trends," *Journal of King Saud University*, vol. 16, no. 1, 2004.
- [6] M. Bolca, B. Turkyilmaz, Y. Kurucu, U. Altinbas, M. T. Esetlili, and B. Gulgun, "Determination of impact of urbanization on agricultural land and wetland land use in Balçovas' Delta by remote sensing and GIS technique," *Environmental monitoring and assessment*, vol. 131, no. 1-3, pp. 409-419, 2007.
- [7] M. L. Zellner and H. W. Reeves, "Examining the contradiction in 'sustainable urban

- growth': an example of groundwater sustainability," *Journal of Environmental Planning and Management*, vol. 55, no. 5, pp. 545-562, 2012.
- [8] E. K. Albalawi and L. Kumar, "Using remote sensing technology to detect, model and map desertification: a review," *J Food Agric Environ*, vol. 11, pp. 791-797, 2013.
- [9] J. B. Campbell and R. H. Wynne, *Introduction to remote sensing*. Guilford Press, 2011.
- [10] T. Lillesand, R. W. Kiefer, and J. Chipman, *Remote sensing and image interpretation*. New York: John Wiley & Sons, 2014.
- [11] V. Walter, "Object-based classification of remote sensing data for change detection," *ISPRS Journal of photogrammetry and remote sensing*, vol. 58, no. 3, pp. 225-238, 2004.
- [12] S. Lang, "Object-based image analysis for remote sensing applications: modeling reality-dealing with complexity," in *Object-based image analysis*: Springer, 2008, pp. 3-27.
- [13] S. W. Myint, P. Gober, A. Brazel, S. Grossman-Clarke, and Q. Weng, "Per-pixel vs. object-based classification of urban land cover extraction using high spatial resolution imagery," *Remote Sensing of Environment*, vol. 115, no. 5, pp. 1145-1161, 5/15/ 2011.
- [14] C. S. Galletti and S. W. Myint, "Land-use mapping in a mixed urban-agricultural arid landscape using object-based image analysis: A case study from Maricopa, Arizona," *Remote Sensing*, vol. 6, no. 7, pp. 6089-6110, 2014.
- [15] M. Herold, J. Scepan, and K. C. Clarke, "The use of remote sensing and landscape metrics to describe structures and changes in urban land uses," *Environment and Planning A*, vol. 34, no. 8, pp. 1443-1458, 2002.
- [16] W. Ji, J. Ma, R. W. Twibell, and K. Underhill, "Characterizing urban sprawl using multi-stage remote sensing images and landscape metrics," *Computers, Environment and Urban Systems*, vol. 30, no. 6, pp. 861-879, 2006.
- [17] S. Angel, J. Parent, and D. Civco, "Urban sprawl metrics: an analysis of global urban expansion using GIS," in *Proceedings of ASPRS 2007 Annual Conference*, Tampa, Florida May, 2007, vol. 7, no. 11: Citeseer.
- [18] P. S. Chavez, "Image-based atmospheric corrections-revisited and improved," *Photogrammetric engineering and remote sensing*, vol. 62, no. 9, pp. 1025-1035, 1996.
- [19] J. R. Anderson, *A land use and land cover classification system for use with remote sensor data*. US Government Printing Office, 1976.
- [20] C. James, *Introduction to Remote Sensing*. New York: The Guilford Press; 3 edition, 2002.
- [21] D. Lu and Q. Weng, "A survey of image classification methods and techniques for improving classification performance," *International journal of Remote sensing*, vol. 28, no. 5, pp. 823-870, 2007.
- [22] G. Rees, *The Remote Sensing Data Book*. Cambridge University Press, 1999.
- [23] *Millennium Ecosystem Assessment*, "Ecosystems and human well-being," in "Washington, DC," 2005.
- [24] Z. Makhmreha and N. Almanasyeha, "Analyzing the State and Pattern of Urban Growth and City Planning in Amman Using Satellite Images and GIS," *European Journal of Social Sciences*, vol. 24, no. 2, pp. 225-264, 2011.
- [25] S. Eckert, "Urban expansion and its impact on urban agriculture-remote sensing based change analysis of Kizinga and Mzingu valley-DAR ES SALAAM, Tanzania," in *European Association of Remote Sensing Laboratories, EARSeL Proceedings*, Strasbourg, France, 2011, vol. 10, no. 1, pp. 46-55.
- [26] J. Harte, "Human population as a dynamic factor in environmental degradation," *Population and Environment*, vol. 28, no. 4-5, pp. 223-236, 2007.
- [27] L. Wang and J. J. Qu, "Satellite remote sensing applications for surface soil moisture monitoring: A review," *Frontiers of Earth Science in China*, vol. 3, no. 2, pp. 237-247, 2009.
- [28] S. Maisel, *Saudi Arabia and the Gulf Arab States Today: An Encyclopedia of Life in the Arab States* (no. 1). Greenwood Press, 2009.
- [29] The Kingdom of Saudi Arabia, "Trade Policy Review," in "World Trade Organization," 2011.
- [30] P. Vincent, *Saudi Arabia: An Environmental Overview*. CRC Press, 2008.
- [31] F. Gassert, P. Reig, I. Tianyi, and m. Andrew, "Aqueduct country and river basin rankings a weighted aggregation of spatially distinct hydrological i," *World Resources Institute*, , vol. Working Paper, 2013.
- [32] E. DeNicola, O. S. Aburizaiza, A. Siddique, H. Khwaja, and D. O. Carpenter, "Climate Change and Water Scarcity: The Case of Saudi Arabia," *Annals of Global Health*, vol. 81, no. 3, pp. 342-353, 5// 2015.

## COMPARISON OF LUNG DAMAGES DUE TO PETROL AND DIESEL CAR SMOKE EXPOSURES: HISTOLOGICAL STUDY

Wardoyo, Arinto Y.P.<sup>1</sup>, Juswono, Unggul P.<sup>2</sup>, Noor, Johan A. E.<sup>3</sup>

<sup>1</sup>Laboratory of Air Quality, Physics Department, Brawijaya University, Indonesia  
Jl. Veteran, Malang, Indonesia

### ABSTRACT

**Background;** Motor vehicles have significantly recognized to have a role in air pollution. The emissions regarding particles and gasses have identified to affect human health depending on the concentration, constituents, kind of vehicles, and fuels. This study investigated the impacts of the petrol and diesel car smoke on mice lung. The aims were to observe the mice lung injury caused by the smoke exposures emitted by petrol and diesel car. The lung injury was identified by using the histological images. The mice were exposed to the smoke with a particular concentration conducted by introducing the smoke into the chamber with the dimension of 30x20x20 cm<sup>3</sup> as long as 40 seconds. The mice exposures were carried out daily for eight days. The lung injury was observed using a Binocular BX-51 Computer Microscope with the 400x magnification to the histological images. We identified the healthy cells and damage cells to determine the lung damage showed by the destructive index. The results showed that the mice exposed to diesel cars have higher index rather than those with the petrol car exposures.

*Keywords: Smoke exposures, Petrol cars, Diesel cars, Lung damage.*

### INTRODUCTION

The traffic pollutants have significantly contributed to the air quality and adverse on health effects. The car emissions contained some dangerous compounds have triggered health problems [1] based on the type of the pollutant itself [2]. There are two kinds of the fuel used to run the engine such as diesel and gasoline. The emissions are in the form of Both types of engine produced compounds that are in the form of gasses [3] and particles [8]. The emission compounds consist of polycyclic aromatic hydrocarbon [4], nitro polycyclic aromatic hydrocarbon [5], black carbon [6], NO<sub>x</sub> [7], particulate matter in various size (PM<sub>25</sub>, PM<sub>10</sub>, PM<sub>2.5</sub>, PM<sub>1.0</sub>, and PM<sub>0.1</sub>) [8] in the different concentration depended on their composition, blended, driving methods, [9], engine type [10], and compression ratio [11].

Fine particles (PM<sub>2.5</sub>) and ultrafine particles (PM<sub>0.1</sub>) are commonly found in the car smoke [12]. The problem of these particles is due to their size, made them possible to be in their airborne and inhaled by the human [13]. The result is a health problem [2] that has reported mostly in respiratory diseases because of the particle emissions [14]. The concentration of fine particle and ultrafine particles was found high in the area close to Highway [15]. This resulted in the increase of the risk for the people living near the highway that had to be exposed daily [16]. Based on the previous research about the effect of the vehicles smoke for the traffic

assistance that increased the chance of development cancer [17].

In general, the vehicle smoke exposures have identified to affect to a lung damage. Previous studies showed that particle exposures have resulted in the respiratory inflammation response [18], alveolar enlargement [19], oxidative stress [20], and alveolar lavage fluids [21]. The allergy response was the most reported cases [22], [23]. The other circumstances were influenza-like illness [24], alveolar emphysema [25], lung cancer [26], and chronic obstructive pulmonary disease (COPD) [27]. The impacts of the vehicle emissions on lung, there is less information available, especially for the emissions from the car using a different fuel. In this study, we tried to observe the effects of the car smoke exposures on lung damage to better understanding the impacts of the emissions emitted by the car operate using diesel and petrol fuel.

### METHODS

#### General Method

Three different cars were used as the samples based on their popularity in the Indonesia. The sample 1 was that the car with the engine capacity of 2000cc was operated using petrol fuel. The sample 2 and 3 were powered using a diesel engine. To characterize the effect of petrol and diesel car emission, we prepared 4 groups of mice. The mice were chosen by their similar characteristic in the

response of the lungs to reveal the effect of the smoke with the human respiratory system [28]. The first group acted as a control that we named the control group. The second group was exposed to petrol car smoke as petrol group, the third labeled diesel 1 and the fourth called diesel 2 were the samples overcoming diesel car smoke exposures. Each of the group excepted control group was experienced for 100-second exposures with the dose concentration that was set up by introducing the smoke into a chamber as long as 40 seconds. The lung of the mice was taken after the 8 exposure days and observed using a Binocular BX-51 Computer Microscope with the 400x magnification. Each histological images of the lung were identified to determine the damage.

To know the concentration of the ultrafine particles and the fine particles in the smoke, we measured the concentration using a *P-Track type* 8525 and a *Kanomax model* 2443 dust monitor. The smoke of the car was collected by the airbag; then the smoke was injected into the chamber with the dimension of 30x20x20 cm<sup>3</sup> with the rate of 2 m/s for 40 seconds. The total concentration of the particles in the smoke was calculated by the summing of the measured particle concentrations.

### Mice Preparation

The mice were treated by following the standard of humane animal care and the guidelines by the Ethics Committee of Experimental Animal of the University of Brawijaya. The mice were kept in the quarantine chamber to isolate from any external pollutant source to avoid the contamination in the standard light (12:12 dark-light) and standard RH-temperature conditions [29]. To reduce the mice stress during exposures, the acclimation processes were done for 3 days by putting the mice into the exposure chamber for 100 seconds.

### Histological Analysis

The histological damage analysis was conducted by observing the lung sample images by using the microscope with the magnification of 400 times and were identified by a counting method. The lung injuries were found as alveolar geometrical damage [30], loss of alveolar wall [31], hemorrhage [32], and the inflammation responses [33]. The destructive index [34] was used to analyze the damage level by following the equation (1)

$$D_e = \frac{D_c}{T_c} \quad (1)$$

With  $D_e$  is destructive index,  $D_c$  is the damage cell counted,  $T_c$  is total cells counted by adding the damage cell with the normal once [35].

### RESULT AND DISCUSSIONS;

The total concentrations of the ultrafine and fine particles contained in the smoke presented in Table 1. The particle concentrations are found low for the petroleum car of  $(14.88 \pm 0.24 \times 10^{11})$  particles/cm<sup>3</sup> for ultrafine and  $(1.54 \pm 0.09) \times 10^{-3}$  mg/m<sup>3</sup> for fine particles. In the diesel car, the total concentration of the ultrafine is found much higher than the petrol car of  $(60.00 \pm 3.20) \times 10^{11}$  and  $(102.40 \pm 5.60) \times 10^{11}$  particles/cm<sup>3</sup>. In case of fine particles, we also found the similar result by  $(162.06 \pm 6.90) \times 10^{-3}$  mg/m<sup>3</sup> and  $(376.30 \pm 7.73) \times 10^{-3}$  mg/m<sup>3</sup>. The increase of the concentration of ultrafine and fine particle in the diesel cars was found directly proportional to the engine capacity. In the measurement results for both type of particulate, the higher engine capacity resulted in the increase of the ultrafine and fine particles contained in the smoke.

Table 1 Total concentrations of ultrafine and fine particles

Fuel Type	Engine capacity (cc)	Total Concentration			
		UFPs (x10 <sup>11</sup> particles)		FPs(x10 <sup>-3</sup> mg/m <sup>3</sup> )	
		Mean	Dv	Mean	Dv
Petrol	2000	14.9	0.2	1.5	0.1
Diesel 1	2238	60.0	3.2	162.1	6.9
Diesel 2	2500	102.4	5.6	376.3	7.7

In the table, one of the factors that were found affecting the smoke ultrafine and fine particle concentration is the engine capacity. The increase of the engine size increases both of ultrafine and fine particles in the smoke. However, between the petrol and the diesel car was found the concentrations differ in the large number. This indicates that the engine type affects the concentration of ultrafine and fine particles in the smoke [36]. This data are supported by the fact that the properties of the fuel used in the combustion system emitting the significant different amount of particles [37], [38]. The diesel engine vehicles had a more significant contribution in the particulate matter concentration than the petrol ones in the road.



### Lung Damage Identification

The lung damages identified in the histological images are found similarly. The alveolus damages (blue dots) that are the geometrical changes both the shape and size, the inflammation (red circle), and loss of alveolus wall (yellow circle) may as the result of the oxidative response by the particles [39].

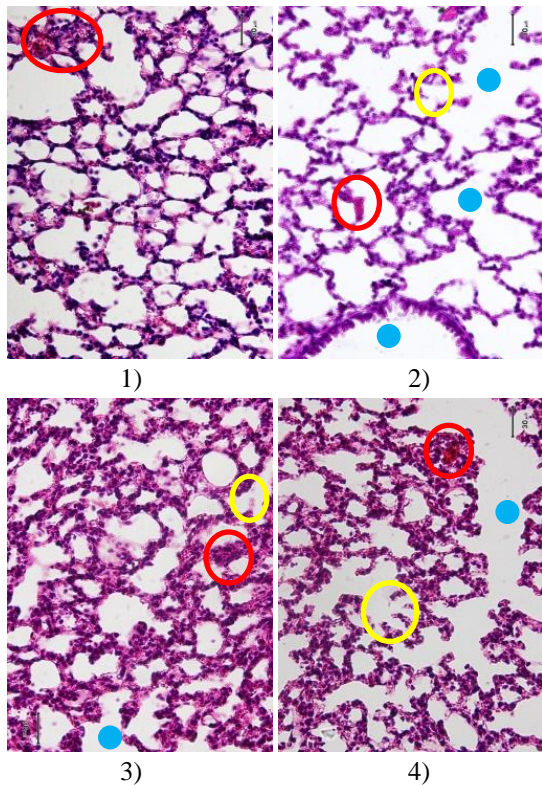


Fig. 1 The mice lung condition after exposed to the smoke. (1) Control; (2) Petrol; (3) Diesel 1; (4) Diesel 2

This results in the development of emphysema in the lung by the work of pro-inflammation cytokine and anti-inflammation cytokine [40]. The emphysema is predicted because of the release of reactive oxygen series (ROS) [41] that loss of the alveolar septum [42], triggered the pro-inflammatory cytokine [43]. The result is the inflammation in the lung tissues. However, the inflammation itself has not triggered the development of alveolar damage [44]. The release of anti-inflammation [45] repairs the alveolar and results in the elaboration of the emphysema. In Fig 1, the alveolar damage can be seen as the irregular shape of alveolar and the enlargement of the area [19]. In the same figure also identified the inflammation area that is believed to trigger the emphysema itself [46]. The depleted of the

alveolar septum is also found in the image by observing the loosening of the alveolar wall. The hemorrhage is also found in the figure by the appearance of the erythrocytes in particular area.

### Damage Analyst

The damages of the lung are analyzed to relate to the effect engine type. Figure 2 displays the lung damage indicated by the destructive index for the car samples. The petrol car has the lowest index among the samples of 0.45. The diesel car with the engine capacity of 2238 cc has the index of 0.47 and the other diesel car sample with the engine capacity of 2500 cc causes the lung damage with the index of 0.46. The different damage of the lung posed by the diesel car smoke exposure does not show a significant different.

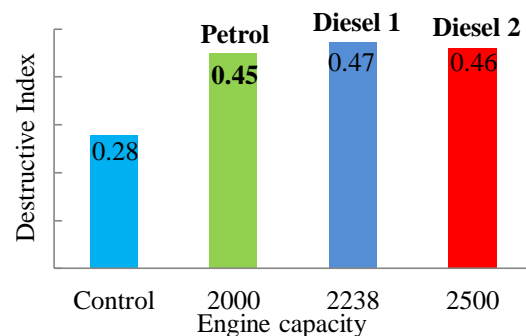


Fig. 2 The destructive lung index for the car samples.

The lung damage between the control and the exposed samples give a large difference of the destructive index. This indicates that the car smoke surely damages the lung tissues. The limitation of the samples may not show many differences of the lung damage between the petrol and diesel car. The engine technology may affect the lung damage due to the particle emission production [47].

### CONCLUSION

The different fuel and engine capacity result in the different concentration of the ultrafine and fine particles in the smoke. The diesel fuel cars produce the large particle concentration than the petrol car. Exposures diesel car smoke to mice cause more the lung damage than petrol car smoke exposures.

### ACKNOWLEDGEMENT

All the authors are grateful to Directorate General of Higher Education, for providing funding for this research project. The kind hands of Eko Teguh,



Arif Budianto, Mia Anggun, involving in this study are gratefully acknowledged.

## REFERENCES

- [1] M. Kampa and E. Castanas, "Human health effects of air pollution," *Environ. Pollut.*, vol. 151, pp. 362–367, 2008.
- [2] K. Kim, E. Kabir, and S. Kabir, "A review on the human health impact of airborne particulate matter," *Environ. Int.*, vol. 74, pp. 136–143, 2015.
- [3] I. M. Kooter, M. A. T. M. Van Vugt, A. D. Jedynska, P. C. Tromp, M. M. G. Houtzager, R. P. Verbeek, G. Kadijk, M. Mulderij, and C. A. M. Krul, "Toxicological characterization of diesel engine emissions using biodiesel and a closed soot filter," *Atmos. Environ.*, vol. 45, no. 8, pp. 1574–1580, 2011.
- [4] I. Ferecatu, M. Borot, C. Bossard, M. Leroux, N. Boggetto, F. Marano, A. Baeza-Squiban, and K. Andreau, "Polycyclic aromatic hydrocarbon components contribute to the mitochondria-antiapoptotic effect of fine particulate matter on human bronchial epithelial cells via the aryl hydrocarbon receptor," *Part. Fibre Toxicol.*, vol. 7, p. 18, 2010.
- [5] C. Thuy, T. Kameda, A. Toriba, and K. Hayakawa, "Polycyclic aromatic hydrocarbons and nitro polycyclic aromatic hydrocarbons in particulates emitted by motorcycles," *Environ. Pollut.*, vol. 183, pp. 175–183, 2013.
- [6] A. L. Holder, G. S. W. Hagler, T. L. B. Yelverton, and M. D. Hays, "On-road black carbon instrument intercomparison and aerosol characteristics by driving environment," *Atmos. Environ.*, vol. 88, pp. 183–191, 2014.
- [7] L. Cédric, M. Goriaux, P. Tassel, P. Perret, M. André, and Y. Liu, "Impact of after-treatment device and driving conditions on black carbon, ultrafine particle and NO<sub>x</sub> emissions for Euro 5 Diesel and gasoline vehicles," *Transp. Res. Procedia*, vol. 14, no. 2, pp. 3079–3088, 2016.
- [8] F. J. Kelly and J. C. Fussell, "Size, source and chemical composition as determinants of toxicity attributable to ambient particulate matter," *Atmos. Environ.*, vol. 60, pp. 504–526, 2012.
- [9] Y. Yao, J. Tsai, and I. Wang, "Emissions of gaseous pollutant from motorcycle powered by ethanol – gasoline blend," *Appl. Energy*, vol. 102, pp. 93–100, 2013.
- [10] Y. Liu, P. Tassel, P. Perret, and M. Andr, "PAH, BTEX, carbonyl compound, black-carbon, NO<sub>2</sub> and ultrafine particle dynamometer bench emissions for Euro 4 and Euro 5 diesel and gasoline passenger cars," *Atmos. Environ.*, vol. 141, no. 2, pp. 80–95, 2016.
- [11] T. Lattimore, J. M. Herreros, H. Xu, and S. Shuai, "Investigation of compression ratio and fuel effect on combustion and PM emissions in a DISI engine," *FUEL*, vol. 169, pp. 68–78, 2016.
- [12] B. Srimuruganandam and S. M. S. Nagendra, "Characteristics of particulate matter and heterogeneous traffic in the urban area of India," *Atmos. Environ.*, vol. 45, no. 18, pp. 3091–3102, 2011.
- [13] M. G. Perrone, M. Gualtieri, V. Consonni, L. Ferrero, G. Sangiorgi, E. Longhin, D. Ballabio, E. Bolzacchini, and M. Camatini, "Particle size, chemical composition, seasons of the year and urban, rural or remote site origins as determinants of biological effects of particulate matter on pulmonary cells," *Environ. Pollut.*, vol. 176, pp. 215–227, 2013.
- [14] H. Lin, W. Ma, H. Qiu, M. G. Vaughn, E. J. Nelson, Z. Qian, and L. Tian, "Is standard deviation of daily PM<sub>2.5</sub> concentration associated with respiratory mortality?," *Environ. Pollut.*, vol. 216, pp. 208–214, 2016.
- [15] S. Fu and Y. Gu, "Highway toll and air pollution: Evidence from Chinese Cities," *J. Environ. Econ. Manage.*, vol. 83, pp. 32–49, 2017.
- [16] D. Goto, K. Ueda, C. Fook, S. Ng, A. Takami, T. Ariga, K. Matsushashi, and T. Nakajima, "Estimation of excess mortality due to long-term exposure to PM<sub>2.5</sub> in Japan using a high-resolution model for present and future scenarios," *Atmos. Environ.*, vol. 140, pp. 320–332, 2016.
- [17] X. Xue, Y. You, J. Wu, B. Han, Z. Bai, N. Tang, and L. Zhang, "Exposure measurement, risk assessment and source identification for exposure of traffic assistants to particle-bound PAHs in Tianjin, China," *J. Environ. Sci.*, vol. 26, no. 2, pp. 448–457, 2014.
- [18] Y. Han, T. Zhu, T. Guan, Y. Zhu, J. Liu, Y. Ji, S. Gao, F. Wang, H. Lu, and W. Huang, "Science of the Total Environment Association between size-segregated particles in ambient air and acute respiratory inflammation," *Sci. Total Environ.*, vol. 565, pp. 412–419, 2016.
- [19] K. Yoshizaki, J. M. Brito, H. T. Moriya, A. C. Toledo, S. Ferzilan, A. Paula, L. De Oliveira, I. D. Machado, S. H. P. Farsky, L. F. F. Silva, M. A. Martins, P. H. N. Saldiva, T. Mauad, and M. Macchione, "Chronic exposure of diesel exhaust particles induces alveolar enlargement in mice," *Respir. Res.*, pp. 1–10, 2015.
- [20] J. O. Ogunbileje, R. S. Nawgiri, J. I. Anetor, O. M. Akinosun, E. O. Farombi, and A. O. Okorodudu, "Particles internalization, oxidative stress, apoptosis and pro-inflammatory cytokines in alveolar macrophages exposed to cement dust," *Environ.*

- Toxicol. Pharmacol.*, vol. 37, no. 3, pp. 1060–1070, 2014.
- [21] S. Robertson, G. a Gray, R. Duffin, S. G. McLean, C. a Shaw, P. W. F. Hadoke, D. E. Newby, and M. R. Miller, “Diesel exhaust particulate induces pulmonary and systemic inflammation in rats without impairing endothelial function ex vivo or in vivo.,” *Part. Fibre Toxicol.*, vol. 9, no. 1, p. 9, 2012.
- [22] L. Bråbäck and B. Forsberg, “Does traffic exhaust contribute to the development of asthma and allergic sensitization in children: findings from recent cohort studies.,” *Environ. Health*, vol. 8, p. 17, 2009.
- [23] N. Li, S. Georas, N. Alexis, P. Fritz, T. Xia, and M. A. Williams, “Task force report A work group report on ultrafine particles ( American Academy of Allergy , Asthma & Immunology ): Why ambient ultrafine and engineered nanoparticles should receive special attention for possible adverse health outcomes in human subjects,” *J. Allergy Clin. Immunol.*, vol. 138, no. 2, pp. 386–396, 2016.
- [24] C. Feng, J. Li, W. Sun, Y. Zhang, and Q. Wang, “Impact of ambient fine particulate matter ( PM<sub>2.5</sub> ) exposure on the risk of influenza- like-illness : a time-series analysis in Beijing , China,” *Environ. Heal.*, pp. 1–12, 2016.
- [25] J. Kravchenko, I. Akushevich, A. P. Abernethy, S. Holman, W. G. Ross, and H. Kim Lyerly, “Long-term dynamics of death rates of emphysema, asthma, and pneumonia and improving air quality,” *Int. J. COPD*, vol. 9, pp. 613–627, 2014.
- [26] C. Liao, C. Chio, W. Chen, Y. Ju, W. Li, Y. Cheng, V. H. Liao, S. Chen, and M. Ling, “Lung cancer risk in relation to traffic-related nano / ultrafine particle-bound PAHs exposure : A preliminary probabilistic assessment,” *J. Hazard. Mater.*, vol. 190, no. 1–3, pp. 150–158, 2011.
- [27] J. Li, S. Sun, R. Tang, H. Qiu, Q. Huang, T. G. Mason, and L. Tian, “Major air pollutants and risk of COPD exacerbations : a systematic review and,” *Int. J. COPD*, vol. 11, pp. 3079–3091, 2016.
- [28] T. Maes, S. Provoost, E. a Lanckacker, D. D. Cataldo, J. a J. Vanoirbeek, B. Nemery, K. G. Tournoy, and G. F. Joos, “Mouse models to unravel the role of inhaled pollutants on allergic sensitization and airway inflammation.,” *Respir. Res.*, vol. 11, p. 7, 2010.
- [29] N. K. Iversen, S. Frische, K. Thomsen, C. Laustsen, M. Pedersen, P. B. L. Hansen, P. Bie, J. Fresnais, J. F. Berret, E. Baatrup, and T. Wang, “Superparamagnetic iron oxide polyacrylic acid coated  $\gamma$ -Fe<sub>2</sub>O<sub>3</sub> nanoparticles do not affect kidney function but cause acute effect on the cardiovascular function in healthy mice,” *Toxicol. Appl. Pharmacol.*, vol. 266, no. 2, pp. 276–288, 2013.
- [30] B. Phillips, E. Veljkovic, S. Boué, W. K. Schlage, G. Vuillaume, F. Martin, B. Titz, P. Leroy, A. Buettner, A. Elamin, A. Oviedo, M. Cabanski, H. De León, E. Guedj, T. Schneider, M. Talikka, N. V. Ivanov, P. Vanscheeuwijck, M. C. Peitsch, and J. Hoeng, “An 8-month systems toxicology inhalation/cessation study in Apoe<sup>-/-</sup> mice to investigate cardiovascular and respiratory exposure effects of a candidate modified risk tobacco product, THS 2.2, compared with conventional cigarettes,” *Toxicol. Sci.*, vol. 149, no. 2, pp. 411–432, 2016.
- [31] G. Vlahovic, M. L. Russell, R. R. Mercer, and J. D. Crapo, “Cellular and Connective Tissue Changes in Alveolar Septal Walls in Emphysema.”
- [32] M. Durga, S. Nathiya, A. Rajasekar, and T. Devasena, “Effects of ultrafine petrol exhaust particles on cytotoxicity , oxidative stress generation , DNA damage and inflammation in human A549 lung cells and murine RAW 264 . 7 macrophages,” *Environ. Toxicol. Pharmacol.*, vol. 38, no. 2, pp. 518–530, 2014.
- [33] K. M. Gowdy, Q. T. Krantz, C. King, E. Boykin, I. Jaspers, W. P. Linak, and M. I. Gilmour, “Role of oxidative stress on diesel-enhanced influenza infection in mice,” *Part Fibre Toxicol*, vol. 7, p. 34, 2010.
- [34] M. Saetta, R. J. Shiner, G. E. Angus, W. O. N. D. Kim, N. Wang, M. King, H. Ghezzi, and M. G. Cosio, “Destructive Index: A Measurement of Lung Parenchymal Destruction in,” no. 5.
- [35] A. a Robbesom, E. M. M. Versteeg, J. H. Veerkamp, J. H. J. M. van Krieken, H. J. Bulten, H. T. J. Smits, L. N. a Willems, C. L. a van Herwaarden, P. N. R. Dekhuijzen, and T. H. van Kuppevelt, “Morphological quantification of emphysema in small human lung specimens: comparison of methods and relation with clinical data.,” *Mod. Pathol.*, vol. 16, no. 1, pp. 1–7, 2003.
- [36] K. Mathivanan, J. M. Mallikarjuna, and A. Ramesh, “Influence of multiple fuel injection strategies on performance and combustion characteristics of a diesel fuelled HCCI engine – An experimental investigation,” *Exp. Therm. Fluid Sci.*, vol. 77, pp. 337–346, 2016.
- [37] Z. Zhang and R. Balasubramanian, “Physicochemical and toxicological characteristics of particulate matter emitted from a non-road diesel engine : Comparative evaluation of biodiesel-diesel and butanol-diesel blends,” *J. Hazard. Mater.*, vol. 264, pp. 395–402, 2014.
- [38] X. Cao, Z. Yao, X. Shen, Y. Ye, and X. Jiang, “On-road emission characteristics of

- VOCs from light-duty gasoline vehicles in Beijing, China,” *Atmos. Environ.*, 2015.
- [39] J. A. Araujo and A. E. Nel, “Particulate matter and atherosclerosis : role of particle size , composition and oxidative stress,” *Part. Fibre Toxicol.*, vol. 19, pp. 1–19, 2009.
- [40] A. T. Saber, N. R. Jacobsen, J. Bornholdt, S. L. Kjær, M. Dybdahl, L. Risom, S. Loft, U. Vogel, and H. Wallin, “Cytokine expression in mice exposed to diesel exhaust particles by inhalation. Role of tumor necrosis factor,” *Part. Fibre Toxicol.*, vol. 8, pp. 1–8, 2006.
- [41] A. Baulig, M. Garlatti, V. Bonvallot, A. Marchand, R. Barouki, F. Marano, and A. Baeza-Squiban, “Involvement of reactive oxygen species in the metabolic pathways triggered by diesel exhaust particles in human airway epithelial cells,” *Am. J. Physiol. Cell. Mol. Physiol.*, vol. 285, no. 3, pp. L671–L679, 2003.
- [42] R. M. Tuder, T. Yoshida, W. Arap, R. Pasqualini, and I. Petrache, “State of the Art Cellular and Molecular Mechanisms of Alveolar An Evolutionary Perspective,” vol. 3, 2006.
- [43] A. Kode, S.-R. Yang, and I. Rahman, “Differential effects of cigarette smoke on oxidative stress and proinflammatory cytokine release in primary human airway epithelial cells and in a variety of transformed alveolar epithelial cells,” *Respir. Res.*, vol. 7, no. 1, p. 132, 2006.
- [44] G. Arunachalam, I. K. Sundar, J.-W. Hwang, H. Yao, and I. Rahman, “Emphysema is associated with increased inflammation in lungs of atherosclerosis-prone mice by cigarette smoke: implications in comorbidities of COPD,” *J. Inflamm. (Lond.)*, vol. 7, p. 34, 2010.
- [45] X. Huang, Y. Liu, Y. Lu, and C. Ma, “Anti-inflammatory effects of eugenol on lipopolysaccharide-induced inflammatory reaction in acute lung injury via regulating inflammation and redox status,” *Int. Immunopharmacol.*, vol. 26, no. 1, pp. 265–271, 2015.
- [46] H. Parameswaran, A. Majumdar, S. Ito, A. M. Alencar, and B. Suki, “Quantitative characterization of airspace enlargement in emphysema,” *J. Appl. Physiol.*, vol. 100, no. September 2005, pp. 186–193, 2006.
- [47] M. Fiebig, A. Wiartalla, B. Holderbaum, and S. Kiesow, “Particulate emissions from diesel engines: correlation between engine technology and emissions,” *J. Occup. Med. Toxicol.*, vol. 9, no. 1, p. 6, 2014.

## SPATIAL VARIATIONS OF SURFACE WATER QUALITY AND POLLUTION SOURCES IN KHLONG U-TAPAO RIVER BASIN

Saudee Maprasit<sup>1</sup>, Chaisri Suksaroj<sup>2</sup>, Vichit Rangpan<sup>3</sup>, and Rotchanatch Darnsawadi<sup>4</sup>

<sup>1</sup>Department of Applied Science, Faculty of Science, Technology and Agriculture, Yala Rajabhat University, Thailand; <sup>2</sup>Faculty of Engineering, <sup>3</sup>Faculty of Environmental Management, Prince of Songkhla University, Thailand

### ABSTRACT

Multivariate statistical analysis, cluster analysis, parametric analysis, as well as factor analysis were applied to analyze water quality dataset including 9 parameters at 21 sites of the Khlong U-Tapao river basin in Songkhla province, Thailand, from 2007–2015 to investigate spatial variations of water quality and identify potential sources of pollution. Using cluster analysis to classify the three-periods of water quality variation in each monitoring site has shown 3 water quality measures: high, moderate and low. Using parametric study to describe variations of water quality and the significantly identified land use variables affecting water quality, such as urbanization and industrial land use which are sources of pollution in upstream. However, in midstream, Economical urbanization is the pollution source while agricultural land use is the pollution source in downstream. Factor analysis identified that the major pollutants in the upstream were turbidity and conductivity matter from soil erosion in rainy season and industrial wastewater, in the midstream, biochemical oxygen demand of organic matters from wastewater discharge from domestic settlements were the main pollutants while in downstream, nutrients from agricultural practices were the major pollutants. From upstream to downstream, bacterial pollutants were the main pollutants from all activities. These results provide fundamental information for developing better water pollution control strategies for the Khlong U-Tapao river basin.

*Key words:* Water quality; Spatial variations; Multivariate statistical analysis; Khlong U-Tapao river basin

### INTRODUCTION

Water, the one fourth natural resources for develop human life quality. The drive source of various systems for example socio-political-economical system of human activities. There are urbanization, agricultures, aquacultures and industries. Water quality, the indicator was pointed suitability which relevant to characteristics of physical-chemical-biological properties for use in each activities of human life execution. A development is related to water quality degradation [1]. One of the Nation significance natural resource concern issue is water quality management [2]. The execution contains various components and uncertainty of qualitative and quantitative information from the interrelationship in their [3], [4]. The main component influence water quality to degradation is products from point-nonpoint source of human life development, a pollution source to water quality. The various land use leachate is a major issue in study and management [2].

The obstacle of water quality management is large scale and plenty of factors, including population growth, land use in each pattern and practice of urbanization, agriculture, aquaculture and industry comprehensive all activity in water supply system [5]. Therefore, to evaluate the state of water quality, the spatio-temporal influential factors such

as season and land use change are considered to investigate impact on water quality [6]. Seasonal change and urban land use change is the impacts on surface water quality, for example how urban scenarios encourages in low, normal and commercial urban growth are impacts on water quality [7]. Furthermore, water quality changes by seasonal change and nutrients loading from land degradation, sediment with nutrients from agricultural land use is damaging to catchment aquatic systems, almost of pollutants from point source of industrial land use such as wastewater discharge. Population growth, unplanned domestic, deforestation, farming and livestock intension, agriculture expansion and infrastructure are human activity which differently impact on water quality.

Land use is the major source of pollution in river water basin. All relationship there are the question what is the affection land use change to water quality, what is the season factors causing different land use and transformation and what is the consequence of the results to water quality. Land use type, occupation and transformation causing to different hydrology and what is the water quality outcome. Therefore, the study in water quality management must to know how the relationship of water quality by land use change with seasonal change.

Water quality studies and management in Khlong U-Tapao river basin for problem solving are complex system education that focused on related factors based on temporal-spatial change. Study in water quality and management just to study behavior and trends of dynamic change include relationship and interaction of variables in the system under different of spatial and temporal including land use change and seasonal parameter. The objectives of this study are quantified the contributions impact of spatial-temporal change to water quality and recognize water quality system. In addition to discuss and point pollution sources for how to solve the impact of land use practice and human driven force on water quality and what feasible actions should be taken from causing adverse effects in each season.

## STUDY AREA

Khlong U-tapao is a sub-basin of Songkhla lake basin located at southern part of Thailand. The basin is about 60 km long from north to south, and 40 km wide from west to east, and total coverage is about 2,805 square kilometers [8], [9], [10] (Fig.1). There are 7 district such as Sadao, Namom, Hatyai, Khlong hoi kong, Bangklam, Ratpum and Kuanniang.

Pollution sources in Khlong U-Tapao river basin come from various land use which divided that, there are; 1) Residential Land Uses which are more found in plain area or low land for example in Hatyai municipality, Khohong sub-district municipality, Banpru municipality, Sadao municipality and comprehensive area of sub-district administrative organization. 2) Agricultural Land Uses, for example para-rubber plantation, paddy field, fruit plantation, palm plantation, farm of cows, buffalos and goats including shrimp farms. The area of paddy field is on low land of the north or upstream of basin, para-rubber and palm plantation is on the south or begin from midstream to downstream of basin. Fruit plantation is distribution around of rural community area. 3) Forestry, which are area of tropical rain forest, swamp forest, bother peat swamp and mangrove swamp and deciduous forest. Almost of tropical rain forest is found on the west of basin. 4) Industrial land use is a main of various para-rubber process and frozen foods. All is found most in urban community. 5) Water resources and 6) Lowland and bare land.

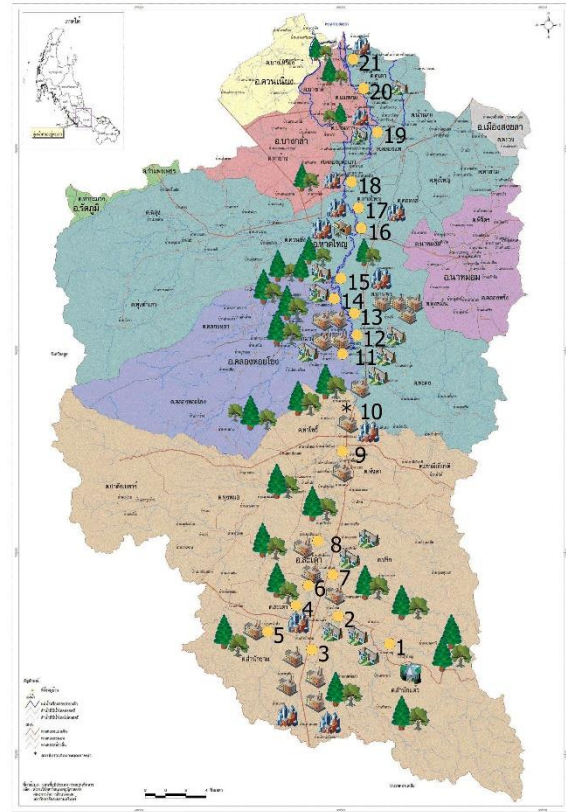


Fig.1 Khlong U-tapao river basin Map and land-use

Table 1 water quality monitoring sites

station	Geographic Co-System		Location area
	Longitude (Easting)	Latitude (Northing)	
UT01	100.490	6.593	Samnak Tao SAO
UT02	100.439	6.636	
UT03	100.410	6.599	
UT04	100.417	6.632	Sadao TM
UT05	100.396	6.632	
UT06	100.430	6.665	
UT07	100.436	6.670	Prik SM
UT08	100.436	6.702	
UT09	100.446	6.776	
UT10	100.441	6.820	Tha Poh SAO
UT11	100.466	6.853	Phatong SM
UT12	100.459	6.865	
UT13	100.460	6.881	
UT14	100.457	6.897	Ban Phru TM
UT15	100.442	6.928	
UT16	100.466	6.977	
UT17	100.465	6.984	Khohong SM
UT18	100.455	7.029	Khuan Lang SM
UT19	100.471	7.070	Khlong Hae TM
UT20	100.468	7.105	Mae Tom SAO
UT21	100.458	7.124	Ku Tao SM

**Note:** SAO: Subdistrict Administration Organization, SM: Subdistrict Municipality, TM: Town Municipality (Department of Provincial Administration, Ministry of Interior, 2013).

The secondary data of water quality come from 21 stations along the Khlong U-Tapo river basin (Fig.1, table 1) and cover 13 administrative districts, there are 4 sub-district administration organization (SAO), 6 sub-district municipality (SM) and 3 town municipalities (TM) [10].

In this basin area was separated in to 3 part such as upstream part, it started from station UT01 to UT09, midstream from UT10-UT17 and downstream from UT18-UT21.

## MATERIALS AND METHODS

### Data

Water quality parameters was collected from secondary data of pH, water temperature (WT), turbidity (TB), dissolved-oxygen (DO), conductivity (CD), biochemical-oxygen-demand (BOD), Total-Coliform-Bacteria (TCB), Nitrogen-Ammonia ( $\text{NH}_3\text{-N}$ ) and Fecal-Coliform-Bacteria (FCB) from Regional Environmental Office 16, Songkhla from 2007-2015. Land use was separated into 3 types of agriculture, industry and urbanization. Agricultural data was gathered from Provincial Agricultural Extension Office, Sadao district, Songkhla. Industrial data was gathered from Songkhla Provincial Industry Office. Urbanization was gathered from Department of Provincial Administration, Ministry of Interior,

### Statistical analysis

A statistical analysis is used for a normal distribution. Correlation is studied for variable relationship by multiple independents [11], [12]. Cluster analysis is used to identify variations of water quality. Factor analysis is applied to use for identified pollution factors which related to pollution sources of river basin and performed this suitable method by Kaiser-Meyer-Olkin (KMO) and Barlett's test [13].

## RESULT AND DISCUSSION

### Water Quality Variations by Seasonal Change

The variations of water quality by seasonal change presented in fig.2 and table 2, in all the year, WT varied from 26.0-34.0  $^{\circ}\text{C}$ , pH from 4.4-9.2, TB from 3.0-307.48 NTU, CD from 0.01-15,064.0  $\mu\text{S}/\text{cm}$ , DO from 0.10-7.60 mg/L, BOD from 0.40-32.20 mg/L, TCB and FCB from 20.0- 1.60E+05 MPN/100mL and  $\text{NH}_3\text{-N}$  from 0.00-0.68 mg/L.

Table 2 water quality variations in dry and rainy season

Season / parameter	WT	pH	TB	CD	DO	BOD	TCB	FCB	NH <sub>3</sub> -N	
Dry	Min.	26.6	4.4	4.3	0.18	0.50	0.40	78.00	78.00	0.00
	Max.	34.0	9.2	110.0	15064.0	7.00	16.20	1.60E+05	1.6E+05	0.51
	Mean	30.0	6.9	50.8	357.26	4.01	4.33	1.19E+04	1.1E+04	0.07
	SD.	1.6	0.7	24.2	1667.67	1.40	3.40	2.73E+04	2.7E+04	0.11
Rain	Min.	26.0	4.6	3.0	0.01	0.10	0.50	20.00	20.00	0.00
	Max.	33.0	8.9	357.0	10680.0	7.60	32.20	1.60E+05	1.6E+05	0.68
	Mean	28.7	6.9	77.3	277.85	3.95	3.78	1.83E+04	1.8E+04	0.06
	SD.	1.3	0.9	76.9	987.07	1.36	3.03	4.01E+04	4.0E+04	0.11
All-year	Min.	26.0	4.4	3.0	0.01	0.10	0.40	20.00	20.00	0.00
	Max.	34.0	9.2	357.0	15064.0	7.60	32.20	1.60E+05	1.6E+05	0.68
	Mean	29.2	6.9	68.2	307.48	3.97	3.99	1.61E+04	1.6E+04	0.06
	SD.	1.5	0.9	65.0	1282.40	1.37	3.18	3.62E+04	3.6E+04	0.11

The result showed that WT, pH, DO and  $\text{NH}_3\text{-N}$  in dry season was higher than rainy season. In another parameter, BOD, CD, TB, TCB and FCB was higher during rainy than dry season because of climatic and hydrologic change [8].

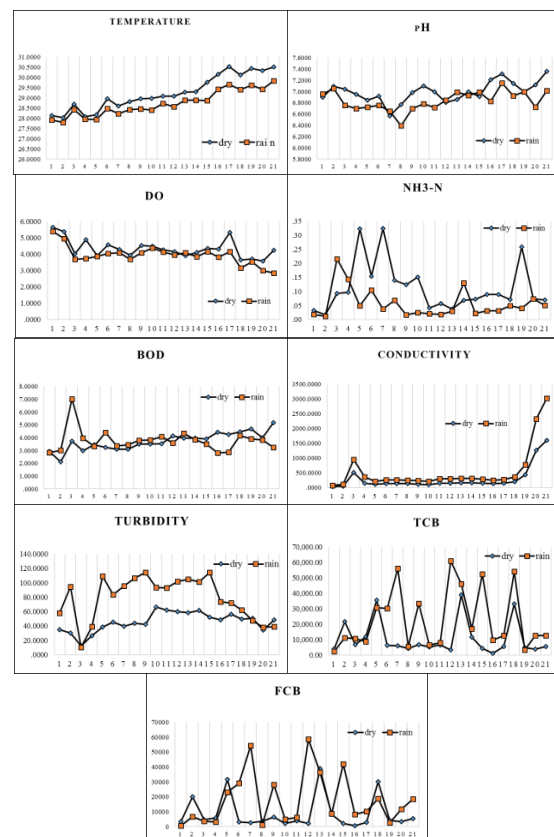


Fig. 2 water quality variations in dry and rainy season

### Cluster Analysis of Water Quality Variations

Two-step Cluster analysis for continuous data was applied to classify the set of water quality variations into 3 variations periods follow by fig.3 and table 3, WT, CD, TCB and FCB were classified into 2 periods but pH, BOD, DO, TB and NH<sub>3</sub>-N were classified into 3 periods.

Table 3 Water quality period by cluster analysis

parameters	Water quality variations period		
	Period 1	Period 2	Period 3
	Low	Moderate	High
WT	-	29.78	28.49
pH	7.02	6.94	6.72
TB	77.10	69.25	30.26
CD	574.34	136.30	-
DO	3.89	4.00	4.80
BOD	4.82	3.85	3.03
TCB	27977	8497.5	-
FCB	17607.89	6790.73	-
NH <sub>3</sub> -N	0.152	0.070	0.057

Water quality in period 1 presented low quality by high value of pH, TB, CD, BOD, TCB, FCB, NH<sub>3</sub>-N and low value of DO whereas high water quality was presented by contrary.

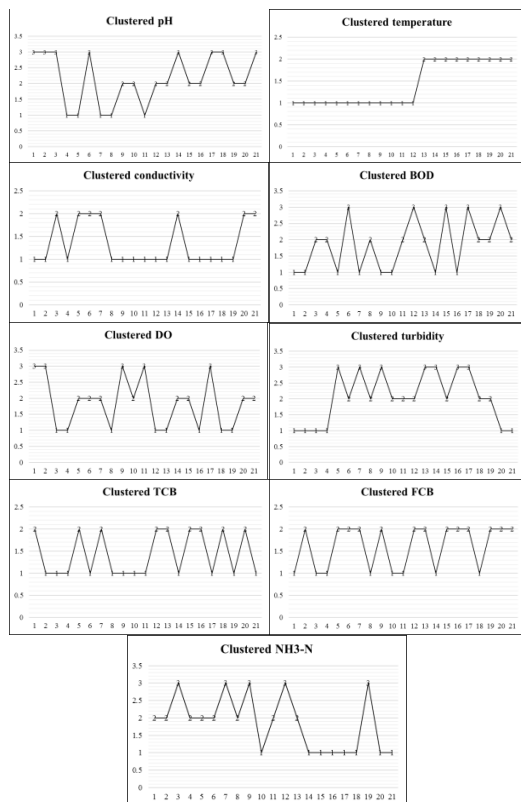


Fig. 3 water quality variations in dry and rainy season

Clustered water quality variations were presented in fig.3 and identified site station of pollution sources that upstream zone was site UT5 and UT7, midstream zone was site UT12, UT15 and downstream was UT19. Follow by table 4.

Table 4 pollution source in each zone.

Water quality	Site station of pollution sources in each basin zone		
	upstream	midstream	downstream
Low	5, 7	12,15	19
Moderate	3,6,9	13,16,17	18,20,21
High	8,4	14	-

### Factor Analysis of Water Quality Variations

Factor analysis to identify group of water quality variation and the main pollution factors which showed results in table 5 and table 6;

Table 5 results of KMO and Bartlett's sphericity tests

Parameter	Mean	SD.	Bartlett's Test of Sphericity	KMO
WT	29.23	1.48	Approx	
pH	7.13	0.61	. Chi-	586.901
TB	61.12	58.74	Square	
CD	349.88	1017.75	df	36
DO	4.45	1.42		
BOD	3.38	2.54		0.516
TCB	1.69E+0	3.57E+0		
FCB	1.34E+0	3.23E+0	Sig.	0.000
NH <sub>3</sub> -N	0.09	0.16		

In factor analysis, the KMO and Bartlett's sphericity test results are 0.516 and 586.901 (df=105, p<0.001), respectively, showing that this method was effective in reducing dimensionality [13].

Table 6 water quality factors on rotated component matrix during dry and rainy season

Variables	Non-rotated Component matrix				Rotated Component matrix			
	1	2	3	4	1	2	3	4
TCB	.944				.962			
FCB	.927			.242	.970			
WT		.738	.219			.729		
pH		.630		-.328		.707		
NH <sub>3</sub> -N			-.721	.373		-.569	.416	
DO	-.294	-.341	.589	.247			-.766	
BOD	.201	.274	-.485	-.310			.657	
CD		.406	.221	.543		.208	-.281	.646
TB	.358	-.460	.249	-.489				-.771
Eigenvalue					1.961	1.417	1.342	1.217
% of variance					21.789	15.742	14.916	14.120



Cumulative % 21.789 37.530 52.446 66.566

The first fourth rotated factors with eigenvalue of 1 or greater are extracted using Varimax with Kaiser normalization, which can explain the total variance in water quality data set amount 66.565%.

Factor analysis identified 4 factors such as factor 1, which accounted for 21.8 % of the total variance, was strong correlation with TCB and FCB. This factor could be interpreted as “bacterial pollutants” influenced by point sources such as urbanization with surrounding urban rim and human made area such planted forest, agro-pastoral land and barren land [14]. Factor 2, which implied 15.7 % of the total variance with moderate correlation on WT and pH and primarily negative correlation on  $\text{NH}_3\text{-N}$ . Factor 2 suggests “nutrient pollution and transform”, It presented natural factors impacted by seasonal change [8], [15]. The inverse relationship between temperature and nitrogen forms is natural process of nitrogen cycle because warmer water is cause of nitrogen transformation by biological process [14]. Almost of this pollutant could be cause by non-point sources such as agricultural runoff and or domestic sewage discharge directly into river basin without treatment [16].

Factor 3 explained 14.9% of the total variance and had moderate correlation with BOD and strong negative loading on DO. This factor represented as “organic pollutants” which influenced by point source such as municipal and industrial effluents [16], [17] resulting from rapid urbanization as well as economical area.

The last factor, factor 4 accounted for 14.1% of the total variance and had moderate correlation with CD and strong negative correlation on TB which represented “solids pollutants” and explained by influenced pollution originating from industrial sewage [16], [17].

### Pollution Source Identification

In upstream area, main pollution sources were from site monitoring UT05 and UT07 which factor 4 reflects the solids pollutants both of dissolved and non-dissolved solids. Almost turbidity in this area discharged during rainy season which eroded soil from land surface to river. Electrical conductivity is high by industrial wastewater discharge from many para-rubber factories including rubber sheet, glove and latex.

In midstream area, main pollution sources were from UT12 and UT15 that factor 3 displays

pollution of organic matter which almost discharge from large and economical urbanization. This zone is in Hatyai district where is a tourist attraction. Some of part are factories of palm-oil, animal-feed and frozen food.

In downstream, main pollution source was UT19 which factor 2 represents pollution of nutrients in agriculture and aquaculture area. In this area is cover of small urbanization with paddy farm and agro-pastoral land.

FCB and TCB are bacterial pollution along river basin. There is problem in many part of river from upstream to downstream which influenced by wastewater discharge from domestic settlements. The management should be concentrate in rainy season more than dry season.

Spatio-temporal pollution sources can conclude in table 7. In rainy season, upstream should be consider site 5 and 7 areas, midstream should be concentrate site 12 and 15 areas and in dry season, downstream should be intensify site 19 areas.

Table 7 Source and season identification of pollution

Basin zone	Site	factor	Season
upstream	UT05, 07	4	Rainy
Midstream	UT12, 15	3	Rainy
downstream	UT19	2	Dry

### CONCLUSION

Water quality variations by spatial patterns could presented various periods of water quality by multivariate statistical analysis, moreover, this method could explain group of water quality variation in each part of land use. Upstream zone should be consideration in area of industry and urbanization, midstream zone should be concentrate in area of economical urbanization and downstream zone should be management in area of agricultural land use as seasonal strategies. Rainy season, rainfall and level of water are main cause of organic pollutants from land surface to river surface both of rural and urban area. Pollutants and waste controlling in these areas may be could reduce water quality degradation. For example, sufficiently construct waste water treatment plant in urbanization, wastewater discharge controlling from industry and agricultural area restricting.

### ACKNOWLEDGEMENTS

The authors are extremely grateful to the Office of the Higher Education Commission, Thailand's ministry of education, Prince of Songkhla University (PSU) and Yala Rajabhat University (YRU). Finally, we would like to thank to the Songkhla's state

agency for making available their all data such as Regional Environmental Office 16, Songkhla Meteorological department, Regional Irrigation Office 16, Provincial Agricultural Extension Office, Sadao district, Songkhla, Songkhla Provincial Industry Office and Department of Provincial Administration, Ministry of Interior.

## REFERENCES

- [1] Praxedes KM, "Water quality management and sustainability: the experience of Lake Victoria Environmental Management Project (LVEMP), Tanzania", Physics and Chemistry of the Earth, Vol.28, 2003, pp. 1111–1115.
- [2] United State Department of Agriculture (USDA), National water quality handbook, 2003, introduction.
- [3] UNESCO/WHO/UNEP, "Water Quality Assessments - A Guide to Use of Biota, Sediments and Water in Environmental Monitoring" Second Edition. Published by E&FN Spon, an imprint of Chapman & Hall, 1992, 1996.
- [4] Li YP, and Huang GH, "Two-stage planning for sustainable water-quality management under uncertainty", J. of Environmental Management, Vol.8, 2009, pp. 2402–2413.
- [5] UNICEF/WHO, "UNICEF Handbook on Water Quality", New York, 2008, pp. 1-2.
- [6] Kannel PR, Lee S, Lee YS, "Assessment of spatial-temporal patterns of surface and ground water qualities and factors influencing management strategy of groundwater system in an urban river corridor of Nepal", J. of Environmental Management, Vol.86, 2008, pp. 595-604.
- [7] Cyril O, Wilson and Qihao W, "Simulating the impacts of future land use and climate changes on surface water quality in the Des Plaines River watershed, Chicago Metropolitan Statistical area, Illinois", Science of the Total Environment, Vol.409, 2011, pp. 4387–4405.
- [8] Maprasit S, Suksaroj C and Darnsawasdi R, "Temporal patterns of water quality variation in Khlong U-Tapao river basin, Thailand", Int. J. of GEOMATE, Vol.11, 2016, pp.2763-2770.
- [9] Gyawali S, Techato K, Yuangyai C and Monprapussom S, "Assessment of Surface Water Quality Parameters and Their Variations for Effective River Monitoring System: A Case Study of U-Tapao River Basin", J. of Environ. Res. Vol.34 (2), 2012, pp. 89-106.
- [10] Regional Environmental Office 16, Songkhla, "Water quality in Khlong U-Tapao river basin", year reports of 2006-2014.
- [11] Ethington B., "Things to know about regression, EDPR 7/8542, Spring, Retrieved on 07 June 2013 from <https://umdrive.memphis.edu/yxu/public/Bunty's%20REGKNOW.pdf>
- [12] Patrasinee P, "chapter7: multiple linear regression analysis", Statistics for Scientific research, 1<sup>st</sup> ed. Bangkok: Chulalongkorn University, 2007, pp. 279-302.
- [13] Vanichbuncha K, "Statistics for research. Faculty of commerce and accountancy. Chulalongkorn University, 2009, pp. 202-228.
- [14] Maillard P and Pinheiro Santos NA, "A spatial-statistical approach for modeling the effect of non-point source pollution on different water quality parameters in the Velhas river watershed-Brazil", Journal of Environmental Management, Vol.86, 2008, pp. 158-170.
- [15] Singh K P, Malik A and Sinha S, "Water quality assessment and apportionment of pollution sources of Gomti river (India) using multivariate statistical technique: a case study", Analytica Chimica Acta, Vol.538, 2005, pp. 355-374.
- [16] Mei K, Liao L, Zhu Y, Lu P, Wang Z, A.Dahlgren R, Zhang M, "Evaluation of spatial-temporal variations and trends in surface water quality across a rural-suburban-urban interface", Environ Sci Pollut Res. Vol.21, 2014, pp. 8036-8051.
- [17] Zhao J, Fu G, Lei K and Li Y, "Multivariate analysis of surface water quality in the Three Georges area of China and implications for water management", Journal of Environmental Sciences, Vol.23(9), 2011, pp. 1460-1471.

## DIVESIRY AND POLLEN MORPHOLGY OF IMPORTANT TREE SPECIES OF RANIKOT FORT, SINDH, PAKISTAN.

Nabila Shah Jilani<sup>1</sup>, S.S Hassney<sup>2</sup>, Muhammad Tahir Rajput<sup>3</sup> and Feroza shar Baloch<sup>4</sup>  
*Institute of Plant Sciences, University of Sindh, Jamshoro, Sindh, Pakistan.*

### ABSTRACT

Ranikot Fort is a talismanic wonder of Sindh, Pakistan. This fort is one of the largest forts of the world and approximately of 35 km in length. Visitors and researchers can reach at this beautiful location and historical mystery via Hyderabad to Sann by travelling about 90 kilometers north of Hyderabad 30 kilometers from town of Sann. All construction in the Ranikot has its own distinctiveness and magnificence. The exploration for the tree plant diversity of fort area was carried out to find out range of important tree plants diversification in this fort area because two species reported threatened in my pervious publication. Frequent survey was conducted throughout the years to record vegetation diversity present in Ranikot fort area. Plant materials were collected from the site area, herbarium sheets were prepared by using slandered techniques. Pollen morphology of important tree species has been investigated by Scanning electron microscope. Considerable pollen diversity has been particularly pollen shape, size, aperture and exine ornamentation.

*Key words: Pollen, Diversity, Ranikot Fort.*

### INTRODUCTION

The exploration for the tree plant diversity and pollen morphology of fort area was carried out to find out range of tree plants diversification in this fort area. Experts of archeology and history have an opinion that Ranikot was built some 500 BC before. Talpur in 1819 refurbished this fort late on. Settler used the fresh spring water to irrigate the field for growing of their food. This is the only fresh water found in the area. There are very few tree plants present in Ranikot, main reason is shortage of water, local people of Ranikot are totally dependent on plants for their survival. They cut, chop trees for making their homes and for fuel. There are very few threes left. Two of tree species reported threatened due to extreme use of local people. (Jilani et al., 2014). A large numbers of plants and animal fossils have been reported by many scholars, historian and plaeobiologist (Khan & Rehmatullah 1968; Khan and Rajput 1976; Rajput & Khan 1982; Rajput et al 1985 & Ahmed et al, 2001).



**Figure. 1: Beautiful picture showing the view of Ranikot fort entrance.**



**Figure.2: Ranikot Fort wall showing resemblance with the great wall of China.**



**Figure. 3: Tribal people of Ranikot Fort**

The people of Ranikot live very simple life without having any facilities of life. They might unaware of the advancement of the world. Their kids don't get education, no medical facility, no roads no transport is available for them. Their homes are made up of four pillars of wood, covered with dry grass roof. They cut trees to get wood for different purposes. This is the reason of disappearing trees from Ranikot.



## MATERIAL AND METHODS

Frequent survey was conducted throughout the years to record vegetation diversity present in Ranikot fort area. Plant materials were collected from the site area, herbarium sheets were prepared by using slandered techniques. All the plants were documented using protocol of plant identification described in the flora of Pakistan, Nasir & Ali (1970 - 1989), Ali & Nasir (1989 - 1993), Ali & Qaiser (1993 - 2008), flora of Karachi, Jafri (1966) and flora of Indian desert, Bhandari (1987). Scanning Electron Microscopic examination of pollen was carried out by using Jeol (JSM-T-200) microscope.

## RESULTS AND DISCUSSIONS

Fig. 4:

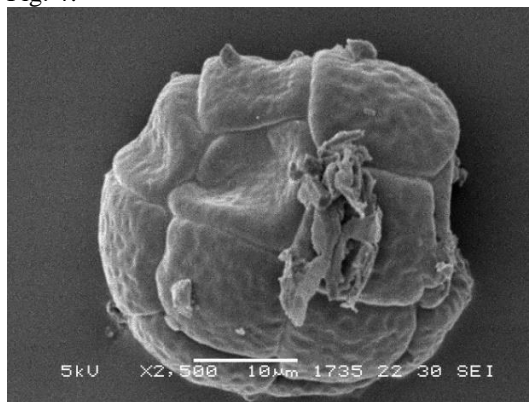


Fig. 5:



Fig. 6:

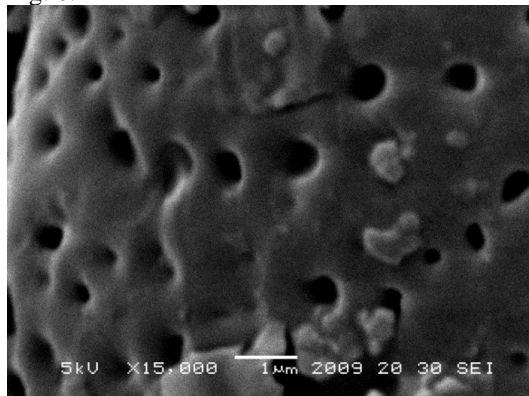


Figure.7:

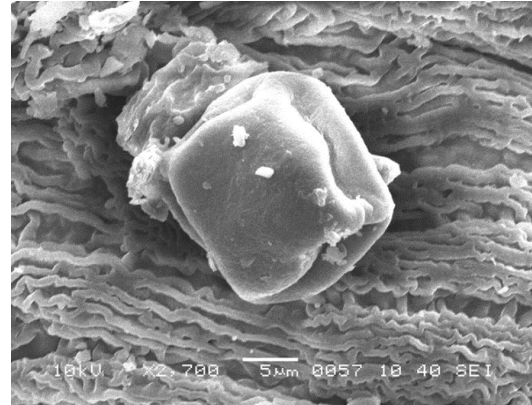


Fig. 8:

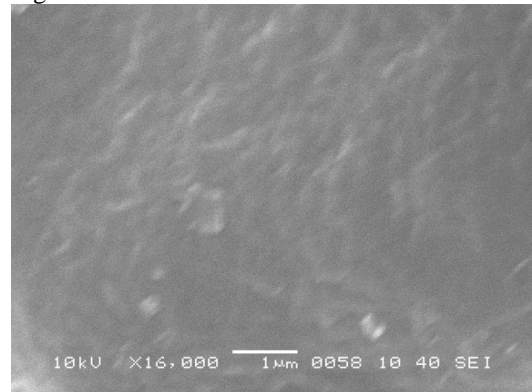


Fig. 9:

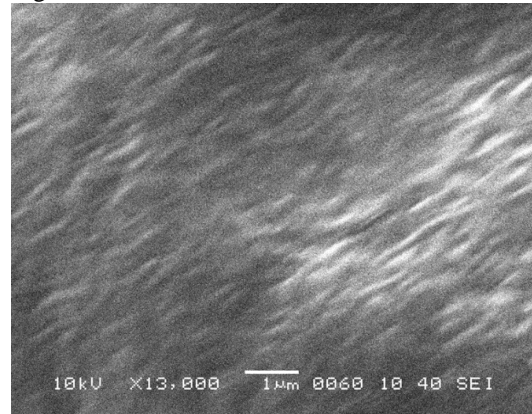


Fig. 10:

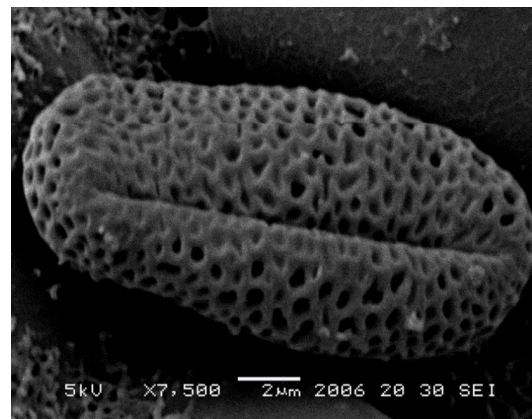
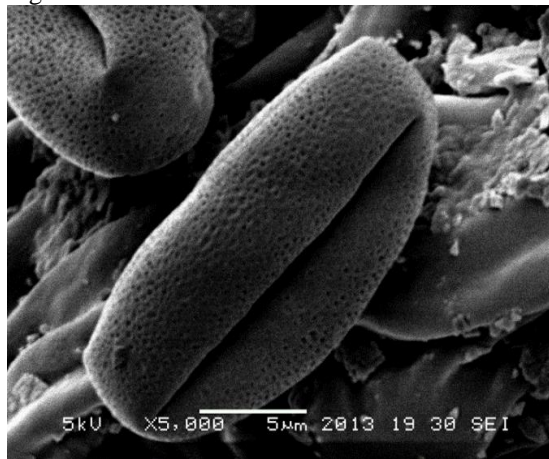


Fig. 11:



(Fig 4, *Acacia Senegal* (Linn.), Fig 5, 6, equatorial view and exine pattern *Prosopis Sineneria* (Linn.), Fig 7, 8, 9 *Ziziphus nummularia* (Burm. f.) Wight & Arn., Fig10, *Tamarix dioica* Roxb. ex. Roth. Fig 11, *Salvadora oleoides* Decne.)

SEM study of five tree species was conducted, considerable diversity have been observed among pollen characters particularly type, shape, size and aperture. *Acacia Senegal* (Linn.), Pollen grain in polyads 12 celled, 40-45  $\mu\text{m}$  in diameter. Pollen grains present in polyads, non aperturate, each polyads consists of 12 cells. *Prosopis Sineneria* (Linn.) Prolate Tricolporate, 35  $\mu\text{m}$  length, 22 $\mu\text{m}$  width. Tricolporate grain with linear, long, narrow colpi. *Ziziphus nummularia* (Burm. f.) Wight & Arn., Pollen Spheroidal, tetracolpate, 22.2  $\mu\text{m}$  diameter. Grain is spheroidal, tetracolpate, due to the broad four colpi folds it gives appearance like a broad rhomboid grain. *Tamarix dioica* Roxb. ex. Roth. Prolate, Tricolpate grain 16  $\mu\text{m}$  long, 6  $\mu\text{m}$  wide. *Salvadora oleoides* Decne. Grain is prolate to sub-prolate, Tricolpate, 15.2  $\mu\text{m}$ , 8.2  $\mu\text{m}$  wide. Tricolpate grain, colpi elongated, tectum reticulate with murate pattern.

## REFERENCES

1. Jilani, N., Tahir, S. and Rajput, M. (2014) Vegetation of Ranikot Fort Area, a Historical Heritage of Sindh, Pakistan. *American Journal of Plant Sciences*, **5**, 2207-2214.
2. Jilani. N.S, S. S. Hassney, M.T. Rajput (2015) Threatened species of Ranikot Fort area a Historical heritage of Sindh, Pakistan. *Sindh University Research Journal*. 149-152.
3. Ahmed, B, MTM Rajput & K.M. Khan (1989), *Laurinoxylonellipticum* Sp. Nov., a new petrified taxon of lauraceae from Tertiary deposits of Sindh, Pakistan. *Pak. J. Bot.*40(1).

4. Akhter R. (2003) A plant guide to National Park Khirthar and adjoining areas. Premier – Kufpec, Pakistan B.V. 1
5. Ahmed Sultan & B.B. Steverd. Grasses of west Pakistan Lahore 1958.
6. Ali, S.I. & M. Qaiser (1986) A phytogeographic analysis of the Phanerogams of Pakistan and Kashmir. *Proc. Roy. Soc. Edinb*; 89B: 89 – 101.
7. Ali, S.I. & M. Qaiser (Eds), 1993 – 2008, *Flora of Pakistan* – Karachi.
8. Ali, S.I. & Y. J. Nasir (Eds), 1989 – 1993, *Flora of Pakistan* – Islamabad, Karachi.
9. Bhnadari, M.M. (1975), *Flora of Indian Desert*. Scientific publishers, Jodhpur.
10. Jafri S.M.H (1966). *The Flora of Karachi* – The book corporation, Karachi, Pakistan.
11. [http://pakistanpaedia.com/landmarks/ranikot/ranikot\\_fort.htm](http://pakistanpaedia.com/landmarks/ranikot/ranikot_fort.htm)
12. Nasir E, and Ali S.I. (Eds), 1970 – 1989, *Flora of Pakistan*.
13. Rajput MTM & K.M. Khan (1984), *Araucarioxylan*Sp. nov. A new species of gymnosperm wood from Manchhar Formation. *Pak. J. Bot.* 16(1); 53-76.

## RELATIONSHIP BETWEEN PAVEMENT TEXTURE AND MOVEMENT

Yuki OGIMOTO<sup>1</sup>, Kazunari TANAKA<sup>2</sup> and shin YOSHIKAWA<sup>3</sup>

<sup>1</sup>Engineering, Osaka Institute of Technology, Japan; <sup>2,3</sup>Osaka Institute of Technology, Japan

### ABSTRACT

The purpose of this research is to design pavement taking pedestrians into consideration, especially the elderly, which is the fastest growing age group in Japan. In recent years, the awareness of street landscape has increased, and the development of roads taking pedestrians into consideration has become more common. It is considered that the walking path of people is changing due to the design of sidewalks and the walking environment. By analyzing the pavement, we believe that we can utilize this for urban planning, by clarifying the route according to individual's age. In previous studies, walkability tests and analysis were performed for each type of pavement. There are few studies on public spaces. If it is possible to grasp the respective walking route by attributes such as age group, then this can lead to improve functional design universally. It will potentially allow people to be able to more easily walk on pavement.

*Keywords: stationary people, pavement, open space, public space*

### INTRODUCTION

Designers are trying to create space that various people can use easily. However, there are actually various aspects to consider for design.

For example, some people are sitting on the chair or bench, others are leaning walls etc., these actions are usually performed unconsciously.

A difference arises from how to use the space considered at the planning stage, stemming from unconscious behavior. People select places from space, at that given time, it is influenced by physical factors and human factors. There is a difference in influence, depending on number of people, sex and age.

In this research, we focus on human behavior and space shape for busy places that many people use, and to understand human behavior and grasp the influence of space shape by classifying attributes such as age and sex. Therefore, from a human behavior point-of-view it becomes possible to visualize, by discovering the influence range and influence of people and space shapes. It would be one of the effective means for making new town planning.

### Purpose and method of research

We find the relationship between the characteristics of space shape and pedestrian features, grasp the relationship with the place of each action and the shape of the surrounding space. It is ultimately best to propose a design taking into consideration human behavior.

In this research, we will quantitatively find the influence of invisible design, utilizing physical and pedestrian behavior data obtained from a field survey.

Ultimately, we will refine it to detailed analysis that finds how space design affects pedestrian influence, we will obtain basic knowledge of analysis using physical data, while acquiring a large amount of pedestrian behavior data.

In order to grasp the influence of the spatial shape and the influence range, first, we shoot a moving image and capture the behavior of the person.

We extract external factors that appear to be affecting people. Furthermore, we will calculate specific figures and analyze them. Analysis is made on the relationship between the elements of the spatial shape extracted by the survey and human attributes. We then express the influence range and influence of the grasped space shape on the map, using GIS from pedestrian data.

### Target area

For the target area, we wanted to use a space that had various features common in public places such as; pillars, walls, stairs, monuments etc.

Also, we wanted to consider the number of users around the ground, rather than only paying attention to the design part of the space.

In this research, we will cover a space used mainly by pedestrians. A preliminary survey was conducted in the open space around Osaka station, and a place considered to be similar was set as the target site. In addition, this survey is a place with many railway stations.



Fig1 An example stationary people



## Investigation

For the survey, first, we shot video to capture the location and constituent elements of the people standing around, then we plot this on CAD and consider this place as a place where people are likely to be stationary, and the hypothesis of the cause from the plot (Figure 2). For the flooring surface, it was concrete tiles, and its pattern consisted of different colors at equal intervals. Braille guide blocks for the visual impaired were also present.

What we noticed when plotting is that when one person arrives and stands in place, they tend to it at a wall etc.

On the other hand, when multiple people stood in place, it was noticed that the distance from any feature (such as a wall) was far compared to the case of a solo individual. The surface was not unified, and each place had different patterns.

We focused on two things here. The first was on the existence of a feature and the spatial shape of the pavement, and the second was the relationship of the number of people at the time of capture and looking at these two points of interest. As a result, when it comes to staying in one spot, people decided to stay at a place that they feel "a sense of security".

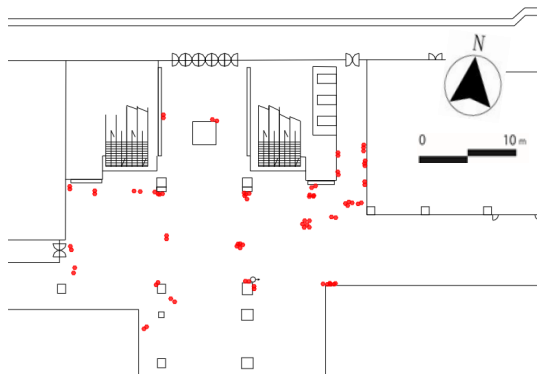


Fig2 stationary people  
(two or more)

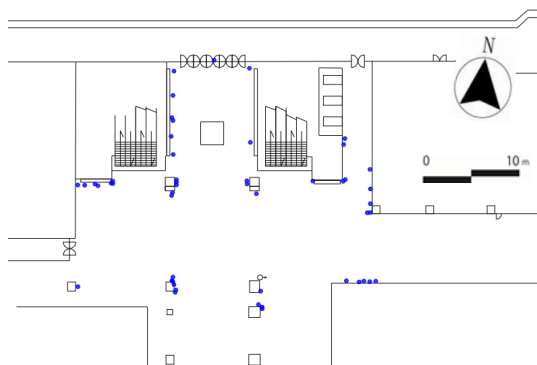


Fig3 stationary people

## analysis

In order to grasp this "sense of security" from the results of the survey, two points of interest were analyzed and quantified. In the analysis, seven kinds of actions were used; the composition of the number of people, the time, the distance to the surrounding features etc. For the attribute information of the person, I converted the strength of the relationship by correlation analysis. The stationary person and the distance from the wall became the strong correlation element. A significant correlation is seen. We graphed the results, when an individual is stationary alone, they are often near to the wall compared to the case when there are two or more people stationary (Fig.3, Fig.4 )

From this result, it can be said that when being alone, the individual wants a feeling of being "secure".

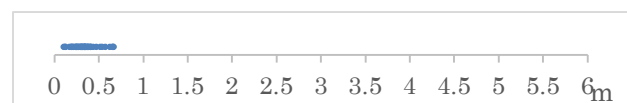


Fig4 Relation between a Stationary  
person (individual) and the Nearest  
Distance to a feature/object

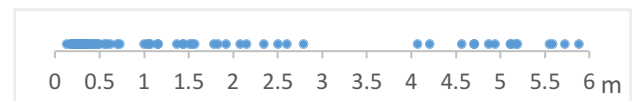


Fig.5 Relation between stationary people (two or more)  
and the Nearest Distance to a feature/object

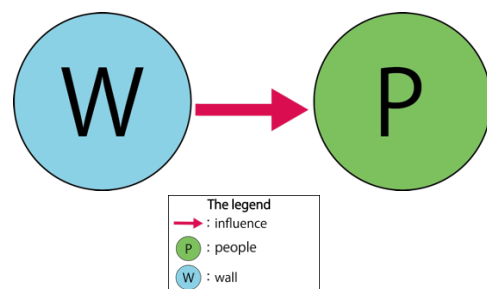


Fig.6 The influence for the people by the wall



### Analysis that replaced walls with people

According to the previous analysis, it is assumed that when a small group of people are standing together they can feel "relief" similar to standing near a wall.

Therefore, when two or more people were stationary, we analyzed them with the same layer as a wall. As a result, it was possible to obtain a graph showing the same tendency as in the case of standing alone by one person. From these results, it was possible for residents to feel that they feel "secure" where they are unconsciously standing.

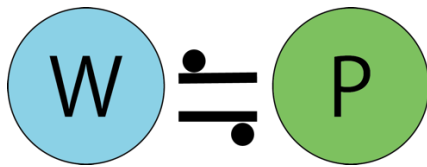


Fig.7 Wall and People

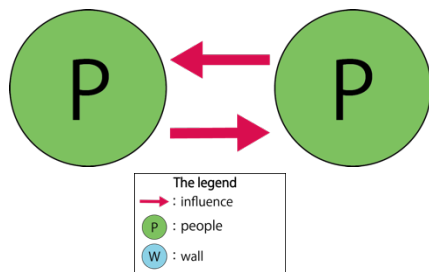


Fig.8 Wall substituted with People



Fig.9 Relation between a Stationary person (individual) and the Nearest Distance to a feature/object



Fig.10 Relation between stationary people (two or more) and the Nearest Distance to a feature/object

### Floor design

In the previous study, the walking trajectories of pedestrians were caught. The pavement; the pattern of the floor surface was not uniform from the photograph, it was different in section B (Figure 11). On the other hand, the floor surface of section A and section C was the same pattern.

Figure 12 is a diagram in which the area shown in the photograph is meshed with the tile of the floor surface with the camera angle adjusted to directly above. The trajectory at this time is caught in 15 seconds. Focusing on the number of trajectories, we see that the interval of B is smaller than that of A and C. That is, from Figure 12, pedestrians do not walk along the center of the road relatively. They tend to walk along it in a parallel manner, or across it in a perpendicular manner.

There is a possibility that the pedestrian selects the space which they like and avoid space which they don't unconsciously considering the pattern of the floor surface from these two figures.

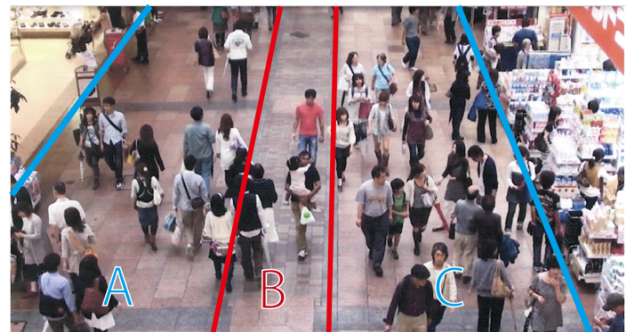


Fig.11 Example: Pavement and Movement in Market Place

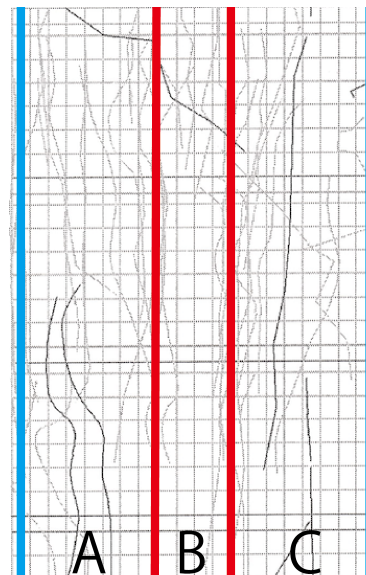
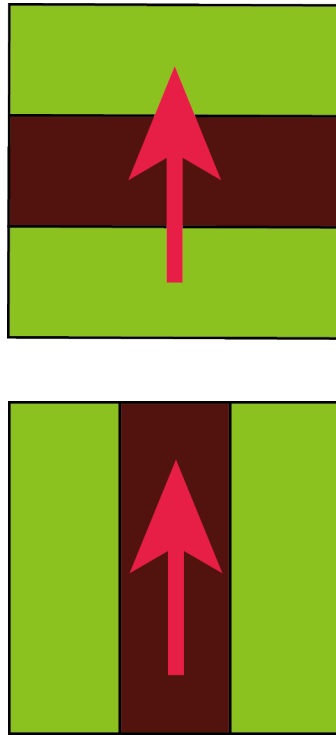


Fig.12 The Trajectory of the People



[3] Sattoshi AMAGAI Zyun HIROTA Evaluation of diversity in walking space Crowd flow and personal space

Fig.13 Relation of the Movement and Pattern of the Pavement

## CONCLUSION

In this research, we focused attention on pedestrians in public spaces in the city and observed and analyzed them. In the analysis, we clarified the tendency of the number of people in stationary positions and found the selection by conditioning of being stationary. In addition, with walking they draw different trajectories for each floor surface, so it is conceivable that the features. The floor surface may have a psychological influence on route selection at the time of walking and selection of stationary position. When creating space for pedestrians, it is necessary to consider the characteristics of the floor surface for designing.

## REFERENCES

- [1] Co., Ltd.New construction company  
: New building July 2011 issue: Osaka station design drawing
- [2] Yurika YOGO, Kazuto HAYASHIDA, Hitoshi WATABE Spatial usage behavior by age in station concourse pp651 ~ pp652 2012

## REMOVAL AMMONIA FROM LANDFILL LEACHATE USING ULTRASONIC IRRADIATION PROCESS

Sartaj M.<sup>1</sup>, Tobalt A.<sup>2</sup>, and Kennedy K.<sup>3</sup>

<sup>1</sup> University of Ottawa, Ottawa, Ont., Canada K1N6N5

### ABSTRACT

Landfill leachate could contain high concentrations of ammonia, which results in environmental consequences if not removed before discharge. Ultrasonic (US) irradiation has been reported to be a promising technology for removing ammonia from aqueous solution. The main objective of this study was to investigate the efficiency of US technology for removal of ammonia from landfill leachate. A series of laboratory batch experiments using synthetic solution (3,000 mg TAN/L) as well as two real landfill leachates (1,730 and 3,440 mg TAN/L) were carried out in triplicates. Heat only experiments using a hot water bath evaporation tests with samples open to the surrounding atmosphere were carried out to quantify the contribution of different mechanisms. Statistical analysis of the TAN removal data showed that there was no significant difference between the two leachate sources tested in this study for total TAN removals. The contribution from non-thermal effect (US), thermal effect (WB), and volatilization was estimated to be 61.5%, 36.7%, and 1.8% of total TAN removal respectively.

*Keywords: Anaerobic Digestion, Biogas, Municipal Solid Waste, Organic Loading Rate, Leachate.*

### INTRODUCTION

Anthropogenic sources of pollution such as agricultural, industrial, and municipal wastewaters contribute to the degradation of water resources [1]-[2]. Discharge of such wastewaters with high ammonia-nitrogen contents can result in eutrophication and algal blooms, depletion of dissolved oxygen, and toxicity to fish even at low concentrations in receiving water bodies, and inhibitory effects on microbial activity of microorganisms responsible for biological treatment of wastewater [2]-[5]. Total ammonia nitrogen (TAN) exists in liquid phase either in unionized form ( $\text{NH}_3$ ) or ionized form ( $\text{NH}_4^+$ ), with toxicity being mainly attributed to  $\text{NH}_3$  form [6]. The  $\text{NH}_3/\text{NH}_4^+$  equilibrium ( $\text{pK}_a$  of  $\text{NH}_4^+$  is 9.25 at standard conditions) depends on temperature and pH; the higher the pH of a solution, the higher the concentration of  $\text{NH}_3$  [7].

Landfill leachate varies in strength and composition depending on several factors such as the age of the landfill, composition of waste, and design and operation of landfill [8]. Ammonia is mainly produced during the anaerobic biodegradation of organic fraction of solid waste and there is no mechanism for its degradation under methanogenic conditions. This process, known as ammonification, results in accumulation of ammonia in leachate, which intensifies its toxicity. As such, ammonia is considered to be the one of the most significant long-term pollutant found in landfill leachate [6]. The range of ammonia concentrations in landfill leachate has been reported to be very wide, from a few hundreds to more than 10 thousands mg/L.

Conventional treatment processes to remove ammonia from aqueous solution include biological

treatment, microwave radiation, air stripping, chemical precipitation, adsorption/ion-exchange, and ultrasonic irradiation [2], [3], [9]. Ultrasonic (US) irradiation has been reported to be a promising technology for removing ammonia from aqueous solution and compared to the conventional methods, it can bring several benefits such as environmentally friendly, low cost, selectivity and compact. Contrary to other processes which are negatively affected by presence of suspended solids, US efficiency may even improve by increase of turbidity or suspended solids.

Considering the above, the main objective of this study was to investigate the application of US technology for removal of ammonia from landfill leachate under high ammonia concentration in the range of 2,000- 3,000 mg/L where the inhibitory effects of ammonia in treatment of landfill leachate and anaerobic digestion process has been reported to occur. Additionally, it was intended to assess the contribution of thermal and non-thermal effects through statistical analysis of the data.

### MATERIALS AND METHODS

A series of laboratory batch experiments using two real landfill leachate were carried out. All tests were carried out in triplicate. Table 1 shows the characteristics of the two leachates collected from two local landfills. While both leachates had high ammonia nitrogen content they were selected to represent both old and new leachates – leachate 1 being more characteristic of a newer landfill's leachate and leachate 2 more characteristic of an older landfill's leachate.

Table 1. Characteristics of leachates used to assess ammonia nitrogen removal by ultrasound irradiation.

	Leachate 1	Leachate 2
BOD <sub>5</sub> (mg/L)	18600	345
Alkalinity (mg CaCO <sub>3</sub> /L)	6690	15300
COD (mg/L)	55000	6200
TKN (mg N/L)	3190	4670
TAN (mg N/L)	1730	3440
pH	5.1	8.2

The schematic of the experimental setup is illustrated in Figure 1. For each test, 165 mL of leachate was added to a 500 mL beaker, with a removable lid used during the cooling stage to limit water loss. The pH of solution was then adjusted to an initial pH of 10 (above the pK<sub>a</sub> of NH<sub>4</sub><sup>+</sup> = 9.25) using a 10 N NaOH solution. The initial TAN, pH, and temperature of the sample were measured. Afterwards, the sample was exposed to US irradiation using Branson digital sonifier 450 with a ½" disruptor horn and ½" disruptor tip for the time duration of 15 minutes. The US vibration was generated by a 20 kHz ultrasonic converter and was transferred into the leachate by putting the US probe into it. The power output could be adjusted from 10 to 100% in 5% increments and ranged from 0 to 400 W. Temperature was measured immediately after this stage. The sample was allowed to cool to room temperature before distilled water was added to account for water loss. TAN and pH were measured again and energy output recorded (KJ).

In order to study the amount of ammonia removed due to temperature rise during the process, heat only experiments were conducted. This method involved the same procedure outlined above; however, instead of being sonicated, the samples were placed into a 20 L/120 V Stable Temp hot water bath set at a temperatures that correlated to the final temperatures achieved after sonication for the desired durations. The contribution of evaporation on the ammonia removal was also investigated by leaving some samples open to the surrounding atmosphere for the same duration time of 15 min instead of being heated in water bath or sonicated.

## RESULTS AND DISCUSSIONS

The ammonia removal efficiency was calculated using the Equation below:

$$\text{TAN removal (\%)} = (C_0 - C_e) / C_0 \times 100\%$$

where: C<sub>0</sub> and C<sub>e</sub> are initial and equilibrium TAN concentration (mg/L), respectively.

Table 2 shows the results of the one-way ANOVA tests that compares the total TAN removal efficiencies for the two leachate sources. Looking at the results in Table 2 it can be seen that there are no significant differences in the total TAN removal efficiencies

between the two synthetic solutions ( $P > 0.05$  and  $F > F_{crit}$ ).

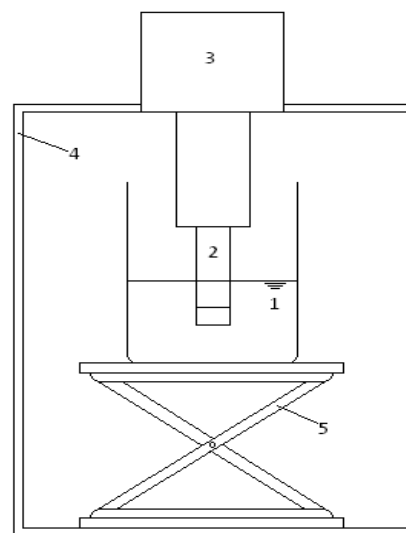


Figure 1 - Schematic of experimental setup.

(1) Synthetic solution or leachate, (2) disruptor horn and tip, (3) US converter, (4) case, (5) stand.

To determine the contribution of thermal and non-thermal effects of US process the TAN removals obtained by water bath was subtracted from the total TAN removal efficiencies. The difference is identified as non-thermal effect (US) effect. It should be noted that the TAN removal in water bath samples shows the combined effect of thermal (due to temperature increase) and volatilization. By subtracting contributions by volatilization from water bath removal, the net thermal effect contribution was also calculated and identified as WB. As such, it is possible to estimate the sonication or non-thermal effect (US), thermal effect (WB), and volatilization (Volat.) contributions. These are presented in Figure 2.

Table 2. One-Way ANOVA for TAN removal efficiencies for two leachate sources

Source of Variation	SS	df	MS	F	P	F <sub>crit</sub>
Between Groups	10.98	1	10.98	2.52	0.19	7.71
Within Groups	17.43	4	4.36			
Total	28.41	5				

The percent removal for Total as well as US, WB and Volat. contributions were compared using t-Test. The results for US removal comparison are presented in Table 3 as an example. As it can be observed, no significant difference was observed between the two leachate sources tested, showing the same performance and removal efficiency. Similar results were obtained for comparison of WB and Volat. contributions.

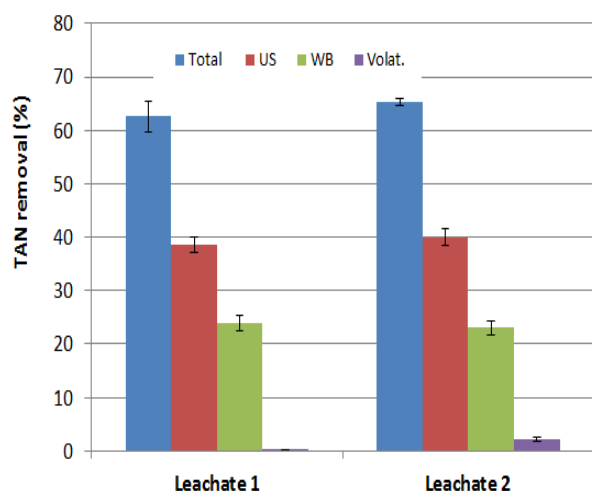


Figure 2 - Average TAN removal by non-thermal (US), thermal (WB), volatilization (Volat.) at pH =10 and duration time of 15 min

Comparing the average contributions from US, WB, and Volat. processes to Total TAN removals indicates that on average 61.5%, 36.7%, and 1.8% of total TAN removal is contributed to US, WB, and Volat. mechanisms.

Table 3. t-Test results for comparisons of Total TAN removal between the two leachate sources

	<i>Leachate 1</i>	<i>Leachate 2</i>
Mean	38.61	40.02
Variance	3.81	2.27
Observations	3	3
Pooled Variance	3.04	
Hypothesized Mean Difference	0	
df	4	
t Stat	-0.991477279	
P(T<=t) one-tail	0.188787797	
t Critical one-tail	2.131846786	
P(T<=t) two-tail	0.377575594	
t Critical two-tail	2.776445105	

## CONCLUSIONS

The results obtained for laboratory batch experiments for TAN removal using ultrasonic irradiation indicated that this process is effective in TAN removal from landfill leachate. The main mechanisms for TAN removal were non-thermal effects accounting for approximately 2/3 of total removal with the remaining 1/3 mainly due to thermal effects.

## REFERENCES

- [1] Arabgol R., Sartaj M., Asghari K. Predicting Nitrate Concentration and Its Spatial Distribution in Groundwater Resources Using Support Vector Machines (SVMs) Model. *Environmental Modeling & Assessment*, 21 (2016), 71-82.
- [2] Ozturk E., Bal N. Evaluation of ammonia–nitrogen removal efficiency from aqueous solutions by ultrasonic irradiation in short sonication periods. *Ultrasonics Sonochemistry*, 26 (2015), 422-427.
- [3] Dong S., Sartaj D. Statistical analysis of thermal and non-thermal effects of sequential microwave/aeration process for the removal of ammonia from aqueous solution. *Desalination and Water Treatment*, 57(2016), 20005-20015.
- [4] Faryadi M., Rahimi M., Moradi N., Safari S. Ammonia removal using 1.7 MHz high frequency ultrasound in batch and novel dam-weir falling systems, *Desalination and Water Treatment*, 54 (2015), 3412–3421.
- [5] Lee S.M., Jung J.Y., Chung Y.C. Measurement of ammonia inhibition of microbial activity in biological wastewater treatment process using dehydrogenase assay. *Biotechnology Letters*, 22(2000), 991-994.
- [6] Nair A., Sartaj M., Kennedy K., Coelho N.M. Enhancing biogas production from anaerobic biodegradation of the organic fraction of municipal solid waste through leachate blending and recirculation. *Waste Management and Research*, 32(2014), 939-946.
- [7] Ding Y., Sartaj M. Optimization of ammonia removal by ion-exchange resin using response surface methodology. *International Journal of Environmental Science and Technology*, 13(2016), 985-994.
- [8] Sartaj M., Ahmadifar M., Jashni A.K., Assessment of in-situ aerobic treatment of municipal landfill leachate at laboratory scale. *Iranian Journal of Science and Technology B*. 34(2010), 107-116.
- [9] Dong S., Sartaj M., Statistical analysis and optimization of ammonia removal from landfill leachate by sequential microwave/aeration process using factorial design and response surface methodology. *Journal of Environmental Chemical Engineering*, 4(2016), 10-108.

## **THE IMPLEMENTATION OF WATER SENSITIVE CITY AT DEPOK - MIDDLE CITY IN INDONESIA**

Firdaus Ali<sup>1</sup>, Irene Sondang<sup>2</sup> Esty Suyanti<sup>3</sup> and Ahmad Zubair<sup>4</sup>

<sup>1</sup>School of Strategic and Global, Universitas Indonesia, Indonesia; <sup>2</sup>Center for Urban and Regional Research, Indonesia

### **ABSTRACT**

The city has increasingly be burdened with the increase of urbanization. The effect of this dynamic is the pressure to urban environment, specifically on the supply of water and the number of water space. The city of Depok as a middle-city continuously experience infrastructure development as the consequences of the capital city, Jakarta's spill over. It resulted in the diminishing amount and quality of water supply and space. Water Sensitive Cities is an innovative approach that is based on similar experience in similar surroundings within Australian cities. The approach integrates the concept of water cycle with urban development dynamics that consider to environment equilibrium. To what extent the concept is implemented in one of the middle cities in Indonesia will therefore then be significant for the study of urban developments and water studies in Indonesia. Specifically for the case of Depok, Water Sensitive City studies will provide a guideline as to what will be required to be done with regards to current condition of water supply and space in the middle city context. The research takes advantage of mix-method approach combined with GIS mapping to identify water space capacities and supply as well as gauge what can be done from a social economic aspects. The research will outline the degree of Water Sensitive City implementation in Depok and what still required to be done. The research will also highlight the extent of which Water Sensitive City as an approach can be applicable in Depok and Indonesia in general.

*Keywords: Water Sensitive City, Water Supply, Water Space, Middle City*

### **INTRODUCTION**

Since the world's urban population has increased rapidly in the past few years, approximately 54% of the world's population now live in urban areas, limitless of resources become an urban issues. Water is one of the most important natural resources and plays an irreplaceable role in human survival and in the ecosystem. In urban areas, many water resources are now facing threats from nutrient enrichment, organic, and inorganic pollution. Besides, with the rapid urban expansion and population growth, water resources in urban areas are also gradually decreasing. With some of the main issues of urbanization in mind, urban entities will need to take further consideration to maintain balance between the different spaces in land, air and water. The numerous dimension that is involved within urban water management portrays the complexities of managing issues in the urban area. This complexity carries with it a multi-dimensional issue that involves a large area of solution that includes the need for technological, urban planning and design, empowerment of urban communities as well as social and institutional development solution [4]. Urban dynamics will have to be able to provide a balance between economic and physical development with the availability or sources, management and fresh water space.

To comprehensively examine and provide effective solutions for the issue of sustainable water management within a certain urban context, a concept of an ideal system of urban water managements will be used. One of this concepts is water sensitive city, a concept that presents an integrative approach of urban water management that does not only provide sufficient supply for urban water requirements, but equally provide numerous other benefits to increase the urban live ability and resilience of the city [1]. The Water Sensitive City approach provides a "Leapfrogging" mechanism that indicates the different stages that a city needs to fulfill in order to achieve Sensitive Water Management in the urban context.

The implementation of Water Sensitive City in the urban areas of Indonesia becomes a challenge in itself due to specific characteristics that tropical urban context in the case of Indonesia. The developmental nature of the urban areas, the ever-increasing population and the rise of land and water use issues as well as continuous development of its governance system provides Indonesian cities an interesting case for the implementation of Water Sensitive City concept. As the concept itself has mainly been implemented in Australian cities, it serves a valid reference from which Indonesian cities may be able to consult from.

One of cities that implemented WSC in

Australia is Melbourne. This city threatened various elements not only growth pressure but also climate changing risk. Drought and flood happened at Melbourne. 40% reduction in livestock production, 80% reduction in grain production, 10-20% reduction in rainfall in autumn/winter and Melbourne's largest reservoir got down to 16% (Thompson Dam). Floods made most region at Melbourne had inundated. Hence city government deal it with short term plan like disaster response unit. They also doing long term plan by implement 10,000 raingardens, planning scheme amendment and maintaining sport grounds.

The implementation on Water Sensitive City Concept at Melbourne city that stated before, become best practice to other city in Indonesia. Depok is the city for the study case of this research. The characteristic similar with Melbourne with a small scale.

We need to know the sustainability of water management after more than 30 years of rapidly changing in Depok. Simple question like: "How the water management to fulfill the needs of the Depok's residents?" becoming our aim in doing this research. By asking this question the research tries to examine the extent of which the concept of Water Sensitive City (WSC) as has been implemented in Australia, is applicable in the context of Indonesian urban environment in Indonesian cities. This investigation is conducted as another effort to achieve an integrated and sustainable urban water management in Indonesia.

#### THE POSSIBILITY OF WATER SENSITIVE CITY CONCEPT WOULD IMPLEMENTED AT DEPOK

Depok is one of middle city in Indonesia that have changing urbanize rapidly. Since earlier 1970 until now there are massive development, since many campuses move from Jakarta to the periphery area. The land use changing made the changing of water usage too. It impacted not only by the availability of fresh water but also the services of fresh water per households at Depok.

Depok city, in this sense serves as a perfect example of a middle city that also serves as waterway through Ciliwung main river and buffer city connecting the capitol Jakarta and water catchment area Bogor city.

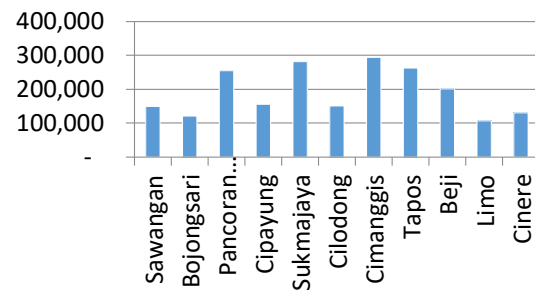


Fig.1 Population of Depok City in 2015

Population of Depok City is 2,106, 100 people with population growth of 3.57 in 2015 [3]. Cimanggis sub-district is the region with the highest population, about 292,132 people lives in the region. But the most dense sub-district in Depok City is Sukmajaya sub-district with population density of 15,600 people per kilometer square.

Total area of Depok City is 20,029 hectares. Residential areas dominating land use in Depok City that reach 58% areas of Depok City. Mixed agricultural is the second largest land use in Depok only have 8.95% of total area. Water bodies such as rivers, lakes and ponds only reach 3% of total area

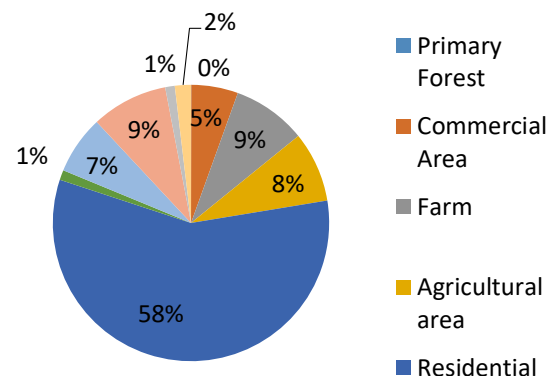


Fig.2 Total Area of Land use in Depok City

Water bodies such as rivers, ponds, lakes and others in Depok City can't works well to receive rainwater or runoff due to insufficient area. This can cause floods in many location in Depok City. Massive housing development can be a contributing factor to decrease area of water catchment area. Increased housing area causes the change of others landuses to residential area.

Despite their importance in water managements, land use between Jakarta, Depok and Bogor city also vary with both urban and rural characteristics developments constantly providing alterations. As many of the developments occurred within the past 5 years, urban management of the city neglected water



management from being integrated to the development plan. As a result, water supply demands increased, while water space decreased. If Depok city government had fully under-stood and implemented Water Sensitive city concept, this may be averted effectively. In addition, such developments have subsequent effects to water catchment areas in Depok, and particularly Jakarta. Despite its status as the centre of economic activity in Indonesia, sustaining close to 10 million residents of different nationalities, cultural backgrounds and social economic power, Jakarta may suffer diminishing supply of water in the next few years to come.

The concepts of Water Sensitive Cities are emerging in response to a general consensus that existing water services and planning processes have been poorly equipped to support the discussed urban challenges (projected population growth, and climate and economic challenges) [2]. Integrated solutions to deliver services for supply, sewerage and flood protection, as well as green and live able urban environments, are a requirement for future cities and towns. In a Water Sensitive City this will be achieved by:

1. Using the city as water supply catchments: diversity of sources and diversity of centralized and decentralized solutions.
2. Assuring its healthy environments: clean rivers and ground water, with cool, green and beautiful urban landscapes.
3. Developing resilient, water-conscious citizens: communities that accept and support new water solutions.

While Australian cities are on their (rather slow) path to transform to water sensitive futures the possibility exists in Indonesian developing cities to leapfrog certain traditional stages in building the urban water infrastructure. For example, rather than investing in a massive centralized sewerage system, it may be more practical in some areas to implement decentralized, efficient and cost-effective treatment and recycling systems at neighborhood scale, leading to direct development of a water sensitive city. In this way developing Indonesian cities will avoid repeating the mistakes that westernized cities made on sustainability.

#### **WATER AVAILABILITY AND MANAGEMENT AT DEPOK CITY**

24 rivers cross Depok City with the longest river are Kali Grogol and Kali Psanggrahan. Length of Kali Grogol crossed Depok City is 35.2 kilometers and Kali Psanggrahan is 20.75 kilometers. But the most important river in Depok City is Ci Liwung, the river has 14 kilometer length throughout Depok City.

Clean water in Depok City provided by PDAM Tirta Asasta, a company owned by the city. PDAM Tirta Asasta established in 2013, before 2013 the needs of clean water provided by PDAM Tirta Kahuripan that owned by Bogor Municipality. In 2015, PDAM Tirta Asasta has 52,255 customers with clean water supply of 1,172,883 cubic meters. The biggest customer of PDAM Tirta Asasta are residential. The middle residential are the biggest with total 26,759 customers and low residential with 18,120 customers.

Needs of drinking water in Depok City is not only provided by PDAM Tirta Asasta but also from other sources. Surprisingly, source of drinking water in Depok City is from ground water pumps with total of 51.31%. Water meter from PDAM Tirta Asasta only supplied 2.96% needs of drinking water.

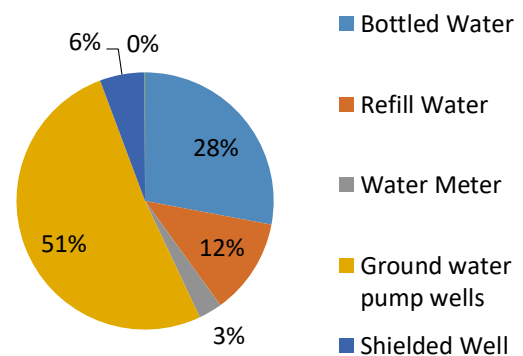


Fig.3 Graphic Source of Drinking Water

Groundwater used to meet needs of drinking water in Depok . Local companies such as PDAM Tirta Asasta was not able to meet the needs of clean water, especially drinking water for residents of Depok city. Excessive use of groundwater can lead to rapid groundwater degradation resulting in an imbalance in the groundwater flow system.

#### **GAP OF WATER ISSUES AT DEPOK CITY**

The issues of water in Depok City are dominated by flood and clean water issues. Floods in many areas of Depok City became major issues especially in the rainy season where rainfall is rising. This flooding issue is usually accompanied by information of clogged waterways caused by garbage and mud sediment. Siltation and constriction of water bodies are also the cause of floods in the city of Depok.

The number of settlements increased, causing an increase in the need for clean water for the people of Depok City. The issue of clean water became the

second biggest issue after the flood, where the need of clean water supplied by PDAM Tirta Asasta has not been able to meet all the needs of the people of Depok City. This causes the use of other sources, especially groundwater pumps become the main source of Depok City residents to get clean water.

## CONCLUSION

Depok city is under pressure from Jakarta's spillover and the internal development of Depok city itself. This is evidenced by the increasingly urbanized land use rather than rural area. This condition causes water demand to increase but water availability decreases. Based on the Water Sensitive indicator, that Depok City is still included in the "Sewered City" stage. Depok City has not been able to manage the water needs and the availability of water in its area. The issue of flooding and clean water is still emerging in many parts of Depok City. Therefore, if the WSC concept wants to be implemented, leapfrogging is necessary so that sustainable development of Depok City does not take a long time to execute.

## ACKNOWLEDGEMENTS

This article is part of Superior Research of Universities (Ministry of Research, Technology and Higher Education)

## REFERENCES

- [1] Brown, R., Keath, N., & Wong, T. (2008). Transitioning to water sensitive cities: historical, current and future transition states. Paper presented at the 11th international conference on urban drainage. Edinburgh, Scotland, UK
- [2] Brown, R. R., & Clarke, J. M. (2007). Transition to water sensitive urban design: The story of Melbourne, Australia (Vol. 7): Facility for Advancing Water Biofiltration, Monash University Melbourne
- [3] BPS, 2016. Kota Depok Dalam Angka 2016. BPS Kota Depok
- [4] Johnstone, P., Adamowicz, R., de Haan, F. J., Ferguson, B., & Wong, T. (2012). Water Sensitive City.

## RISK MAPPING STUDIES OF HYDRO-METEOROLOGICAL HAZARD IN DEPOK MIDDLE CITY

R. Jachrizal Soemabrata<sup>1</sup>, Ahmad Zubair<sup>2</sup>, Irene Sondang<sup>3</sup> and Esty Suyanti<sup>4</sup>

<sup>1</sup>School of Strategic and Global, Universitas Indonesia, Indonesia; <sup>2</sup>Center for Urban and Regional Research, Indonesia

### ABSTRACT

Rapid population makes rapid activity at limitation space. It will increase the potential of conflict within natural or environment resources. Urbanization in Indonesia cities result tight competition of resources between urban dwellers, especially in satellite city like Depok as the consequences Jakarta's spill over. Depok more experiences with flood and landslide since the rapid population pressure. Instead of doing curative action deal with disaster, this city should do preventive action by doing risk mapping. This research will guideline to identify the vulnerability and capacity of it city in dealing with hydro-meteorological hazard. It will conduct by mix method approach using GIS technique and statistical analysis to determine the risk mapping. This research will show the spatial variety of risk that (potential) occurred related with hydro-meteorological in Depok City. Through risk mapping studies, this study will examine the balancing of population growth with the environment acceptances at middle city in Indonesia.

*Keywords: Risk Mapping, Hydro—Meteorological Hazard, Vulnerability, Capacity, Middle City*

### INTRODUCTION

Geographically, Indonesia is located among three tectonic plates of earth, they are Eurasian, Pacific and Indo-Australian plates. Indonesia is also located in the ring of fire area. This location causes 62 % of 497 cities in Indonesia have a high risk level of disaster [1]

Since 2011, Indonesia has entered a period of development, called urban millennia, a situation where the number of urban residents is greater than rural areas. This condition can be seen from the population in big cities such as Jakarta which continues to increase every year.

Indonesia's major cities have a strategic role to play in the development of the region as a service, collection and distribution node, which has a backward relationship with its intermediate and hinterland cities as well as forward relationships with other big cities [2]. Unfortunately, the growth rate and growth of middle cities are relatively uneven and tend to be uncontrolled then causing many problems.

One of the middle cities in Indonesia is Depok. Depok's development tends not to look at the characteristics of the city itself, consequently the physical burden that need to be borne by the city even increases. If this situation still exists, it will lead to large of potential disasters and run down the growth process that will make the slow pace of urban development.

Responding to the importance of disaster and urban issues in Indonesia's development, it is necessary that every city in Indonesia has a tool that can measure disaster risks, one of them through

making maps. Map can give several disaster information by linking 3 aspects. These aspects are the potential disasters occurring in the city, the vulnerability of cities and the roles and capacities of both communities, NGO and governments.

### LITERATURE REVIEW

Disaster risk assessment is an approach to show potential negative impacts that may arise from a potential disaster. Disaster risk assessment in the previous research was conducted on a provincial scale using GIS by the government. The disaster threats experienced by middle cities in Indonesia are hydro meteorological disasters. It is hydro meteorological (i.e., floods, landslides) and climatological disasters (i.e., droughts and heat waves), rather than the geophysical disasters (i. e., earthquakes and volcanic eruptions), that have been trending upwards in recent decades. This rising trend of climate-related hazards suggests a possible connection between these hazards and in turn disasters on the one side and climate change on the other [3].

Hydro meteorological disasters greatly affect the resilience of communities within middle city. The characteristics and circumstances of a community, system or asset that make it susceptible to the damaging effects of a hazard. Figure 1 shows many aspects of vulnerability, arising from various physical, social, economic, and environmental factors. Examples may include poor design and construction of buildings, inadequate protection of assets, lack of public information and awareness, limited official

recognition of risks and preparedness measures, and disregard for wise environmental management. [4]

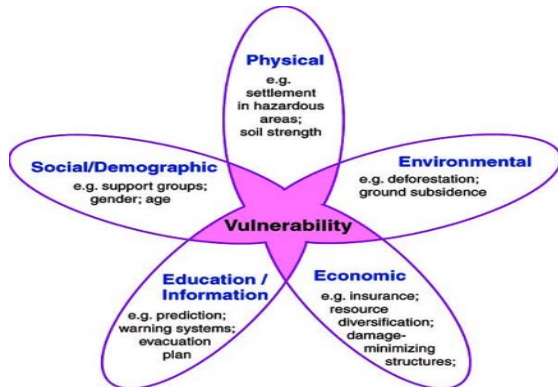


Fig. 1 5 Aspects to Assess Vulnerability

Souza [5], stated that potential damage and risk maps are automatically built up within the GIS (any other geo processing software may be used), then any change in environmental characteristics might be easily updated, allowing that all of the thematic maps involving the Risk Assessment be rapidly modified too.

Hydro meteorological disaster risk reduction is not only done with the construction and management of facilities and infrastructures, in accordance with National Law Number 26, 2007 about Spatial Planning, Republic of Indonesia located in disaster prone areas requires spatial planning based on disaster mitigation as an effort to improve the safety and comfort of life and preserve the environment [6].

## METHODOLOGY

There are 3 components of indicators for calculating the disaster risk of a region. Those indicators are hazard, vulnerability and capacity. At this stage, the study will be conducted to explore the risk assessment methods that used in government guidelines through the Head of National Board for Disaster Management Regulation No 2/2011 as well as recommendations from the United Nation International Strategy for Disaster Reduction (UNISDR).

$$R = \frac{H \times V}{C} \quad (1)$$

R = Risk  
H = Hazard  
V = Vulnerability  
C = Capacity

Based on National Board for Disaster Management [8], equation (1) is a risk assessment method linking potential hazard and vulnerability in Depok City, then divide by its capacity. The review

will be followed by a case study conducted in Depok City. It is hoped that by studying the application in the case study, some learning outcomes will be useful for the improvement of the formulation.

## Hazard Assessment

Hydro-Meteorological hazards are caused by extreme meteorological and climate events, such as floods, droughts, hurricanes, tornadoes, or landslides [7]. The focus of research are floods and landslides. Flood disaster can be calculated and classified into

Table 1 Flood Classification and Score

Depth (m)	Class	Value	Weight (%)	Score
<0.76	Low	1		0.3
0.76-1.5	Mid	2	100	0.6
>1.5	High	3		1

Source: National Board for Disaster Management

Landslides can be calculated and classified into:

Table 2 Landslide Classification and Score

Threat Zone	Class	Value	Weight (%)	Score
Low				
Ground Movement	Low	1		0.3
Medium				
Ground Movement	Mid	2	100	0.6
High				
Ground Movement	High	3		1

Source: National Board for Disaster Management

## Vulnerability Assessment

The vulnerabilities that can be identified in this study are economic and social vulnerability. Indicators used in vulnerability analysis are primarily exposure and loss information. The sources of information used for analysis can come from Central Agency on Statistics data and basic map information.

Economic vulnerability can be calculated through the following equation:

Table 3 Economic Vulnerability Classification

Parameter	Weight (%)	Class (Million)			Score
		Low	Mid	High	

PL	60	<50	50-200	>200	Class/Max
GDRP	40	<100	100-300	>300	Score

Source: National Board for Disaster Management

$$EV = (0.6 \times PL \text{ score}) + (0.4 \times GDRP \text{ Score}) \quad (2)$$

EV = Economic Vulnerability  
 PL = Productive Land  
 GDRP = Gross Domestic Regional Product

Social vulnerability can be calculated through the following equation [8]:

Table 4 Social Vulnerability Classification

Parameter	Weight (%)	Class			Score
		Low	Mid	High	
PD	60	<500	500-1000	>1000	Class/Max Score
SR	40	<	20-	>	
PR		20%	40%	40%	
DR					
AR					

Source: National Board for Disaster Management

$$SV = \left( 0.6 \times \frac{\log\left(\frac{PD}{100}\right)}{\log\left(\frac{100}{100}\right)} \right) + (0.1 \times SR) + (0.1 \times PR) + (0.1 \times DR) + (0.1 \times AR) \quad (3)$$

SV = Social Vulnerability  
 PD = Population Density  
 SR = Sex Ratio  
 PR = Poverty Ratio  
 DR = Disabled Ratio  
 AR = Age Ratio

### Capacity Assessment

The capacity index is calculated based on indicators in the Hyogo Framework for Actions (HFA). The HFA agreed by more than 160 countries in the world consists of 5 Priority DRR programs. Achieving these disaster risk reduction priorities is measured by 22 indicators of achievement [8].

Table 5 Capacity Classification and Score

Parameter	Weight (%)	Class			Score
		Low	Mid	High	
RADMI	100	<0.3	0.3-0.6	>0.6	Class/Max Score
EWS					
DE					
BRFR					

### DODP

Source: National Board for Disaster Management

$$Capacity \text{ Index} = (1 \times Capacity \text{ Score}) \quad (4)$$

RADMI = Rules and Disaster Management Institution  
 EWS = Early Warning System  
 DE = Disaster Education  
 BRFR = Basic Risk Factor Reduction  
 DOP = Development of Disaster Preparedness

## RESULT AND DISCUSSION

### Hazard

#### Flood

Floods are overflow water that exceeds the capacity of rivers in their canals that are usually preceded by high rainfall or high flow water from upstream areas. Due to its vast territory, flood in different areas manifest themselves in different types and with various characteristics [9]. Flood and inundation problems are caused by high rainfall, modified or disturbed river morphological conditions, poor drainage systems, and other external factors such as high river sedimentation and landslides.

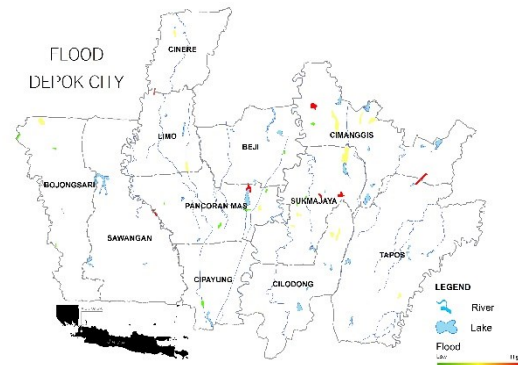


Fig. 2 Flood Area in Depok City in 2015

Some district are potentially affected by flood. The flooded districts spread throughout Depok City and is dominated in the eastern of city. Some areas prone to flooding tend to be passed by large streams such as Ciliwung and Pesangrahan River. Average depth of flood in Depok city is about 50-100 cm, or even reach 200 cm in certain area.

Floods are indirectly related to so massive land use changes. Land use / land cover will be given for making land use monitoring system [10]. It is understood that floods occur because of the unplanned rapid urbanization, change in land use and poor watershed management mainly in flood plains become important issues for consideration as the flood causes [11].

Flood also affects the availability of water. Study of the run-off transformation on the land surface is especially important in built-over areas, where basic natural landscapes are modified [12]. In addition to the area being a reservoir of water, many ponds and fish ponds are both consumption and aquaculture that can become a water reservoir when heavy rains so that the overflow of river water can still be handled.

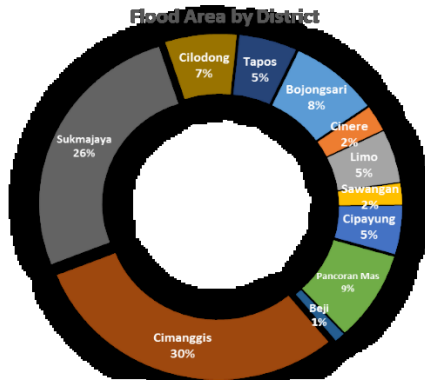


Fig. 3 Flood Areas Percentage by District in 2015

Based on Soemabrata [13], figure 3 shows that Depok City has a flood prone area of 126.4 Hectares, Sukmajaya District became the most potentially affected by floods with estimated total area of 32.8 Hectares. In addition, flood-prone areas in Depok City tend to be located at an altitude of less than 100 meters which includes a declivous area.

#### Landslide

Landslide in Depok City occurs due to several factors both from the physical condition of the region and the natural factors of Depok and human activity in it. According to Matheus [14], measuring the level of landslide hazard can be determined based on seven natural physical parameters consisting of slope, soil, rocks making up the slope, rainfall, land use, seismicity and fault.

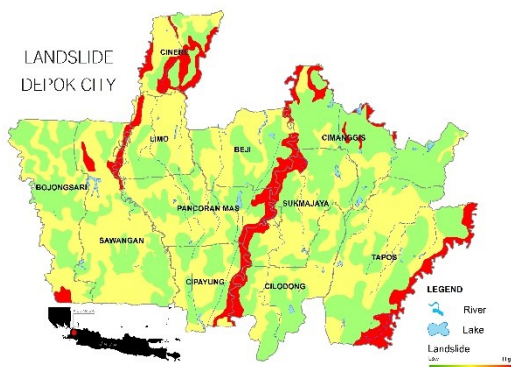


Fig. 4 Landslide Area in Depok City in 2015

Factors caused by humans can be in the form of piles of garbage and the accumulation of material caused by the expansion of settlements so that piling up the soil around the valley leads to overloaded land, and there are farms on the slopes. Potentially landslide-prone areas are located along large rivers that have a fairly steep slope. Geological and geomorphological conditions (e.g., material type, strength and structure, and slope angle) predispose slopes to failure; knowledge of these conditions can help to predict the location, types, and volumes of potential failures [15].

Figure 4 shows the landslide prone area in Depok City is on slope between 8-15% which means that the slope condition is quite steep and has a steep hill or valley. This region is often found along a large river flow that has a river width of more than 10 m. The steeper the slope, the higher the landslide potential, but this can't be separated from the type of rock and soil type in the area.

#### Landslide Area by District

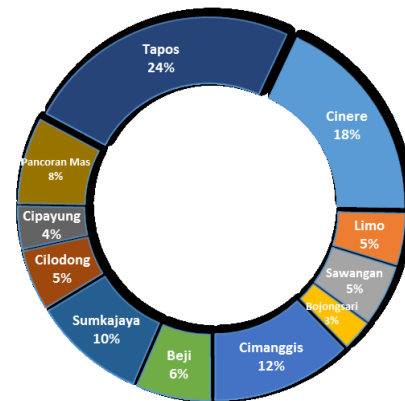


Fig. 5 Landslide Areas Percentage by District in 2015

Based on Soemabrata [13], figure 5 shows areas prone to landslides in the city of Depok reach 1807 Hectares in area. The most vulnerable areas of landslides are Tapos and Cinere Districts with a total of 7 vulnerable villages. This region has a fairly steep slope along the stream.

#### Vulnerability

Vulnerability can simply be defined as exposure x sensitivity [16]. Vulnerability is considered as a result of the interactions between physical (territorial) characteristics and the susceptibility and the capacities of the socioeconomic system to adapt and cope with a specific hazard, expressed as a nondimensional index ranging between 0 and 1 [17]. The vulnerability of Depok City can be divided into economic, social, physical and environmental vulnerabilities.



### Economic Vulnerability

Indicators used to measure the economic vulnerability of Depok City is the area of productive land and GDP of the city. The area of productive land can be obtained from land use maps and district / city or sub-district books in figures and converted into rupiah, whereas GRDP can be obtained from sector or district reports in figures. The weight of the index of economic vulnerability is almost the same for all types of threats, except for building fire and residential and settlement fires.

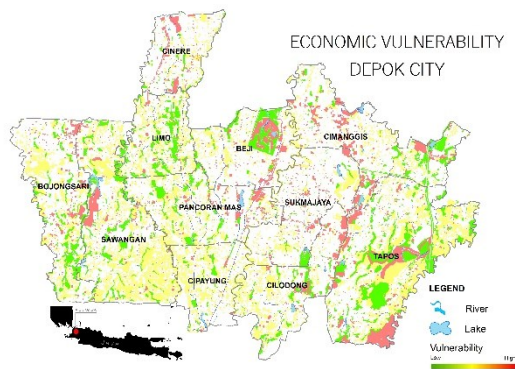


Fig. 6 Economic Vulnerability Area in Depok City in 2015

Figure 6 shows the area with the highest level of economic vulnerability is located in the suburbs with total area of 629 Hectares. Based on the data and field observations that have been done, there are 8 most vulnerable districts. One of them is located in the vital areas of the city. Most of them have productive land (e.g. offices, services and trading area, plantations) that play an important role in economic activity. The rise of land use change has also become one of the causes of economic vulnerability index which is still continuously increasing every year.

### Social Vulnerability



Fig. 7 Social Vulnerability Area in Depok City in 2015

Indicators used for social vulnerability are population density, sex ratio, poverty ratio, disabled ratio and age group ratio. Figure 7 illustrates the distribution of areas with levels of social vulnerability. Where each indicator of each districts has different vulnerability lift. Areas with high social vulnerability are only in Sukmajaya District. This is consistent with the high population density in the region. In addition to population density, the more disability and the number of vulnerable age groups, the more vulnerable the District to Hydro-Meteorological hazard.

Areas with low social vulnerability are located in some districts located in the suburbs. In addition, in the region in some indicators also shows are in low grade. Broadly speaking, it can be said that the more towards the center of the city, the level of social vulnerability is increasing. Vice versa, the more towards the suburbs, the lower the social vulnerability.

### Capacity

The policies and regulations on disaster in Depok City are still overlapping. This is due to the absence of agencies that focus on disaster management affairs. Unlike other cities such as Jakarta that already have Regional Board for Disaster Management (BPBD DKI Jakarta), BPBD Depok needs to be completed because the level of disaster threat is increasing every year. For now, disaster-related policies are downgraded into several plans and programs can be identified through urban planning regulation (RDTR Depok City in City Regulation No.1 Year 2015). The plans and programs are as follows:

Table 6 Flood and Landslide Management Program

Item	Program
Flooded Area Plan	Normalization of drainage channels Building new channels to the river Building embankments
Landslided Area Plan	Protecting and building of river/lake walls Normalization of riverbank and lake with mmud dredging and develop jogging track Building an evacuation road Reforestation by planting landslide prevention plants along riverbank Limit the utilization of space around riverbank



Source: Urban Planning of Depok City

Several programs can also be identified through a series of Focus Group Discussions (FGD) with the Local Government of Depok City and field findings.

## CONCLUSION

Depok City based on the identification of potential hazard threat variables and have historical data related to Hydro-Meteorological hazard that are floods and landslides. Meanwhile, the susceptibility variable successfully identifies two aspects, those are economic and social aspect. Two other aspects (environmental and physical vulnerability) have not been identified due to data limitation. While the capacity variables successfully identified that there have been disaster management programs even though the activities that are preventive are still small. One of them is due to the lack of focus on disaster management because it does not have BPBD yet. The future research should be more focus on the measuring the risk index. Governments need to work with communities to build capacity and reduce vulnerability levels with more planned mitigation programs. In addition, the establishment of disaster management in the city-level is urgently needed.

## ACKNOWLEDGEMENTS

This article is part of Superior Research of Universities (Ministry of Research, Technology and Higher Education) titled "Measuring the Risk of Hydro-Meteorological Disasters on Urban Slums From Health, Adaptive Capacity of Citizens, and Availability of Basic Infrastructure Aspects"

## REFERENCES

- [1] State Ministry for Development Planning, "Disaster Index Reduction in Indonesia", Jakarta: National Board for Disaster Management, 2014.
- [2] Soemabrata. J, "Hidro-Meteorological Hazard Risk Assessment in Slum Area Depok City through Health Aspects, Community Adaptation Capacity, and Availability of Basic Infrastructure", Depok: Universitas Indonesia, 2016, ch 1.
- [3] Thomas V, "Confronting Climate-Related Disasters in Asia and Pacific", *Jahrbuch für Wirtschaftswissenschaften Review of Economics*, Vol. 2, 2014, pp. 121-135.
- [4] United Nations International Strategy for Disaster Reduction (UNISDR), "Global Platform for Disaster Risk Reduction", 2nd Session, Geneva, Switzerland, June 2009.
- [5] Souza, C.R. de G, "Flood Risk Assessment in Coastal Drainage Basins through Multivariate Analysis within a GIS-Based Model", *J. of Coastal Research*, Vol.1, 2009, pp. 900-904.
- [6] M.R. Amri *et al*, "Resiko Bencana Indonesia". Jakarta: Indonesian National Board for Disaster Management, 2016, ch. 2.
- [7] Huan Wu *et al*, "Hydrometeorological Hazards: Monitoring, Forecasting, Risk Assessment, and Socioeconomic Responses", *J. of Advances in Meteorology*, Vol. 2016, Aug. 2016, pp. 1-3.
- [8] M.R. Amri *et al*, "Resiko Bencana Indonesia", Jakarta: National Board for Disaster Management Regulation, 2016 ch 3.
- [9] Zhong Guihui *et al*, "Urban Flood Mapping for Jiaxing City Based on Hydrodynamic Modeling and GIS Analysis", *J. of Coastal Research*, Vol. 1, 2014, pp. 168-175.
- [10] K. Djaja *et al*, "The Integration of Geography Information System (GIS) and Global Navigation Satellite System-Real time Kinematic (GNSS-RTK) For Land Use Monitoring", *International Journal of GEOMATE*, Vol.13, Aug, 2017, pp.31-34.
- [11] N.F Ibrahim *et al*, "Identification of Vulnerable Areas to Floods in Kelantan River Sub-Basins By Using Flood Vulnerability Index", *International Journal of GEOMATE*, Vol. 12, Jan, 2017, pp. 107-114.
- [12] A.V. Bobylev, A.V. Malaev, N.S. Rasskazova, "The Geoecological Modelling of Small Water Reservoirs and River Catchment Areas as a Procedure in Urban Development", *Procedia Engineering*, Vol. 150, 2016, pp. 2067-2072.
- [13] Soemabrata. J, "Hidro-Meteorological Hazard Risk Assessment in Slum Area Depok City through Health Aspects, Community Adaptation Capacity, and Availability of Basic Infrastructure", Depok: Universitas Indonesia, 2016, ch 4.
- [14] S. Matheus, H. Lilik, H. Gunawan "Landslide Hazard and Risk Assessment for Ambon City using Landslide Inventory and GIS", *J. Of Physics: Conference Series* 739, 2016, pp. 1-11.
- [15] Samuel T. McColl, "Landslide Causes and Triggers", *Landslide Hazards, Risk and Disasters*. Amsterdam: Elsevier, 2015, pp. 17-42.
- [16] R.R. Putra, J. Kiyono, A. Furukawa, "Vulnerability Assessment of Non Engineered Houses Based on Damage Data of The 2009 Padang Earthquake in Padang City, Indonesia", *Int. J. of GEOMATE*, Vol. 7, Dec. 2014, pp. 1076-1083.
- [17] Giupponi Carlo *et al*, "Integrated Risk Assessment of Water-Related Disasters", *Hydro-Meteorological Hazards, Risks, and Disasters*. Amsterdam: Elsevier, 2015, pp. 163-200.

## ROLE OF GOVERNMENT AND PRIVATE SECTOR IN MARINE ECOTOURISM RELATED TO CONSERVATION OF BIODIVERSITY IN SERIBU ISLANDS

Lily Surayya Eka Putri<sup>1</sup> and Kristiyanto<sup>2</sup>

<sup>1</sup>Department of Biology, Faculty of Science and Technology, State Islamic University Syarif Hidayatullah  
Jakarta, Indonesia

<sup>2</sup>UNINDRA, Indonesia

### ABSTRACT

Ecotourism have relation with conservation of biodiversity which recently shows bad condition on marine ecosystem. This research analyzed how the role of government compared to private sector was conducted in Pramuka and Air Island based on diversity of marine biota and conformity of ecotourism. Line Intercept Transect method was used in this study stretched along the parallel 85 m into the coastline with three replications over 25 m. Interview with local people surrounding islands was also conducted to get the information of anthropogenic activities. The study showed that coral diversity in Pramuka and Air Island were in moderate level ( $1.00 < H' < 3.00$ ), nevertheless live coral coverage in Pramuka Island was 29.17% of 73.44% total coral coverage lower than Air Island (49% of 55.62%). Sea grass species found in Pramuka Island were 6 species and only 3 species were found in Air Island whereas mangrove species was lower in Pramuka Island than Air Island. For ecotourism conformity, Pramuka Island was only suitable for sea grass tourism whereas snorkeling and diving tourism were more suitable in Air Island. Hence, despite ecotourism in both islands were likely destroyed the environment, conservation of biodiversity on marine ecosystem seemed ineffectively managed or even ignored by government neither private sector. Education and raise awareness for local people is the main priority in order to conserve the uniqueness of the ecosystems in Seribu Islands.

*Keywords: Marine Biodiversity, Marine Ecotourism Conformity, Seribu Islands*

### INTRODUCTION

Indonesia is the largest archipelago country with more than 17,000 small islands which is called Seribu Islands. The Seribu Islands has the unique natural resources, both in terrestrial and marine areas providing environmental services for local people to support economic and social development sustainably [1], [2].

The richness of biodiversity in Seribu Islands provides <sup>ecotourism</sup> activities which serves an interesting tourism destination, including white sandy beach, beauty of under water, and unique culture. Nevertheless, such ecotourism activities are conducted so far in Seribu Islands has some negative impacts on the conservation of biodiversity, including use of coral for building, destruction of coral as water sport activities, exploitation sands for building. Many studies have reported the degradation marine diversity, including corals in Seribu Island [3-6] and sea grass [7].

Most of management of the small islands in Seribu Islands is run by government and some of them are by private. There are 12 islands managed by government of DKI Jakarta which are in primary zone and 11 islands in inhabitant zone, while 34 islands managed by private for tourism destination and no inhabitants in those islands. Unfortunately,

less study is conducted regarding to evaluate role of government and private sector in conserving biodiversity related to tourism activities and other anthropogenic activities in the mainland. Therefore, this study was conducted at Pramuka and Air Island representing government and private sector management in order to analyze the role of both management in marine diversity conservation and evaluated the impact of ecotourism activities to biodiversity in the islands. The ecological data was collected and analyzed as the important information in monitoring the condition of the ecosystem at both islands, including diversity of marine (corals and sea grass) and conformity of ecotourism assessment.

### MATERIALS AND METHODS

This research used the qualitative and quantitative methods, including collecting data through field survey methods, interviews and observations in Pramuka and Air Islands, Seribu Islands, Indonesia, from June to November 2013. Diversity of marine biota was collected including coral and sea grass, and the analysis was conducted at the Laboratory of Biology, Center for Integrated Laboratory, State Islamic University (UIN) Syarif Hidayatullah Jakarta. The sampling point at

Pramuka Island was at North, South, and West (Pier) sites, while Northern sites of Air Island which coral ecosystem found. Interview with local people was also conducted to get more information about the contribution given by government and private sector for conservation program in both islands.

Furthermore, the data of diversity index of various marine species is determined using the formula of Shannon-Wiener index [8].

$$H' = - \sum_{n=1}^{\infty} \left( \frac{ni}{N} + \ln \frac{ni}{N} \right)$$

Description:

H' = Shannon-Wiener diversity index

ni = Number of individuals of a species to-i

N = Total number of individuals of all species

The value of Shannon Wiener Diversity Index has a range of categories is defined as follows:

H' < 1.00 : Diversity of species is low.

1.00 ≤ H' ≤ 3.00 : Diversity of species is moderate.

H' > 3.00 : Diversity of species is high

For coral reef monitoring, it was used LIT (Line Intercept Transect) method to collect data which was made of 3 transects. The length of transect was each 25 m with 5 m interval between each transect, so it was about 85 meters length of line toward the sea. Observation was conducted at two depths, which were at 3 and 10 meters depth, with 3 replications. The depth of 3 m represented shallow waters while the 10 m depth for a relatively deepest water, assuming two conditions represent the depth of the reef where coral can grow well [9]. Observation was conducted in the morning or during the day depending on the condition of weather [10].

Installation of transect was parallel to the shoreline and follow the contours of corals. Transect is placed on top of the coral colony and recorded the coral form, live and dead coral, abiotic form, coral cover, and the form of the substrate (sand, mud and rocks), along 85 m length.

These measurements were performed with an accuracy approach which always considered the colony form as a single individual. If a colony of the same type is separated by one or several parts of the dead corals, the living part of each regarded as a separate individual. If two or more colonies are growing on top of the other colonies, then each colony was still counted as a colony separately [11]. The length of overlapping colonies were recorded and used to analyze the species richness.

The percentage of coral cover was used to estimate the condition of coral reefs in an environment which was obtained from the measurement of life form of corals using the formula [12] below:

$$L = \frac{Li}{N} \times 100\%$$

Description:

L = The percentage of coral cover (%)

Li = Length of life form (intercept colony) categories

to-i

N = Length of transect (m)

Percentage of coral coverage is the area covered by growing corals which was developed by Gomez and Yap [13] the criteria as follow:

Table 1 Percentage of live coral coverage

Coverage (%)	Category
75 – 100	Very good
50 – 74.9	Good
25 – 49.9	Moderate
0 – 24.9	Bad

Measurement of physical parameters at each station of each transect was also considered. The physical parameters of water measured were pH, temperature, and clarity

## Data Analysis

The data of this study is the qualitative and quantitative data. Data obtained from this study was analyzed quantitatively descriptively using simple mathematic formula, so it can provide an overview of the ecological condition of Pramuka and Air Island. Furthermore, ecological data from both study sites was analyzed to evaluate the conformity index of ecotourism, including type of ecotourism for recreation, snorkeling, diving, and sea grass tourism. Assessment for conformity of ecotourism was adapted from Yulianda [14] and Baksir [15]. Based on the results obtained, it can be further evaluated the role of government and the private sector in managing the region-based biodiversity conservation.

## RESULT AND DISCUSSION

Management in Seribu Islands is the important factor in determining the condition of biodiversity in this area. Based on ecological data, there were differences between Pramuka Island which was managed by local governments and Air Island which was managed by private company (Table 2). The differences were very closely related to conservation activities carried out by the stakeholders.

The quality of the environment and the level of diversity in Air Island as the resort's island which

was run by the private company were relatively better than Pramuka Island. There was not found people living in this island resulted in little waste produced which in further lead to better environmental quality of the surrounding waters. However, less waste production in the island did not significantly impact to the quality of environment in Air Island. This assumes that lack of contribution was given by the management in marine conservation leading to moderate to low diversity of corals and sea grass (Table 3) which should have high diversity as no residential in this island.

Table 2 Comparison of Pramuka and Air Island profile

Parameter	Management	
	Pramuka Island	Air Island
Management	Government	Private
Residential	Yes	No
Wastes	Many domestic wastes and without treatment	Less domestic wastes and with treatment
Environmental awareness	- Cleanliness bad - Low awareness of government - Low Awareness of people	- Cleanliness keep well - Low awareness of management
Transportation	Ships dock everyday	Ships dock only weekend, prefer big private ships
Exploitation of natural resources	Corals for building materials	Corals for water front development on large scale
Research	Many studies done by universities, government, and NGO's	Less research done

#### Marine Biodiversity in Pramuka and Air Island

Based on ecological quality, level of biodiversity in Air Island was relatively similar to Pramuka Island that was in moderate level ( $1.00 < H' < 3.00$ ) (Table 3). As resort's island, the diversity index in Air Island has to have high diversity index ( $H' > 3$ ). This was suggested that the external factor were also contributed to the quality

of the ecosystem, such as research and conservation activities. Those activities which are often carried out by the external parties, including universities, NGO's and government as governors had a positive impact on the conservation in Pramuka Island's ecosystems. Instead of Air Island, it was very few and even might not have conservation and education programs for the tourists that come to the island leading to degradation to the ecosystem. It seems that management of Air Island was dependent on natural condition instead of giving proper contribution in conservation.

However, it does not mean that the island run by the government was better than the private island. Based on surveys and interviews conducted in Pramuka Island were acquired the information that most of the contribution of conservation programs was from the outsiders such as universities, researchers and NGO's compared to the local people itself and government. The marine biota diversity has to be consider as an important parameter to assess the success of conservation program in the islands

Regarding to the marine diversity, in recent study, diversity index of corals decreased to 1.38 (Table 3) compared to the study conducted by Efrinawati [3] that found diversity index of coral was 2.07-2.82. This was so bad and it can be assumed that all activities done did not give significantly impact to the marine environment, such as coral transplantation. Rifqi [4] observed that coral transplantation had already conducted in Pramuka Island since 2005, but live coral coverage was only 23-50% in 2016 due to water pollution come from mainland and diesel spill from ships. This condition was almost the same as reported by Mujiyanto et al [16] in 2009 that live coral coverage was 30-50%. More attention for corals conservation is needed for environmental sustainability in the future.

Table 3 Comparison of Diversity Index ( $H'$ ) and Number of Species at Pramuka and Air Island

No	Parameter	Pramuka Island	Air Island
A	$H'$ index		
-	Corals	1,38 (moderate)	1,52 (moderate)
-	Seagrass	1,60 (moderate)	0,82 (low)
B	Number of Species		
-	Life form of corals	10	6
-	Sea grass	6	3
-	Macroalgae	2	3
-	Coral fish	<61	<61

The low diversity index in Pramuka Island was also strengthened by the low coverage of live corals was 29.17%. The coral coverage in Pramuka Island was 73.44% however 44.27% was dominated by dead coral algae (DCA) (Fig. 1). In Air Island, 49.22% of 55.62 % live coral dominated coral coverage and only 6.4% of dead corals found. Nevertheless, there was not any contribution given by the resort management for marine conservation. Thus, the good condition of live coral coverage was solely because of the dynamics of nature. This was proved by the study conducted by Subhan et al [6] in 2008 and Yosephine et al [5] in 2010 found that live coral coverage in Air Island was 27.18%-37.88% and 43.16% lower than the recent study in 2013.

Regarding to sea grass ecosystems, the diversity index in Pramuka Island was better than Air Island (Table 3). There were 6 species of sea grass found in Pramuka Island, including *Cymodocea rotundata*, *Cymodocea serrulata*, *Enhalus acoroides*, *Halodule uninervis*, *Halophila ovalis*, dan *Thalassia hemprichii*, whereas 3 species in Air Island, *Cymodocea rotundata*, *Enhalus acoroides*, and *Thalassia hemprichii*. *Enhalus acoroides* (37%-43%) and *Cymodocea rotundata* (31%-58%) were the most dominant species grown in both islands (Fig. 2). Both species are a hardy species and it is adaptable to marginal conditions. Just like other intertidal species,

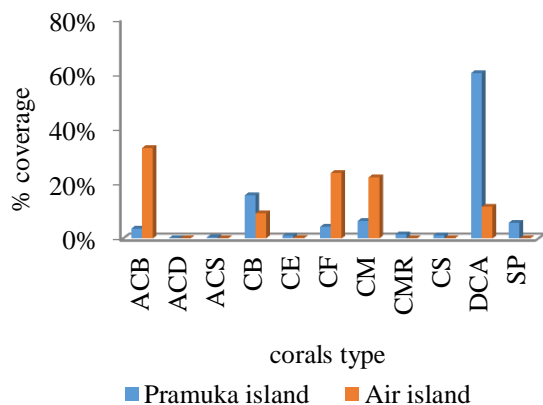


Fig. 1 Percentage of coral coverage at Pramuka and Air Island. Note: ACB (Acropora Branching), ACD (Acropora Digitate), ACS (Acropora Submassive), CB (Branching Coral), CE (Encrusting Coral), CF (Foliose Coral), CM (Massive Coral), CMR (Mushroom Coral), CS (Submassive Coral), DCA (Dead Coral Algae), SP (Sponge)

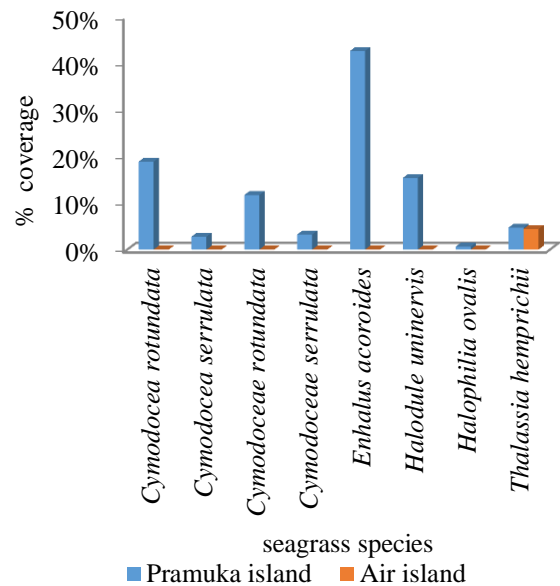


Fig. 2 Percentage of sea grass coverage at Pramuka and Air Island

*Enhalus acoroides* and *Cymodocea rotundata* are common and widespread, especially in embayments. Based on criteria of ecology developed by Salm et al. [17] and Soselisa [18], diversity of sea grass was high (>5 species) in Pramuka Island, but it was categorized low (1-3 species) in Air Island.

Macroalgae was also found in Pramuka and Air Island, they were *Padina* sp., *Sargassum* sp., and only *Halimeda* sp. was in Air Island, but in small quantities due to anthropogenic wastes that have an impact on water quality degradation. Very low clarity was observed that was only 1.5 m in Pramuka Island and 2 m in Air Island (Table 4). This was resulted in interference of marine biota including corals, sea grass and macroalgae diversity. Based on criteria of ecology [17], [18], diversity of macroalgae was low (<10 species) in both islands.

Table 4 Physical parameter

Parameter	Pramuka Island	Air Island
pH	8	7.6
Temperature (°C)	29.66	31.2
Clarity (m)	1.5	2

### Conformity of Ecotourism

From the field observation, in general the condition of Pramuka and Air Island was not in good condition, however with high awareness and efforts from all stakeholders especially government, resort management, and local community, ecotourism in both islands still have good potential to be developed because of the underwater

uniqueness in both islands. This factor is very important to attract tourists visiting the islands.

In order to analyze the conformity of Pramuka and Air Island as ecotourism destination, it is necessary to use the matrix of conformity [14],[15]. The conformity of ecotourism category is divided into recreational, snorkeling, diving and sea grass tourism. The value of matrix is defined as 3 categories: value 1 means not suitable, value 2 means suitable, and value 3 means very suitable.

Analysis of ecotourism conformity on Pramuka and Air Island was showed at Table 5. The conformity of Pramuka Island was only suitable for sea grass tourism which was supported by the higher diversity of

Table 5 The conformity of ecotourism at Pramuka and Air Island

No	Parameter	Pramuka Island	Air Island
1	Recreation	1.84	1.46
2	Snorkling	1.63	2.29
3	Diving	1.54	2.29
4	Sea grass	2.12	1.8

sea grass in Pramuka Island than Air Island. Fortunately, the presence of coral fish in the sea grass ecosystems was such an attractively scenery for tourist in shallow water activities as the main habitat for sea grass. Various types of sea grass can be found in Pramuka Island at depths between 50-100 cm at low tide and 2 m at high tide.

For Air Island, snorkeling and diving tourism were more suitable to be develop. This was supported by higher live coral coverage in Air Island than Pramuka Island. Deep depth water was also considered which can dive until 18 m deep in Air Island. Although, diversity of coral fish was low based on Salm et al. [17] and Soselisa [18], the live coral coverage still attract tourist to dive or snorkel. The diversity of fish is closely related to the quality of the waters and the presence of the inhabitants in Island. Waste production in Air Island as a Resort Island with no inhabitants, was not so many as Pramuka Island with large residents which could pollute the water if it was disposed directly to water without treatment.

Recreation tourism was not suitable in both island due to muddy sand in the beach and the presence of sea urchins and lepu fish that can injure tourists while doing activities on the beach.

In general, ecotourism are not are suitable in Pramuka and Air Island and also not meet the criteria of ecotourism itself of which environmental protection and biodiversity conservation are imperatively considered. To develop ecotourism in the islands, the authorities should focus on consultation and participation between all stakeholders involved in ecotourism to ensure the economic and socio-cultural benefits are shared

between government, private sector, tourists and local communities.

This study has already shown that it is quite difficult to expect local communities with low awareness to support and implement conservation. Hence, it is up to the political will of the government to develop and implement policies that strike a balance between economic gains and environmental conservation. Clifton [19] suggested that if the activities do not reflect the needs between local communities and the environment, local people will not participate in conservation activities which finally will not result in environmental benefits.

The efforts in scientific research activities, conservation and management, environmental education, awareness, and community action have done successfully in Tamar project at Brazil [20], in Brunei Darussalam [21] and also in South Korea [22]. The high level of interaction develops awareness about the importance of field research and the importance of conservation and research in the islands.

## CONCLUSION

The role of the private sector and government is still limited in conservation of biodiversity in Pramuka and Air Island. However, if they make good collaboration with other parties including university, research centre and NGO's, and have open minded to others, in future, both Islands will be getting better environment as habitats for marine organisms.

Meanwhile, the government needs to give seriously attention in population growth in Pramuka Island which tends to enhance waste production resulted in water quality declined. Bad water quality is related to low-moderate level of marine diversity in Pramuka and Air Island. This also results in less conformity of ecotourism. Air Island was suitable for snorkeling and diving tourism while Pramuka Island was only suitable for recreation tourism.

With good efforts and collaboration among all stakeholders, ecotourism activities will further provide positive impacts in economic, socio-culture and environmental benefits in Seribu Islands. Research and education are the first step concerned in order to develop the ecotourism in small islands, like Seribu Island. Finally, the quality of marine environment will increase in between with biodiversity conservation activities, so environmental sustainability will be achieved in the future.

## ACKNOWLEDGEMENTS

Authors would like to thank to State Islamic University (UIN) Syarif Hidayatullah Jakarta which had given financial support for this research. We also thank to students and laboratory staff of Biology Department who had given technical support in the field and laboratory.

## REFERENCES

- [1] Clark JR, "Coastal Zone Management Handbook". Lewis Publisher, Boca Raton, Florida, 1996.
- [2] Dahuri R, "Marine Diversity as The Asset of Indonesian Sustainable Development". PT Gramedia Pustaka Utama, Jakarta, 2003.
- [3] Efrinawati, "Coral reefs in Pramuka Island, Panggang Island District, National Park of Seribu Island". [Thesis], Science and Technology Faculty, UIN Syarif Hidayatullah Jakarta, 2012.
- [4] Bahri RS, "Coral coverage in coral transplantation in Pramuka Island, Seribu Islands". [Thesis], Marine Science & Technology, Faculty of Fisheries and Marine Science, Bogor Agricultural Institute, Bogor, 2016.
- [5] Tuti MIY, Suharsono, Giyanto, Manogar, "Effect of turbidity to coral ecosystem in Seribu Island. Centre for Oseanography Reseach, Institution of
- [6] Subhan B, Arafat D, Andono G, Mursalin, Madduppa H, "Study of substrate basis in corals reef at Karang Beras, Air, Panggang and Pramuka Island, Seribu Islands, Jakarta", in Proc. National Seminar and Conference in Water Resources Utilization, 2008.
- [7] Wahab I, Maduppa H, Mujizat K, "Seagrass species distribution, density and coverage at Panggang Island, Jakarta", Earth & Environmental Science, 54, 2017, pp. 1-8.
- [8] Shannon CE, Wiener W, "The Mathematical Theory of Communication". University of Juionis Press, Urbana, 1963.
- [9] Anggoro AW, "Coral reef condition in Weh Island, Sabang, Nangroe Aceh Darussalam. [Thesis], Department of Science and Marine Technology, Faculty of Fisheries and Marine Science, Institute of Agriculture Bogor, 2005.
- [10] English S, Wilkinson, Baker V, "Survey Manual for Tropical Marine Resources, Second Edition". Australian Institute of Marine Science-AIMS, Townnville, Australia, 1997.
- [11] Hidayat A, "Concept and Policy of Marine Tourism Development". Seawatch Indonesia, BPPT, Jakarta, 2000.
- [12] Fachrul MF, "Sampling Method for Bioekology". Bumi Aksara, Jakarta, 2008.
- [13] Gomez ED and Yap HT, "Monitoring Reef Condition", Coral Reef Management Hand Book, Kenchington RA and Hudson BE T (ed)., UNESCO: Regional Office for Science and Technology for South East Asia, Jakarta, 1988.
- [14] Yulianda F, "Marine ecotourism as an alternative to conservation-based coastal resource utilization". Paper in Seminar of Science, MSP Department, February 21, 2007, Bogor, 2007.
- [15] Baksir A, "Development of small islands for sustainable ecotourism at South and West Morotai district, North Maluku Province". [Dissertation], Bogor Agricultural Institute, 2010.
- [16] Mujiyanto BI, Baiq I, Purwanti, Hartati ST, "Relation between coral coverage percentage and coral fish community in Seribu Island", in Proc. National Forum of Fish Resources II, Cooperation LRPSI-PRPT, Institute of Agriculture Bogor, Institute of Science Indonesia and MII, 2009.
- [17] Salm RV, Clark JR, Siirila E, "Marine and Coastal Protected Areas: A Guide for Planners and Managers", 3<sup>rd</sup> ed. International Union for Conservation of Nature and Natural Resources, Bland, Switzerland, 2000.
- [18] Soselisa A, "Study of coastal and marine resources in Padaido Island, Padaido District, Biak Numfor, Papua". [Dissertation]: Institute of Agriculture Bogor, Bogor, 2006.
- [19] Clifton, J. 2004. Ecotourism: Theory, reality and challenges. Chan, N.W. (Ed.). Ecotourism: issues and challenges: 1-10. Penang: School of Humanities, Universiti Sains Malaysia,
- [20] Moreira JC, Robles RA, "Tamar Project: Conservation and Education in Ecotourism Activities Related to Turtles in Fernando de Noronha Archipelago, Brazil", Wildlife Tourism, Environmental Learning and Ethical Encounters, Borges de Lima I, Green R. (eds). Geoheritage, Geoparks and Geotourism (Conservation and Management Series), Springer, Cham, 2017.
- [21] Ahmad A, "Conservation of island biodiversity in Brunei Darussalam: The role of ecotourism in environmental education", International Journal of Ecology & Development, 30 (1), 2015, pp. 51-63.
- [22] Shin I, "Ecotourism Policies in Korea: Pursuing nature conservation & Making Communities more vibrant", Special Session on Challenges and Opportunities for Sustainable Development of Tourism in Small Island Developing States (SIDS), Busan, 18 April 2014.



## **SEISMIC MICROZONATION FOR URBAN PLANNING AND VULNERABILITY ASSESSMENT OF NON-ENGINEERED STRUCTURE IN EARTHQUAKE PRONE AREA, PADANG, INDONESIA**

\*Rusnardi Rahmat Putra<sup>1</sup>, Junji Kiyono<sup>2</sup>, Ganefri<sup>3</sup> Fahmi Rijal<sup>4</sup> and Syahril<sup>5</sup>

<sup>1,4</sup>Civil Engineering, Engineering Faculty, Universitas Negeri Padang, Indonesia, <sup>3</sup>Graduate School of Engineering, Kyoto University, Japan, <sup>2</sup>Elect<sup>4</sup>Mechanical Engineering, Engineering Faculty, Universitas Negeri Padang, Indonesia

**Abstract:** Padang city is located at earthquake prone area, several powerful earthquakes have struck Padang during recent years, one of the largest of which was an M 7.6 event that occurred on September 30, 2009 and caused more than 1000 casualties. The basic purpose of seismic microzonation is to produce input for urban planning and to supply site specific ground motion data to be used for the assessment of the vulnerability of the non-structure houses stock. A very detailed geological and geotechnical studies were conducted to evaluate the variation of site characterization within the city of Padang. We performed single observations of microtremors at 110 sites in Padang. The results enabled us to estimate the site-dependent amplification characteristics of earthquake ground-motion. We also conducted a 12-site microtremor array investigation to gain a representative determination of the soil condition of subsurface structures in Padang. Based on soil characteristic in whole Padang, We simulated the recorded ground motion of earthquake 2009 to obtain ground motion whole Padang. This seismic microzonation is a parameter for vulnerability assessment to non-engineered houses. We conducted vulnerability assessment to non-engineered structure of houses stock to estimate current structure condition to face predicted earthquake event in near future. About 1400 non-engineered structure were assessed and interviewed. The residents received explanations for each item on the questionnaire from the interviewers, and answers were filled in directly on the answer sheets. This survey produced a map of the shaking intensity and houses' vulnerability distribution in Padang. From the dispersion curve of microtremor array observations, the central business district of Padang corresponds to relatively soft soil condition with  $V_{s30}$  less than 400 m/s, the predominant periods due to horizontal vertical ratios (HVSRS) are in the range of 2.0 to 4.0 s, and 98% of houses in high risk due to predicted earthquake. These results enable produce clear information to Padang people including local government of Padang how to create a mitigation system to reduce earthquake risk.

**Keywords:** array observation, vulnerability assessment, non-engineered structure, seismic microzonation

### **1. INTRODUCTION**

The city of Padang is located on the west coast of Sumatra in western Indonesia, lies close to the Sumatran subduction zone that is formed by the subduction of the Indo-Australian Plate beneath the Eurasian Plate. Relative motion of the plates occurs at a rate of about 50 to 70 mm/year and this is the main source of subduction-related seismicity in the area [1]. Based on our catalog, several giant earthquakes have occurred in this region since records began: 1779 (Mw 8.4), 1833 (Mw 9.2), 1861 (Mw 8.3), 2004 (Mw 9.2), 2007 (Mw 7.9 and 8.4), 2009 (Mw 7.6), and 2017 (6.4). The hypocenter of the Padang earthquake that occurred on September 30, 2009 was located in the ocean slab of the Indo-Australian Plate at  $-0.81^{\circ}\text{S}$ ,  $99.65^{\circ}\text{E}$  and at a depth of 80 km. It produced a high degree of shaking and the tremor was felt in the

Indonesian capital, Jakarta, about 923 km from the epicenter. The tremors also were felt in neighboring countries such as Malaysia and Singapore [2]. The earthquake caused landslides and collateral debris flows in the hills surrounding Lake Maninjau. A major landslide in Gunung NanTigo, Padang Pariaman completely destroyed some villages and forced road closures.

This 1900-km-long active strike-slip fault zone that runs along the backbone of Sumatra poses seismic and fault hazards to a dense population distributed on and around the fault zones [3]. The Sumatran Fault is highly segmented. It consists of 20 major geometrically defined segments and the slip rate along the fault increase to the northwest, from about 5 mm/yr [3].

This fault also has generated large destructive earthquakes, e.g., 1892 (Mw 7.1), 1943 (Mw 7.6) and 2007 (Mw 6.4). These faults are

capable of generating strong ground motion in the future that would greatly affect vulnerable structures. Based on the latest earthquake events catalogs from USGS (2017) showed the number of earthquake events with magnitude from 3 to 6 is creasing within one month for each month in 2017. It shows how the activity of plate currently is.

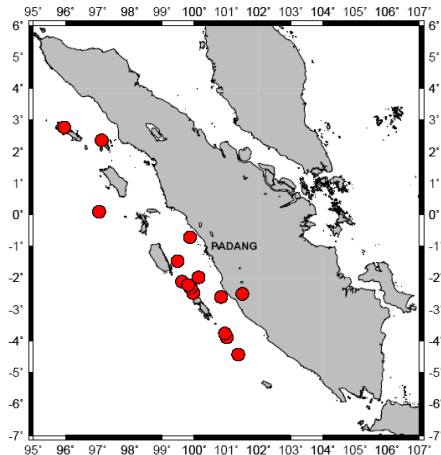


Fig.1 Seismicity of Sumatra Island from 2005 to 2010,  $M_w > 6.5$ ,  $< 100$  km depth of hypocenter, and Padang City

### Regional Geology and Recent Earthquake

The city of Padang, with a population of 914,968 people as of 2016, is the capital of West Sumatra province. The location of the city center is at  $100.38^\circ\text{E}$ ,  $0.95^\circ\text{S}$ . The main part of Padang is situated on an alluvial plain between the Indian Ocean and the mountains. For the most part, the countainous area is formed of Tertiary sedimentary rocks with outcrops of metamorphic rocks seen in some places. The alluvial plain spreads along the base of the mountains and is roughly 10 km wide in the east-west direction and 20 km wide in the north-south direction.

The topography of the Padang region is very similar to the tsunami-damaged area of Miyagi Prefecture in Japan, that was inundated by as much as 4-5 km from the coast after the March 11, 2011  $M_w$  9.0 Tohoku earthquake off the east coast of Honshu. In Padang, about 650,000 people live in the coastal area (covering about  $60 \text{ km}^2$ ). The population density is very high, about  $10,833 \text{ people/km}^2$ . The city is located on the coast of the Indian Ocean between the Sumatran Fault and the Sunda Trench Fault. Both faults are active with slip rate ranging from 10 to 27 mm/year [3]. According to our catalog, 3,174 events with a magnitude greater than 4 occurred in this region from AD 1779 to 2017 [4]. The several giant earthquakes mentioned previously have all been strongly felt here. For example, the source of the 2009 Padang earthquake was located in the ocean slab of the

Indo-Australian Plate. It produced extensive shaking and severe damage to houses and buildings in Padang and Padang Pariaman, because its epicenter was about 60 km offshore from Padang. As the Padang earthquake was an intra-slab earthquake at intermediate depth with a comparable magnitude, the event did not generate a tsunami of significance [5]. Due to this earthquake, 1117 people were reported killed, 1214 severely injured, 1688 slightly injured, and 3 were left missing in West Sumatra. The earthquake also destroyed many houses, buildings and infrastructure (heavily damaged houses numbered 114,797, with 67,198 moderately damaged and 67,837 slightly damaged). In Padang, 5458 buildings sustained damage [6]. This event occurred at the end of the working day, just 15 minutes after offices and schools closed; if it had struck earlier, the number of casualties would definitely have been higher as a result of building collapses. Several hours after Padang earthquake, 1<sup>st</sup> October 2009, Sumatran fault line generated  $M_w$  7.1 and 10 km depth. Due to this earthquake destroyed many houses and building (heavily damaged houses numbered 600, with 550 moderately damaged). Since Padang has high potential to great earthquake shaking in near future with great acceleration too compare with previous earthquake in 2009 [7]. With great potential shaking occur in Padang for several return period of earthquake events, Padang has highest vulnerability to non engineered structure in Indonesia [8]. Based on observation in Palu city, Palu its self has the same soil characteristic as Padang city [9],[10].

There are four accelerometers in Padang. Three were donated by Engineers Without Borders Japan (EWBJ) and installed in 2008, and the other was installed by the Indonesian Government's Bureau of Meteorology, Climatology and Geophysics (BMKG). However, only one ground motion record is available for the Padang earthquake. Due to an electric power cut during the earthquake, only the BMKG device recorded the time history of the earthquake. The observed record shows about 20 s of strong shaking with a peak ground acceleration (PGA) of 0.3 g and a predominant period of 0.5 s [11]. Response spectra at low period is greater then Indonesia code for rock condition (0.83g). The location of this station is a mountainous suburb about 12 km in from the coast. The subsurface condition at this station is rocky; the average shear wave velocity for the upper 30 m of the subsurface here,  $V_{s30}$ , is 1200 m/s [10].

### DAMAGE FROM THE 2009 PADANG EARTHQUAKE

The city of Padang covers an area of about  $695 \text{ km}^2$  and is divided into 11 districts: B. T. Kabung, K. Tangah, Kuranji, L. Begalung, L. Kilangan, Nanggalo, P. Barat, P. Selatan, P. Timur,

P. Utara, and Pauh. 51.0% of the land is forested, 28.52% is used for farming, 9.54% for housing and 7.1% for rice fields [12]. The population of more than 914,968 is increasing by 1%-2% per year. The K. Tengah district has the highest population and most extensive area compared with the other districts in the city.

The central business area of Padang is close to the coast and consist of several district: P. Barat, P. Utara, P. Selatan and P. Timur, B.T. Kabung, K. Tengah. The downtown area is utilized as a center of political and commercial activities. Although the Padang earthquake affected all districts of the city, the major damage occurred downtown, because about 80% of population lives near the coast. The majority of houses in the city are one- and two-storey non-engineered structures. These structures are typically built of confined masonry, with reinforced-concrete (RC) frames acting as confinement for the brick masonry walls. There are three general categories of houses in Padang: permanent houses (RC), semi-permanent houses (mix of RC and wood) and traditional houses (wood). Unfortunately, no detailed damage statistics are available for each type of building, so we cannot classify the category of the house. This earthquake also affected lifelines in Padang. The strong ground shaking destroyed public water distribution pipes leading to 2,906 reported leakage points in total [13]. Damage to pipelines forced the cessation of water delivery to consumers for several weeks.

## 2. SITE CHARACTERIZATION BY MICROTREMOR OBSERVATION

### Single Microtremor Observation

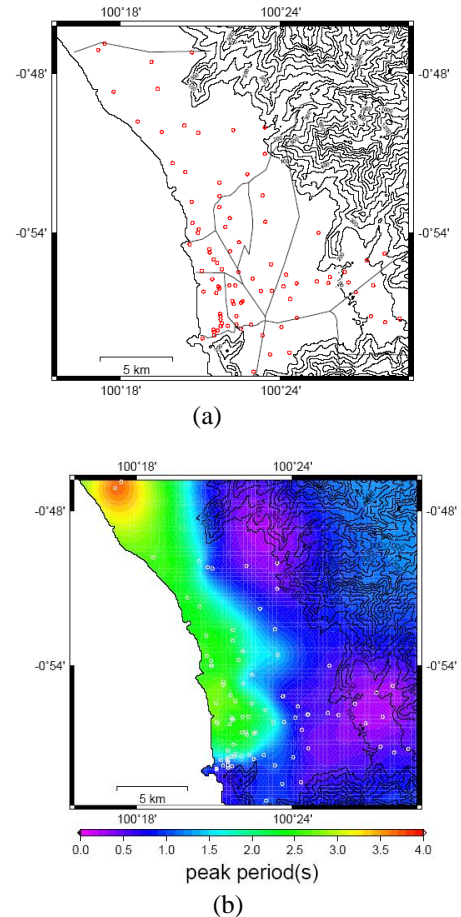
A microtremor is a very small ground motion that can be recorded on the ground surface. It can be produced by a variety of excitations (e.g., wind, traffic, breaking sea waves). A full microtremor record can be described by one vertical and two horizontal components. Our analysis was conducted using the recorded microtremor. First, the horizontal and vertical spectrum ratios (HVSr) were computed for all sites (**Fig. 2**). HVSr (Horizontal-Vertical Spectra Ratio) is consists in estimating the ratio between the Fourier amplitude spectra of the horizontal (H) to vertical (V) components of ambient noise vibrations recorded at one single station.

The peak period of the HVSr is known to correspond to the resonant period of the site. This method postulates the shape of the Fourier spectrum. Equation. (1) shows the method used to calculate HVSr using the observed records.

$$HVSr = \frac{\sqrt{F_{NSi}(\omega)^2 + F_{EWi}(\omega)^2}}{F_{UDI}(\omega)^2} \quad (1)$$

where  $F_{NSi}(\omega)$  and  $F_{EWi}(\omega)$  denote the Fourier amplitude of the NS, EW and UD components of each interval, respectively, and  $\omega$  is the frequency.

We performed 140 single site surveys that sampled every district of the city of Padang. These observations were carried out in November 2008, September, November, and December 2009 and January 2010. The locations of observations are plotted in Fig.3. Microtremor was measured using a GPL- 6A3P sensor. The two horizontal (NS and EW) and the vertical (UD) components were



**Fig. 2** Observation sites and results of HVSR.(a) Microtremor single observation sites at every district in Padang, (b) Distributed HVSR ratio.

The recorded simultaneously for 10 minutes with a 100 Hz sampling frequency. We estimated the distribution of the peak periods of the HVSRs for all sites in Padang using the ordinary kriging technique. From single observations, we obtained a predominant period of 2.0 to 4.0 s in the central business district and less than 1.0 s in the

mountainous areas. These results indicate an affect related to the thickness of alluvium in the coastal area of Padang city, which decreases in thickness inland.

### 3. SITE CHARACTERIZATION BY MICROTREMOR OBSERVATION

#### Microtremor Array Observations

The velocity of surface waves is well known to vary as a function of frequency (or period) due to dispersion. Since dispersion is a function of subsurface structure, the substructure can be estimated from a Rayleigh wave dispersion curve. We carried out microtremor array investigations using 12 sites at several districts in Padang (Fig.3). Dispersion curves were calculated using the SPAC method [13] to obtain a velocity structure from the microtremor recordings. An outline of the procedure follows. It is necessary to simultaneously record microtremors with an instrument array of at least three stations. The dispersion of a measured surface wave is a response to the subsurface structure directly below the array, and the estimation of the subsurface structure causing the dispersion is determined by means of inversion of Rayleigh waves. The basic principles of the SPAC method assume that the complex wave motions of microtremors are stochastic processes in time and space. A spatial autocorrelation coefficient for a circular array can then be defined when the waves composing the microtremor (i.e., the surface waves) are dispersive. Hence, the spatial autocorrelation is a function of phase velocity and frequency. Rayleigh wave records were measured for the 12-array observation sites using the SPAC method and inversion analysis was undertaken on the observed dispersion curves to estimate the soil profiles. In the inversion analysis, the Particle Swarm Optimization (PSO) algorithm was adopted to solve the nonlinear optimization problem [14]. The basic procedures of PSO are outlined below. The particle swarm concept originated as a simulation of simplified social system. The original intent was to graphically simulate the choreography of bird of a bird flock or fish school. However, it was found that particle swarm model can be used as an optimizer, PSO simulates the behaviors of bird flocking. Suppose the following scenario: a group of birds are randomly searching food in an area. There is only one piece of food in the area being searched. All the birds do not know where the food is. But they know how far the food is in each iteration. So what's the best strategy to find the food? The effective one is to follow the bird which is nearest to the food. PSO learned from the scenario and used it to solve the optimization problems. In PSO, each single solution is a "bird" in

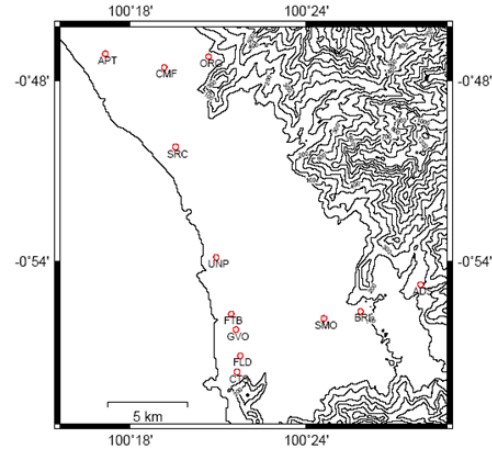


Fig.3 Array observation sites

the search space. We call it "particle". All of particles have fitness values which are evaluated by the fitness function to be optimized, and have velocities which direct the flying of the particles. The particles fly through the problem space by following the current optimum particles. PSO is initialized with a group of random particles (solutions) and then searches for optima by updating generations. In every iteration, each particle is updated by following two "best" values. The first one is the best solution (fitness) it has achieved so far. (The fitness value is also stored.) This value is called pbest. Another "best" value that is tracked by the particle swarm optimizer is the best value, obtained so far by any particle in the population. This best value is a global best and called gbest. When a particle takes part of the population as its topological neighbors, the best value is a local best and is called lbest.

We estimate the subsurface structure of the model by solving a nonlinear minimization problem with the fitness function below.

$$v_{id}^{t+1} = \omega v_{id}^t + c_1 r_1 (p_{id}^t - x_{id}^t) + c_2 r_2 (p_{gd}^t - x_{id}^t) \quad (1)$$

$$x_{id}^{t+1} = x_{id}^t + v_{id}^{t+1} \quad (2)$$

where  $v_{id}^t$  is particle velocity of the  $i^{th}$  component in dimension d in the interaction,  $x_{id}^t$  is the particle position of the  $i^{th}$  component in dimension d in interaction,  $c_1$  and  $c_2$  are constant weight factors,  $p_i$  is the best position achieved by particle  $i$ ,  $p^g$  is the best position found by the neighbor of particle  $i$ ,  $r_1$  and  $r_2$  are random factors in the [0,1] interval and  $\omega$  is the inertia weight. Before performing the inversion analysis, the subsurface structure was assumed to consist of horizontal layers of elastic and homogeneous media above a semi-infinite elastic body. The shear wave velocity and thickness of each layer are the parameters determined by the inversion analysis. The results enable us to determine the condition of



shallow subsurface structures (Ono et al., 2010). The outline of the SPAC method for the phase velocity calculation of Rayleigh waves follows.

$$F(\omega) = \frac{1}{2\pi} \int_{-\infty}^{\infty} f(t) \cdot \exp(-i\omega t) dt$$

$$= A_f(\omega) \cdot \exp(-i\phi_f(\omega)) \quad (3)$$

$$G(\omega) = \frac{1}{2\pi} \int_{-\infty}^{\infty} g(t) \cdot \exp(-i\omega t) dt$$

$$= A_g(\omega) \exp(-i\phi_g(\omega)) \quad (4)$$

$A_f(\omega)$ ,  $A_g(\omega)$  and  $\phi_f(\omega)$ , are difference between the amplitude of  $\phi_g(\omega)$ ,  $F(\omega)$ ,  $G(\omega)$  respectively. Further cross correlation in the frequency region of the two waveforms will be as follows.

$$= F(\omega) \cdot \overline{G(\omega)} = A_f(\omega) \cdot A_g(\omega) \cdot i\Delta\phi(\omega) \quad (5)$$

It shows the phase difference of  $\Delta\phi(\omega)$

$$\Delta\phi(\omega) = \frac{\omega r}{c(\omega)} \quad (6)$$

$c(\omega)$  is the phase velocity from the phase

difference.

$$CC_{fg} = A_f(\omega) \cdot A_g(\omega) \cdot \exp\left(i \frac{\omega r}{c(\omega)}\right) \quad (7)$$

The complex coherence of two waveforms is defined by the following equation.

$$COH_{fg}(\omega) = \frac{CC_{fg}(\omega)}{A_f(\omega) \cdot A_g(\omega)}$$

$$= \exp\left(i \frac{\omega r}{c(\omega)}\right) \quad (8)$$

$$Re(COH_{fg}(\omega)) = \cos\left(\frac{\omega r}{c(\omega)}\right) \quad (9)$$

$$c(\omega, \varphi) = \frac{c(\omega)}{\cos\varphi} \quad (10)$$

$$SPAC(\omega, r) = \frac{1}{2\pi} \int_0^{2\pi} \exp\left(i \frac{\omega r}{c(\omega)} \cos\varphi\right) d\varphi \quad (11)$$

$$Re(SPAC(\omega, r)) = \frac{1}{2\pi} \int_0^{2\pi} \cos\left(i \frac{\omega r}{c(\omega)} \cos\varphi\right) d\varphi \quad (12)$$

$$J\left(\frac{\omega r}{c(\omega)}\right) = \frac{1}{2\pi} \int_0^{2\pi} \exp\left(\frac{\omega r}{c(\omega)} \cos\varphi\right) d\varphi \quad (13)$$

where  $J_0(x)$  is the zero-order Bessel function of the first kind of  $x$ , and  $c(\omega)$  is the phase velocity at frequency  $\omega$ . The SPAC coefficient  $\rho(r, \omega)$  can be obtained in the frequency domain using the Fourier transform of the observed microtremors.

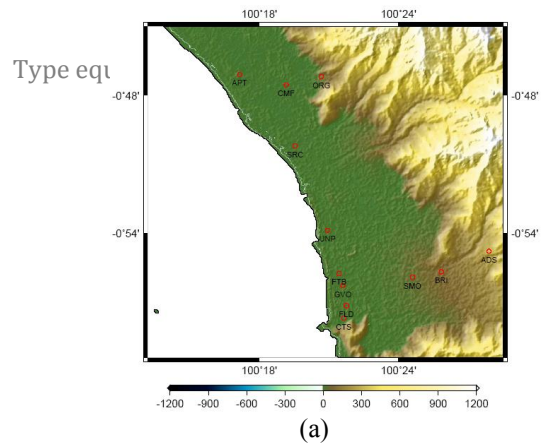
From the SPAC coefficient  $\rho(r, \omega)$ , the phase velocity is calculated for every frequency from the Bessel function argument of equation. 15 and the velocity model can be invert. The layer thickness and the average S-wave velocity in Figure 6 each array site. For the average S wave velocity model obtained by averaging the estimated ground structure of the array site was to be calculated by a weighted average using a S-wave velocity structure is estimated as a weighted layer thickness.

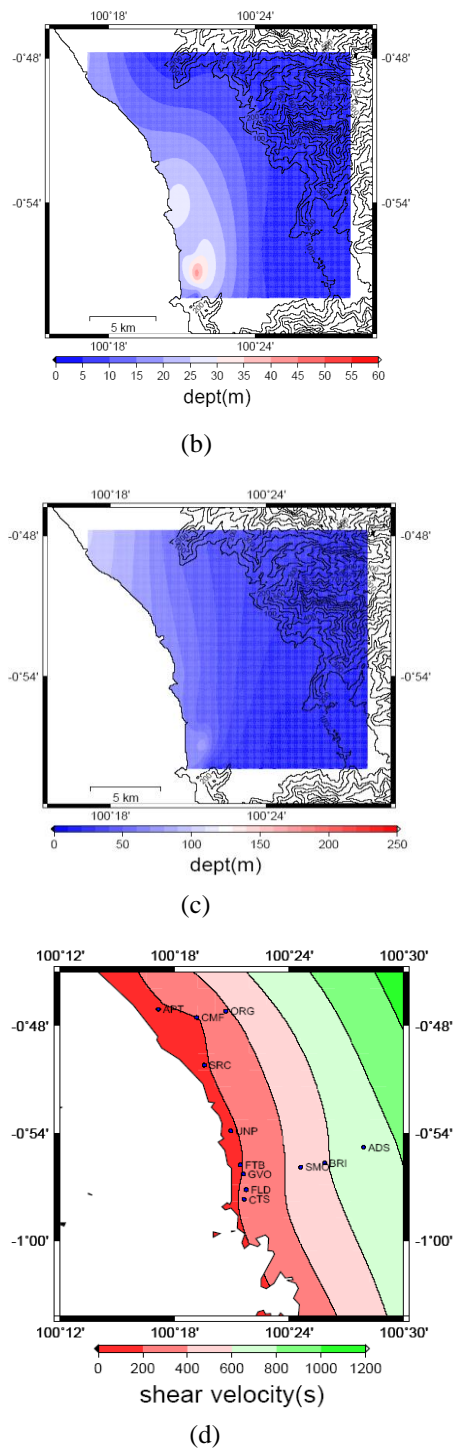
$$Re(SPAC(\omega, r)) = J\left(\frac{\omega r}{c(\omega)}\right) \quad (14)$$

From the SPAC coefficient  $\rho(r, \omega)$ , the phase velocity is calculated for every frequency from the Bessel function argument of equation. 15 and the velocity model can be invert. The layer thickness and the average S-wave velocity in Figure 6 each array site. For the average S wave velocity model obtained by averaging the estimated ground structure of the array site was to be calculated by a weighted average using a S-wave velocity structure is estimated as a weighted layer thickness.

$$\overline{V_s} = \sum V_{st} \cdot \frac{H_i}{H} \quad (15)$$

From the dispersion curve, we can produce an interpretation  $V_{s30}$  (average shear wave velocity for the upper 30 m) as show in Table 4, shows the contours of  $V_{s30}$  for every 200 m/s increment and soil characteristic every layer.



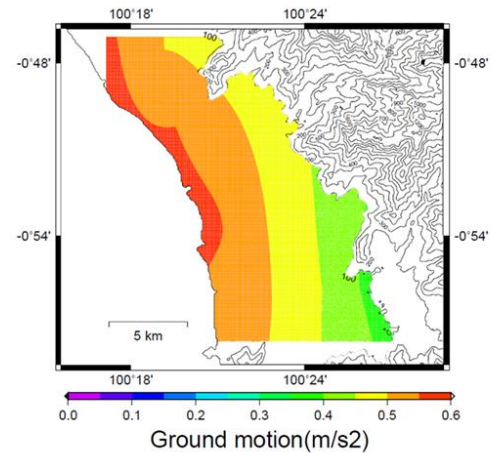


**Fig.4** Observation sites, soil profile and distribution of average shear wave velocity, (a) Array observation sites, (b) layer 1 ( $V_s < 400$  m/s) and (c) layer 2 ( $V_s > 400$  m/s), (d) Distribution of  $V_{s30}$  (m/sec).

#### 4. VULNERABILITY ASSESSMENT

Vulnerability can simply be defined as the sensitivity of the exposure to seismic hazard(s).

The vulnerability of an element is usually expressed as a percentage loss (or as a value between zero and one) for a given hazard severity level [16]. In a large number of elements, like building stocks, vulnerability may be defined in terms of the damage potential to a class of similar structures subjected to a given seismic hazard.



**Fig.5** Ground motion whole Padang city.

Vulnerability analysis reveals the damageability of the structure(s) under varying intensity or magnitudes of ground motion. Multiple damage states are typically considered in the analysis. Based on the data of damaged houses by ground shaking of Padang earthquake in 2009.

#### 5. ASSESSMENT TO RESIDENTIAL HOUSES

##### Survey Outline

The main purpose of assessment of housing has been used to quantify the structural condition after giant earthquake based on observed or interviewed to the owner its self. Since Padang has been conducted for seismic intensity in 2011 [11]. The method was originally developed by Japan architecture disaster prevention association earthquake. This method widely applied to assess houses for preventing future ground shaking due to predicted earthquake. It has been useful for estimating house condition such as the earthquake resistant performance and earthquake resistant repair to improve earthquake-resistant performance the observed houses by knowing the weak point at the structural. The original questionnaire sheet was written in Japanese (juutaku day taishinnshinndan); however, it was translated into Indonesian language for its application to Padang city. The questionnaire has 10 items that cover recognition of structural condition in general, had experience past giant earthquake and strengthened after struck by earthquake. Some sentences were modified to make

it more relevant to local people while not changing

the city The interviewers explained each item of the

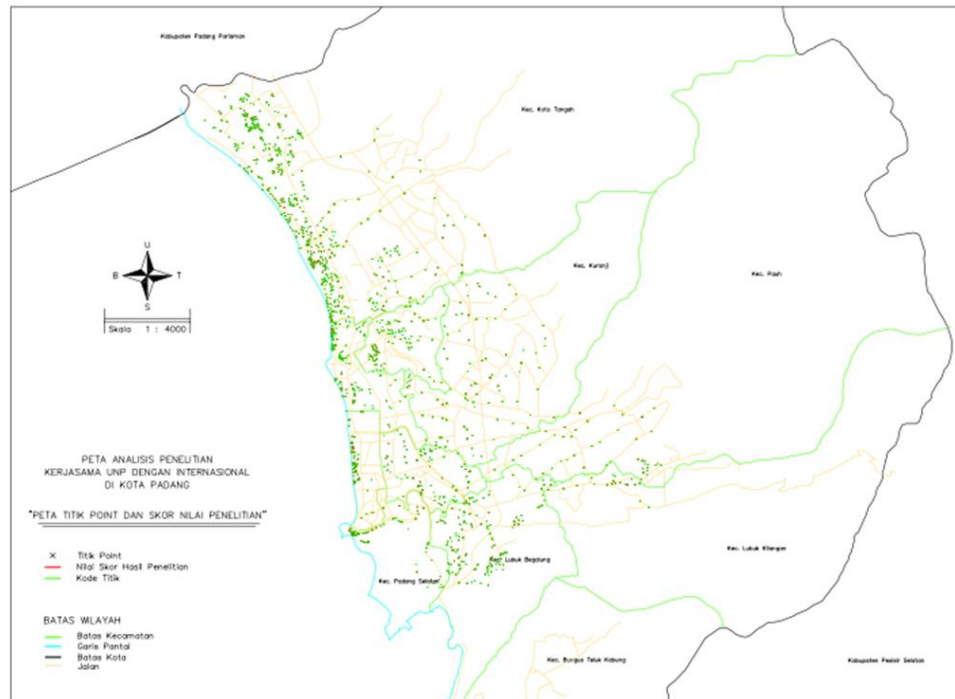


Fig. 6 Assessment distribution map in Padang

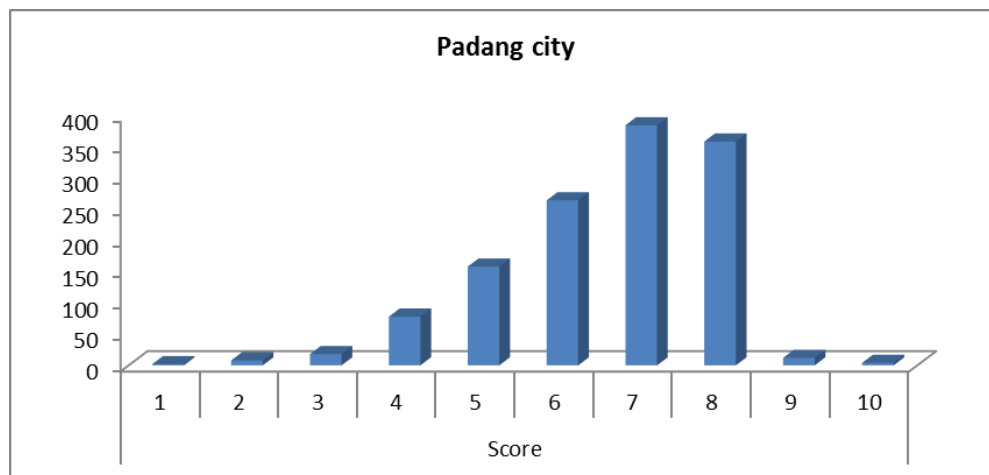


Fig. 7 Survey result show residential condition distribution in Padang city

the original topics covered by questionnaire. People living near the observation points were interviewed using the questionnaire [17][18]. The questionnaire survey was conducted from October 2<sup>nd</sup> to November 23<sup>rd</sup>, 2016. The survey was carried out in all districts of Padang by distributing and completing 1235 the questionnaire. People living near the observation points were interviewed using the questionnaire. The questionnaire survey was conducted from October 2<sup>nd</sup> to November 23<sup>rd</sup>, 2016. The survey was carried out in all districts of Padang by distributing and completing 1235 questionnaires through a direct interview process with residents of

questionnaire to residents, discussed the responses given, and documented the answers on the standard answer sheets. The results of the questionnaire survey conducted to estimate the houses condition distribution in Padang after earthquake in Padang 2009. The interview distribution showed in figure 11 and its result showed in figure 12, the interview result is indicated 98% of houses in Padang with score < 8 (Japan architecture disaster prevention association), its means the houses need to consult and discuss with experts directly soon as possible.



## 6. CONCLUSION

According to microtremor observations, downtown Padang is underlain by soft soil conditions ( $V_{s30} < 400$  m/s). Consistent results concerning the soil condition were found based on predominant period observations.

In both cases, the coastal area was determined to have a soft soil conditions ( $V_{s30} < 400$  m/s), a longer predominant period, and a greater seismic intensity.

Padang has a thick alluvial layer in the coastal area (with a predominant period between 2.0 and 4.2 s) that thins toward the mountains (with a predominant period less than 2.0 s). The subsurface geology also changes slowly from soft soil in the coastal area to rocky conditions in the mountains.

The results show clear information on soil condition especially at the downtown and residential houses current condition with 98% of houses need to consult to expert as soon as possible as a way to mitigate future earthquake event.

## 7. ACKNOWLEDGEMENTS

The author would like to thank to Professor Junji Kiyono from Kyoto University who provided strong support throughout the period. Thanks also go to Professor Yusuke Ono and Professor Noguchi from Tottori University, Japan for their great assistance during the field survey. Thanks to Dr. Safriani from Universitas Negeri Padang as research partner. Finally would like to thanks Indonesian government DIKTI who provided financial support on research schema Penelitian Unggulan Perguruan Tinggi year 2016.

## 8. REFERENCES

- [1] Prawirodirjo, L., Y. Bock, J.F. 2000, "One century of tectonic deformation along the Sumatran fault from triangulation and global positioning system surveys", J. of Geophysical research, 105, 28, 343-28,363.
- [2] Aislinn Laing, 2009, "More than 1000 feared dead in Sumatra earthquake", [www.telegraph.co.id](http://www.telegraph.co.id).
- [3] Natawidjaja and WahyuTriyoso 2007. "The Sumatran fault Zone-from Source to Hazard", J. of Earthquake and Tsunami, Vol. 1 No. 1, 21-47.
- [4] Rusnardi Rahmat Putra, J. Kiyono, Y. Ono, H Parajuli, "Seismic Hazard Analysis For Indonesia". Journal of Natural Disaster Science, Vol. 33, No.3 pp.59-70, June 2012.
- [5] EERI 2009. "The Mw 7.6 Western Sumatra Earthquake of September 30, 2009", Special report.
- [6] BNPB 2009 (National Disaster Management Agency of Indonesian Government). "Total damage report and verification for West Sumatra due to Padang earthquake", [www.bnpb.go.id](http://www.bnpb.go.id).
- [7] Rusnardi Rahmat Putra, J. Kiyono, Y. Ono, H Parajuli. 2012, *Seismic Hazard Analysis for Indonesia*, Journal of Natural Disaster Science, Vol. 33, No.3 pp.59-70, June 2012.
- [8] Rusnardi Rahmat Putra, Junji Kioyono, Aiko Furukawa, *Vulnerability Assessment of Non Engineering Houses Based on Ddamage Data of the 2009 Padang Earthquake in Padang City*, International Journal of Geomate, Vol 7, No.2 (SI.No.14) pp.1076-1083,2014
- [9] Rusnardi Rahmat Putra, Junji Kiyono, Yusuke Ono, Yasuo Yoshimoto, Syharil, *Determined Soil Characteristic of Palu in Indonesia by Using Microtremor Observation*, International Journal of Geomate, Vol. 10, No.2 (SI. No. 20) 1737-1742, 2016.
- [10] Rusnardi Rahmat Putra, *Estimation of Vs30 Based on Soil Investigation by Using Microtremor Observation in Padang, Indonesia*, International Journal of Geomate, Oct., 2017, Vol.13, Issue 38, pp.135-140, 2017
- [11] Rusnardi Rahmat Putra, J. Kiyono, Y. Ono, *Estimation of Earthquake Ground Motion in Padang City, Indonesia*. International Journal of GEOMATE, Vol..1 (S1.No.1), pp.71-77, October, 2011.
- [12] Padang City Statistic Center Agency of Local Government, [www.padangkota.bps.go.id](http://www.padangkota.bps.go.id). 2017.
- [13] Aki, K. 1957."Space and time spectra of stationary stochastic waves, with special reference to microtremor", Bull. Earth. Res. Inst., Vol. 35, No. 3, 415-456.
- [14] Keneddy, J. and Eberhart, R. C. *Particle swarm optimization*, Proc. Of IEEE International Conference on Neural Networks, Vol.4,pp.1942-1948, 1995
- [15] Ono, Y., Kiyono, J., Rusnardi, P. R. and Noguchi, T. 2010. *Microtremor Observation in Padang City, Indonesia to Estimate Site Amplification of Seismic Ground Motion*, Proc. of International Symposium on a Robust and Resilient Society against Natural Hazards and Environmental Disasters and the third AUN/SEED-Net Regional Conference on Geodisaster Mitigation, pp.386-391.
- [16] Baker, Jack W. 2008. "Introduction Probabilistic Hazard Analysis", handbook. Version 1.3 Oct 1st 2008.
- [17] Fallahi, A, P. Teymourzadeh, M. Miyajima, T. Tobita and R. Alaghebandian (2008). *Statistical Study to Determine JMA Earthquake Intensity by Questionnaire Survey in 2003 Bam (Iran) Earthquake*, The 14 World conference on earthquake engineering,

October 12-17, Beijing, China.

- [18] Sutrisno, Rusnardi, Ganefri, A *Comparative Study on Structure in Building Using Different Partition receiving expense earthquake*, International Journal of Geomate, Vol.13, Issue 37, pp.34-39, 2017.

## **RAINWATER HARVESTING STUDY AT MASJID JAMEK RIYAH DUS SOLIHIN, PINTAS PUDING, BATU PAHAT JOHOR MALAYSIA**

Amir Hashim Mohd Kassim<sup>1</sup>, Siti Mariam Sulaiman<sup>2</sup>, Radin Maya Saphira Radin Mohamed<sup>3</sup> and Adel Ali Saeed Al Gheethi<sup>4</sup>

<sup>1,2,3,4</sup> Department of Water & Environmental Engineering, Faculty of Civil & Environmental Engineering, Universiti Tun Hussein Onn Malaysia, 86400 Pt. Raja, Batu Pahat, Johor, Malaysia.

### **ABSTRACT**

Harvesting rainwater contribute towards a sustainable living. It eliminate the wastage and reduce the dependency of potable water. The demand of potable water increases in accordance to the population. Rainwater harvesting is capable to combat water crisis and serves as an alternative water resources during water shortage. The present study proposed a rainwater harvesting system for the mosque and obtain the rainfall amount at study area. The method used for designing the rainwater harvesting system is referred to MSMA 2<sup>nd</sup> Edition. The system is consists of downpipe filter (4"/ Ø150 mm), Eaves gutter (16, 000 mm<sup>2</sup>) first flush diverter 150 mm (63 liter; 1.78 length) and: taper tank (600 liters). Rainfall data for study area was recorded by HOBO tipping rain gauge for four months. Rainwater was calculated and harvested 116.7% yield to the water demand for the study area. The rainfall for four months at the study area showed that the rainwater demand was sufficient to be collected and used for the mosque activities. The highest rainfall data collected was 75.2 mm. This study would help to initiate a starting point to create a green mosque concept into reality. Furthermore, this system applied the concept of green building that create environmental friendly surrounding as a stepping stone to educate and at the same time save the environment and minimize the energy wastage.

*Keywords: Design of rainwater harvesting system, MSMA, Rainfall data*

### **INTRODUCTION**

The rainwater is a precious gift for us by nature. Since the creation of the Earth, rain has helped nourish the growth of myriad of flora and fauna and has provided precious drinking water for all creatures. Rainwater harvesting is as old as mankind. About 4,000 years ago in Rome, the Romans have been used rainwater for domestic purposes. Roman villages and cities of that time planned to take advantage of rainwater for drinking [1]

Clean water is a valuable and important source. Since clean water is important, it is seen as a waste for it to be used for flushing of toilets and watering plants. Rainwater is one of reliable source of clean water it can be used as a substitute by collecting and utilize it rather than let it go to waste. A part from that, by collecting rainwater from roof, flash flood affect can be reduced as few percentage of rainfall is retained and thus reduce the volume of surface runoff. Besides, by using rainwater as an alternative, clean water can be saved and used for other purposed and simultaneously decrease of demand of clean water resulted in lower cost of water bill and cost of operation in the water treatment plants. The use of untreated rainwater for non – potable uses that would otherwise be supplied by potable water ultimately conserves municipally supplied potable water [2].

Water shortage is becoming the number one problem in the world today. Moreover, the problem of water scarcity is strongly connected to the

problem of water quality. Urban development, human activities and industrialization deteriorate the quality of water and, in some cases, make it unsafe for consumption [3]. Some effort has been made to reuse ablution water from mosques (masjid), which it has low contaminant and consist of high volume from the cleansing ritual [4] [5]. However, the utilization of the rainwater harvesting in mosque has not widely discussed in the case study.

Developing of region increase the water demand and reduce capability of drainage area to maintain overland flow judging the increasing of runoff coefficient. Fast growing development in Parit Raja especially at Pintas Puding area now has begun to increase of the water demand due to the rapid urbanization and dependence on main water supply.

In order to overcome the water crisis, domestic rainwater harvesting has been carried out which is an alternative solution for these problem. Rainwater harvesting is a simple ancient technique of collect water and storage. This technique has been practiced in Sri Lanka to meet the growing water demand on water supply; a good example is the sophisticated rainwater cum reservoir system in 5<sup>th</sup> century Sigiriya fortress complex. In Malaysia, a study on rainwater harvesting and utilization system (for non potable household use), coupled with detention storage (to reduce peak storm runoff), for double storey terrace house at Taman Wangsa Melawati, Kuala Lumpur was carried out. Therefore, all of the advantages of using rainwater harvesting will be

combined in this further study to overtake the water crisis besides reducing water bills for the mosque.

Rainwater harvesting is a technology used for collecting and storing rainwater from rooftops, the land surface of rock catchments using simple techniques such as jars and pots as well as more complex techniques such as underground check dams and ponds. Commonly used systems are constructed of three principal components; which are the catchments area, the collection device and the conveyance system. The captured rainwater could be used for domestic usage such as drinking, cooking, toilet flushing, and other public facilities.

This study was conducted to propose a rainwater harvesting system at the study area with the collected data.

## METHODOLOGY

### Design of Rainwater Harvesting System

The study area is located at Masjid Jamek Riyahdus Solihin in Batu Pahat, Johor, Malaysia. This mosque is located nearby to Sekolah Kebangsaan Pintas Puding, and Kolej Jururawat Masyarakat Batu. Rainwater harvesting is a technique of collecting rainfall as a source of water supply for household, commercial and industrial premises. The planning and development of rainwater harvesting system shall be carried out adhering to the principles and guideline describes in MSMA (Urban Stormwater Management). The value of rainwater as the primary source of clean water is always ignored. Rainwater harvesting using roof catchments is the easiest and most common method.

### Determine Average Rainfall Intensity

Average rainfall intensity determined by referring to the intensity – duration – frequency (IDF) curves at study area city or the nearest. Basically, to obtain the most accurate amount of the rainfall intensity, Eq. (1) can be used.

$$i = \frac{\lambda T^K}{(d + \theta)^{\eta}} \quad (Eqn. 1)$$

Where,

$i$  = Average rainfall intensity (mm/hr);

$T$  = Average recurrence interval-ARI ( $0.5 \leq T \leq 12$  month and  $2 \leq T \leq 100$  years)

$d$  = Storm duration (hours),  $0.0833 \leq d \leq 72$ ; and

$\lambda, K, \theta$  and  $\eta$  = Fitting constants dependent on the rain gauge location

### Determine the Catchment Area

The rooftop act as the catchment area for this

study. Rooftop dimension such as width, base and slope was taken by measure at the study area. The total catchment area can be determined by using Eq 2.

$$\text{Total catchment area} = Ah \times Ar \quad (Eqn. 2)$$

Where,

$Ah$  = plan area ( $m^2$ )

$Ar$  = rise vertical area ( $m^2$ )

### Gutter and RWDP Sizing

Gutter and downpipe size was determined by referring to the design chart from MSMA 2<sup>nd</sup> Edition (Chapter 6) [6]. The size determine by considering the rooftop gradient and the total flow of the rainfall.

### First Flush Diverter

First flush diverter is a must component in rainwater harvesting. It separate debris from entering the storage tank to control the quality of the rainwater. First flush diverter was determined according to standard as stated in MSMA 2<sup>nd</sup> Edition (Chapter 6) [6]. First flush volume requirement are based on the roof area or the catchment area. Figure 1 shows the illustration of the first flush diverter.

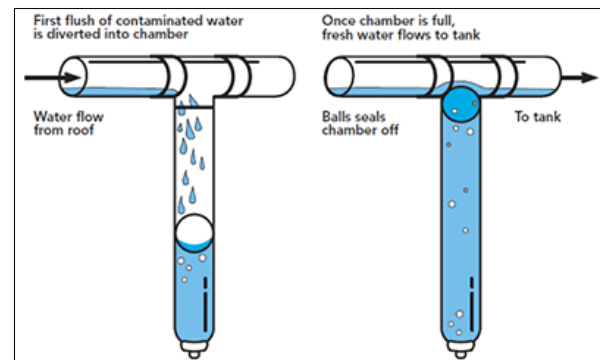


Fig 1 Illustration of first flush diverter

### Tank size Estimation

There are various types of rainwater harvesting tank. In general, the rainwater tank can be divided into either above – ground tank or below – tank. The tank shapes can be circular, or rectangular. The tank sizing was determined based on the Yield Before Spillage (YBS) model. Tank size of 1  $m^3$  is for roof area of 100  $m^2$ . Tank size ( $m^3$ ) can be determined according to Eq. 3.

$$St = 0.01 Ar \quad (Eqn. 3)$$

Where,

$St$  = Tank Size ( $m^3$ )

$Ar$  = Rooftop Catchment Area ( $m^2$ ).

### Determine the Water Demand

Water demand was determined based on the average consumption, and average total rainwater demand at the study area. Total use per day and the annual rainwater demand need to be determined in unit of m<sup>3</sup> and in percentage. Water demand determination is important to determine whether the rainwater supplied is sufficient to fulfill the water demand at study area. Table 1 shows the estimation amount of water used for different application.

Table 1 Amount of Water Uses for Different Applications (DID, 2009)

Use (Appliance)	Type	Average Consumption	Average total Rainwater Demand
Indoor Toilet	Single Flush	9 litres per flush	120 litres per day
	Dual Flush	6 or 3 litres per flush	40 litres per day
Washing Machine	Twin Tub (semi – auto)		40 litres per wash
	Front Loading		80 litres per wash
	Top Loading		170 litres per wash
Dishwasher	-		20 – 50 litres per load
General Cleaning	-	10 – 20 litres per minutes	150 litres per day
Outdoor Sprinkler	or	10 – 20 litres per minute	1000 litres per hour
handheld hose			
Drip System	Paths/	4 litres per hour	200 litres per wash
Hosing	Driveways	20 litres per minute	
Washing car with a Running hose		100 – 300 litres per minute	

### Collection of Rainfall Data

Collection of rainfall data at the study area is taken for almost four months at the study area. The rainfall data collected using the rain gauge that was installed a few meters from the location of the RWH system. The rainfall data and temperature for every 3 minutes from 28<sup>th</sup> August 2016 were recorded until 20<sup>th</sup> November 2016 using HOBO tipping rain gauge.

## RESULTS AND ANALYSIS

### Average Rainfall Intensity

In order to maximize the error in estimating the amount of rainfall intensity values from the IDF curves, the empirical equation 1 was applied. The fitting constants dependent on the rain gauge location (Table 2)

The system designed using the average recurrence interval – ARI, T is for 10 years with 10 minutes of storm duration, d.

Johor	$\Lambda$	$\kappa$	$\theta$	$\eta$
Stor JPS Johor Bahru	59.972	0.163	0.121	0.793
Pusat Kem. Pekan Nenas	54.265	0.179	0.1	0.756
Johor Silica	59.06	0.202	0.128	0.66
Balai Polis Kg. Seelong	50.115	0.191	0.099	0.763
SM Bukit Besar	50.554	0.193	0.117	0.722
Setor JPS BatuPahat	64.099	0.174	0.201	0.826
Ladang Ulu Remis	55.864	0.166	0.174	0.81
Simpang Masai K. Sedili	61.562	0.191	0.103	0.701
Emp. Semberong	60.568	0.163	0.159	0.821
Pintu Kaw. Tg. Agas	80.936	0.187	0.258	0.89
JPS Kluang	54.428	0.192	0.108	0.74
Ladang Chan Wing	57.188	0.186	0.093	0.777
Ladang Kekayaan	53.457	0.18	0.094	0.735
Ibu Bekalan Kahang	52.177	0.186	0.055	0.652
JalanKluang–Mersing	56.966	0.19	0.144	0.637
LadangLabis	45.808	0.222	0.012	0.713
Rmh. Tapis Segamat	45.212	0.224	0.039	0.711
Kg Peta Hulu Sg Endau	59.5	0.185	0.129	0.623
Setor JPS Endau	62.04	0.215	0.103	0.592

Table 2 Fitting constants dependent on the rain gauge (MSMA 2<sup>nd</sup> Edition)

$$i = \frac{(64.099)(10)^{0.174}}{(0.1666 + 0.201)^{0.826}}$$

$$i = 218.71 \text{ mm/hr}$$

### Catchment Area

Plan area, Ah = 25 m×22 m= 550m<sup>2</sup>

Rise Vertical area, Ar =25×0.5 m=12.5m<sup>2</sup>

$$\begin{aligned}
 \text{Total catchment area} &= A_h \times A_r \quad (\text{Eqn. 2}) \\
 &= 550 + (12.5/2) \\
 &= 556.3 \text{ m}^2
 \end{aligned}$$

### Calculation of Gutter and Downpipe Size

As the gradient of the rooftop surface is flatter than 1:500, with the calculated value of average rainfall intensity and total catchment area, the sizing of the eaves gutter is able to be identified as 15.75 m<sup>2</sup> with 4.0L/s total flow. Therefore, 150 mm diameter of circular downpipe was taken from Table 3.

Table 3 Required Size of Downpipe for Eaves Gutter (AS/NZS 3500.3, 2003)

Eaves Gutter Size (mm <sup>2</sup> )	Minimum Nominal Size of Downpipe (mm)	
	Circular	Rectangular
4,000	75	65 x 50
4,200		
4,600		75 x 50
4,800	85	100 x 50
5,900		
6,400	90	75 x 70
6,600		
6,700	100	100 x 75
8,200		
9,600	125	100 x 100
12,800		
16,000	150	125 x 100
18,400		
19,200	Not applicable	150 x 100
20,000		125 x 125
22,000		150 x 125

This study determines the size of the down pipe by using the size of the gutter. However, it is different for other researcher. Study by Villarreal and Dixon (2005)[7] determine the size of the downpipe by referring to the material of the downpipe itself. Villarreal and Dixon (2005) [7] use concrete pipe with diameter of 300 mm compare to other researcher with the use PVC pipe with diameter of 65 mm. The pipe size for this study is within the range from the previous study which shows that the size is suitable to be used.

### First Flush Volume

The first flush need to install with suitable volume according to its standard as suggested in the MSMA 2nd Edition (Chapter 6). This is important to prevent

the contaminants and debris collected from the roof surface from entering the storage tank.

Table 4 First Flush Requirement According To Roof Area (DID, 2009)

Roof Area (m <sup>2</sup> )	First Flush Volume (m <sup>3</sup> )
Less than 100	0.025 – 0.05
100 – 4356	0.05 – 2.5
Greater than 4356	2.5

Note: Adopt first flush of 5 m<sup>3</sup> if surface contains excessive soil, dust or debris.

### Tank Size Estimation

Based on the Yield Before Spillage (YBS) model suggested for the procedures in estimating the rainwater availability, the estimation of the Average Annual Rainwater Yield (AARY) was carried out by using the water balance model for the selected towns in Malaysia and summarize that tank size for Malaysia regardless of location is 1m<sup>3</sup> for roof area of 100m<sup>2</sup>. With the 10 mm of rainfall is equivalent to be stored from 100 m<sup>2</sup> of rooftop area. The tank size was determined by using Equation 3.

$$St = 0.01Ar \quad (\text{Eqn. 3})$$

Where,

St = Tank Size (m<sup>3</sup>); and

Ar = Rooftop Catchment Area (m<sup>2</sup>).

$$St = 0.01 (556.3)$$

$$St = 5.563 \text{ m}^3$$

### Water Demand

The rainwater demand depends on the number of people using the water, average consumption and also the range of uses by the consumer. The water demand for the rainwater influences the effectiveness and availability of designed rainwater storage tank.

Table 5 Rainwater Demand for Domestic Application (DID, 2009)

Use (Application)	Type	Average Consumption	Average Total Rainwater Demand
Toilet	Single Flush	9 litres per flush	120 litres per day
General washing	-	10-20 litres per minute	150 litres per day

$$\begin{aligned}
 \text{Total use per day} &= 120 \text{ l/day} + 150 \text{ L/day} \\
 &= 270 \text{ l/day}
 \end{aligned}$$

The annual rainwater demand = 365 days  $\times$  300 L/day = 98.55 m

Compute the Average Annual Rainwater Yield for town ( $\text{m}^3$ )

From Table 5, take the nearest Kluang, The AARY for 1m3 tank size =  $1 \times 115 = 115\text{m}^3$

Compute the percentage of water yield over rainwater demand

Percentage of rainwater yield over rainwater demand =  $(115/98.55) \times 100 = 116.7\%$

### Rainfall Data

The rainfall data was collected for almost four months (August until November) using the rain gauge that installed few meters from the location of the RWH system. The rainfall data and temperature for every 3 mins from 28<sup>th</sup> August 2016 were recorded until 20<sup>th</sup> November 2016 using HOBO tipping rain gauge. Figure 6 shows the rainfall amount and temperature collected at study area.

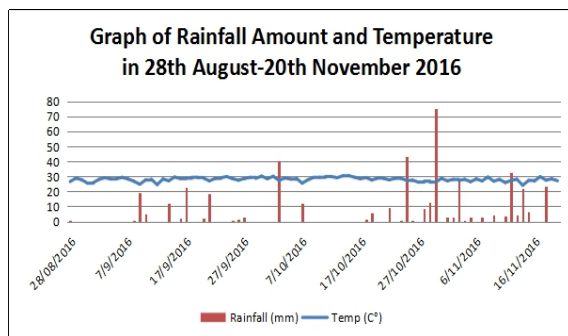


Fig. 2 Rainfall amount and temperature collected

According to website from the Department of Irrigation and Drainage Malaysia (DID), <http://infokemarau.water.gov.my/realtime.cfm>, 2017), the rainfall data that were recorded at Sri Medan show that the highest rainfall data recorded is 77.00 mm which is the same as the rainfall data in Figure 3. The data are comparable due to Malaysia's equatorial climate. Equatorial climate can be defined as the climate where there is a constant temperature, high moisture content and generally high rainfall intensity. Figure 3 shows the rainfall amounts that were obtained from infokemarau website <http://infokemarau.water.gov.my/realtime.cfm>, 2017),

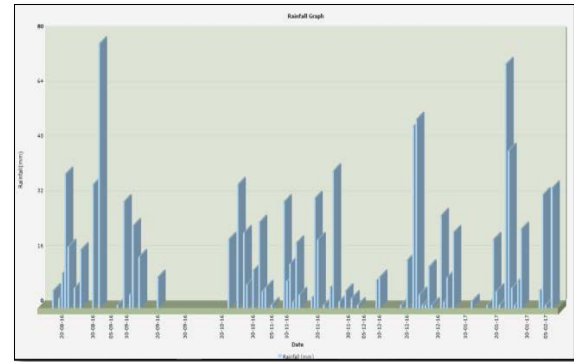


Fig. 3 Recorded rainfall data from infokemarau (2017)

### CONCLUSION

From the study, it is promising if the rainwater harvesting is practices in mosque, it serves as a substitution for non – potable water usage for domestic activities such as flushing and irrigation and supplying freshwater in the face of increasing water scarcity and escalating demand. The component that needs to be used for this RWH system is design based on the MSMA 2<sup>nd</sup> Edition. The components proposed Downpipe filter (4"/Ø150mm), Eaves gutter (16, 000mm<sup>2</sup>), First flush diverter 150mm (63 liter; 1.78 length), : taper tank (600liters) and Outgoing Distributions Pipe from RWH Tank Main Discharge Point to Nearest Irrigation Tap or Usage Points (Ø35mm). The rainwater is calculated 116.7% yield to the water demand for the study area. The rainfall for four months at the study area shows that the rainwater demand is sufficient to be collected and used for the mosque activities. The highest rainfall collect is recorded to be 75.2 mm.

By using rainwater, many benefits can be seen economically and environmentally where water can be saved and can reduce impacts from flash flood phenomena respectively. It is important that mosque would take rainwater harvesting system seriously in realizing its objectives to become a green mosque that creates an environmental friendly surroundings and the same time save the environment and minimize the energy usage.

### ACKNOWLEDGEMENT

We wish to thank research grant FRGS 1453 and IGSP vot U682 for financial assistance during the study.

### REFERENCES

- [1] Amir Hashim Mohd Kassim (2006), Improvement of Rainwater Quality using the Bio-sand Filtration, Department of Water Resources and Environmental Engineering, Faculty of Civil and



Environmental Engineering, Kolej Universiti Teknologi Tun Hussein Onn (KUiTTHO).

[2] Persyn R., Russell A., Porter D. O. and Silvy V.A., (2004). Rainwater Harvesting, Texas Cooperative Extension, Texas agricultural and Mechanical University System.

[3] Nazahiyah Rahmat, Zarina Md Ali, Sabariah Musa (2008), Treatment of Rainwater Quality Using Sand Filter. Department of Water and Environmental Engineering, Faculty of Civil and Environmental Engineering University Tun Hussein Onn Malaysia (UTHM, Malaysia).

[4] RMSR Mohamed, MN Adnan, MA Mohamed, AHM Kassim Conventional Water Filter (Sand and Gravel) for Ablution Water Treatment, Reuse Potential, and Its Water Savings, Journal of Sustainable Development 9 (1), 35 (2016).

[5] RMSR Mohamed, AA Al-Gheethi, JA Rahman, AHM Kassim, S Musa, Reuse of Ablution Water to Improve Peat Soil Characteristics for Ornamental Landscape Plants Cultivation, MATEC Web of Conferences 103, 05003 (2017).

[6] Manual Mesra Saliran Alam (MSMA) 2<sup>nd</sup> Edition (Chapter 2 to 6), Department of Irrigation and Drainage Malaysia.

[7] Villarreal, E. L. and Dixon, A. (2005). Analysis of a rainwater collection system for domestic water supply in Ringdansen, Norrköping, Sweden. Building and Environment, 40(9), 1174-1184.

## *Authors Index*

<b>A</b>		ChitsanuphongThanutong	332
A. Sivaruban	124	Choo Yong	283
A.A.S. Al-Gheethi	417	Chutarat Chompunth	455
A.M. Kostryukova	395,399,405		
Abd El Halim O	299	<b>D</b>	
Adisak Martsri	342	D. K. Weerakoon	124
Agrianti Komalasari	477	Daniela Ionescu	33
Agustinus C. B. Kantale	97	Darga Kumar Nandyala	321
Ahmad Husein Alkaff	97	Darren Newell	283
Ahmad Rasidi Osman	231	David Morgan	426
Ahmad Zubair	524,528	David Thorpe	12,266
Ahmad Zuhdi Ismail	315	Donlaya Promkaew	136
Aki Matsumoto	432	Dr Bandita Mainali	33
Alan Lymbery	426	Dr.Maitree Pakarasang	140
Alex Otieno Owino	172	Dr.Thanarat Sripongngam	140,146
Alireza Rezagholilou	360	Dr.Wichai Eungpinichpong	140
Amir Hashim Kassim	417		
Andreea Maria Chelaru	437	<b>E</b>	
Aniza Ibrahim	214	E.E. Shchelkanova	405
Annisa Novantri	422	Eddy Setiadi Soedjono	462
Apichat Deeminoi	140,146	Eman Albalawi	496
Ashraf Dewan	496	Environment	390
Ashraf Memon	22	Erwin Prasetya Toepak	39,45
Atika Marnolia	45	Esty Suyanti	524,528
		Eungpinichpong W	113
<b>B</b>			
Boontarika T.	391	<b>F</b>	
Bruce W. Melville	202	Fadhil Al-Asadi	309
Buddhapala Wongkaew	51,332	Fadhluhartini Muftah	231,237
Bungorn Sripanidkulchai	150	Faijal Ali	321
<b>C</b>		Fatmah	117
Chaisri Suksaroj	508	Fauzan	224,249
Chan V. K.	449	Febrin Anas Ismail	249
Chaowalit Hamontree	305	Feroza shar Baloch	514
Chee-Loong Wong	488	Firdaus Ali	524
Chihiro Yoshimura	196		

# *Authors Index*

## **G**

G. Kandasamy	124
Guilherme Marins Pessanha	293

## **H**

H.N.P. Singh	159
Hafiz S.A. Yahya	107
Hapsa Husen	214
Harada, H.	172
Hidehiro Koyamada	57,67,72
Hidetaka Noritomi	443
Hiroaki Shigematsu	208
Hiroki Suyama	57,67,72
Hiroshi Kita	338
Hiroyuki Daimon	411
Hong Bum Park	467
Hossain	172

## **I**

I Made Wahyu Wijaya	462
I.V. Mashkova	395,399,405
Ignatius Rendroyoko	184
Irene Sondang	524,528
Irfana Kabir Ahmad	214
Isamu Yoshitake	373

## **J**

Jaime Massaguer Hidalgo Jr	293
Jana VASKOVA	260
Jaruk Keawsod	163
Javad Asad Poor	266
Jeffrey Johns	77
Jestin Jelani1	214
Jim Shiau	309,354
Jingliang Dong	379
Jirapon Kulkham	391

Jiraporn Chuenjai	305
Jiraporn Krasaetep	62
Jiyuan Tu	379
John Russell	33
John Victor Smith	243
Jongprasithporn	342
Jumpei Nishigami	443
Juswono Unggul P.	502

## **K**

Kamarul Ismail	482
Kanaporn Tansriprapasiri	130
Kanchana Nimsuntorn	130
Kansiri Pakkethati	154
Karim Ismail	299
Katipelly, N. D.	449
Katsumi Uchiyama	443
Kazuhiro ODA	327,338
Kazunari TANAKA	473,517
Keigo KOIZUMI	327,338
Kennedy K.	521
Kiao Inthavong	379
Kingsley Osezua Akeme	360
Kittima Vanichkul	391
Koiwanit, J.	254,449
Koji Takasu	57,67,72
Kristiyanto	534
Kunihiko Fukaura	432
Kyeong Mo Lim	467

## **L**

Laojeenwong P	113
Le Ma1	426
Lessandro Estelito O. Garciano	276
Lev Zuev1and Yulia Li	91
Lily Surayya Eka Putri	534

# *Authors Index*

Lindrianasari	477	Ngapuli I Sinisuka	184
Luciana Omar	299	Nicoleta Popa	437
Lyn A. Gettys	432	Niramol Patjanasoontorn	83
		Nobuyuki Endo	443
<b>M</b>		Noor Suraya Romali	315
M. Faisal	411	Noor, Johan A. E.	502
M.M. Prasad	159	Nor Kalsum Mohd Isa	482
M.Z.	172	Nordila Ahmad	196,202
Mahatma Kufepaksi	477	Nurina Fitriani	462
Mamoru Yamada	432	Nutjaree Johns	77
Manutchanok Jongprasithporn	348	Nutthanun Tatchananusorn	136
Maratree Plainsirichai	62		
Maria McCrann	33	<b>O</b>	
Maria Visa	437	Ojiro C.	172
Marthinus Sonnekus	243	Okuyama, S.	172
Mazlini Adnan	482	Ozumi, S.	172
Meysam Banimahd	360		
Mia Nurkanti	422	<b>P</b>	
Mitsuru Komatsu	338	Pachanuporn Sunon	77
Mochammad Fardiansyah	97	Panupong Thanutong	51,332
Mohammad Mirza Hassan	354	Piewkhow L.	449
Mohammed M. Khattab	190	Piyathida Kuhirunyaratn	87,130
Mohd Hairry Ibrahim	482	Poonpakdee P.	254
MohdSyahrul Hisyam Sani	231,237	Porntip Wongkaew	51,77,332
Mohd. Raihan Taha	214	Preetham Kumar	383
Muhammad Isha Ismail	237		
Muhammad Tahir Rajput	514	<b>R</b>	
Muntana Nakornriab	62	R. Jachrizal Soemabrata	528
		Radim CAJKA	260
<b>N</b>		Radin Maya S. Mohamed	417
Nabila Shah Jilani	514	Ravikant R Singh	321
Najeeha Apandi	417	Rendy Pramuda Putra	97
Nantakrit Yodpijit	342,348	Rifda Rahman	462
Nawaporn Chamnanketgorn	305	Rika Oie	67
Nazar K. Oukaili	178,190	Rio Sandi	249
Neneng Suliasih	422	Robert Corner	496

## *Authors Index*

Rotchanatch Darnsawasdi	508	<b>T</b>	
Ruddy Kurniawan	224	T.G. Krupnova	395,399,405
<b>S</b>		Taizo Uchida	432
S.S Hassney	514	Takeshi YAMAMOTO	327
Sam M Dakka	368	Tarmizi Ismail	488
Saming Champasri	391	Thamer Mohammad	202
Sang Kil Park	467	Thuy Thi Thanh LE	287
Sartaj M.	521	Tjut Chamzurni	411
Satoru Kato	443	Tobalt A.	521
Saudee Maprasit	508		
Seezar Sh. Abdullah	178	<b>U</b>	
Seiki KAWAGOE	287	Uraiwan Chatchawan	136,150
Sengheng Hul	196	Usman Sumo Tambunan	39,45,97
Shahjahan Khan	22		
Shahrin Mohammad	231	<b>V</b>	
Sheena I. Better	276	Vanissorn Vimonsatit	373
Shek Poi Ngian	231	Vasundhara Acharya	383
Shin YOSHIKAWA	473,517	Vichit Rangpan	508
Shogo Hashimoto	208		
Shuto Takeuchi	473	<b>W</b>	
Sipanut Silaket	83	Wannapong Yeamma	342
Siravitch Atipatha	348	Warangkana Chompoopan	83
Sisikka Wannajun	62	Wardoyo Arinto Y.P.	502
Siti Hanggita Rachmawati	167	Wichai Eungpinichpong	83,136,150,163
Siti Nor Hidayah Arifin	417	William T. Haller	432
Stephen Beatty	426	Worawut Chompoopan	87
Sunisa Kunarak	219		
Sunita Kumari	159		
Supapat Phuangkaew	342,348	<b>Y</b>	
Suparman	103	Yidan Shang	379
Suwanna Arunpongpaisal	83,150	Yodthong Baimark	154
Suwita Saepaisan	51	YoichiMimura	373
Svetlana Barannikova	91	Yong Goh	266
Syafrida Siregar	39	Yonik Meilawati Yustiani	422
		Yoshifumi Kochi	432
		Yoshio FUKUDA	327

## *Authors Index*

Yuangyai, C.	254
Yuki OGIMOTO	517
Yuki takagi	57
Yuto Murakami	72
Yuya Imamura	432
Yuztitya Asmaranti	477

## **Z**

Zakaria Hossain	167
Zev Al Jauhari	224
Zuliziana Suif	196,202
Zulkifli Yusop	315,488

# SEE-Nagoya 2018

**Fourth International Conference on  
Science, Engineering & Environment  
12-14 November 2018, Nagoya, Japan**

## Invitation to participate

- The "International Journal of GEOMATE" is a Scientific Journal of the GEOMATE International Society that encompasses a broad area in Geotechnique, Construction Materials and Environment.
- The key objective of this journal is to promote interdisciplinary research from various regions of the globe.
- The editorial board of the journal is comprised of extensively qualified researchers, academicians, scientists from Japan and other countries of the world.
- It is peer-reviewed Journal that is published quarterly till 2015 and now bimonthly. All articles published in this journal are available on line.
- Contributors may download the manuscript preparation template for submitting paper or contact to the Editors-in-Chief

[[editor@geomatejournal.com](mailto:editor@geomatejournal.com)].

ISSN: 2186-2990

DOI: <http://dx.doi.org/10.21660/geomate>



Scopus

EBSCO

CENGAGE Learning

U GIF GLOBAL IMPACT FACTOR



VOLUME 00  
Issue 00  
Month, Year

## International Journal of GEOMATE

(Geotechnique, Construction Materials and Environment)



THE GEOMATE INTERNATIONAL SOCIETY

Tsu, Japan

<http://www.geomatejournal.com/>